Cover Picture

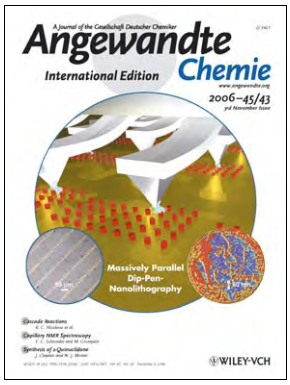

Khalid Salaita, Yuhuang Wang, Joseph Fragala, Rafael A. Vega, Chang Liu, and Chad A. Mirkin*

Massively parallel dip–pen nanolithography is possible when 55000 AFM cantilevers are used to write molecules directly onto a surface. An optical micrograph shows the surface after etching (cover picture, left), and each round feature is a miniature image of the face of Thomas Jefferson (AFM image, right), who helped develop the polygraph, a duplicator based on an array of pens. For more information on the new technique see the Communication by C. A. Mirkin and co-workers on page 7220 ff.

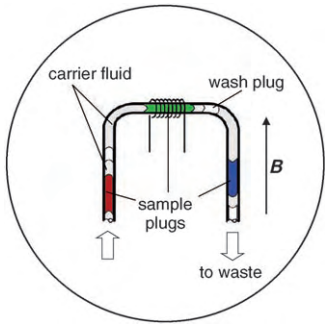

Capillary NMR Spectroscopy
In their Minireview on page 7122 ff., F. C. Schroeder and M. Gronquist discuss capillary NMR technology, its application in the characterization and screening of mass-limited small-molecule and protein samples, and its use in combination with other analytical methods.

Cascade Reactions
Cascade reactions are far from trivial but worth the effort, as K. C. Nicolaou et al. discuss in their Review on page 7134 ff. The advantages of this approach are highlighted with a multitude of applications in total synthesis.

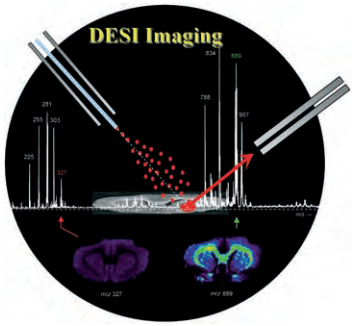

Mass Spectrometry and Imaging
In their Communication on page 7188 ff., R. G. Cooks and co-workers introduce desorption electrospray ionization (DESI) mass spectrometry as a technique to generate images of rat brain tissue under ambient conditions and two-dimensional maps of specific compounds therein.

Contents

VIP *The following Communications have been judged by at least two referees to be "very important papers" and will be published online at www.angewandte.org soon:*

B. V. Popp, J. E. Wendlandt, C. R. Landis, S. S. Stahl**
Reaction of Molecular Oxygen with an NHC-Coordinated Pd^0 Complex: Computational Insights and Experimental Implications

R. Martinez, R. Chevalier, S. Darses, Jean-P. Genet**
A Versatile Ruthenium Catalyst for C–C Bond Formation through C–H Bond Activation

*H. Nuss, M. Jansen**
$Cs_5([12]crown\text{-}4)_2(O_3)_5$: The First Supramolecular Ozonide Compound Containing $^1{}_\infty\{Cs_8(O_3)_{10}\}^2$ Rods

F. Camerel, R. Ziessel, B. Donnio, C. Bourgogne, D. Guillon, M. Schmutz, C. Iacovita, Jean-P. Bucher*
Formation of Gels and Liquid Crystals Induced by Pt···Pt Interactions in Luminescent σ-Alkynyl Platinum(II) Terpyridine Complexes

*R. Matsubara, S. Kobayashi**
Catalytic Asymmetric Amination of Enecarbamates

*N. Borho, Y. Xu**
Lock-and-Key Principle on a Microscopic Scale: The Case of the Propylene Oxide·Ethanol Complex

Web Sites

http://http://www.ochem4free.com — Organic Chemistry Online ... and for Free? — *A. B. Machotta, M. Oestreich* — 7114

Books

Organic Light-Emitting Devices — Klaus Müllen, Ullrich Scherf — *reviewed by C.-S. Hsu* — 7115

The Nanotech Pioneers — Steven A. Edwards — *reviewed by V. Balzani* — 7116

Highlights

Strained Molecules

J. Clayden,* W. J. Moran — 7118 – 7120

The Twisted Amide 2-Quinuclidone: 60 Years in the Making

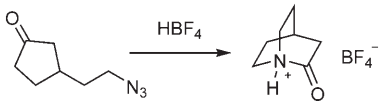

No longer left to the imagination: Non-planar amides have intrigued chemists for decades. This year, a story 60 years in the making came to an end: 2-quinuclidone has finally been synthesized and isolated in the form of its HBF_4 salt (see scheme).

Minireviews

NMR Spectroscopy

F. C. Schroeder,*
M. Gronquist — 7122 – 7131

Extending the Scope of NMR Spectroscopy with Microcoil Probes

... and to cap it off: Capillary NMR (CapNMR) spectroscopy is emerging as a major breakthrough in increasing the mass-sensitivity of NMR spectroscopic analysis. As discussed in the Minireview, not only is the acquisition of the spectra of mass-limited samples getting easier but the quality of CapNMR spectra obtained in many small-molecule applications exceeds what can be accomplished with conventional probe designs.

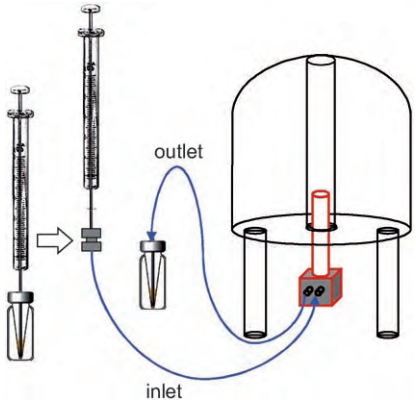

InterScience
© 2006 Wiley-VCH Verlag GmbH & Co. KGaA, Weinheim

Reviews

Well-orchestrated sequences of events: The virtues of cascade reactions are the focus of this Review, which discusses a number of recent total syntheses that feature these processes, highlights developments in the field, and points to its promising future.

Natural Product Synthesis

K. C. Nicolaou,* D. J. Edmonds, P. G. Bulger ——— **7134 – 7186**

Cascade Reactions in Total Synthesis

Communications

Images of the masses: Two-dimensional molecular imaging of intact rat brain tissue under ambient conditions was achieved by using the mass spectrometric technique of desorption electrospray ionization (DESI). The distributions of specific lipids, such as sulfatide 24:1, reveal distinctive subanatomical features of the rat brain (cc = corpus callosum; aca = anterior part of anterior commissure) with spatial resolution of less than 500 μm.

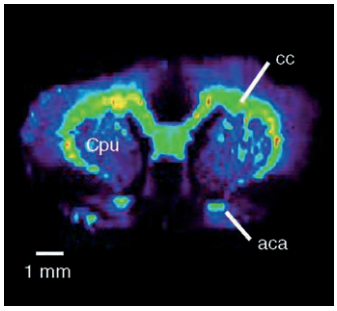

Mass Spectrometry

J. M. Wiseman, D. R. Ifa, Q. Song, R. G. Cooks* ——— **7188 – 7192**

Tissue Imaging at Atmospheric Pressure Using Desorption Electrospray Ionization (DESI) Mass Spectrometry

Room to expand: A rare example of thermal spin crossover in a Mn^{III} complex is accompanied by elongation of the bonds to the equatorial N_4 donor set upon warming (see scheme; Mn purple, N blue, O red), which is consistent with population of the $d_{x^2-y^2}$ orbital. The spin crossover was observed for an $N_4(O^-)_2$ donor set with axial oxygen donors, whereas only a temperature-independent high-spin state was observed with these donors in a *cis* arrangement.

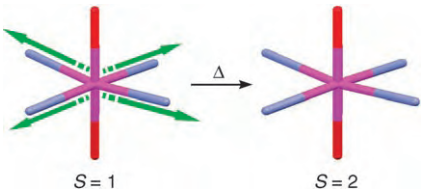

Spin Crossover

G. G. Morgan,* K. D. Murnaghan, H. Müller-Bunz, V. McKee, C. J. Harding ——— **7192 – 7195**

A Manganese(III) Complex That Exhibits Spin Crossover Triggered by Geometric Tuning

For the USA and Canada:
ANGEWANDTE CHEMIE International Edition (ISSN 1433-7851) is published weekly by Wiley-VCH PO Box 191161, D 69451 Weinheim, Germany. Air freight and mailing in the USA by Publications Expediting Inc. 200 Meacham Ave., Elmont, NY 11003. Periodicals postage paid at Jamaica NY 11431. US POSTMASTER: send address changes to *Angewandte Chemie*, Wiley-VCH, 111 River Street, Hoboken, NJ 07030. Annual subscription price for institutions: US$ 5685/5168 (valid for print and electronic / print or electronic delivery); for individuals who are personal members of a national chemical society prices are available on request. Postage and handling charges included. All prices are subject to local VAT/sales tax.

© 2006 Wiley-VCH Verlag GmbH & Co. KGaA, Weinheim

The best in chemistry – for more than hundred years

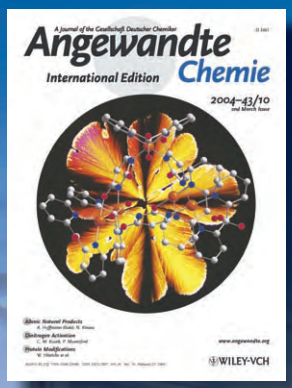

A Journal of the Gesellschaft Deutscher Chemiker

Angewandte
International Edition **Chemie**

www.angewandte.org

1888: ***The beginning of a success story***

Constant Innovations

1962: *First issue of the International Edition*
1976: *Graphical abstracts*
1979: *Cover pictures*
1988: *Centenary of Angewandte*
1989: *Routine use of color*
1991: *New section: Highlights*
1992: *Computerized editorial tracking system*
1995: *Internet service for readers*
1998: *Regular press service; full-text online*
2000: *New section: Essays; EarlyView: Communications available online ahead of the printed version*
2001: *New section: Microreviews*
2002: *Online submission of manuscripts*
2003: *Weekly publication; new section: News; new layout*
2004: *Backfiles (1962-1997); ManuscriptXpress: Online system for authors and referees*

Angewandte's advisors...

K.C. Nicolaou
The Scripps Research Institute and University of California San Diego (La Jolla, USA)

» ***Angewandte Chemie*** *has been highly influential in shaping the art of publishing chemical innovations and I feel privileged to be part of its Advisory Board. Eliciting admiration and respect from both readers and authors alike, its editorial staff should be commended for creating a new and exciting image of this most admired journal.* «

Angewandte Chemie International Edition *is a journal of the German Chemical Society (GDCh)*

GDCh

WILEY InterScience® DISCOVER SOMETHING GREAT

WILEY-VCH

95203123_gu

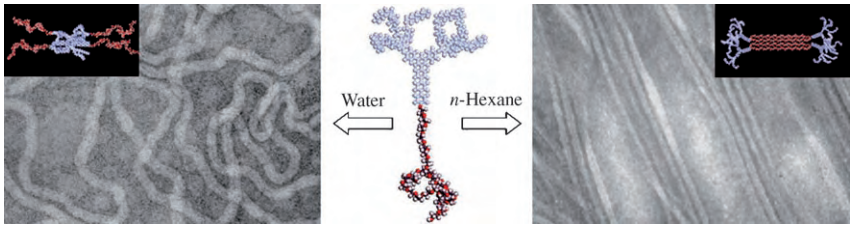

Thin end of the wedge: A block molecule, which consists of a rigid wedge-shaped aromatic segment linked at its apex to a flexible poly(ethylene oxide) chain, self-assembles into cylindrical nanofibers in both polar and nonpolar solvents. The structure of the nanofibers changes reversibly in response to solvent polarity, from highly flexible coil-like cylinders in water to stiff rodlike aggregates in *n*-hexane (see picture).

Nanostructures

J.-K. Kim, E. Lee, M. Lee* — **7195 – 7198**

Nanofibers with Tunable Stiffness from Self-Assembly of an Amphiphilic Wedge–Coil Molecule

Knocking them into shape: The total synthesis of two reported marine natural products containing halogenated pyrano-[3,2-*b*]pyrans (see example in blue) has led to the reassignment of both structures as halogenated 2,2′-bifuranyls (red). Concomitantly an efficient route to pyrano-[3,2-*b*]pyrans is described.

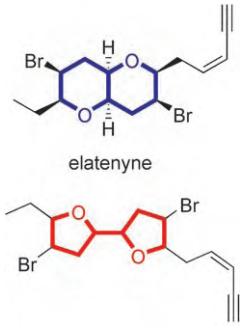

Total Synthesis

H. M. Sheldrake, C. Jamieson, J. W. Burton* — **7199 – 7202**

The Changing Faces of Halogenated Marine Natural Products: Total Synthesis of the Reported Structures of Elatenyne and an Enyne from *Laurencia majuscula*

Seeing red: Highly sensitive and selective chemical sensing systems were developed for the naked-eye detection of toxic ions by the direct and indirect postgrafting of hydrophilic and hydrophobic chromophores into spherically nanosized cavities of cubic *Fm3m* monoliths (HOM-C10). This leads to reliable control over the visual detection of toxic metals such as Pb^{II}, Cd^{II}, Sb^{III}, and Hg^{II} ions at a low concentrations ($\approx 10^{-9}$ M). DZ = diphenylthiocarbazone.

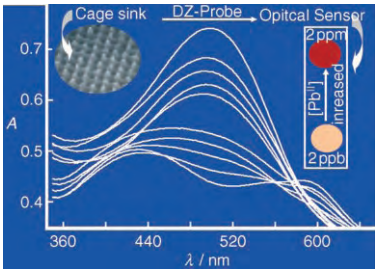

Environmental Chemistry

T. Balaji, S. A. El-Safty,* H. Matsunaga, T. Hanaoka, F. Mizukami — **7202 – 7208**

Optical Sensors Based on Nanostructured Cage Materials for the Detection of Toxic Metal Ions

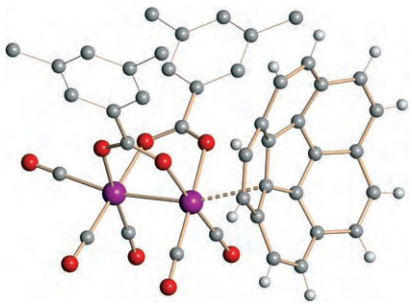

Right to the core: A ruthenium(I) complex of corannulene, prepared in a solvent-free environment, exhibits two coordination modes of the bowl: η^2-rim and η^1-hub (see picture for the hub-coordinated complex; Ru purple, O red, C gray, H white). The latter represents the first example of a transition-metal center binding only to the fullerene-like interior of an open geodesic polyarene.

Polyarene Coordination

M. A. Petrukhina,* Y. Sevryugina, A. Y. Rogachev, E. A. Jackson, L. T. Scott — **7208 – 7210**

Corannulene "Hub" Carbon Coordination by $[Ru_2\{O_2C(3,5\text{-}CF_3)_2C_6H_3\}_2(CO)_5]$

© 2006 Wiley-VCH Verlag GmbH & Co. KGaA, Weinheim

Contents

Metal–Boron Nanotubes

Y. Zhu, F. Liu, W. Ding,* X. Guo,* Y. Chen ——— **7211 – 7214**

Noncrystalline Metal–Boron Nanotubes: Synthesis, Characterization, and Catalytic-Hydrogenation Properties

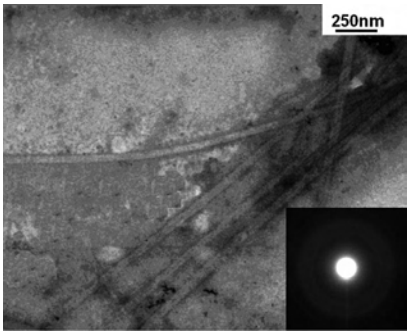

It's all in the mix: A mixed-surfactant-templated synthesis gives noncrystalline metal–boron nanotubes (see picture: TEM image of Fe–B nanotubes; inset: the corresponding selected-area electron diffraction pattern) from simple starting materials under mild conditions. These nanotubes show better catalytic activity for the hydrogenation of *m*-nitrotoluene to *m*-toluidine than the corresponding nanoparticles.

Mixed-Valence Compounds

D. Kawakami, M. Yamashita,* S. Matsunaga, S. Takaishi, T. Kajiwara, H. Miyasaka, K. Sugiura, H. Matsuzaki, H. Okamoto, Y. Wakabayashi, H. Sawa ——— **7214 – 7217**

Halogen-Bridged Pt^{II}/Pt^{IV} Mixed-Valence Ladder Compounds

Chutes and ... Ladders in coordination networks represent a boundary between 1D and 2D systems. Halogen-bridged Pt^{II}/Pt^{IV} mixed-valence ladder compounds have been synthesized for the first time. In these compounds, the band gap is controlled by changing the bridging halide ions. Moreover, by changing counteranions, the charge arrangements of the ladder compounds can be controlled.

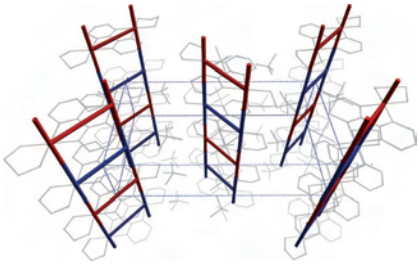

Organic Reactions in Water

Y. Gu, C. Ogawa, J. Kobayashi, Y. Mori, S. Kobayashi* ——— **7217 – 7220**

A Heterogeneous Silica-Supported Scandium/Ionic Liquid Catalyst System for Organic Reactions in Water

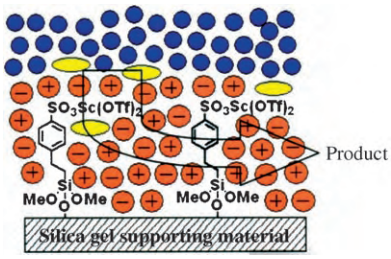

Several carbon–carbon bond-forming reactions are catalyzed by a silica-supported scandium triflate catalyst combined with an ionic liquid. The combination of these two components creates a hydrophobic reaction environment in water (see scheme; blue: water, yellow: substrate, orange: ionic liquid).

Nanofabrication

K. Salaita, Y. Wang, J. Fragala, R. A. Vega, C. Liu, C. A. Mirkin* ——— **7220 – 7223**

Massively Parallel Dip–Pen Nanolithography with 55 000-Pen Two-Dimensional Arrays

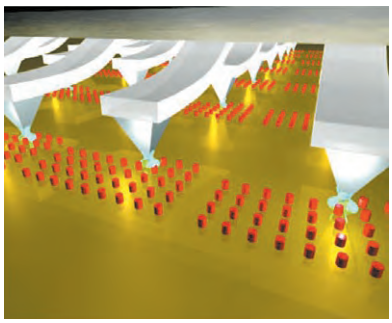

Lots of writing on the wall: A simple and flexible approach for performing high-throughput, large-area, direct-write molecular patterning, without tip feedback, is demonstrated by using a 55 000-pen two-dimensional array of atomic force microscope (AFM) cantilevers. The use of low-aspect-ratio pyramidal tips, curved cantilevers, and a novel gravity-driven alignment method allows parallel patterning of molecules across 1-cm^2 substrate areas at sub-100-nm resolution.

© 2006 Wiley-VCH Verlag GmbH & Co. KGaA, Weinheim

Rewriting the end: Two unmodified oligodeoxyribonucleotides (ODNs) were photochemically ligated through modification of ODNs that contain photosensitive nucleosides at both terminal ends in the presence of a template ODN. Additionally, this method was applied to the synthesis of R-shaped DNA as a unique structure.

DNA Structures

M. Ogino, K. Fujimoto* ____ **7223 – 7226**

Photochemical Synthesis of R-Shaped DNA toward DNA Recombination and Processing In Vitro

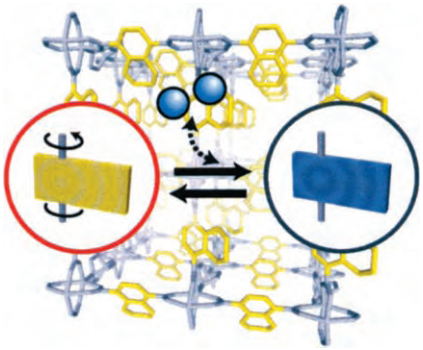

Controlling guests: Porous coordination polymers containing mobile organic groups, such as naphthalene rings (see picture), are synthesized, and their rotational motion is characterized by solid-state ^{2}H NMR spectroscopy. The rotation of the groups can be switched off (blue) by guest (blue spheres) adsorption and switched on (yellow) again by guest desorption.

Metal–Organic Frameworks

S. Horike, R. Matsuda, D. Tanaka, S. Matsubara, M. Mizuno, K. Endo, S. Kitagawa* ____ **7226 – 7230**

Dynamic Motion of Building Blocks in Porous Coordination Polymers

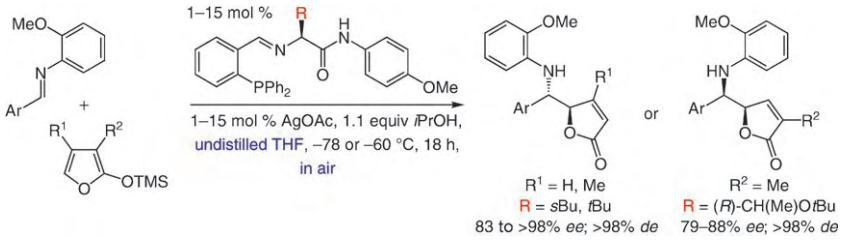

Very selective but very easy: These are two of the attributes of the asymmetric vinylogous Mannich reactions presented herein. These reactions can be run on a gram scale and in undistilled THF and air (see scheme; TMS = $SiMe_3$). All that is needed is commercially available AgOAc, a readily available amino acid derived phosphine, and a commercially available or easily prepared (one step) siloxyfuran.

Asymmetric Catalysis

E. L. Carswell, M. L. Snapper,* A. H. Hoveyda* ____ **7230 – 7233**

A Highly Efficient and Practical Method for Catalytic Asymmetric Vinylogous Mannich (AVM) Reactions

Uranyl interactions: The title compound is the first example of an actinide compound that contains three different actinyl-ion coordination geometries, namely, octahedral, pentagonal bipyramidal, and hexagonal bipyramidal. Strong cation–cation interactions between the uranyl ions lead to pentamers with a rather unusual configuration (see picture; U dark gray, O light gray).

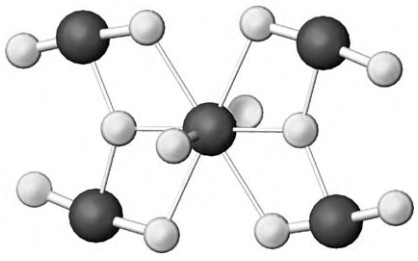

Actinide Chemistry

E. V. Alekseev, S. V. Krivovichev,* W. Depmeier, O. I. Siidra, K. Knorr, E. V. Suleimanov, E. V. Chuprunov ____ **7233 – 7235**

$Na_2Li_8[(UO_2)_{11}O_{12}(WO_5)_2]$: Three Different Uranyl-Ion Coordination Geometries and Cation–Cation Interactions

© 2006 Wiley-VCH Verlag GmbH & Co. KGaA, Weinheim

Contents

Total Synthesis

A. Dömling,* B. Beck, U. Eichelberger, S. Sakamuri, S. Menon, Q.-Z. Chen, Y. Lu, L. A. Wessjohann* ____ **7235 – 7239**

Total Synthesis of Tubulysin U and V

Multicomponent method: Tubulysins are among the most potent cytotoxic agents known. Now the first total synthesis of some members has been achieved by utilizing a rapid three-component reaction for the synthesis of the unusual central thiazole amino acid tubuvaline (see scheme; Boc = *tert*-butoxycarbonyl, Ac = acetyl), thereby opening new perspectives for anticancer drug development.

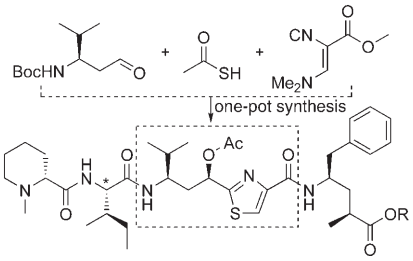

Crystal Growth

N. Kröger,* M. B. Dickerson, G. Ahmad, Y. Cai, M. S. Haluska, K. H. Sandhage, N. Poulsen, V. C. Sheppard **7239 – 7243**

Bioenabled Synthesis of Rutile (TiO_2) at Ambient Temperature and Neutral pH

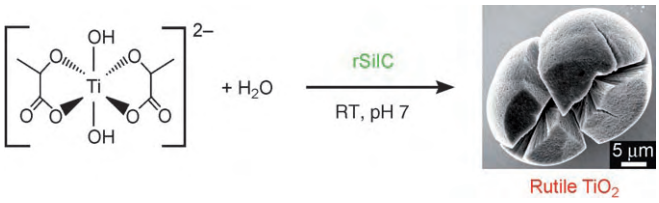

Biomineral-forming organisms provide inspiration for developing new reaction pathways to functional materials, such as rutile for optical devices. A recombinant protein (rSilC) was designed based on the sequence of a silica-forming protein from a diatom. This unique protein induced the formation of hierarchically nanostructured rutile microcrystals under mild reaction conditions (see SEM image).

Dendrimers

S. H. Kim, J. A. Katzenellenbogen* ____ **7243 – 7248**

Hormone–PAMAM Dendrimer Conjugates: Polymer Dynamics and Tether Structure Affect Ligand Access to Receptors

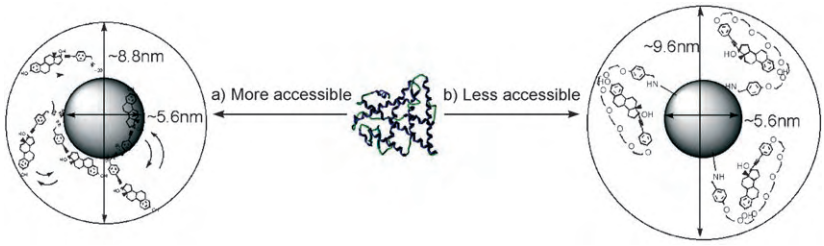

An open and closed case: Estradiol was conjugated to a PAMAM dendrimer (gray circle) through a short (17α-phenylethynyl) or a long (hexaethyleneglycol) tether to evaluate how ligand access to a receptor is affected. With the short tether (a), the hormone is free and solvent exposed, with unimpeded access to the estrogen receptor, while the long tether (b) wraps around the hormone and the dendrimer and markedly reduces access to the receptor.

Phosphanes

R. M. Hiney, L. J. Higham,* H. Müller-Bunz, D. G. Gilheany* ____ **7248 – 7251**

Taming a Functional Group: Creating Air-Stable, Chiral Primary Phosphanes

No rings of fire! Enantiopure primary phosphanes have been developed which are remarkably stable to air oxidation in both solid and solution states (see example). This new class of stable ligand synthon appears to owe its stability to conjugation in their aryl backbones with the extended π ring system. Even one extra ring is good enough.

© 2006 Wiley-VCH Verlag GmbH & Co. KGaA, Weinheim

Steaming ahead: The nonvolatility of ionic liquids is challenged further. Imidazolium(Im)-based ionic liquids composed of supramolecular structures in the condensed phase (see scheme) vaporize at ambient pressure from heated (100–600 °C) solvent droplets as neutral clusters of the type Im_nA_n.

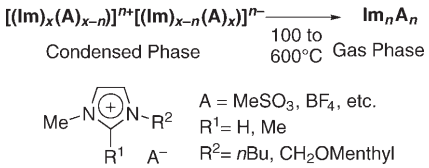

Gas-Phase Ionic Liquids

B. A. DaSilveira Neto, L. S. Santos, F. M. Nachtigall, M. N. Eberlin,* J. Dupont* ——— **7251 – 7254**

On the Species Involved in the Vaporization of Imidazolium Ionic Liquids in a Steam-Distillation-Like Process

An active link: A diglycine-containing linker (cat·linker) was fabricated on Rink amide resin for dual functions: a) attachment of a scaffold and b) capture of metal ions for promoting on-resin reactions (see picture). The metal-catching feature of the linker proves essential for the solid-phase synthesis of indoles through microwave-assisted Cu^{II}-mediated heteroannulation.

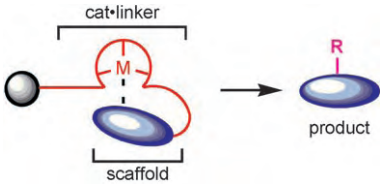

A Metal-Catching Linker

L.-P. Sun, W.-M. Dai* ——— **7255 – 7258**

An Engineered Linker Capable of Promoting On-Resin Reactions for Microwave-Assisted Solid-Phase Organic Synthesis

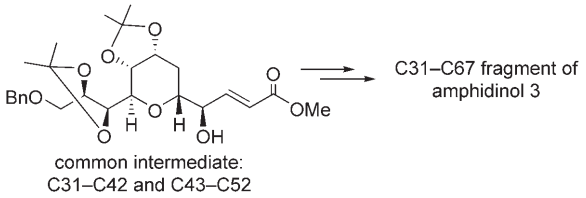

A tetrahydropyran intermediate, prepared from (−)-diethyl tartrate, was used to assemble the C31–C67 fragment of amphidinol 3. Both of the tetrahydropyran rings in the natural product were prepared from this intermediate. The polyene segment was assembled with high selectivity.

Polyketides

J. de Vicente, J. R. Huckins, S. D. Rychnovsky* ——— **7258 – 7262**

Synthesis of the C31–C67 Fragment of Amphidinol 3

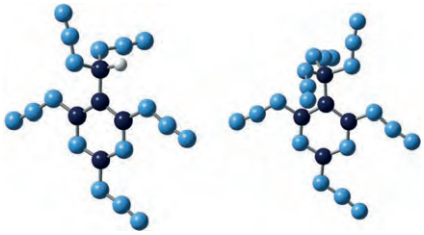

An additional azidomethyl group dramatically decreases the melting points of the corresponding azidopyrimidines. Theoretical calculations show that these polyazido compounds (see picture; N light blue, C dark blue, H white) exhibit highly promising energetic properties. 2,4,6-Triazidopyrimidine was found to be a novel precursor to carbon nanotubes in the presence of $Ni(ClO_4)_2$.

Polyazido Compounds

C. Ye, H. Gao, J. A. Boatz, G. W. Drake, B. Twamley, J. M. Shreeve* **7262 – 7265**

Polyazidopyrimidines: High-Energy Compounds and Precursors to Carbon Nanotubes

Elusive intermediate trapped: γ-Substituted difluoropropargyl groups can stabilize an organoindium(III) complex. The resulting structure is the only known example of an indium atom bonded to a propargylic carbon atom (see picture; F blue, S yellow, C white, H green). Reactions with electrophiles produced a difluoroalkyne or -allene, depending on the type of electrophile.

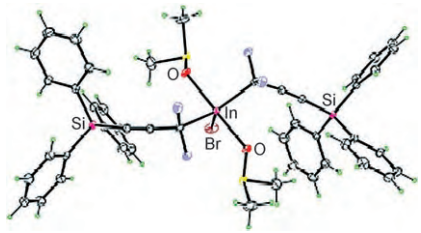

Organoindium Reagents

B. Xu, M. S. Mashuta, G. B. Hammond* ——— **7265 – 7267**

Crystallographic Characterization of Difluoropropargyl Indium Bromide, a Reactive Fluoroorganometallic Reagent

© 2006 Wiley-VCH Verlag GmbH & Co. KGaA, Weinheim

Contents

Negative-Valent Transition Metals

W. W. Brennessel, V. G. Young, Jr., J. E. Ellis* ——— **7268 – 7271**

Towards Homoleptic Naphthalenemetalates of the Later Transition Metals: Isolation and Characterization of Naphthalenecobaltates(1−)

Taming of the wild anions: Highly labile naphthalene complexes of formally negative-valent later transition metals have been obtained in the form of $[Co(\eta^4\text{-}C_{10}H_8)(\eta^4\text{-cod})]^-$ (see picture; cod = 1,5-cyclooctadiene) and $[Co(\eta^4\text{-}C_{10}H_8)_2]^-$. The latter is the first structurally authenticated homoleptic bis(naphthalene)metal anion for any d-block element and promises to be a particularly reactive synthon for the "naked" atomic cobalt anion.

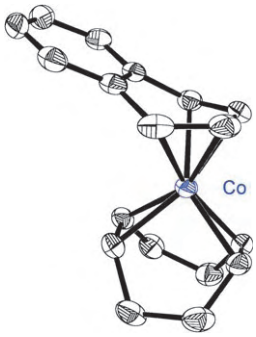

Phosphine Polymers

K. J. T. Noonan, D. P. Gates* ——— **7271 – 7274**

Ambient-Temperature Living Anionic Polymerization of Phosphaalkenes: Homopolymers and Block Copolymers with Controlled Chain Lengths

New kid on the block: Unprecedented polystyrene-*block*-poly(methylenephosphine) copolymers are accessible from the reaction of living polystyrene with the phosphaalkene (see scheme; Mes = 2,4,6-$Me_3C_6H_2$). The living anionic polymerization of P=C bonds represents a new development in phosphorus chemistry and opens up the possibility to synthesize functional phosphorus polymers of controlled architectures.

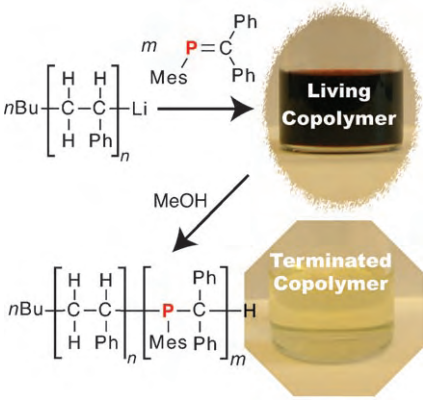

Polycarbonate Synthesis

K. Nakano, T. Kamada, K. Nozaki* ——— **7274 – 7277**

Selective Formation of Polycarbonate over Cyclic Carbonate: Copolymerization of Epoxides with Carbon Dioxide Catalyzed by a Cobalt(III) Complex with a Piperidinium End-Capping Arm

Sidestepping a cyclic side product: Copolymerization of terminal epoxides with CO_2 was investigated by using a cobalt(III) complex bearing a piperidinium end-capping arm and a piperidinyl arm (see scheme; DME = 1,2-dimethoxyethane). The catalyst system can selectively produce copolymers without contaminant formation of cyclic carbonates even at high conversion of the epoxide (> 99%).

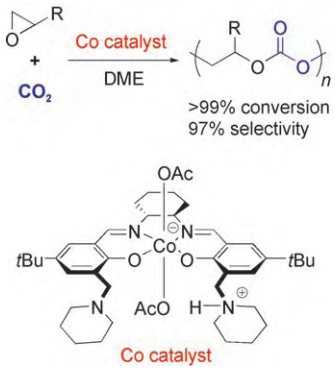

Surface Chemistry

K. Zhu, J. Hu, C. Kübel, R. Richards* ——— **7277 – 7281**

Efficient Preparation and Catalytic Activity of MgO(111) Nanosheets

Preferential growth of MgO(111) nanosheets with a thickness typically between 3 and 5 nm (see TEM image) has been achieved by a simple, efficient, and inexpensive wet chemical route. The MgO(111) nanosheets have been shown to have ultrahigh activity for the Claisen–Schmidt condensation of benzaldehyde and acetophenone.

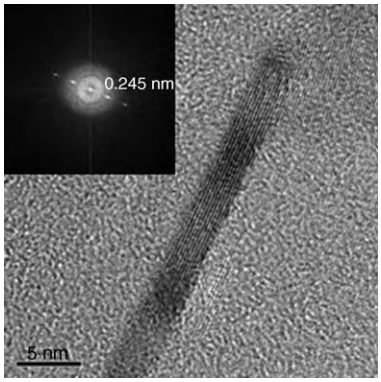

© 2006 Wiley-VCH Verlag GmbH & Co. KGaA, Weinheim

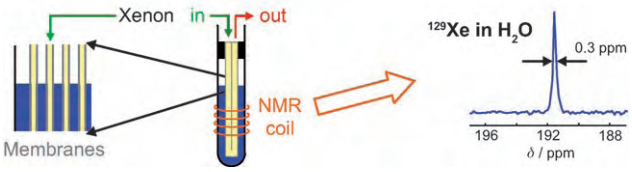

Go with the flow: In many applications of NMR spectroscopy in chemistry, proper sample preparation is absolutely critical for success, in particular in biochemical and biomedical areas. For the NMR spectroscopy of laser-polarized ^{129}Xe, an efficient and robust method for continuous flow of the gas to a NMR tube was developed. Applications to H_2O, DMSO, phospholipid bicelles, and 2D exchange NMR spectroscopy are demonstrated.

^{129}Xe NMR in Biochemistry

D. Baumer, E. Brunner,* P. Blümler, P. P. Zänker, H. W. Spiess* **7282 – 7284**

NMR Spectroscopy of Laser-Polarized ^{129}Xe Under Continuous Flow: A Method To Study Aqueous Solutions of Biomolecules

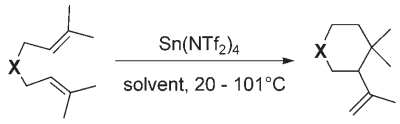

The tin salt $Sn(NTf_2)_4$ (Tf = trifluoromethanesulfonyl) is an efficient catalyst for the selective and ring-size-specific cycloisomerization of highly substituted 1,6-dienes to give six-membered-ring carbocycles (see scheme; $X = C(CO_2Et)_2$, $C(CO_2Me)_2$ $C(CN)(CO_2Et)$, etc.). This is the first Lewis acid catalyzed cycloisomerization of this type of substrate.

Cyclohexane Derivatives

F. Grau, A. Heumann,* E. Duñach* **7285 – 7289**

Cycloisomerization of 1,6-Dienes Mediated by Lewis Super Acids without Additives: Easy Access to Polysubstituted Six-Membered Carbocycles

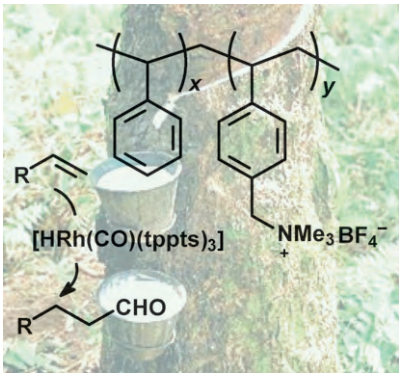

An elegant method for the aqueous-phase hydroformylation of 1-octene with a water-soluble Rh catalyst and amphiphilic latex particles as phase-transfer agents has been developed (see scheme). In this way, substantial concentrations of the olefin in the aqueous catalyst-containing phase were reached, and thus reasonable turnover frequencies under mild reaction conditions could be achieved.

Homogeneous Catalysis

K. Kunna, C. Müller, J. Loos, D. Vogt* **7289 – 7292**

Aqueous-Phase Hydroformylation of 1-Octene: Styrene Latices as Phase-Transfer Agents

Inequivalent in the crystal: The three chemically distinct calculated proton shielding tensors of solid benzene—a consequence of interactions in the crystal—can be described as the superposition of the isolated molecule and the intermolecular shielding contributions. In the ovaloid representations of the shielding tensors *1*, *2*, and *3* indicate the least, intermediate, and most shielded principal axes, respectively.

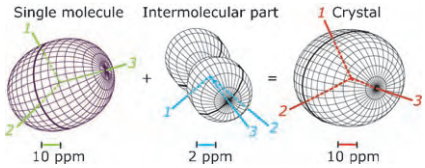

Shielding Tensors of Benzene

T. Heine,* C. Corminboeuf, G. Grossmann, U. Haeberlen **7292 – 7295**

Proton Magnetic Shielding Tensors in Benzene—From the Individual Molecule to the Crystal

© 2006 Wiley-VCH Verlag GmbH & Co. KGaA, Weinheim

Contents

Rotaxanes

M. Radha Kishan, A. Parham, F. Schelhase, A. Yoneva, G. Silva, X. Chen, Y. Okamoto, F. Vögtle* ____ **7296 – 7299**

Bridging Rotaxanes' Wheels—Cyclochiral Bonnanes

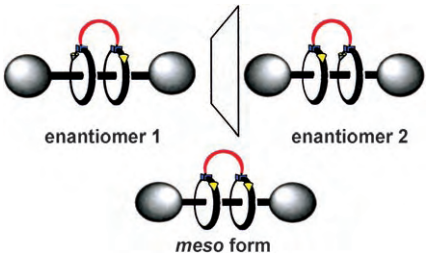

Building bridges: The wheels of [3]rotaxane were intramolecularly tethered to yield the first member of cyclochiral, interlocked architectures named "bonnanes" (after the city Bonn, Germany; see scheme). The enantiomers and *meso* form were separated on an immobilized chiral phase and characterized.

Supporting information available on the WWW (see article for access details).

A video clip is available as Supporting Information on the WWW (see article for access details).

Looking for outstanding employees?

Do you need another expert for your excellent team?
... Chemists, PhD Students, Managers, Professors, Sales Representatives...

Place an advert in the printed version and have it made available online for 1 month, free of charge!

Angewandte Chemie International Edition
Advertising Sales Department: Marion Schulz
Phone: 0 62 01 - 60 65 65
Fax: 0 62 01 - 60 65 50
E-Mail: MSchulz@wiley-vch.de

Service

Keywords ____ *7300*

Authors ____ *7301*

Preview ____ *7303*

RSS Feed

Journal content prior to publication in an issue can be found online on our **Early View** page at www.angewandte.org. Stay updated on the latest journal content by registering for our **free e-mail alerts** at http://interscience.wiley.com/alerts.

Keep up with the latest research with our **RSS feed**, which provides the titles, authors, and the Digital Object Identifiers (DOIs) of Early View articles, including links to the full texts. RSS ("Really Simple Syndication") is an XML-based format for sharing and distributing web content. To receive the RSS feed, just click on the orange feed icon at www.angewandte.org, and visit http://interscience.wiley.com/rss for more information.

© 2006 Wiley-VCH Verlag GmbH & Co. KGaA, Weinheim

Organic Chemistry Online ... and for Free?

At www.ochem4free.com, the well-disposed internet user will find the introductory organic chemistry textbook by Richard F. Daley and Sally J. Daley entitled "Organic Chemistry", organized into chapters that are available as free, pdf-formatted downloads following registration (Figure 1).

The homepage itself is clearly arranged in a somewhat naive design, but, in turn, it is easy to follow and operate. In addition to the downloadable isolated chapters of the textbook, the site also features a couple of extra learning instruments (priced at $30 each or $45 total). A forum provides a platform for mutual exchange of information by posting questions as well as answers. Simple laboratory techniques, such as proper handling of a refractor, are demonstrated in short video clips.

The authors praise their work as being a novel approach to impart organic chemistry by arranging its contents by reaction mechanisms instead of the conventional classification by functional groups. It must be noted that this is not the only textbook on the current market that follows up on this concept. Its contents completely cover very basic organic chemistry, and it will, therefore, mainly appeal to ambitious high school students as well as undergraduates. In the first few chapters, atomic and molecular orbitals are introduced and explained step by step, as well as chemical bonding, nomenclature, conformational analysis, and physical properties of organic compounds. Then, a general chapter on chemical reactions and reaction orders is followed by the chemistry of carbonyl and carboxylate groups. Strangely enough, chapters on IR and NMR spectroscopy then appear before returning to organic chemistry with chirality and nucleophilic substitution reactions. Elimination and addition reactions, aromaticity in connection with the chemistry of aromatic compounds, the chemistry of enolates, and radical reactions complete the standard repertoire. An additional chapter on polymers as well as amino acids, carbohydrates, and nucleic acids provides an introduction to biological chemistry and biochemistry, the chemistry of life. A few digressions, so-called "sidebars", and discussed syntheses liven up the subject.

Unfortunately, schemes and equations are extremely simple if not antiquated in style; they are non-uniform and sometimes flawed. The individual pages are everything but overladen making the entire book extend over 1200 pages, and thus the reader may have serious difficulty to find the desired information. It lacks a complete table of contents and a general index—instead, it merely includes an index on (named) reactions, which only refers to chapters but not to appropriate page numbers; this is also true for references in the main text. This major shortcoming is supposed to be ironed out in the printed version, which costs, however, another $70 for the three-volume set. One would think (or even expect) that an online textbook could allow for cross-linking of key terms by a simple "click".

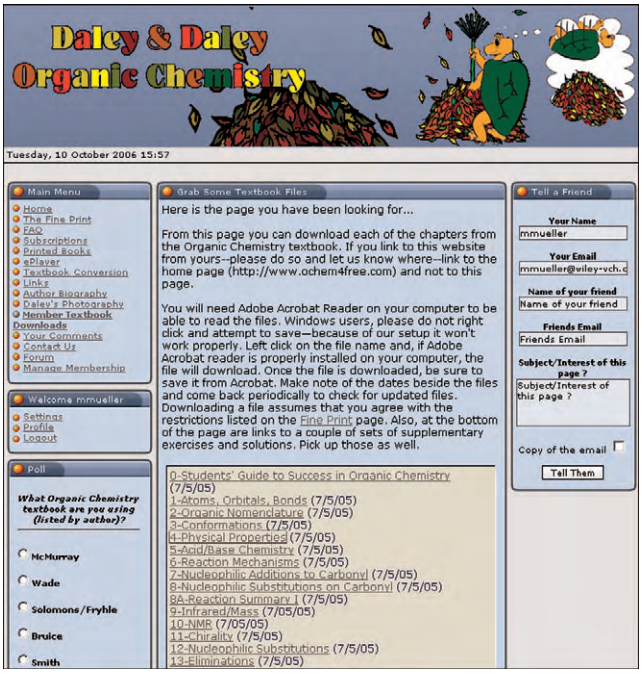

Figure 1. Access to Daley and Daley's textbook of organic chemistry requires only a free registration.

For more information visit
www.ochem4free.com

The authors laid substantial emphasis on repetition and understanding throughout, thus every chapter ends with a summary of the "key ideas" combined with ample exercises, which are highly recommended to do. Again, further exercises and, particularly, the solutions to all exercises must be purchased as two separate books for $30 and $40, respectively.

Making knowledge available at no cost is certainly noble-minded, yet the user will realize fairly quickly that, in this case, it is merely intended to be an appetizer. Efficient use is really only practicable with the full package. When taking into account that the focus of this textbook is basic organic chemistry—there is hardly any discussion of organometallic chemistry or modern (asymmetric) synthetic methods—it is rather expensive, as it will quickly become insufficient for any advanced level. However, it is generally to the students' advantage to scrutinize before buying a textbook whether the offer is what they really need.

Axel B. Machotta, Martin Oestreich
Westfälische Wilhelms-Universität
Münster (Germany)

DOI: 10.1002/anie.200603935

WILEY InterScience DISCOVER SOMETHING GREAT
© 2006 Wiley-VCH Verlag GmbH & Co. KGaA, Weinheim

Strained Molecules

DOI: 10.1002/anie.200603016

The Twisted Amide 2-Quinuclidone: 60 Years in the Making**

Jonathan Clayden and Wesley J. Moran*

Keywords:
amides · penicillin · reactivity · strained molecules · synthetic methods

The remarkable unreactivity of the amide motif is central to its function as the cement in nature's construction work.[1] Amide stability is widely accepted[2] to arise from the delocalization of π electrons over the three constituent amide atoms (N, C, O) as depicted in Scheme 1. As a result, the four substituents around the amide C–N bond must all lie in the same plane.

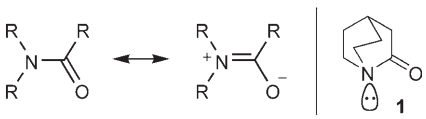

Scheme 1. Delocalization in an amide.

But how important really is delocalization in governing the properties of amides? One way to find out is to make amides in which the nitrogen lone pair is not—and indeed cannot be—delocalized. If an amide is built in which structural constraints do not allow coplanarity, then delocalization would be diminished or impossible.[1,3] Chemical intuition suggests that such "twisted amides" will be less stable and will show increased electrophilicity, closer to that of esters or ketones.

In 1938, Lukeš realized that a straightforward way to build a model amide with a twist is to place the nitrogen atom at a bridgehead position in a bicyclic ring system.[4] 2-Quinuclidone (**1**) is perhaps the simplest and indeed most beautiful of these theoretically twisted amides—"theoretical" because, incredibly, the simple 2-quinuclidone structure remained unknown, thwarting every attempt at synthesis, until early in 2006.[5]

The challenge of twisted amides and their synthesis was first taken up during the Second World War, when rapid production of penicillin was urgently required. At the time penicillin's structure was unknown, but to most chemists its ready hydrolysis in water proved it could not be an amide. However, R. B. Woodward realized otherwise: the proposed (and of course correct) structure contains a β-lactam ring (Scheme 2) in which ring strain forces the amide to adopt a nonplanar conformation. In Woodward's eyes the degradation and hydrolysis data were fully consistent with the presence of a twisted amide.[6] Others disagreed, however, and only after Dorothy Hodgkin had published penicillin's X-ray crystal structure was the β-lactam structure accepted by the scientific community.[6]

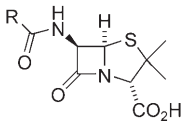

Scheme 2. General structure of penicillins.

Synthetic success followed with the first total synthesis of penicillin V by Sheehan and Henery-Logan at MIT in 1957.[7] In the final synthetic step, the twisted amide (β-lactam) **3** is formed in a dicyclohexylcarbodiimide-mediated ring closure of **2**, but with a yield of just 10–12% (Scheme 3).

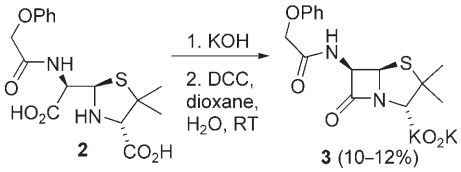

Scheme 3. Synthesis of the potassium salt of penicillin V. DCC = dicyclohexylcarbodiimide.

Amides are highly resistant to "chemical" hydrolysis[8]—but susceptible to much faster cleavage by peptidase enzymes. Could peptidases be exploiting the reactivity gained when delocalization is lost by forcing amides into twisted conformations? Such questions can be answered with model twisted amides, and have driven interest in the synthesis of 2-quinuclidone and its structural analogues.[9]

"Traditional" approaches to amide formation, such as that used by Sheehan and Henery-Logan, have been successful in the synthesis of a number of twisted amides. Somayaji and Brown, for example, prepared twisted amide **5** by a intramolecular coupling reaction of commercially available acid **4** by using dicyclohexylcarbodiimide (Scheme 4).[10] Hydrolysis of **5** was much faster than that of planar amides in both acidic and basic conditions.

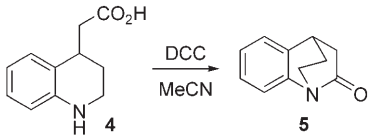

Scheme 4. Twisted amide synthesis.

[*] Prof. J. Clayden, Dr. W. J. Moran
School of Chemistry
University of Manchester
Oxford Road, Manchester M13 9PL (UK)
Fax: (+44) 161-275-4939
E-mail: clayden@manchester.ac.uk

[**] We are grateful to the EPSRC for support.

WILEY InterScience DISCOVER SOMETHING GREAT

© 2006 Wiley-VCH Verlag GmbH & Co. KGaA, Weinheim

Related approaches failed for 2-quinuclidone (**1**) itself, which had remained unknown since it was originally proposed as a structure by Lukeš[4] and became a synthetic target for Woodward. Substituted analogues **6** of 2-quinuclidone were however prepared (Scheme 5).[11] Compound **6d** was surprisingly stable towards base-induced methanolysis, but the presence of the methyl groups hindered the study of reactivity at the amide carbonyl group itself.[10]

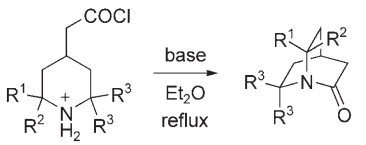

6a: $R^1 = R^2 = H$, $R^3 = Me$
6b: $R^1 = H$, $R^2 = R^3 = Me$
6c: $R^1 = R^3 = Me$, $R^2 = H$
6d: $R^1 = R^2 = R^3 = Me$

Scheme 5. Synthesis of substituted 2-quinuclidones **6**.

In 1998, Kirby et al. succeeded in making 1-aza-2-adamantanone **10** from the known ester imide **7** (Scheme 6).[12] Reduction of **7** with $LiAlH_4$ furnished the amino alcohol **8**, which was acylated and oxidized to the amido acid **9**. Heating in aqueous acid gave twisted amide **10**.

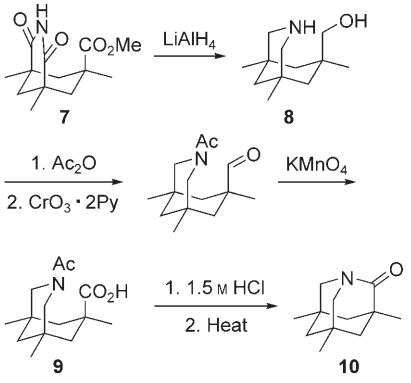

Scheme 6. Synthesis of 1-aza-2-adamantanone **10**. Ac = acetyl; Py = pyridine.

Amide **10** shows unconventional reactivity, taking part in a variety of reactions that amides normally do not undergo (Scheme 7). Wittig olefination and ketal formation of the carbonyl group was successful, as was methylation of the nitrogen atom.

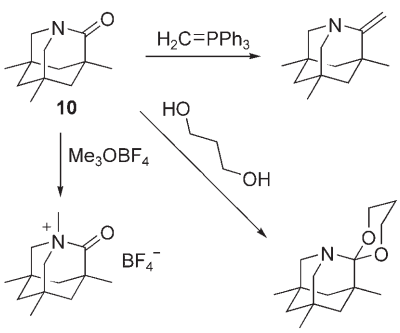

Scheme 7. Unusual reactions of 1-aza-2-adamantanone **10**.

The synthesis of 2-quinuclidone evidently required a new approach, and Tani and Stoltz decided to evade its apparent high susceptibility to hydrolysis by avoiding aqueous conditions and isolating the protonated salt, 2-quinuclidonium tetrafluoroborate (**1**·HBF_4). The approach paid off, and the synthesis of 2-quinuclidone was finally achieved after more than sixty years of interest.[5]

The bicyclic skeleton was formed by elegant use of the Schmidt–Aubé reaction, which required first the preparation of azide **13** (Scheme 8). Bicyclic lactone **11** was prepared by Baeyer–Villiger oxidation of norbornanone and reduced to diol **12** in excellent yield. Chemoselective tosylation of the primary hydroxyl group followed by displacement with sodium azide and oxidation of the remaining secondary alcohol provided key intermediate **13**.

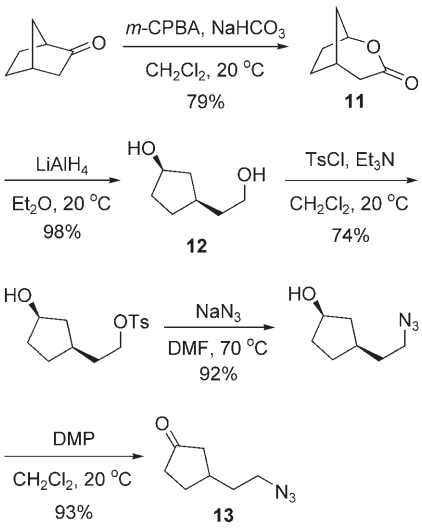

Scheme 8. Preparation of azide **13**. *m*-CPBA = *m*-chloroperoxybenzoic acid; Ts = toluene-4-sulfonyl; DMP = Dess–Martin periodinane.

Screening several different reaction conditions showed that treatment of **13** with tetrafluoroboric acid provided a mixture of two products of nitrene insertion adjacent to the carbonyl group in a 76:24 ratio in favor of the desired isomer. Recrystallization of the mixture of isomers permitted the isolation of pure 2-quinuclidonium tetrafluoroborate (**1**·HBF_4, Scheme 9). Spectroscopic analysis and single-crystal X-ray analysis confirmed the identity of the salt.

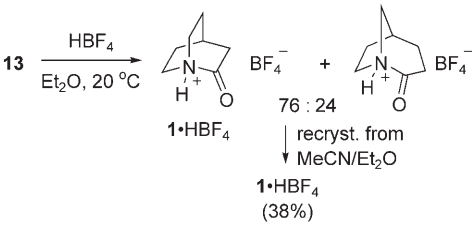

Scheme 9. Formation of **1**·HBF_4.

The reactivity of **1**·HBF_4 is, as expected, remarkable. It is hydrolyzed instantaneously in D_2O; addition of five equivalents of D_2O in CD_3CN leads to hydrolysis, occuring with a half-life of 135 minutes. While **1**·HBF_4 can be handled in acetonitrile or diethyl ether, common nucleophilic solvents such as DMSO, pyridine, and methanol lead to rapid decomposition. Attempts to free-base **1**·HBF_4 to generate 2-quinuclidone itself were unsuccessful and generally resulted in the formation of polymeric material.

The successful synthesis of 2-quinuclidone, the archetypal twisted amide, is the culmination of decades of synthetic interest, and the fact that only in 2006 have chemists managed to make such a simple structure is testament to the challenge posed by strained molecules. Natural products have traditionally been seen as the pinnacle of synthetic achievement, but maybe it is in the form of unnatural products—indeed, products only of chemists' imaginations—that greater challenges lie.

Published online: September 29, 2006

 © 2006 Wiley-VCH Verlag GmbH & Co. KGaA, Weinheim

[1] A. Greenberg, C. M. Breneman, J. F. Liebman, *The Amide Linkage: Selected Structural Aspects in Chemistry, Biochemistry, and Materials Science*, Wiley, New York, **2000**.

[2] But see: a) A. J. Bennet, Q. P. Wang, H. Slebocka-Tilk, V. Somayaji, R. S. Brown, B. Santarsiero, *J. Am. Chem. Soc.* **1990**, *112*, 6383; b) H. Slebocka-Tilk, R. S. Brown, *J. Org. Chem.* **1987**, *52*, 805.

[3] A. Greenberg, *Mol. Struct. Energ.* **1989**, *7*, 139.

[4] R. Lukeš, *Coll. Czech. Chem. Commun.* **1938**, *10*, 148.

[5] K. Tani, B. M. Stoltz, *Nature* **2006**, *441*, 731.

[6] *The Chemistry of Penicillin* (Eds.: H. T. Clark, J. R. Johnson, R. Robinson), Princeton University Press, Princeton, **1949**, p. 440.

[7] a) J. C. Sheehan, K. R. Henery-Logan, *J. Am. Chem. Soc.* **1957**, *79*, 1262; b) J. C. Sheehan, K. R. Henery-Logan, *J. Am. Chem. Soc.* **1959**, *81*, 3089.

[8] a) J. K. Young, S. Pazhanisamy, R. L. Schowen, *J. Org. Chem.* **1984**, *49*, 4148; b) R. M. Pollack, M. L. Bender, *J. Am. Chem. Soc.* **1970**, *92*, 7190; c) M. L. Bender, R. J. Thomas, *J. Am. Chem. Soc.* **1961**, *83*, 4183; d) M. L. Bender, *Chem. Rev.* **1960**, *60*, 53, and references therein.

[9] a) W. L. Mock, *Bioorg. Chem.* **1976**, *5*, 403; b) G. M. Blackburn, C. J. Skaife, I. T. Kay, *J. Chem. Res. Miniprint* **1980**, 3650; c) X. Lopez, J. I. Mujika, G. M. Blackburn, M. Karplus, *J. Phys. Chem. A* **2003**, *107*, 2304; d) J. I. Mujika, J. M. Mercero, X. Lopez, *J. Am. Chem. Soc.* **2005**, *127*, 4445; see also reference [5] and references therein.

[10] V. Somayaji, R. S. Brown, *J. Org. Chem.* **1986**, *51*, 2676.

[11] a) H. Pracejus, *Chem. Ber.* **1959**, *92*, 988; b) H. Pracejus, *Chem. Ber.* **1965**, *98*, 2897; c) H. Pracejus, M. Kehlen, H. Kehlen, H. Matschiner *Tetrahedron* **1965**, *21*, 2257; d) A. Greenberg, G. Wu, J.-C. Tsai, Y.-Y. Chui, *Struct. Chem.* **1993**, *4*, 127.

[12] A. J. Kirby, I. V. Komarov, P. D. Wothers, N. Feeder, *Angew. Chem.* **1998**, *110*, 830; *Angew. Chem. Int. Ed.* **1998**, *37*, 785; See also K. M. Morgan, M. L. Rawlings, M. N. Montgomery, *J. Phys. Org. Chem.* **2005**, *18*, 310.

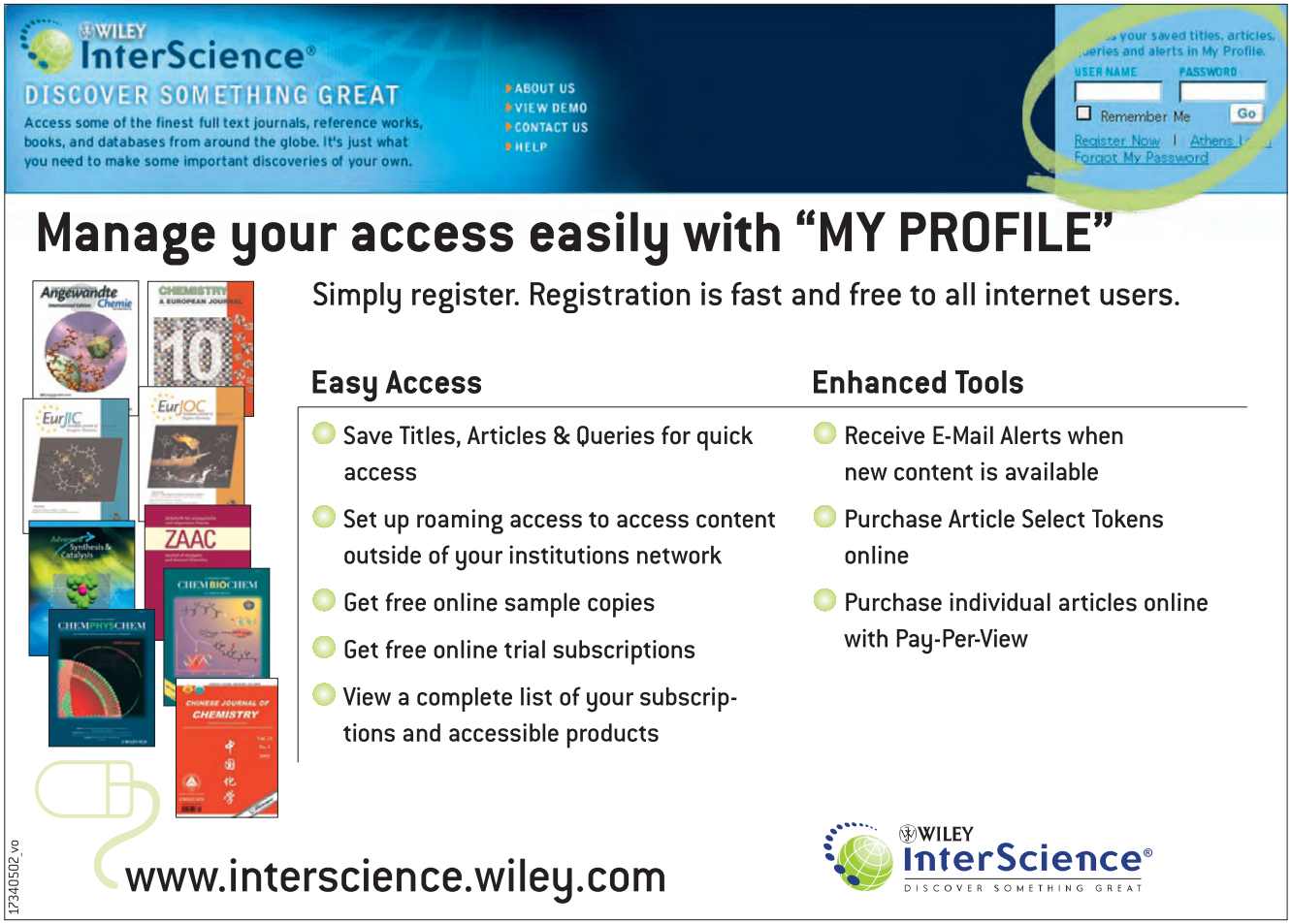

 © 2006 Wiley-VCH Verlag GmbH & Co. KGaA, Weinheim

DOI: 10.1002/anie.200601789

NMR Spectroscopy

Extending the Scope of NMR Spectroscopy with Microcoil Probes**

Frank C. Schroeder and Matthew Gronquist*

Keywords:
analytical methods · capillary NMR spectroscopy · mass-sensitivity · NMR spectroscopy · structure elucidation

Dedicated to Dr. Volker Sinnwell on the occasion of his 63rd birthday

Capillary NMR (CapNMR) spectroscopy has emerged as a major breakthrough for increasing the mass-sensitivity of NMR spectroscopic analysis and enabling the combination of NMR spectroscopy with other analytical techniques. Not only is the acquisition of high-sensitivity spectra getting easier but the quality of CapNMR spectra obtained in many small-molecule applications exceeds what can be accomplished with conventional designs. This Minireview discusses current CapNMR technology and its applications for the characterization of mass-limited, small-molecule and protein samples, the rapid screening of small-molecule or protein libraries, as well as hyphenated techniques that combine CapNMR with other analytical methods.

1. Introduction

In the spectroscopic characterization of small (or large) molecules, NMR spectra most closely reflect how we casually think about organic structures as ball-and-stick models. First-order interpretation of NMR spectra allows us to think of each NMR signal as representing individual hydrogen or carbon atoms (more precisely, groups of nonequivalent atoms), which comes as close as one can get to "seeing" each individual hydrogen or carbon atom in a molecule. Homo- and heteronuclear correlation spectra such as COSY, HSQC (heteronuclear single-quantum correlation), or HMBC (heteronuclear multiple-bond correlation) then provide additional signals, which, with little abstraction, translate into bonds that connect the atoms.[1] It is this close analogy to molecular models that makes the interpretation of NMR spectra so satisfying and intuitive. A detailed understanding of the physical background of solution NMR spectroscopy is much more difficult to attain but is not required for most small-molecule chemists. Generally, organic chemists and chemical biologists are able to use NMR spectroscopy very effectively without worrying much about quantum mechanics or statistics, as a basic understanding of pulse sequences and data processing is entirely sufficient to maximize the utility of available NMR spectrometers. However, just about anybody who has used NMR spectroscopy for the characterization of molecular structures or dynamics has at one point or another encountered the Achilles' heel of NMR spectroscopy: its limited sensitivity. For example, NMR spectroscopic analyses typically require several orders of magnitude more material than mass spectrometry.[2–4] That NMR spectroscopy, as opposed to mass spectrometry, is nondestructive is of little comfort to those who simply cannot isolate enough material to obtain sufficiently good NMR spectra. Examples of mass-limited applications include the identification of new natural products, the analysis of metabolites or breakdown products of pharmaceuticals and agrochemicals, as well as the characterization of large libraries of synthetic compounds from combinatorial chemistry.

The sensitivity of NMR spectroscopy depends primarily on three instrumental parameters: the strength of the magnetic field (the use of stronger magnets results in higher sensitivity), the size and fill factor of the receiver coil (mass-sensitivity increases with increasing fill factor and decreasing coil diameter), and the amount of noise introduced during detection.[5,6] After NMR spectrometers became widely

[*] Dr. F. C. Schroeder
Biological Chemistry and Molecular Pharmacology
Harvard Medical School
250 Longwood Avenue, Boston, MA 02115 (USA)
Fax: (+1) 617-432-6424
E-mail: frank_schroeder@hms.harvard.edu
Dr. M. Gronquist
Department of Chemistry
SUNY College at Fredonia
Fredonia, NY 14063 (USA)

[**] We thank Professor Jerrold Meinwald and Dr. Ivan Keresztes, Cornell University, as well as Tim Peck and Dean Olson, Protasis-MRM, for helpful suggestions and discussions.

InterScience
© 2006 Wiley-VCH Verlag GmbH & Co. KGaA, Weinheim

available in the 1960s, the development during the subsequent two decades of superconducting magnets allowed a dramatic increase in field strengths and thus sensitivity. However, in the past 15 years the field strengths of commercially available NMR spectrometers have increased more and more slowly, as current magnet designs approach the limits of existing superconducting-wire technology and as the costs associated with installing higher-field spectrometers rise more than exponentially with field strength. For example, the costs for the purchase and installation of a 900-MHz spectrometer can easily reach $10000000 (ca. €8000000), whereas less than 10% of this amount would be required for a standard configured 600-MHz instrument.[7] Meanwhile, the sensitivity at 900 MHz increases only by a relatively modest factor of roughly two as compared to at 600 MHz.[7] More recently, efforts to improve the sensitivity of NMR spectroscopy have therefore focused on probe design, aimed at reducing thermal noise in the receiver and developing probe geometries that allow for smaller receiver coils with better fill factors. The introduction of cryogenic probes, in which thermal noise is greatly reduced by cooling the receiver coil and preamplifiers to 25 K or below, resulted in sensitivity gains of roughly a factor of three to four as compared to conventional probe designs.[8,9] However, the design of cryogenic probes places extremely high demands on thermal insulation and cooling capacity, as the 25-K receiver coil is separated from the room-temperature NMR sample by only a few millimeters. The required refrigerated helium-based cooling system makes the acquisition and maintenance of cryogenic probes rather expensive, and installation of a cryogenic probe usually necessitates that the spectrometer be dedicated exclusively to this probe.

Cryogenic probes offer significant sensitivity gains and therefore, despite the aforementioned drawbacks, have become indispensable for the characterization of biological macromolecules by NMR spectroscopy. For the analysis of mass-limited samples, however, microcoil probe designs[10] offer a viable alternative by providing significant gains in mass-sensitivity at a fraction of the cost of cryogenic probes. In this Minireview, we describe some of the physical concepts relevant to understanding the advantages and limitations of microcoil probe designs and provide a general estimate of how the mass-sensitivity of microcoil probes compares with that of conventional probes. We also discuss the applications of microcoil NMR spectroscopy as a stand-alone technique and in conjunction with other analytical techniques such as HPLC or electrophoresis, and consider recent progress towards incorporating microcoil probes in high-throughput applications.

2. Microcoil NMR Probes

2.1. Background and Design

The rationale for the development of microcoil NMR probes was presented by the fact that for a given mass of analyte, a reduction in the diameter of the receiver coil increases the signal-to-noise ratio (S/N).[5,10–12] Because a reduction in coil diameter inevitably results in a decrease in the sample volume, microcoil NMR probes will only provide a sensitivity advantage in cases where the mass-limited sample is fully soluble in the smaller volume of solvent. On the other hand, for concentration-limited samples microcoil designs offer no advantage, as a smaller probe accommodates much less of a concentration-limited sample than conventional designs. Accordingly, the concentration sensitivity of microcoil NMR probes is generally lower than that of conventional 5-mm probes (Table 1).[10]

Designing NMR probes with smaller receiver coils has been a challenging task. A smaller coil requires the sample to be in closer proximity to the coil, which can result in

Table 1: Comparison of the concentration-sensitivity (S_c) and mass-sensitivity (S_m) for a test sample of sucrose using a CapNMR microcoil probe and a 5-mm H{C,N} probe at 600 MHz with a Shigemi tube.[a]

Probe	Sample volume [μL]	S_c (S/N per mM) (normalized)	S_m (S/N per μmol) (normalized)
5 mm	260[b]	10.4	1
CapNMR	5	1	5.0

[a] A single scan was acquired for samples of a solution of sucrose (17.2 μg, 50 nmol) in D_2O.[18] Signal-to-noise ratios were determined using the anomeric proton and VNMR (VARIAN) software. For a similar comparison see Ref. [12]. [b] A slightly smaller volume of 200–220 μL could have been used for the Shigemi tube, which could have increased the mass-sensitivity for the 5-mm probe by up to 25% and thus reduce the advantage of CapNMR in mass-sensitivity to a factor of roughly four.

Frank C. Schroeder studied chemistry and physics at the University of Hamburg and completed his PhD in 1997 with Wittko Francke. He carried out postdoctoral studies with Jerrold Meinwald at Cornell University, where he further developed his interests in the spectroscopic characterization of small molecules and their role in chemical biology. In 2004, he took his current position as Director of the Natural Products Initiative at Harvard Medical School. His research encompasses NMR spectroscopic approaches for the characterization of small-molecule mixtures and identification and function of signaling molecules in plants and higher animals.

Matthew Gronquist completed his PhD in 2002 at Cornell University, where he carried out studies under the guidance of Jerrold Meinwald into the characterization and synthesis of natural products. Following graduation he moved to the State University of New York (SUNY) College at Cortland, where he was appointed an assistant professor. In 2006, he moved to the SUNY College at Fredonia and is currently an assistant professor of chemistry. His research interests include small-molecule signaling in bacteria and the chemical ecology of arthropods.

© 2006 Wiley-VCH Verlag GmbH & Co. KGaA, Weinheim

significant line-broadening as a result of differences in magnetic susceptibility between the sample, coil material, and surrounding environment.[13–16] Furthermore, smaller coil diameters also require reconsideration of how the sample is introduced into the probe because conventional sample tube designs cannot be miniaturized indefinitely and maintaining a high fill factor for the coil is necessary to take full advantage of the sensitivity gain that results from reducing its size. A major breakthrough came with the introduction of probes that feature a receiver coil directly wrapped around a capillary-scale flow cell, which is embedded in a fluid whose magnetic susceptibility closely matches that of the coil material.[17] Careful susceptibility matching made it possible to drastically reduce magnetic field inhomogeneities in the vicinity of the coil and resulted in greatly improved lineshapes suitable for high-resolution NMR spectroscopy. Linewidths of the most recent generation of commercial capillary microcoil NMR (CapNMR) probes now easily match those of 5-mm cryogenic probes. As CapNMR flow cells are extremely small, they can be oriented horizontally, perpendicular to the magnetic field, which allows the use of solenoidal receiver coils (Figure 1). Compared to the "saddle"-type coil designs necessary for vertically oriented samples, solenoidal coils

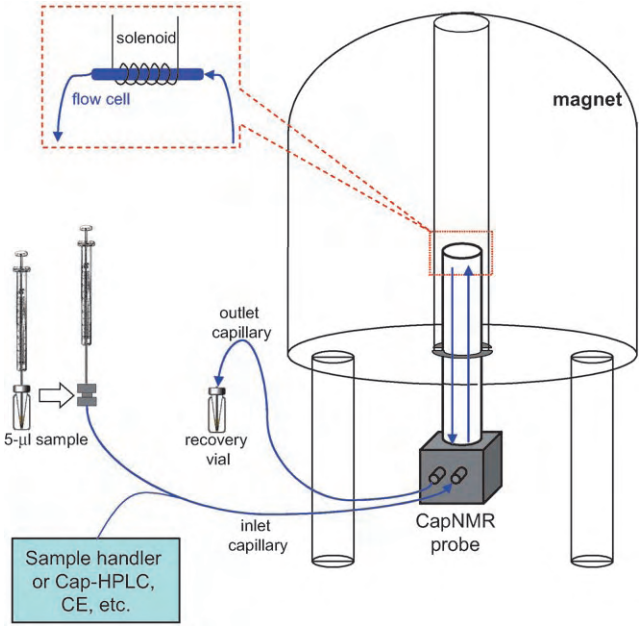

Figure 1. Schematic of the setup and probe design for CapNMR spectroscopy. CE = capillary electrophoresis.

provide roughly twofold higher intrinsic sensitivity as a result of their stronger coupling to the sample.[10] The solenoidal design thus further increases overall sensitivity of the probe, in addition to the improvement gained from miniaturizing the coil. Another consequence of working with an extremely small sample volume is that shimming is very fast and usually involves little more than adjusting a few first-order shims.[12] Frequently, when one is dealing with a series of samples in the same solvent, shimming is needed for the first sample only.

Microcoil NMR probes typically employ a single coil for the deuterium lock, proton, and X-nuclei (X = ^{13}C, ^{15}N) channels. In its most common—and most mass-sensitive—design, the CapNMR probe features a very small 5-µL flow cell with an active volume of only about 2.5 µL.[12] In addition, a slightly less mass-sensitive 10-µL version is available, with an active volume of roughly 5 µL. In either case, the flow cell is connected to gas-chromatography-type fused-silica capillaries or FEP (fluorinated ethylene propylene) tubing (inner diameter (i.d.): 75–100 µm), which serve as the inlet and outlet. For loading of the flow cell, the sample is injected into the inlet line either manually by syringe or automatically by a liquid-handling system. There are many advantages of using a capillary-scale flow path. First, employing flow cells allows somewhat higher fill factors to be achieved than with sample-tube-based microcoil designs. The use of very narrow capillaries virtually eliminates mixing within the outlet and inlet and thus reduces problems associated with sample management, such as peak dispersion and sample carryover, that are commonly encountered with larger-scale flow probes.[12] Furthermore, the inlet and outlet lines can be easily connected to other analytical instrumentation, for example, capillary LC, for "online" hyphenated applications. Perhaps more importantly, the compatibility of CapNMR with standard laboratory titer plates and microvials makes it well-suited for the high-throughput analysis of compound libraries and allows for facile combination with analytical platforms that include analytical-scale HPLC or capillary electrophoresis (CE) and mass spectrometry (MS).

2.2. A Comparison of Mass-Sensitivity

As should be evident from the preceding section, using the CapNMR system requires a new approach to sample preparation and loading. Instead of preparing a glass NMR tube containing the sample as a solution in 200–600 µL of solvent (depending on the type of probe and glass tube), in CapNMR the sample has to be dissolved in only 5–10 µL of solvent, and the solution must subsequently be transferred, without significant losses, manually by syringe or under automation using a liquid-handling system for injection into the probe. To compare the utility of CapNMR as a flow-cell design to that of traditional sample-tube-based probes, these differences must be carefully considered, especially if one is primarily interested in using CapNMR for manual injection of samples that otherwise could be analyzed by using traditional probes. The primary motivation for using CapNMR in this case would be its significantly higher mass-sensitivity,[12] but exactly how much of a difference does it make compared to using a "normal" 5-mm probe for real samples? The use of solvent-specific susceptibility-matched NMR tubes (e.g. Shigemi tubes) in 5-mm probes already results in a two- to threefold net increase in mass-sensitivity. To assess the degree to which using CapNMR could improve the sensitivity of NMR spectroscopy beyond that achieved by using Shigemi-type tubes, Gronquist et al. directly compared spectra obtained with both probe designs by using a 10 mM sucrose solution and a series of natural product extracts as test samples.[18] In

© 2006 Wiley-VCH Verlag GmbH & Co. KGaA, Weinheim

one series of experiments, one-dimensional ^{1}H NMR spectra as well as two-dimensional (^{1}H,^{13}C) HMQC and (^{1}H,^{13}C) HMBC[19] spectra were acquired for a 5-μL sample of a solution of sucrose (10 mM), which was injected into the CapNMR probe by syringe. In a second series of experiments, the same amount of sucrose was dissolved in the volume of solvent (D_2O) required for using a 5-mm Shigemi tube, followed by acquisition of an equivalent set of spectra using a conventional 5-mm H{C,N} probe and the same spectrometer. A comparison of the ^{1}H spectra reveals that the signal-to-noise ratio is about five times better for the CapNMR spectrum (Figure 2). In addition, the HDO solvent peak in the CapNMR spectrum is smaller by several orders of magnitude than in the spectrum obtained using a 5-mm probe as a consequence of the fact that the active volume of the 5-mm probe is more than 100-times greater than that of the CapNMR probe. The much smaller solvent signal allowed the use of a higher receiver gain for acquisition of the CapNMR spectrum, which contributed to the observed sensitivity gain.

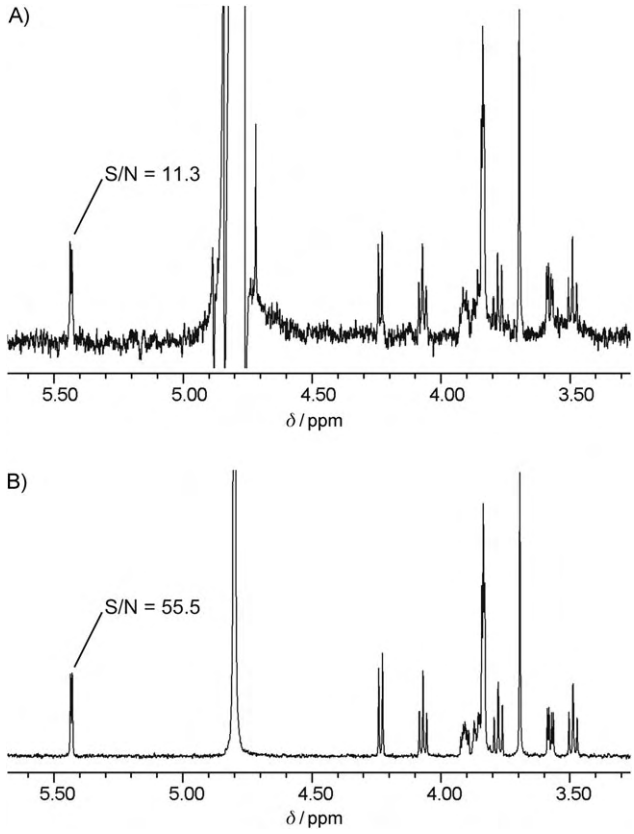

Figure 2. ^{1}H NMR spectra (1 scan each) of sucrose (17.2 μg) dissolved in A) D_2O (260 μL) using a Shigemi tube and a 5-mm H{C,N} probe, and B) 5 μL of D_2O using a 5-μL CapNMR probe. S/N ratios were determined by using VNMR (Varian Inc.) software.

Of particular relevance for the NMR spectroscopic characterization of small molecules are the indirect-detection carbon–proton correlations HMQC, HSQC, and HMBC. Owing to the low natural abundance of ^{13}C the sensitivity of these experiments is significantly lower than that of proton–proton correlations, and insufficient signal-to-noise ratios of HMQC/HSQC and especially HMBC spectra is what ultimately limits structure determination of mass-limited, small-molecule samples. CapNMR probes are commonly equipped with gradient coils and thus allow the acquisition of both the gradient and the slightly more sensitive nongradient versions of HMQC and HMBC. For these spectra, CapNMR probes can also provide significant sensitivity advantages, as shown for the nongradient HMBC spectra in Figure 3.[18] The nongradient versions of indirect-detection carbon–proton correlations, in which signals from ^{12}C-bound protons are suppressed through phase-cycling and which, in some cases, can provide higher sensitivity than the corresponding gradient-based versions[20] (see also Ref. [21]), especially benefit from the much smaller solvent signals acquired with CapNMR probes.

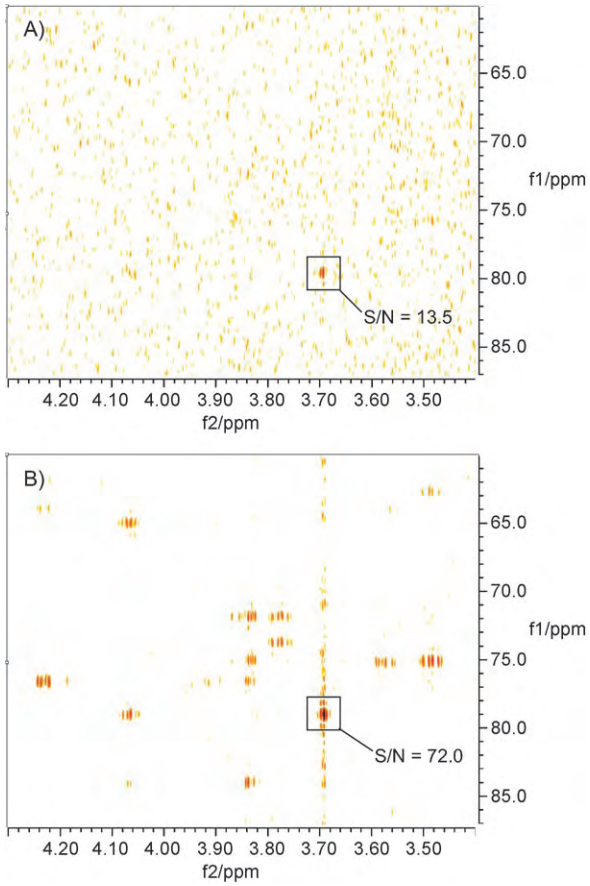

Figure 3. A) Nongradient (^{1}H,^{13}C) HMBC spectrum of sucrose (17.2 μg) dissolved in D_2O (260 μL) using a Shigemi tube and a 5-mm H{C,N} probe. B) Nongradient (^{1}H,^{13}C) HMBC spectrum of sucrose (17.2 μg) dissolved in D_2O (5 μL) using a 5-μL CapNMR probe. The total acquisition time for each spectrum was 14 h.[18] S/N ratios were determined on slices in f2 by using VNMR (Varian Inc.) software.

 © 2006 Wiley-VCH Verlag GmbH & Co. KGaA, Weinheim

3. Stand-Alone Applications

3.1. Offline Characterization of Small Molecules

There are relatively few reports on the use of microcoil NMR probes for the offline characterization of mass-limited small-molecule samples, such as precious natural products or other biologically active materials that cannot be obtained in sufficient quantity to enable structure determination by using conventional NMR probes. Nonetheless, natural product chemists can expect to benefit greatly from the introduction of microcoil probes. Simply because of their scarcity, many organisms with potentially interesting secondary metabolites are effectively placed off limits for natural product exploration based on conventional NMR spectroscopy, as the amounts of sample isolated would likely not be sufficient to obtain spectra of suitable quality for identification. The relatively slow adoption of microcoil NMR technology for natural products applications might in part be related to its flow-cell design, which requires a dedicated approach to sample preparation and might deter chemists who are used to using glass NMR tubes. However, manual injection[18,22] or automated loading[23] of individual samples into the CapNMR probes is entirely feasible. For loading of a 5-μL CapNMR flow cell, the sample dissolved in 5 μL of deuterated solvent is injected into the inlet line, either by using a dedicated liquid-handling system or simply by syringe. The injection of the sample is then followed by injection of a small amount of additional deuterated solvent, which serves to push the sample through the inlet line into the flow cell. The volume of solvent needed to push the sample into the flow cell depends on the length of the inlet line and is easily calibrated upon initial installation of the probe by using a test sample. For recovery of the sample after completion of NMR spectroscopic analysis, the sample is simply flushed from the probe into a recovery vial by injecting a larger volume of solvent (typically around 50 μL). Offline sample injection as described here is highly reproducible and can be used for the routine characterization of many kinds of mass-limited samples. However, it requires that all samples be carefully filtered prior to injection to avoid blockages in the capillaries that might result from insoluble contaminants. Accordingly, inline filtration is a standard procedure (standard filter size: 2 μm).

The identification of two antibacterial glycosides **1** and **2** by Hu and co-workers represented the first example of structure elucidation of new natural products by using CapNMR spectroscopy (Figure 4).[24] Glycosides **1** and **2** were isolated by automated high-throughput fractionation of a library of plant extracts. Following fractionation, those fractions that displayed antibacterial activity were characterized offline by using the CapNMR probe with manual injection. Similarly, the antibacterial plant metabolites suaveolindole[25] (**3**) and a group of partially acetylated oligorhamnosides[26] such as **4** were identified by using CapNMR spectroscopy. The amount of glycoside **2** isolated (70 μg) would clearly have been insufficient for identification by using a conventional 5-mm probe, and although **1** and **3** were isolated in amounts large enough to warrant identification by

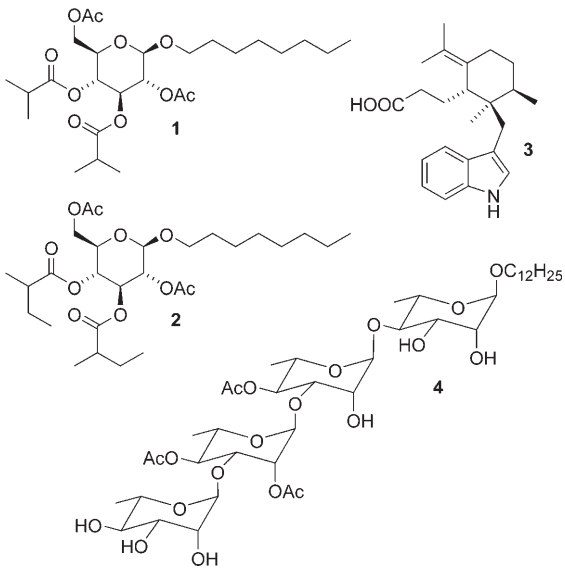

Figure 4. Plant-derived natural products identified by Hu and co-workers by using CapNMR spectroscopy.

using conventional 5-mm probes, use of the CapNMR probe significantly reduced the times required for the acquisition of ^{13}C NMR, gCOSY (gradient-selected COSY), HSQC, and HMBC spectra.

In a study aimed at exploring natural product diversity in rare organisms, Gronquist et al. used a 5-μL CapNMR probe to characterize and identify a series of novel steroidal pyrones isolated from a small collection of specimens of a rare firefly species.[18] Thirteen different cardenolides and related steroids, for example, **5** and **6**, were identified, all of which represented new natural products (Figure 5). The compounds

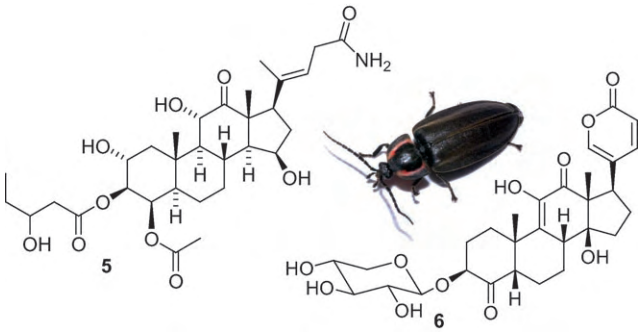

Figure 5. Steroids identified from *Lucidota atra* fireflies by using CapNMR spectroscopy.

were identified on the basis of data from routine dqf-COSY (double quantum filtered COSY), NOESY, HMQC, and HMBC spectra. Nongradient HMBC spectra of sufficient quality for structure determination were obtained for samples containing as little as 40 nmol of material. By directly comparing the sensitivity achieved by CapNMR spectroscopy with that of a 5-mm H{C,N} probe with a Shigemi tube, it was found that CapNMR provided a roughly threefold gain in sensitivity while maintaining very high spectral quality.

© 2006 Wiley-VCH Verlag GmbH & Co. KGaA, Weinheim

Spectral characteristics such as good line shapes and a low level of artifacts were essential for the spectroscopic characterization of the steroid samples, as several of these constituted mixtures of two or three compounds. The observed sensitivity gain of roughly a factor of three is significantly smaller than the increase in sensitivity determined in the sucrose experiments described in Section 2.2. The reason for the lower sensitivity gain in the case of the steroid example lies in the specific details of the sample preparation procedure. When using the Shigemi tube, the sample can be transferred into the tube almost without loss, as the relatively large volume of the NMR tube permits multiple rinses of the original sample vial. With CapNMR, however, a small amount of sample is inevitably left behind in the original sample vial, because the sample has to be transferred by a single 5-μL injection. Nevertheless, the use of the CapNMR probe for characterization of the firefly-derived cardenolides allowed the identification of at least twice as many compounds as would have been possible by using the 5-mm probe/Shigemi tube combination.

In addition to its value for the identification of new natural products, Hu et al. demonstrated the utility of capillary NMR spectroscopy for the dereplication of natural product libraries.[27] As generally only about 10 nmol (about 5 μg for a compound with a molecular weight of 500 $g\,mol^{-1}$) of material is required for the acquisition of 1D ^1H and (^1H,^1H) COSY spectra, even trace amounts of known natural products can easily be identified. CapNMR probes also hold great promise for the identification of known metabolites in pharmacology or of synthetic products in combinatorial chemistry (see Section 5).

3.2. Protein Structure Determination

While CapNMR probes have been commercially available for a few years, their utility for the characterization of biological macromolecules has been realized only recently. The relatively low concentration-sensitivity of microcoil probes makes their use for the characterization of proteins and nucleic acids non-intuitive, because most biological macromolecules are generally much more concentration-limited than organic small molecules. However, in 2004, Peti et al. showed that the use of microcoil probes for protein structure determination offers distinct advantages.[22] NMR spectroscopic characterization of a protein usually starts with assignment of the protein backbone by using well-established triple-resonance experiments such as HNCOCA and HNCA.[28] This step is followed by the acquisition of additional spectra aimed at assignment of the aliphatic and aromatic side chains. Compared to the characterization of the protein backbone, the assignment of the side chain, especially aromatic amino acid side chains, is much less straightforward and often very time-consuming because it relies on interpretation of 2D (^1H,^1H) NOESY, COSY, and TOCSY spectra that suffer from poor signal dispersion and are thus prone to cross-peak overlap, which results in ambiguous assignments. As the hydrophobic aromatic side chains play a key role in protein stability, there is considerable interest in improving methods for their characterization. Peti et al. showed that the distinctive physical properties of microcoil probes allow side-chain assignments to be dramatically simplified. In addition to providing high mass-sensitivity, microcoil probes exhibit excellent radiofrequency (RF) characteristics as a direct result of the solenoidal coil design, and only very low transmitter power is needed to achieve short proton and carbon 90-degree pulses. These specific qualities of microcoils allowed for the first time the acquisition of aliphatic–aromatic HCCH-TOCSY spectra, which can be used to assign the aromatic and aliphatic side chains of a fully ^{13}C-labeled protein in a single experiment (Figure 6). By using conventional room-temperature or cryogenic 5-mm probes the acquisition of such spectra would not be feasible because the RF power required to induce TOCSY transfer over the entire chemical shift range of aromatic and aliphatic carbon atoms would be prohibitively high. Using their full-range HCCH-TOCSY version, Peti et al. completely assigned the side chains for a sample of only 500 μg of a 9.7-kDa protein. The 3D HNCO and HNCOCA spectra required for assignment of the backbone were also obtained by using the CapNMR probe.

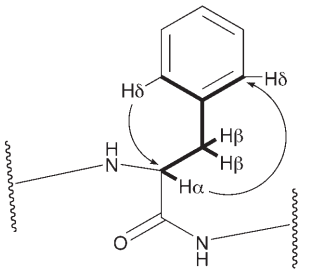

Figure 6. An important step in the NMR spectroscopic characterization of proteins consists of connecting Cα/Hα and Cβ/Hβ atoms of aromatic amino acids with the Hδ protons in the corresponding aromatic ring system. HCCH-TOCSY correlations between Hα and Cδ atoms and between Hδ and Cα atoms in a phenylalanine residue are shown.[22]

In another recent example, Peti et al. outlined the utility of capillary NMR systems in structural genomics.[29] To identify promising targets for structure determination by X-ray crystallography, structural genomics researchers increasingly resort to NMR spectroscopic screening of protein libraries for proteins that exhibit substantial folding in solution. In combination with high-throughput methods for protein expression and purification, implementing CapNMR techniques allows for a substantial miniaturization of structural genomics pipelines. By using ^1H NMR and 2D (^1H,^{15}N) COSY spectra, Peti et al. demonstrated the effectiveness of their miniaturized pipeline by comparing the results obtained for nine mouse homologue protein targets with those obtained by using traditional "large-scale" methodology. This comparison indicated that the quality of structural information obtained through CapNMR-based structural genomics pipelines was similar to that achieved by using conventional methods. Thus, capillary NMR spectroscopy allows implementation of a miniaturized structural

© 2006 Wiley-VCH Verlag GmbH & Co. KGaA, Weinheim

genomics pipeline without compromising data quality, thus significantly reducing the costs associated with protein production as, for example, the requirements for labeled ^{15}N media decrease by about 20-fold.

4. Hyphenated Techniques

The design and performance parameters of capillary probes offer distinct advantages over earlier flow-through NMR probe designs and make them well suited for direct coupling to various chromatographic methods, resulting in so-called "hyphenated" techniques.[30] CapNMR probes are especially well matched to capillary-based separations, which operate with compatible flow rates and give peak volumes similar to the volume of the flow cell, a necessary condition for fully exploiting the increased mass-sensitivity of the microcoil probe. The higher peak concentrations generally realized in capillary separations provide further gains in sensitivity when compared to larger bore separations.[31] The very low flow rates used in capillary-based systems translate into lower consumption of deuterated solvents, thus reducing costs and decreasing the need for solvent suppression. Capillary NMR spectroscopy has been coupled online to capillary HPLC (CapLC-NMR), as well as to capillary electrophoretic techniques such as capillary isotachophoresis (cITP-NMR)[32] and capillary electrochromatography (CEC-NMR).[33]

4.1. Capillary LC-NMR (CapLC-NMR)

Capillary HPLC is the most common separation technique to be coupled online with the CapNMR probe, largely as a result of the popularity and applicability of HPLC as the method of choice for a wide range of separation problems. As with earlier versions of LC-NMR,[34,35] various modes of operation are possible depending on the nature of the sample and specific time requirements. In continuous-flow mode (also referred to as on-flow), transients are collected continuously over the course of the separation. The continuous introduction of fresh polarized nuclei into the flow cell benefits the sensitivity by reducing the need for relaxation delays in the pulse sequences, but also results in additional line-broadening as flow rates increase.[36] As each eluting peak occupies the active volume of the flow cell for only a short period of time, relatively few transients are collected for each component and this mode is thus necessarily relatively insensitive.[33] Sensitivity can be improved by decreasing flow rates[37] and increasing sample loading, but a point of diminishing returns is quickly reached where the chromatographic separation begins to suffer. Nonetheless, the increased mass-sensitivity of the CapNMR probe makes continuous-flow LC-NMR a viable technique for applications in which rapid analysis yielding detailed structural information is required. The feasibility of CapLC-NMR for continuous-flow analysis of mixtures of natural products was demonstrated by Krucker et al.[38] In their analysis, a 200-nL aliquot containing approximately 1.3 μg each of four tocopherol homologues was separated and each elution peak was positively identified based solely on its ^1H NMR spectrum. Note that two of the components, β- and γ-tocopherol, were indistinguishable by their mass spectra. Comparison to previous work by the same authors using classical HPLC-NMR showed the CapLC-NMR system to achieve comparable performance while decreasing the amount of sample required by a factor of 200.[39]

For most mass-limited applications, longer acquisition times are required than can be achieved by using a continuous-flow mode. In stopped-flow mode, selected elution peaks are stored in the flow cell for extended periods of time, allowing the acquisition of longer 1D or 2D spectra. Large improvements in the signal-to-noise ratio are realized, but total run times necessarily become longer. Online UV/Vis detection is generally incorporated immediately upstream from the NMR probe to identify peaks prior to their entry into the capillary probe flow cell, and the proper time delay required to correctly position the eluting analyte bands in the active volume of the flow cell must be calibrated. The continuous-flow-path construction of the narrow diameter (50–100 μm i.d.) inlet/outlet feed lines of the flow cell minimizes sample dilution caused by diffusion, while the small sample volume and relatively larger diameter of the flow cell facilitate rapid equilibration of the samples stored in the flow cell.[12] As a result, acquisitions lasting several hours are possible with negligible sample diffusion. The potential of stopped-flow CapLC-NMR has been demonstrated recently for a variety of mass-limited applications in natural product analysis,[40,41] metabolite identification,[42,43] and as a potential technique for monitoring protein phosphorylation in cellular signaling pathways.[44]

These analyses show CapLC-NMR to be a promising technique for the rapid extraction of detailed structural information from mass-limited samples. However, as previously noted for stand-alone applications, the benefits of using CapLC-NMR as opposed to other online and offline NMR techniques are only fully realized for samples that are truly mass-limited. In a recent comparison of CapLC-NMR with alternate methods, CapLC-NMR was shown to be an effective technique for distinguishing among diastereomeric adamantane metabolites present in a urine sample.[41] However, the authors noted that limitations inherent in the CapLC-NMR system, such as the loading potential of the column and difficulties in targeting the desired elution peaks for stopped-flow acquisitions, will often warrant the use of alternate techniques in cases where the sample size is not severely limited. In these cases, a larger-scale fractionation followed by offline collection of the fractions of interest and subsequent manual or automated injection into the CapNMR probe can provide better results. Although most applications of CapLC-NMR reported to date have been demonstrations of feasibility, the technique seems well on its way to becoming routine, as underscored by the recent introduction of a commercially available CapLC-NMR system that comes complete with autosampler and integrated diode-array UV/Vis detection.[45]

© 2006 Wiley-VCH Verlag GmbH & Co. KGaA, Weinheim

4.2. Capillary Electrophoresis Hyphenated to Capillary NMR (CE-NMR)

Capillary electrophoresis and its many variants have developed into important separation techniques that frequently prove effective in situations where HPLC is not suitable.[46] Although a wide variety of detection strategies are possible (UV/Vis spectroscopy, MS, etc.), the lack of sensitivity inherent to NMR spectroscopy has previously precluded its coupling to capillary electrophoretic separations. Microcoil NMR spectroscopy for the first time provides a viable way to combine the powerful separation capabilities of capillary electrophoresis with the detailed structural and molecular dynamic information afforded by NMR spectroscopy.[14] The most promising variant of microcoil CE-NMR described to date is capillary isotachophoresis-NMR (cITP-NMR).[32] Capillary isotachophoresis (cITP) separates and concentrates charged species based on their electrophoretic mobilities through the application of a high voltage across a capillary containing a two-buffer system comprised of a leading electrolyte (LE) and a trailing electrolyte (TE; Figure 7). Under optimal conditions, cITP has the ability to concentrate charged analytes by two to three orders of magnitude over the course of the separation. When hyphenated to capillary NMR spectroscopy, cITP allows focusing of sample components precisely in the active volume of the capillary probe to maximize the potential of the microcoil design. The focusing of the sample realized with cITP-NMR allows the use of probes with active volumes on the order of tens of nanoliters, thus providing even greater gains in mass-sensitivity and making cITP-NMR the most mass-sensitive NMR technique yet realized. The potential of cITP-NMR for the online separation and analysis of nanomolar quantitities of biologically relevant small molecules was demonstrated by Korir et al.[47] A mixture containing 2.5 nmol each of three sulfated heparin disaccharides was separated, and ^{1}H NMR spectra suitable for identification were acquired for each component as the focused bands passed through the 25-nL active volume of a custom-built microcoil probe.

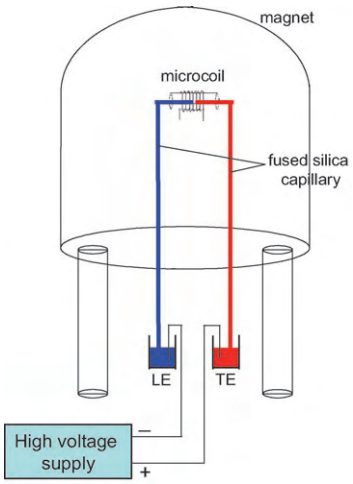

Figure 7. Schematic of cITP-NMR. Charged analytes are focused through the application of high voltage across a capillary that contains a two-buffer system. Focused bands are detected as they move through the microcoil probe.[47,49]

In contrast to CapLC-NMR, which seems to be on the verge of entering the mainstream as a routine analytical method, capillary electrophoresis-NMR (CE-NMR) is still in the early stages of development. Most results reported to date are based on custom-built, "in-house" probes, which often use internally modified capillaries and very small active volumes.[48,49] Nonetheless, the preliminary results seem promising and suggest that CE-NMR will continue to develop and may become the technique of choice for specific applications in chemical, biochemical, and environmental analysis.

5. High-Throughput Capillary NMR Spectroscopy

Capillary NMR spectroscopy holds particular promise for use in high-throughput applications, such as in the analysis of natural product or synthetic compound libraries. A continuing problem in characterizing large libraries has been the lack of a universal detector. Whereas various combinations of MS, UV, and evaporative light-scattering detectors (ELSD) have been used extensively in high-throughput applications, these methods often suffer from response bias or a general lack of structural information. The detailed structural and stereochemical information afforded by NMR spectroscopy is thus often necessary for the comprehensive characterization of natural product and synthetic library compounds.[50] In addition, NMR spectroscopic techniques have been used to screen small-molecule libraries for weak ligand–protein interactions that are difficult to observe with traditional fluorescence-based techniques but which may hold important clues for drug development.[51–53] While automated high-throughput NMR systems are not novel,[54] the increased mass-sensitivity realized with microcoil capillary probes greatly extends the scope and applicability of high-throughput NMR spectroscopy as it facilitates faster acquisitions on smaller amounts of sample while consuming far less deuterated solvent. The flow-through design of capillary probes makes them well suited for automation either hyphenated online to analytical separations or offline as stand-alone analyzers. The general trend appears to be toward offline analyses facilitated through the use of common sample formats across complementary analytical platforms. The ease of shimming and the shim stabilities that are intrinsic to the microcoil design translate into further efficiency for overall sample throughput. Finally, as NMR spectroscopy is non-destructive, incorporating it into an online analysis enables further coupling to a fraction collector or other detection techniques, such as MS, UV, and ELSD, thus allowing the acquisition of complementary structural information.

Preliminary evaluations carried out on test libraries by using microcoil probes with various system configurations were recently reported. Bailey and Marshall recently reported a method utilizing continuous flow for the rapid analysis of a test library comprised of *p*-hydroxybenzoic acid esters.[55] Individual samples were automatically loaded sequentially from a 96-well plate and pumped through the capillary flow

 © 2006 Wiley-VCH Verlag GmbH & Co. KGaA, Weinheim

cell as a steady sample stream. Transients were collected continuously and stored as a pseudo-2D file, from which increments corresponding to individual samples were extracted and pooled to give individual 1D spectra. By this means, ^{1}H NMR spectra suitable for structure confirmation were obtained for injection amounts corresponding to approximately 3.4 μg of sample per injection. Analysis of a 96-well plate could be completed in less than 1 hour, and consumption of the deuterated solvent was less than 4.0 mL per plate. Alternatively, Kautz et al. described a stopped-flow method based on segmented flow analysis (SFA).[56] In this method, library compounds are injected as discrete plugs separated by an immiscible, susceptibility-matched fluorocarbon carrier fluid. Sample plugs are detected by their NMR signal upon entering the flow cell and then stopped for spectral acquisition. The carrier fluid serves to wet the capillary walls, decreasing adhesion and limiting the resultant carryover and loss of sample. The immiscible nature of the carrier fluid also limits sample dispersion, allowing 2D acquisitions with durations of up to several days when necessary. The potential of the technique was demonstrated through the unambiguous identification of all members of a test library containing such structurally diverse elements as reserpine, erythromycin, and uracil (green, red, and blue structures, respectively, in Figure 8). Sample amounts were on the order of 10 μg per

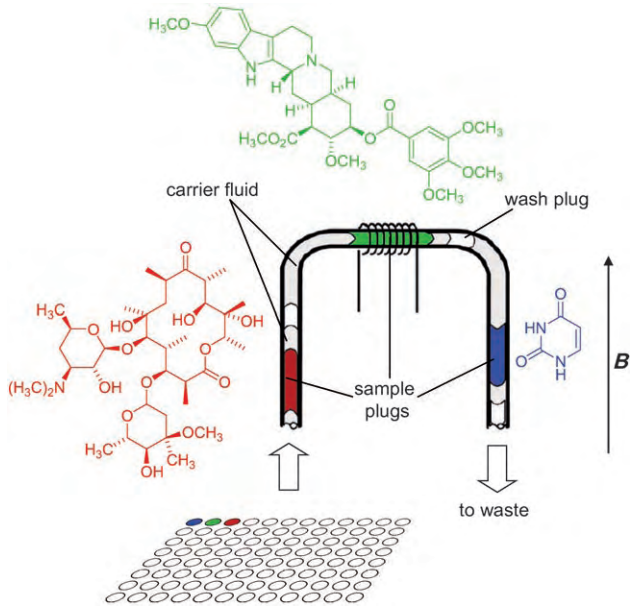

Figure 8. Schematic of SFA-NMR.[56] Library samples are advanced as discrete 1 μL sample plugs, separated by an immiscible carrier fluid. [D_6]DMSO wash plugs containing 1% trimethylsilylpropionate are included to further limit sample carryover and facilitate sample detection and positioning.

injection, and analysis of a 96-well plate could be completed in less than 3 h while consuming less than 0.5 mL of deuterated solvent per plate. Most recently, a flexible automated system capable of accepting both open-access samples in vials as well as library samples prepared in 384-well plates was described and evaluated.[23] The system, which is controlled and monitored by using web-based software, allows walk-up analysis of priority samples prepared in microliter vials anytime during library analyses.

6. Summary and Outlook

NMR spectroscopy is clearly one of the most valuable analytical techniques for organic chemists and biochemists. The introduction of microcoil probes is likely to further extend its scope and utility as they offer improved mass-sensitivity and are easily combined with almost any chromatographic technique. For a technology so radically different from that of conventional NMR probes, current microcoil designs have been astonishingly successful and, within only a few years of their original inception, have evolved into a serious alternative to cryogenic probes, as for many situations they offer comparable sensitivity at a fraction of the cost. Moreover, CapNMR probes can be installed and exchanged with conventional 5- or 3-mm NMR probes very quickly and thus, as opposed to cryogenic probes, do not require a spectrometer to be solely dedicated to their use. As the technology is still young, further improvements in sensitivity and overall design are likely. Chemists interested in microcoil NMR spectroscopy will have to adjust to specific requirements for sample preparation and handling. Current sample injection procedures require careful filtration, and complete transfer of mass-limited samples into the flow cell cannot always be achieved. However, improved routines for both manual and automated sample injection continue to be developed. High-throughput combinatorial chemistry as well as pharmacological applications and high-throughput natural products chemistry will benefit from the availability of probes with two or more flow cells.[57]

At this time, microcoil probes appear particularly well suited for small-molecule NMR spectroscopy, whereas their utility for the characterization of biological macromolecules is somewhat limited because for many proteins or nucleic acids sufficiently high sample concentrations cannot be obtained. For such concentration-limited samples, cryogenic probes will remain the obvious choice. However, as recent examples by Peti et al. have illustrated, the use of microcoil probes for protein structure determination is entirely feasible and in certain situations can offer distinct advantages (see Section 3.2).

There are additional benefits of using miniaturized NMR probes, some of which have not yet become fully apparent. Because of their small sample volumes, microcoil NMR probes require far smaller homogeneous magnetic field regions than traditional 5-mm probes. One consequence is the relative ease of shimming of microcoil probes, which usually requires adjusting only a few first-order shims. More importantly, the less stringent requirements for the homogenous region of the magnetic field may allow the development of smaller magnets, which could lead to significant cost savings, but might also hold promise for the introduction of magnets with higher field strengths or the use of alternative materials for magnet design, including the use of room-temperature superconducting materials. Introduction of

© 2006 Wiley-VCH Verlag GmbH & Co. KGaA, Weinheim

smaller highfield magnets suitable for high-resolution NMR spectroscopy would dramatically reduce space requirements for NMR spectrometers and might ultimately lead to the development of benchtop instruments.

Received: May 8, 2006
Published online: September 22, 2006

[1] R. R. Ernst, *Angew. Chem.* **1992**, *104*, 817; *Angew. Chem. Int. Ed. Engl.* **1992**, *31*, 805.
[2] A. E. Derome, *Modern NMR Techniques for Chemistry Research*, Pergamon, New York, **1987**.
[3] C. L. Putzig, *Anal. Chem.* **1994**, *66*, 26R.
[4] M. E. Lacey, R. Subramanian, D. L. Olson, A. G. Webb, J. V. Sweedler, *Chem. Rev.* **1999**, *99*, 3133.
[5] D. I. Hoult, R. E. Richards, *J. Magn. Reson.* **1976**, *24*, 71.
[6] A. Abraham, *The Principles of Nuclear Magnetism*, Clarendon Press, Oxford, **1961**.
[7] P. L. Rinaldi, *Analyst* **2004**, *129*, 687.
[8] D. J. Russell, C. E. Hadden, G. E. Martin, A. A. Gibson, A. P. Zens, J. L. Carolan, *J. Nat. Prod.* **2000**, *63*, 1047.
[9] M. Spraul, A. S. Freund, R. E. Nast, R. S. Withers, W. E. Maas, O. Corcoran, *Anal. Chem.* **2003**, *75*, 1546.
[10] A. G. Webb, *Prog. Nucl. Magn. Reson. Spectrosc.* **1997**, *31*, 1.
[11] J. N. Shoolery, *Top. Carbon-13 NMR Spectrosc.* **1979**, *2*, 28.
[12] D. L. Olson, J. A. Norcross, M. O'Neil-Johnson, P. F. Molitor, D. J. Detlefsen, A. G. Wilson, T. L. Peck, *Anal. Chem.* **2004**, *76*, 2966.
[13] N. Wu, T. L. Peck, A. G. Webb, R. L. Magin, J. V. Sweedler, *Anal. Chem.* **1994**, *66*, 3849.
[14] N. Wu, T. L. Peck, A. G. Webb, R. L. Magin, J. V. Sweedler, *J. Am. Chem. Soc.* **1994**, *116*, 7929.
[15] T. L. Peck, R. L. Magin, P. C. Lauterbur, *J. Magn. Reson. Ser. B* **1995**, *108*, 114.
[16] A. G. Webb, S. C. Grant, *J. Magn. Reson. Ser. B* **1996**, *113*, 83.
[17] D. L. Olson, T. L. Peck, A. G. Webb, R. L. Magin, J. V. Sweedler, *Science* **1995**, *270*, 1967.
[18] M. Gronquist, J. Meinwald, T. Eisner, F. C. Schroeder, *J. Am. Chem. Soc.* **2005**, *127*, 10810.
[19] For a detailed explanation of two-dimensional NMR spectroscopy and commonly used NMR spectroscopic acronyms, see: H. Kessler, M. Gehrke, C. Griesinger, *Angew. Chem.* **1988**, *100*, 507; *Angew. Chem. Int. Ed. Engl.* **1988**, *27*, 490.
[20] R. Hurd, B. K. John, *J. Magn. Reson.* **1991**, *91*, 648.
[21] P. L. Rinaldi, P. A. Keifer, *J. Magn. Reson. Ser. A* **1994**, *108*, 259.
[22] W. Peti, J. Norcross, G. Eldridge, M. O'Neil-Johnson, *J. Am. Chem. Soc.* **2004**, *126*, 5873.
[23] A. Jansma, T. Chuan, R. W. Albrecht, D. L. Olson, T. L. Peck, B. H. Geierstanger, *Anal. Chem.* **2005**, *77*, 6509.
[24] J.-F. Hu, H.-D. Yoo, C. T. Williams, E. Garo, P. A. Cremin, L. Zeng, H. C. Vervoort, C. M. Lee, S. M. Hart, M. G. Goering, M. O'Neil-Johnson, G. R. Eldridge, *Planta Med.* **2005**, *71*, 176.
[25] H.-D. Yoo, P. A. Cremin, L. Zeng, E. Garo, C. T. Williams, C. M. Lee, M. G. Goering, M. O'Neil-Johnson, G. R. Eldridge, J.-F. Hu, *J. Nat. Prod.* **2005**, *68*, 122.
[26] J.-F. Hu, E. Garo, G. W. Hough, M. G. Goering, M. O'Neil-Johnson, G. R. Eldridge, *J. Nat. Prod.* **2006**, *69*, 585.
[27] J.-F. Hu, E. Garo, H.-D. Yoo, P. A. Cremin, L. Zeng, M. G. Goering, M. O'Neil-Johnson, G. R. Eldridge, *Phytochem. Anal.* **2005**, *16*, 127.
[28] J. Cavanagh, W. J. Fairbrother, A. G. Palmer III, N. J. Skelton, *Protein NMR Spectroscopy*, Academic Press, San Diego, CA, **1996**.
[29] W. Peti, R. Page, K. Moy, M. O'Neil-Johnson, I. A. Wilson, R. C. Stevens, K. Wüthrich, *J. Struct. Funct. Genomics* **2005**, *6*(4), 259.
[30] D. A. Jayawickrama, J. V. Sweedler, *J. Chromatogr. A* **2003**, *1000*, 819.
[31] J. P. C. Vissers, *J. Chromatogr. A* **1999**, *856*, 117.
[32] R. A. Kautz, M. E. Lacey, A. M. Wolters, F. Foret, A. G. Webb, B. L. Karger, J. V. Sweedler, *J. Am. Chem. Soc.* **2001**, *123*, 3159.
[33] E. Rapp, A. Jakob, A. B. Schefer, E. Bayer, K. Albert, *Anal. Bioanal. Chem.* **2003**, *376*, 1053.
[34] V. Exarchou, M. Krucker, T. A. van Beek, J. Vervoort, I. P. Gerothanassis, K. Albert, *Magn. Reson. Chem.* **2005**, *43*, 681.
[35] S. H. Hansen, A. G. Jensen, C. Cornett, I. Bjornsdottir, S. Taylor, B. Wright, I. D. Wilson, *Anal. Chem.* **1999**, *71*, 5235.
[36] A. G. Webb, *Magn. Reson. Chem.* **2005**, *43*, 688.
[37] M. Sandvoss in *Online NMR and Related Techniques* (Ed.: K. Albert), Wiley, Chichester, **2002**, p. 111.
[38] M. Krucker, A. Lienau, K. Putzbach, M. D. Grynbaum, P. Schuler, K. Albert, *Anal. Chem.* **2004**, *76*, 2623.
[39] A. Lienau, T. Glaser, M. Krucker, D. Zeeb, F. Ley, F. Curro, K. Albert, *Anal. Chem.* **2002**, *74*, 5192.
[40] H. B. Xiao, M. Krucker, K. Putzbach, K. Albert, *J. Chromatogr. A* **2005**, *1067*, 135.
[41] P. Hentschel, M. D. Grynbaum, P. Molnar, K. Putzbach, J. Rehbein, J. Deli, K. Albert, *J. Chromatogr. A* **2006**, *1112*, 285.
[42] R. J. Lewis, M. A. Bernstein, S. J. Duncan, C. J. Sleigh, *Magn. Reson. Chem.* **2005**, *43*, 783.
[43] M. Sandvoss, A. D. Roberts, I. M. Ismail, S. E. North, *J. Chromatogr. A* **2004**, *1028*, 259.
[44] P. Hentschel, M. Krucker, M. D. Grynbaum, K. Putzbach, R. Bischoff, K. Albert, *Magn. Reson. Chem.* **2005**, *43*, 747.
[45] http://www.bruker-biospin.de/NMR/hyphenation/caplc.html.
[46] L. DeFrancesco, *Anal. Chem.* **2001**, *73*, 497A.
[47] A. K. Korir, V. K. Almeida, D. S. Malkin, C. K. Larive, *Anal. Chem.* **2005**, *77*, 5998.
[48] A. M. Wolters, D. A. Jayawickrama, J. V. Sweedler, *J. Nat. Prod.* **2005**, *68*, 162.
[49] V. K. Almeida, C. K. Larive, *Magn. Reson. Chem.* **2005**, *43*, 755.
[50] D. Raftery, *Anal. Bioanal. Chem.* **2004**, *378*, 1403.
[51] S. B. Shuker, P. J. Hajduk, R. P. Meadows, S. W. Fesik, *Science* **1996**, *274*, 1531.
[52] A. D. Chen, M. J. Shapiro, *J. Am. Chem. Soc.* **2000**, *122*, 414.
[53] A. H. Siriwardena, F. Tian, S. Noble, J. H. Prestegard, *Angew. Chem.* **2002**, *114*, 3604; *Angew. Chem. Int. Ed.* **2002**, *41*, 3454.
[54] P. A. Keifer, *Curr. Opin. Chem. Biol.* **2003**, *7*, 388.
[55] N. J. C. Bailey, I. R. Marshall, *Anal. Chem.* **2005**, *77*, 3947.
[56] R. A. Kautz, W. K. Goetzinger, B. L. Karger, *J. Comb. Chem.* **2005**, *7*, 14.
[57] M. A. Macnaughtan, T. Hou, J. Xu, D. Raftery, *Anal. Chem.* **2003**, *75*, 5116.

 © 2006 Wiley-VCH Verlag GmbH & Co. KGaA, Weinheim

DOI: 10.1002/anie.200601872

Natural Product Synthesis

Cascade Reactions in Total Synthesis

K. C. Nicolaou, David J. Edmonds, and Paul G. Bulger*

Keywords:
cascade reactions · domino reactions · natural products · tandem reactions · total synthesis

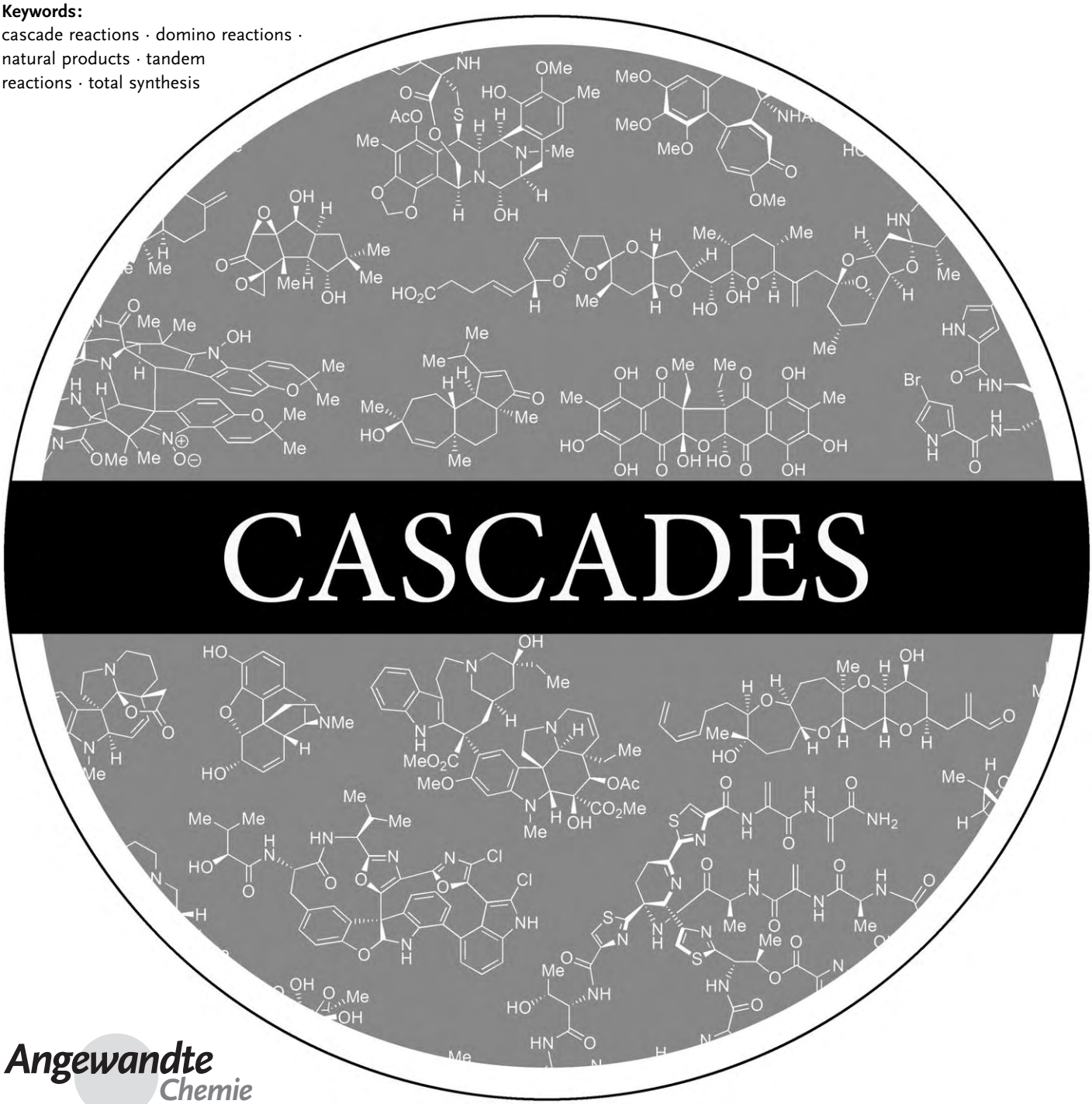

Angewandte Chemie

© 2006 Wiley-VCH Verlag GmbH & Co. KGaA, Weinheim

The design and implementation of cascade reactions is a challenging facet of organic chemistry, yet one that can impart striking novelty, elegance, and efficiency to synthetic strategies. The application of cascade reactions to natural products synthesis represents a particularly demanding task, but the results can be both stunning and instructive. This Review highlights selected examples of cascade reactions in total synthesis, with particular emphasis on recent applications therein. The examples discussed herein illustrate the power of these processes in the construction of complex molecules and underscore their future potential in chemical synthesis.

From the Contents

1. Introduction	7135
2. Nucleophilic Cascades	7137
3. Electrophilic Cascades	7144
4. Radical Cascades	7150
5. Pericyclic Cascades	7155
6. Transition-Metal-Catalyzed Cascades	7167
7. Summary and Outlook	7174

1. Introduction

Cascade reactions constitute a fascinating branch of organic chemistry, and one which has been the subject of intense research in recent years, as witnessed by the number of reviews that have appeared covering various aspects of these processes.[1] The undeniable benefits of cascade reactions are well established, having been recounted on numerous occasions, and include atom economy,[2] as well as economies of time, labor, resource management, and waste generation. As such, cascade reactions can be considered to fall under the banner of "green chemistry",[3] as the savings involved when one carries out several transformations in one synthetic operation can be considerable. For example, only a single reaction solvent, workup procedure, and purification step may be required to provide a product that would otherwise have to be made over the course of several individual steps. Such considerations will become increasingly important in years to come, as both chemists and society in general strive for evermore effective and responsible methods for the management of Earth's precious resources.

Target-oriented synthesis provides the ultimate test of reaction design and applicability. The design of cascades to provide specific targeted molecules of considerable structural and stereochemical complexity poses a significant intellectual challenge and can be one of the most impressive activities in natural product synthesis. Cascade reactions therefore contribute immeasurably to both the science and art of total synthesis, bringing not only improved practical efficiency but also enhanced aesthetic appeal to synthetic planning. The recognition of these dual benefits is, of course, by no means an exclusively modern phenomenon. Indeed, cascade reactions (either as designed sequences or serendipitous discoveries) have attracted the attention of organic chemists since the formative years of total synthesis, with Robinson's one-pot synthesis of tropinone (**4**, Scheme 1) in 1917 standing as the seminal work in this field.[4] Subsequent classic examples include the cationic polyolefin cyclization approach to progesterone (**11**, Scheme 2) developed by Johnson and co-

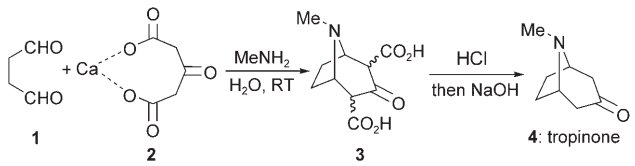

Scheme 1. Robinson's seminal total synthesis of tropinone (**4**).[4]

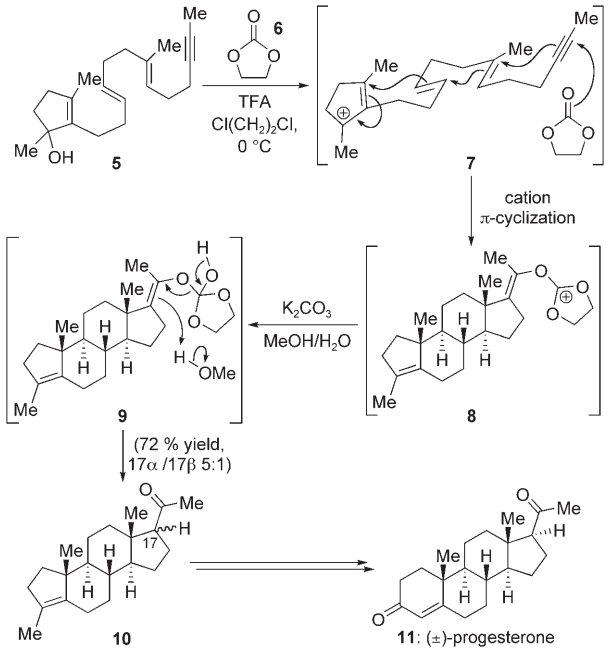

Scheme 2. The total synthesis of (±)-progesterone (**11**) involving a polyolefin cyclization (Johnson et al., 1971).[5]

[*] Prof. Dr. K. C. Nicolaou, Dr. D. J. Edmonds, Dr. P. G. Bulger
Department of Chemistry
and The Skaggs Institute for Chemical Biology
The Scripps Research Institute
10550 North Torrey Pines Road, La Jolla, CA 92037 (USA)
Fax: (+1) 858-784-2469
E-mail: kcn@scripps.edu
and
Department of Chemistry and Biochemistry
University of California, San Diego
9500 Gilman Drive, La Jolla, CA 92093 (USA)

© 2006 Wiley-VCH Verlag GmbH & Co. KGaA, Weinheim

workers[5] on the basis of the Stork–Eschenmoser hypothesis,[6] the "endiandric acid cascade" (Scheme 3) proposed by Black and co-workers[7] and reduced to practice by the Nicolaou group,[8] and the radical-based synthesis of hirsutene (**22**, Scheme 4) and other triquinane natural products by Curran and co-workers.[9,10]

As masterful as each of the syntheses illustrated in Schemes 1–4 is, they should by now be familiar to most students of organic chemistry. Therefore, rather than dwell further on the triumphs of the past, this Review will highlight and discuss a selection of more recent examples of cascade reactions employed in the total synthesis of natural products, offering fresh evidence for the utility of these types of processes in chemical synthesis. We do not aim to present a comprehensive survey of the literature, but rather to highlight a broad variety of strategies developed for the construction of complex molecules using cascade reactions. Where possible, we have tried to avoid duplicating the content of previous reviews, although some examples are covered again in cases where they serve to illustrate a particular reaction class or strategy. Of course, in selecting only representative examples from the extensive literature in the field, and then further restricting the candidate pool to applications in the total synthesis of natural products, we will inevitably be omitting discussion of a wealth of impressive cascade processes, such as the landmark rational chemical synthesis of C_{60} (**24**, Scheme 5) by L. T. Scott et al.[11] Apologies are therefore due in advance to those whose work has been omitted.

The very nature of cascade reactions, which often involve many distinct steps, can at times make them rather hard to classify. For convenience, we have grouped the examples that follow into five sections: nucleophilic, electrophilic, radical-mediated, pericyclic, and transition-metal-catalyzed processes. This classification scheme is rather arbitrary, particularly in the case of examples that feature more than one class of reaction, but we have tried to place each cascade according to

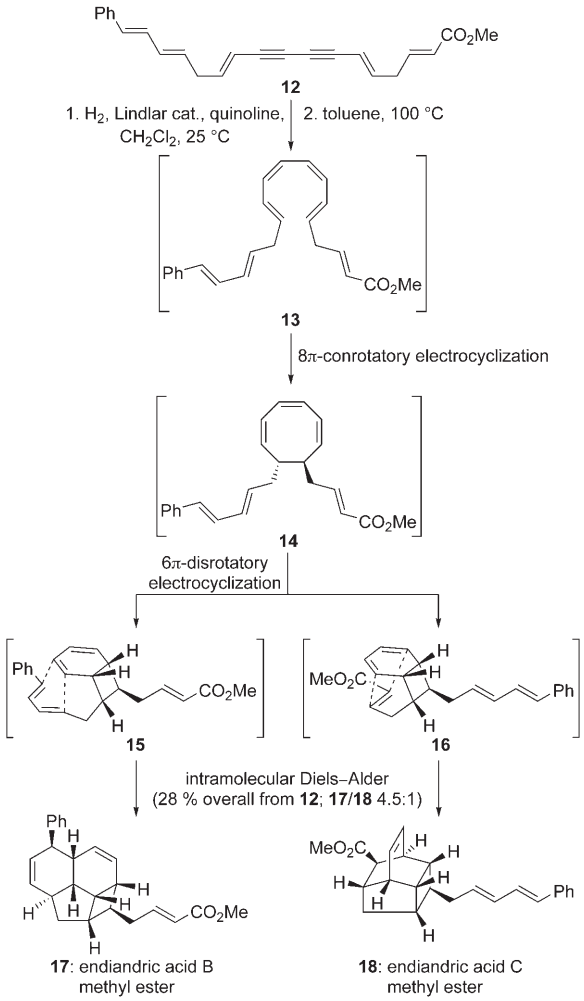

Scheme 3. The endiandric acid cascade (Nicolaou et al., 1982).[8]

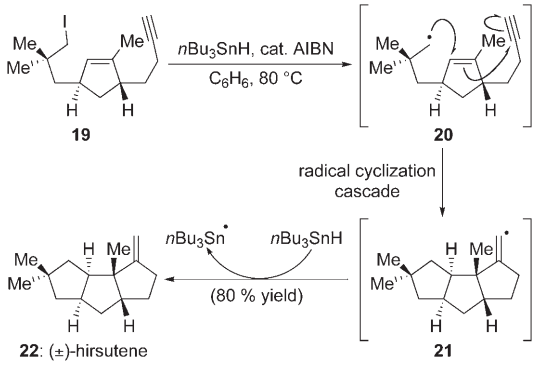

Scheme 4. A radical cyclization cascade in the total synthesis of (±)-hirsutene (**22**; Curran and Chen, 1985).[10]

*K. C. Nicolaou, born in Cyprus and educated in England and the United States, is currently Chairman of the Department of Chemistry at The Scripps Research Institute, where he holds the Darlene Shiley Chair in Chemistry and the Aline W. and L. S. Skaggs Professorship in Chemical Biology. He is also Professor of Chemistry at the University of California, San Diego, and Program Director at the Chemical Synthesis Laboratories at Biopolis, A*STAR, Singapore. His series "Classics in Total Synthesis", which he has co-authored with Erik J. Sorensen and Scott A. Snyder, is used worldwide as a teaching tool and source of inspiration for students and practitioners of chemical synthesis.*

David J. Edmonds was born in Glasgow (UK) in 1980. He received his MSci in Chemistry with Medicinal Chemistry from the University of Glasgow in 2001. He was awarded a University Scholarship for postgraduate research, and carried out his PhD work at Glasgow under the supervision of Dr. D. J. Procter on the application of samarium(II)-mediated reactions to total synthesis. In early 2005, he joined Professor K. C. Nicolaou's group, supported by a European Merck Postdoctoral Fellowship, where he has continued to pursue his research interests in the total synthesis of natural products..

 © 2006 Wiley-VCH Verlag GmbH & Co. KGaA, Weinheim

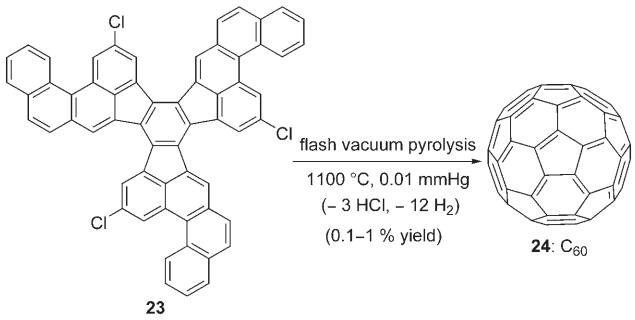

Scheme 5. The total synthesis of C_{60} (**24**; Scott et al., 2002).[11]

what can be argued as being the major theme of the sequence. Within each section, we have ordered the examples so as to provide a continuous discussion, rather than in chronological fashion. On the basis of space considerations, we shall not discuss the important class of enzyme-catalyzed cascade reactions,[12] except to highlight the current "gold standard" in this field by the group of A. I. Scott; namely the conversion of 5-aminolevulinic acid (**25**) into hydrogenobyrinic acid (**26**, Scheme 6) by treatment with a genetically engineered 12-enzyme cocktail in a process that involves 17 steps and the formation of nine stereocenters in a single reaction vessel![13] A further four chemical transformations enable the elaboration of hydrogenobyrinic acid to vitamin B_{12} (**27**).[14]

Before tackling the chosen examples, however, some discussion regarding the terminology and organization of this Review is warranted. Different authors use varying definitions as to what constitutes a cascade process. A variety of terms, including "cascade", "domino", "tandem", and "sequential", are used in the literature, often seemingly interchangeably and with liberal abandon, although efforts have been made to restore order to this area of reaction terminology.[1b,c] For our subjective purposes, we shall employ the term "cascade" to encompass all of the above descriptors. We have also adopted a rather inclusive attitude in order to capture as broad a spectrum of creative reaction design as possible. For example, the strictest definition of a cascade process would discount any example in which the reaction conditions are altered during the process; we will include not only these but also sequences in which further reagents are added at various points ("one-pot" transformations). We will, however, exclude multidirectional reactions (also sometimes termed "tandem" reactions) in which two or more reactions occur on the same substrate, but essentially in isolation of one another.

Paul G. Bulger was born in London (UK) in 1978. He completed his MChem degree in 2000 at the University of Oxford, where he carried out undergraduate research under the supervision of M. G. Moloney. He remained at the University of Oxford for his graduate studies, obtaining his DPhil in Chemistry in 2003 for research conducted under the supervision of Professor Sir J. E. Baldwin. In late 2003, he joined Professor K. C. Nicolaou's group at The Scripps Research Institute as a postdoctoral researcher. His research interests encompass reaction mechanism and design, and their application to complex natural product synthesis and chemical biology.

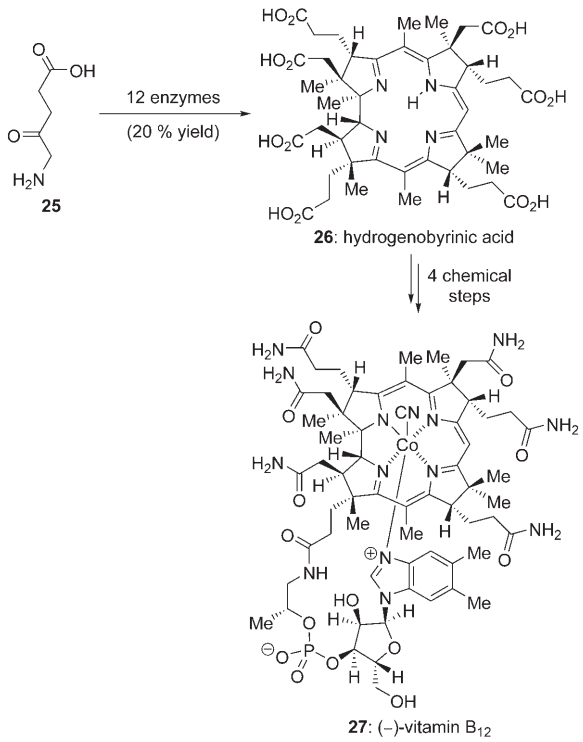

Scheme 6. The enzymatic synthesis of hydrogenobyrinic acid (**26**; Scott et al., 1994).[13]

Many of the examples highlighted here are based on the use of biosynthetic considerations to guide synthetic strategy (biomimetic synthesis), a paradigm that has witnessed a renaissance in recent years.[15] Others feature novel strategies by combining several known reactions that would normally be executed independently into a single-pot cascade, or by developing completely new reaction pathways altogether. Nevertheless, the common feature of all these examples is their inspired use of cascade reactions to generate molecular complexity in a concise fashion. It is hoped that this Review will serve not only to put into perspective recent accomplishments in the field but also to provide further impetus and inspiration for the implementation of new cascade strategies of broader generality and scope in the future.

2. Nucleophilic Cascades

In defining a nucleophilic cascade, we have adopted a policy whereby the key step in each case involves a nucleophilic attack. This section includes a variety of conjugate addition reactions, which are often employed in conjunction with other reactions.[16] Also included here are several organometallic addition processes, which are followed by pericyclic or anionic rearrangements, such as the anionic oxy-Cope reaction or Brook rearrangement.

 © 2006 Wiley-VCH Verlag GmbH & Co. KGaA, Weinheim

The polyketide ionophore natural product tetronasin (**31**, Scheme 7) is of commercial importance as an antibiotic, antiparasitic, and growth-promoting agent for use in ruminants. The interesting structure of tetronasin, which includes

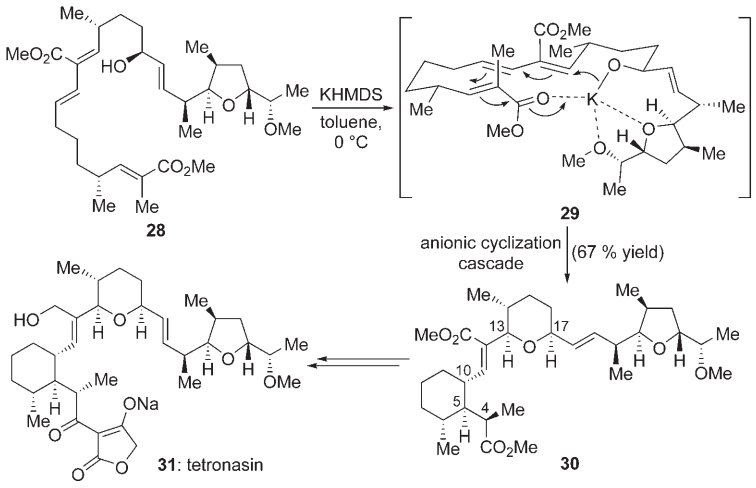

Scheme 7. An anionic cyclization cascade in the total synthesis of tetronasin (**31**; Ley et al., 1998).[18]

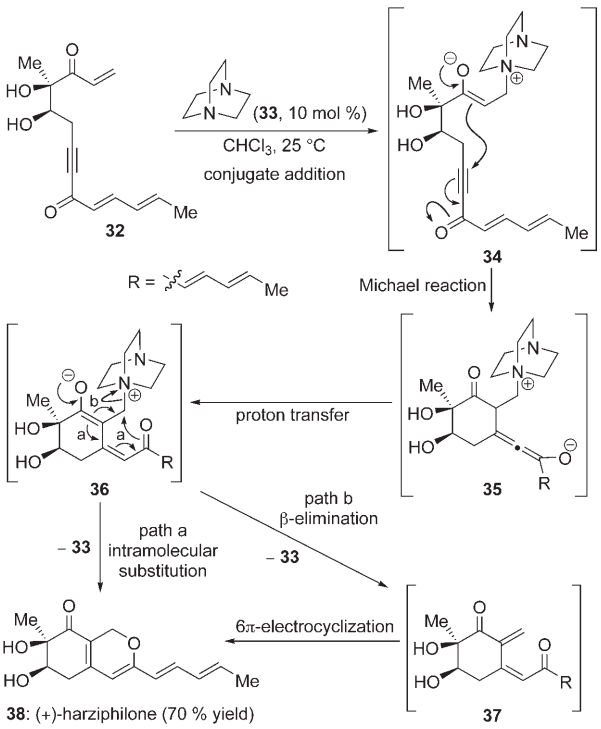

Scheme 8. Total synthesis of (+)-harziphilone (**38**) via a nucleophile-catalyzed cycloisomerization (Sorensen et al., 2004).[20]

tetronic acid, tetrahydrofuran, tetrahydropyran, and cyclohexane rings, prompted the groups of Ley and Staunton to investigate its biosynthesis. They proposed that both the tetrahydropyran and cyclohexane six-membered rings might be formed in a single step, and with the correct configuration, through a nucleophilic cascade triggered by the addition of an alcohol group to a suitably disposed activated triene.[17] The intriguing question of whether this process could be replicated in the laboratory was also answered by Ley and coworkers, who developed a biomimetic total synthesis of tetronasin incorporating the proposed biosynthetic cyclization cascade (Scheme 7).[18] They found that exposure of the putative cascade precursor **28** to potassium hexamethyldisilazide (1.1 equiv) in toluene at 0 °C indeed led to efficient cyclization to give **30** in a respectable yield of 67 %. This cyclization is thought to proceed via potassium salt **29**, in which the oxygen-based functional groups coordinate to the metal center in a manner resembling the ionophoric characteristics of the natural product, orienting the reacting groups in a favorable manner for cyclization. The structural order in this intermediate led to formation of **30** as a single diastereoisomer, in which three of the newly formed stereogenic centers (at C5, C10, and C13) were installed with the required configuration as found in the natural product **31**. Although the stereogenic center at C4 was formed with the incorrect *R* configuration, this site was readily epimerized to the natural *S* configuration in the closing stages of the synthesis.[19]

The group of Sorensen recently reported the nucleophilic catalysis of a cascade reaction in the enantioselective total synthesis of harziphilone (**38**, Scheme 8).[20] They devised a clever strategy for the construction of the required bicyclic ring system of the target molecule through the conjugate addition of a ketone enolate onto an acetylenic ketone to form the cyclohexane ring, followed by a 6π-electrocyclization of a dienone to generate the pyran ring. This second step was based on precedent from work by Büchi and Marvell on the cycloisomerization of *cis*-dienones.[21] Thus, treatment of enone **32** with DABCO (**33**, 10 mol %) in $CHCl_3$ at ambient temperature led to the initial formation of enolate **34** in a process resembling the first step of the Baylis–Hillman reaction.[22] Subsequent conjugate addition of enolate **34** onto the proximal triple bond established the cyclohexane ring (**34**→**35**), and was presumably followed by proton transfer to give the isomeric enolate **36**. A further cyclization process then generated the target natural product **38** and concomitantly liberated a molecule of DABCO (**33**), which could then re-enter the catalytic cycle. Two mechanistic pathways can be envisaged for this second ring formation. The first involves a single step, intramolecular substitution of the quaternary ammonium ion by the ketone carbonyl oxygen atom (path a). Alternatively, elimination of DABCO from **36** would give *cis*-dienone **37**, which would be expected to undergo a facile 6π-electrocyclization (path b).[21] Interestingly, model studies indicated that the cyclization cascade proceeded significantly faster in substrate **32**, which bears an unprotected 1,2-diol, as opposed to one in which the diol group was protected as the corresponding acetonide. This disparity may be due to activation of the enone to 1,4-addition by intramolecular hydrogen bonding.

The growing family of bisanthraquinone natural products includes a number of dimeric structures, such as rugulosin (**47**, Scheme 9), in which the monomeric anthraquinone units are united by between one and four single bonds to form cagelike skeletons. Following the biosynthetic proposals and prelimi-

 © 2006 Wiley-VCH Verlag GmbH & Co. KGaA, Weinheim

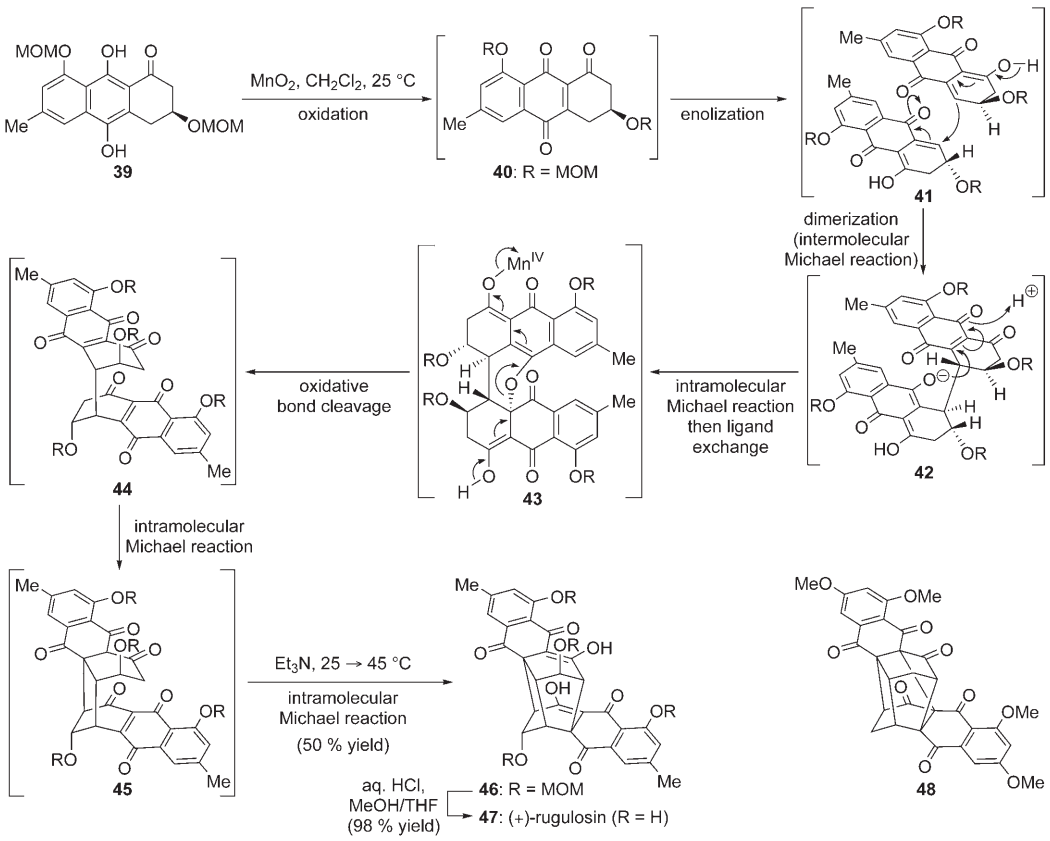

Scheme 9. The total synthesis of (+)-rugulosin (**47**) through an oxidative coupling/Michael reaction cascade (Nicolaou et al., 2005).[26]

nary experimental results of Shibata and co-workers,[23] the groups of Nicolaou[24] and Snider[25] independently developed biomimetic approaches to this class of natural products by employing cascade sequences to prepare model systems and analogues. A major obstacle to the preparation of the natural compounds is the presence of β-hydroxy or alkoxy ketone groups in both the monomeric tricyclic units (such as **39**) and the dimeric intermediates, as these motifs are very prone to elimination and subsequent aromatization of the resulting cyclohexenone ring. The conditions developed by Nicolaou et al. proved to be mild enough to overcome this hurdle and allowed for the preparation of (+)-rugulosin (**47**) in a highly efficient cascade process.[26] It was found that the complete polycyclic architecture of the target compound, **47**, could be prepared from readily available ketone **39** in a single reaction vessel through a sequence of oxidative, bond-forming and bond-breaking events (Scheme 9). Exposure of monomeric ketone **39** to MnO_2 in CH_2Cl_2 resulted in oxidation to the corresponding anthraquinone, **40**, followed by dimerization to give heptacyclic compound **43**. Although **43** is formally the product of a hetero-Diels–Alder reaction between two molecules of the corresponding enolized species **41** of anthraquinone **40**, compound **43** is believed to be formed via sequential inter- and intramolecular Michael reactions (i.e. **40**→**41**→**42**→**43**), as the use of the bulkier TBS hydroxy-protecting group (R = TBS) allows for the isolation of the first Michael adduct (corresponding to **42**). Oxidative bond cleavage (**43**→**44**) and Michael reaction steps then led to the formation of doubly bridged structure **45**. Addition of Et_3N to the reaction mixture at this point, followed by gentle warming to 45 °C, not only facilitated the final intramolecular Michael reaction to establish the complete core structure (**45**→**46**) but also hindered further oxidative carbon–carbon bond formation between the enol groups. In earlier model studies,[24] Nicolaou et al. observed a related oxidative bond formation in the absence of Et_3N to form the strained product **48**, which comprises the carbon framework of the related natural product rugulin. With compound **46** in hand, acidic hydrolysis of the hydroxy-protecting groups then completed the total synthesis of (+)-rugulosin (**47**). If so desired, any one of **43**, **44**, or **45** could be isolated at the appropriate stage. In this case, however, the rugulosin structure **46** was the desired endpoint, and it transpired that it was, in fact, more efficient to conduct the whole seven-step sequence (**39**→**46**) in one pot rather than to adopt a stepwise approach to bond construction.

The facile dimerization of the alkaloid avrainvillamide (**49**) has been exploited by the groups of Myers and Baran in their total syntheses of stephacidin B (**51**, Scheme 10).[27] Both groups observed that **49** dimerized upon treatment with triethylamine at room temperature. The interconversion of **49** and **51** was also observed during preparative TLC or upon concentration or dissolution. A plausible mechanism for this dimerization involves the nucleophilic attack by the amide nitrogen atom of one molecule of **49** onto the α,β-unsaturated nitrone group of another to give **50**, with conjugate addition of the resulting hydroxyenamine onto the other α,β-unsaturated nitrone then forming the second bond.[27a,28] An alternative

 © 2006 Wiley-VCH Verlag GmbH & Co. KGaA, Weinheim

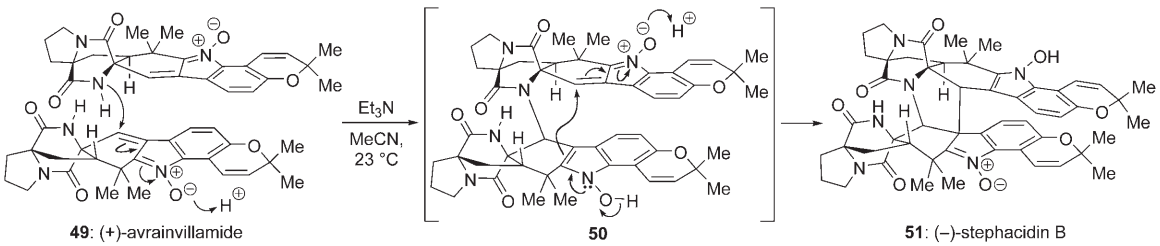

Scheme 10. Dimerization of (+)-avrainvillamide (**49**) to give (−)-stephacidin B (**51**) through a double conjugate addition (Herzon and Myers, 2005; Baran et al., 2005).[27]

mechanism in which the two bonds are formed in the reverse order has also been proposed,[29] however, this seems less likely in light of the observations by Myers and Herzon regarding the electrophilicity of the α,β-unsaturated nitrone functionality.[30]

The groups of Myers and Baran both also employed cascade reactions in their respective routes to avrainvillamide (Scheme 11 and Scheme 12). The synthesis by Herzon and Myers (Scheme 11),[27a] which led to the unnatural enantiomers (−)-avrainvillamide (**57**) and (+)-stephacidin B (**58**), featured a radical cyclization cascade approach to the diazabicyclooctane ring system. Acyl radical **55** was generated from cyclohexadienyl carboxamide **52** by employing a method developed by Walton and co-workers.[31] Heating of a mixture of amide **52** and peroxide-based initiator **53** resulted in radical generation followed by hydrogen-atom abstraction from the bis-allylic methylene site in **52** to generate cyclohexadienyl radical **54**. The latter species fragments through the enthalpically and entropically favored loss of a molecule of toluene to give acyl radical **55**; 6-*exo*-trig cyclization and expulsion of a phenylsulfinyl radical then furnished the desired tetracyclic product **56** in good overall yield (62%). Fusion of the remaining three rings of the avrainvillamide structure onto compound **56**, over the course of five more steps, then completed the synthesis of the monomeric unit **57**.[32]

The synthesis of (+)-avrainvillamide (**49**) by Baran et al. involved a deprotection–cyclization cascade initiated by heating of **59** at 240 °C (Scheme 12).[27b,33] The first step is the loss of the Boc protecting group from the indole nitrogen atom, which occurs by a retro-ene mechanism under thermal

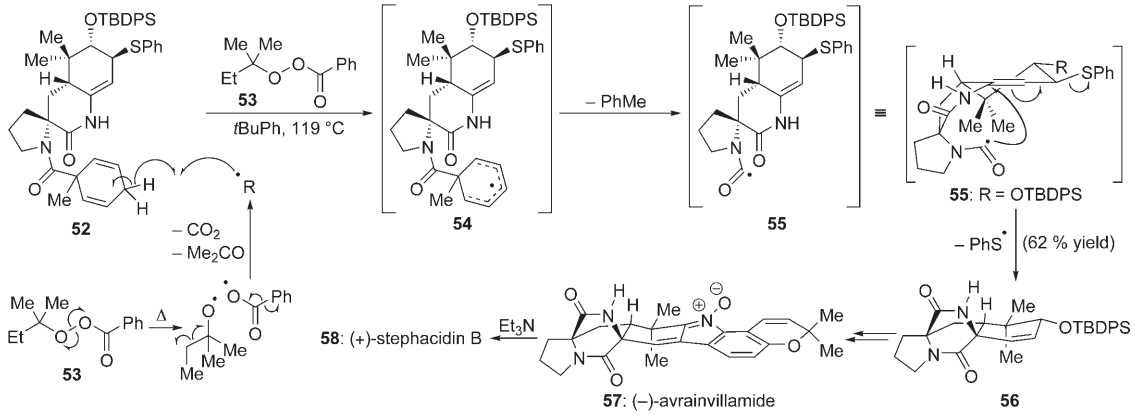

Scheme 11. Acyl radical generation and cyclization in the total synthesis of (−)-avrainvillamide (**57**) and (+)-stephacidin B (**58**; Herzon and Myers, 2005).[27a]

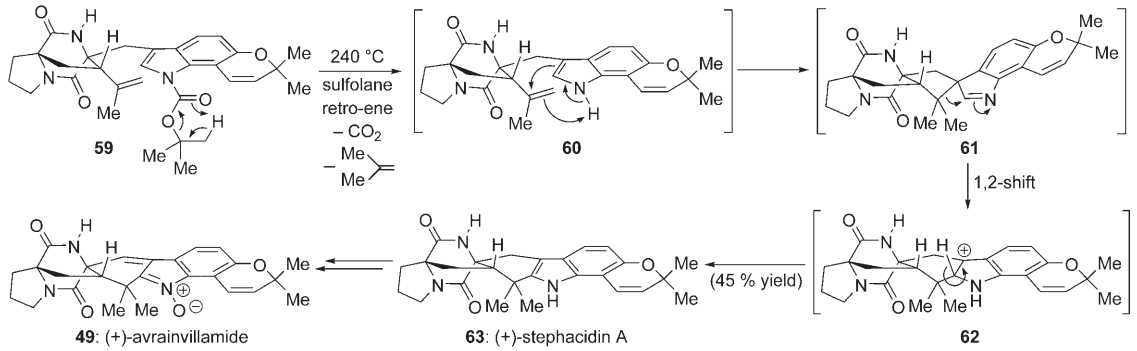

Scheme 12. The total synthesis of (+)-stephacidin A (**63**) and (+)-avrainvillamide (**49**) by a thermal cascade (Baran et al., 2005).[27b]

 © 2006 Wiley-VCH Verlag GmbH & Co. KGaA, Weinheim

conditions with the extrusion of isobutene and carbon dioxide to afford **60**. At the elevated temperature of the reaction, a formal ene reaction between the indole ring and the isopropenyl group of **60** then ensues, yielding spirocyclic imine **61** as a fleeting intermediate, which then undergoes a selective 1,2-shift of the more highly substituted alkyl group to give (+)-stephacidin A (**63**). This material was converted into the natural enantiomers of avrainvillamide (**49**) and stephacidin B (**51**), thus establishing their absolute configurations as those shown in Scheme 10.[34]

Ecteinascidin 743 (**72**, Scheme 13) is a marine-derived natural product isolated from the Caribbean tunicate *Ecteinascidia turbinata*.[35,36] It is a potent antitumor agent and has entered clinical trials for the treatment of a number of different types of human cancer.[37] Inspired by its promising biological activity, scarcity, and intriguing molecular structure, the Corey group initiated investigations that culminated in the efficient total synthesis of ecteinascidin 743 (**72**).[38] A prominent feature of the route was the ingenious method devised for the installation of the unusual bridging 10-membered sulfur-containing ring, as shown in Scheme 13. Advanced hexacyclic intermediate **64** was prepared from two amino acid derivatives through a series of iminium ion cyclizations. This set the stage for the introduction of the bridging sulfide through the 1,4-addition of a thiolate anion to an intermediate *ortho*-quinone methide (**67**).[39] This highly reactive species was generated by treatment of hydroxy ketone **64** with a Swern-type reagent to generate the *O*-dimethylsulfonium ion intermediate **65**. Triflic anhydride was used in place of the more conventional oxalyl chloride in order to avoid any interference by chloride ions during subsequent steps. The addition of an amine base (iPr$_2$NEt) led to the cyclo-elimination of DMSO, via ylide species **66**, to afford *ortho*-quinone methide **67**. Following the addition of tBuOH to quench any excess Swern reagent, a guanidine base **68** was used to release a thiolate anion from the fluorenyl sulfide moiety. The liberated thiolate anion **69** was then trapped by the *ortho*-quinone methide to give the 10-membered sulfide ring. This intramolecular conjugate addition was rendered irreversible by the addition of acetic anhydride, to trap the resulting phenolate **70** as the corresponding acetate **71**. This amazing one-pot cascade proceeded in excellent overall yield (79%) and, significantly, without the need for isolation of any of the sensitive intermediates along the pathway. A similar cascade sequence has since been employed in an efficient semisynthesis of ecteinascidin 743 (**72**), thereby securing the supply of larger quantities of this previously scarce compound.[40]

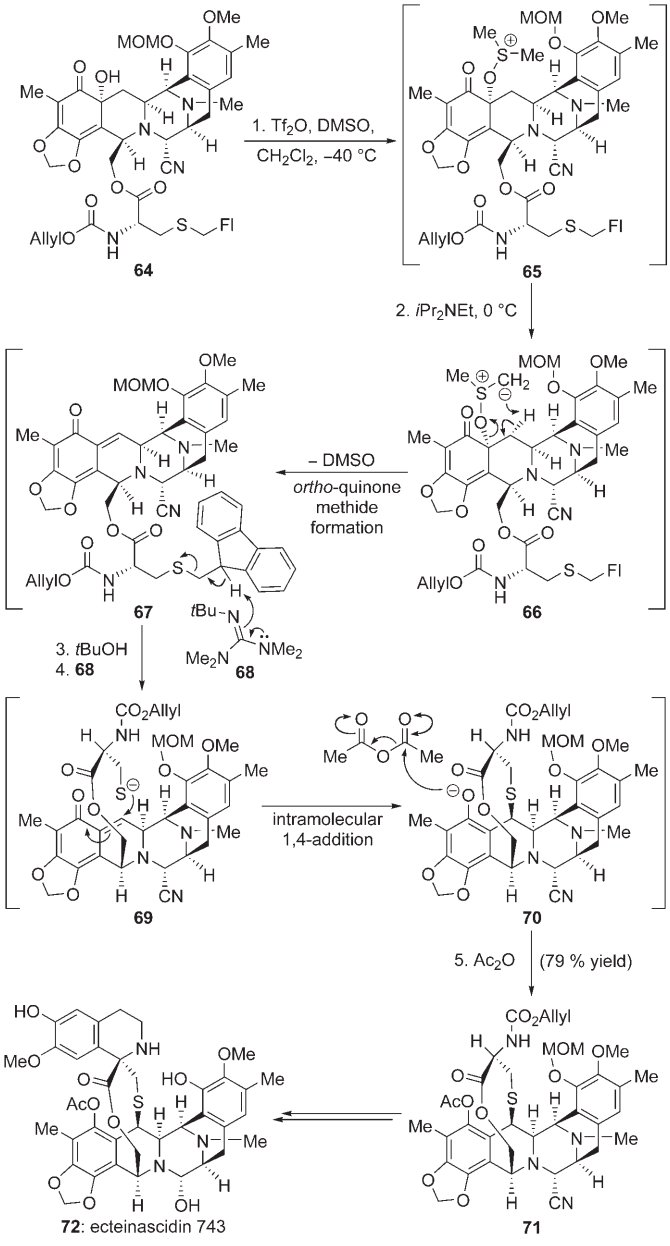

Scheme 13. *ortho*-Quinone methide generation and trapping in the total synthesis of ecteinascidin 743 (**72**; Corey et al., 1996).[38]

Multicomponent reactions offer means to construct complex and structurally diverse compounds rapidly from relatively simple building blocks.[41,42] The Ugi reaction is a powerful four-component coupling reaction and one of several such processes that employ an isocyanide as one of the reactants.[43] Although popular in the field of combinatorial synthesis,[44] applications of Ugi reactions in total synthesis are comparatively rare.[45] One of the most advanced applications of an Ugi reaction to date can be found in the total synthesis of ecteinascidin 743 (**72**) by Fukuyama and coworkers, who employed this four-component process to couple two major fragments, whilst simultaneously incorporating the remaining three carbon atoms needed for the hexacyclic core structure of the target.[46] Amine **73**, carboxylic acid **74**, isocyanide **75**, and acetaldehyde (**76**) were heated in methanol to give amide **80** (Scheme 14). Reversible acid-catalyzed iminium ion formation (**73** + **76** → **77**) is followed by nucleophilic attack of the isocyanide component and capture of the resulting nitrilium ion **78** by the carboxylate anion to generate neutral intermediate **79**. This species then undergoes a rapid O → N acyl transfer to afford **80** as the observed product. Amide **80** was formed in high yield (90%), albeit as a mixture of epimers at the newly generated C4 stereocenter. Indeed, satisfactory control of the stereochemistry of the newly formed stereocenter in the Ugi reaction remains an

© 2006 Wiley-VCH Verlag GmbH & Co. KGaA, Weinheim

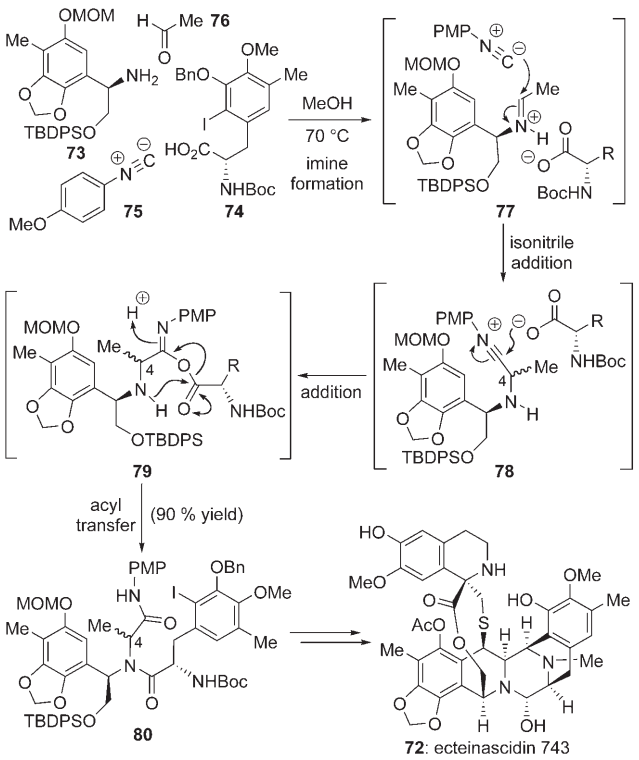

Scheme 14. The Ugi four-component coupling reaction in the total synthesis of ecteinascidin 743 (**72**; Fukuyama et al., 2002).[46]

unresolved problem in general. In the context of this synthesis, however, this lack of stereocontrol was immaterial, as the planned route required the subsequent destruction of this stereocenter followed by its later reinstallation with the required configuration.[47]

Triquinane natural products, such as hypnophilin (**91**), coriolin (**92**), and ceratopicanol (**93**, Scheme 15) have been, and continue to be, popular targets for total synthesis endeavors, inspiring the development of a number of cascade processes.[48] The Paquette group has exploited the squarate ester cascade[49] for the total syntheses of all three of the aforementioned targets, as shown in Scheme 15.[50] This anionic cascade is triggered by the addition of two vinyllithium species to the squarate ester **81**, and can proceed by two pathways, depending on whether the second nucleophile adds in a *cis* or *trans* fashion relative to the first. With a *cis* mode of addition, favored by chelation between the incoming nucleophile and the ketal oxygen atoms, the 1,5-diene-dialkoxide **84** is formed. This undergoes a facile dianionic oxy-Cope rearrangement, via a boatlike transition state, to form cyclooctatriene species **85**. Alternatively, a *trans* mode of addition, favored by steric considerations, leads to dialkoxide **86**, which, on stereoelectronic grounds, cannot undergo a [3,3] sigmatropic reaction. Instead, a charge-driven 4π-conrotatory electrocyclic ring opening occurs, with electrostatic repulsion favoring rotation of the two alkoxide oxygen centers away from each other. The resulting octatetraene **87** then converges on cyclooctatriene intermediate **85** through an 8π-conrotatory ring closure. In cases where both

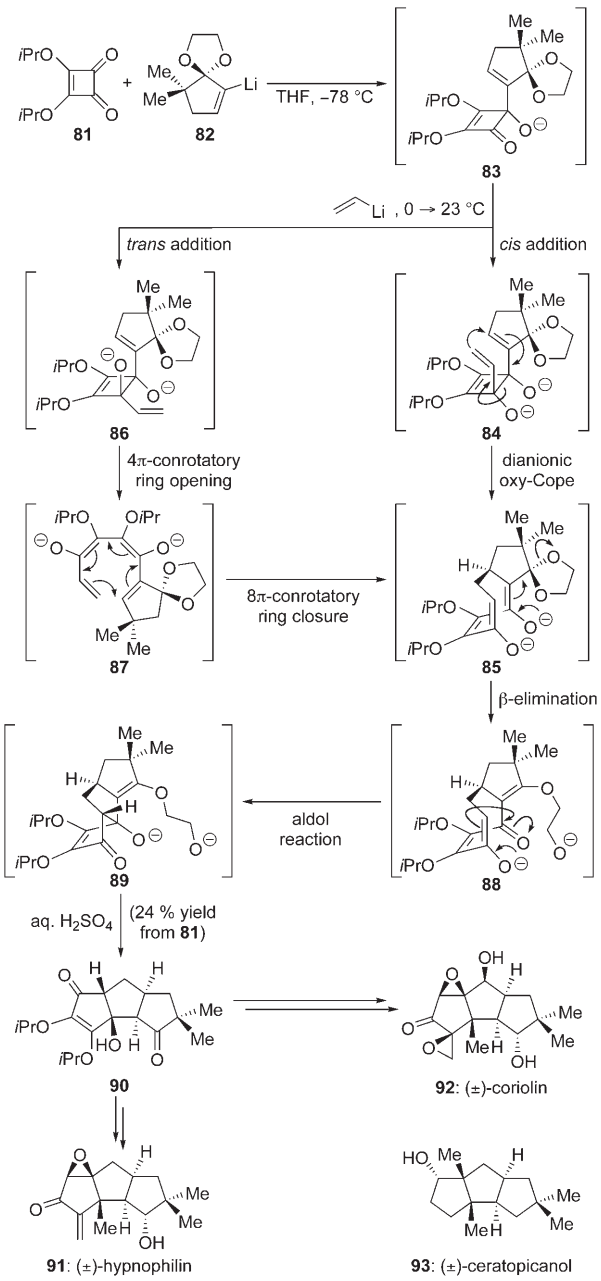

Scheme 15. The squarate ester cascade as used in the total synthesis of (±)-hypnophilin (**91**) and (±)-coriolin (**92**), and the structure of (±)-ceratopicanol (**93**; Paquette and Geng, 2002).[50]

vinyllithium species are substituted on the distal end of the olefin, it is possible to distinguish between these mechanisms and, to some extent, control which pathway is followed.[49] In this case, it is likely that both modes are operative, each giving the same final product. From dianion intermediate **85**, the cascade continues with the β-elimination of one of the ketal oxygen groups by the adjacent enolate, leading to regioselective formation of ketone **88**. An intramolecular aldol reaction between this ketone and the remaining enolate, followed by hydrolysis, then gave tricyclic product **90**, which could be converted into hypnophilin (**91**) or coriolin (**92**) over

 © 2006 Wiley-VCH Verlag GmbH & Co. KGaA, Weinheim

several more steps. A similar cascade led to the total synthesis of ceratopicanol (**93**).[50b]

Paquette and Geng employed a related approach for the preparation of the angular triquinane pentalenene (**100**, Scheme 16).[51] In this cascade, the second nucleophile is an acetylide anion and the *trans* addition route dominates, generating the highly strained 1,2,4,6-cyclooctatetraene intermediate **97**. As expected, this species was formed with high stereoselectivity due to the more facile 8π-conrotatory electrocyclic ring closure of conformer **96**, in which the cyclopentane methyl substituent is on the exterior of the helical pitch of the dienolate. In this case, there is no leaving group available to differentiate the two enolate groups, but relief of strain favors the selective protonation of the allenoate to give ketone **98**. A transannular aldol reaction then gives the product **99**, which was elaborated to give the target natural product **100**.[52]

In their approach to (+)-CP-263,114 (phomoidride B, **112**), Shair and co-workers also employed an organometallic addition/Cope rearrangement strategy.[53a] Their variant involved the addition of Grignard reagent **101** to β-keto ester **102** (Scheme 17). The addition proceeds with complete selectivity for the desired diastereoisomer **103** under chelation control. 1,5-Diene **103** then undergoes a facile oxy-Cope rearrangement upon warming to room temperature to give the cyclononene enolate **104**. Interestingly, the use of organolithium or organocerium reagents in model studies of this addition step failed to give the desired products.[53b] The final step in this cascade is the transannular Dieckmann cyclization of **104** to form ketone **105** and generate the characteristic

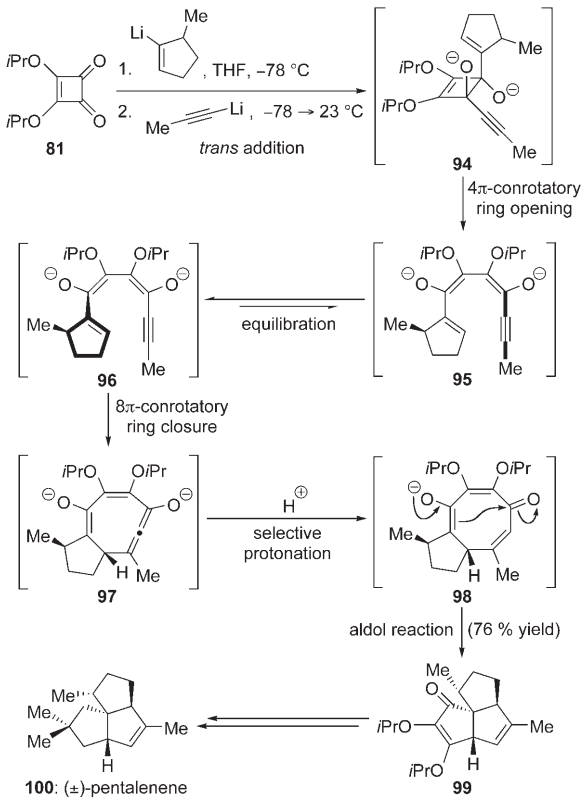

Scheme 16. The total synthesis of (±)-pentalenene (**100**) using the squarate ester cascade (Paquette and Geng, 2002).[51]

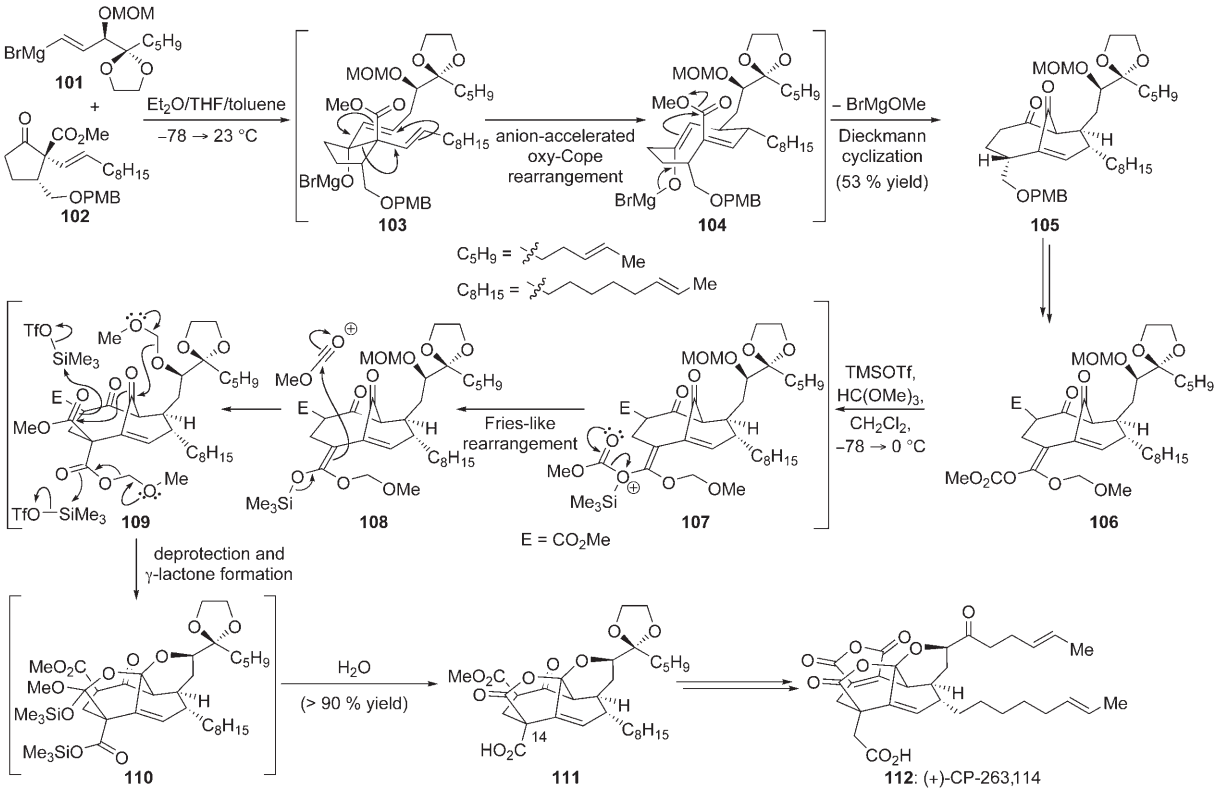

Scheme 17. Anionic oxy-Cope/Dieckmann cascade and Fries-like rearrangement in the total synthesis of (+)-CP-263,114 (**112**; Shair et al., 2000).[53]

 © 2006 Wiley-VCH Verlag GmbH & Co. KGaA, Weinheim

strained bicyclic core of the target compound. Following the advancement of ketone **105** to β-ketoester **106**, a novel electrophilic cascade was effected by treatment of this material with TMSOTf (2.0 equiv) and $HC(OMe)_3$ (2.0 equiv) in CH_2Cl_2 to give lactone **111** in over 90% yield. A plausible mechanism for this transformation is shown in Scheme 17 and commences with the initial ionization of the enol carbonate with TMSOTf to provide silylketeneacetal **108**, a species poised for reaction with the liberated acylium ion, leading to the assembly of **109**. Lewis acid mediated deprotection of the MOM groups and hydrolytic workup then gave the product **111**. In addition to providing an interesting solution to the problem of generating the γ-lactone cage structure, the concomitant unveiling of the carboxylic acid group at C14 during the conversion of **106** into **111** provided a convenient handle for the installation of the one remaining carbon atom required to reach the target structure **112** through a modified Arndt–Eistert protocol. Subsequent studies by Shair and co-workers of this addition/Cope rearrangement strategy using related systems revealed the potential for retro-aldol/aldol equilibration of the organometallic addition product (corresponding to magnesium alkoxide **103**), with implications for the dynamic kinetic resolution of substrates with chiral all-carbon quaternary stereocenters.[54]

Nicolaou et al. also employed a cascade reaction in their total synthesis of CP-225,917 (phomoidride A, **122**) and CP-263,114 (phomoidride B, **112**).[55] This cascade was used to introduce the challenging maleic anhydride moiety from nitrile precursor **114**. In preparation for the cascade process, **113** was selectively mesylated on the primary alcohol group. Mesylate **114** was then exposed to mildly basic conditions, which initiated the presumed chain of events delineated in Scheme 18. Base-induced epoxide formation (**114**→**115**) is followed by fragmentation to give an intermediate alkoxide, which immediately closes onto the proximal nitrile functionality to give iminobutenolide **116**. Subsequent tautomerization, oxidation, and hydrolysis steps afforded maleic anhydride **121** via intermediates **117**–**120**. Several further functional group manipulations then completed the syntheses of both CP-225917 (**122**) and CP-263114 (**112**).[56]

The dithiane lynchpin strategy,[57] developed by the Smith group based on precedent noted by Tietze et al.,[58] makes use of the Brook rearrangement[59] to regenerate a lithiated dithiane, following the opening of an epoxide by a lithiated silyl dithiane nucleophile. The new lithiated dithiane can then capture a second, different electrophile, provided that the timing of migration of the silyl group can be controlled. Smith and Kim recently extended this strategy to the synthesis of the poison frog alkaloids (−)-indolizidine 223AB and (−)-205B (**129**, Scheme 19) by using an aziridine electrophile in the second step.[60] Thus, lithiation of silyl dithiane **123** with *t*BuLi in diethyl ether and addition of epoxide **124** led to lithium alkoxide **125** (Scheme 19). Aziridine **126** was then added in a mixture of THF and DME, the polar solvent triggering a 1,4-Brook rearrangement to generate lithiated dithiane **127**. Nucleophilic opening of the aziridine then gave the sulfonamide product **128**, which was subsequently converted into alkaloid (−)-205B (**129**).[61]

3. Electrophilic Cascades

The first synthesis described in this section could equally have been included in the previous section, as it includes both nucleophilic and electrophilic cascades. The approach of Corey and co-workers to the dimeric triterpene (+)-α-onocerin (**137**, Scheme 20) involved a sequential addition/dimerization, four-component coupling sequence to assemble a precursor for a two-directional electrophilic tetracyclization.[62] Addition of vinyllithium to acyl silane **130** gave

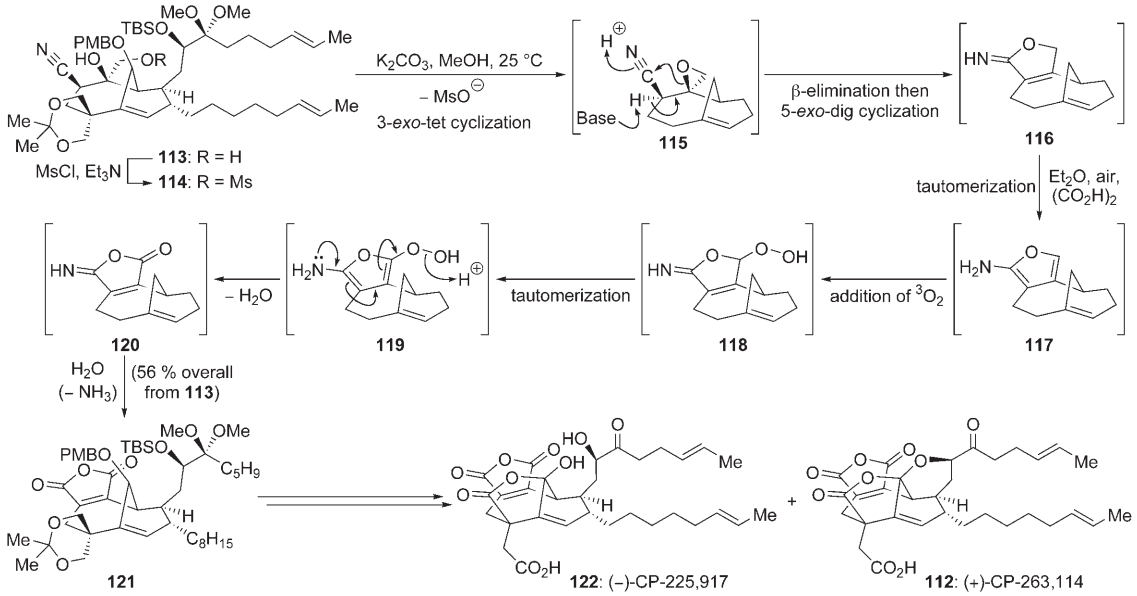

Scheme 18. Construction of the maleic anhydride unit during the total synthesis of the CP molecules (Nicolaou et al., 1999).[55] Substituents in intermediates **115**–**120** are omitted for clarity.

 © 2006 Wiley-VCH Verlag GmbH & Co. KGaA, Weinheim

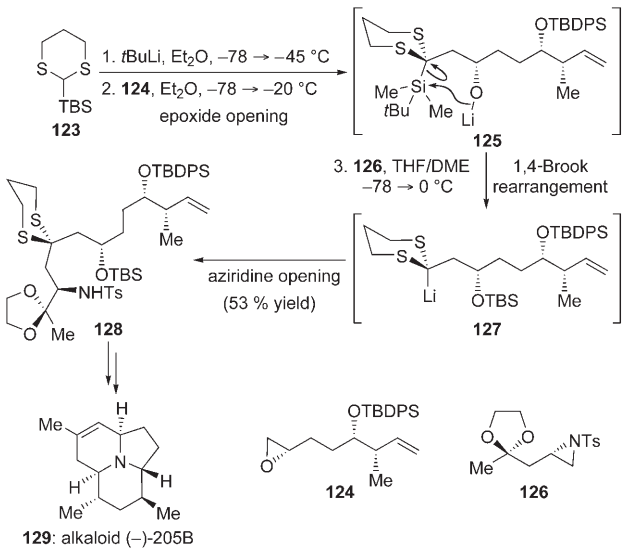

Scheme 19. Dithiane linchpin coupling through a 1,4-Brook rearrangement, as applied to the total synthesis of poison-frog alkaloid (–)-205B (**129**; Smith and Kim, 2005).[60]

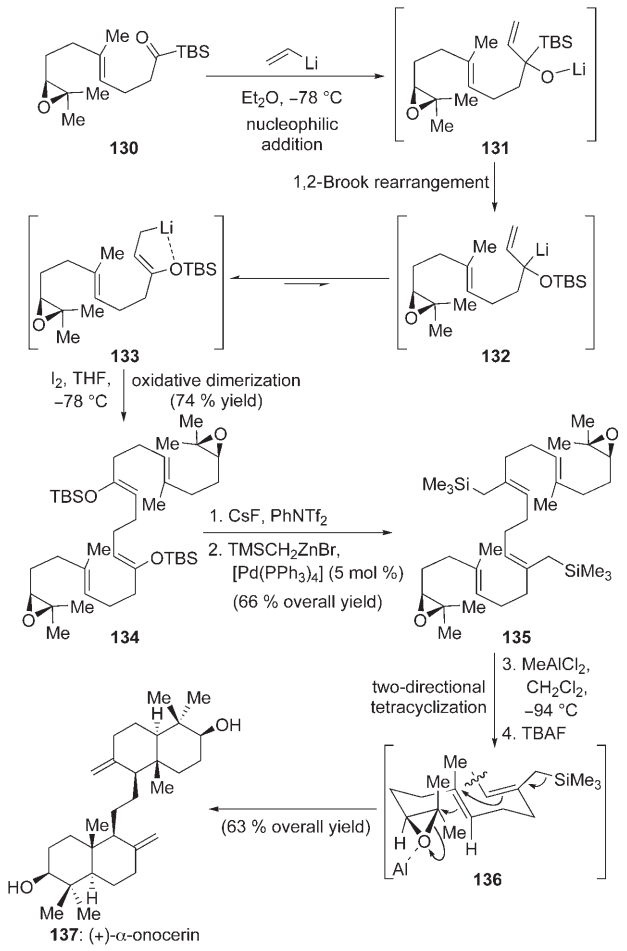

Scheme 20. Application of the 1,2-Brook rearrangement and a two-directional epoxy-olefin cyclization in the total synthesis of (+)-α-onocerin (**137**; Corey et al., 2002).[62]

chelated *Z*-allylic lithium intermediate **133** through the 1,2-Brook rearrangement of alkoxide **131** followed by allylic rearrangement (**132**→**133**).[63] Addition of iodine gave the dimer **134** in excellent yield (74%). Conversion of the silyl enol ether groups into the corresponding enol triflates was accomplished in a single operation through the action of cesium fluoride and phenyl ditriflimide, and was followed by Negishi coupling to give dimeric allylsilane **135** in 66% yield from **134**. Exposure of **135** to $MeAlCl_2$ (2.5 equiv) in CH_2Cl_2 at −94°C followed by treatment with TBAF (to cleave any TMS ethers of **137** which may have been present) then gave (+)-α-onocerin (**137**, 63% yield from **135**). In addition to the desired tetracyclic product, which arose from the chair–chair transition-state arrangement **136**, a minor non-C_2-symmetric product (not shown) was also formed in 9% yield, presumably as a result of one cyclization proceeding through a chair–boat transition state. This remarkable synthesis demonstrates the great power of cascade reactions in the rapid construction of complex molecules; indeed, the two cascades described here enabled the formation of four rings, nine carbon–carbon bonds, and six new stereogenic centers in just four steps.[64]

The opening of epoxide rings under (Brønsted or Lewis) acidic catalysis forms the basis of many spectacular cascade processes. Corey and Xiong used a two-directional epoxide-opening cascade in their total synthesis of the C_2-symmetric pentacyclic tetrahydrofuran natural product glabrescol (**142**), in an endeavor which also served to determine the true stereochemical identity of the natural material.[65] They had previously prepared several *meso* isomers, including that originally proposed for the natural product, and found that the original structure was incorrect.[66] All the isomers were prepared by using cascade cyclizations of polyepoxides; the cascade used to prepare natural glabrescol is illustrated in Scheme 21. The tetra-epoxide precursor **138** was prepared by oxidative dimerization and epoxidation using the protocol of Shi and co-workers.[67] Treatment of **138** with camphorsulfonic acid gave the desired tetracyclic product **139** in good overall

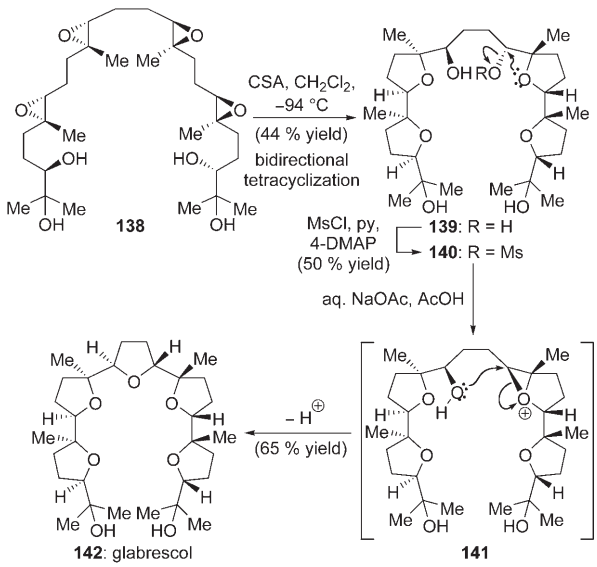

Scheme 21. Poly-epoxide cyclizations in the total synthesis of glabrescol (**142**; Xiong and Corey, 2000).[65]

 © 2006 Wiley-VCH Verlag GmbH & Co. KGaA, Weinheim

yield. At each site, opening of the corresponding epoxide ring occurred at the more substituted terminus, a corollary of the stereoelectronic preference for five-membered-ring formation, and with inversion of configuration. Selective monomesylation of **139**, followed by treatment with acetic acid gave the desired C_2-symmetric product **142** by the double-inversion mechanism shown (**140**→**141**→**142**). The use of acetic acid, a good ionizing solvent, combined with the steric shielding around the secondary mesylate group, discourages the direct S_N2-type displacement by the hydroxy group (which would form the undesired product stereochemistry as the result of a single inversion), and enables neighboring-group participation from the vicinal ether oxygen to form epoxonium ion intermediate **141**. This species is then opened in a kinetically favored 5-*exo* mode by the pendant hydroxy group. Comparison of synthetic **142** and natural glabrescol revealed the two materials to be identical.[68]

A biomimetic electrophilic cascade[69] was employed by Holton and co-workers in their total synthesis of hemibrevetoxin B (**147**, Scheme 22).[70] Their plan of attack called for the formation of the B and C rings of the target structure through the double cyclization of a suitable hydroxy epoxide precursor.[71] They eventually settled on epoxy alkene **143** as a suitable substrate, with the alkene serving as a trigger for the cascade upon activation by an electrophile. In the event, treatment of **143** with *N*-phenylselenophthalimide led to sequential ring closure to give the advanced intermediate **146** in 83% yield and as a single stereoisomer. This cyclization is thought to proceed through attack of the epoxide oxygen atom on the *epi*-selenonium ion of intermediate **144** to generate a bicyclic epoxonium ion **145**. Subsequent attack by the hydroxy group then proceeds selectively to give the *trans*-fused oxepane product **146**. The highly polar but non-

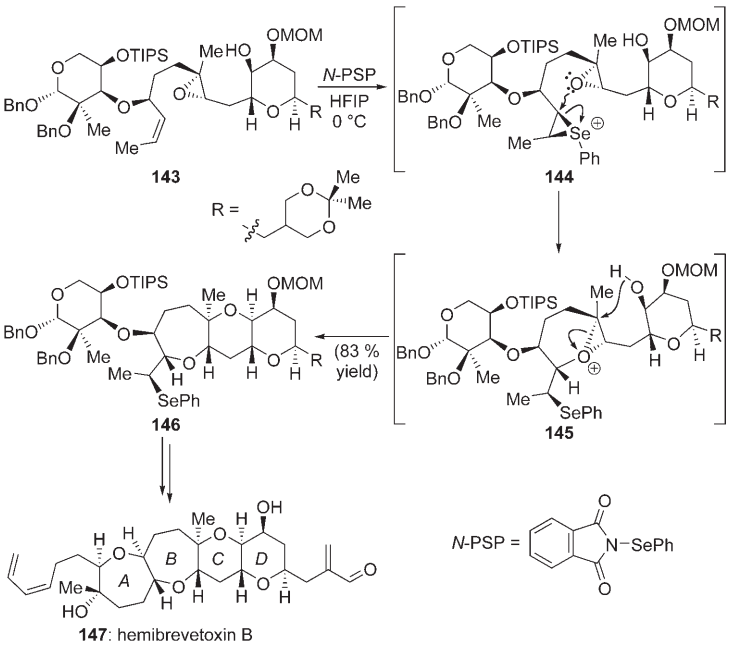

Scheme 22. Total synthesis of hemibrevetoxin B (**147**) using an epoxy-olefin cyclization (Holton et al., 2003).[70]

nucleophilic solvent 1,1,1,3,3,3-hexafluoro-2-propanol was chosen for its ability to stabilize such charged species without interfering in the progress of the reaction. Fusion of the oxepane A ring onto intermediate **146** followed by the appropriate side-chain manipulations then completed the total synthesis.[72]

The pinacol-terminated Prins cyclization was developed by the group of Overman as an effective technology for the synthesis of natural products.[73] One such application is found in their general approach to the cladiellin family of diterpene metabolites, as represented by the synthesis of the revised structure of sclerophytin A (**153**, Scheme 23.[74] The sequence

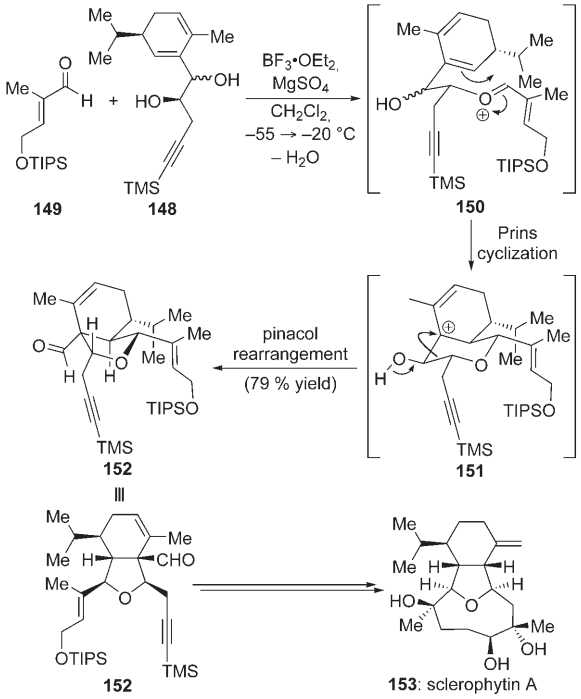

Scheme 23. The Prins-pinacol reaction in the total synthesis of sclerophytin A (**153**; Overman et al., 2001).[74]

begins with the Lewis acid catalyzed condensation of diol **148** with aldehyde **149** to form oxocarbenium ion **150**. It is not necessary to specifically control which alcohol group engages the aldehyde in this step, as only **150** can participate in the Prins cyclization reaction and all the possible condensation products are in equilibrium. The Prins cyclization of **150** proceeds stereoselectively, with the approach of the oxocarbenium ion dictated by the bulky isopropyl substituent. The cyclization generates stabilized allylic carbocation **151**, which undergoes a pinacol rearrangement to give the bicyclic product **152** in 79% isolated yield. Tetrahydrofuran **152** proved to be a versatile platform for the synthesis of various members of this class of natural products, including sclerophytin A (**153**), its originally proposed structure, deacetoxyalcyonin acetate, and cladiell-11-ene-3,6,7-triol.[74–76]

Oxocarbenium ion species are commonly employed in total synthesis as intermediates in the preparation of acetal and ketal protecting groups, and also in the formation of spiroketal structural units.[77,78] The construction of such

 © 2006 Wiley-VCH Verlag GmbH & Co. KGaA, Weinheim

motifs using cascade processes is exemplified by two syntheses of the trioxadispiroketal ABCD-ring fragment of the shellfish toxin azaspiracid-1 (**156**, Scheme 24). In their second-generation synthesis of the azaspiracids, Nicolaou et al. prepared bis-spiroketal **155** from precursor **154** in a one-step deprotection–cyclization cascade sequence.[79] Treatment of **154** with excess TMSOTf at low temperature effected removal of the TES ether, acetonide, and dioxolane protecting groups, and the formation of three rings, with the thermodynamically favored anomeric configuration at the C10 and C13 positions, to give **155** in 65% yield.[80] In a conceptually different approach to the ABCD-ring fragment, Forsyth and co-workers prepared acetylenic ketone **158**, which, upon exposure to $TsOH{\cdot}H_2O$ (1.0 equiv) in toluene at room temperature, underwent cleavage of the two TES protecting groups followed by a double intramolecular conjugate addition.[81] The use of acid catalysis under equilibrating conditions ensured the formation of the desired, thermodynamically favored ketal **159**, which was isolated as a single stereoisomer in 55% yield from alcohol **157**.[81–83]

Heathcock and co-worker's famous one-step synthesis of dihydro-*proto*-daphniphylline (**168**), the proposed biogenetic precursor to the *Daphniphylum* polycyclic alkaloids, is perhaps the most striking example of a cascade involving iminium ion intermediates.[84] The process begins with dihydrosqualene dialdehyde **160** (Scheme 25) and represents the culmination of several years of careful development combined with a chance discovery.[85] Treatment of acyclic di-aldehyde **160** with methylamine and warm acetic acid gave the target compound **168** in 65% yield through a process that formed five new rings and installed eight new stereogenic centers in a completely diastereoselective fashion. The first step in the cascade involves the condensation of methylamine with the most reactive aldehyde group to give secondary enamine **161**. Intramolecular Michael addition of enamine **161** onto the enal group establishes the first carbon–carbon bond and ring of the sequence (**161**→**162**), and is followed by further condensation and cyclization events to form iminium ion **164**. A formal hetero-Diels–Alder reaction then gives tetracyclic

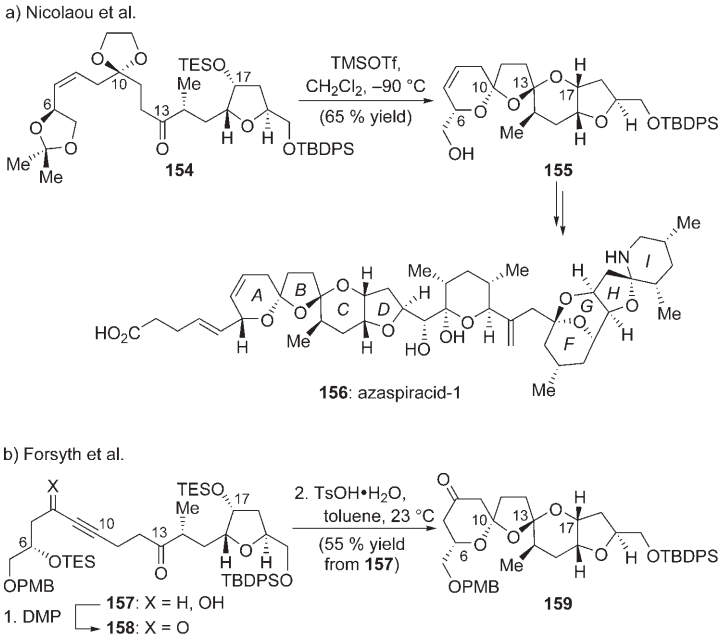

Scheme 24. a) Use of a deprotective polycyclization en route to the total synthesis of azaspiracid-1 (**156**; Nicolaou et al., 2006).[79] b) Construction of the azaspiracid-1 ABCD ring framework through an acid-catalyzed nucleophilic addition cascade (Forsyth et al., 2004).[81]

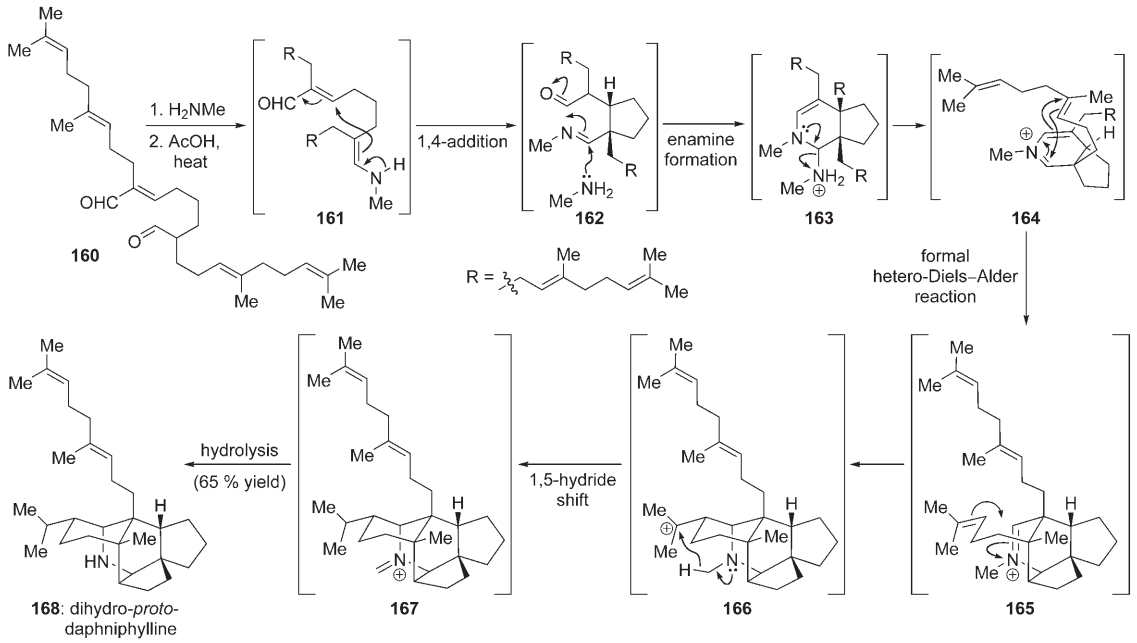

Scheme 25. Biomimetic synthesis of dihydro-*proto*-daphniphylline (**168**; Heathcock et al., 1992).[84]

© 2006 Wiley-VCH Verlag GmbH & Co. KGaA, Weinheim

iminium ion **165**, although this step most likely proceeds in a stepwise manner through a Prins cyclization to form the second five-membered ring, followed by ring closure between the resulting enamine and tertiary carbocation species. The final ring is then formed by another Prins cyclization to generate carbocation **166**. A 1,5-hydride shift from the methyl group of the tertiary amine to the carbocation, followed by hydrolysis on workup, completes the synthesis of dihydro-*proto*-daphniphylline (**168**). When ammonia is used in place of methylamine, the dehydro product with an isopropenyl side chain in place of the isopropyl group, is formed in a rather lower yield. Thus, in addition to differentiating what would be one of three similar olefins in the polycyclic product, the use of methylamine also aids the progress of the cascade as the substituted imine and enamine intermediates are more stable.

Another example of the power of iminium ions as intermediates in cascade reactions can be found in the highly efficient and convergent synthesis of aspidophytine (**177**, Scheme 26) by Corey and co-workers. Reductive condensation of tryptamine derivative **169** and chiral di-aldehyde **170** gave pentacyclic amine **176** with the formation of three new rings, three new stereogenic centers, and four new sigma bonds.[86] This transformation proceeds through condensation of primary amine **169** with dialdehyde **170** to give the cyclic iminium ion **172**, presumably via enamine **171**. A Pictet–Spengler cyclization generates the pyrrolidine ring and the new quaternary stereocenter. The stereocontrol obtained in this step is notable and may arise through interaction between the iminium ion carbon atom and the ester carbonyl oxygen atom of **172**, leading to preferential attack by the indole from the opposite face of the molecule. The stereochemistry of the resulting spirocyclic intermediate **173** then governs the facial selectivity in the attack of the allylsilane substituent[87] on the newly formed iminium ion to generate the pentacyclic system **174**. Following completion of this cascade, sodium cyanoborohydride was added to effect reduction of the enamine group to give **176**, which was converted into aspidophytine.[88]

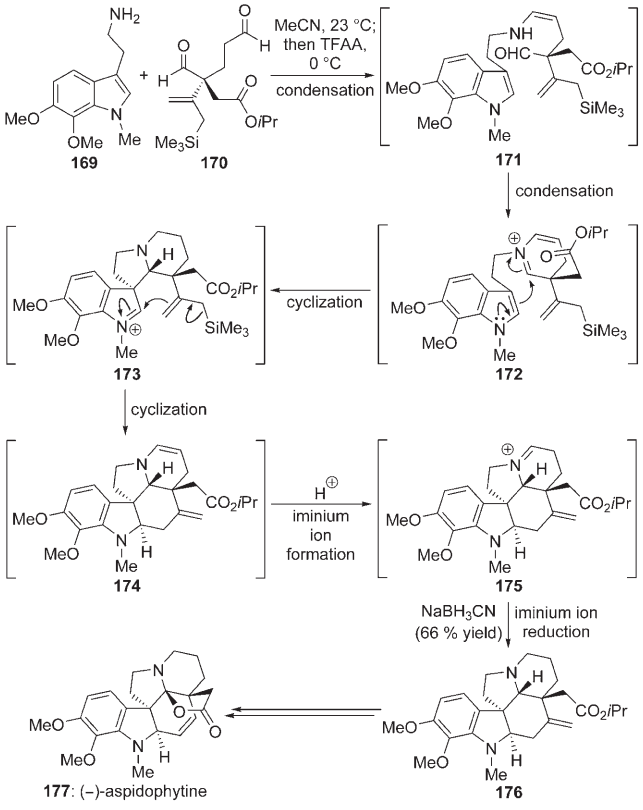

Scheme 26. The total synthesis of (−)-aspidophytine (**177**) through a series of iminium ion cyclizations (Corey et al., 1999).[86]

The total synthesis of (+)-vinblastine (**184**, Scheme 27) by Fukuyama and co-workers makes use of an electrophilic aromatic substitution reaction for the late-stage coupling of the "northern" and "southern" halves of the target (**178** and **181**, respectively), along the lines of the biosynthesis of this clinically important anticancer drug.[89] Treatment of indole **178** with *t*BuOCl in CH_2Cl_2 led to the initial formation of imine **179**, followed by tautomerization to the corresponding chloroindolene species **180**. Exposure of a mixture of chloroindolene **180** and synthetic indole **181** (itself a natural product, (−)-vindoline, which had previously been synthesized by the Fukuyama group)[90] in CH_2Cl_2 to excess TFA led to the formation of the desired adduct **183** as a single regio- and stereoisomer in remarkable yield (97% for the two steps from "northern" indole **178**) by addition of the vindoline aromatic nucleus to the highly reactive electrophilic species **182**.[91] The stereochemical outcome of the coupling was anticipated not only on the basis of precedent provided by model studies from Schill and co-workers,[92] but also by molecular modeling calculations, which suggested that the 11-membered ring of intermediate **182** would preferentially

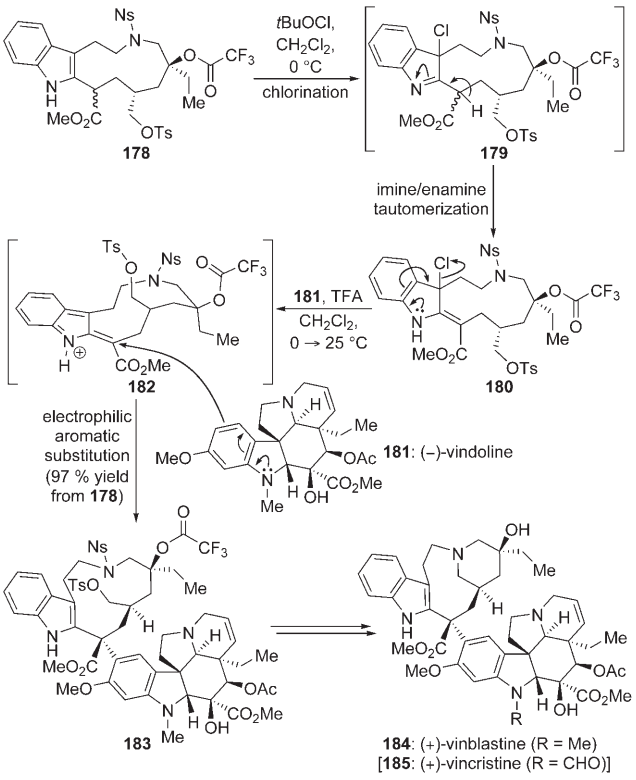

Scheme 27. The total synthesis of (+)-vinblastine (**184**) through electrophilic aromatic substitution (Fukuyama et al., 2002).[89]

 © 2006 Wiley-VCH Verlag GmbH & Co. KGaA, Weinheim

adopt the conformation shown. Attack of (−)-vindoline (**181**) from the convex face of this ring would then lead to the formation of coupled product **183** with the correct stereochemistry at the C16 position as required for the target natural product **184**.[93] Fukuyama and co-workers have also applied this strategy to the synthesis of the related alkaloid (+)-vincristine (**185**).[94]

The Padwa group has employed a Pummerer/Pictet–Spengler cascade reaction,[95–97] involving both thionium and iminium ion intermediates, in the preparation of the alkaloid jamtine (**191**, Scheme 28).[98] This synthesis also serves to demonstrate the versatility of sulfoxides in total synthesis. Treatment of sulfoxide **186** (as a 4:1 mixture of *Z*/*E* isomers) with CSA in refluxing toluene generated sulfonium ion **187**, which underwent cyclization to form *N*-acyl iminium ion **189**. This species was then intercepted by the electron-rich aromatic ring in a Pictet–Spengler cyclization to form the tricyclic core of the target natural product **191**. This cyclization cascade in fact led to the formation of a 5:2:1:1 mixture of diastereoisomers in an overall yield of 88%, with the major product being the desired diastereoisomer **190**. To rationalize the preferential formation of tricyclic stereoisomer **190**, Padwa et al. suggested that a 4π-Nazarov-type electrocyclization controls the direction of ring closure from the α-acylthionium ion intermediate (i.e. **188**→**189**). The subsequent Pictet–Spengler step involves attack of the aromatic ring from the less hindered side of the iminium ion framework. The resulting sulfide group in cascade product **190** was put to further use later in the synthetic route to introduce the trisubstituted alkene through the thermal elimination of a sulfoxide. This strategy allowed the rapid construction of the polycyclic alkaloid jamtine (**191**) from simple building blocks.[99]

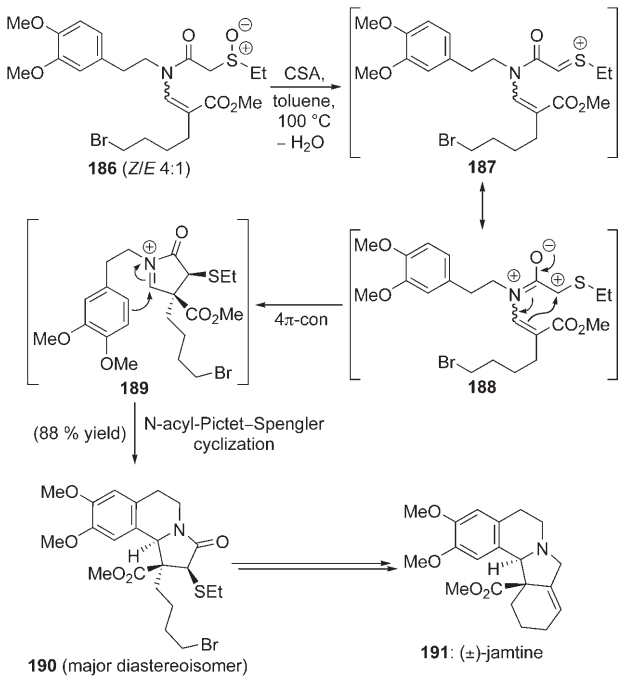

Scheme 28. The total synthesis of (±)-jamtine (**191**) through a Pummerer/Pictet–Spengler cascade (Padwa and Danca, 2002).[98]

Two distinct cascade reactions involving carbocationic intermediates can be found in the total syntheses of sceptrin (**197**) and ageliferin (**202**, Scheme 29), reported by Baran and

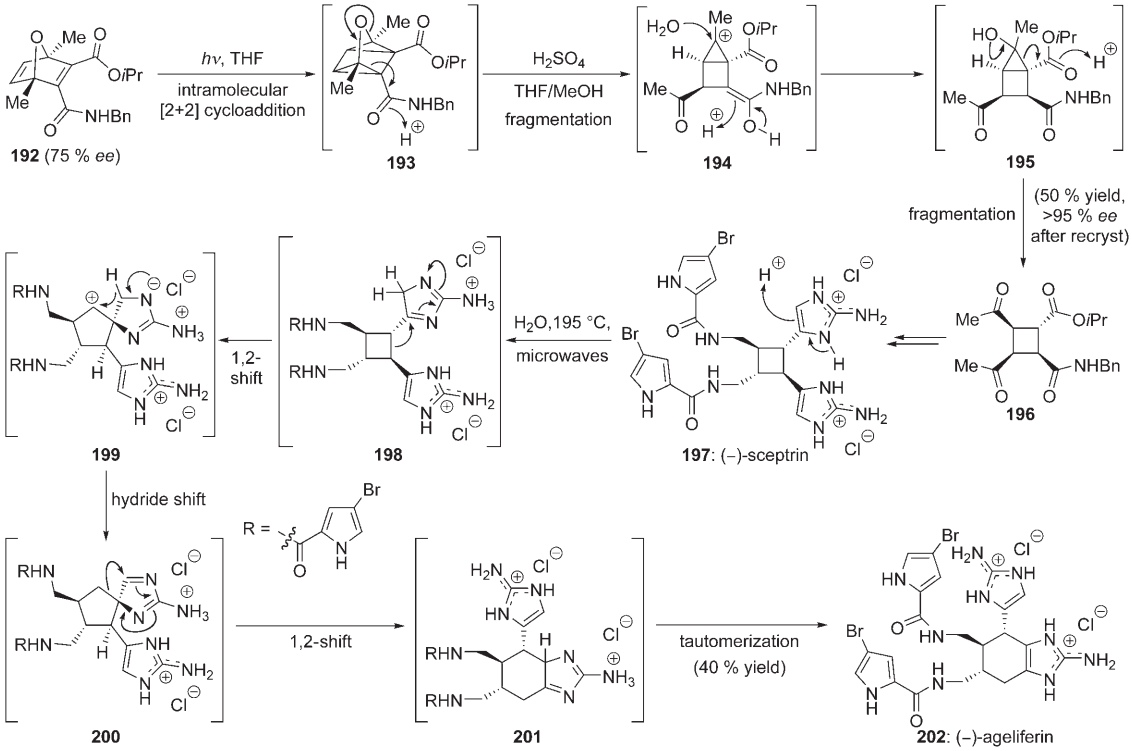

Scheme 29. The total synthesis of (−)-sceptrin (**197**) and (−)-ageliferin (**202**) by a controlled quadricyclane fragmentation and cationic ring expansion (Baran et al., 2006).[103]

© 2006 Wiley-VCH Verlag GmbH & Co. KGaA, Weinheim

co-workers. In their synthesis of racemic sceptrin,[100] they made use of the fragmentation of a 3-oxaquadricyclane system, first reported by the groups of McInnes[101] and Nelson,[102] to prepare the required all-*trans*-tetrasubstituted cyclobutane ring. The problem of preparing enantiopure sceptrin by an analogous route was far from simple, especially in light of the poorly understood mechanism of the quadricyclane fragmentation. Indeed, initial attempts to prepare non-racemic cyclobutanes from enantiomerically enriched chiral 3-oxaquadricyclanes resulted in significant loss of enantiopurity. However, by employing monobenzylamide **193**, prepared in situ by irradiation of non-racemic diene **192**, Baran et al. were able to access tetrasubstituted cyclobutane **196** with clean transfer of chirality (Scheme 29).[103] They proposed a mechanism involving initial cleavage of the oxygen bridge to give cyclopropyl carbocation **194**. The regioselectivity of this step is crucial to the transfer of chirality during the cascade and is correlated with the greater stability of amide enols as compared to ester enols.[104] Addition of a molecule of water to **194** yields cyclopropanol **195**, which subsequently undergoes retroaldol fragmentation, driven by relief of ring strain, to give cyclobutane **196**. Interestingly, the product of this cascade has the *cis*,*trans*,*trans* configuration, in contrast to that observed earlier using *meso*-quadricyclanes. Fortunately, a facile epimerization gave the correct all-*trans* arrangement required for natural (−)-sceptrin (**197**).[105] Suspecting that (−)-sceptrin (**197**) may be the true natural precursor of the related natural product (−)-ageliferin (**202**), rather than a product of a divergent pathway, Baran et al. began to investigate the rearrangement of **197** to **202**. After screening a number of conditions, they discovered that the required transformation could be achieved by brief heating of an aqueous solution of **197** under microwave irradiation.[106,107] The most direct route from **197** to **202** would involve a concerted [1,3]-sigmatropic shift followed by tautomerization, but the possibility of this pathway occurring can be excluded on the basis that it would require inversion of configuration at the migrating center, whereas retention is observed experimentally. Several other more plausible mechanisms for the conversion of **197** into **202** can be envisioned, including the one illustrated in Scheme 29 which features a series of 1,2-shifts. Initial enamine–imine tautomerization of (−)-sceptrin (**197**) gives **198**, which undergoes the first alkyl 1,2-shift to give 5,5-spiro carbocation **199**. A hydride shift followed by a second alkyl 1,2-shift gives cyclohexane **201**, and a final tautomerization affords (−)-ageliferin (**202**) in moderate overall yield (40% from **197**). The synthesis by Baran et al. of (−)-sceptrin (**197**) and (−)-ageliferin (**202**) served to highlight a new possibility for the biosynthetic relationship of these natural products and to define the absolute stereochemistry of natural (−)-ageliferin.

4. Radical Cascades

The reactivity profiles of organic radicals[108] are well suited to the development of cascade reactions, and a wide variety have been designed and executed.[109] In this section, we will discuss a selection of radical-based cascades from recent total synthesis campaigns, with the aim of highlighting a broad scope of radical processes. The use of carbon- and heteroatom-centered radicals is exemplified, as are a range of methods for radical generation, including single electron transfer and photochemical processes in addition to the more traditional AIBN/tin hydride protocols.

In their synthesis of (−)-morphine (**208**, Scheme 30), Parker and Fokas used a cascade radical process to form two rings and install the all-carbon quaternary stereocenter in a single step. Treatment of bromide **203** with tri-*n*-butyltin hydride and AIBN in refluxing benzene gave tetracyclic

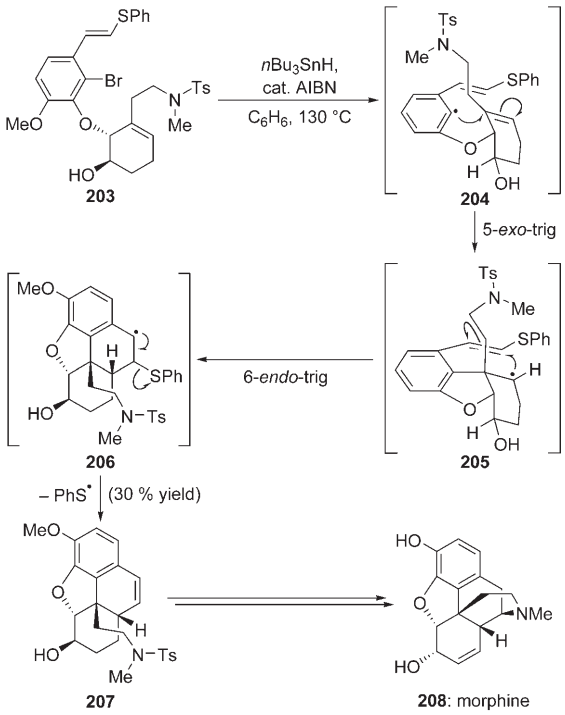

Scheme 30. Radical cyclizations in the total synthesis of (−)-morphine (**208**; Parker and Fokas, 2006).[110]

product **207** in moderate yield.[110] The reaction proceeds by the initial generation of aryl radical **204**, which cyclizes onto the tethered cyclohexene to form the dihydrobenzofuran system and the quaternary center. The approach of the aryl radical to the lower face of the alkene (as drawn in **204**) is governed by the stereochemistry of the ether linkage. Secondary radical **205** then cyclizes in a 6-*endo*-trig fashion to generate benzylic radical **206**. The geometric constraints imposed by the tricyclic framework of **205** discourage the alternative, and otherwise generally kinetically favored, 5-*exo*-trig mode of cyclization. Finally, elimination of phenylsulfinyl radical forms the olefin required for completion of this formal total synthesis of morphine.[111] Notably, a model substrate that lacks the vinylic 2-aminoethyl substituent underwent an analogous radical-based cyclization to generate the corresponding tetracyclic system in a much improved yield of 85%, illustrating the difficulties often encountered in the installation of congested all-carbon quaternary centers.

 © 2006 Wiley-VCH Verlag GmbH & Co. KGaA, Weinheim

Zard and co-workers have developed a mild method for the generation of nitrogen-centered amidyl radicals from *O*-acyl hydroxamic acids.[112] This technology was central to their synthesis of the *Lycopodium* alkaloid 13-deoxyserratine (**215**, Scheme 31).[113] Treatment of benzoate **209** with tri-*n*-butyltin

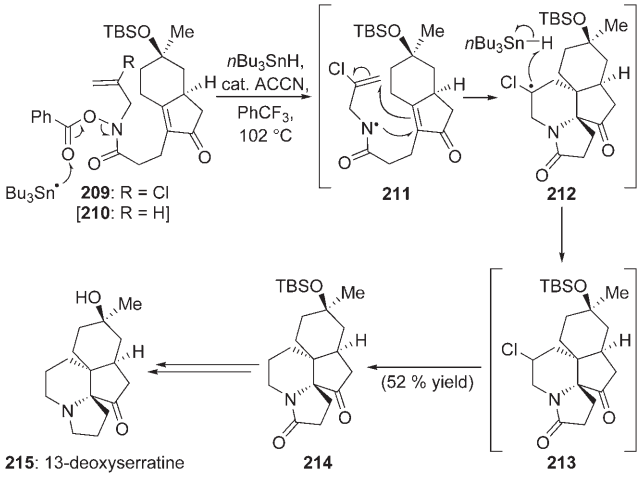

Scheme 31. Nitrogen-centered radical cyclization in the total synthesis of 13-deoxyserratine (**215**; Zard et al., 2002).[113]

hydride and the radical initiator 1,1′-azobis(cyclohexanecarbonitrile) led to generation of amidyl radical **211**. This species underwent sequential 5-*exo*-trig and 6-*endo*-trig cyclizations, followed by hydrogen abstraction from tri-*n*-butyltin hydride, to furnish a tetracyclic intermediate (**211**→**212**→**213**). In this reaction, the vinyl chloride substituent acts as a disposable directing group.[114] Substrate **210**, which lacks this control element, was found to give the product arising from two 5-*exo*-trig cyclizations. The chlorine atom encourages the desired switch in regiochemical outcome by disfavoring the 5-*exo*-trig ring closure on steric grounds and by stabilizing the radical that results from the 6-*endo* cyclization. The overall efficiency of the synthesis does not suffer as a result of this tactic, as no extra step was required for the introduction of the chlorine substituent and it is cleanly removed in situ to give **214**, which was converted into 13-deoxyserratine (**215**) in just a few more steps. The yield for this cascade is impressive if it is considered that two vicinal quaternary stereocenters are formed in a single step from a relatively simple starting material. Zard and Sharp have recently applied a similar strategy to the total synthesis of the alkaloid aspidospermidine.[115]

The use of radical rearrangements and fragmentations can allow for the construction of complex systems in remarkable ways, providing that the timing of the elementary steps in the cascade can be controlled in the desired manner.[109] One instructive example can be found in the synthesis of lubiminol (**223**, Scheme 32) by Crimmins et al.[116] The synthetic strategy called for a radical fragmentation/ring expansion of a tricyclic cyclobutane such as **216**. This plan allowed for the formation of the spirocyclic system, including the challenging C5 quaternary center, by a stereocontrolled [2+2] photocycloaddition. Indeed, the cyclobutane substrate **216** could be prepared as a single diastereoisomer in this manner. Treatment of **216** with tri-*n*-butyltin hydride and AIBN led to fragmentation of the thiocarbamate to give secondary radical **218**. This process is driven by the affinity of tin for the sulfur atom of the thiocarbonyl group and the formation of a stronger C=O bond in place of the C=S linkage. Strain-driven fragmentation of the cyclobutane ring in **218** then proceeded regioselectively to give the primary radical **219**. This species then underwent a Dowd–Beckwith ring expansion,[117] involving 3-*exo*-trig cyclization onto the ketone carbonyl group followed by fragmentation of the resulting oxygen-centered radical **220**, with regioselective cleavage giving the observed cyclohexanone product **222** after reduction of **221**. Ketone **222** was then converted into (±)-lubiminol (**223**).[118] A more direct approach to this target would involve the radical fragmentation of substrate **224**, in which the required C10 methyl substituent has already been installed. Surprisingly, under the conditions that worked so effectively for **216**, cyclobutane **224** failed to give any cyclohexanone products.[116] The reason for the dramatic and deleterious effect of this seemingly benign methyl group on the radical process is not clear. It may be that the Dowd–Beckwith fragmentation step is disfavored by the increased steric hindrance imposed

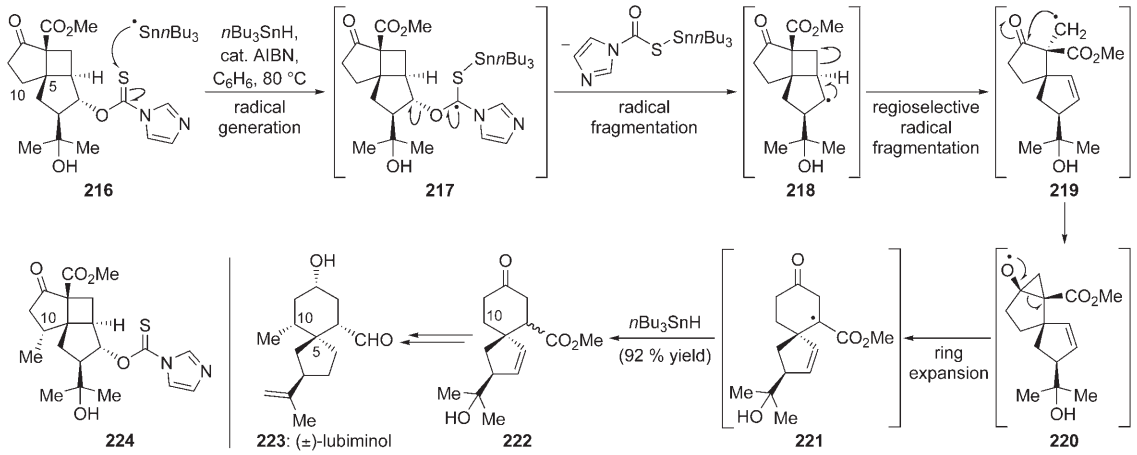

Scheme 32. The total synthesis of lubiminol (**223**) through a cyclobutane fragmentation/ring-expansion cascade (Crimmins et al., 1998).[116]

 © 2006 Wiley-VCH Verlag GmbH & Co. KGaA, Weinheim

by the methyl group, or that intramolecular hydrogen-atom transfer from this group is a competing process. However, as another substrate bearing the epimeric 10*S*-methyl-substituted center also failed to proceed efficiently through the cascade, more subtle conformational effects may also be at work.

The chemical synthesis of steroids has been a central feature of organic chemistry research for much of the last century.[119] The rigid steroid framework has inspired a number of elegant and inventive cascade reactions, from the landmark biomimetic synthesis of progesterone (**11**) by Johnson and co-workers (see Scheme 2),[5] and the cobalt-catalyzed synthesis of estrone (**232**) by Vollhardt and co-workers,[120] to more recent accomplishments, including the palladium-catalyzed sequences developed by the groups of Tietze[121] and Negishi,[122] and Grubbs and co-workers' enyne metathesis cascade.[123] Pattenden et al. recently completed a short synthesis of (±)-estrone (**232**) using an imaginative radical cascade (Scheme 33).[124] Radical precursor **225** was

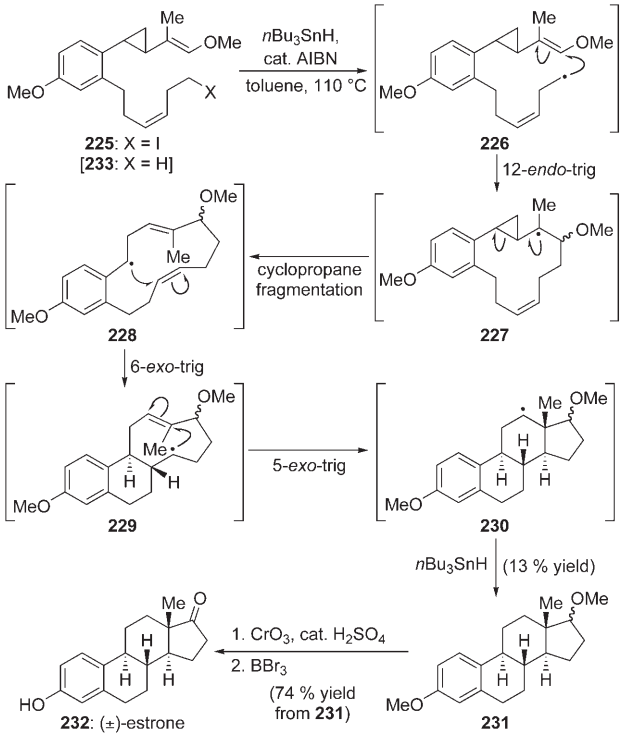

Scheme 33. Total synthesis of (±)-estrone (**232**) through a radical cascade cyclization (Pattenden et al., 2004).[124]

treated with AIBN and tri-*n*-butyltin hydride to give the tetracyclic steroid precursor **231**. This reaction proceeds by the initial macrocyclization of the primary radical **226** to give tertiary radical **227** (note that, in contrast to carbanion chemistry, carbon-centered radicals generally tolerate oxygenated functionality in the β-position). Fragmentation of the cyclopropane ring (**227**→**228**) then serves to move the radical site to the benzylic position. Two sequential transannular cyclizations (**228**→**229**→**230**) followed by quenching of the resulting secondary radical (**230**) then gave **231**. Although the overall yield of this cascade was very modest, it nevertheless enabled the diastereoselective formation of three rings and four stereocenters in a single maneuver. From tetracyclic compound **231**, a simple two-step procedure then led to (±)-estrone (**232**).[125] The low overall yield of this cascade can be attributed largely to the difficulty in achieving the initial macrocyclization step. The relatively slow rate of macrocyclization allows side reactions, such as simple quenching of primary radical **226** by tri-*n*-butyltin hydride, to compete. Indeed, the major product of this reaction was the reduced species **233**, which was isolated in 52% yield. However, once the macrocyclization event had occurred, the remaining steps of the cascade were comparatively efficient.

Radical cascades can also be initiated by treating suitable substrates with various single-electron-transfer reagents. Samarium(II) iodide has been employed as a mild and selective reductant in many cascade reactions, in which it can mediate both radical and anionic processes.[126] Kilburn and co-workers employed this reagent in the synthesis of paeonilactone B (**239**, Scheme 34),[127] which featured a cascade

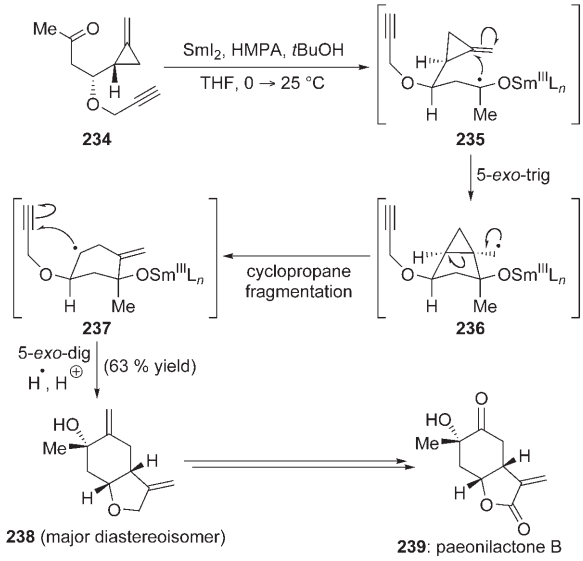

Scheme 34. The use of a Sm^{II}-mediated cyclization/fragmentation cascade in the total synthesis of paeonilactone B (**239**; Kilburn et al., 2001).[127]

cyclization involving a methylene cyclopropane group. Treatment of ketone **234** with samarium(II) iodide in the presence of HMPA and *t*BuOH results in one-electron reduction to give ketyl radical anion **235**. A 5-*exo*-trig cyclization of **235** onto the methylene cyclopropane unit generates cyclopropyl carbinyl radical **236**, which undergoes a facile ring-expanding fragmentation to give homoallylic radical species **237**. Subsequent 5-*exo*-dig cyclization of **237**, followed by hydrogen-atom capture, gives the bicyclic product **238** in good yield (63%) as a 10:1 mixture of diastereoisomers at the hydroxy-substituted center (only the major diastereoisomer is shown in Scheme 34). Elaboration of bicyclic product **238** over a short sequence of steps then completed the total synthesis.[128] The relatively high level of diastereoselectivity observed in the conversion of **235** to **236** was found to be critically dependent

 © 2006 Wiley-VCH Verlag GmbH & Co. KGaA, Weinheim

on the reaction solvent mixture. The use of the highly coordinating cosolvent HMPA was crucial, with the selectivity thought to result from the bulky solvated samarium alkoxide adopting a pseudoequatorial position in the cyclization of **235**.[129]

Radical species can also be generated oxidatively by one-electron transfer from the substrate to a metal center. Lee et al. employed the Mn^{III}–Cu^{II} system in their total synthesis of the guaianolide sesquiterpene (−)-estafiatin (**247**, Scheme 35).[130] Treatment of allylic chloromalonate **240** with a mixture of manganese(III) acetate and copper(II) acetate in ethanol at 80 °C led to a stereoselective 5-*exo*-trig,7-*endo*-trig radical cyclization cascade, which gave tricyclic product **246** in 65% yield. The chloride substituent was specifically incorporated into cascade precursor **240** in order to prevent further oxidation of product lactone by the excess manganese(III) acetate and was easily removed during the subsequent completion of the total synthesis of (−)-estafiatin (**247**).[131] The radical cyclization proceeds by ligand exchange to generate the manganese(III) enolate **241** in the rate-determining step.[132] A rapid redox reaction then generates the electrophilic radical **242**, which undergoes a 5-*exo*-trig cyclization to generate primary radical **243**. This species then undergoes a selective 7-*endo*-trig cyclization to afford tertiary radical **244**. The generally moderate intrinsic *endo* selectivity found in related reactions[133] is enhanced in this case by the presence of the vinylic methyl substituent, which hinders the trajectory of approach required for 6-*exo* cyclization and encourages the 7-*endo* pathway. A reluctance towards formation of a more strained *trans*-fused 6,5-ring system may also contribute to the high *endo* selectivity in this case. In the final step, tertiary radical **244** is oxidized by the copper(II) acetate to give the tertiary carbocation **245**, which loses a proton to give the *exo*-methylene product **246**.

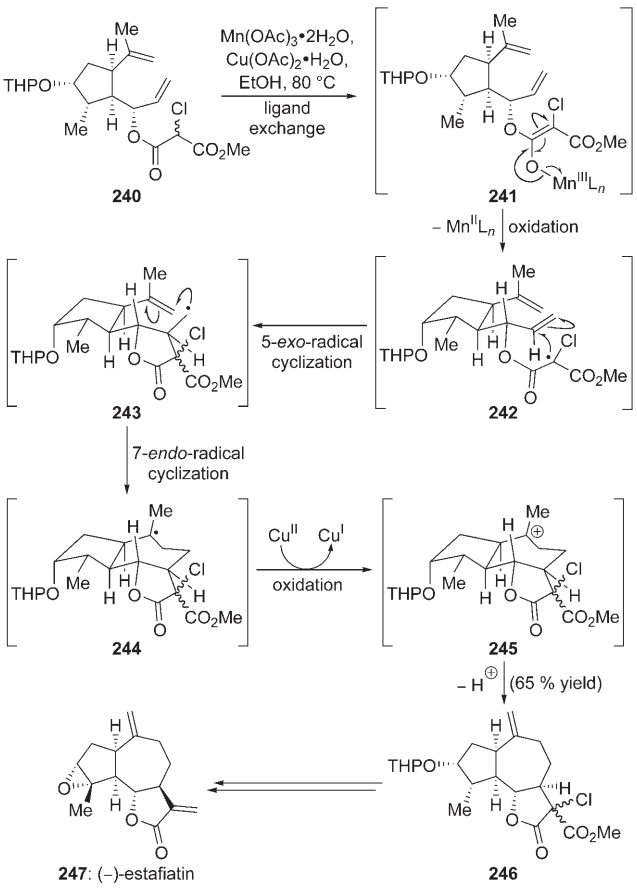

Scheme 35. Total synthesis of (−)-estafiatin (**247**) through an oxidative radical cyclization cascade (Lee et al., 1997).[130]

The lanthanide salt, cerium(IV) ammonium nitrate (CAN), is another single-electron oxidant that is widely used in organic synthesis.[126,134] Nicolaou and Gray employed CAN to effect the key dimerization step in their total synthesis of hybocarpone (**256**).[135] Their approach involved the use of two separate cascade sequences, as shown in Scheme 36. The first was used to prepare the monomeric naphthazarin unit of hybocarpone (**256**) through photoenolization of benzaldehyde derivative **248** in the presence of acrylate **249**. Thus, irradiation of **248** generated *ortho*-quinodimethane enol **250**, which was trapped in situ by dienophile **249** to give the cyclohexanol product **251** in high yield.[136] Alcohol **251** was then converted into quinone **252** in preparation for the crucial dimerization event. After screening a range of electron-transfer agents, it was discovered that

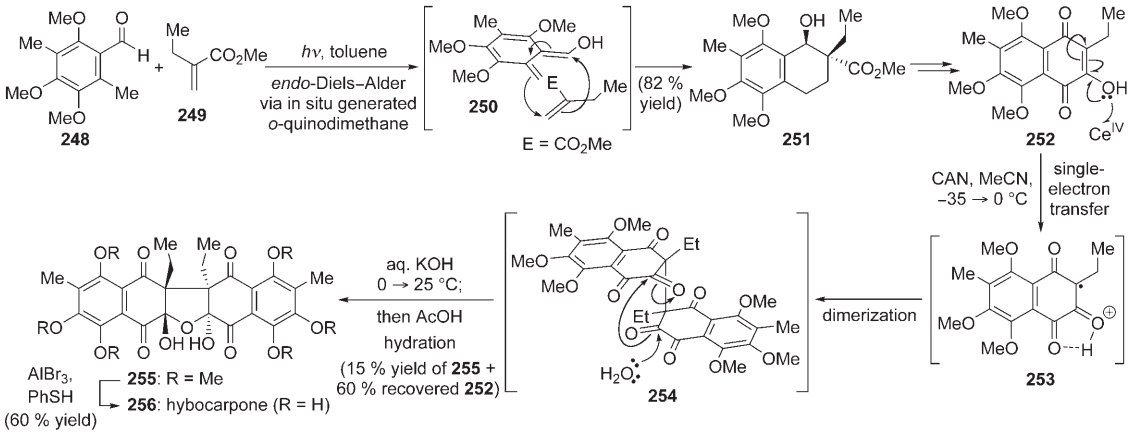

Scheme 36. Total synthesis of hybocarpone (**256**) through photochemical enolization/Diels–Alder and oxidative coupling cascades (Nicolaou and Gray, 2001).[135]

 © 2006 Wiley-VCH Verlag GmbH & Co. KGaA, Weinheim

brief treatment of **252** with CAN at low temperature effected the desired carbon–carbon bond-forming reaction. Oxidation of **252** by CAN is believed to lead to tertiary radical **253**, which undergoes stereoselective dimerization to give the C_2-symmetric diketone **254**. Quenching of the reaction with base completed the process by triggering hydration of the 1,4-diketone to give pentacyclic product **255**. Hydrate **255** was formed along with a minor quantity of an unsymmetrical stereoisomer, as predicted by molecular modeling studies, which could be epimerized to give **255** on treatment with mild acid. Global deprotection of **255** with aluminum bromide and benzene thiol gave hybocarpone (**256**).[137]

Harran and co-workers employed a photochemically initiated radical coupling in the total synthesis of the revised structure of diazonamide A (**270**, Scheme 37).[138] They also made use of an oxidative annulation reaction of a phenol precursor, mediated by a hypervalent iodine(III) reagent. The core architecture of diazonamide A (**270**) comprises two macrocyclic domains: the "left-hand" macrolactam peptide-containing portion and the "right-hand" heterocyclic sector. The macrolactam portion of the target was prepared first, through the oxidative cyclization of peptidic precursor **257**. Thus, treatment of **257** with $PhI(OAc)_2$ and LiCl in CF_3CH_2OH gave the desired macrocycle **261** in moderate yield (20–25%), accompanied by lesser amounts of the diastereomeric product **262** (7–8%) and a mixture of epimeric spirodienones **263** (ca. 15%). A number of mechanistic pathways could be invoked to explain this result,[139] but a likely pathway[140] involves the reaction of the phenol group with the iodoso species to generate **258**, which fragments with the loss of acetate and iodobenzene to give phenonium ion intermediate **259**. Reaction of **259** through path b (Scheme 37) involves attack of the amide group at C4 of the phenonium ion, leading to spirocycle **263**. Alternatively, attack of the nucleophilic indole (path a) gives macrocyclic intermediate **260**, which re-aromatizes with concomitant ring closure to generate the required aminal ring system in **261**. The minor diastereomeric product **262** arises from attack of the indole ring and subsequent ring closure occurring on the opposite face of the indole C2–C3 double bond to that depicted in Scheme 37. The observed stereocontrol in the formation of the macrocyclic products is thought to be relayed

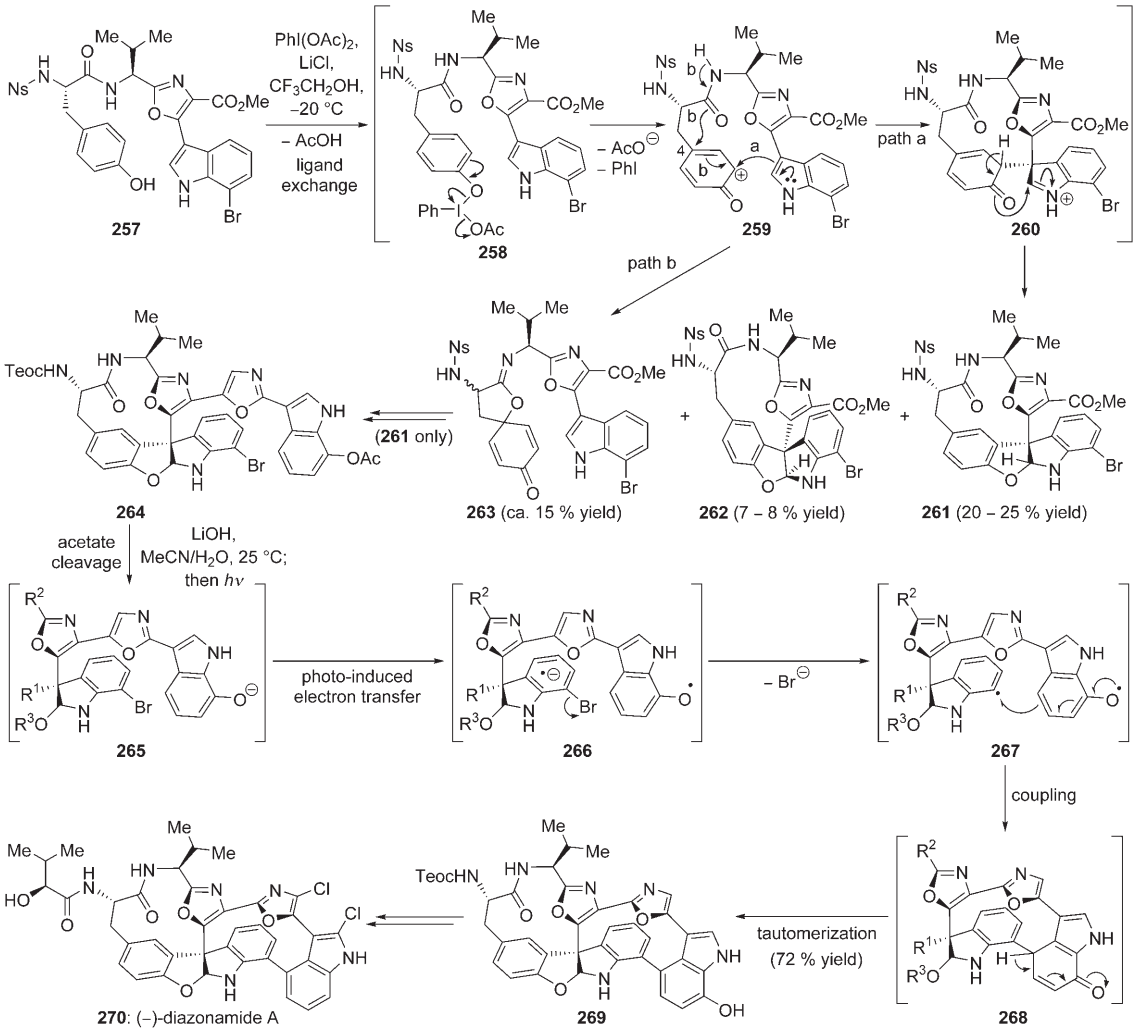

Scheme 37. Oxidative phenolic coupling and photolytic aromatic coupling reactions in the total synthesis of (−)-diazonamide A (**270**; Harran et al., 2003).[138]

 © 2006 Wiley-VCH Verlag GmbH & Co. KGaA, Weinheim

from the two backbone stereocenters, which endow precursor **257** with a helical character. This helical character also brings the phenol and indole rings into close proximity to one another, enabling macrocyclization to dominate over an ostensibly more favorable five-membered ring closure to afford spirodienones **263**. After separation from the accompanying by-products, macrocycle **261** was elaborated to give bromide **264**, in preparation for the photochemical macrocyclization event. Treatment of compound **264** with aqueous lithium hydroxide in acetonitrile served to cleave the phenolic acetate group and afford phenolate anion **265**. Irradiation of this solution then triggered the crucial Witkop cyclization[141] to generate macrocyclic product **269** in 72% overall yield. This process involves a photoinduced electron transfer between the phenoxide group and the less electron-rich bromoindoline aromatic ring. Loss of bromide from the resulting radical anion **266** then gives a radical pair **267**, which couples (**267**→**268**) and tautomerizes (**268**→**269**) to generate the required biaryl linkage in high yield and complete the macrocyclic framework.[142] These two very different cyclization procedures therefore provided both elegant and creative solutions to the synthesis of the respective macrocyclic domains of diazonamide A (**270**). Having reached the advanced staging area represented by compound **269** in this concise manner, Harran and co-workers were able to complete the total synthesis of this fascinating target in short order.[143]

5. Pericyclic Cascades

Pericyclic reactions are perhaps the most common processes encountered in cascade reactions. This broad class includes cycloadditions, sigmatropic rearrangements, and electrocyclic reactions, all of which have been employed in cascades en route to natural product targets. This section begins with cascades that incorporate Diels–Alder reactions,[144] coupled with a variety of other pericyclic and nonpericyclic processes, in both inter- and intramolecular settings. Several other cascades that hinge upon sigmatropic and electrocyclic transformations then follow. Additionally, a number of pericyclic reactions can be found throughout this Review as components of other cascades.

The first example in this section is taken from the total synthesis of the indole alkaloid hirsutine (**280**, Scheme 38) by Tietze and Zhou.[145] As with several of the reactions covered in this Review, this process is rather difficult to classify, as it combines several individual reaction types in an elegant cascade. The first step in this three-component coupling reaction is the Knoevenagel condensation of chiral aldehyde **271** with Meldrum's acid (**272**), which proceeds under very mild conditions.[146] The resulting alkylidene intermediate **274** then reacts with enol-ether **273** in an intermolecular hetero-Diels–Alder reaction to give dihydropyran **275** with excellent diastereoselectivity. This is then followed by a retro-[4+2] cycloaddition reaction to expel a molecule of acetone and generate a reactive ketene intermediate **276**. Hydration of **276** gives a new 1,3-diacid derivative **277**, which undergoes thermal decarboxylation to form **278** in excellent overall yield

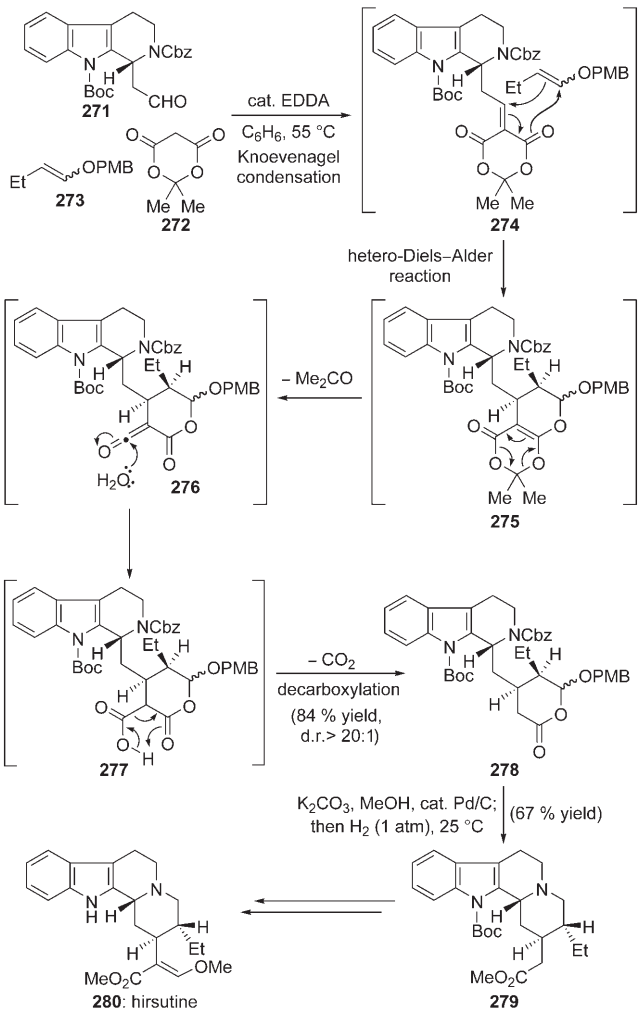

Scheme 38. Knoevenagel/hetero-Diels–Alder reaction cascade in the total synthesis of hirsutine (**280**; Tietze and Zhou, 1999).[145]

(84%). In a second cascade step, treatment of **278** with K_2CO_3 in methanol followed by hydrogenation under palladium catalysis led to methanolysis of the lactone, loss of the PMB and Cbz protecting groups, iminium ion formation, and finally reduction to form tetracyclic amine **279**, a precursor to hirsutine (**280**).[147]

Another cascade sequence involving a hetero-Diels–Alder reaction can be found in the total synthesis by Nicolaou et al. of the veterinary antibiotic thiostrepton (**289**, Scheme 39),[148] the most structurally complex member of the thiopeptide class of natural products.[149] Inspired by the biosynthetic proposals of Floss and co-workers,[150] Nicolaou et al. began investigating the [4+2] dimerization of azadienes for the construction of the dehydropiperidine core structure that lies at the heart of the target natural product. It was found that treatment of thiazolidine **281** with silver(I) carbonate and a catalytic amount of DBU in pyridine led to a formal elimination of hydrogen sulfide to generate the highly reactive aza-diene **282**. The Diels–Alder dimerization of **282** then proceeded through an *endo* transition state to give the dihydropiperidine system **283** with excellent control of stereoselectivity at the newly formed piperidine C5 and C6

 © 2006 Wiley-VCH Verlag GmbH & Co. KGaA, Weinheim

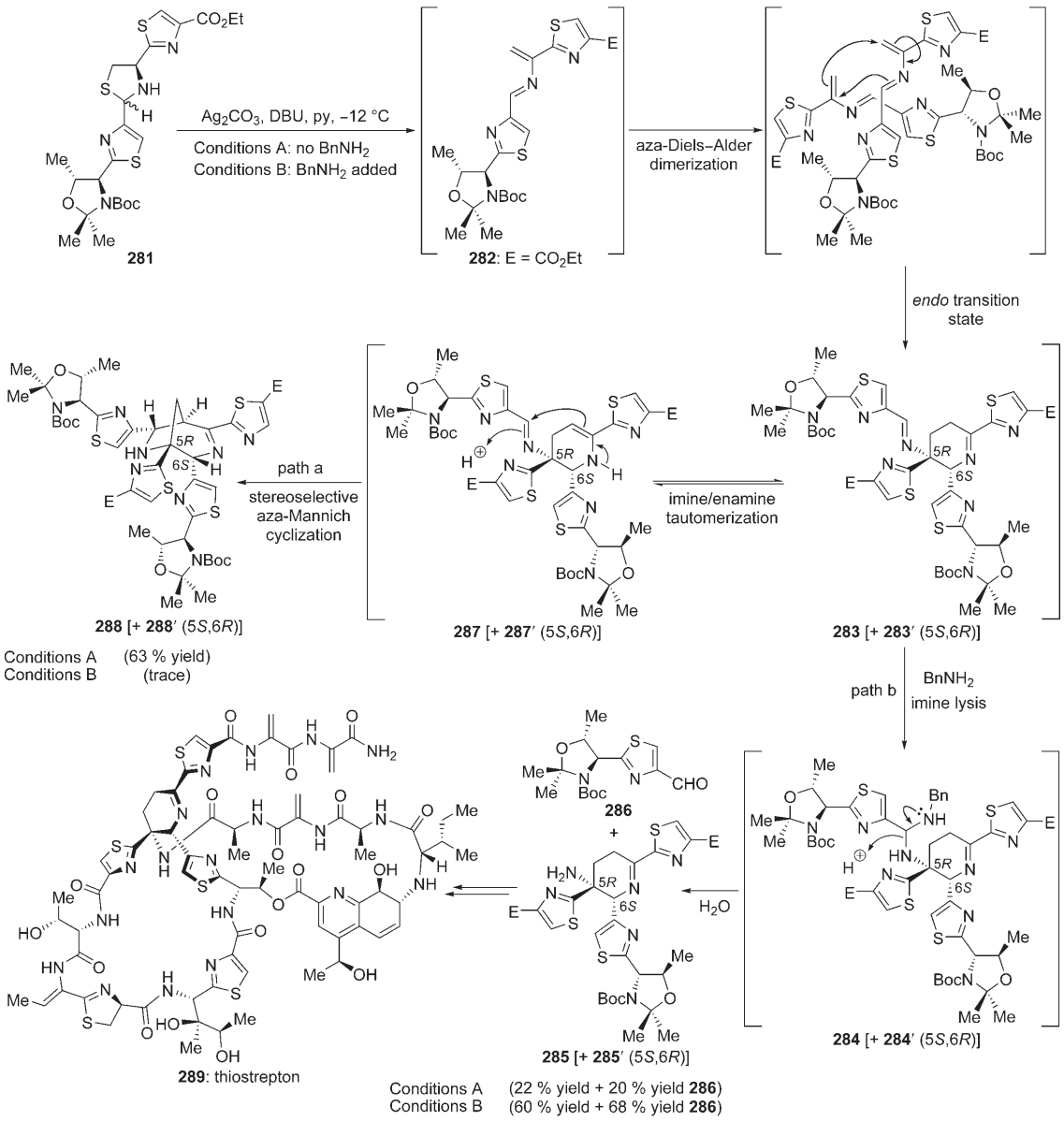

Scheme 39. aza-Diels–Alder dimerization and aza-Mannich reactions in the total synthesis of thiostrepton (**289**; Nicolaou et al., 2004).[148]

stereocenters. However, the reaction was not influenced by the remote stereocenters of the substrate, so **283** was formed as a 1:1 mixture of 5*R*,6*S*/5*S*,6*R* diastereoisomers (**283** and **284**, respectively). In the initial investigation of this reaction, the addition of water to the reaction mixture at the end of the cascade sequence, with the intention of hydrolyzing the exocyclic imine group of **283**, led to a low yield (20%) of the desired amine product **285**. Under these conditions, the major reaction product was found to be the interesting bicyclic imine **288**, which presumably arises as the result of tautomerization of the initial [4+2] adduct **283** to the corresponding enamine species **287**, followed by a highly stereoselective aza-Mannich cyclization (path a).[151] Fortunately, inclusion of benzylamine in the reaction mixture successfully diverted the course of the reaction in favor of the desired imine lysis pathway (path b). Thus, imine hydrolysis, through initial aminolysis (**283**→**284**→**285**), gave a good yield of the dihydropiperazine product **285** (60%), along with a similar quantity of aldehyde **286**, which could be recycled for the synthesis of thiazolidine **281**.[152,153]

The complex polycyclic architectures of the bisorbicillinoids belie their considerably simpler biosynthetic precursor. The groups of Nicolaou and Corey have investigated the biosynthesis and total synthesis of a number of these fascinating fungal metabolites.[154,155] Quinol **291** (Scheme 40) was identified as a potential precursor to several of these natural products, however, such a compound was anticipated to be highly unstable.[156] Therefore, acetate **290** was prepared through oxidation of the corresponding phenol using $Pb(OAc)_4$ in AcOH to serve as a more stable precursor to the required quinol species **291**. It was anticipated that hydrolysis of the acetate group, under either basic or acidic conditions, could then lead to the formation of reactive intermediate **291** in situ. As shown in Scheme 40, acid-

 © 2006 Wiley-VCH Verlag GmbH & Co. KGaA, Weinheim

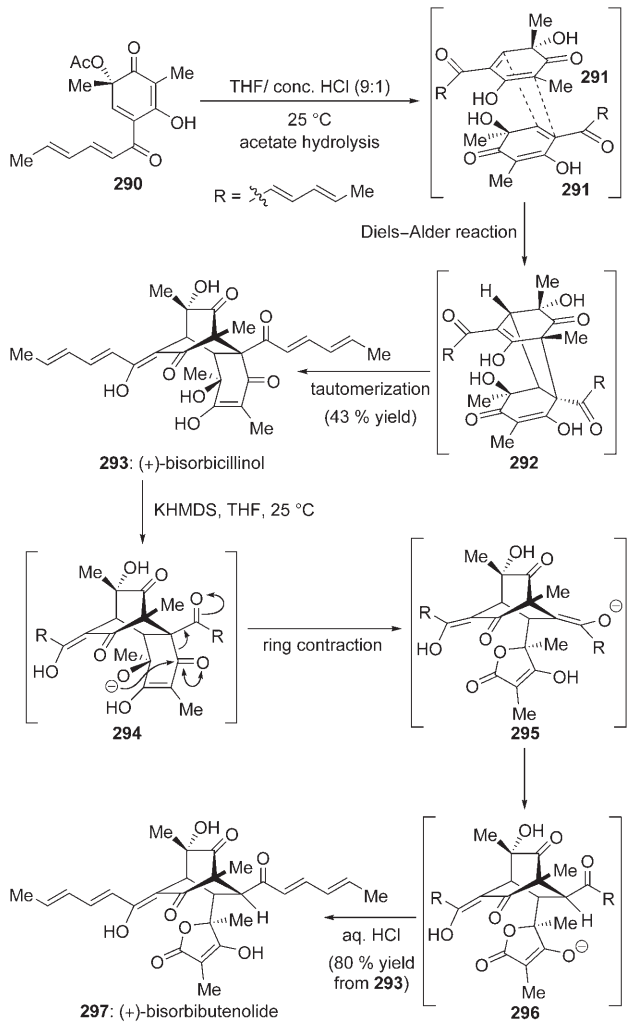

Scheme 40. Diels–Alder dimerization and base-catalyzed isomerization reactions to form (+)-bisorbicillinol (**293**) and (+)-bisorbibutenolide (**297**; Nicolaou et al., 1999).[154]

catalyzed hydrolysis of **290** led to the Diels–Alder dimerization of quinol **291** to give **292**, tautomerization of which afforded (+)-bisorbicillinol **293** in 43% yield.[154] Under basic conditions (10 equiv KOH, 9:1 THF/H_2O), the potassium salt of **291** could be observed by ^{1}H NMR spectroscopy, and only dimerized to give **293** on acidification, indicating the increased stability of the quinoxide. Nicolaou et al. also found that (+)-bisorbicillinol (**293**) could be converted into another member of this class through a base-mediated ring-contraction sequence. Deprotonation of **293** using KHMDS (1.1 equiv) in THF at room temperature led to intramolecular attack of the alkoxide group of anion **294** onto the ketone group, followed by a retro-aldol fragmentation to give butenolide anion **296**. Protonation of this species upon quenching the reaction mixture with 1N aqueous HCl then furnished (+)-bisorbibutenolide (**297**). The conversion of bisorbicillinol (**293**) into bisorbibutenolide (**297**) is attended by a significant relief in the ring strain and overall steric crowding present in the former compound, which provides the necessary driving force for this transformation.

The conditions under which acetate **290** is hydrolyzed and the resulting quinolate anion is neutralized have a dramatic impact on the product distribution. The groups of Corey and Nicolaou have both used **290** as a precursor to the intricate pentacyclic cage structure of trichodimerol (**302**, Scheme 41).

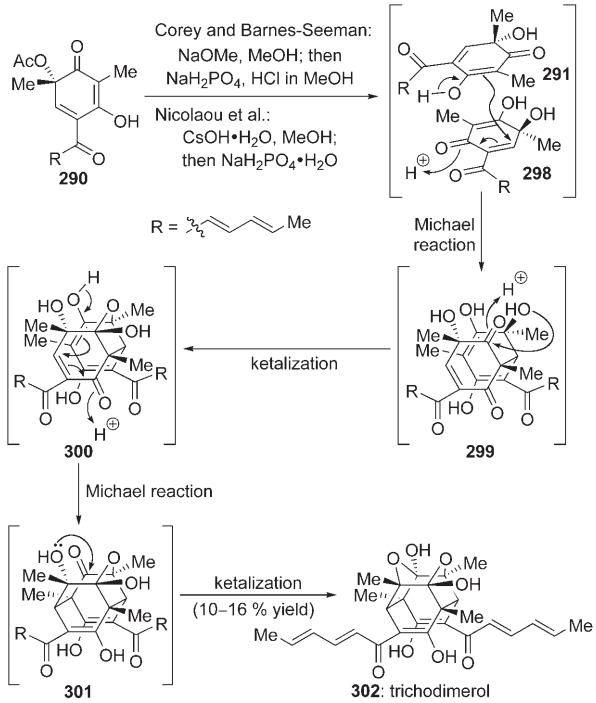

Scheme 41. A Michael reaction and ketalization cascade to form trichodimerol (**302**; Nicolaou et al., 1999; Corey and Barnes-Seeman, 1999).[154,155]

Basic hydrolysis of the acetate, followed by careful neutralization with sodium dihydrogen phosphate, gave the target natural product **302**. The yield of trichodimerol (**302**) isolated from this sequence may seem low (10–16%), but should be judged in light of the great molecular complexity generated; the sequence forms four new sigma bonds and generates eight new stereocenters (six of which are quaternary). Under these reaction conditions, quinol **291** enters a sequence of Michael additions and ketalizations rather than a Diels–Alder process. Addition of enol tautomer **291** to keto tautomer **298** initially yields dimeric species **299**. A ketalization event then provides tricyclic intermediate **300**, which is poised for a succession of Michael addition (**300**→**301**) and further ketalization steps (**301**→**302**) to afford the target product **302**. In addition to the formation of trichodimerol (**302**), Nicolaou et al. also isolated a similar proportion of bisorbicillinol (**293**) from the reaction mixture, indicating the degree of crossover between the competing Michael addition/ketalization and Diels–Alder dimerization pathways.

Aubé and co-workers have designed a number of cascade processes based on sequential Diels–Alder and intramolecular Schmidt reactions, using either keto-azides or azido-dienes under Lewis acid catalysis.[157] They applied this strategy for nitrogen heterocycle construction to the total synthesis of the *Stemona* alkaloid stenine (**310**, Scheme 42). Their first-

 © 2006 Wiley-VCH Verlag GmbH & Co. KGaA, Weinheim

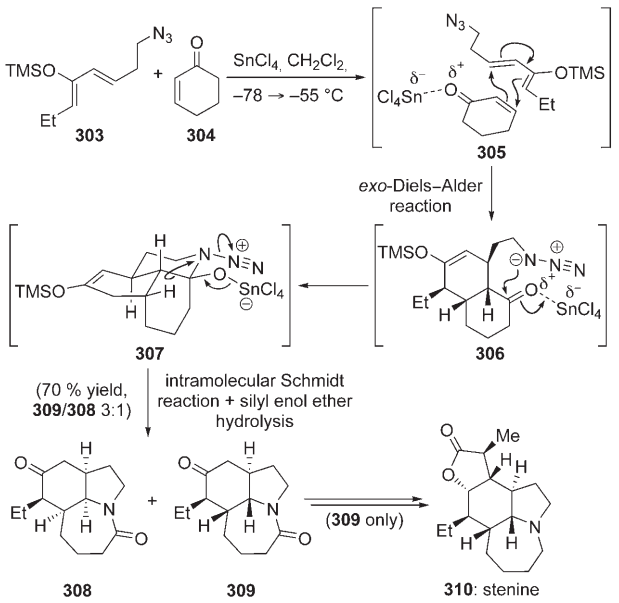

Scheme 42. Total synthesis of stenine (**310**) through a Diels–Alder/Schmidt cascade (Zeng and Aubé, 2005).[159]

generation approach to this target employed an intramolecular Diels–Alder/Schmidt reaction sequence,[158] however, not only was the cascade precursor difficult to prepare, but the cascade itself generated several undesired by-products, limiting its efficiency. In their second-generation synthesis,[159] a Lewis acid catalyzed intermolecular Diels–Alder reaction was utilized to couple azido-diene **303** with cyclohexenone **304** to give *cis*-decalin **306**, as shown in Scheme 42. The moderate *exo* selectivity of this reaction was ascribed to unfavorable steric interactions between the cyclic dienophile and the bulky TMS enol ether of the diene (only the *exo* mode of [4+2] cycloaddition is depicted in Scheme 42). Subsequent attack of the tethered azide onto the ketone proceeded stereoselectively due to the constraints of the fused ring system to give **307**.[160] Selective migration of the carbon–carbon bond antiperiplanar to the equatorially aligned N_2 leaving group in **307** led to formation of the desired tricyclic product **309**, accompanied by the corresponding diastereoisomer **308** (which results from the minor *endo* mode of [4+2] cycloaddition), in 3:1 ratio and a combined yield of 70%. After the separation of **308** and **309**, the latter could be converted into stenine (**310**) through a short sequence of steps.[161]

In their approach to the same target, Padwa and Ginn employed an intramolecular Diels–Alder reaction of a 2-methylthio-5-amido-substituted furan to fuse the 6,5-bicyclic system onto a preexisting seven-membered ring.[162] The required activated furan system was prepared in situ as part of an impressive cascade reaction (Scheme 43), which also included the rearrangement of the Diels–Alder product. The sequence begins with dithioacetal **311**, which was treated with DMTSF to form furan **316**. Methylsulfenylation of **311** by DMTSF gives methylthiosulfonium ion **312**, which fragments to give sulfonium ion **313**. A Pummerer cyclization of **313** with the nearby amide group, followed by loss of a proton and elimination of acetic acid, gives the required furan ring (**314**→**315**→**316**).[163] The electron-rich furan group then undergoes an intramolecular Diels–Alder reaction with the pendant olefin[164] to generate tetracyclic intermediate **317**. Interestingly, this Diels–Alder reaction proceeded smoothly at room temperature, while the reaction of the corresponding six-membered lactam substrate required heating at 110°C. The rate difference can be explained by the greater flexibility of the seven-membered lactam, which allows the furan to adopt a reactive conformation at ambient temperature.[165] Opening of the strained oxygen bridge (**317**→**318**), assisted by the nitrogen atom, is accompanied by a 1,2-shift of the methylthio substituent onto the activated iminium ion species to give tricyclic enamide **319**, a species which now comprised much of the structural and stereochemical complexity of the target natural product **310**.[166]

Boger et al. have developed a number of cascade processes based on the hetero-Diels–Alder reactions of azadienes.[167] Recent examples of this work can be found in their use of 1,3,4-oxadiazoles in the total syntheses of several alkaloid natural products, including that of vindorosine (**324**, Scheme 44) described here.[168] 1,3,4-Oxadiazoles had previously been employed in Diels–Alder reactions with olefins to

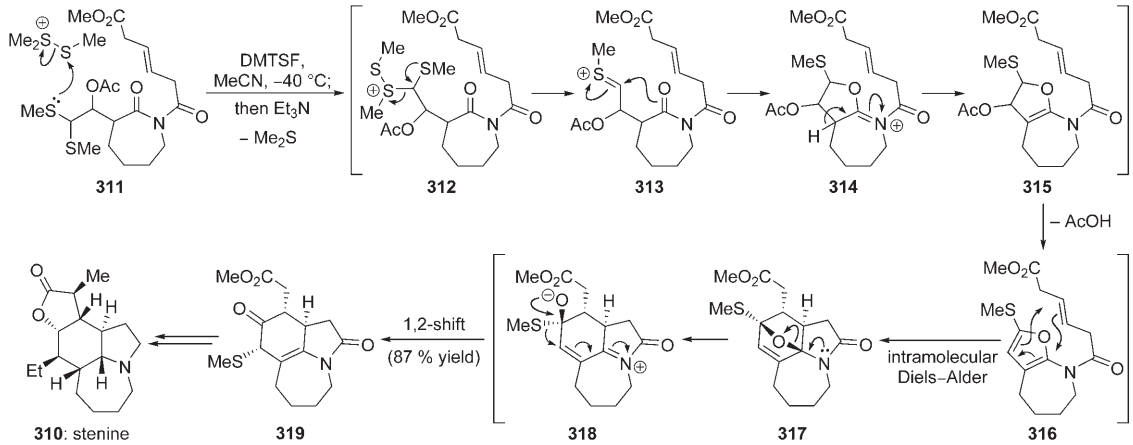

Scheme 43. A heterocyclization/Diels–Alder reaction/rearrangement cascade in the total synthesis of stenine (**310**; Ginn and Padwa, 2002).[162]

 © 2006 Wiley-VCH Verlag GmbH & Co. KGaA, Weinheim

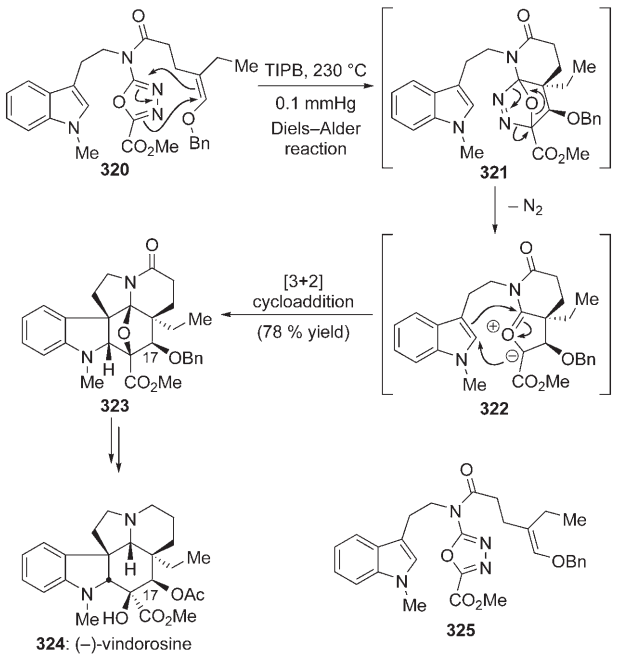

Scheme 44. Diels–Alder and [3+2] cycloadditions in the total synthesis of vindorosine (**324**; Boger et al., 2006).[168]

produce bicyclic intermediates. These intermediates lose nitrogen to generate 1,3-dipoles, which undergo a second cycloaddition with another equivalent of the olefin to give symmetrical 2:1 adducts.[169] Boger and co-workers have extended this technology by developing cascade processes in which 1,3,4-oxadiazoles are employed in intramolecular cycloadditions, giving access to nonsymmetrical products.[170] Work by Padwa and Price had demonstrated that vindorosine (**324**) and related alkaloids could be accessed through the 1,3-dipolar cycloaddition of a carbonyl ylide species and a tethered indole dipolarophile.[171] By tethering both the olefin and the indole ring to a suitably substituted 1,3,4-oxadiazole, Boger and co-workers found that the pentacyclic skeleton of vindorosine (**324**) could be accessed rapidly from the relatively simple precursor **320** in a single step.[172] Heating of a solution of **320** in triisopropylbenzene at 230 °C led to its slow, but efficient, conversion into hexacyclic product **323** (Scheme 44). An inverse-electron-demand Diels–Alder reaction between the oxadiazole ring and the tethered enol ether substituent leads to the initial formation of **321**, followed by extrusion of nitrogen to form carbonyl ylide intermediate **322**. A stereoselective 1,3-dipolar cycloaddition then ensues, to give the desired product **323**. In all, three rings, four carbon–carbon bonds, and six stereocenters (four of them quaternary) are formed in this cascade. The *endo* selectivity observed in this case,[172] and also in the work of Padwa and Price,[171] is attributed to the conformational preference of the tethered dipolarophile. Interestingly, the efficiency of this cascade sequence was found to be strongly dependent on the concentration of the reaction mixture, with dilute solutions giving the best results. The use of the corresponding *E*-enol ether **325** (which led to the formation of the undesired 17*S* epimer of hexacyclic product **323**) gave higher yields in the cascade sequence at higher reaction concentrations. As precursor **320** is achiral, hexacyclic product **323** was formed as a racemate; however, it could be resolved by HPLC on a chiral stationary phase, thus providing access to (−)-vindorosine.[171] Besides vindorosine, Boger and co-workers have used analogous cascades to prepare a number of other members of this class of alkaloids.[173,174]

Several groups have prepared the class 1 *Galbulimina* alkaloid himbacine (**334**) by means of an intramolecular Diels–Alder reaction.[175] In an extension of this approach, Baldwin et al. designed and executed a biomimetic cascade to install three of the four rings of the target molecule in a single step (Scheme 45 a). They postulated that reductive condensation of diketone **326** with an appropriate amine would generate a cyclic unsaturated iminium ion **327**, which would undergo a Diels–Alder reaction to form the tetracyclic structure (Scheme 45 b).[176,177] With this hypothesis as both

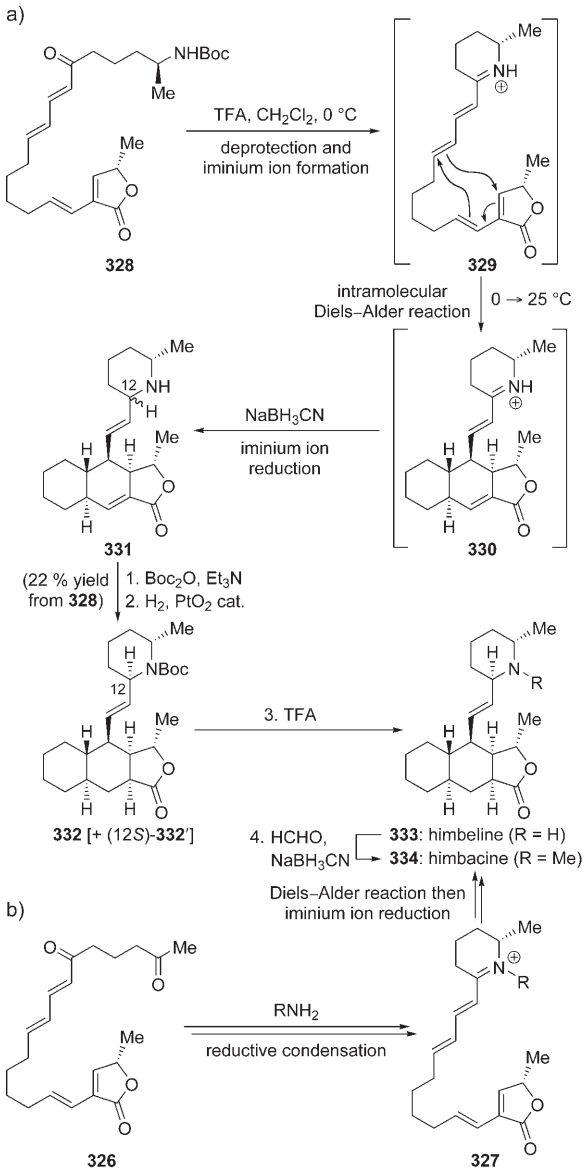

Scheme 45. Cyclization/cycloaddition cascades in the total synthesis of himbeline (**333**) and himbacine (**334**): a) biomimetic approach; b) proposed biosynthesis (Baldwin et al., 2005).[176]

 © 2006 Wiley-VCH Verlag GmbH & Co. KGaA, Weinheim

their guide and inspiration, the team prepared tetraene **328**, in which the chiral secondary amine was already incorporated in a protected form. Exposure of **328** to TFA in CH_2Cl_2 effected the cleavage of the Boc protecting group and catalyzed the formation of the cyclic iminium ion **329**. Conjugation with the iminium ion species served to activate the adjacent diene system (through the lowering of the LUMO energy) towards intramolecular Diels–Alder reaction with the other diene unit, forming tetracyclic species **330**. Brief treatment of the reaction mixture with sodium cyanoborohydride then gave amine **331**. While the Diels–Alder event was highly diastereoselective, forming a single 6,6,5-tricyclic system, the final reductive quench of iminium ion **330** displayed no facial selectivity, with amine **331** produced as a 1:1 mixture of epimers at the C12 position. Separation of this epimeric mixture was postponed until after Boc protection of the secondary amine and selective hydrogenation of the trisubstituted olefin to give **332**, along with its C12 epimer, in modest overall yield from **328**. Amine **332** was converted into himbeline (**333**) and then himbacine (**334**) through standard procedures. The other epimer of the cascade product, (12*S*)-**332′**, could similarly be transformed into another member of this class of natural products, namely himandravine (not shown), the C12 epimer of himbacine (**334**).[178]

Transannular Diels–Alder reactions have been used widely in the synthesis of complex natural products. The conformational constraints imposed by the macrocyclic nature of the substrates often provide a high degree of stereocontrol in these processes. This area was the subject of a recent review by Deslongchamps, a pioneer of the transannular Diels–Alder reaction.[179] Two striking examples that have appeared in the literature since that survey are included here to demonstrate the power of the reaction in cascade sequences. The first is the total synthesis of the insecticide spinosyn A (**338**, Scheme 46) by Roush and co-workers.[180] In their total synthesis of this target, Evans and Black had previously observed that the natural conformational preference of an intramolecular Diels–Alder substrate favored formation of the undesired *endo* adduct.[181] This was successfully overcome in their synthesis by the use of a chiral auxiliary, however, this strategy would not be possible in the context of a transannular cycloaddition. Roush and co-workers combined the use of a fully functionalized macrocyclic substrate with a bromide stereodirecting substituent on the diene to achieve excellent stereocontrol in favor of the correct isomer. As shown in Scheme 46, the cascade begins from the linear precursor **335**, which undergoes an *E*-selective Horner–Wadsworth–Emmons macrocyclization[182] to give pentaene **336**. This intermediate spontaneously undergoes a transannular Diels–Alder reaction to form **337**, with the correct stereochemistry for spinosyn A (**338**). Steric repulsion between the vinylic bromide and the C9 alkoxy substituent helps to ensure that **336** reacts through the conformation shown,[183] while the overall conformation of the macrocyclic ring improves the selectivity through the influence of distant stereogenic centers, such as that at C21. This highly efficient conversion (**335**→**337**) facilitated the completion of the total synthesis of (−)-spinosyn A (**338**).

The total synthesis of the antitumor polyketide (−)-FR182877 (**344**, Scheme 47) was completed by the groups of Sorensen and Evans, with both employing a transannular Diels–Alder cascade sequence. Sorensen and co-workers proposed that the polycyclic ring system of (−)-FR182877 (**344**) could be formed through two Diels–Alder processes

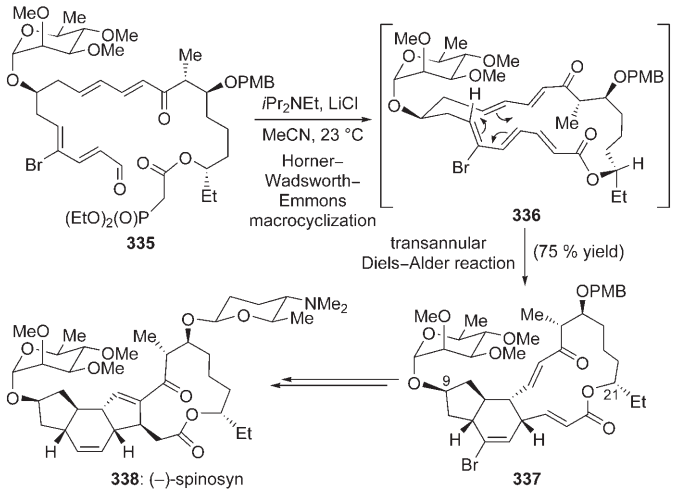

Scheme 46. Total synthesis of spinosyn (**338**) using a macrocyclization/transannular Diels–Alder cascade (Roush et al., 2004).[180]

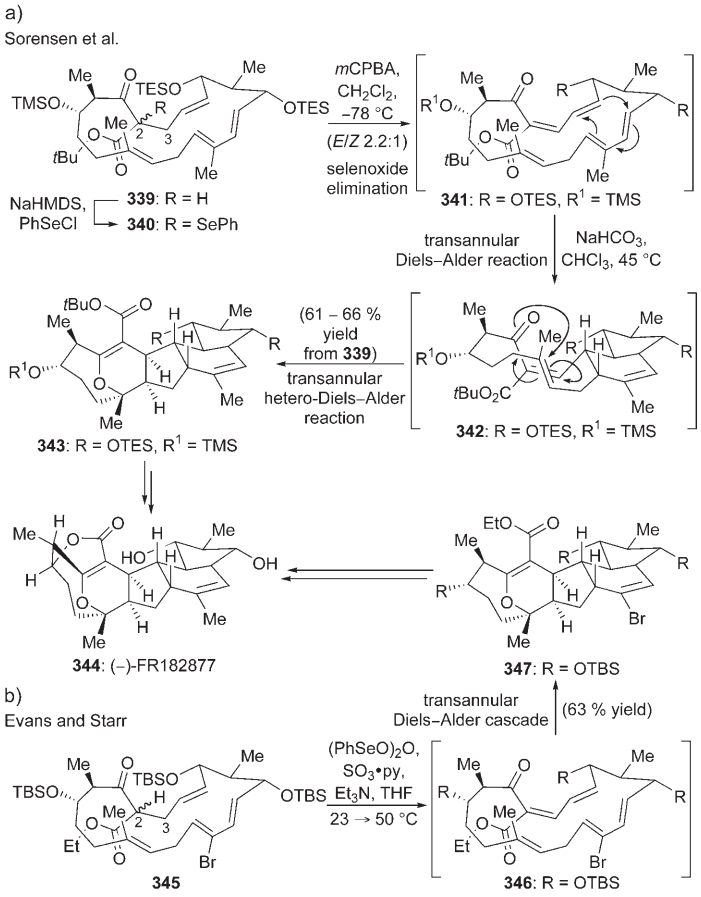

Scheme 47. Transannular Diels–Alder cascades in the total synthesis of (−)-FR182877 (**344**; Sorensen et al., 2002; Evans and Starr, 2002).[188,189]

 © 2006 Wiley-VCH Verlag GmbH & Co. KGaA, Weinheim

and a condensation event to form a large ring,[184] a hypothesis that was supported by the isolation and biosynthetic investigation of the related natural product hexacyclinic acid.[185] Their initial synthetic studies focused on a sequence involving an intramolecular Diels–Alder reaction followed by formation of a macrocycle and eventual hetero-Diels–Alder reaction.[186] Ultimately, their successful synthetic plan was based upon the construction of a polyketide macrocycle, which would undergo transannular Diels–Alder and hetero-Diels–Alder reactions to form the complex pentacyclic framework of the target compound. Their first total synthesis of FR182877 yielded the unnatural (+)-enantiomer,[187] however, their optimized sequence gave the natural (−)-antipode **344** (Scheme 47a).[188] The efficiency of the transannular Diels–Alder cascade hinged on the selectivity of the oxidation reaction used to introduce the crucial C2−C3 double bond into precursor **341**. In the absence of this element of unsaturation, macrocycle **339** did not undergo transannular cycloaddition, as the dienophile is not activated by conjugation. It was found that selenation of keto-ester **339**, using phenyl selenium chloride and sodium hexamethyldisilazide in diethyl ether at room temperature gave a 10:1 ratio of selenide products in favor of the desired epimer. Oxidation led to facile selenoxide elimination to generate pentaene **341**. Warming of the reaction mixture to 45 °C triggered the cycloaddition sequence (**341**→**342**→**343**), giving a good overall yield of the desired pentacyclic stereoisomer **343**. The selenoxide elimination step also formed a smaller amount of the alkene with a *Z*-configured C2=C3 bond (not shown), which in turn followed its own divergent cycloaddition pathways, yielding by-products which account for most of the mass balance in this reaction. Nevertheless, this optimized route allowed the Sorensen group to prepare multigram quantities of advanced intermediate **343**, ensuring a reliable supply of the natural product **344**.

Evans and Starr also identified a Diels–Alder cascade as a potential route to (−)-FR182877 (**344**).[189] They prepared a similar precursor, **345**, which underwent oxidation to **346** and the transannular Diels–Alder cascade in an efficient one-pot procedure (Scheme 47b). Their advanced cascade product **347** was formed as a single diastereoisomer in good yield. As both groups of researchers had observed poor selectivity in intramolecular Diels–Alder reactions of related substrates, Evans and Starr calculated the effect of the macrocycle on the selectivity of the cascade sequence. They found that the C6-C7-C8 stereotriad alone had little effect on the facial selectivity of the cycloaddition, even within a macrocyclic environment, due to its local symmetry. However, including either of the C18 or C19 stereocenters in the calculations led to a preference for the desired selectivity. The reinforcing effect of having both stereocenters present was shown to be responsible for the excellent selectivity observed in the initial transannular cycloaddition, further emphasizing the ability of a macrocyclic framework to transmit stereochemical control from seemingly remote stereocenters.

Highlighting the various syntheses of (−)-colombiasin A (**350**, Scheme 48–Scheme 50) serves to illustrate a compendium of pericyclic cascade processes. As shown in Scheme 48b, the final stages in the biosynthesis of **350** have been proposed to involve the stepwise formation of the bridged bicyclic system from bicyclic compound **348** through initial C1–C9 cyclization to give elisabethin A (**349**) followed by subsequent C2−C12 bond formation.[190] The concomitant isolation of **348**,[191] **349**,[192,193] and **350**,[190] all produced from the same organism (*Pseudopterogorgia elisabethae*), lends credence to this hypothesis (although, of course, not constituting definitive proof for it).

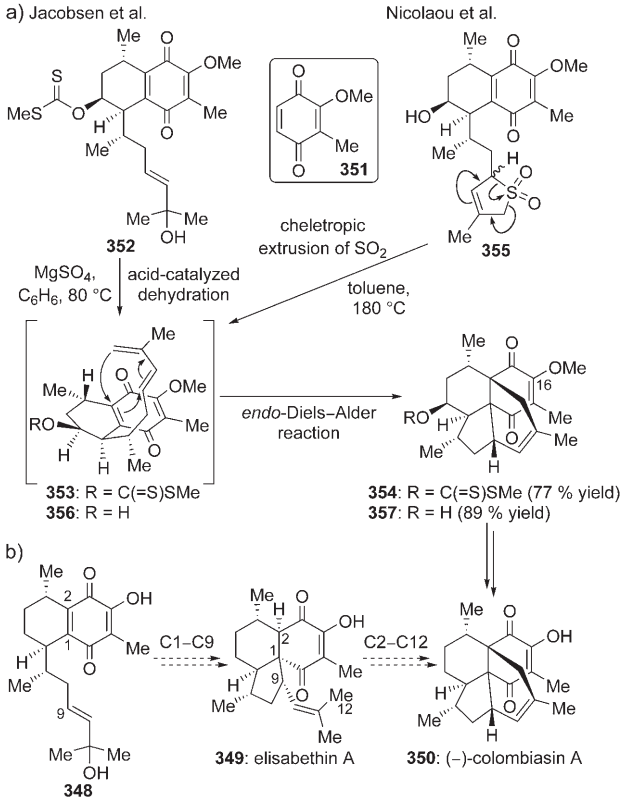

Scheme 48. a) Diene formation/Diels–Alder reactions in the synthesis of (−)-colombiasin A (**350**; Nicolaou et al., 2001; Jacobsen et al., 2005).[194,195] b) Proposed biosynthesis of elisabethin A (**349**) and (−)-colombiasin A (**350**) from bicyclic compound **348**.

Jacobsen and co-workers were keen to investigate a more direct method for the formation of the C1−C9 and C2−C12 bonds from a precursor such as **348**, and to this end they prepared advanced intermediate **352** (Scheme 48a). Heating a mixture of this material and $MgSO_4$ in benzene to reflux initiated a tandem dehydration/*endo*-intramolecular Diels–Alder reaction (**352**→**353**→**354**) to assemble the tetracyclic framework of the target natural product in 77% yield. Barton–McCombie reduction of the xanthate ester group to the corresponding alkane (nBu$_3$SnH/cat. AIBN) followed by demethylation of the C16 hydroxy group ($AlCl_3$, $PhNMe_2$) then completed the concise total synthesis of (−)-colombiasin A (**350**).[194] A related intramolecular Diels–Alder cascade approach had previously been employed by Nicolaou et al. in their approach to the same target.[195] In this case, the in situ generation of diene **353** was achieved through the cheletropic extrusion of SO_2 from sulfone **355**.[196] Note that the initial masking of the sensitive diene as the corresponding sulfone

 © 2006 Wiley-VCH Verlag GmbH & Co. KGaA, Weinheim

was essential in order to enable the generation of the quinone portion of the cascade precursor **355**.

The most recently reported total synthesis of (−)-colombiasin A (**350**) came from Davies et al., who deployed their combined C–H insertion/Cope rearrangement methodology[197] as one of the defining transformations.[198] Slow addition of methyl vinyl diazoacetate (**358**, 3.0 equiv) to a solution of racemic dihydronaphthalene **359** and chiral rhodium(II) catalyst **360** (2 mol%) in 2,2-dimethylbutane at room temperature triggered the sequence of events shown in Scheme 49. Initial rhodium carbenoid formation (**358**→**362**) was followed by enantioselective intermolecular C–H insertion to give β,γ-unsaturated ester **363** as a fleeting intermediate which, under the conditions of the reaction, underwent Cope ([3,3] sigmatropic) rearrangement to form **364** (presumably via the expected chairlike transition conformation shown). Isolation of the cascade product was postponed until after hydrogenation of both alkenes and reduction of the ester group to the corresponding primary alcohol to give **365** in 34% overall yield from dihydronaphthalene **359** and, perhaps more significantly, as a single diastereoisomer and with over 95% *ee*! Three new stereogenic centers were therefore formed in a single operation from achiral starting materials employing only 2 mol% of a chiral catalyst, which demonstrates the enormous potential of this C–H activation methodology. The C–H functionalization step (**359**→**363**) is particularly noteworthy as a result of the discrimination between the two enantiomers of dihydronaphthalene **359** by the chiral rhodium carbenoid **362**. Thus, while the (*S*)-dihydronaphthalene enantiomer undergoes the desired C–H insertion, the corresponding *R* enantiomer preferentially undergoes cyclopropanation to give **366** in 36% yield and with over 95% *ee* following hydrogenation and ester reduction. As such, the conversion of racemic **359** into enantiomerically enriched **364** can be regarded as a kinetic resolution.[199]

The syntheses of (−)-colombiasin A (**350**) by the groups of Nicolaou, Jacobsen, and Davies all began with the same quinone starting material, **351** (Scheme 48), onto which the remainder of the polycyclic architecture was cleverly appended. In another highly original approach, Harrowven et al. introduced the quinone ring at a late stage in the synthetic sequence through the domino process illustrated in Scheme 50.[200] Heating of a solution of squarate derivative

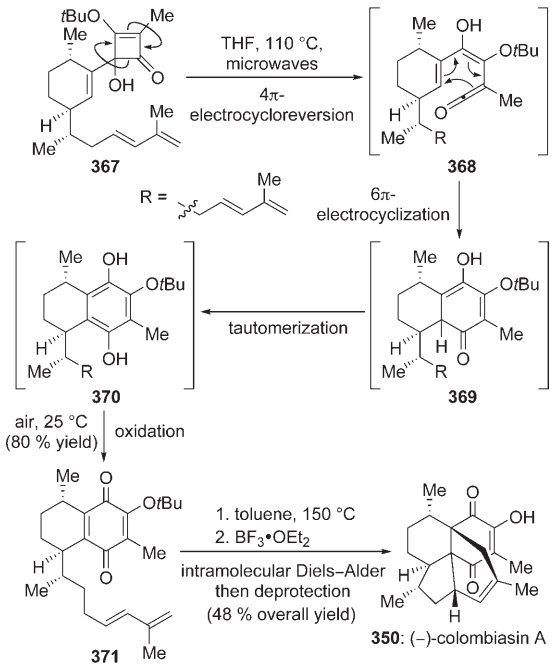

Scheme 50. Electrocyclization reactions in the synthesis of (−)-colombiasin A (**350**; Harrowven et al., 2005).[200]

367 in THF to 110°C under microwave irradiation[107] triggered a Moore rearrangement,[201] involving sequential 4π-electrocycloreversion (**367**→**368**), 6π-electrocyclization (**368**→**369**), and tautomerization (**369**→**370**) steps to deliver the fully substituted aromatic derivative **370** as a single regioisomer. Following the complete conversion of **367** into **370**, exposure of the crude reaction mixture to air resulted in facile oxidation to form quinone **371**, which was isolated in

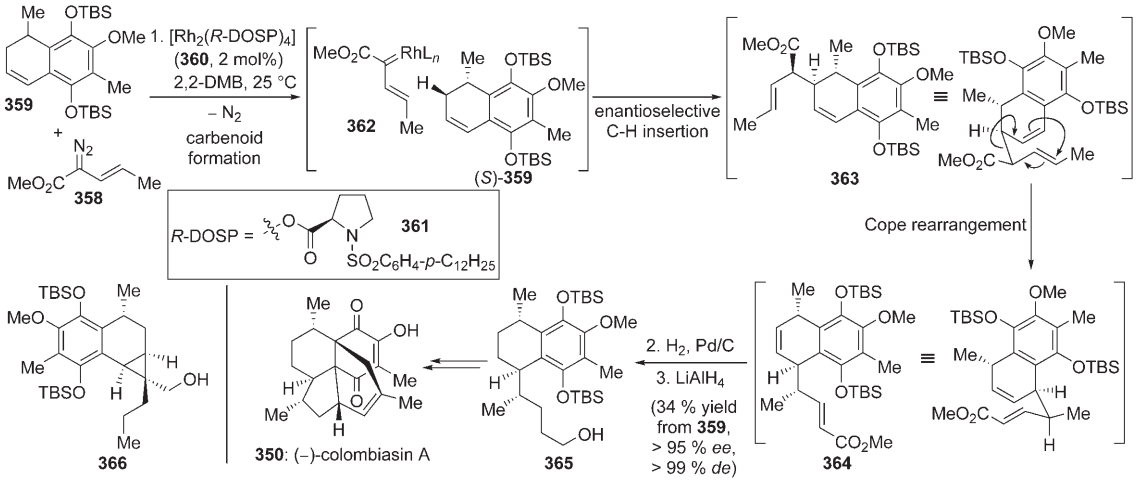

Scheme 49. Enantioselective C–H insertion/Cope rearrangement cascade in the synthesis of (−)-colombiasin A (**350**; Davies et al., 2006).[198]

 © 2006 Wiley-VCH Verlag GmbH & Co. KGaA, Weinheim

80% overall yield from cyclobutenone **367**. With **371** in hand, intramolecular Diels–Alder reaction followed by cleavage of the *tert*-butyl protecting group was all that was required to complete the total synthesis of this intriguing marine natural product.

The close structural relationships between various members of this family of marine-derived diterpenes was underscored by the conversion of (−)-colombiasin A (**350**) into (−)-elisapterosin B[202] (**375**, Scheme 51) reported by Jacobsen and co-workers.[194] One plausible mechanistic rationale for this transformation invokes a retro [4+2] cycloaddition to give quinone **372**, followed by Lewis acid catalyzed [5+2] cycloaddition[203] to generate the rearranged carbocyclic framework in a remarkable yield of 94%. Proof of the validity of the [5+2] cycloaddition step had already been provided in the pioneering total synthesis of (−)-elisapterosin B (**375**) by Rychnovsky and Kim,[204a] who converted quinone **376** into the natural product **375** in 41% yield by treatment with a large excess of $BF_3{\cdot}OEt_2$ (25 equiv) in CH_2Cl_2 at −78 °C. By analogy with Lewis acid catalysis of the Nazarov cyclization,[204b] Rychnovsky and Kim proposed that coordination of the boron species to the quinone generates a 4π-electron pentadienyl cation intermediate (e.g. **373**) which can undergo a thermally allowed cycloaddition with the pendant alkene. A similar protocol was subsequently applied by Harrowven and co-workers on the related *tert*-butyl ether **370**, to give (−)-elisapterosin B (**375**) in 71% yield.[200]

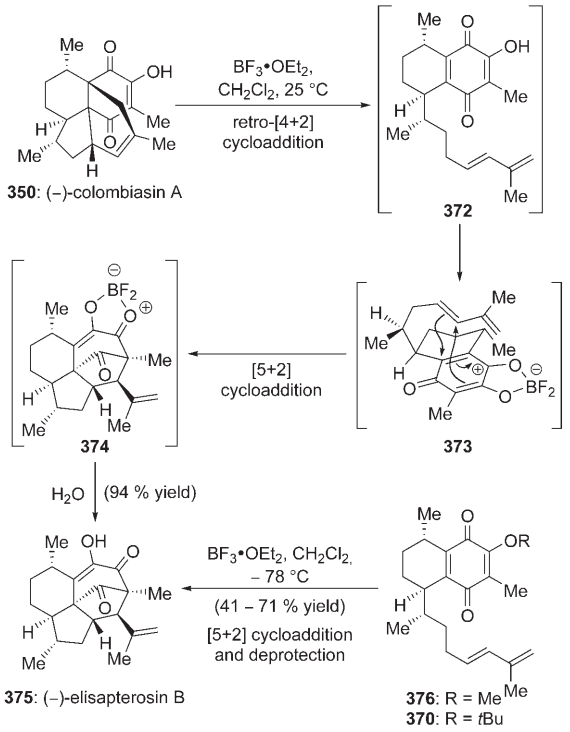

Scheme 51. Conversion of (−)-colombiasin A (**350**) into (−)-elisapterosin B (**374**) by a retro-Diels–Alder/[5+2] cycloaddition cascade (Jacobsen et al., 2005),[194] and formation of (−)-elisapterosin B from a quinone precursor (Rychnovsky and Kim, 2003; Harrowven et al., 2005; Davies et al., 2006).[198,200,204]

For the sake of completeness, we shall conclude our foray into the chemistry of gorgonian diterpene metabolites by highlighting the elegant biogenetically inspired synthesis of (+)-elisapterosin B (**385**, Scheme 52a) by Rawal and co-workers that features a conceptually different approach to formation of the bridged bicyclic system.[205] Treatment of tricyclic compound **381** (*ent*-2-*epi*-elisabethin A), in which the C1–C9 bond is already in place, with CAN in acetonitrile at 0 °C resulted in oxidative cyclization (possibly by the pathway shown)[206] to create the final ring junction and install the remaining two stereocenters, leading to the formation of triketone **384**. At this point, addition of pyridine and triethylamine to the reaction mixture, followed by gentle warming to 50 °C, resulted in enolization to give (+)-elisapterosin B (**385**, the enantiomer of the natural product) in 84% overall yield from **381**. A key step in the synthesis of tricyclic compound

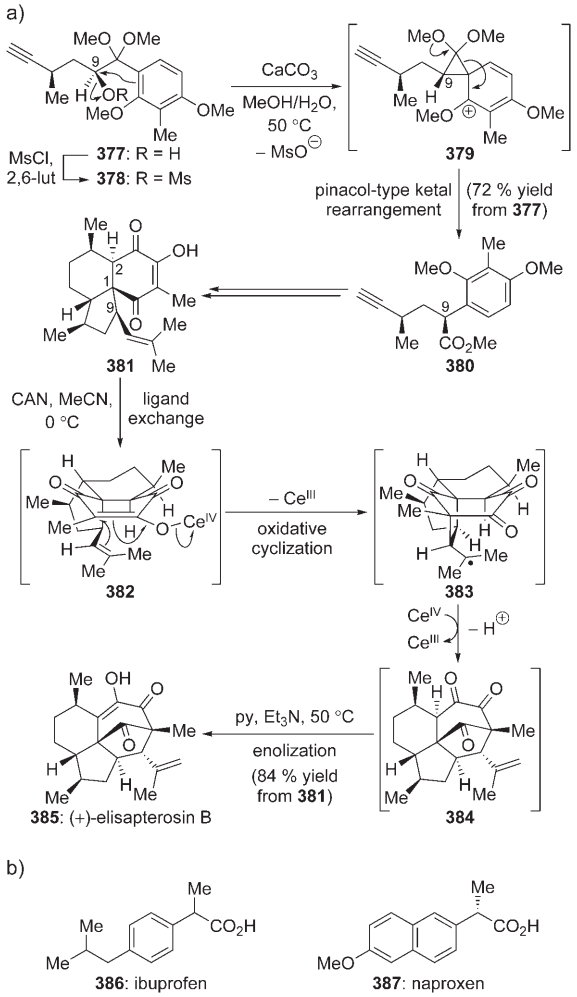

Scheme 52. a) Pinacol-type rearrangement and oxidative cyclization cascades in the total synthesis of (+)-elisapterosin B (**385**; Rawal et al., 2003).[205] b) Structures of the nonsteroidal anti-inflammatory drugs ibuprofen (**386**) and naproxen (**387**).

 © 2006 Wiley-VCH Verlag GmbH & Co. KGaA, Weinheim

381 was the pinacol-type ketal rearrangement of mesylate **378** to give α-aryl ester **380**, involving migration of the electron-rich aryl ring (with inversion of stereochemistry at the C9 position) via bridged phenonium ion **379**. This type of rearrangement, initially developed by Tsuchihashi and co-workers,[207] provides a potentially useful stereocontrolled entry to the α-aryl alkanoic acid class of compounds, which includes the widely used nonsteroidal anti-inflammatory drugs ibuprofen (**386**) and naproxen (**387**) shown in Scheme 52b.[208]

As demonstrated by the syntheses of the endiandric acids (Scheme 3) and (−)-FR182877 (**344**, Scheme 47), the linking of sequential pericyclic processes into a single cascade can lead to rapid and dramatic increases in molecular complexity. Another example is provided by the novel anti-angiogenic fungal metabolites epoxyquinols A (**392**) and B (**393**, Scheme 53). These molecules have been proposed, by Osada and co-workers, to arise through oxidation of quinol **388** to give dienal **389**, followed by 6π-electrocyclization to give a mixture of diastereomeric 2*H*-pyrans **390** and **391** and subsequent intermolecular cycloaddition.[209] Epoxyquinol A (**392**) would be formed through an *endo*-Diels–Alder heterodimerization between one molecule of **390** and one molecule of **391**, while the formation of epoxyquinol B requires a [4+2] homodimerization between two molecules of **390** in an *exo* alignment. Interest in this class of compounds was heightened by the isolation, at a later date, of epoxytwinol A (**394**) from the same fungus.[210] This C_2-symmetric pentaketide dimer would arise from a formal [4+4] cycloaddition between two molecules of **390**.

The challenge of reducing these biosynthetic hypotheses to practice inspired a number of groups to tackle the total synthesis of these natural products. Hayashi and co-workers were the first to disclose their route to the epoxyquinols,[211] followed shortly thereafter by the groups of Porco,[212] Mehta,[213] and Kuwahara.[214,215] Each of these elegant syntheses featured a different route to the monomeric precursor **388**, but all then successfully employed the key oxidation/electrocyclization/Diels–Alder cascade.[216]

Studies by the groups of Hayashi[217] and Porco[218] also culminated in the enantioselective synthesis of epoxytwinol A (**394**). For the sake of brevity, however, we shall highlight only the results from Porco and co-workers, as summarized in Scheme 53 and Scheme 54. Selective oxidation of the primary hydroxy group in diol **388** using conditions developed by Semmelhack et al. (cat. TEMPO, cat. CuCl, 1 atm O_2, DMF, 25 °C)[219,220] provided a 9:1 equilibrium mixture of 2*H*-pyran epimers **390**/**391** and aldehyde **389**. Stirring this crude oxidation product mixture in CH_2Cl_2/MeOH (100:7) at room temperature triggered the various modes of dimerization, to give epoxyquinols A (**392**, 16% yield from **388**) and B (**393**, 21%) and epoxytwinol A (**394**, 10%). The fact that these oxidation/dimerization cascades occur spontaneously under ambient conditions suggest that they need not be enzyme-controlled.

Detailed mechanistic studies by Hayashi and co-workers indicate that the particular transition-state arrangements leading to epoxyquinols A (**392**) and B (**393**) are favored not only by approach of the larger methyl substituents *anti* to one another, but are also stabilized by intermolecular hydro-

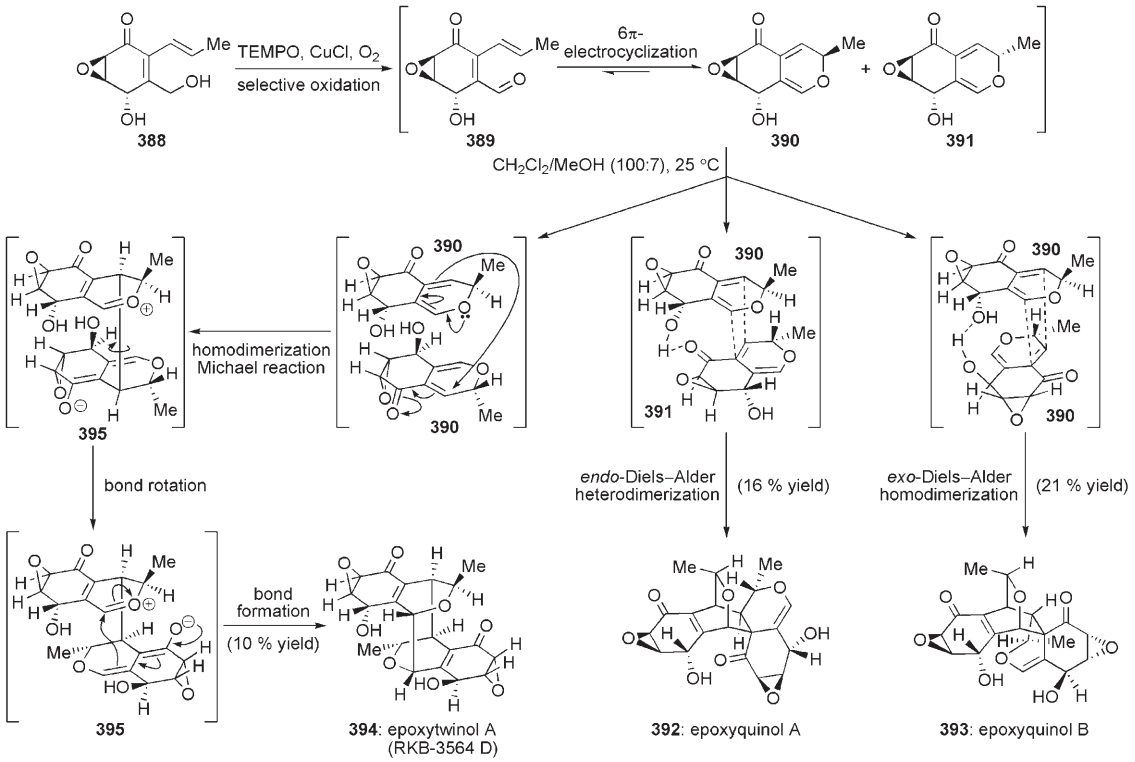

Scheme 53. Pericyclic and Michael reaction cascades in the total synthesis of epoxyquinols A (**392**) and B (**393**) and epoxytwinol A (**394**; Hayashi et al., 2002; Porco et al., 2002).[211,212,218]

 © 2006 Wiley-VCH Verlag GmbH & Co. KGaA, Weinheim

gen-bonding interactions as shown.[221] The [4+2] homodimerization of two molecules of 2*H*-pyran epimer **391** is apparently very unfavorable, and was not observed by Porco and co-workers.[222]

Of particular interest is the dimerization pathway leading to epoxytwinol A (**394**). [4+4] Cycloaddition reactions are electronically forbidden processes under thermal conditions and are generally conducted under photochemical irradiation[223] or with transition-metal catalysts.[224,225] A stepwise, ionic mechanism for the formation of epoxytwinol A (**394**) has therefore been invoked.[218] Intermolecular Michael reaction between two molecules of **390** initially gives zwitterionic intermediate **395**, which then undergoes rotation about the newly formed carbon–carbon bond to enable subsequent ring closure of the dienolate species onto the oxonium ion.

Whilst the cascades described above provided a concise approach to the target natural products (**392**, **393**, and **394**), Porco and co-workers were still interested in developing reaction conditions which would favor [4+4] cycloaddition over the predominant [4+2] Diels–Alder pathways. As shown in Scheme 54, it was found that the use of an alkoxysilanol

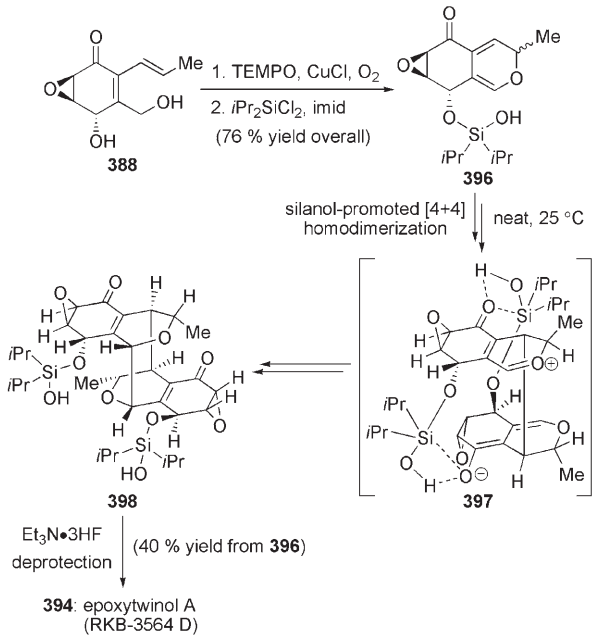

Scheme 54. Silanol-promoted formal [4+4] dimerization reaction for the selective formation of epoxytwinol A (**394**; Li and Porco, 2004).[226]

protecting group on the secondary alcohol redirected the inherently favored [4+2] dimerization pathway to a [4+4] manifold to exclusively generate the epoxytwinol molecular architecture in respectable overall yield.[226] The reasons behind the choice of a seemingly rather exotic silanol protecting group[227,228] are twofold: 1) the Diels–Alder reactions to form **392** or **393** (Scheme 53) place the hydroxy group(s) in more sterically encumbered positions than required in the corresponding [4+4] pathway, thus bulky protecting groups might be expected to discourage the [4+2] cycloadditions, and 2) formation of a templated intermediate such as **397** (Scheme 54), which is stabilized by both hydrogen bonding and interaction of the oxygen anion and carbonyl oxygen center with the electropositive silicon atoms, could facilitate the initial Michael addition in the [4+4] pathway. Whatever the precise mechanistic basis, this innovative use of a silanol as a directing group provided an elegant solution to the problem at hand.

The total syntheses of the immunosuppressant agents SNF4435 C (**399**) and D (**400**, Scheme 55), reported independently by the groups of Parker,[229] Baldwin,[230] and Trauner,[231] represent an "endiandric acid cascade" for the 21st century.[232] By analogy with the endiandric acids, the bicyclo[4.2.0]octadiene core of SNF4435 C (**399**) and D (**400**) would be derived from sequential 8π-conrotatory and 6π-disrotatory electrocyclizations of the appropriately configured tetraene precursor **401**.[233] In comparing the three total syntheses, one of the most striking observations is their common reliance on palladium-catalyzed cross-coupling reactions to assemble the tetraene backbone. These processes compare favorably with the more laborious preparation of the endiandric acid cascade precursor **13** (Scheme 3) more than twenty years earlier (when such cross-couplings were still a nascent technology) through a classical Glaser acetylene coupling[234,235] followed by several further manipulations (a route which in any case would not be amenable to the production of methyl-substituted derivatives of tetraene systems such as **13**).

Parker and Lim effected the Stille coupling of vinyl iodide **402** with stannane **403** to furnish the putative tetraene intermediate **401**, which, under the conditions of the reaction, spontaneously underwent the electrocyclization cascade to afford a 3.8:1 mixture of SNF3345 C (**399**) and D (**400**). Trauner and Beaudry subsequently coupled the complementary reaction partners **404** and **405** under modified Stille conditions[236] to provide the target products (**399** and **400**) in an improved overall yield. Baldwin and co-workers extended the proposed biosynthesis of SNF back a further step by speculating that the *Z*,*Z*,*Z*,*E*-tetraene **401** arises from isomerization of the corresponding *Z*,*E*,*E*,*E*-configured precursor **406**,[237] itself a natural product (named spectinabilin) isolated from the same actinomycete strain (*Streptomyces spectabilis*).[238] To their delight, they found that this extended cascade (**406**→**401**→**399** + **400**) could indeed be triggered by heating a solution of synthetic spectinabilin **406** (prepared through Suzuki coupling of **407** and **408** followed by a Negishi coupling to install the remaining vinyl methyl group) in DMF at 70 °C. The modest overall yield for this isomerization/electrocyclization cascade is counterbalanced by the more straightforward synthesis of the key cross-coupling fragments **407** and **408**, compared to that of **402** and **403** or **404** and **405**.

The ratio of synthetic SNF4435 C (**399**) and D (**400**) formed in these cascades (3.0–3.8:1.0) closely parallels that of the compounds found in nature.[239] The origin of this diastereoselectivity lies in the conrotatory 8π-electrocyclization of tetraene **401**, which can proceed through either of the helical transition states **410** or **412**;[240,241] the former is evidently favored to a degree, because in this arrangement the bulky pyrone substituent is orientated away from the interior of the helix. Related 8π-/6π-electrocyclization

 © 2006 Wiley-VCH Verlag GmbH & Co. KGaA, Weinheim

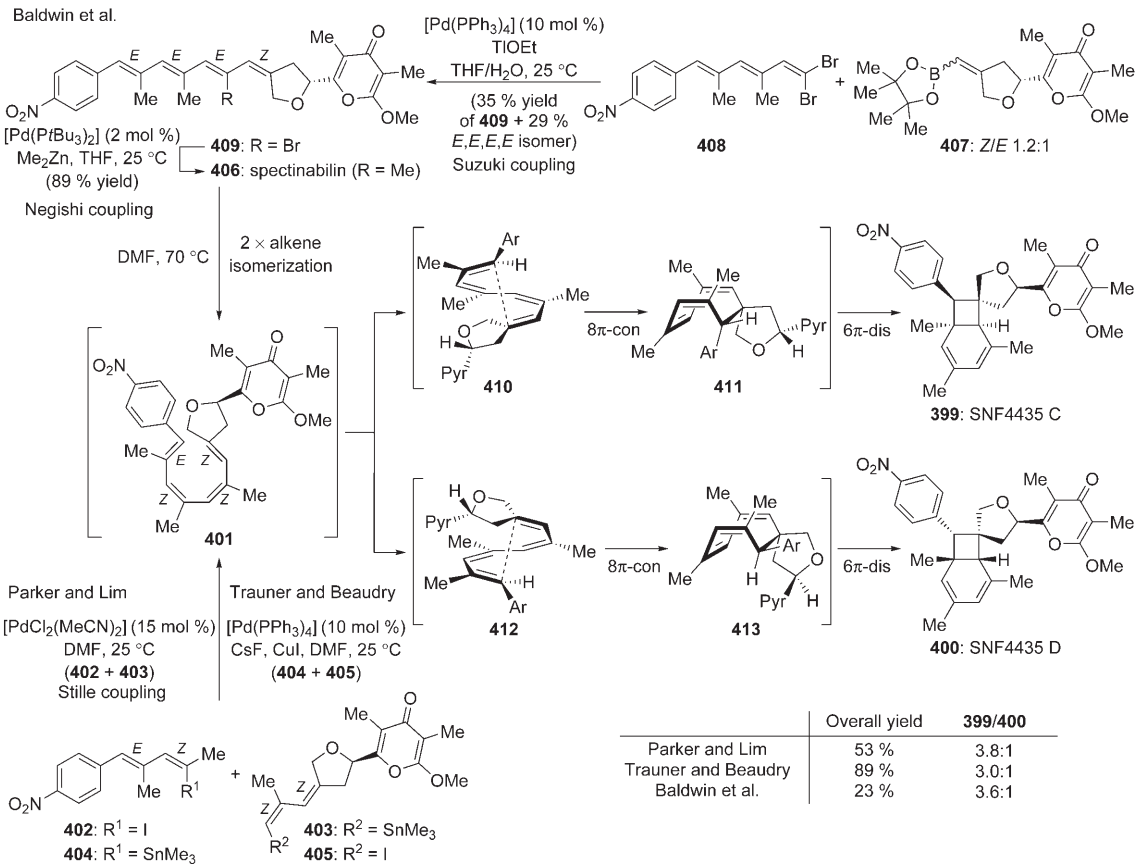

	Overall yield	399/400
Parker and Lim	53 %	3.8:1
Trauner and Beaudry	89 %	3.0:1
Baldwin et al.	23 %	3.6:1

Scheme 55. Total syntheses of SNF4435 C (**399**) and D (**400**) through electrocyclization cascades (Parker and Lim, 2004; Baldwin et al., 2005; Trauner et al., 2005).[229–231]

domino processes have been applied in the total syntheses of several other structurally intriguing natural products.[242–244]

Further proof, if any were needed, of the value of biomimetically inspired synthetic strategies towards natural products is provided by the total syntheses of 1-*O*-methylforbesione (**418**, Scheme 56) reported by Nicolaou and Li[245] and by Theodorakis and co-workers.[246] Heating a solution of readily available xanthone derivative **414** in DMF to 120 °C initiated the Claisen rearrangement/Diels–Alder/Claisen rearrangement cascade, illustrated in Scheme 56 a, to form four new stereogenic centers and two new rings to directly provide the target natural product (**418**) in 51–63 % yield. Most of the mass balance of this reaction comprised the regioisomeric polycyclic structure **419**, which results from the initial [3,3]-sigmatropic rearrangement of the C5, as opposed to C6, allyloxy group, followed by the corresponding intramolecular Diels–Alder reaction. Claisen rearrangement of the C3 allyloxy group was site-selective, with migration occurring exclusively towards the C4 terminus. Circumstantial evidence provided by both groups justifies the sequence of events being as depicted in Scheme 56 a, in which the Claisen/Diels–Alder cascade of ring C precedes the Claisen rearrangement of ring A. This biomimetic route to the 4-oxatricyclo[4.3.1.0]decan-2-one system, first proposed by Quillinan and Scheinmann in 1971,[247] provides access to this formidable cagelike structure with an unrivalled elegance and efficiency, and has found use in the synthesis of the related compounds gambogin[248] (**420**) and 1-*O*-methyllateriflorone (**421**, Scheme 56 b).[249]

The aza-Cope rearrangement/Mannich reaction cascade provides a useful access to 3-acylpyrrolidine systems (Scheme 57 a), which are a common substructure of a diverse collection of alkaloids.[250] Overman and co-workers employed this process in their recent synthesis of the *Stemona* alkaloids didehydrostemofoline (**429**) and isodidehydrostemofoline (**430**, Scheme 57 b).[251,252] Identification of an aza-Cope/Mannich cascade as a key operation en route to the rather unusual polycyclic framework of the target compounds **429** and **430** is aided by their retrosynthetic simplification to common precursor **428**, in which a 3-acylpyrrolidine motif is more clearly visible as part of the tricyclic skeleton. Despite being itself a formidable synthetic target, ketone **428** could be prepared in a single operation from the more readily available bicyclic compound **425**. Treatment of compound **425** with an excess of paraformaldehyde in toluene/MeCN (3:1) at 80 °C led to the initial formation of iminium ion **426**, which then underwent a (reversible) charge-accelerated [3,3]-sigmatropic arrangement[253] to afford enol **427**, with a subsequent irreversible and highly exothermic intramolecular Mannich reaction terminating the sequence. This cascade proceeded in a remarkable overall yield of 94 %, with the stereochemical information in bicyclic precursor **425** being transferred with high fidelity to the more structurally complex rearranged product **428**. Overman and co-workers have been instrumen-

 © 2006 Wiley-VCH Verlag GmbH & Co. KGaA, Weinheim

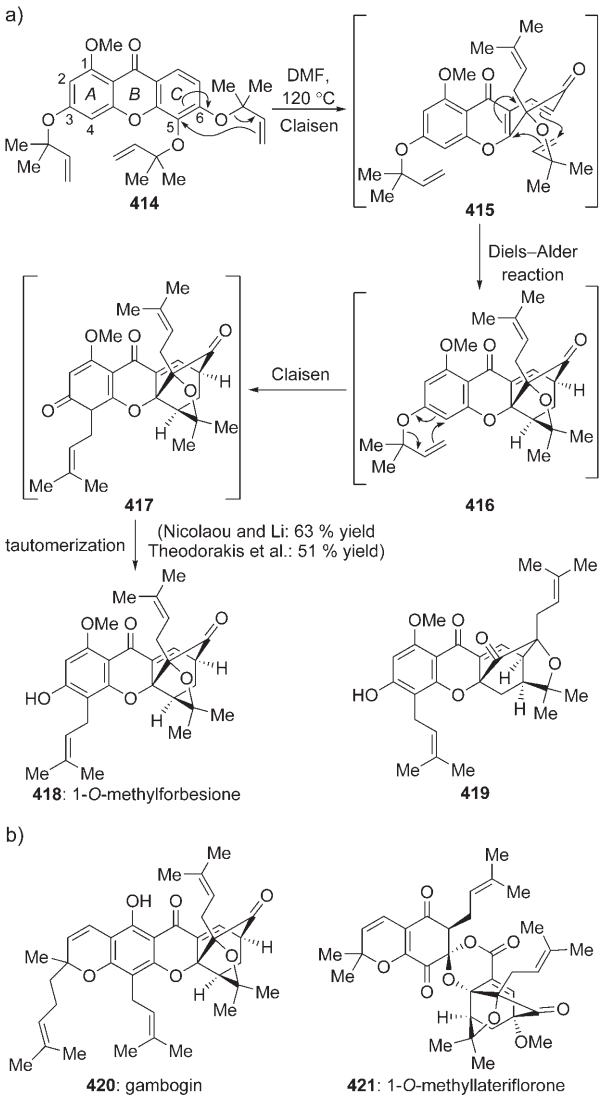

Scheme 56. a) A Claisen/Diels–Alder/Claisen cascade in the total synthesis of 1-*O*-methylforbesione (**418**; Nicolaou and Li, 2001; Theodorakis et al., 2004).[245,246] b) Structures of gambogin (**420**) and 1-*O*-methyllateriflorone (**421**).

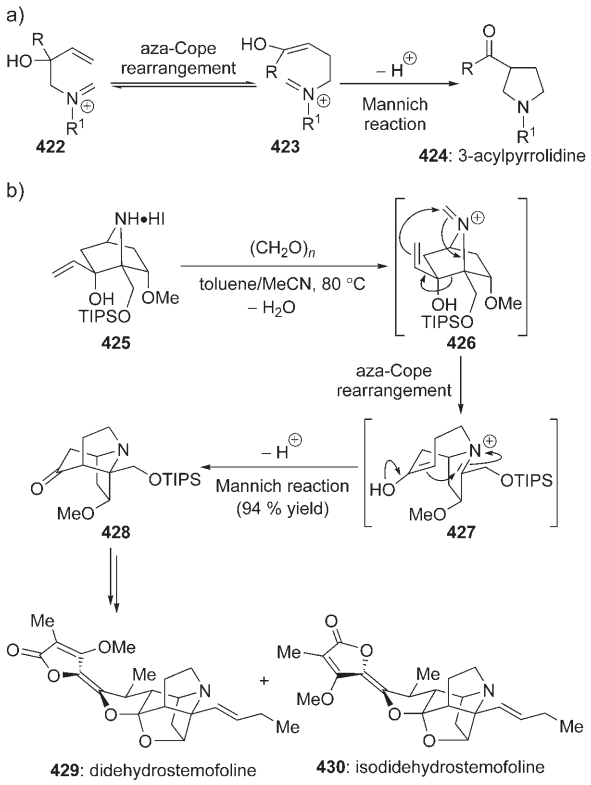

Scheme 57. The aza-Cope/Mannich cascade approach to 3-acylpyrrolidine structures: a) general principles and b) application to the total synthesis of didehydrostemofoline (**429**) and isodidehydrostemofoline (**430**; Overman et al., 2003).[251]

tal in the design and development of the aza-Cope/Mannich cascade[254] and have demonstrated the utility of this methodology in the synthesis of a number of other structurally complex targets, including strychnine,[255] dehydrotubifoline,[256] and 16-methoxytabersonine.[257]

6. Transition-Metal-Catalyzed Cascades

The development of new transition-metal-catalyzed reactions is one of the most vibrant areas of chemical research, and one which is likely to become increasingly important in years to come.[258] Together with organocatalytic reactions[259] and enzymatic processes,[260] transition-metal-mediated reactions offer the potential for generating molecular complexity, and often in an enantioselective fashion, by employing only catalytic amounts of mediators. In doing so, they also meet many of the well-rehearsed criteria required to be labeled "atom-economical transformations".[2] Additionally, whilst many of the cascades described so far have been predicated on the use of biomimetic strategies, transition-metal-catalyzed processes provide synthetic chemists with tools for bond construction for which there are no direct parallels in nature. An enormous variety of transition-metal-mediated cascades have been developed in recent years, but our self-imposed restriction to applications in total synthesis will limit our discussion here to exemplars of just some of the more widely used processes.

It would certainly be hard to overstate the impact that the development of palladium-catalyzed cross-coupling reactions has had on synthetic organic chemistry. Within the last 25 years, these processes have blossomed into extraordinarily powerful tools for carbon–carbon and carbon–heteroatom bond formation, and research in this field continues apace.[261] A wide variety of highly inventive palladium-catalyzed cascades have been applied in total synthesis, but we shall limit our discussion here to just a few instructive examples. For more details on this topic, the reader is directed to several more specific reviews.[262]

Amongst the palladium-catalyzed carbon–carbon bond-forming reactions, the Heck reaction[263] has undoubtedly found the most applications in cascade processes. In particular, the utility of the intramolecular Heck reaction for the generation of tertiary or quaternary stereocenters (in both a

 © 2006 Wiley-VCH Verlag GmbH & Co. KGaA, Weinheim

diastereo- and enantioselective fashion) and multiple-ring systems, even in sterically crowded environments, has been well documented.[264] Keay and co-workers employed an asymmetric polyene Heck cyclization in their enantioselective synthesis of (+)-xestoquinone[265] (**440**, Scheme 58), in which

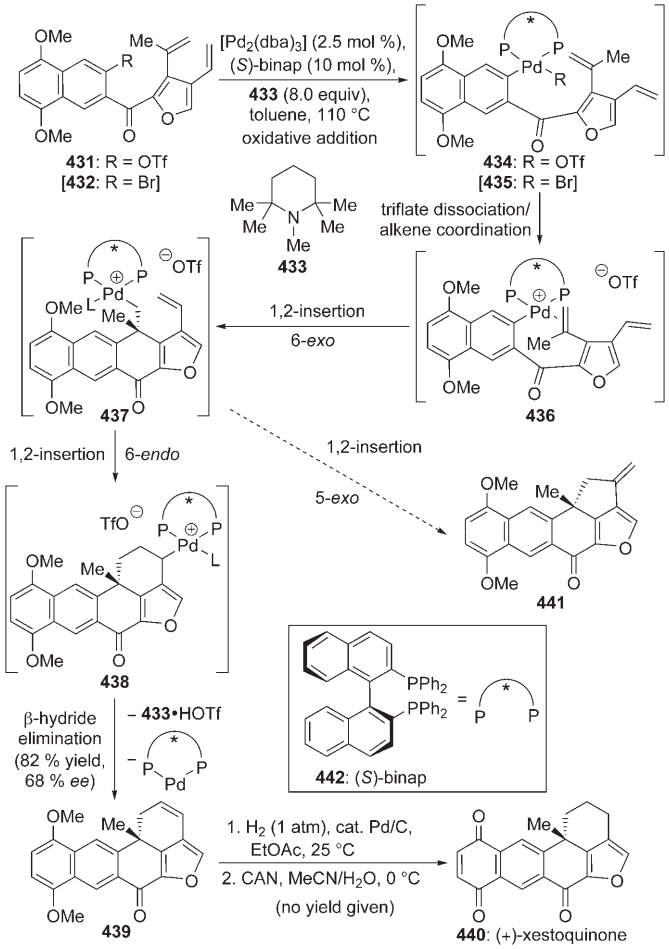

Scheme 58. Use of a catalytic asymmetric Heck polyene cyclization in the total synthesis of (+)-xestoquinone (**440**; Keay et al., 1996).[266]

achiral aryl triflate **431** was converted in a single step into pentacyclic compound **439** under the conditions shown.[266,267] Although the enantioselectivity of this reaction was not optimal, the conversion of **431** into **439** nevertheless provided an elegant solution to both the problems of generation of the imposing polycyclic ring structure and the installation of the isolated all-carbon quaternary stereocenter. This polyene cyclization was originally attempted using aryl bromide **432**, which led to the formation of **439** with poor enantioselectivity (13% *ee* or less). Identification of the corresponding aryl triflate **431** as the optimal substrate for this reaction followed from insights provided by Hayashi and co-workers[268] and Cabri et al.[269] on the mechanism of Heck reactions of aryl triflates employing diphosphine ligands.[270] As shown in Scheme 58, oxidative addition of a Pd^0 species into aryl triflate **431** initially generates Pd^{II} complex **434**. Owing to the kinetic lability of the Pd–OTf bond, dissociation of the triflate counterion followed by alkene π coordination then yields cationic complex **436**. That the chiral binap ligand **442** remains anchored to the metal center through both the alkene coordination event and subsequent 1,2-insertion step to generate σ-alkylpalladium(II) intermediate **437** ensures a higher level of enantioselectivity. Once formed, intermediate **437** can then undergo another migratory insertion reaction (**437**→**438**) followed by β-hydride elimination to deliver pentacyclic compound **439** and regenerate the Pd^0 catalyst. Formation of the 5-*exo* product **441** during the second 1,2-insertion is apparently disfavored by the greater strain energy of the resulting ring system, to the extent that the 6-*endo* mode of ring closure predominates. In contrast, reaction of aryl bromide **432** presumably requires partial dissociation of the diphosphine ligand from the palladium center in the corresponding oxidative addition complex **435**, due to the lower lability of the Pd–Br bond, in order to generate a vacant coordination site for the pendant alkene. This can lead to the substantially diminished enantioselectivity observed experimentally.[271–273]

The Stille reaction has become a well-established method for effecting both intermolecular fragment couplings and intramolecular cyclizations of highly functionalized substrates under mild conditions.[274] The combination of these two processes into a single operation results in a Stille "stitching cyclization" cascade for the generation of macrocyclic structures. Pioneered by Nicolaou et al. in the total synthesis of rapamycin,[275] a more recent application of the stitching cyclization cascade can be found in the synthetic route to the novel ansamycin antibiotic mycotrienin I[276] (**447**, Scheme 59a) developed by Panek and co-workers.[277] Having overcome a number of unanticipated synthetic hurdles en route to bis-*E*,*E*-vinyl iodide **443**, the team was gratified to find that the most daring step in the whole sequence was to proceed with remarkable efficiency. Thus, sequential addition of bis-iodide **443**, enedistannane **444**[278] (1.2 equiv), and iPr_2NEt (1.5 equiv) to a solution of [$PdCl_2$-$(MeCN)_2$] (20 mol%) in DMF/THF (1:1) at room temperature led to the formation of macrocyclic triene **445** over the course of 24 h. Treatment of macrocycle **445** with TsOH in MeOH then resulted in the selective cleavage of the C11 TIPS protecting group (an outcome anticipated by the authors on the basis of earlier model studies, and a maneuver which would subsequently allow for the installation of the amino acid derived side chain on the correct hydroxy group) to give alcohol **446** in 90% overall yield from bis-iodide **443**. The crucial stitching cyclization therefore served to incorporate the missing C6–C7 unit, generate the complete macrocyclic structure, and form the C4–C9 triene with the required *E*,*E*,*E* geometry, all in a single operation![279]

A conceptually similar stitching cyclization cascade had been employed by Smith et al. two years earlier in their approach to the structurally related trienomycin family of metabolites,[280,281] in this case employing Wittig reactions as the key carbon–carbon bond-forming processes. As shown in Scheme 59b for the synthesis of (+)-trienomycin A (**451**), bis-olefination of dialdehyde **448** with phosphonium salt **449**[282] provided the macrocyclic *E*,*E*,*E*-triene in 21% yield, accompanied by a mixture of other triene isomers in a combined

 © 2006 Wiley-VCH Verlag GmbH & Co. KGaA, Weinheim

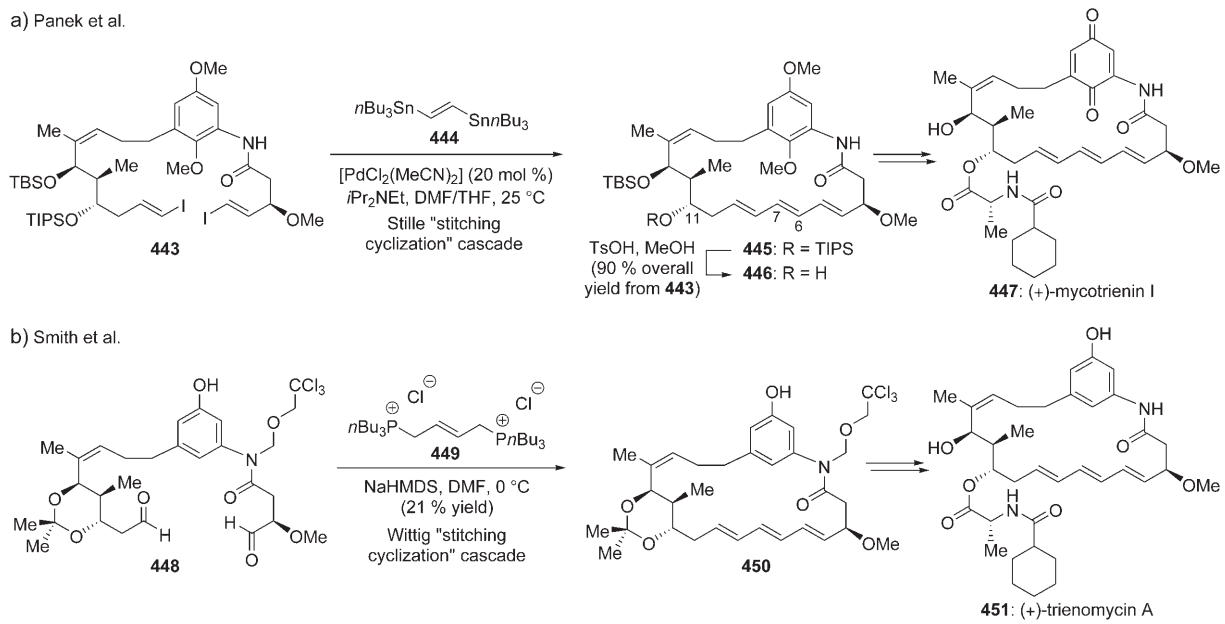

Scheme 59. a) A Stille "stitching cyclization" cascade in the total synthesis of (+)-mycotrienin I (**447**; Panek et al., 1998).[277] b) A Wittig "stitching cyclization" cascade approach to (+)-trienomycin A (**451**; Smith et al., 1996).[280]

yield of 34%. This case illustrates one potential advantage of cross-coupling reactions for the synthesis of polyene systems over more traditional olefination procedures, namely the (generally) reliable and predictable formation of alkene systems of well-defined geometry.

An alternative Stille-based cascade approach to macrocyclic structures, pioneered by Baldwin et al. in 1992[283] and exemplified by the synthesis of elaiolide (**456**, Scheme 60) by Paterson et al., involves the one-pot cyclodimerization of an α-iodo-ω-stannane monomeric precursor.[284] As illustrated in Scheme 60, treatment of ester **452** with copper(I) thiophene-2-carboxylate (10 equiv) in NMP (Liebeskind "palladium-free" Stille coupling conditions)[285,286] led to the formation of the 16-membered C_2-symmetric macrolide **455** in an impressive 80% yield. Note that the reaction proceeded to completion within 15 minutes at room temperature with no trace of the presumed intermediate **454** being isolated. Geometric constraints preclude intramolecular cyclization of precursor **452**, while intramolecular cyclization of the open-chain dimerization intermediate **454** is evidently faster than competing oligomerization processes, at least at the particular concentration used.[287] This one-step cyclodimerization approach to macrolides offers an appealing alternative to conventional esterification/macrolactonization strategies.[288]

One of the most widespread and versatile uses of palladium in organic synthesis is in the generation of heterocyclic ring systems.[289] Flynn and co-workers reported an interesting palladium-catalyzed multicomponent coupling approach to benzo[*b*]furan structures,[290,291] and subsequently applied this methodology to the synthesis of the norsesquiterpenoid frondosin B (**467**, Scheme 61).[292] This well-orchestrated sequence of events began with the treatment of a mixture of readily available *ortho*-bromophenol **457** and alkyne **458** with MeMgBr (2.1 equiv) in THF, leading to the initial formation of the corresponding magnesium phenolate **459** and magnesium acetylide **460**, respectively. Subsequent addition of $[PdCl_2(PPh_3)_2]$ (5 mol%) and heating to 65°C triggered a Kumada cross-coupling reaction[293,294] to give *ortho*-alkynylphenolate intermediate **461**. At this point, dilution of the reaction mixture with DMSO, addition of vinyl bromide **462**, and further heating to 80°C promoted the

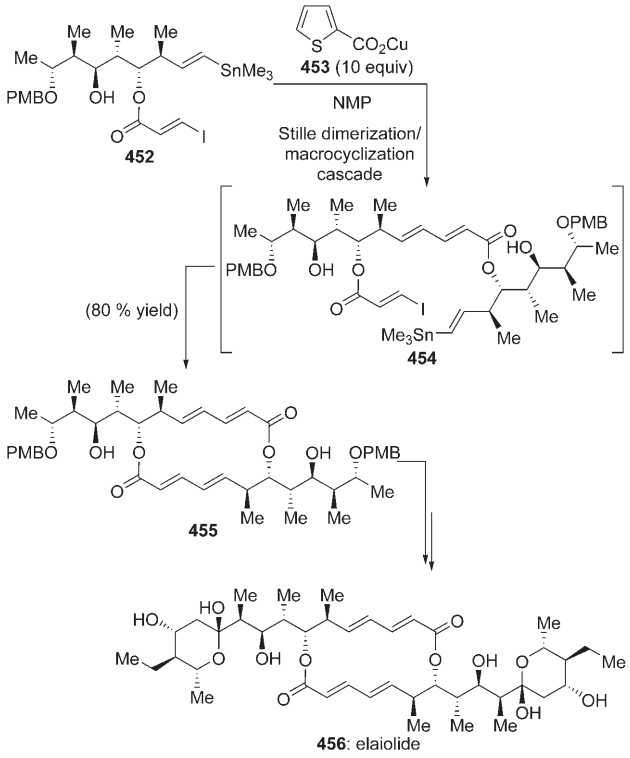

Scheme 60. A "palladium-free" Stille dimerization/macrocyclization approach to the synthesis of elaiolide (**456**; Paterson et al., 1999).[284]

 © 2006 Wiley-VCH Verlag GmbH & Co. KGaA, Weinheim

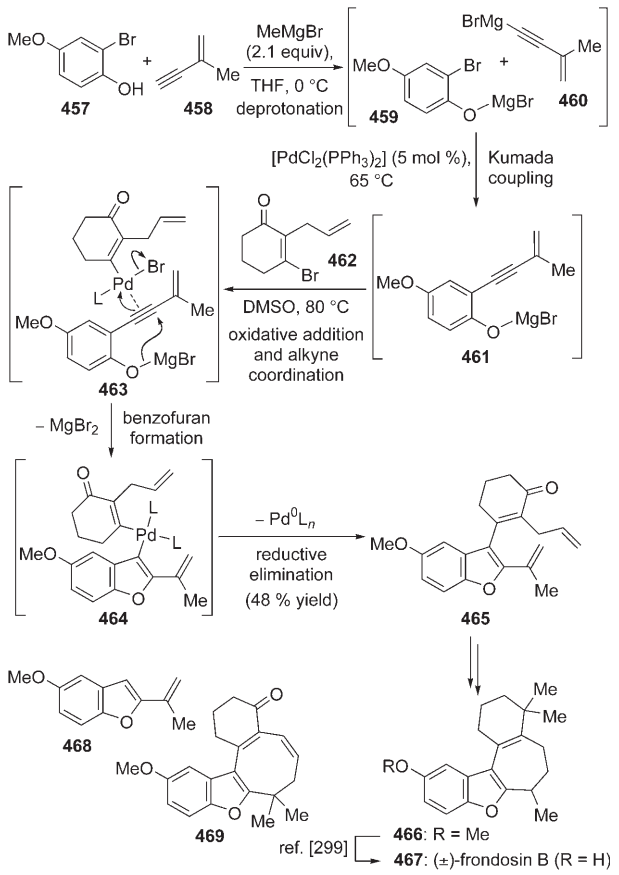

Scheme 61. A palladium-catalyzed multicomponent coupling approach to benzo[*b*]furan structures in the synthesis of (±)-frondosin B (**467**; Flynn et al., 2004).[292]

heteroannulation cascade, via the presumed intermediacy of species **463** and **464**, to afford the 2,3-disubstituted benzo[*b*]-furan product **465** in 48% overall yield.[295–297] Minor by-products concomitantly formed in this reaction were the protocyclized material **468** (12% yield) and tetracyclic compound **469** (11% yield); whilst the former would derive from the direct cyclization of *ortho*-alkynylphenolate intermediate **461**, the latter was speculated to arise from cascade product **465** by a further sequence consisting of an antarafacial 1,7-hydrogen shift followed by conrotatory 8π-electrocyclization.[298] Despite these competing side reactions, the multicomponent coupling cascade enabled the preparation of tricyclic compound **465** in just two steps from commercially available starting materials, with only a further three operations required to reach the complete framework of frondosin B (**467**), as represented by the phenolic methyl ether **466**. Deprotection of **466** to give the target natural product **467** had previously been reported by Danishefsky and co-workers[299] and by Trauner and Hughes[300] in their respective total syntheses.

Over the last 15 years, metathesis-based reactions have made the transition from emerging methodologies to established synthetic techniques in the research laboratory, although, as with palladium-catalyzed cross-couplings, the field is still far from maturity.[301] The ring-opening metathesis polymerization of cyclic olefins, a well-established method for the industrial production of a variety of polymers, can in a sense be viewed as the pinnacle of metathesis-based cascades.[302] In the context of total synthesis, however, a number of elegant cascades triggered by the initial ring-opening metathesis of a strained ring system have also been developed. Selected examples include ring-opening metathesis/sigmatropic rearrangement processes,[303] ring-opening/cross-metathesis cascades,[304–306] and, in particular, ring-opening/ring-closing metathesis ("ring-rearrangement metathesis") strategies.[307] In their recent synthesis of (+)-cyanthiwigin U (**477**, Scheme 62), Phillips and Pfeiffer employed an elegant

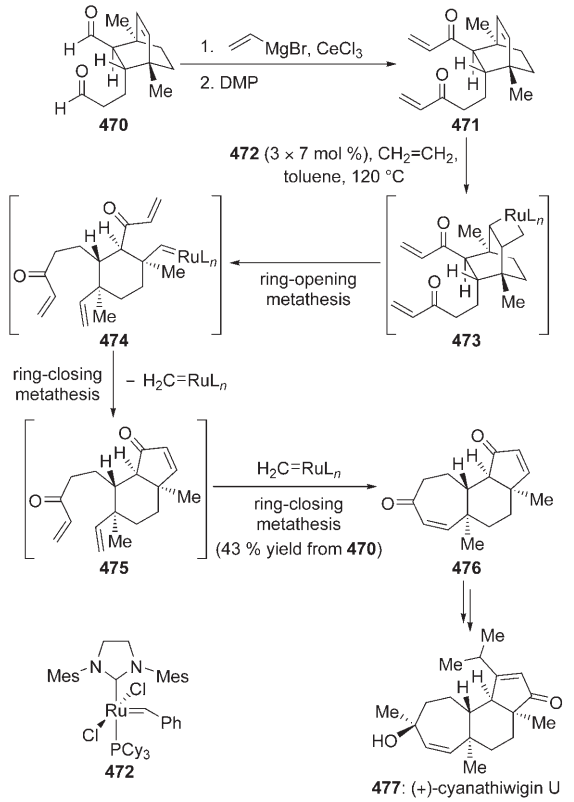

Scheme 62. Total synthesis of (+)-cyanathiwigin U (**477**) via a two-directional ring-opening/ring-closing olefin-metathesis cascade (Pfeiffer and Phillips, 2005).[308]

two-directional ring-opening metathesis/ring-closing metathesis tandem reaction to fashion the tricyclic core structure of the targeted natural product.[308] A chiral-auxiliary-mediated asymmetric Diels–Alder reaction[309] was used to construct bicyclic dialdehyde **470** in enantiopure form, treatment of which with vinylmagnesium bromide and subsequent Dess–Martin oxidation gave bis-enone **471**. Exposure of **471** to ruthenium carbene **472**[310] in refluxing toluene under an atmosphere of ethylene[311] led to the desired rearrangement, giving tricyclic compound **476** in 43% overall yield from dialdehyde **470**. Tricyclic product **476** has the correct relative and absolute stereochemistry at the four contiguous stereogenic centers around the crowded cyclohexane ring required to complete the total synthesis, which was then achieved in only five further steps. There are several possible mechanistic scenarios for the conversion of **471** into **476**, of which only one

 © 2006 Wiley-VCH Verlag GmbH & Co. KGaA, Weinheim

is illustrated in Scheme 62. Note that all the steps in the catalytic cycle are, in principle, reversible, but this reaction benefits from a powerful thermodynamic driving force with favorable contributions from both enthalpic (release of ring strain) and entropic (release of ethylene) terms. This example is illustrative of a key enabling ability of ring-rearrangement metathesis, namely the transfer of easily installed stereochemical information on a precursor molecule (in this case **471**) to a polycyclic product (**476**) in which such chiral information would be difficult to encode with equal facility.

Cascade reactions figure prominently in the masterful synthesis of (−)-cylindrocyclophane F (**490**, Scheme 63) reported by Smith et al. in 2000.[312,313] Having already synthesized this target through conventional stepwise approaches,[314] they turned to the far more challenging, but inherently more tantalizing, prospect of effecting the synthesis of the [7,7]-paracyclophane core structure through olefin-metathesis dimerization. Specifically, cross-metathesis between two molecules of functionalized rescorcinol monomer **486**, in a head-to-tail fashion, followed by a ring-closing metathesis event could afford the complete [7,7]-cyclophane skeleton, as represented by **489**, in a single operation. Monomeric precursor **486** was prepared by the thermal combination of silyloxyacetylene **478** and cyclobutenone **479** to give phenol **484**, followed by routine protecting-group adjustments. This initial annulation reaction, first developed by Danheiser et al.,[315] presents a convenient regiocontrolled approach to highly substituted aromatic compounds,[316] and proceeds through a cascade of four pericyclic reactions, as illustrated in Scheme 63.[317] To their delight, Smith et al. found that treatment of a solution of precursor **486** in benzene with the Schrock molybdenum carbene **487**[318] (30 mol%) cleanly generated the desired 22-membered macrocyclic compound **489** within two hours at 20°C in 72% yield and as a single *E*,*E* isomer. The same transformation could also be effected by using the Grubbs second-generation carbene **472** (15 mol% catalyst, benzene, 40°C, 27 h, 58% yield). Two further steps then completed the total synthesis of (−)-cylindrocyclophane F (**490**). To rationalize this remarkable metathesis cascade, the researchers performed molecular modeling calculations, which revealed that the observed product **489** was the thermodynamically most stable entity amongst the possible seven cyclic dimers of **486** (including head-to-head [8,6]-cyclophanes and *Z*-configured isomers). This suggested that the dimerization/macrocyclization of **486** actually proceeds through a cascade of reversible olefin metatheses,[319] which drives the reaction towards formation of the thermodynamically most stable product, *E*,*E*-[7,7]-paracyclophane **489**. Lending weight to this rationale was the observation that either the *E* or *Z* isomer of the tail-to-tail dimer **491** could be employed as a metathesis substrate, giving only the *E*,*E*-[7,7]-paracyclophane head-to-tail product **489**. This second-generation metathesis-based approach almost halved the number of steps (11 versus 20), and proceeded in nearly three times the overall yield (22% versus 8%) compared to the original stepwise strategy, once again highlighting the potential of cascade processes for the streamlining of synthetic routes.[320,321]

The spectacular results of the application of ruthenium carbine based systems such as **472** as olefin- and enyne-metathesis catalysts over the last decade has, to a certain degree, overshadowed the concomitant development of a number of other useful ruthenium-catalyzed carbon–carbon bond-forming reactions.[322] One such reaction is the ruthe-

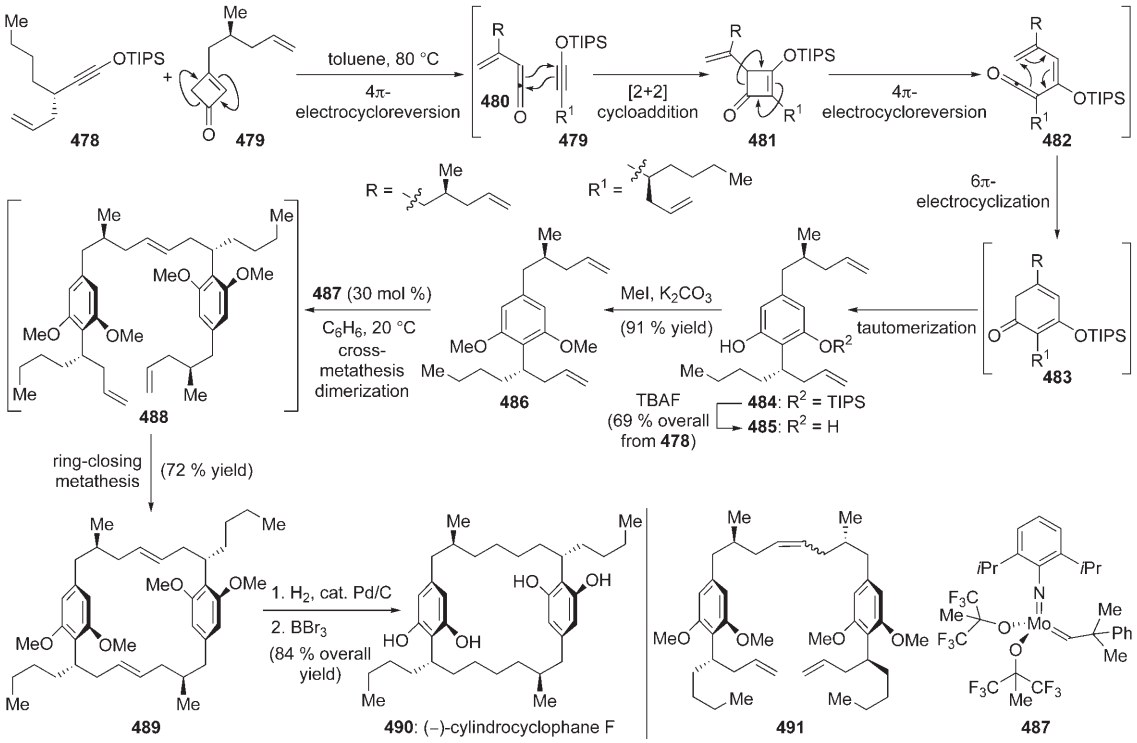

Scheme 63. Selective olefin cross-metathesis/ring-closing metathesis in the synthesis of (−)-cyclindrocyclophane F (**490**; Smith et al., 2000).[312]

© 2006 Wiley-VCH Verlag GmbH & Co. KGaA, Weinheim

nium-catalyzed intermolecular coupling of alkynes and terminal alkenes to give 1,4-dienes (Scheme 64a) developed by Trost et al.[323] Through the judicious placement of appropriate functional groups on the alkene and alkyne partners, this coupling reaction has been extended to the one-step synthesis of substituted butenolides.[324,325] Trost et al. showcased this methodology in the total synthesis of squamocins E (**504**) and K (**505**, Scheme 64b),[326] whereby heating a solution of alkene **495** (1.0 equiv), γ-hydroxyalkynoate **496** (1.0–1.6 equiv), and ruthenium complex **497** (5 mol%) in MeOH at 60°C led to the formation of butenolide **503** as a single regioisomer and in yields of up to 98%! The mechanism of this protecting-group-free transformation is believed to proceed through the sequence shown in Scheme 64b. Formation of the presumed active ruthenium species **498** from precatalyst **497** is followed by ligand exchange and coordination of the alkene and alkyne components (**498**→**499**), oxidative cyclization to generate ruthenacyclopentene **500**, *syn*-β-hydride elimination (**500**→**501**), and then reductive elimination to extrude 1,4-diene **502** and regenerate catalyst **498**.[327] Diene **502** is suitably arranged to undergo lactonization to give butenolide **503** as the observed product. Simple manipulations of the 1,2-disubstituted alkene then completed the synthesis of the target natural products **504** and **505**.[328] The regioselectivity of butenolide formation is set during the coordination and cyclization steps of the catalytic cycle and is dictated primarily by coordination and steric effects, rather than electronic factors. This reaction provides a concise approach to the target butenolide ring system, a structural motif present in a large number of biologically active natural products.[329] In a more general context, the ruthenium-catalyzed alkene–alkyne coupling offers a mild, highly chemoselective, and atom-economical method for effecting fragment couplings.[330]

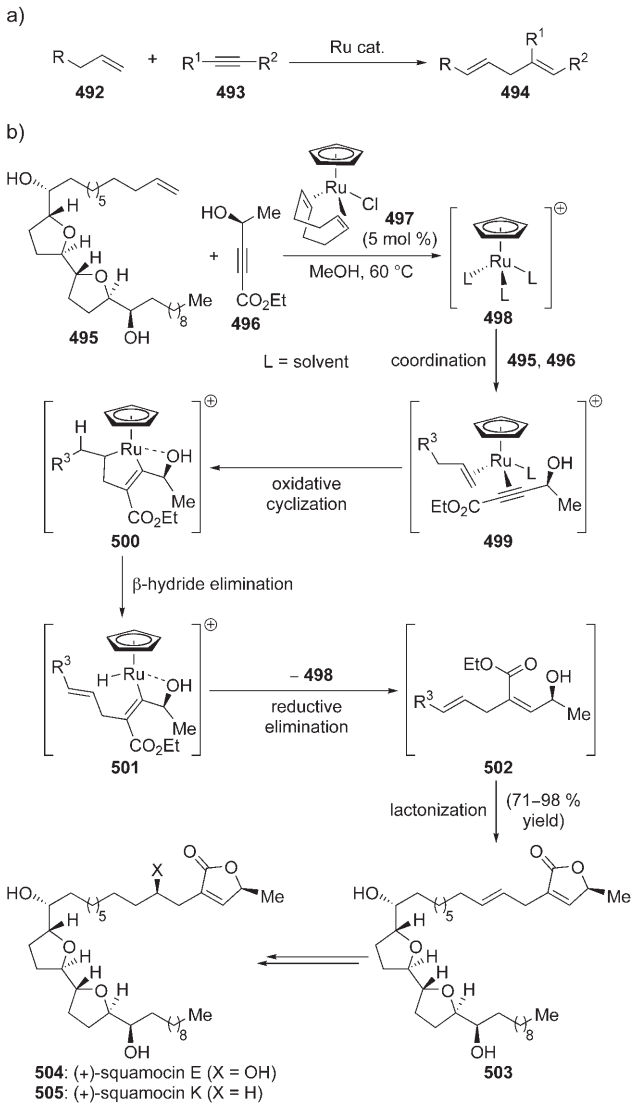

Scheme 64. Ruthenium-catalyzed alkene–alkyne coupling: a) general principles and b) application to butenolide formation in the total synthesis of (+)-squamocin E (**504**) and (+)-squamocin K (**505**; Trost et al., 1997).[326]

It is significant that the uncatalyzed reaction of simple alkenes with alkynes to give 1,4-dienes (Scheme 64a), a formal variant of the Alder-ene reaction, generally only occurs under forcing conditions ($T > 150$°C) and has consequently found little application in the synthesis of complex molecules.[331] Indeed, a notable feature of transition-metal catalysis is that it offers the potential for effecting a variety of pericyclic processes which would be difficult, if not impossible, to achieve under purely thermal conditions.[332]

In particular, a litany of higher-order and multicomponent [m+n+o…(+x)] cycloaddition reactions (where m, n, etc. refer to the number of atoms of each component participating in the reaction), many of which were unimaginable before the advent of transition-metal catalysis, have been, and continue to be, developed.[333] Classic examples include the [2+2+1] carbocyclization of an alkene, alkyne, and CO to generate cyclopentenones (the Pauson–Khand reaction),[334] and the [2+2+2] cyclotrimerization of alkynes to form benzenoid rings.[335–338] Wender et al. have been the key instigators in the development of a homologue of the venerable Diels–Alder reaction for the synthesis of seven-membered rings, namely the formal [5+2] cycloaddition between vinylcyclopropanes (VCPs) and π systems. Originally described as the intramolecular cyclization of alkynes and VCPs (e.g. **506**→**507**, Scheme 65a),[339] the scope of this reaction has subsequently been extended to include alkenes,[340] allenes,[341] and even intermolecular processes.[342] Given the prevalence of seven-membered rings in a wide range of natural and designed molecules,[343] it is perhaps unsurprising that this versatile reaction has begun to find application in target-oriented synthesis, an example of which being the approach to the bicyclo[5.3.0]decane skeleton of the tremulane sesquiterpenes recently reported by Martin and Ashfeld.[344] Exposure of alkyne **508** to dimeric rhodium species **509** (10 mol%) in refluxing toluene triggered the sequence of events depicted in Scheme 65b, leading to the formation of two new rings and two new stereocenters in a completely diastereoselective fashion and generating bicyclic aldehyde **514** in 85% yield. The initial steps in the mechanism bear close parallel to the ruthenium-catalyzed alkene–alkyne

 © 2006 Wiley-VCH Verlag GmbH & Co. KGaA, Weinheim

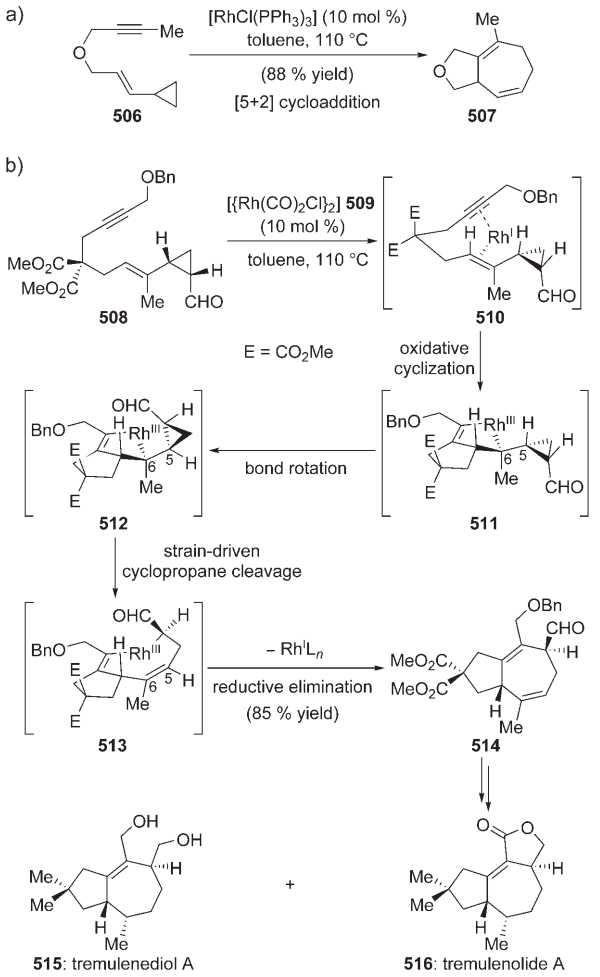

Scheme 65. Rhodium-catalyzed [5+2] cycloadditions: a) first examples (Wender et al., 1995)[339] and b) application to the total syntheses of tremulenediol (**515**) and tremulenolide A (**516**; Martin and Ashfeld, 2005).[344]

coupling discussed above (but this time occurring through a $Rh^{I}\leftrightarrow Rh^{III}$ manifold), that is, formation of a coordinatively unsaturated Rh^{I} species followed by complexation of the alkene and alkyne groups (**508**→**510**) and oxidative cyclization to give Rh^{III} metallacyclopentene **511**.[345] In this case, however, intermediate **511** can undergo a strain-driven cyclopropane cleavage reaction to form the ring-expanded metallacycle **513** and, finally, reductive elimination to provide bicyclic product **514**.[346] Importantly, note that cyclopropane cleavage from the initially formed metallacyclopentene **511** requires rotation about the C5–C6 bond to give the alternative conformer **512** (i.e. **511**→**512**→**513**). This ensures the correct alignment of not only the carbon–rhodium and carbon–carbon bonds required for concerted ring expansion, but also of the C5 hydrogen and C6 methyl substituents required for formation of the *Z*-configured C5–C6 double bond. The net result is that only one of the cyclopropyl carbon–carbon bonds undergoes cleavage to form **514** as a single regio- and diastereoisomer, an outcome anticipated by Martin and Ashfeld on the basis of elegant mechanistic studies by Wender et al.[347] Having assembled the bicyclic core structure in this manner, Martin and Ashfeld were then able to complete the enantioselective syntheses of tremulenediol A (**515**) and tremulenolide A (**516**) over the course of several more steps.[348–350]

The final class of transition-metal-catalyzed reactions that we shall highlight involves the formation and subsequent reactivity of metal carbenoid species from α-carbonyldiazo compounds. Coordination to the metal center (usually a Rh^{II} or Cu^{I} species) tempers, to a degree, the generally high reactivity associated with free carbenes and allows for potentially selective further transformations.[351] From a practical synthetic perspective, such metal carbenes undergo three main types of reaction, as summarized in a very simplistic form in Scheme 66 a. Cyclopropanation with alkenes and C–H insertion reactions are both areas that have witnessed spectacular advances in recent years, particularly with regards to intermolecular and asymmetric processes, and have been extensively reviewed.[352,353] An example of each was illustrated in the synthesis of (–)-colombiasin

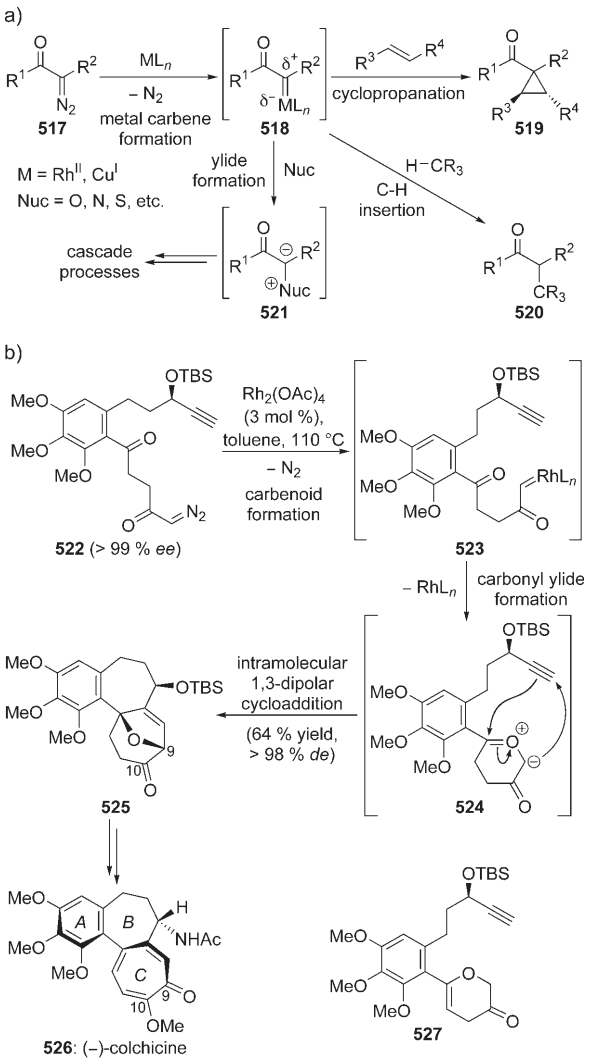

Scheme 66. a) Formation and fate of metal–carbene species **518** derived from α-carbonyl diazo compounds **517**. b) A tandem carbonyl ylide formation/1,3-dipolar cycloaddition approach to the total synthesis of (–)-colchicine (**526**; Schmalz et al., 2005).[355]

 © 2006 Wiley-VCH Verlag GmbH & Co. KGaA, Weinheim

(**350**) by Davies et al. (Scheme 49). However, the electrophilic character of the metal-bound carbon atom also renders this site susceptible to nucleophilic attack to generate a variety of ylide species, which, in turn, can undergo subsequent reactions.

A number of elegant cascades have been designed on the basis of this sequence,[354] one of which was employed by Schmalz and co-workers in an enantioselective synthesis of (−)-colchicine (**526**, Scheme 66b) reported in 2005.[355,356] Colchicine (**526**) has proven to be a tempting target for generations of synthetic chemists and has inspired the development of many ingenious syntheses over the last 50 years.[357] However, a common feature of these routes is that they all adopt a stepwise linear approach to the construction of the tricyclic ring system (i.e. A→AB→ABC, A→AC→ABC, etc.), with the regiocontrolled synthesis of the tropolone C ring often being a particularly thorny issue.[358] As illustrated in Scheme 66b, Schmalz and co-workers employed a Rh-triggered cycloaddition cascade of α-diazoketone **522** to generate both the seven-membered B and C rings in a single step, and with complete control of diastereoselectivity, in a unique A→ABC ring approach. The mechanism of this transformation[359] begins with the generation of electrophilic rhodium carbene **523**, followed by intramolecular cyclization of the proximal Lewis basic carbonyl group to form a reactive carbonyl ylide **524**, which then undergoes intramolecular 1,3-dipolar cycloaddition onto the tethered alkyne to give the observed product **525** in 64% yield.[360] The elevated temperature (110°C) at which this reaction was run was crucial to the success of this venture, as at ambient temperature the uncyclized enol ether **527**, formally derived from carbonyl ylide **524** via a 1,4-hydrogen shift, was the exclusive product. In addition to establishing the complete carbon skeleton of the target natural product **526**, this sequence also regioselectively installed oxygen functionality at the C9 and C10 positions in what would become the tropolone C ring, thereby allowing the completion of the total synthesis in short order.[361]

An intermolecular variant of this cycloaddition cascade was applied by Hashimoto and co-workers en route to their second-generation synthesis of zaragozic acid C (**532**, Scheme 67).[362] Slow addition of a solution of the D-tartrate-derived α-diazoester **528** to a solution of alkyne **529** (3.0 equiv) and rhodium(II) acetate dimer (5 mol%) in refluxing benzene led to the formation of bicyclic compound **530** as a single stereoisomer in 72% yield. The stereoselectivity of this reaction is dictated by approach of the alkyne dipolarophile to the top face of carbonyl ylide intermediate **530** (as drawn in Scheme 67), so as to avoid steric interactions with the pseudoaxial OTMS group at C4. The regioselectivity of the cycloaddition can be rationalized in terms of frontier molecular orbital theory,[363] assuming that the dominant electronic interaction is between the ylide HOMO and alkyne LUMO.[364] This cycloaddition provides an concise approach to the densely functionalized 2,8-dioxabicyclo[3.2.1]octane core structure of the zaragozic acids, and avoids some of the potential problems associated with the formation of this motif through intramolecular acid-catalyzed ketalization of an open-chain 1,3-diol precursor.[365–367]

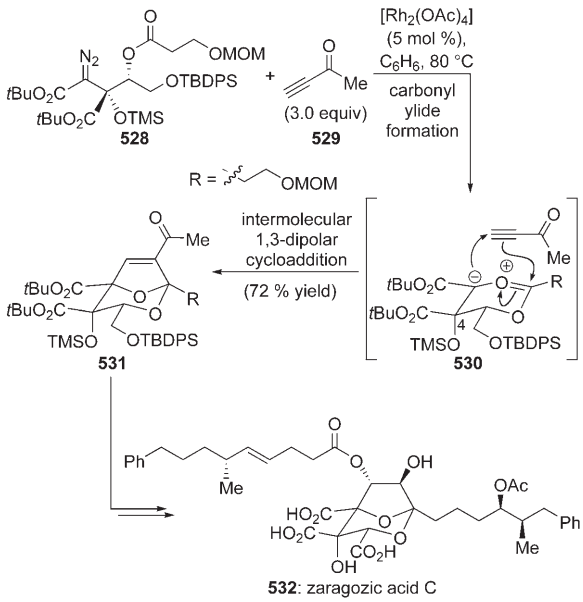

Scheme 67. Carbonyl ylide generation and cycloaddition in the total synthesis of zaragozic acid C (**532**; Hashimoto et al., 2003).[362]

7. Summary and Outlook

The enormous benefits associated with cascade reactions have ensured that they continue to be developed and exploited in organic synthesis. That most of the beautiful and ingenious examples described in this Review have been reported within only the last five years serves to emphasize this point. Of course, in highlighting only successful applications from total synthesis, we neglect a great many cascades developed for other applications, or without a natural product target in mind. Additionally, countless examples of cascades that have gone awry or failed altogether have been omitted. The synthesis of the cascade precursors themselves may also be far from trivial, and considerable experimental skill (and perseverance) is often required to unearth suitable conditions under which the desired cascade can be effected with success.

There are currently relatively few examples of catalytic enantioselective cascade reactions, and it is likely that asymmetric catalysis of cascade processes will become increasingly prominent in years to come, with enzymatic, organocatalytic, and transition-metal-catalyzed processes at the vanguard of this movement. With the increasing pressures to fashion diverse and increasingly complex molecular architectures rapidly through efficient and economical means, cascade reactions are destined to assume an integral position in many synthetic endeavors. In order to push the state of the art of these sequences, contemporary as well as future generations of synthetic practitioners will require an increasingly precise understanding of the mechanism and kinetics of organic transformations. Gains in this fundamental knowledge, combined with a large dose of intellectual flexibility and creativity, will undoubtedly lead to even more spectacular applications of cascade reactions in the future.

 © 2006 Wiley-VCH Verlag GmbH & Co. KGaA, Weinheim

Abbreviations

Ac	acetyl
ACCN	1,1′-azobis(cyclohexanecarbonitrile)
AIBN	2,2′-azobis(2-methylpropionitrile)
BINAP	2,2′-diphenylphosphino-1,1′-binaphthyl
Bn	benzyl
Boc	*tert*-butyloxycarbonyl
CAN	ammonium cerium(IV) nitrate
Cbz	benzyloxycarbonyl
CSA	10-camphorsulfonic acid
2,2-DMB	2,2-dimethylbutane
DBU	1,8-diazabicyclo[5.4.0]undec-7-ene
4-DMAP	4-dimethylaminopyridine
DME	ethylene glycol dimethyl ether
DMF	*N*,*N*-dimethylformamide
DMP	Dess–Martin periodinane
DMSO	dimethyl sulfoxide
DMTSF	dimethyl(methylthio)sulfonium tetrafluoroborate
EDDA	ethylenediamine diacetate
Fl	9-fluorenyl
HFIP	1,1,1,3,3,3-hexafluoro-2-propanol
HMPA	hexamethylphosphoramide
HOMO	highest occupied molecular orbital
imid	imidazole
KHMDS	potassium bis(trimethylsilyl)amide
LUMO	lowest unoccupied molecular orbital
2,6-lut	2,6-lutidine
*m*CPBA	*meta*-chloroperoxybenzoic acid
MOM	methoxymethyl
Ms	methanesulfonyl
NaHMDS	sodium bis(trimethylsilyl)amide
NMP	1-methyl-2-pyrrolidinone
Ns	2-nitrobenzenesulfonyl
PMB	4-methoxybenzyl
PMP	4-methoxyphenyl
N-PSP	*N*-(phenylseleno)phthalimide
py	pyridine
TBAF	tetra-*n*-butylammonium fluoride
TBDPS	*tert*-butyldiphenylsilyl
TBS	*tert*-butyldimethylsilyl
TEMPO	2,2,6,6-tetramethylpiperidine 1-oxide
Teoc	2-(trimethylsilyl)ethoxycarbonyl
TES	triethylsilyl
Tf	trifluoromethanesulfonyl
TFA	trifluoroacetic acid
TFAA	trifluoroacetic anhydride
THF	tetrahydrofuran
THP	2-tetrahydropyranyl
TIPB	triisopropylbenzene
TIPS	triisopropylsilyl
TMS	trimethylsilyl
Ts	4-toluenesulfonyl
TsOH	4-toluenesulfonic acid

It is with enormous pride and great pleasure that we wish to thank our collaborators whose names appear in the references cited and whose contributions made the described work so rewarding and enjoyable. We also thank Dr. David M. Shaw for proofreading this manuscript. We gratefully acknowledge the National Institutes of Health (USA), the Skaggs Institute for Chemical Biology, the George E. Hewitt Foundation, Amgen, Merck, Novartis, and Pfizer for supporting our research programs. D.J.E. thanks Merck for postdoctoral fellowship support.

Received: May 11, 2006

[1] a) L. F. Tietze, G. Brasche, K. Gericke, *Domino Reactions in Organic Synthesis*, Wiley-VCH, Weinheim, **2006**, p. 672; b) L. F. Tietze, U. Beifuss, *Angew. Chem.* **1993**, *105*, 137–170; *Angew. Chem. Int. Ed. Engl.* **1993**, *32*, 131–163; c) L. F. Tietze, *Chem. Rev.* **1996**, *96*, 115–136; d) H. Pellissier, *Tetrahedron* **2006**, *62*, 1619–1665; e) H. Pellissier, *Tetrahedron* **2006**, *62*, 2143–2173; f) T.-L. Ho, *Tandem Organic Reactions*, Wiley, New York, **1992**, p. 502; g) R. A. Bunce, *Tetrahedron* **1995**, *51*, 13103–13159.

[2] a) B. M. Trost, *Science* **1991**, *254*, 1471–1477; b) B. M. Trost, *Angew. Chem.* **1995**, *107*, 285–307; *Angew. Chem. Int. Ed. Engl.* **1995**, *34*, 259–281.

[3] a) P. T. Anastas, J. C. Warner, *Green Chemistry: Theory and Practice*, Oxford University Press, Oxford, **2000**, p. 135; b) A. S. Matlack, *Introduction to Green Chemistry*, Marcel Dekker, New York, **2001**, p. 570.

[4] R. Robinson, *J. Chem. Soc. Trans.* **1917**, 762–768.

[5] a) W. S. Johnson, M. B. Gravestock, B. E. McCarry, *J. Am. Chem. Soc.* **1971**, *93*, 4332–4334; b) M. B. Gravestock, W. S. Johnson, B. E. McCarry, R. J. Parry, B. E. Ratcliffe, *J. Am. Chem. Soc.* **1978**, *100*, 4274–4282.

[6] a) G. Stork, A. W. Burgstahler, *J. Am. Chem. Soc.* **1955**, *77*, 5068–5077; b) A. Eschenmoser, L. Ruzicka, O. Jeger, D. Arigoni, *Helv. Chim. Acta* **1955**, *38*, 1890–1904; c) P. A. Stadler, A. Eschenmoser, H. Schinz, G. Stork, *Helv. Chim. Acta* **1957**, *40*, 2191–2198.

[7] a) W. M. Bandaranayake, J. E. Banfield, D. St. C. Black, G. D. Fallon, B. M. Gatehouse, *J. Chem. Soc. Chem. Commun.* **1980**, 162–163; b) W. M. Bandaranayake, J. E. Banfield, D. St. C. Black, *J. Chem. Soc. Chem. Commun.* **1980**, 902–903; c) W. M. Bandaranayake, J. E. Banfield, D. St. C. Black, *Aust. J. Chem.* **1981**, *34*, 1655–1667; d) W. M. Bandaranayake, J. E. Banfield, D. St. C. Black, *Aust. J. Chem.* **1982**, *35*, 557–565; e) W. M. Bandaranayake, J. E. Banfield, D. St. C. Black, G. D. Fallon, B. M. Gatehouse, *Aust. J. Chem.* **1982**, *35*, 567–579; f) J. E. Banfield, D. St. C. Black, S. R. Johns, R. I. Willing, *Aust. J. Chem.* **1982**, *35*, 2247–2256.

[8] a) K. C. Nicolaou, N. A. Petasis, R. E. Zipkin, J. Uenishi, *J. Am. Chem. Soc.* **1982**, *104*, 5555–5557; b) K. C. Nicolaou, N. A. Petasis, J. Uenishi, R. E. Zipkin, *J. Am. Chem. Soc.* **1982**, *104*, 5557–5558; c) K. C. Nicolaou, R. E. Zipkin, N. A. Petasis, *J. Am. Chem. Soc.* **1982**, *104*, 5558–5560; d) K. C. Nicolaou, N. A. Petasis, R. E. Zipkin, *J. Am. Chem. Soc.* **1982**, *104*, 5560–5562.

[9] a) D. P. Curran, D. M. Rakiewicz, *J. Am. Chem. Soc.* **1985**, *107*, 1448–1449; b) D. P. Curran, D. M. Rakiewicz, *Tetrahedron* **1985**, *41*, 3943–3958.

[10] D. P. Curran, M.-H. Chen, *Tetrahedron Lett.* **1985**, *26*, 4991–4994.

[11] L. T. Scott, M. M. Boorum, B. J. McMahon, S. Hagen, J. Mack, J. Blank, H. Wegner, A. de Meijere, *Science* **2002**, *295*, 1500–1503.

[12] a) S. F. Mayer, W. Kroutil, K. Faber, *Chem. Soc. Rev.* **2001**, *30*, 332–339; b) C.-H. Wong, G. M. Whitesides, *Enzymes in Synthetic Organic Chemistry*, Elsevier, Oxford, **1994**, p. 370.

[13] a) C. A. Roessner, J. B. Spencer, N. J. Stolowich, J. Wang, G. P. Nayar, P. J. Santander, C. Pichon, C. Min, M. T. Holderman,

 © 2006 Wiley-VCH Verlag GmbH & Co. KGaA, Weinheim

A. I. Scott, *Chem. Biol.* **1994**, *1*, 119 – 124; b) A. I. Scott, *Synlett* **1994**, 871 – 883; c) A. I. Scott, *J. Org. Chem.* **2003**, *68*, 2529 – 2539.

[14] a) F. Blanche, D. Thibaut, D. Frechet, M. Vuilhorgne, J. Crouzet, B. Cameron, K. Hlineny, U. Traub-Eberhard, M. Zboron, G. Müller, *Angew. Chem.* **1990**, *102*, 947 – 949; *Angew. Chem. Int. Ed. Engl.* **1990**, *29*, 884 – 886; b) A. Eschenmoser, *Angew. Chem.* **1988**, *100*, 5 – 40; *Angew. Chem. Int. Ed. Engl.* **1988**, *27*, 5 – 39.

[15] For recent discussions of various aspects of biomimetic synthesis, see: a) R. A. Yoder, J. N. Johnston, *Chem. Rev.* **2005**, *105*, 4730 – 4756; b) M. C. de la Torre, M. A. Sierra, *Angew. Chem.* **2004**, *116*, 162 – 184; *Angew. Chem. Int. Ed.* **2004**, *43*, 160 – 181; c) K. C. Nicolaou, T. Montagnon, S. A. Snyder, *Chem. Commun.* **2003**, 551 – 564; d) U. Scholz, E. Winterfeldt, *Nat. Prod. Rep.* **2000**, *17*, 349 – 366.

[16] For a recent review of asymmetric processes triggered by conjugate additions, see: H.-C. Guo, J.-A. Ma, *Angew. Chem.* **2006**, *118*, 362 – 375; *Angew. Chem. Int. Ed.* **2006**, *45*, 354 – 366.

[17] a) H. C. Hailes, C. M. Jackson, P. F. Leadlay, S. V. Ley, J. Staunton, *Tetrahedron Lett.* **1994**, *35*, 307 – 310; b) H. C. Hailes, S. Handa, P. F. Leadlay, I. C. Lennon, S. V. Ley, J. Staunton, *Tetrahedron Lett.* **1994**, *35*, 311 – 314; c) H. C. Hailes, S. Handa, P. F. Leadlay, I. C. Lennon, S. V. Ley, J. Staunton, *Tetrahedron Lett.* **1994**, *35*, 315 – 318.

[18] a) G.-J. Boons, D. S. Brown, J. A. Clase, I. C. Lennon, S. V. Ley, *Tetrahedron Lett.* **1994**, *35*, 319 – 322; b) G.-J. Boons, I. C. Lennon, S. V. Ley, E. S. E. Owen, J. Staunton, D. J. Wadsworth, *Tetrahedron Lett.* **1994**, *35*, 323 – 326; c) S. V. Ley, D. S. Brown, J. A. Clase, A. J. Fairbanks, I. C. Lennon, H. M. I. Osborn, E. S. E. Stokes (née Owen), D. J. Wadsworth, *J. Chem. Soc. Perkin Trans. 1* **1998**, 2259 – 2276.

[19] For an earlier total synthesis of tetronasin that proceeded through the same late-stage intermediates downstream of tricyclic product **30**, see: K. Hori, H. Kazuno, K. Nomura, E. Yoshii, *Tetrahedron Lett.* **1993**, *34*, 2183 – 2186.

[20] L. M. Stark, K. Pekari, E. J. Sorensen, *Proc. Natl. Acad. Sci. USA* **2004**, *101*, 12064 – 12066.

[21] a) G. Büchi, N. C. Yang, *J. Am. Chem. Soc.* **1957**, *79*, 2318 – 2323; b) E. N. Marvell, G. Caple, T. A. Gosink, G. Zimmer, *J. Am. Chem. Soc.* **1966**, *88*, 619 – 620; c) E. N. Marvell, T. Chadwick, G. Caple, T. Gosink, G. Zimmer, *J. Org. Chem.* **1972**, *37*, 2992 – 2997.

[22] D. Basavaiah, A. J. Rao, T. Satyanarayana, *Chem. Rev.* **2003**, *103*, 811 – 891.

[23] a) Y. Ogihara, N. Kobayashi, S. Shibata, *Tetrahedron Lett.* **1968**, *9*, 1881 – 1886; b) S. Seo, U. Sankawa, S. Shibata, *Tetrahedron Lett.* **1972**, *13*, 731 – 734; c) S. Seo, Y. Ogihara, U. Sankawa, S. Shibata, *Tetrahedron Lett.* **1972**, *13*, 735 – 736; d) S. Shibata, *Pure Appl. Chem.* **1972**, *33*, 109 – 127; e) S. Seo, U. Sankawa, Y. Ogihara, Y. Iitaka, S. Shibata, *Tetrahedron* **1973**, *29*, 3721 – 3726; f) N. Takeda, S. Seo, Y. Ogihara, U. Sankawa, I. Iitaka, I. Kitagawa, S. Shibata, *Tetrahedron* **1973**, *29*, 3703 – 3719; g) D.-M. Yang, U. Sankawa, Y. Ebizuka, S. Shibata, *Tetrahedron* **1976**, *32*, 333 – 335.

[24] K. C. Nicolaou, C. D. Papageorgiou, J. L. Piper, R. K. Chadha, *Angew. Chem.* **2005**, *117*, 5996 – 6001; *Angew. Chem. Int. Ed.* **2005**, *44*, 5846 – 5851.

[25] B. B. Snider, X. Gao, *J. Org. Chem.* **2005**, *70*, 6863 – 6869.

[26] K. C. Nicolaou, Y. H. Lim, C. D. Papageorgiou, J. L. Piper, *Angew. Chem.* **2005**, *117*, 8131 – 8135; *Angew. Chem. Int. Ed.* **2005**, *44*, 7917 – 7921.

[27] a) S. B. Herzon, A. G. Myers, *J. Am. Chem. Soc.* **2005**, *127*, 5342 – 5344; b) P. S. Baran, C. A. Guerrero, B. D. Hafensteiner, N. B. Ambhaikar, *Angew. Chem.* **2005**, *117*, 3960 – 3963; *Angew. Chem. Int. Ed.* **2005**, *44*, 3892 – 3895; c) P. S. Baran, B. D. Hafensteiner, N. B. Ambhaikar, C. A. Guerrero, J. D. Gallagher, *J. Am. Chem. Soc.* **2006**, *128*, 8678 – 8693; for a more detailed discussion of these syntheses, see: d) C. Escolano, *Angew. Chem.* **2005**, *117*, 7844 – 7847; *Angew. Chem. Int. Ed.* **2005**, *44*, 7670 – 7673.

[28] F. von Nussbaum, *Angew. Chem.* **2003**, *115*, 3170 – 3179; *Angew. Chem. Int. Ed.* **2003**, *42*, 3068 – 3071.

[29] J. Qian-Cutrone, S. Huang, Y.-Z. Shu, D. Vyas, C. Fairchild, A. Menendez, K. Krampitz, R. Dalterio, S. E. Klohr, Q. Gao, *J. Am. Chem. Soc.* **2002**, *124*, 14556 – 14557.

[30] A. G. Myers, S. B. Herzon, *J. Am. Chem. Soc.* **2003**, *125*, 12080 – 12081.

[31] a) L. V. Jackson, J. C. Walton, *Chem. Commun.* **2000**, 2327 – 2328; b) A. F. Bella, L. V. Jackson, J. C. Walton, *Org. Biomol. Chem.* **2004**, *2*, 421 – 428.

[32] For other approaches to the stephacidins, see: a) L. A. Adams, C. R. Gray, R. M. Williams, *Tetrahedron Lett.* **2004**, *45*, 4489 – 4493; b) A. W. Grubbs, G. D. Artman III, R. M. Williams, *Tetrahedron Lett.* **2005**, *46*, 9013 – 9016.

[33] P. S. Baran, C. A. Guerrero, N. B. Ambhaikar, B. D. Hafensteiner, *Angew. Chem.* **2005**, *117*, 612 – 615; *Angew. Chem. Int. Ed.* **2005**, *44*, 606 – 609.

[34] A similar strategy has been reported for the synthesis of the related alkaloid paraherquamide, see: a) T. D. Cushing, J. F. Sanz-Cervera, R. M. Williams, *J. Am. Chem. Soc.* **1993**, *115*, 9323 – 9324; b) R. M. Williams, J. Cao, H. Tsujishima, *Angew. Chem.* **2000**, *112*, 2640 – 2644; *Angew. Chem. Int. Ed.* **2000**, *39*, 2540 – 2544.

[35] a) A. E. Wright, D. A. Forleo, G. P. Gunawardana, S. P. Gunasekera, F. E. Koehn, O. J. McConnell, *J. Org. Chem.* **1990**, *55*, 4508 – 4512; b) K. L. Rinehart, T. G. Holt, N. L. Fregeau, J. G. Stroh, P. A. Keifer, F. Sun, L. H. Li, D. G. Martin, *J. Org. Chem.* **1990**, *55*, 4512 – 4515; c) R. Sakai, K. L. Rinehart, Y. Guan, A. H.-J. Wang, *Proc. Natl. Acad. Sci. USA* **1992**, *89*, 11456 – 11460; d) R. Sakai, E. A. Jares-Erijman, I. Manzanares, M. V. Silva Elipe, K. L. Rinehart, *J. Am. Chem. Soc.* **1996**, *118*, 9017 – 9023.

[36] For a recent review of this field, see: J. D. Scott, R. M. Williams, *Chem. Rev.* **2002**, *102*, 1669 – 1730.

[37] a) K. L. Rinehart, *Med. Res. Rev.* **2000**, *20*, 1 – 27; b) L. Lau, J. G. Supko, S. Blaney, L. Hershon, N. Seibel, M. Krailo, W. Qu, D. Malkin, J. Jimeno, M. Bernstein, S. Baruchel, *Clin. Cancer Res.* **2005**, *11*, 627 – 677.

[38] a) E. J. Corey, D. Y. Gin, R. S. Kania, *J. Am. Chem. Soc.* **1996**, *118*, 9202 – 9203; b) E. J. Martinez, E. J. Corey, *Org. Lett.* **2000**, *2*, 993 – 996.

[39] For a review of *ortho*-quinone methides, see: R. W. Van de Water, T. R. R. Pettus, *Tetrahedron* **2002**, *58*, 5367 – 5405.

[40] C. Ceuvas, M. Pérez, M. J. Martín, J. L. Chicharro, C. Fernández-Rivas, M. Flores, A. Francesch, P. Gallego, M. Zarzuelo, F. de la Calle, J. García, C. Polanco, I. Rodríguez, I. Manzanares, *Org. Lett.* **2000**, *2*, 2545 – 2548.

[41] For selected reviews on multicomponent reactions, see: a) *Multicomponent Reactions* (Eds.: J. Zhu, H. Bienaymé), Wiley-VCH, Weinheim, **2005**, p. 468; b) D. J. Ramón, M. Yus, *Angew. Chem.* **2005**, *117*, 1628 – 1661; *Angew. Chem. Int. Ed.* **2005**, *44*, 1602 – 1634; c) A. Ulaczyk-Lesanko, D. G. Hall, *Curr. Opin. Chem. Biol.* **2005**, *9*, 266 – 276; d) D. Tejedor, D. González-Cruz, A. Santos-Expósito, J. J. Marrero-Tellado, P. de Armas, F. García-Tellado, *Chem. Eur. J.* **2005**, *11*, 3502 – 3510.

[42] For selected recent examples of multicomponent reactions in total syntheses, see: a) P. R. Sebahar, R. M. Williams, *J. Am. Chem. Soc.* **2000**, *122*, 5666 – 5667; b) D. A. Powell, R. A. Batey, *Org. Lett.* **2002**, *4*, 2913 – 2916; c) K. Inanaga, K. Takasu, M. Ihara, *J. Am. Chem. Soc.* **2004**, *126*, 1352 – 1353.

[43] a) A. Dömling, I. Ugi, *Angew. Chem.* **2000**, *112*, 3300 – 3344; *Angew. Chem. Int. Ed.* **2000**, *39*, 3168 – 3210; b) J. Zhu, *Eur. J.*

 © 2006 Wiley-VCH Verlag GmbH & Co. KGaA, Weinheim

Org. Chem. **2003**, 1133 – 1144; c) A. Dömling, *Chem. Rev.* **2006**, *106*, 17 – 89.

[44] A. Dömling, *Comb. Chem. High Throughput Screening* **1998**, *1*, 1 – 22.

[45] For selected examples, see: a) S. M. Bauer, R. W. Armstrong, *J. Am. Chem. Soc.* **1999**, *121*, 6355 – 6366; b) S. E. de Laszlo, P. G. Williard, *J. Am. Chem. Soc.* **1985**, *107*, 199 – 203; c) J. E. Semple, P. C. Wang, Z. Lysenko, M. M. Joullié, *J. Am. Chem. Soc.* **1980**, *102*, 7505 – 7510.

[46] A. Endo, A. Yanagisawa, M. Abe, S. Tohma, T. Kan, T. Fukuyama, *J. Am. Chem. Soc.* **2002**, *124*, 6552 – 6554.

[47] Williams and co-workers have reported a cascade reaction for the synthesis of the ecteinascidin 743 pentacyclic core; see: a) W. Jin, S. Metobo, R. M. Williams, *Org. Lett.* **2003**, *5*, 2095 – 2098; two recent total syntheses have been reported; see: b) J. Chen, X. Chen, M. Bois-Choussy, J. Zhu, *J. Am. Chem. Soc.* **2006**, *128*, 87 – 89; c) S. Zheng, C. Chan, T. Furuuchi, B. J. D. Wright, B. Zhou, J. Guo, S. J. Danishefsky, *Angew. Chem.* **2006**, *118*, 1786 – 1791; *Angew. Chem. Int. Ed.* **2006**, *45*, 1754 – 1759; d) C. Chan, S. Zheng, B. Zhou, J. Guo, R. M. Heid, B. J. D. Wright, S. J. Danishefsky, *Angew. Chem.* **2006**, *118*, 1781 – 1786; *Angew. Chem. Int. Ed.* **2006**, *45*, 1749 – 1754.

[48] For a review of syntheses in this field, see: G. Mehta, A. Srikrishna, *Chem. Rev.* **1997**, *97*, 671 – 719.

[49] L. A. Paquette, *Eur. J. Org. Chem.* **1998**, 1709 – 1728.

[50] a) F. Geng, J. Liu, L. A. Paquette, *Org. Lett.* **2002**, *4*, 71 – 73; b) L. A. Paquette, F. Geng, *J. Am. Chem. Soc.* **2002**, *124*, 9199 – 9203.

[51] L. A. Paquette, F. Geng, *Org. Lett.* **2002**, *4*, 4547 – 4549.

[52] For details of other total syntheses of pentalenene, see Ref. [48], and references 4–26 in Ref. [51].

[53] a) C. Chen, M. E. Layton, S. M. Sheehan, M. D. Shair, *J. Am. Chem. Soc.* **2000**, *122*, 7424 – 7425; for earlier model studies, see: b) C. Chen, M. E. Layton, M. D. Shair, *J. Am. Chem. Soc.* **1998**, *120*, 10784 – 10785.

[54] K. Xu, G. Lalic, S. M. Sheehan, M. D. Shair, *Angew. Chem.* **2005**, *117*, 2299 – 2301; *Angew. Chem. Int. Ed.* **2005**, *44*, 2259 – 2261.

[55] a) K. C. Nicolaou, P. S. Baran, Y.-L. Zhong, H.-S. Choi, W. H. Yoon, Y. He, K. C. Fong, *Angew. Chem.* **1999**, *111*, 1774 – 1781; *Angew. Chem. Int. Ed.* **1999**, *38*, 1669 – 1675; b) K. C. Nicolaou, P. S. Baran, Y.-L. Zhong, K. C. Fong, Y. He, W. H. Yoon, H.-S. Choi, *Angew. Chem.* **1999**, *111*, 1781 – 1784; *Angew. Chem. Int. Ed.* **1999**, *38*, 1676 – 1678; c) K. C. Nicolaou, J.-K. Jung, W. H. Yoon, Y. He, Y.-L. Zhong, P. S. Baran, *Angew. Chem.* **2000**, *112*, 1899 – 1902; *Angew. Chem. Int. Ed.* **2000**, *39*, 1829 – 1832; d) K. C. Nicolaou, J. Jung, W. H. Yoon, K. C. Fong, H.-S. Choi, Y. He, Y.-L. Zhong, P. S. Baran, *J. Am. Chem. Soc.* **2002**, *124*, 2183 – 2189; e) K. C. Nicolaou, P. S. Baran, Y.-L. Zhong, K. C. Fong, H.-S. Choi, *J. Am. Chem. Soc.* **2002**, *124*, 2190 – 2201; f) K. C. Nicolaou, Y.-L. Zhong, P. S. Baran, J. Jung, H.-S. Choi, W. H. Yoon, *J. Am. Chem. Soc.* **2002**, *124*, 2202 – 2211.

[56] The Fukuyama and Danishefsky groups have also reported total syntheses of the CP molecules; see: a) N. Waizumi, T. Itoh, T. Fukuyama, *J. Am. Chem. Soc.* **2000**, *122*, 7825 – 7826; b) Y. Hayashi, T. Itoh, T. Fukuyama, *Org. Lett.* **2003**, *5*, 2235 – 2238; c) D. Meng, Q. Tan, S. J. Danishefsky, *Angew. Chem.* **1999**, *111*, 3393 – 3397; *Angew. Chem. Int. Ed.* **1999**, *38*, 3197 – 3201; d) Q. Tan, S. J. Danishefsky, *Angew. Chem.* **2000**, *112*, 4683 – 4685; *Angew. Chem. Int. Ed.* **2000**, *39*, 4509 – 4511; for a review of synthetic efforts in this field, see: e) D. A. Spiegel, J. T. Njardarson, I. M. McDonald, J. L. Wood, *Chem. Rev.* **2003**, *103*, 2691 – 2727.

[57] a) A. B. Smith III, A. M. Boldi, *J. Am. Chem. Soc.* **1997**, *119*, 6925 – 6926; b) A. B. Smith III, S. M. Pitram, A. M. Boldi, M. J. Gaunt, C. Sfouggatakis, W. H. Moser, *J. Am. Chem. Soc.* **2003**, *125*, 14435 – 14445; for an account of this strategy in total synthesis endeavors, see: c) A. B. Smith III, C. M. Adams, *Acc. Chem. Res.* **2004**, *37*, 365 – 377.

[58] L. F. Tietze, H. Geissler, J. A. Gewert, U. Jakobi, *Synlett* **1994**, 511 – 512.

[59] For a review of the Brook rearrangement, see: W. H. Moser, *Tetrahedron* **2001**, *57*, 2065 – 2084.

[60] a) A. B. Smith III, D.-S. Kim, *Org. Lett.* **2004**, *6*, 1493 – 1495; b) A. B. Smith III, D.-S. Kim, *Org. Lett.* **2005**, *7*, 3247 – 3250; c) A. B. Smith III, D.-S. Kim, *J. Org. Chem.* **2006**, *71*, 2547 – 2557.

[61] For an earlier total synthesis of this alkaloid, see: N. Toyooka, A. Fukutome, H. Shinoda, H. Nemoto, *Angew. Chem.* **2003**, *115*, 3938 – 3940; *Angew. Chem. Int. Ed.* **2003**, *42*, 3808 – 3810.

[62] Y. Mi, J. V. Schreiber, E. J. Corey, *J. Am. Chem. Soc.* **2002**, *124*, 11290 – 11291.

[63] a) E. J. Corey, S. Lin, *J. Am. Chem. Soc.* **1996**, *118*, 8765 – 8766; b) E. J. Corey, S. Lin, G. Luo, *Tetrahedron Lett.* **1997**, *38*, 5771 – 5774.

[64] For previous syntheses of α-onocerin, see: a) G. Stork, J. E. Davies, A. Meisels, *J. Am. Chem. Soc.* **1959**, *81*, 5516 – 5517; b) G. Stork, A. Meisels, J. E. Davies, *J. Am. Chem. Soc.* **1963**, *85*, 3419 – 3425; c) N. Danieli, Y. Mazur, F. Sondheimer, *Tetrahedron* **1967**, *23*, 509 – 514.

[65] Z. Xiong, E. J. Corey, *J. Am. Chem. Soc.* **2000**, *122*, 9328 – 9329.

[66] Z. Xiong, E. J. Corey, *J. Am. Chem. Soc.* **2000**, *122*, 4831 – 4832.

[67] Z.-X. Wang, Y. Tu, M. Frohn, J.-R. Zhang, Y. Shi, *J. Am. Chem. Soc.* **1997**, *119*, 11224 – 11235.

[68] For other total syntheses of glabrescol, see: a) Y. Morimoto, T. Iwai, T. Kinoshita, *J. Am. Chem. Soc.* **2000**, *122*, 7124 – 7125; b) H. Hioki, C. Kanehara, Y. Ohnishi, Y. Umemori, H. Sakai, S. Yoshio, M. Matsushita, M. Kodama, *Angew. Chem.* **2000**, *112*, 2652 – 2654; *Angew. Chem. Int. Ed.* **2000**, *39*, 2552 – 2554; for a review of approaches to oligotetrahydrofurans, see: c) U. Koert, *Synthesis* **1995**, 115 – 132.

[69] a) M. S. Lee, G. Qin, K. Nakanishi, M. G. Zagorski, *J. Am. Chem. Soc.* **1989**, *111*, 6234 – 6241; b) A. V. K. Prasad, Y. Shimizu, *J. Am. Chem. Soc.* **1989**, *111*, 6476 – 6477; c) D. E. Cane, W. D. Celmer, J. W. Westley, *J. Am. Chem. Soc.* **1983**, *105*, 3594 – 3600.

[70] A. Zakarian, A. Batch, R. A. Holton, *J. Am. Chem. Soc.* **2003**, *125*, 7822 – 7824.

[71] For a review of hydroxy-epoxide cyclization and ether ring-expansion approaches to *trans*-fused polycyclic ethers, see: K. Fujiwara, A. Murai, *Bull. Chem. Soc. Jpn.* **2004**, *77*, 2129 – 2146.

[72] For other total syntheses of hemibrevetoxin B, and related natural products, see: a) T. Nakata, *Chem. Rev.* **2005**, *105*, 4314 – 4347; b) M. Inoue, *Chem. Rev.* **2005**, *105*, 4379 – 4405.

[73] L. E. Overman, L. D. Pennington, *J. Org. Chem.* **2003**, *68*, 7143 – 7157.

[74] D. W. C. MacMillan, L. E. Overman, L. D. Pennington, *J. Am. Chem. Soc.* **2001**, *123*, 9033 – 9044.

[75] a) D. W. C. MacMillan, L. E. Overman, *J. Am. Chem. Soc.* **1995**, *117*, 10391 – 10392; b) L. E. Overman, L. D. Pennington, *Org. Lett.* **2000**, *2*, 2683 – 2686; c) F. Gallou, D. W. C. MacMillan, L. E. Overman, L. A. Paquette, L. D. Pennington, J. Yang, *Org. Lett.* **2001**, *3*, 135 – 137.

[76] For other total syntheses of sclerophytin A and related compounds, see: a) L. A. Paquette, O. M. Moradei, P. Bernardelli, T. Lange, *Org. Lett.* **2000**, *2*, 1875 – 1878; b) P. Bernardelli, O. M. Moradei, D. Friedrich, J. Yang, F. Gallou, B. P. Dyck, R. W. Doskotch, T. Lange, L. A. Paquette, *J. Am. Chem. Soc.* **2001**, *123*, 9021 – 9032; c) O. Corminboeuf, L. E. Overman, L. D. Pennington, *J. Am. Chem. Soc.* **2003**, *125*, 6650 – 6652; d) O. Corminboeuf, L. E. Overman, L. D. Pennington, *Org. Lett.* **2003**, *5*, 1543 – 1546; e) G. A. Molander, D. J. St. Jean, Jr., J. Hass, *J. Am. Chem. Soc.* **2004**, *126*, 1642 – 1643; f) M. T.

 © 2006 Wiley-VCH Verlag GmbH & Co. KGaA, Weinheim

Crimmins, B. H. Brown, *J. Am. Chem. Soc.* **2004**, *126*, 10264 – 10266.
[77] For a review of the chemistry of spiroketals, see: F. Perron, K. F. Albizati, *Chem. Rev.* **1989**, *89*, 1617 – 1661.
[78] For a review of the synthesis of bis-spiroacetal ring systems, see: M. A. Brimble, F. A. Farès, *Tetrahedron* **1999**, *55*, 7661 – 7706.
[79] a) K. C. Nicolaou, M. O. Frederick, G. Petrovic, K. P. Cole, E. Loizidou, *Angew. Chem.* **2006**, *118*, 2671 – 2677; *Angew. Chem. Int. Ed.* **2006**, *45*, 2609 – 2615; b) K. C. Nicolaou, M. O. Frederick, E. Z. Loizidou, G. Petrovic, K. P. Cole, T. V. Koftis, Y. M. A. Yamada, *Chem. Asian J.* **2006**, *1*, 245 – 263.
[80] For another striking example of a deprotection/ketalization, which also involves epoxide-opening cyclizations, see: I. Paterson, R. D. Tillyer, J. B. Small, *Tetrahedron Lett.* **1993**, *34*, 7137 – 7140.
[81] L. K. Geisler, S. Nguyen, C. J. Forsyth, *Org. Lett.* **2004**, *6*, 4159 – 4162.
[82] For the total synthesis and structural revision of azaspiracid-1, see: a) K. C. Nicolaou, S. Vyskocil, T. V. Koftis, Y. M. A. Yamada, T. Ling, D. Y.-K. Chen, W. Tang, G. Petrovic, M. O. Frederick, Y. Li, M. Satake, *Angew. Chem.* **2004**, *116*, 4412 – 4418; *Angew. Chem. Int. Ed.* **2004**, *43*, 4312 – 4318; b) K. C. Nicolaou, T. V. Koftis, S. Vyskocil, G. Petrovic, T. Ling, Y. M. A. Yamada, W. Tang, M. O. Frederick, *Angew. Chem.* **2004**, *116*, 4418 – 4424; *Angew. Chem. Int. Ed.* **2004**, *43*, 4318 – 4324; c) K. C. Nicolaou, P. M. Pihko, F. Bernal, M. O. Frederick, W. Qian, N. Uesaka, N. Diedrichs, J. Hinrichs, T. V. Koftis, E. Loizidou, G. Petrovic, M. Rodriquez, D. Sarlah, N. Zou, *J. Am. Chem. Soc.* **2006**, *128*, 2244 – 2257; d) K. C. Nicolaou, D. Y.-K. Chen, Y. Li, N. Uesaka, G. Petrovic, T. V. Koftis, F. Bernal, M. O. Frederick, M. Govindasamy, T. Ling, P. M. Pihko, W. Tang, S. Vyskocil, *J. Am. Chem. Soc.* **2006**, *128*, 2258 – 2267; e) K. C. Nicolaou, T. V. Koftis, S. Vyskocil, G. Petrovic, W. Tang, M. O. Frederick, D. Y.-K. Chen, Y. Li, T. Ling, Y. M. A. Yamada, *J. Am. Chem. Soc.* **2006**, *128*, 2859 – 2872.
[83] For other recent approaches to the azaspiracids, see: a) X.-T. Zhou, R. G. Carter, *Angew. Chem.* **2006**, *118*, 1819 – 1822; *Angew. Chem. Int. Ed.* **2006**, *45*, 1787 – 1790; b) X.-T. Zhou, R. G. Carter, *Chem. Commun.* **2004**, 2138 – 2140; c) Y. Ishikawa, S. Nishiyama, *Heterocycles* **2004**, *63*, 885 – 893; d) C. J. Forsyth, J. Hao, J. Aiguade, *Angew. Chem.* **2001**, *113*, 3775 – 3779; *Angew. Chem. Int. Ed.* **2001**, *40*, 3663 – 3667.
[84] a) C. H. Heathcock, M. M. Hansen, R. B. Ruggeri, J. C. Kath, *J. Org. Chem.* **1992**, *57*, 2544 – 2553; b) C. H. Heathcock, S. Piettre, R. B. Ruggeri, J. A. Ragan, J. C. Kath, *J. Org. Chem.* **1992**, *57*, 2554 – 2566.
[85] For accounts of the development of this process, see: a) C. H. Heathcock, *Angew. Chem.* **1992**, *104*, 675 – 691; *Angew. Chem. Int. Ed. Engl.* **1992**, *31*, 665 – 681; b) C. H. Heathcock, *Proc. Natl. Acad. Sci. USA* **1996**, *93*, 14323 – 14327.
[86] F. He, Y. Bo, J. D. Altom, E. J. Corey, *J. Am. Chem. Soc.* **1999**, *121*, 6771 – 6772.
[87] For a review of recent developments in the use of allylsilanes in organic synthesis, see: L. Chabaud, P. James, Y. Landais, *Eur. J. Org. Chem.* **2004**, 3173 – 3199.
[88] For other total syntheses of aspidophytine, see: a) S. Sumi, K. Matsumoto, H. Tokuyama, T. Fukuyama, *Org. Lett.* **2003**, *5*, 1891 – 1893; b) S. Sumi, K. Matsumoto, H. Tokuyama, T. Fukuyama, *Tetrahedron* **2003**, *59*, 8571 – 8587; c) J. M. Mejia-Oneto, A. Padwa, *Org. Lett.* **2006**, *8*, 3275 – 3278.
[89] a) S. Yokoshima, T. Ueda, S. Kobayashi, A. Sato, T. Kuboyama, H. Tokuyama, T. Fukuyama, *J. Am. Chem. Soc.* **2002**, *124*, 2137 – 2139; b) S. Yokoshima, T. Ueda, S. Kobayashi, A. Sato, T. Kuboyama, H. Tokuyama, T. Fukuyama, *Pure Appl. Chem.* **2003**, *75*, 29 – 38.
[90] S. Kobayashi, T. Ueda, T. Fukuyama, *Synlett* **2000**, 883 – 886.
[91] Funk and Fuchs have employed a similar species in the total synthesis of perophoramidine; see: J. R. Fuchs, R. L. Funk, *J. Am. Chem. Soc.* **2004**, *126*, 5068 – 5069.
[92] G. Schill, C. U. Priester, U. F. Windhövel, H. Fritz, *Tetrahedron* **1987**, *43*, 3765 – 3786.
[93] Four other syntheses of vinblastine, using natural vindoline, have been reported; see: a) P. Mangeney, R. Z. Andriamialisoa, N. Langlois, Y. Langlois, P. Potier, *J. Am. Chem. Soc.* **1979**, *101*, 2243 – 2245; b) J. P. Kutney, L. S. L. Choi, J. Nakano, H. Tsukamoto, M. McHugh, C. A. Boulet, *Heterocycles* **1988**, *27*, 1845 – 1853; c) M. E. Kuehne, P. A. Matson, W. G. Bornmann, *J. Org. Chem.* **1991**, *56*, 513 – 528; d) P. Magnus, J. S. Mendoza, A. Stamford, M. Ladlow, P. Willis, *J. Am. Chem. Soc.* **1992**, *114*, 10232 – 10245.
[94] T. Kuboyama, S. Yokoshima, H. Tokuyama, T. Fukuyama, *Proc. Natl. Acad. Sci. USA* **2004**, *101*, 11966 – 11970.
[95] A. Padwa, T. M. Heidelbaugh, J. T. Kuethe, M. S. McClure, *J. Org. Chem.* **1998**, *63*, 6778 – 6779.
[96] For reviews of the use of Pummerer reactions in the synthesis of heterocyclic compounds, see: a) A. Padwa, D. E. Gunn, Jr., M. H. Osterhout, *Synthesis* **1997**, 1353 – 1377; b) A. Padwa, D. M. Danca, J. D. Ginn, S. M. Lynch, *J. Braz. Chem. Soc.* **2001**, *12*, 571 – 585; c) S. K. Bur, A. Padwa, *Chem. Rev.* **2004**, *104*, 2401 – 2432.
[97] For an overview of the use of tandem methodology in heterocycle synthesis, see: A. Padwa, *Pure Appl. Chem.* **2004**, *76*, 1933 – 1952.
[98] a) A. Padwa, M. D. Danca, *Org. Lett.* **2002**, *4*, 715 – 717; b) A. Padwa, M. D. Danca, K. I. Hardcastle, M. S. McClure, *J. Org. Chem.* **2003**, *68*, 929 – 941.
[99] Another synthesis of jamtine was published recently; see: a) N. S. Simpkins, C. D. Gill, *Org. Lett.* **2003**, *5*, 535 – 537; b) C. D. Gill, D. A. Greenhalgh, N. S. Simpkins, *Tetrahedron* **2003**, *59*, 9213 – 9230.
[100] P. S. Baran, A. L. Zografos, D. P. O'Malley, *J. Am. Chem. Soc.* **2004**, *126*, 3726 – 3727.
[101] J. Laing, A. W. McCulloch, D. G. Smith, A. G. McInnes, *Can. J. Chem.* **1971**, *49*, 574 – 582.
[102] S. F. Nelson, J. C. Calabrese, *J. Am. Chem. Soc.* **1973**, *95*, 8385 – 8388.
[103] P. S. Baran, K. Li, D. P. O'Malley, C. Mitsos, *Angew. Chem.* **2006**, *118*, 255 – 258; *Angew. Chem. Int. Ed.* **2006**, *45*, 249 – 252.
[104] a) N. Heinrich, W. Koch, G. Frenking, H. Schwarz, *J. Am. Chem. Soc.* **1986**, *108*, 593 – 600; b) R. E. Rosenberg, *J. Org. Chem.* **1998**, *63*, 5562 – 5567.
[105] For another synthesis of sceptrin, see: V. B. Birman, X.-T. Jiang, *Org. Lett.* **2004**, *6*, 2369 – 2371.
[106] P. S. Baran, D. P. O'Malley, A. L. Zografos, *Angew. Chem.* **2004**, *116*, 2728 – 2731; *Angew. Chem. Int. Ed.* **2004**, *43*, 2674 – 2677.
[107] For selected reviews of microwave-assisted synthesis, see: a) A. de la Hoz, A. Diaz-Ortiz, A. Moreno, *Chem. Soc. Rev.* **2005**, *34*, 164 – 178; b) P. Lidström, J. Tierney, B. Wathey, J. Westman, *Tetrahedron* **2001**, *57*, 9225 – 9283; c) C. O. Kappe, A. Stadler, *Microwaves in Organic and Medicinal Chemistry*, Wiley-VCH, Weinheim, **2005**, p. 410; d) J. P. Tierney, P. Lidström, *Microwave Assisted Organic Synthesis*, Blackwell, Oxford, **2005**, p. 296; e) C. O. Kappe, *Angew. Chem.* **2004**, *116*, 6408 – 6443; *Angew. Chem. Int. Ed.* **2004**, *43*, 6250 – 6284; f) *Microwaves in Organic Synthesis* (Ed.: A. Loupy), Wiley-VCH, Weinheim, **2002**, p. 499.
[108] For general reviews of radical chemistry, see: a) B. Giese, *Radicals in Organic Synthesis: Formation of Carbon-Carbon Bonds*, Pergamon, Oxford, **1986**, p. 294; b) *Radicals in Organic Synthesis, Vols. 1&2* (Eds.: P. Renaud, M. P. Sibi), Wiley-VCH, Weinheim, **2001**, p. 1110; c) S. Z. Zard, *Radical Reactions in Organic Synthesis*, Oxford University Press, Oxford, **2003**, p. 256.

 © 2006 Wiley-VCH Verlag GmbH & Co. KGaA, Weinheim

[109] a) M. Albert, L. Fensterbank, E. Lacôte, M. Malacria, *Top. Curr. Chem.* **2006**, *264*, 1 – 62; b) A. J. McCarroll, J. C. Walton, *Angew. Chem.* **2001**, *113*, 2282 – 2307; *Angew. Chem. Int. Ed.* **2001**, *40*, 2224 – 2248.

[110] a) K. A. Parker, D. Fokas, *J. Am. Chem. Soc.* **1992**, *114*, 9688 – 9689; b) K. A. Parker, D. Fokas, *J. Org. Chem.* **2006**, *71*, 449 – 455.

[111] For reviews of the synthesis of morphine, see: a) L. M. Mascavage, M. L. Wilson, D. R. Dalton, *Curr. Org. Synth.* **2006**, *3*, 99 – 120; b) J. Zezula, T. Hudlicky, *Synlett* **2005**, 388 – 405; c) T. Hudlicky, G. Butora, S. P. Fearnley, A. G. Gum, M. R. Stabile, *Stud. Nat. Prod. Chem.* **1996**, *18*, 43 – 154.

[112] a) A.-C. Callier, B. Quiclet-Sire, S. Z. Zard, *Tetrahedron Lett.* **1994**, *35*, 6109 – 6112; b) J. Boivin, A.-C. Callier-Dublanchet, B. Quiclet-Sire, A.-M. Schiano, S. Z. Zard, *Tetrahedron* **1995**, *51*, 6517 – 6528; for a review of nitrogen-centered radicals, see: c) A. G. Fallis, I. M. Brinza, *Tetrahedron* **1997**, *53*, 17543 – 17594.

[113] J. Cassayre, F. Gagosz, S. Z. Zard, *Angew. Chem.* **2002**, *114*, 1861 – 1863; *Angew. Chem. Int. Ed.* **2002**, *41*, 1783 – 1785.

[114] S. Knapp, F. S. Gibson, Y. H. Choe, *Tetrahedron Lett.* **1990**, *31*, 5397 – 5400.

[115] L. A. Sharp, S. Z. Zard, *Org. Lett.* **2006**, *8*, 831 – 834; for previous syntheses of aspidospermidine, see reference [1] therein.

[116] a) M. T. Crimmins, Z. Wang, L. A. McKerlie, *Tetrahedron Lett.* **1996**, *37*, 8703 – 8706; b) M. T. Crimmins, Z. Wang, L. A. McKerlie, *J. Am. Chem. Soc.* **1998**, *120*, 1747 – 1756.

[117] P. Dowd, W. Zhang, *Chem. Rev.* **1993**, *93*, 2091 – 2115.

[118] For other total syntheses of lubiminol, see: a) A. Murai, S. Sato, T. Masamune, *J. Chem. Soc. Chem. Commun.* **1982**, 513 – 514; b) A. Murai, S. Sato, T. Masamune, *Bull. Chem. Soc. Jpn.* **1984**, *57*, 2286 – 2290; c) A. Murai, S. Sato, T. Masamune, *Bull. Chem. Soc. Jpn.* **1984**, *57*, 2291 – 2294; d) C. Iwata, H. Kubota, M. Yamada, Y. Takemoto, S. Uchida, T. Tanaka, T. Imanishi, *Tetrahedron Lett.* **1984**, *25*, 3339 – 3342; e) C. Iwata, Y. Takemoto, H. Kubota, T. Kuroda, T. Imanishi, *Chem. Pharm. Bull.* **1990**, *38*, 361 – 365.

[119] For two recent reviews of steroid synthesis, see: a) R. Skoda-Földes, L. Kollár, *Chem. Rev.* **2003**, *103*, 4095 – 4129; b) Ref. [15a].

[120] a) R. L. Funk, K. P. C. Vollhardt, *J. Am. Chem. Soc.* **1980**, *102*, 5253 – 5261; b) R. L. Funk, K. P. C. Vollhardt, *J. Am. Chem. Soc.* **1979**, *101*, 215 – 217; c) R. L. Funk, K. P. C. Vollhardt, *J. Am. Chem. Soc.* **1977**, *99*, 5483 – 5484.

[121] L. F. Tietze, T. Nöbel, M. Spescha, *J. Am. Chem. Soc.* **1998**, *120*, 8971 – 8977.

[122] Y. Zhang, G. Wu, G. Angel, E. Negishi, *J. Am. Chem. Soc.* **1990**, *112*, 8590 – 8592.

[123] W. J. Zuercher, M. Scholl, R. H. Grubbs, *J. Org. Chem.* **1998**, *63*, 4291 – 4298.

[124] a) G. Pattenden, L. K. Reddy, A. Walter, *Tetrahedron Lett.* **2004**, *45*, 4027 – 4030; b) G. Pattenden, M. A. Gonzalez, S. McCulloch, A. Walter, S. J. Woodhead, *Proc. Natl. Acad. Sci. USA* **2004**, *101*, 12024 – 12029.

[125] For the first total synthesis of estrone, see: G. Anner, K. Miescher, *Helv. Chim. Acta* **1948**, *31*, 2173 – 2183.

[126] For selected reviews of the use of samarium diiodide in synthesis, see: a) G. A. Molander, *Chem. Rev.* **1992**, *92*, 29 – 68; b) G. A. Molander, C. R. Harris, *Chem. Rev.* **1996**, *96*, 307 – 338; c) G. A. Molander, C. R. Harris, *Tetrahedron* **1998**, *54*, 3321 – 3354; d) H. B. Kagan, *Tetrahedron* **2003**, *59*, 10351 – 10372; e) D. J. Edmonds, D. Johnston, D. J. Procter, *Chem. Rev.* **2004**, *104*, 3371 – 3403.

[127] a) R. J. Boffey, M. Santagostino, W. G. Whittingham, J. D. Kilburn, *Chem. Commun.* **1998**, 1875 – 1876; b) R. J. Boffey, W. G. Whittingham, J. D. Kilburn, *J. Chem. Soc. Perkin Trans. 1* **2001**, 487 – 496.

[128] For other syntheses of paeonilactone B, see: a) S. Kadota, M, Takeshita, K. Kiyoshi, T. Kikuchi, *Chem. Pharm. Bull.* **1989**, *37*, 843 – 845; b) D. P. Richardson, T. E. Smith, W. W. Lin, C. N. Kiser, B. R. Mahon, *Tetrahedron Lett.* **1990**, *31*, 5973 – 5976; c) S. Hatakeyama, M. Kawamura, E. Shimanuki, S. Takano, *Tetrahedron Lett.* **1992**, *33*, 333 – 336; d) S. Hatakeyama, M. Kawamura, Y. Mukugi, H. Irie, *Tetrahedron Lett.* **1995**, *36*, 267 – 268; e) C. Jonasson, M. Rönn, J.-E. Bäckvall, *J. Org. Chem*, **2000**, *65*, 2122 – 2126.

[129] Selected other examples of the use of samarium diiodide-mediated cascades in total synthesis include a ketyl-olefin cyclization cascade in the total synthesis of hypnophilin and coriolin by the Curran group; see: a) T. L. Fevig, R. L. Elliott, D. P. Curran, *J. Am. Chem. Soc.* **1988**, *110*, 5064 – 5067; a stereocontrolled reductive double alkylation of an unsaturated bis-oxindole in the total synthesis of *meso*-chimonanthine and *meso*-calycanthine by Link and Overman; see: b) J. T. Link, L. E. Overman, *J. Am. Chem. Soc.* **1996**, *118*, 8166 – 8167; a heteropinacol macrocyclization, N–O bond cleavage, *N*-acylation cascade in the Nicolaou group's second total synthesis of diazonamide; see: c) K. C. Nicolaou, P. Bheema Rao, J. Hao, M. V. Reddy, G. Rassias, X. Huang, D. Y.-K. Chen, S. A. Snyder, *Angew. Chem.* **2003**, *115*, 1795 – 1800; *Angew. Chem. Int. Ed.* **2003**, *42*, 1753 – 1758; d) K. C. Nicolaou, J. Hao, M. V. Reddy, P. Bheema Rao, G. Rassias, S. A. Snyder, X. Huang, D. Y.-K. Chen, W. E. Brenzovich, N. Giuseppone, P. Giannakakou, A. O'Brate, *J. Am. Chem. Soc.* **2004**, *126*, 12897 – 12906.

[130] E. Lee, J. W. Lim, C. H. Yoon, Y. Sung, Y. K. Kim, *J. Am. Chem. Soc.* **1997**, *119*, 8391 – 8392.

[131] For other syntheses of estafiatin, see: a) M. T. Edgar, A. E. Greene, P. Crabbé, *J. Org. Chem.* **1979**, *44*, 159 – 160; b) M. Demuynck, A. A. Devreese, P. J. De Clercq, M. Vandewalle, *Tetrahedron Lett.* **1982**, *23*, 2501 – 2504; c) A. A. Devreese, M. Demuynck, P. J. De Clercq, M. Vandewalle, *Tetrahedron* **1983**, *39*, 3049 – 3054; d) M. Ando, A. Akahane, H. Yamaoka, K. Takase, *J. Org. Chem.* **1982**, *47*, 3909 – 3916; e) J. H. Rigby, J. Z. Wilson, *J. Am. Chem. Soc.* **1984**, *106*, 8217 – 8224.

[132] For reviews of manganese(III)-mediated radical cyclizations, see: a) B. B. Snider, *Chem. Rev.* **1996**, *96*, 339 – 363; b) B. B. Snider, *Transition Metals for Organic Synthesis* (Eds.: M. Beller, C. Bolm), 2nd ed., Wiley-VCH, Weinheim, **2004**, pp. 483 – 490.

[133] a) B. B. Snider, J. E. Merritt, *Tetrahedron* **1991**, *47*, 8663 – 8678; b) B. B. Snider, B. A. McCarthy, *Tetrahedron* **1993**, *49*, 9447 – 9452.

[134] For the use of cerium(IV) reagents in synthesis, see: a) Ref. [126a]; b) V. Nair, J. Mathew, J. Prabhakaran, *Chem. Soc. Rev.* **1997**, *26*, 127 – 132.

[135] a) K. C. Nicolaou, D. Gray, *Angew. Chem.* **2001**, *113*, 783 – 785; *Angew. Chem. Int. Ed.* **2001**, *40*, 761 – 763; b) K. C. Nicolaou, D. L. F. Gray, *J. Am. Chem. Soc.* **2004**, *126*, 607 – 612.

[136] For a review of photoenolization, see: a) P. G. Sammes, *Tetrahedron* **1976**, *32*, 405 – 422; for a review of *ortho*-quinodimethane chemistry, see: b) J. L. Charlton, M. M. Alauddin, *Tetrahedron* **1987**, *43*, 2873 – 2889.

[137] For a recent formal synthesis of hybocarpone, see: C. L. L. Chai, J. A. Elix, F. K. E. Moore, *J. Org. Chem.* **2006**, *71*, 992 – 1001.

[138] a) A. W. G. Burgett, Q. Li, Q. Wei, P. G. Harran, *Angew. Chem.* **2003**, *115*, 5111 – 5116; *Angew. Chem. Int. Ed.* **2003**, *42*, 4961 – 4966; for the total synthesis of the proposed structure of diazonamide A and its structural revision, see: b) J. Li, S. Jeong, L. Esser, P. G. Harran, *Angew. Chem.* **2001**, *113*, 4901 – 4906; *Angew. Chem. Int. Ed.* **2001**, *40*, 4765 – 4770; c) J. Li, A. W. G. Burgett, L. Esser, C. Amezcua, P. G. Harran, *Angew. Chem.*

 © 2006 Wiley-VCH Verlag GmbH & Co. KGaA, Weinheim

2001, *113*, 4906 – 4909; *Angew. Chem. Int. Ed.* **2001**, *40*, 4770 – 4773.

[139] For a review of the oxidation of phenolic compounds with hypervalent iodine reagents, see: a) R. M. Moriarty, O. Prakash, *Org. React.* **2001**, *57*, 327 – 415; for more general reviews of the use of hypervalent iodine reagents in synthesis, see: b) T. Wirth, *Angew. Chem.* **2005**, *117*, 3722 – 3731; *Angew. Chem. Int. Ed.* **2005**, *44*, 3656 – 3665; c) V. V. Zhdankin, P. J. Stang, *Chem. Rev.* **2002**, *102*, 2523 – 2584; d) R. M. Moriarty, O. Prakash, *Org. React.* **1999**, *54*, 273 – 418; e) P. J. Stang, V. V. Zhdankin, *Chem. Rev.* **1996**, *96*, 1123 – 1178.

[140] For discussions of the possible mechanisms of oxidation of phenolic compounds using hypervalent iodine reagents, see: a) L. Kürti, P. Herczegh, J. Visy, M. Simonyi, S. Antus, A. Pelter, *J. Chem. Soc. Perkin Trans. 1* **1999**, 379 – 380; b) D. Magdziak, S. J. Meek, T. R. R. Pettus, *Chem. Rev.* **2004**, *104*, 1383 – 1429, and references therein.

[141] O. Yonemitsu, P. Cerutti, B. Witkop, *J. Am. Chem. Soc.* **1966**, *88*, 3941 – 3945.

[142] For reviews of substitution reactions that proceed by electron-transfer mechanisms, see: a) J.-M. Savéant, *Tetrahedron* **1994**, *50*, 10117 – 10165; b) R. A. Rossi, A. B. Pierini, A. B. Peñéñory, *Chem. Rev.* **2003**, *103*, 71 – 167.

[143] For other total syntheses of diazonamide A, see: a) K. C. Nicolaou, M. Bella, D. Y.-K. Chen, X. Huang, T. Ling, S. A. Snyder, *Angew. Chem.* **2002**, *114*, 3645 – 3649; *Angew. Chem. Int. Ed.* **2002**, *41*, 3495 – 3499; b) K. C. Nicolaou, D. Y.-K. Chen, X. Huang, T. Ling, M. Bella, S. A. Snyder, *J. Am. Chem. Soc.* **2004**, *126*, 12888 – 12896. See also Refs. [129c] and [129d].

[144] For a review of tandem Diels–Alder reactions, see: J. D. Winkler, *Chem. Rev.* **1996**, *96*, 167 – 176.

[145] L. F. Tietze, Y. Zhou, *Angew. Chem.* **1999**, *111*, 2076 – 2078; *Angew. Chem. Int. Ed.* **1999**, *38*, 2045 – 2047.

[146] For an account of the development and application of this and similar cascade reactions, see Ref. [1c] and L. F. Tietze, N. Rackelmann, *Pure Appl. Chem.* **2004**, *76*, 1967 – 1983.

[147] For other total syntheses of hirsutine, see: a) E. Wenkert, Y. D. Vankar, J. S. Yadav, *J. Am. Chem. Soc.* **1980**, *102*, 7971 – 7972; b) R. T. Brown, M. F. Jones, M. Wingfield, *J. Chem. Soc. Chem. Commun.* **1984**, 847 – 848; c) T. Naito, O. Miyata, I. Ninomiya, *Heterocycles* **1987**, *26*, 1739 – 1742; d) M. Lounasmaa, J. Miettinen, P. Hanhinen, R. Jokela, *Tetrahedron Lett.* **1997**, *38*, 1455 – 1458; e) M. Lounasmaa, R. Jokela, C. Laine, P. Hanhinen, *Heterocycles* **1998**, *49*, 445 – 450.

[148] a) K. C. Nicolaou, M. Nevalainen, B. S. Safina, M. Zak, S. Bulat, *Angew. Chem.* **2002**, *114*, 2021 – 2025; *Angew. Chem. Int. Ed.* **2002**, *41*, 1941 – 1945; b) K. C. Nicolaou, B. S. Safina, M. Zak, A. A. Estrada, S. H. Lee, *Angew. Chem.* **2004**, *116*, 5197 – 5202; *Angew. Chem. Int. Ed.* **2004**, *43*, 5087 – 5092; c) K. C. Nicolaou, M. Zak, B. S. Safina, S. H. Lee, A. A. Estrada, *Angew. Chem.* **2004**, *116*, 5202 – 5207; *Angew. Chem. Int. Ed.* **2004**, *43*, 5092 – 5097; d) K. C. Nicolaou, B. S. Safina, M. Zak, S. H. Lee, M. Nevalainen, M. Bella, A. A. Estrada, C. Funke, F. J. Zécri, S. Bulat, *J. Am. Chem. Soc.* **2005**, *127*, 11159 – 11175; e) K. C. Nicolaou, M. Zak, B. S. Safina, A. A. Estrada, S. H. Lee, M. Nevalainen, *J. Am. Chem. Soc.* **2005**, *127*, 11176 – 11183.

[149] For a review of the thiopeptide antibiotics, see: M. C. Bagley, J. W. Dale, E. A. Merritt, X. Xiong, *Chem. Rev.* **2005**, *105*, 685 – 714.

[150] U. Mocek, Z. Zeng, D. O'Hagan, P. Zhou, L.-D. G. Fan, J. M. Beale, H. G. Floss, *J. Am. Chem. Soc.* **1993**, *115*, 7992 – 8001.

[151] For a similar dimerization/aza-Mannich sequence, see: G. Wulff, H. Böhnke, *Angew. Chem.* **1986**, *98*, 101 – 102; *Angew. Chem. Int. Ed. Engl.* **1986**, *25*, 90 – 92.

[152] For an advanced approach to thiostrepton, see: a) T. Mori, Y. Satouchi, H. Tohmiya, S. Higashibayashi, K. Hashimoto, M. Nakata, *Tetrahedron Lett.* **2005**, *46*, 6417 – 6422; b) T. Mori, H. Tohmiya, Y. Satouchi, S. Higashibayashi, K. Hashimoto, M. Nakata, *Tetrahedron Lett.* **2005**, *46*, 6423 – 6427.

[153] For the application of an aza-Diels–Alder reaction in the total synthesis of the related antibiotic amythiamicin D, see: a) R. A. Hughes, S. P. Thompson, L. Alcaraz, C. J. Moody, *Chem. Commun.* **2004**, 946 – 948; b) R. A. Hughes, S. P. Thompson, L. Alcaraz, C. J. Moody, *J. Am. Chem. Soc.* **2005**, *127*, 15644 – 15651.

[154] a) K. C. Nicolaou, K. B. Simonsen, G. Vassilikogiannakis, P. S. Baran, V. P. Vidali, E. N. Pitsinos, E. A. Couladouros, *Angew. Chem.* **1999**, *111*, 3762 – 3766; *Angew. Chem. Int. Ed.* **1999**, *38*, 3555 – 3559; b) K. C. Nicolaou, G. Vassilikogiannakis, K. B. Simonsen, P. S. Baran, Y.-L. Zhong, V. P. Vidali, E. N. Pitsinos, E. A. Couladouros, *J. Am. Chem. Soc.* **2000**, *122*, 3071 – 3079.

[155] D. Barnes-Seeman, E. J. Corey, *Org. Lett.* **1999**, *1*, 1503 – 1504.

[156] For biosynthetic proposals for the oxidative dimerization route to the bisorbicillinoids, see: a) N. Abe, T. Murata, A. Hirota, *Biosci. Biotechnol. Biochem.*, **1998**, *62*, 661 – 666; b) N. Abe, T. Murata, A. Hirota, *Biosci. Biotechnol. Biochem.* **1998**, *62*, 2120 – 2126; c) K. C. Nicolaou, R. Jautelat, G. Vassilikogiannakis, P. S. Baran, K. B. Simonsen, *Chem. Eur. J.* **1999**, *5*, 3651 – 3665.

[157] Y. Zeng, S. Reddy, E. Hirt, J. Aubé, *Org. Lett.* **2004**, *6*, 4993 – 4995.

[158] J. E. Golden, J. Aubé, *Angew. Chem.* **2002**, *114*, 4492 – 4494; *Angew. Chem. Int. Ed.* **2002**, *41*, 4316 – 4318.

[159] Y. Zeng, J. Aubé, *J. Am. Chem. Soc.* **2005**, *127*, 15712 – 15713.

[160] For the first report of the intramolecular Schmidt reaction, see: a) J. Aubé, G. L. Milligan, *J. Am. Chem. Soc.* **1991**, *113*, 8965 – 8966; for selected applications of this reaction in total synthesis, see: b) R. Iyengar, K. Schildknegt, J. Aubé, *Org. Lett.* **2000**, *2*, 1625 – 1627; c) R. Iyengar, K. Schildknegt, M. Morton, J. Aubé, *J. Org. Chem.* **2005**, *70*, 10645 – 10652; d) B. T. Smith, J. A. Wendt, J. Aubé, *Org. Lett.* **2002**, *4*, 2577 – 2579; e) A. Wrobleski, K. Sahasrabudhe, J. Aubé, *J. Am. Chem. Soc.* **2002**, *124*, 9974 – 9975; f) A. Wrobleski, K. Sahasrabudhe, J. Aubé, *J. Am. Chem. Soc.* **2004**, *126*, 5475 – 5481.

[161] For a similar strategy for the synthesis of the stenine ring system involving a Beckmann rearrangement, see: S. H. Jung, J. E. Lee, H. J. Joo, S. H. Kim, H. Y. Koh, *Bull. Korean Chem. Soc.* **2000**, *21*, 159 – 160.

[162] a) J. D. Ginn, A. Padwa, *Org. Lett.* **2002**, *4*, 1515 – 1517; b) A. Padwa, J. D. Ginn, *J. Org. Chem.* **2005**, *70*, 5197 – 5206.

[163] A. Padwa, J. D. Ginn, M. S. McClure, *Org. Lett.* **1999**, *1*, 1559 – 1561.

[164] a) A. Padwa, M. A. Brodney, M. Dimitroff, *J. Org. Chem.* **1998**, *63*, 5304 – 5305; for selected examples of the use of the intramolecular Diels–Alder reactions of activated furans, see: b) A. Padwa, M. A. Brodney, S. M. Lynch, *J. Org. Chem.* **2001**, *66*, 1716 – 1724; c) H. Zhang, A. Padwa, *Org. Lett.* **2006**, *8*, 247 – 250.

[165] S. K. Bur, S. M. Lynch, A. Padwa, *Org. Lett.* **2002**, *4*, 473 – 476.

[166] For other total syntheses of stenine, see: a) C. Chen, D. J. Hart, *J. Org. Chem.* **1990**, *55*, 6236 – 6240; b) C. Chen, D. J. Hart, *J. Org. Chem.* **1993**, *58*, 3840 – 3849; c) P. Wipf, Y. Kim, D. M. Goldstein, *J. Am. Chem. Soc.* **1995**, *117*, 11106 – 11112; d) Y. Morimoto, M. Iwahashi, K. Nishida, Y. Hayashi, H. Shirahama, *Angew. Chem.* **1996**, *108*, 968 – 970; *Angew. Chem. Int. Ed. Engl.* **1996**, *35*, 904 – 906; e) Y. Morimoto, M. Iwahashi, T. Kinoshita, K. Nishida, *Chem. Eur. J.* **2001**, *7*, 4107 – 4116.

[167] For selected examples, see: a) D. L. Boger, J. S. Panek, *J. Am. Chem. Soc.* **1985**, *107*, 5745 – 5754; b) D. L. Boger, R. S. Coleman, *J. Am. Chem. Soc.* **1987**, *109*, 2717 – 2727; c) D. L. Boger, R. S. Coleman, *J. Am. Chem. Soc.* **1988**, *110*, 1321 – 1323; d) H. H. Wasserman, R. W. DeSimone, D. L. Boger, C. M. Baldino, *J. Am. Chem. Soc.* **1993**, *115*, 8457 – 8458; e) D. L.

 © 2006 Wiley-VCH Verlag GmbH & Co. KGaA, Weinheim

Boger, C. M. Baldino, *J. Am. Chem. Soc.* **1993**, *115*, 11418 – 11425.

[168] G. I. Elliot, J. Velcicky, H. Ishikawa, Y. Li, D. L. Boger, *Angew. Chem.* **2006**, *118*, 636 – 638; *Angew. Chem. Int. Ed.* **2006**, *45*, 620 – 622.

[169] R. N. Warrener, D. Margetic, E. R. T. Tiekink, R. A. Russell, *Synlett* **1997**, 196 – 198.

[170] S. E. Wolkenberg, D. L. Boger, *J. Org. Chem.* **2002**, *67*, 7361 – 7364.

[171] a) A. Padwa, A. T. Price, *J. Org. Chem.* **1995**, *60*, 6258 – 6259; b) A. Padwa, A. T. Price, *J. Org. Chem.* **1998**, *63*, 556 – 565.

[172] G. D. Wilkie, G. I. Elliott, B. S. J. Blagg, S. E. Wolkenberg, D. R. Soenen, M. M. Miller, S. Pollack, D. L. Boger, *J. Am. Chem. Soc.* **2002**, *124*, 11292 – 11294.

[173] Minovine: a) Z. Q. Yuan, H. Ishikawa, D. L. Boger, *Org. Lett.* **2005**, *7*, 741 – 744; vindoline: b) Y. Choi, H. Ishikawa, J. Velcicky, G. I. Elliot, M. M. Miller, D. L. Boger, *Org. Lett.* **2005**, *7*, 4539 – 4542.

[174] For selected syntheses of vindorosine and vindoline, see: a) G. Büchi, K. E. Matsumoto, H. Nishimura, *J. Am. Chem. Soc.* **1971**, *93*, 3299 – 3301; b) M. Ando, G. Büchi, T. Ohnuma, *J. Am. Chem. Soc.* **1975**, *97*, 6880 – 6881; c) J. P. Kutney, U. Bunzli-Trepp, K. K. Chan, J. P. de Souza, Y. Fujise, T. Honda, J. Katsube, F. K. Klein, A. Leutwiler, S. Morehead, M. Rohr, B. R. Worth, *J. Am. Chem. Soc.* **1978**, *100*, 4220 – 4224; d) R. Z. Andriamialisoa, N. Langlois, Y. Langlois, *J. Org. Chem.* **1985**, *50*, 961 – 967; e) M. E. Kuehne, D. E. Podhorez, T. Mulamba, W. G. Bornmann, *J. Org. Chem.* **1987**, *52*, 347 – 353; f) P. L. Feldman, H. Rapoport, *J. Am. Chem. Soc.* **1987**, *109*, 1603 – 1604; g) K. Cardwell, B. Hewitt, M. Ladlow, P. Magnus, *J. Am. Chem. Soc.* **1988**, *110*, 2242 – 2248; h) ref. [90]; i) ref. [89].

[175] a) D. J. Hart, W.-L. Wu, *J. Am. Chem. Soc.* **1995**, *117*, 9369 – 9370; b) D. J. Hart, J. Li, W.-L. Wu, *J. Org. Chem.* **1997**, *62*, 5023 – 5033; c) S. Chackalamannil, R. J. Davies, T. Asberom, D. Doller, D. Leone, *J. Am. Chem. Soc.* **1996**, *118*, 9812 – 9813; d) S. Chackalamannil, R. J. Davies, Y. Wang, T. Asberom, D. Doller, J. Wong, D. Leone, *J. Org. Chem.* **1999**, *64*, 1932 – 1940; e) M. Takadoi, T. Katoh, A. Ishiwata, S. Terashima, *Tetrahedron Lett.* **1999**, *40*, 3399 – 3402; f) L. S.-M. Wong, M. S. Sherburn, *Org. Lett.* **2003**, *5*, 3603 – 3606.

[176] J. E. Baldwin, R. Chesworth, J. S. Parker, A. T. Russell, *Tetrahedron Lett.* **1995**, *36*, 9551 – 9554.

[177] For a review of biosynthetic Diels–Alder reactions, see: E. M. Stocking, R. M. Williams, *Angew. Chem.* **2003**, *115*, 3186 – 3223; *Angew. Chem. Int. Ed.* **2003**, *42*, 3078 – 3115.

[178] a) K. Tchabanenko, R. M. Adlington, A. R. Cowley, J. E. Baldwin, *Org. Lett.* **2005**, *7*, 585 – 588; b) K. Tchabanenko, R. Chesworth, J. S. Parker, N. K. Anand, A. T. Russell, R. M. Adlington, J. E. Baldwin, *Tetrahedron* **2005**, *61*, 11649 – 11656.

[179] E. Marsault, A. Toró, P. Nowak, P. Deslongchamps, *Tetrahedron* **2001**, *57*, 4243 – 4260.

[180] a) D. J. Mergott, S. A. Frank, W. R. Roush, *Proc. Natl. Acad. Sci. USA* **2004**, *101*, 11955 – 11959; b) S. A. Frank, W. R. Roush, *J. Org. Chem.* **2002**, *67*, 4316 – 4324; c) D. J. Mergott, S. A. Frank, W. R. Roush, *Org. Chem.* **2002**, *4*, 3157 – 3160.

[181] a) D. A. Evans, W. C. Black, *J. Am. Chem. Soc.* **1993**, *115*, 4497 – 4513; the Paquette group has also completed a total synthesis of spinosyn A; see: b) L. A. Paquette, Z. Gao, Z. Ni, G. F. Smith, *J. Am. Chem. Soc.* **1998**, *120*, 2543 – 2552; c) L. A. Paquette, I. Collado, M. Purdie, *J. Am. Chem. Soc.* **1998**, *120*, 2553 – 2562.

[182] For reviews, see: a) W. S. Wadsworth, Jr., *Org. React.* **1977**, *25*, 73 – 253; b) K. B. Becker, *Tetrahedron* **1980**, *36*, 1717 – 1745; c) B. E. Maryanoff, A. B. Reitz, *Chem. Rev.* **1989**, *89*, 863 – 927.

[183] a) W. R. Roush, M. Kageyama, *Tetrahedron Lett.* **1985**, *26*, 4327 – 4330; b) R. K. Boeckman, Jr., T. E. Barta, *J. Org. Chem.* **1985**, *50*, 3421 – 3423; c) W. R. Roush, M. Kageyama, R. Riva, B. B. Brown, J. S. Warmus, K. J. Moriarty, *J. Org. Chem.* **1991**, *56*, 1192 – 1210.

[184] C. D. Vanderwal, D. A. Vosburg, S. Weiler, E. J. Sorensen, *Org. Lett.* **1999**, *1*, 645 – 648.

[185] R. Höfs, M. Walker, A. Zeeck, *Angew. Chem.* **2000**, *112*, 3400 – 3403; *Angew. Chem. Int. Ed.* **2000**, *39*, 3258 – 3261.

[186] C. D. Vanderwal, D. A. Vosburg, E. J. Sorensen, *Org. Lett.* **2001**, *3*, 4307 – 4310.

[187] D. A. Vosburg, C. D. Vanderwal, E. J. Sorensen, *J. Am. Chem. Soc.* **2002**, *124*, 4552 – 4553.

[188] C. D. Vanderwal, D. A. Vosburg, S. Weiler, E. J. Sorensen, *J. Am. Chem. Soc.* **2003**, *125*, 5393 – 5407.

[189] a) D. A. Evans, J. T. Starr, *Angew. Chem.* **2002**, *114*, 1865 – 1868; *Angew. Chem. Int. Ed.* **2002**, *41*, 1787 – 1790; b) D. A. Evans, J. T. Starr, *J. Am. Chem. Soc.* **2003**, *125*, 13531 – 13540.

[190] A. D. Rodríguez, C. Ramírez, *Org. Lett.* **2000**, *2*, 507 – 510.

[191] a) R. S. Thornton, R. G. Kerr, *J. Chem. Ecol.* **2002**, *28*, 2083 – 2090; b) W. O'Neal, J. R. Pawlik, *Mar. Ecol. Prog. Ser.* **2002**, *240*, 117 – 126.

[192] For the isolation of elisabethin A, see: A. D. Rodríguez, E. González, S. D. Huang, *J. Org. Chem.* **1998**, *63*, 7083 – 7091.

[193] a) T. J. Heckrodt, J. Mulzer, *J. Am. Chem. Soc.* **2003**, *125*, 4680 – 4681; b) G. Zanoni, M. Franzini, *Angew. Chem.* **2004**, *116*, 4942 – 4946; *Angew. Chem. Int. Ed.* **2004**, *43*, 4837 – 4841.

[194] A. A. Boezio, E. R. Jarvo, B. M. Lawrence, E. N. Jacobsen, *Angew. Chem.* **2005**, *117*, 6200 – 6204; *Angew. Chem. Int. Ed.* **2005**, *44*, 6046 – 6050.

[195] a) K. C. Nicolaou, G. Vassilikogiannakis, W. Mägerlein, R. Kranich, *Angew. Chem.* **2001**, *113*, 2543 – 2547; *Angew. Chem. Int. Ed.* **2001**, *40*, 2482 – 2486; b) K. C. Nicolaou, G. Vassilikogiannakis, W. Mägerlein, R. Kranich, *Chem. Eur. J.* **2001**, *7*, 5359 – 5371.

[196] For a review highlighting similar cheletropic extrusion/IMDA cascades, see: A. Ichihara, *Synthesis* **1987**, 207 – 222.

[197] a) H. M. L. Davies, Q. Jin, *Proc. Natl. Acad. Sci. USA* **2004**, *101*, 5472 – 5475; b) H. M. L. Davies, Q. Jin, *J. Am. Chem. Soc.* **2004**, *126*, 10862 – 10863; c) H. M. L. Davies, R. E. J. Beckwith, *J. Org. Chem.* **2004**, *69*, 9241 – 9247.

[198] H. M. L. Davies, X. Dai, M. S. Long, *J. Am. Chem. Soc.* **2006**, *128*, 2485 – 2490.

[199] For reviews of kinetic resolution, see: E. Vedejs, M. Jure, *Angew. Chem.* **2005**, *117*, 4040 – 4069; *Angew. Chem. Int. Ed.* **2005**, *44*, 3974 – 4001, and references therein.

[200] D. C. Harrowven, D. D. Pascoe, D. Demurtas, H. O. Bourne, *Angew. Chem.* **2005**, *117*, 1247 – 1248; *Angew. Chem. Int. Ed.* **2005**, *44*, 1221 – 1222.

[201] a) J. O. Karlsson, N. V. Nguyen, L. D. Foland, H. W. Moore, *J. Am. Chem. Soc.* **1985**, *107*, 3392 – 3393; b) S. T. Perri, H. J. Dyke, H. W. Moore, *J. Org. Chem.* **1989**, *54*, 2032 – 2034; c) A. Enhsen, K. Karabelas, J. M. Heerding, H. W. Moore, *J. Org. Chem.* **1990**, *55*, 1177 – 1185.

[202] A. D. Rodríguez, C. Ramírez, I. I. Rodríguez, C. L. Barnes, *J. Org. Chem.* **2000**, *65*, 1390 – 1398.

[203] a) P. Joseph-Nathan, M. E. Garibay, R. L. Santillan, *J. Org. Chem.* **1987**, *52*, 759 – 763; b) I. H. Sanchez, R. Yanez, R. Enriquez, P. Joseph-Nathan, *J. Org. Chem.* **1981**, *46*, 2818 – 2819; c) P. Joseph-Nathan, V. Mendoza, E. Garcia, *Tetrahedron* **1977**, *33*, 1573 – 1576.

[204] a) A. I. Kim, S. D. Rychnovsky, *Angew. Chem.* **2003**, *115*, 1305 – 1308; *Angew. Chem. Int. Ed.* **2003**, *42*, 1267 – 1270. For selected recent reviews of the Nazarov cyclization, see: b) A. J. Frontier, C. Collison, *Tetrahedron* **2005**, *61*, 7577 – 7606; c) H. Pellissier, *Tetrahedron* **2005**, *61*, 6479 – 6517; d) M. A. Tius, *Eur. J. Org. Chem.* **2005**, 2193 – 2206; e) K. L. Habermas, S. E. Denmark, T. K. Jones, *Org. React.* **1994**, *45*, 1 – 158.

[205] N. Waizumi, A. R. Stankovic, V. H. Rawal, *J. Am. Chem. Soc.* **2003**, *125*, 13022 – 13023.

 © 2006 Wiley-VCH Verlag GmbH & Co. KGaA, Weinheim

[206] For discussions of the possible mechanisms of this and related reactions, see: a) Ref. [193b]; b) T. Linker, *J. Organomet. Chem.* **2002**, *661*, 159 – 167.
[207] a) G. Tsuchihashi, K. Kitajima, S. Mitamura, *Tetrahedron Lett.* **1981**, *22*, 4305 – 4308; b) Y. Honda, A. Ori, G. Tsuchihashi, *Bull. Chem. Soc. Jpn.* **1987**, *60*, 1027 – 1036.
[208] For a review of the synthesis of α-arylalkanoic acids by 1,2-aryl shift reactions, see: C. Giordano, G. Castaldi, F. Uggeri, *Angew. Chem.* **1984**, *96*, 413 – 419; *Angew. Chem. Int. Ed. Engl.* **1984**, *23*, 413 – 419.
[209] a) H. Kakeya, R. Onose, H. Koshino, A. Yoshida, K. Kobayashi, S.-I. Kageyama, H. Osada, *J. Am. Chem. Soc.* **2002**, *124*, 3496 – 3497; b) H. Kakeya, R. Onose, A. Yoshida, H. Koshino, H. Osada, *J. Antibiot.* **2002**, *55*, 829 – 831.
[210] H. Kakeya, R. Onose, H. Koshino, H. Osada, *Chem. Commun.* **2005**, 2575 – 2577.
[211] a) M. Shoji, J. Yamaguchi, H. Kakeya, H. Osada, Y. Hayashi, *Angew. Chem.* **2002**, *114*, 3324 – 3326; *Angew. Chem. Int. Ed.* **2002**, *41*, 3192 – 3194; b) M. Shoji, S. Kishida, M. Takeda, H. Kakeya, H. Osada, Y. Hayashi, *Tetrahedron Lett.* **2002**, *43*, 9155 – 9158.
[212] a) C. Li, S. Bardham, E. A. Pace, M.-C. Liang, T. D. Gilmore, J. A. Porco, Jr., *Org. Lett.* **2002**, *4*, 3267 – 3270.
[213] a) G. Mehta, K. Islam, *Tetrahedron Lett.* **2003**, *44*, 3569 – 3572; b) G. Mehta, K. Islam, *Tetrahedron Lett.* **2004**, *45*, 3611 – 3615.
[214] S. Kuwahara, S. Imada, *Tetrahedron Lett.* **2005**, *46*, 547 – 549.
[215] For reviews of the synthesis of natural products containing an epoxyquinone structure, see: a) K. Miyashita, T. Imanishi, *Chem. Rev.* **2005**, *105*, 4515 – 4536; b) J. Marco-Contelles, M. T. Molina, S. Anjum, *Chem. Rev.* **2004**, *104*, 2857 – 2899.
[216] This type of oxidation/electrocyclization/Diels–Alder dimerization cascade had previously been pioneered by the Porco group in the total synthesis of torreyanic acid; see: a) C. Li, E. Lobkovsky, J. A. Porco, Jr., *J. Am. Chem. Soc.* **2000**, *122*, 10484 – 10485; b) C. Li, R. P. Johnson, J. A. Porco, Jr., *J. Am. Chem. Soc.* **2003**, *125*, 5095 – 5106; for a more recent synthesis of torreyanic acid, see: c) G. Mehta, S. C. Pan, *Org. Lett.* **2004**, *6*, 3985 – 3988.
[217] M. Shoji, H. Imai, M. Mukaida, K. Sakai, H. Kakeya, H. Osada, Y. Hayashi, *J. Org. Chem.* **2005**, *70*, 79 – 91.
[218] C. Li, J. A. Porco, Jr., *J. Org. Chem.* **2005**, *70*, 6053 – 6065.
[219] M. F. Semmelhack, C. R. Schmid, D. A. Cortés, C. S. Chou, *J. Am. Chem. Soc.* **1984**, *106*, 3374 – 3376.
[220] For selected reviews of oxidations mediated by nitroxyl radicals, see: a) R. A. Sheldon, I. W. C. E. Arends, *Adv. Synth. Catal.* **2004**, *346*, 1051 – 1071; b) N. Merbouh, J. M. Bobbitt, C. Bruekner, *Org. Prep. Proced. Int.* **2004**, *36*, 3 – 31.
[221] a) M. Shoji, S. Kishida, Y. Kodera, I. Shiina, H. Kakeya, H. Osada, Y. Hayashi, *Tetrahedron Lett.* **2003**, *44*, 7205 – 7207; b) M. Shoji, H. Imai, I. Shiina, H. Kakeya, H. Osada, Y. Hayashi, *J. Org. Chem.* **2004**, *69*, 1548 – 1556.
[222] Trace amounts of this mode of [4+2] dimerization, to afford another natural product called epoxyquinol C, were observed by Hayashi and co-workers; see Ref. [217].
[223] For reviews of photocycloadditions, see: a) F. Müller, J. Mattay, *Chem. Rev.* **1993**, *93*, 99 – 117; b) J. J. McCullough, *Chem. Rev.* **1987**, *87*, 811 – 860.
[224] a) P. A. Wender, N. C. Ihle, *J. Am. Chem. Soc.* **1986**, *108*, 4678 – 4679; b) M. Murakami, K. Itami, Y. Ito, *Synlett* **1999**, 951 – 953.
[225] For reviews of [4+4] cycloaddition reactions in natural products synthesis, see: a) S. M. Sieburth, N. T. Cunard, *Tetrahedron* **1996**, *52*, 6251 – 6282; b) G. Kaupp, *Angew. Chem.* **1992**, *104*, 435 – 437; *Angew. Chem. Int. Ed. Engl.* **1992**, *31*, 422 – 424.
[226] C. Li, J. A. Porco, Jr., *J. Am. Chem. Soc.* **2004**, *126*, 1310 – 1311.
[227] For reviews of the synthesis and structure of silanols, see: a) V. Chandrasekhar, R. Boomishankar, S. Nagendran, *Chem. Rev.* **2004**, *104*, 5847 – 5910; b) P. D. Lickiss, *Adv. Inorg. Chem.* **1995**, *42*, 147 – 262.
[228] For selected applications of organosilanols in organic synthesis, see: a) S. Özçubukçu, F. Schmidt, C. Bolm, *Org. Lett.* **2005**, *7*, 1407 – 1409 (catalysts for asymmetric organozinc additions); b) S. E. Denmark, M. H. Ober, *Adv. Synth. Catal.* **2004**, *346*, 1703 – 1714; c) S. E. Denmark, R. F. Sweis, *Acc. Chem. Res.* **2002**, *35*, 835 – 846 (Hiyama cross-couplings); d) A. Mori, Y. Danda, T. Fujii, K. Hirabayashi, K. Osakada, *J. Am. Chem. Soc.* **2001**, *123*, 10774 – 10775 (conjugate additions); e) S. M. Sieburth, L. Fensterbank, *J. Org. Chem.* **1993**, *58*, 6314 – 6318 (*ortho*-metalation directing group).
[229] K. A. Parker, Y.-H. Lim, *J. Am. Chem. Soc.* **2004**, *126*, 15968 – 15969.
[230] a) M. F. Jacobsen, J. E. Moses, R. M. Adlington, J. E. Baldwin, *Org. Lett.* **2005**, *7*, 2473 – 2476; b) M. F. Jacobsen, J. E. Moses, R. M. Adlington, J. E. Baldwin, *Tetrahedron* **2006**, *62*, 1675 – 1689.
[231] C. M. Beaudry, D. Trauner, *Org. Lett.* **2005**, *7*, 4475 – 4477.
[232] For a review of biosynthetic and biomimetic electrocyclizations, see: C. M. Beaudry, J. P. Malerich, D. Trauner, *Chem. Rev.* **2005**, *105*, 4757 – 4778.
[233] C. M. Beaudry, D. Trauner, *Org. Lett.* **2002**, *4*, 2221 – 2224.
[234] For a review of acetylene coupling reactions, see: K. Sonogashira, *Comprehensive Organic Synthesis*, *Vol. 3* (Eds.: B. M. Trost, I. Fleming), Pergamon, Oxford, **1991**, pp. 551 – 561.
[235] For selected recent developments in Glaser-type coupling reactions, see: a) G. W. Kabalka, L. Wang, R. M. Pagni, *Synlett* **2001**, 108 – 110; b) J. Li, H. Jiang, *Chem. Commun.* **1999**, 2369 – 2370; c) S. Höger, A.-D. Meckenstock, H. Pellen, *J. Org. Chem.* **1997**, *62*, 4556 – 4557.
[236] S. P. H. Mee, V. Lee, J. E. Baldwin, *Angew. Chem.* **2004**, *116*, 1152 – 1153; *Angew. Chem. Int. Ed.* **2004**, *43*, 1132 – 1136.
[237] J. E. Moses, J. E. Baldwin, R. Marquez, R. M. Adlington, A. R. Cowley, *Org. Lett.* **2002**, *4*, 3731 – 3734.
[238] K. Kakinuma, C. A. Hanson, K. L. Rinehart, Jr., *Tetrahedron* **1976**, *32*, 217 – 222.
[239] a) K. Kurosawa, K. Takahashi, E. Tsuda, *J. Antibiot.* **2001**, *54*, 541 – 547; b) K. Takahashi, E. Tsuda, K. Kurosawa, *J. Antibiot.* **2001**, *54*, 548 – 553.
[240] B. E. Thomas IV, J. D. Evanseck, K. N. Houk, *J. Am. Chem. Soc.* **1993**, *115*, 4165 – 4169.
[241] F. L. Ansari, R. Qureshi, M. L. Qureshi, *Electrocyclic Reactions*, Wiley-VCH, Weinheim, **1999**, p. 288.
[242] Total synthesis of ocellapyrone A: J. E. Moses, R. M. Adlington, R. Rodriguez, S. J. Eade, J. E. Baldwin, *Chem. Commun.* **2005**, 1687 – 1689.
[243] Total synthesis of ocellapyrones A and B: A. K. Miller, D. Trauner, *Angew. Chem.* **2005**, *117*, 4678 – 4682; *Angew. Chem. Int. Ed.* **2005**, *44*, 4602 – 4606.
[244] Total synthesis of elysiapyrones A and B: J. E. Barbarow, A. K. Miller, D. Trauner, *Org. Lett.* **2005**, *7*, 2901 – 2903.
[245] K. C. Nicolaou, J. Li, *Angew. Chem.* **2001**, *113*, 4394 – 4398; *Angew. Chem. Int. Ed.* **2001**, *40*, 4264 – 4268.
[246] a) E. J. Tisdale, I. Slobodov, E. A. Theodorakis, *Proc. Natl. Acad. Sci. USA* **2004**, *101*, 12030 – 12035; b) E. J. Tisdale, I. Slobodov, E. A. Theodorakis, *Org. Biomol. Chem.* **2003**, *1*, 4418 – 4422; for earlier model studies by the same group, see: c) E. J. Tisdale, C. Chowdhury, B. G. Vong, H. Li, E. A. Theodorakis, *Org. Lett.* **2002**, *4*, 909 – 912.
[247] A. J. Quillinan, F. Scheinmann, *Chem. Commun.* **1971**, 966 – 967.
[248] K. C. Nicolaou, H. Xu, M. Wartmann, *Angew. Chem.* **2005**, *117*, 766 – 771; *Angew. Chem. Int. Ed.* **2005**, *44*, 756 – 761.
[249] a) K. C. Nicolaou, P. K. Sasmal, H. Xu, K. Namoto, A. Ritzén, *Angew. Chem.* **2003**, *115*, 4357 – 4361; *Angew. Chem. Int. Ed.*

 © 2006 Wiley-VCH Verlag GmbH & Co. KGaA, Weinheim

2003, *42*, 4225 – 4229; b) K. C. Nicolaou, P. K. Sasmal, H. Xu, *J. Am. Chem. Soc.* **2004**, *126*, 5493 – 5501.

[250] For a brief review of the aza-Cope/Mannich cascade, see: L. E. Overman, *Acc. Chem. Res.* **1992**, *25*, 352 – 359.

[251] M. Brüggemann, A. I. McDonald, L. E. Overman, M. D. Rosen, L. Schwink, J. P. Scott, *J. Am. Chem. Soc.* **2003**, *125*, 15284 – 15285.

[252] For a review of the chemistry of the *Stemona* alkaloids, see: R. A. Pilli, M. C. Ferreira de Oliveira, *Nat. Prod. Rep.* **2000**, *17*, 117 – 127.

[253] For a review covering charge-accelerated [3,3] sigmatropic rearrangements, see: R. P. Lutz, *Chem. Rev.* **1984**, *84*, 205 – 247.

[254] L. A. Overman, M. Kakimoto, M. E. Okazaki, G. P. Meier, *J. Am. Chem. Soc.* **1983**, *105*, 6622 – 6629.

[255] a) S. D. Knight, L. E. Overman, G. Pairaudeau, *J. Am. Chem. Soc.* **1993**, *115*, 9293 – 9294; b) S. D. Knight, L. E. Overman, G. Pairaudeau, *J. Am. Chem. Soc.* **1995**, *117*, 5776 – 5788.

[256] a) J. M. Fevig, R. W. Marquis, Jr., L. E. Overman, *J. Am. Chem. Soc.* **1991**, *113*, 5085 – 5086; b) S. R. Angle, J. M. Fevig, S. D. Knight, R. W. Marquis, Jr., L. E. Overman, *J. Am. Chem. Soc.* **1993**, *115*, 3966 – 3976.

[257] L. E. Overman, M. Sworin, R. M. Burk, *J. Org. Chem.* **1983**, *48*, 2685 – 2690.

[258] a) *Transition Metals for Organic Synthesis* (Eds.: M. Beller, C. Bolm), 2nd ed., Wiley-VCH, Weinheim, **2004**, p. 1344; b) L. S. Hegedus, *Transition Metals in the Synthesis of Complex Organic Molecules*, 2nd ed., University Science Books, Sausalito, **1999**, p. 337; c) *Comprehensive Organometallic Chemistry II*, *Vol. 12* (Eds.: E. W. Abel, F. G. A. Stone, G. Wilkinson), Pergamon, Oxford, **1995**, p. 1359.

[259] a) *Asymmetric Organocatalysis* (Eds.: A. Berkessel, H. Gröger), Wiley-VCH, Weinheim, **2005**, p. 440; b) J. Seayad, B. List, *Org. Biomol. Chem.* **2005**, *3*, 719 – 724; c) P. I. Dalko, L. Moisan, *Angew. Chem.* **2004**, *116*, 5248 – 5286; *Angew. Chem. Int. Ed.* **2004**, *43*, 5138 – 5175.

[260] a) *Enzyme Catalysis in Organic Synthesis*, *Vols. 1–3* (Eds.: K. Drauz, H. Waldmann), 2nd ed., Wiley-VCH, Weinheim, **2002**, p. 1556; b) B. G. Davis, V. Boyer, *Nat. Prod. Rep.* **2001**, *18*, 618 – 640.

[261] a) *Metal-Catalyzed Cross-Coupling Reactions*, *Vols. 1 and 2* (Eds.: F. Diederich, P. J. Stang), 2nd ed., Wiley-VCH, Weinheim, **2004**, p. 916; b) *Handbook of Organopalladium Chemistry for Organic Synthesis* (Ed.: E. Negishi), Wiley Interscience, New York, **2002**, p. 3350; c) "Cross-Coupling Reactions: A Practical Guide": *Top. Curr. Chem.* **2002**, *219*, 248 (Ed.: N. Miyaura).

[262] a) K. C. Nicolaou, P. G. Bulger, D. Sarlah, *Angew. Chem.* **2005**, *117*, 4516 – 4563; *Angew. Chem. Int. Ed.* **2005**, *44*, 4442 – 4489; b) L. F. Tietze, H. Ila, H. P. Bell, *Chem. Rev.* **2004**, *104*, 3453 – 3516; c) G. Poli, G. Giambastiani, A. Heumann, *Tetrahedron* **2000**, *56*, 5959 – 5989; d) A. de Meijere, S. Bräse, *J. Organomet. Chem.* **1999**, *576*, 88 – 110; e) A. Heumann, M. Réglier, *Tetrahedron* **1996**, *52*, 9289 – 9346.

[263] a) R. F. Heck, J. P. Nolley, Jr., *J. Org. Chem.* **1972**, *37*, 2320 – 2322; b) T. Mizoroki, K. Mori, A. Ozaki, *Bull. Chem. Soc. Jpn.* **1971**, *44*, 581; c) I. P. Beletskaya, A. V. Cheprakov, *Chem. Rev.* **2000**, *100*, 3009 – 3066; d) M. Shibasaki, E. M. Vogl, T. Ohshima, *Adv. Synth. Catal.* **2004**, *346*, 1533 – 1552.

[264] a) A. B. Dounay, L. E. Overman, *Chem. Rev.* **2003**, *103*, 2945 – 2963; b) J. T. Link, *Org. React.* **2002**, *60*, 157 – 534; c) M. Shibasaki, E. M. Vogl, *J. Organomet. Chem.* **1999**, *576*, 1 – 15; d) M. Shibasaki, C. D. J. Boden, A. Kojima, *Tetrahedron* **1997**, *53*, 7371 – 7395; e) E. Negishi, C. Copéret, S. Ma, S.-Y. Liou, F. Liu, *Chem. Rev.* **1996**, *96*, 365 – 393; f) L. E. Overman, *Pure Appl. Chem.* **1994**, *66*, 1423 – 1430.

[265] H. Nakamura, J. Kobayashi, M. Kobayashi, Y. Ohizumi, Y. Hirata, *Chem. Lett.* **1985**, 713 – 716.

[266] a) S. P. Maddaford, N. G. Andersen, W. A. Cristofoli, B. A. Keay, *J. Am. Chem. Soc.* **1996**, *118*, 10766 – 10773; for model studies by the same group, see: b) W. A. Cristofoli, B. A. Keay, *Synlett* **1994**, 625 – 627.

[267] The use of intramolecular polyene Heck cyclizations in natural product synthesis, at least in a diastereoselective fashion, had been pioneered by the Overman group in their approach to the scopadulcic acid family of diterpenes; see: a) M. E. Fox, C. Li, J. P. Marino, Jr., L. E. Overman, *J. Am. Chem. Soc.* **1999**, *121*, 5467 – 5480; b) L. E. Overman, D. J. Ricca, V. D. Tran, *J. Am. Chem. Soc.* **1997**, *119*, 12031 – 12040; c) L. E. Overman, D. J. Ricca, V. D. Tran, *J. Am. Chem. Soc.* **1993**, *115*, 2042 – 2044; d) D. J. Kucera, S. J. O'Connor, L. E. Overman, *J. Org. Chem.* **1993**, *58*, 5304 – 5306.

[268] F. Ozawa, A. Kubo, T. Hayashi, *J. Am. Chem. Soc.* **1991**, *113*, 1417 – 1419.

[269] a) W. Cabri, I. Candiani, *Acc. Chem. Res.* **1995**, *28*, 2 – 7; b) W. Cabri, I. Candiani, S. DeBernardinis, F. Francalanci, S. Penco, R. Santi, *J. Org. Chem.* **1991**, *56*, 5796 – 5800.

[270] For a more detailed discussion, see Ref. [264a].

[271] Subsequently, Shibasaki and co-workers reinvestigated the asymmetric cyclization of bromide **432** to give alkene **439** and found that, under significantly modified conditions, this transformation could be effected in 39% yield and 63% *ee*; see: F. Miyazaki, K. Uotsu, M. Shibasaki, *Tetrahedron* **1998**, *54*, 13073 – 13078.

[272] For other total synthesis of xestoquinone, see: a) H. S. Sutherland, K. C. Higgs, N. J. Taylor, R. Rodrigo, *Tetrahedron* **2001**, *57*, 309 – 317; b) R. Carlini, K. Higgs, C. Older, S. Randhawa, R. Rodrigo, *J. Org. Chem.* **1997**, *62*, 2330 – 2331; c) N. Harada, T. Sugioka, H. Uda, T. Kuriki, *J. Org. Chem.* **1990**, *55*, 3158 – 3163.

[273] An elegant palladium-catalyzed process, consisting of an intermolecular Suzuki coupling/intramolecular asymmetric Heck reaction cascade, has been employed by the Shibasaki group in their enantioselective synthesis of (+)-halenaquinone; see: a) A. Kojima, T. Takemoto, M. Sodeoka, M. Shibasaki, *J. Org. Chem.* **1996**, *61*, 4876 – 4877; b) A. Kojima, T. Takemoto, M. Sodeoka, M. Shibasaki, *Synthesis* **1998**, 581 – 589.

[274] For reviews of the Stille reaction, see: a) V. Farina, V. Krishnamurthy, W. J. Scott, *Org. React.* **1997**, *50*, 1 – 652; b) P. Espinet, A. M. Echavarren, *Angew. Chem.* **2004**, *116*, 4808 – 4839; *Angew. Chem. Int. Ed.* **2004**, *43*, 4704 – 4734; c) J. K. Stille, *Angew. Chem.* **1986**, *98*, 504 – 520; *Angew. Chem. Int. Ed. Engl.* **1986**, *25*, 508 – 524.

[275] The "stitching cyclization" cascade was pioneered by the Nicolaou group in their total synthesis of rapamycin; see: a) K. C. Nicolaou, T. K. Chakraborty, A. D. Piscopio, N. Minowa, P. Bertinato, *J. Am. Chem. Soc.* **1993**, *115*, 4419 – 4420; b) K. C. Nicolaou, A. D. Piscopio, P. Bertinato, T. K. Chakraborty, N. Minowa, K. Koide, *Chem. Eur. J.* **1995**, *1*, 318 – 333.

[276] M. Sugita, Y. Natori, T. Sasaki, K. Furihata, A. Shimazu, H. Seto, N. Otake, *J. Antibiot.* **1982**, *35*, 1460 – 1466.

[277] a) J. S. Panek, C. E. Masse, *J. Org. Chem.* **1997**, *62*, 8290 – 8291; b) C. E. Masse, M. Yang, J. Solomon, J. S. Panek, *J. Am. Chem. Soc.* **1998**, *120*, 4123 – 4134.

[278] E. J. Corey, R. H. Wollenberg, *J. Am. Chem. Soc.* **1974**, *96*, 5581 – 5583.

[279] For the application of the "stitching cyclization" cascade to the generation of an enediyne system in the total synthesis of dynemicin A, see: a) M. D. Shair, T. Y. Yoon, K. K. Mosny, T. C. Chou, S. J. Danishefsky, *J. Am. Chem. Soc.* **1996**, *118*, 9509 – 9525; b) M. D. Shair, T. Yoon, S. J. Danishefsky, *Angew. Chem.* **1995**, *107*, 1883 – 1885; *Angew. Chem. Int. Ed. Engl.* **1995**, *34*, 1721 – 1723; c) M. D. Shair, T. Yoon, S. J. Danishefsky, *J. Org. Chem.* **1994**, *59*, 3755 – 3757.

 © 2006 Wiley-VCH Verlag GmbH & Co. KGaA, Weinheim

[280] a) A. B. Smith III, J. Barbosa, W. Wong, J. L. Wood, *J. Am. Chem. Soc.* **1995**, *117*, 10777 – 10778; b) A. B. Smith III, J. Barbosa, W. Wong, J. L. Wood, *J. Am. Chem. Soc.* **1996**, *118*, 8316 – 8328.

[281] For the isolation and structure elucidation of the trienomycin antibiotics, see: a) I. Umezawa, S. Funayama, K. Okada, K. Iwasaki, J. Satoh, K. Masuda, K. Komiyama, *J. Antibiot.* **1985**, *38*, 699 – 705; b) S. Funayama, K. Okada, K. Komiyama, I. Umezewa, *J. Antibiot.* **1985**, *38*, 1107 – 1109; c) S. Funayama, K. Okada, K. Iwasaki, K. Komiyama, I. Umezawa, *J. Antibiot.* **1985**, *38*, 1677 – 1683; d) H. Nomoto, S. Katsumata, K. Takahashi, S. Funayama, K. Komiyama, I. Umezawa, S. Omura, *J. Antibiot.* **1989**, *42*, 479 – 481; e) A. B. Smith III, J. L. Wood, A. E. Gould, S. Ōmura, K. Komiyama, *Tetrahedron Lett.* **1991**, *32*, 1627 – 1630; f) A. B. Smith III, J. L. Wood, W. Wong, A. E. Gould, C. J. Rizzo, J. Barbosa, K. Komiyama, S. Ōmura, *J. Am. Chem. Soc.* **1996**, *118*, 8308 – 8315.

[282] C. W. Spangler, R. K. McCoy, A. A. Dembek, L. S. Sapochak, B. D. Gates, *J. Chem. Soc. Perkin Trans. 1* **1989**, 151 – 154.

[283] a) J. E. Baldwin, R. M. Adlington, S. H. Ramcharitar, *Tetrahedron* **1992**, *48*, 2957 – 2976; b) J. E. Baldwin, R. M. Adlington, S. H. Ramcharitar, *Synlett* **1993**, 875 – 877.

[284] a) I. Paterson, H.-G. Lombart, C. Allerton, *Org. Lett.* **1999**, *1*, 19 – 22; b) I. Paterson, J. Man, *Tetrahedron Lett.* **1997**, *38*, 695 – 698.

[285] G. D. Allred, L. D. Liebeskind, *J. Am. Chem. Soc.* **1996**, *118*, 2748 – 2749.

[286] For a brief review of the utility of copper(I) thiophene carboxylate in organic synthesis, see: A. Innitzer, *Synlett* **2005**, 2405 – 2406.

[287] At a higher substrate concentration of 0.2 M, monomer **452** was converted into a mixture of macrodimer **455** (42% yield) and macrotrimers (47% yield).

[288] For an alternative synthesis of elaiolide, see: D. A. Evans, D. M. Fitch, *J. Org. Chem.* **1997**, *62*, 454 – 455.

[289] J. J. Li, G. W. Gribble, *Palladium in Heterocyclic Chemistry*, Pergamon, New York, **2000**, p. 413.

[290] J. H. Chaplin, B. L. Flynn, *Chem. Commun.* **2001**, 1594 – 1595.

[291] For reviews of the synthesis of benzo[*b*]furans, see: a) X.-L. Hou, Z. Yang, H. N. C. Wong, *Prog. Heterocycl. Chem.* **2003**, *15*, 167 – 205; b) C. P. Dell, *Sci. Synth.* **2001**, *10*, 11 – 86; for more recent developments in the synthesis of benzo[*b*]furans, see: c) C. Chen, P. G. Dormer, *J. Org. Chem.* **2005**, *70*, 6964 – 6967, and references therein.

[292] D. J. Kerr, A. C. Willis, B. L. Flynn, *Org. Lett.* **2004**, *6*, 457 – 460.

[293] For selected recent developments in the palladium-catalyzed cross-coupling of organomagnesium reagents, see: M. E. Limmert, A. H. Roy, J. F. Hartwig, *J. Org. Chem.* **2005**, *70*, 9364 – 9370.

[294] For the development of practical iron-catalyzed cross-coupling reactions, see: a) A. Fürstner, R. Martin, *Chem. Lett.* **2005**, *34*, 624 – 629; b) C. Bolm, J. Legros, J. Le Paih, L. Zani, *Chem. Rev.* **2004**, *104*, 6217 – 6254.

[295] For the synthesis of benzo[*b*]furans and related heterocycles thorough palladium-catalyzed annulation of internal alkynes, see: R. C. Larock, E. K. Yum, M. J. Doty, K. K. C. Sham, *J. Org. Chem.* **1995**, *60*, 3270 – 3271.

[296] For a review of the synthesis of heterocycles through palladium π-olefin and π-alkyne chemistry, see: G. Zeni, R. C. Larock, *Chem. Rev.* **2004**, *104*, 2285 – 2309.

[297] For a more general review of transition metal-catalyzed reactions in heterocyclic synthesis, see: I. Nakamura, Y. Yamamoto, *Chem. Rev.* **2004**, *104*, 2127 – 2198.

[298] For examples of [1,7]-hydrogen shift/8π-electrocyclization cascades, see: G. Pohnert, W. Boland, *Tetrahedron* **1994**, *50*, 10235 – 10244.

[299] a) M. Inoue, A. J. Frontier, S. J. Danishefsky, *Angew. Chem.* **2000**, *112*, 777 – 780; *Angew. Chem. Int. Ed.* **2000**, *39*, 761 – 764; b) M. Inoue, M. W. Carson, A. J. Frontier, S. J. Danishefsky, *J. Am. Chem. Soc.* **2001**, *123*, 1878 – 1889.

[300] a) C. C. Hughes, D. Trauner, *Angew. Chem.* **2002**, *114*, 1639 – 1642; *Angew. Chem. Int. Ed.* **2002**, *41*, 1569 – 1572; b) C. C. Hughes, D. Trauner, *Tetrahedron* **2004**, *60*, 9675 – 9686.

[301] For a comprehensive treatise of metathesis reactions and applications, see: *Handbook of Metathesis*, *Vols. 1*, *2*, *and 3* (Ed.: R. H. Grubbs), Wiley-VCH, Weinheim, **2003**, p. 1234.

[302] a) C. Slugovc, *Macromol. Rapid Commun.* **2004**, *25*, 1283 – 1297; b) J. C. Mol, *J. Mol. Catal. A* **2004**, *213*, 39 – 45; c) M. Schuster, S. Blechert, *Angew. Chem.* **1997**, *109*, 2124 – 2145; *Angew. Chem. Int. Ed. Engl.* **1997**, *36*, 2036 – 2056.

[303] For an application in the total synthesis of (+)-asteriscanolide, see: J. Limanto, M. L. Snapper, *J. Am. Chem. Soc.* **2000**, *122*, 8071 – 8072.

[304] For the use of a ring-opening/cross-metathesis cascade in the total synthesis of bistramide A, see: A. V. Statsuk, D. Liu, S. A. Kozmin, *J. Am. Chem. Soc.* **2004**, *126*, 9546 – 9547.

[305] For the development of asymmetric ring-opening metathesis/cross-metathesis reactions, see: D. S. La, E. S. Sattely, J. G. Ford, R. R. Schrock, A. H. Hoveyda, *J. Am. Chem. Soc.* **2001**, *123*, 7767 – 7778.

[306] For the application of a tandem ring-closing metathesis/cross-metathesis cascade to the total synthesis of (−)-muricatacin, see: K. J. Quinn, A. K. Issacs, R. A. Arvary, *Org. Lett.* **2004**, *6*, 4143 – 4145.

[307] For selected applications in total synthesis, see: a) J. R. Stille, R. H. Grubbs, *J. Am. Chem. Soc.* **1986**, *108*, 855 – 856; b) M. Schaudt, S. Blechert, *J. Org. Chem.* **2003**, *68*, 2913 – 2920; c) Ref. [160f]; d) C. Stapper, S. Blechert, *J. Org. Chem.* **2002**, *67*, 6456 – 6460; e) R. Stragies, S. Blechert, *J. Am. Chem. Soc.* **2000**, *122*, 9584 – 9591; f) R. Stragies, S. Blechert, *Tetrahedron* **1999**, *55*, 8179 – 8188; for asymmetric approaches, see: g) G. S. Weatherhead, G. A. Cortez, R. R. Schrock, A. H. Hoveyda, *Proc. Natl. Acad. Sci. USA* **2004**, *101*, 5805 – 5809; h) S. D. Burke, N. Müller, C. M. Beaudry, *Org. Lett.* **1999**, *1*, 1827 – 1829.

[308] M. W. B. Pfeiffer, A. J. Phillips, *J. Am. Chem. Soc.* **2005**, *127*, 5334 – 5335.

[309] C. Palomo, M. Oiarbide, J. M. García, A. González, A. Lecumberri, A. Linden, *J. Am. Chem. Soc.* **2002**, *124*, 10288 – 10289.

[310] M. Scholl, S. Ding, C. W. Lee, R. H. Grubbs, *Org. Lett.* **1999**, *1*, 953 – 956.

[311] Model studies by the Phillips group had shown an ethylene atmosphere to be beneficial to this type of ring-rearrangement metathesis, presumably by helping to maintain active catalyst species; see: T. L. Minger, A. J. Phillips, *Tetrahedron Lett.* **2002**, *43*, 5357 – 5359.

[312] a) A. B. Smith III, S. A. Kozmin, C. M. Adams, D. V. Paone, *J. Am. Chem. Soc.* **2000**, *122*, 4984 – 4985; b) A. B. Smith III, C. M. Adams, S. A. Kozmin, D. V. Paone, *J. Am. Chem. Soc.* **2001**, *123*, 5925 – 5937.

[313] The Hoye group simultaneously and independently reported an alternative dimerization/macrocyclization strategy in the total synthesis of the structurally related congener (−)-cylindrocyclophane A, based on a double Horner–Wadsworth–Emmons olefination, see: T. R. Hoye, P. E. Humpal, B. Moon, *J. Am. Chem. Soc.* **2000**, *122*, 4982 – 4983.

[314] A. B. Smith III, S. A. Kozmin, D. V. Paone, *J. Am. Chem. Soc.* **1999**, *121*, 7423 – 7424.

[315] a) R. L. Danheiser, A. Nishida, S. Savariar, M. P. Trova, *Tetrahedron Lett.* **1988**, *29*, 4917 – 4920; b) R. L. Danheiser, S. K. Gee, *J. Org. Chem.* **1984**, *49*, 1672 – 1674; c) R. L. Danheiser, S. K. Gee, J. L. Perez, *J. Am. Chem. Soc.* **1986**, *108*, 806 – 810.

 © 2006 Wiley-VCH Verlag GmbH & Co. KGaA, Weinheim

[316] For a review of the synthesis of benzenoid compounds from acyclic precursors, see: P. Bamfield, P. F. Gordon, *Chem. Soc. Rev.* **1984**, *13*, 441 – 488.

[317] A "second generation" version of this aromatic annulation strategy was subsequently developed by the Danheiser group, in which the vinylketene intermediate is generated in situ through the photochemical Wolff rearrangement of an α,β-unsaturated α′-diazo ketone precursor; see: a) R. L. Danheiser, R. G. Brisbois, J. L. Kowalczyk, R. F. Miller, *J. Am. Chem. Soc.* **1990**, *112*, 3093 – 3100; b) R. L. Danheiser, D. D. Cha, *Tetrahedron Lett.* **1990**, *31*, 1527 – 1530.

[318] R. R. Schrock, J. S. Murdzek, G. C. Bazan, J. Robbins, M. DiMare, M. O'Regan, *J. Am. Chem. Soc.* **1990**, *112*, 3875 – 3886.

[319] It should be recalled, however, that in many cases the reverse reaction is kinetically slow, due to the fact that the product alkene is typically more hindered than the starting material alkenes. For a discussion, see: a) A. Fürstner, O. R. Thiel, L. Ackermann, *Org. Lett.* **2001**, *3*, 449 – 451; b) A. Fürstner, K. Radkowski, C. Wirtz, R. Goddard, C. W. Lehmann, R. Mynott, *J. Am. Chem. Soc.* **2002**, *124*, 7061 – 7069.

[320] For other selected examples of cross-metathesis/ring-closing-metathesis cascades, see: a) Ref. [319a]; b) T. D. Clark, M. R. Ghadiri, *J. Am. Chem. Soc.* **1995**, *117*, 12364 – 12365; c) K. Arakawa, T. Eguchi, K. Kakinuma, *J. Org. Chem.* **1998**, *63*, 4741 – 4745.

[321] For more detailed reviews of the use of metathesis-based reactions in total synthesis, see: a) K. C. Nicolaou, P. G. Bulger, D. Sarlah, *Angew. Chem.* **2005**, *117*, 4564 – 4601; *Angew. Chem. Int. Ed.* **2005**, *44*, 4490 – 4527; b) J. Mulzer, E. Öhler, *Top. Organomet. Chem.* **2004**, *7*, 269 – 366.

[322] For reviews of non-metathesis-based ruthenium-catalyzed carbon–carbon bond-forming reactions, see: a) B. M. Trost, M. U. Frederiksen, M. T. Rudd, *Angew. Chem.* **2005**, *117*, 6788 – 6825; *Angew. Chem. Int. Ed.* **2005**, *44*, 6630 – 6666; b) S. Dérien, F. Monnier, P. H. Dixneuf, *Top. Organomet. Chem.* **2004**, *7*, 1 – 44; c) B. Schmidt, *Angew. Chem.* **2003**, *115*, 5146 – 5149; *Angew. Chem. Int. Ed.* **2003**, *42*, 4996 – 4999; d) B. M. Trost, F. D. Toste, A. B. Pinkerton, *Chem. Rev.* **2001**, *101*, 2067 – 2096; e) T. Naota, H. Takaya, S.-I. Murahashi, *Chem. Rev.* **1998**, *98*, 2599 – 2660.

[323] B. M. Trost, A. F. Indolese, T. J. J. Müller, B. Treptow, *J. Am. Chem. Soc.* **1995**, *117*, 615 – 623.

[324] a) B. M. Trost, T. J. J. Müller, *J. Am. Chem. Soc.* **1994**, *116*, 4985 – 4986; b) B. M. Trost, T. J. J. Müller, J. Martinez, *J. Am. Chem. Soc.* **1995**, *117*, 1888 – 1899.

[325] For a palladium-catalyzed coupling of γ-hydroxyalkynoates and terminal alkynes to give β-substituted butenolides, see: B. M. Trost, M. C. McIntosh, *J. Am. Chem. Soc.* **1995**, *117*, 7255 – 7256.

[326] B. M. Trost, T. L. Calkins, C. G. Bochet, *Angew. Chem.* **1997**, *109*, 2746 – 2748; *Angew. Chem. Int. Ed. Engl.* **1997**, *36*, 2632 – 2635.

[327] For a more detailed discussion of the mechanism of this coupling process, see: a) Ref. [323]; b) Ref. [322a].

[328] For an alternative total synthesis of squamocin E, see: a) T. R. Hoye, Z. Ye, *J. Am. Chem. Soc.* **1996**, *118*, 1801 – 1802; for the total synthesis of squamocins A and D, see: b) U. Emde, U. Koert, *Tetrahedron Lett.* **1999**, *40*, 5979 – 5982; c) U. Emde, U. Koert, *Eur. J. Org. Chem.* **2000**, 1889 – 1904.

[329] For reviews of synthetic approaches to butenolides, see: a) R. Brückner, *Curr. Org. Chem.* **2001**, *5*, 679 – 718; b) D. W. Knight, *Contemp. Org. Synth.* **1994**, *1*, 287 – 315.

[330] The Trost group has recently extended the scope of the alkene–alkyne coupling to include macrocyclization processes, as demonstrated in their total synthesis and structure revision of amphidinolide A; see: a) B. M. Trost, P. E. Harrington, *J. Am. Chem. Soc.* **2004**, *126*, 5028 – 5029; b) B. M. Trost, S. T. Wrobleski, J. D. Chisholm, P. E. Harrington, M. Jung, *J. Am. Chem. Soc.* **2005**, *127*, 13589 – 13597; c) B. M. Trost, P. E. Harrington, J. D. Chisholm, S. T. Wrobleski, *J. Am. Chem. Soc.* **2005**, *127*, 13598 – 13610.

[331] For selected reviews of ene reactions, see: a) K. Mikami, T. Nakai, *Catalytic Asymmetric Synthesis* (Ed.: I. Ojima), 2nd ed., Wiley-VCH, New York, **2000**, pp. 543 – 568; b) K. Mikami, M. Shimizu, *Chem. Rev.* **1992**, *92*, 1021 – 1050; c) B. B. Snider, *Comprehensive Organic Synthesis*, *Vol. 2* (Eds.: B. M. Trost, I. Fleming), Pergamon, London, **1991**, pp. 527 – 581; d) B. B. Snider, *Comprehensive Organic Synthesis*, *Vol. 5* (Eds.: B. M. Trost, I. Fleming), Pergamon, London, **1991**, pp. 1 – 27; e) H. M. R. Hoffmann, *Angew. Chem.* **1969**, *81*, 597 – 618; *Angew. Chem. Int. Ed. Engl.* **1969**, *8*, 556 – 577.

[332] For an early review, see: F. D. Mango, *Coord. Chem. Rev.* **1975**, *15*, 109 – 205.

[333] For reviews of transition-metal-catalyzed cycloadditions (carbocyclizations), see: a) I. Nakamura, Y. Yamamoto, *Chem. Rev.* **2004**, *104*, 2127 – 2198; b) C. Aubert, O. Buisine, M. Malacria, *Chem. Rev.* **2002**, *102*, 813 – 834; c) H.-W. Frühauf, *Chem. Rev.* **1997**, *97*, 523 – 596; d) I. Ojima, M. Tzarmarioudaki, Z. Li, R. J. Donovan, *Chem. Rev.* **1996**, *96*, 635 – 662; e) M. Lautens, W. Klute, W. Tam, *Chem. Rev.* **1996**, *96*, 49 – 92.

[334] a) I. U. Khand, G. R. Knox, P. L. Pauson, W. E. Watts, M. I. Foreman, *J. Chem. Soc. Perkin Trans. 1* **1973**, 977 – 981; for reviews of the Pauson–Khand reaction, see: b) S. E. Gibson, N. Mainolfi, *Angew. Chem.* **2005**, *117*, 3082 – 3097; *Angew. Chem. Int. Ed.* **2005**, *44*, 3022 – 3037, and references therein.

[335] K. P. C. Vollhardt, *Acc. Chem. Res.* **1977**, *10*, 1 – 8.

[336] For selected recent advances in [2+2+2] cycloadditions, see: a) L. V. R. Boñaga, H.-C. Zhang, A. F. Moretto, H. Ye, D. A. Gauthier, J. Li, G. C. Leo, B. E. Maryanoff, *J. Am. Chem. Soc.* **2005**, *127*, 3473 – 3485; b) Y. Yamamoto, K. Kinpara, T. Saigoku, H. Takagishi, S. Okuda, H. Nishiyama, K. Itoh, *J. Am. Chem. Soc.* **2005**, *127*, 605 – 613; c) P. A. Evans, K. W. Lai, J. R. Sawyer, *J. Am. Chem. Soc.* **2005**, *127*, 12466 – 12467; d) H. A. Duong, M. J. Cross, J. Louie, *J. Am. Chem. Soc.* **2004**, *126*, 11438 – 11439; e) M. J. Eichberg, R. L. Dorta, K. Lamottke, K. P. C. Vollhardt, *Org. Lett.* **2000**, *2*, 2479 – 2481; f) J. Seo, H. M. P. Chui, M. J. Heeg, J. Montgomery, *J. Am. Chem. Soc.* **1999**, *121*, 476 – 477.

[337] For a review of recent advances in transition-metal-catalyzed annulations, see: M. Rubin, A. W. Sromek, V. Gevorgyan, *Synlett* **2003**, 2265 – 2291.

[338] For a review of transition-metal-mediated cycloaddition reactions of alkynes, see: N. E. Schore, *Chem. Rev.* **1988**, *88*, 1081 – 1119.

[339] P. A. Wender, H. Takahashi, B. Witulski, *J. Am. Chem. Soc.* **1995**, *117*, 4720 – 4721.

[340] P. A. Wender, C. O. Husfeld, E. Langkopf, J. A. Love, *J. Am. Chem. Soc.* **1998**, *120*, 1940 – 1941.

[341] P. A. Wender, F. Glorius, C. O. Husfeld, E. Langkopf, J. A. Love, *J. Am. Chem. Soc.* **1999**, *121*, 5348 – 5349.

[342] a) P. A. Wender, H. Rieck, M. Fuji, *J. Am. Chem. Soc.* **1998**, *120*, 10976 – 10977; b) P. A. Wender, C. O. Husfeld, E. Langkopf, J. A. Love, N. Pleuss, *Tetrahedron* **1998**, *54*, 7203 – 7220; c) P. A. Wender, C. M. Barzilay, A. J. Dyckman, *J. Am. Chem. Soc.* **2001**, *123*, 179 – 180; d) P. A. Wender, A. J. Dyckman, C. O. Husfeld, M. J. C. Scanio, *Org. Lett.* **2000**, *2*, 1609 – 1611; See also: e) P. Binger, P. Wedemann, S. I. Kozhushkov, A. de Meijere, *Eur. J. Org. Chem.* **1998**, 113 – 119.

[343] For selected reviews of the synthesis of seven-membered rings, see: a) J. B. Bremner, *Prog. Heterocycl. Chem.* **2003**, *15*, 385 – 430; b) E. J. Kantorowski, M. J. Kurth, *Tetrahedron* **2000**, *56*, 4317 – 4353; c) P. A. Wender, J. A. Love, *Adv. Cycloaddit.* **1999**, *5*, 1 – 45; d) J. O. Hoberg, *Tetrahedron* **1998**, *54*, 12631 – 12670.

[344] B. L. Ashfeld, S. F. Martin, *Org. Lett.* **2005**, *7*, 4535 – 4537.

 © 2006 Wiley-VCH Verlag GmbH & Co. KGaA, Weinheim

[345] The Trost group has subsequently developed ruthenium-catalyzed intramolecular [5+2] cycloadditions using the same catalyst systems as in the alkene–alkyne couplings; see: B. M. Trost, H. C. Shen, D. B. Horne, F. D. Toste, B. G. Steinmetz, C. Koradin, *Chem. Eur. J.* **2005**, *11*, 2577 – 2590.

[346] An alternative mechanistic scenario, involving initial metallacyclohexene formation from the VCP moiety followed by migratory insertion into the alkyne group to give intermediate **513**, may also be operative. For a discussion of the mechanism of this reaction, see Ref. [342a].

[347] a) P. A. Wender, A. J. Dyckman, C. O. Husfeld, D. Kadereit, J. A. Love, H. Rieck, *J. Am. Chem. Soc.* **1999**, *121*, 10442 – 10443; b) P. A. Wender, A. J. Dyckman, *Org. Lett.* **1999**, *1*, 2089 – 2092.

[348] Davies and Doan previously reported concise syntheses of (±)-tremulenediol A and (±)-tremulenolide A employing an elegant cyclopropanation/Cope rearrangement cascade; see: H. M. L. Davies, B. D. Doan, *J. Org. Chem.* **1998**, *63*, 657 – 660.

[349] For other total syntheses using this type of [5+2] cycloaddition, see: a) P. A. Wender, L. Zhang, *Org. Lett.* **2000**, *2*, 2323 – 2326; b) P. A. Wender, M. Fuji, C. O. Husfeld, J. A. Love, *Org. Lett.* **1999**, *1*, 137 – 139.

[350] For a conceptually different approach to transition-metal-catalyzed [5+2] cycloadditions, see: Y. Zhang, L. S. Liebeskind, *J. Am. Chem. Soc.* **2006**, *128*, 465 – 472, and references therein.

[351] a) M. P. Doyle, *Top. Organomet. Chem.* **2004**, *7*, 203 – 222; b) F. Zaragoza Dörwald, *Metal Carbenes in Organic Synthesis*, Wiley-VCH, Weinheim, **1999**, p. 283; c) M. P. Doyle, M. A. McKervey, T. Ye, *Modern Catalytic Methods for Organic Synthesis with Diazo Compounds: From Cyclopropanes to Ylides*, Wiley, New York, **1998**, p. 652.

[352] For selected reviews of metal-catalyzed carbenoid cyclopropanations, see: a) A. Pfalz, *Transition Metals for Organic Synthesis, Vol. 1* (Eds.: M. Beller, C. Bolm), 2nd ed., Wiley-VCH, Weinheim, **2004**, pp. 157 – 170; b) A. J. DelMonte, E. D. Dowdy, D. J. Watson, *Top. Organomet. Chem.* **2004**, *6*, 97 – 122; c) H. M. L. Davies, E. G. Antoulinakis, *Org. React.* **2001**, *57*, 1 – 326; for a special issue of *Chemical Reviews* dedicated to cyclopropanes and related rings, see: *Chem. Rev.* **2003**, *103*, 931 – 1648.

[353] For selected reviews of metal-carbenoid C–H insertion reactions, see: a) H. M. L. Davies, M. S. Long, *Angew. Chem.* **2005**, *117*, 3584 – 3586; *Angew. Chem. Int. Ed.* **2005**, *44*, 3518 – 3520; b) D. F. Taber, P. V. Joshi, *Modern Rhodium-Catalyzed Organic Reactions* (Eds.: P. A. Evans, J. Tsuji), Wiley-VCH, Weinheim, **2005**, pp. 357 – 377; c) H. M. L. Davies, R. E. J. Beckwith, *Chem. Rev.* **2003**, *103*, 2861 – 2903.

[354] a) G. Mehta, S. Muthusamy, *Tetrahedron* **2002**, *58*, 9477 – 9504; b) A. Padwa, M. D. Weingarten, *Chem. Rev.* **1996**, *96*, 223 – 269.

[355] T. Graening, V. Bette, J. Neudörfl, J. Lex, H.-G. Schmalz, *Org. Lett.* **2005**, *7*, 4317 – 4320.

[356] For earlier model studies by the same group, see: T. Graening, W. Friedrichsen, J. Lex, H.-G. Schmalz, *Angew. Chem.* **2002**, *114*, 1594 – 1597; *Angew. Chem. Int. Ed.* **2002**, *41*, 1524 – 1526.

[357] For a recent review of total syntheses of colchinine, see: T. Graening, H.-G. Schmalz, *Angew. Chem.* **2004**, *116*, 3292 – 3318; *Angew. Chem. Int. Ed.* **2004**, *43*, 3230 – 3256.

[358] For reviews of tropolone chemistry, see: a) G. Fischer, *Adv. Heterocycl. Chem.* **1996**, *66*, 285 – 403; b) G. Fischer, *Adv. Heterocycl. Chem.* **1995**, *64*, 81 – 157; c) F. Pietra, *Acc. Chem. Res.* **1979**, *12*, 132 – 138; d) F. Pietra, *Chem. Rev.* **1973**, *73*, 293 – 364.

[359] For initial studies and development of this type of cascade, see: a) K. Ueda, T. Ibata, M. Takebayashi, *Bull. Chem. Soc. Jpn.* **1972**, *45*, 2779 – 2782; b) A. Padwa, S. P. Carter, H. Nimmesgern, *J. Org. Chem.* **1986**, *51*, 1157 – 1158; c) A. Padwa, S. P. Carter, H. Nimmesgern, P. D. Stull, *J. Am. Chem. Soc.* **1988**, *110*, 2894 – 2900; d) A. Padwa, G. E. Fryxell, L. Zhi, *J. Am. Chem. Soc.* **1990**, *112*, 3100 – 3109.

[360] For selected reviews of 1,3-dipolar cycloaddition chemistry, see: a) *Cycloaddition Reactions in Organic Synthesis* (Eds.: S. Kobayashi, K. A. Jørgensen), Wiley-VCH, Weinheim, **2002**, p. 344; b) *Synthetic Applications of 1,3-Dipolar Cycloaddition Chemistry Toward Heterocycles and Natural Products* (Eds.: A. Padwa, W. H. Pearson), Wiley, New York, **2002**, p. 940; c) S. Karlsson, H.-E. Högberg, *Org. Prep. Proced. Int.* **2001**, *33*, 103 – 172.

[361] For related cycloaddition cascade approached to benzotropolone structures, see: a) C. Plüg, W. Friedrichsen, *Tetrahedron Lett.* **1992**, *33*, 7509 – 7510; b) C. Plüg, W. Friedrichsen, *J. Chem. Soc. Perkin Trans. 1* **1996**, 1035 – 1040; c) C. Plüg, W. Friedrichsen, T. Debaerdemaeker, *J. Prakt. Chem.* **1997**, *339*, 205 – 216; d) J. E. Baldwin, A. V. W. Mayweg, K. Neumann, G. J. Pritchard, *Org. Lett.* **1999**, *1*, 1933 – 1935.

[362] a) S. Nakamura, Y. Hirata, T. Kurosaki, M. Anada, O. Kataoka, S. Kitagaki, S. Hashimoto, *Angew. Chem.* **2003**, *115*, 5509 – 5513; *Angew. Chem. Int. Ed.* **2003**, *42*, 5351 – 5355; b) S. Nakamura, *Chem. Pharm. Bull.* **2005**, *53*, 1 – 10.

[363] I. Fleming, *Frontier Orbitals and Organic Chemical Reactions*, Wiley, New York, **1976**, p. 249.

[364] O. Kataoka, S. Kitagaki, N. Watanabe, J. Kobayashi, S. Nakamura, M. Shiro, S. Hashimoto, *Tetrahedron Lett.* **1998**, *39*, 2371 – 2374.

[365] For other carbonyl ylide cycloaddition approaches towards the zaragozic acids, see: a) D. M. Hodgson, J. M. Bailey, C. Villalonga-Barber, M. G. B. Drew, T. Harrison, *J. Chem. Soc. Perkin Trans. 1* **2000**, 3432 – 3443; b) D. M. Hodgson, C. Villalonga-Barber, *Tetrahedron Lett.* **2000**, *41*, 5597 – 5600; c) D. M. Hodgson, J. M. Bailey, T. Harrison, *Tetrahedron Lett.* **1996**, *37*, 4623 – 4626; d) H. Koyama, R. G. Ball, G. D. Berger, *Tetrahedron Lett.* **1994**, *35*, 9185 – 9188.

[366] For other total syntheses of zaragozic acid C, see: a) E. M. Carreira, J. Du Bois, *J. Am. Chem. Soc.* **1994**, *116*, 10825 – 10826; b) E. M. Carreira, J. Du Bois, *J. Am. Chem. Soc.* **1995**, *117*, 8106 – 8125; c) D. A. Evans, J. C. Barrow, J. L. Leighton, A. J. Robichaud, M. Sefkow, *J. Am. Chem. Soc.* **1994**, *116*, 12111 – 12112; d) H. Sato, S. Nakamura, N. Watanabe, S. Hashimoto, *Synlett* **1997**, 451 – 454; e) A. Armstrong, L. H. Jones, P. A. Barsanti, *Tetrahedron Lett.* **1998**, *39*, 3337 – 3340; f) A. Armstrong, P. A. Barsanti, L. H. Jones, G. Ahmed, *J. Org. Chem.* **2000**, *65*, 7020 – 7032.

[367] For total syntheses of the related metabolite zaragozic acid A, see: a) K. C. Nicolaou, A. Nadin, J. E. Leresche, E. W. Yue, S. La Greca, *Angew. Chem.* **1994**, *106*, 2312 – 2313; *Angew. Chem. Int. Ed. Engl.* **1994**, *33*, 2190 – 2191; b) K. C. Nicolaou, E. W. Yue, S. La Greca, A. Nadin, Z. Yang, J. E. Leresche, T. Tsuri, Y. Naniwa, F. De Riccardis, *Chem. Eur. J.* **1995**, *1*, 467 – 494; c) S. Caron, D. Stoermer, A. K. Mapp, C. H. Heathcock, *J. Org. Chem.* **1996**, *61*, 9126 – 9134; d) K. Tomooka, M. Kikuchi, K. Igawa, M. Suzuki, P.-H. Keong, T. Nakai, *Angew. Chem.* **2000**, *112*, 4676 – 4679; *Angew. Chem. Int. Ed.* **2000**, *39*, 4502 – 4505.

 © 2006 Wiley-VCH Verlag GmbH & Co. KGaA, Weinheim

VIP Mass Spectrometry

DOI: 10.1002/anie.200602449

Tissue Imaging at Atmospheric Pressure Using Desorption Electrospray Ionization (DESI) Mass Spectrometry**

*Justin M. Wiseman, Demian R. Ifa, Qingyu Song, and R. Graham Cooks**

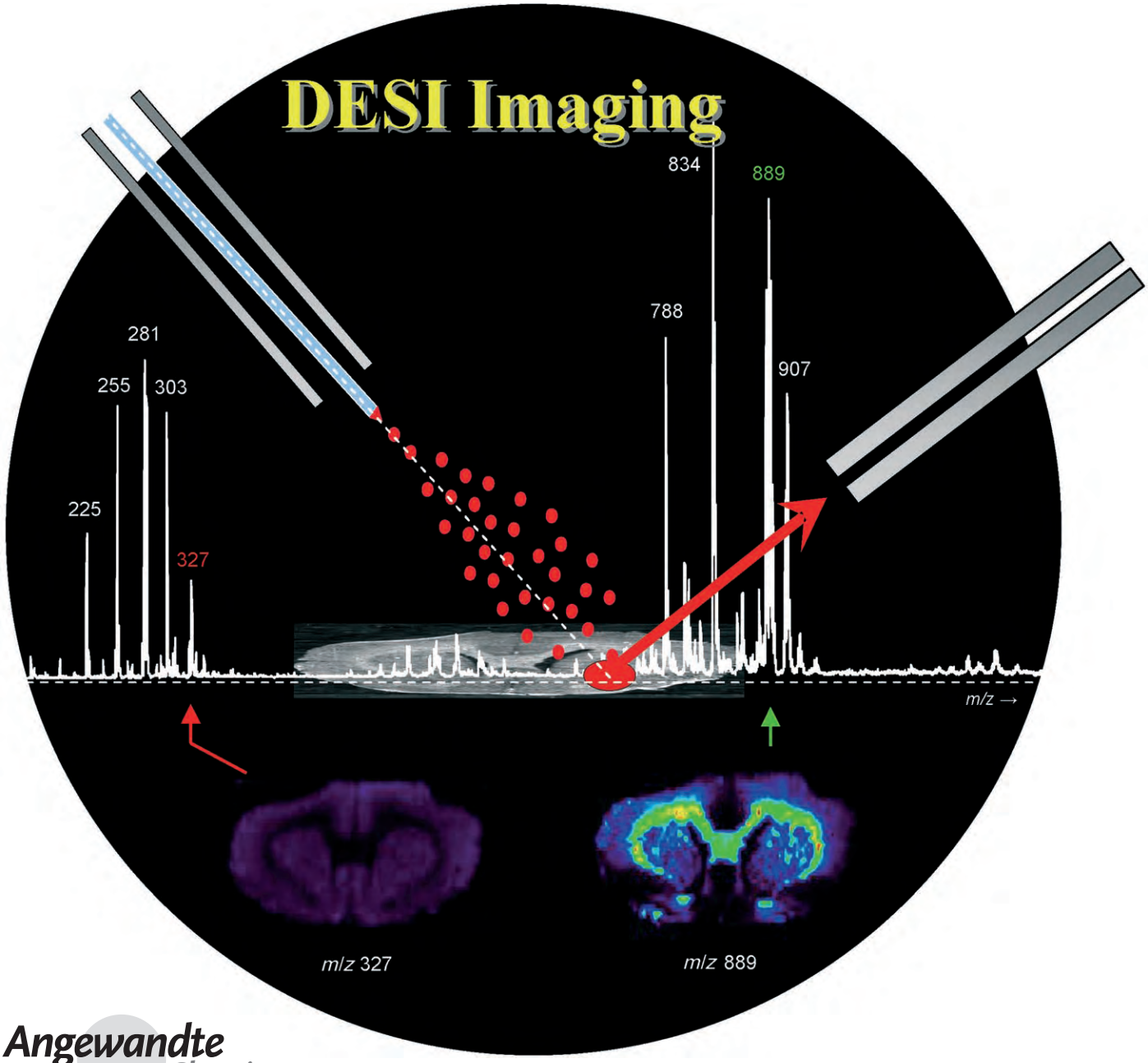

WILEY InterScience DISCOVER SOMETHING GREAT

© 2006 Wiley-VCH Verlag GmbH & Co. KGaA, Weinheim

Mass spectrometry (MS) is an increasingly indispensable tool in the biological sciences. Innovations in methods of creating, analyzing (mass), dissociating, reacting, and collecting ions are allowing the identification of increasingly complex biomolecules and molecular complexes, and some of these innovations hold the promise of implementation in a clinical setting. We report on one such new development, imaging of biological tissue sections at atmospheric pressure without prior chemical treatment of the tissue. The experiment uses a new mass spectrometry technique, desorption electrospray ionization (DESI),[1,2] introduced as one of a family of methods that have extended the applications of mass spectrometry to ordinary samples in the ambient environment. The DESI methodology is demonstrated here to allow mapping of the distribution of specific lipids directly from thin histological sections of rat brain with spatial resolution of less than 500 μm and with unit-mass resolution.

DESI is a novel ionization technique that permits the analysis of surfaces without the addition of a matrix or other treatment while the sample is held under ambient conditions.[1] It is a desorption ionization (DI) method in which the surface being analyzed is impacted by charged droplets of solvent generated from an electrospray. With this method, high-throughput surface analysis is achieved at atmospheric pressure. An analogous method uses charged droplets of glycerol and ammonium acetate, although the sample is maintained under vacuum.[3]

The potential of DESI for molecular imaging was recognized early.[4] Direct analysis of histological tissue sections was demonstrated recently,[5] where profiling of liver adenocarcinoma tissue sections revealed differences in the phospholipid profiles along a scan line extending from the tumor to nontumor regions. The presence of specific sphingomyelins marked the tumor margin, and this has implications for the underlying biochemistry of sphingomyelin metabolism in adenocarcinomas.

The present study reports the first 2D molecular images of biological samples using ambient mass spectrometry. Elemental or molecular images of samples, including biological tissue samples examined under vacuum, have been reported using DI techniques, specifically secondary-ion mass spectrometry (SIMS) and matrix-assisted laser desorption ionization (MALDI). The earliest experiments[6] used finely focused primary-ion beams as probes, and these were rastered across a surface to record images showing elemental or small-molecule distributions. At the end of 1970s, SIMS studies in this lab successfully mapped cocaine and cinnamoylcocaine in whole coca plant tissues[7] and muscarine in fungal tissues.[8] Recently, imaging mass spectrometry has emerged as a powerful technique in the biological sciences and is based on MALDI[9,10] and SIMS.[11] SIMS has the advantage of very high (micron scale) spatial resolution, while MALDI is applicable to larger molecules and is faster but gives lower resolution and requires the addition of a matrix to the sample. MALDI imaging of histological sections of biological tissues has been demonstrated previously, especially in the case of peptides and proteins.[12] The method, as developed by Caprioli et al.,[9,13] permits the analysis of peptides and proteins directly from tissue sections after matrix deposition and introduction of the sample into the vacuum system. Thus the quality of data obtained in these studies depends on the choice of the matrix compound, the matrix solvent, and the homogeneity of the matrix coating. There would be advantages to methods that require no sample treatment prior to sample analysis to allow a true in situ measurement; DESI-MS provides this capability. DESI is also complementary to MALDI imaging in that lipids are more readily ionized by DESI while peptides and proteins are more readily examined by MALDI (although in neither case do these represent intrinsic restrictions in the methodology).

The spot size in the DESI-MS imaging experiment depends on the capillary diameter and the tip-to-surface distance, among other parameters.[14] However, the achievable spatial resolution appears to be significantly poorer than the impacting spot diameter; in some experiments a spatial resolution of 250 μm is achieved at a signal/noise ratio (S/N) of 10:1 (see Supporting Information). In the DESI imaging experiment the sample (placed onto a target such as a microscope slide, or it is analyzed in situ) is moved under the fixed spray nozzle to study an area of interest. This process generates a mass spectrum for each exposed area or pixel on the surface. Ion images of the sampled area showing the spatial (2D) distribution of the intensity of a selected ion (or set of ions) are created from the data.

The negative-ion DESI mass spectrum from a rat brain section is shown in Figure 1 a and represents the average mass spectrum recorded from the tissue section. In the low mass/charge region ($m/z < 400$), ions corresponding to deprotonated free fatty acids palmitate (m/z 255), oleate (m/z 281), stearate (m/z 283), arachidonate (m/z 303), and docosohexaenoate (DHA; m/z 327) are present, along with other ions. In the high m/z region ($m/z > 600$), ions corresponding to the deprotonated forms of various lipids are present. The lipid species detected directly from the brain tissue in the m/z range 600–900 consist mainly of sulfatides, phosphatidylserines, and phosphatidylinositols. The less abundant species detected in the m/z range 700–800 are identified as phosphatidylethanolamines. The inset of Figure 1 a displays an MS/MS product-ion mass spectrum of the peak at m/z 885.6 which

[*] J. M. Wiseman, Dr. D. R. Ifa, Q. Song, Prof. R. G. Cooks
Department of Chemistry
Purdue University
West Lafayette, IN 47907 (USA)
Fax: (+1) 765-494-0239
E-mail: cooks@purdue.edu
Homepage: http://www.chem.purdue.edu/cooks/

[**] This work was supported by Prosolia Inc. (Indianapolis, IN) and the Office of Naval Research, and performed in the Bindley Biosciences Center. The authors gratefully thank Candice Kissinger, James Woods, and Peter Kissinger (Bioanalytical Systems Inc., West Lafayette, IN) for advice and for providing rat brain specimens for these studies. The authors also thank Shannon Cornett (Vanderbilt University) for information on data conversion. In addition, we thank Dominik Lenz (Purdue University, Bindley Bioscience Center) for providing optical images of rat brain sections. Frontispiece artwork by D.R.I. and J.M.W.

Supporting information for this article is available on the WWW under http://www.angewandte.org or from the author.

 © 2006 Wiley-VCH Verlag GmbH & Co. KGaA, Weinheim

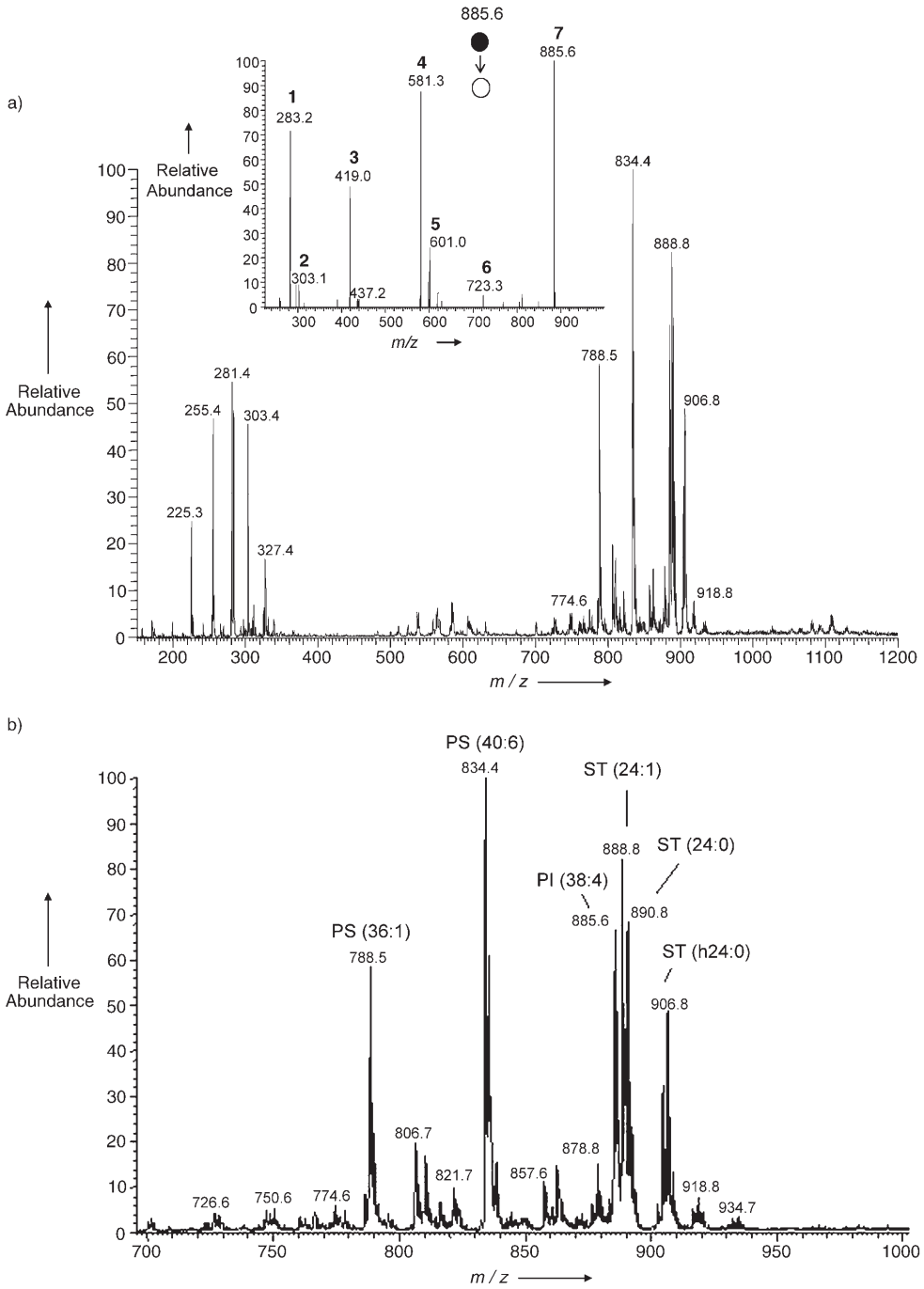

Figure 1. Negative-ion DESI mass spectrum recorded on a 4-μm thick coronal rat brain section examined using methanol/water (1:1 v/v) as the spray solvent. a) Full mass spectrum. The inset shows the MS/MS investigation of phosphatidylinositol (38:4). 1) $[C_{17}H_{36}COO]^-$; 2) $[C_{19}H_{32}COO]^-$; 3) $[M-H-(C_{17}H_{36}CH{=}C{=}O)-\text{Inositol}]^-$; 4) $[M-H-(C_{19}H_{32}COOH)]^-$; 5) $[M-H-(C_{17}H_{36}COOH)]^-$; 6) $[M-H-\text{Inositol}-H_2O]^-$; 7) $[M-H]^-$. b) Expanded view of the mass range from *m/z* 700–1000 including the molecular ion, $[M-H]^-$, signals from several specific phosphatidylserines (PSs), sulfatides (STs), and phosphatidylinositols (PIs).

shows fragment ions that identify it as phosphatidylinositol (38:4). Figure 1b shows an expanded view of the DESI mass spectrum in the *m/z* range 700–1000. Confirmation of the lipid assignments was achieved by tandem mass spectrometry (MS/MS), spectral comparisons with authentic lipid standards, and comparison to existing ESI mass spectra.[15] As the fragmentations of many different lipid species have been studied extensively,[15] lipids detected directly from the tissue surface could be identified through the MS/MS data. (A summary of the peak assignments and relative abundances for negative ions detected from the rat brain is provided in the Supporting Information.)

The spatial images of specific lipids (distributions of signal intensity) in the rat brain tissue are shown in Figure 2. For comparison, an optical image is provided in Figure 2a and major structural features are indicated. The negative ions detected from the tissue were deprotonated molecules of the form $[M-H]^-$. The ion images of the phospholipids phosphatidylinositol (PI), phosphatidylserine (PS), and sulfatide (ST) corresponding to peaks at *m/z* 885.6 (PI), *m/z* 834.4 and 788.5 (PS), and *m/z* 888.8 and 906.8 (ST), respectively, represent specific lipids at or near the surface of the tissue. The image of the ion at *m/z* 885.6, identified as PI 38:4, shows a relatively homogeneous distribution across the entire brain tissue section, except in the lateral ventricles where no signal is observed (Figure 2b). The ventricles in the rat brain are clearly resolved in the corresponding ion images, indicating that a lateral spatial resolution of less than 500 μm is achieved. The ion image of the peak at *m/z* 834.4, identified as PS 40:6 (Figure 2c), shows a homogeneous distribution in areas of the brain corresponding to gray matter (i.e. cerebral cortex). Its signal is less intense in the areas corresponding to white matter (e.g. corpus callosum). In contrast, the ion image in Figure 2f, corresponding to the peak at *m/z* 788.4 (PS 36:1), shows complementary localization with the ion image of PS 40:6. Distinctly different spatial intensity distributions are observed for the sulfatide peaks at *m/z* 888.8 and 906.8 (Figure 2d,e) than seen for the PI 38:4 ion image in Figure 2b. The sulfatide distributions show complementary localization with PS 40:6, and their intensity distributions resemble the distinctive corpus callosum and striatum anatomic structures in the brain section. In addition, the sulfatide intensity distributions (Figure 2d,e) are also localized in an anatomic substructure of the brain representing the anterior commissure.

 © 2006 Wiley-VCH Verlag GmbH & Co. KGaA, Weinheim

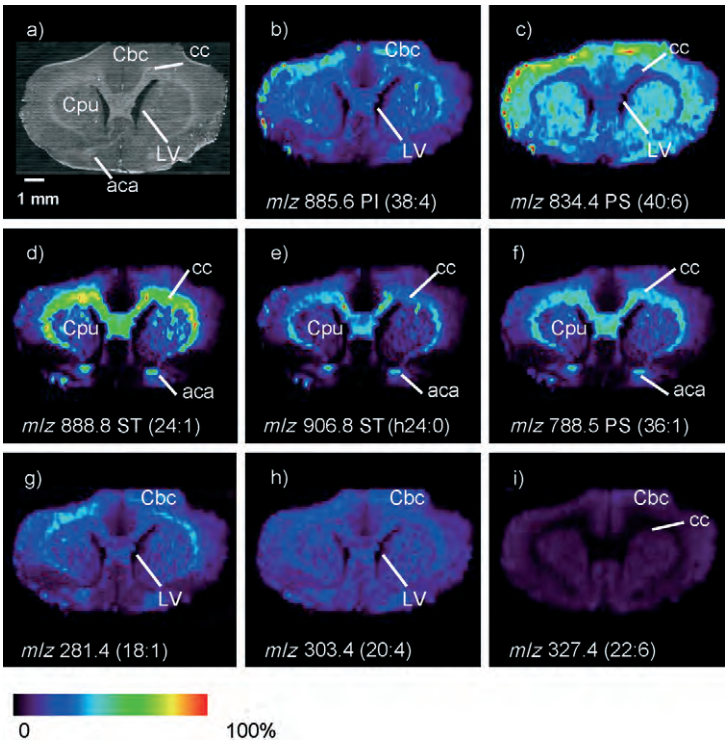

Figure 2. Selected molecular ion $[M-H]^-$ images of specific lipids from analysis of a 13×10 mm^2 area of rat brain tissue section. a) Optical image of the coronal section of the rat brain prior to analysis. cc = corpus callosum; CPu = striatum; Cbc = cerebral cortex; LV = lateral ventricle; aca = anterior part of anterior commissure. b–i) Ion images of PI (38:4; b), PS (40:6; c), ST (24:1; d), ST (h24:1; e), PS (36:1; f), oleate (18:1; g), arachidonate (20:4; h), and docosahexaenoate (22:6; i).

Homogeneous spatial intensity distributions across the entire tissue section are observed for the deprotonated ions of oleic acid (18:1; Figure 2g) and arachidonic acid (20:4; Figure 2h). However, the intensity of the ion at *m/z* 327 corresponding to DHA (22:6), an *n*−3 polyunsaturated fatty acid, is lower in the region of the brain corresponding to the corpus callosum.

These results are in qualitative agreement with the reported literature on lipid composition and distribution in brain tissue, suggesting that the spatial signal intensity distributions reflect relative concentration differences of the lipids in the brain tissue.[16] Specifically, sulfatides are known to be enriched in white matter but also present in neurons and astrocytes, and represent approximately 5% of the total lipids in adult brain myelin.[17] The selected ion images for the long-chain fatty-acid-containing sulfatides reflect these concentration differences in the brain and directly correlate with anatomic features corresponding to the corpus callosum and the striatum.

The results presented here represent the first application of DESI-MS to two-dimensional molecular-ion imaging of biological tissues. The capability of DESI-MS in providing spatial information about specific molecules on the tissue surface was demonstrated with a spatial resolution of less than 500 μm and with unit-mass resolution. The resulting ion images reflect the relative concentrations of the species detected from the tissue surface. The spatial resolution in these initial experiments is not as good as in MALDI and significantly poorer than in SIMS imaging, however, there are offsetting advantages in terms of ease of implementation and ambient analysis. Note also that the unit-mass resolved imaging data is complemented by tandem mass spectrometry information, which is used to confirm the identities of individual compounds or even to scan the tissue for groups of compounds that have a functional group of interest. These capabilities open the way to studies of drug distributions in tissue, diagnostic applications, biochemical investigations of anatomic substructures in tissue, and eventually to in vivo mass spectrometry.

Received: June 18, 2006
Published online: September 26, 2006

Keywords: lipids · mass spectrometry · microscopy · phospholipids · surface analysis

[1] Z. Takats, J. M. Wiseman, B. Gologan, R. G. Cooks, *Science* **2004**, *306*, 471.
[2] R. G. Cooks, Z. Ouyang, Z. Takats, J. M. Wiseman, *Science* **2006**, *311*, 1566.
[3] a) J. F. Mahoney, E. S. Parilis, T. D. Lee, *Nucl. Instrum. Methods Phys. Res. Sect. B* **1995**, *88*, 154; b) J. F. Mahoney, J. Perel, S. A. Ruatta, P. A. Martino, S. Husain, T. D. Lee, *Rapid Commun. Mass Spectrom.* **1991**, *5*, 441.
[4] Z. Takats, B. Gologan, J. M. Wiseman, R. G. Cooks, Purdue Research Foundation (West Lafayette, IN), US, **2003**.
[5] J. M. Wiseman, S. M. Puolitaival, Z. Takats, R. G. Cooks, R. M. Caprioli, *Angew. Chem.* **2005**, *117*, 7256; *Angew. Chem. Int. Ed.* **2005**, *44*, 7094.
[6] A. Benninghoven, F. G. Rudenauer, H. W. Werner, *Secondary Ion Mass Spectrometry: Basic Concepts, Instrumental Aspects, Applications and Trends*, Wiley, New York, **1987**.
[7] R. J. Day, S. E. Unger, R. G. Cooks, *J. Am. Chem. Soc.* **1979**, *101*, 501.
[8] R. J. Day, S. E. Unger, R. G. Cooks, *Anal. Chem.* **1980**, *52*, A557.
[9] R. M. Caprioli, T. B. Farmer, J. Gile, *Anal. Chem.* **1997**, *69*, 4751.
[10] L. A. McDonnell, S. R. Piersma, A. F. M. Altelaar, T. H. Mize, S. L. Luxembourg, P. D. E. M. Verhaert, J. van Minnen, R. M. A. Heeren, *J. Mass Spectrom.* **2005**, *40*, 160.
[11] a) M. L. Pacholski, N. Winograd, *Chem. Rev.* **1999**, *99*, 2977; b) D. Touboul, F. Kollmer, E. Niehuis, A. Brunelle, O. Laprevote, *J. Am. Soc. Mass Spectrom.* **2005**, *16*, 1608; c) P. J. Todd, T. G. Schaaff, P. Chaurand, R. M. Caprioli, *J. Mass Spectrom.* **2001**, *36*, 355; d) R. D. Harris, M. J. Van Stipdonk, E. A. Schweikert, *Int. J. Mass Spectrom.* **1998**, *174*, 167.
[12] a) K. Yanagisawa, Y. Shyr, B. G. J. Xu, P. P. Massion, P. H. Larsen, B. C. White, J. R. Roberts, M. Edgerton, A. Gonzalez, S. Nadaf, J. H. Moore, R. M. Caprioli, D. P. Carbone, *Lancet* **2003**, *362*, 433; b) P. Chaurand, S. A. Schwartz, R. M. Caprioli, *Anal. Chem.* **2004**, *76*, 86a; c) P. Chaurand, B. B. DaGue, R. S. Pearsall, D. W. Threadgill, R. M. Caprioli, *Proteomics* **2001**, *1*, 1320.
[13] M. Stoeckli, P. Chaurand, D. E. Hallahan, R. M. Caprioli, *Nat. Med.* **2001**, *7*, 493.
[14] Z. Takats, J. M. Wiseman, R. G. Cooks, *J. Mass Spectrom.* **2005**, *40*, 1261.

 © 2006 Wiley-VCH Verlag GmbH & Co. KGaA, Weinheim

[15] a) M. Pulfer, R. C. Murphy, *Mass Spectrom. Rev.* **2003**, *22*, 332; F.-F. Hsu, J. Turk, *J. Am. Soc. Mass Spectrom.* **2000**, *11*, 986; b) F.-F. Hsu, J. Turk, *J. Am. Soc. Mass Spectrom.* **2004**, *15*, 536.
[16] B. W. Argonoff, J. A. Benjamins, A. K. Hajra, *Basic Neurochemistry* (Ed.: G. J. Seigel), Lippincott-Raven, Philadelphia, **1994**, p. 48.
[17] I. Ishizuka, *Prog. Lipid Res.* **1997**, *36*, 245.

 © 2006 Wiley-VCH Verlag GmbH & Co. KGaA, Weinheim

Spin Crossover

DOI: 10.1002/anie.200601823

A Manganese(III) Complex That Exhibits Spin Crossover Triggered by Geometric Tuning**

Grace G. Morgan, Kevin D. Murnaghan, Helge Müller-Bunz, Vickie McKee, and Charles J. Harding*

Dedicated to Professor Jane Nelson

The design and synthesis of molecules with potential for information storage and processing is a focus in current materials research, an area in which bulk metal oxides still predominate. The potential of discrete transition-metal spin-crossover (SCO) complexes in this area is now starting to be realized as photoinduced switching emerges as an increasingly efficient trigger for spin conversion.[1] As the field continues to grow, it is important to identify new candidates with improved thermal or optical responses and also to fine-tune the molecular design for successful incorporation into devices.

Although the phenomenon is theoretically possible for octahedral d^4–d^7 ions, it is routinely observed only in Fe^{II} and Fe^{III} complexes, and to a lesser extent in Co^{II} complexes. This situation highlights the delicate balance between ligand-field strength, ionic charge, and the number of d electrons in determining SCO activity. For example, the contrast between the spin-labile Fe^{II} center and its d^6 analogue Co^{III} lies in the higher nuclear charge of Co^{III}, which stabilizes the $S = 0$ state. Similarly, SCO is rarely observed in Mn^{II} (d^5) complexes, in which the high-spin (HS) state is usually stabilized, in contrast to the isoelectronic Fe^{III} ion, for which many examples of spin conversion exist.[2]

Spin transitions in d^4 ions are, however, the most rare. The two potential candidates are Mn^{III} and Cr^{II} and although thermal SCO has been reported for both ions[3,4] it is considered exceptional. The best-known example is [Mn(trp)] (trp^{3-} = tris{1-(2-azolyl)-2-azabuten-4-yl}amine),[3] and investigations of its physical properties continue.[5,6] The only other well-characterized example $[CrI_2(depe)_2]$[4] (depe = 1,2-bis-(diethylphosphino)ethane) also continues to attract attention.[7] An early report of some Mn^{III} complexes, which were not structurally characterized, attributes the temperature dependence of the magnetic moment to exchange interactions, although SCO is a more likely interpretation.[8]

An important driving force for SCO is the change in metal–ligand bond length arising from the increased vibrational entropy in the HS state. The concomitant decrease in ligand-field splitting energy reduces the ligand-field stabilization energy (LFSE) associated with the maximum population of the t_{2g} orbitals. The reluctance of octahedral d^4 ions to undergo thermal SCO may be due to the very minor gain in LFSE on crossover from ^5E to ^3T as only one electron is transferred. In most crystal fields, the small LFSE gain for d^4 ions is outweighed by the energetic penalty of pairing two electrons, which results in both an increase in the destabilizing Coulomb repulsion energy π_c and a decrease in the stabilizing exchange energy π_e.[9]

Schiff base ligands with $N_4(O^-)_2$, $N_2(O^-)_2$, and $N_3(O^-)_3$ donor sets that are known to generate ligand fields close to the crossover value for Fe^{III} [10] tend to stabilize manganese in its +III oxidation state, in which it is normally HS. Recently, however, we have observed that modulation of the orientation of the $N_4(O^-)_2$ donors in a series of hexadentate ligands has a dramatic effect on the spin state of Mn^{III} complexes and that gradual thermal SCO may be attained when the phenolate oxygen donors are *trans* to each other. This geometry is achieved by varying the length of the alkyl chains in the starting tetraamine. The use of a triethylene-tetraamine link (in L1) orients the oxygen donors *cis* to each other and produces a HS Mn^{III} complex, whereas lengthening the link by two methylene groups (L2) orients the oxygen donors in *trans* geometry and thermal SCO results.

To illustrate this phenomenon, we report the structures and temperature dependence of the magnetic susceptibility of $[MnL1]NO_3{\cdot}EtOH$ (**1**) and $[MnL2]NO_3$ (**2**), which exhibit different geometries of the $N_4(O^-)_2$ donor set. The syntheses of the perchlorate salts of both complexes have been reported as part of an investigation into their electron-transfer activity.[11]

L1 forms a temperature-independent HS complex with Mn^{III} (**1**), which has a magnetic moment of 4.8 μ_B between 80 and 300 K. In contrast, the magnetic moment of complex **2** has significant temperature dependence (Figure 1). The absence of a plausible pathway for intermolecular exchange

[*] Dr. G. G. Morgan, Dr. K. D. Murnaghan, Dr. H. Müller-Bunz
Centre for Synthesis and Chemical Biology
Conway Institute for Biomedical and Biomolecular Research and
School of Chemistry and Chemical Biology
University College Dublin
Belfield, Dublin 4 (Ireland)
Fax: (+353) 1-716-2127
E-mail: grace.morgan@ucd.ie
Prof. V. McKee
Department of Chemistry
Loughborough University
Leicestershire, LE11 3TU (UK)
Dr. C. J. Harding
Department of Chemistry
The Open University
Walton Hall, Milton Keynes, MK7 6AA (UK)

[**] The authors would like to thank the University College Dublin, Enterprise Ireland, and the Royal Society of New Zealand (ISAT Linkages Fund) for financial support and the University of Otago for hosting a sabbatical visit (to G.G.M.) during manuscript preparation.

InterScience
© 2006 Wiley-VCH Verlag GmbH & Co. KGaA, Weinheim

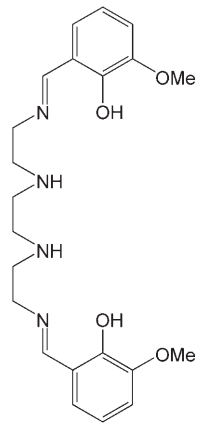

H_2L1

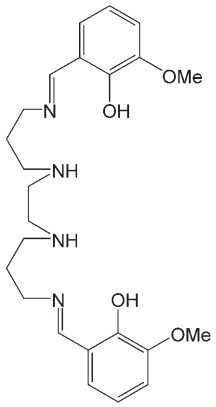

H_2L2

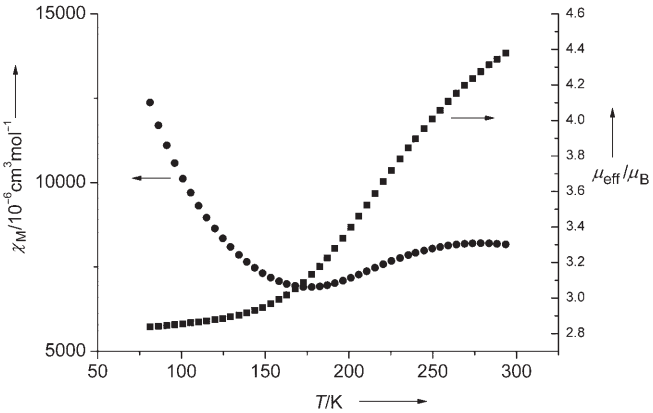

Figure 1. χ_M and μ_{eff} versus T for **2**.

and the sigmoid form of this temperature dependence confirms this process as SCO. At 80 K, the magnetic moment converges close to the expected LS value of 2.8 μ_B whereas at 300 K the HS limit is entropically inaccessible, as this is a one-electron SCO.[12] The gradual nature of the crossover reflects the inefficient communication between discrete Mn^{III} sites which is mediated only by weak hydrogen bonding.

Crystallographic data for **1** were collected at 100 K and for **2** at 100 and 300 K;[13] selected bond lengths for all structural determinations are given in Table 1, and structures of **1** and **2** (100 K) are shown in Figure 2 with a comparison of the Mn coordination spheres in both complexes shown in Figure 3.

Table 1: Selected bond lengths [Å] for **1** at 100 K and for **2** at 100 K and 300 K and differences in bond lengths for **2** between 100 K and 300 K (Δr_{HL}).

	1 100 K	**2** 100 K	**2** 300 K	**2** Δr_{HL}
Mn–N_{imine}	1.992(2) 2.051(2)	1.9883(11)	2.0723(19)	0.0840
Mn–N_{amine}	2.064(2) 2.301(2)	2.0501(11)	2.161(2)	0.1109
Mn–O	2.0889(18) 1.8873(18)	1.8719(9)	1.8679(13)	−0.0040

HS octahedral complexes of d^4 transition-metal ions are expected to display larger radii, and hence longer metal–ligand bonds, than their LS counterparts. Additionally, distortions due to Jahn–Teller splitting are expected for the ^5E state. In the HS complex **1**, the geometry around Mn is distorted octahedral with two *cis* oxygen donors (O1 and O3), two *cis* amines (N2 and N3), and two *trans* imine nitrogen donors (N1 and N4). The long bonds to one of the oxygen atoms (O3) and one of the amine nitrogen atoms (N3) are in accordance with the expected static axial elongation. Structural data for the SCO complex **2** at both collection temperatures show that the geometry around Mn is again pseudooctahedral but now with the two oxygen donors oriented *trans* to each other and with more regular geometry. A twofold rotation axis through the Mn center bisects the ethylene linkage between the two amine nitrogen atoms N2 and N2a to generate geometrically equivalent pairs of *cis* imine (N1 and N1a), *cis* amine (N2 and N2a), and *trans* phenolate (O1 and O1a) donors.

Comparison of the bond lengths in **1** and **2** at 100 K (Figure 3) reveals a significant increase in the average Mn–donor bond lengths in the HS complex **1** over those in the LS

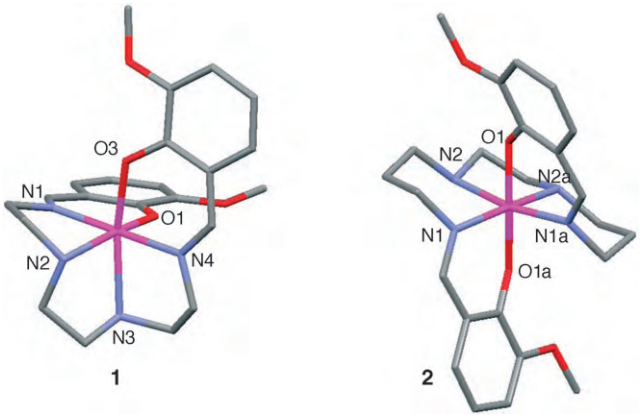

Figure 2. Structures of **1** and **2** at 100 K ($a = 0.5-x, 0.5-y, z$).

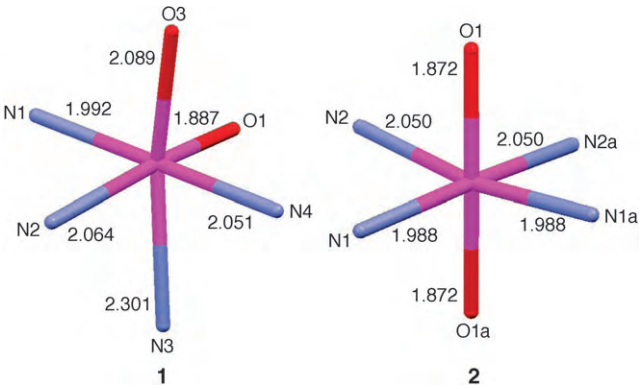

Figure 3. Comparison of Mn–donor bond lengths in **1** and **2** at 100 K ($a = 0.5-x, 0.5-y, z$).

© 2006 Wiley-VCH Verlag GmbH & Co. KGaA, Weinheim

SCO complex **2**, and the significant change in the sum of the bond lengths (12.384 Å for **1** compared with 11.821 Å for **2**) is consistent with different orbital populations for the two complexes at 100 K.

Of greater significance is the comparison between the bond lengths of **2** at the two collection temperatures (Figure 4). The most striking feature is the significant

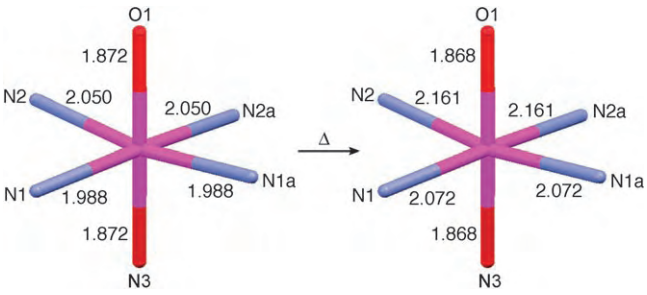

Figure 4. Comparison of Mn–donor distances in **2** at 100 K and 300 K ($a = 0.5-x, 0.5-y, z$).

elongation of all four equatorial Mn–N bond lengths in sharp contrast to the axial Mn–O bond lengths, which remain unchanged. This structural change is in good agreement with population of the antibonding $d_{x^2-y^2}$ orbital upon switching to the HS state (Figure 5), which should result in longer equatorial distances relative to the ^{3}T state.

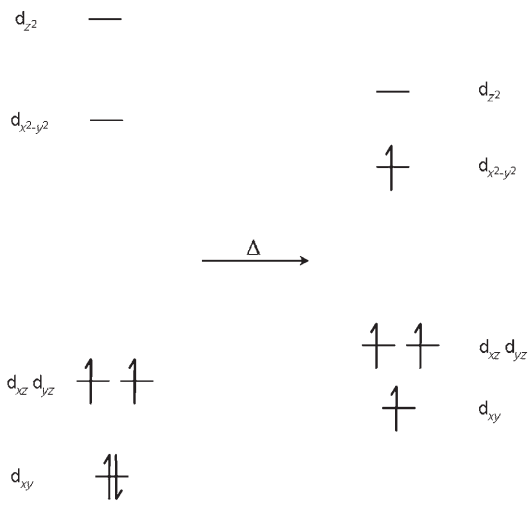

Figure 5. Orbital populations for the $S = 1$ and $S = 2$ states of **2**.

Thermal population of the $d_{x^2-y^2}$ orbital rather than the d_{z^2} orbital as a result of the SCO produces an unusual axial compression in the predominantly HS form of **2** at 300 K. Axially compression in HS Mn^{III} complexes is rare and is often associated with significant geometric distortion, which is not observed here.[14]

The bond length difference between the high- and low-spin ions (Δr_{HL}) is not expected to be as large for d^4 metals as it is for ions with d^5 and d^6 configurations, as only one electron is removed from an antibonding orbital upon transition to the $S = 1$ state in d^4 complexes. In Fe^{II} complexes, the bond-length change may be as large as 0.2 Å, whereas the smaller changes upon crossover in Fe^{III} complexes (typically ca. 0.1 Å) are ascribed to the asymmetric population of the t_{2g} orbital set in the LS state, in which one electron hole exists.[14]

The change in bond lengths for d^4 SCO complexes upon moving from $S = 2$ to $S = 1$ should therefore be expected to be significantly less than for d^5 complexes, as only one electron is removed from the e_g* orbital set and two electron holes remain in the t_{2g} orbitals upon switching to the ^{3}T state. The bond-length change in **2** is 0.06 Å (averaged over all six donors), which is in line with the expected trend.

The flexible open-chain chelating ligand L2 can readily accommodate the necessary structural changes that accompany SCO. This situation is more difficult to achieve with a macrocylic ligand such as cyclam (1,4,8,11-tetraazacyclotetradecane), which also coordinates Mn^{III} with an N_4 equatorial donor set, and with various exogenous axial donors.[15] When these are cyano ligands, the LS state of the Mn^{III} complex is stabilized with short axial bonds but surprisingly long equatorial bonds.[15b] Presumably the more rigid macrocycle constrains the contraction of the equatorial bonds that is expected in LS Mn^{III} complexes.

In conclusion, we have demonstrated that thermal SCO in Mn^{III} complexes is accessible with the $N_4(O^-)_2$ donor set of L2 and that the effect was triggered by orienting the methoxy-substituted phenolate donors *trans* to each other in the more flexible ligand. No crossover was observed when the phenolate donors were *cis*, and orientation of the donors, and thus the SCO phenomenon, was controlled by modification of the chain length of the chelating ligand. This result opens up a route to the synthesis of a new family of d^4 SCO candidates, and work is already underway to establish the series.

Experimental Section

1: 3-Methoxy-2-hydroxy-benzaldehyde (0.92 g, 6 mmol) in ethanol (30 mL) was added to triethylenetetraamine (0.73 g, 3 mmol) in ethanol (15 mL), and then solid $Mn(NO_3)_2{\cdot}6H_2O$ (0.54 g, 3 mmol) was added. Dark-brown crystals precipitated from the filtered solution after 48 h. Yield: 220 mg (13.5 %). Elemental analysis (%) calcd for $C_{24}H_{34}N_5O_8Mn$: C 50.09, H 5.95, N 12.17; found: C 49.72, H 5.91, N 12.09.

2: Neat *N*,*N*′-Bis(3-aminopropyl)ethylenediamine (0.54 g, 3.1 mmol) was added to a solution of 3-methoxy-2-hydroxy-benzaldehyde (0.99 g, 6.5 mmol) in ethanol (25 mL), and then solid $Mn(NO_3)_2{\cdot}6H_2O$ (0.54 g, 3 mmol) was added. The solution was heated to reflux for 20 minutes and filtered while hot. Black crystals formed almost instantly on cooling. Yield: 650 mg (39 %). Elemental analysis (%) calcd for $C_{24}H_{32}N_5O_7Mn$: C 51.71, H 5.79, N 12.56; found: C 51.67, H 5.75, N 12.52.

Magnetic susceptibilities were measured between 80 and 300 K on a Faraday balance calibrated with $Hg[Co(NCS)_4]$. Experimental susceptibilities were corrected for the diamagnetism of the constituent atoms by using Pascal's constants. Crystal data for **1** and **2** were collected at 100 K on a Bruker SMART APEX CCD area detector diffractometer and for **2** at 300 K on a Bruker SMART 1000 diffractometer. Crystal-structure pictures were generated with Mercury.[16]

Received: May 9, 2006
Published online: October 9, 2006

 © 2006 Wiley-VCH Verlag GmbH & Co. KGaA, Weinheim

Keywords: ligand design · magnetic properties · manganese · molecular switches · spin crossover

[1] a) A. Hauser, *Top. Curr. Chem.* **2004**, *234*, 155 – 198; b) S. Bonhommeau, G. Molnár, A. Galet, A. Zwick, J.-A. Real, J. J. McGarvey, A. Bousseksou, *Angew. Chem.* **2005**, *117*, 4137 – 4141; *Angew. Chem. Int. Ed.* **2005**, *44*, 4069 – 4073.

[2] P. J. van Konigsbruggen, Y. Maeda, H. Oshio, *Top. Curr. Chem.* **2004**, *233*, 259 – 324.

[3] P. G. Sim, E. Sinn, *J. Am. Chem. Soc.* **1981**, *103*, 241 – 243.

[4] D. M. Halepoto, D. G. L. Holt, L. F. Larkworthy, G. L. Leigh, D. C. Povey, G .W. Smith, *J. Chem. Soc. Chem. Commun.* **1989**, 1322 – 1323.

[5] Y. Garcia, O Kahn, J-P. Ader, A. Buzdin, Y. Meurdesoif, M. Guillot, *Phys. Lett.* A **2000**, *271*, 145 – 154.

[6] a) M. Nakano, G. Matsubayashi, T. Matsuo, *Phys. Rev. B* **2002**, *66*, 212412 – 212415; b) S. Kimura, Y. Narumi, D. Kindo, M. Nakano and G. Matsubayashi, *Phys. Rev. B* **2005**, *72*, 064448.

[7] V. Ksenofontov, A. B. Gaspar, G. Levchenko, B. Fitzsimmons, P. Gütlich, *J. Phys. Chem.* B **2004**, *108*, 7723.

[8] V. V. Zelentsov, I. K. Somova, *Zh. Obshch. Khim.* **1974**, *44*, 1309 – 1313.

[9] Y. Garcia, P. Gütlich, *Top.Curr.Chem.* **2004**, *234*, 49 – 62.

[10] J.-P. Costes, F. Dahan, J.-P. Laurent, *Inorg. Chem.* **1990**, *29*, 2448 – 2452.

[11] a) A. Panja, N. Shaikh, R. J. Butcher, P. Banerjee, *Inorg. Chim. Acta* **2003**, *352*, 27 – 33; b) A. Panja, N. Shaikh, S. Gupta, R. J. Butcher, P. Banerjee, *Eur. J. Inorg. Chem.* **2003**, 1540 – 1547.

[12] P. Gütlich, Y. Garcia, H. Spiering, *Magnetism: Molecules to Materials*, *Vol. IV* (Ed.: J. S. Miller, M. Drillon), Wiley-VCH, Weinheim, **2002**, Chapter 8.

[13] Crystal data for **1** (at 100(2) K): $0.30 \times 0.05 \times 0.02\ mm^3$, monoclinic, $P2_1/c$, $a = 17.661(2)$, $b = 11.836(1)$, $c = 12.863(1)$ Å, $\beta = 105.595(2)°$, $V = 2589.8(5)$ Å^3, $\rho_{calcd} = 1.476\ Mg\,m^{-3}$, $2\theta_{max} = 50.00°$, $Mo_{K\alpha}$ ($\lambda = 0.71073$ Å), φ-ω-scans, 18064 reflections collected, 4548 unique (all included in refinement), correction for Lorentzian polarization and absorption: semi-empirical from equivalents (program SADABS,[17a] $\mu = 0.568\ mm^{-1}$, max. and min. transmission 0.9887 and 0.8583), solution: direct methods (SHELXS-97[17b]), refinement: full-matrix least-squares against $|F^2|$ (SHELXL-97-2[17c]), 346 parameters, hydrogen atoms were added at calculated positions and refined by using a riding model, $R_1 = 0.059$, $wR_2 = 0.099$, residual electron density: $0.431\ e^-$ Å^{-3}. Crystal data for **2** (at 100(2) K): $0.5 \times 0.4 \times 0.2\ mm^3$, orthorhombic, *Pccn*, $a = 17.837(1)$, $b = 8.4113(6)$, $c = 16.813(1)$ Å, $V = 2589.8(5)$ Å^3, $\rho_{calcd} = 1.468\ Mg\,m^{-3}$, $2\theta_{max} = 57.19°$, $Mo_{K\alpha}$ ($\lambda = 0.71073$ Å), ϕ-ω-scans, 20136 reflections collected, 3078 independent (all included in refinement), correction for Lorentzian polarization and absorption: semi-empirical from equivalents (program SADABS,[17a] $\mu = 0.577\ mm^{-1}$, max. and min. transmission 0.8933 and 0.7764), solution: direct methods (SHELXS-97[17b]), refinement: full-matrix least-squares against $|F^2|$ (SHELXL-97-2[17c]), 233 parameters, hydrogen atoms were located in the difference Fourier map and allowed to refine freely, $R_1 = 0.034$, $wR_2 = 0.083$, residual electron density: $0.461\ e^-$ Å^{-3}. Crystal data for **2** (at 300(2) K): $0.65 \times 0.15 \times 0.10\ mm^3$, orthorhombic, *Pccn*, $a = 17.833(2)$, $b = 8.914(1)$, $c = 16.504(2)$ Å, $V = 2623.8(6)$ Å^3, $\rho_{calcd} = 1.411\ Mg\,m^{-3}$, $2\theta_{max} = 50.00°$, $Mo_{K\alpha}$ ($\lambda = 0.71073$ Å), φ-ω-scans, 17576 reflections collected, 2314 independent (all included in refinement), correction for Lorentzian polarization and absorption: semi-empirical from equivalents (programs SADABS,[16d] SMART,[16e] and SAINT,[16e] $\mu = 0.555\ mm^{-1}$, max. and min. transmission 1.0000 and 0.8363). The structure was solved by direct methods and refined by full-matrix least-squares on F^2 by using the SHELXTL suite of programs.[16f] 172 parameters, hydrogen atoms bonded to carbon were added at calculated positions and refined by using a riding model. The hydrogen atom bonded to N2 was located from a difference map and refined with a fixed, isotropic displacement parameter. $R_1 = 0.048$, $wR_2 = 0.089$, residual electron density: $0.185\ e^-$ Å^{-3}. CCDC-605565 (**1** at 100 K), -605564 (**2** at 100 K), and -605566 (**2** at 300 K) contain the supplementary crystallographic data for this paper. These data can be obtained free of charge from The Cambridge Crystallographic Data Centre via www.ccdc.cam.ac.uk/data_request/cif.

[14] a) C. Mantel, A. K. Hassan, J. Pécaut, A. Deronzier, M.-N. Collomb, C. Duboc-Toia, *J. Am. Chem. Soc.* **2003**, *125*, 12337 – 12344; b) A. K. Gregson, D. M. Doddrell, P. C. Healy, *Inorg. Chem.* **1978**, *17*, 1216 – 1219.

[15] a) S. Mossin, H. Osholm Sørensen, H. Weihe, J. Glerup, I. Sotofte, *Inorg. Chim. Acta* **2005**, *358*, 1096 – 1106; b) S. Mossin, H. Osholm Sørensen, H. Weihe, *Acta Crystallogr. Sect. C* **2002**, *58*, m204 – m206.

[16] I. J. Bruno, J. C. Cole, P. R. Edgington, M. K. Kessler, C. F. Macrae, P. McCabe, J. Pearson, R. Taylor, *Acta Crystallogr. Sect. B* **2002**, *58*, 389 – 397.

[17] a) G. M. Sheldrick, SADABS, Bruker AXS Inc., Madison, WI 53711, USA, **2000**; b) G. M. Sheldrick, SHELXS-97, University of Göttingen, **1997**; c) G. M. Sheldrick SHELXL-97-2, University of Göttingen, **1997**; d) G. M. Sheldrick, SADABS, Bruker AXS Inc., Madison, WI 53711, USA, **2003**; e) Bruker **1998** SMART (version 5.625 and SAINT (version 6.02), Bruker AXS, Madison, WI 53711, USA; f) G. M. Sheldrick, SHELXTL version 6.12, **2001**, Bruker AXS, Madison, WI 53711, USA.

 © 2006 Wiley-VCH Verlag GmbH & Co. KGaA, Weinheim

Nanostructures

DOI: 10.1002/anie.200602298

Nanofibers with Tunable Stiffness from Self-Assembly of an Amphiphilic Wedge–Coil Molecule**

*Jung-Keun Kim, Eunji Lee, and Myongsoo Lee**

Self-assembly of amphiphilic block molecules can lead to a variety of nanostructures, which include spherical micelles, vesicles, nanofibers, and tubes.[1] Extensive efforts have thus been made toward the design of novel molecular architec-

[*] J.-K. Kim, E. Lee, Prof. M. Lee
Center for Supramolecular Nanoassembly and
Department of Chemistry
Yonsei University
Shinchon 134, Seoul 120-749 (Korea)
Fax: (+82) 2-393-6096
E-mail: mslee@yonsei.ac.kr

[**] This work was supported by the National Creative Research Initiative Program of the Korean Ministry of Science and Technology. We acknowledge the Pohang Accelerator Laboratory, Korea, for use of the synchrotron radiation source. E.L. thanks the Seoul Science Fellowship Program.

Supporting information for this article is available on the WWW under http://www.angewandte.org or from the author.

© 2006 Wiley-VCH Verlag GmbH & Co. KGaA, Weinheim
InterScience

tures consisting of incompatible components that are able to assemble into nanostructures with desired functions. Among the nanostructures formed by self-assembly of designed molecules, a 1D fibrillar assembly has proved to be particularly interesting for applications such as nanowires and biomimetic macromolecules.[2] The 1D structures with stimuli-responsive features are likely to further enhance their scope as intelligent materials. Although stimuli-responsive nanostructures have been extensively studied with spherical objects,[3] switching of the properties triggered by external stimuli with 1D fibrillar objects remains challenging.[4] In this context, we have been interested in the preparation of a stimulus-responsive 1D cylindrical assembly with tunable properties triggered by the solvent environment.

Herein, we report the formation of cylindrical micelles from the self-assembly of a wedge–coil block molecule, and reversible switching between rigid rodlike aggregates and flexible coil-like aggregates triggered by a change in solvent polarity (Figure 1). The wedge–coil molecule, **1**, that forms

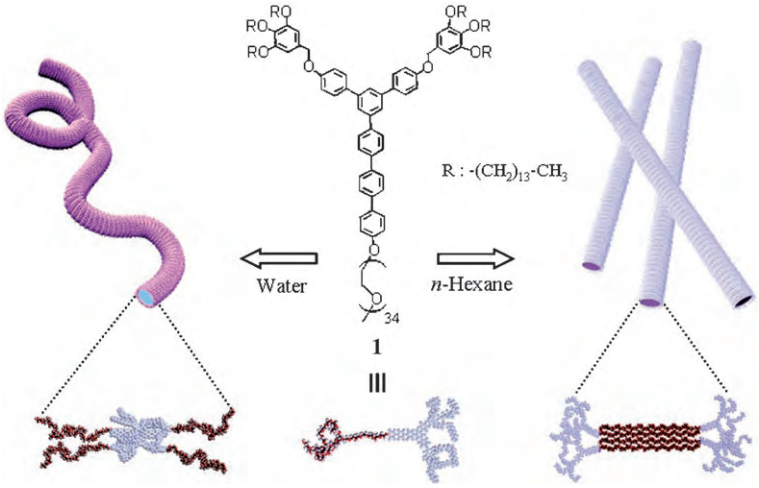

Figure 1. Schematic representation of the flexible coil-like and stiff rodlike nanofibers.

the cylindrical aggregates consists of a wedge-shaped rigid aromatic segment containing a tetradecyloxy periphery, and a flexible poly(ethylene oxide) (PEO) chain (degree of polymerization, DP = 34; volume fraction of PEO, $f_{PEO} = 0.43$), which are covalently linked at the apex of the wedge segment. The synthesis of the wedge–coil molecule was achieved in a stepwise fashion according to the procedures described previously.[5] The resulting molecule was characterized by ^{1}H NMR spectroscopy, elemental analysis, gel-permeation chromatography, and MALDI-TOF mass spectrometry, and was shown to be in full agreement with the structures presented.

The wedge–coil molecule **1**, when dissolved in a solvent selective for one of the blocks, can self-assemble into an aggregate structure because of its amphiphilic characteristics. Dynamic light scattering (DLS) experiments were performed with **1** in water (0.01 wt %), a selective solvent for the PEO chains, and *n*-hexane (0.01 wt %), a selective solvent for the hydrophobic wedge segments, to investigate the aggregation behavior. The wedge–coil molecule showed aggregation behavior in both water and *n*-hexane, as revealed by the autocorrelation functions (see Supporting Information). The angular dependence of the apparent diffusion coefficient (D_{app}) was measured because the slope is related to the shape of the diffusing species.[6] The slopes measured in water and *n*-hexane were 0.033 and 0.025, respectively, consistent with the value predicted for nonspherical micelles with an elongated shape (0.03). The formation of cylindrical micelles in both solvents was further confirmed by the Kratky plots, which show a linear angular dependence on the scattered light intensity of the aggregates.[7] A CONTIN analysis of the autocorrelation function in aqueous solution shows a broad peak corresponding to an average hydrodynamic radius (R_h) of approximately 138 nm. This result suggests the formation of highly flexible cylindrical micelles in aqueous solution.[8] In contrast, a CONTIN size distribution analysis in *n*-hexane shows two sharp peaks corresponding to R_h values of 12 and 45 nm, characteristic of two relaxation modes as a result of the coupling of translational and rotational diffusion of rigid rodlike micelles.[9]

Evidence for the formation of the cylindrical aggregates in both polar and apolar solvents was also provided by transmission electron microscopy (TEM) experiments (Figure 2). The micrographs negatively stained with an aqueous solution of uranyl acetate (2 wt %; Figure 2a) show highly curved cylindrical objects with a uniform diameter of about 15 nm, which indicates the formation of flexible coil-like nanofibers. To obtain more information on these nanofibers, we additionally performed TEM experiments with an ultramicrotomed film dried from aqueous solution (positively stained with RuO_4). The cross-sectional image of the fibers shows more stained dark aromatic domains surrounded by lighter PEO segments (Figure 2b).[10a] The diameter of the core was measured as approximately 5 nm, which is the estimated

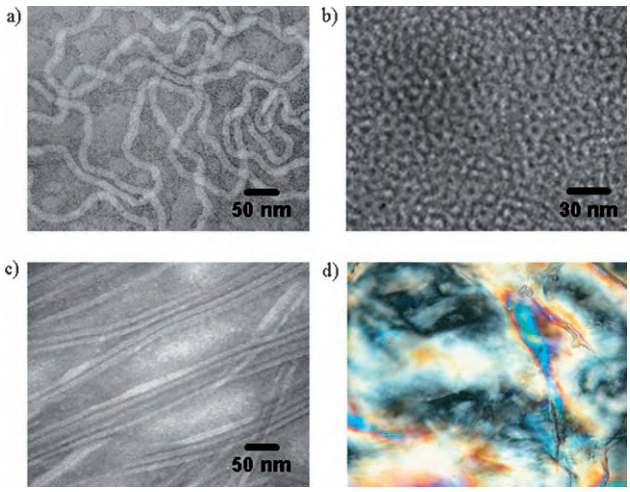

Figure 2. a) TEM image of nanofibers of **1** in aqueous solution (negatively stained with uranyl acetate); b) cross-sectional TEM image of nanofibers of **1** in aqueous solution (positively stained with RuO_4); c) TEM image of nanofibers of **1** in *n*-hexane solution (positively stained with RuO_4); and d) a representative optical polarized micrograph of the nematic phase in *n*-hexane solution.

 © 2006 Wiley-VCH Verlag GmbH & Co. KGaA, Weinheim

length of an aromatic part together with a tetradecyl group (5.4 nm, by Corey–Pauling–Kultin (CPK) modeling). This result suggests that the core of the fiber formed from aqueous solution consists of an aromatic segment and tetradecyl groups, which are fully interdigitated with each other.

Similar to the aqueous solution, the wedge–coil block molecule in *n*-hexane was also observed to form cylindrical objects. However, the curvature of the cylindrical micelles formed in *n*-hexane is significantly different from that in water. The micrographs positively stained from RuO_4 showed bundles of the cylindrical aggregates aligned parallel to each other. These cylinders have lengths up to several micrometers and a uniform diameter of about 16 nm (Figure 2c). Notably, there is clear contrast between the periphery and center of the cylindrical object, which indicates that the cylinders consist of a light coil interior and dark aromatic exterior in *n*-hexane solution.[10] Considering the extended molecular length (13.8 nm by CPK), the diameter of 16 nm indicates that the PEO chains within the core are fully interdigitated with each other. The formation of bundles of the micelles could be attributed to the existence of stiff rodlike micelles, consistent with the DLS results.

A rodlike shape with a high aspect ratio is a crucial prerequisite to form liquid-crystalline ordering,[11] and thus the *n*-hexane solution was further investigated with polarized optical microscopy. As expected for stiff rodlike aggregates, the solution (8 wt%) is highly birefringent with a threadlike texture (Figure 2d), indicative of the formation of a lyotropic nematic liquid crystal. Evidence for the formation of rigid rodlike nanofibers is also provided by X-ray scattering experiments. In contrast to the small-angle X-ray scattering (SAXS) pattern of the aggregates formed from aqueous solution, which showed only a weak reflection (Figure 3a), the SAXS pattern of the dried liquid crystal formed from *n*-hexane solution showed a strong reflection corresponding to a spacing of 16.2 nm, thus demonstrating the presence of an ordered structure (Figure 3b). Notably, this dimension is consistent with the diameter determined from TEM.

These results demonstrate that the wedge–coil molecule self-assembles into highly flexible coil-like cylinders in polar solvents such as water, whereas stiff rodlike cylinders are formed in nonpolar solvents such as *n*-hexane. This remarkable contrast in stiffness of the cylindrical objects depending on solvent polarity can be understood by considering the packing arrangements of the molecular segments within the cylindrical core. In aqueous solution, the core of the cylindrical micelles consists of hydrophobic dendritic wedge segments, because water is a selective solvent for PEO.[12] The bulky dendritic architecture of the hydrophobic part in the cylindrical core frustrates the crystallization process, which prevents the dense packing of the dendritic segments.[13] As a result, this loose distribution of the hydrophobic segments in the cylindrical core leads to highly flexible cylindrical micelles.

In *n*-hexane solution, however, the micelles consist of a PEO core surrounded by hydrophobic wedge segments. Within the cylindrical domains, the hydrophilic chains with linear geometry crystallize to result in the dense packing of the core. This crystalline nature of the PEO segments within

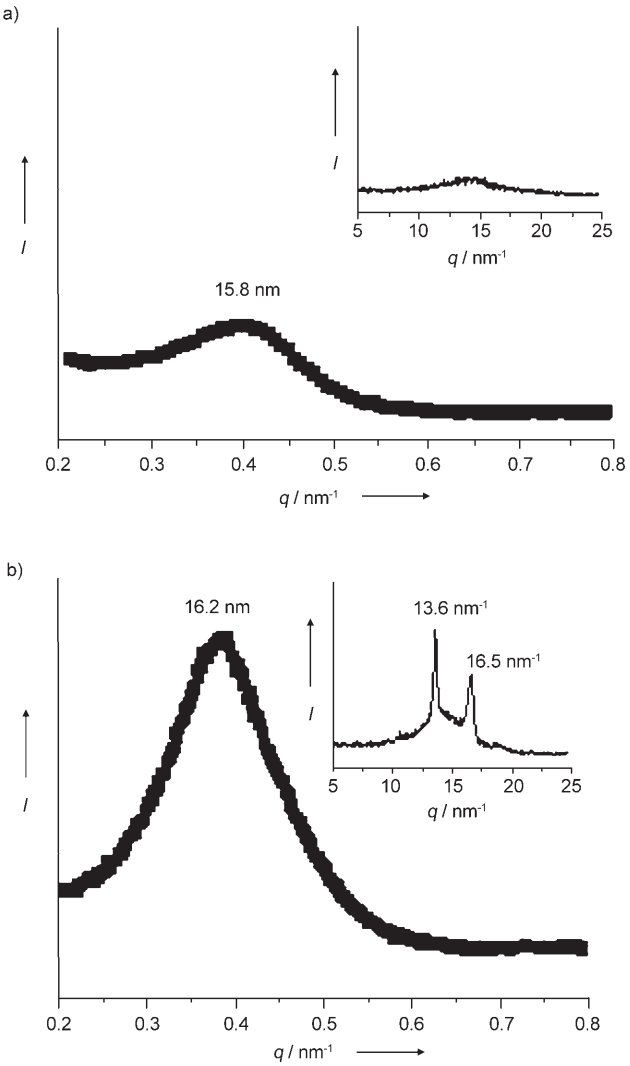

Figure 3. a) SAXS pattern of molecule **1** formed from aqueous solution (inset: wide-angle X-ray scattering (WAXS) pattern); and b) SAXS pattern of molecule **1** formed from *n*-hexane solution (inset: WAXS pattern).

the cylindrical core is reflected in wide-angle X-ray scattering (WAXS) measurements (Figure 3b, inset). The WAXS pattern of the dried liquid-crystal gel formed from *n*-hexane solution showed two sharp reflections, which indicate crystalline packing of the PEO segments within the domains.[5] To further confirm the PEO packing within the cylindrical aggregates, FTIR spectroscopic experiments were performed because this technique has already been successfully used to investigate fundamental questions of PEO morphology.[14] FTIR spectra corresponding to the CH_2 wagging mode, which is sensitive to the crystalline packing, are shown in Figure 4. The film cast from *n*-hexane solution showed two peaks at 1360 and 1343 cm^{-1} (see Table 1), which contribute to modes in the crystalline phase of PEO. Upon exchange of the solvent to water, however, these peaks transformed into a single peak centered at 1350 cm^{-1} which is assigned to amorphous PEO. These results together with the WAXS patterns demonstrate that the PEO core in hexane solution is

 © 2006 Wiley-VCH Verlag GmbH & Co. KGaA, Weinheim

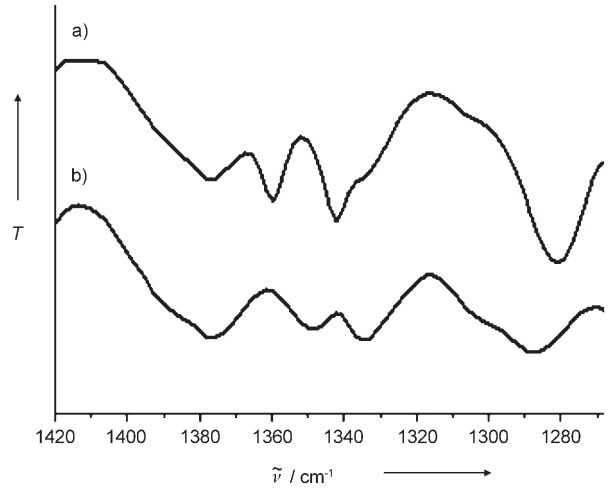

Figure 4. FTIR spectra of molecule **1** formed from a) *n*-hexane solution and b) aqueous solution in the 1270–1400 cm^{-1} region.

Table 1: Frequencies and peak assignments of the FTIR bands of **1** at 1270–1400 cm^{-1}.

$\tilde{\nu}$ [cm^{-1}]		Assignment
1 in water	**1** in *n*-hexane	
1377	1377	CH_3 deformation
	1360	CH_2 wag, C–C stretch
1350		
	1343	CH_2 wag
1334	1334	ring C–C stretch
1305	1305	ring C–H in-plane bending, ring C–C stretch
1288		
	1280	CH_2 twist

a highly ordered crystalline material, which is responsible for the formation of stiff rodlike cylindrical fibers.

The notable feature of the amphiphilic wedge–coil block molecule investigated here is its ability to self-assemble into cylindrical nanofibers in both polar and nonpolar solvents. Remarkably, as the solvent polarity changes from water to *n*-hexane, the resulting nanofibers change from a highly flexible coil-like character to a stiff rodlike nature. This switching in the stiffness of the nanofibers in response to solvent polarity is attributed to the structural inversion of the cylindrical core from bulky dendritic segments with an amorphous nature to crystallizable linear PEO segments. This structural inversion opens up the possibility of using this block molecule for applications such as encapsulation and/or release of molecules of interest, stimuli-sensitive templating media, and smart surfaces.

Received: June 8, 2006
Revised: July 27, 2006
Published online: September 29, 2006

Keywords: amphiphiles · nanostructures · self-assembly · solvent effects · supramolecular chemistry

[1] a) S. Förster, T. Plantenberg, *Angew. Chem.* **2002**, *114*, 712–739; *Angew. Chem. Int. Ed.* **2002**, *41*, 688–714; b) S. Jain, F. S. Bates, *Science* **2003**, *300*, 460–464; c) D. E. Discher, A. Eisenberg, *Science* **2002**, *297*, 967–973; d) W.-Y. Yang, E. Lee, M. Lee, *J. Am. Chem. Soc.* **2006**, *128*, 3484–3485; e) T. Shimizu, M. Masuda, H. Minamikawa, *Chem. Rev.* **2005**, *105*, 1401–1444; f) M. Antonietti, C. Göltner, *Angew. Chem.* **1997**, *109*, 944–964; *Angew. Chem. Int. Ed. Engl.* **1997**, *36*, 910–928.

[2] a) I. Manners, *Science* **2001**, *294*, 1664–1666; b) J. D. Hartgerink, E. Beniash, S. I. Stupp, *Science* **2001**, *294*, 1684–1688; c) T. Koga, M. Higuchi, T. Kinoshita, N. Higashi, *Chem. Eur. J.* **2006**, *12*, 1360–1367; d) A. Aggeli, I. A. Nyrkova, M. Bell, R. Harding, L. Carrick, T. C. B. McLeish, A. N. Semenov, N. Boden, *Proc. Natl. Acad. Sci. USA* **2001**, *98*, 11857–11862; e) W. Meier, C. Nardin, M. Winterhalter, *Angew. Chem.* **2000**, *112*, 4747–4750; *Angew. Chem. Int. Ed.* **2000**, *39*, 4599–4602.

[3] a) M. Lee, S.-J. Lee, L.-H. Jiang, *J. Am. Chem. Soc.* **2004**, *126*, 12724–12725; b) J. Rodríguez-Hernández, S. Lecommandoux, *J. Am. Chem. Soc.* **2005**, *127*, 2026–2027; c) Z. Hu, A. M. Jonas, S. K. Varshney, J.-F. Gohy, *J. Am. Chem. Soc.* **2005**, *127*, 6526–6527; d) D. R. Vutukuri, S. Basu, S. Thayumanavan, *J. Am. Chem. Soc.* **2004**, *126*, 15636–15637; e) E. R. Gillies, T. B. Jonsson, J. M. J. Fréchet, *J. Am. Chem. Soc.* **2004**, *126*, 11936–11943.

[4] a) H.-J. Kim, J.-H. Lee, M. Lee, *Angew. Chem.* **2005**, *117*, 5960–5964; *Angew. Chem. Int. Ed.* **2005**, *44*, 5810–5814; b) J.-H. Ryu, M. Lee, *J. Am. Chem. Soc.* **2005**, *127*, 14170–14171; c) D. J. Hill, M. J. Mio, R. B. Prince, T. S. Hughes, J. S. Moore, *Chem. Rev.* **2001**, *101*, 3893–4011; d) M. Barboiu, J.-M. Lehn, *Proc. Natl. Acad. Sci. USA* **2002**, *99*, 5201–5206; e) J. Xu, E. R. Zubarev, *Angew. Chem.* **2004**, *116*, 5607–5612; *Angew. Chem. Int. Ed.* **2004**, *43*, 5491–5496.

[5] a) J.-K. Kim, M.-K. Hong, J.-H. Ahn, M. Lee, *Angew. Chem.* **2005**, *117*, 332–336; *Angew. Chem. Int. Ed.* **2005**, *44*, 328–332; b) S. Peleshanko, J. Jeong, V. V. Shevchenko, K. L. Genson, Yu. Pikus, M. Ornatska, S. Petrash, V. V. Tsukruk, *Macromolecules* **2004**, *37*, 7497–7506.

[6] a) M. Schmidt, W. H. Stockmayer, *Macromolecules* **1984**, *17*, 509–514; b) J. Massey, K. N. Power, I. Manners, M. A. Winnik, *J. Am. Chem. Soc.* **1998**, *120*, 9533–9540.

[7] J. Boersma, *J. Chem. Phys.* **1981**, *74*, 6989–6990.

[8] J. F. Gohy, B. G. G. Lohmeijer, A. Alexeev, X.-S. Wang, I. Manners, M. A. Winnik, U. S. Schubert, *Chem. Eur. J.* **2004**, *10*, 4315–4323.

[9] a) M. Al-Hussein, B. G. G. Lohmeijer, U. S. Schubert, W. H. de Jeu, *Macromolecules* **2003**, *36*, 9281–9284; b) R. Pecora, *J. Chem. Phys.* **1968**, *48*, 4126–4128.

[10] a) J. Bae, J.-K. Kim, N.-K. Oh, M. Lee, *Macromolecules* **2005**, *38*, 4226–4230; b) M. Lee, B.-K. Cho, K. J. Ihn, W.-K. Lee, N.-K. Oh, W.-C. Zin, *J. Am. Chem. Soc.* **2001**, *123*, 4647–4648.

[11] S. M. Yu, V. P. Conticello, G. Zhang, C. Kayser, M. J. Fournier, T. L. Mason, D. A. Tirrell, *Nature* **1997**, *389*, 167–170.

[12] This finding was also confirmed by dye encapsulation experiments (see Supporting Information).

[13] The amorphous nature within the cylindrical micelles formed in aqueous solution was conformed by X-ray scattering experiments that showed only a broad halo in the wide-angle range (see Figure 3a, inset).

[14] a) M. A. K. L. Dissanayaket, R. Frech, *Macromolecules* **1995**, *28*, 5312–5319; b) Y. Su, J. Wang, H. Liu, *Langmuir* **2002**, *18*, 5370–5374.

 © 2006 Wiley-VCH Verlag GmbH & Co. KGaA, Weinheim

Total Synthesis

DOI: 10.1002/anie.200602211

The Changing Faces of Halogenated Marine Natural Products: Total Synthesis of the Reported Structures of Elatenyne and an Enyne from *Laurencia majuscula***

*Helen M. Sheldrake, Craig Jamieson, and Jonathan W. Burton**

The structures of complex natural products are best confirmed by independent synthesis or X-ray crystallography. Advances in NMR spectroscopy over the last 20 years have greatly improved the ease with which the structures of complex molecules are solved; however, in cases where crystallography is not possible, regio- and stereocontrolled synthesis remains the best method for structure confirmation. In many cases, determining the connectivity through heteroatoms becomes a significant challenge in structure assignment by NMR spectroscopy, especially in otherwise closely related molecules. For example, consider the two natural products (*E*)-dactomelyne (**1**) and notoryne (**2**).[1,2] They both contain the same carbon and proton connectivity, and hence unambiguous structure assignment would be challenging on the basis of NMR experiments alone. The natural products **1** and **2** belong to a much wider group of C_{15} metabolites isolated from red algae and from marine organisms that feed on *Laurencia* species.[3] In 1986, the dibrominated natural product elatenyne was isolated by Hall and Reiss, and was assigned the pyrano[3,2-*b*]pyran structure **3** on the basis of extensive ^{1}H and ^{13}C NMR spectroscopic analyses.[4] More recently, the structure of a halogenated C_{15} natural product isolated from *L. majuscula* was disclosed as the pyrano[3,2-*b*]pyran **4**, again on the basis of extensive NMR spectroscopic analyses and by comparison with the structures **3** (reported for elatenyne) and (*E*)-dactomelyne (**1**).[5]

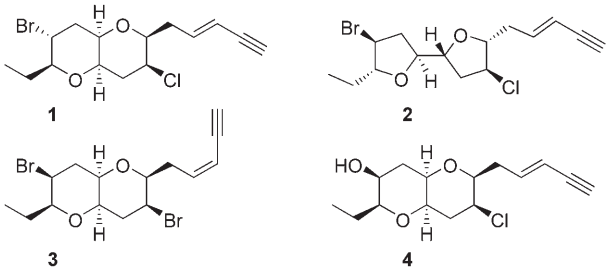

Elatenyne and the *L. majuscula* enyne were attractive targets for total synthesis because of their densely functionalized pyrano[3,2-*b*]pyran cores and embedded C_2 symmetry.[6,7] Herein, we report an efficient two-directional route to these halogenated secondary metabolites which rapidly established the central pyrano[3,2-*b*]pyran core and culminated in the total synthesis of structures **3** and **4**.[8,9] The spectroscopic data for the synthetic pyrano[3,2-*b*]pyrans **3** and **4** are inconsistent with those reported for the natural products, and we propose that both natural products are structurally related to notoryne **2** by having a core 2,2′-bifuranyl structure.

Our approach to the fused bicycles **3** and **4** is delineated in Scheme 1. The known bislactone **5**[10] was reduced with diisobutylaluminum hydride and the resulting intermediate aluminum alkoxides were trapped with acetic anhydride to give a mixture of the anomeric acetates **6**.[11] Exposure of the acetates **6** to acidic methanol gave a mixture of the methyl glycosides **7**, which on treatment with iodotrimethylsilane in acetonitrile gave solely the pyrano[3,2-*b*]pyran **8**.[12] ^{1}H NMR spectroscopic studies have demonstrated that this rearrangement proceeds by way of the corresponding anomeric iodides, with the pyrano[3,2-*b*]pyran bis(anomeric) iodide being greatly favored over the 2,2′-bifuranyl bis(anomeric) iodide at equilibrium.[13] Subsequent epoxidation under mild con-

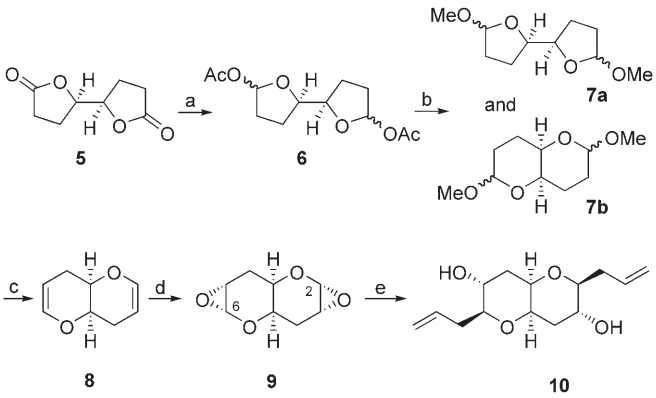

Scheme 1. Synthesis of the pyrano[3,2-*b*]pyran core **10**. a) Diisobutylaluminum hydride, CH_2Cl_2, −78 °C, then Ac_2O, pyridine, DMAP, CH_2Cl_2, −78 °C, 14 h, then −78→−20 °C, 83%; b) MeOH, HCl, 90%; c) Me_3SiI, MeCN, RT, then $(Me_3Si)_2NH$; d) 3,3-dimethyldioxirane, $NaHCO_3$, CH_2Cl_2; e) $(CH_2{=}CHCH_2)_2Mg$, Et_2O, THF, −78 °C→RT, 57% overall from **7**. DMAP = 4-dimethylaminopyridine.

[*] Dr. H. M. Sheldrake, Dr. J. W. Burton
Department of Chemistry
University of Cambridge
Lensfield Road, Cambridge CB21EW (UK)
Fax: (+44) 1223-336-362
E-mail: jwb1004@hermes.cam.ac.uk
Dr. C. Jamieson
Organon Laboratories Ltd.
Newhouse, Lanarkshire, ML15SH (UK)

[**] We thank Prof. J. Reiss (La Trobe University) and Prof. G. König (Universität Bonn) for supplying spectroscopic data for elatenyne and the enyne isolated from *L. majuscula*, respectively; Dr. J. Davies and Dr. S. Pascu for X-ray crystallography; Dr. D. Fox for helpful discussions; GlaxoSmithKline (CASE award to H.M.S.); the Royal Society (Research Fellowship to J.W.B.); and the EPSRC for funding, including financial assistance towards the purchase of the Nonius CCD diffractometer. AstraZeneca UK are gratefully acknowledged for some unrestricted funds.

Supporting information for this article is available on the WWW under http://www.angewandte.org or from the author.

 © 2006 Wiley-VCH Verlag GmbH & Co. KGaA, Weinheim

ditions provided the bis(epoxide) **9** as a relatively stable white crystalline solid. X-ray analysis of **9** confirmed that epoxidation had occurred on the more accessible convex face of the bis(enol ether) **8** as expected (see Supporting Information).

The bis(epoxide) **9** was opened with inversion of stereochemistry at C2 and C6 by treatment with diallylmagnesium to provide the corresponding C_2-symmetric diol **10**;[14] approximately 8% of an asymmetric diol is also formed under these conditions and corresponds to one epoxide of **9** being opened with inversion (an S_N2-like mechanism) and the other epoxide being opened with overall retention (an S_N1-like mechanism).[15] The sequence shown in Scheme 1 rapidly establishes the central pyrano[3,2-*b*]pyran system of **3** and **4** in five steps from the known lactone **5**.

The conversion of the diol **10** into the *cis*-enyne **3** is shown in Scheme 2. Protection of the diol **10** gave the bis(silyl ether) **11**, which on ozonolysis with a reductive workup yielded the diol **12**. Many attempts were made to desymmetrize **12** by formation of a monoiodide, -tosylate, or -aldehyde. Ultimately, the most efficient method for breaking the C_2 symmetry of **12** involved statistical protection using chlorotriethylsilane, which provided the unsymmetric alcohol **13** in good yield after one recycle.[16] The primary alcohol was readily reduced via the corresponding tosylate **14**[17] to provide the ethyl-substituted pyrano[3,2-*b*]pyran **15**, which was then transformed into the aldehyde **17** by using standard procedures.[18] The enyne side chain was installed with exclusive *Z* selectivity by using a Yamamoto–Peterson reaction to give **18**.[19] Removal of the two oxygen-protecting groups gave the bromination substrate **19**. The introduction of halogen atoms into tetrahydropyrans by substitution from the corresponding hydroxy groups has been reported to be very challenging.[20] After screening a wide variety of reagents, we discovered that exposure of the bis(triflate) **20**, derived from the diol **19**, to tetrabutylammonium bromide in toluene at reflux delivered the desired dibromide **21**, albeit in low yield.[21,22] Removal of the acetylene-protecting group gave the *cis*-enyne **3**.

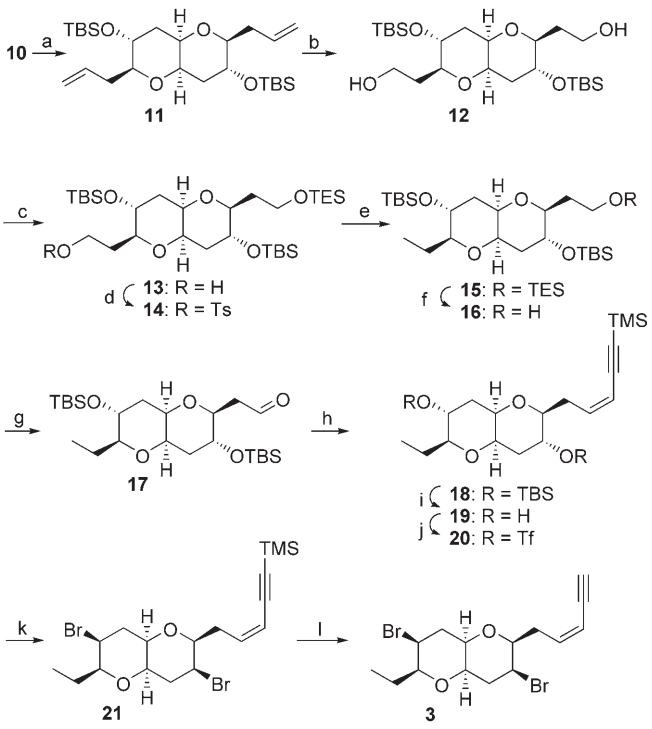

Scheme 2. Synthesis of the reported structure of elatenyne (**3**). a) TBSOTf, Et_3N, CH_2Cl_2, 99%; b) O_3/O_2, CH_2Cl_2, MeOH, −78 °C, then Ph_3P, −78 °C, 2 h, then $NaBH_4$, −78 °C→RT, 2 h, 82%; c) Et_3SiCl, Et_3N, CH_2Cl_2, 70% after one recycle; d) TsCl, DMAP, Et_3N, CH_2Cl_2, 93%; e) $LiBHEt_3$, Et_2O, RT, 91%; f) K_2CO_3, MeOH, 98%; g) nPr_4NRuO_4, NMO, CH_2Cl_2, 4-Å MS, 95%; h) $Me_3SiC{\equiv}CCH_2SiMe_2tBu$, *t*BuLi, $Ti(OiPr)_4$, THF, −78 °C, add **17**, −78 °C→RT, 0.5 h, then $(Me_3Si)_2NK$, 75%; i) TsOH, MeOH, 22 h, 75%; j) Tf_2O, pyridine, CH_2Cl_2; k) nBu_4NBr, toluene, reflux, 2 h, 14% from **19**; l) nBu_4NF, THF, −5 °C, 98%. TBS = *tert*-butyldimethylsilyl, TES = triethylsilyl, Ts = toluene-4-sulfonyl, NMO = 4-methylmorpholine *N*-oxide, MS = molecular sieves, Tf = trifluoromethanesulfonyl.

The broader applicability of this synthetic strategy towards *cis*-fused pyrano[3,2-*b*]pyrans is illustrated by our synthesis of the enyne **4** (Scheme 3). Desymmetrization of the C_2-symmetric diol **10** was again achieved by silylation (with recycling) to provide the unsymmetric alcohol **22**.[23] The axial chlorine atom was introduced from the corresponding triflate **23** on exposure to tetrabutylammonium chloride in toluene at reflux to

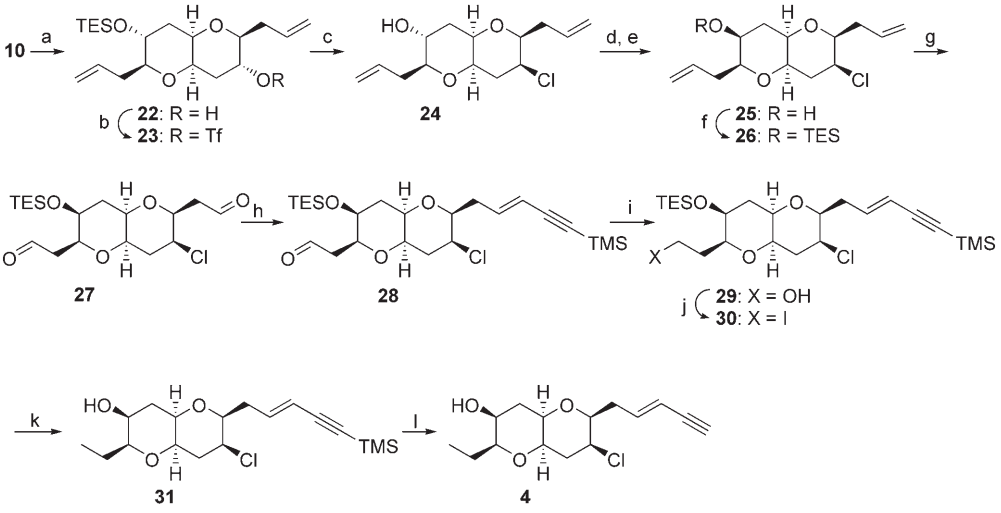

Scheme 3. Synthesis of the reported structure of the enyne from *L. majuscula* **4**. a) Et_3SiCl, imidazole, DMF, 64% after one recycle; b) Tf_2O, pyridine, CH_2Cl_2; c) nBu_4NCl, toluene, reflux, 2 h, then amberlite resin IR-120, MeOH, 45% from **22**; d) nPr_4NRuO_4, NMO, CH_2Cl_2, 4-Å MS, 65%; e) $NaBH_4$, MeOH, 87%; f) Et_3SiOTf, Et_3N, CH_2Cl_2, 99%, g) O_3/O_2, CH_2Cl_2, −78 °C, then Ph_3P, −78 °C, 0.5 h, then RT, 8 h, 95%; h) $Ph_3P^+CH_2C{\equiv}C\text{-}SiMe_3\text{-}Br^-$, *n*BuLi, THF, add **27**, −78→0 °C, 45%, (15% recovered **27**); i) $NaBH_4$, MeOH, 100%, j) I_2, PPh_3, imidazole, Et_2O, MeCN, RT, 72%; k) Zn, AcOH, MeOH, Et_2O, RT, then HCl, 96%; l) nBu_4NF, THF, RT, 92%.

© 2006 Wiley-VCH Verlag GmbH & Co. KGaA, Weinheim

yield the chloro alcohol **24** after acid treatment. This is a remarkable transformation given that a previous attempted synthesis of the dactomelynes had failed because the introducion of the axial chlorine atom through a substitution reaction from the corresponding hydroxy group proved impossible.[7]

The remaining secondary hydroxy group in **24** was inverted by an oxidation[18]/reduction sequence to give **25**; thus all of the required stereochemistry for the synthesis of **4** was set. Crystals of alcohol **25** suitable for X-ray analysis were obtained and the crystal structure confirmed that all the substituents were on the concave face of the pyran[3,2-*b*]pyran system, with the chlorine atom and hydroxy groups being oriented axially (see Supporting Information). Protection of the hydroxy group of **25** to give the silyl ether **26** followed by ozonolysis (with triphenylphosphane workup) gave the bis(aldehyde) **27** in excellent yield.

Addition of one equivalent of a preformed solution of the ylide derived from (3-trimethylsilyl-2-propynyl)triphenylphosphonium bromide to a cold solution of the bis(aldehyde) **27** delivered the enyne **28** with high *E* selectivity (*E*/*Z* > 7:1).[24] The only other product isolated from this reaction was the corresponding bis(enyne) (17%). Reduction of the aldehyde **28**, conversion of the resulting alcohol **29** into the corresponding primary iodide **30**, and reductive removal of the iodine with zinc[25] provided the ethyl-substituted pyranopyran **31**. Removal of the acetylene-protecting group gave the *trans*-enyne **4**.[26]

Neither the spectroscopic data for synthetic **3** nor synthetic **4** corresponded with the literature data reported for their respective natural products.[4,5] The difficulty in unequivocally assigning the structures of complex natural products has recently been reviewed by Nicolaou and Snyder, and is further highlighted by the work described here.[27] During our synthetic studies towards the enynes **3** and **4**, we synthesized a large number of pyrano[3,2-*b*]pyran and 2,2′-bifuranyl compounds. Careful analysis of the ^{13}C NMR data of all of these compounds revealed that the ^{13}C NMR chemical shifts of the central oxygen-bearing carbon atoms fall into two distinct groups: for the pyrano[3,2-*b*]pyran, the ^{13}C NMR chemical shift of the C8a and C4a carbon atoms resonate at less than $\delta = 76$ ppm, whereas the corresponding carbon atoms (C2 and C2′) in the 2,2′-bifuranyls resonate at greater than $\delta = 76$ ppm (Scheme 4).[28] For elatenyne, the relevant carbon atoms resonate at $\delta = 79.5$ and 80 ppm, whereas for the pyrano[3,2-*b*]pyran **3** they resonate at $\delta = 71.3$ and 71.4 ppm. For the *L. majuscula* enyne the relevant carbon atoms resonate at $\delta = 77.9$ and 79.2 ppm, whereas for the synthetic pyrano[3,2-*b*]pyran **4** they resonate at $\delta = 73.9$ and 70.5 ppm. The difficulty in distinguishing between closely related structures (for example, **1** and **2**) by using NMR spectroscopic techniques alone, coupled with the general pattern of the ^{13}C NMR chemical shifts of the pyrano[3,2-*b*]pyran and 2,2′-bifuranyl units has led us to conclude that the overall structures of elatenyne and the enyne from *L. majuscula* are the 2,2′-bifuranyls **32** and **33**, respectively (Scheme 5). Further analysis of all the spectroscopic data for the natural products supports this proposal.[29–31]

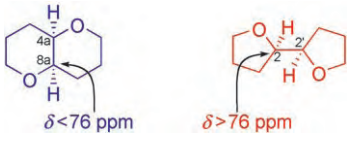

Scheme 4. ^{13}C chemical shifts for pyrano[3,2-*b*]pyran and 2,2′-bifuranyl compounds.

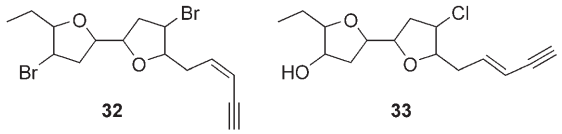

Scheme 5. Proposed structures for elatenyne and the enyne from *L. majuscula*.

In summary, we have reported an efficient synthetic route to halogenated pyrano[3,2-*b*]pyrans which has culminated in the total synthesis of the putative structures of elatenyne **3** and an enyne isolated from *L. majuscula* **4**. Key features of our two-directional synthesis include: the rapid construction of the central pyrano[3,2-*b*]pyran core of **3** and **4** through a novel rearrangement of the anomeric acetates **6**, a regioselective Wittig reaction for the formation of the enyne **28**, and the introduction of the halogen atoms through substitution from the corresponding activated hydroxy groups. The spectroscopic data for **3** and **4** did not correspond with those reported for the natural products, which led us to propose revised structures for the natural products based upon a central 2,2′-bifuranyl core (Scheme 5). Reisolation of the natural products would allow further spectroscopic analysis to aid full structure determination. In the meantime, work is underway to predict the structures of elatenyne and the enyne from *L. majuscula* on the basis of a rational biosynthetic pathway and to confirm the stereochemistry of the natural products by stereoselective total synthesis.

Received: June 2, 2006
Revised: August 15, 2006
Published online: October 6, 2006

Keywords: fused-ring systems · natural products · revised structures · structure elucidation · total synthesis

[1] For an isolation and structure determination of the dactomelynes, see: Y. Gopichand, F. J. Schmitz, J. Shelly, A. Rahman, D. van der Helm, *J. Org. Chem.* **1981**, *46*, 5192; reisolation: Z. Aydogmus, S. Imre, L. Ersoy, V. Wray, *Nat. Prod. Res.* **2004**, *18*, 43.
[2] For the isolation and structure determination of notoryne, see: H. Kikuchi, T. Suzuki, E. Kurosawa, M. Suzuki, *Bull. Chem. Soc. Jpn.* **1991**, *64*, 1763.
[3] K. L. Erickson in *Marine Natural Products*, *Vol. 5* (Ed.: P. J. Scheuer), Academic Press, New York, **1983**, p. 131.
[4] J. G. Hall, J. A. Reiss, *Aust. J. Chem.* **1986**, *39*, 1401.
[5] A. D. Wright, G. M. König, R. De Nys, O. Sticher, *J. Nat. Prod.* **1993**, *56*, 394.

 © 2006 Wiley-VCH Verlag GmbH & Co. KGaA, Weinheim

[6] For a notable previous total synthesis of the dactomelynes, see: E. Lee, C. M. Park, J. S. Yun, *J. Am. Chem. Soc.* **1995**, *117*, 8017.
[7] For an attempted synthesis of the dactomelynes, see: A. P. Kozikowski, J. Lee, *J. Org. Chem.* **1990**, *55*, 863.
[8] For a summary of the advantages of two-directional synthesis, see: C. S. Poss, S. L. Schreiber, *Acc. Chem. Res.*, **1994**, *27*, 9.
[9] For an excellent review on desymmetrization and the two-directional synthesis of natural products, see: S. R. Magnuson, *Tetrahedron* **1995**, *51*, 2167.
[10] The bis(lactone) **5** has been synthesized in two steps from commercially available materials: M. E. Maier, S. Reuter, *Synlett* **1995**, 1029.
[11] D. J. Kopecky, S. D. Rychnovsky, *J. Org. Chem.* **2000**, *65*, 191.
[12] For the formation of *endo*-glycals using iodotrimethylsilane and hexamethyldisilazane, see: D. Craig, M. W. Pennington, P. Warner, *Tetrahedron Lett.* **1995**, *36*, 5815; L. A. Paquette, J. A. Oplinger, *J. Org. Chem.* **1988**, *53*, 2953.
[13] The anomeric acetates **6** gave the pyrano[3,2-*b*]pyran **8** in low yield on treatment with iodotrimethylsilane in acetonitrile.
[14] J. D. Rainier, S. P. Allwein, J. M. Cox, *J. Org. Chem.* **2001**, *66*, 1380.
[15] The asymmetric diol was inseparable at this stage and was removed after ozonolysis of **11**.
[16] The use of silyl protection to desymmetrize C_2-symmetric diols was reported by Poss and Schreiber[8].
[17] H. C. Brown, S. Krishnamurthy, *J. Am. Chem. Soc.* **1973**, *95*, 1669. Solvent effects in the reduction of halides and tosylates: S. Krishnamurthy, *J. Org. Chem.* **1980**, *45*, 2550.
[18] S. V. Ley, J. Norman, W. P. Griffith, S. P. Marsden, *Synthesis* **1994**, 639.
[19] Y. Yamakado, M. Ishiguro, N. Ikeda, H. Yamamoto, *J. Am. Chem. Soc.* **1981**, *103*, 5568.
[20] L.-X. Gao, A. Murai, *Heterocycles* **1996**, *42*, 745.
[21] Bromination of the bis(triflate) **20** cannot occur from the ground state, O-inside conformation, and will be further slowed by the β-oxygen effect, see: S. S. Shaik, *J. Am. Chem. Soc.* **1983**, *105*, 4359. For discussion of the conformational preferences of pyrano[3,2-*b*]pyrans and related systems, see: R. W. Hoffmann, I. Münster, *Ann. Chem.* **1997**, 1143; A. G. Santos, R. W. Hoffmann, *Tetrahedron: Asymmetry* **1995**, *6*, 2767; M. Grabarnik, N. G. Lemcoff, R. Madar, S. Abramson, S. Weinman, B. Fuchs, *J. Org. Chem.* **2000**, *65*, 1636.
[22] The stereochemistry of the dibromide was established by analysis of the coupling constants (see the Supporting Information).
[23] The diol **10** contained an inseparable impurity which was removed after chlorination of **23**.
[24] The connectivity of the pyrano[3,2-*b*]pyran **28** (and hence the regiochemistry of the Wittig reaction) was firmly established by ^{1}H NMR COSY experiments. The origin of the regioselectivity of the Wittig reaction may be steric in nature because of the larger size of an OTES group with respect to a chlorine atom.
[25] The reported conditions were particularly effective: Z.-H. Peng, K. A. Woerpel, *J. Am. Chem. Soc.* **2003**, *125*, 6018.
[26] The enyne **4** was isolated as an inseparable 8:1 mixture of *E* and *Z* isomers.
[27] For an excellent review regarding recent misassigned natural products, see: K. C. Nicolaou, S. A. Snyder, *Angew. Chem.* **2005**, *117*, 2086; *Angew. Chem. Int. Ed.* **2005**, *44*, 1012.
[28] In the vast majority of cases (> 98 %) C-4a and C-8a atoms in the pyrano[3,2-*b*]pyrans resonate below $\delta = 76$ ppm, and C-2 and C-2′ atoms in the 2,2′-bifuranyls resonate above $\delta = 76$ ppm. See the Supporting Information for key ^{13}C NMR chemical shifts for 74 synthetic pyrano[3,2-*b*]pyran and 27 synthetic 2,2′-bifuranyl compounds.
[29] In particular the mass spectra for both elatenyne and the enyne isolated from *L. majuscula* contain fragment ions which are readily explicable on the basis of a 2,2′-bifuranyl structure and are in close agreement with the fragmentation pattern reported and discussed for notoryne[2].
[30] It should be noted that at the time of the isolation of elatenyne no C_{15} halogenated 2,2′-bifuranyl natural products had been reported. A 2,2′-bifuranyl structure for elatenyne was considered less likely than the corresponding pyrano[3,2-*b*]pyran: J. G. Hall, PhD Thesis, La Trobe University (Australia), **1984**.
[31] Unlike a number of pyrano[3,2-*b*]pyrans we synthesized, neither elatenyne nor the enyne from *L. majuscula* are crystalline which may be partly because of the extra degree of freedom around the central C–C bond in 2,2′-bifuranyl units.

 © 2006 Wiley-VCH Verlag GmbH & Co. KGaA, Weinheim

Environmental Chemistry

DOI: 10.1002/anie.200602453

Optical Sensors Based on Nanostructured Cage Materials for the Detection of Toxic Metal Ions**

Tatineni Balaji, Sherif A. El-Safty, Hideyuki Matsunaga, Takaaki Hanaoka, and Fujio Mizukami*

Chemical sensors are molecular receptors that transform their chemical information into analytically useful signals upon binding to specific guests. These sensors are attracting attention owing to their potential for easy detection and quantification of the pollutant species in many fields of application, such as waste management, environmental chemistry, clinical toxicology, and bioremediation of radionuclides.[1–6] Among these, the sensitive detection of heavy-metal ions, such as mercury and lead, is critical for monitoring the environment as they are highly toxic and common environmental pollutants. Although instrumental analyses such as atomic absorption or atomic emission spectroscopy are currently used in applications relevant to the detection of toxic metal ions, there is still a need to develop inexpensive and easy methods for the detection of these toxic ions. In view of these sophisticated experimental methods, emphasis is currently being placed on the development of sensor materials for the detection of toxic ions that offer high sensitivity,

[*] Dr. T. Balaji,[+] Dr. S. A. El-Safty,[+] Dr. H. Matsunaga, Dr. T. Hanaoka, Dr. F. Mizukami
National Institute of Advanced Industrial Science & Technology (AIST)
Research Center for Compact Chemical Process (CCP)
4-2-1, Nigatake, Miyagino-ku, Sendai 983-8551 (Japan)
Fax: (+81) 22-237-5226
E-mail: sherif.el-safty@aist.go.jp

[+] Both authors contributed equally to the practical work.

[**] We thank Dr. Y. Kiyozumi, Dr. T. Ikeda, and Dr. A. Kawai (CCP-AIST) for the measurements of Ar isotherms.

Supporting information for this article is available on the WWW under http://www.angewandte.org or from the author.

WILEY InterScience DISCOVER SOMETHING GREAT
© 2006 Wiley-VCH Verlag GmbH & Co. KGaA, Weinheim

short response times, and selectivity.[7,8] Among all these sensor approaches, the optical sensors that allow on-site, real-time qualitative or semiquantitative detection without the use of any substantial or complicated spectroscopic instrumentation have received a great deal of attention as promising methods for the determination of pollutant species in environmental analysis.[9–11] However, most of the sensors developed so far were kinetically slow with a limited sensitivity for detection below the permissible level of toxic ions, indicating a lack of possibility to control the remote sensing of pollutant species.

With recent advances in mesostructured materials and nanotechnologies, new methods are emerging to design optical sensors and biosensors, and to develop highly sensitive solid-state sensors.[12–14] However, in recent years, large-scale nanostructured materials such as SBA-15 and MCM-41 have attracted significant interest for the development of optical chemical sensors.[15–19] Although these materials offer considerable advantages over other methods in the area of sensing technologies, there is still a growing demand to solve one of the major technological challenges in nano-optical sensors: the detection and determination of environmentally important toxic species at a low level of concentration with a rapid-assessment process. In this respect, we report herein the use of newly synthesized cubic *Fm3m* nanostructured cage-monolith-based optical sensors for highly sensitive and selective detection of Pb^{II}, Cd^{II}, Sb^{III}, and Hg^{II} toxic ions at subnanomolar concentrations in a few minutes. To the best of our knowledge, this is the first visual detection method to detect toxic ions at low-level concentrations based on the color change of the probe sensors (Scheme 1). Such cage monoliths with spherical nanosized cavities show evidence for a high adsorption capacity of probe molecules, efficient transport of toxic species through much more direct and easier diffusion to the network sites, and a high degree of detection functionality for these toxic ions without loss of cage character (i.e. uniformly shaped and sized cavity and entrance pores).

Instant direct-templating methods that apply a microemulsion system of F108 ($EO_{141}PO_{44}EO_{141}$) copolymer as a template were used to affect the rapid synthesis of highly ordered, and optically transparent cage silica monoliths (Scheme 1) with cubic *Fm3m* (HOM-C10) structures, as evidenced by X-ray diffraction (XRD) and N_2 isothermal profiles (see the Supporting Information).[20a,b] The potential use of these cage materials as colorimetric sensors **1**–**4** for the naked-eye detection of metal ions has generated considerable evidence for the accessibility and retainability of probe molecules in the three-dimensional cage cavity (Scheme 1). Several successful immobilization strategies that use direct and indirect postgrafting techniques of hydrophilic and hydrophobic chromophores into the cubic *Fm3m* cage monoliths were preformed to design sinklike sensors **1**–**4** (Scheme 2). However, the functionalized cage sensors were fabricated by following a direct immobilization for probe **1** and a two-step inclusion procedures for probes **2**–**4** through graft-controlled surface modification of the cage monoliths

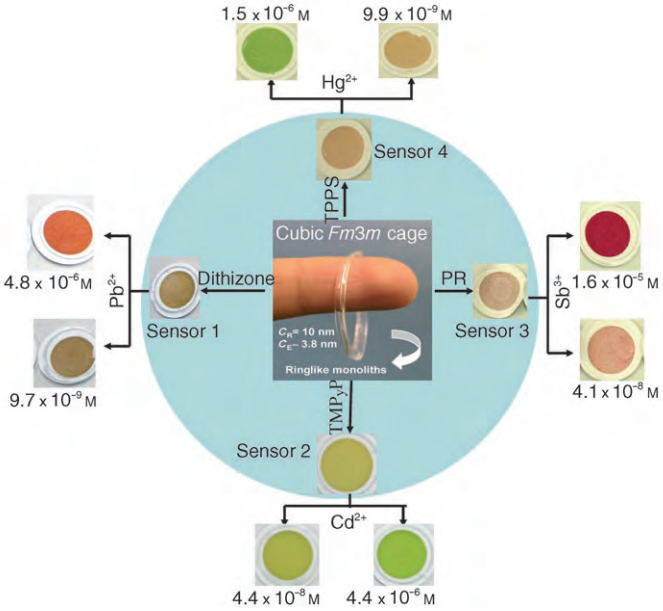

Scheme 1. A schematic representation of the colorimetric detection systems of optically monolithic cage sensors and the respective color changes over a tunable and wide detection range of the toxic analyte ions. C_R = pore cavity size, C_E = pore entrance size.

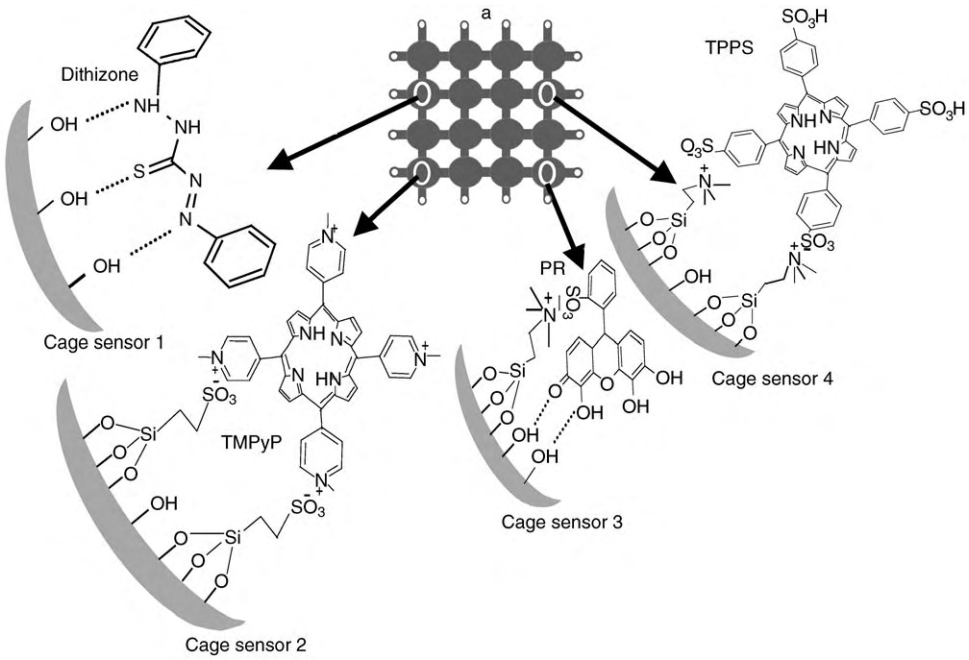

Scheme 2. Representative of the structures of the optical probe sinks **1**–**4** based on chromophore–cage cubic *Fm3m* nanostructures (a).

© 2006 Wiley-VCH Verlag GmbH & Co. KGaA, Weinheim

with amine- or thiol-coupling agents (see the Supporting Information). Our experimental results show that the coupling agents mercaptopropyl trimethoxysilane (MPTS) and *N*-trimethoxysilylpropyl-*N*,*N*,*N*-trimethylammonium chloride (TMAC) can be used to tune the polarity of the HOM surfaces on which the high accessibility of the α,β,γ,δ-tetrakis(1-methylpyridinium-4-yl)porphine *p*-toluenesulfonate (TMPyP), pyrogallol red (PR), and tetraphenylporphine tetrasulfonic acid (TPPS) moieties were observed (see Table 1 and the Supporting Information),[19,21,22] and therefore led to the generation of the long-term-stable sensors **2**, **3**, and **4** with a high selectivity for Cd^{II}, Sb^{III}, and Hg^{II} target ions, respectively, with sensitive detection and rapid-assessment analysis (≤ 1 min).

In these sensing designs, despite the hydrophilic and hydrophobic character and grafting strategies of the immobilized probe moieties, the cage-monolithic materials exhibited higher adsorption integrity of the probes in terms of capacity and fast-loading kinetics than those of silica materials with amorphous or even-ordered structures (such as SBA-15).[20c] The excellent accessibility and functionality of the chromophore molecules into the 3D cubic *Fm*3*m* cage monoliths (see the Supporting Information) led to the creation of a new type of material for colorimetric detection, namely, optical probe sinks. This allowed for sensitivity over a wide and tunable detection range and simple detection by the naked eye without the use of high amounts of materials and annealing experiments (Scheme 1). To investigate the successful immobilizations of the probes without loss of the cage regularity and functionality, the optical probe sinks were characterized by a number of techniques such as ^{29}Si NMR spectroscopy, FTIR spectroscopy, thermogravimetric analysis (TG), and energy-dispersive X-ray (EDX) microanalysis (see the Supporting Information).[21,22] In general, our findings revealed that the chromophore moieties effectively bind to the HOM cage monoliths, as evidenced from the large adsorption value (Q) of the probe molecules (Table 1).

TEM images (Figure 1), in general, reveal well-organized mesopore arrays over a large area of the cubic *Fm*3*m* cage sensors, despite the harsh synthesis conditions required by batch contact–time experiments during the embedding/grafting techniques. Although the existence of undulating or curvelike channels was observed among the clear [110] and [111] incidences, which indicated the degree of distortion in the cage pores (Figure 1b), sufficiently large-scale ordered

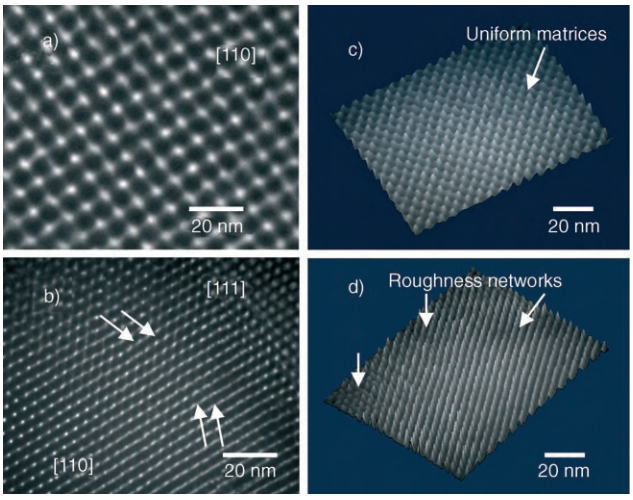

Figure 1. Representative TEM images of uniformly shaped cage mesochannels of the optical sensor **1** (a) and **2** (b) recorded along the [110] (a) and distorted [110]/[111] incidences (b). The 3D surfaces of these TEM micrographs (c and d) with a tilt of 45° revealed, in general, smooth and well-ordered network surfaces over wide-range domains. However, the TEM image (b) indicated that the grafting of the cage monoliths during the batch embedding experiments might induce the orientationally distorted portion, but this does not lead to significant collapse in the mesoscopic frameworks.

domains were retained for all cage-network surfaces. In addition, the regular and continuous extension in the network cage surfaces (Figure 1c,d) might permit the homogenous and fast diffusion of pollutant species into the sensing matrices.[23] AFM patterns (see the Supporting Information) clearly provide further evidence of topological defect-free surfaces associated with the organization of well-defined cagelike pores over large-scale regions. This indicates the retention of periodically ordered nanoscale cage structures with immobilization of the probe molecules (Scheme 2). Such retention led to a significant increase in the response time of the sensing systems (≤ 1 min, Table 1), indicating the effectiveness of the 3D ordered pore surfaces of these optical probe sinks for facile transport of analyte ions during the detection process.

Figure 2 reveals that dominant face-centered cubic (fcc) *Fm*3*m* structures with a highly ordered structure and a large lattice constant in the range of 21–22 nm are characteristic of the sensors **1**–**4**. The well-resolved XRD patterns of sensor **1**–

Table 1: Structural parameters[a] of the optical-sensor-based cubic *Fm*3*m* cage monoliths, and characteristics of the sensing systems[b] during the colorimetric detection of toxic metal ions by using these cage probe sinks.

Optical sensors		a	C_R	S_{BET}	V_p	V_m	Q	$10^9\,D_L$	D_R	n	t [s]	pH range
Probe	Ions	[nm]	[nm]	[$m^2\,g^{-1}$]	[$cm^3\,g^{-1}$]	[$cm^3\,g^{-1}$]	[mmol g^{-1}]	[mol dm^{-3}]	[mol dm^{-3}]			
1	Pb^{2+}	22.0	14.9	702	1.05	0.1	0.012	2.38	9.7×10^{-9} to 4.8×10^{-6}	1:2	150	6–7.5
2	Cd^{2+}	21.2	14.3	500	0.90	0.05	0.0031	13.5	1.78×10^{-8} to 4.4×10^{-6}	1:1	40	7–10
3	Sb^{3+}	21.2	14.2	457	0.87	0.04	0.019	33.7	4.1×10^{-8} to 1.6×10^{-6}	1:1	60	2.7–3.6
4	Hg^{2+}	21.2	14.3	410	0.89	0.04	0.0054	6.34	9.9×10^{-9} to 1.5×10^{-6}	1:1	60	8–10

[a] Unit lattice constant ($a_{Fm3m} = d_{111}\sqrt{3}$), pore cavity sizes [$C_R = a\,(6/\vartheta\pi)^{1/3}(V_p\rho/1 + V_p\rho + V_m\rho)^{1/3}$], where ϑ is the number of cavities in the unit cell; $\vartheta = 4$ for cubic *Fm*3*m*, ρ is the density of the silica framework and equal to 2.2 g cm^{-3}, S_{BET} = specific surface area, and mesopore (V_p))/micropore (V_m) volumes. [b] Adsorption amount (Q) of the probe molecules at the saturation point within the cage structures, detection limit (D_L) and range (D_R), stoichiometry of the ion/chromophore complex formation (n), and kinetic responding times (t). S_{BET} = specific surface area.

 © 2006 Wiley-VCH Verlag GmbH & Co. KGaA, Weinheim

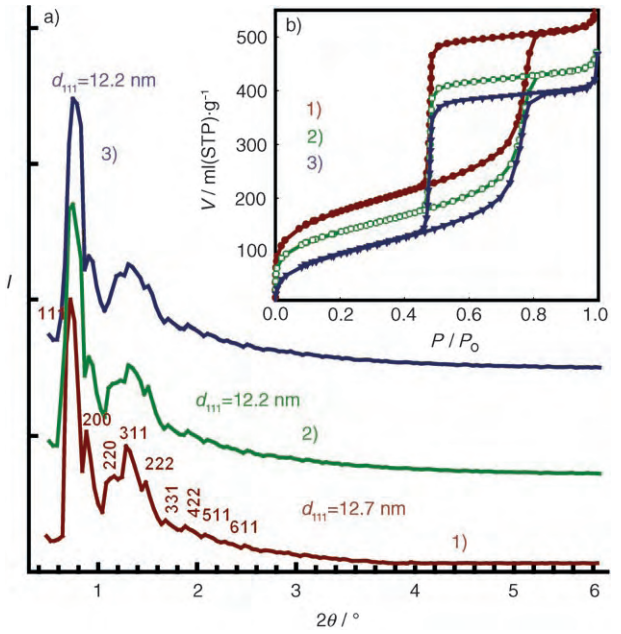

Figure 2. XRD patterns (a) and N_2 adsorption/desorption isotherms at 77 K (b) of cage sensors **1** (1), **2** (2), and **4** (3) before detection of Pb^{II}, Cd^{II}, and Hg^{II} analyte targets, respectively. STP = standard temperature and pressure.

4, which are similar to that of original cubic *Fm*3*m* cage monoliths HOM-C10 (see the Supporting Information),[20] provide strong evidence for a high degree of mesoscopically ordered sensors. The N_2 (Figure 2B and the Supporting Information) and Ar (see the Supporting Information) isothermal shapes indicated the stability of the cagelike pore domains with entrance sizes ≤ 5.0 nm (see reference [24] for extensive discussion). However, the decrease in the pore sizes of spherical cavities (Table 1) was observed by inclusion of the probe molecules and evidenced by the shift in the capillary condensation to a lower relative pressure P/P_o in both sets of N_2 and Ar isotherms (see the Supporting Information).[24] In addition, the decrease in the specific surface area and micropore/mesopore volumes (see Table 1) indicated that a large amount of the probes might be grafted into the large pore cavity; however, a significant amount might also anchor on the outer surfaces of the cage. It was evident that the cage character was maintained even after embedding of the sensing probe molecules, despite the extensive grafting process (Scheme 2). Such wide-range functionalities of the optical hybrid cage probes make these sensing systems technologically promising for colorimetric detection of toxic ions at a low concentration level, namely, subnanomolar (see Scheme 1).

The colorimetric detection of Pb^{II}, Cd^{II}, Sb^{III}, and Hg^{II} ions was revealed in the detection range of 9.9×10^{-9}–1.5×10^{-6} M by using the cage sensors **1**–**4**. The applicability of our sensing techniques, which are based on the design of 3D cage monoliths with the ability to act as an optical probe, was confirmed by the quantitative determination of these toxic metals (Scheme 1).[18,21] The color changes of the sensors **1**–**4**, induced by metal ions, can be easily visualized and quantified rapidly without any instrumentation, although UV/Vis spectroscopy was used for monitoring the changes in the absorption spectra that were observed when the metal ions complexed with the molecular probes (Figure 3). Although the cubic *Fm*3*m* cage structure had an influence on the color

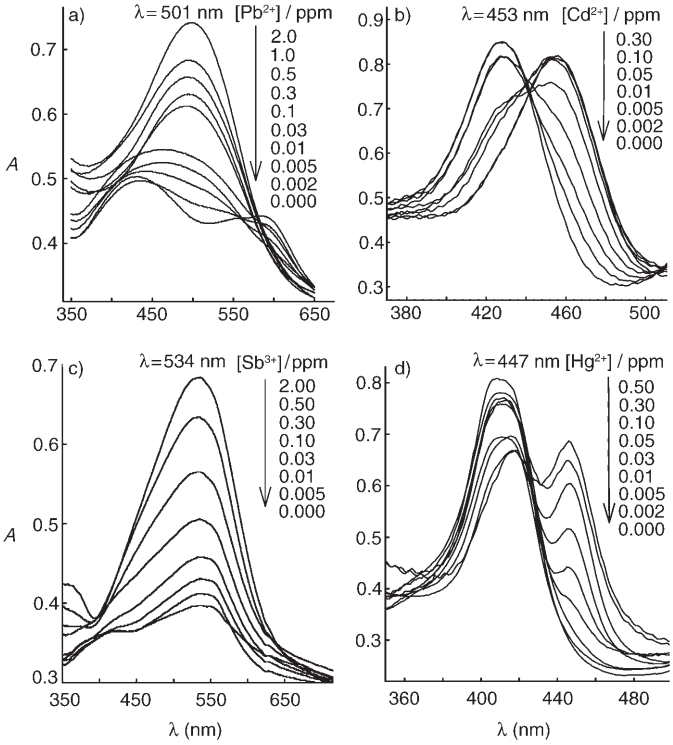

Figure 3. Concentration-dependent changes of UV/Vis absorption spectra of cage sensors **1** (a), **2** (b), **3** (c), and **4** (d) after detection of Pb^{II}, Cd^{II}, Sb^{III}, and Hg^{II} analyte targets, respectively.

changes of the sensors **1**–**4**,[18,21] these classes of cage sensing sinks offered several advantages in view of the long-term (several months) stability of the sensing probes[25] and the high adsorption capacity of the probes. This increases the utility of the probes as sensors in terms of sensitivity and fast kinetic detections.[6]

The ability to use naked-eye detection over the wide and tunable detection range of the analyte ions was clarified by UV/Vis spectroscopy (Figure 3). Our control experiments showed that sensitive colorimetric detection of metal ions required specific conditions, such as pH values and specific amounts of the cage sensor. The variation in these detection conditions was mainly dependent on the nature of the sensing system and the formation of the ion–chromophore complex (see Table 1). The calibration plots (see the Supporting Information) of these sensing systems show a liner correlation at low concentration ranges of analyte ions. However, in all detection designs, the liner correlation was varied depending upon the characteristics of the complex formation with the sensing systems. Furthermore, the stoichiometry of the metal–chromophore complexes can be derived from the deviation from linearity at the inflection point, as listed in Table 1.[18] From the calibration plot (see the Supporting Information),

 © 2006 Wiley-VCH Verlag GmbH & Co. KGaA, Weinheim

the ion detection limit (D_L) of the cage sensors was estimated (Table 1).[18] In all sensing systems, the D_L values are the first evidence of a higher degree of sensitivity than ever previously reported for visual detection techniques.[8–18,21] This evidence confirms that the cage sensing monolithic designs can be used effectively to detect very low concentrations of toxic ions with very simple instrumentation or even the naked eye.

The key result in our study is that naked-eye detection was found to be possible for subnanomolar concentrations of metal ions (Scheme 1), although the interference of anionic and cationic species, namely, effective disturbance sensing, was influenced by the selectivity of the optical probe sinks.[21] The results herein show that the cage sensors **1**–**4** revealed highly selective sensing systems of Pb^{II}, Cd^{II}, Sb^{III}, and Hg^{II} target ions despite the presence of interference ions, such as cations, anions, or complexing agents, at concentrations up to 300 times that of analyte targets (for extensive studies, see the Supporting Information). In addition, no significant changes in the color developed maps of the chromophore–metal complexes were visually observed after the addition of effectively interfered ions, indicating that our sensing systems did not undergo integrated disturbance effects in their selective functions towards targets (see the Supporting Information).

The kinetic response was studied by continuously monitoring the colored complex spectra of cage sensors after the addition of analyte ions at varying times. Our results show that fast responding times t (where, $30\,s \le t \le 3$ min) were characteristic of the complexation reactions of the metal ions and chromophore probes in our sensing systems (Table 1). Spectrophotometric studies (data not shown) reveal that the optical density of the sensors reached the maximum plateau within a minute, indicating significant accessibility and diffusion of the analyte into the well-ordered probe sinks.[25,26] Despite the rapid response at high analyte concentrations in our sensing systems, the sensitive color detection, in particular at low analyte concentrations, was substantially influenced by the concentration of the chromophore (the amount of sensor used). Within these sensing systems, the amount of the sensors used ($\approx$2–5 mg) was optimized to find the ideal optical density and response time at low analyte concentrations.

Furthermore, the reusability and reproducibility of the cage sensors are of particular interest in developing recyclable hybrid optical sensors, highlighting their important characteristic features and desirability for industrial applications.[23] Both sets of parameters were extensively studied by repeated exquisite-detection regeneration cycles. In these treatment procedures, the use of specific concentrations of stripping agents, such as EDTA or Cl^-, SCN^-, and CN^- anions, made the removal of the metal ions (decomplexation) possible. For example, EDTA (0.1%) was an effective stripping agent for the removal of Pb^{II} from a complex with the dithizone probe (sensor **1**) without resulting in a reduced response. Our experiments show that more than four cycles of Pb^{2+} analyte removal resulted in a 90% reduction in the sensitive recognition (Figure 4). The decrease in the degree of sensitive recognition is due to the intensive effect of the stripping agents on the sensing functions during several cycles.[27]

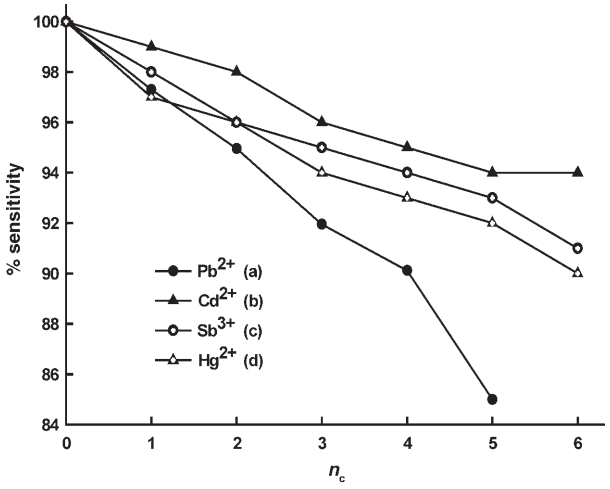

Figure 4. Reproducibility of the cage sensors **1** (a), **2** (b), **3** (c), and **4** (d) after complexation–regeneration cycles of analyte ions. Note the calculated percent variability with respect to the efficiency of the optical sensors after cycling of analyte ions (0.3 ppm). n_c = number of cycles.

In conclusion, cage monolithic silica materials with their uniformly nanosized cavities and entrances and highly ordered 3D cubic *Fm*3*m* structures show promise for the development of low-cost, rapid-response, and highly sensitive optical sensors. Our cage sensing systems exhibit exquisite sensitivity, long-term stability, and kinetically fast yet reliable detection of low concentrations (subnanomolar range) of several biologically toxic ions. These cage sensors could be used as optical sensing sinks that enable colorimetric detection (naked eye) with a high quantification limit. The effective use of these sensors as remote sensing operators on a real-time basis would significantly open up general and simple approachs for the identification of various biological and chemical toxic species without using sophisticated instruments.

Experimental Section

All materials were used without further purification. TMAC and MPTS were supplied from Gelest Co., Ltd. Japan. Diphenylthiocarbazone (dithizone), PR, TMPyP, and TPPS were obtained from Tokyo Kasei Kogyo Co., Ltd. Japan. Buffer solutions were prepared by mixing KCl/HCl (0.2 M) with CH_3COOH/CH_3COONa, 2-(cyclohexylamino)ethane sulfonic acid (CHES), 3-morpholinopropane sulfonic acid (MOPS), and *N*-cyclohexyl-3-aminopropane sulfonic acid (CAPS); a NaOH solution was employed to adjust the pH of the solutions (pH 6–10).

Fabrication of cubic *Fm*3*m* cage sensors: 1) Cage–dithizone sensor **1**: Dithizone was immobilized through direct dissolution and impregnation onto cubic *Fm*3*m* cage monoliths (HOM-C10) in ethanol. The stepwise impregnation was carried out under vacuum at 40 °C to reach probe saturation. The supported solid was washed with deionized water and dried at 80 °C.

2) Cage–TMPyP sensor **2:** The anchoring of MPTS onto the cage cavity was achieved by the addition of suspended MPTS to freshly prepared cubic *Fm*3*m* cage monoliths in refluxing toluene for 15 h.[28] The formation of cage-SO_3H monoliths was carried out by the addition of H_2O_2 (8%) solution to cage-SH materials at 50 °C with

 © 2006 Wiley-VCH Verlag GmbH & Co. KGaA, Weinheim

continuous stirring for 15 h. The modified cage-SO_3H solid was filtered, washed with deionized water, and then dried at 60–70 °C for 5 h. The incorporation of the TMPyP chromophore was formed by addition of an aqueous solution of TMPyP (3.4×10^{-3} g L^{-1}) to 1 g of cage-SO_3H solid with continuous stirring for 3 h. The cage-TMPyP sensor **2** was collected by suction and washed with deionized water several times without resulting in elution of the TMPyP chromophore.

3) Cage–PR sensor **3:** The TMAC ligand was grafted into the cubic *Fm3m* cage cavity as previously described with the incorporation of MPTS. The immobilization of the PR chromophore onto cage-TMAC occurred under aqueous acidic conditions (pH ≈ 3) with continuous stirring for 2 h. The cage PR solid was collected and washed with acidified water to determine if there was any elution of the PR chromophore. The cage-PR sensor **3** was dried under vacuum at 65 °C for 5 h.

4) Cage–TPPS sensor **4**: The functionalized TPPS chromophore in cage-TMAC materials was preformed by addition of an aqueous solution of TPPS (2.8×10^{-6} g L^{-1}) to 1 g cage-TMAC solid under stirring for 4 h.[28] The cage-TPPS solid was collected and washed with deionized water several times and then dried in an oven at 65 °C for 5 h. Note that the adsorption capacity of the probe molecules at the saturation point (Table 1) was determined by monitoring the absorbance of the probe with the fabricated sensors.

Detection of metal ions by using cage sensors: Toxic metal ions, such as Pb^{II}, Cd^{II}, Sb^{III}, and Hg^{II}, were detected by using sensors **1**, **2**, **3**, **4** at various pH values (≈7, 9.5, 3, and 9) by using MOPS, CHES, HCl/KCl, and CAPS buffer solutions, respectively. pH Studies show that the color changes of the sensors were suitable at these specific pH values. All solid sensor monoliths were grinded into a fine powder, approximately 80–90 μm in size, before the detection of analyte ions was performed. The colorimetric detection was performed by mixing various concentrations of toxic ions to the solid sensors at a constant volume (20 cm^3) with shaking; after an interval of time (1–5 min) depending on the nature of the sensor systems, the solid sensors were collected by suction with cellulose acetate filter paper (25 mm; Sibata filter holder) or a 25-mm glass microfiber filter (lock-type syringe). The collected films were used for color assessment with the naked eye and for absorbance measurements with UV/Vis spectroscopy. The absorbance spectra of sensor **1** at 596 nm exhibited a blue shift to 501 nm through the addition of Pb^{II} ions. In sensing systems **2** and **4**, a bathchromic shift was revealed from 429 and 410 nm to 453 and 447 nm during the detection of Cd^{II} and Hg^{II} ions, respectively. However, absorbance spectra of sensor **3** showed a hyperchromic effect at 534 nm upon the addition of Sb^{III} ions. These results indicated the formation of charge-transfer complexes between the metal ions and the probes (Figure 4). The concentrations of toxic metal ions were calculated by comparing the color intensity of the target samples with that of the standard samples, which were prepared with known concentrations of ion solutions. Note that the elution of TPPS might be observed from the sensor **4** monoliths during the reaction with Hg^{II} ions, indicating the nature of the structural character of the TPPS chromophore on the formation of Hg^{II}/TPPS complex. To avoid this elution, the addition of TMAC solution (2 mL) to sensor **4** with stirring for 6 h was required.

Instrumentation: The metal ion concentration was determined with a Seiko SPS-1500 inductively coupled plasma atomic emission spectrometer (ICP-AES). The absorbance spectrum of the solid material was recorded by using a UV/Vis spectrometer (Shimadzu 3150, Japan). Small-angle powder XRD patterns were measured by using an MXP 18 diffractometer (Mac Science Co. Ltd.) with monochromated CuKα radiation. N_2 and Ar adsorption–desorption isotherms were measured by using a BELSORP36 analyzer (JP. BEL Co. Ltd) at 77 K. The surface area was measured by using the Brunauer–Emmett–Teller (BET) method, whereas the microporosity was assessed by using the α_s-plot method. The spherical cavity of the cage cubic *Fm3m* sensors was determined as previously reported.[24] Energy-dispersive X-ray microanalysis (DS-130S) was used to determine the elemental compositions. FTIR spectra were recorded with a Prestige-21 instrument (Shimadzu, Japan). TG analyses were conducted with Thermo Plus TG8120 (Rigaku, Japan). The AFM measurements were performed on a SPA300/SPI3700 (Seiko Instruments). TEM images were obtained by using a JEOL TEM (JEM-2000EXII) operating at 200 kV with a side-mounted CCD camera (Mega View III from Soft Imaging System Co.). ^{29}Si magic-angle spinning (MAS) NMR spectra were measured at room temperature on a Bruker AMX-500 spectrometer operatingat 125.78 MHz with a 90° pulse length of 4.7 μs. For all samples the repetition delay was 180 s with a rotor spinning at 4 kHz.

Received: June 19, 2006
Revised: August 9, 2006
Published online: October 9, 2006

Keywords: cage monoliths · colorimetry · environmental chemistry · sensors · toxic metal ions

[1] G. K. Walkup, B. Imperiali, *J. Am. Chem. Soc.* **1996**, *118*, 3053–3054.
[2] A. Miyawaki, J. Llopis, R. Helm, J. M. McCaffery, J. A. Adams, M. Ikura, R. Y. Tsien, *Nature* **1997**, *388*, 882–887.
[3] M. M. Henary, C. J. Fahrni, *J. Phys. Chem. A* **2002**, *106*, 5210–5220.
[4] J. Homola, S. S. Yee, G. Gauglitz, *Sens. Actuators B* **1999**, *54*, 3–15.
[5] F. Turner, *Science* **2000**, *290*, 1315–1317.
[6] P. Chen, C. He, *J. Am. Chem. Soc.* **2004**, *126*, 728–729.
[7] X. Wang, C. Drew, S. H. Lee, K. J. Senecal, J. Kumar, L. A. Samuelson, *Nano Lett.* **2002**, *2*(11), 1273–1275.
[8] R. Metivier, I. Leray, B. Valeur, *Chem. Eur. J.* **2004**, *10*, 4480–4490.
[9] E. Palomares, R. Vilar, J. R. Durrant, *Chem. Commun.* **2004**, 362–363.
[10] a) J. Liu, Y. Lu, *J. Am. Chem. Soc.* **2004**, *126*, 12298–12305; b) J. Liu, Y. Lu, *Anal. Chem.* **2004**, *76*, 1627–1632.
[11] J. M. Nam, C. S. Thaxton, C. A. Mirkin, *Science* **2003**, *301*, 1884–1886.
[12] E. Palomares, R. Vilar, A. Green, J. R. Durrant, *Adv. Funct. Mater.* **2004**, *14*, 111–114.
[13] J. Shi, Y. Zhu, X. Zhang, W. R. G. Baeyens, A. M. Garcia-Campana, *Trends Anal. Chem.* **2004**, *23*, 351–360.
[14] S. O. Obare, R. E. Hollowell, C. J. Murphy, *Langmuir* **2002**, *18*, 10407–10410.
[15] G. Wirnsberger, B. J. Scott, G. D. Stucky, *Chem. Commun.* **2001**, 119–120.
[16] L. Mercier, T. J. Pinnavaia, *Adv. Mater.* **1997**, *9*, 500.
[17] R. Metivier, I. Leray, B. Lebeau, B. Valeur, *J. Mater. Chem.* **2005**, *15*, 2965–2973.
[18] T. Balaji, M. Sasidharan, H. Matsunaga, *Anal. Bioanal. Chem.* **2006**, *384*, 488–494.
[19] a) A. B. Desacalzo, D. Jimenez, M. D. Marcos, R. M. Manez, J. Soto, J. El Haskouri, C. Guillem, D. Beltran. P. Amoros, M. V. Borrachero, *Adv. Mater.* **2002**, 14, 966; b) M. Boiocchi, M. Bonizzoni, L. Fabbrizzi, G. Piovani, A. Taglietti, *Angew. Chem.* **2004**, *116*, 3935–3940; *Angew. Chem. Int. Ed.* **2004**, *43*, 3847–3852; c) M. Comes, G. R. Lopez, M. D. Marcos, R. M. Manez, F. Sancenon, J. Soto, L. A. Villaescusa, P. Amoros, D. Beltran, *Angew. Chem.* **2005**, *117*, 2978–2982; *Angew. Chem. Int. Ed.* **2005**, *44*, 2918–2922.
[20] a) S. A. El-Safty, T. Hanaoka, F. Mizukami, *Chem. Mater.* **2005**, *17*, 3137–3145; b) S. A. El-Safty, T. Hanaoka, F. Mizukami, *J. Phys. Chem. B* **2005**, *109*, 9255–9264; c) D. Zhao, J. Feng, Q.

 © 2006 Wiley-VCH Verlag GmbH & Co. KGaA, Weinheim

Huo, N. Melosh. G. H. Fredrickson, B. F. Chmelka, G. D. Stucky, *Science* **1998**, *279*, 548.
[21] C. W. Clavier, D. L. Rodman, J. F. Sinski, L. R. Allain, H.-J. Im, Y. Yang, J. C. Clark, Z-L. Xue, *J. Mater. Chem.* **2005**, *15*, 2356 – 2361.
[22] A. M. Liu, K. Hidajat, S. Kawi, D. Y. Zhao, *Chem. Commun.* **2000**, 1145 – 1146.
[23] a) J. Xiao, J. Wei, *Chem. Eng. Sci.* **1992**, *47*, 1123; b) L. Nicole, C. Boissiere, D. Grosso, P. Hesemann, J. Moreau, C. Sanchez, *Chem. Commun.* **2004**, 2312 – 2313.
[24] a) P. I. Ravikovitch, A. V. Neimark, *Langmuir* **2002**, *18*, 1550 – 1560; b) J. R. Matos, M. Kruk, L. P. Mercuri, M. Jaroniec, L. Zhao, T. Kamiyama, O. Terasaki, T. J. Pinnavaia, Y. Liu, *J. Am. Chem. Soc.* **2003**, *125*, 821 – 829; c) T. W. Kim, R. Ryoo, M. Kruk, K. P. Gierszal, M. Jaroniec, S. Kamiya, O. Terasaki, *J. Phys. Chem. B* **2004**, *108*, 11480 – 11489.
[25] M. Plaschke, R. Czolk, H. J. Ache, *Anal. Chim. Acta* **1995**, *304*, 107 – 113.
[26] L. Rodman, H. Pan, C. W. Clavier, X. Feng, Z.-L. Xue, *Anal. Chem.* **2005**, *77*, 3231 – 3237.
[27] A. Sayari, S. Hamoudi, Y. Yang, *Chem. Mater.* **2005**, *17*, 212 – 216.
[28] J. Evans, A. B. Zaki, M. Y. El-Sheikh, S. A. El-Safty, *J. Phys. Chem. B* **2000**, *104*, 10271 – 10282.

 © 2006 Wiley-VCH Verlag GmbH & Co. KGaA, Weinheim

Polyarene Coordination

DOI: 10.1002/anie.200602568

Corannulene "Hub" Carbon Coordination by $[Ru_2\{O_2C(3,5\text{-}CF_3)_2C_6H_3\}_2(CO)_5]$**

Marina A. Petrukhina, Yulia Sevryugina, Andrey Yu. Rogachev, Edward A. Jackson, and Lawrence T. Scott*

Transition-metal complexes of fullerenes have attracted considerable attention since 1991, when Fagan et al. reported the synthesis and structure of the first complex, $[Pt(PPh_3)_2(\eta^2\text{-}C_{60})]$.[1] A great number of *exo*-bound transition-metal complexes of fullerenes have been synthesized since then.[2] By contrast, bowl-shaped polycyclic aromatic hydrocarbons that constitute fragments of fullerenes[3] could not be coaxed to function as ligands for transition metals until 1997, when Seiders et al. finally isolated and spectroscopically characterized the first cationic metal complex of corannulene, $[(\eta^6\text{-}C_{20}H_{10})Ru(C_5Me_5)]^+$.[4] Corannulene, the smallest open geodesic polyarene that maps onto the ring system of C_{60} (Scheme 1), has served as the primary model for theoretical and experimental coordination studies since then. NMR evidence for η^6 complexation of corannulene by $[Ir(C_5Me_5)]^{2+}$ was reported in 2003,[5] but structural characterization of the first η^6 corannulene complex by X-ray crystallography was not achieved until 2004.[6] Last year, Elliott et al. reported three silver complexes of corannulene, all having extended networks built on η^2 and η^1 binding of Ag^+ centers to the rim CH sites of the hydrocarbon bowl.[7]

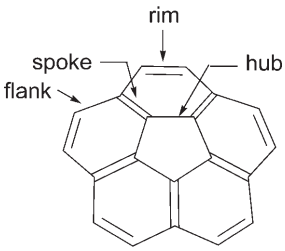

Scheme 1. Four types of C–C bonds in corannulene ($C_{20}H_{10}$).

The first crystalline η^2 complexes of corannulene were synthesized and structurally characterized by X-ray crystallography in our laboratory in 2003.[8] Using gas-phase coordination reactions,[9] we prepared two rhodium(II) complexes having different compositions $[\{Rh_2(O_2CCF_3)_4\}_m\cdot(C_{20}H_{10})_n]$ ($m/n = 1{:}1$ and $3{:}2$) in a solvent-free environment. The compounds exhibit extended 1D and 2D structures built on the rim $\mu_2\text{-}\eta^2{:}\eta^2$ and $\mu_3\text{-}\eta^2{:}\eta^2{:}\eta^2$ coordination modes, respectively, of corannulene. More recently, we have prepared a discrete bis(corannulene) ruthenium(I) complex, $[Ru_2(O_2CCF_3)_2(CO)_4\cdot(C_{20}H_{10})_2]$, which has terminally η^2-rim-bound $C_{20}H_{10}$ molecules.[10] This work demonstrates that the preference exhibited by corannulene for η^2 coordination on the rim by strongly Lewis acidic rhodium(II) centers[8,9] extends also to isoelectronic ruthenium(I) centers.

As this field has blossomed, we have become increasingly intrigued by the continued absence of any structurally characterized transition-metal complexes of corannulene, or of any other geodesic polyarene, in which a metal center coordinates to one or more of the interior, "fullerene-like" quaternary carbon atoms in preference to the methine atoms on the rim. Taking into consideration some basic principles of chemical bonding, we speculated that fine-tuning the electrophilic properties of metal sites should affect the nature of their coordination to bowl-shaped polyarenes. More specifically, we reasoned that softening the Lewis acidity of the metal complexes used[8–10] should decrease the preference for complexation to corannulene rim carbon atoms, since a weak Lewis acid should not strongly differentiate between the rim

[*] Prof. Dr. M. A. Petrukhina, Y. Sevryugina, Dr. A. Y. Rogachev
Department of Chemistry
University at Albany, State University of New York
Albany, NY 12222 (USA)
Fax: (+1) 518-442-3462
E-mail: marina@albany.edu
E. A. Jackson, Prof. Dr. L. T. Scott
Department of Chemistry
Merkert Chemistry Center, Boston College
Chestnut Hill, MA 02467-3860 (USA)

[**] M.P. is grateful to the Donors of the American Chemical Society Petroleum Research Fund (PRF no. 42910-AC3) and the National Science Foundation Career Award (NSF-0546945) for the support of this work. Additional support from the Department of Energy is gratefully acknowledged.

Supporting information for this article is available on the WWW under http://www.angewandte.org or from the author.

InterScience DISCOVER SOMETHING GREAT
© 2006 Wiley-VCH Verlag GmbH & Co. KGaA, Weinheim

and hub corannulene sites. Importantly, the coefficients of the highest-occupied molecular orbitals (HOMOs, doubly degenerate, see the Supporting Information) are greatest in corannulene at the five interior carbon atoms. However, the coefficients of the lowest-unoccupied molecular orbitals (LUMOs, doubly degenerate, see the Supporting Information) are greater at the rim (Figure 1). Clearly both HOMOs and LUMOs should be taken into account in metal–arene complexes, since ligand-to-metal donation and metal-to-ligand back-donation equally contribute to bonding in such systems.

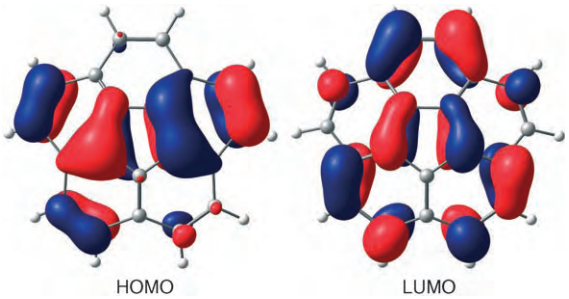

Figure 1. HOMO and LUMO of corannulene (PBE0/6-31G(d)//6-311G(d,p)). One of the two doubly degenerate orbitals is shown in each case.

Pursuing this line of thought, we turned our attention to the gas-phase reactions of corannulene with a single-end Lewis acidic site, the diruthenium(I,I) mixed carbonyl 3,5-bis(trifluoromethyl)benzoate, $[Ru_2\{O_2C(3,5\text{-}CF_3)_2C_6H_3\}_2(CO)_5]$.[11] According to our DFT charge-distribution analysis, this complex should behave as a much softer Lewis acid than the dimetal trifluoroacetate complexes used previously,[8–10] and our experimental results seem to confirm this conclusion. We report herein a new transition-metal complex in which one corannulene is η^1-coordinated to ruthenium at an interior "hub" carbon atom while another is η^2-rim-bound.

The gas-phase codeposition of corannulene with $[Ru_2\{O_2C(3,5\text{-}CF_3)_2C_6H_3\}_2(CO)_5]$ was performed at 165 °C. This reaction resulted in the formation of the new corannulene-based product $[Ru_2\{O_2C(3,5\text{-}CF_3)_2C_6H_3\}_2(CO)_5\cdot(C_{20}H_{10})]\cdot(^1/_4\,C_{20}H_{10})$, which was isolated in moderate yield. The crystals are air-stable at room temperature but show a slight sensitivity to moisture. They were characterized by elemental analysis, IR, UV/Vis, and NMR spectroscopy, and by X-ray crystallography (Supporting Information).

X-ray structural characterization reveals that one corannulene molecule functions as a guest, occupying a cavity in the crystal lattice (Figure 2), whereas the others function as ligands coordinated to diruthenium units. In contrast to the coordinated corannulene, the clathrated bowl is severely disordered and may even be undergoing bowl-to-bowl inversion in the crystal.

There are two crystallographically independent diruthenium(I,I) units with bound corannulene molecules in the same crystal. A comparison of these complexes reveals two different coordination modes of the $C_{20}H_{10}$ bowl. One has an

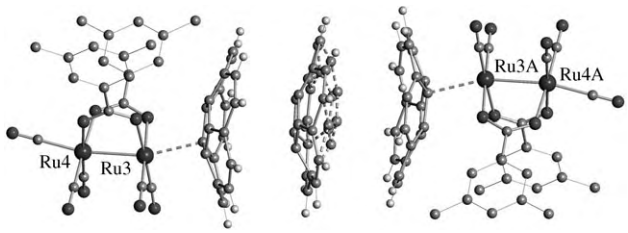

Figure 2. A fragment of the structure showing two types of corannulene. The fluorine and hydrogen atoms of the benzoate ligands are omitted.

η^2-rim-bound corannulene, with Ru1–C1 and Ru1–C2 bond lengths of 2.517(3) and 2.573(3) Å (Figure 3).

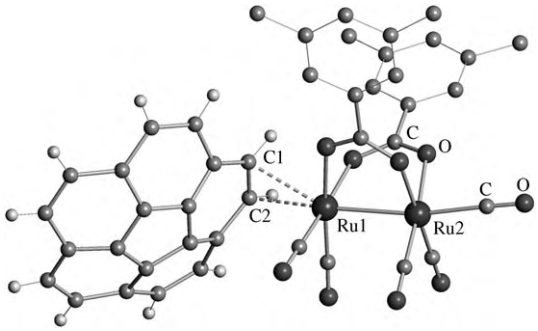

Figure 3. A rim-coordinated corannulene unit.

In the other complex, the open ruthenium end of the dimetal unit is η^1-bound to a single interior "hub" carbon atom on the convex surface of corannulene, with a Ru3–C12B bond length of 2.611(3) Å (Figure 4). The much longer Ru3–

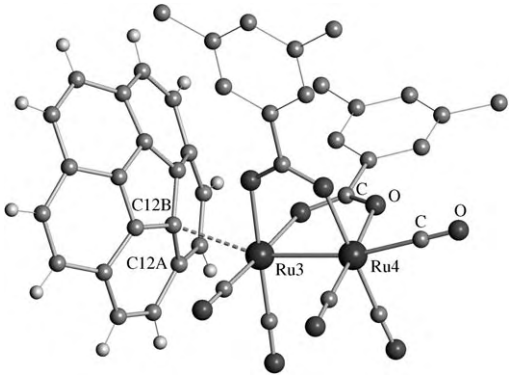

Figure 4. A hub-coordinated corannulene unit.

C12A separation (2.965(4) Å) leads us to classify the metal–ligand interaction in this complex as η^1 binding to a single interior "hub" carbon atom, rather than as η^2 binding to a "spoke" double bond. The C12A-C12B-Ru3 bond angle (90.26°) is very close to the angle one would expect for pure η^1 binding.

It is noteworthy that the Ru–C bond lengths of 2.547 (rim-complex average) and 2.611 Å (hub-carbon complex) are appreciably longer than the average bond length observed in

 © 2006 Wiley-VCH Verlag GmbH & Co. KGaA, Weinheim

the recently isolated bis(corannulene) adduct $[Ru_2(O_2CCF_3)_2(CO)_4\cdot(C_{20}H_{10})_2]$ (2.508 Å).[10] Interestingly, metal centers in all three ruthenium(I)–corannulene complexes bind the bowl from the *exo* face.

A comparison between the geometrical parameters of the coordinated corannulenes in these two complexes with those in the uncomplexed $C_{20}H_{10}$ molecule[12] (Supporting Information) shows that there is little perturbation of the corannulene core upon complexation with ruthenium(I) in the η^2 complex (Figure 3); however, one noticeable perturbation can be seen in the η^1 complex (Figure 4). The carbon atom bound to ruthenium in the η^1 complex is significantly more pyramidalized than the other four hub carbon atoms of the complexed ligand. The p-orbital axis vector (POAV) analysis of Haddon[13] provides an excellent method for quantifying this degree of pyramidalization. As reference points, we note that a planar trigonal carbon atom (such as that in benzene) has a POAV angle of 0.0°, whereas the highly pyramidalized carbon atoms of C_{60} have POAV angles of 11.6°. The four uncomplexed hub carbon atoms of the ligand in the η^1 complex (Figure 4) have POAV angles of 8.3° ± 0.2°, a value which is indistinguishable from that in unbound corannulene (POAV angle also 8.3°). The hub carbon atom that is η^1-bound, on the other hand, has a POAV angle of 10.6°. This increase in pyramidalization by nearly 30% constitutes compelling experimental evidence for a bonding interaction between the metal center and the hub carbon atom.

To compare the binding energies of the η^2-rim and the η^1-hub corannulene $[Ru_2\{O_2C(3,5\text{-}CF_3)_2C_6H_3\}_2(CO)_5\cdot(C_{20}H_{10})]$ complexes, we performed density functional theory (DFT) calculations (Supporting Information).[14] Our calculations predict a small preference of 2.5 kcal mol^{-1} for the rim-bound structure over the hub complex. The absolute binding energies for the rim (11.5 kcal mol^{-1}) and hub (9.0 kcal mol^{-1}) isomers, however, fall significantly below the value for the $[Ru_2(O_2CCF_3)_2(CO)_4\cdot(C_{20}H_{10})]$ complex (20.3 kcal mol^{-1}).[10] Consistently, the latter shows the shortest Ru–C bonding interactions in this ruthenium(I)–corannulene series. Importantly, a molecular-orbital analysis of the two optimized gas-phase structures confirms both the η^2 binding in the rim isomer and the η^1 hapticity in the hub complex.

In summary, the use of a very soft, single-end diruthenium(I,I) Lewis acid has resulted in the isolation of a unique ruthenium(I)–corannulene complex with two crystallographically independent units cocrystallized in one crystal. One unit is an η^2-rim-bound complex, while the other represents the first example of metal coordination exclusively to the interior region on the convex surface of a geodesic polyarene. The formation of a hub-coordinated complex in this work demonstrates for the first time a degree of similarity between the convex carbon surfaces of corannulene and of fullerenes in metal-binding reactions.

Received: June 27, 2006
Published online: October 6, 2006

Keywords: coordination modes · corannulene · density functional calculations · ruthenium · structure elucidation

[1] P. J. Fagan, J. C. Calabrese, B. Malone, *Science* **1991**, *252*, 1160.
[2] a) P. J. Fagan, J. C. Calabrese, B. Malone, *Acc. Chem. Res.* **1992**, *25*, 134; b) A. Balch, M. M. Olmstead, *Chem. Rev.* **1998**, *98*, 2123; c) K. Lee, H. Song, J. T. Park, *Acc. Chem. Res.* **2003**, *36*, 78.
[3] Recent reviews: a) L. T. Scott, *Pure Appl. Chem.* **1996**, *68*, 291; b) P. W. Rabideau, A. Sygula, *Acc. Chem. Res.* **1996**, *29*, 235; c) G. Mehta, H. S. P. Rao, *Tetrahedron* **1998**, *54*, 13325; d) L. T. Scott, *Angew. Chem.* **2004**, *116*, 5102; *Angew. Chem. Int. Ed.* **2004**, *43*, 4994.
[4] T. J. Seiders, K. K. Baldridge, J. M. O'Connor, J. S. Siegel, *J. Am. Chem. Soc.* **1997**, *119*, 4781.
[5] C. A. Alvarez, R. J. Angelici, A. Sygula, R. Sygula, P. W. Rabideau, *Organometallics* **2003**, *22*, 624.
[6] a) P. A. Vecchi, C. M. Alvarez, A. Ellern, R. J. Angelici, A. Sygula, R. Sygula, P. W. Rabideau, *Angew. Chem.* **2004**, *116*, 4597; *Angew. Chem. Int. Ed.* **2004**, *43*, 4497; b) P. A. Vecchi, C. M. Alvarez, A. Ellern, R. J. Angelici, A. Sygula, R. Sygula, P. W. Rabideau, *Organometallics* **2005**, *24*, 4543.
[7] E. L. Elliott, G. A. Hernandez, A. Linden, J. S. Siegel, *Org. Biomol. Chem.* **2005**, *3*, 407.
[8] M. A. Petrukhina, K. W. Andreini, J. Mack, L. T. Scott, *Angew. Chem.* **2003**, *115*, 3497; *Angew. Chem. Int. Ed.* **2003**, *42*, 3375.
[9] a) M. A. Petrukhina, L. T. Scott, *Dalton Trans.* **2005**, 2969; b) M. A. Petrukhina, K. W. Andreini, L. Peng, L. T. Scott, *Angew. Chem.* **2004**, *116*, 5593; *Angew. Chem. Int. Ed.* **2004**, *43*, 5477.
[10] M. A. Petrukhina, Y. Sevryugina, A. Yu. Rogachev, E. A. Jackson, L. T. Scott, *Organometallics* **2006**, in press.
[11] Y. Sevryugina, A. V. Olenev, M. A. Petrukhina, *J. Cluster Sci.* **2005**, *16*, 217.
[12] a) J. C. Hanson, C. E. Nordman, *Acta Crystallogr. Sect. B* **1976**, *32*, 1147; b) M. A. Petrukhina, K. W. Andreini, J. Mack, L. T. Scott, *J. Org. Chem.* **2005**, *70*, 5713.
[13] a) R. C. Haddon, L. T. Scott, *Pure Appl. Chem.* **1986**, *58*, 137; b) R. C. Haddon, *J. Am. Chem. Soc.* **1987**, *109*, 1676; c) R. C. Haddon, *J. Am. Chem. Soc.* **1990**, *112*, 3385.
[14] Molecular-geometry optimizations were performed at the DFT level by using the hybrid exchange-correlation functional PBE0 as implemented in the PC GAMESS version of the GAMESS-US program package. The Hay and Wadt effective core potential (ECP) and the LANL2DZ basis set were used for Ru atoms, the 3-21G(d) basis sets were used for the benzene rings and the CF_3 groups of the carboxylate ligands, and the 6-31G(d) basis sets were employed for all other atoms.

 © 2006 Wiley-VCH Verlag GmbH & Co. KGaA, Weinheim

Metal–Boron Nanotubes

DOI: 10.1002/anie.200602610

Noncrystalline Metal–Boron Nanotubes: Synthesis, Characterization, and Catalytic-Hydrogenation Properties**

Yan Zhu, Fuping Liu, Weiping Ding, Xuefeng Guo,* and Yi Chen*

Much attention has been focused recently on one-dimensional (1D) nanostructures, such as nanowires, nanorods, nanobelts, and nanotubes owing to their unique applications in, for example, energy storage, transistors, biochips, sensors. Several different synthetic strategies have been explored for generating 1D nanostructures, for example, self-assembly of 0D building blocks and size reduction of 1D microstructures.[1,2] Furthermore, appropriate capping reagents have been used to control the growth rates of various facets of a solid kinetically.[3] In the vapor–-liquid–-solid (VLS) process, the symmetry is broken by the introduction of a flat solid–liquid interface.[4] The supersaturation of a system can also be controlled below a certain level to effectively induce 1D growth.[5] Since the discovery of carbon nanotubes,[6] a variety of inorganic nanotubes have also been synthesized,[7–16] and template-directed methods have been found to be an elegant and straightforward route for the formation of nanotubular materials.[17–21]

Noncrystalline transition-metal–boron alloys with short-range-ordered and long-range-disordered structures have been intensively investigated owing to their important practical or potential applications in various fields, such as ferrofluids, powder metallurgy, magnetic applications, composite materials, and catalysis.[22–24] Although noncrystalline metal–boron alloys prepared by melt-quenching or chemical reduction date back to the 1950s—pure boron nanotubes have been reported only recently[9–11]—no studies have been reported on the chemical preparation of 1D morphologies of noncrystalline metal–boron alloys. Considering the unusual characteristics of these artificially synthesized 1D nanostructures, it is desirable to explore methods to obtain 1D noncrystalline metal–boron (M–B) alloys. Owing the isotropic structures of noncrystalline alloys it is difficult for them to be grown into 1D nanostructures. Herein we report the first synthesis of nanotubes of noncrystalline M–B (M = Fe, Co, and Ni) alloys involving the use of lyotropic liquid crystals (LCs) of non-ionic–anionic mixed surfactants as templates. The non-ionic surfactants used are Tween 40 (polyoxyethylene sorbitan monopalmitate), Tween 60 (polyoxyethylene sorbitan monostearate), and Tween 80 (polyoxyethylene sorbitan monooleate), and the anionic surfactant is CSA (camphorsulfonic acid). The noncrystalline M–B nanotubes thus prepared are more effective than the corresponding nanoparticles for the catalytic hydrogenation of *m*-nitrotoluene.

Figure 1a shows the X-ray diffraction (XRD) patterns of the as-synthesized nanotubes of noncrystalline M–B alloys. The three samples keep their noncrystalline features, as indicated by a broad peak located at a 2θ value of around 45° and the lack of other diffraction peaks from crystalline phases.[25]

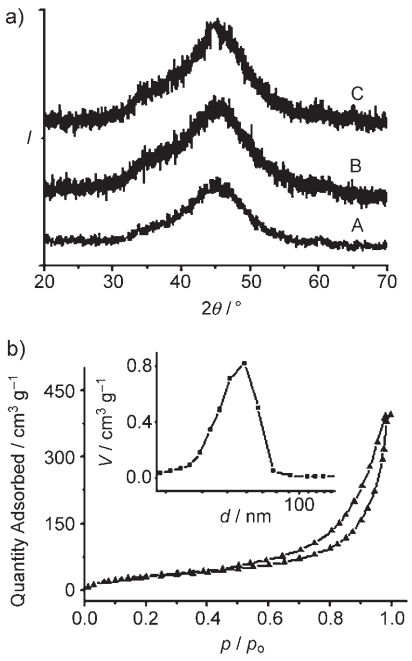

Figure 1. a) XRD patterns of Fe–B (A), Co–B (B), and Ni–B (C) nanotubes; b) nitrogen absorption isotherms of Fe–B nanotubes measured at 77 K; the inset shows the corresponding pore size distribution curve determined by the BJH method from the desorption isotherm; V = pore volume, d = pore width.

Figure 1b shows the N_2 sorption isotherms and pore size distribution of Fe–B nanotubes; similar results were obtained for Co–B and Ni–B nanotubes. The porous characteristics of the three noncrystalline M–B alloys are summarized in Table 1. Their surface areas measured by N_2 sorption are basically consistent with those evaluated from the size of the nanotubes measured by transmission electron microscopy (TEM).

These noncrystalline nanotubes are fragile under high-energy electron-beam irradiation. Therefore a low voltage of 80 kV was adopted for most of the TEM measurements. Unfortunately, such a low voltage can only provide the

[*] Y. Zhu, Prof. W. Ding, Prof. X. Guo, Prof. Y. Chen
Lab of Mesoscopic Chemistry
School of Chemistry and Chemical Engineering
Nanjing University
Nanjing 210093 (P.R. China)
Fax: (+86) 258-331-7761
E-mail: dingwp@nju.edu.cn
guoxf@nju.edu.cn
Dr. F. Liu
Changzhou Sunlight Fine Chemical Co., Ltd.
Changzhou 213134 (P.R. China)

[**] We are grateful for financial support from MOST (China) (grant no. 2003CB615804) and the NSF (China) (grant no. 20403008).

© 2006 Wiley-VCH Verlag GmbH & Co. KGaA, Weinheim

Table 1: Porous texture of the samples detected by N_2 sorption isotherms,[a] and their catalytic performance for the hydrogenation of *m*-nitrotoluene to *m*-toluidine.[b]

Samples	S_{BET} [$m^2 g^{-1}$]	Pore size [nm]	Pore volume [$cm^3 g^{-1}$]	Yield [%]
Fe–B NTs	118.3	46.2	0.6	79.2
Co–B NTs	98.9	55.9	0.5	93.8
Ni–B NTs	92.6	59.7	0.5	93.1
Fe–B NPs	39.6	10.2	0.2	10.7
Co–B NPs	33.5	10.6	0.1	83.5
Ni–B NPs	31.9	8.2	0.1	80.0
Pd/C (3%)	1100.1	–	–	96.0

[a] Surface area: BET method; pore diameter: BJH method from the desorption branch; pore volume: single-point adsorption total pore volume at a relative pressure of 0.97. NTs: nanotubes; NPs: nanoparticles prepared according to ref. [26]. [b] The reaction was performed at 393 K and 2.0 MPa of hydrogen pressure for 2 h for all samples except Fe–B NTs and NPs, for which a hydrogen pressure of 3.5 MPa was used.

morphology of the nanotubes (as shown in Figure 2a) rather than any further details regarding their local structures. TEM images (Figure 2a) of Fe–B nanotubes prepared using Tween 40 and CSA as template reveal that the nanotubes are several micrometers in length and have inner and outer diameters of around 50–55 and 60–65 nm, respectively. The continuous broad halo rings (inset of Figure 2a) resulting from selected-area electron diffraction (SAED) further support the noncrystalline nature of the Fe–B nanotubes and are consistent with the magnified TEM image taken at 200 kV shown in Figure 2b. To avoid damaging the nanotubes this image was taken in the shortest possible time. Energy dispersive spectrometry (EDS) of a single nanotube revealed the coexistence of Fe and B in the sample at an atomic ratio

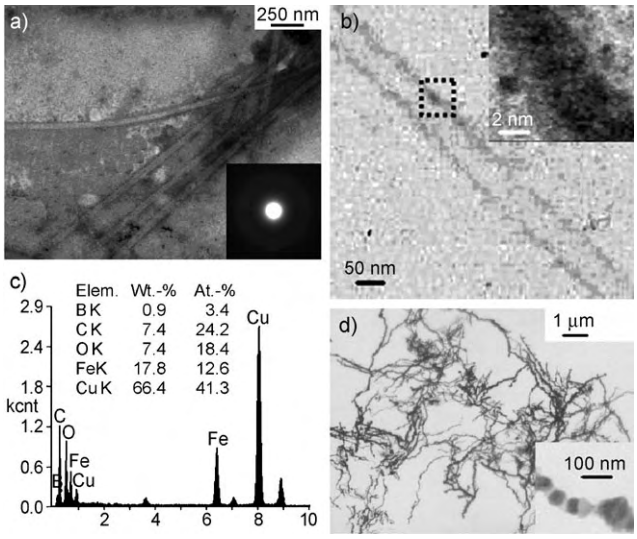

Figure 2. a) TEM image (80 kV) of Fe–B nanotubes; inset: the corresponding SAED pattern; b) HRTEM image (200 kV) of one isolated Fe–B nanotube inset: expansion of marked section; c) EDS spectrum of a single Fe–B nanotube (kcnt = kilocounts); d) TEM image of Fe–B noncrystalline chains of beads obtained with only CSA as the template, inset: enlargement.

about 3.7:1 (Figure 2c). In contrast, when only CSA was used as surfactant chains were observed resulting from assembly of nanoparticles through the magnetism of Fe–B (Figure 2d), whereas with Tween 40, Tween 60, or Tween 80 as the sole template sheet-like structures were obtained (not shown).

The Co–B and Ni–B nanotubes obtained with Tween 60 and CSA as template are also noncrystalline. Their TEM, SAED, and EDS images (Figure 3) reveal the noncrystalline

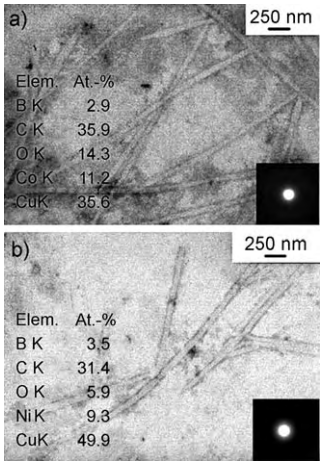

Figure 3. TEM images (80 kV) and corresponding SAED (inset) and EDS analyses of a) Co–B nanotubes and b) Ni–B nanotubes.

nature of these nanotubes and the reasonable M:B ratios obtained. Elemental analysis by inductively coupled plasma (ICP) spectroscopy indicated that the Fe:B, Co:B, and Ni:B atomic ratios in the as-prepared samples are 3.2:1, 2.9:1, and 2.5:1, respectively, which are basically consistent with the EDS results and are close to the composition of the nanoparticulate counterparts selected for comparison.[26]

A few M–B nanoparticles can often be seen in the TEM images of the noncrystalline nanotube samples. It seems difficult to avoid having these nanoparticles present, this is tentatively attributed to there being only weak interactions between the metal ions and surfactants in the soft-template method used. However, the noncrystalline nanotubes are always the major product, with an estimated percentage of more than 70% according to microscopic observation on various samples.

The template has a strong impact on the morphology of the product. It is likely that the lyotropic nematic nature of the non-ionic–anionic surfactant mixture provides a template for the growth of 2D lamellar mesostructures, and the synthesis of the nanotubes might consist of two steps. The first step should be the formation of a lamellar structure by the condensation of the mixed surfactants and metal cations. The cations are likely to be located in the spaces between the head groups of the anionic surfactant. This arrangement is a result of the formation of CSA–M ion pairs stabilized by the non-ionic surfactant LCs, and means that the metallic ions are confined to the aqueous interface of the mixed-surfactant lamellar micelles. The second step, which is induced by the addition of sodium borohydride, is the reduction of these metal ions, which results in the loosening of the lamellar

 © 2006 Wiley-VCH Verlag GmbH & Co. KGaA, Weinheim

nanosheets and the rolling-up of the 2D nanosheets, driven by a decrease in their surface free energy, similar to the formation of cylindrical nanotubes from layered materials. The reduction process is strongly exothermic and is responsible for the ultimate formation of nanotubular M–B alloys. However, one question remains unanswered, namely why different Tween surfactants have to be used for different M–B nanotubes (Tween 40 gives Fe–B and Tween 60 gives Co–B and Ni–B, while Tween 80 is not effective at all). This observation suggests that the interactions between the transition-metal ions and surfactants are rather complicated and probably vary with the nature of the metal ion.

Noncrystalline metal–boron alloys have been used as hydrogenation catalysts for a long time and their use in magnetically stabilized bed reactors for hydrogenation reactions has made great progress recently.[27] To elucidate the shape-specific effects of nanotubes, the ability of our noncrystalline nanotubes to catalyze the hydrogenation of *m*-nitrotoluene was investigated (see Table 1; the catalytic properties of noncrystalline M–B nanoparticles are also included for comparison). When Fe–B nanotubes were employed as the catalyst the yield of *m*-toluidine in the first reaction cycle was 79.2%, compared with 10.7% for conventional Fe–B nanoparticles under the same reaction conditions. The catalytic activity of the noncrystalline Fe–B nanotubes is evidently much higher than that of Fe–B nanoparticles. The higher catalytic activity of the nanotubes can be partially ascribed to their larger surface area, although this cannot entirely account for the better catalytic performance of the nanotubes. The structure of the nanotube must also have some effect. The negative curvature of the nanotube's inner surface may enhance the coordination of reaction molecules by the multiple active centers. Gubbins et al. have simulated the chemical reaction of N_2 and three equivalents of H_2 under confining conditions, especially in nanotubes, and have found that the fluid molecules in the nanotubes experience a strong interaction with the walls.[28,29] In the current hydrogenation reaction the noncrystalline alloy catalysts strongly adsorb hydrogen, and *m*-nitrotoluene, which is capable of wetting and selectively adsorbing onto the solid surfaces, should experience a large attractive potential energy because of the combined interactions in the tubes. These effects must affect the reaction equilibrium and result in an increase in the yield of *m*-toluidine through Le Chatelier's principle as a result of the decrease in the total number of molecules in the reaction system.[30]

Noncrystalline Co–B and Ni–B nanotubes provide an interesting comparison with the Fe–B nanotubes since the primary factors determining their activity are somewhat different. Conventional noncrystalline Co–B and Ni–B nanoparticles display high resistivity to poisoning as well as good activity and selectivity for certain hydrogenation reactions. Consequently, the increased surface area and nanotube effects cause an increase of *m*-toluidine yields for these two nanotube samples, although this increase is not as remarkable as for the Fe–B nanotubes. As seen from Table 1, the catalytic activities of Co–B and Ni–B nanotubes are similar to that of Pd/C (Pd content of 3% and a surface area of 1100 $m^2 g^{-1}$.). Figure 4 shows the TEM image and the corresponding SAED and EDS results for the Fe–B nanotubes after two catalytic cycles. (The yield of *m*-toluidine in the second cycle is 75.3%.) The structure of the nanotubes appears to have changed very little after two catalytic cycles. The nanotubular morphologies are still observed and their structures are still noncrystalline, as determined by SAED. These results are inspiring and further work in this area is in progress.

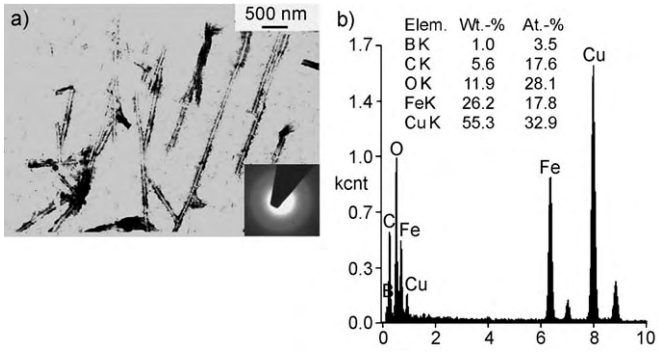

Figure 4. TEM image (a) and EDS spectrum (b) of Fe–B nanotubes after two catalytic cycles. The inset of (a) is the corresponding SAED pattern.

In summary, metal–boron nanotubes with a uniform size have been fabricated by using lyotropic non-ionic–anionic mixed-surfactant liquid crystals as templates. This method provides a route for the synthesis of metal–boron nanotubes and can also be extended to other tubular materials or noncrystalline alloys. The results of catalytic studies show that these metal–boron nanotubes exhibit superior catalytic activities to the corresponding metal–boron nanoparticles. They are therefore promising for future applications in catalysis and might become a new class of industrial material.

Experimental Section

In a typical synthesis, $FeCl_3 \cdot 6H_2O$ (0.01 mol, 2.7 g) was dissolved in H_2O (18 mL) containing (1*S*)-(+)-10-camphorsulfonic acid (0.01 mol, 2.3 g) and Tween 40 (0.01 mol, 12.8 g) at 333 K. The mixture was then cooled to 293 K and allowed to stand at that temperature for 1 h. A mixture of 4 M $NaBH_4$ and 0.1 M NaOH was added to the above homogeneous mixture and kept for 48 h under an inert gas atmosphere (N_2). The resulting solid was collected, washed with distilled water and ethanol, and dried in flowing nitrogen. The noncrystalline Co–B and Ni–B nanotubes were prepared from $CoCl_2 \cdot 6H_2O$ or $NiCl_2 \cdot 6H_2O$ and Tween 60 in place of $FeCl_3 \cdot 6H_2O$ and Tween 40 under otherwise identical experimental conditions.

Hydrogenation of *m*-nitrotoluene was used to measure the catalytic performance. Thus, a 250-mL autoclave loaded with methanol (200 mL), *m*-nitrotoluene (10 g, 0.07 mol), and catalyst (0.5 g, 0.008 mol) was filled with hydrogen (2 MPa; 3.5 MPa was used for Fe–B) after purging to remove air, stirred vigorously, and heated to 393 K. After 2 h the products were analyzed by gas chromatography.

Powder XRD measurements were performed with a Philips X'Pert MPD Pro X-ray diffractometer with graphite-monochromated high-intensity $Cu_{K\alpha}$ radiation at 50 kV. TEM and EDS images were recorded with a JEM-100S Electron Microscope (JEOL) at an accelerating voltage of 80 kV. HRTEM was performed with a JEOL JEM-2010 instrument at an acceleration voltage of 200 kV. An aliquot of the sample suspended in ethanol was dropped on a polymer-coated copper grid for TEM observation. ICP spectroscopy was performed

 © 2006 Wiley-VCH Verlag GmbH & Co. KGaA, Weinheim

with a J-A1100 spectrometer (Jarrell–Ash). The nitrogen sorption isotherms were measured at liquid-nitrogen temperature on an ASAP 2020 apparatus.

Received: June 30, 2006
Revised: August 7, 2006
Published online: October 9, 2006

Keywords: alloys · heterogeneous catalysis · liquid crystals · nanotubes · surfactants

[1] C. A. Mirkin, R. L. Letsinger, R. C. Mucic, J. J. Storhoff, *Nature* **1996**, *382*, 607.
[2] R. M. Penner, M. J. Heben, T. L. Longin, N. S. Lewis, *Science* **1990**, *250*, 1118.
[3] X. G. Peng, L. Manna, W. D. Yang, J. Wickham, E. Scher, A. Kadavanich, A. P. Alivisatos, *Nature* **2000**, *404*, 59.
[4] J. D. Holmes, K. P. Johnston, R. C. Doty, B. A. Korgel, *Science* **2000**, *287*, 1471.
[5] X. Wang, Y. Li, *J. Am. Chem. Soc.* **2002**, *124*, 2880.
[6] S. Iijima, *Nature* **1991**, *354*, 56.
[7] N. G. Chopra, R. J. Ruyken, K. Cherry, V. H. Crespi, M. L. Cohen, S. G. Louie, A. Zettl, *Science* **1995**, *269*, 966.
[8] R. Ma, Y. Bando, D. Golberg, T. Sato, *Angew. Chem.* **2003**, *115*, 1880; *Angew. Chem. Int. Ed.* **2003**, *42*, 1836.
[9] D. Ciuparu, R. F. Klie, Y. Zhu, L. Pfefferle, *J. Phys. Chem. B* **2004**, *108*, 3967.
[10] A. Quandt, A. Y. Liu, I. Boustani, *Phys. Rev. B* **2001**, *64*, 125422.
[11] A. Quandt, I. Boustani, *ChemPhysChem.* **2005**, *6*, 2001.
[12] W. Tremel, *Angew. Chem.* **1999**, *111*, 2311; *Angew. Chem. Int. Ed.* **1999**, *38*, 2175.
[13] G. R. Patzke, F. Krumeich, R. Nesper, *Angew. Chem.* **2002**, *114*, 2554; *Angew. Chem. Int. Ed.* **2002**, *41*, 2446.
[14] R. Tenne, *Angew. Chem.* **2003**, *115*, 5280; *Angew. Chem. Int. Ed.* **2003**, *42*, 5124.
[15] M. Remskar, *Adv. Mater.* **2004**, *16*, 1497.
[16] R. Tenne, C. N. R. Rao, *Philos. Trans. R. Soc. London Ser. A* **2004**, *362*, 2099.
[17] C. R. Martin, *Science* **1994**, *266*, 1961.
[18] M. E. Spahr, P. Bitterli, R. Nesper, M. Muller, F. Krumeich, H. U. Nissen, *Angew. Chem.* **1998**, *110*, 1339; *Angew. Chem. Int. Ed.* **1998**, *37*, 1263.
[19] H. P. Lin, C. Y. Mou, S. B. Liu, *Adv. Mater.* **2000**, *12*, 103.
[20] Y. D. Li, X. L. Li, R. R. He, J. Zhu, Z. X. Deng, *J. Am. Chem. Soc.* **2002**, *124*, 1411.
[21] T. Kijima, T. Yoshimura, M. Uota, T. Ikeda, D. Fujikawa, S. Mouri, S. Uoyama, *Angew. Chem.* **2004**, *116*, 230; *Angew. Chem. Int. Ed.* **2004**, *43*, 228.
[22] W. L. Johnson, *Prog. Mater. Sci.* **1986**, *30*, 81.
[23] A. Molnar, G. V. Smith, M. Bartoâk, *Adv. Catal.* **1989**, *36*, 329.
[24] Y. Chen, *Catal. Today* **1998**, *44*, 3.
[25] S. Mûrup, S. A. Sethi, S. Linderoth, C. B. Koch, M. D. Bentzon, *J. Mater. Sci.* **1992**, *27*, 3010.
[26] J. Y. Shen, Z. Hu, L. F. Zhang, Z. Y. Li, Y. Chen, *Appl. Phys. Lett.* **1991**, *59*, 3545.
[27] X. K. Meng, X. H. Mu, B. N. Zong, E. Z. Min, Z. H. Zhu, S. B. Fu, Y. B. Luo, *Catal. Today* **2003**, *79*, 21.
[28] C. H. Turner, J. K. Johnson, K. E. Gubbins, *J. Chem. Phys.* **2001**, *114*, 1851.
[29] O. Byl, P. Kondratyuk, J. T. Yates, *J. Phys. Chem. B* **2003**, *107*, 4277.
[30] M. S. Bartkowiak, G. Dudziak, R. Sikorski, R. Gras, R. Rodhakrishnan, K. E. Gubbins, *J. Chem. Phys.* **2001**, *114*, 950.

 © 2006 Wiley-VCH Verlag GmbH & Co. KGaA, Weinheim

Mixed-Valence Compounds

DOI: 10.1002/anie.200602987

Halogen-Bridged Pt^{II}/Pt^{IV} Mixed-Valence Ladder Compounds**

Daisuke Kawakami, Masahiro Yamashita, Satoshi Matsunaga, Shinya Takaishi, Takashi Kajiwara, Hitoshi Miyasaka, Ken-ichi Sugiura, Hiroyuki Matsuzaki, Hiroshi Okamoto, Yusuke Wakabayashi, and Hiroshi Sawa*

Low-dimensional electronic systems have been attracting much attention for a long time in solid-state chemistry and physics. Among them, one-dimensional (1D) electronic systems have been an attractive target because many characteristic physical properties have been observed in them, such as Mott–Hubbard, charge-density-wave (CDW), and spin-density-wave (SDW) states in organic (semi)conductors,[1,2] as well as nonlinear excitations such as solitons and polarons in π-conjugated polymers [3,4] and slow relaxation of magnetization in several Ising-type ferro- or ferrimagnetic compounds.[5–7] Two-dimensional (2D) electronic systems have also been of interest for the past several decades. Many materials with Perovskite structures have been the target of research. To date, many attractive physical properties have been reported, such as colossal magnetoresistance (CMR) in manganese oxides[8,9] and high-temperature superconductivity in copper oxides, among others.[10,11]

[*] D. Kawakami, Prof. M. Yamashita, Dr. S. Takaishi, Dr. T. Kajiwara, Prof. H. Miyasaka
Department of Chemistry
Graduate School of Science
Tohoku University
and
Core Research for Evolutional Science and Technology (CREST)
6-3 Aza-Aoba, Aramaki, Aoba-ku, Sendai 980-8578 (Japan)
Fax: (+81) 22-795-6548
E-mail: yamasita@agnus.chem.tohoku.ac.jp

S. Matsunaga, Prof. K. Sugiura
Department of Chemistry
Graduate School of Science
Tokyo Metropolitan University
1-1 Minamiosawa, Hachioji, Tokyo 192-0397 (Japan)

Dr. H. Matsuzaki, Prof. H. Okamoto
Department of Advanced Material Science
Graduate School of Frontier Science
The University of Tokyo
5-1-5 Kashiwanoha, Kashiwa, Chiba 277-8561 (Japan)

Dr. Y. Wakabayashi, Prof. H. Sawa
Institute of Materials Structure Science
High-Energy Accelerator Research Organization
1-1 Oho, Tsukuba 305-0801 (Japan)

[**] This work was partly supported by a Grant-in Aid for Creative Scientific Research from the Ministry of Education, Culture, Sports, Science and Technology.

Supporting information for this article is available on the WWW under http://www.angewandte.org or from the author.

WILEY InterScience DISCOVER SOMETHING GREAT
© 2006 Wiley-VCH Verlag GmbH & Co. KGaA, Weinheim

In ladder systems, which can be classified as the boundary region between 1D and 2D systems, on the other hand, only a few studies have been made although further interesting physical properties are expected. Our purpose in this study is to establish a synthetic strategy for ladder compounds.

Our target compounds are the halogen-bridged 1D metal compounds (MX chains). These compounds have been attractive materials because of their highly isolated 1D electronic structures, which are formed by d_{z^2} orbitals of the metal centers and p_z orbitals of the bridging halides. In these compounds, various electronic states can be realized by substituting components such as central metals (M), in-plane ligands (L), bridging halides (X), and counteranions (Y). The MX-chain compounds with a mixed-valence structure -X···M^{2+}···X-M^{4+}- (M = Pd, Pt; X = Cl, Br, I) have been extensively studied as 1D materials with strong electron–phonon interactions (S). Their Peierls-distorted 1D compounds show unique optical and dynamical properties such as progressive overtones in resonance Raman spectra[12] and luminescence with a large Stokes shift,[13] as well as the long-range migration of spin solitons and polarons along 1D chains.[14]

If a single-chain system can be expanded to a ladder-chain system, it is expected that the system can take two valence arrangements, namely in-phase and out-of-phase types (Figure 1). Such a variety in the valence arrangements is

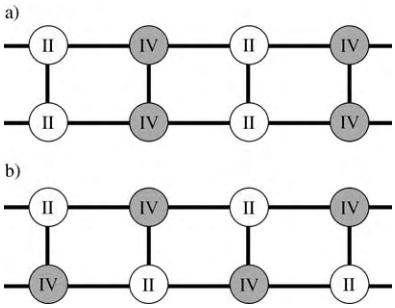

Figure 1. In-phase (a) and out-of-phase (b) valence arrangements in the mixed-valence ladder system.

interesting in the fields of chemistry and physics. Moreover, novel interactions are expected through connection of the 1D chains. Although more than 300 halogen-bridged MX-chain compounds have been synthesized so far, all compounds have single-chain structures. We have succeeded in synthesizing ladder-type, halogen-bridged platinum complexes for the first time in which 1D chains are connected by the 2,2′-bipyrimidine (bpym) ligand: {(μ-bpym)[Pt^{II}(en)]$_2$}{(μ-bpym)-[$Pt^{IV}X_2$(en)]$_2$}$X_2(ClO_4)_6\cdot 2H_2O$ (X = Br (**1**), Cl (**2**); en = ethylenediamine) and {(μ-bpym)[Pt^{II}(en)]$_2$}{(μ-bpym)-[$Pt^{IV}X_2$(en)]$_2$}$X_8\cdot 4H_2O$ (X = I (**3**), Br (**4**)). Herein, we report the syntheses, crystal structures, and optical properties of these complexes.

Figure 2 shows two perspective views of the crystal structure of bromide-bridged platinum compound **1**. The {Pt(en)} moiety is connected by a bpym ligand, thus forming a binuclear {(μ-bpym)[Pt(en)]$_2$} unit. This unit is bridged by bromide ions to form a ladder structure. Each ladder is

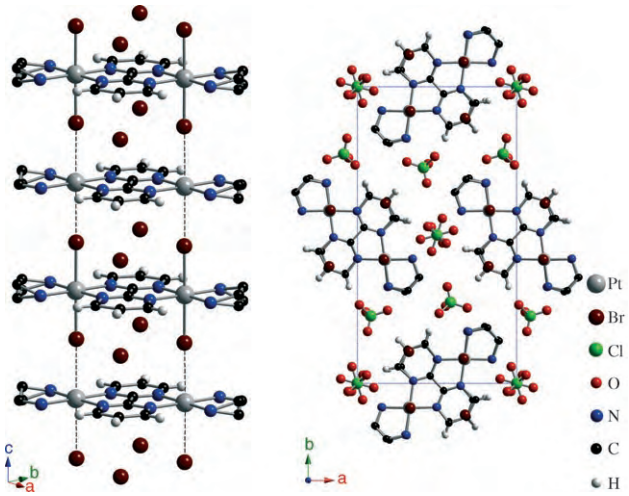

Figure 2. Perspective views of the 3D packing of **1**. H atoms of the en ligands have been omitted for clarity.

weakly connected through the hydrogen bond between the amino protons of the en ligands and perchlorate ions of the counteranions. The shortest Pt–Pt separations along the leg and rung directions within the ladder are 5.534 and 5.466 Å, respectively, whereas that between the ladders is 8.561 Å, thus indicating that each ladder is isolated from one other. The bridging bromide ions lie closer to the Pt^{IV} centers, thus indicating the Pt^{II}/Pt^{IV} mixed valence or CDW state of this compound. Therefore, this compound belongs to the class II compounds of the Robin–Day classification.[15] This compound has an in-phase valence arrangement as shown in Figure 1 a. Generally, in the 2D mixed-valence compounds, the out-of-phase valence arrangements are stabilized rather than the in-phase valence arrangements owing to Coulomb interactions. This trend is inconsistent with our result. In compound **1**, nonbonded bromide anions are located at the sandwich position between two bpym ligands with half occupancies. Usually, a negative charge stabilizes the high oxidation state. The bromide anions lie closer to the Pt^{IV} centers; therefore, these bromide anions can stabilize the in-phase valence arrangement.

Figure 3 shows two perspective views of the crystal structure of iodide-bridged platinum compound **3**. The fundamental intraladder structure is almost the same as that of **1**. The shortest Pt–Pt separations along the leg and rung directions within the ladder are 5.833 and 5.468 Å, respectively, whereas that between the ladders is 7.933 Å. Compared with the crystal structure of compound **1**, two significant differences are found, depending on the counteranions: 1) two water molecules are located at the sandwich position between two bpym ligands (no halide anions) and 2) the bridging halide ions are disordered. The valence arrangement of this compound has not been clarified as yet because of the disorder of the bridging halide ions. However, because nonbonded halide anions that were found in compound **1** are absent in compound **3**, this compound might have out-of-phase valence arrangement (Figure 1 b).

Figure 4 shows an X-ray oscillation photograph of **1** and **3**. In the case of compound **1**, very weak superlattice reflections

 © 2006 Wiley-VCH Verlag GmbH & Co. KGaA, Weinheim

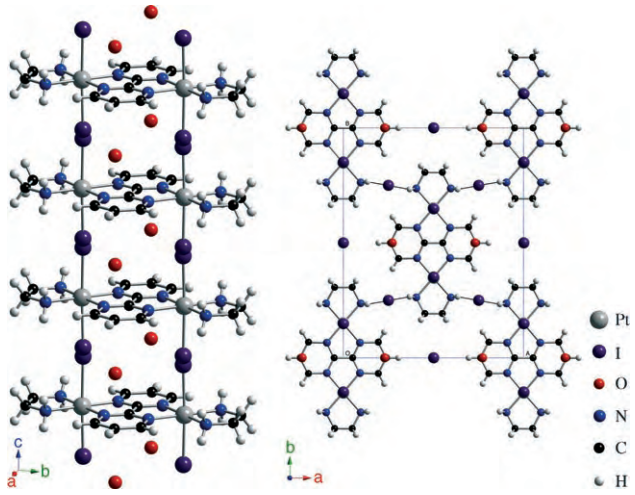

Figure 3. Perspective views of the 3D packing of **3**.

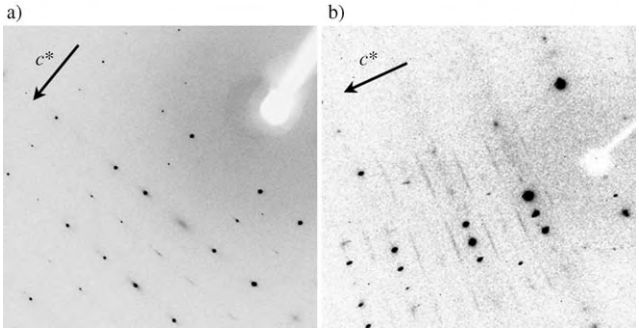

Figure 4. X-ray oscillation photograph in **1** (a) and **3** (b).

at $h,k,l+^1/_2$ were observed which correspond to the two-fold periodicity along the c^* direction (leg direction). The line width of these superlattice reflections is as sharp as those of the main reflections, thus indicating that this compound has a long-range ordered charge arrangement. On the other hand, in the case of compound **3**, diffuse scatterings with finite line width at $h,k,l+^1/_2$ were observed. This finding suggests that compound **3** has some short-range ordered charge arrangement. We have succeeded in controlling the charge arrangement of ladder compounds by variation of the counteranions.

The selected interatomic separations and the distortion parameter (d) of the described compounds, defined as $\{r(Pt^{II}\cdots X)-r(Pt^{IV}\text{-}X)\}/\{r(Pt^{II}\cdots Pt^{IV})\}$, are listed in Table 1. Here, the d parameter shows the degree of displacement of the bridging halide ions from the midpoints between the two neighboring Pt ions. In other words, this value is an index to estimate the electron–phonon interaction and the band gap. In the described ladder compounds, the d parameters are dependent on the bridging halide ions and increase in the order I, Br, Cl. This result suggests that the band gap was controlled by changing bridging halide ions.

Table 1: Comparison of the interatomic separations [Å] and the distortion parameter (d) for **1**–**4**.

Compound	$Pt^{II}\cdots Pt^{IV}$	$Pt^{II}\cdots X$	Pt^{IV}–X	d[a]
1	5.534	3.057	2.478	0.105
2	5.435	3.119	2.317	0.148
3	5.833	3.156	2.678	0.082
4	5.482	3.008	2.474	0.097

[a] Defined as $\{r(Pt^{II}\cdots X)-r(Pt^{IV}\text{–}X)\}/\{r(Pt^{II}\cdots Pt^{IV})\}$.

To acquire information about the band gap, optical conductivity spectra (Figure 5) were obtained from Kramers–Kronig transformation of the single-crystal reflectance

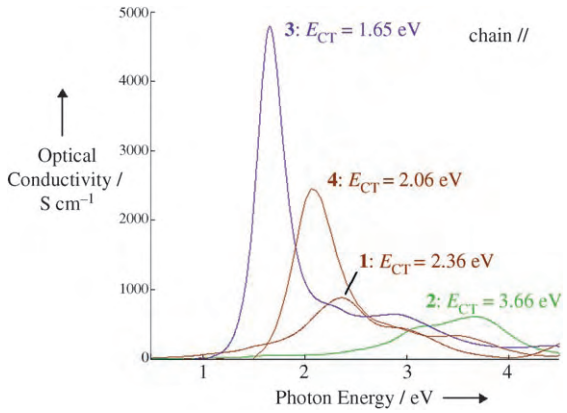

Figure 5. Optical conductivity spectra with polarization of light parallel to the chain axis compounds **1**–**4** at room temperature.

spectra. Broad bands were observed at about 2.4, 3.7, 1.7, and 2.1 eV with shoulders (ca. 3.0 eV) in **1, 2, 3**, and **4**, respectively. By considering the trends of a series of the single-chain MX compounds,[16] these broad bands are attributable to the charge-transfer (CT) transition from Pt^{II} to Pt^{IV} species. The E_{CT} value outstandingly depends on the bridging halide ion and increases in the order I, Br, Cl. This tendency is similar to single-chain MX compounds, thus indicating that the band gap can be controlled by changing bridging halide ions. This finding is consistent with the argument of the d parameter. However, shoulders of the CT bands have not been observed in the single-chain MX chains. Although the origin of such behavior has not been clarified at the present stage, investigations on the assignment of such transitions are now in progress.

In the resonance Raman spectra (Figure 6), intense peaks attributable to the X-Pt^{IV}-X stretching modes are observed, where the stretching modes of **1**, **2**, **3**, and **4** are at $\tilde{\nu}=191.7$, 325.7, 124.3, and 174.4 cm^{-1}, respectively. The Raman shifts clearly depend on the bridging halide ions, which is in good agreement with the X-ray and optical conductivity results.

In summary, we have succeeded in synthesizing halogen-bridged Pt^{II}/Pt^{IV} mixed-valence ladder compounds for the first time. In these compounds, the band gap is controlled by changing bridging halide ions. Moreover, by changing counteranions, the charge arrangements of ladder compounds can be controlled. Therefore, ladder-type MX compounds have strong advantages for studying the boundary region between 1D and 2D electronic systems. Our results will greatly contribute to the realization of attractive physical properties in the ladder system.

 © 2006 Wiley-VCH Verlag GmbH & Co. KGaA, Weinheim

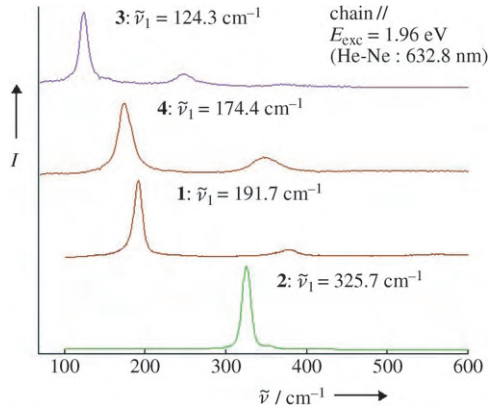

Figure 6. Polarized Raman spectra for the polarization of $z(x,x)z(x||c$ axis) at room temperature.

Experimental Section

1: $HClO_4$ (3 mL) was added to an aqueous solution (10 mL) containing {(μ-bpym)[Pt^{II}(en)]$_2$}$(NO_3)_4$ (50 mg, 0.055 mmol) and {(μ-bpym)[$Pt^{IV}Br_2$(en)]$_2$}$(NO_3)_4$ (67 mg, 0.054 mmol). Needle-shaped crystals were obtained after a week. Elemental analysis (%) calcd for $C_{12}H_{22}N_8Br_3Cl_3O_{12}Pt_2{\cdot}H_2O$: C 11.77, H 1.98, N 9.15, Br 19.57, Cl 8.69; found: C 11.77, H 2.04, N 8.94, Br 19.47, Cl 8.49.

3: I_2 vapor was allowed to slowly diffuse into a H_2O/MeOH solution containing {(μ-bpym)[Pt^{II}(en)]$_2$}$(NO_3)_4$ (50 mg, 0.055 mmol) and excess KI. Needle-shaped crystals were obtained after a week. Elemental analysis (%) calcd for $C_{12}H_{22}N_8I_6Pt_2{\cdot}2H_2O$: C 9.83, H 1.79, N 7.64; found: C 9.66, H 2.14, N 7.41.

The syntheses of **2** and **4** are provided in the Supportiong Information.

X-ray crystal structure determinations were made by using a Bruker SMART 1000 (**1**, **2**) and a Rigaku Saturn CCD diffractometer (**3**, **4**) with graphite-monochromated $Mo_{K\alpha}$ radiation ($\lambda = 0.7107$ Å). Crystal data of these compounds are provided in the Supporting Information. CCDC-611172, 604141, 610578, and 610579 contain the supplementary crystallographic data for this paper. These data can be obtained free of charge from The Cambridge Crystallographic Data Centre via www.ccdc.cam.ac.uk/data_request/cif.

Received: July 25, 2006
Published online: October 9, 2006

Keywords: charge transfer · coordination modes · ladder polymers · mixed-valent compounds · valence structures

[1] A. Andrieux, D. Jerome, K. Bechgaard, *J. Phys. Lett.* **1981**, *42*, 87 – 90.
[2] L. Forro, S. Bouffard, J. P. Pouget, *J. Phys. Lett.* **1984**, *45*, 453 – 459.
[3] I. B. Goldberg, H. R. Crowe, P. R. Newman, A. J. Heeger, A. G. MacDiarmid, *J. Chem. Phys.* **1979**, *70*, 1132 – 1136.
[4] W. P. Su, J. R. Schrieffer, A. J. Heeger, *Phys. Rev. B* **1980**, *22*, 2099 – 2111.
[5] A. Caneschi, D. Gatteschi, N. Lalioti, C. Sangregorio, R. Sessoli, G. Venturi, A. Vindigni, A. Rettori, M. G. Pini, M. A. Novak, *Angew. Chem.* **2001**, *113*, 1810 – 1813; *Angew. Chem. Int. Ed.* **2001**, *40*, 1760 – 1763.
[6] R. Clérac, H. Miyasaka, M. Yamashita, C. Coulon, *J. Am. Chem. Soc.* **2002**, *124*, 12837 – 12844.
[7] R. Lescouezec, J. Vaissermann, C. Ruiz-Perez, F. Lloret, R. Carrasco, M. Julve, M. Verdaguer, Y. Dromzee, D. Gatteschi, W. Wernsdorfer, *Angew. Chem.* **2003**, *115*, 1521 – 1524; *Angew. Chem. Int. Ed.* **2003**, *42*, 1483 – 1486.
[8] R. von Helmholt, J. Wecker, B. Holzapfel, L. Schultz, K. Samwer, *Phys. Rev. Lett.* **1993**, *71*, 2331 – 2333.
[9] S. Jin, T. H. Tiefel, *Science* **1994**, *264*, 413 – 415.
[10] J. G. Bednorz, K. A. Muller, *Z. Phys. B* **1986**, *64*, 189 – 194.
[11] Y. Tokura, H. Takagi, S. Uchida, *Nature* **1989**, *337*, 345 – 347.
[12] R. J. H. Clark, M. L. Franks, W. R. Trumble, *Chem. Phys. Lett.* **1976**, *41*, 287 – 292.
[13] H. Tanino, K. Kobayashi, *J. Phys. Soc. Jpn.* **1983**, *52*, 1446 – 1456.
[14] N. Kimura, S. Ishimaru, R. Ikeda, M. Yamashita, *J. Chem. Soc. Faraday Trans.* **1998**, *94*, 3659—3663.
[15] M. B. Robin, P. Day, *Adv. Inorg. Chem. Radiochem.* **1967**, *9*, 247 – 422.
[16] H. Okamoto, M. Yamashita, *Bull. Chem. Soc. Jpn.* **1998**, *71*, 2023 – 2039.

 © 2006 Wiley-VCH Verlag GmbH & Co. KGaA, Weinheim

Organic Reactions in Water

DOI: 10.1002/anie.200603070

A Heterogeneous Silica-Supported Scandium/Ionic Liquid Catalyst System for Organic Reactions in Water**

*Yanlong Gu, Chikako Ogawa, Juta Kobayashi, Yuichiro Mori, and Shū Kobayashi**

Organic reactions in water are of current interest in organic synthesis.[1] In addition to environmental and economical advantages, unique reactivity and selectivity that are not achieved in organic solvents are often observed in water, and several interesting and useful reactions have been exploited with water as the solvent. Lewis acids are frequently used to accelerate organic transformations,[2] but the moisture sensitivity of the majority of Lewis acids render them unsuitable for use in aqueous solvent systems. To address this stability issue, water-compatible Lewis acids have been developed,[3] and several Lewis acid catalyzed reactions, including asymmetric reactions, have been studied in aqueous media.[4] However, many of these reactions proceed sluggishly in pure water, presumably because most organic materials are not soluble in the medium. We solved this problem by generating hydrophobic reaction environments in water by

[*] Y. Gu, C. Ogawa, J. Kobayashi, Y. Mori, Prof. S. Kobayashi
Graduate School of Pharmaceutical Sciences
The University of Tokyo
The HFRE Division, ERATO, Japan Science and Technology Agency (JST)
Hongo, Bunkyo-ku, Tokyo 113-0033 (Japan)
Fax: (+81) 3-5684-0634
E-mail: skobayas@mol.f.u-tokyo.ac.jp

[**] This work was partially supported by a Grant-in-Aid for Scientific Research from the Japan Society of the Promotion of Science (JSPS).

Supporting information (experimental details and spectral data of products) for this article is available on the WWW under http://www.angewandte.org or from the author.

© 2006 Wiley-VCH Verlag GmbH & Co. KGaA, Weinheim
InterScience

utilizing Lewis acid–surfactant combined catalysts (LASCs)[5] or styrene-based hydrophobic polymer-supported catalysts.[6] In these cases, however, substrate scope, catalysts loadings, and recovery and reuse of catalysts are not yet satisfactory. In the course of our investigations into the development of more efficient catalysts in water, we reasoned that hydrophobic ionic liquids (ILs) might interact with silica-supported metal catalysts to create hydrophobic reaction environments in water.[7] Herein we describe a silica gel supported scandium system with an ionic liquid, a novel heterogeneous catalyst that works very efficiently in several carbon–carbon bond-forming reactions in water.[8] An asymmetric version of this system involving a chiral scandium catalyst is also reported.

The silica gel supported scandium catalysts were prepared according to a modified literature method (Scheme 1, Figure 1a).[9] The scandium catalysts thus prepared were added to a solution of ionic liquid in ethyl acetate, and the solvent

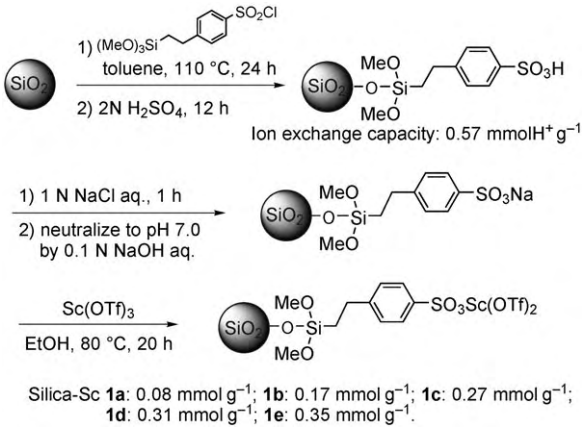

Scheme 1. Preparation of silica gel supported Sc.

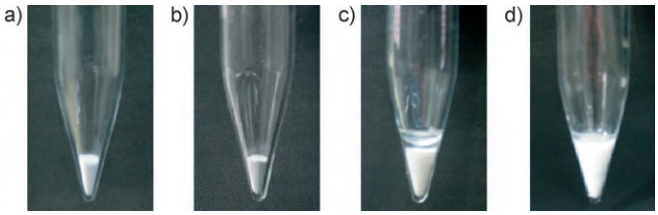

Figure 1. View of catalyst and reaction systems. a) Silica-Sc; b) silica-Sc-IL; c) silica-Sc-IL, water, and substrates before mixing; d) mixture from (c) during the reaction (after mixing).

was removed under reduced pressure to afford powdery and free-flowing solid silica-Sc-IL (Figure 1b). Interestingly, silica-Sc and silica-Sc-IL could not be differentiated by sight. When substrates and water were added to silica-Sc-IL, the phases did not mix (Figure 1c), but formed a colloidal suspension upon stirring (Figure 1d).

Silica-Sc-IL (**1**) was first tested in Mukaiyama aldol reactions. Several reaction conditions were examined in the model reaction of benzaldehyde with 1-ethylthio-1-trimethylsiloxy-2-methyl-1-propene (**2a**) (Table 1). To our great delight, the reaction took place smoothly in water, and the best yields were obtained with 0.27 mmol g^{-1} loading of

Table 1: Mukaiyama reaction conditions with silica-Sc-IL.

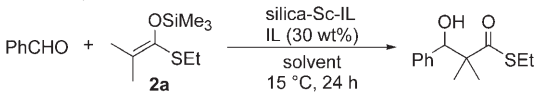

Entry	Catalyst	Sc [mol%]	Solvent	IL[e]	Yield [%]
1	**1a**	1.6	H_2O	[DBIm]SbF_6	50
2	**1b**	3.4	H_2O	[DBIm]SbF_6	81
3	**1c**	5.4	H_2O	[DBIm]SbF_6	97
4	**1d**	6.2	H_2O	[DBIm]SbF_6	73
5[a]	–	0	H_2O	[DBIm]SbF_6	0
6	**1c**	5.4	hexane	[DBIm]SbF_6	26
7	**1c**	5.4	Et_2O	[DBIm]SbF_6	22
8[b]	**1c**	5.4	–	[DBIm]SbF_6	25
9[c]	**1c**	5.4	H_2O	–	31
10	**1c**	5.4	H_2O	[DBIm]NTf_2	64
11	**1c**	5.4	H_2O	[DBIm]PF_6	76
12	**1c**	5.4	H_2O	[BMIm]SbF_6	54
13[d]	**1c**	5.4	H_2O	[DBIm]SbF_6	69

[a] Without catalyst; [b] without solvent; [c] without IL; [d] 15 wt% of IL was used; [e] [DBIm] = 1-butyl-3-decylimidazolium; [BMIm] = 1-butyl-3-methylimidazolium.

scandium (**1c**; Table 1, entry 3). The reaction proceeded sluggishly in hexane, ether, and also under solvent-free conditions (Table 1, entries 6–8). These results clearly show that the reaction progressed much faster in water than in organic solvents or in the absence of solvent, and that the use of water as a solvent is essential for the silica-Sc-IL-catalyzed aldol reaction. Although the reaction also proceeded sluggishly without ionic liquid (Table 1, entry 9), moderate to good yields were obtained by using other ionic liquids (Table 1, entries 10–12). When half the amount of ionic liquid was used, the reaction was accelerated relative to the background level; however, the reaction was not complete within 24 h (Table 1, entry 13). These experiments clearly showed that silica-Sc-IL and ionic liquid formed a hydrophobic reaction environment in water. It should be noted that water-labile reagents such as **2a** can be used effectively in water under the conditions, and that, to the best of our knowledge, this is the first demonstration of the combination of silica gel supported metal catalysts with ionic liquids to create an efficient hydrophobic environment for organic reactions in water.[10]

A range of other substrates were surveyed for Mukaiyama aldol reactions with silica-Sc-IL **1c** (Table 2). In all cases, aldehydes reacted smoothly with silicon enolates in water to afford the desired aldol adducts in high yields. The scandium catalyst was reused at least three times with only a slight decrease in yields (Table 2, entry 1). In a typical experimental procedure,[11] hexane was added to extract the product after the reaction was completed. We carefully checked both the water and organic phases for evidence of metal leaching. Inductively coupled plasma (ICP) analysis revealed that 0.1% of the Sc (relative to the total Sc content) had leached into the water phase, whereas no leaching into the organic phase was detected.

We then tested Michael reactions of indole derivatives with enones (Table 3). The reactions also proceeded smoothly in water to afford the desired Michael adducts in high yields. Turnover numbers as high as 4560 were obtained (Table 3,

 © 2006 Wiley-VCH Verlag GmbH & Co. KGaA, Weinheim

Table 2: Mukaiyama aldol reactions in water.

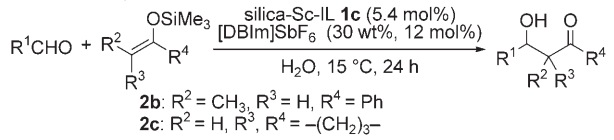

2b: $R^2 = CH_3$, $R^3 = H$, $R^4 = Ph$
2c: $R^2 = H$, R^3, $R^4 = -(CH_2)_3-$

Entry	R^1	Enolate	Yield [%]
1	Ph	**2a**	97 (95[a], 90[b])
2	4-$MeOC_6H_4$	**2a**	81
3	4-ClC_6H_4	**2a**	90
4	(*E*)-PhCH=CH_2	**2a**	87
5	$PhCH_2CH_2$	**2a**	64
6[c]	Ph	**2b**	71[d]
7	Ph	**2c**	84[e]

[a] Reused in the second run; [b] reused in the third run; [c] 50 wt% of IL and **2a** (0.75 mmol) were used at 20°C; [d] *syn*/*anti* = 49:51; [e] *syn*/*anti* = 60:40.

Table 3: Silica-Sc-IL-catalyzed Michael reactions of indoles.[a]

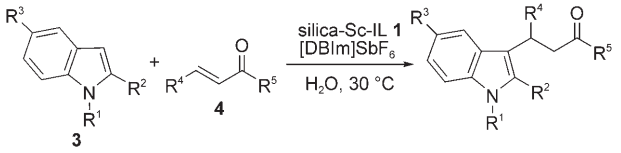

Entry	Sc [mol%]	**3**[b]	**4**[c]	*t* [h]	Yield [%]
1	**1a** (1.6)	**3a**	**4a**	4	96
2	**1f**[d] (0.02)	**3a**	**4a**	12	93
3	**1a** (1.6)	**3b**	**4a**	4	92
4	**1a** (1.6)	**3c**	**4a**	4	88
5	**1a** (1.6)	**3d**	**4a**	4	87
6	**1a** (1.6)	**3e**	**4a**	4	74
7	**1a** (1.6)	**3a**	**4b**	4	89
8	**1a** (1.6)	**3a**	**4c**	4	88
9	**1e** (7.0)	**3a**	**4d**	20	70

[a] 50 wt%, 20 mol%; [b] **3a**: indole; **3b**: 5-bromoindole; **3c**: 5-methoxyindole; **3d**: 1-methylindole; **3e**: 2-methylindole; [c] **4a**: methyl vinyl ketone; **4b**: ethyl vinyl ketone; **4c**: pheny propenyl ketone; **4d**: cyclopenten-2-one; [d] **1f**: silica-Sc$(OSO_2C_8F_{17})_2$ (0.001 mmol g^{-1}).

entry 2). Other substrates were treated under standard conditions, and in all cases the desired Michael adducts were obtained in high yields.

We further investigated the applicability of the catalyst system to other reactions in water. We selected a three-component Mannich reaction of aldehydes, amines, and silicon enolates, and an allylation reaction of a ketone with tetraallyl tin (Scheme 2).[12] In all cases, the reactions proceeded smoothly in water to afford the desired products in high yields. It is noted that silica-Sc-IL can be widely used as a Lewis acid catalyst in several important carbon–carbon bond-forming reactions in water.

Finally, a catalytic asymmetric version of this system was tested with silica-Sc-IL and a chiral ligand (Scheme 3). In the presence of silica-Sc-IL and chiral bipyridine **5**,[13] the silicon enolate derived from propiophenone was treated with an aqueous solution of formaldehyde in water.[14] Remarkably, the reaction proceeded at 35°C to afford the desired hydroxymethylated ketone in 47% yield and 49% *ee*.[15] Although the yield and the enantioselectivity were moderate,

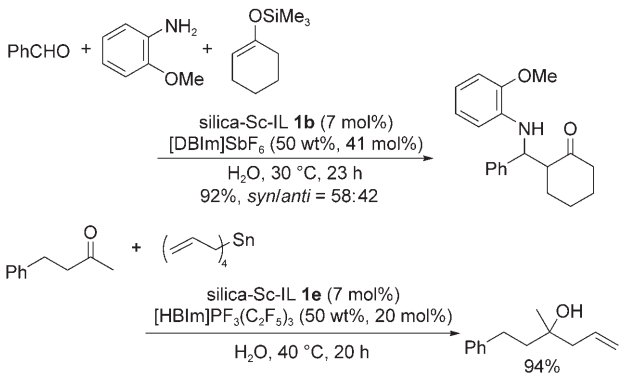

Scheme 2. Mannich (top) and allylation (bottom) reactions.

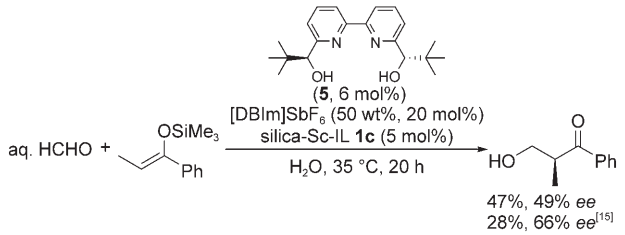

Scheme 3. Catalytic asymmetric hydroxymethylation.

this is the first example of an enantioselective reaction with a supported chiral scandium catalyst in water. Investigations aimed at improving the yield and enantiomeric excess of the reaction are now in progress.

In summary, we developed a novel heterogeneous scandium catalyst system, which works well in several carbon–carbon bond-forming reactions in water and has been applied to a catalytic asymmetric reaction. It has been shown for the first time that the combination of silica gel supported metal catalysts with an ionic liquid creates a hydrophobic reaction environment in water. This concept may be applicable to other catalysts based, for example, on metal complexes, and investigations along this line are underway.

Received: July 29, 2006
Published online: October 6, 2006

Keywords: heterogeneous catalysis · hydrophobic effect · ionic liquids · Lewis acids · scandium

[1] a) *Organic Synthesis in Water* (Ed.: P. A. Grieco), Blackie A&P, London, **1998**; b) C.-J. Li, T.-H. Chan, *Organic Reactions in Aqueous*, Media, Wiley, New York, **1997**; c) U. M. Lindstroem, *Chem. Rev.* **2002**, *102*, 2751–2772; d) C.-J. Li, *Chem. Rev.* **2005**, *105*, 3095–3166.

[2] a) *Selectivities in Lewis Acid Promoted Reactions* (Ed.: D. Schinzer), Kluwer Academic Publishers, Dordrecht, **1989**; b) *Lewis Acids in Organic Synthesis*, (Ed.: H. Yamamoto), Wiley-VCH, Weinheim, **2000**.

[3] a) S. Kobayashi, *Chem. Lett.* **1991**, 2187–2188; b) S. Kobayashi, I. Hachiya, *J. Org. Chem.* **1994**, *59*, 3590–3596; c) S. Kobayashi, S. Nagayama, T. Busujima, *J. Am. Chem. Soc.* **1998**, *120*, 8287–8288; d) S. Kobayashi, C. Ogawa, *Chem. Eur. J.* **2006**, *12*, 5954–5960.

 © 2006 Wiley-VCH Verlag GmbH & Co. KGaA, Weinheim

[4] a) S. Kobayashi, K. Manabe, *Acc. Chem. Res.* **2002**, *35*, 209 – 217; b) S. Kobayashi, K. Manabe, *Chem. Eur. J.* **2002**, *8*, 4094 – 4101; c) S. Kobayashi, T. Ogino, H. Shimizu, S. Ishikawa, T. Hamada, K. Manabe, *Org. Lett.* **2005**, *7*, 4729 – 4731.
[5] a) S. Kobayashi, T. Wakabayashi, *Tetrahedron Lett.* **1998**, *39*, 5389 – 5392; b) K. Manabe, Y. Mori, T. Wakabayashi, S. Nagayama, S. Kobayashi, *J. Am. Chem. Soc.* **2000**, *122*, 7202 – 7207.
[6] a) S. Nagayama, S. Kobayashi, *Angew. Chem.* **2000**, *112*, 578 – 581; *Angew. Chem. Int. Ed.* **2000**, *39*, 567 – 569; for other supported scandium catalysts used in water, see: b) S. Kobayashi, S. Nagayama, *J. Org. Chem.* **1996**, *61*, 2256 – 2257; c) H.-Y. Tian, Y.-J. Chen, D. Wang, C.-C. Zeng, C.-J. Li, *Tetrahedron Lett.* **2000**, *41*, 2529 – 2532; d) M. T. Reetz, D. Giebel, *Angew. Chem.* **2000**, *112*, 2614 – 2617; *Angew. Chem. Int. Ed.* **2000**, *39*, 2498 – 2501; e) W. Gu, W.-J. Zhou, D. L. Gin, *Chem. Mater.* **2001**, *13*, 1949 – 1951; f) T. Kawabata, T. Mizugaki, K. Ebitani, K. Kaneda, *J. Am. Chem. Soc.* **2003**, *125*, 10486 – 10487; g) S. Iimura, K. Manabe, S. Kobayashi, *Tetrahedron* **2004**, *60*, 7673 – 7678.
[7] Reviews of ILs and recent works on ILs related to materials chemistry: a) T. Welton, *Chem. Rev.* **1999**, *99*, 2071 – 2084; b) J. D. Holbrey, K. R. Seddon, *Clean Prod. Process* **1999**, *1*, 223 – 236; c) P. Wasserscheid, W. Keim, *Angew. Chem.* **2000**, *112*, 3926 – 3945; *Angew. Chem. Int. Ed.* **2000**, *39*, 3772 – 3789; d) R. Sheldon, *Chem. Commun.* **2001**, 2399 – 2407; e) J. Dupont, R. F. de Souza, P. A. Z. Suarez, *Chem. Rev.* **2002**, *102*, 3667 – 3692; f) C. Gordon, *Appl. Catal. A* **2001**, *222*, 101 – 117; g) M. Antonietti, D. Kuang, B. Smarsly, Y. Zhou, *Angew. Chem.* **2004**, *116*, 5096 – 5100; *Angew. Chem. Int. Ed.* **2004**, *43*, 4988 – 4992; h) B. S. Lee, Y. S. Chi, J. K. Lee, I. S. Choi, C. E. Song, S. K. Namgoong, S. Lee, *J. Am. Chem. Soc.* **2004**, *126*, 480 – 481; i) J. N. A. C. Lopes, A. A. H. Padua, *J. Phys. Chem. B* **2006**, *110*, 3330 – 3335.
[8] Scandium Lewis acids are often used in organic synthesis. See: a) S. Kobayashi, *Eur. J. Org. Chem.* **1999**, 15 – 27; b) S. Kobayashi, M. Sugiura, H. Kitagawa, W. W.-L. Lam, *Chem. Rev.* **2002**, *102*, 2227 – 2302.
[9] a) C. W. Jones, K. Tsuji, M. E. Davis, *Nature* **1998**, *393*, 52 – 54; b) B. Sow, S. Hamoudi, H. Zahedi-Niaki, S. Kaliaguine, *Microporous Mesoporous Mater.* **2005**, *79*, 129 – 136.
[10] Although supported ionic liquid catalysis has been investigated recently, there are no examples of the combination of silica-supported metal catalysts with ionic liquids. It is reported that silica gel supported ionic liquids and additional nonsupported ionic liquids form ionic-liquid phases on the surface of silica gel owing to interactions between supported and nonsupported ionic liquids. See a) C. P. Mehnert, R. A. Cook, N. C. Dispenziere, M. Afeworki, *J. Am. Chem. Soc.* **2002**, *124*, 12932 – 12933; b) A. Riisager, R. Fehrmann, S. Flicker, R. van Hal, M. Haumann, P. Wasserscheid, *Angew. Chem.* **2005**, *117*, 826 – 830; *Angew. Chem. Int. Ed.* **2005**, *44*, 815 – 819; c) H. Hagiwara, Y. Sugawara, T. Hoshib, T. Suzukib, T. *Chem. Commun.* **2005**, 2942 – 2944; d) M. Gruttadauria, S. Riela, C. Aprile, P. L. Meo, F. Anna, R. Noto, *Adv. Synth. Catal.* **2006**, *348*, 82 – 92; e) C. P. Mehnert, *Chem. Eur. J.* **2005**, *11*, 50 – 56.
[11] See the Supporting Information.
[12] Other examples are shown in the Supporting Information.
[13] a) C. Bolm, M. Zehnder, D. Bur, *Angew. Chem.* **1990**, *102*, 206 – 208; *Angew. Chem. Int. Ed. Engl.* **1990**, *29*, 205 – 207; b) C. Bolm, M. Ewald, M. Felder, G. Schlingloff, *Chem. Ber.* **1992**, *125*, 1169 – 1190.
[14] S. Ishikawa, T. Hamada, K. Manabe, S. Kobayashi, *J. Am. Chem. Soc.* **2004**, *126*, 12236 – 12237.
[15] The product was obtained in 28% yield with 66% *ee* under the following conditions: **4** (6.5 mol%), $[HBIm]NTf_2$ (50 wt%, 20 mol%), Silica-Sc-IL (0.24 mmol g^{-1}, 5 mol%), H_2O, 35 °C, 24 h.

 © 2006 Wiley-VCH Verlag GmbH & Co. KGaA, Weinheim

Nanofabrication

DOI: 10.1002/anie.200603142

Massively Parallel Dip–Pen Nanolithography with 55 000-Pen Two-Dimensional Arrays**

*Khalid Salaita, Yuhuang Wang, Joseph Fragala, Rafael A. Vega, Chang Liu, and Chad A. Mirkin**

The last decade has witnessed the development of a dichotomy in scanning-probe lithographic (SPL) approaches and systems.[1–4] These techniques are either: 1) constructive, such as dip–pen nanolithography (DPN),[1,2] and involve the delivery of molecules or other materials that can chemically or physically anchor to the underlying substrate, or 2) destructive (e.g. anodic oxidation[5,6] and nanografting[7]) and involve the delivery of energy (in the form of heat, force, or current) to a surface that results in the physical change, chemical transformation, or displacement of the underlying material.[3,4] The design demands for parallelization of the two approaches are daunting but extremely different because of the fundamental difference between delivering energy and chemical materials. In fact, the only example of massively parallel SPL is the "millipede", which has been limited to destructive patterning involving polymer thermal indentation and annealing.[8–10] Since throughput is the biggest limitation of the constructive DPN technology, large area parallelization capabilities must be developed to realize its full potential.[3,4,11,12] However, parallelization must be accomplished with the constraints and capabilities of the DPN technique in mind. Herein, we describe a solution to DPN parallelization through the development, fabrication, and use of a novel 55 000-pen two-dimensional (2D) array to pattern gold

[*] K. Salaita,[+] Y. Wang,[+] R. A. Vega, Prof. C. A. Mirkin
Department of Chemistry, Department of Materials Science and Engineering, Department of Medicine, and International Institute for Nanotechnology
Northwestern University
2145 Sheridan Road, Evanston, IL 60208-3113 (USA)
Fax: (+1) 847-467-5123
E-mail: chadnano@northwestern.edu

J. Fragala
NanoInk, Inc.
215 E. Hacienda Avenue, Campbell, CA 95008-6616 (USA)

Prof. C. Liu
Micro and Nanotechnology Laboratory
University of Illinois at Urbana-Champaign
208 North Wright Street, IL 61801-2355 (USA)

[+] These authors contributed equally to this work.

[**] C.A.M. acknowledges the Defense Advanced Research Projects Agency, Air Force Office of Scientific Research, the National Science Foundation, and the National Institutes of Health (through a Director's Pioneer Award) for support of this work. The authors thank Tsuyohiko Fujigaya for the 3D graphic in Scheme 1, and Roger Shile and Pam Simao for fabrication of pen arrays.

Supporting information for this article is available on the WWW under http://www.angewandte.org or from the author.

WILEY InterScience DISCOVER SOMETHING GREAT
© 2006 Wiley-VCH Verlag GmbH & Co. KGaA, Weinheim

substrates with sub-100-nm resolution over square centimeter areas (Scheme 1).

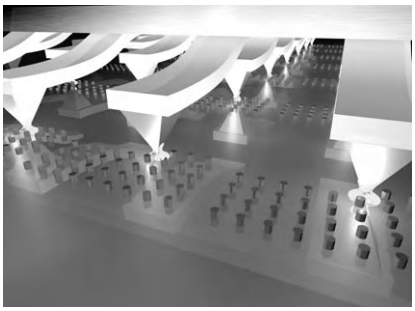

Scheme 1. Massively parallel DPN with a passive, wire-free, 2D cantilever array.

Using photolithographic techniques,[13] we have fabricated a 55 000-pen 2D array (yield > 98 %; Figure 1 A). With a pen spacing of 90 and 20 μm in the *x* and *y* directions, respectively, this array occupies 1 cm^2 and has the highest density and largest total number of cantilevers reported to date.[2] The 55 000-pen array was developed so that it would be amenable to a lithographic approach that does not require independent feedback from each tip.

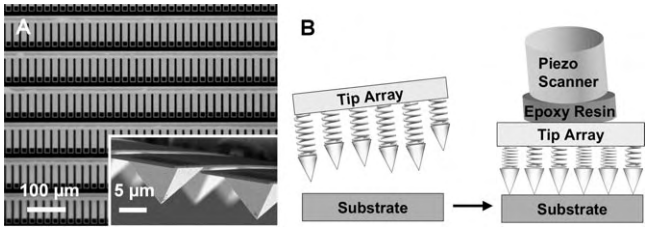

Figure 1. A) Optical micrograph of part of the 2D array of cantilevers used for patterning. Inset: SEM image of the cantilever arrays at a different viewing angle. B) Schematic of the gravity-driven alignment method used for massively parallel DPN with a 2D cantilever array. Each pen was brought into contact with the substrate under the weight of the whole pen array. Subsequently, the exact position of the pen array was locked to the AFM scanner head by an epoxy resin.

Large-area DPN is possible with this 2D array because of several features associated with the array architecture and a novel but easily adoptable gravity-driven alignment procedure (Figure 1 B). First, the cantilevers were fabricated such that the apex of each pyramidal tip is (7.6 ± 0.2) μm taller than the cantilever base, and each tip has a square base with an edge length comparable to the cantilever width (Figure 1 A). This pen structure gives the tip adequate spatial clearance for approaching the substrate. Second, the cantilevers are bent at an angle of approximately 20° (or a tip deflection of approximately 20 μm) from the supporting base by coating them with 25 nm of Au (and a 5-nm Ti adhesion layer) and then annealing at 300 °C for 2 h.[13] This curvature is a result of the different thermal expansion of gold and silicon nitride, and intrinsic stress arising from the annealing-induced restructuring of the Au/Ti/Si_xN_y multilayer.[14,15] The bent cantilever architecture provides greater tolerance to substrate morphology and inherent tip misalignment within the array (up to ± 10 μm). Third, gravity (ca. 20 nN/tip), instead of a complex set of feedback systems, is used to bring all of the tips in contact with a sacrificial substrate prior to use. Finally, the tip array is locked into position with respect to the piezo scanner head by taking advantage of the malleability of a rapidly curing epoxy resin (Figure 1 B). This remarkably simple alignment procedure allows all of the tips within the array to be engaged and disengaged in a deliberate and controlled fashion without a feedback system or independent cantilever addressability. Once engaged, the pen array can be used to directly write virtually any pattern of molecules on the underlying substrate and simultaneously generate approximately 55 000 duplicates at the resolution of single-pen DPN.

Structures made of several molecules (e.g. 1-mercaptohexadecanoic acid, 1-octadecanethiol (ODT), phospholipids[16]) in many different physical forms on vastly different substrates (gold and glass) have been fabricated using this array and alignment procedure.[13] As an illustration of the control afforded by the technique, we have uniformly coated the pen arrays with ODT and subsequently used them to pattern a polycrystalline gold-coated (25–50-nm thick with a 5-nm Ti adhesion layer) silicon substrate with one-molecule high features. The resulting ODT molecular patterns were converted, by wet chemical etching, to raised gold features with in-plane dimensions defined by DPN.[13,17–19] By converting molecular patterns into gold nanostructures, we could use an optical microscope to rapidly characterize the patterns over the entire 1-cm^2 area. Higher resolution scanning electron microscopy and AFM were used to analyze the fine structure of representative duplicates. Alternatively, the ODT patterns can be used as affinity templates to assemble proteins, such as fibronectin, to form arrays of such materials with feature size control on the sub-100-nm to many micrometer length scale (see Supporting Information).

In an initial experiment, the 55 000-pen array was used to generate approximately 88 million dot features (Figure 2). Each pen generated 1600 dots in a 40 × 40 array, where the dot-to-dot distance was 400 nm. The dots had a diameter of (100 ± 20) nm, a height of 30 nm, and were spaced by 20 μm in the *x* direction and 90 μm in the *y* direction corresponding to the distances determined by the array architecture. Although smaller dots could be generated by reducing the hold time, the diameter of these features approaches the ultimate resolution

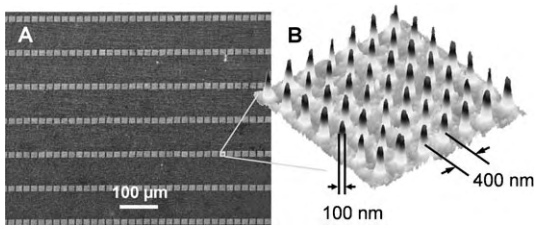

Figure 2. A) Large-area SEM image of part of an 88 000 000-gold-dot array (40 × 40 within each block) on an oxidized silicon substrate. B) Representative AFM topographical image of part of one of the blocks, where the dot-to-dot distance is 400 nm, and the dot diameter is (100 ± 20) nm.

 © 2006 Wiley-VCH Verlag GmbH & Co. KGaA, Weinheim

under these conditions, which is limited by the radius of curvature of the tip apex (ca. 60 nm), as well as the grain size of evaporated Au (30–50 nm).

A remarkable attribute of this 2D DPN patterning approach is the rapid prototyping capability that can be used to, for example, generate a combinatorial array of molecular and solid-state features that systematically vary in size, spacing, and shape.[13] One can even generate very sophisticated structures using this approach along with integrated software that controls the relative movement of the tip array over the underlying substrate. Indeed, we were able to take the likeness of Thomas Jefferson from a 2005 US five-cent coin and duplicated it 55000 times by depositing 80 nm features of ODT according to a $14.5 \times 14.5\ \mu m^2$ bit map that contains 8773 dots (Figure 3A). The pattern was created

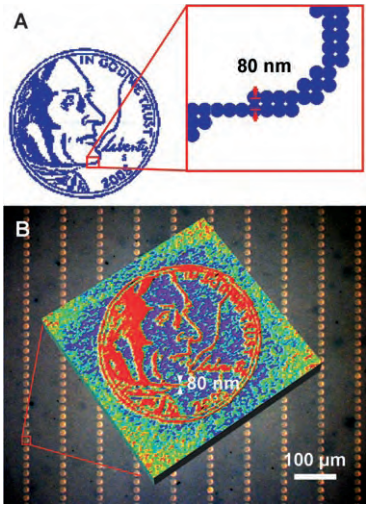

Figure 3. A) Dot matrix map representing the front face of the 2005 US five-cent coin. The coin bears a picture of Thomas Jefferson, who helped develop the polygraph, a letter duplicator that relies on an array of macroscopic pens. The lines of the chin are composed of dots of 80-nm diameter . B) Optical micrograph of a representative region of the substrate on which the approximately 55000 duplicates were generated. Each of the circular features is a miniaturized replica of the face of the five-cent coin. Inset: High-resolution topographical AFM image of a representative replica.

by holding the pen array at each spot for 0.08 s and traveling between spots at a speed of $60\ \mu m\,s^{-1}$. Figure 3B shows a representative portion of the approximately 55000 copies of gold structures (yield > 99%) across an area of $1 \times 1\ cm^2$. Importantly, approximately 4.7×10^8 features were used to generate the replicas, and the total time required to perform this fabrication was less than 30 min.

The bent-cantilever architecture and large pyramidal tip size provides for a very simple method of tolerating substrate roughness and thickness variations. To demonstrate this tolerance a gold-coated glass microscope slide (total thickness variation ca. $2.6\ \mu m\,cm^{-2}$) was patterned in place of a single-crystal silicon substrate (total thickness variation ca. $0.05\ \mu m\,cm^{-2}$). Figure 4A is an optical image showing the iridescent reflection from arrays of gold disks of approximately 600-nm diameter patterned on a glass microscope

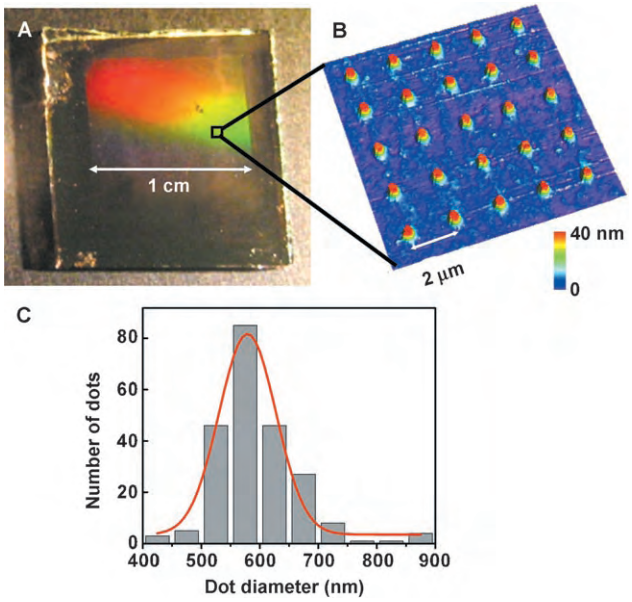

Figure 4. A) Iridescent reflection from arrays of gold disks patterned across a $1 \times 1\text{-}cm^2$ area of a glass slide. Each pen generated a 5×20 square-lattice array of disks of approximately 600-nm diameter at a pitch of 2 μm. B) Representative AFM image of part of a gold-disk array. C) Histogram analysis of the diameter of 240 disks randomly but uniformly selected from the sample shown in (A).

slide. To quantify the patterning fidelity, 240 features were randomly selected across the entire $1\text{-}cm^2$ area and imaged by AFM, and histograms were constructed using the full-width at half maximum height (FWHM) of the height profile of the features (Figure 4). Significantly, > 99% of the pens (excluding 1–2% of pens damaged during processing) are in operation. The standard deviation of the dot diameters for the features generated by the 55000 different pens was 16% across the $1\text{-}cm^2$ area, which is a combined result of minor variations in substrate etching, tip morphology, and ink coating. In all patterning experiments AFM and SEM images confirm that registry and alignment are maintained within the field of view of each tip and between tips as well. This degree of registry and pattern fidelity are maintained even when the single-crystal silicon substrate is replaced with a glass microscope slide, thus confirming the flexibility and robustness of this molecular patterning technique.

Although still in its infancy, this parallel 2D DPN approach should be particularly useful for fabricating combinatorial libraries of structures, especially once independent tip-inking strategies have been developed. It is also useful for creating the types of structures that can be fabricated with a nanostamping approach but without the distortion effects that plague stamping and the need to fabricate a mask each time a new design is required.[3]

Received: August 3, 2006
Published online: September 25, 2006

Keywords: dip–pen nanolithography · lithography · nanofabrication · parallelization · scanning probe

 © 2006 Wiley-VCH Verlag GmbH & Co. KGaA, Weinheim

[1] R. D. Piner, J. Zhu, F. Xu, S. H. Hong, C. A. Mirkin, *Science* **1999**, *283*, 661 – 663.
[2] D. S. Ginger, H. Zhang, C. A. Mirkin, *Angew. Chem.* **2004**, *116*, 30 – 46; *Angew. Chem. Int. Ed.* **2004**, *43*, 30 – 45.
[3] B. D. Gates, Q. B. Xu, M. Stewart, D. Ryan, C. G. Willson, G. M. Whitesides, *Chem. Rev.* **2005**, *105*, 1171 – 1196.
[4] S. Kramer, R. R. Fuierer, C. B. Gorman, *Chem. Rev.* **2003**, *103*, 4367 – 4418.
[5] S. C. Minne, S. R. Manalis, A. Atalar, C. F. Quate, *J. Vac. Sci. Technol. B* **1996**, *14*, 2456 – 2461.
[6] S. C. Minne, J. D. Adams, G. Yaralioglu, S. R. Manalis, A. Atalar, C. F. Quate, *Appl. Phys. Lett.* **1998**, *73*, 1742 – 1744.
[7] G. Y. Liu, S. Xu, Y. L. Qian, *Acc. Chem. Res.* **2000**, *33*, 457 – 466.
[8] P. Vettiger, M. Despont, U. Drechsler, U. Durig, W. Haberle, M. I. Lutwyche, H. E. Rothuizen, R. Stutz, R. Widmer, G. K. Binnig, *IBM J. Res. Dev.* **2000**, *44*, 323 – 340.
[9] P. Vettiger, G. Cross, M. Despont, U. Drechsler, U. Durig, B. Gotsmann, W. Haberle, M. A. Lantz, H. E. Rothuizen, R. Stutz, G. K. Binnig, *IEEE Trans. Nanotechnol.* **2002**, *1*, 39 – 55.
[10] E. Eleftheriou, T. Antonakopoulos, G. K. Binnig, G. Cherubini, M. Despont, A. Dholakia, U. Durig, M. A. Lantz, H. Pozidis, H. E. Rothuizen, P. Vettiger, *IEEE Trans. Magn.* **2003**, *39*, 938 – 945.
[11] S. H. Hong, C. A. Mirkin, *Science* **2000**, *288*, 1808 – 1811.
[12] K. Salaita, S. W. Lee, X. F. Wang, L. Huang, T. M. Dellinger, C. Liu, C. A. Mirkin, *Small* **2005**, *1*, 940 – 945.
[13] See the Supporting Information.
[14] L. A. Wenzler, G. L. Moyes, T. P. Beebe, *Rev. Sci. Instrum.* **1996**, *67*, 4191 – 4197.
[15] D. C. Miller, C. F. Herrmann, H. J. Maier, S. M. George, C. R. Stoldt, K. Gall, *Scr. Mater.* **2005**, *52*, 873 – 879.
[16] S. Lenhert, P. Sun, Y. Wang, H. Fuchs, C. A. Mirkin, unpublished work.
[17] Y. N. Xia, X. M. Zhao, E. Kim, G. M. Whitesides, *Chem. Mater.* **1995**, *7*, 2332 – 2337.
[18] M. Geissler, H. Schmid, A. Bietsch, B. Michel, E. Delamarche, *Langmuir* **2002**, *18*, 2374 – 2377.
[19] H. Zhang, S. W. Chung, C. A. Mirkin, *Nano Lett.* **2003**, *3*, 43 – 45.

 © 2006 Wiley-VCH Verlag GmbH & Co. KGaA, Weinheim

DNA Structures

DOI: 10.1002/anie.200603161

Photochemical Synthesis of R-Shaped DNA toward DNA Recombination and Processing In Vitro**

*Masayuki Ogino and Kenzo Fujimoto**

Ligation of DNA is widely used in DNA repair, replication, and recombination in biomedicine and molecular biology. DNA ligases are enzymes that catalyze formation of the phosphodiester bond between the adjacent 5′-phosphate and 3′-OH groups of two DNA fragments. It is able to join between two single-stranded (ss) DNA fragments annealed on the complementary DNA strand.[1] Although enzymatic ligation methods have advantages, the strategy is limited under certain conditions (such as pH, temperature, and the metal cation) and unique structures, such as branched DNA, cannot be formed. There are methods for nonenzymatic template-directed chemical ligation.[2] These methods use DNA or RNA templates to mediate ligation reactions that generate oligomers of DNA, RNA, or structural analogues of nucleic acids. Modified nucleosides containing various DNA functional groups that react after hybridization by the addition of reagents or by photoirradiation and extended sequence-specific small-molecule synthesis, have been investigated in addition to that of polymerization and single nucleotide polymorphism detection systems.[3,4f] We previously reported a highly efficient and reversible template-directed DNA photoligation of an oligodeoxyribonucleotide (ODN) containing a 5-vinyldeoxyuridine derivative at the 5′ end and an ODN that contains thymine at the 3′ end.[4] In addition, we recently disclosed an efficient template-directed photoligation ODN by using a 5-cyanovinyl-1′-α-2′-deoxyuridine (α^{C}U)-containing ODN at the 3′ end with an ODN that contains thymine at the 5′ end.[5] By using these methods, we succeeded in the synthesis of complex DNA structures, such as branched DNA, end-capped DNA, or padlocked plasmid

[*] M. Ogino, Prof. Dr. K. Fujimoto
School of Materials Science
Japan Advanced Institute of Science and Technology
Asahidai, Nomi, Ishikawa 923-1292 (Japan)
Fax: (+81) 761-51-1671
E-mail: kenzo@jaist.ac.jp
Homepage: http://www.jaist.ac.jp/ms/labs/fujimoto/
Prof. Dr. K. Fujimoto
PRESTO
Japan Science and Technology Agency (JST)
Kawaguchi 332-0012 (Japan)

[**] This work was supported by Precursory Research for Embryonic Science and Technology (PRESTO), the Japan Science and Technology Agency (JST). Partial support by a Grant-in-Aid for Scientific Research from the Ministry of Education, Culture, Sports, Science, and Technology, Japan is also acknowledged.

Supporting information for this article is available on the WWW under http://www.angewandte.org or from the author.

© 2006 Wiley-VCH Verlag GmbH & Co. KGaA, Weinheim

DNA, at desired sites.[6] Although template-directed chemical ligation and photoligation connect modified DNA to natural DNA, they are not able to connect two natural DNA molecules. Therefore, these methods are subject to limitation with respect to the applications such as biotechnological techniques. If two natural DNA molecules can be connected, the photoligation method would become a useful strategy for biotechnological application in combination with the usual gene manipulation. Thus, we developed a new ligation method that cross-links two natural DNA molecules. Herein, we report template-directed photoligation by using ODNs that contain α^{C}U and β^{C}U at both terminal ends. By using this method, two unmodified ODNs as natural DNA were photochemically ligated through a modified ODN in the presence of template ODN. Furthermore, we developed a method that can directly process DNA in a method similar to RNA processing. We applied the method to the synthesis of R-Shaped DNA as a unique structure to resemble lariat DNA.[7]

The synthesis of the photoreactive nucleosides and the corresponding phosphoramidite building block of α^{C}U and 5-cyanovinyl-1′-β-2′-deoxyuridin (β^{C}U) as well as the synthesis of the corresponding ODN followed standard routes in DNA chemistry. α^{C}U was synthesized from Hoffer's chlorosugar; the method was reported previously,[5] and the synthesis of β^{C}U is shown in the Supporting Information. The modified ODNs containing α^{C}U and β^{C}U (5′-d(β^{C}UGTGCα^{C}Up)-3′ (ODN **1**) and 5′-d(β^{C}UGCATGTGCα^{C}Up)-3′ (ODN **5**)) were synthesized by using a 3′-phosphate controlled pore glass (CPG) solid-phase support.[8] After purification with reversed-phase HPLC, ODN **1** was characterized by MALDI-TOF MS (*m*/*z* calcd for $[M-H]^-$: 1950.2828; found: 1950.5432). The modified ODN **5** was characterized by MALDI-TOF MS (*m*/*z* calcd for $[M-H]^-$: 3189.0578; found: 3189.0632). The ODNs used in this study are summarized in Table 1.

Table 1: ODNs used in this study.

ODN	Sequences
ODN **1**	5′-d(β ^{C}UGTGCα^{C}Up)-3′
ODN **2**	5′-d(GACAGC)-3′
ODN **3**	5′-d(TGCGTG)-3′
ODN **4**	5′-d(CACGCAAGCACAGCTGTC)-3′
ODN **5**	5′-d(β?^{C}UGCATGTGCα^{C}Up)-3′
ODN **6**	5′-d(GAGACGTGAT)d(A)$_{20}$(TGGCAGTACG)-3′
ODN **7**	5′-d(CGTACTGCCAAGCACATGCAATCACGTCTC)-3′

We determined the feasibility of the template-directed photoligation through ODNs that contain α^{C}U and β^{C}U at the 3′ and 5′ ends, respectively (Scheme 1). 5′-d(GACAGC)-3′ (ODN **2**), 5′-d(TGCGTG)-3′ (ODN **3**), and ODN **1** were irradiated at 366 nm for 1 h at 0 °C in the presence of template ODN **4**. Capillary-gel-electrophoresis (CGE) analysis of this mixture indicated a clean and efficient formation of ligated ODN **8** and the concomitant disappearance of ODN **1**, ODN **2**, and ODN **3** (Figure 1). We observed the appearance of the peak of ligated product ODN **8** in 95 % yield as determined by CGE analysis. The yield was calculated based on the average

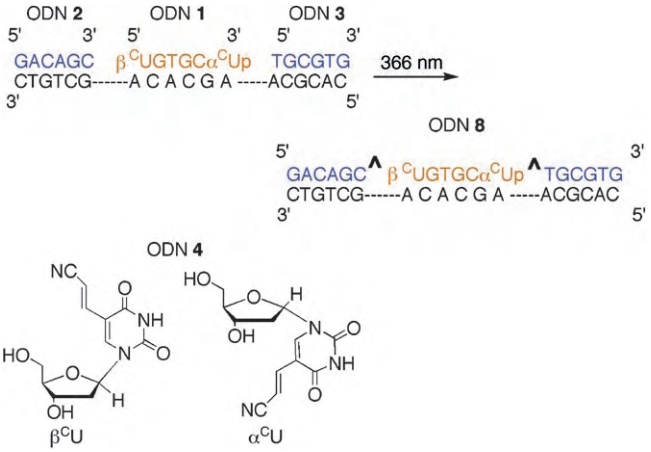

Scheme 1. Template-directed photoligation of ODNs through α^{C}U and β^{C}U. The connections made by photoirradiation in ODN **8** are indicated (**Λ**).

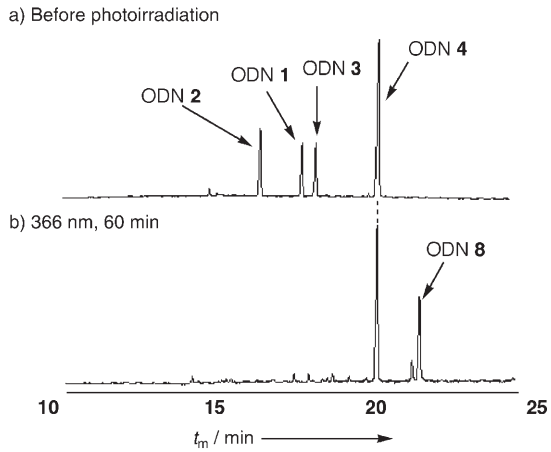

Figure 1. CGE of ODN **1**, ODN **2**, and ODN **3** irradiated at 366 nm in the presence of template ODN **4**. a) Before photoirradiation, and b) after irradiation at 366 nm for 60 min, 95 % yield. t_m = migration time.

of ODN **2** and ODN **3**. MALDI-TOF MS indicated that ODN **8** was a ligated product of ODN **1**, ODN **2**, and ODN **3** (*m*/*z* calcd for $[M-H]^-$: 5575.73; found: 5575.70). The molecular weight of ODN **8** was equal to the sum of the molecular weights of ODN **1**, ODN **2**, and ODN **3**. Enzymatic digestion of isolated ODN **8** with P1 nuclease, snake venom phosphodiesterase, and alkaline phosphatase showed the formation of deoxycytidine (dC), deoxyguanosine (dG), thymidine (T), and deoxyadenosine (dA) in a ratio of 3:7:2:2 together with new products (see Supporting Information). Spectroscopic data, including MALDI-TOF MS, indicated that these new products were the α^{C}U-T (*m*/*z* calcd for $[M+H]^+$: 522.1836; found: 522.1999) and dC-β^{C}U (*m*/*z* calcd for $[M+H]^+$: 507.1839; found: 507.2011) photoadducts. The structure of α^{C}U-T and dC-β^{C}U was expected to be a [2+2] adduct on the basis of previous reports.[4c,5] Although two unmodified 6-mer ODNs were ligated to modified ODN **1** in the presence of template ODN, this result suggests that the new method could

 © 2006 Wiley-VCH Verlag GmbH & Co. KGaA, Weinheim

apply to the ligation of two DNA or RNA fragments, such as DNA recombination in vitro.[9]

To expand the new system, we performed template-directed photoligation at two positions in the middle of the DNA structures, and synthesized R-shaped DNA as a novel structure (Scheme 2). ODN **5** and ODN **6** were irradiated at 366 nm for 2 h at 0 °C in the presence of template ODN **7**. Figure 2b shows a CGE analysis of a photoirradiated mixture with clean and efficient formation of the expected ligated 50-mer R-shaped ODN **9** and the complete disappearance of ODN **5** and ODN **6**. We observed the appearance of the peak of the ligated product ODN **9** in 90% yield as determined by CGE analysis. The yield was calculated based on the average yield of ODN **5** and ODN **6**. As shown in Figure 3, the generation of the product with one end connected is confirmed by priority for the first 20 minutes (as the slope of residual ratio for one-end-connected product (red line) in the first 20 min in Figure 3 is steeper than the slope of yield for R-shaped DNA (orange line)). The increase of ODN **9** was more gradual than the product with one end connected. These results suggest that photoligation progressed stepwise from the product with one side connected to ODN **9**. We considered that the second reaction was promoted by an increase in the stability of the duplex that is formed by the product with one end connected. The isolated new product was characterized by MALDI-TOF MS (m/z calcd for $[M+H]^+$: 15676.36; found: 15676.76) and enzymatic digestion (see Supporting Information). As a result, we confirmed that ODN **9** is R-shaped DNA. The method of R-shaped DNA synthesis may offer novel DNA processing in vitro that is modelled on pre-mRNA splicing.

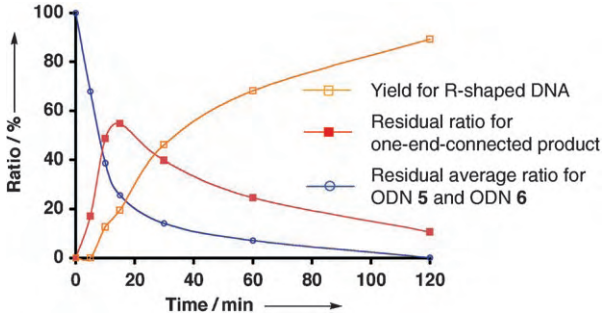

Figure 3. Yield for R-shaped DNA and residual ratio for ODN **5**, ODN **6**, and the one-end-connected product as determined by CGE.

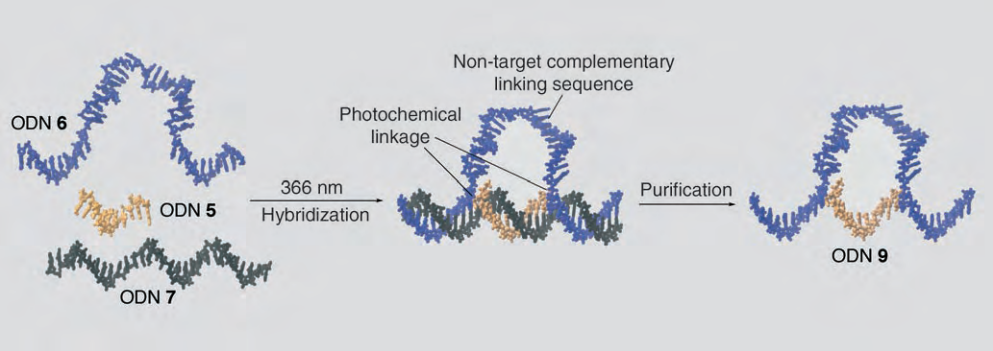

Scheme 2. Template-directed photoligation synthesis of R-shaped DNA through $\alpha^{C}U$ and $\beta^{C}U$

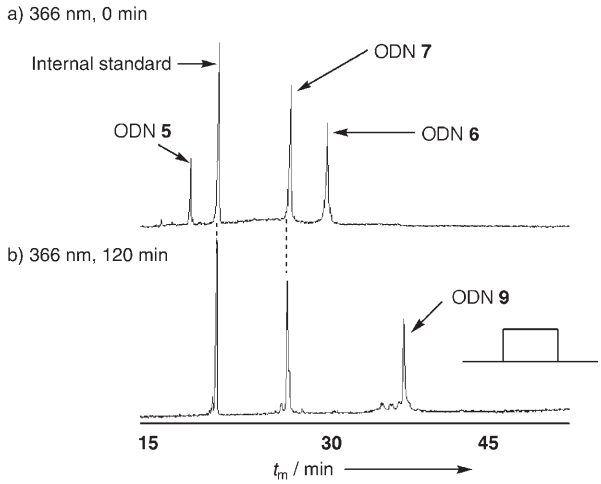

Figure 2. CGE of ODN **5** and ODN **6** irradiated at 366 nm in the presence of template ODN **7**. a) Before photoirradiation, and b) after irradiation at 366 nm for 120 min, 90% yield.

In conclusion, we demonstrated a novel strategy for connecting DNA strands by using ODNs that contain $\alpha^{C}U$ and $\beta^{C}U$ at the 3′ and 5′ ends, respectively. Two DNA fragments were ligated to the modified ODN that contains $\alpha^{C}U$ and $\beta^{C}U$ in the presence of template ODN. These methods can be used for recombination that mutually connects two or more genes of different kinds. We have also shown the synthesis of a novel unique DNA structure by R-shaped ODN. These methods may be used for the in vitro DNA processing of any DNA, such as genome DNA and plasmid DNA. Additionally, R-shaped DNA may construct the periodically controlled rod- and sheet-type nanoarrays[10] and DNA nanodevices[11] as part of the nanostructures. These unique structures are a powerful tool for easy and accurate DNA handling, leading to the development of DNA nanoarchitecture as represented by various crossover DNA motifs.

Experimental Section

Photoligation of ODNs as monitored by CGE: The reaction mixture (total volume = 100 μL) containing ODN **1**, ODN **2**, and ODN **3** (each with a strand concentration of 30 μM) in the presence of template ODN **4** (strand concentration of 33 μM,) in sodium cacodylate buffer (50 mM; pH 7.0) and sodium chloride (100 mM) was irradiated with a 25-W transilluminator (366 nm) at 0 °C for 1 h. After irradiation, the progress of photoreaction was monitored by CGE on a BECKMAN COULTER, P/ACE™ MDQ Capillary Electrophoresis system. The denaturing gel (eCAP™ ssDNA 100-R

 © 2006 Wiley-VCH Verlag GmbH & Co. KGaA, Weinheim

Kit) purchased from BECKMAN COULTER containing Tris-Borate buffer solution and urea was prepared according to the instruction manual. The enzymatic digestion was carried out with alkaline phosphatase, phosphodiesterase in NaCl (100 mM), Tris-HCl (100 mM; pH 8.9), 50% glycerol, $MgCl_2$ (15 mM), and P1 nuclease at 37°C for 4 h.

Spectroscopic measurements: The absorbance of the hybrid duplexes was monitored at 260 nm from 10 to 80°C with a heating rate of 1.0°C min^{-1} by using a BECKMAN COULTER DU 800 UV/Vis spectrophotometer.

Received: August 4, 2006
Revised: September 1, 2006
Published online: September 29, 2006

Keywords: DNA · ligation · oligodeoxyribonucleotides · photochemistry

[1] a) R. C. Alexander, A. K. Johnson, J. A. Thorpe, T. Gevedon, S. M. Testa, *Nucleic Acids Res.* **2003**, *31*, 3208–3216; b) A. V. Cherepanov, S. de Vries, *Eur. J. Biochem.* **2003**, *270*, 4315–4325.

[2] a) T. Wu, L. E. Orgel, *J. Am. Chem. Soc.* **1992**, *114*, 5496–5501; b) C. Bohler, P. E. Nielsen, L. E. Orgel, *Nature* **1995**, *376*, 578–581; c) M. K. Herrlein, J. S. Nelson, R. L. Letsinger, *J. Am. Chem. Soc.* **1995**, *117*, 10151–10152; d) R. K. Bruick, P. E. Dawson, S. B. Kent, N. Usman, G. F. Joyce, *Chem. Biol.* **1996**, *3*, 49–55; e) A. Luther, R. Brandsch, G. von Kiedrowski, *Nature* **1998**, *396*, 245–248; f) Y. Xu, E. T. Kool, *Nucleic Acids Res.* **1998**, *26*, 3159–3164; g) J. Leu, J.-S. Taylor, *Nucleic Acids Res.* **1998**, *26*, 3300–3304; h) J. Ye, Y. Gat, G. T. Lynn, *Angew. Chem.* **2000**, *112*, 3787–3789; *Angew. Chem. Int. Ed.* **2000**, *39*, 3641–3643; i) X. Wu, S. Guntha, M. Ferencic, R. Krishnamrthy, A. Eschenmoser, *Org. Lett.* **2002**, *4*, 1279–1282.

[3] a) Y. Xu, N. B. Karalkar, E. T. Kool, *Nat. Biotechnol.* **2001**, *19*, 148–152; b) Z. J. Gartner, D. R. Liu, *J. Am. Chem. Soc.* **2001**, *123*, 6961–6963.

[4] a) K. Fujimoto, S. Matsuda, N. Takahashi, I. Saito, *J. Am. Chem. Soc.* **2000**, *122*, 5646–5647; b) K. Fujimoto, S. Matsuda, M. Hayashi, I. Saito, *Tetrahedron Lett.* **2000**, *41*, 7897–7900; c) K. Fujimoto, N. Ogawa, M. Hayashi, S. Matsuda, I. Saito, *Tetrahedron Lett.* **2000**, *41*, 9437–9440; d) Y. Yoshimura, Y. Noguchi, H. Sato, K. Fujimoto, *ChemBioChem* **2006**, *7*, 598–601; e) S. Ogasawara, K. Fujimoto, *Angew. Chem.* **2006**, *118*, 4624–4627; *Angew. Chem. Int. Ed.* **2006**, *45*, 4512–4515.

[5] M. Ogino, Y. Yoshimura, A. Nakazawa, I. Saito, K. Fujimoto, *Org. Lett.* **2005**, *7*, 2853–2856.

[6] a) S. Ogasawara, K. Fujimoto, *ChemBioChem* **2005**, *6*, 1756–1760; b) K. Fujimoto, Y. Yoshimura, T. Ikemoto, A. Nakazawa, M. Hayashi, I. Saito, *Chem. Commun.* **2005**, *25*, 3177–3179; c) K. Fujimoto, S. Matsuda, N. Ogawa, M. Hayashi, I. Saito, *Tetrahedron Lett.* **2000**, *41*, 6451–6454.

[7] a) C. B. Reese, Q. Song, *Nucleic Acids Res.* **1999**, *27*, 2672–2681; b) S. Carriero, M. J. Damha, *Org. Lett.* **2003**, *5*, 273–276; c) S. Carriero, M. J. Damha, *J. Org. Chem.* **2003**, *68*, 8328–8338.

[8] T. A. Walton, M. H. Lyttle, D. J. Dick, R. M. Cook, *Bioconjugate Chem.* **2002**, *13*, 1155–1158.

[9] a) K. Murashima, A. Kosugi, R. H. Doi, *Mol. Microbiol.* **2002**, *45*, 617–626; b) Y. An, J. Ji, W. Wu, A. Lv, R. Huang, Z. Xiu, *Mol. Biol.* **2006**, *40*, 486–492.

[10] A. Chworos, I. Severcan, A. Y. Kyofman, P. Weinkam, E. Oroudjev, H. G. Hansma, L. Jaeger, *Science* **2004**, *306*, 2068–2072.

[11] H. A. Becerril, R. M. Stoltenberg, D. R. Wheeler, R. C. Davis, J. N. Harb, A. T. Woolley, *J. Am. Chem. Soc.* **2005**, *127*, 2828–2829.

 © 2006 Wiley-VCH Verlag GmbH & Co. KGaA, Weinheim

Metal–Organic Frameworks

DOI: 10.1002/anie.200603196

Dynamic Motion of Building Blocks in Porous Coordination Polymers**

*Satoshi Horike, Ryotaro Matsuda, Daisuke Tanaka, Seijiro Matsubara, Motohiro Mizuno, Kazunaka Endo, and Susumu Kitagawa**

The design and construction of metal–organic crystal architectures have been widely studied, and a variety of frameworks have been prepared through self-assembly processes.[1] In particular, porous coordination polymers (PCPs) are currently receiving considerable attention in view of their possible functions in sorption, separation, and guest alignment.[2]

The characteristics of the increasing number of PCPs have been extensively studied. Crystal structures of PCPs with and without guests, and thermodynamic sorption isotherms are typical research topics; however, these topics investigate static aspects of the frameworks. The unique advantages of PCPs are their increased flexibility and dynamics compared to inorganic porous materials.[3] The nature of the flexibility depends strongly on the characteristics of the organic ligands used to build the frameworks. When the ligands contain mobile parts (for example, groups that undergo rotation or libration), dynamic motion may occur inside the frameworks in the solid state, even at room temperature.

Molecular motion in crystalline solids has received much attention, and various solids containing mobile groups have been designed and synthesized.[4] Compounds that are capable of rotational motion in response to outside driving forces such as light, heat, or electric fields are intriguing for the development of nanoscale devices. Studies of such solids have mainly focused on the construction of discrete molecular

[*] S. Horike, Dr. R. Matsuda, D. Tanaka, Prof. Dr. S. Kitagawa
Department of Synthetic Chemistry and Biological Chemistry
Graduate School of Engineering, Kyoto University
Katsura, Nishikyo-ku, Kyoto 615-8510 (Japan)
Fax: (+81) 75-383-2732
E-mail: kitagawa@sbchem.kyoto-u.ac.jp
Prof. Dr. S. Matsubara
Department of Material Chemistry
Graduate School of Engineering, Kyoto University
Katsura, Nishikyo-ku, Kyoto 615-8510 (Japan)
Prof. Dr. M. Mizuno, Prof. Dr. K. Endo
Department of Chemistry
Graduate School of Natural Science & Technology
Kanazawa University
Kakuma, Kanazawa, Ishikawa 920-1192 (Japan)

[**] This work was supported by the Ministry of Education, Culture, Sports, Science, and Technology of the Government of Japan through a Grant-in-Aid for Scientific Research on a Priority Area, "Chemistry of Coordination Space" (#434), and the Core Research for Evolutional Science and Technology (CREST) program.

Supporting information for this article is available on the WWW under http://www.angewandte.org or from the author.

WILEY InterScience DISCOVER SOMETHING GREAT
© 2006 Wiley-VCH Verlag GmbH & Co. KGaA, Weinheim

compounds; however, extended networks containing not only a mobile component, but also a rigid framework that maintains the integrity of the lattice are considered to be ideal structures for nanoscale applications.[5] From this point of view, we have investigated PCPs as a basis for creating crystalline polymer networks with responsive rotational groups. The large void space and easily modified designs of PCPs make these materials suitable for this purpose. Herein, we synthesize PCPs containing rotational organic parts and characterize their dynamic behavior with solid-state ^{2}H NMR spectroscopy, sorption measurements, and differential scanning calorimetry (DSC). In addition, we regulate their dynamic motion by guest sorption.

A pillared layer structure is a useful topology for the construction and modification of porous frameworks.[6] We first explored the solid-state dynamics of such a compound, in which the layers consist of Cd^{2+} and 2-sulfoterephthalate (2-stp) ions, and the pillars are pyrazine (pyz) molecules.[7] $\{[CdNa(2\text{-stp})(pyz)_{0.5}(H_2O)](H_2O)\}_n$ ($\mathbf{1}\supset H_2O$) was synthesized by the reaction of $Cd(NO_3)_2\cdot 4H_2O$ with 2-sulfoterephthalate, NaOH, and pyrazine in water/ethanol. Figure 1a shows the structure of $\mathbf{1}\supset H_2O$ determined by single-crystal X-ray diffraction at 223 K. The neutral layers consisting of Cd^{2+}, Na^+, and 2-sulfoterephthalate ions are parallel to the *ac* plane, and the pyrazine ligands connect the layers to form the 3D pillared layer structure. The structure of $\mathbf{1}\supset H_2O$ contains channels (filled by water molecules) with dimensions of 5×5 Å^2 that run along the *a* direction. The distance between the nitrogen atoms of adjacent pyrazine ligands along the *a* direction is 7.04 Å.

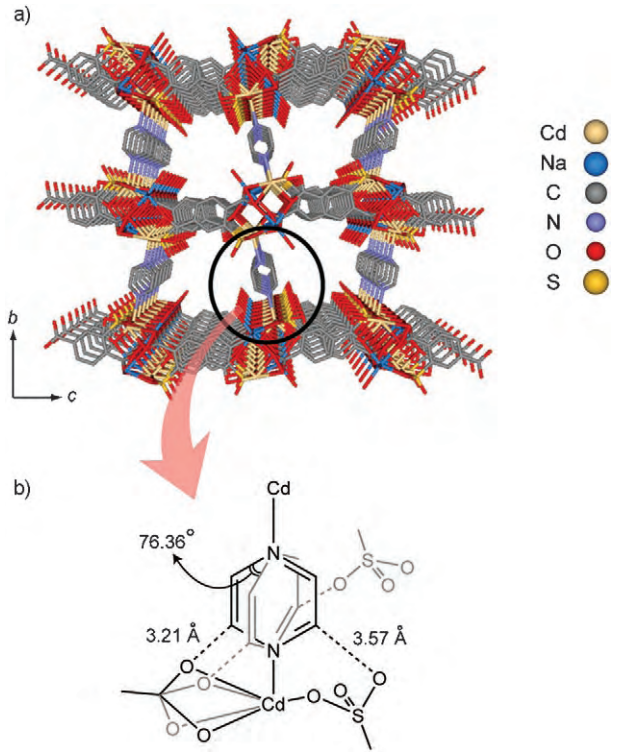

Figure 1. Crystal structure of $\mathbf{1}\supset H_2O$ at 223 K. a) The pillared layer structure viewed down the *a* direction. Hydrogen atoms and guest water molecules are omitted. b) Illustration of the disorder of a pyrazine molecule (circled in (a)) and a 2-sulfoterephthalate ion around a Cd^{2+} center. Dashed lines indicate C–H···O interactions.

The pyrazine molecule and the 2-sulfoterephthalate ion are disordered over two conformations, each with an occupancy of 0.5 (Figure 1b). In each conformation, two C–H···O interactions[8,9] occur between the pyrazine ring and oxygen atoms from one carboxylate group (3.21 Å) and the sufonate group (3.57 Å) of the 2-sulfoterephthalate ion. The dihedral angle between the planes of the pyrazine rings in the two conformations is 76.36°. Thus, the pyrazine pillars are isolated enough from the rest of the framework to rotate about their N–N axes.

For solid-state ^{2}H NMR spectroscopy experiments, partially deuterated $\mathbf{1}\supset H_2O$, $\{[CdNa(2\text{-stp})([D_4]pyz)_{0.5}(H_2O)](H_2O)\}_n$ ($\mathbf{1d}\supset H_2O$) was synthesized by using [D$_4$]pyrazine in the procedure described above. The powder X-ray diffraction (XRD) patterns of $\mathbf{1}\supset H_2O$ and $\mathbf{1d}\supset H_2O$ both match the powder XRD pattern simulated from the single-crystal structure of $\mathbf{1}\supset H_2O$ (see Supporting Information). This result demonstrates that the topology of the framework in $\mathbf{1d}\supset H_2O$ is identical to that in $\mathbf{1}\supset H_2O$.

To study the dynamics of the empty framework, we dried $\mathbf{1d}\supset H_2O$ under reduced pressure at 323 K for 12 h to remove guest water molecules. The ^{2}H NMR spectra of anhydrous **1d** recorded at 193–293 K are displayed in Figure 2a. The line shape changes significantly with temperature. At 293 K, a splitting of 21 kHz is observed. At 193 K, the experimental spectrum is axially symmetric, with a splitting of 123 kHz between opposite edges, which agrees with the quadrupole coupling constant observed for a pyrazine ring in a rigid lattice.[10] To explain the changes in line shape, spectral simulations were carried out by describing the motion of the pyrazine ring as a four-site jump between orientations at angles of 0, 76.4, 180, and 256.4° about the N–N axis (chosen based on the disordered structure of $\mathbf{1}\supset H_2O$) at a single jump frequency (Figure 2c). The population of each site was defined as 0.25. The simulated spectra (Figure 2b) are in good agreement with the observed spectra over the temperature range studied, confirming the validity of this rotation model. The ring undergoes jumps at a rate of 2.0×10^4 s^{-1} at 193 K and at a rate of 1.0×10^5 s^{-1} at 293 K. A pre-exponential factor of 2.4×10^6 s^{-1} and an activation energy of 7.7 kJ mol^{-1} for the four-site jump motion were determined from an Arrhenius plot (see Supporting Information). The activation energy is quite small and is nearly identical to the C–H···O bond energy reported previously.[9,11]

We also analyzed the dynamics of as-synthesized $\mathbf{1d}\supset H_2O$, in which the pores are filled with guest water molecules. The mobility is identical that of anhydrous **1d** over the same temperature range. This result suggests that the potential barrier for rotation of the pyrazine pillars in **1d** is too small for guest sorption to interrupt the rotation.

Therefore, to make a guest-responsive dynamic framework, we prepared a PCP containing bulkier rotational groups, $[Zn_2(1,4\text{-ndc})_2(dabco)]_n$ (**2**; 1,4-ndc = 1,4-naphthalenedicarboxylate, dabco = 1,4-diazabicyclo[2,2,2]octane).[12] In this framework, paddle-wheel Zn^{2+} dimers are linked by 1,4-naphthalenedicarboxylate ions, resulting in regular square-grid-type layers parallel to the *ab* plane, and these layers are

 © 2006 Wiley-VCH Verlag GmbH & Co. KGaA, Weinheim

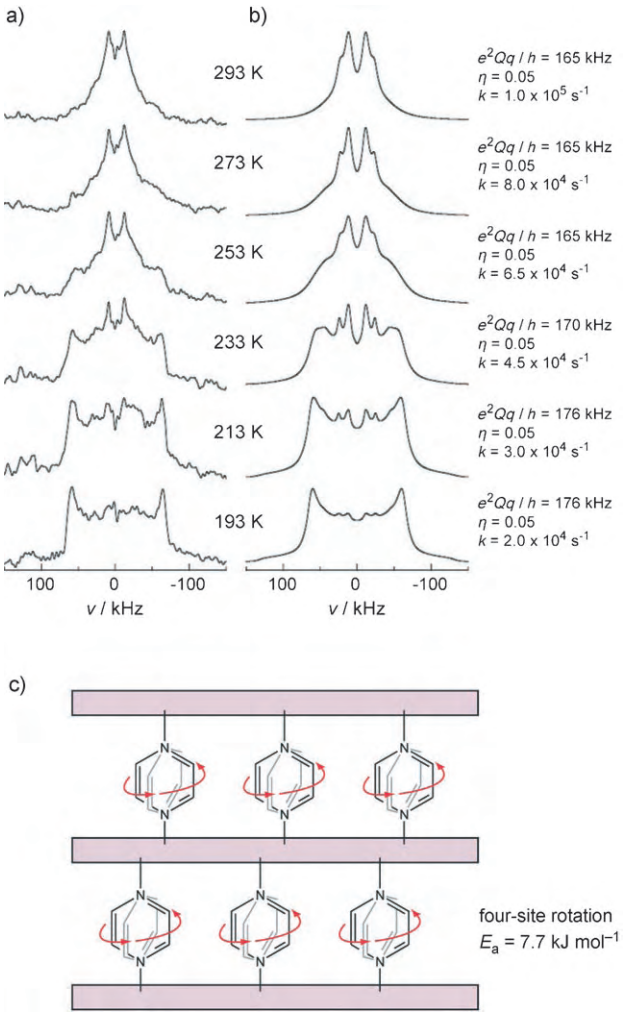

Figure 2. a) Experimental and b) simulated ^{2}H NMR spectra of **1d** at 193–293 K. The jump rates of the pyrazine rings (k), and the nuclear quadrupole coupling constants (e^2Qq/h) and asymmetry parameters (η) are indicated. c) Illustration of the four-site rotation of the pyrazine rings in **1**. The activation energy (E_a) is indicated.

pillared by 1,4-diazabicyclo[2,2,2]octane molecules (Figure 3a). Rectangular channels of 5.7×5.7 Å^2 run along the c direction. At 296 K, the naphthalene ring of the dicarboxylate ion is disordered over four positions (Figure 3b). Even though the naphthalene ring in **2** is larger than the pyrazine ring in **1**, there is enough void space in the framework of **2** for rotation about the C1–C4 axis of the naphthalene ring.

We synthesized partially deuterated **2** (**2d**) by using [D_6]1,4-naphthalenedicarboxylate and confirmed that the topology of the framework is identical to that of **2** by XRD (see Supporting Information). The ^{2}H NMR spectra for anhydrous **2d** at 193–293 K each consist of a superposition of three Pake doublets with different quadrupole coupling constants (see Supporting Information), which arise from the three types of deuterium atoms of the naphthalene ring. The spectra are temperature-dependent below 223 K, and we carried out simulations for the spectra recorded at 203–223 K. In these simulations, we modeled the motion of the naphthalene rings as a four-site flip between orientations at angles of

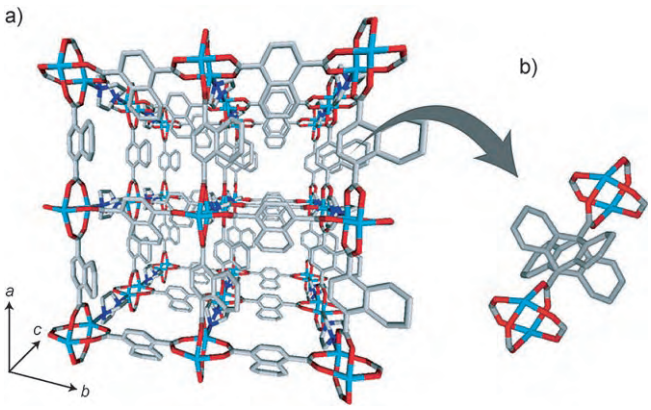

Figure 3. Crystal structure of **2** at 296 K.[12] a) The pillared layer structure viewed down the c direction. b) Four-site disorder of the naphthalene ring. Hydrogen atoms are omitted; Zn blue, C gray, O red, N dark blue.

0, 70, 180, and 250° about the C1–C4 axis (based on the disordered structure of **2**). Rotation rates ranging from 3.0×10^6 s^{-1} at 203 K to 5×10^7 s^{-1} at 223 K were determined from the fitting. Although the mode of motion in **2** is the same as that in **1**, the activation energy of 53 kJ mol^{-1} of **2**, determined from an Arrhenius plot, is approximately six times larger than that of **1**, because of differences in packing and in the size of the mobile group.

The sorption isotherm for benzene on **2** was measured at 298 K (see Supporting Information). The isotherm displays a Type I profile, indicative of a typical physisorption process for a microporous compound. The maximum amount of benzene adsorbed is only 3 molecules per pore (100 mL g^{-1}). Considering the van der Waals volume of the benzene molecule (ca. 89 Å^3),[13] the volume occupied by the benzene molecules in the pore is $3 \times 89 = 267$ Å^3. However, the total volume of the potential solvent area in the disordered structure of **2** is 195 Å^3 per pore, as calculated using the PLATON program.[14] This value is smaller than the volume of 3 benzene molecules, suggesting that the molecules are densely adsorbed inside the pores. Thus, the benzene molecules could interfere with the free rotation of the naphthalene rings about their C1–C4 axes. The ^{2}H NMR spectra of **2d** after benzene adsorption (**2d**⊃C_6H_6) recorded at 193–293 K (see Supporting Information) are drastically different from those of anhydrous **2d**. Over the whole temperature range, peaks with a frequency separation of 126 kHz are observed. The associated rate of less than 10^3 s^{-1} corresponds to the slow-exchange or static limit. Thus, the rotational motion of **2d**⊃C_6H_6 is immediately decelerated by guest adsorption. After desorption of the benzene molecules, the four-site rotation of the naphthalene rings in **2d** restarts. Therefore, the rotational behavior is reversible by guest adsorption/desorption (Figure 4a).

Thermogravimetric analysis (TGA) of **2**⊃C_6H_6 shows a gradual weight loss corresponding to the loss of nearly 3 benzene molecules per pore (observed 24.1%, calculated 25.9%) over 25–150°C, without any clear steps (see Supporting Information). However, in the heating cycle of the DSC curve of **2**⊃C_6H_6 over 25–150°C, a sharp endothermic transition with an enthalpy of 4.32 kJ mol^{-1} is observed at

 © 2006 Wiley-VCH Verlag GmbH & Co. KGaA, Weinheim

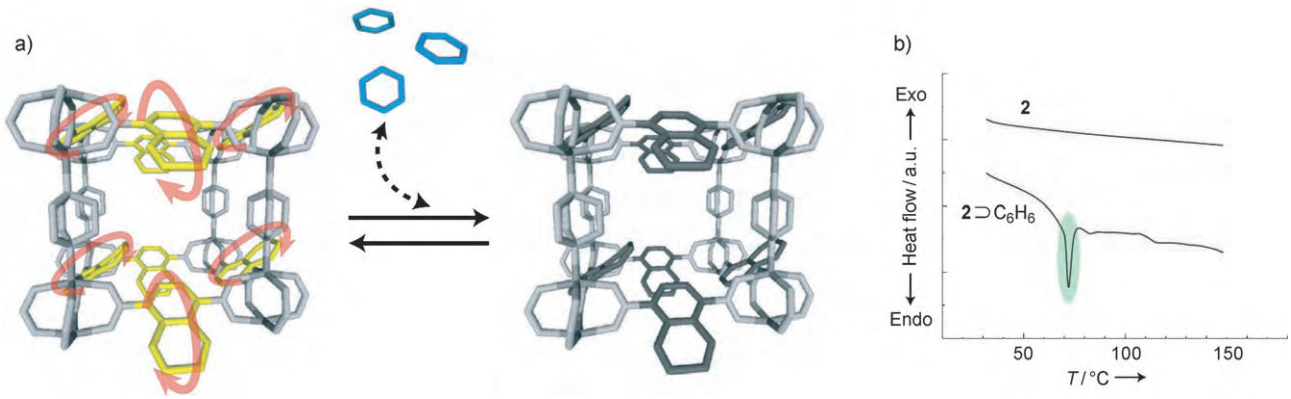

Figure 4. a) Illustration of the guest-induced reversible rotation in **2**. Benzene guests are blue; rotationally free naphthalene rings are yellow. b) DSC curves for **2** and **2**⊃C_6H_6 (scan rate of 5 K min^{-1}). The endothermic peak corresponding to the transition between the static and dynamic states of **2**⊃C_6H_6 is highlighted.

72 °C, in addition to the broad endothermic peak corresponding to the gradual desorption of benzene molecules (Figure 4b). The DSC profile of guest-free **2** shows no obvious peaks over the same temperature range. The difference between the profiles of **2**⊃C_6H_6 and **2** indicates that an abrupt change in network dynamics accompanies guest desorption. The enthalpy associated with the peak in the DSC curve of **2**⊃C_6H_6 corresponds to the enthalpy difference between the equilibrium static and dynamic states of the framework. Similar behavior was observed when acetone was used as a guest.

In conclusion, we have synthesized PCPs with rotational groups and have characterized their dynamic behavior by ^{2}H NMR spectroscopy and DSC. The designable open frameworks of PCPs can provide an organized arrangement of rotational groups in the solid state. This approach could allow the development of new types of functional crystalline solids with mobile groups for electro-optic or dielectric applications.

Experimental Section

1⊃H_2O. $Cd(NO_3)_2{\cdot}4H_2O$ (1.11 g, 3.6 mmol) in ethanol (60 mL) was slowly added to a water/ethanol (1:1) solution (120 mL) containing 2-sulfoterephthalate (0.97 g, 3.6 mmol), pyrazine (0.40 g, 3.6 mmol), and NaOH (0.29 g, 7.2 mmol). The white microcrystals obtained were collected by filtration, washed with ethanol, and dried under reduced pressure for 1 h. Elemental analysis (%) calcd for $C_{10}H_{11}NO_{10}NaSCd$: C 25.41, H 2.35, N 2.96; found: C 25.55, H 2.69, N 2.91.

Physical measurements: Powder XRD patterns were collected on a Rigaku RINT 2000 (Ultima) diffractometer using $Cu_{K\alpha}$ radiation. TGA was carried out in a nitrogen atmosphere with a Rigaku ThermoPlus TG 8120 instrument. Elemental analysis was performed with a Thermo Finnigan EA1112 instrument. DSC was performed with a Mettler DSC822e calorimeter. The sorption isotherm of benzene (in the gaseous state) at 298 K was measured using BELSORP18-Plus volumetric adsorption equipment (BEL Japan). Solid-state ^{2}H NMR spectra were recorded on a Varian Chemagnetics CMX-300 spectrometer operated at 45.826 MHz, by using a quadrupole pulse sequence. Simulated spectra were produced with FORTRAN programs written by us.

X-ray structure determination: XRD data for a single crystal were collected on a Rigaku Mercury CCD system with $Mo_{K\alpha}$ radiation. The structure was solved by direct methods (SIR97) and refined on F^2 (SHELXL-97). Non-hydrogen atoms, except for disordered coordinated water molecules and guest molecules, were refined anisotropically. All hydrogen atoms were placed geometrically and refined with a riding model (with U_{iso} constrained to be 1.2 times U_{eq} of the carrier atom). Crystal data for **1**⊃H_2O: $C_{10}H_3NO_{10}SCdNa$, $M_r = 464.58$, $0.20 \times 0.05 \times 0.05$ mm^3, orthorhombic, *Cmca*, $a = 7.038(5)$, $b = 23.12(3)$ Å, $c = 20.675(12)$ Å, $V = 3363(6)$ Å^3, $Z = 8$, $\rho_{calcd} = 1.835$ g cm^{-3}, $\lambda(Mo_{K\alpha}) = 0.71070$ Å, $T = 223$ K, $2\theta_{max} = 50.0°$, 15089 reflections collected, 1622 unique ($R_{int} = 0.0401$), 147 parameters, $R = 0.0646$ ($I > 2\sigma(I)$), $R_w = 0.1886$ ($I > 2\sigma(I)$), GOF = 1.232. CCDC-615500 contains the supplementary crystallographic data for this paper. These data can be obtained free of charge from The Cambridge Crystallographic Data Centre via www.ccdc.cam.ac.uk/data_request/cif.

Received: August 7, 2006
Published online: October 2, 2006

Keywords: cadmium · coordination polymers · metal–organic frameworks · molecular dynamics · NMR spectroscopy

[1] a) C. Janiak, *Dalton Trans.* **2003**, 2781–2804; b) R. J. Hill, D. L. Long, N. R. Champness, P. Hubberstey, M. Schröder, *Acc. Chem. Res.* **2005**, *38*, 335–348; c) B. Moulton, M. J. Zaworotko, *Chem. Rev.* **2001**, *101*, 1629–1658.

[2] a) D. Bradshaw, J. B. Claridge, E. J. Cussen, T. J. Prior, M. J. Rosseinsky, *Acc. Chem. Res.* **2005**, *38*, 273–282; b) C. J. Kepert, *Chem. Commun.* **2006**, 695–700; c) A. C. Sudik, A. R. Millward, N. W. Ockwig, A. P. Côté, J. Kim, O. M. Yaghi, *J. Am. Chem. Soc.* **2005**, *127*, 7110–7118; d) X. C. Huang, Y. Y. Lin, J. P. Zhang, X. M. Chen, *Angew. Chem.* **2006**, *118*, 1587–1589; *Angew. Chem. Int. Ed.* **2006**, *45*, 1557–1559; e) G. Férey, C. Mellot-Draznieks, C. Serre, F. Millange, J. Dutour, S. Surblé, I. Margiolaki, *Science* **2005**, *309*, 2040–2042; f) S. Kitagawa, R. Kitaura, S. Noro, *Angew. Chem.* **2004**, *116*, 2388–2430; *Angew. Chem. Int. Ed.* **2004**, *43*, 2334–2375.

[3] a) E. Y. Lee, S. Y. Jang, M. P. Suh, *J. Am. Chem. Soc.* **2005**, *127*, 6374–6381; b) R. Kitaura, K. Seki, G. Akiyama, S. Kitagawa, *Angew. Chem.* **2003**, *115*, 444–447; *Angew. Chem. Int. Ed.* **2003**, *42*, 428–431; c) R. Kitaura, K. Fujimoto, S. Noro, M. Kondo, S. Kitagawa, *Angew. Chem.* **2002**, *114*, 141–143; *Angew. Chem. Int. Ed.* **2002**, *41*, 133–135.

[4] a) G. S. Kottas, L. I. Clarke, D. Horinek, J. Michl, *Chem. Rev.* **2005**, *105*, 1281–1376; b) T.-A. V. Khuong, G. Zepeda, R. Ruiz, S. I. Khan, M. A. Garcia-Garibay, *Cryst. Growth Des.* **2004**, *4*, 15–18; c) Z. Dominguez, H. Dang, M. J. Strouse, M. A. Garcia-Garibay, *J. Am. Chem. Soc.* **2002**, *124*, 7719–7727; d) T. Shima, F. Hampel, J. Gladysz, *Angew. Chem.* **2004**, *116*, 5653–5656;

 © 2006 Wiley-VCH Verlag GmbH & Co. KGaA, Weinheim

Angew. Chem. Int. Ed. **2004**, *43*, 5537 – 5540; e) T. Akutagawa, K. Shitagami, S. Nishihara, S. Takeda, T. Hasegawa, T. Nakamura, Y. Hosokoshi, K. Inoue, S. Ikeuchi, Y. Miyazaki, K. Saito, *J. Am. Chem. Soc.* **2005**, *127*, 4397 – 4402.
[5] C. E. Godinez, G. Zepeda, C. J. Mortko, H. Dang, M. A. Garcia-Garibay, *J. Org. Chem.* **2004**, *69*, 1652 – 1662.
[6] a) V. A. Russell, C. C. Evans, W. Li, M. D. Ward, *Science* **1997**, *276*, 575 – 579; b) M. Kondo, T. Okubo, A. Asami, S. Noro, T. Yoshitomi, S. Kitagawa, T. Ishii, H. Matsuzaka, K. Seki, *Angew. Chem.* **1999**, *111*, 190 – 193; *Angew. Chem. Int. Ed.* **1999**, *38*, 140 – 143.
[7] S. Horike, R. Matsuda, D. Tanaka, M. Mizuno, K. Endo, S. Kitagawa, *J. Am. Chem. Soc.* **2006**, *128*, 4222 – 4223.
[8] Z. S. Derewenda, L. Lee, U. Derewenda, *J. Mol. Biol.* **1995**, *252*, 248 – 262.
[9] G. Desiraju, *Acc. Chem. Res.* **1996**, *29*, 441 – 449.
[10] M. Bach-Vergés, S. J. Kitchin, G. B. Hix, K. D. M. Harris, A. E. Aliev, *Chem. Mater.* **2002**, *14*, 2656 – 2663.
[11] T. Steiner, *J. Phys. Chem. A* **2000**, *104*, 433 – 435; P. Seiler, J. D. Dunitz, *Helv. Chim. Acta* **1989**, *72*, 1125 – 1135.
[12] H. Chun, D. N. Dybtsev, H. Kim, K. Kim, *Chem. Eur. J.* **2005**, *11*, 3521 – 3529.
[13] a) C. E. Webster, R. S. Drago, M. C. Zerner, *J. Am. Chem. Soc.* **1998**, *120*, 5509 – 5516; b) H. B. Cui, K. Takahashi, Y. Kano, H. Kobayashi, Z. M. Wang, A. Kobayashi, *Angew. Chem.* **2005**, *117*, 6666 – 6670; *Angew. Chem. Int. Ed.* **2005**, *44*, 6508 – 6512.
[14] A. L. Spek, *J. Appl. Crystallogr.* **2003**, *36*, 7 – 13.

 © 2006 Wiley-VCH Verlag GmbH & Co. KGaA, Weinheim

Asymmetric Catalysis

DOI: 10.1002/anie.200603496

A Highly Efficient and Practical Method for Catalytic Asymmetric Vinylogous Mannich (AVM) Reactions**

Emma L. Carswell, Marc L. Snapper, and Amir H. Hoveyda**

Stereoselective vinylogous Mannich reactions[1] are of significant utility in organic synthesis.[2] Through diastereoselective addition of vinylogous enol equivalents to enantiomerically enriched imines, α,β-unsaturated, δ-amino carbonyls have been synthesized and used as chiral building blocks. A catalytic asymmetric vinylogous Mannich (AVM) process would constitute a more efficient strategy, one that does not require pre-existing chirality.[3] As illustrated in Equation (1)

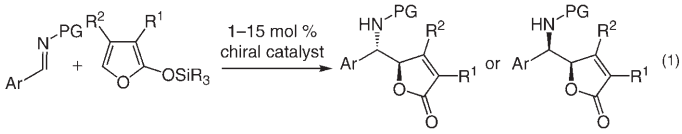

(1)

(PG = protecting group), a catalytic AVM involving a siloxyfuran can deliver synthetically versatile, enantiomerically enriched products that bear two stereogenic centers appended to a γ-butenolide.

In 1999, Martin and Lopez reported a method (Ti-catalyzed) for addition of siloxyfurans to 2-aminophenol-derived imines; reactions proceeded in 40–92% *de* but in only up to 54% *ee*.[4] Terada and co-workers have outlined an enantioselective (up to 97% *ee*) protocol for Brønsted acid catalyzed Friedel–Crafts reactions of *N*-Boc aldimines with 2-methoxyfuran. Enantiomerically enriched furan-2-ylamines may be oxidized to afford alkylamine-substituted γ-butenolides [Eq. (1)] by a two-step sequence that generates the carbinol stereogenic center with moderate diastereoselectivity (70% *de*).[5]

Herein we report the first highly diastereo- and enantioselective protocol for catalytic AVM reactions. Ag-catalyzed transformations[6] proceed in >98% *de*, in 79 to >98% *ee* and 60–98% isolated yield. The catalytic method is practical: transformations are carried out in air with undistilled solvent and undistilled additive, in the presence of 1–15 mol% commercially available AgOAc (not purified) and an easily accessible chiral phosphine (three steps, 50% yield). Siloxyfurans are commercially available and/or readily prepared (one step, 90% yield).

As the data summarized in entry 1 of Table 1 illustrate, in the presence of 1 mol% **1a**,[6b–d] 1 mol% AgOAc, 1.1 equivalents *i*PrOH, in undistilled THF and in air, reaction of aldimine **2a** and commercial siloxyfuran **3** affords γ-butenolide **4a** in >98% *de*, 95% *ee*,[7] and 82% yield. When **1b**, bearing a *t*Leu (vs. *i*Leu) unit (entry 2) or ligand **1c**, containing the less expensive Val (entry 3) is used, similar reactivity and selectivity is observed.[8] The efficient reaction with **3** is especially noteworthy and was somewhat surprising, since we had previously established that silylketene acetals do not participate (<2% conv.) in this class of catalytic Mannich reactions.[6d] It is likely that this change in reactivity, in spite of somewhat lower nucleophilicity of siloxyfurans (vs. ketene acetals)[9] is the result of reduced steric hinderance at the reacting carbon. As represented by catalytic AVM in entries 4–5 (Table 1), one of the chiral phosphines (**1a**, **1b**, or **1c**) can deliver slightly higher efficiency (90% vs. 85% conv.) and enantioselectivity (97% vs. 93% *ee*); others are shown in entries 12–13 and 15–16. Reactions proceed readily and with high enantioselectivity with electron-rich (entries 4–5 and 15–16) and electron-poor (entries 6–9 and 14) arylimines. Sterically demanding *ortho*-substituted aldimines, such as **2f** (entries 10–11), **2g** (entries 12–13), and **2h** (entry 14)

[*] E. L. Carswell, Prof. M. L. Snapper, Prof. A. H. Hoveyda
Department of Chemistry
Merkert Chemistry Center
Boston College
Chestnut Hill, MA 02467 (USA)
Fax: (+1) 617-552-1442
E-mail: marc.snapper@bc.edu
amir.hoveyda@bc.edu

[**] This work was generously supported by a grant from the United States NIH (GM-57212). We thank Dr. R. J. Staples and Mr. S. J. Malcolmson for X-ray determinations; X-ray facilities at Boston College are supported by Schering-Plough.

Supporting information for this article is available on the WWW under http://www.angewandte.org or from the author.

InterScience
© 2006 Wiley-VCH Verlag GmbH & Co. KGaA, Weinheim

Table 1: Ag-catalyzed AVM with siloxyfuran **3**.

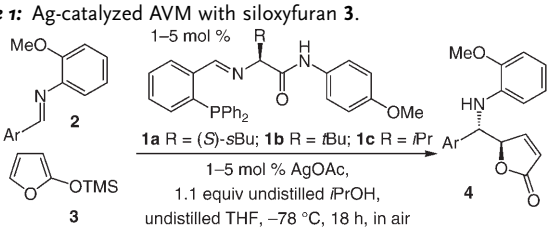

Entry	Ar		Ligand (mol%)	Conv. [%][a]	Yield [%][b]	*de* [%][b]	*ee* [%][c]
1	Ph	**a**	**1a** (1)	91	82	>98	95
2	Ph	**a**	**1b** (1)	94	82	>98	96
3	Ph	**a**	**1c** (1)	85	77	>98	92
4	*p*-MeOC$_6$H$_4$	**b**	**1a** (1)	85	76	>98	93
5	*p*-MeOC$_6$H$_4$	**b**	**1b** (1)	90	85	>98	97
6	*p*-NO$_2$C$_6$H$_4$	**c**	**1a** (1)	>98	98	>98	91
7	*p*-ClC$_6$H$_4$	**d**	**1a** (1)	94	89	>98	93
8	*p*-ClC$_6$H$_4$	**d**	**1c** (1)	98	86	>98	92
9	*m*-NO$_2$C$_6$H$_4$	**e**	**1a** (1)	94	75	>98	93
10	2-naphthyl	**f**	**1a** (1)	96	94	>98	98
11	2-naphthyl	**f**	**1b** (1)	>98	94	>98	>98
12	*o*-MeC$_6$H$_4$	**g**	**1a** (5)	86	73	>98	93
13	*o*-MeC$_6$H$_4$	**g**	**1b** (5)	73	65	>98	94
14	*o*-BrC$_6$H$_4$	**h**	**1a** (3)	89	60	>98	93
15	2-furyl	**i**	**1a** (1)	98	77	>98	84
16	2-furyl	**i**	**1b** (1)	98	78	>98	90

[a] Determined by analysis of 400-MHz ^{1}H NMR spectra. [b] Isolated yields of purified products. [c] Determined by chiral HPLC analysis; see the Supporting Information for details.

can be used; higher catalyst loadings, however, may be required (3–5 vs. 1 mol%). The presence of *i*PrOH as an additive is required for high conversions,[10] particularly with larger-scale processes where adventitious moisture is less available (H_2O is an effective additive[11]).

Reactions of 4-Me-substituted **5**, prepared from the commercially available lactone precursor (TMSOTf, Et_3N, 0°C; 90% yield; TMS = $SiMe_3$, OTf = OSO_2CF_3) have been examined. As the data in Table 2 indicate, with 5 mol% **1a** and AgOAc, **6a–b**, **6d**, **6h**, and **6j** are obtained in >98% *de*, 64–97% yield, and 83–90% *ee*.[12] Phosphine **1c**, bearing the less expensive Val moiety, can be used, but products are obtained in slightly lower selectivities (e.g., 93% conv., 90% yield, 84% *ee* for **6a** in entry 1). Higher catalyst loadings are needed for synthetically useful conversions and yields (5 mol% vs. 1 mol% typically required for **3**).

Table 2: Ag-catalyzed AVM reactions with substituted siloxyfuran **5**.

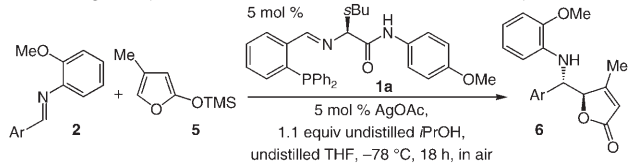

Entry	Ar		Conv. [%][a]	Yield [%][b]	*de* [%][a]	*ee* [%][c]
1	Ph	**a**	92	85	>98	87
2	*p*-MeOC$_6$H$_4$	**b**	80	70	>98	83
3	*p*-ClC$_6$H$_4$	**d**	>98	97	>98	90
4	*o*-BrC$_6$H$_4$	**h**	98	64	>98	89
5	*p*-BrC$_6$H$_4$	**j**	>98	90	>98	88

[a]–[c] See Table 1.

Catalytic AVM of 3-substituted siloxyfuran **7** (Table 3) proved more complicated, requiring identification of a new optimal chiral ligand. Catalytic AVM of **7** and **2a** with **1a** or **1b** (5 mol% loading, −78°C, 18 h) resulted in diastereoselective (>98% *de*) but inefficient transformations (25% and 34% conv., respectively); furthermore, enantioselectivity was disappointingly low (35% and 23% *ee*, respectively). Examination of alternative chiral ligands was thus performed, leading us to discover that **1d**, bearing a Thr(*t*Bu) residue, delivers the AVM product in 79% *ee* (48% conv.). Subsequent optimization led us to establish that at −60°C, **8a** is obtained in >98% *de*, 85% *ee*, and 70% yield. Ag-catalyzed AVM of **7** with electron-rich **2b** and electron-poor **2d** and **2h** gives **8b**, **8d**, and **8h** in 66–82% isolated yield and 79–88% *ee* (entries 2–4, Table 3). Two additional points merit mention: 1) Ligand **1d** is ineffective for reactions of **3** or **5**. For example, with 3 mol% **1d** (−78°C), formation of **6a** (entry 1, Table 2) proceeds to 91% conversion but in <5% *ee*. 2) In contrast to catalytic AVM of **3** (Table 1) and **5** (Table 2), with 3-substituted **7**, it is the *syn* diastereomer that is formed exclusively (Table 3). Determination of the absolute stereochemistry of **8**[13] indicates that the opposite aldimine enantioface undergoes addition.

Table 3: Ag-catalyzed AVM reactions with substituted siloxyfuran **7**.

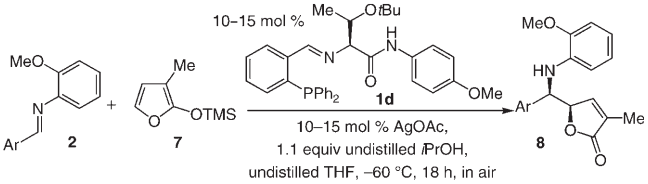

Entry	Ar		Mol%	Conv. [%][a]	Yield [%][b]	*de* [%][a]	*ee* [%][c]
1	Ph	**a**	10	88	70	>98	85
2	*p*-MeOC$_6$H$_4$	**b**	15	71	66	>98	88
3	*p*-ClC$_6$H$_4$	**d**	10	93	82	>98	83
4	*o*-BrC$_6$H$_4$	**h**	10	>98	65	>98	79

[a]–[c] See Table 1.

Preliminary mechanistic models are shown in Scheme 1. The Lewis acidic[14] chiral complex may associate with the aldimine substrate through bidentate chelation (cf. **I**, Scheme 1). In the activated complex, to minimize steric interactions, the substrate is bound *anti* to the bulky amino acid substituent (R). The catalyst-bound imine may react with the siloxyfuran by an *endo*-type addition (**I**)[15] to generate **II**.[16] Intramolecular desilylation by the Lewis basic amide terminus of the chiral ligand delivers **III**. Product release is facilitated by *i*PrOH by desilylation of the amide terminus and protonation of the N–Ag bond. Such a pathway should be unfavorable for siloxyfuran **7** because of steric repulsion in the catalyst-bound imine (**V**). Thus, in reactions involving **7**, the *exo*-type mode of addition **VI** may be favored, leading to **8** (Table 3). Additions of **7** may be more sluggish because of a transition structure that requires positioning of the imine's

 © 2006 Wiley-VCH Verlag GmbH & Co. KGaA, Weinheim

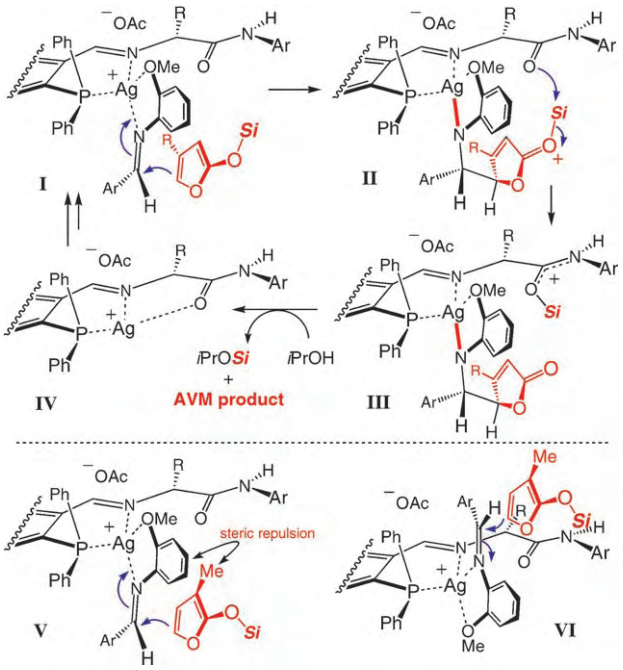

Scheme 1. Mechanistic models. ***Si*** = trimethylsilyl group.

aryl group and the siloxyfuran in the proximity of the amino acid substituent (R).[17] The origin of the dependence of specific catalyst classes for reactions of particular siloxyfurans (e.g., inefficiency of **1a** for AVMs of **7** or of **1d** for additions of **5**) is unclear.

The above hypotheses suggest that C-terminal amide Lewis basicity is critical to reactivity and enantioselectivity of catalytic AVM reactions; this is supported by the data in Table 4. In contrast to the AVM of **2a** and **3** promoted by **1a** (>98% conv., 94% *ee*), the ligand bearing a *p*-trifluoromethylaniline amide (**9**; entry 2, Table 4) gives 55% conversion into **4a** in 85% *ee*. Ligand **10** (entry 3), with an *n*-butylamide terminus, is equally active (>98% conv.) but initiates a less enantioselective AVM (87% vs. 94% *ee* with **1a**). The less Lewis basic methyl ester of **11** (entry 4) is less effective (70% conv.) than **1a** and delivers nearly racemic **4a** (−13% *ee*). The amide moiety might prolong catalyst longevity by providing stabilization of cationic Ag complexes (e.g., **IV**). Moreover, amide termini can stabilize intermediates (e.g., **III**, Scheme 1), which contain a positively charged C terminus. The lower activity of electron-rich phosphine **12** (entry 5) points to the importance of a Lewis acidic phosphine·Ag complex.

Anisidyl groups are removed by a one-pot procedure with $PhI(OAc)_2$ (commercial, used directly).[18] Synthetically versatile derivatives, such as amine **13** and Cbz amide **14**, can be obtained in >98% *de* (Scheme 2). Conversion into enantiomerically enriched **15** (Scheme 2) illustrates one of several functionalization possibilities that the butenolide moiety offers.

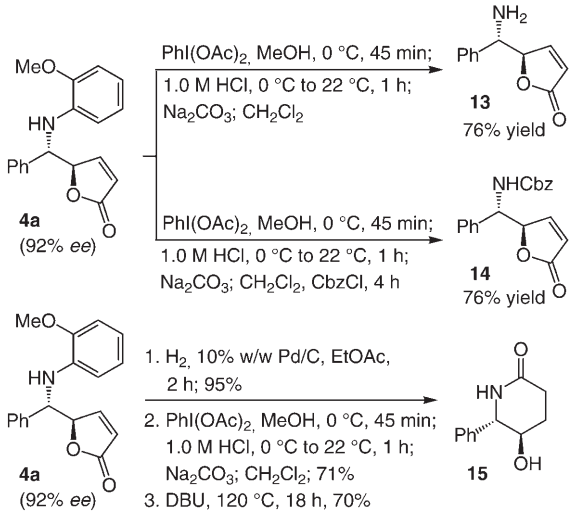

Scheme 2. Functionalizations of catalytic AVM products. Cbz = benzyloxycarbonyl; DBU = 1,8-diazabicyclo[5.4.0]undec-7-ene.

The present catalytic asymmetric protocol is exceptionally practical. As shown in Equation (2), Ag-catalyzed AVM and unmasking of the enantiomerically enriched amine can be carried out efficiently on a multigram scale with only 1 mol% catalyst loading.

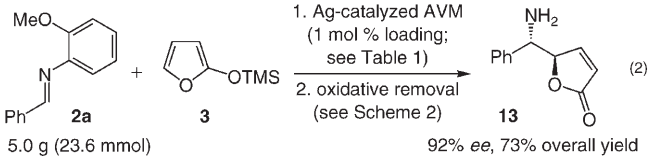

Applications to reactions of enolizable aldimines[19] and mechanistic studies are in progress.

Table 4: Effect of ligand structure on efficiency of catalytic AVM.

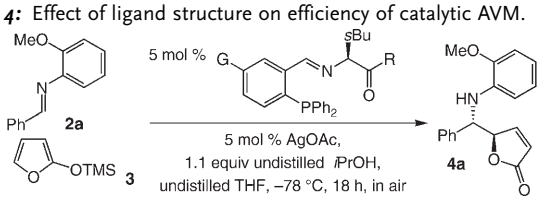

Entry	G	R	Ligand	Conv. [%][a]	*de* [%][a]	*ee* [%][b]
1	H	N(H)-*p*-$MeOC_6H_4$	**1a**	>98	>98	94
2	H	N(H)-*p*-$CF_3C_6H_4$	**9**	55	>98	85
3	H	N(H)*n*Bu	**10**	>98	>98	87
4	H	OMe	**11**	70	>98	−13
5	OMe	N(H)-*p*-$MeOC_6H_4$	**12**	86	>98	82

[a] Determined by analysis of 400-MHz ^{1}H NMR spectra of unpurified products. [b] Determined by chiral HPLC analysis; see the Supporting Information for details.

Received: August 26, 2006
Published online: October 16, 2006

Keywords: asymmetric catalysis · enantioselective synthesis · imines · silver · vinylogous Mannich reactions

 © 2006 Wiley-VCH Verlag GmbH & Co. KGaA, Weinheim

[1] For reviews on utility of stereoselective vinylogous Mannich reactions, see: a) G. Casiraghi, F. Zanardi, G. Appendino, G. Rassu, *Chem. Rev.* **2000**, *100*, 1929 – 1972; b) S. F. Martin, *Acc. Chem. Res.* **2002**, *35*, 895 – 904.

[2] For example, see: a) S. F. Martin, S. Liras, *J. Am. Chem. Soc.* **1993**, *115*, 10450 – 10451; b) S. Liras, C. L. Lynch, A. M. Fryer, B. T. Vu, S. F. Martin, *J. Am. Chem. Soc.* **2001**, *123*, 5918 – 5924; c) M. V. Spanedda, M. Ourévitch, B. Crousse, J.-P. Bégué, D. Bonnet-Delopn, *Tetrahedron Lett.* **2004**, *45*, 5023 – 5025.

[3] For a review of Mannich reactions, see: a) A. Córdova, *Acc. Chem. Res.* **2004**, *37*, 102 – 112; for select recent reports of catalytic asymmetric Mannich reactions (not AVM), see: b) T. Hamada, K. Manabe, S. Kobayashi, *J. Am. Chem. Soc.* **2004**, *126*, 7768 – 7769; c) S. Matsunaga, T. Yoshida, H. Morimoto, N. Kumagai, M. Shibasaki, *J. Am. Chem. Soc.* **2004**, *126*, 8777 – 8785; d) Y. Hamashima, N. Sasamoto, D. Hotta, H. Somei, N. Umebayashi, M. Sodeoka, *Angew. Chem.* **2005**, *117*, 1549 – 1553; *Angew. Chem. Int. Ed.* **2005**, *44*, 1525 – 1529; e) P. G. Cozzi, E. Rivalta, *Angew. Chem.* **2005**, *117*, 3666 – 3669; *Angew. Chem. Int. Ed.* **2005**, *44*, 3600 – 3603; f) J. Song, Y. Wang, L. Deng, *J. Am. Chem. Soc.* **2006**, *128*, 6048 – 6049; g) Y. Chi, S. H. Gellman, *J. Am. Chem. Soc.* **2006**, *128*, 6804 – 6805.

[4] S. F. Martin, O. D. Lopez, *Tetrahedron Lett.* **1999**, *40*, 8949 – 8953.

[5] D. Uraguchi, K. Sorimachi, M. Terada, *J. Am. Chem. Soc.* **2004**, *126*, 11804 – 11805.

[6] For related Ag-catalyzed Mannich-type reactions (not AVM), see: a) D. Ferraris, B. Young, T. Dudding, T. Lectka, *J. Am. Chem. Soc.* **1998**, *120*, 4548 – 4549; b) N. S. Josephsohn, M. L. Snapper, A. H. Hoveyda, *J. Am. Chem. Soc.* **2003**, *125*, 4018 – 4019; c) N. S. Josephsohn, M. L. Snapper, A. H. Hoveyda, *J. Am. Chem. Soc.* **2004**, *126*, 3734 – 3735; d) N. S. Josephsohn, E. L. Carswell, M. L. Snapper, A. H. Hoveyda, *Org. Lett.* **2005**, *7*, 2711 – 2713.

[7] For determination of relative and absolute stereochemical identity of AVM products from reactions of **3**, see the Supporting Information.

[8] See the Supporting Information for all data.

[9] For relative p nucleophilicity of various enol silanes, see: H. Mayr, B. Kempf, A. R. Ofial, *Acc. Chem. Res.* **2003**, *36*, 66 – 77.

[10] For a similar effect in Cr-catalyzed enantioselective aldol additions of siloxyfurans to aldehydes, see: S. Onitsuka, Y. Matsuoka, R. Irie, T. Katsuki, *Chem. Lett.* **2003**, *32*, 974 – 975.

[11] For example, when carried out on a 0.5-g (2.4-mmol) scale, AVM of **2a** and **3** proceeds to only 43% conversion (93% *ee*) in the absence of *i*PrOH (> 98% conv., 82% yield, 91% *ee* with 1.1 equiv of the alcohol additive). Ag-catalyzed AVM to afford **4a** proceeds to 97% conversion (87% yield) in 92% *ee* with 1.1 equivalents H_2O (conditions in Table 1).

[12] Relative and absolute stereochemical identity of products derived from **5** was established through an X-ray crystal structure of **6j** (entry 5, Table 2). See the Supporting Information for details.

[13] For relative and absolute stereochemical identity of products derived from **7**, see the Supporting Information.

[14] Preliminary data indicate that the chiral Ag complex likely serves as a Lewis acid catalyst (vs. Ag enolate). For example, there is ca. 30% conversion in the presence of 20 mol% of Et_3N (synthesis of **4a** with 1 mol% **1a**, −78 °C).

[15] Preference for *endo*-type ("Diels–Alder"-type) transition states has been suggested for diastereoselective (non-asymmetric) vinylogous Mannich reactions; see: S. K. Burr, S. F. Martin, *Org. Lett.* **2000**, *2*, 3445 – 3447.

[16] The C=N bond of chiral ligands do not undergo addition likely because of steric hinderance provided by the amino acid substituent.

[17] Pre-association of the amide moiety with the siloxyfuran is also feasible; such an interaction would enhance enolsilane nucleophilicity and facilitate delivery; see: a) S. E. Denmark, G. L. Beutner, T. Wynn, M. D. Eastgate, *J. Am. Chem. Soc.* **2005**, *127*, 3774 – 3789, and references therein; b) Y. Zhao, J. Rodrigo, A. H. Hoveyda, M. L. Snapper, *Nature* **2006**, *443*, 67 – 70.

[18] a) J. R. Porter, J. F. Traverse, A. H. Hoveyda, M. L. Snapper, *J. Am. Chem. Soc.* **2001**, *123*, 10409 – 10410; b) L. C. Akullian, M. L. Snapper, A. H. Hoveyda, *Angew. Chem.* **2003**, *115*, 4376 – 4379; Angew. *Chem. Int. Ed.* **2003**, *42*, 4244 – 4247.

[19] Preliminary results show that the present procedure is applicable to AVM of aldimines derived from aliphatic aldehydes.

 © 2006 Wiley-VCH Verlag GmbH & Co. KGaA, Weinheim

Actinide Chemistry

DOI: 10.1002/anie.200601207

$Na_2Li_8[(UO_2)_{11}O_{12}(WO_5)_2]$: Three Different Uranyl-Ion Coordination Geometries and Cation–Cation Interactions**

Evgeny V. Alekseev, Sergey V. Krivovichev, Wulf Depmeier, Oleg I. Siidra, Karsten Knorr, Evgeny V. Suleimanov, and Evgeny V. Chuprunov*

Synthetic and natural actinide compounds are of great environmental concern[1] and have also been of interest to materials scientists because of their unique electronic properties.[2] The structural chemistry of actinides is very diverse because of the possibility of different oxidation states and the large number of coordination geometries. Whereas actinides in low oxidation states sometimes mimic rare-earth elements, actinides in higher oxidation states possess unique coordination chemistry owing to their tendency to form linear actinyl

[*] Prof. Dr. S. V. Krivovichev, O. I. Siidra
Department of Crystallography
St.Petersburg State University
University Emb. 7/9, 199034 St. Petersburg (Russia)
Fax: (+43) 512-507-2926
E-mail: skrivovi@mail.ru

Dr. E. V. Alekseev, Prof. Dr. W. Depmeier, Dr. K. Knorr
Institut für Geowissenschaften
Universität Kiel
24118 Kiel (Germany)

Dr. E. V. Alekseev, Prof. Dr. E. V. Suleimanov,
Prof. Dr. E. V. Chuprunov
Nizhny Novgorod State University
603950 Nizhny Novgorod (Russia)

[**] This work was financially supported by a DFG research grant to W.D. (De412/30-1) and an Alexander von Humboldt Institutional Cooperation grant (to W.D. and S.V.K.). S.V.K. thanks the Russian Ministry of Science and Education for financial support (grants RNP 2.1.1.3077 and 02.442.11.7301). E.V.A. was supported in this work by a DAAD postdoctoral fellowship and the President of the Russian Federation program for young candidates of science (grant MK-1669.2005.2).

© 2006 Wiley-VCH Verlag GmbH & Co. KGaA, Weinheim

ions. The typical coordination geometries of the actinyl ions are octahedral, pentagonal bipyramidal, and hexagonal bipyramidal.[3] Herein we report the synthesis and structure of $Na_2Li_8[(UO_2)_{11}O_{12}(WO_5)_2]$ (**1**), the first actinide compound that contains three different actinyl-ion coordination geometries.

The orange crystals of **1** were obtained by high-temperature solid-state reactions of uranyl acetate, lithium and sodium carbonates, and tungsten(VI) oxide.[4] The structure solution[5] revealed elaborate 1.2-nm-thick layers with Na^+ and Li^+ ions within and in between these layers (Figure 1).

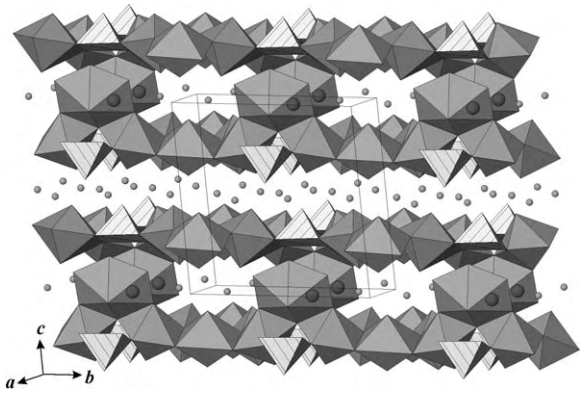

Figure 1. Crystal structure of **1**. U polyhedra gray; W polyhedra lined; Na^+ large circles; Li^+ small circles.

The layers have the composition $[(UO_2)_{11}O_{12}(WO_5)_2]^{10-}$ and consist of two equivalent sublayers (Figure 2) that are formed by edge-sharing $[UO_7]$ pentagonal bipyramids, $[UO_6]$ octahedra (see below), and $[WO_6]$ octahedra. The coordination polyhedra are arranged according to the β-U_3O_8 anion topology that has been recognized for many U^{VI} compounds. The sublayers are linked into double layers by the $[UO_2]^{2+}$ uranyl cations. The interior space of the layers is filled by the Na^+ and Li^+ ions. There are also Li^+ ions that are located in between the layers, thus providing three-dimensional integrity of the structure.

The coordination of the U atoms in **1** is of particular interest. There are six symmetry-independent U^{VI} centers.

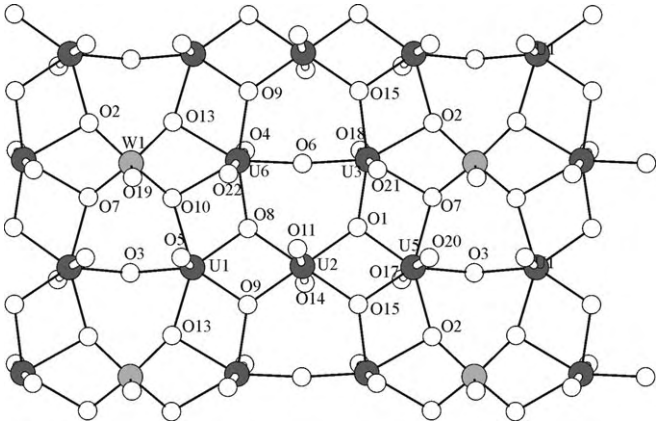

Figure 2. Structure of the uranyl tungstate sublayer in **1**.

Each U^{6+} cation is coordinated by two O atoms, thus forming linear $[O{=}U{=}O]^{2+}$ uranyl ions. The U=O bond lengths are in the range 1.813–1.868 Å. The uranyl cations of the U1, U3, U5, and U6 centers are coordinated in equatorial planes by five O atoms (O_{eq}) each, which results in the formation of $[UO_7]$ pentagonal bipyramids. The U–O_{eq} bond lengths in these polyhedra are in the range 2.162–2.518 Å, which indicates a quite high degree of coordinative distortion. The $[O{=}U2{=}O]^{2+}$ ion is coordinated by four O_{eq} atoms with U2–O_{eq} bond lengths ranging from 2.218 to 2.266 Å. The uranyl cation of the U4 atom is coordinated by six O atoms, which leads to a $[UO_8]$ hexagonal bipyramid. The U4–O_{eq} bonds can be clearly separated into two groups: two bonds with lengths of 2.230 Å, and four bonds with lengths of 2.632 to 2.679 Å. Thus, the structure of **1** contains all three coordination geometries of uranyl ions. To our knowledge, this has not been observed previously in uranyl compounds.

Another particular feature of the structure of **1** is the presence of strong cation–cation interactions between the uranyl ions. Cation–cation interactions were discovered by Sullivan et al. in 1961[6] and imply coordination of the actinide center of an actinyl ion $[AnO_2]^{n+}$ by the O atom of an adjacent actinyl ion. The cation–cation interactions are well-recognized in Np^V, Pu^V, and Am^V chemistry,[7] but are rather rare for U^{VI}.[8] In the structure of **1**, the $[U1\,O_2]^{2+}$, $[U4\,O_2]^{2+}$, and $[U5\,O_2]^{2+}$ ions interact with each other to form pentamers as shown in Figure 3. The central group of the pentamer is the

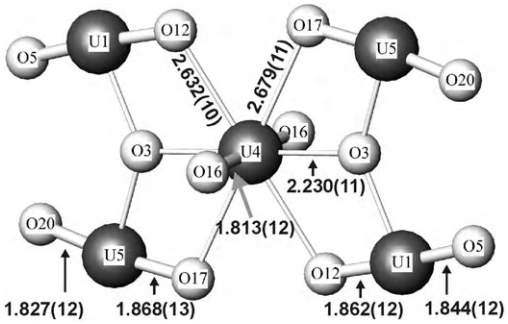

Figure 3. Pentamer of the uranyl ions UO_2^{2+} and cation–cation interactions in **1**.

U4 center, which has hexagonal bipyramidal geometry. The U=O bonds within this uranyl cation are 1.813 Å long. Further, the U4 atom has two short U4–O3 bonds (2.230 Å) and four U–O bonds to the O12 and O17 atoms, which are the parts of the $[U1\,O_2]^{2+}$ and $[U5\,O_2]^{2+}$ ions, respectively. These bonds are relatively long (2.632–2.679 Å) in comparison with the usual U–O_{eq} bond length within $[UO_8]$ hexagonal bipyramids (2.47 Å).[3] The U1=O12 and U5=O17 bonds are rather elongated (1.862 and 1.868 Å, respectively). Thus, the general geometrical configuration of the pentamer is rather unusual. The O16 atom of the $[O{=}U4{=}O]^{2+}$ ion also forms a rather long bond to the W atom of the uranyl tungstate sublayer (2.507 Å).

In conclusion, we note that the thickness of the $[(UO_2)_{11}O_{12}(WO_5)_2]^{10-}$ layer in **1** is about 1.2 nm, which, along with reports on similar uranyl compounds, makes it

 © 2006 Wiley-VCH Verlag GmbH & Co. KGaA, Weinheim

possible to suggest the occurence of further uranyl-based layered compounds formed by intercalation of additional uranyl cations in between single sheets of uranium and other high-valent cation polyhedra such as Mo^{VI} and W^{VI}.

Received: March 27, 2006
Published online: September 15, 2006

Keywords: actinides · coordination modes · structure elucidation · tungsten · uranium

[1] a) R. J. Finch, T. Murakami, *Rev. Mineral.* **1999**, *38*, 91; b) E. C. Buck, D. J. Wronkiewicz, P. A. Finn, J. K. Bates, *J. Nucl. Mater.* **1997**, *249*, 70; c) N. L. Misra, K. L. Chawla, V. Venugopal, N. C. Jayadevan, D. D. Sood, *J. Nucl. Mater.* **1995**, *226*, 120.

[2] a) P. C. Burns, K.-A. Hughes Kubatko, G. Sigmon, B. J. Fryer, J. E. Gagnon, M. R. Antonio, L. Soderholm, *Angew. Chem.* **2005**, *117*, 2173; *Angew. Chem. Int. Ed.* **2005**, *44*, 2135; b) S. V. Krivovichev, V. Kahlenberg, R. Kaindl, E. Mersdorf, I. G. Tananaev, B. F. Myasoedov, *Angew. Chem.* **2005**, *117*, 1158; *Angew. Chem. Int. Ed.* **2005**, *44*, 1134; c) S. V. Krivovichev, V. Kahlenberg, R. Kaindl, E. Mersdorf, I. G. Tananaev, B. F. Myasoedov, *J. Am. Chem. Soc.* **2005**, *127*, 1072; d) T. Albrecht-Schmitt, *Angew. Chem.* **2005**, *117*, 4914; *Angew. Chem. Int. Ed.* **2005**, *44*, 4836.

[3] P. C. Burns, M. L. Miller, R. C. Ewing, *Can. Mineral.* **1996**, *34*, 845; P. C. Burns, *Rev. Mineral.* **1999**, *38*, 23; P. M. Almond, T. E. Albrecht-Schmitt, *Inorg. Chem.* **2003**, *42*, 5693; P. C. Burns, *Can. Mineral.* **2005**, *43*, 1839.

[4] The synthesis of **1** was carried out using mixture of Li_2CO_3, Na_2CO_3, WO_3, and $UO_2(CH_3COO)_2(H_2O)_2$ in a ratio of 10:1:10:10. The mixture was heated to 950 °C at a rate of 60 °C h^{-1}, kept at 950 °C for 40 min, and then cooled down to 200 °C at a rate of 4 °C h^{-1}. Crystals of **1** grew in the melt of $Li_2(UO_2)_4(WO_4)_4$. Powder of **1** can be obtained by keeping a mixture of the same reagents in a ratio of 8:2:2:11 at 800 °C for 7 days. In the latter case, the reaction yield can be estimated as 80 %. Electron dispersive spectroscopy (EDS) analysis confirmed the presence of Na, U, and W. The infrared spectrum was collected within the range 350–1000 cm^{-1}. The band at 934 cm^{-1} can be assigned to the vibrations of the W=O bond; the bands at 808 and 840–870 cm^{-1} can be attributed to the symmetrical and asymmetrical vibrations of the UO_2^{2+} ion, respectively. The bands at 773, 676, 587, and 448 cm^{-1} can be interpreted as corresponding to the U-O-U and W-O-U bonds.

[5] Crystallographic data for $Li_8Na_2W_2U_{11}O_{44}$: plate-like crystal ($0.13 \times 0.13 \times 0.03$ mm^3), triclinic, $P\bar{1}$, $a = 6.946(2)$, $b = 11.207(3)$, $c = 12.054(5)$ Å, $\alpha = 99.525(17)$, $\beta = 106.21(2)$, $\gamma = 90.223(12)°$, $V = 887.4(5)$ $Å^3$, $Z = 1$, $\rho_{calcd} = 7.095$ g cm^{-3}, $2\theta_{max} = 60°$, λ-($Mo_{K\alpha}$) = 0.71073 Å, $\omega/2\theta$ scan (STOE STADI-4), 293 K, 10268 measured reflections, 5168 independent reflections, 3891 reflections with $|F_o| = 4\sigma_F$ ($R_{int} = 0.0542$, $R_\sigma = 0.0645$), structure solution by direct methods, full-matrix least-square refinement (176 parameters) on $|F^2|$, (programs SHELXS-97 (G. M. Sheldrick, program for crystal structure solution, Göttingen, **1997**) and SHELXL-97 (G. M. Sheldrick, program for the refinement of crystal structures, Göttingen, **1997**)), $R_1 = 0.0567$, $wR_2 = 0.1347$ for observed reflections, $R_1 = 0.0793$, $wR_2 = 0.1427$ for all data, max/min electron density = 6.60/−6.18. Further details on the crystal-structure investigations may be obtained from the Fachinformationszentrum Karlsruhe, 76344 Eggenstein-Leopoldshafen, Germany (fax: (+49) 7247-808-666; e-mail: crysdata@fiz-karlsruhe.de), on quoting the depository number CSD-416364.

[6] J. C. Sullivan, J. C. Hindman, A. J. Zielen, *J. Am. Chem. Soc.* **1961**, *83*, 3373.

[7] N. N. Krot, M. S. Grigoriev, *Russ. Chem. Rev.* **2004**, *73*, 89; T. E. Albrecht-Schmitt, P. M. Almond, R. E. Sykora, *Inorg. Chem.* **2003**, *42*, 3788.

[8] N. P. Brandenburg, B. O. Loopstra, *Acta Crystallogr. Sect. B* **1978**, *34*, 3734; S. Obbade, S. Yagoubi, C. Dion, M. Saadi, F. Abraham, *J. Solid State Chem.* **2004**, *177*, 1681; T. A. Sullens, R. A. Jensen, T. Y. Shvareva, T. E. Albrecht-Schmitt, *J. Am. Chem. Soc.* **2004**, *126*, 2676.

 © 2006 Wiley-VCH Verlag GmbH & Co. KGaA, Weinheim

Total Synthesis

DOI: 10.1002/anie.200601259

Total Synthesis of Tubulysin U and V**

Alexander Dömling, Barbara Beck, Uwe Eichelberger, Sukumar Sakamuri, Sanjay Menon, Quin-Zene Chen, Yingchun Lu, and Ludger A. Wessjohann**

In memory of Ivar Ugi

Tubulysins (**1**) are compounds of extraordinary potency, rapidly degrading the tubulin cytoskeleton, with tubulysin D being the most active tubulin-modifier known so far.[1,2] The tubulysins were first described by Höfle, Reichenbach, and co-workers in 2000.[3,4] Several representatives are active with GI_{50} values (growth inhibition of 50%) in the low picomolar range against the NCI-60 cancer cell-line panel, and some are highly antiangiogenic.[5] Semisynthetic tubulysins, derived from isolated material, show promising in vivo anticancer properties and are candidates for antibody conjugates. Thus, tubulysins are attractive leads as novel anticancer agents.[5] However, so far, tubulysins can only be produced by a fermentation process that yields less than 10 mg L^{-1} by several rather tedious chromatographic purification steps. Thus, and

[*] Priv.-Doz. Dr. A. Dömling, Dr. B. Beck
R&D Biopharmaceuticals GmbH
Am Klopferspitz 19a, 82152 Martinsried (Germany)
Fax: (+49) 89-7007-6499
E-mail: alexander.doemling@rdbiopharma.de
Dr. U. Eichelberger, Prof. L. A. Wessjohann
Leibniz-Institut für Pflanzenbiochemie
Abteilung für Natur- und Wirkstoffchemie
Weinberg 3, 06120 Halle (Germany)
Fax: (+49) 345-5582-1309
E-mail: wessjohann@ipb-halle.de
Dr. B. Beck, Dr. S. Sakamuri, Dr. S. Menon, Dr. Q.-Z. Chen, Dr. Y. Lu
Morphochem Inc.
11 Deer Park Drive, Suite 116, Monmouth Junction, NJ 08852 (USA)

[**] U.E. and L.A.W. acknowledge support from the State of Saxony-Anhalt as part of a HWP grant. We thank Dr. A. Porzel for special NMR analysis and Prof. G. Höfle for providing reference spectra and preliminary activity and isolation information.

Supporting information for this article is available on the WWW under http://www.angewandte.org or from the author.

© 2006 Wiley-VCH Verlag GmbH & Co. KGaA, Weinheim

in order to reveal the structure–activity relationship for these compounds, a total synthesis is highly desirable.

Tubulysins are structurally related to the marine natural product class of dolastatins and the anticancer drug LU 103793. Similar to dolastatins 10[6] and 15,[7] tubulysins are unusual peptides, mainly composed of the uncommon or hydrophobic amino acids *N*-methylpipecolic acid (Mep), isoleucine (Ile), tubuvaline (Tuv), and tubuphenylalanine (Tup) or tubutyrosine (Tut), with an N- to C-terminal distance of ≈18 Å, an aromatic amino acid at the C terminus, and a tertiary amino terminus. Two major series of tubulysins can be distinguished (Table 1). Those with labels from the beginning

Table 1: Selected members of the tubulysin family.[a] [8]

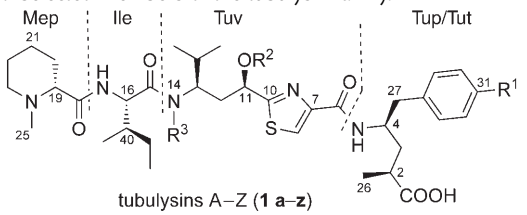

Tubulysin	R^1	R^2	R^3
A	OH	Ac	$CH_2O-(CO)-CH_2CH(CH_3)_2$
...			
D	H	Ac	$CH_2O-(CO)-CH_2CH(CH_3)_2$
E	H	Ac	$CH_2O-(CO)-CH_2CH_2CH_3$
F	H	Ac	$CH_2O-(CO)-CH_2CH_3$
G	H	Ac	$CH_2O-(CO)-CH_3$
...			
U	H	Ac	H
V	H	H	H
...			
Z	OH	H	H

[a] Mep = *N*-methylpipecolinic acid, Ile = isoleucine, Tuv = tubuvaline, Tup = tubuphenylalanine, Tut = tubutyrosine.

of the alphabet (for example, the tubulysin A or D series, with Tut or Tup, respectively) have both the Tuv hydroxy group (R^2) and an *N*,*O*-acetal involving the amide nitrogen atom of tubuvaline (R^3) acylated. The series with labels from later in the alphabet (for example, tubulysins U–Z) has these two functions partially or completely missing (Table 1).[9] Usually, this latter series is less active, but the members studied so far (tubulysins W–Z) reach the activity range of, for example, taxol or the epothilones.

Despite several attempts, no complete synthesis of a tubulysin has been described so far.[10,11] The total synthesis is challenging for several reasons. Only one amino acid of the tetrapeptide (Ile) occurs naturally as a separate compound. The central fragment, Tuv, constitutes a complex, thiazole-containing amino acid with two stereocenters. In the series labeled with earlier alphabet letters, the bis-acyl *N*,*O*-acetal at Tuv makes a total synthesis more difficult, since this functional group is not compatible with most protecting-group strategies. The C-terminal amino acid, Tup, constitutes a γ-amino acid comprising two stereocenters as well. Most importantly, the middle part of all tubulysins is sterically highly crowded, and peptide-bond formation often fails to properly connect either the Ile or Mep residues to the rest of the molecule.

Herein we report the first stereoselective total synthesis of two members of the tubulysin family. A retrosynthetic analysis of the "pentapeptidic" tubulysin U (**1u**, Scheme 1)

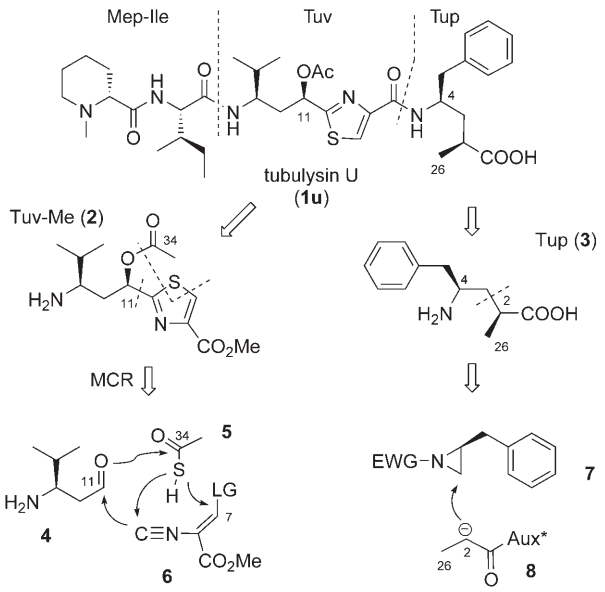

Scheme 1. Retrosynthesis of tubulysin U (**1u**). LG = leaving group, EWG = electron-withdrawing group, Aux* = chiral auxiliary, MCR = multicomponent reaction.

leads to the four amino acids Mep, Ile, Tuv, and Tup, of which Tuv is biosynthetically derived from valine, an acetate equivalent, and cysteine as a hidden fifth amino acid. For the chemical synthesis, we introduced two disconnections to yield three equally complex and large substructures. For the C-terminal moiety, the stereocontrolled alkylation of aziridine **7** by using a chiral auxiliary (such as **8**) appeared most useful. Tubuvaline, the complex-looking centerpiece of all tubulysins, resolves unexpectedly into a set of three easily available building blocks (**4**–**6**) if one considers a recently discovered thiazole synthesis,[12] an isonitrile-based multicomponent reaction (MCR) based on the multiple reactivity of Schöllkopf type isonitriles, **6**.[13] The N terminus contains the commercially available amino acids pipecolinic acid and Ile. When earlier attempts toward the synthesis of tubulysins are considered, the formation of the Ile–Tuv amide bond is expected to constitute the most severe problem. According to the established C- to N-terminus peptide-assembly routine, the successive coupling of Ile and Mep should be preferred, due to the lower propensity for racemization. However, coupling of a preformed Mep–Ile dipeptide is more convergent and may be more attractive if racemization is not an issue or if the central Ile–Tuv amide bond formation reaction gives only a low yield.

According to the retrosynthesis, tubuphenylalanine (**3**) is available from commercial (*S*)-*N*-Ts-2-benzylaziridine (**7a**; Ts = toluene-4-sulfonyl), by ring opening with a propanoyl anion under the control of pseudoephedrine as a chiral auxiliary connected to propionic acid, as in amide **10**

 © 2006 Wiley-VCH Verlag GmbH & Co. KGaA, Weinheim

(Scheme 2).[14,15] The desired *syn* diastereomer is formed in 70% relative yield and is separated from the minor *anti* isomer by chromatography. Amide hydrolysis and removal of the tosylate paves the way to Tup and its various protected

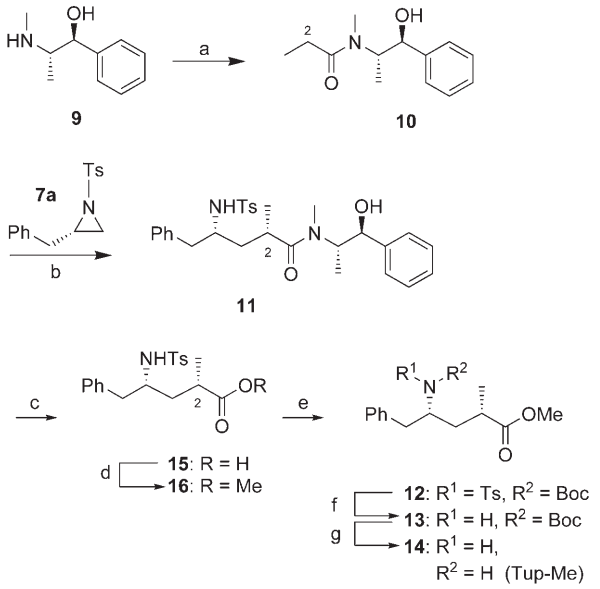

Scheme 2. Synthesis of differently protected tubuphenylalanine (Tup) derivatives by the pseudoephedrine route. a) Propionic anhydride, Et_3N, CH_2Cl_2, 93%; b) 1. LDA, LiCl, THF, −78°C; 2. (*S*)-(+)-2-benzyl-1-(toluene-4-sulfonyl)-aziridine, THF, −20°C, 86% (81:19 d.r. mixture of C-2 diastereomers, major isomer shown separated and processed further); c) 4 M H_2SO_4/dioxane, reflux, 91%; d) MeOH, conc. HCl, reflux, 85%; e) Boc_2O, DMAP, CH_3CN, 100%; f) Mg (powder), MeOH, ultrasound, 70%; g) 4 N HCl in dioxane, 100%. Boc = *tert*-butoxycarbonyl, DMAP = 4-dimethylaminopyridine, LDA = lithium diisopropylamide, THF = tetrahydrofuran.

forms **12**–**16**, of which the Tup methyl ester hydrochloride, **14**·HCl, was used for the further synthesis. Racemization was not observed. Several alternative routes to this building block, for example, the use of Evans methodology, were tried but did not lead to the product at all or gave lower yields and significantly lower *de* values (see also reference [3]).

Tubuvaline is available as its Boc-protected methyl ester **17** in a very straightforward one-pot process following a newly discovered three-component synthesis of 2-hydroxymethylthiazoles (Scheme 3).[12] Thus, Schöllkopf isonitrile (**6a**, available in one step from glycine isonitrile),[13] Boc-protected L-homovaline aldehyde (Boc-**4**),[16] and thioacetic acid (**5**) gave **17** in 40% yield, with a 3:1 ratio of diastereomers. These values constitute considerable improvements over both the first thiazole MCRs[12] and the alternative routes.[11] The major diastereomer shows the right configuration at C-11, as determined by comparison with data for the Cbz-Tuv ethyl ester (Cbz = benzyloxycarbonyl) published by Wipf et al.[11] and the original NMR data for tubulysin A.[2] Basic hydrolysis allows cleavage of the ester to give building block **18**, which is also suitable for the synthesis of tubulysins V and U (see below). The selective hydrolysis of the methyl ester (R^1), while leaving the acetate (R^2) intact, is possible by enzymatic

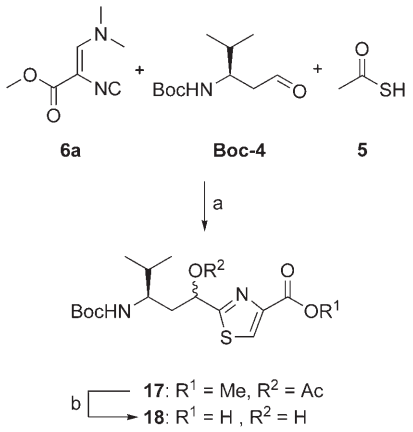

Scheme 3. One-pot synthesis of protected L-tubuvaline by a new MCR to form 2-hydroxymethyl thiazoles. a) 1. $BF_3{\cdot}Et_2O$, Boc-L-homovaline aldehyde, THF, −78°C; 2. simultaneous addition of thioacetic acid and Schöllkopf isonitrile in THF by syringe pump over 30 min; then room temperature overnight; 40%, 3:1, major isomer separated; b) NaOH, THF/H_2O (3:1), 62%.

catalysis (see below), as has been demonstrated with tubulysin A.[8]

D-Mep-L-Ile is the third major building block (Scheme 4). The commercial isoleucine 4-nitrophenyl (*p*NP) ester, Boc-

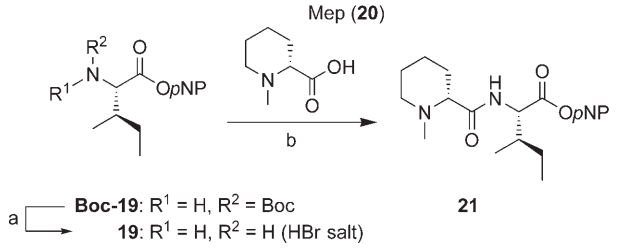

Scheme 4. Synthesis of D-Mep–L-Ile as the activated *p*NP ester. a) HBr in acetic acid (33%), 0°C, 91%; b) 1. *N*-methyl D-pipecolic acid, Et_3N, CH_2Cl_2, −15°C; 2. ethyl chloroformate, −10°C; 3. L-Ile-*p*NP, −10°C, 43%. *p*NP = 4-nitrophenyl.

19, can be *N*-deprotected. Activated as a mixed anhydride, D-Mep[17] reacts chemoselectively and without detectable racemization with **19** to give the Mep–Ile dipeptide already activated at the C terminus. The coordinated levels of carbonyl activation and careful control of the reaction temperature save several steps of protection–deprotection–activation, by utilizing *p*NP as a carboxyl-protecting moiety in the first coupling and as an activation moiety in the second, upcoming amide coupling.

Finally, suitably monoprotected Tup **14** and Tuv **18** were coupled without racemization with 3-(diethoxyphosphoryloxy)-1,2,3-benzotriazin-4-(3*H*)-one (DEPBT, Scheme 5).[18] After Boc deprotection of **22**, the second coupling step (Scheme 5) with Cbz-Ile activated as a *p*NP-ester, Cbz-**19**, also proceeds in very good yield and without racemization. The subsequent deprotection of the benzyloxycarbonyl group is clean. However, the final coupling step with D-Mep (**20**), activated by various methods (for example, TBTU, 2(-7-aza-

 © 2006 Wiley-VCH Verlag GmbH & Co. KGaA, Weinheim

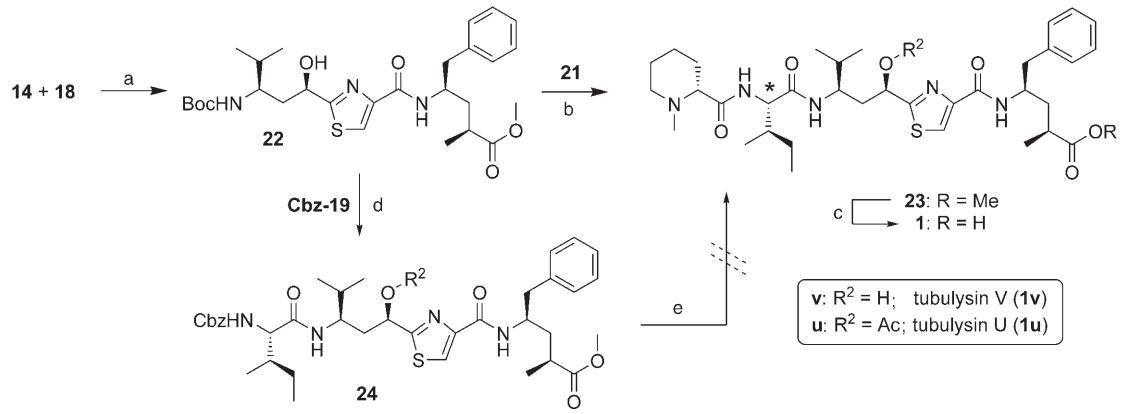

Scheme 5. Assembly of tubulysin U (**1u**) by prolongation of the N terminus. a) 1. **18**, DIPEA, DEPBT, DMF, 0°C; 2. **14**, DMF, 78%; b) 3-step 1-pot procedure: 1. TFA, CH_2Cl_2; 2. D-Mep–L-Ile-*p*NP (**21**), Et_3N, DMF; 3. Ac_2O, pyridine, 83%, 1:1 mixture of diastereomers; c) porcine liver esterase, phosphate buffer (pH 7.2), 36°C, 61%. Alternative route: d) 3-step procedure (b) with Cbz-Ile-*p*NP (step 2), only one diastereomer detected, 85%; e) 1. Pd/C/H_2, MeOH, 93%; 2. TBTU, DIPEA, DMF, D-Mep, only one diastereomer detected, 10%. DIPEA = diisopropylethylamine, DMF = *N*,*N*-dimethylformamide, TBTU = 2-(1H-benzotriazol-1-yl)-1,1,3,3-tetramethyluronium tetrafluoroborate, TFA = trifluoroacetic acid

1*H*-benzotriazole)-1,1,3,3-tetramethyluronium tetrafluoroborate (TATU), or 1-hydroxy-1*H*-benzotriazole (HOBt)), gave protected tubulysins as complex mixtures with a maximum 10% yield of isolated product. These were separable by GC but hardly by preparative LC. This was not satisfactory, and thus the more convergent direct coupling of Boc-Tuv–Tup-Me, **22**, with Mep–Ile-*p*NP, **21**, was tried. A one-pot procedure, including amino deprotection of the Tuv–Tup part, coupling, and reacetylation of the resulting methyl ester of tubulysin V, **23v**, gave the corresponding tubulysin U ester **23u** in an excellent 83% yield. Unfortunately, but not unexpectedly, quantitative epimerization occurs at the α-carbon atom of Ile during dipeptide transfer (indicated by an asterisk in Scheme 5). Nevertheless, separation of the 1:1 diasteromeric mixture gives over 40% of the desired tubulysin U ester **23u** with the correct stereochemistry; this more convergent process is thus much more efficient than the less-racemization-prone stepwise route.

Finally, selective methyl ester hydrolysis in the presence of the acetate and, most importantly, without epimerization or other acid- or base-induced deterioration of tubulysin U was achieved by selective enzymatic hydrolysis with porcine liver esterase to give the title compound **1u** in 61% yield. Tubulysin V (**1v**), the deacetylated derivative, is likewise obtainable by either full ester hydrolysis, and indeed it forms as a minor byproduct even under controlled enzyme hydrolysis conditions, or by omitting the reacetylation step after the first coupling.

Overall, we have developed a short, stereoselective, and convergent route to selected tubulysin family members. The rapid access will form the basis for further structure–activity relationship and biological studies of this promising class of anticancer natural products.

Experimental Section

MCR synthesis of **17**: Boc-**4** (1 g, 4.64 mmol) in THF (1.5 mL) was added to $BF_3{\cdot}Et_2O$ (1.16 mL, 9.29 mmol) in THF (2.5 mL) at −78°C. The resulting mixture was stirred for 5 min at −78°C. Thioacetic acid (**5**, 0.33 mL, 4.64 mmol) in THF (1.5 mL) and a solution of **6a**[13] (0.72 g, 4.64 mmol) in THF (1.5 mL) were added simultaneously by using a double-syringe pump over a period of 30 min. The reaction mixture was stirred for 1 h at −78°C, allowed to come to room temperature, and stirred overnight. The reaction was quenched with water (15 mL) and, after addition of Et_2O (15 mL), the resulting mixture was stirred for 30 min. After separation of the phases, the aqueous layer was washed with Et_2O (3 × 10 mL). The combined organic layers were washed with a solution of citric acid (5%, 2 × 10 mL), sat. $NaHCO_3$ solution (2 × 10 mL), and brine (2 × 10 mL), dried over Na_2SO_4, filtered, and concentrated in vacuo. The obtained oil was purified by flash chromatography on silica (hexanes/EtOAc 7:3) to yield two diastereomers: **17a** (0.60 g) and **17b** (0.21 g) in 43% combined yield (diastereomeric ratio 3:1). For further data, see the Supporting Information.

Synthesis of **1u/v** by coupling of Tup–Tuv-Me with Mep–Ile-pNP and selective enzymatic methyl ester hydrolysis:

Synthesis of **23**: TFA (300 μL, 1.77 mmol) was added to **22** (66 mg, 0.12 mmol) in CH_2Cl_2 (3.5 mL). The mixture was stirred for 1 h at room temperature and all volatile matter was removed in vacuo. The residue was dissolved in DMF (3.5 mL) and this was followed by subsequent addition of Et_3N (150 μL, 1 mmol) and **21** (60 mg, 0.16 mmol). After stirring for 38 h at room temperature, the solvent was evaporated under high vacuum ($p < 1$ mbar, 25°C). The crude residue was dissolved in pyridine (3.5 mL) and, after addition of acetic acid (0.7 mL), the mixture was stirred for 3 h at room temperature. Evaporation of all volatile matter in vacuo yielded the crude product, which was purified by reversed-phase HPLC (RP-18, MeOH/H_2O/TFA 65:35:0.1). Yield = 71 mg (83%).

Synthesis of **1u**: A phosphate buffer (2 mL, pH 7.3, 0.02 M) was added to **23** (6 mg, 8.2 μmol) in dimethylsulfoxide (0.15 mL) and the mixture was vigorously stirred for 5 min. The temperature was kept constant at 36°C and porcine liver esterase (0.15 mL, 250 units mg^{-1}) was added. After stirring for 4 h (detection of only one product; careful TLC control), the mixture was extracted with EtOAc (2 × 15 mL) and the combined organic extracts were freed of solvent in vacuo without heating. The crude product was purified by reversed-phase HPLC (RP-18, MeOH/H_2O/TFA 65:35:0.1). Yield = 3.6 mg (61%) of **1u**. Longer treatment with porcine liver esterase yielded increasing amounts of **1v**.

Received: March 31, 2006
Revised: July 7, 2006
Published online: October 2, 2006

 © 2006 Wiley-VCH Verlag GmbH & Co. KGaA, Weinheim

Keywords: antitumor agents · multicomponent reactions · natural products · peptide coupling · thiazoles

[1] G. Kaur, M. Hollingshead, S. Holbeck, V. Schauer-Vukašinović, R. F. Camalier, A. Dömling, S. Agarwal, *Biochem. J.* **2006**, *396*, 235 – 242; M. W. Khalil, F. Sasse, H. Lünsdorf, Y. A. Elnakady, H. Reichenbach, *ChemBioChem* **2006**, *7*, 678 – 683.
[2] H. Steinmetz, N. Glaser, E. Herdtweck, F. Sasse, H. Reichenbach, G. Höfle, *Angew. Chem.* **2004**, *116*, 4996 – 5000; *Angew. Chem. Int. Ed.* **2004**, *43*, 4888 – 4892.
[3] "Compounds with antimycotic and cytostatic effect, preparation method, agent containing these compounds and DSM 11 092": H. Reichenbach, G. Höfle, F. Sasse, H. Steinmetz, WO 98/13375, **1998**.
[4] F. Sasse, H. Steinmetz, J. Heil, G. Höfle, H. Reichenbach, *J. Antibiot.* **2000**, *53*, 879 – 885.
[5] For a recent review, see: A. Dömling, W. Richter, *Mol. Diversity* **2005**, *9*, 141 – 147.
[6] G. R. Pettit, Y. Kamano, C. L. Herald, A. A. Tuinman, F. E. Boettner, H. Kizu, J. M. Schmidt, L. Baczynskyj, K. B. Tomer, R. J. Bontems, *J. Am. Chem. Soc.* **1987**, *109*, 6883 – 6885.
[7] G. R. Pettit, Y. Kamano, C. Dufresne, R. L. Cerny, C. L. Herald, J. M. Schmidt, *J. Org. Chem.* **1989**, *54*, 6005 – 6006.
[8] G. Höfle, N. Glaser, T. Leibold, U. Karama, F. Sasse, H. Steinmetz, *Pure Appl. Chem.* **2003**, *75*, 167 – 178.
[9] N. Glaser, H. Steinmetz, G. Höfle, personal communication.
[10] G. K. Friestad, J. C. Marie, A. M. Deveau, *Org. Lett.* **2004**, *6*, 3249 – 3252.
[11] P. Wipf, T. Takada, M. J. Rishel, *Org. Lett.* **2004**, *6*, 4057 – 4060.
[12] B. Henkel, B. Beck, B. Westner, B. Mejat, A. Dömling, *Tetrahedron Lett.* **2003**, *44*, 8947 – 8950.
[13] U. Schöllkopf, *Angew. Chem.* **1977**, *89*, 351 – 360; *Angew. Chem. Int. Ed. Engl.* **1977**, *16*, 339 – 348.
[14] A. G. Myers, B. H. Yang, H. Chen, L. McKinstry, *J. Am. Chem. Soc.* **1997**, *119*, 6496 – 6511.
[15] J. L. Vicario, D. Badia, L. Carrillo, *J. Org. Chem.* **2001**, *66*, 5801 – 5807.
[16] J. L. Toujas, E. Jost, M. Vaultier, *Bull. Soc. Chim. Fr.* **1997**, *134*, 713 – 717.
[17] R. Ledger, F. H. C. Stewart, *Aust. J. Chem.* **1967**, *20*, 2509 – 2516.
[18] H. Li, X. Jiang, Y. Ye, C. Fan, T. Romoff, M. Goodman, *Org. Lett.* **1999**, *1*, 91 – 93.

 © 2006 Wiley-VCH Verlag GmbH & Co. KGaA, Weinheim

Crystal Growth

DOI: 10.1002/anie.200601871

Bioenabled Synthesis of Rutile (TiO_2) at Ambient Temperature and Neutral pH**

Nils Kröger, Matthew B. Dickerson, Gul Ahmad, Ye Cai, Michael S. Haluska, Kenneth H. Sandhage, Nicole Poulsen, and Vonda C. Sheppard*

Biomineralizing organisms are unmatched in their ability to form micro- to nanoscale hierarchically structured 3D inorganic materials under ambient conditions. Although the genetic foundations of the species-specific 3D architectures of biominerals are not well understood, specific organic molecules (mostly proteins) are known to guide their deposition and morphogenesis.[1–3] It has been suggested that the molecules and mechanisms of biomineralization may provide new paradigms for the environmentally benign syntheses of advanced nanopatterned materials.[4–6] Indeed, pioneering work by Morse and co-workers demonstrated that proteins (named silicateins) involved in the biomineralization of sponge silica spicules are able to catalyze in vitro the formation of silica and amorphous or partially crystallized, non-biological inorganic materials (titanium dioxide, titanium phosphates, gallium oxohydride, and gallium oxide).[7–12] Also, the hydrolytic enzyme lysozyme has been shown to induce formation of amorphous titania and silica.[13,14]

A different family of silica-forming proteins (named silaffins) has been characterized from diatoms, which are a group of unicellular microalgae (phytoplankton) that form intricately structured 3D silica microshells. Silaffins represent a unique family of phosphoproteins that share no sequence homology with sponge silicateins and exhibit a different mechanism of silica formation.[15a–c] Recently, poly(allylamine)[16a] and the synthetic non-phosphorylated 19-mer peptide R5, which corresponds to a repeat sequence of the silaffin

[*] Prof. Dr. N. Kröger, Dr. N. Poulsen, V. C. Sheppard
School of Chemistry and Biochemistry
Georgia Institute of Technology
770 State Street, Atlanta, GA 30332-0400 (USA)
Fax: (+1) 404-894-7452
E-mail: nils.kroger@chemistry.gatech.edu
M. B. Dickerson, Dr. G. Ahmad, Dr. Y. Cai, Dr. M. S. Haluska, Prof. Dr. K. H. Sandhage
School of Materials Science and Engineering
Georgia Institute of Technology
771 Ferst Drive, Atlanta, GA 30332-0245 (USA)

[**] This work was supported by the Office of Naval Research, the Air Force Office of Scientific Research, the Georgia Tech Research Corporation, and the Colleges of Science and Engineering of the Georgia Institute of Technology. We thank Matije Crne and Mohan Srinivasarao for help with polarized light microscopy. The authors acknowledge the FIB2 Center at Georgia Tech established under NSF, CRIF project number: 0343028.

Supporting information for this article is available on the WWW under http://www.angewandte.org or from the author.

 © 2006 Wiley-VCH Verlag GmbH & Co. KGaA, Weinheim InterScience

precursor polypeptide sil1p, have been employed for silica and titania syntheses.[16b–d]

Despite these achievements, only amorphous or partially nanocrystalline minerals have been produced to date through in vitro mineralization, and the formation of hierarchical structures—a hallmark of biominerals—has not been achieved. It is reasonable to assume that silaffin proteins may exhibit improved mineral-forming activities, as compared with short peptides (such as the R5 peptide), owing to possible cooperative effects between the mineral-interacting protein domains. To investigate this possibility, selected regions of silaffin genes were expressed in *Escherichia coli* and purified to homogeneity (see Supporting Information). Their mineral-forming activities were then analyzed. The characteristic properties of recombinant silaffins rSilC, rSil1L, rSil3, and rSilN are listed in Table 1. Analyses by mass spectroscopy confirmed that the amino acid side chains of recombinant silaffins carry no post-translational modifications (data not shown).

Table 1: Properties of recombinant silaffins.[a]

	rSilC	rSil1L	rSil3	rSilN
M_{theor} [kDa]	17.6	11.8	22.1	9.9
pI	11.8	10.6	9.4	3.8
K + R	45 (27%)	15 (14%)	33 (16%)	2 (2%)
D + E	0	4 (4%)	30 (14%)	23 (27%)

[a] The theoretical molecular masses of the unmodified polypeptides are listed. pI = isolectric point. K + R = content of lysine and arginine residues, respectively. D + E = content of aspartate and glutamate residues, respectively.

Initial experiments were conducted to determine whether recombinant silaffins retained silica-formation activity. The silaffins rSilC, rSil1L, and rSil3 induced the precipitation of silica in the pH range 6–10, whereas no silica was deposited within the assay time (10 min) in the presence of rSilN or in the absence of silaffins. The complete amount of silaffin added to the silicic acid solution was incorporated into the precipitates, and the amount of silica produced increased linearly with the amount of recombinant silaffin added to the silicic acid solution. The silica precipitates were composed of aggregates of spherical particles that exhibited different sizes depending on the recombinant silaffin used (rSilC: 200–400 nm; rSil3: 50–250 nm; rSil1L: < 50 nm; see Supporting Information). These morphologies were similar to the silica precipitates formed previously by polycationic peptides and proteins (e.g. R5 peptide, poly-L-lysine, lysozyme), which is consistent with a common mineralization mechanism. The proposed mechanism involves the flocculation of polysilicic acid particles (that form rapidly at pH ≥ 6) by polycationic peptide/protein molecules.[17–19]

It was then investigated whether recombinant silaffins were also able to induce the formation of TiO_2 (titania). Titania-based materials have a wide variety of applications in (photo)catalysis, gas sensing, and photovoltaics, and are used as pigments and phosphors.[20,21] The twofold negatively charged complex titanium(IV) bis-(ammonium lactato)-dihydroxide (TiBALDH) was used as a substrate for titania formation in buffered aqueous solutions. In the absence of silaffins, the solutions remained clear and homogenous for several hours, as did the solutions containing rSil3 and rSilN. However, when rSilC or rSil1L were added, the TiBALDH solutions instantly became turbid, and precipitates were formed after only a few minutes under all pH conditions tested (pH 3–10). Energy-dispersive X-ray (EDX) analyses yielded strong signals for Ti and O in the rSilC- and rSil1L-induced precipitates, indicating the presence of titania (see Supporting Information). The precipitates also contained the complete amount of recombinant silaffin added to the TiBALDH solutions (see Supporting Information). Thermogravimetric analyses (TGA) indicated an organic content of 56 wt% for rSilC–titania and 50 wt% for rSil1L–titania.

The rSil1L–titania was composed of large aggregates of randomly arranged nanospheres (diameters of 100–300 nm) that were partially fused together to form an interconnected network of particles (Figure 1a). The rSilC–titania contained two different types of structures (Figure 1b). One type consisted of aggregates of round particles (diameters of

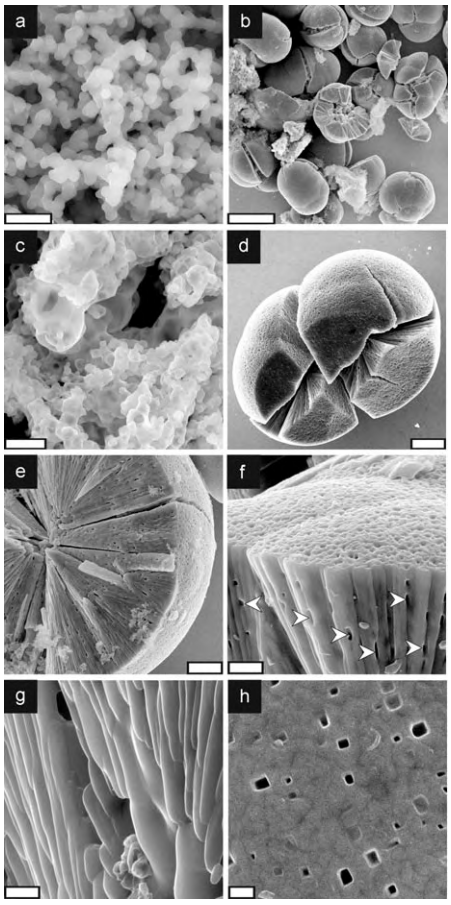

Figure 1. Titania formation by recombinant silaffins. a) SEM images of the precipitates formed by 53 μM rSil1L, and b–h) 32 μM rSilC in sodium phosphate/citrate buffer solution (50 mM; pH 7). The images in parts e–h were taken from fractured hemispheres. e) Part of the fractured hemisphere. f) Detail from the region near the external surface region; the arrowheads indicate some of the pores inside the microspheres. g) Detail of the central core region. h) Detail of the external surface. Scale bars: 20 μm (b), 5 μm (d, e), 1 μm (a, c, f), and 500 nm (g, h).

 © 2006 Wiley-VCH Verlag GmbH & Co. KGaA, Weinheim

100 nm–1 μm) that were interconnected and, in many cases, appeared to be partially collapsed, which suggested that they were hollow (Figure 1c). This was indeed confirmed by scanning electron microscopy (SEM) analysis of focused ion beam (FIB) milled cross sections (see Supporting Information) as well as by transmission electron microscopy (TEM; see below). The second type of rSilC–titania structure consisted of large microspheres (diameters 20–50 μm) that were frequently cracked and/or fragmented (Figure 1b,d,e). Higher-magnification images revealed a remarkable hierarchical architecture (Figure 1e–h). The microspheres were comprised of radially arranged, densely packed columns of tapered cross-section. The columns revealed thicknesses of 400–800 nm on the larger ends (i.e. at the external surface; Figure 1f) and 100–200 nm on the smaller ends (i.e. at the central core; Figure 1g). Both on the external surfaces, and throughout the cross-sections of the microspheres, numerous rectangular pores with long edge lengths between 100–200 nm were observed (Figure 1f,h).

Selected-area electron diffraction (SAED) analyses of the columnar subunits of the microspheres yielded well-defined diffraction spots that could all be assigned to lattice planes of the titania polymorph rutile (Figure 2a,b). High-resolution (HR) TEM confirmed this result by revealing exclusively crystalline regions with a lattice spacing characteristic for (110) rutile (Figure 2c). In contrast, the aggregates of hollow particles (i.e. the second type of structure present in the rSilC–titania precipitate) were composed of an amorphous titania matrix containing a dispersion of anatase nanocrystals (Figure 2d–f).

Powder X-ray diffraction (XRD) analysis of rSilC–titania yielded diffraction peaks only for rutile (Figure 2g), presumably because the anatase nanocrystals (Figure 2f) were so low in abundance that they escaped detection. The XRD pattern obtained from the rSil1L–titania precipitate revealed broad diffraction peaks of low intensity, which were consistent with nanocrystals of a monoclinic titania polymorph (TiO_2–B)[22] (see Supporting Information).

The presence of oriented rutile microcrystals in the rSilC–titania precipitate is highly surprising. Conventional syntheses of microcrystalline rutile require high temperatures (e.g. 600–800 °C), and the formation of nanocrystalline rutile has so far only been achieved at extremely acidic pH values ($pH < 1$) and elevated temperatures.[23–36]

To further study the rSilC-induced formation of rutile microspheres, the process was followed by polarized light microscopy. The addition of rSilC to the aqueous TiBALDH solution rapidly induced formation of large, irregularly shaped aggregates (Figure 3a), which were consistent with the aggregates of round hollow particles observed by SEM analysis (see Figure 1c). These partially amorphous, partially crystalline particles (see Figure 2f) represented the end product in aqueous solution, even after prolonged incubation times (up to 24 h). In contrast, removal of the mother liquor 10 minutes after precipitation and subsequent dehydration—either by incubation in methanol or drying for 30 minutes in vacuo—induced the formation of rutile microspheres (Figure 3b,c). After extended periods of drying (≥ 24 h), the relative abundance of the irregularly shaped particle aggregates was strongly reduced, and crystalline microspheres were almost exclusively observed (Figure 3d).

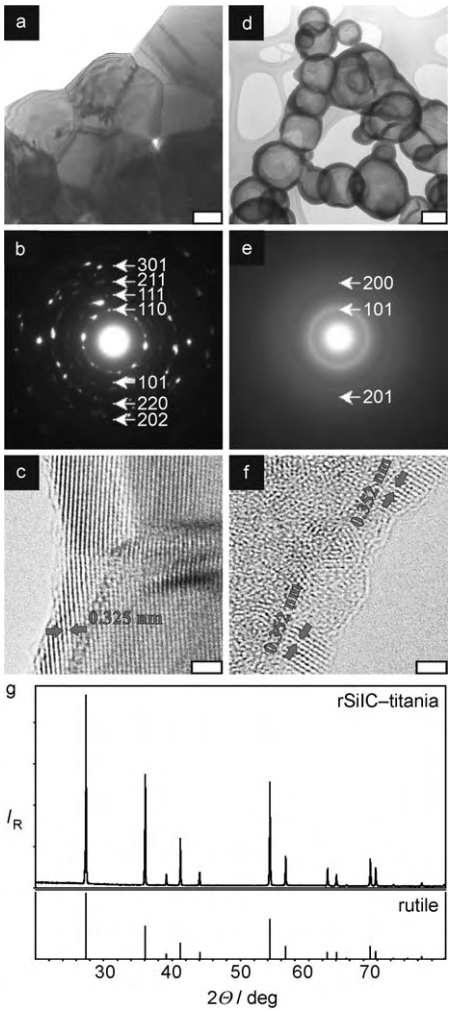

Figure 2. Structural analyses of rSilC–titania. TEM images obtained from microspheres (a) and the aggregates of hollow particles (d). SAED analyses obtained from a microsphere (b) and the shell of a hollow particle (e). Diffraction rings corresponding to rutile (b) and anatase (e) are assigned. HR-TEM analysis of a microsphere fragment showing the (110) lattice fringes of rutile (c, arrows), and from the shell region of a hollow particle showing the (101) lattice fringes of anatase (f, arrows). g) Powder X-ray diffraction analysis obtained from the rSilC–titania precipitate (I_R = relative intensity). Scale bars: 100 nm (a), 200 nm (d), 2 nm (c,f).

The transformation process from partially amorphous titania aggregates into highly organized rutile microspheres requires the reorganization of the condensed TiO_6 octahedra. This can usually only be achieved at high temperatures or under extremely acidic conditions.[23–36] We hypothesize that the rSilC molecules entrapped within the hydrated, partially amorphous titania mediate rutile crystallization by 1) acting as an acid–base catalyst in the hydrolysis and condensation reactions between TiO_6 octahedra, and 2) guiding the rearrangement of these units into a crystal lattice. The molecular characteristics of rSilC are well suited for these functions. The numerous lysine residues can donate and accept protons, and the highly repetitive spacing of functional groups in rSilC (see

 © 2006 Wiley-VCH Verlag GmbH & Co. KGaA, Weinheim

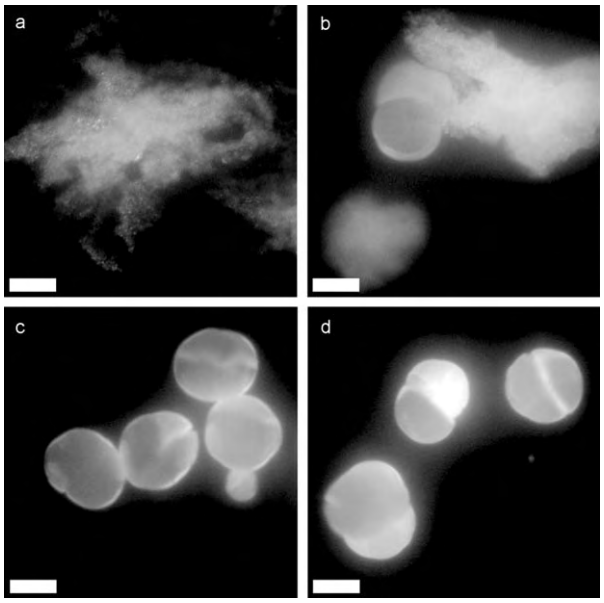

Figure 3. Analysis of microsphere formation by polarized light microscopy. The structures of rSilC–titania were documented at different processing stages: a) In mother liquor after 10-min reaction time; b) after subsequent washing with H_2O and methanol; c) after washing (with H_2O and methanol) and drying for 30 min in vacuo; and d) after continued drying for 24 h in vacuo. Scale bars: 20 μm.

Supporting Information) may lower the activation energy for the alignment of TiO_6 octahedra into a rutile lattice. In contrast, rSil1L, which is unable to induce rutile formation, contains only a short repetitive sequence region with less conserved repeated units (see Supporting Information). The synthetic homopolypeptide poly-L-lysine ($M_w = 15$–30 kDa) is also incapable of directing the formation of rutile and led rather to the deposition of anatase titania as the predominant crystalline phase (see Supporting Information). This indicates that the distribution of positive charges, the amino acid sequence/composition, the 3D polypeptide conformation, or a combination of these factors is crucial for rSilC's ability to induce rutile formation. The influence of these factors can be experimentally tested by site-directed mutagenesis of the rSilC polypeptide sequences.

The transformation of amorphous mineral deposits into crystalline phases has also been observed in biological mineralization processes. Many $CaCO_3$-forming organisms employ specific proteins to deposit structures made of amorphous $CaCO_3$, which in later stages crystallize as calcite.[37] By using a system in vitro that is based on self-assembled monolayers, Aizenberg et al. have mimicked this strategy and demonstrated that the transformation of amorphous $CaCO_3$ into calcite required sufficient removal of the H_2O associated with the amorphous phase. This was achieved by introducing closely spaced channels into which the H_2O was expelled during the crystallization process.[38] As shown in the present study, the removal of H_2O is also critical for the rSilC-induced transformation of the hydrated, partially amorphous titania aggregates into rutile microspheres (see Figure 3). It is suggested that the numerous pores present within the rutile microspheres (Figure 1 f,h) may act as H_2O release channels that enable the crystallization process to occur. The mechanism of pore formation within the rutile microspheres is currently unclear.

The ability of recombinant silaffin rSilC to induce the formation of rutile under ambient conditions and neutral pH is unprecedented, and opens up new possibilities to produce functional hybrid materials for optical applications.

Experimental Section

Selected regions of silaffin genes were amplified by PCR, cloned into pET16 plasmids, and introduced into *E. coli* by transformation. After induction of protein expression (1 mM isopropyl thiogalactoside, 3 h, 37 °C), cells were washed (150 mM NaCl) and lysed by sonication in buffer A (1M NaCl, 50 mM Tris-HCl (pH 8.0), 6M guanidine-HCl). Recombinant silaffins were isolated from the centrifuged supernatant (4 °C, 30 min, 10000 g) by Ni-NTA chromatography. Recombinant silaffin rSilC was subjected to an additional purification step by using cation exchange chromatography. Column eluates containing recombinant silaffins were dialyzed against ammonium acetate (50 mM), lyophyllized, and the residues were dissolved in H_2O. The yield was approximately 5 mg recombinant silaffin per liter of *E. coli* culture. Quantification of recombinant silaffins was performed after complete acid hydrolysis (6M HCl, 110 °C, 24 h) by reversed-phase HPLC of the phenylthiocarbamyl derivatives as described previously.[15b]

For titania formation, sodium phosphate/citrate buffer solution (20 μL of 500 mM) of the desired pH, TiBALDH (in H_2O; 20 μL of 2M), and H_2O (140 μL) were mixed and kept for 20 minutes at room temperature. Precipitation was initiated by adding recombinant silaffin (20 μL), and the reaction mixture was incubated for 10 minutes at room temperature. The precipitate was collected by centrifugation, washed three times each with H_2O (1 mL), and finally two times with methanol (1 mL). After the last centrifugation step, the precipitate was dried in a vacuum centrifuge overnight.

Silica precipitation was performed from freshly prepared silicic acid solutions (100 mM) that were adjusted to the desired pH by sodium phosphate/citrate buffer solution mixture (50 mM) as described previously.[15a] Silica quantification was performed by using the β-silicomolybdate assay.[17]

SEM was conducted with a field-emission gun microscope (Leo 1530 FEG SEM, Carl Zeiss SMT Ltd., Cambridge, UK) equipped with an EDX spectrometer (INCA EDS, Oxford Instruments, Bucks, UK). Precipitates were dried on a gold-coated aluminum SEM stub or silicon wafer. FIB-SEM was performed with a Nova 200 DBFIB FE-SEM equipped with a gallium ion FIB (FEI Company, Hillsboro, USA). TEM analysis was conducted with a JEOL 4000 EX instrument. HR-TEM analysis was conducted at an operating voltage of 400 kV. For TEM analysis, a drop of suspended precipitate was dried on a carbon-film-coated copper grid. Alternatively, the precipitate was resuspended in ethanol and ground with a mortar and pestle prior to drying.

Thermogravimetric analyses were conducted with a Netzsch 449C simultaneous thermal analyzer (Selb, Germany). Prior to analysis, samples were dried for 16 h at 65 °C.

Powder XRD was performed by using a PANalytical X-Pert Pro Alpha 1 diffractometer with an incident beam Johannsen monochromator, with 1/2° divergence slits, 0.04° soller slits, and an Xcelerator linear detector. The powder sample was loaded on a zero-background sample holder, and the measurement was performed over a 20–60° 2θ range by using a continuous scan with a 0.167° 2θ step size.

For polarized light microscopy, a Leica RDX microscope was used with the polarizer oriented 90° with respect to the analyzer.

Received: May 11, 2006
Revised: August 30, 2006
Published online: September 29, 2006

 © 2006 Wiley-VCH Verlag GmbH & Co. KGaA, Weinheim

Keywords: biomimetic synthesis · crystal growth · proteins · sol–gel processes · titanium

[1] H. A. Lowenstam, S. Weiner, *On Biomineralization*, Oxford University Press, New York, **1989**.
[2] S. Mann, *Biomineralization*, Oxford University Press, Oxford, New York, **2001**.
[3] E. Bäuerlein, *Biomineralization*, Wiley-VCH, Weinheim, **2004**.
[4] A. H. Heuer, D. J. Fink, V. J. Laraia, J. L. Arias, P. D. Calvert, K. Kendall, G. L. Messing, J. Blackwell, P. C. Rieke, D. H. Thompson, A. P. Wheeler, A. Veis, A. I. Caplan, *Science* **1992**, *255*, 1098 – 1105.
[5] S. Mann, G. A. Ozin, *Nature* **1996**, *382*, 313 – 318.
[6] D. E. Morse, *Trends Biotechnol.* **1999**, *17*, 230 – 232.
[7] J. L. Sumerel, D. E. Morse in *Silicon Biomineralization* (Ed.: W. E. G. Müller), Springer, Berlin, **2003**, pp. 225 – 247.
[8] J. L. Sumerel, W. Yang, D. Kisailus, J. C. Weaver, J. H. Choi, D. E. Morse, *Chem. Mater.* **2003**, *15*, 4804 – 4809.
[9] D. Kisailus, M. Najarian, J. C. Weaver, D. E. Morse, *Adv. Mater.* **2005**, *17*, 1234 – 1239.
[10] P. Curnow, P. H. Bessette, D. Kisailus, M. M. Murr, P. S. Daugherty, D. E. Morse, *J. Am. Chem. Soc.* **2005**, *127*, 15749 – 15755.
[11] M. N. Tahir, P. Théato, W. E. G. Müller, H. C. Schröder, A. Janshoff, J. Zhang, J. Huth, W. Tremel, *Chem. Commun.* **2005**, 5533 – 5535.
[12] M. N. Tahir, P. Théato, W. E. G. Müller, H. C. Schröder, A. Borejko, S. Faiß, A. Janshoff, J. Huth, W. Tremel, *Chem. Commun.* **2004**, 2848 – 2849.
[13] T. Coradin, A. Coupé, J. Livage, *Colloids Surf. B* **2003**, 189 – 196.
[14] H. R. Luckarift, M. B. Dickerson, K. H. Sandhage, J. Spain, *Small* **2006**, *2*, 640 – 643.
[15] a) N. Kröger, R. Deutzmann, M. Sumper, *Science* **1999**, *286*, 1129 – 1132; b) N. Poulsen, M. Sumper, N. Kröger, *Proc. Natl. Acad. Sci. USA* **2003**, *100*, 12075 – 12080; c) N. Poulsen, N. Kröger, *J. Biol. Chem.* **2004**, *279*, 42993 – 42999.
[16] a) K. E. Cole, A. N. Ortiz, M. A. Schoonen, A. M. Valentine, *Chem. Mater.*, DOI: 10.1021cm060807b; b) R. R. Naik, M. O. Stone, *Mater. Today* **2005**, *8*, 18 – 26; c) M. J. Pender, L. A. Sowards, J. D. Hartgerink, M. O. Stone, R. R. Naik, *Nano Lett.* **2006**, *6*, 40 – 44; d) S. L. Sewell, D. W. Wright, *Chem. Mater.* **2006**, *18*, 3108 – 3113.
[17] R. K. Iler, *The Chemistry of Silica*, Wiley, New York, **1979**.
[18] S. V. Patwardhan, J. Clarson, C. C. Perry, *Chem. Commun.* **2005**, 1113 – 1121.
[19] P. J. Lopez, C. Gautier, J. Livage, T. Coradin, *Curr. Nanosci.* **2005**, 1, 73 – 83.
[20] U. Diebold, *Surf. Sci. Rep.* **2003**, *48*, 53 – 229.
[21] J. Ovenstone, P. J. Titler, R. Withnall, J. Silver, *J. Mater. Res.* **2002**, *17*, 2524 – 2531.
[22] A. R. Armstrong, G. Armstrong, J. Canales, P. G. Bruce, *Angew. Chem.* **2004**, *116*, 2336 – 2338; *Angew. Chem. Int. Ed.* **2004**, *43*, 2286 – 2288.
[23] M. Gopal, W. J. M. Chan, L. C. DeJonghe, *J. Mater. Sci.* **1997**, *32*, 6001 – 6008.
[24] J. Ovenstone, K. Yanagisawa, *Chem. Mater.* **1999**, *11*, 2770 – 2774.
[25] M. Wu, J. Long, A. Huang, Y. Luo, S. Feng, R. Xu, *Langmuir* **1999**, *15*, 8822 – 8825.
[26] S. T. Aruna, S. Tirosh, A. Zaban, *J. Mater. Chem.* **2000**, *10*, 2388 – 2391.
[27] W. P. Huang, X. H. Tang, Y. Q. Wang, Y. Koltypin, A. Gedanken, *Chem. Commun.* **2000**, 1415 – 1416.
[28] C. Wang, Z. X. Deng, Y. D. Li, *Inorg. Chem.* **2001**, *40*, 5210 – 5214.
[29] H. Yin, Y. Wada, T. Kitamura, S. Kambe, S. Murasawa, H. Mori, T. Sakata, S. Yanagida, *J. Mater. Chem.* **2001**, *11*, 1694 – 1703.
[30] W. W. So, S. B. Park, K. J. Kim, C. H. Shin, S. J. Moon, *J. Mater. Sci.* **2001**, *36*, 4299 – 4305.
[31] M. Andersson, L. Osterlund, S. Ljungstrom, A. Palmqvist, *J. Phys. Chem. B* **2002**, *106*, 10674 – 10679.
[32] D. B. Zhang, L. M. Qi, J. M. Ma, H. M. Cheng, *J. Mater. Chem.* **2002**, *12*, 3677 – 3680.
[33] S. Yin, R. X. Li, Q. L. He, T. Sato, *Mater. Chem. Phys.* **2002**, 75, 76 – 80.
[34] S. Yang, Y. Liu, Y. Guo, J. Zhao, H. Xu, Z. Wang *Mater. Chem. Phys.* **2003**, 77, 501 – 506.
[35] Z. L. Tang, J. Y. Zhang, Z. Cheng, Z. T. Zhang, *Mater. Chem. Phys.* **2003**, 77, 314 – 317.
[36] J. Yang, S. Mei, J. M. Ferreira, P. Norby, S. Quaresma, *J. Colloid Interface Sci.* **2005**, *283*, 102 – 106.
[37] L. Addadi, S. Raz, S. Weiner, *Adv. Mater.* **2003**, *15*, 959 – 970.
[38] J. Aizenberg, D. A. Muller, J. L. Grazul, D. R. Hamann, *Science* **2003**, *299*, 1205 – 1208.

 © 2006 Wiley-VCH Verlag GmbH & Co. KGaA, Weinheim

Dendrimers

DOI: 10.1002/anie.200601923

Hormone–PAMAM Dendrimer Conjugates: Polymer Dynamics and Tether Structure Affect Ligand Access to Receptors**

*Sung Hoon Kim and John A. Katzenellenbogen**

The development of ligand–polymer conjugates as diagnostic and therapeutic agents raises an interesting question: In what way do the conformational and dynamic features of the macromolecular carrier influence ligand access to its target receptor? Poly(amide)polyamine (PAMAM) dendrimers, in particular, are being widely adapted to biomedical applica-

[*] Dr. S. H. Kim, Prof. J. A. Katzenellenbogen
Department of Chemistry
University of Illinois
600 South Mathews Avenue, Urbana, IL 61801 (USA)
Fax: (+1) 217-333-7325
E-mail: jkatzene@uiuc.edu

[**] We are grateful for support of this research through grants from the National Institutes of Health (PHS 5R37 DK15556). We thank Kathryn Carlson for determining the receptor binding affinities. NMR spectra were obtained in the Varian Oxford Instrument Center for Excellence in NMR Laboratory. Funding for this instrumentation was provided in part by the W. M. Keck Foundation, the National Institutes of Health (PHS 1 S10 RR104444-01), and the National Science Foundation (NSF CHE 96-10502). Mass spectra were obtained on instruments supported by grants from the National Institute of General Medical Sciences (GM 27029), the National Institutes of Health (RR 01575), and the National Science Foundation (PCM 8121494). PAMAM = poly(amide)polyamine.

Supporting information for this article (details of the preparation and characterization of estrogen–dendrimer conjugates) is available on the WWW under http://www.angewandte.org or from the author.

© 2006 Wiley-VCH Verlag GmbH & Co. KGaA, Weinheim
InterScience

tions,[1–5] yet little is known about how their complex, pH-dependent conformation and flexibility[6–8] affects the accessibility of covalently attached ligands. We have used spectroscopic and physical methods to characterize ligand dynamics and access to the receptor in four estrogen–dendrimer conjugates (EDCs) that were prepared to study pathways of estrogen signaling.[9] Curiously, EDCs having long or hydrophobic tethers engender considerable ligand shielding that results in poor access to the receptor, whereas those with short tethers expose the ligand so it binds to the receptor with little impediment from the dendrimer carrier.

The four EDCs (Scheme 1) are based on a generation six (G6) PAMAM dendrimer, with a molecular weight of approximately 58000,[1] comparable to that of bovine serum albumin (67000) used to construct other estrogen–protein conjugates.[10,11] Three are linked to estradiol, either through 17α-ethynyl (**Ia** and **IIa**) or 7α sites (**IVa**), which are known to tolerate substitution,[12] while the fourth is based on the nonsteroidal ligand cyclofenil (**IIIa**).[13] The linking tethers are short (**Ia** and **IIIa**), moderate (**IVa**), or long (**IIa**, hexaethylene glycol). Four compounds (**Ib**–**IVb**) in which the tether chain was terminated by an (acetamido)ethylamine function, which mimicks the first dendrimer attachment site, were prepared for reference.

The EDCs were prepared by reductive amination of the appropriate estrogen aryl carboxaldehyde with the primary amine termini of the G6 PAMAM. Imine formation proceeded spontaneously, and reduction with borohydride was quantitative; these steps could be followed by ^{1}H NMR spectroscopy. The final ligand:dendrimer ratio (18:1–20:1, Scheme 1), determined by MALDI MS, simply reflected the reaction stoichiometry. The resulting EDCs were purified by ultrafiltration.[9]

Although conformationally mobile, G6 PAMAMs are believed to be roughly spherical up to the generation five layer.[6,7] Conformation and flexibility are predicted to be pH-dependent,[6,8] with low pH values favoring rigid, extended forms (because of Coulombic repulsion) and high pH values producing more dense compact forms. At neutral pH, the peripheral amine groups are partially protonated, with the outer layers constituting a relatively flexible framework having pockets,[6–8] a characteristic through which PAMAMs can be used as drug and gene delivery systems.[14,15] In our EDCs we have added a peripheral hydrophobic group (estrogen) to a macromolecule that has a relatively hydrophilic surface, but which is also porous with a more hydrophobic interior. Thus, the disposition of the ligand with respect to the surface—Is it extended outward and thus

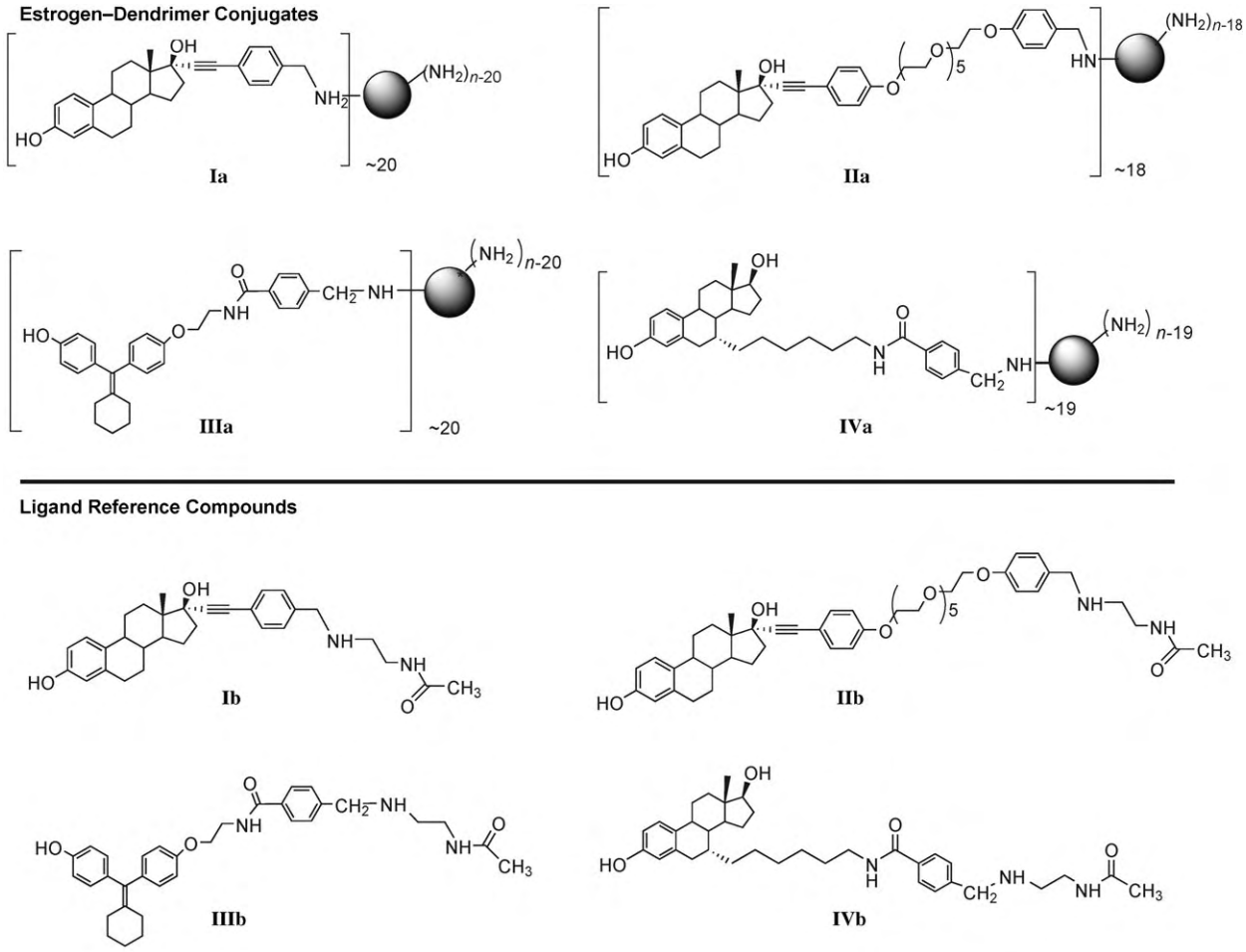

Scheme 1. Estrogen–dendrimer conjugates (EDCs, **Ia**–**IVa**) and reference compounds (**Ib**–**IVb**).

 © 2006 Wiley-VCH Verlag GmbH & Co. KGaA, Weinheim

available to a receptor, or is it buried within the G6 layer and inaccessible to other proteins?—becomes an important issue.

NOESY spectra show interactions between the ligand and the dendrimer backbone (and sometimes tether). In both the short- and long-tether EDCs the aromatic signals (C-1, 2, 4; a–d) show strong cross-peaks in D_2O with 4/5 resonances that can be assigned to the dendrimer backbone (f–k); these cross-peaks are very weak in methanol (Figures 1 and 2, top versus bottom spectrum). Significantly, the long-tether EDC in D_2O (**IIa**, Figure 2, bottom) shows there are strong interactions between the resonances of the ethylene glycol spacer (eg) and the aromatic resonances of the ligand (C-1, 2, 4), even though

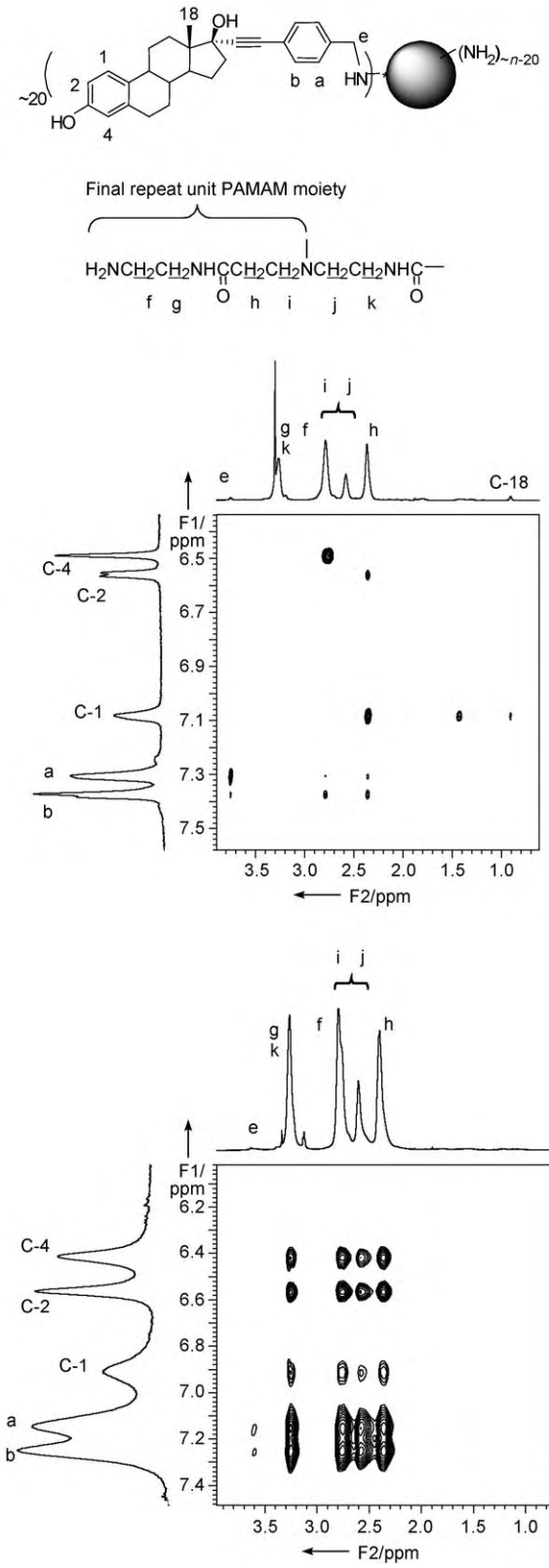

Figure 1. Aliphatic and aromatic region of the ^{1}H NMR NOESY spectra of short-tether EDC **Ia** in CD_3OD (top) and in D_2O (bottom).

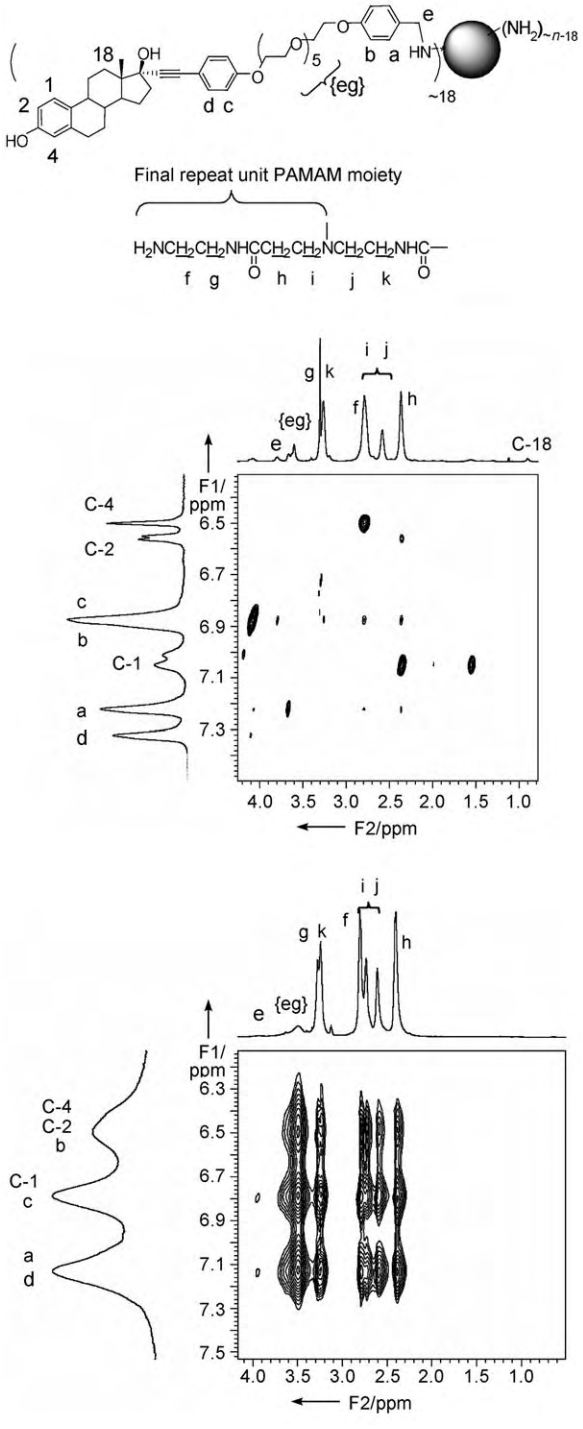

Figure 2. Aliphatic and aromatic region of the ^{1}H NMR NOESY spectra of long-tether EDC **IIa** in CD_3OD (top) and in D_2O (bottom).

 © 2006 Wiley-VCH Verlag GmbH & Co. KGaA, Weinheim

they are at opposite ends of the ligand. Thus, in an aqueous environment, but not in methanol, the ligand portion of the long-tether EDC becomes enwrapped by the ethylene glycol tether and buried within the dendrimer with sufficient stability to generate large NOE signals. Although oligoethylene glycol derivatives are water compatible and flexible, they have a coiled structure, engendered by the gauche preference of the glycol unit,[16–19] which probably contributes to this ligand-tether-dendrimer interaction.

Spin–lattice and spin–spin relaxation times T_1 and T_2 for the C-4 proton of the EDCs **Ia** and **IIa**, as well as their reference compounds **Ib** and **IIb**, are given in Figure 3. The

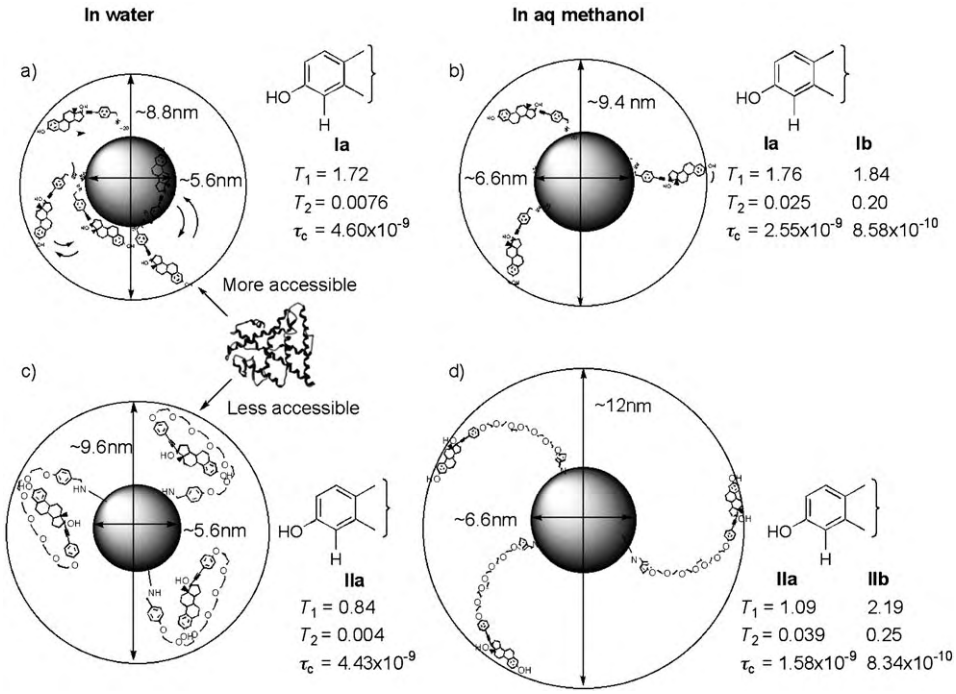

Figure 3. ^{1}H NMR relaxation and rotational correlation times (in seconds) and hydrodynamic diameter measurements for the short-tether (**Ia**) and long-tether (**IIa**) EDCs: a) EDC **Ia** in water, b) EDC **Ib** in 20% MeOH in water, c) EDC **IIa** in water, d) EDC **IIb** in 20% MeOH in water. The diameters, measured by dynamic light scattering studies, are shown schematically; the inner circle represents the PAMAM and the outer circle the EDC diameter. The spin–lattice and spin–spin relaxation times (T_1 and T_2) and the rotational correlation time (τ_c) are given for the C-4 proton of the 17α-ethynylestradiol in the EDCs and control compounds. The abbreviated structure of the ligand is meant to represent the degree to which the ligand is extended or enveloped relative to the PAMAM.

T_1 value for the C-4 ligand proton in the long-tether EDC (**IIa**) in D_2O is considerably less than that in CD_3OD; in the latter solvent, the T_1 value is very similar to that of the monomeric ligand analogue **IIb**. In contrast, there was little difference in the T_1 value for the short-tether EDC (**Ia**) in the two solvent systems, both values being similar to those of the monomeric ligand analogue **Ib**. This finding suggests that in hydrophilic solvents, only the ligand in the long-tether EDC (**IIa**) undergoes a change of environment, which causes its motion to become more restricted (increasing spin–lattice relaxation; smaller T_1 values). The T_2 values of both the short- and long-tether EDCs decrease upon shifting from CD_3OD to D_2O, but the decrease was more pronounced for the long-tether EDC (**IIa**). The T_2 values for the monomeric ligand analogues (**Ib** and **IIb**) are, as expected, much larger.

The rotational correlation times of the C-4 proton on the A ring of the steroid, calculated from the T_1 and T_2 values,[20] show that the tumbling motion of two monomeric ligands (**Ib** and **IIb**) in CD_3OD is very similar, whereas the tumbling motion of the two EDCs showed a twofold difference in methanol, but only a 1.3-fold difference in D_2O. We interpret the effect of solvent on the rotational correlation times to mean the following: in CD_3OD, the size difference between the short- and long-tether EDCs is pronounced because the long-tether EDC (**IIa**) has an extended structure; by contrast, in water, the ligand of the long-tether EDC becomes encapsulated in the dendrimer interior, so its molecular size is less different from that of the short-tether EDC.

To further evaluate the apparent size of the EDCs, we determined the hydrodynamic diameter of the G6 PAMAM and the EDCs in water and 20% aqueous methanol solution by dynamic light scattering (DLS; Figure 3). In all cases, the diameters are smaller in water than in aqueous methanol, but the two EDCs show very different solvent effects. The radius of the short-tether EDC (**Ia**) in both solvents is nearly the same as the sum of the PAMAM radius and the length of the ligand moiety (ca. 1.5 nm, determined by molecular modeling studies). By contrast, the radius of the long-tether EDC (**IIa**) in aqueous MeOH is much larger, consistent with a stretched-out conformation, whereas in water its radius is much smaller, similar to that of the short-tether EDC. Thus, the short-tether EDC (**Ia**) appears to have a more rigid structure, with the ligand projecting outward from the peripheral region of the dendrimer in a relatively solvent-insensitive manner. By contrast, the long linker in EDC **IIa** allows the hydrophobic ligand to reach back into the interior region of the PAMAM in aqueous media.

The hydrodynamic diameters of the other two EDCs (**IIIa** and **IVa**) were approximately 8.6 nm and 45 nm in water, respectively. The cyclofenil-functionalized EDC (**IIIa**), with a short linker, has a radius close to that of the dendrimer plus the length of the cyclofenil moiety (1.4 nm), as was the case with **Ia**. The unexpectedly large diameter measured for the

 © 2006 Wiley-VCH Verlag GmbH & Co. KGaA, Weinheim

Table 1: Relative binding affinity (RBA) values for the EDCs and reference compounds for ERα and ERβ.

EDC or reference compound	I		II		III		IV	
	a	**b**	**a**	**b**	**a**	**b**	**a**	**b**
RBA[a] (ERα)	3.8 ± 0.8	3.6 ± 0.2	0.9 ± 0.1	3.3 ± 0.5	2.9 ± 0.2	2.8 ± 0.3	2.4 ± 0.3	10.3 ± 0.4
RBA[a] (ERβ)	1.9 ± 0.3	2.3 ± 0.4	0.2 ± 0.1	1.2 ± 0.4	5.8 ± 0.1	10.2 ± 0.4	2.7 ± 0.3	14.4 ± 3.8
ligand–receptor access ratio[b]	83–106 %		17–27 %		60–104 %		19–23 %	
nature of tether explanation	**short**		**long**		**short**		**medium**; **hydrophobic**	
	Good ligand–receptor access		ligand access restricted by encapsulation by PAMAM and tether		good ligand–receptor access		ligand access restricted by EDC aggregation	

[a] RBA = relative binding affinity determined in competitive radiometric binding assays.[21,22] RBA = {IC_{50}[estradiol]/IC_{50}[compound]} × 100. Values are the mean ± range or SD of 2 or more independent experiments. The RBA for estradiol is 100; K_d value for estradiol is 0.2 nM for ERα and 0.5 nM for ERβ. [b] Ligand–receptor access ratio is defined as {RBA[EDC]/RBA[reference compound]} × 100.

EDC **IVa**, with a moderate length but hydrophobic pentamethylene group linker, is most likely the result of aggregation.

We determined the ligand access to the receptor in all four EDCs by comparing their binding affinities for the estrogen receptors with those of their reference compounds, which were designed to mimic the EDC ligand in all respects except not having the dendrimer attached (Scheme 1). Binding affinities, determined by a known method,[21,22] are expressed in Table 1 as relative binding affinity (RBA) values, where the affinity of estradiol is set at 100. The values for the EDCs are based on the ligand-equivalent concentration, which corrects for the fact that multiple ligands are attached to each dendrimer.

All of the compounds have RBA values in the range 0.2–14.4. Most notably, the short-tether EDCs (**Ia**, **IIIa**) have RBA values for the estrogen receptors (ERs) that are very close to those of the corresponding model compounds (**Ib** and **IIIb**). In contrast, both the long and moderate tether length EDCs (**IIa** and **IVa**) have much lower affinities than the reference compounds. The ratio of EDC to reference compound affinity, expressed in percent, can be termed the "ligand–receptor access index" and provides a direct measurement of ligand access to the receptor. The two short-tether EDCs **Ia** and **IIIa** have ligand–receptor access indices of 83–106 % and 60–104 %, respectively, whereas the EDCs with either long- or medium-length tethers (**IIa** and **IVa**) have indices of only 17–27 % and 19–23 %, respectively. Thus, as expected from the spectroscopic and hydrodynamic measurement studies, the short-tether EDCs (**Ia** and **IIIa**) provide much better ligand access to the receptor than do the longer tether EDCs (**IIa** and **IVa**), for the reasons summarized in the Table 1.

We have shown that tethering ligands to polymeric macromolecules can significantly affect ligand access to a receptor. In our EDCs, where the ligand is hydrophobic (for example, an estrogen) and is attached to a macromolecule having a flexible structure with surface invaginations (for example, PAMAM), ligand access becomes a function of the tether: Short-tether EDCs are able to maintain ligand exposure, thus providing essentially unimpeded access to the ERs; in contrast, ligands attached through long or hydrophobic tethers experience masking by burrowing into the PAMAM or by aggregation and thus result in poor access of the ligand to the receptor. Our findings hold important implications for the future design of drug– or hormone–polymer conjugates where receptor interaction by the polymer-bound ligand is the goal, and our investigation provides approaches that can be used to evaluate the behavior of new ligand–polymer conjugates. We believe that these principles will help ensure success in the future development of such novel polymer-based biological reagents.

Received: May 15, 2006
Revised: August 24, 2006
Published online: October 6, 2006

Keywords: dendrimers · estrogen · hormones · receptors · solvent effects

[1] R. Esfand, D. A. Tomalia, *Drug Discovery Today* **2001**, *6*, 427.
[2] C. C. Lee, J. A. MacKay, J. H. Frechet, F. C. Szoka, *Nat. Biotechnol.* **2005**, *23*, 1517.
[3] T. D. McCarthy, P. Karellas, S. A. Henderson, M. Giannis, D. F. O'Keefe, G. Heery, J. R. Paull, B. R. Matthews, G. Holan, *Mol. Pharm.* **2005**, *2*, 312.
[4] S. Svenson, D. A. Tomalia, *Adv. Drug Delivery Rev.* **2005**, *57*, 2106.
[5] T. P. Thomas, I. J. Majoros, A. Kotlyar, J. F. Kukowska-Latallo, A. Bielinska, A. Myc, J. R. Baker, Jr., *J. Med. Chem.* **2005**, *48*, 3729.
[6] I. Lee, B. D. Athey, A. W. Wetzel, W. Meixner, J. R. J. Baker, *Macromolecules* **2002**, *35*, 4510.
[7] P. K. Maiti, T. Cagin, G. Wang, W. A. I. Goddard, *Macromolecules* **2004**, *37*, 6236.
[8] W. Chen, D. A. Tomalia, J. L. Thomas, *Macromolecules* **2000**, *33*, 9196.
[9] W. R. Harrington, S. H. Kim, C. C. Funk, Z. Madak-Erdogan, R. Schiff, J. A. Katzenellenbogen, B. S. Katzenellenbogen, *Mol. Endocrinol.* **2006**, *20*, 491.
[10] P. E. Stevis, D. C. Deecher, L. Suhadolnik, L. M. Mallis, D. E. Frail, *Endocrinology* **1999**, *140*, 5455.
[11] J. L. Temple, S. Wray, *Endocrinology* **2005**, *146*, 558.
[12] G. M. Anstead, K. E. Carlson, J. A. Katzenellenbogen, *Steroids* **1997**, *62*, 268.
[13] R. S. Muthyala, S. Sheng, K. E. Carlson, B. S. Katzenellenbogen, J. A. Katzenellenbogen, *J. Med. Chem.* **2003**, *46*, 1589.
[14] S. Kannan, P. Kolhe, V. Raykova, M. Glibatec, R. M. Kannan, M. Lieh-Lai, D. Bassett, *J. Biomater. Sci. Polym. Ed.* **2004**, *15*, 311.
[15] C. Kojima, K. Kono, K. Maruyama, T. Takagishi, *Bioconjugate Chem.* **2000**, *11*, 910.

 © 2006 Wiley-VCH Verlag GmbH & Co. KGaA, Weinheim

[16] H. J. Kreuzner, R. L. C. Wang, M. Grunze, *New J. Phys.* **1999**, *1*, 21.1.
[17] S. Wolfe, *Acc. Chem. Res.* **1972**, *5*, 102.
[18] K. B. Wiberg, M. A. Murcko, K. E. Laidig, P. MacDougall, *J. Phys. Chem.* **1990**, *94*, 6956.
[19] M. Sundaralingam, *Nature* **1968**, *217*, 35.
[20] H. Pfeifer, *NMR: Basic Principles and Progress*, *Vol. 7*, Springer, New York, **1972**.
[21] K. E. Carlson, I. Choi, A. Gee, B. S. Katzenellenbogen, J. A. Katzenellenbogen, *Biochemistry* **1997**, *36*, 14897.
[22] J. A. Katzenellenbogen, H. J. Johnson, Jr., K. E. Carlson, *Biochemistry* **1973**, *12*, 4092.

 © 2006 Wiley-VCH Verlag GmbH & Co. KGaA, Weinheim

Phosphanes

DOI: 10.1002/anie.200602143

Taming a Functional Group: Creating Air-Stable, Chiral Primary Phosphanes**

Rachel M. Hiney, Lee J. Higham, Helge Müller-Bunz, and Declan G. Gilheany**

Primary phosphanes, unlike their nitrogen counterparts, have a reputation as being toxic, volatile compounds that often spontaneously ignite in air.[1] Accordingly, despite an impressive range of applications as asymmetric ligand precursors,[2] biomedicines,[3] polymers,[4] carbohydrates,[5] and macrocycles,[6] as well as possessing two reactive P–H bonds for functionalization, they remain under-used. Some of the few primary phosphanes reported to be air stable[7] are shown in Scheme 1. There appears to be more than one factor that can confer stability. Thus supermesitylphosphane (**1a**),[8] triptycylphosphane (**1b**),[9] and various related compounds[7] undoubtedly owe their stability to steric factors. More

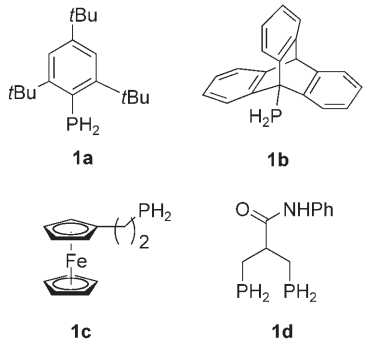

Scheme 1. Phosphanes possessing a high degree of air stability.

puzzling is **1c**, which is stable in air indefinitely, whereas $FcPH_2$ and 1,1′-Fc′$(PH_2)_2$ (Fc = $[(\eta^5\text{-}C_5H_4)Fe^{II}(\eta^5\text{-}C_5H_5)]$, Fc′ = $[Fe^{II}(\eta^5\text{-}C_5H_4)_2)]$) are oxidized in three–five days.[10a] Clearly the alkyl spacer groups are important, but their significance is not currently understood. The reasons for the air-stability of the compounds $[R^2R^1N(CH_2)_nPH_2]I$,[11] $S(CH_2SCH_2CH_2PH_2)_2$,[3] and the related **1d**[12a] are also unclear; the authors suggested that the remote heteroatom might confer stability through negative hyperconjugation.[11,12] Herein we report a potentially larger class of air-stable phosphanes, which possess extended π conjugation, and we suggest that stability may be more the norm than the exception.

As part of our research into P-stereogenic 2-methoxy-2′-diphenylphosphanyl-1,1′-binaphthyl (mop) ligands,[13] we required precursor chiral primary phosphanes, which have rarely been used in the design of asymmetric ligands.[14,2c] Our initial target was (*R*)-2-phosphanyl-2′-methoxy-1,1′-binaphthyl (**4**). We also recognized that **4** might provide a test of whether the local heteroatom conferred air stability.

Compound (*R*)-**4** was prepared in a straightforward manner (Scheme 2) in high yield as a white powder, and its ^{31}P NMR ($\delta = -126.3$ ppm, average $^1J_{P\text{-}H} = 202.6$ Hz) and IR data (ν(P-H) = 2291 cm^{-1}) were as expected.

More gratifying was that (*R*)-**4** did indeed show remarkable stability towards air oxidation: no oxidation was observed for (*R*)-**4** after seven-days exposure to air. Suitable crystals of (*R*)-**4** for X-ray crystallography[15] were obtained from acetonitrile, and the resulting structure (Figure 1) represents, to the best of our knowledge, the first such characterization of an optically pure primary phosphane. The P–C bond length (1.811(6) Å) correlates with the few other crystal structures reported for uncoordinated primary-phosphanes.[9,10b,11,12a,16,17]

On closer examination of the solid-state molecular structure we noted that the environment around the P atom is not crowded, nor does there appear to be any interaction between the P atom and the O atom of the methoxy substituent, apparently ruling out the ether group as being a

[*] R. M. Hiney, Dr. L. J. Higham,[+] Dr. H. Müller-Bunz, Dr. D. G. Gilheany
School of Chemistry and Chemical Biology
Centre for Synthesis and Chemical Biology
Conway Institute for Biomolecular and Biomedical Research
University College Dublin, Belfield, Dublin 4 (Ireland)
Fax: (+353) 1-716-2127
E-mail: lee.higham@ucd.ie
declan.gilheany@ucd.ie

[+] Current address:
School of Natural Sciences-Chemistry, Bedson Building
Newcastle University, Newcastle upon Tyne, NE1 7RU (UK)

[**] We thank the Irish Research Council for Science, Engineering, and Technology (IRCSET) for a scholarship for R.M.H. and the EU for a Marie Curie Host Development Fellowship (HMPD-CT-2000-00053) for L.J.H. We also thank Prof. R. O'Neill for electrochemistry advice and apparatus as well as Dr. G. Docherty (Rhodia) for discussions on phenylphosphane.

Supporting information for this article is available on the WWW under http://www.angewandte.org or from the author (detailed preparations of (*R*)-**2a**, (*S*)-**2b** , (*R*)-**3a**, (*S*)-**3b**, (*R*)-**4**, (*S*)-**5**, **6**, **7** and **8** are included, together with the method for preparing the *cis*-$[Mo(RPH_2)_2(CO)_4]$ complexes. Further details of the electrochemical experiments, oxidation protocols and safety precautions may also be found therein).

WILEY InterScience DISCOVER SOMETHING GREAT
© 2006 Wiley-VCH Verlag GmbH & Co. KGaA, Weinheim

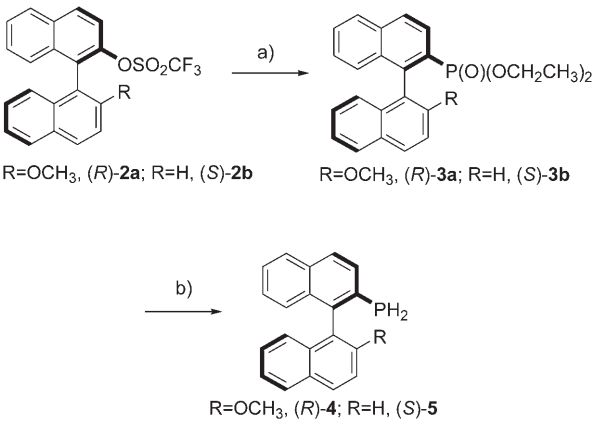

Scheme 2. Synthesis of (*R*)-**4** and (*S*)-**5**. a) $Pd(OAc)_2$, 1,4-bis(diphenylphosphanyl)butane, $((CH_3)_2CH)_2N(CH_2CH_3)$, NaCOOH, HP(O)$(OCH_2CH_3)_2$, DMSO, 100 °C; b) $LiAlH_4$, $(CH_3)_3SiCl$, THF, −78 → −40 °C.

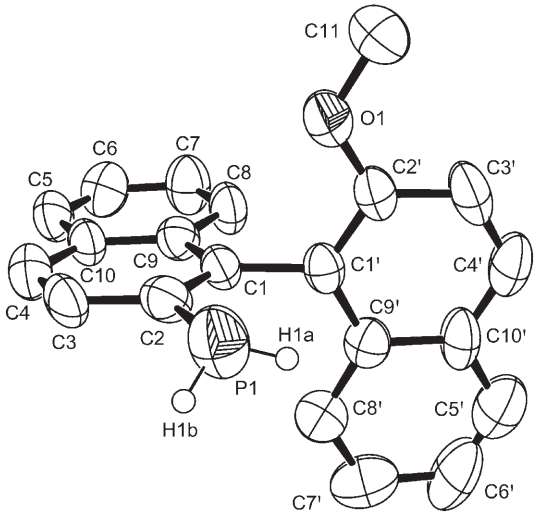

Figure 1. The X-ray crystal structure of (*R*)-**4**. Hydrogen atoms attached to carbon atoms are omitted for clarity.

contributor to the air stability. To confirm this latter point, we prepared the analogous phosphane lacking the 2′-methoxy substituent, (*S*)-2-phosphanyl-1,1′-binaphthyl (**5**, Scheme 2), again as a white solid in high yield (^{31}P NMR: $\delta = -126.7$ ppm, $^1J_{P\text{-}H} = 203.8$ Hz; IR: ν(P-H) = 2297 cm^{-1}). Remarkably, samples of (*S*)-**5** in the solid state were also stable over the same timeframe (Figure 2). Additionally, (*S*)-**5** is a novel chiral ligand precursor.[18]

Having discounted the relevance of the ether group, we sought to simplify the structure even further and we found that 2-naphthylphosphane (**6**), a white solid prepared by using a similar route, exhibited good air stability (88% phosphane remained after seven days, Figure 2). For comparison, the regioisomer of **6**, 1-naphthylphosphane (**7**) showed significantly more oxidation than **6** (Figure 2), but we attribute this result to the fact that it is an oil under ambient conditions. We also prepared the related compound 5,6,7,8-tetrahydro-2-naphthylphosphane (**8**) where the ring without the phosphorus substituent is hydrogenated and conjugation thereby

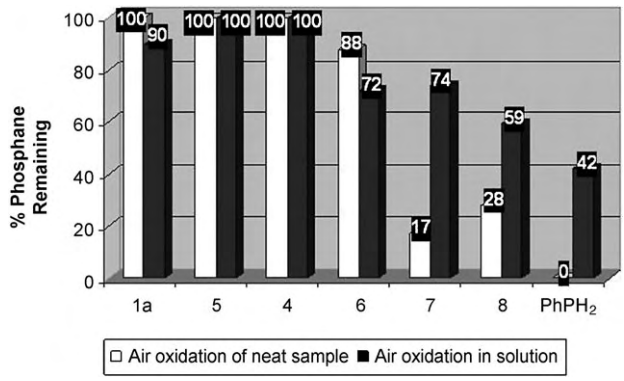

Figure 2. Oxidation profiles of RPH_2 of neat (left bar) and in $CDCl_3$ solution (right bar) after seven days.

reduced. Compound **8**, also an oil, had very low air stability commensurate with that of $PhPH_2$.

It is important to note that in previous reports the air stability of primary phosphanes often only referred to the neat samples. We were concerned that the nature of the sample (crystalline solid or oil) would influence the rate of oxidation. Therefore, we examined the solution behavior of our primary phosphanes in $CDCl_3$ on exposure to air over seven days in uncapped NMR tubes (a method rarely performed[10b,11]; Figure 2).

Under these conditions, there was a small quantity of oxidation in the case of supermesitylphosphane (**1a**), but remarkably even without the steric stabilization of **1a**, **4** and **5** exhibited no oxidation. Thus their stability in air is not simply a result of the slow rate of solid-state reactions. Even when the solution of **5** was enriched with dioxygen, we observed no oxidation after 24 h. In solution, the naphthylphosphanes **6** and **7** showed similar levels of oxidation, with notable quantities of the oxides and H-phosphinic acids produced.[19]

This observation indicates that the sensitivity of neat **7** relates to it being an oil at ambient temperature. The monoarenes **8** and $PhPH_2$ had oxidized to a large extent by the end of the seven days in solution, but were still more stable than in their neat state as oils.

As steric factors do not appear significant in the stabilization of **4** and **5** to oxidation, we wished to examine their electronic nature. Unfortunately, the low basicity of the phosphanes (**5** was unprotonated with 6 M HCl) and solubility difficulties precluded the measurement of pK_a values. Some insight into their basicity was obtained from IR studies following the protocol of Henderson and Alley,[10a] in which two equivalents of $FcCH_2PH_2$ were treated with *cis*-$[Mo(C_5H_{10}N)_2(CO)_4]$ to give *cis*-$[Mo(FcCH_2PH_2)_2(CO)_4]$ (Table 1).

Comparison of entries 3, 4, and 7 in Table 1 shows there is no apparent correlation between the oxidative stability of the primary phosphanes and the $\nu_{(CO)}$ (A_1) stretching frequency. This routine method to assess the basicity of the phosphanes cannot therefore be extrapolated to predict their stability in air.

We turned next to the electrochemical behavior of the phosphanes, which was examined by voltammetry using a Pt-disk electrode. We believe that this is the first report of such

 © 2006 Wiley-VCH Verlag GmbH & Co. KGaA, Weinheim

Table 1: The oxidation potentials of the phosphanes and their $\nu_{(CO)}$ (A_1) vibrations in *cis*-[Mo(RPH$_2$)$_2$(CO)$_4$].

	RPH_2	$E_{s,max}$ [mV[a]]	$\nu_{(CO)}$ [cm^{-1}]
1	$FcCH_2PH_2$	–	2020[b]
2	**1a**	960	–[c]
3	(*R*)-**4**	1005[d]	2023
4	(*S*)-**5**	1170	2025
5	**6**	850	2027
6	**7**	845	2027
7	**8**	770[e]	2025
8	$PhPH_2$	795	2025

[a] Tetrabutylammonium tetrafluoroborate (0.1 M) as the supporting electrolyte, scan rate 100 mV s^{-1}, 20 °C; potential in mV, measured with a Pt disk working electrode in degassed dichloromethane solution; the values are referenced to ferrocene/ferrocinium. [b] See Ref. [10b]. [c] The *cis* compound was not formed. [d] This value is attributable to the ether group, as (*R*)-2,2′-dimethoxy-1,1′-binaphthylene gave a value of 1030 mV. [e] Partially masked by the wave of the oxidation product at 1160 mV.

studies on uncomplexed primary phosphanes. We have used the potential of maximum slope $E_{s,max}$[20] to quantify the position of the waves on the potential axis because of the irreversibility of the phosphane oxidation under these experimental conditions. In this case the values obtained do appear to indicate a trend with oxidative stability (Table 1). The lowest potentials are observed for the most readily oxidized compounds **8** and $PhPH_2$. Intermediate in value and very similar in magnitude are the naphthylphosphanes **6** and **7**, again emphasizing that the difference observed in the oxidation of the neat samples is directed by kinetic factors (a solid versus an oil), but also confirming that the position of substitution has little effect. Finally, the oxidation-resistant **5** and **1a** show high $E_{s,max}$ values. These results indicate a correlation between the ease of generation of a radical such as $[RPH_2]^{+\bullet}$ and air stability.[21] This finding is consistent with the reported[22] mechanism of phosphorus oxidation by triplet oxygen having a radical nature.[23]

Our results show that the simple addition of a benzene ring to phenylphosphane imparts stability towards oxidation. In discussing the source of this remarkable stability, we note that there are no steric factors and no remote heteroatom. Therefore the source of this stabilization must be a type of conjugative effect. This is confirmed by the fact that when the additional ring is saturated, the stability was not affected.[24] The conjugative effect could be between the phosphorus lone pair of electrons and the aromatic system, simply within the aromatic system itself, or both. In considering this, we take into account the following: 1) conjugation of phosphanyl groups and aromatic rings has been a most contentious issue in the literature;[25] 2) both 1-naphthyl and 2-naphthyl substitution lead to a similar stabilization, whereas a conjugative effect to the lone pair of electrons might be expected to show a difference; 3) there appears to be no relation between the stabilization and the basicity of the phosphane, which would again imply that the lone pair of electrons is not involved in imparting stability; 4) a lower oxidation potential of the phosphane seems to correlate with the stability observed; and 5) studies from photoelectron spectroscopy (PES)[25a–c] have established that the highest occupied molecular orbital (HOMO) of phenylphosphane is a perturbed π orbital of the benzene ring. We believe therefore that the conjugative effect is related to the aromatic system and that the greater conjugation in (*R*)-**4** and (*S*)-**5** either raises the energy required to form a $[RPH_2]^{+\bullet}$-type radical cation, or conversely stabilizes it, thereby rendering it less reactive in the next stage of the oxidation. However, the manner in which the conjugation operates in exerting such effects is unclear and indeed this still may not be the critical factor controlling the oxidation. We will report in due course on theoretical, PES, and microwave studies of this intriguing system which we hope will allow us to elucidate the origin of the air stability.

In conclusion, we have synthesized the first air-stable chiral primary phosphanes and have attributed their stability to conjugation in their aryl backbones. Our findings suggest that many, perhaps most, primary phosphanes have no greater air sensitivity than moderately reactive aldehydes.[26] We hope that this will prompt a renaissance in the use of primary phosphanes as synthetic precursors; for example, (*R*)-**4** and (*S*)-**5** are convenient starting materials for previously inaccessible asymmetric phosphanes, such as phospholane–mop hybrids. More generally we note that 2-naphthylphosphane (**6**) could be used as a safe and convenient replacement for phenylphosphane.

Received: May 30, 2006
Revised: August 28, 2006
Published online: October 5, 2006

Keywords: air stability · asymmetric catalysis · conjugation · electrochemistry · phosphanes

[1] a) L. Maier in *Organic Phosphorus Compounds*, *Vol. 1* (Eds.: G. M. Kosolapoff, L. Maier), Wiley-Interscience, New York, **1972**, chap. 1, pp. 4–16; b) For example, Rhodia created a safety video for internal use showing spontaneous combustion of primary phosphanes in air to illustrate their pyrophoricity; c) K. V. Katti, N. Pillarsetty, K. Raghuraman, *Top. Curr. Chem.* **2003**, *229*, 121–141.
[2] a) T. P. Clarke, C. R. Landis, *Tetrahedron: Asymmetry* **2004**, *15*, 2123–2137; b) G. Hoge, B. Samas, *Tetrahedron: Asymmetry* **2004**, *15*, 2155–2157; c) D. J. Brauer, K. W. Kottsieper, S. Roßenbach, O. Stelzer, *Eur. J. Inorg. Chem.* **2003**, 1748–1755; d) A. Herrbach, A. Marinetti, O. Baudoin, D. Guénard, F. Guéritte, *J. Org. Chem.* **2003**, *68*, 4897–4905, and references therein; e) S. Chatterjee, M. D. George, G. Salem, A. C. Willis, *J. Chem. Soc. Dalton Trans.* **2001**, 1890–1896.
[3] K. V. Katti, H. Gali, C. J. Smith, D. E. Berning, *Acc. Chem. Res.* **1999**, *32*, 9–17.
[4] H. Dorn, R. A. Singh, J. A. Massey, A. J. Lough, I. Manners, *Angew. Chem.* **1999**, *111*, 3540–3543; *Angew. Chem. Int. Ed.* **1999**, *38*, 3321–3323.
[5] T. Hanaya, H. Yamamoto, *Bull. Chem. Soc. Jpn.* **1989**, *62*, 2320–2327.
[6] E. P. Kyba, S.-T. Liu, *Inorg. Chem.* **1985**, *24*, 1613–1616.
[7] M. Brynda, *Coord. Chem. Rev.* **2005**, *249*, 2013–2034.
[8] a) M. Yoshifuji, K. Shibayama, N. Inamoto, T. Matsushita, K. Nishimoto, *J. Am. Chem. Soc.* **1983**, *105*, 2495–2497; b) M. Yoshifuji, K. Shibayama, K. Toyota, N. Inamoto, *Tetrahedron Lett.* **1983**, *24*, 4227–4228.
[9] G. Ramakrishnan, A. Jouaiti, M. Geoffroy, G. Bernardinelli, *J. Phys. Chem.* **1996**, *100*, 10861–10868.

 © 2006 Wiley-VCH Verlag GmbH & Co. KGaA, Weinheim

[10] a) W. Henderson, S. R. Alley, *J. Organomet. Chem.* **2002**, *656*, 120–128. b) N. J. Goodwin, W. Henderson, B. K. Nicholson, J. Fawcett, D. R. Russell, *J. Chem. Soc. Dalton Trans.* **1999**, 1785–1793.

[11] D. J. Brauer, J. Fischer, S. Kucken, K. P. Langhans, O. Stelzer, N. Weferling, *Z. Naturforsch. B* **1994**, *49*, 1511–1524.

[12] a) N. Pillarsetty, K. Raghuraman, C. L. Barnes, K. V. Katti, *J. Am. Chem. Soc.* **2005**, *127*, 331–336; b) H. Gali, S. R. Karra, V. S. Reddy, K. V. Katti, *Angew. Chem.* **1999**, *111*, 2152–2155; *Angew. Chem. Int. Ed.* **1999**, *38*, 2020–2023.

[13] L. J. Higham, E. F. Clarke, H. Müller-Bunz, D. G. Gilheany, *J. Organomet. Chem.* **2005**, *690*, 211–219.

[14] a) R. Schmid, E. A. Broger, M. Cereghetti, Y. Crameri, J. Foricher, M. Lalonde, R. K. Müller, M. Scalone, G. Schoettel, U. Zutter, *Pure Appl. Chem.* **1996**, *68*, 131–138; b) L. Dahlenburg, A. Kaunert, *Eur. J. Inorg. Chem.* **1998**, 885–887.

[15] Crystal data: (*R*)-**4**: $C_{21}H_{17}OP$, $M_r = 316.32$; $0.30 \times 0.20 \times 0.20\ mm^3$; triclinic; space group: $P\bar{1}$; $a = 7.7975(11)$, $b = 13.1619(18)$, $c = 16.220(2)$ Å, $\alpha = 92.165(3)$, $\beta = 91.324(3)$, $\gamma = 97.985(3)°$, $V = 1646.7(4)$ Å^3; $\rho_{calcd} = 1.276\ Mg\,m^{-3}$; $2\Theta_{max} = 42.00°$; radiation: $Mo_{K\alpha}$ ($\lambda = 0.71073$ Å); scan mode: ϕ-ω scans; measurement temperature: 293(2) K; 12670 reflections collected, (6654 independent, $R_{int} = 0.0411$); correction for Lorentzian polarization and absorption: semi-empirical from equivalents (program SADABS;[27a] $\mu = 0.169\ mm^{-1}$, max. and min. transmission 0.9670 and 0.7351); solution: direct methods (SHELXS-97[27b]); refinement: full-matrix least-squares against $|F^2|$ (SHELXL-97-2[27c]), 837 parameters; hydrogen atoms were added at calculated positions and refined using a riding model; $R_1 = 0.0790$ and $wR_2 = 0.1312$ (all data); residual electron density: $0.169\ e^-$ Å^{-3}; CCDC-281451 contains the supplementary crystallographic data for this paper. These data can be obtained free of charge from The Cambridge Crystallographic Data Centre via www.ccdc.cam.ac.uk/data_request/cif.

[16] R. A. Bartlett, M. M. Olmstead, P. P. Power, G. A. Sigel, *Inorg. Chem.* **1987**, *26*, 1941–1946.

[17] Several references with no comment on air stability but giving crystal structure data are given in the Supporting Information.

[18] We note 2′-diphenylphosphanyl-1,1′-binaphthyl (Y. Uozumi, N. Suzuki, A. Ogiwara, T. Hayashi, *Tetrahedron* **1994**, *50*, 4293–4302) is highly effective in asymmetric hydrosilylation (K. Kitayama, Y. Uozumi, T. Hayashi, *J. Chem. Soc. Chem. Commun.* **1995**, 1533–1534) and cross-coupling reactions (Y. H. Cho, A. Kina, T. Shimada, T. Hayashi, *J. Org. Chem.* **2004**, *69*, 3811–3823).

[19] The first oxidation products formed from **6** and **7** over the time frame of Figure 2 are the corresponding primary phosphane oxides (^{31}P NMR: $\delta = 0.8$ ppm for **6**; $\delta = 0.4$ ppm for **7**) consistent with the case of supermesitylphosphane.[8b] Compounds **4** and **5** are not oxidized over the same time frame but behave similarly if left for very much longer or subjected to more harsh conditions.

[20] a) K. B. Oldham, *J. Electroanal. Chem.* **1985**, *184*, 257–267; b) P. D. Lyne, R. D. O'Neill, *Anal. Chem.* **1990**, *62*, 2347–2351.

[21] Although these measurements are indicative of a one-electron process at an electrode and not necessarily applicable to oxidation by an oxygen molecule, they do however indicate the relative HOMO energies of the different primary phosphanes.

[22] a) H. R. Hudson in *The Chemistry of Organophosphorus Compounds*, *Vol. 1* (Ed.: F. R. Hartley), Wiley, New York, **1990**, pp. 438–439, and references therein; b) P. D. Bartlett, E. F. Cox, R. E. Davis, *J. Am. Chem. Soc.* **1961**, *83*, 103–109.

[23] It should be noted that **1a** and **5** were easily oxidized by peroxides in reaction grade THF, but this is an oxidation that takes place by a different mechanistic process; see reference [22a].

[24] One other suggested possibility for the stability of **4**/**5** relative to $PhPH_2$ is that the latter is ordinarily contaminated by a species that assists oxidation. However, when **5** was spiked with $PhPH_2$ no oxidation of **5** was observed after 25 days.

[25] a) D. E. Cabelli, A. H. Cowley, M. J. S. Dewar, *J. Am. Chem. Soc.* **1981**, *103*, 3286–3289; b) L. Nyulaszi, D. Szieberth, G. I. Csonka, J. Reffy, J. Heinicke, T. Veszpremi, *Struct. Chem.* **1995**, *6*, 1–7; c) K. Miqueu, J-M. Sotiropoulos, G. Pfister-Guillouzo, V. Rudzevich, V. Romanenko, G. Bertrand, *Eur. J. Inorg. Chem.* **2004**, 381–387; d) T. P. Debies, J. W. Rabalais, *Inorg. Chem.* **1974**, *13*, 308–312; e) D. G. Gilheany in *The Chemistry of Organophosphorus Compounds*, *Vol. 1* (Ed.: F. R. Hartley), Wiley, **1990**, chap. 1, pp. 9–49.

[26] We stress that oxidation of neat and dissolved primary phosphanes by air, oxygen, and peroxide are not trivial experiments and stringent safety precautions against fire must be adopted.

[27] a) G. M. Sheldrick, SADABS, Bruker AXS Inc., Madison, WI 53711, USA, **2000**; b) G. M. Sheldrick, SHELXS-97, University of Gottingen, **1997**; c) G. M. Sheldrick SHELXL-97-2, University of Gottingen, **1997**.

 © 2006 Wiley-VCH Verlag GmbH & Co. KGaA, Weinheim

Gas-Phase Ionic Liquids

DOI: 10.1002/anie.200602219

On the Species Involved in the Vaporization of Imidazolium Ionic Liquids in a Steam-Distillation-Like Process**

Brenno A. DaSilveira Neto, Leonardo S. Santos, Fabiane M. Nachtigall, Marcos N. Eberlin, and Jairton Dupont**

Among the various outstanding properties exhibited by ionic liquids (ILs), two of the most peculiar are their very low vapor pressure[1] and pronounced supramolecular self-organization both in the condensed[2–5] and gas phases.[6] This unique set of properties make ionic liquids very attractive alternatives to classical organic solvents and water, opening also a wealth of

[*] Dr. L. S. Santos,[+] F. M. Nachtigall, Prof. M. N. Eberlin
Thomson Mass Spectrometry Laboratory
Institute of Chemistry–UNICAMP
Campinas, SP-13083-970 (Brazil)
Fax: (+55) 19-3521-3073
E-mail: eberlin@iqm.unicamp.br

Dr. B. A. DaSilveira Neto, Prof. J. Dupont
Laboratory of Molecular Catalysis
Institute of Chemistry–UFRGS
Porto Alegre, RS-91501-970 (Brazil)
Fax: (+55) 51-3316-7304
E-mail: dupont@iq.ufrgs.br

[+] Permanent address: Chemistry Institute of Natural Resources
Talca University
Casa Central 2, Norte 685, Talca (Chile)

[**] This research was supported in part by FAPESP, FINEP-MCT, CNPq, and CAPES.

© 2006 Wiley-VCH Verlag GmbH & Co. KGaA, Weinheim
WILEY InterScience DISCOVER SOMETHING GREAT

other applications.[7–11] Owing to the (so-far indisputable) nonvolatility of ILs, rather atypical investigations of molecular properties in solution are possible under high-vacuum conditions.[12,13] Very recently, however, the "nonvolatility paradigm" of ILs has been challenged. It was found that some highly thermally stable ILs based on ammonium salts such as imidazolium cations may be distilled under high-vacuum conditions.[14] Based on the observed distillation profiles, it was postulated that for both protic and aprotic ILs volatilization occurs most likely by transfer to the gas phase of multiple ion clusters (probably discrete neutral clusters), which further aggregate and recondense as pure IL at lower temperatures. It was also argued against a proton-transfer mechanism that could facilitate vaporization of ILs as single neutral species, such as the respective imidazole carbenes.[14] Herein experimental evidence is provided for the mechanism of the long-overlooked IL vaporization process.

We chose to investigate IL distillation by means of atmospheric-pressure chemical ionization mass spectrometry experiments[15,16] (APCI-MS and APCI-MS/MS). During the electrohydrodynamic spraying process of APCI,[17] the sample vaporizes together with the solvent by an interesting steam-distillation-like process.[18] This process promotes gentle ambient vaporization at temperatures considerably lower than the boiling point or decomposition temperature of the sample. An electron beam produced by a corona-discharge needle at the end of a metal capillary (Figure 1) creates the

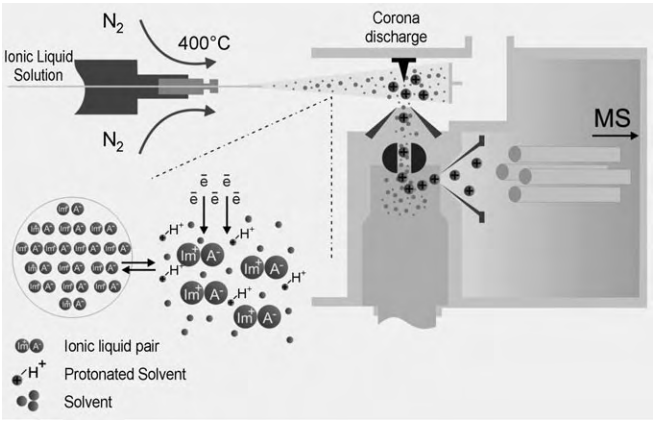

Figure 1. Schematic representation of ambient vaporization, ionization, and detection of ILs under APCI conditions. As seen in the expanded region, under the positive-ion mode, $[Im_nA_{n-1}]^+$ ions are proposed to be formed in the APCI plasma by abstraction of A^- from Im_nA_n gaseous clusters by proton-transfer reactions with the protonated solvent.

APCI plasma. In this plasma, protonated and deprotonated solvent molecules are formed, and proton-transfer or proton-abstraction reactions with the gaseous analyte molecules (M) create the major ions detected by MS, either $[M+H]^+$ or $[M-H]^-$.[19] We therefore envisaged that this gentle steam-distillation-like process could promote ambient vaporization of IL followed by soft chemical ionization of the putative IL neutral clusters for further detection and characterization by MS.

Gratifyingly, when acetonitrile solutions of the six ILs investigated[20] (Scheme 1) were subjected to APCI-MS with the APCI heater set to 100–600 °C and the corona-discharge voltage set to 3000 V or more, all of the IL clusters were

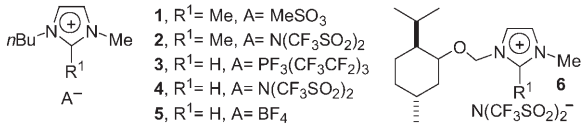

Scheme 1. Imidazolium-based ILs investigated by APCI-MS.

indeed detected (Figure 2). In the positive-ion mode, at temperatures close to 100 °C the imidazolium cation started to be detected, and at higher temperatures supramolecular

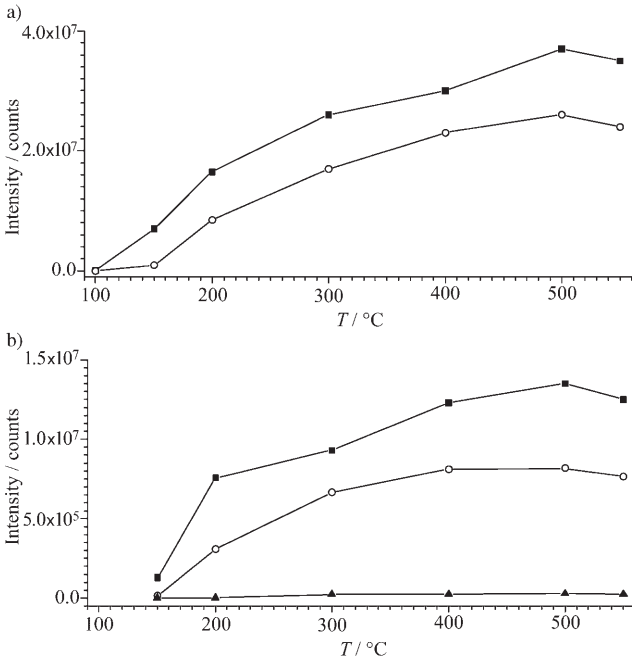

Figure 2. Detection of ionic clusters from ionic liquid **4** in a) positive-ion mode: Im^+ (■), $[Im_2A]^+$ (○) and b) negative-ion mode A^- (■), $[ImA]^-$ (○) $[Im_2A_3]^-$ (▲) with increasing temperature.

clusters of the type $[Im_2A]^+$ (Im = imidazolium unit, A = anion) were also observed (Figure 2). Similar behavior was observed in negative-ion mode: $[NTf_2]^-$ (Tf = trifluoromethanesulfonyl) was detected at around 150 °C, and when the temperature was increased, higher supramolecular aggregates such as $[ImA_2]^-$ and $[Im_2A_3]^-$ were observed. Therefore higher temperatures tend to favor the distillation of heavier clusters up to near 500 °C, at which temperature the ion abundance decreases somewhat probably as a result of IL decomposition and/or decreased efficiency of the APCI process at elevated temperatures.

As Figure 3 illustrates for ILs **2** and **3**, APCI(+)-MS (in the positive-ion mode) detects mainly the ImA and $[Im_2A_2]$ clusters as the cation Im^+ (m/z 153 and 139, respectively) and the supramolecular cationic species $[Im_2A]^+$ (m/z 451 and

 © 2006 Wiley-VCH Verlag GmbH & Co. KGaA, Weinheim

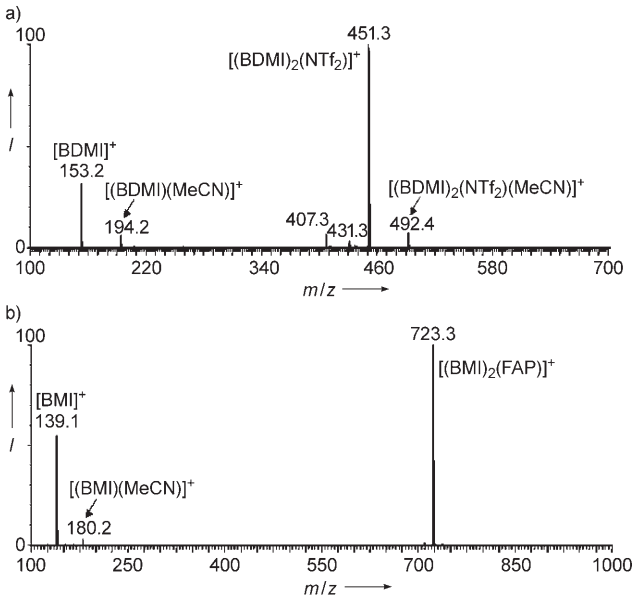

Figure 3. APCI(+)-MS of solutions of a) **2** and b) **3**in MeCN.

723) as well as eventually their corresponding solvent (acetonitrile) adducts. When no or low voltages were applied at the corona-discharge capillary (no discharge), and when the metal capillary was simply isolated, no ions were detected at all. This result indicates that neutral species are being distilled, and that ionization of these species is facilitated by the APCI plasma. When APCI(−)-MS was applied, three important and correlated species were detected: A^-, $[ImA_2]^-$ and $[Im_2A_3]^-$, as Figure 4 illustrates for **3** (*m*/*z* 279.9, 699.1, and 1118.3, respectively).

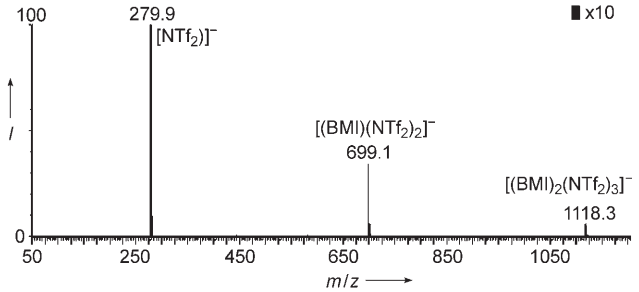

Figure 4. APCI(−)-MS of a solution of **2** in MeCN.

The abundances of the negatively charged trimer $[Im_2A_3]^-$ under APCI(−)-MS were very low, and it is quite possible that the positively charged trimer cluster was formed but to an undetectable amount for APCI(+)-MS. The abundance of negative and positive ions for the same cluster may vary considerably owing to the different energetics of the ion/molecule reactions leading to their formation, protonation, and deprotonation.

We also note that the APCI-MS results are very distinct from those from fast-atom bombardment (FAB) MS[21] and electrospray ionization (ESI) MS[6] for imidazolium ion based ILs; these methods generate a much more diverse set of singly, doubly, and triply charged higher ionic clusters with magic-number aggregation. In FAB and ESI, these larger aggregates are formed by different processes. In FAB, preformed ions in the matrix solution are desorbed by a localized nonequilibrium vibrational process or evaporate from the splash droplets.[22] In ESI, ions evaporate from highly charged droplets, or tiny droplets containing a single ion evaporate to produce the gaseous ions.[17]

The composition of these IL clusters was also investigated by tandem mass spectrometry. For example, the supramolecular species $[Im_2A]^+$ (*m*/*z* 723) from **2** dissociates upon collisions with argon as expected by the loss of a neutral ImA cluster to form Im^+ (*m*/*z* 139). Similarly, $[Im_2A_3]^-$ (*m*/*z* 1118.3; also from **2**), dissociates by sequential loss of ImA to form the fragment ions $[ImA_2]^-$ (*m*/*z* 699.1) and A^- (*m*/*z* 279.9; Figure 5).

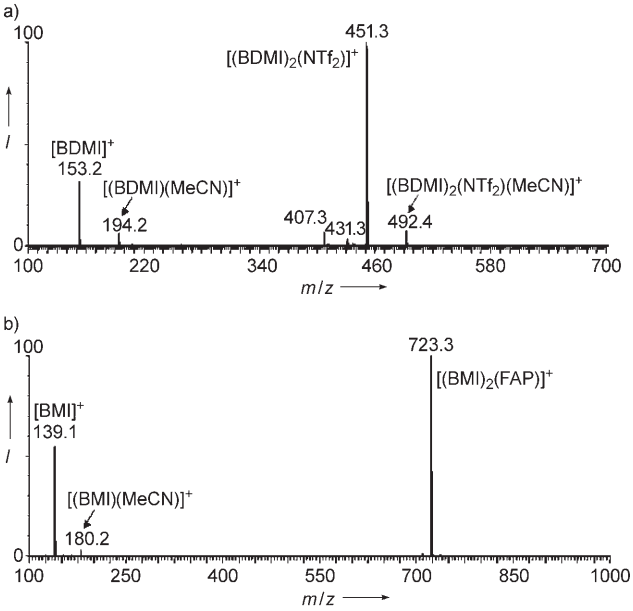

Figure 5. a) APCI(+)-MS/MS for collision(15 eV)-induced dissociation of $[X_2A]^+$ from **2**; b) APCI(−)-MS/MS for collision(15 eV)-induced dissociation of $[Im_2A_3]^-$ from **3**.

We therefore rationalize that during APCI(+)-MS, Im^+ and $[Im_2A]^+$ are formed by proton transfer from $[S+H]^+$ to the gaseous ImA and Im_2A_2 clusters, respectively, as summarized in Equations (1) and (2) and represented schematically in Figure 3.

$$ImA + [S+H]^+ \rightarrow Im^+ + AH + S \quad (1)$$

$$Im_2A_2 + [S+H]^+ \rightarrow [Im_2A]^+ + AH + S \quad (2)$$

Analogously, during APCI(−)-MS, the homologous anions A^-, $[ImA_2]^-$, and $[Im_2A_3]^-$ are formed either by direct electron attachment to the respective neutral clusters (the most plausible event for the aprotic IL) or by deprotonation reactions with the $[S-H]^-$ species [Eqs. (3)–(5)].

$$ImA + [S-H]^- \rightarrow [Im+H] + A^- + S \quad (3)$$

 © 2006 Wiley-VCH Verlag GmbH & Co. KGaA, Weinheim

$$Im_2A_2 + [S{-}H]^- \rightarrow [Im{+}H] + [ImA_2]^- + S \quad (4)$$

$$Im_3A_3 + [S{-}H]^- \rightarrow [Im{+}H] + [Im_2A_3]^- + S \quad (5)$$

Note that, like the distillation profiles observed by Earle and co-workers,[14] the present APCI-MS data are also in opposition with IL volatilization via neutral single species. For the ILs **1**–**6**, the neutral species would be the respective imidazole carbenes[23] and the protonated anions AH. Both unsubstituted (**3**–**6**) and substituted (**1**, **2**) ILs produces abundant ions with similar distributions upon APCI-MS in both negative- and positive-ion modes. In addition, the neutral AH species such as $[BF_4 + H]$ and $[FAP + H]$ ($FAP = PF_3(CF_3CF_2)_3$) would hardly be stable in the APCI plasma, probably decomposing by the loss of HF. We also failed to observe any detectable amounts of $[AH + H]^+$ species during APCI(+)-MS particularly when $A^- = NTf_2^-$.

Recently the atmospheric-pressure thermal desorption ion mass spectrometry (APTDI-MS) of organic salts, including two ionic liquids, was reported. For ILs, ionic species, such as the 1,3-dimethylimidazolium ion (Im^+) and its aggregate $[Im_2A]^+$ were detected.[24] This observation was interpreted as the thermal emission of ions directly from the viscous ionic liquids, suggesting that the desorption of ions could also be used to support distillation and volatility of ionic liquids. In view of the present results from the gentle steam-distillation-like process of APCI, we rationalize that ILs distill indeed as discrete neutral aggregates of the general formula $[ImA]_n$ ($n \approx 1$–3). As the interactions of the lighter gaseous supramolecules are weaker than those observed in the condensed phase (where much larger supramolecular assemblies dominate), they can therefore be disrupted either thermally during APTDI or by ion/molecule reactions during APCI to form the $[Im_nA_{n-1}]^+$ or $[Im_{n-1}A_n]^-$ species observed by both techniques. Therefore, when heated, imidazolium ILs composed of supramolecular structures $[(Im)_x(A)_{x-n})]^{n+}[(Im)_{x-n}(A)_x)]^{n-}$ in the condensed phase vaporize as discrete neutral clusters of the type Im_nA_n. We are currently investigating the APCI-MS behavior of several types of ILs including thermally unstable ones in the search for similar clusters.

Experimental Section

APCI mass spectra and tandem mass spectra were acquired using a Micromass (Manchester, UK) Qtof instrument. Typical operating conditions: APCI corona probe current: 3 kV; cone voltage: 2 V; vaporizer temperature: 400 °C. APCI tandem MS were collected using collision(15 eV)-induced dissociation with argon of selected ions.

Received: June 2, 2006
Revised: June 27, 2006
Published online: October 9, 2006

Keywords: distillation · imidazolium · ionic liquids · mass spectrometry

[1] P. Wasserscheid, *Nature* **2006**, *439*, 797 – 797.
[2] M. Antonietti, D. B. Kuang, B. Smarsly, Z. Yong, *Angew. Chem.* **2004**, *116*, 5096 – 5100; *Angew. Chem. Int. Ed.* **2004**, *43*, 4988 – 4992.
[3] J. Dupont, *J. Braz. Chem. Soc.* **2004**, *15*, 341 – 350.
[4] C. S. Consorti, P. A. Z. Suarez, R. F. de Souza, R. A. Burrow, D. H. Farrar, A. J. Lough, W. Loh, L. H. M. da Silva, J. Dupont, *J. Phys. Chem. B* **2005**, *109*, 4341 – 4349.
[5] J. Dupont, P. A. Z. Suarez, *Phys. Chem. Chem. Phys.* **2006**, *8*, 2441 – 2452.
[6] F. C. Gozzo, L. S. Santos, R. Augusti, C. S. Consorti, J. Dupont, M. N. Eberlin, *Chem. Eur. J.* **2004**, *10*, 6187 – 6193.
[7] P. Wasserscheid, T. Welton, *Ionic Liquids in Synthesis*, Wiley-VCH, Weinheim, **2003**.
[8] P. Wasserscheid, W. Keim, *Angew. Chem.* **2000**, *112*, 3926 – 3945; *Angew. Chem. Int. Ed.* **2000**, *39*, 3772 – 3789.
[9] J. Dupont, R. F. de Souza, P. A. Z. Suarez, *Chem. Rev.* **2002**, *102*, 3667 – 3691.
[10] T. Welton, *Coord. Chem. Rev.* **2004**, *248*, 2459 – 2477.
[11] B. A. D. Neto, G. Ebeling, R. S. Goncalves, F. C. Gozzo, M. N. Eberlin, J. Dupont, *Synthesis* **2004**, 1155 – 1158.
[12] C. W. Scheeren, G. Machado, J. Dupont, P. F. P. Fichtner, S. R. Texeira, *Inorg. Chem.* **2003**, *42*, 4738 – 4742.
[13] E. F. Smith, I. J. V. Garcia, D. Briggs, P. Licence, *Chem. Commun.* **2005**, 5633 – 5635.
[14] M. J. Earle, J. Esperanca, M. A. Gilea, J. N. C. Lopes, L. P. N. Rebelo, J. W. Magee, K. R. Seddon, J. A. Widegren, *Nature* **2006**, *439*, 831 – 834.
[15] S. J. Bos, S. M. van Leeuwen, U. Karst, *Anal. Bioanal. Chem.* **2006**, *384*, 85 – 99.
[16] E. C. Horning, M. G. Horning, D. I. Carroll, I. Dzidic, R. Stillwell, *Anal. Chem.* **1973**, *45*, 936 – 943.
[17] A. G. Harrison, *Chemical Ionization Mass Spectrometry*, 2nd ed., CRC Press, NY, **1992**.
[18] W. L. F. Armarego, D. D. Perrin;, *Purification of Laboratory Chemicals*, 4th ed., Butterworth-Heinemann, Oxford, **1997**.
[19] T. J. Kauppila, T. Kuuranne, E. C. Meurer, M. N. Eberlin, T. Kotiaho, R. Kostiainen, *Anal. Chem.* **2002**, *74*, 5470 – 5479.
[20] C. C. Cassol, G. Ebeling, B. Ferrera, J. Dupont, *Adv. Synth. Catal.* **2006**, *348*, 243 – 248.
[21] A. K. AbdulSada, A. E. Elaiwi, A. M. Greenway, K. R. Seddon, *Eur. Mass Spectrom.* **1997**, *3*, 245 – 247.
[22] C. Fenselau, R. J. Cotier, *Chem. Rev.* **1987**, *87*, 501 – 512.
[23] J. Dupont, J. Spencer, *Angew. Chem.* **2004**, *116*, 5408 – 5409; *Angew. Chem. Int. Ed.* **2004**, *43*, 5296 – 5297.
[24] H. Chen, O. Y. Zheng, R. G. Cooks, *Angew. Chem.* **2006**, *118*, 3738 – 3742; *Angew. Chem. Int. Ed.* **2006**, *45*, 3656 – 3660.

 © 2006 Wiley-VCH Verlag GmbH & Co. KGaA, Weinheim

A Metal-Catching Linker

DOI: 10.1002/anie.200602523

An Engineered Linker Capable of Promoting On-Resin Reactions for Microwave-Assisted Solid-Phase Organic Synthesis**

*Li-Ping Sun and Wei-Min Dai**

Solid-phase organic synthesis (SPOS)[1] has emerged as one of the key tools in combinatorial chemistry[2] for generating libraries of small organic molecules. In order to transfer the versatile reaction types established in solution to solid-phase synthesis, numerous classes of linkers[1–3] have been developed, including traceless and multifunctional linkers.[4] The latter enable the generation of diversity in the end products upon cleavage (R in Figure 1A). If a linker possesses elements of chirality, reactions occurring on the tethered scaffold are induced to form chiral molecules.

In a different approach from the resin-bound chiral auxiliaries,[5] the immobilization of chiral ligands and metal complexes has been advanced in recent years, to allow easy recovery of resin-bound chiral catalysts from the reaction solution (Figure 1B).[6] In such heterogeneous catalysis, the substrate is not loaded onto the resin and conventional purification is required for product separation. Despite the fact that many metal-catalyzed reactions have been carried out on resin-bound scaffolds,[1d] there is virtually no example of a solid-phase reaction promoted by a metal species that is covalently bound in close proximity to the scaffold. We report herein an engineered linker (cat·linker) with the dual functions of a normal linker for attachment of a scaffold and a promoter for facilitating the reaction occurring on the tethered scaffold (Figure 1C). It has been proven essential for performing Cu^{II}-mediated heteroannulation on a cat·linker-conjugated scaffold under microwave irradiation.[7]

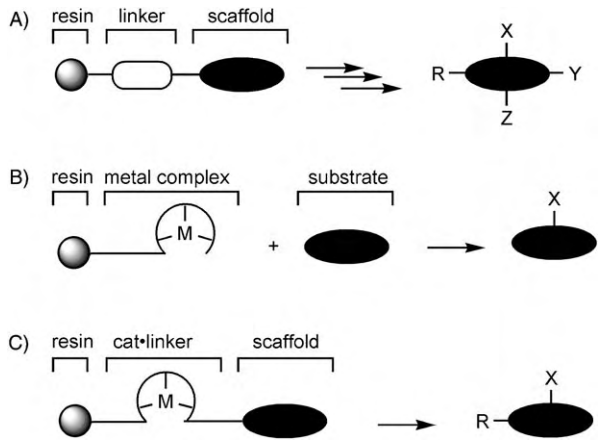

Figure 1. Schematic representations of A) solid-phase synthesis, B) solution synthesis by using supported metal complexes, and C) solid-phase synthesis with a novel linker capable of on-resin activation. M = metal ion, cat·linker = a linker capable of catching metal ions and promoting on-resin reactions.

In connection with our previous solid-phase synthesis of an indole library[8] through Pd^{II}-[9] or Cu^{II}-catalyzed[10] intramolecular heteroannulation under controlled microwave heating,[11] we designed the solid-phase synthesis of 2,5-disubstituted indoles **4** by anchoring 2-bromo-4-nitroaniline onto Rink amide resin through a diacid spacer (Scheme 1).

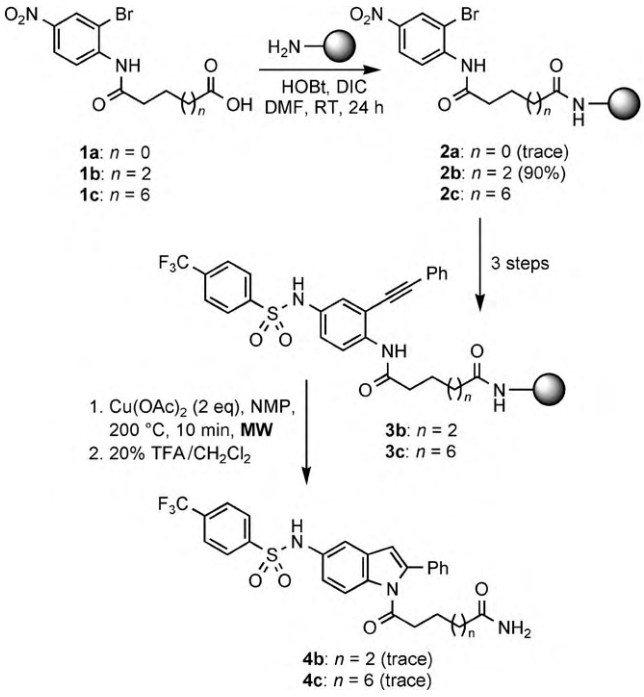

Scheme 1. Initial attempts to form 1-acyl indoles **4** by using diacid-modified linkers. DIC = *N*,*N*-diisopropylcarbodiimide, DMF = *N*,*N*-dimethylformamide, HOBt = *N*-hydroxybenzotriazole, **MW** = microwave, NMP = *N*-methylpyrrolidinone, TFA = trifluoroacetic acid.

This approach differed from our reported solid-phase synthesis employing resin-bound 1-alkynes.[8] We envisaged that the *N*-acyl chains in **4** could be easily removed during postcleavage modification upon exposure to a base,[12] which would result in an indirect traceless synthesis.[4]

We found that the diacid chain length influenced the solid-phase reactions at different stages. First, the succinic acid derived **1a** failed[13] to couple with the Rink amide resin while

[*] Dr. L.-P. Sun, Prof. W.-M. Dai
Department of Chemistry
The Hong Kong University of Science and Technology
Clear Water Bay, Kowloon, Hong Kong SAR (P.R. China)
Fax: (+852) 2358-1594
E-mail: chdai@ust.hk
Homepage: http://ihome.ust.hk/~chdai/index.html

[**] This work was supported in part by the Innovation and Technology Fund (ITS/119/00) from the Innovation and Technology Commission and an Earmarked Research Grant (600904) from the Research Grants Council, The Hong Kong Special Administrative Region, P.R. China. Support from the Department of Chemistry, The Hong Kong University of Science and Technology, is also acknowledged.

Supporting information for this article is available on the WWW under http://www.angewandte.org or from the author.

 © 2006 Wiley-VCH Verlag GmbH & Co. KGaA, Weinheim

1b and **1c**, with their longer chains, could be successfully loaded onto the resin. For example, cleavage of **2b** supplied the resin-free product in 90% yield. From **2b** and **2c**, the resin-bound 2-alkynyl anilides **3b** and **3c** were prepared in good purities and yields by following our established procedures.[8] To our surprise, the Cu^{II}-mediated cyclization under controlled microwave heating at 200 °C[8] did not produce indoles **4b** and **4c**, as confirmed by cleavage of the materials from the resin. We reasoned that the failure in the cyclization might result from an inferior contact of Cu^{II} with the resin-bound alkynes.

In order to enhance the efficiency of solid-phase reactions by running them in a more "solution-like" environment, poly(ethylene glycol) (PEG) grafted polystyrene supports and other resins have been introduced.[1a] We took a different approach to improve the heterogeneous reaction profiles by building a metal-capture unit onto the linker in close proximity to the scaffold. Scheme 2 illustrates our design and the fabrication of the polyglycine-derived engineered linkers. We built the polyglycine chains on the Rink amide resin (0.70 mmol g^{-1}) through microwave-assisted polypeptide synthesis.[14] A 93% yield was estimated for **5** based on a loading of 0.65 mmol g^{-1}. By iterative peptide synthesis, the glycine-modified resins **6** and **7** were prepared. Removal of Fmoc in **5**–**7** followed by coupling with the acid **1b** furnished **8a**–**c** in excellent overall yields.

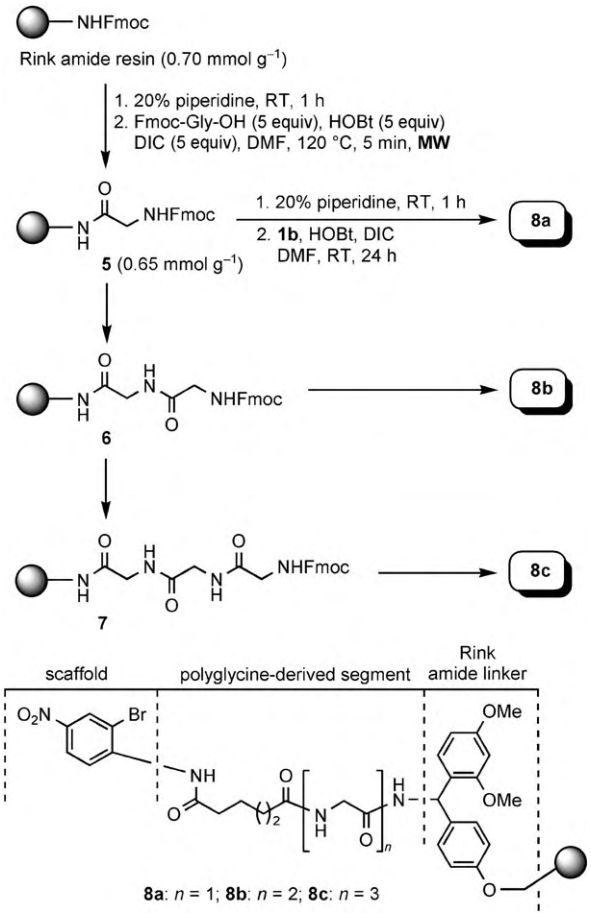

Scheme 2. Design and synthesis of three examples of the new system cat·linker (polyglycine-derived segment + Rink amide linker). Fmoc = (9-fluorenylmethyloxy)carbonyl.

With **8a**–**c** in hand, we synthesized the resin derivatives **9a**–**c** by a) Sonogashira cross-coupling, b) nitro reduction, and c) sulfonamide formation (Scheme 3).[8] Upon exposure

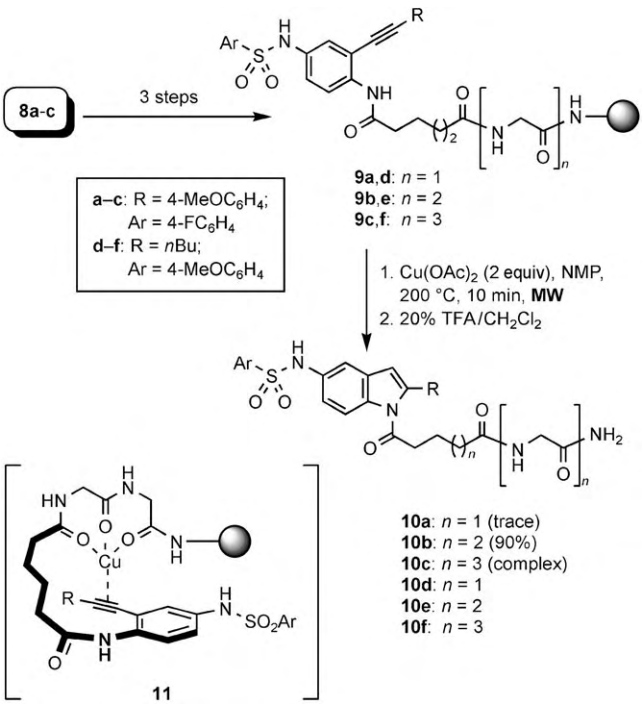

Scheme 3. Effect of glycine units on cat·linker performance.

of **9a**–**c** to $Cu(OAc)_2$ in NMP under controlled microwave heating at 200 °C for 10 min, the desired product **10b** was obtained in 90% yield after cleavage from the resin. By contrast, compound **10a** was hardly detected in the resin cleavage mixture and **10c** was a trace component of a complex mixture. The remarkable effect of the built-in glycine units on the heteroannulation might be explained by a metal-catching and activation mechanism. That is, the dipeptide moiety in **9a** was not efficient for fishing Cu^{II} from the solution onto the resin, while the coordination sites of Cu^{II} were mostly occupied by the tetrapeptide in the case of **9c**, thereby rendering activation of the alkyne difficult.[15] As depicted in the structure of **11**, the tripeptide unit of **9b** may form a Cu^{II} complex through the amide carbonyl oxygen donors[16] and the Cu ion also chelates with the neighboring alkyne to promote the heteroannulation. It should be emphasized that the formation of stable Cu^{II} complexes is not necessary for activating the alkyne moiety toward heteroannulation because excess Cu^{II} was used for the solid-phase reaction. Instead, any factor, such as diffusion, which improves transfer of Cu^{II} onto the resin is beneficial to the heterogeneous reaction.

In order to gain support for the above assumption, we carried out control experiments with the resin-bound alkynes **9d**–**f**, prepared from **8a**–**c**. First, **9d**–**f** were subjected to microwave heating in NMP at 200 °C for 10 min *in the absence of* $Cu(OAc)_2$. After cleavage, the resin-free alkynes were

 © 2006 Wiley-VCH Verlag GmbH & Co. KGaA, Weinheim

essentially recovered, as confirmed by ^{1}H NMR spectroscopy (see S37–S39 in the Supporting Information). In a separate set of experiments, the resin-bound alkynes **9d–f** were sopped in an NMP solution of $Cu(OAc)_2$ at room temperature for 24 h, thereby allowing Cu^{II} to diffuse onto the resin. After washing and drying, the Cu^{II}-treated alkynes were subjected to the same microwave heating in NMP at 200 °C for 10 min *without additional $Cu(OAc)_2$*. Formation of indole **10e** was clearly demonstrated by ^{1}H NMR analysis of the crude reaction mixture. Indoles **10d** and **10f** were also formed but to a much lesser extent (see S35–S36 in the Supporting Information). On the basis of these findings, we can conclude that: a) a combination of microwave heating and Cu^{II} is essential for the heteroannulation,[8,10] b) once Cu^{II} is sopped up onto the resin, heteroannulation takes place upon heating, and c) the diglycine-derived cat·linker in **8b** is superior for promoting on-resin heteroannulation, although the exact mode of Cu intake may be subject to further discussion.

As an application of the cat·linker, we synthesized a 16-member library of indoles **14** from the scaffold **8b** by using 4 terminal alkynes and 4 arylsulfonyl chlorides. The results are summarized in Scheme 4 and Table 1. The solid-phase synthesis of **12** was carried out by using the IRORI radio frequency (R_f)-encoded MicroKan reactors.[8] Then, an individual library member **12** was transferred from the MicroKan reactor along with the R_f tag to a 10-mL pressurized process vial for the Cu^{II}-mediated heteroannulation, heated with a technical microwave reactor. Attempts to directly release indole **14** from the resin-bound product were not successful. Therefore, **13** was cleaved from the support at the site of the Rink amide linker and was converted into **14** by treatment with a mixed pyrrolidine/THF solution at 60 °C for 12 h. The peptide residue could be easily removed from the product by filtration through a short silica gel plug. The overall yields of indoles **14** are 38–60%, as calculated from the loading of **5** (0.65 mmol g^{-1}). To our delight, the purities of **14** are excellent (89–100%), as determined by LC–MS analysis (Table 1).[17]

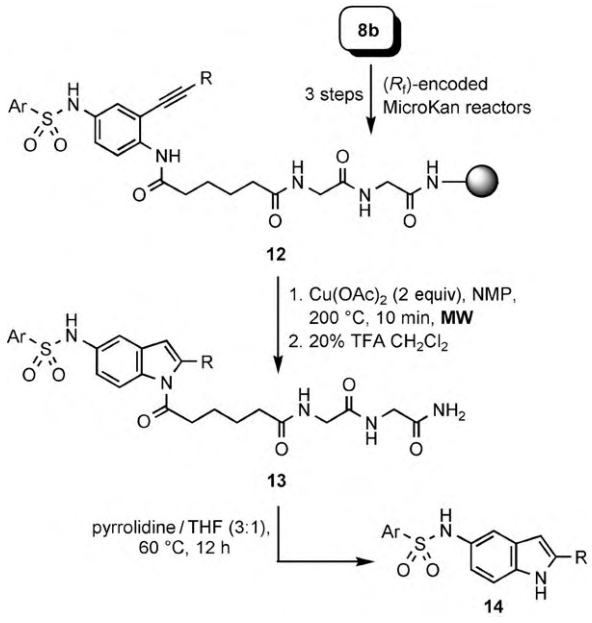

Scheme 4. Synthesis of a library of indoles **14** (see Table 1).

Table 1: Synthesis of a 16-member indole library.

14: R; Ar	Yield [%][a]	Purity [%][b]
a: 4-MeC$_6$H$_4$; 4-FC$_6$H$_4$	49	93[c]
b: 4-MeC$_6$H$_4$; 4-MeOC$_6$H$_4$	38	98
c: 4-MeC$_6$H$_4$; 4-*i*PrC$_6$H$_4$	45	97
d: 4-MeC$_6$H$_4$; 2-thienyl	45	93
e: 4-MeOC$_6$H$_4$; 4-FC$_6$H$_4$	48	90[c]
f: 4-MeOC$_6$H$_4$; 4-MeOC$_6$H$_4$	60	96
g: 4-MeOC$_6$H$_4$; 4-*i*PrC$_6$H$_4$	53	97
h: 4-MeOC$_6$H$_4$; 2-thienyl	43	98
i: Ph; 4-FC$_6$H$_4$	51	95[c]
j: Ph; 4-MeOC$_6$H$_4$	44	89
k: Ph; 4-*i*PrC$_6$H$_4$	56	97
l: Ph; 2-thienyl	46	98
m: *n*Bu; 4-FC$_6$H$_4$	47	96[c]
n: *n*Bu; 4-MeOC$_6$H$_4$	51	100
o: *n*Bu; 4-*i*PrC$_6$H$_4$	43	99
p: *n*Bu; 2-thienyl	59	99

[a] Calculated based on the loading of **5** (0.65 mmol g^{-1}). [b] Determined by HPLC. The structures were characterized by ^{1}H NMR spectroscopy and MS. [c] The fluorine atom was replaced by pyrrolidine.

In summary, we have developed an engineered linker with dual functions for anchoring the scaffold onto a solid support and for promoting a metal-mediated reaction at an appropriate stage of the solid-phase synthesis. Incorporation of the Cu^{II}-capturing tripeptide segment into the so-called cat·linker proves essential for the microwave-assisted indole synthesis through heteroannulation. We consider that diffusion of Cu^{II} from the solution onto the support may be a main path, but distribution of Cu^{II} on the resin surface is influenced by the linker structure. Only Cu^{II} species located close to the attached scaffold and capable of complexation with the alkyne can promote the heteroannulation. In addition to easy on-resin fabrication, the cat·linker has no influence on the Pd^0–Cu^I-catalyzed Sonogashira cross-coupling reaction or the $SnCl_2{\cdot}H_2O$ reduction of NO_2. The cat·linker-modified polystyrene support retains the same resin profile and can be used, as in the current study, for IRORI MicroKan reactor-based R_f-encoded split-pool combinatorial synthesis.

Received: June 22, 2006
Published online: October 6, 2006

Keywords: heteroannulation · heterocycles · heterogeneous catalysis · microwave-assisted reactions · solid-phase synthesis

[1] a) F. Zaragoza Dörwald, *Organic Synthesis on Solid Phase. Supports, Linkers, Reactions*, Wiley-VCH, Weinheim, **2000**; b) *Solid-Phase Organic Synthesis* (Ed.: K. Burgess), Wiley-Interscience, New York, **2000**; c) P. Seneci, *Solid-Phase Synthesis and Combinatorial Technologies*, Wiley-Interscience, New York, **2000**; d) S. Bräse, J. H. Kirchhoff, J. Köbberling, *Tetrahedron* **2003**, *59*, 885–939.

[2] a) *Handbook of Combinatorial Chemistry* (Eds.: K. C. Nicolaou, R. Hanko, W. Hartwig), Wiley-VCH, Weinheim, **2002**; b) *Combinatorial Chemistry. A Practical Approach* (Eds.: W. Bann-

 © 2006 Wiley-VCH Verlag GmbH & Co. KGaA, Weinheim

warth, E. Felder), Wiley-VCH, Weinheim, **2000**; c) *Combinatorial Chemistry. Synthesis, Analysis, Screening* (Ed.: G. Jung), Wiley-VCH, Weinheim, **1999**.
[3] F. Guillier, D. Orain, M. Bradley, *Chem. Rev.* **2000**, *100*, 2091 – 2157.
[4] a) A. C. Comely, S. E. Gibson, *Angew. Chem.* **2001**, *113*, 1042 – 1063; *Angew. Chem. Int. Ed.* **2001**, *40*, 1012 – 1032; b) C. W. Phoon, M. M. Sim, *Curr. Org. Chem.* **2002**, *6*, 937 – 964; c) P. Blaney, R. Grigg, V. Sridharan, *Chem. Rev.* **2002**, *102*, 2607 – 2624; d) A. J. Wills, S. Balasubramanian, *Curr. Opin. Chem. Biol.* **2003**, *7*, 346 – 352; e) S. Bräse, *Acc. Chem. Res.* **2004**, *37*, 805 – 816; f) C. Gil, S. Bräse, *Curr. Opin. Chem. Biol.* **2004**, *8*, 230 – 237.
[5] a) C. W. Y. Chung, P. H. Toy, *Tetrahedron: Asymmetry* **2004**, *15*, 387 – 399; b) Y. Zhang, Y. Wang, W.-M. Dai, *J. Org. Chem.* **2006**, *71*, 2445 – 2455, and references therein.
[6] a) N. E. Leadbeater, M. Marco, *Chem. Rev.* **2002**, *102*, 3217 – 3274; b) C. A. McNamara, M. J. Dixon, M. Bradley, *Chem. Rev.* **2002**, *102*, 3275 – 3300.
[7] The results are taken in part from L.-P. Sun, PhD thesis, The Hong Kong University of Science and Technology (P.R. China), **2004**.
[8] W.-M. Dai, D.-S. Guo, L.-P. Sun, X.-H. Huang, *Org. Lett.* **2003**, *5*, 2919 – 2922.
[9] B. C. J. van Esseveldt, F. L. van Delft, R. de Gelder, F. P. J. T. Rutjes, *Org. Lett.* **2003**, *5*, 1717 – 1720, and references therein.
[10] a) M. G. Saulnier, D. B. Frennesson, M. S. Deshpande, D. M. Vyas, *Tetrahedron Lett.* **1995**, *36*, 7841 – 7844; b) K. Hiroya, S. Itoh, M. Ozawa, Y. Kanamori, T. Sakamoto, *Tetrahedron Lett.* **2002**, *43*, 1277 – 1280; c) K. Hiroya, S. Itoh, T. Sakamoto, *J. Org. Chem.* **2004**, *69*, 1126 – 1136.
[11] a) M. Nüchter, B. Ondruschka, W. Bonrath, A. Gum, *Green Chem.* **2004**, *6*, 128 – 141; b) C. O. Kappe, *Angew. Chem.* **2004**, *116*, 6408 – 6443; *Angew. Chem. Int. Ed.* **2004**, *43*, 6250 – 6284; c) C. O. Kappe, A. Stadler, *Microwaves in Organic and Medicinal Chemistry*, Wiley-VCH, Weinheim, **2005**.
[12] a) W.-M. Dai, D.-S. Guo, L.-P. Sun, *Tetrahedron Lett.* **2001**, *42*, 5275 – 5278; b) W.-M. Dai, L.-P. Sun, D.-S. Guo, *Tetrahedron Lett.* **2002**, *43*, 7699 – 7702; c) L.-P. Sun, X.-H. Huang, W.-M. Dai, *Tetrahedron* **2004**, *60*, 10983 – 10992, and references therein.
[13] For an example of intramolecular imide formation from a resin-bound succinic acid monoamide, see: F. Stieber, U. Grether, H. Waldmann, *Chem. Eur. J.* **2003**, *9*, 3270 – 3281.
[14] H. J. Olivos, P. G. Alluri, M. M. Reddy, D. Salony, T. Kodadek, *Org. Lett.* **2002**, *4*, 4057 – 4059.
[15] Strong coordination of Cu^{II} with polypeptides such as polyglycines requires an efficient anchoring donor and involves the amide nitrogen atom, thereby resulting in facile amide deprotonation; see: a) H. Sigel, R. B. Martin, *Chem. Rev.* **1982**, *82*, 385 – 426; b) K.-E. Falk, H. C. Greeman, T. Jansson, B. G. Malmstrom, T. Vanngard, *J. Am. Chem. Soc.* **1967**, *89*, 6071 – 6077; c) M. P. Youngblood, K. L. Chellappa, C. E. Bannister, D. W. Margerum, *Inorg. Chem.* **1981**, *20*, 1742 – 1747; d) I. Sóvágó in *Biocoordination Chemistry* (Ed.: K. Burger), Ellis Horwood, New York, **1990**, chap. 4. In addition, Cu^{II} complexes bound through amide oxygen atoms have been reported; see reference [16].
[16] a) J. C. Pessoa, I. Correia, T. Kiss, T. Jakusch, M. M. C. A. Castro, C. G. G. C. Geraldes, *J. Chem. Soc. Dalton Trans.* **2002**, 4440 – 4450; b) Y. Rodríguez-Martín, P. A. L. Luis, C. Ruiz-Pérez, *Inorg. Chim. Acta* **2002**, *328*, 169 – 178; c) K. B. Girma, V. Lorenz, S. Blaurock, F. T. Edelmann, *Inorg. Chim. Acta* **2006**, *359*, 364 – 368.
[17] The LC–MS charts can be found in the Supporting Information.

 © 2006 Wiley-VCH Verlag GmbH & Co. KGaA, Weinheim

Polyketides

DOI: 10.1002/anie.200602742

Synthesis of the C31–C67 Fragment of Amphidinol 3**

*Javier de Vicente, John R. Huckins, and Scott D. Rychnovsky**

The amphidinols are a structurally unique group of metabolites isolated from the marine dinoflagellates *Amphidinium klebsii* and *Amphidinium carterae*.[1] Amphidinol 3 (AM3; **1**) is one of the most biologically active compounds in this class, as it exhibits potent hemolytic activity against human erythrocytes and antifungal activity against *Aspergillus niger*.[1] Key structural features of AM3 include two highly substituted tetrahydropyran (THP) rings, a long irregular polyol domain, and a skipped polyene chain all distributed over a flexible 67-carbon backbone. The absolute stereochemistry of AM3 was elucidated by Murata and co-workers by using a new and powerful *J*-based NMR spectroscopic technique.[1d,2] Because of its complex molecular architecture and substantial biological activity, AM3 has emerged as an important synthetic target, and a number of recent efforts toward AM3 have been reported.[3] Herein, we disclose the synthesis of the fully protected C31–C67 fragment.

Our approach to AM3 dissects the molecule into three main fragments: polyene **2**, bisTHP core **3**, and the lower polyol fragment (Scheme 1). The union of these segments relies on two sequential olefination reactions. To take advantage of the partial symmetry present in the molecule, both THP rings in the C31–C52 core fragment **3** will be derived from a common intermediate. Synthesis of the C53–C67 polyene fragment **2** will rely on Pd-catalyzed cross-coupling and the Horner–Wadsworth–Emmons reaction to establish the all-*E*-alkene geometries.

Synthesis of core fragment **3** began with known 2,6-*cis*-THP **4** (Scheme 2), which is available in 11 steps from (D)-(−)-diethyl tartrate.[3a] TMSOTf-mediated allylation of the oxocarbenium ion derived from acetoxy ether **4** proceeded in excellent yield and furnished the desired 2,6-*trans*-THP ring as a 10:1 mixture of diastereomers, which were separated by column chromatography. Axial addition predominated, as expected for the addition to a THP oxocarbenium ion.[4] Protection of the diol as the acetonide and subsequent

[*] Dr. J. de Vicente, J. R. Huckins, Prof. S. D. Rychnovsky
Department of Chemistry
University of California, Irvine
1102 Natural Sciences 2, Irvine, CA 92697-2025 (USA)
Fax: (+1) 949-824-6379
E-mail: srychnov@uci.edu

[**] This study was supported by the National Institutes of General Medicine (GM 43854). J.d.V. acknowledges the Spanish Ministry of Education and Science for a postdoctoral fellowship.

Supporting information for this article is available on the WWW under http://www.angewandte.org or from the author.

InterScience
© 2006 Wiley-VCH Verlag GmbH & Co. KGaA, Weinheim

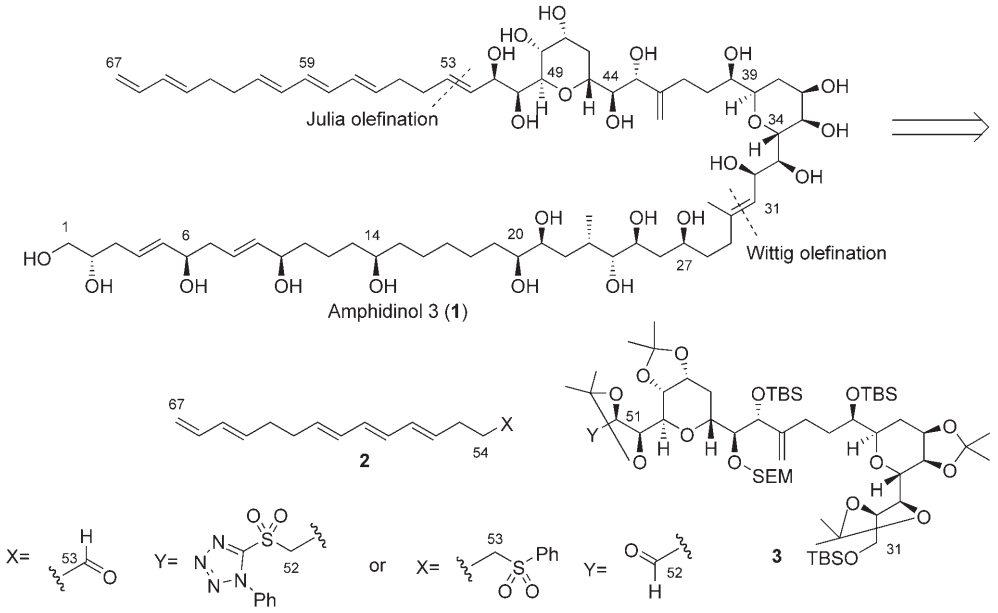

Scheme 1. Retrosynthetic analysis of amphidinol 3 (**1**). TBS = *tert*-butyldimethylsilyl; SEM = β-(trimethylsilyl)ethoxymethyl.

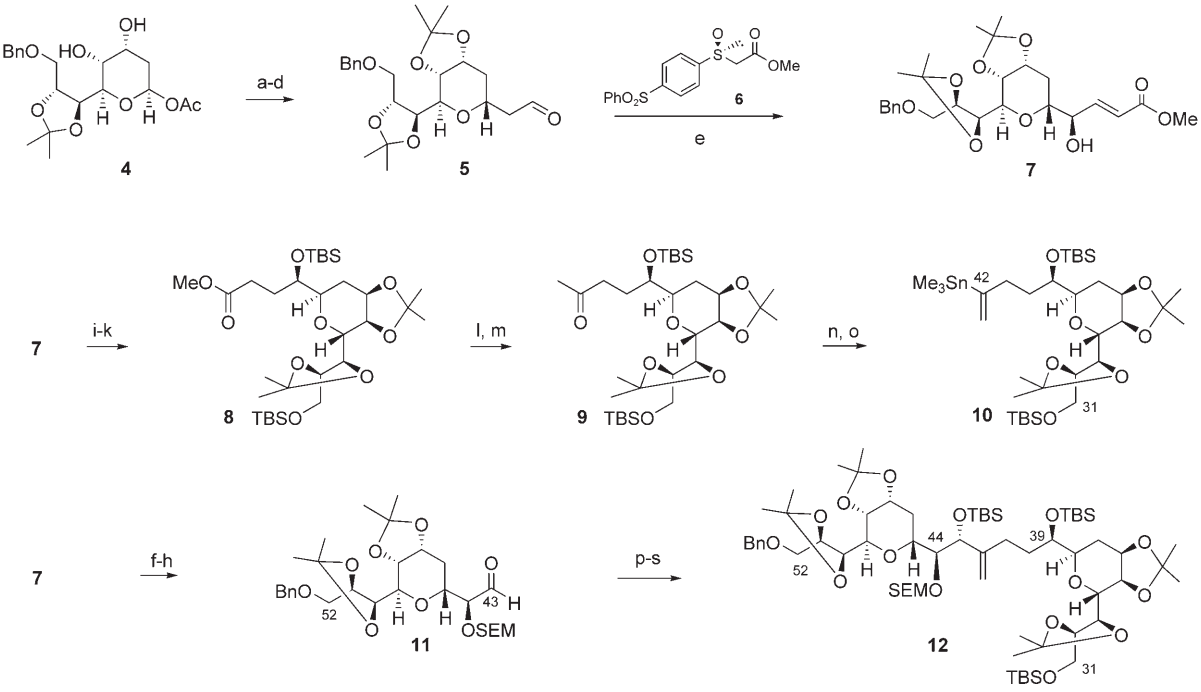

Scheme 2. Synthesis of the C31–C52 fragment **12**. Reagents and conditions: a) allyltrimethylsilane, DTBMP, TMSOTf, CH_2Cl_2, −78 °C; b) K_2CO_3, MeOH (82% over two steps); c) 2,2-DMP, TsOH, C_6H_6 (82%); d) 1. O_3, sudan III, CH_2Cl_2; 2. PPh_3, −78 °C→RT (94%); e) **5**, piperidine, CH_3CN, −5 °C (80%); f) SEMCl, iPr_2NEt, CH_2Cl_2, 40 °C (85%); g) OsO_4, NMO, acetone/H_2O (8:1); h) $NaIO_4$, THF/H_2O (1:1; 82% over two steps); i) TBSOTf, 2,6-lutidine, CH_2Cl_2, 0 °C→RT (97%); j) H_2 (90 psi), Pd/C, THF; k) TBSOTf, 2,6-lutidine, CH_2Cl_2, 0 °C→RT (84% over two steps); l) 1. Me(OMe)NH·HCl, *n*BuLi, THF, −78→0 °C; 2. **8**, −78 °C; m) MeMgBr, THF, 0 °C (98% for two steps); n) 1. LDA, THF, −78 °C; 2. *N*-(5-chloro-2-pyridyl)triflimide, −70 °C (74%); o) $Me_3SnSnMe_3$, LiCl, $[Pd(PPh_3)_4]$, THF, 80 °C in a sealed tube (85%); p) 1. **10**, *n*BuLi, THF, −78 °C; 2. **11**; q) Dess–Martin periodinane, pyridine, CH_2Cl_2; r) $Zn(BH_4)_2$, Et_2O, −35 °C (43% over three steps); s) TBSOTf, 2,6-lutidine, CH_2Cl_2 (73%). Bn = benzyl, 2,2-DMP = 2,2-dimethoxypropane, DTBMP = 2,6-di-*tert*-butyl-4-methylpyridine, LDA = lithium diisopropylamide, NMO = *N*-methylmorpholine-*N*-oxide, OTf = trifluoromethanesulfonate, TMS = trimethylsilyl, TsOH = *para*-toluenesulfonic acid.

ozonolysis provided aldehyde **5**. Sulfoxide **6** was prepared as reported[5] and coupled with aldehyde **5** under the hydroxylative Knoevenagel conditions detailed by Trost and Mallart.[6] This crucial [2,3] sulfoxide/sulfenate rearrangement established the last stereogenic center in the THP core of AM3 and furnished allylic alcohol **7** as a 85:15 mixture of

 © 2006 Wiley-VCH Verlag GmbH & Co. KGaA, Weinheim

diastereomers at C39/C44. The configuration of the major isomer was confirmed by using the advanced Mosher's analysis.[7]

With common intermediate **7** in hand, preparation of both halves of the core section was initiated (Scheme 2). To arrive at the nucleophilic coupling partner **10**, the alcohol **7** was first protected as the TBS ether. A strategic protecting-group exchange was effected by hydrogenolysis of the benzyl group, which was accompanied by reduction of the enoate alkene, followed by silylation of the primary alcohol. The C44 epimers of ester **8**, which arise from the hydroxylative Knoevenagel reaction, were readily separated by column chromatography. Methyl ketone **9** was obtained from ester **8** via the intermediate Weinreb amide.[8] Kinetic deprotonation with LDA followed by trapping with Comins reagent[9] furnished the enol triflate, which was then transformed into vinyl stannane **10** by a Stille cross-coupling with hexamethylditin.[10] Stannane **10** serves as a precursor to a vinyl lithium reagent that will be used to couple the fragments.

With the desired nucleophilic coupling partner in hand, common intermediate **7** was next converted into the requisite aldehyde **11** (Scheme 2). The free alcohol was protected as a SEM ether, and the C39 diastereomers were separated by medium-pressure liquid chromatography (MPLC). Oxidative cleavage of the alkene by using the Johnson–Lemieux protocol afforded aldehyde coupling partner **11**.[11]

Union of the two THP fragments **10** and **11** was accomplished by treatment of stannane **10** with *n*BuLi to afford the nucleophilic vinyl lithium species and subsequent addition to aldehyde **11**. This reaction furnished the C31–C52 bisTHP core of AM3 as a 1:1 mixture of diastereomers. Oxidation of the allylic alcohol mixture with Dess–Martin periodinane[12] followed by chelation-controlled reduction of the resultant ketone with $Zn(BH_4)_2$ afforded the desired *R* alcohol as the sole product. This transformation highlights the selection of the SEM protecting group for the C44 alcohol, which can be removed with other silyl groups, but participates in chelation. The yield over these three steps was 43%, and the stereochemistry at C43 was verified by using the advanced Mosher's analysis.[7] Protection of the alcohol as the TBS ether afforded the complete, fully protected core fragment **12**.

Synthesis of the C53–C67 skipped polyene is detailed in Scheme 3 and began from *E* vinyl iodide **13**, available after triisopropylsilyl (TIPS) etherification and hydrozirconation/iodinolysis of the corresponding alkynol. Sonagashira cross-coupling[13] of iodide **13** and (trimethylsilyl)acetylene followed by methanolysis of the TMS group furnished the terminal enyne. Selective hydroboration of the alkyne with catecholborane and subsequent iodinolysis afforded the *E*,*E* dienyl iodide with complete geometric selectivity.[14] A simple protecting-group interchange provided iodide **14**.

A Negishi cross-coupling procedure was employed to form the central all-*E* triene.[15] Treatment of another equivalent of vinyl iodide **13** with two equivalents of *t*BuLi followed by transmetallation to zinc furnished the requisite nucleophile. Addition of vinyl iodide **14** in the presence of $[Pd(PPh_3)_4]$ afforded the all-*E* triene with excellent (>20:1) geometric selectivity in 91% yield. Hydrolysis of the acetate

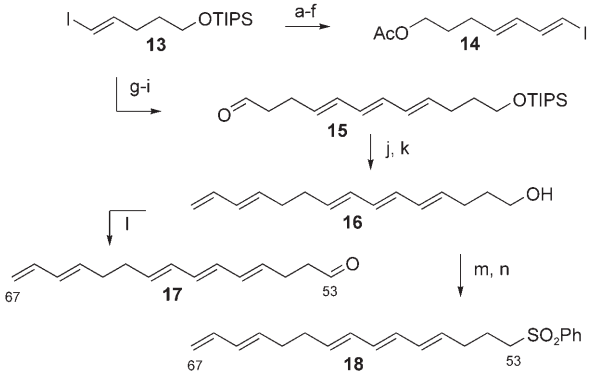

Scheme 3. Synthesis of the C53–C67 fragments **17** and **18**. Reagents and conditions: a) (trimethylsilyl)acetylene, $[Pd(PPh_3)_4]$, pyrrolidine (98%); b) K_2CO_3, MeOH (99%); c) 1. catecholborane (74°C); 2. H_2O; d) 1. NaOH, Et_2O, 0°C; 2. I_2, 0°C (70% over two steps); e) TBAF, THF (100%); f) Ac_2O, DMAP, pyridine, CH_2Cl_2 (95%); g) 1. **13**, *t*BuLi, THF, −78°C; 2. $ZnCl_2$, −78°C→RT; 3. **14**, $[Pd(PPh_3)_4]$, −20→7°C (91%); h) K_2CO_3, MeOH (100%); i) 1. $(COCl)_2$, DMSO, CH_2Cl_2, −78°C; 2. NEt_3, −78°C→RT (87%); j) diethylallyl phosphonate, *n*BuLi, HMPA, THF, −78→−10°C (62%); k) TBAF, THF (100%); l) SO_3·pyridine, DMSO, iPr_2NEt, CH_2Cl_2 (87%); m) PPh_3, LiBr, DIAD, THF, 0°C→RT (ca. 72%); n) benzenesulfinic acid sodium salt, NaI, $NaHCO_3$, DMF, 45°C (84%). DIAD = diisopropyl azodicarboxylate, DMAP = 4-dimethylaminopyridine, HMPA = hexamethylphosphoramide, TBAF = tetrabutylammonium fluoride.

group followed by a Swern oxidation delivered aldehyde **15**.[16]

With the all-*E* triene portion of the polyene in place, a semistabilized Horner–Wadsworth–Emmons olefination was utilized to install the terminal *E*-1,3-diene moiety.[17] Treatment of diethylallyl phosphonate with *n*BuLi in the presence of HMPA, followed by addition of trienal **15** led to the formation of the all-*E* pentaene in 62% yield. Removal of the TIPS ether moiety furnished alcohol **16**. Note that polyene **16** was synthesized with excellent control over the *E*/*Z* geometry of each double bond. We anticipated that undesired alkene isomers would likely be difficult or impossible to separate. Alcohol **16** was further elaborated to aldehyde **17** and sulfone **18** as potential coupling partners with the bisTHP core.

A report from Paquette and Chang, which describes the union of the polyene segment to one of the protected THP rings of the core of AM3, drew our attention.[3e] They described a highly selective Julia–Kocienski olefination using aldehyde **17** and a β-alkoxy sulfone core fragment. We were intrigued by this result because we too had explored this strategy on several model systems, one of which was very similar to the core fragment prepared by Paquette and Chang. This strategy had proved unselective in our hands, and we chose to pursue an alternate route. The disclosure was interesting enough, however, to prompt us to attempt that same coupling on the fully elaborated core.

Further elaboration of bisTHP fragment **12** to the desired sulfone nucleophile began with reductive debenzylation using LiDBB to reveal the primary alcohol (Scheme 4).[18] No reduction of the allylic ether at C43 was observed under the reaction conditions. The phenyltetrazole sulfide was introduced under conditions developed by Mitsunobu,[19] followed

 © 2006 Wiley-VCH Verlag GmbH & Co. KGaA, Weinheim

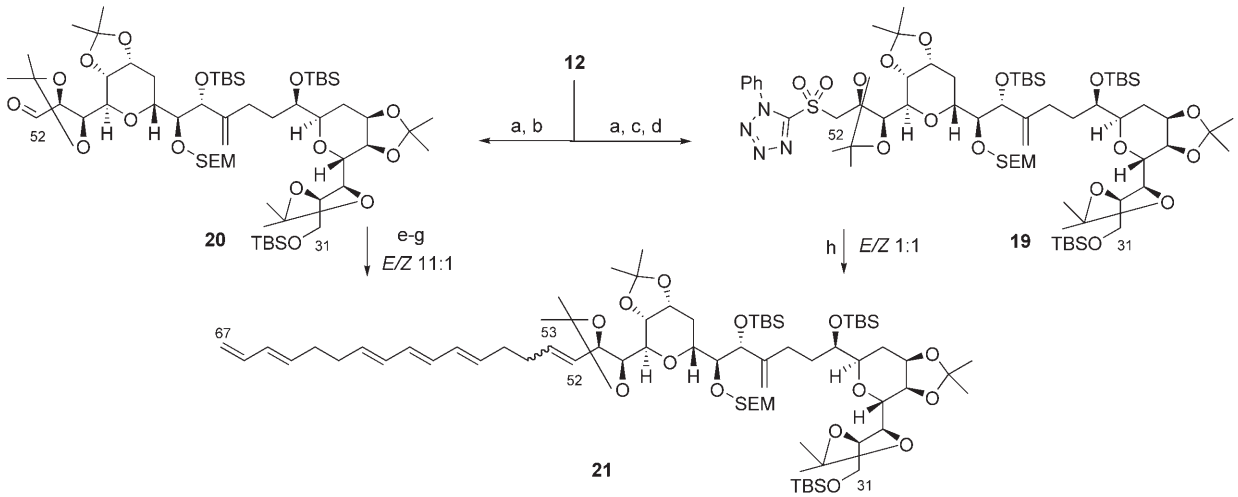

Scheme 4. The union of the polyene and core fragments. Reagents and conditions: a) LiDBB, THF, −78 °C (98%); b) Dess–Martin periodinane, pyridine, CH_2Cl_2 (100%); c) PPh_3, phenyltetrazole thiol, DIAD, THF, 0 °C→RT (86%); d) $[Mo_7O_{24}(NH_4)_6]\cdot 4H_2O$, H_2O_2, EtOH (59%); e) 1. **18**, LDA, THF, −78 °C; 2. **20**, −78 °C→RT (76%); f) Bz_2O, DMAP, pyridine, CH_2Cl_2 (89%); g) Na(Hg), Na_2HPO_4, THF/MeOH (3:1), −20 °C (72%); h) 1. **19**, KHMDS, THF, −78 °C; 2. **17**, −78 °C→RT (40%). Bz_2O = benzoic anhydride, KHMDS = potassium bis(trimethylsilyl)amide, LiDBB = lithium di-*tert*-butylbiphenylide.

by molybdate-mediated oxidation[20] to provide sulfone **19**. A suitable electrophile was generated by Parikh–Doering oxidation of alcohol **16**[21] to furnish aldehyde **17** (Scheme 3).

The Julia–Kocienski olefination[22] was carried out by treating a solution of sulfone **19** in THF at −78 °C with KHMDS, followed by addition of aldehyde **17**. In accord with our model studies, the coupling of these two fragments proceeded in an unselective manner to furnish the C31–C67 fragment of AM3 (**21**) in 40% yield as a 1:1 mixture of *E*/*Z* isomers. These results stand in contrast to those obtained by Paquette and Chang. Subtle differences between substrates, reagents, and even the scale of the reactions may be responsible for these divergent outcomes.

An alternate strategy we explored for uniting the polyene with the core relied on the Julia–Lythgoe olefination.[23] The required sulfone **18** (Scheme 3) was synthesized from alcohol **16** by using the Mitsunobu reaction to provide the primary bromide followed by displacement with the sodium salt of benzenesulfinic acid. The requisite aldehyde **20** was available by Dess–Martin oxidation of the alcohol revealed by debenzylation of core fragment **12** (Scheme 4).

In agreement with our earlier model studies, metalation of sulfone **18** with LDA followed by addition of aldehyde **20** afforded the coupled β-hydroxy sulfone product in 76% yield (Scheme 4). Acylation of the alcohol with benzoic anhydride followed by elimination with sodium amalgam afforded the C31–C67 section of AM3 (**21**) with a satisfying 11:1 *E*/*Z* ratio. This sequence proceeded in good yield, was very selective, and afforded the product cleanly. In our hands, the Julia–Lythgoe procedure was reproducible and led to fewer by-products than the Julia–Kocienski strategy for this coupling.

In summary, the fully protected C31–C67 fragment of amphidinol 3 (**21**), the largest portion of this challenging natural product yet to be disclosed, has been synthesized in a very convergent manner. Key features of the synthesis are the use of common intermediate **7** for the construction of both halves of the bisTHP core (**12**), a highly stereoselective polyene synthesis, and the union of those fragments by a stereoselective Julia–Lythgoe olefination. Our efforts in the total synthesis of amphidinol 3 are ongoing.

Received: July 10, 2006
Published online: October 2, 2006

Keywords: Julia olefination · natural products · polyenes · polyketides · tetrahydropyran

[1] a) G. K. Paul, N. Matsumori, M. Murata, K. Tachibana, *Tetrahedron Lett.* **1995**, *36*, 6279; b) M. Satake, M. Murata, T. Yasumoto, T. Fujita, H. Naoki, *J. Am. Chem. Soc.* **1991**, *113*, 9859; c) T. Houdai, S. Matsuoka, M. Murata, M. Satake, S. Ota, Y. Oshima, L. L. Rhodes, *Tetrahedron* **2001**, *57*, 5551; d) M. Murata, S. Matsuoka, N. Matsumori, G. K. Paul, K. Tachibana, *J. Am. Chem. Soc.* **1999**, *121*, 870; e) G. K. Paul, N. Matsumori, K. Konoki, M. Murata, K. Tachibana, *J. Mar. Biotech.* **1997**, *5*, 124; f) G. K. Paul, N. Matsumori, K. Konoki, M. Sasaki, M. Murata, K. Tachibana in *Harmful and Toxic Algal Blooms. Proceedings of Seventh International Conference on Toxic Phytoplankton* (Eds.: T. Yasumoto, Y. Oshima, Y. Fukuyo), UNESCO, Sendai, Japan, **1996**, p. 503.

[2] N. Matsumori, D. Kaneno, M. Murata, H. Nakamura, K. Tachibana, *J. Org. Chem.* **1999**, *64*, 866.

[3] a) J. de Vicente, B. Betzemeier, S. D. Rychnovsky, *Org. Lett.* **2005**, *7*, 1853; b) S. BouzBouz, J. Cossy, *Org. Lett.* **2001**, *3*, 1451; c) E. M. Flamme, W. R. Roush, *Org. Lett.* **2005**, *7*, 1411; d) J. D. Hicks, E. M. Flamme, W. R. Roush, *Org. Lett.* **2005**, *7*, 5509; e) L. A. Paquette, S.-K. Chang, *Org. Lett.* **2005**, *7*, 3111; f) S.-K. Chang, L. A. Paquette, *Synlett* **2005**, 2915; g) C. Dubost, I. E. Marko, J. Bryans, *Tetrahedron Lett.* **2005**, *46*, 4005.

[4] a) L. Ayala, C. G. Lucero, J. A. C. Romero, S. A. Tobacco, K. A. Woerpel, *J. Am. Chem. Soc.* **2003**, *125*, 15521; b) R. V. Stevens, A. W. M. Lee, *J. Am. Chem. Soc.* **1979**, *101*, 7032; c) R. V. Stevens, *Acc. Chem. Res.* **1984**, *17*, 289; d) P. Deslongchamps, *Stereoelectronic Effects in Organic Chemistry*, Pergamon, New York, **1983**, pp. 209–221.

 © 2006 Wiley-VCH Verlag GmbH & Co. KGaA, Weinheim

[5] J.-M. Brunel, P. Diter, M. Deutsch, H. B. Kagan, *J. Org. Chem.* **1995**, *60*, 8086.
[6] B. M. Trost, S. Mallart, *Tetrahedron Lett.* **1993**, *34*, 8025.
[7] The major isomer of **7** was purified by MPLC before the Mosher analysis: a) M. J. Rieser, Y. H. Hui, J. K. Rupprecht, J. F. Kozlowski, K. V. Wood, J. L. McLaughlin, P. R. Hanson, Z. Zhuang, T. R. Hoye, *J. Am. Chem. Soc.* **1992**, *114*, 10203; b) J. A. Dale, H. S. Mosher, *J. Am. Chem. Soc.* **1973**, *95*, 512; c) G. R. Sullivan, J. A. Dale, H. S. Mosher, *J. Org. Chem.* **1973**, *38*, 2143; d) I. Ohtani, T. Kusumi, Y. Kashman, H. Kakisawa, *J. Am. Chem. Soc.* **1991**, *113*, 4092.
[8] a) A. Basha, M. Lipton, S. M. Weinreb, *Tetrahedron Lett.* **1977**, *18*, 4171; b) J. I. Levin, E. Turos, S. M. Weinreb, *Synth. Commun.* **1982**, *12*, 989.
[9] D. L. Comins, A. Dehghani, *Tetrahedron Lett.* **1992**, *33*, 6299.
[10] W. J. Scott, J. K. Stille, *J. Am. Chem. Soc.* **1986**, *108*, 3033.
[11] R. Pappo, D. S. Allen, Jr., R. U. Lemieux, W. S. Johnson, *J. Org. Chem.* **1956**, *21*, 478.
[12] D. B. Dess, J. C. Martin, *J. Org. Chem.* **1983**, *48*, 4155.
[13] a) K. Sonagashira, Y. Todah, N. Hagihara, *Tetrahedron Lett.* **1975**, *16*, 4467; b) M. Alami, F. Ferri, G. Linstrumelle, *Tetrahedron Lett.* **1993**, *34*, 6403.
[14] a) H. C. Brown, S. K. Gupta, *J. Am. Chem. Soc.* **1972**, *94*, 4370; b) H. C. Brown, T. Hamaoka, N. Ravindran, *J. Am. Chem. Soc.* **1973**, *95*, 5786.
[15] a) E.-I. Negishi, *Acc. Chem. Res.* **1982**, *15*, 340; b) E.-I. Negishi, T. Takahashi, S. Baba, D. E. Van Horn, N. Okukado, *J. Am. Chem. Soc.* **1987**, *109*, 2393.
[16] a) S. L. Huang, K. Omura, D. Swern, *J. Org. Chem.* **1976**, *41*, 3329; b) T. T. Tidwell, *Org. React.* **1990**, *39*, 297.
[17] Y. Wang, F. G. West, *Synthesis* **2002**, 99.
[18] LiDBB is a reducing agent for arene radical anions, first reported by Freeman et al.: P. K. Freeman, L. L. Hutchinson, *J. Org. Chem.* **1980**, *45*, 1924.
[19] O. Mitsunobu, *Synthesis* **1981**, 1.
[20] H. S. Schultz, H. B. Freyermuth, S. R. Buc, *J. Org. Chem.* **1963**, *28*, 1140.
[21] J. R. Parikh, W. v. E. Doering, *J. Am. Chem. Soc.* **1967**, *89*, 5505.
[22] a) P. R. Blakemore, W. J. Cole, P. J. Kocienski, A. Morley, *Synlett* **1998**, 26; b) P. R. Blakemore, *J. Chem. Soc. Perkin Trans. 1* **2002**, 2563.
[23] M. Julia, J. M. Paris, *Tetrahedron Lett.* **1973**, *14*, 4833.

 © 2006 Wiley-VCH Verlag GmbH & Co. KGaA, Weinheim

Polyazido Compounds

DOI: 10.1002/anie.200602778

Polyazidopyrimidines: High-Energy Compounds and Precursors to Carbon Nanotubes**

*Chengfeng Ye, Haixiang Gao, Jerry A. Boatz, Gregory W. Drake, Brendan Twamley, and Jean'ne M. Shreeve**

Organic polyazido-substituted compounds are at the forefront of high-energy research. Polyazido organic compounds have high relative heats of formation as one azido group adds about 87 kcal mol^{-1} of endothermicity to a hydrocarbon compound.[1] In this family of compounds, 3,6-diazido-1,2,4,5-tetrazine (**1**) has the highest reported heat of formation, about 1101 kJ mol^{-1} (6709 kJ kg^{-1}).[2] The compound 4,4′,6,6′-tetraazido-2,2′-azo-1,3,5-triazine (**2**) has a heat of formation of 2171 kJ mol^{-1} (6164 kJ kg^{-1}; Scheme 1).[3] Recently it was demonstrated that **1** and **2** are good precursors to carbon nitride nanomaterials. Thermal decomposition of **1**[4] and **2**[5] yields nitrogen-rich nanolayered,

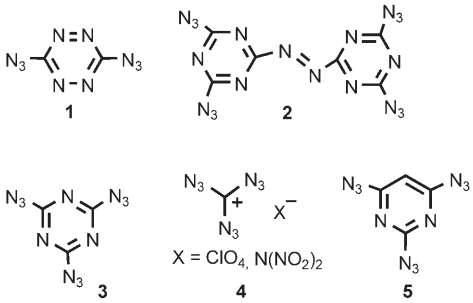

Scheme 1. Examples of reported polyazido compounds.

[*] Dr. C. Ye, Dr. H. Gao, Dr. B. Twamley, Prof. J. M. Shreeve
Department of Chemistry
University of Idaho
Moscow, ID 83844-2343 (USA)
Fax: (+1) 208-885-9146
E-mail: jshreeve@uidaho.edu
Dr. J. A. Boatz
Space and Missile Propulsion Division
Air Force Research Laboratory
10 East Saturn Blvd.
Edwards AFB, CA 93524 (USA)
Dr. G. W. Drake
NASA Solid Propellants Branch ER22
Marshall Space Flight Center
Huntsville, AL 34812 (USA)

[**] J.M.S., H.G., and C.Y. gratefully acknowledge the financial support of the AFOSR (Grant F49620-03-1-0209), NSF (Grant CHE0315275), and ONR (Grant N00014-02-1-0600). The Bruker (Siemens) SMART APEX diffraction facility was established at the University of Idaho with the assistance of the NSF-EPSCoR program and the M. J. Murdock Charitable Trust, Vancouver, WA (USA).

Supporting information for this article is available on the WWW under http://www.angewandte.org or from the author.

WILEY InterScience DISCOVER SOMETHING GREAT
© 2006 Wiley-VCH Verlag GmbH & Co. KGaA, Weinheim

nanoclustered, and nanodendritic carbon nitrides, depending on the different heating processes.

To date, many of the reported polyazido compounds are based on C/N heteroaromatic cycles, including tetrazine (as in **1**),[4] triazine (as in **3**),[6] heptazine,[7] triazole,[8] and tetrazole[9], and inorganic anions, including $[P(N_3)_6]^-$,[10] $[B(N_3)_4]^-$,[11] $[Si(N_3)_6]^{2-}$,[12] $[Te(N_3)_5]^-$,[13] $[Ti(N_3)_5]^-$,[14] $[Sb(N_3)_6]^-$,[15] and $[U(N_3)_7]^{3-}$,[16] as well as triazidocarbenium perchlorate and dinitramide (**4**; Scheme 1).[1] Few reports focus on pyrimidine as a basic building block. Although 2,4,6-triazidopyrimidine (**5**) has been known since 1979, [17] it has mainly been used for photochemical reactions. Few physical properties of this compound are known.

Preliminary calculations show that **5** has a positive heat of formation comparable to that of 2,4,6-triazido-1,3,5-triazine (**3**). Herein, we report the synthesis of a series of polyazidopyrimidine compounds, their calculated heats of formation, and their role as a source of carbon nanotubes by detonation generation.

Currently, except for the triazidocarbon cation in **4**,[1] molecules with three or four azido groups on the same carbon atom have not been available because of their instability, high sensitivity, and difficulty in synthesis. Only a few geminal diazido compounds have been prepared from the $SnCl_2$- or $ZnCl_2$-catalyzed reaction of substituted benzaldehyde or acetophenone with $TMSN_3$.[18] However, heterocycles based on geminal diazido compounds have not been reported. We have prepared pentaazidopyrimidine **7** starting from 5-carboxyaldehyde-2,4,6-triazidopyrimidine (**6**; Scheme 2). The best yield of 35% could be achieved by first substituting the three chlorine atoms on the pyrimidine ring with azido groups and subsequently transforming the aldehyde group into a geminal diazido functionality by using $TMSN_3/SnCl_2$. Remarkably, this pentaazido compound is a liquid at room temperature with a melting point at about −48 °C and has good thermal stability up to about 179 °C. It is noteworthy that **7** can be purified by column chromatography and routine handling while avoiding external heating. This suggests that **7** is not as detonation-sensitive as **1**. However, extreme care is absolutely necessary!

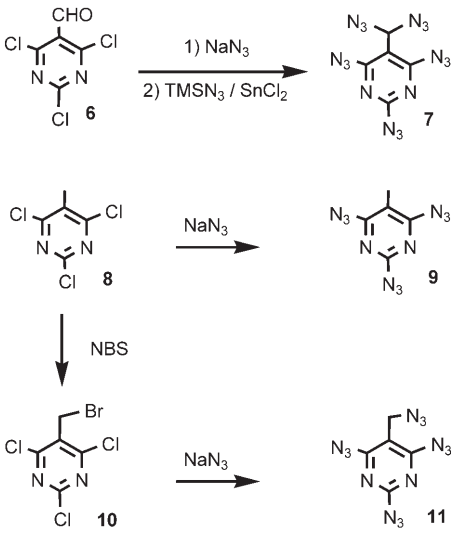

Scheme 2. Synthesis of polyazidopyrimidines; TMS = $SiMe_3$.

For purposes of comparison, triazido- and tetraazidopyrimidine derivatives **9** and **11** were prepared as outlined in Scheme 2. The solid-state structures of these two compounds were established by single-crystal X-ray analysis (Figure 1).[19]

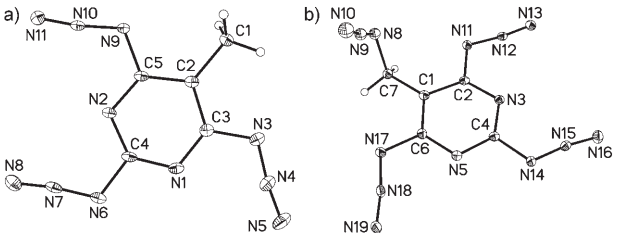

Figure 1. Thermal ellipsoid plot (ellipsoids at 30% probability) of **9** (a) and **11** (b). Hydrogen atoms have been included but not labelled.

Compound **9** is planar and packs in layers, in a fashion similar to the packing of **3**.[6a] However, in **9** the molecules have significant overlap with the adjacent layer. The layers are also farther apart (3.19 Å) as the steric bulk of the methyl group prevents closer association. There are no significant intermolecular interactions in either **3** or **9**. The structure of **11** is quite different. The packing no longer displays flat, planar sheets, but stacks along the *a* axis. These stacks are composed of two alternating molecules. The gap between the molecules in these stacks is about 3.26 Å at the maximum separation with 10° angles between the heterocycles. There are also weak nonclassical hydrogen bonds between the methylene group and terminal azido nitrogen atoms, both within the stacks (C7–N13, ca. 3.31 Å) and between the stacks (C7–N19, ca. 3.41 Å). This compound was difficult to crystallize and exhibits disorder in the azidomethyl group as well as rotational twinning.[19]

The melting point of the triazido analogue **9** is 103 °C, while the addition of one extra azido group reduces the melting point drastically by about 80 °C to 22.5 °C in **11** (Table 1). The introduction of this fourth azido group does not result in any obvious decrease in thermal stability. The presence of a fifth azido group in **7** led to a decrease in the melting point by an additional 70 °C with just a slight decrease in thermal stability (Table 1).

A possible rationale for the lower melting point observed for the (azidomethyl)pyrimidine compound is the inefficient packing caused by the azidomethyl group. The azido group in **11** is disordered (see above) and exhibits free rotation around

Table 1: Physical properties of polyazido compounds.

Compd.	Density [g cm^{-3}]	M.p. [°C]	T_d (DSC) [°C]	$\Delta_f H°_{298}$[a] [kJ mol^{-1}]
1	1.72	130	130	1121.7[b]
3	1.72	94	180	1136.0[c]
7	1.71	−48	179	1807.1
9	1.55	103	195	1087.4
11	1.65	22.5	193	1452.7
12				2192.0

[a] Calculated value in the gas phase. [b] $\Delta_f H°_{298}$ (solid) = 1101 kJ mol^{-1}, reference [2]. [c] $\Delta_f H°_{298}$ (solid) = 1050 kJ mol^{-1}, reference [6b].

 © 2006 Wiley-VCH Verlag GmbH & Co. KGaA, Weinheim

the methylene carbon atom C7. This phenomenon has also been confirmed with other examples; for example, 3,5-diazidomethyl-4-amino-triazole (m.p. 92 °C) and its perchlorate salt (m.p. 75 °C) have much lower melting points than 3,5-dimethyl-4-amino-triazole (m.p. 196 °C)[20] and its perchlorate salt (m.p. 94 °C; see the Supporting Information). Thus, introducing azidoalkyl groups could be an efficient way to reduce the melting point and increase the heat of formation, both of which are essential for the preparation of energetic ionic liquids.[21]

The heats of formation of **7**, **9**, **11**, and 5-triazidomethyl-2,4,6-triazidopyrimidine (**12**) were predicted using quantum chemical calculations (see the Supporting Information for computation details). The optimized geometries of pentaazidopyrimidine **7** and hexaazidopyrimidine **12** are shown in Figure 2; both geometries are proven to be at local minima in

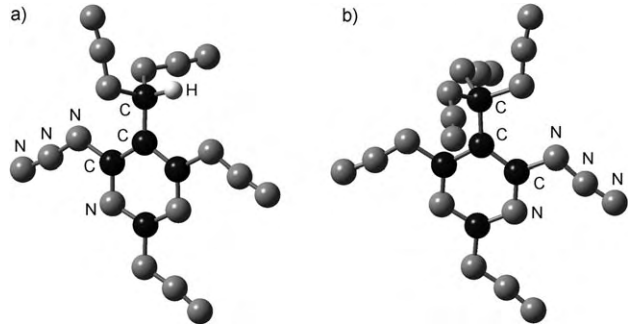

Figure 2. Optimized geometries at the B3LYP/6-311G(d,p) level of **7** (a) and **12** (b).

the potential-energy surface. The incremental contribution of each additional azido ligand to the heat of formation in the sequence **9**→**11**, **11**→**7**, and **7**→**12** is +365, +354, and +385 kJ mol^{-1}, respectively (Table 1). Similar behavior is observed in the corresponding sequence of isodesmic reference compounds $CH_3CH_{3-n}(N_3)_n$ (n = 0–3), in which the incremental changes in heats of formation as a function of n are +351, +337, and +323 kJ mol^{-1}, respectively. For **7**, using 20 kcal as its heat of sublimation, the heat of formation for the solid state was estimated to be 1723.2 kJ mol^{-1} (5764 kJ kg^{-1}), which would be the third-highest heat of formation reported for energetic materials, just lower than those of **2** (6164 kJ kg^{-1}) and **1** (6709 kJ kg^{-1}).

The formation of carbon nanotubes (CNTs) was investigated by catalytic detonation of the polyazidopyrimidines above. Since their discovery in 1990, CNTs have been shown to be extremely promising for applications in materials science and medicinal chemistry owing to interesting electronic, mechanical, and structural properties. Synthesis of nanomaterials on a large scale by detonation of explosive precursors is a new promising method owing to its low cost. Polyazido compounds with little or no hydrogen content are regarded as such ideal precursors for nanomaterials. Kroke first reported the preparation of CNTs using **3** by this detonation method in 1999,[22] but the yield was only about 2%. Optimization of the detonation conditions in the presence of transition metals, for example, Fe, Ni, Cu, and Ti, improved the yields to greater than 60%.[23]

Compound **3** is very detonation-sensitive, and its explosive nature increases with higher purity and crystal size.[6a] We found **5** to be much less sensitive to detonation than **3**. Therefore, **5** was examined as the carbon source and self-heating producer for CNTs. Among the catalysts explored, for example, Cu powder, $Cu(OAc)_2$,[24] $AgNO_3$, and $Ni(ClO_4)_2$, we found that $Ni(ClO_4)_2$ was the best catalyst for the production of CNTs. The synthetic method is straightforward. Compound **5** (0.3 g 1.47 mmol) and $Ni(ClO_4)_2$ (0.02 g, 0.07 mmol) were placed in a 75-mL stainless-steel vessel, which was then closed with a valve and heated to 250 °C over the course of about 20 minutes. The vessel was then allowed to cool to room temperature. The product was observed as a fleecy, puffy, fiber-like black residue, which could easily be removed from the vessel with forceps. On touching with a glass vial, the black residue agglomerated. This material floats and disperses well in ethanol. SEM and TEM pictures of as-prepared samples clearly show the presence of characteristic hollow-channel CNT structures (lengths ca. 3–20 μm, diameters ca. 60–80 nm and up to 100 nm; Figure 3). The yield of CNTs is estimated to be greater than 90%. They have a bamboo-like morphology (Figure 3c), and these "compartmentalized nanotubes" are segmented with a relatively uniform segment length of about 90 nm.

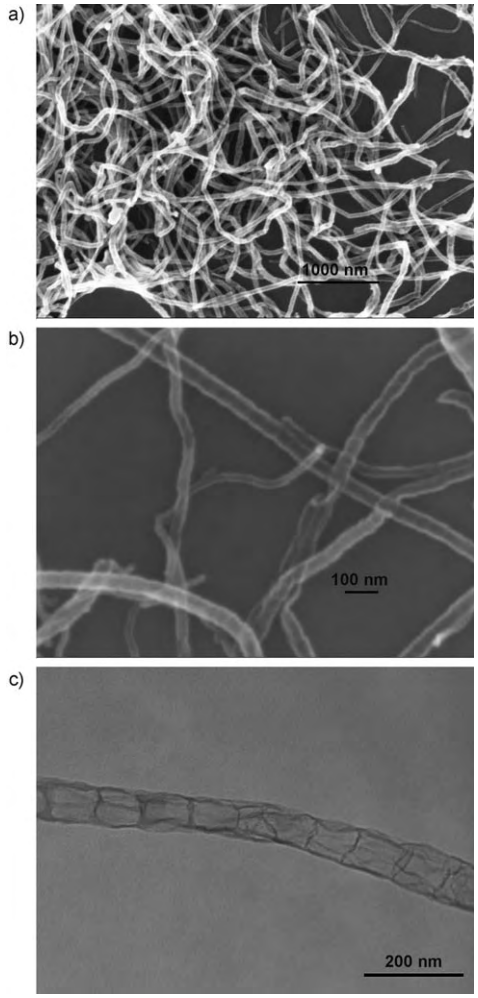

Figure 3. SEM (a, b) and TEM (c) images of CNTs generated by catalytic detonation of **5**.

 © 2006 Wiley-VCH Verlag GmbH & Co. KGaA, Weinheim

In conclusion, we have successfully synthesized a series of polyazidopyrimidine compounds, in which the azidomethyl group dramatically decreases the melting points. Theoretical calculations show that these compounds exhibit highly promising energetic properties. 2,4,6-Triazidopyrimidine was found to be a novel and less sensitive precursor for the formation of carbon nanotubes in high yields.

Caution! All polyazides must be handled with extreme care and with appropriate safety precautions.

Received: July 13, 2006
Published online: September 13, 2006

Keywords: azides · explosives · heats of formation · nanotubes · nitrogen

[1] M. A. Petrie, J. A. Sheehy, J. A. Boatz, G. Rasul, G. K. S. Prakash, G. A. Olah, K. O. Christe, *J. Am. Chem. Soc.* **1997**, *119*, 8802 – 8808.
[2] M. H. V. Huynh, M. A. Hiskey, D. E. Chavez, D. L. Naud, R. D. Gilardi, *J. Am. Chem. Soc.* **2005**, *127*, 12537 – 12543.
[3] M. H. V. Huynh, M. A. Hiskey, E. L. Hartline, D. P. Montoya, R. Gilardi, *Angew. Chem.* **2004**, *116*, 5032 – 5036; *Angew. Chem. Int. Ed.* **2004**, *43*, 4924 – 4928.
[4] M. H. V. Huynh, M. A. Hiskey, J. G. Archuleta, E. L. Roemer, R. Gilardi, *Angew. Chem.* **2004**, *116*, 5776 – 5779; *Angew. Chem. Int. Ed.* **2004**, *43*, 5658 – 5661.
[5] M. H. V. Huynh, M. A. Hiskey, J. G. Archuleta, E. L. Roemer, *Angew. Chem.* **2005**, *117*, 747 – 749; *Angew. Chem. Int. Ed.* **2005**, *44*, 737 – 739.
[6] a) E. Kebenich, T. M. Klapötke, J. Knizek, H. Noth, A. Schulz, *Eur. J. Inorg. Chem.* **1998**, 2013 – 2016; b) E. G. Gillan, *Chem. Mater.* **2000**, *12*, 3906 – 3912.
[7] D. R. Miller, D. C. Swenson, E. G. Gillan, *J. Am. Chem. Soc.* **2004**, *126*, 5372 – 5373.
[8] H. Xue, Y. Gao, B. Twamley, J. M. Shreeve, *Chem. Mater.* **2005**, *17*, 191 – 198.
[9] A. Hammerl, T. M. Klapötke, *Inorg. Chem.* **2002**, *41*, 906 – 912.
[10] R. Haiges, S. Schneider, T. Schroer, K. O. Christe, *Angew. Chem.* **2004**, *116*, 5027 – 5032; *Angew. Chem. Int. Ed.* **2004**, *43*, 4919 – 4924.
[11] W. Frank, T. Habereder, A. Hammerl, T. M. Klapötke, B. Krumm, P. Mayer, H. Noth, M. Warchhold, *Inorg. Chem.* **2001**, *40*, 1334 – 1340.
[12] A. C. Filippou, P. Portius, G. Schnakenburg, *J. Am. Chem. Soc.* **2002**, *124*, 12396 – 12397.
[13] T. M. Klapötke, B. Krumm, P. Mayer, I. Schwab, *Angew. Chem.* **2003**, *115*, 6024 – 6026; *Angew. Chem. Int. Ed.* **2003**, *42*, 5843 – 5846.
[14] R. Haiges, J. A. Boatz, S. Schneider, T. Schroer, M. Yousufuddin, K. O. Christe, *Angew. Chem.* **2004**, *116*, 3210 – 3214; *Angew. Chem. Int. Ed.* **2004**, *43*, 3148 – 3152.
[15] R. Haiges, J. A. Boatz, A. Vij, V. Vij, M. Gerken, S. Schneider, T. Schroer, M. Yousufuddin, K. O. Christe, *Angew. Chem.* **2004**, *116*, 6844 – 6848; *Angew. Chem. Int. Ed.* **2004**, *43*, 6676 – 6680.
[16] M.-J. Crawford, A. Ellern, P. Mayer, *Angew. Chem.* **2005**, *117*, 8086 – 8090; *Angew. Chem. Int. Ed.* **2005**, *44*, 7874 – 7878.
[17] V. Y. Pochinok, L. F. Avramenko, A. V. Pochinok, P. A. Kondratenko, V. I. Nagornyi, T. P. Naidenova, N. P. Chibisova, *Ukr. Khim. Zh.* **1979**, *45*, 1074 – 1077.
[18] a) K. Nishiyama, T. Yamaguchi, *Synthesis* **1988**, 106 – 108; b) K. Nishiyama, M. Oba, A. Watanabe, *Tetrahedron* **1987**, *43*, 693 – 700.
[19] Crystal data for **9**: $C_5H_3N_{11}$, $M_r = 217.18.$, $T = 89(2)$ K, monoclinic, space group $P21/c$, $a = 9.838(3)$, $b = 15.295(4)$, $c = 6.3070(16)$ Å, $\beta = 100.683(4)°$, $V = 932.5(4)$ Å^3, $Z = 4$, $\rho_{calcd} = 1.547$ g cm^{-3}, $\mu = 0.118$ mm^{-1}, reflections collected/unique 13723/1690, $R1 = 0.0337$, $wR2 = 0.0932$ ($I > 2\sigma I$), GOF = 1.032. Crystal data for **11**: $C_5H_2N_{14}$, $M_r = 258.21$, $T = 89(2)$ K, monoclinic, space group $P21/a$, $a = 6.5156(14)$, $b = 22.149(5)$, $c = 7.2649(16)$ Å, $\beta = 97.540(4)°$, $V = 1039.3(4)$ Å^3, $Z = 4$, $\rho_{calcd} = 1.650$ g cm^{-3}, $\mu = 0.128$ mm^{-1}, reflections collected/unique 27871/2123, $R1 = 0.0370$, $wR2 = 0.0936$ ($I > 2\sigma I$), GOF = 1.055, sample was rotationally twinned (179.8° about reciprocal (0,0,1) with a refined BASF of 0.252(3)), and the azidomethyl group was disordered 50 %. CCDC-612107 and CCDC-612108 contain the supplementary crystallographic data for this paper. These data can be obtained free of charge from The Cambridge Crystallographic Data Centre via www.ccdc.cam.ac.uk/data_request/cif.
[20] P. C. Wade, B. R. Vogt, T. P. Kissick, L. M. Simpkins, D. M. Palmer, R. C. Millonig, *J. Med. Chem.* **1982**, *25*, 331 – 333.
[21] R. P. Singh, R. D. Verma, D. T. Meshri, J. M. Shreeve, *Angew. Chem.* **2006**, *118*, 3664 – 3682; *Angew. Chem. Int. Ed.* **2006**, *45*, 3584 – 3601.
[22] E. Kroke, M. Schwarz, *Adv. Mater.* **1999**, *11*, 158 – 161.
[23] T. Utschig, M. Schwarz, G. Miehe, E. Kroke, *Carbon* **2004**, *42*, 823 – 828.
[24] a) Y. Lu, Z. P. Zhu, W. Wu, Z. Y. Liu, *Chem. Commun.* **2002**, 2740 – 2741; b) Y. Lu, Z. P. Zhu, Z. Y. Liu, *Carbon* **2004**, *42*, 361 – 370.

 © 2006 Wiley-VCH Verlag GmbH & Co. KGaA, Weinheim

Organoindium Reagents

DOI: 10.1002/anie.200602823

Crystallographic Characterization of Difluoropropargyl Indium Bromide, a Reactive Fluoroorganometallic Reagent**

*Bo Xu, Mark S. Mashuta, and Gerald B. Hammond**

Dedicated to Professor Raymond G. Plevey on the occasion of his 66th birthday

Indium-promoted reactions and their application to synthetic methodologies based on green chemistry have grown exponentially in recent years.[1] The interaction of allylic or propargylic halides with indium metal—through metal/halo-

[*] B. Xu, Dr. M. S. Mashuta, Prof. G. B. Hammond
Department of Chemistry
University of Louisville
Louisville, KY 40292 (USA)
Fax: (+1) 508-852-3899
E-mail: gb.hammond@louisville.edu

[**] Financial support by the National Science Foundation (CHE-0513483) is gratefully acknowledged. We are grateful to Professor Craig A. Grapperhaus (University of Louisville) for his collaboration. M.S.M. thanks the Kentucky Research Challenge Trust Fund for an upgrade of the X-ray facilities.

Supporting information for this article is available on the WWW under http://www.angewandte.org or from the author.

© 2006 Wiley-VCH Verlag GmbH & Co. KGaA, Weinheim

gen exchange or transmetalation—and their subsequent reaction with electrophiles continue to be actively pursued.[2] Initially, an indium sesquihalide ($R_3In_2X_3$) was regarded as a synthetic intermediate.[3] On the basis of recent NMR data, researchers have proposed that indium(I) and indium(III) complexes, or a combination thereof, could mediate allylation[4] and propargylation reactions.[5] Owing to their short-lived nature, the structure of the transient organoindium species is still a matter of debate. By incorporating fluorine on the propargylic carbon atom of **1** prior to its reaction with indium, we were able to stabilize the resulting organoindium complex. Herein we report the first crystallographic characterization of a reactive propargyl indium species.

Earlier, we had reported that the reaction of a silylfluoropropargyl bromide **1** with indium in predominantly aqueous media produced a stable complex, which is loosely represented as **2** (Scheme 1).[6] The organoindium compound **2** yielded **3** or **4**, depending on the nature of the electrophile (E) used.[7,8]

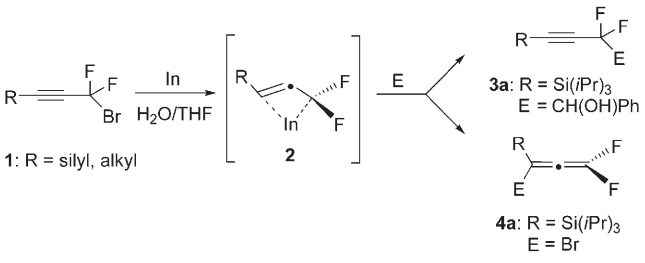

Scheme 1. Indium-mediated difluoroallenylation and -propargylation.

With the purpose of elucidating the structure of **2**, a 1:1 mixture of **1a** ($R = Si(iPr)_3$) and indium metal in predominantly aqueous media was sonicated at 5–10 °C and monitored by ^{19}F NMR spectroscopy (Scheme 2). Two slowly

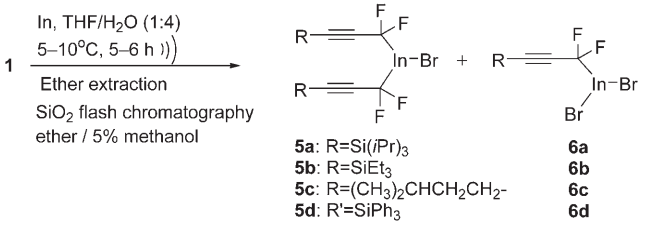

Scheme 2. Synthesis of difluoropropargyl indium bromides.

increasing resonance signals, centered at $\delta = -89$ ppm, were detected after 0.5 hours, and all the starting material was consumed after five to six hours. After ether extraction, the resulting solution was relatively stable toward treatment with a mild acid, but the complex decomposed if concentrated to dryness. We isolated each species by using SiO_2 flash chromatography and found that DMSO stabilized the resulting white solids. These compounds could be kept at room temperature for several weeks without decomposition, and could be stored for months in the refrigerator. Elemental analyses indicated that the indium/fluorine/bromine ratios were very close to 1:4:1 (1.03:4:1.11) and 1:2:2 (0.98:2.02:2) for the two compounds; satisfactory carbon and hydrogen analyses were also obtained. IR absorption as well as ^{19}F and ^{13}C NMR signals supported the presence of a propargyl species in solution. On the basis of this evidence, we proposed structures **5a** and **6a**. In a similar fashion, we isolated **5b–d** and **6b–d**.

Although attempts to obtain suitable single crystals of **5a–c** and **6a–c** failed, we succeeded in obtaining X-ray quality crystals of **5d** by slow evaporation of a saturated solution in DMSO and dichloromethane at room temperature. This compound crystallized as colorless prisms in the *C*2/*c* space group. Its ORTEP[9a] view (Figure 1) illustrates the first

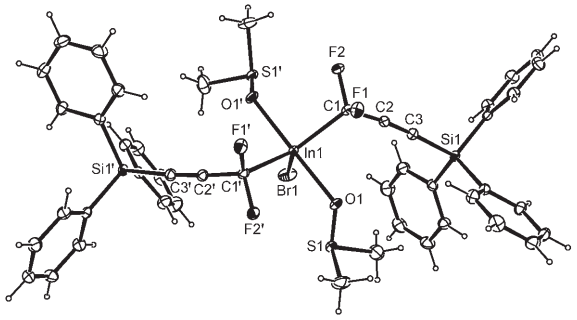

Figure 1. ORTEP showing 45 % displacement ellipsoids. H atoms are shown as spheres of arbitrary radii. Selected bond lengths [Å] and angles [°]: In1-C1 2.217(2), In1-Br1 2.5363(5), In1-O1 2.2432(18), F1-C1 1.398(3), F2-C1 1.392(3), C1-C2 1.456(3), C2-C3 1.201(4); C1-In1-C1 129.12(13), C1-In1-Br1 115.44(6), O1-In1-Br1 91.76(5), C2-C3-Si1 176.0(2), C3-C2-C1 174.3(3).

example of a crystallographically characterized In-C-C≡C complex. Indeed, no crystal structures have been reported to date in the Cambridge Structural Database for an indium atom that is bonded to sp^3 allylic or propargylic carbon atoms.[10] Compound **5d** adopts a trigonal-bipyramidal geometry about the central indium atom with the two 1,1-difluoro-3-triphenylsilylprop-2-ynyl ligands and the Br atom coordinating in the trigonal plane while two dmso ligands occupy axial positions. The In–C bond length (2.217(2) Å) is typical of trigonal-bipyramidal CH_3In complexes, and the In–Br (2.5363(5) Å) and In–O bond lengths (2.2432(18) Å) are also standard.[11] The C1-In-C1′ bond angle (129.12(13)°) is significantly greater than the ideal 120° while the Br1-In-C1 and Br1-In-C1′ angles are contracted (115.44(6)°) to accommodate the large C1-In-C1′ bond angle. To complete the trigonal bipyramid, the coordination of the axial dmso ligands is distorted slightly from linearity (O1-In-O1′ 176.48(10)°). Most significantly the $CF_2C{\equiv}C$ group shows the unprecedented presence of sp hybridization (C2–C3 1.201(4) Å; nearly linear C2-C3-Si1 (176.0(2)°) and C1-C2-C3 (174.3(3)°) angles) located in a position alpha to the CF_2 group.

To demonstrate the reactive nature of these fluoroorganometallic complexes, we treated the obtained mixture of **5a** and **6a** (Scheme 2) with different electrophiles. With a less reactive electrophile (benzaldehyde), the reaction produced **3a** in 51 % yield after two hours in refluxing ether. With a

 © 2006 Wiley-VCH Verlag GmbH & Co. KGaA, Weinheim

more reactive electrophile such as bromine, **4a** was obtained in 76% yield under very mild conditions (−20°C, 0.5 hours).

In conclusion, we have synthesized and structurally characterized a hitherto unknown propargyl indium reagent, and we have used it to prepare a difluoroalkyne or -allene. The mechanism of formation of fluoroorganoindium complexes, their regiochemistry, and synthetic applications are currently under investigation.

Experimental Section

Indium powder (1 equiv) was added to a 0.15 M solution of **1a** (5 mmol) in a mixture of water and THF (4:1). This mixture was sonicated at 5–10°C for 6–8 h. The temperature in the ultrasound bath was adjusted by addition of ice, and the reaction was periodically monitored by ^{19}F NMR. After the starting material was consumed, the reaction mixture was extracted by ether, and the organic layer was washed with brine, dried over $MgSO_4$, and concentrated. The crude indium complex was dissolved in ether (5 mL) and separated by flash chromatography (80 g SiO_2). The column was eluted with ether (300 mL), then by 5% methanol in ether (300 mL). DMSO (1 mL) was added to each of the two fractions before complete solvent removal. The mixtures were filtered, and the solvent removed from the filtrate by rotary evaporation. The two white solids were washed with hexane and dried in vacuum to give **5a** (750 mg, 37%) and **6a** (400 mg, 13%).

5a·3 dmso: M.p. 53–55°C; ^{1}H NMR (500 MHz, $CDCl_3$, 25°C, TMS): $\delta = 1.00$–1.04 (m, 42 H, $CH(CH_3)_2$), 2.73 ppm (s, 18 H, dmso); ^{13}C NMR (126 MHz, $CDCl_3$, 25°C, TMS): $\delta = 11.3$, 18.8, 39.5 (dmso), 92.5, 104.0 (t, $J = 24.4$ Hz), 131.0 ppm (t, $J = 285$ Hz); ^{19}F NMR (470 MHz, $CDCl_3$, 25°C, CF_3Cl): $\delta = -88.8$ ppm (s, 2 F). Elemental analysis (%) calcd for $C_{30}H_{60}BrF_4InO_3S_3Si_2$: C 40.40, H 6.78; found: C 40.59, H 6.52.

6a·3 dmso: M.p. 90–92°C; ^{1}H NMR (500 MHz, $CDCl_3$, 25°C, TMS): $\delta = 1.00$–1.07 (m, 21 H, $CH(CH_3)_2$), 2.73 ppm (s, 18 H, dmso); ^{13}C NMR (126 MHz, $CDCl_3$, 25°C, TMS): $\delta = 11.3$, 18.8, 39.5 (dmso), 93.5, 103.0 (m), 130.0 ppm (m); ^{19}F NMR (470 MHz, $CDCl_3$, 25°C, CF_3Cl): $\delta = -89.1$ ppm (s, 2 F). Elemental analysis (%) calcd for $C_{18}H_{39}Br_2F_2InO_3S_3Si$: C 29.20, H 5.31; found: C 29.43, H 5.23.

A colorless crystal of **5d** (dimensions $0.21 \times 0.19 \times 0.16$ mm^3) was mounted on a glass fiber for collection of X-ray data on a Bruker SMART APEX CCD diffractometer. The SMART[9b] software package (version 5.628) was used to acquire a total of 1868 thirty-second-frame ω-scan exposures of data at 100 K ($2\theta_{max} = 56.18°$) using monochromated $Mo_{K\alpha}$ radiation (0.71073 Å) from a sealed tube and a monocapillary. Frame data were processed using SAINT[9c] (version 6.36) to determine the final unit cell parameters ($a =$ 34.025(3) Å, $b = 10.1163(9)$ Å, $c = 13.1193(11)$ Å, $\beta = 95.925(2)°$, $V = 4491.6(7)$ Å^3, $Z = 4$, $\rho_{calcd} = 1.505$ Mg m^{-3}) to produce raw *hkl* data that were then corrected for absorption (transmission min./max. = 0.700/0.764, $\mu = 1.615$ mm^{-1}) by using SADABS.[9d] The structure was solved by Patterson methods in the space group *C*2/*c* by using SHELXS-90[9e] and refined by least-squares methods on F^2 by using SHELXL-97[9f] as part of the SHELXTL[9g] suite of programs. All nonhydrogen atoms were refined anisotropically. Hydrogen atoms were placed in their geometrically generated positions and refined as a riding model. Methyl H atoms were included as fixed contributions with $U(H) = 1.5 \times U_{eq}$ (attached C atom) while the torsion angle which defines its orientation was allowed to refine on the attached C atom. Phenyl H atoms were assigned $U(H) = 1.2 \times U_{eq}$. For all 5225 unique reflections (R(int) = 0.0381) the final anisotropic full-matrix least-squares refinement on F^2 for 265 variables converged at $R1 = 0.0363$ and $wR2 = 0.0896$ with a GOF of 1.05.

CCDC-614782 contains the supplementary crystallographic data for this paper. These data can be obtained free of charge from The Cambridge Crystallographic Data Centre via www.ccdc.cam.ac.uk/data_request/cif.

Received: July 15, 2006
Revised: August 22, 2006
Published online: October 6, 2006

Keywords: difluoropropargyl groups · fluorine · indium · metalation · structure elucidation

[1] Reviews: a) J. Podlech, T. C. Maier, *Synthesis* **2003**, 633; b) K. K. Chauhan, C. G. Frost, *J. Chem. Soc Perkin Trans. 1* **2000**, 3015; c) A. N. Pae, Y. S. Cho, *Curr. Org. Chem.* **2002**, *6*, 715.
[2] a) K. Lee, D. Seomoon, P. H. Lee, *Angew. Chem.* **2002**, *114*, 4057; *Angew. Chem. Int. Ed.* **2002**, *41*, 3901; b) W. Miao, W. Lu, T. H. Chan, *J. Am. Chem. Soc.* **2003**, *125*, 2412; c) S. A. Babu, M. Yasuda, I. Shibata, A. Baba, *J. Org. Chem.* **2005**, *70*, 10408.
[3] S. Araki, H. Ito, Y. Butsugan, *J. Org. Chem.* **1988**, *53*, 1831.
[4] T. H. Chan, Y. Yang, *J. Am. Chem. Soc.* **1999**, *121*, 3228.
[5] a) W. Miao, L. W. Chung, Y.-D. Wu, T. H. Chan, *J. Am. Chem. Soc.* **2004**, *126*, 13326; b) M.-J. Lin, T.-P. Loh, *J. Am. Chem. Soc.* **2003**, *125*, 13042; c) M. R. Isaac, T. H. Chan, *J. Chem. Soc. Chem. Commun.* **1995**, 1003.
[6] S. Arimitsu, B. Xu, T. Kishbaugh, L. Griffin, G. B. Hammond, *J. Fluorine Chem.* **2004**, *125*, 641.
[7] Z. Wang, G. B. Hammond, *J. Org. Chem.* **2000**, *65*, 6547.
[8] B. Xu, G. B. Hammond, *Angew. Chem.* **2005**, *117*, 7570; *Angew. Chem. Int. Ed.* **2005**, *44*, 7404.
[9] a) ORTEP-3 for Windows, L. J. Farrugia, *J. Appl. Crystallogr.* **1997**, *30*, 565; b) SMART, V. 5.625, Bruker Advanced X-ray Solutions, Inc., Madison, WI, **2001**; c) SAINT, V. 6.22, Bruker Advanced X-ray Solutions, Inc., Madison, WI, **2001**; d) G. M. Sheldrick, SADABS, V. 2.02, Area Detector Absorption Correction, University of Göttingen, Göttingen, Germany, **1997**; e) SHELXS-90 G. M. Sheldrick, *Acta Crystallogr. Sect. A* **1990**, *46*, 467; f) G. M. Sheldrick, SHELXL-99, Program for the Refinement of Crystal Structures, University of Göttingen, Göttingen, Germany, **1997**; g) SHELXTL 6.12, Program Library for Structure Solution and Molecular graphics, Bruker Advanced X-ray Solutions, Madison, WI, **2001**.
[10] F. H. Allen, *Acta Crystallogr. Sect. B* **2002**, *58*, 380.
[11] a) R. J. Baker, M. L. Cole, C. Jones, M. F. Mahon, *J. Chem. Soc. Dalton Trans.* **2002**, 1992; b) C. Peppe, J. A. Nobrega, M. Z. Hernandes, R. L. Longo, D. G. Tack, *J. Organomet. Chem.* **2001**, *626*, 68; c) G. R. Willey, D. R. Aris, J. V. Haslop, W. Errington, *Polyhedron* **2001**, *20*, 423.

 © 2006 Wiley-VCH Verlag GmbH & Co. KGaA, Weinheim

Negative-Valent Transition Metals

DOI: 10.1002/anie.200602937

Towards Homoleptic Naphthalenemetalates of the Later Transition Metals: Isolation and Characterization of Naphthalenecobaltates(1−)**

*William W. Brennessel, Victor G. Young, Jr., and John E. Ellis**

Dedicated to Professor Christoph Elschenbroich

Storable sources of transition-metal atoms, or "naked-metal-atom" reagents, were first discovered in the pioneering research of Wilke and co-workers, which involved spectacular homoleptic alkene nickel(0) complexes, including [Ni(cod)$_2$],[1] (cod = 1,5-cyclooctadiene) and [Ni(C_2H_4)$_3$].[2] Subsequently, Jonas et al. isolated related anionic alkene complexes, [Co(cod)$_2$]$^-$[3] and [Co(C_2H_4)$_4$]$^-$,[4] which proved to be extremely useful synthons for the atomic cobalt anion. Kündig and Timms[5] and Elschenbroich and Möckel[6] then independently discovered that early-transition-metal "naked-atom" reagents could be isolated in the form of quite labile neutral homoleptic naphthalene complexes, [M($C_{10}H_8$)$_2$] (M = V, Cr, Mo). Anionic early-transition-metal homoleptic naphthalene complexes were later established for zirconium ([Zr(η^4-$C_{10}H_8$)$_3$]$^{2-}$)[7] and tantalum ([Ta(η^4-$C_{10}H_8$)$_3$]$^-$)[8] and have been shown to function as sources of atomic Zr^{2-} and Ta^- ions in their reactions with carbon monoxide and similar ligands. However, no compounds of this class are presently known for the later transition metals. Indeed, even *heteroleptic* naphthalene complexes containing formally negative-valent metals are unknown for d-block elements to the right of manganese,[9] and also unknown for the corresponding heavier metals within each triad. For these reasons, we report herein on the isolation, structural characterization, and some chemical properties of the first compound of this type, [Co(η^4-$C_{10}H_8$)(η^4-cod)]$^-$ (**1**). Also, two other naphthalenecobaltate(1−) complexes were unexpectedly obtained in the course of developing a "noncobaltocene" route to alkenecobaltates(1−).

Recently, we disclosed that the reaction of cobalt(II) bromide with three equivalents of potassium naphthalene gave a thermally unstable deep-red species, which functioned as a convenient source of atomic Co^{1-} ions, but defied all attempts at isolation or characterization.[10] However, when identical reactions were carried out in the presence of one equivalent of cod, bright-red and quite air-sensitive microcrystals of thermally stable (at 20 °C) anion **1** were isolable as [K(L)(thf)$_x$] salts (L = [18]crown-6) in 60–65 % yields [Eq. (1)], where x is 0.5 or 0, depending on the method

$$CoBr_2 + 3\ KC_{10}H_8 + 1{,}5\text{-cod} \xrightarrow[-78 \rightarrow +20\ ^\circ C,\ -2\ KBr]{THF} \xrightarrow[L]{Et_2O} [K(L)(thf)_x][\mathbf{1}] + 2\ C_{10}H_8 \quad (1)$$

of purification (see the Experimental Section). Interestingly, analogous reactions that were conducted with cobaltocene as the Co^{II} precursor also provided **1** in yields of about 85 %. Thus, both reactions may involve a common intermediate, perhaps a homoleptic naphthalenecobaltate(1−)[11] that is analogous to the known bis(1,2,3,4-η^4-anthracene)cobaltate(1−) (**2**).[10]

^{1}H and ^{13}C NMR spectra of **1** in solution are unexceptional and entirely consistent with its formulation, and showed resonances characteristic of η^4-naphthalene[7,8] and η^4-1,5-cyclooctadiene[3,12] groups bound in a 1:1 ratio to an electron-rich metal center. A single-crystal X-ray study on **1**, as the [K([18]crown-6)] salt, revealed an undistorted cation that was well-separated from the cobalt center of the anion and had no significant effect on its structure.[13] The latter showed a nearly tetrahedral environment about the cobalt center,[14] which is appropriate for a d^{10} cobalt(−I) complex (Figure 1). Indeed, the Co–C and C–C bond lengths of the η^4-diene units in **1** and **2**[10] are nearly identical, thus indicating that there are no great differences in the η^4-polyarene–cobalt interactions in the two anions.[15] However, the average Co–C

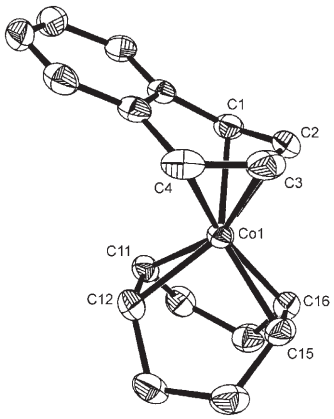

Figure 1. Molecular structure of **1**; cation is not shown. Thermal ellipsoids are set at the 50 % probability level, with hydrogen atoms omitted for clarity. Selected bond lengths [Å] and angles [°]: Co-C1 2.142(1), Co-C2 2.008(1), Co-C3 2.012 (2), Co-C4 2.158(2), Co-C11 2.017(1), Co-C12 2.028(1), Co-C15 2.009(1), Co-C16 2.021(2), C1-C2 1.424(2), C2-C3 1.400(2), C3-C4 1.414(2), C11-C12 1.400(2), C15-C16 1.412(2), Co-centroid(η^4) 1.67, Co-centroid(cod) 1.30; centroid(η^4)-Co-centroid(cod) 175.2.

[*] W. W. Brennessel, Dr. V. G. Young, Jr., Prof. J. E. Ellis
Department of Chemistry
University of Minnesota
Minneapolis, Minnesota 55455 (USA)
Fax: (+1) 612-626-7541
E-mail: ellis@chem.umn.edu

[**] Highly Reduced Organometallics, part 58. This work was supported by the U.S. National Science Foundation and the donors of the Petroleum Research Fund, administered by the American Chemical Society. We thank Ms. Christine Lundby for expert assistance in the preparation of this manuscript. Part 57: reference [8].

Supporting information for this article is available on the WWW under http://www.angewandte.org or from the author.

InterScience
© 2006 Wiley-VCH Verlag GmbH & Co. KGaA, Weinheim

bond length of the η^4-cod group in **1** (2.019(8) Å) is slightly shorter than the corresponding value found in $[(thf)_2Li][Co(cod)_2]$ (2.05(2) Å),[3] thus suggesting that the cod ligand is a somewhat better donor in **1** than it is in $[Co(cod)_2]^-$. Thus, the relative stability of **1** compared to a homoleptic naphthalenecobaltate is likely a result, in part, of the synergy of its mixed cod/naphthalene ligand set, where cod is expected to be a better donor and weaker acceptor than naphthalene.[15,16]

Several reactions of **1** are shown in Scheme 1 to illustrate its utility as a precursor to other Co^{1-} complexes. Very good acceptor ligands, such as 1,2-bis(diphenylphosphano)ethane

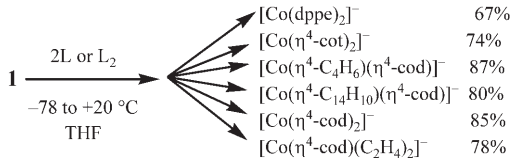

Scheme 1. Reactions of **1** with L_2 = dppe, cot, C_4H_6 (1,3-butadiene), $C_{14}H_{10}$ (anthracene), cod (1,5-cyclooctadiene), and L = C_2H_4 (ethene), with yields of isolated products, obtained as [K([18]crown-6)] salts.

(dppe) or 1,3,5,7-cyclooctatetraene (cot), react with **1** to provide the identical homoleptic cobaltates in about the same yields as those obtained from analogous reactions with **2**.[10] New cobaltates that are derived from **1** include $[Co(\eta^4\text{-}C_4H_6)(\eta^4\text{-cod})]^-$ (**3**) and $[Co(\eta^4\text{-}C_{14}H_{10})(\eta^4\text{-cod})]^-$ (**4**), which were structurally characterized[17] and provide unprecedented examples of mixed 1,3-butadiene–alkene and anthracene–alkene metalates. In contrast to **4**, compound **1** readily reacts with excess cod or ethylene to afford $[Co(cod)_2]^-$ (**5**)[3] or $[Co(cod)(C_2H_4)_2]^-$ (**6**)[4] in good yields, thus indicating that the naphthalene ligand in **1** is more labile than the anthracene ligand in **4**. These reactions are noteworthy because **5** and **6** were previously available only from reductions involving cyclopentadienylcobalt precursors, such as cobaltocene.[4,18] It is clear that the naphthalene ligand in **1** fulfills the same important role of a supporting ligand, as Jonas previously established for the cyclopentadienyl group in his prior routes to these alkenecobaltates.[4,19–22]

The ability of ethylene to readily displace naphthalene from **1** to produce **6** was an exciting result because it suggested that the long-known $[Co(C_2H_4)_4]^-$ complex[4,23] should also be accessible from reductions of $CoBr_2$ mediated by alkali metal–naphthalene reagents in the presence of excess ethylene. Indeed, a pale gray solid, identical to the previously reported $[K(thf)_x][Co(C_2H_4)_4]$ (**7**),[4] was obtained in about 80% yield by this facile procedure, which is identical to the synthesis of **1**, except excess ethylene was first added rather than cod. Treatment of **7** with [18]crown-6 or [2.2.2]cryptand in THF/pentane at 0 °C afforded $[K([18]crown\text{-}6)][Co(C_2H_4)_4]$ (**8**) as a beige solid or $[K([2.2.2]cryptand)][Co(C_2H_4)_4]$ (**9**) as light yellow needles. The formulation of **9** was confirmed by a single-crystal X-ray study, which revealed the presence of discrete $[Co(C_2H_4)_4]^-$ units in the solid state for the first time.[24]

When a light-yellow solution of **8** and three equivalents of naphthalene in THF were evaporated in vacuo at 20 °C, the concentrated solution/slurry acquired a distinct reddish appearance. Addition of diethyl ether caused precipitation of a red solid.[25] Crystallization of this product from THF/pentane at 0 °C *reproducibly* gave both yellow and red-black single crystals, in variable amounts. The crystals were manually separated under an inert atmosphere and identified by X-ray crystallography as **8** and **10**, respectively. The latter was found to be the remarkable "triple salt" $[K([18]crown\text{-}6)]_3[Co(\eta^4\text{-}C_{10}H_8)(C_2H_4)_2]_2[Co(\eta^4\text{-}C_{10}H_8)_2]$, which contained the new naphthalenecobaltates $[Co(\eta^4\text{-}C_{10}H_8)(C_2H_4)_2]^-$ (**11**) and $[Co(\eta^4\text{-}C_{10}H_8)_2]^-$ (**12**) in a 2:1 ratio.[25] Anion **12** is of particular significance because it represents the first homoleptic naphthalenemetalate of a later transition metal. Attempts to isolate pure salts of **11** and **12** have so far failed.

The asymmetric unit of **10**[26] contains two independent anions of **11** and one of **12**, which interact weakly with and appear to be largely unperturbed by essentially undistorted [K([18]crown-6)] cations. The independent anions of **11** are almost superimposable, and one of these is shown in Figure 2.

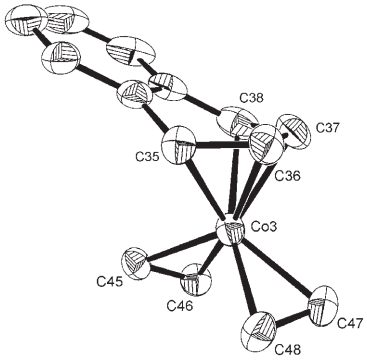

Figure 2. Molecular structure of **11**; cation is not shown. Thermal ellipsoids are set at the 50% probability level, with hydrogen atoms omitted for clarity. Selected bond lengths [Å]: Co3-C35 2.166(2), Co3-C36 2.011(3), Co3-C37 2.016(3), Co3-C38 2.158(3), Co3-C45 2.017(2), Co3-C46 2.007(2), Co3-C47 2.039(3), Co3-C48 2.012(3), C35-C36 1.416(4), C36-C37 1.402(4), C37-C38 1.405(4), C45-C46 1.399(4), C47-C48 1.405(4), Co-centroid(η^4) 1.68.

Anion **12** is depicted in Figure 3. The structural properties of **11** are nearly identical to those of closely related **1**[27] and only differ significantly in the twist angle,[14] which has an average value of 68(1)° for **11**. The corresponding twist angles for **2** and **12** are 62°[10] and 70°, respectively. Thus, the geometry about the cobalt center in these anions is distorted tetrahedral, which is indicative of d^{10} cobalt(−I). In view of the relatively robust character of **2**[10] and the prior difficulties in accessing bona fide **12**,[28] it is noteworthy that the η^4-diene–cobalt units in both compounds are nearly identical.[29] Although the structural data suggest that the anthracene and naphthalene units bind about as strongly to cobalt in **2** and **12**, respectively, interatomic distances may prove to be rather insensitive measures of metal–arene binding in these complexes. For example, a recent computational study on low-valent molybdenum–arene complexes showed that the Mo–(η^4-arene) bond energy increased in the order naphthalene < anthracene, owing, in part, to the greater acceptor

 © 2006 Wiley-VCH Verlag GmbH & Co. KGaA, Weinheim

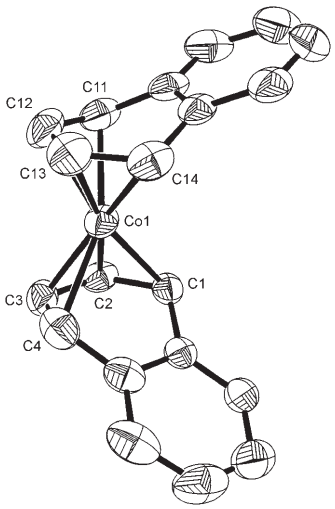

Figure 3. Molecular structure of **12**; cation is not shown. Thermal ellipsoids are set at the 50% probability level, with hydrogen atoms omitted with clarity. Selected bond lengths [Å] and angles [°]: Co1-C1 2.116(3), Co1-C2 1.960(3), Co1-C3 1.989(3), Co1-C4 2.131(3), Co1-C11 2.139(3), Co1-C12 1.992(3), Co1-C13 1.961(3), Co1-C14 2.106(3), C1-C2 1.433(4), C2-C3 1.418(4), C3-C4 1.421(5), C11-C12 1.407(5), C12-C13 1.406(5), C13-C14 1.413(5), Co-centroid(η^4) 1.63; centroid(η^4)-Co-centroid(η^4) 167.5.

ability of anthracene. However, corresponding average Mo–C and C–C bond lengths for the η^4-diene–molybdenum units in these two compounds were only marginally different.[30]

In summary, we have prepared, isolated, and fully characterized the first naphthalenecobaltate(1−) complex, $[Co(\eta^4\text{-}C_{10}H_8)(cod)]^-$ (**1**), and have shown that it functions as an effective storable source of the atomic cobalt anion in several reactions. Two related species, $[Co(\eta^4\text{-}C_{10}H_8)(C_2H_4)_2]^-$ (**11**) and $[Co(\eta^4\text{-}C_{10}H_8)_2]^-$ (**12**), were also identified in the unusual triple salt **10**. Compound **12** is of special interest because it is the first structurally characterized homoleptic bis(naphthalene)metal anion for any d-block element, and it promises to be a particularly reactive source of atomic cobalt anions in chemical reactions. Extension of this investigation to other polyarenes and transition metals is in progress.

Experimental Section

1: A bright-blue solution of anhydrous $CoBr_2$ (0.500 g, 2.29 mmol) and 1,5-cod (0.247 g, 2.29 mmol) in THF (40 mL, −78 °C) was added to a forest-green solution of $KC_{10}H_8$ (6.86 mmol) in THF (40 mL, −78 °C). The resulting red-brown solution was warmed to room temperature over a 12-hour period and then filtered to remove KBr. After the solvent was removed in vacuo, diethyl ether (50 mL) was added to extract the product. The reaction mixture was filtered into a flask containing [18]crown-6 (0.604 g, 2.29 mmol) in diethyl ether, whereupon a bright red microcrystalline product formed within seconds. The product was separated by filtration, washed thoroughly with diethyl ether, and dried in vacuo. Pure magenta microcrystals of $[K([18]crown\text{-}6)(thf)_{0.5}][Co(C_{10}H_8)(cod)]$ were thereby obtained (0.936 g, 64%). Elemental analysis (%) calcd for $C_{32}H_{48}CoKO_{6.5}$: C 60.55, H 7.62; found: C 61.15, H 7.61; m.p. 124–126 °C (decomp); ^{1}H NMR (300 MHz, [D$_8$]THF, 20 °C, cation resonances omitted; Np = naphthalene) $\delta = 0.94$ (br, 2H, CH, cod), 1.25, 1.75, 1.94, 2.44 (br m, 2H; CH_2, cod), 2.83 (m, 2H, H1,H4 of Np), 4.13 (br m, 2H, CH, cod), 4.91 (m, 2H, H2,H3 of Np), 5.49 ppm (m, 4H, H5–H8 of Np); ^{13}C NMR (75.5 MHz [D$_8$]THF, 20 °C) $\delta = 33.4$ (t, CH_2, cod), 54.3 (d, CH, cod), 60.2 (d, C1,C4 of Np), 69.9 (d, CH, cod), 84.8 (d, C2,C3 of Np), 114.7, 118.4 (d, C5,C8 and C6,C7 of Np), 149.2 ppm (s, C9,C10 of Np). Identification of C,H resonances was established by ^{1}H–^{13}C HMQC, COSY 2D NMR and trends previously established for η^4-naphthalene complexes,[7,8] but no unique assignment of C5,C8 or C6,C7 on the naphthalene ligand was possible. X-ray quality single-crystals of **1**, as a [(K[18]crown-6)] salt, were grown as red-brown plates from a pentane-layered THF solution at 0 °C.[13]

Received: July 21, 2006
Published online: October 6, 2006

Keywords: alkene ligands · arene ligands · cobalt · cobaltates · subvalent compounds

[1] a) G. Wilke, *Angew. Chem.* **1960**, *72*, 581; b) B. Bogdanovic, M. Kröner, G. Wilke, *Justus Liebigs Ann.* **1966**, *699*, 1.
[2] K. Fischer, K. Jonas, G. Wilke, *Angew. Chem.* **1973**, *85*, 620; *Angew. Chem. Int. Ed. Engl.* **1973**, *12*, 565.
[3] K. Jonas, R. Mynott, C. Krüger, J. C. Sekutowski, Y.-H. Tsay, *Angew. Chem.* **1976**, *88*, 808; *Angew. Chem. Int. Ed. Engl.* **1976**, *15*, 767.
[4] K. Jonas, C. Krüger, *Angew. Chem.* **1980**, *92*, 513; *Angew. Chem. Int. Ed. Engl.* **1980**, *19*, 520.
[5] E. P. Kündig, P. L. Timms, *J. Chem. Soc. Chem. Commun.* **1977**, 912.
[6] C. Elschenbroich, R. Möckel, *Angew. Chem.* **1977**, *89*, 908; *Angew. Chem. Int. Ed. Engl.* **1977**, *16*, 870.
[7] M. Jang, J. E. Ellis, *Angew. Chem.* **1994**, *106*, 2036; *Angew. Chem. Int. Ed. Engl.* **1994**, *33*, 1973.
[8] W. W. Brennessel, J. E. Ellis, M. K. Pomije, V. J. Sussman, E. Urnezius, V. G. Young, Jr., *J. Am. Chem. Soc.* **2002**, *124*, 10258.
[9] a) $[Mn(\eta^4\text{-}C_{10}H_8)(PMe_3)_3]^-$: K. Jonas, G. Burkart, C. Häselhoff, P. Betz, C. Krüger, *Angew. Chem.* **1990**, *102*, 291; *Angew. Chem. Int. Ed. Engl.* **1990**, *29*, 323; b) $[Mn(\eta^4\text{-}C_{10}H_8)(CO)_3]^-$: R. L. Thompson, S. Lee, A. L. Rheingold, N. J. Cooper, *Organometallics* **1991**, *10*, 1657; c) $[Mn(\eta^4\text{-}C_{10}H_8)(\eta^6\text{-biphenyl})]^-$: K. Jonas, C.-C. Häselhoff, R. Goddard, C. Krüger, *Inorg. Chim. Acta* **1992**, *198–200*, 533.
[10] W. W. Brennessel, V. G. Young, Jr., J. E. Ellis, *Angew. Chem.* **2002**, *114*, 1259; *Angew. Chem. Int. Ed.* **2002**, *41*, 1211.
[11] P. A. Leach, S. J. Geib, J. A. Corella, G. F. Warnock, N. J. Cooper, *J. Am. Chem. Soc.* **1994**, *116*, 8566.
[12] K. Jonas, L. Schieferstein, *Angew. Chem.* **1979**, *91*, 590; *Angew. Chem. Int. Ed. Engl.* **1979**, *18*, 549.
[13] Crystal structure analysis of **1**: $C_{30}H_{44}CoKO_6$, $M_r = 598.68$, monoclinic, space group $P2_1/c$, red-brown plates, $a = 12.954(1)$, $b = 14.038(1)$, $c = 16.213(2)$ Å, $\beta = 96.399(2)°$, $V = 2930.0(5)$ Å^3, $Z = 4$, $T = 173(2)$ K, $\lambda = 0.71073$ Å, 22987 reflections, 6702 independent, $R1 = 0.0275$ ($I > 2\sigma(I)$), $wR2 = 0.0654$ (for all data), $\mu = 0.768$ mm^{-1} (SADABS), full-matrix least-squares refinement on F^2. CCDC-614823 (**1**) and CCDC-614824 (**10**) contain the supplementary crystallographic data for this paper. These data can be obtained free of charge from The Cambridge Crystallographic Data Centre via www.ccdc.cam.ac.uk/data_request/cif.
[14] Coordination geometry is determined by a twist angle, θ, corresponding to the intersection of planes that are defined by the midpoints of the bound C–C groups of the coordinated diene units and cobalt center. For **1** the θ angle is 84°, compared to 90° for tetrahedral geometry.
[15] Average Co–C1,C4 and Co–C2,C3 bond lengths for the η^4-1,3-diene groups in **1** are 2.15(1) and 2.010(3) Å, respectively, and the corresponding values for **2** are 2.13(1) and 1.99(2) Å.[10] The

 © 2006 Wiley-VCH Verlag GmbH & Co. KGaA, Weinheim

average outer C1–C2 and inner C2–C3 bond lengths in **1** are 1.419(7) and 1.400(2), whereas corresponding values in **2** are 1.416(8) and 1.420(6) Å. A definite, albeit weak, long-short-long pattern in the diene C–C bond lengths in **1**, but not **2**, suggests that slightly more back-bonding is present in the cobalt–arene interaction in **1** compared to **2**, likely because of the presence of cod in the naphthalene complex. Interestingly, Zenneck and co-workers have observed nearly identical diene C–C bond lengths for naphthalene in the X-ray structure of $[Fe(\eta^6\text{-}C_6Me_6)(\eta^4\text{-}C_{10}H_8)]$, where the presence of the good donor hexamethylbenzene is critical in the stabilization of this complex, relative to a possible homoleptic naphthaleneiron(0) complex, which decomposes at about −60 °C.[16]

[16] C. Brodt, S. Niu, H. Pritzkow, M. Stephan, U. Zenneck, *J. Organomet. Chem.* **1993**, *459*, 283, and references therein.

[17] See the Supporting Information for syntheses and characterization of **3** and **4**. Details on the X-ray studies on **3** and **4** will be described elsewhere: W. W. Brennessel, J. E. Ellis, unpublished results. Crystal data for [K([18]crown-6)][Co(C_4H_6)(cod)] (**3**): $C_{24}H_{42}CoKO_6$, $M_r = 524.61$, triclinic, space group $P\bar{1}$, orange blocks, $a = 8.6632(7)$, $b = 10.9612(9)$, $c = 14.924(1)$ Å, $\alpha = 90.952(1)$, $\beta = 93.574(1)$, $\gamma = 112.826(1)°$, $Z = 2$, $wR2$ (all data) = 0.0988 with GOF on F^2 of 1.037. Crystal data for [K([2.2.2]cryptand)][Co($C_{14}H_{10}$)(cod)] (**4**): $C_{40}H_{58}CoKN_2O_6$, $M_r = 760.91$, triclinic, space group $P\bar{1}$, red-violet plates, $a = 12.104(1)$, $b = 13.158(1)$, $c = 14.411(1)$ Å, $\alpha = 108.664(2)$, $\beta = 107.142(2)$, $\gamma = 106.915(2)°$, $Z = 2$, $wR2$ (all data) = 0.0955 with GOF on F^2 of 1.022.

[18] K. Jonas, *Angew. Chem.* **1985**, *97*, 292; *Angew. Chem. Int. Ed. Engl.* **1985**, *24*, 295.

[19] Jonas et al. were the first to prepare and examine the reactivity of non-carbonyl-containing heteroleptic naphthalenemetalates, including Mn^{-I} species[9a,c] and the M^0 complexes $[C_5H_5M(C_{10}H_8)]^-$ (M = V,[20,21] Cr,[22] Fe[22]).

[20] K. Jonas, V. Wiskamp, *Z. Naturforsch. B* **1983**, *38*, 1113.

[21] K. Jonas, W. Rüsseler, C. Krüger, E. Raabe, *Angew. Chem.* **1986**, *98*, 902; *Angew. Chem. Int. Ed. Engl.* **1986**, *25*, 925.

[22] K. Jonas, *Pure Appl. Chem.* **1990**, *62*, 1169.

[23] J. E. Ellis, *Inorg. Chem.* **2006**, *45*, 3167.

[24] Details on the syntheses of **7**, **8**, and **9** and the X-ray study on **9** will be described elsewhere: W. W. Brennessel, J. E. Ellis, unpublished results. Crystal data for [K([2.2.2]cryptand)][Co(C_2H_4)$_4$]: $C_{26}H_{52}CoKN_2O_6$, $M_r = 586.73$, orthorhombic, space group *Pbcn*, light-yellow needles, $a = 25.836(3)$, $b = 10.4820(12)$, $c = 22.544(3)$ Å, $Z = 8$, $wR2$ (all data) = 0.0734 with GOF on F^2 of 1.017.

[25] Interestingly, exposure of a suspension of the red product to excess ethylene in diethyl ether at 20 °C caused it to rapidly revert to pale yellow, slightly soluble **8**.

[26] Crystal structure analysis of **10**: $C_{84}H_{120}Co_3K_3O_{18}$, $M_r = 1711.89$, triclinic, space group $P\bar{1}$, red-black blocks, $a = 15.228(1)$, $b = 15.938(1)$, $c = 19.098(1)$ Å, $\alpha = 84.505(1)$, $\beta = 67.115(1)$, $\gamma = 88.147(1)°$, $V = 4250.5(5)$ Å^3, $Z = 2$, $T = 173(2)$ K, $\lambda = 0.71073$ Å, 41889 reflections, 17834 independent, $R1 = 0.0382$ ($I > 2\sigma(I)$), $wR2 = 0.0977$ (for all data), $\mu = 0.791$ mm^{-1} (SADABS), full-matrix least-squares refinement on F^2. See reference [13] for CCDC number and related information.

[27] Average C–C bond lengths for the η^4-diene and η^2-alkene groups in **1** are 1.413(12) and 1.406(8) Å, respectively. Corresponding values for **11** are 1.408(7) and 1.402(4) Å. Average Co–C1,C4, Co–C2,C3, and Co–C(alkene) bond lengths in **1** are 2.15(1), 2.010(3), and 2.019(8) Å, respectively. Corresponding values for **11** are 2.162(6), 2.014(3), and 2.019(14) Å. Finally, the fold angles for coordinated naphthalenes in **1** and **11** are 27 and 30°.

[28] In this regard, it is important to stress that there is no proof presently for the formation of **12** in the alkali metal naphthalene reductions of cobalt(II) bromide[10] or cobaltocene[11] in THF.

[29] Average C–C bond lengths for the η^4-diene groups in **2** and **12** are 1.417(7) and 1.416(10) Å. Average Co–C1,C4 and Co–C2,C3 bond lengths for both η^4-diene groups in **2** are 2.13(1) and 1.99(2) Å, and corresponding values for **12** are 2.12(1) and 1.98(1) Å. Average fold angles for the anthracene ligands in **2** are 28°, and those for the naphthalene ligands in **12** are 32°. The twist angles[14] in **2** and **12** are 62° and 70°, respectively.

[30] G. Zhu, K. E. Janak, J. S. Figueroa, G. Parkin, *J. Am. Chem. Soc.* **2006**, *128*, 5452.

 © 2006 Wiley-VCH Verlag GmbH & Co. KGaA, Weinheim

Phosphine Polymers

DOI: 10.1002/anie.200602955

Ambient-Temperature Living Anionic Polymerization of Phosphaalkenes: Homopolymers and Block Copolymers with Controlled Chain Lengths**

*Kevin J. T. Noonan and Derek P. Gates**

Living polymerization is a powerful synthetic tool that enables the construction of well-defined macromolecules possessing controlled architectures and tailor-made properties.[1,2] Despite considerable recent activity in the synthesis of polymers composed of inorganic elements,[3,4] living polymerization methods remain primarily the domain of organic polymer chemistry.[5] The prospect of accessing macromolecules of controlled architecture possessing the unique properties imparted by inorganic functionalities is particularly attractive.[6] The addition polymerization of the C=C bond of substituted olefins (for example, styrene) is the prototypical example of a living polymerization,[7] yet the living polymerization of inorganic multiple bonds is unprecedented.

Inspired by the fascinating chemistry of phosphaalkenes and the established parallels between P=C and C=C bonds in molecular chemistry,[8] we have embarked on a program to extend this analogy to polymer science.[9] Building on the well-known addition polymerization of olefins, we have recently discovered that P=C bonds can also be polymerized to afford macromolecules with chemically functional phosphine moieties.[10,11] To polymerize phosphaalkene **1a**, high temperatures (up to 150 °C), long reaction times (about

[*] K. J. T. Noonan, Prof. D. P. Gates
Department of Chemistry
University of British Columbia
2036 Main Mall, Vancouver, BC, V6T 1Z1 (Canada)
Fax: (+1) 604-822-2847
E-mail: dgates@chem.ubc.ca

[**] This work was supported by the Natural Sciences and Engineering Research Council of Canada (Discovery and Research Tools grants to D.G. and a graduate fellowship to K.N.), the Canada Foundation for Innovation, and the BC Knowledge Development Fund. We thank Dr. Nick Burlinson for assistance with the ^{31}P NMR experiments.

Supporting information for this article is available on the WWW under http://www.angewandte.org or from the author.

© 2006 Wiley-VCH Verlag GmbH & Co. KGaA, Weinheim

24 hours), and minimal solvent were required, even in the presence of radical or anionic initiators. Under these conditions, low monomer conversions and several unidentified phosphorus by-products are observed, thus resulting in poor yields of isolated poly(methylenephosphine). Clearly, improved methods are necessary for the polymerization of **1**. It has been noted that **1a** reacts rapidly with alkyl lithium reagents (for example, MeLi) to afford $MesP(Me)CPh_2Li$ ($\delta(^{31}P) = -45$ ppm; Mes = 2,4,6-$Me_3C_6H_2$)[10,12] which in the presence of additional **1a** forms short-chain oligomers.[13] Prompted by these observations, we speculated that the anionic polymerization of **1** may be living under the right conditions.

Herein, we report the first living anionic polymerization of a heteroatom-containing multiple bond; namely, treating phosphaalkene **1** with *n*BuLi at ambient temperatures in solution gives living poly(methylenephosphine) **2** (Scheme 1). This new chemistry facilitates the construction of monodisperse homopolymers and unprecedented styrene–phosphaalkene block copolymers with controlled molecular weights.

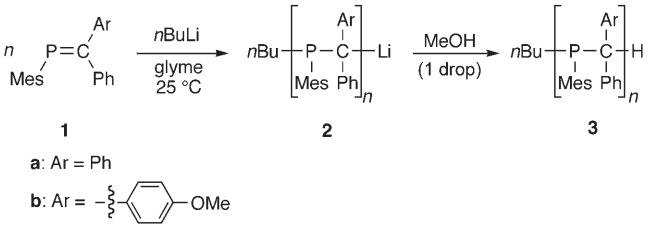

Scheme 1. Living anionic polymerization of **1**.

Monomers **1a** and **1b** are readily synthesized following literature procedures[14,15] and, for this work, must be carefully purified using distillation and recrystallization methods. The addition of the anionic initiator *n*BuLi (2 mol%) to a pale yellow solution of phosphaalkene **1a** in glyme[16] at 25°C resulted in an immediate color change to deep red. Remarkably, monitoring the reaction progress over several hours using ^{31}P NMR spectroscopy revealed that monomer **1a** ($\delta =$ 234 ppm) is entirely consumed and that polymer **2a** ($\delta =$ −7 ppm) is formed quantitatively (Figure 1). The reaction is very clean and no side-products are observed. This finding is in stark contrast to our earlier investigations involving the high-temperature polymerization of neat **1a** where a number of phosphorus-containing by-products were observed.[10] Interestingly, analysis of the ^{31}P NMR spectroscopic data shows that the polymerization follows pseudo-first-order kinetics for up to 60% conversion (inset, Figure 1). This extremely slow measured propagation rate ($k_p =$ 21 $L\,mol^{-1}\,h^{-1}$) is extraordinary. For comparison, the k_p value of styrene in glyme (1.4×10^7 $L\,mol^{-1}\,h^{-1}$)[1] is higher by several orders of magnitude. Presumably, the small k_p value for **1a** is a consequence of the steric hindrance associated with the addition of a bulky propagating carbanion (that is, in **2a**) to bulky **1a**.

The red color of the solution of polymer **2a** persists even in the absence of monomer; however, an immediate loss of color is observed when methanol (one drop) is added. The

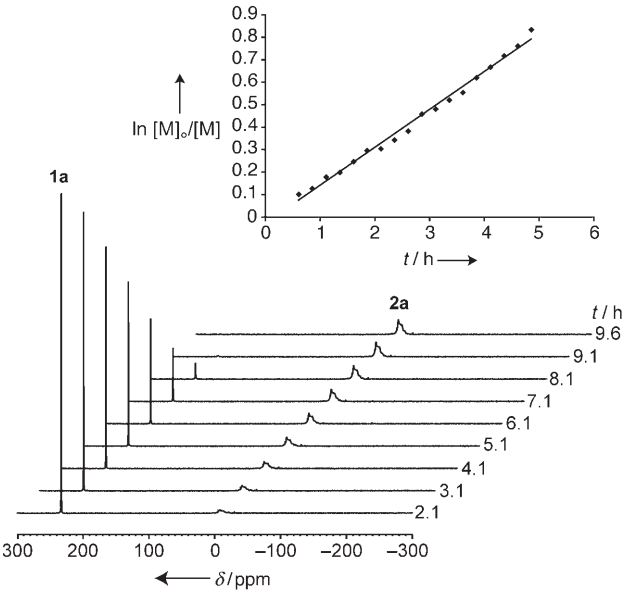

Figure 1. Selected ^{31}P NMR spectra and first-order kinetic plot (inset) showing the progress of the polymerization of **1a** in glyme using *n*BuLi (2 mol%); ^{31}P NMR measurement times are given in hours. Kinetic data: monomer/initiator (M/I) = 50:1, $k_p = 21$ $L\,mol^{-1}\,h^{-1}$. Concentrations determined by relative integration of the ^{31}P NMR signals for **1a** and **2a** (relaxation time (t_1) for **1a** is 1.33 s; relaxation delay for NMR experiment is 2 s with a 30° tip angle).

subsequent addition of hexanes to this quenched solution results in the precipitation of H-terminated polymer **3a** (74% yield). Analysis of **3a** using triple-detection gel permeation chromatography (GPC) reveals a very narrow polydispersity index (PDI, $M_w/M_n = 1.04$). Moreover, the measured absolute molecular weight ($M_n = 14\,800$ $g\,mol^{-1}$) is very close to the theoretical molecular weight ($M_n = 15\,900$ $g\,mol^{-1}$; Table 1, entry 3). On the basis of the observed narrow PDI and the excellent correlation of the measured molecular weight of **3a** to that predicted from the ratio of **1a**/*n*BuLi, we postulate that this polymerization reaction is living.

A classic characteristic of a living polymerization is that a plot of M_n versus monomer conversion will be linear. The combination of the slow propagation rate for **1a** with the

Table 1: Synthesis of poly(methylenephosphine)s **3** with controlled molecular weight. Initiator (I) = *n*BuLi.

Entry[a]	M	M/I	M_n (calcd)[b] [$g\,mol^{-1}$]	M_n (abs)[c] [$g\,mol^{-1}$]	M_w/M_n[c]	r_{hyd}[c] [nm]
1	**1a**	25:1	8000	8900	1.08	1.8
2	**1a**	33:1	10500	10500	1.08	1.9
3	**1a**	50:1	15900	14800	1.04	2.3
4	**1a**	100:1	31700	29600	1.15	3.4
5	**1b**	33:1	11500	11500	1.09	1.8
6	**1b**	50:1	17400	14600	1.11	2.5

[a] Conditions: glyme, 25°C in N_2 atmosphere (glovebox). Upon complete consumption of monomer (confirmed by ^{31}P NMR), the reactions were quenched with MeOH. [b] Predicted M_n value from M/I ratio. [c] GPC (triple detection) equipped with differential refractometer (Waters), viscometer, and laser-light-scattering detectors (Wyatt); refractive index increment (d*n*/d*c*) determined off-line (0.223 $mL\,g^{-1}$ for both **1a** and **1b**); r_{hyd} = hydrodynamic radius.

 © 2006 Wiley-VCH Verlag GmbH & Co. KGaA, Weinheim

^{31}P NMR handle makes this system ideal for analysis of molecular weight versus conversion. Aliquots were taken over a period of about eight hours, and each aliquot was analyzed using ^{31}P NMR spectroscopy and triple-detection GPC. The monomer conversion for each aliquot was determined from the relative integration of the signals resulting from monomer (**1a**) and polymer (**2a**) in the ^{31}P NMR spectrum. The plot of M_n versus conversion for two separate experiments correlates well with the theoretical trend line, and the polydispersities determined were below 1.05 (Figure 2). The absence of data at low monomer conversion (< 50 %) is a consequence of the similar solubilities of low-molecular-weight **3a** and monomer **1a**, which renders these species inseparable using precipitation techniques. Nevertheless, the data obtained clearly support our hypothesis that the ambient-temperature anionic polymerization of **1a** is living.

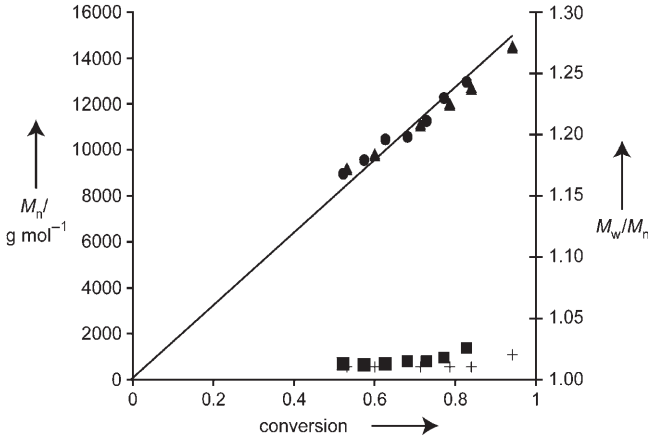

Figure 2. A graph of molecular weight (M_n) and polydispersity index (PDI, M_w/M_n) for **3a** versus conversion of monomer (conditions: glyme, 2 mol% *n*BuLi, 25 °C). The solid line shows the theoretical trend. Data are presented for two separate experiments with each point representing an aliquot taken from the reaction mixture (absolute M_n from GPC; % conversion from ^{31}P NMR). Experiment 1: ● (M_n) and ■ (PDI); Experiment 2: ▲ (M_n) and + (PDI).

The preparation of **3a** with molecular weights that are dependent upon the monomer-to-initiator ratio (M/I) that was used provides the final confirmation that the anionic polymerization of **1a** is living (Table 1). Importantly, all these polymers have narrow polydispersities and are isolated in high yield (≥ 70 %). We have also extended this living polymerization reaction to a 4-methoxyphenyl-substituted monomer **1b** (Table 1, entries 5 and 6).

Once the living nature of the anionic polymerization of **1a** was confirmed, we attempted to prepare a block copolymer from **1a** and styrene (Scheme 2). Living polystyrene was generated by treating a solution of styrene in toluene with *n*BuLi (M/I = 100:1; 25 °C). An aliquot was removed from the reaction mixture, quenched with MeOH, and analyzed by GPC ($M_n = 13300\ g\,mol^{-1}$, $M_w/M_n = 1.07$). This experimentally determined molecular weight is close to the theoretical molecular weight ($M_n = 10500\ g\,mol^{-1}$). To the orange solution of living polystyrene was added a solution of **1a** (M/I = 28:1) in glyme.[17] The color of the solution immediately

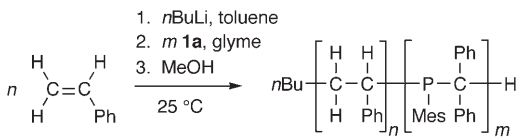

4

Scheme 2. Living anionic copolymerization of styrene and **1a**.

changed to deep red, thus suggesting rapid initiation of **1a** by the living polystyrene. After 24 hours, the ^{31}P NMR spectrum of the reaction mixture showed that **1a** had been entirely converted to polymer. The living copolymer was quenched with MeOH, and hexanes was subsequently added to precipitate block copolymer **4** (60 % yield). The molecular weight of polystyrene-*block*-poly(methylenephosphine) **4**, as determined using GPC ($M_n = 20900\ g\,mol^{-1}$, $M_w/M_n = 1.03$), correlates reasonably well with the predicted molecular weight ($M_n(\text{calcd}) = 19300\ g\,mol^{-1}$). Similar results were obtained in a second experiment to prepare block copolymer **4** ($n = 100$, $m = 50$, $M_n(\text{calcd}) = 26300\ g\,mol^{-1}$; GPC: $M_n = 29600\ g\,mol^{-1}$; $M_w/M_n = 1.06$). Importantly, the block copolymers from both experiments show monomodal GPC traces, and their $^{13}C\{^1H\}$ and ^{1}H NMR spectra are consistent with the assigned structures.

In conclusion, living anionic polymerization techniques, common for C=C bonds, have been extended to P=C bonds. This chemistry further illustrates the remarkable parallel between P=C and C=C bonds. Interestingly, we have utilized this new methodology to prepare unprecedented polystyrene-*block*-poly(methylenephosphine) copolymers with narrow polydispersities and controlled molecular weights. These synthetic breakthroughs pave the way to phosphorus-containing macromolecules with novel chemical functionalities and properties.

Received: July 23, 2006
Published online: September 29, 2006

Keywords: block copolymers · inorganic polymers · living polymerization · phosphaalkenes · phosphorus

[1] G. Odian, *Principles of Polymerization*, Wiley, New York, **1991**.
[2] O. W. Webster, *Science* **1991**, *251*, 887.
[3] a) J. E. Mark, H. R. Allcock, R. West, *Inorganic Polymers*, 2nd ed., Oxford University Press, Oxford, **2005**; b) V. Chandrasekhar, *Inorganic and Organometallic Polymers*, Springer, Berlin, **2005**; c) I. Manners, *Angew. Chem.* **1996**, *108*, 1712; *Angew. Chem. Int. Ed. Engl.* **1996**, *35*, 1602.
[4] Selected recent developments in phosphorus polymer chemistry: M. Raab, G. Schick, R. Fondermann, M. Dolg, W. Henze, U. Weynand, R. M. Gschwind, K. Fischer, M. Schmidt, E. Niecke, *Angew. Chem.* **2006**, *118*, 3154; *Angew. Chem. Int. Ed.* **2006**, *45*, 3083; L. A. Vanderark, T. J. Clark, E. Rivard, I. Manners, J. C. Slootweg, K. Lammertsma, *Chem. Commun.* **2006**, 3332; T. Baumgartner, W. Bergmans, T. Karpati, T. Neumann, M. Nieger, L. Nyulaszi, *Chem. Eur. J.* **2005**, *11*, 4687; T. J. Clark, J. M. Rodezno, S. B. Clendenning, S. Aouba, P. M. Brodersen, A. J. Lough, H. E. Ruda, I. Manners, *Chem. Eur. J.* **2005**, *11*, 4526; Z. Jin, B. L. Lucht, *J. Am. Chem. Soc.* **2005**, *127*, 5586; S. Kawasaki,

 © 2006 Wiley-VCH Verlag GmbH & Co. KGaA, Weinheim

J. Ujita, K. Toyota, M. Yoshifuji, *Chem. Lett.* **2005**, *34*, 724; R. C. Smith, J. D. Protasiewicz, *J. Am. Chem. Soc.* **2004**, *126*, 2268; Y. Morisaki, Y. Aiki, Y. Chujo, *Macromolecules* **2003**, *36*, 2594; C. Marmillon, F. Gauffre, T. Gulik-Krzywicki, C. Loup, A.-M. Caminade, J.-P. Majoral, J.-P. Vors, E. Rump, *Angew. Chem.* **2001**, *113*, 2696; *Angew. Chem. Int. Ed.* **2001**, *40*, 2626; C. Hay, C. Fischmeister, M. Hissler, L. Toupet, R. Réau, *Angew. Chem.* **2000**, *112*, 1882; *Angew. Chem. Int. Ed.* **2000**, *39*, 1812.

[5] Inorganic systems that polymerize in a living fashion are relatively rare. Examples include ring-opening polymerization (ROP) methods (for polysiloxanes, polyferrocenylsilanes, polyferrocenylphosphines, polysilanes, polycarbosilanes) and condensation methods (for polyphosphazenes). See, for example: R. Rulkens, Y. Ni, I. Manners, *J. Am. Chem. Soc.* **1994**, *116*, 12121; M. Tanabe, I. Manners, *J. Am. Chem. Soc.* **2004**, *126*, 11434; C. H. Honeyman, T. J. Peckham, J. A. Massey, I. Manners, *Chem. Commun.* **1996**, *22*, 2589; T. Sanji, K. Kawabata, H. Sakurai, *J. Organomet. Chem.* **2000**, *611*, 32; K. Matsumoto, H. Yamaoka, *Macromolecules* **1995**, *28*, 7029; H. R. Allcock, C. A. Crane, C. T. Morrissey, J. M. Nelson, S. D. Reeves, C. H. Honeyman, I. Manners, *Macromolecules* **1996**, *29*, 7740.

[6] Inorganic–organic block copolymers that are prepared using living techniques possess exciting properties such as supramolecular self-assembly. For representative examples, see: X. S. Wang, M. A. Winnik, I. Manners, *Angew. Chem.* **2004**, *116*, 3789; *Angew. Chem. Int. Ed.* **2004**, *43*, 3703; J. F. Gohy, B. G. G. Lohmeijer, A. Alexeev, X. S. Wang, I. Manners, M. A. Winnik, U. S. Schubert, *Chem. Eur. J.* **2004**, *10*, 4315; H. R. Allcock, E. S. Powell, Y. Chang, C. Kim, *Macromolecules* **2004**, *37*, 7163; T. Sanji, K. Takase, H. Sakurai, *J. Am. Chem. Soc.* **2001**, *123*, 12690.

[7] M. Szwarc, *Nature* **1956**, *178*, 1168.

[8] a) K. B. Dillon, F. Mathey, J. F. Nixon, *Phosphorus: The Carbon Copy*, Wiley, New York, **1998**; b) F. Mathey, *Angew. Chem.* **2003**, *115*, 1616; *Angew. Chem. Int. Ed.* **2003**, *42*, 1578; c) P. Le Floch, *Coord. Chem. Rev.* **2006**, *250*, 627; d) L. Weber, *Angew. Chem.* **2002**, *114*, 583; *Angew. Chem. Int. Ed.* **2002**, *41*, 563; e) M. Yoshifuji, *J. Chem. Soc. Dalton Trans.* **1998**, 3343; f) L. Weber, *Angew. Chem.* **1996**, *108*, 292; *Angew. Chem. Int. Ed. Engl.* **1996**, *35*, 271; g) F. Mathey, *Acc. Chem. Res.* **1992**, *25*, 90; h) R. Appel, in *Multiple Bonds and Low Coordination in Phosphorus Chemistry* (Eds.: M. Regitz, O. J. Scherer), Thieme, Stuttgart, **1990**, p. 157; i) R. Appel, F. Knoll, *Adv. Inorg. Chem.* **1989**, *33*, 259; j) J. F. Nixon, *Chem. Rev.* **1988**, *88*, 1327.

[9] D. P. Gates, *Top. Curr. Chem.* **2005**, *250*, 107.

[10] C.-W. Tsang, M. Yam, D. P. Gates, *J. Am. Chem. Soc.* **2003**, *125*, 1480.

[11] C.-W. Tsang, B. Baharloo, D. Riendl, M. Yam, D. P. Gates, *Angew. Chem.* **2004**, *116*, 5800; *Angew. Chem. Int. Ed.* **2004**, *43*, 5682.

[12] T. A. van der Knaap, F. Bickelhaupt, *Tetrahedron Lett.* **1982**, *23*, 2037.

[13] B. H. Gillon, D. P. Gates, *Chem. Commun.* **2004**, 1868.

[14] G. Becker, W. Uhl, H.-J. Wessely, *Z. Anorg. Allg. Chem.* **1981**, *479*, 41.

[15] M. Yam, J. H. Chong, C.-W. Tsang, B. O. Patrick, A. E. Lam, D. P. Gates, *Inorg. Chem.* **2006**, *45*, 5225.

[16] Glyme (1,2-dimethoxyethane) was chosen as the solvent for the anionic polymerization of **1** in an effort to increase the rate of propagation. For example, it is known that styrene polymerizes at a much higher rate in glyme than in THF; see: G. Odian, *Principles of Polymerization*, Wiley, New York, **1991** p. 412.

[17] Homopolymerizations of styrene using *n*BuLi were performed in several different solvents, including glyme, THF, and toluene. We obtained the most consistent results for toluene because of the slower rate of propagation in this solvent. P=C monomer **1a** was added in glyme since polymerization of **1a** is extremely slow in toluene.

 © 2006 Wiley-VCH Verlag GmbH & Co. KGaA, Weinheim

Polycarbonate Synthesis

DOI: 10.1002/anie.200603132

Selective Formation of Polycarbonate over Cyclic Carbonate: Copolymerization of Epoxides with Carbon Dioxide Catalyzed by a Cobalt(III) Complex with a Piperidinium End-Capping Arm**

*Koji Nakano, Toshihiro Kamada, and Kyoko Nozaki**

The copolymerization of epoxides with CO_2[1] has been intensively studied in the last decade as one of the most promising processes for CO_2 utilization.[2–11] The concomitant production of cyclic carbonate is an incidental problem in the reaction of terminal epoxides such as propylene oxide (PO). Recently, the [Co(salcy)OAc] complex (salcyH_2 = *trans*-*N*,*N*′-bis(3,5-di-*tert*-butylsalicylidene)-1,2-cyclohexanediamine) was reported to copolymerize PO with CO_2 without the production of cyclic propylene carbonate (PC) in up to approximately 75% conversion with a turnover frequency (TOF) of 51 [in moles of repeating unit per mol Co per hour ($mol_{ru}\,mol_{Co}^{-1}\,h^{-1}$)].[12] Further enhancement of the catalytic activity was achieved with anionic cobaltate complexes such as $[Co(salcy)Cl(OBzF_5)]^-[PPN]^+$ (BzF_5 = $C(=O)C_6F_5$, $[PPN]^+$ = bis(triphenylphosphoranylidene)ammonium), which release the reactive anionic propagating species more readily than neutral cobalt complexes.[13–15] However, such a high reactivity also leads to the formation of PC at a higher degree of conversion (> 50%): the polymerization mixture solidifies to retard the intermolecular propagation, thus resulting in relative acceleration of intramolecular degradation, so-called back-biting.[16] Thus, high catalytic activity has been incompatible with the suppression of the formation of cyclic carbonate. Herein, we report the copolymerization of terminal epoxides with CO_2 by using a new cobalt complex that can selectively produce the copolymer, even at high monomer conversion.

To achieve a high epoxide conversion without production of cyclic carbonate, we designed cobaltate complex **1** with two acetate ligands and a salcy-type ligand (Scheme 1). The key of the catalyst design is in the piperidinyl and piperidinium arms.

[*] Dr. K. Nakano, T. Kamada, Prof. Dr. K. Nozaki
Department of Chemistry and Biotechnology
Graduate School of Engineering
The University of Tokyo
7-3-1 Hongo, Bunkyo-ku, Tokyo 113-8656 (Japan)
Fax: (+81) 3-5841-7263
E-mail: nozaki@chembio.t.u-tokyo.ac.jp

[**] This study was supported by a Grant-in-Aid for Scientific Research on Priority Areas "Advanced Molecular Transformations of Carbon Resources" from the Ministry of Education, Culture, Sports, Science and Technology, Japan. We are grateful to Prof. Yoshiaki Nishibayashi and Dr. Yoshihiro Miyake (The University of Tokyo) for high-resolution (HR) mass-spectrometric measurements.

Supporting information for this article is available on the WWW under http://www.angewandte.org or from the author.

WILEY InterScience DISCOVER SOMETHING GREAT
© 2006 Wiley-VCH Verlag GmbH & Co. KGaA, Weinheim

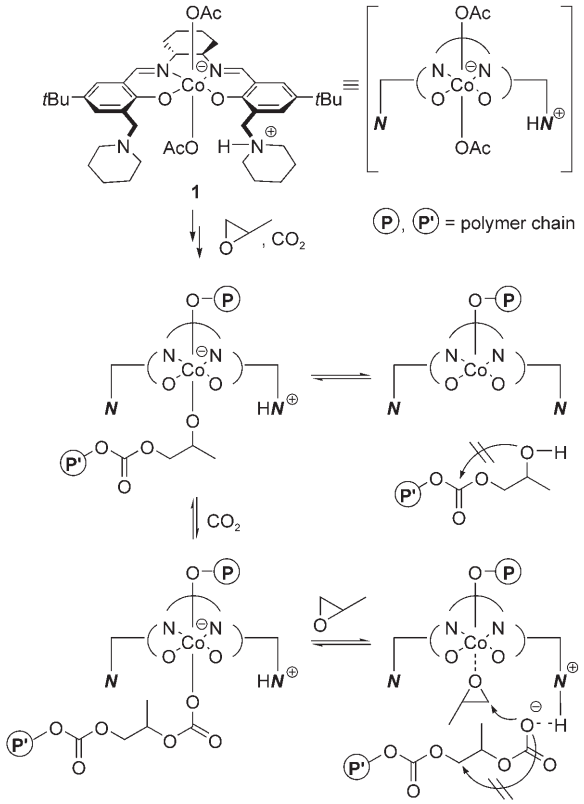

Scheme 1. Catalyst design to suppress the production of cyclic carbonate.

When the two acetate ligands initiate the copolymerization, a piperidinium arm should control the nucleophilicity of the propagating species by protonating the anionic propagating species that is released from the cobaltate center. The protonated propagating species is not nucleophilic enough to form cyclic carbonate through back-biting, but it can react with carbon dioxide[16b,c] or activated epoxide[16a] once it is deprotonated by one of the two piperidinyl groups.

Complex **1** was synthesized by the reaction of $Co(OAc)_2$ with the corresponding disalicylidenediamine[17] and subsequent oxidation in the presence of an excess amount of AcOH and air, and the product was sufficiently dried under reduced pressure. The formation of **1** was spectroscopically confirmed as follows.[18] The ^1H NMR spectrum of **1** and the ^1H and ^2H NMR spectra of partially deuterated **1**, which was obtained by using an excess mount of CD_3COOD, clearly show that complex **1** contains two acetate ligands. Accordingly, one of the two piperidinyl groups should be protonated. Moreover, the simple pattern of the ^1H NMR spectrum of **1** reflects the symmetrical structure of **1** in solution, thus indicating that a proton is exchanged rapidly between the two piperidinyl groups. Thus, the two piperidinyl groups should contribute equally to the copolymerization.

By using complex **1**, high catalytic activity and high epoxide conversion were accomplished. The copolymerization of PO with CO_2 (1.4 MPa), catalyzed by complex **1** (PO/**1** = 2000), gave the completely alternating copolymer, poly(propylene carbonate) (PPC) in 38% yield (TOF(PPC) = 254 $mol_{ru}\,mol_{Co}^{-1}\,h^{-1}$, $M_n = 12\,600\ g\,mol^{-1}$, $M_w/M_n = 1.13$) without a significant production of PC (PPC/PC = 99:1; Table 1, entry 1).[19] Interestingly, high conversion of epoxide did not result in the formation of PC. The copolymer with a higher M_n value ($23\,900\ g\,mol^{-1}$) and narrow polydispersity

Table 1: Copolymerization of epoxides with CO_2 catalyzed by cobalt complex **1**.[a]

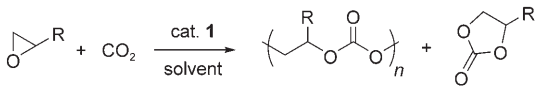

Entry	R	Solvent	t [h]	Yield of **2**+**3** [%][b]	**2**/**3**[b]	M_n [g mol^{-1}][c]	M_w/M_n[c]
1	Me	–	3	38	99:1	12 600	1.13
2	Me	–	12	77	99:1	23 900	1.14
3	Me	–	116	79	96:4	83 700	1.28
4	Me	–	1	34	90:10	7100	1.22
5	Me	DME	6	53	99:1	13 200	1.10
6	Me	DME	48	>99	97:3	26 500	1.10
7[d]	Me	DME	20	95	95:5	5100	1.06
8	Et	DME	48	89	97:3	31 000	1.12
9	Bu	DME	48	89	98:2	34 300	1.14

[a] Reaction conditions: epoxide (14.3 mmol in entries 1, 2, and 4–9; 47.2 mmol in entry 3), **1** (epoxide/**1** = 2000 in entries 1, 2, and 4; 6500 in entry 3; 1000 in entries 5–9), CO_2 (initial pressure: 1.4 MPa), DME (1.0 mL in entries 5–9), at 25 °C (entries 1–3 and 5–9) or 60 °C (entry 4). [b] Determined on the basis of ^1H NMR spectroscopy of the crude product by using phenanthrene as an internal standard. [c] Determined by size-exclusion chromatography analysis using a polystyrene standard. [d] Methanol (20 equivalents based on **1**) was added.

index (PDI) of 1.14 was selectively produced in 76% yield (TOF(PPC) = 127 $mol_{ru}\,mol_{Co}^{-1}\,h^{-1}$; Table 1, entry 2). Copolymerization at a higher PO/**1** ratio of 6500 also gave the alternating copolymer with a much higher M_n value ($83\,700\ g\,mol^{-1}$) with high selectivity (PPC/PC = 96:4; Table 1, entry 3). The efficient suppression of the back-biting process allowed high-temperature copolymerization (60 °C), thereby giving PPC selectively with higher activity (PPC/PC = 90:10, TOF(PPC) = 602 $mol_{ru}\,mol_{Co}^{-1}\,h^{-1}$; Table 1, entry 4). It is essential that the piperidinium group is tethered to the salcy-type ligand framework. In fact, the copolymerization of PO with CO_2 by using the reported $[Co(salcy)Cl(OBzF_5)]^-$-$[PPN]^+$ system[14] in the presence of *N*-methylpiperidinium acetate resulted in low selectivity for the copolymer (PO/Co = 6000, 34% yield of PPC, 37% yield of PC, PPC/PC = 42:58).[20] Thus, the highest level of activity together with suppression of PC formation and high conversion of PPC have been accomplished using complex **1**.[21]

The complete consumption of epoxide was attained by adding solvents. Since the polymerization mixture becomes viscous with increase of conversion, the addition of solvent is necessary for effective diffusion of the reactant. Copolymerizations of PO with CO_2 (PO/**1** = 1000) in the presence of an organic solvent such as 1,2-dimethoxyethane (DME), toluene, or dichloromethane gave the copolymer. Particularly, employment of DME resulted in the quantitative conversion with high copolymer selectivity (PPC/PC = 97:3, >99% conversion; Table 1, entries 5 and 6). Very recently, a similar

 © 2006 Wiley-VCH Verlag GmbH & Co. KGaA, Weinheim

solvent effect was reported for the copolymerization with $[Co(salcy)Cl(OBzF_5)]^-[PPN]^+$, where the use of DME as a solvent achieved the high PPC yield of 75% without a contaminating amount of PC (PPC/PC = 98:2).[22] Under the same reaction conditions, terminal epoxides with a longer alkyl chain were also copolymerized with CO_2 by using complex **1** (Table 1, entries 8 and 9). Although the longer alkyl substituents slightly decreased the catalytic activities,[13] completely alternating copolymers were obtained in high yields without formation of a significant amount of cyclic carbonate.

The successful complete consumption of an epoxide without production of cyclic carbonate allowed the synthesis of block polymer. Thus, the block terpolymer was produced by stepwise addition of the two different epoxides, PO and 1-hexene oxide, without significant production of cyclic carbonates (Scheme 2). Such a selective synthesis of a block terpolymer is characteristic of the present catalyst system. Since the previously reported catalysts hardly achieve the complete consumption of an epoxide, the polymerization for a block terpolymer should result in the production of a tapered one.

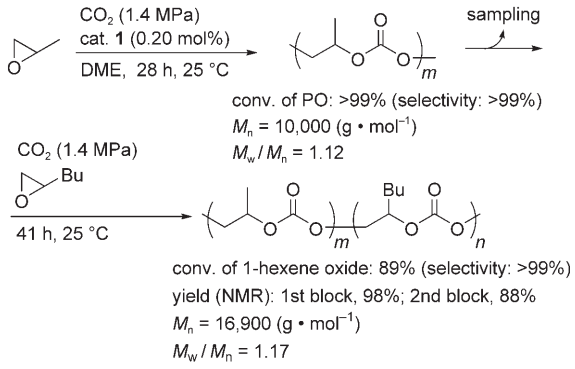

Scheme 2. Synthesis of a block terpolymer.

Immortal polymerization is indicated in the present PO/CO_2 copolymerization system.[23] In all experiments, gel permeation chromatography (GPC) analyses of the obtained copolymers gave bimodal traces. The M_n values of both higher- and lower-molecular-weight copolymers increased linearly in proportion to conversion in the range of 0–99%, and the PDIs remained narrow (1.10–1.11). Moreover, for each conversion, the M_n value of the higher-molecular-weight copolymer was twice as large as that of the lower-molecular-weight one. This difference can be attributed to the chain transfer by contaminant water, which works as a bifunctional initiating group to give a telechelic polymer, as previously demonstrated by Sugimoto et al.[24] MALDI-TOF mass spectrometry of the copolymer revealed the formation of the telechelic copolymer in addition to the copolymer initiated by the acetate group. These results clearly demonstrate the reversible and rapid chain transfer of the propagating species, which is characteristic of successful "immortal" polymerization.[25] To confirm such an immortal nature of the present system, copolymerization of PO with CO_2 was carried out in the presence of methanol as a chain-transfer reagent (Table 1, entry 7). When a large excess of methanol (20 equivalents based on **1**) was added, an alternating copolymer with a methoxy initiating group was obtained as a main component. The M_n value of the obtained copolymer was estimated to be 5100 g mol^{-1}, which agrees with the theoretical M_n value of 4300 g mol^{-1} that was calculated from the copolymer yield and the monomer/(methanol+acetate) ratio. Furthermore, the PDI remained narrow (1.06).

In conclusion, the cobaltate complex with a piperidinium arm was found to copolymerize terminal epoxides with CO_2 with high activity and without a significant amount of associated cyclic carbonate. In particular, complete consumption of the epoxide was accomplished with high copolymer selectivity. This feature is the key to the successful synthesis of the block terpolymer.

Experimental Section

Representative procedure for the copolymerization of propylene oxide with CO_2 (Table 1, entry 1). A 50-mL autoclave was charged with propylene oxide (1.0 mL, 14.3 mmol) and **1** (5.8 mg, 7.2×10^{-3} mmol) under argon. After CO_2 (1.4 MPa) was introduced, the reaction mixture was stirred at 25 °C for 3 h. The CO_2 pressure was released, and the polymerization mixture was quenched with methanol, diluted with CH_2Cl_2, and transferred into a round-bottom flask. Phenanthrene (34 mg, 0.19 mmol) was added as an internal standard to the resulting solution. A small aliquot of the mixture was taken out and concentrated under reduced pressure by rotary evaporation. Analyses by ^{1}H NMR spectroscopy and GPC gave the yields of copolymer (38%) and propylene carbonate (< 0.1%), the ratio of them (99:1), as well as the molecular weight (12600 g mol^{-1}) and molecular-weight distribution (1.13) of the copolymer.

Received: August 2, 2006
Published online: October 6, 2006

Keywords: carbon dioxide · cobalt · copolymerization · epoxides · homogeneous catalysis

[1] S. Inoue, H. Koinuma, T. Tsuruta, *J. Polym. Sci. Part B* **1969**, *7*, 287–292.
[2] For recent reviews, see: a) G. W. Coates, D. R. Moore, *Angew. Chem.* **2004**, *116*, 6784–6806; *Angew. Chem. Int. Ed.* **2004**, *43*, 6618–6639; b) H. Sugimoto, S. Inoue, *J. Polym. Sci. Part A* **2004**, *42*, 5561–5573; c) D. J. Darensbourg, R. M. Mackiewicz, A. L. Phelps, D. R. Billodeaux, *Acc. Chem. Res.* **2004**, *37*, 836–844; d) K. Nakano, N. Kosaka, T. Hiyama, K. Nozaki, *Dalton Trans.* **2003**, 4039–4050; e) M. S. Super, E. J. Beckman, *Trends Polym. Sci.* **1997**, *5*, 236–240.
[3] D. J. Darensbourg, R. M. Mackiewicz, *J. Am. Chem. Soc.* **2005**, *127*, 14026–14038.
[4] D. J. Darensbourg, A. L. Phelps, *Inorg. Chem.* **2005**, *44*, 4622–4629.
[5] M. H. Chisholm, Z. P. Zhou, *J. Am. Chem. Soc.* **2004**, *126*, 11030–11039.
[6] H. Sugimoto, H, Ohshima, S. Inoue, *J. Polym. Sci. Part A* **2003**, *41*, 3549–3555.
[7] R. Eberhardt, M. Allmendinger, B. Rieger, *Macromol. Rapid Commun.* **2003**, *24*, 194–196.
[8] S. D. Allen, D. R. Moore, E. B. Lobkovsky, G. W. Coates, *J. Am. Chem. Soc.* **2002**, *124*, 14284–14285.

 © 2006 Wiley-VCH Verlag GmbH & Co. KGaA, Weinheim

[9] D. R. Moore, M. Cheng, E. B. Lobkovsky, G. W. Coates, *Angew. Chem.* **2002**, *114*, 2711 – 2714; *Angew. Chem. Int. Ed.* **2002**, *41*, 2599 – 2602.
[10] S. Mang, A. I. Cooper, M. E. Colclough, N. Chauhan, A. B. Holmes, *Macromolecules* **2000**, *33*, 303 – 308.
[11] T. Sarbu, T. Styranec, E. J. Beckman, *Nature* **2000**, *405*, 165 – 168.
[12] Z. Q. Qin, C. M. Thomas, S. Lee, G. W. Coates, *Angew. Chem.* **2003**, *115*, 5642 – 5645; *Angew. Chem. Int. Ed.* **2003**, *42*, 5484 – 5487.
[13] X. B. Lu, L. Shi, Y. M. Wang, R. Zhang, Y. J. Zhang, X. J. Peng, Z. C. Zhang, B. Li, *J. Am. Chem. Soc.* **2006**, *128*, 1664 – 1674.
[14] C. T. Cohen, T. Chu, G. W. Coates, *J. Am. Chem. Soc.* **2005**, *127*, 10869 – 10878.
[15] X. B. Lu, Y. Wang, *Angew. Chem.* **2004**, *116*, 3658 – 3661; *Angew. Chem. Int. Ed.* **2004**, *43*, 3574 – 3577.
[16] a) G. A. Luinstra, G. R. Haas, F. Molnar, V. Bernhart, R. Eberhardt, B. Rieger, *Chem. Eur. J.* **2005**, *11*, 6298 – 6314; b) W. Kuran, T. Listos, *Macromol. Chem. Phys.* **1994**, *195*, 1011 – 1015; c) P. Gorecki, W. Kuran, *J. Polym. Sci. Polym. Lett.* **1985**, *23*, 299 – 304.
[17] a) M. W. Fennie, E. F. DiMauro, E. M. O'Brien, V. Annamalai, M. C. Kozlowski, *Tetrahedron* **2005**, *61*, 6249 – 6265; b) E. F. DiMauro, M. C. Kozlowski, *J. Am. Chem. Soc.* **2002**, *124*, 12668 – 12669; c) E. F. DiMauro, M. C. Kozlowski, *Org. Lett.* **2001**, *3*, 3053 – 3056.
[18] See the Supporting Information.
[19] The M_n value is not close to the estimated value. This difference could be a result of the chain transfer by concomitant water.
[20] The copolymerization using $[Co(salcy)Cl(OBzF_5)]^-[PPN]^+$ in the absence of *N*-methylpiperidinium acetate (PO/Co = 6000, 1.4 MPa of CO_2, 3 h) was also carried out, and resulted in a high catalytic activity (yield of **2** + **3** = 25 %, TOF(PPC) = 492 $mol_{ru}\,mol_{Co}^{-1}\,h^{-1}$, M_n = 36000 $g\,mol^{-1}$, M_w/M_n = 1.12) and high selectivity (PPC/PC = 99:1) as reported in reference [14]. The prolonged copolymerization (68 h), however, led to the partial degradation to PC (yield of **2** + **3** = 84 %, PPC/PC = 72:28) and a broader molecular-weight distribution (M_w/M_n = 1.71).
[21] High catalytic activity (500–1000 $mol_{ru}\,mol_{Co}^{-1}\,h^{-1}$) was reported by using cobaltate complexes.[13,14] However, such a system was found to produce PC in greater than 50 % conversion. Other systems using chromium complexes or zinc complexes also show high activity of 100–200 $mol_{ru}\,mol_{Co}^{-1}\,h^{-1}$ and are classified into a highly active catalyst system, although a contaminant amount of PC is produced even at low conversion.[4,8] As mentioned above, the use of a [Co(salcy)OAc] complex has been the successful example which achieves both the high catalytic activity (51 $mol_{ru}\,mol_{Co}^{-1}\,h^{-1}$) and suppression of PC formation even at high monomer conversion.[12]
[22] Although the employment of DME improved the yield of PPC, the prolonged reaction did not result in a yield higher than 75 %; see: C. T. Cohen, G. W. Coates, *J. Polym. Sci. Part A* **2006**, *44*, 5182 – 5191.
[23] Immortal polymerization is a living polymerization that involves rapid, reversible chain transfer; that is, the chain transfer does not lead to simple chain termination, and the dormant chain end can repropagate when activated on a catalyst center. Because the chain-transfer reaction proceeds much faster than the propagation reaction, polymers are obtained with low PDI values. See reference [25].
[24] H. Sugimoto, H. Ohtsuka, S. Inoue, *J. Polym. Sci. Part A* **2005**, *43*, 4172 – 4186.
[25] S. Inoue, *J. Polym. Sci. Part A* **2000**, *38*, 2861 – 2871.

 © 2006 Wiley-VCH Verlag GmbH & Co. KGaA, Weinheim

Surface Chemistry

DOI: 10.1002/anie.200602393

Efficient Preparation and Catalytic Activity of MgO(111) Nanosheets**

*Kake Zhu, Juncheng Hu, Christian Kübel, and Ryan Richards**

MgO has a typical rocksalt structure and possesses a high melting point and high ionic character. Although the stoichiometry and crystallinity are nearly constant, the morphology can vary in terms of shape, particle size, and surface structure. The MgO(100) facet is unambiguously the most stable because of its low surface energy, and it is therefore normally a product after cleavage, and it is the sole surface generated by current wet chemical methods. Numerous studies have demonstrated that the shape and size of crystalline MgO is highly influential on the adsorption properties and the configuration of the surface species formed during chemical adsorption. For example, SO_2 is found to bind in a monodentate fashion at the edge/corner sites of the aerogel nanocrystal but prefers bidentate adsorption on flat (microcrystalline) surfaces.[1,2] This selectivity is also found for acetylene in theoretical ab initio calculations and solid-state NMR experimental studies in which no stable dissociation products on the flat (100)-like surface could be obtained theoretically or experimentally.[3] Furthermore, nanostructured MgO has been reported to be extremely effective for the destructive adsorption of numerous environmental toxins and several chemical warfare agents (VX, sarin, mustard gas).[4–6] However, the (111) surface consists of alternating polar monolayers of oxygen anions and magnesium cations and thus, a strong electrostatic field perpendicular to the (111) surface is created.[7] Such a surface has provided a prototype for the study of surface structure and surface reactions, and has attracted a great geal of attention from both experimental and theoretical studies.[8,9] These studies indicate the importance of size and shape control in MgO synthesis for its applications: it is not only the surface

[*] Dr. K. Zhu,[+] Dr. J. Hu, Prof. Dr. R. Richards
International University Bremen
28759 Bremen (Germany)
Fax: (+49) 421-200-3229
E-mail: r.richards@iu-bremen.de
Dr. C. Kübel
Fraunhofer Institut für Fertigungstechnik und angewandte Materialforschung (IFAM)
Wiener Strasse 12, 28359 Bremen (Germany)
[+] Current address:
Center for Sustainable and Green Chemistry
Technical University of Denmark
2800 Lyngby (Denmark)

[**] We would like to thank the International University Bremen for financial support. K.Z. and J.H. contributed equally to this work.

Supporting information for this article is available on the WWW under http://www.angewandte.org or from the author.

© 2006 Wiley-VCH Verlag GmbH & Co. KGaA, Weinheim

area that matters, but also the surface chemistry. Herein we report for the first time an efficient wet chemical method to synthesize MgO nanosheets that possess the (111) lattice plane as the main surface.

The MgO(111) nanosheets reported herein are likely to serve as catalysts, catalyst supports, or adsorbents with high activity and selectivity because of their unique surface chemistry. Theoretical studies on MgO(111) have suggested that the polar oxide surface may be of interest for splitting water and/or hydrogen storage.[10] When MgO(111) nanosheets were employed for the Claisen–Schmidt condensation of benzaldehyde and acetophenone, they were found to exhibit activity superior to other systems, such as $AlCl_3$, BF_3, $POCl_3$, alumina, and recently reported nanocrystalline MgO samples.[11]

The traditional method for preparing MgO is the thermal decomposition of either magnesium salts or magnesium hydroxides, which results in an inhomogeneous morphology and crystallite size as well as a low surface area. Many attempts were therefore made to tailor the texture and morphology of MgO. One of the most fruitful methods has been an adapted aerogel preparation by high-temperature supercritical drying of a toluene/methanol solvent system to yield approximately 4-nm cubic MgO polyhedron crystallites with {100} surfaces that were rich in edge and corner sites and with a surface area of 300–500 $m^2 g^{-1}$.[12–14] Furthermore, mesoporous carbon aerogels and hexagonal arrays of mesoporous carbon have been employed as hard templates for the formation of MgO during thermal decomposition of magnesium nitrate. These templates have resulted in ordered mesoporous MgO that mimic the structure of the templates and have a surface area of 150 and 306 $m^2 g^{-1}$, respectively.[15,16] Recently, a chemical vapor deposition (CVD) method was developed which produces MgO cubes with controllable particle size; however, the surface of these cubes all possess {100} surfaces and demonstrates size-dependent optical properties.[17] Preparations and studies of MgO(111) have thus far been limited to deposition on substrates such as Si(100), Ag(111), and GaAs(001),[18–20] or alternatively by mechanical polishing followed by acid etching, ion bombardment, and electron beam annealing (1000 °C) in an ultrahigh vacuum (UHV), high-temperature annealing (800 °C) in air, and also after oxygen plasma cleaning and annealing in a UHV as well as various other etching and reconstruction processes.[21–23] These studies show the diversity and complexity of MgO in terms of its shape and particle size; however, as far as surface orientation is concerned, to the best of our knowledge, neither selectivity nor controlled growth of MgO(111) has been reported for substrate-free systems.

Benzyl alcohol has been found to be a successful medium for tailoring selected metal oxides with well-controlled shapes, sizes, and crystallinity under anhydrous conditions. For example, anatase TiO_2 nanoparticles in the 4–8-nm size range,[24] vanadium oxide nanorods, and tungsten oxide nanoplatelets and nanowires with uniform morphology[25,26] were synthesized in such a medium from metal chloride precursors. We present here a simple method for preparing a sheetlike MgO with a thickness of less than 10 nm and, more interestingly, which exhibits the highly ionic (111) facet as the major surface of the "nanosheet". In our system, a mixture of water and methanol was added slowly to hydrolyze the magnesium methoxide/benzyl alcohol solution to produce the nanosheets. Theoretical studies suggest that water plays an important role: as chemisorption of water forms a hydroxy surface which stabilizes the otherwise unstable (111) surface of MgO,[27] similar interactions can occur in our system.

To synthesize these MgO(111) nanosheets, a stoichiometric amount of 4-nitro- or 4-methoxybenzyl alcohol was added to 10 wt% $Mg(OCH_3)_2$ in methanol. This was followed by the addition of a water/methanol mixture to the system and subsequent supercritical treatment and calcination in air. 4-Nitro- and 4-methoxybenzyl alcohol were chosen for their strong interaction with the inorganic intermediate $Mg(OH)(OCH_3)$, in which the hydroxy groups can interact strongly with benzyl alcohol molecules (as the latter are stronger acids than methanol), therefore, facilitating the spontaneous substitution on the interface during mixing and supercritical treatment.

The MgO nanosheets have been shown to possess the (111) plane as the main surface through a combination of bright-field transmission electron microscopy (BF-TEM), high-resolution transmission electron microscopy (HRTEM), and electron diffraction studies. BF-TEM analysis of the $Mg(OH)(OCH_3)$ precursor and the calcined MgO samples reveal that the material crystallizes with the formation of nanosheets with a typical diameter of 50–200 nm and a typical thickness of 3–5 nm (see the Supporting Information and Figure 1). The majority of the sheetlike nanoparticles are oriented almost parallel to the support film. However, some of the sheets are imaged edge on, for example, in the marked area in Figure 1.

Local energy-dispersive X-ray microanalysis (EDX) measurements on thin aggregates of the calcined MgO nanosheets on the carbon support film show that only Mg and O are present in the sample. Quantification of the Mg and O intensities reveals an Mg:O composition close to 1:2 for the sample before calcination, which is in agreement with the

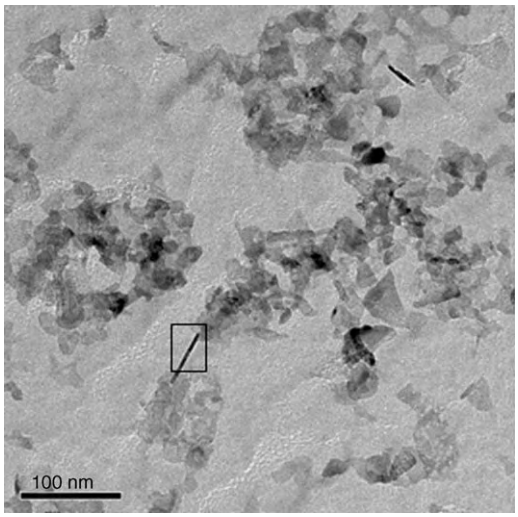

Figure 1. BF-TEM images showing larger aggregates and scattered small aggregates of MgO(111) from 4-methoxybenzyl alcohol.

 © 2006 Wiley-VCH Verlag GmbH & Co. KGaA, Weinheim

formulation $Mg(OH)_2$ or $Mg(OH)(OCH_3)$. An Mg:O composition close to 1:1 has been measured for the nanosheets after calcination, which is in agreement with the formulation MgO (see the Supporting Information).

Electron diffraction studies on thin MgO aggregates proves that the MgO nanosheets crystallize in the well-known periclase structure. The observed lattice spacings are in excellent agreement with the literature *d*-spacings for periclase[28] (see the Supporting Information).

HRTEM analysis of isolated MgO nanosheets shows that their main surface is parallel to the (111) lattice planes. The MgO(111) facet is composed exclusively of oxygen in one layer and exclusively magnesium atoms in the other (Figure 2), thus, the surface of MgO(111) has a strong

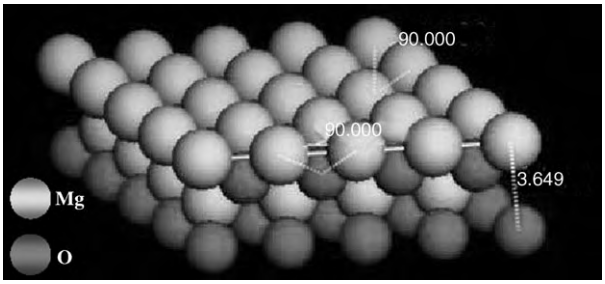

Figure 2. Illustration of the (111) facet of MgO (note the alternating layers of Mg^{2+} and O^{2-} ions).

electropolarity, either positive or negative. The HRTEM images of nanosheets viewed edge-on exhibit lattice fringes with a distance of 0.24–0.25 nm parallel to the main surface of the nanosheet, which is in good agreement with the {111} lattice spacings in MgO (Figure 3). The HRTEM images of isolated nanosheets oriented parallel to the support film typically exhibit the characteristic lattice fringes of the 111 zone, thus indicating that the sheets lie on the (111) plane, which is oriented perpendicular to the 111 zone (see the Supporting Information).

Since the addition of toluene was found to make a dramatic difference to the aerogels,[5,6] we also investigated the effect of adding toluene to our systems. TEM analysis of $Mg(OH)(OCH_3)$ nanosheets prepared with toluene added to the mixture shows similar features to those prepared without toluene. However, the nanosheets are typically larger, with a thickness of up to 25 nm and a diameter of up to 500 nm (see the Supporting Information). These larger sheets do not form uniform MgO sheets on calcination, but instead form highly porous sheets of MgO (Figure 4). Nevertheless, these porous sheets exhibit the same preference for the (111) lattice plane that forms the surface of the nanosheets (see the Supporting Information). Even though the 220, 422, and 440 reflections observed (see the Supporting Information) correspond to an almost single-crystalline domain, in most cases the crystals exhibit a rotational disorder around the [111] zone axis. Furthermore, part of the MgO is typically hydrolyzed to give rise to the weak set of {220} and {420} diffraction spots of $Mg(OH)_2$, which presumably arise from hydrolysis of the MgO nanosheets during preparation of the TEM sample. Our

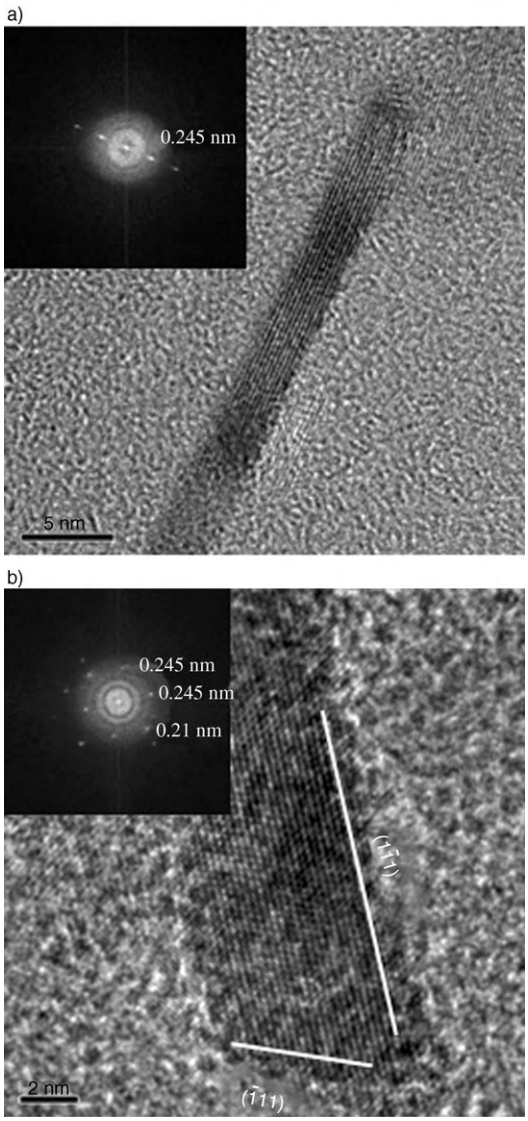

Figure 3. HRTEM images and local Fourier transforms of two isolated MgO nanosheets obtained with 4-methoxybenzyl alcohol (Figure 3 a corresponds to the marked area in Figure 1).

comparitive studies indicate that a water-free mixture does not produce MgO(111) nanosheets (see the Supporting Information).

TEM provides compelling evidence for the existence of MgO nanosheets. It seems water plays an important role in the formation of such nanosheets because a C–C bond-formation mechanism can prevail in the water-free system[29,30] instead of an acid–base interaction between the solid powder and the benzyl alcohol. Although we are still not sure of the surface species formed during the formation of $Mg(OH)(OCH_3)$, comparison of our work and that of literature studies[12–14] strongly suggest that an acid–base interaction between $Mg(OH)(OCH_3)$ and benzyl alcohol is essential for the formation of MgO nanosheets, which implies that we can tailor the preferential growth of metal oxides by careful choice of the media. As many defined oxide surfaces are a result of acid or base etching, we may use either a mild

 © 2006 Wiley-VCH Verlag GmbH & Co. KGaA, Weinheim

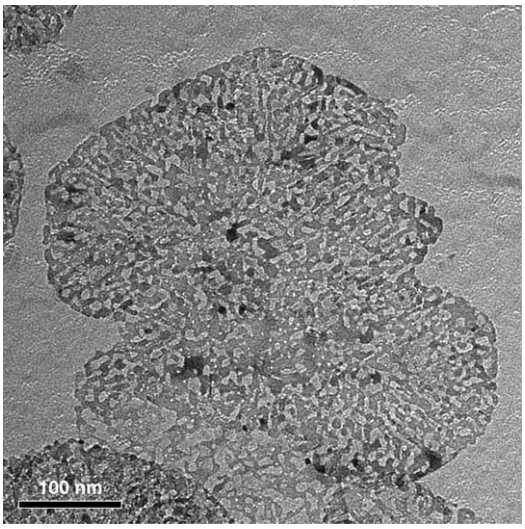

Figure 4. BF-TEM image of highly porous MgO nanosheets obtained by calcination of $Mg(OH)(OCH_3)$ nanosheets prepared in the presence of toluene and 4-methoxybenzyl alcohol.

acid or base in the precursor solution and heat the system to the supercritical phase to strengthen the acidity/basicity so that we can control the growth of a preferential surface.

It has been established for the base-catalyzed Claisen–Schmidt condensation reaction that the shape and the presence of exposed crystal facets are crucial parameters for the utilization of magnesium oxide as a solid base catalyst.[11] Polar anionic surfaces are of particular interest for the reaction, and therefore we have evaluated the catalytic activity of the MgO(111) nanosheets. Catalytic activities were determined for the Claisen–Schmidt condensation of benzaldehyde with acetophenone at 110 °C over magnesium oxide samples with different crystallites (Figure 5). CM-MgO samples are generally large cubic crystals, the NA-MgO samples are thin hexagonal platelets about 150 nm in diameter and 10 nm thick with large exposed areas of the (100) crystal facet, while the NAP-MgO samples are very small, irregular stacks of square plates with numerous crystal faces, edges, and corners. As shown in Figure 5, NAP-MgO displays higher activity in the reaction than NA-MgO and CM-MgO. This result has been attributed to the NAP-MgO possesing a single-crystallite polyhedral structure[11] which has high surface concentrations of edges and corners and various exposed crystal planes (such as (001) and (111)), hence leading to inherently high surface reactivity per unit area. It is notable that the MgO(111) nanosheets prepared from the present method display a much higher catalytic activity for the Claisen–Schmidt condensation of benzaldehyde with acetophenone than the best of the reported NAP-MgO catalysts.[11] Previous studies[11] indicate that the Claisen–Schmidt condensation is largely driven by Lewis basic O^{2-} sites, with the Bronsted basic -OH surface groups being less important in the reaction. The pronounced activity of benzaldehyde with acetophenone in the Claisen–Schmidt condensation taken together with temperature-programmed desorption studies of CO_2 (see the Supporting Information) demonstrates clearly that the MgO(111) nanosheets are Lewis basic and the MgO(111) face, which has O^{2-} ions on the surface, is particularly important for the reaction. Structure analysis based on the simulation of transmission electron micrographs has led to a proposal that structures involving oxygen trimers exist on the surface of MgO(111), thus providing a possible explanation for the excellent catalytic activity observed in the Claisen–Schmidt condensation.[9]

In summary, we have demonstrated for the first time experimentally the direct synthesis by an efficient wet chemical synthetic approach of MgO nanosheets in which (111) facets form the main surfaces. The obtained MgO nanosheets can be used as highly active solid base catalysts and may provide a prototype for the study of surface structure and surface reactions of polar oxide surfaces. The present approach may open up new simple routes to prepare well-defined crystal surfaces of metal oxides.

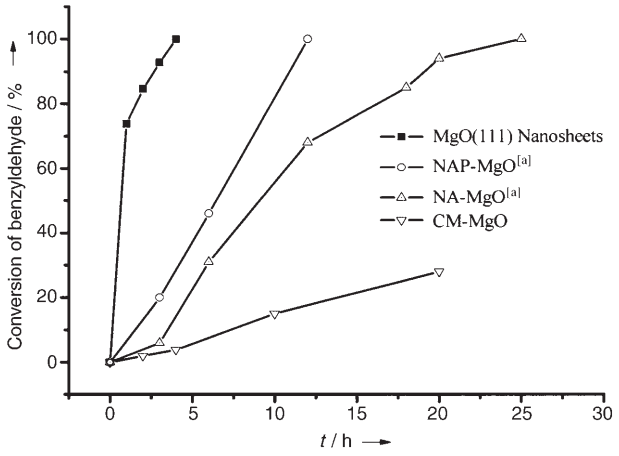

Figure 5. Claisen–Schmidt condensation of benzaldehyde with acetophenone using different crystallites of magnesium oxide at 110 °C. (NAP-MgO: aerogel-prepared MgO; NA-MgO: conventionally prepared MgO; CM-MgO: commercial MgO.) [a] From reference [11].

Experimental Section

Synthesis: In a typical synthesis of the MgO nanosheet structure (referred to here as IUB-Z-MgO), Mg belt (1.0 g) was cleaned with sandpaper and acetone. The belt was then cut into small pieces and dissolved in absolute methanol under a static argon atmosphere. After the Mg belt had totally dissolved, 4-methoxybenzyl alcohol (BZ) was added to the mixture in a Mg/BZ ratio of 2:1. After stirring the mixture for 5 h, a solution of H_2O (molar ratio of 2:1 with respect to Mg) in methanol (30.0 mL) was added dropwise with stirring. The mixture was then stirred for 12 h before being transferred to an autoclave. The autoclave containing the reaction mixture was purged with Ar for 10 min, and then a pressure of 10 bars Ar was imposed before initiation of heating. The mixture was heated at 265 °C for 15 h, and then the vapor inside vented (thereby removing the solvent in the supercritical state). A dry white powder was collected and calcined with a ramp rate of 3 °C min^{-1} to 500 °C, then maintained at 500 °C for 6 h. The ultrafine white powder produced contained solely IUB-Z-MgO, with the MgO nanoplates possessing the (111) surface on the edges.

TEM characterization of the $Mg(OH)(OCH_3)$ and MgO samples was carried out on an FEI Tecnai F20 S-Twin operated at 200 kV. The

 © 2006 Wiley-VCH Verlag GmbH & Co. KGaA, Weinheim

samples were prepared by spreading an ultrasonicated suspension in ethanol on carbon-coated copper grids. TEM and high-resolution images of the nanosheets were acquired with a Gatan 794 CCD camera. Electron diffraction simulation was performed using the software MS Modeling (MS Modeling V3.0 by Accelrys).

N_2 adsorption/desorption isotherms at −196 °C were performed with a Quantachrome Autosorb 1-C system, the data were analyzed by employing the Barrett–Joyner–Halenda (BJH) method; pore volume and pore size distribution curves were obtained from the desorption branch of the isotherm.

Catalytic reactions: A mixture of acetophenone (3 mmol), benzaldehyde (2.5 mmol), and catalyst (0.175 g) was introduced into a 50-mL round-bottomed flask containing dry toluene (10 mL) and stirred in an argon atmosphere at 110 °C. Samples were taken at regular times and analyzed by GC with a flame-ionization detector. The response factors were calculated for each reactive agent from pure samples. The reaction products were identified by GC-MS.

Received: June 14, 2006
Published online: October 6, 2006

Keywords: condensation reactions · heterogeneous catalysis · magnesium oxide · nanostructures · surface chemistry

[1] E. Lucas, S. Decker, A. Khaleel, A. Seitz, S. Fultz, A. Ponce, W. Li, C. Carnes, K. J. Klabunde, *Chem. Eur. J.* **2001**, *7*, 2505.
[2] H. Itoh, S. Utampanya, J. V. Stark, K. J. Klabunde, J. R. Schulp, *Chem. Mater.* **1993**, *5*, 71.
[3] J. B. Nicholas, A. A. Kheir, T. Xu, T. R. Krawietz, J. F. Haw, *J. Am. Chem. Soc.* **1998**, *120*, 10471.
[4] J. V. Stark, D. G. Park, I. Lagadic, K. J. Klabunde, *Chem. Mater.* **1996**, *8*, 1904.
[5] J. V. Stark, K. J. Klabunde, *Chem. Mater.* **1996**, *8*, 1913.
[6] K. J. Klabunde, J. Stark, O. Koper, C. Mohs, D. G. Park, S. Decker, Y. Jiang, I. Lagadic, D. J. Zhang, *J. Phys. Chem.* **1996**, *100*, 12142.
[7] P. W. Tasker, *J. Phys. C* **1979**, *12*, 4977.
[8] J. M. Zuo, M. O'Keeffe, P. Rez, J. C. H. Spence, *Phys. Rev. Lett.* **1997**, *78*, 4777.
[9] R. Plass, K. Egan, C. Collazo-Davila, D. Grozea, E. Landree, L. D. Marks, M. Gajdardziska-Josifovska, *Phys. Rev. Lett.* **1998**, *81*, 4891.
[10] V. K. Lazarov, R. Plass, H. C. Poon, D. K. Saldin, M. Weinert, S. A. Chambers, M. Gajdardziska-Josifovska, *Phys. Rev. B* **2005**, *71*, 115434-1.
[11] B. M. Choudary, M. L. Kantam, K. V. S. Ranganath, K. Mahendar, B. Sreedhar, *J. Am. Chem. Soc.* **2004**, *126*, 3396.
[12] S. Utamapanya, K. J. Klabunde, J. R. Schlup, *Chem. Mater.* **1991**, *3*, 175.
[13] Y. Diao, W. P. Walawander, C. M. Sorensen, K. J. Klabunde, T. Rieker, *Chem. Mater.* **2002**, *14*, 362.
[14] K. T. Ranjit, K. J. Klabunde, *Chem. Mater.* **2005**, *17*, 65.
[15] W. C. Li, A. H. Lu, C. Weidenthaler, F. Schueth, *Chem. Mater.* **2004**, *16*, 5676.
[16] J. Roggenbuck, M. Tiemann, *J. Am. Chem. Soc.* **2005**, *127*, 1096.
[17] S. Stankic, M. Mueller, O Dewald, M. Sterrer, E. Knoezinger, J. Bernardi, *Angew. Chem.* **2005**, *117*, 4996; *Angew. Chem. Int. Ed.* **2005**, *44*, 4917.
[18] X. Y. Chen, K. H. Wong, C. L. Mak, X. B. Yin, M. Wang, J. M. Liu, Z. G. Liu, *J. Appl. Phys.* **2002**, *91*, 5728.
[19] R. Arita, Y. Tanida, S. Entani, M. Kiguchi, K. Saiki, H. Aoki, *Phys. Rev. B* **2004**, *69*, 235423.
[20] E. J. Tarsa, M. Degraef, D. R. Clarke, A. C. Gossard, J. S. Speck, *J. Appl. Phys.* **1993**, *73*, 3276.
[21] S. Shinozak, H. Sato, *J. Appl. Phys.* **1972**, *43*, 701.
[22] V. E. Henrich, *Surf. Sci.* **1976**, *57*, 385.
[23] V. K. Lazarov, S. A. Chambers, M. Gajdardziska-Josifovska, *Phys. Rev. Lett.* **2003**, *90*, 216108.
[24] M. Niederberger, M. H. Bartl, G. D. Stucky, *Chem. Mater.* **2002**, *14*, 4364.
[25] M. Niederberger, M. H. Bartl, G. D. Stucky, *J. Am. Chem. Soc.* **2002**, *124*, 13642.
[26] J. Polleux, A. Gurlo, N. Barsan, U. Weimar, M. Antonietti, M. Niederberger, *Angew. Chem.* **2006**, *118*, 267; *Angew. Chem. Int. Ed.* **2006**, *45*, 261.
[27] A. Wander, I. J. Besh, N. M. Harrison, *Phys. Rev. B* **2003**, *68*, 233405.
[28] S. Sasaki, K. Fujino, Y. Takeuchi, *Proc. Jpn. Acad.* **1979**, *55*, 43.
[29] M. Niederberger, N. Pinna, J. Polleux, M. Antonietti, *Angew. Chem.* **2004**, *116*, 2320; *Angew. Chem. Int. Ed.* **2004**, *43*, 2270.
[30] M. Niederberger, G. Garnweitner, N. Pinna, M. Antonietti, *J. Am. Chem. Soc.* **2004**, *126*, 9120.

 © 2006 Wiley-VCH Verlag GmbH & Co. KGaA, Weinheim

^{129}Xe NMR in Biochemistry

DOI: 10.1002/anie.200601008

NMR Spectroscopy of Laser-Polarized ^{129}Xe Under Continuous Flow: A Method To Study Aqueous Solutions of Biomolecules**

Daniela Baumer, Eike Brunner, Peter Blümler, Paul Philipp Zänker, and Hans Wolfgang Spiess**

Nuclear magnetic resonance (NMR) spectroscopy of ^{129}Xenon is a valuable tool for studying chemical properties and structures, such as guest–host interactions,[1] novel microporous systems,[2] surfaces,[3] and most importantly, biomolecules.[4–6] Most such studies are carried out in solutions, particularly in aqueous solutions. ^{129}Xe (26.44% natural abundance) has a nuclear spin of 1/2 and its chemical shift is highly sensitive over a range of more than 300 ppm for adducts and adsorbates.[7–9] Owing to the low solubility of xenon in water, however, such measurements suffer from low sensitivity. This problem can, in principle, be overcome by the use of so-called laser-polarized (LP) ^{129}Xe.[10] LP ^{129}Xe is commonly produced by spin-exchange optical pumping and exhibits a spin polarization which is several orders of magnitude higher than that of ^{129}Xe in thermal equilibrium, at common magnetic field strengths (5–25 T), and room temperature. Moreover, LP ^{129}Xe is increasingly applied in magnetic resonance imaging (MRI), for instance in lung and brain imaging[11] and angiography.[12] A major problem, however, is the dissolution of LP ^{129}Xe in aqueous solutions. The drawback of single-batch experiments is the limited time available for experiments since the LP ^{129}Xe loses its polarization on the time scale of the longitudinal relaxation time T_1 (that is, a few tens of seconds). Therefore, the depolarized xenon should be continuously replaced with freshly polarized gas, which in analogy to surface NMR spectroscopy, could be realized by continuous-flow experiments.[13–15] Han et al.[16] recently developed a system which enables LP ^{129}Xe to be dissolved under stopped flow. Microbubbles of LP xenon are injected into the solution through microcapillaries. During the NMR experiment, however, the flow must be switched off to maintain the spectral resolution, which otherwise would be reduced by the large change in magnetic susceptibility at the gas/liquid interface. Recent studies of the interaction between xenon and phospholipid bicelles[17] explicitly report problems related to the dissolution of xenon by the shaking that is required and the resulting formation of stable foams.

Herein, we report the first applications of a membrane-based continuous-flow system which preserves the spectral resolution without the need of interrupting the flow. The polarized xenon (2% polarization in the gas phase) is produced in a polarizer that has been described elsewhere[18] and is transferred into the solutions under continuous flow through a newly developed membrane system using commercially available hollow-fiber membranes (CELGARD, Membrana GmbH, Wuppertal, Germany),[19] for further details see Supporting Information. Another problem which arises on dissolving gases in, for example, solutions of amphiphilic molecules or proteins, is the formation of stable foams. Our method also circumvents this problem, because the gases are dissolved in the liquids in a more "direct way". The gas diffuses continuously through nanopores into the liquid without bubbling, shaking, or other mechanical disturbance. To demonstrate the capabilities of our new approach, we have studied LP ^{129}Xe in water, DMSO, and a solution containing phospholipid bicelles that is used in high-resolution NMR spectroscopy studies of proteins[20] and which is particularly prone to foam formation.

Figure 1 shows characteristic ^{129}Xe NMR spectra of LP ^{129}Xe in pure water and DMSO. The line width of the signals belonging to the dissolved xenon is only 0.3 to 0.4 ppm (insets of Figure 1), allowing chemical shift measurements with an

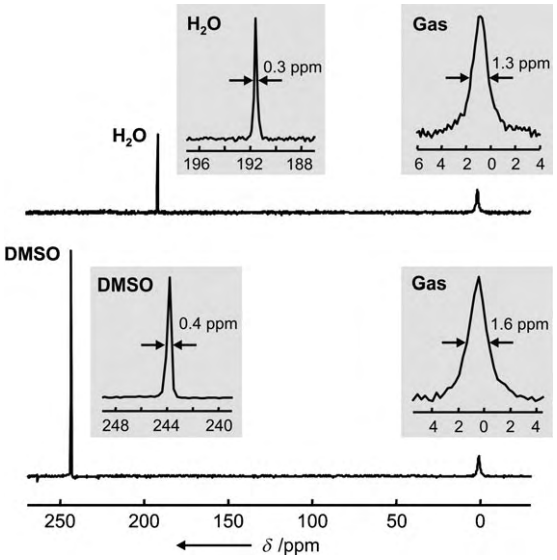

Figure 1. ^{129}Xe NMR spectra of LP ^{129}Xe dissolved in H_2O (top) and DMSO (bottom) obtained with two scans at $T = 298$ K. Chemical shifts are referenced to the gas signal. The line width of the signals is given in the insets.

[*] Dr. D. Baumer, Prof. E. Brunner
Institut für Biophysik und Physikalische Biochemie
Universität Regensburg
Universitätsstrasse 31, 93040 Regensburg (Germany)
Fax: (+49) 941-943-2479
E-mail: eike.brunner@biologie.uni-regensburg.de
Dr. P. Blümler, Dipl.-Phys. P. P. Zänker, Prof. H. W. Spiess
Max-Planck-Institut für Polymerforschung
Ackermannweg 10, 55128 Mainz (Germany)
Fax: (+49) 6131-379-100
E-mail: spiess@mpip-mainz.mpg.de
Dr. P. Blümler
Research Center Jülich
ICG III, 52425 Jülich (Germany)

[**] We thank S. Appelt and W. Häsing (FZ Jülich) for the development of the xenon polarizer and H.-D. Lemke (Membrana GmbH) for the oxygenator fiber membranes. Financial support from the DFG (Br 1278/12-1 and Sp 98/6-2) is gratefully acknowledged.

Supporting information for this article is available on the WWW under http://www.angewandte.org or from the author.

WILEY InterScience DISCOVER SOMETHING GREAT
© 2006 Wiley-VCH Verlag GmbH & Co. KGaA, Weinheim

accuracy of 0.03 to 0.04 ppm. The broadness of the gas peaks on the right hand side of the spectra in Figure 1 originates from the rapidly diffusing gas inside the heterogeneous physical environment of the hollow fibers (membrane/free gas). Control experiments showed that no gaseous xenon is contained in the liquid (see Supporting Information). The dissolution process occurs much faster than T_1 (see below). The dissolved xenon, therefore, reaches the maximum possible spin polarization. Thus, the new membrane system does allow high-resolution NMR spectroscopy of biomolecules to be performed using a continuous-flow of LP ^{129}Xe. The gas signal can be used for internal referencing of the spectra. A chemical shift of $\delta = 0.12$ ppm is expected[7,21] at a xenon partial pressure of 0.03 MPa. The influence of helium in the gas mixture is negligible[8] (this is shown in Figure 2; in contrast to the measurement with LP ^{129}Xe, the other data points were measured without helium). The advantages of our new approach are demonstrated by two new applications.

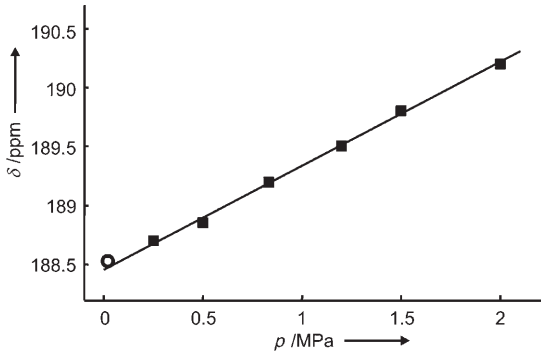

Figure 2. The chemical shift of ^{129}Xe versus xenon partial pressure at $T = 308$ K measured in an aqueous DMPC/DHPC bicelle solution. The open circle indicates the measurement with LP ^{129}Xe under continuous flow using the membrane method, the other points are generated by thermally polarized ^{129}Xe measurements.

Lipid bicelles are of increasing interest[17] in two fields of research. They can be considered as models for biomembranes because these membranes partly consist of lipid-bilayers and they are used in many biomolecular NMR spectroscopic experiments to partially orient the molecules.[20] When using thermally polarized xenon, large gas pressures (up to 2 MPa) have to be applied to generate sufficient signal intensity. However, to obtain the pure xenon–bicelle interaction from such measurements the chemical shift has to be extrapolated to zero xenon partial pressure, to remove the possibility of xenon–xenon interactions. To extract this quantity with thermally polarized xenon, a set of experiments at various pressures is required to generate an experimental curve which can be reliably extrapolated to zero pressure. This is a highly time-consuming procedure. Instead, LP ^{129}Xe offers the possibility to directly measure the chemical shift at very low xenon partial pressure (in this case 0.02 MPa) in a single experiment.

To demonstrate this approach, we have measured the NMR chemical shift of thermally polarized ^{129}Xe in an aqueous solution of the two phospholipids DHPC/DMPC[*] as a function of the xenon pressure from 0.25 MPa to 2 MPa (see Supporting Information) and compared these measurements with the data obtained by using LP ^{129}Xe under continuous flow at 0.02 MPa (see Figure 2). The measured chemical shift increases linearly with the pressure, that is, with increasing xenon concentration. For the ^{129}Xe chemical shift δ at 305 K we found the relationship given in Equation (1) where p is the xenon partial pressure.

$$\delta\,[\mathrm{ppm}] = 188.46 + 0.88\,p\,[\mathrm{MPa}] \quad (1)$$

The chemical shift at low pressure (0.02 MPa), which was measured by using LP ^{129}Xe ($\delta = 188.5$ ppm), fits excellently into the regression line determined for the data measured in thermal equilibrium (Figure 2). This result confirms the reliability and accuracy of chemical shift measurements using LP ^{129}Xe under continuous flow in the membrane system.

Moreover, comparison of the chemical shifts of LP ^{129}Xe in H_2O ($\delta = 190.9$ ppm) and in DHPC/DMPC ($\delta = 188.5$ ppm) demonstrates that xenon interacts with the bicelles. A chemical shift change of -2.4 ppm is induced by the lipid bicelles at 305 K. This chemical shift can be used to investigate xenon–molecule interactions and to determine specific and nonspecific interactions.[4] The relaxation time T_1 measured for xenon in the bicelle-containing sample amounts to 40 s at 311 K. Whereas the experiment with LP ^{129}Xe took about 5 minutes, a single data point in the pressure-dependent measurements took on average 2 h leading to a total measurement time of about 12 h.

This reduced measuring time also enables us to record two-dimensional NMR spectra of ^{129}Xe.[22] In fact, 2D exchange spectroscopy (EXSY) allows us to follow the dissolution process of LP ^{129}Xe in water under continuous flow in real time (see Figure 3). The signal on the diagonal at approximately $\delta = 0$ ppm arises from xenon gas in the microcapillaries, the one at approximately $\delta = 190$ ppm is from xenon dissolved in water. Note that even with a mixing time of only 1 ms a cross-peak appears for dissolved xenon. This result indicates that the dissolution through the membrane happens on a timescale of milliseconds (for details see Supporting Information). The 2D EXSY technique will be very useful to study systems where a slow exchange of xenon between different chemical environments occurs in solution. This situation occurs, for example, in blood[23] or emulsions. The accessible dynamic range covers about five orders of magnitude, from 100 μs to 10 s.

In summary, our method of dissolving LP ^{129}Xe from hollow fiber membranes has the following important advantages. It is fast, reliable, and robust, without the need of special sample preparation. The new system prevents the formation of bubbles and foam and thus minimizes the associated line broadening. There is no observable loss of polarization or shortening of T_1. The continuous operation allows signal averaging and, therefore, multidimensional

[*] dihexanoyl phosphatidylcholine/dimyristoyl phosphatidylcholine; for sample preparation procedure see Supporting Information.

 © 2006 Wiley-VCH Verlag GmbH & Co. KGaA, Weinheim

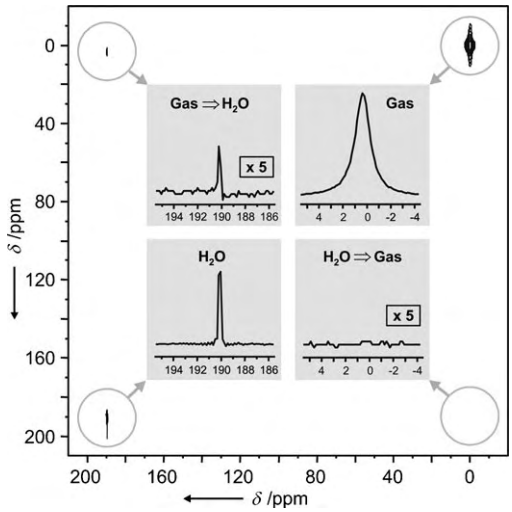

Figure 3. Two-dimensional EXSY spectrum (contour plot) of LP ^{129}Xe dissolved in H_2O at $T = 308$ K and $t_{mix} = 1$ ms. Experiment time is 68 min. Note the asymmetry of the spectrum: the only observed cross-peak can be assigned to gaseous xenon during the evolution time.

NMR measurements. In addition, the membranes are stable in most liquids (water, alcohols, DMSO) used for dissolving biomolecules.

Although laser-polarization increases the NMR signal sufficiently to study small concentrations of adsorbed xenon in biomolecules or host structures, applications remain rare with the dissolution process being the main obstacle. Our method simplifies the application of LP ^{129}Xe (or other gases with short lifetimes) in spectroscopic methods by improving the dissolution process. We have demonstrated that the procedure allows the application of LP ^{129}Xe in biomolecular high-resolution NMR under continuous-flow conditions at low xenon pressures and can be used to record 2D NMR spectra in solution under continuous flow. Hopefully, this will widen the applications of hyperpolarized gases in this growing field of research.

Received: March 14, 2006
Revised: July 27, 2006
Published online: October 2, 2006

Keywords: gas dissolution · laser polarization · lipid bicelles · NMR spectroscopy · xenon

[1] Y.-Q. Song, B. M. Goodson, R. E. Taylor, D. D. Laws, G. Navon, A. Pines, *Angew. Chem.* **1997**, *109*, 2464 – 2466; *Angew. Chem. Int. Ed. Engl.* **1997**, *36*, 2368 – 2370.
[2] D. V. Soldatov, I. L. Moudrakovski, J. A. Ripmeester, *Angew. Chem.* **2004**, *116*, 6468 – 6471; *Angew. Chem. Int. Ed.* **2004**, *43*, 6308 – 6311.
[3] D. Raftery, H. Long, T. Meersmann, P. J. Grandinetti, L. Reven, A. Pines, *Phys. Rev. Lett.* **1991**, *66*, 584 – 587.
[4] S. M. Rubin, M. M. Spence, B. M. Goodson, D. E. Wemmer, A. Pines, *Proc. Natl. Acad. Sci. USA* **2000**, *97*, 9472 – 9475.
[5] C. Landon, P. Berthault, F. Vovelle, H. Desvaux, *Protein Sci.* **2001**, *10*, 762 – 770.
[6] T. J. Lowery, M. Doucleff, E. J. Ruiz, S. M. Rubin, A. Pines, D. E. Wemmer, *Protein Sci.* **2005**, *14*, 848 – 855.
[7] C. J. Jameson, A. K. Jameson, S. M. Cohen, *J. Chem. Phys.* **1973**, *59*, 4540 – 4546.
[8] A. K. Jameson, C. J. Jameson, H. S. Gutowsky, *J. Chem. Phys.* **1970**, *53*, 2310 – 2321.
[9] T. Ito, J. Fraissard, *J. Chem. Phys.* **1982**, *76*, 5225 – 5229.
[10] T. G. Walker, W. Happer, *Rev. Mod. Phys.* **1997**, *69*, 629 – 642.
[11] M. Albert, G. Cates, B. Driehuys, W. Happer, B. Saam, C. S. Springer, A. Wishnia, *Nature* **1994**, *370*, 199 – 201.
[12] H. E. Möller, M. S. Chawla, X. J. Chen, B. Driehuys, L. W. Hedlund, C. T. Wheeler, G. A. Johnson, *Magn. Reson. Med.* **1999**, *41*, 1058 – 1064.
[13] M. Haake, A. Pines, J. A. Reimer, R. Seydoux, *J. Am. Chem. Soc.* **1997**, *119*, 11711 – 11712.
[14] E. Brunner, R. Seydoux, M. Haake, A. Pines, J. Reimer, *J. Magn. Reson.* **1998**, *130*, 145 – 148.
[15] A. Nossov, F. Guenneau, M.-A. Springuel-Huet, E. Haddad, V. Montouillout, B. Knott, F. Engelke, C. Fernandez, A. Gédéon, *Phys. Chem. Chem. Phys.* **2003**, *5*, 4479 – 4483.
[16] S. Han, S. Garcia, T. J. Lowery, E. J. Ruiz, J. A. Seeley, L. Chavez, D. S. King, D. E. Wemmer, A. Pines, *Anal. Chem.* **2005**, *77*, 4008 – 4012.
[17] X. Li, C. Newberry, I. Saha, P. Nikolaou, N. Whiting, B. M. Goodson, *Chem. Phys. Lett.* **2005**, *419*, 233 – 239.
[18] N. J. Shah, T. Ünlü, H.-P. Wegener, H. Halling, K. Zilles, S. Appelt, *NMR Biomed.* **2000**, *13*, 214 – 219.
[19] P. P. Zänker, P. Blümler, H. D. Lemke, H. W. Spiess, German patent application (DE 102005026604.5; PCT/EP2006/005349): Verfahren zum Lösen von Gasen mit kurzlebigen physikalischen Eigenschaften in einer Flüssigkeit (Xenonizer), submitted, **2005**.
[20] N. Tjandra, A. Bax, *Science* **1997**, *278*, 1111 – 1114.
[21] D. Baumer, A. Fink, E. Brunner, *Z. Phys. Chem.* **2003**, *217*, 289 – 293.
[22] J. Jeener, B. H. Meier, P. Bachmann, R. R. Ernst, *J. Chem. Phys.* **1979**, *71*, 4533 – 4546.
[23] A. Bifone, Y.-Q. Song, R. Seydoux, R. E. Taylor, B. M. Goodson, T. Pietrass, T. F. Budinger, G. Navon, *A.* Pines, *Proc. Natl. Acad. Sci. USA* **1996**, 93, 12932 – 12936.

 © 2006 Wiley-VCH Verlag GmbH & Co. KGaA, Weinheim

Cyclohexane Derivatives

DOI: 10.1002/anie.200602020

Cycloisomerization of 1,6-Dienes Mediated by Lewis Super Acids without Additives: Easy Access to Polysubstituted Six-Membered Carbocycles

Fanny Grau, Andreas Heumann, and Elisabet Duñach**

Dedicated to Professor Peter Vollhardt on the occasion of his 60th birthday

Alkyl-substituted carbocycles are a common structural component in a number of naturally occurring and biologically active molecules.[1] One of the challenging problems in the synthesis of compounds containing five- and six-membered rings is the efficient control of the ring size during a cyclization or cycloaddition step. With innumerable applications, the Diels–Alder cycloaddition is the best established reaction leading to six-membered rings exclusively.[2] The advent of stereoselective transition-metal catalysts has stimulated new ways to catalytic cyclization[3] as another important approach for the construction of carbocyclic compounds.[4] Though often highly selective, none of these reactions are really ring-size specific.[5] The cycloisomerization of polyunsaturated substrates has been studied extensively and is well established as an efficient method for the synthesis of five-membered carbocycles.[6,7] Though many metals have been reported to achieve catalytic cycloisomerization reactions,[8] only a few examples are known that lead to the selective formation of six-membered rings. Cyclohexane derivatives have been obtained from 1,6-dienes (e.g. olefinic indoles) with palladium[9] and platinum[10] complexes without special additives. However, other systems require catalyst combinations such as bulky ethylenebis(tetrahydroindenyl)titanium dichloride in association with *n*BuMgBr,[11] $[Cp_2ZrCl_2]$/methylaluminoxane ($[Zr]:[Al] = 0.1$),[12] $[Cp^*_2ZrMe_2]/B(C_6F_5)_3$/$AlMe_3$ ($Cp^* = C_5Me_5$),[13] methylaluminoxane and butylmetallocene scandium hydride complexes.[14] These latter examples involve the use of highly sterically hindered catalysts in association with alkylation or reducing agents. No simple catalytic system has been yet reported for the cycloisomerization of 1,6-dienes to give highly substituted cyclohexane carbocycles.

In the presence of Lewis acids, the intramolecular ene reaction[15] of 1,6-dienes generally leads to five-membered-ring compounds.[16] In a particular example, an alkenylpentenolide was transformed in the presence of pure sulfuric acid into a cyclohexane ring, as a result of a Wagner–Meerwein transposition with the formation of a spirocyclic ring system.[17]

We have recently reported on Lewis acid catalyzed cycloisomerizations of nonactivated and differently substituted olefinic alcohols to give cyclic ethers.[18] We found that the catalyst, tin(IV) triflate, $Sn(OTf)_4$, is involved in the activation of both the hydroxy group and the double bond. The following order of reactivity was observed: trisubstituted $\approx$ 1,1-disubstituted $>$ 1,2-disubstituted $>$ monosubstituted olefins. It seemed to us that enhancing the electrophilicity of a double bond with a strong Lewis acid might also favor intramolecular C–C bond formation within dienes, in a process comparable to the olefin activation by cationic late transition metals.[19] However, in contrast to order of reactivity towards late transition metals, highly substituted double bonds were supposed to be much more reactive with Lewis acids. We now report on our preliminary results on the transformation of 1,6-dienes that are highly substituted at the alkene termini in the presence of catalytic amounts of tin(IV) bis(trifluoromethanesulfonyl)imide, $Sn(NTf)_4$, allowing the selective formation of highly substituted six-membered-ring carbocycles.

The active catalyst, $Sn(NTf_2)_4$, and other metal bis(trifluoromethanesulfonyl)imides and metal triflate salts were prepared by using a simple electrochemical procedure.[20] These metal salts can be considered as Lewis super acids owing to the strong acidity of $HNTf_2$ (pK_a in water estimated at 1.7).[21]

Treatment of diethyl diprenylmalonate (**1a**) in refluxing 1,2-dichloroethane with a 5 mol% $Sn(NTf_2)_4$ afforded the *gem*-dimethyl cyclohexane derivative **1b** in 60% yield (Table 1). The structure of the new compound was easily deduced from the ^1H and ^{13}C NMR spectra.[22] Indeed, the new carbon–carbon bond in cyclohexane derivative **1b** arises from cyclization of diene **1a** occurring nonsymmetrically at two different sites of the two identically substituted double bonds: the first double bond undergoes a nucleophilic attack by the second double bond with Markovnikov-type regiochemistry.

To examine the scope of this novel catalytic system, we investigated the reactions of **1a** using several SnX_n derivatives ($X = Cl$, OTf, NTf_2, $n = 2$ or 4; Table 1, entries 1–4). More classical Lewis acids such as $SnCl_4$ and $SnCl_2$ led to low conversion and low selectivity. The other metal triflates and bistriflimidates tested (e.g. with W^{VI}, Ni^{II}, Sm^{III}, Bi^{III}, Table 1, entries 5–8) were found to be inefficient. Only $Sn(OTf)_4$ and $Sn(NTf_2)_4$ showed interesting activities (Table 1, entries 1 and 4). $Sn(NTf_2)_4$ was by far the most efficient catalyst, since it

[*] F. Grau, Dr. E. Duñach
Laboratoire de Chimie
des Molécules Bioactives et des Arômes
Université de Nice-Sophia Antipolis
CNRS, UMR 6001
Parc Valrose, 06108 Nice Cedex 2 (France)
Fax: (+33) 492-076-151
E-mail: dunach@unice.fr
Dr. A. Heumann
Université Paul Cézanne
UMR CNRS 6180 "Chirotechnologies et Biocatalyse"
Faculté Saint-Jérôme – Case A62
13397 Marseille Cedex 20 (France)
Fax: (+33) 491-288-278
E-mail: andreas.heumann@univ-cezanne.fr
Homepage: http://www.unice.fr/lcmba/

Supporting information for this article is available on the WWW under http://www.angewandte.org or from the author.

 © 2006 Wiley-VCH Verlag GmbH & Co. KGaA, Weinheim

Table 1: Effect of Lewis acid catalysts in the cycloisomerization of **1a** to give **1b**.

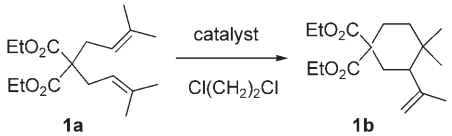

1a **1b**

Entry	Cat. (mol%)	*t*, *T*	Conv. [%]	Yield [%]
1	$Sn(OTf)_4$ (5)	71 h, 50°C	78	60
2	$SnCl_4$ (5)	24 h, 40°C	25	11
3	$SnCl_2$ (5)	28 h, 50°C	28	14
4	$Sn(NTf_2)_4$ (2)	1.5 h, 50°C	100	88
5	$Ni(OTf)_3$ (5)	24 h, 83°C	32	24
6	$W(NTf_2)_6$ (5)	20 h, 83°C	43	36
7	$Bi(OTf)_3$ (5)	7 h, 83°C	31	23
8	$Sm(OTf)_3$ (5)	24 h, 83°C	9	–

could be used in 2-mol% quantities under mild conditions. The rapid and selective cycloisomerization of **1a** led to **1b** in 88% yield. To our knowledge, this is the first example of a selective Lewis acid catalyzed cycloisomerization of a highly (alkene-) substituted 1,6-diene.

A number of 1,6-dienes with different substitution patterns at the double bonds as well as at the homoallylic carbon were prepared from simple starting materials.[23] Table 2 summarizes some representative examples of this reaction using a variety of differently substituted substrates **1a**–**13a**. The conditions were optimized for the different substrates by using a catalytic amount of $Sn(NTf_2)_4$ (5 mol%). Two solvents, nitromethane and dichloroethane, turned out to be the best reaction media. The influence of the malonate unit was first studied with diprenyl-substituted derivatives **1a**–**6a** (Table 2, entries 1–6). In comparing ethyl and methyl malonates **1a** and **2a**, the reactions conducted under several experimental conditions led to similar selectivities and reactivities. Both cyclohexane derivatives **1b** and **2b** were obtained selectively in about 90% yield under mild conditions (from room temperature to 40°C). Under more severe reaction conditions, a cyclization involving one ester group became competitive. Thus, in refluxing dichloroethane (83°C), the cycloisomerization of **2a** led to the corresponding cyclohexane derivative **2b** in lower yield (58%), together with a by-product (10% yield), which was identified as the δ-lactone **2c**. This lactone by-product is the result of an intramolecular cyclization involving one ester unit and one of the double bonds.[24] It is interesting to note that this reaction between an alkene and the ester moiety may become the dominant reaction when less substituted double bonds (with lower nucleophilicity) are present in the diene (see Table 2, entry 12).

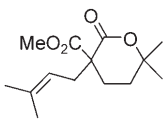

2c

When one malonate ester group was replaced by a nitrile (Table 2, entry 3) or an ethyl ketone (entry 4), the corresponding cycloisomerization products were still obtained selectively in yields of 70–74%. However, the malononitrile analogue (with two nitrile groups) was unreactive. This may indicate that the ester oxygen atom(s) play an important role in the mechanism of the cycloisomerization. Sulfone **5a** and phosphate **6a** (entries 5 and 6) also afforded the corresponding highly substituted cyclohexane structures **5b** and **6b**, respectively, arising from the head-to-tail diene cycloisomerization.

The influence of the double-bond substitution upon cycloisomerization was further examined with substrates **7a**–**12a** (Table 2, entries 7–12).[25] The transformation of these substrates proceeded with satisfactory yields and selectivities. The common structural feature of the cyclic products is the presence of the *gem*-dimethyl group at the cycloalkane skeleton, indicating that the C–C bond-forming step always occurs at the more substituted site of the double bond. It is also worth noting that the substitution pattern of the second (less substituted) double bond influences the cyclization in several ways: 1) When the second allyl group is substituted at the terminal alkene carbon, the usual cyclohexane structures are formed selectively (Table 2, entries 7–10). 2) Substrates with a terminal (mono- or disubstituted) double bond such as **9a** and **11a** (Table 2, entries 9 and 11) yielded cycloheptene and cycloheptane derivatives **9b**[26] and **11b**, respectively. Whereas the *gem*-dimethyl cycloheptene derivative **9b** was obtained selectively, in the case of **11a** the reaction was less efficient: instead of a single carbocyclic product, we could isolate only the bridged bicyclic lactone derivative **11b** in low yields (22%) as the result of a cascade of C–C and C–O couplings, 3) With less substituted (less nucleophilic) double bonds such as in **12a** (Table 2, entry 12), C–C bond formation is disfavoured, and a C–O coupling reaction occurs between one of the double bonds and one of the ester groups (as mentioned before) to give **12b** in selectively 70% yield.

Another point of interest was the competition between olefinic and aromatic double bonds in the C–C bond-forming step. When a phenyl group is present as in **13a** (Table 2, entry 13), a double cyclization occurs very selectively affording tricyclic compound **13b** in 78% yield. Each of the double bonds of the diene reacts preferentially with an aromatic ring by C–H activation in a catalytic process (Table 2, entry 13).[27–28]

To evaluate whether other strong acids are also effective catalysts, the reaction of **1a** was carried out in the presence of $HNTf_2$. The cyclization giving **1b** occurred in 80% yield;[29a] however, no conversion was observed with **3a.**[29b] With other olefins, the presence of this super acid led to partial or complete polymerization. These results indicate that the Lewis acid catalyst $Sn(NTf_2)_4$ has a different reactivity and is more effective than the protic acid $HNTf_2$ for the cycloisomerization of highly substituted 1,6-dienes. We tested a mixture of $Sn(NTf_2)_4$/$HNTf_2$ (1:1, 5 mol% each) for the cyclization of **1a** in a Brønsted acid assisted Lewis acid catalyzed process,[30] but the results were not better than those obtained with $Sn(NTf_2)_4$ alone.

The possibility of a partial hydrolysis of $Sn(NTf_2)_4$ by reaction with traces of water was also considered. Preliminary kinetic studies carried out with **1a** and added water in distinct quantities. Whereas traces of water had almost no effect on either the reaction rate or the yield, the reaction rate decreased notably after the addition of greater amounts of water (up to 2 equiv H_2O with respect to the catalyst). At the

 © 2006 Wiley-VCH Verlag GmbH & Co. KGaA, Weinheim

Table 2: Cycloisomerization of 1,6-dienes with $Sn(NTf_2)_4$ (5 mol%).

Entry	Substrate		*t* [h]	Solvent, *T* [°C]	Conversion [%]	Product (Yield [%])	
1	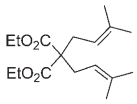	**1a**	4 2.5	$Cl(CH_2)_2Cl$, 40 CH_3NO_2, 25	100 100	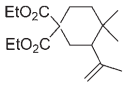	**1b** (92) **1b** (92)
2	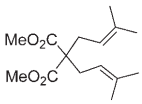	**2a**	5	$Cl(CH_2)_2Cl$, 40	100	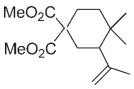	**2b** (88)
3	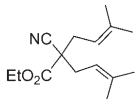	**3a**	2	CH_3NO_2, 101	80	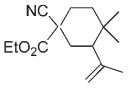	**3b** (70), 1 isomer
4	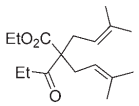	**4a**	5	CH_3NO_2, 25	90	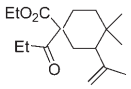	**4b**,**c** (74), 2 diastereomers
5	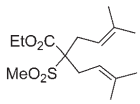	**5a**	5	CH_3NO_2, 40	100	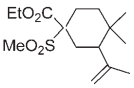	**5b** (74), 1 isomer
6	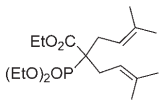	**6a**	5	CH_3NO_2, 101	59	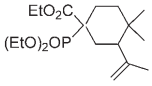	**6b** (46), 1 isomer
7	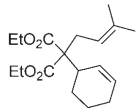	**7a**	3	CH_3NO_2, 60	100	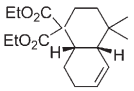	**7b** (88), 1 isomer
8	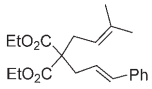	**8a**	5	$Cl(CH_2)_2Cl$, 60	100	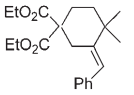	**8b** (70)
9	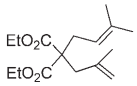	**9a**	1	CH_3NO_2, 101	100	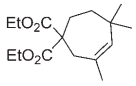	**9b** (61)
10	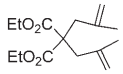	**10a**	1	CH_3NO_2, 101	100	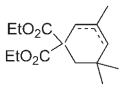	**10b**,**c** (61), 0.69:1
11	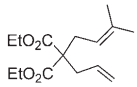	**11a**	5	CH_3NO_2, 101	54	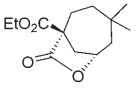	**11b** (22)
12	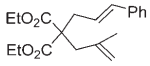	**12a**	6	CH_3NO_2, 101	75	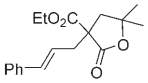	**12b** (70)
13	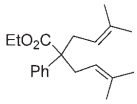	**13a**	130	CH_3NO_2, 101	100	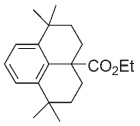	**13b** (78)

same time, the amount of by-products increased considerably. The importance of the acidity of the Sn^{IV} catalyst system was further demonstrated after the addition of 2,6-di-*tert*-butylpyridine as a highly hindered base ($Sn(NTf_2)_4$/base 1:1). Under these conditions, the cyclization of **1a** was completely inhibited.

We do not know yet the exact mechanism of these cycloisomerizations. However, all our results seem to point in favor of a carbocationic-type mechanism. The 1,6-dienes with the more substituted double bonds were the most efficient and selective substrates in the cyclization reaction. The product formation may be explained as the result of a first coordination of the Lewis acid to the more electron-rich double bond, followed by the coupling of the second less electron-rich olefin at the more substituted end of the first olefin (Scheme 1). The ester group present should also participate in the coordination to the Sn^{IV}. Thus, the electrophilic-type addition of the Lewis acid to the isobutenyl group of **14** gives an intermediate zwitterion **14a**, which is stabilized by the second alkene group in **14b**. The ring-closing step (C–C bond formation) is controlled by the stability of the carbocation intermediates **14c** and **14d**, which depends on the

 © 2006 Wiley-VCH Verlag GmbH & Co. KGaA, Weinheim

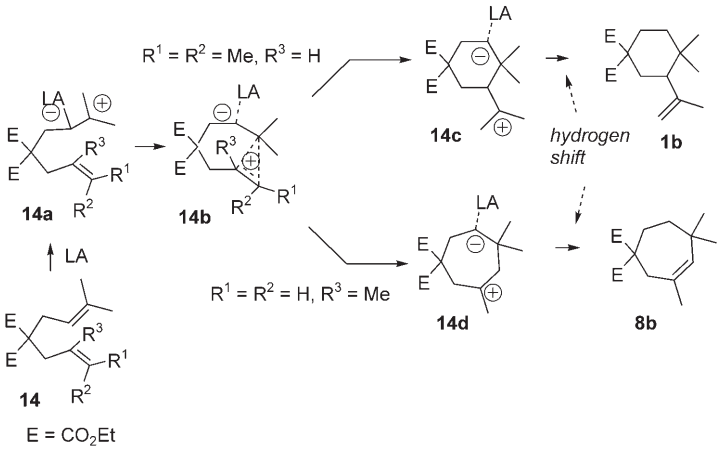

Scheme 1. Cycloisomerization of 1,6-dienes and competition between the formation of six- and seven-membered rings (LA = Lewis acid).

substitution of the second olefin. Though in most reactions a six-membered ring formed, cycloheptanes were obtained in two cases. The ring-size specificity is explained by the predominance of the more stable (tertiary) cationic carbon center in **14c** and **14d**, respectively (Scheme 1).

This mechanistic proposition does not involve protic acids. However, the role of protons (from residual water) in the catalytic process cannot be completely excluded.[30] The combination of Brønsted and Lewis acids has been reported as a particularly useful tool in several efficient reactions in asymmetric catalysis.[31] Nevertheless, for the moment we have no experimental support for the direct interaction of protons in association with Lewis acids in the cycloisomerization of 1,6-dienes.

The enhancement of the electrophilic alkene activation in dimerization reactions by highly charged transition-metal complexes has been recently reported and is now well established.[19] However, the use of Lewis acids for this purpose is much less developed. The role of tin derivatives in olefin polymerization has also been emphasized.[32] Catalyst design is important since the action of strong Lewis acid anions (OTf^-, SbF_5^-) combined with cationic palladium complexes leads to quite uncontrolled isomerization processes in 1,6-dienes.[33]

In conclusion, we have found that $Sn(NTf_2)_4$ is a powerful catalyst for the cycloisomerization of malonate-type highly substituted 1,6-dienes. The present transformation provides simple and selective procedure for the preparation of highly functionalized six-membered-ring carbocyclic systems. Moreover, the development of new catalysts for diene cycloisomerization broadens the field of atom-economic cyclization processes.[34]

Experimental Section

General cyclization procedure: A mixture of the 1,6-diene (1 mmol) and $Sn(NTf_2)_4$ (0.05 mmol) was stirred under nitrogen at the reported temperature in distilled dichloroethane or nitomethane (5 mL). The progress of the reaction was monitored by GC analysis. The reaction products were hydrolyzed by addition of water (10 mL) and extracted with ether (3 × 10 mL). The combined organic phases washed with brine and dried over $MgSO_4$. After filtration and evaporation of the solvent, the products were purified by flash chromatography on silica gel. The compounds **1b**–**13b** were characterized by ^1H and ^{13}C NMR spectroscopy, mass spectrometry, and high-resolution MS or elemental analysis. Compounds **3b**, **5b**, **6b**, and **7b** were obtained as single diastereomers. Compounds **4b,c** were obtained as a 1.2:1 mixture of diastereomers; the configuration could not be determined by NMR experiments. The *cis* configuration of **7b** was established according to the Karplus rules. The *E* configuration of **8b** was established by NOESY NMR experiments.

Received: May 22, 2006
Published online: October 6, 2006

Keywords: cyclization · dienes · Lewis acids · six-membered rings · tin

[1] T. L. Ho, *Carbocycle Construction in Terpene Synthesis*, Wiley-VCH, Weinheim, **1988**.
[2] K. C. Nicolaou, S. A. Snyder, T. Montagnon, G. Vassilikogiannakis, *Angew. Chem.* **2002**, *114*, 1742 – 1773; *Angew. Chem. Int. Ed.* **2002**, *41*, 1668 – 1698.
[3] C. Thebtaranonth, Y. Thebtaranonth, *Tetrahedron* **1990**, *46*, 1385 – 1489.
[4] a) I. Ojima, M. Tzamarioudaki, Z. Li, R. J. Donovan, *Chem. Rev.* **1996**, *96*, 635 – 662; b) C. Aubert, O. Buisine, M. Malacria, *Chem. Rev.* **2002**, *102*, 813 – 834.
[5] A notable exception is the Pd-catalyzed cycloaddition: B. M. Trost, *Angew. Chem.* **1986**, *98*, 1 – 20; *Angew. Chem. Int. Ed. Engl.* **1986**, *25*, 1 – 20.
[6] a) B. M. Trost, M. J. Krische, *Synlett* **1998**, 1 – 16; b) B. Bogdanovic, *Adv. Organomet. Chem.* **1979**, *17*, 105 – 140.
[7] Cycloisomerization of 1,6-dienes: a) R. A. Widenhoefer, *Acc. Chem. Res.* **2002**, *35*, 905 – 913; b) G. Lloyd-Jones, *Org. Biomol. Chem.* **2003**, *1*, 215 – 236.
[8] For representative examples with transition metals, see a) Rh: A. Bright, J. F. Malone, J. K. Nicholson, J. Powell, B. L. Shaw, *Chem. Commun.* **1971**, 712 – 713; b) R. Grigg, J. F. Malone, T. R. B. Mitchell, A. Ramasubbu, R. M. Scott, *J. Chem. Soc. Perkin Trans. 1* **1984**, 1745 – 1754; c) Pd: A. Heumann, L. Giordano, A. Tenaglia, *Tetrahedron Lett.* **2003**, *44*, 1515 – 1518; d) Ru: Y. Yamamoto, Y. Nakagai, K. Itoh, *Chem. Eur. J.* **2004**, *10*, 231 – 236; e) Y. Terada, M. Arisawa, M. Nishida, *Angew. Chem.* **2004**, *116*, 4155 – 4159; *Angew. Chem. Int. Ed.* **2004**, *43*, 4063 – 4067; f) Ni: B. Radetich, T. V. RajanBabu, *J. Am. Chem. Soc.* **1998**, *120*, 8007 – 8008; g) Ti: S. Okamoto, T. Livinghouse, *J. Am. Chem. Soc.* **2000**, *122*, 1223 – 1224.
[9] a) B. M. Trost, J. M. D. Fortunak, *Organometallics* **1982**, *1*, 7 – 13; b) A. F. Barrero, J. E. Oltra, M. Alvarez, *Tetrahedron Lett.* **1998**, *39*, 1401 – 1404.
[10] a) W. D. Kerber, J. H. Koh, M. R. Gagné, *Org. Lett.* **2004**, *6*, 3013 – 3015; b) C. Liu, X. Han, X. Wang, R. A. Widenhoefer, *J. Am. Chem. Soc.* **2004**, *126*, 3700 – 3701.
[11] S. Okamoto, T. Livinghouse, *Organometallics* **2000**, *19*, 1449 – 1451.
[12] S. Thiele, G. Erker, *Chem. Ber.* **1997**, *130*, 201 – 207.
[13] K. H. Shaughnessy, R. M. Waymouth, *J. Am. Chem. Soc.* **1995**, *117*, 5873 – 5874.
[14] a) W. E. Piers, P. J. Shapiro, E. E. Bunel, J. E. Bercaw, *Synlett* **1990**, 74 – 84; b) also see P. W. Chum, S. E. Wilson, *Tetrahedron Lett.* **1976**, 1257 – 1258.
[15] W. Oppolzer, V. Snieckus, *Angew. Chem.* **1978**, *90*, 506 – 516; *Angew. Chem. Int. Ed. Engl.* **1978**, *17*, 476 – 486.
[16] a) L. F. Tietze, U. Beifuss, M. Ruther, A. Rühlmann, J. Antel, G. M. Sheldrick, *Angew. Chem.* **1988**, *100*, 1200 – 1201; *Angew. Chem. Int. Ed. Engl.* **1988**, *27*, 1186 – 1187; b) For the conversion

 © 2006 Wiley-VCH Verlag GmbH & Co. KGaA, Weinheim

of 1,7-dienes to give cyclohexanes, see Ref. [4]; c) For the conversion of 1,5-dienes to give cyclohexanes, see T. Kato, S. Kumazawa, Y. Kitahara, *Synthesis* **1972**, 573 – 575.
[17] V. Jäger, W. Kuhn, U. Schubert, *Tetrahedron Lett.* **1986**, *27*, 2583 – 2586.
[18] L. Coulombel, I. Favier, E. Duñach, *Chem. Commun.* **2005**, 2286 – 2288.
[19] C. Hahn, *Chem. Eur. J.* **2004**, *10*, 5888 – 5899.
[20] I. Favier, E. Duñach, *Tetrahedron Lett.* **2003**, *44*, 2031 – 2032.
[21] A. Vij, R. L. Kirchmeier, J. M. Shreeve, R. D. Verma, *Coord. Chem. Rev.* **1997**, *158*, 413 – 432.
[22] The presence of three nonequivalent CH_3 groups, two at a quaternary carbon (singlets at $\delta = 0.82$ and 0.85 ppm) and another one in a vinylic position ($\delta = 1.7$ ppm) was easily deduced from the ^{1}H NMR spectrum. The two ester ethyl groups and two vinylic protons (two broad singlets at $\delta = 4.6$ and 4.75 ppm) were also magnetically different. The ^{13}C NMR analysis revealed 17 carbon atoms compatible with the structure of the pentasubstituted cyclohexane derivative **1b**. Complete NMR data for **1b:** ^{1}H NMR (500 MHz, $CDCl_3$): $\delta = 4.78$ (1H, brs), 4.55 (1H, brs), 4.12 (2H, brq, $J = 7.2$ Hz), 4.09 (2H, q, $J = 7.2$ Hz), 2.10 (1H, ddd, $J = 13.9$, 6.3, 2.8 Hz), 2.03 (1H, dd, $J = 7.5$, 3.1 Hz), 2.03 (1H, dd, $J = 4.6$, 3.1 Hz), 1.87 (1H, dd, $J = 7.5$, 4.6 Hz), 1.86 (1H, ddd, $J = 13.9$, 11.2, 6.3 Hz), 1.64 (3H, s), 1.49 (1H, ddd, $J = 11.4$, 11.2, 6.3 Hz), 1.27 (1H, ddd, $J = 11.4$, 2.8, 6.3 Hz), 1.17 (3H, t, $J = 7.1$ Hz), 1.14 (3H, t, $J = 7.1$ Hz), 0.81 (3H, s), 0.78 ppm (3H, s); ^{13}C NMR (126 MHz, $CDCl_3$): $\delta =$ 172.86, 171.51, 146.83, 113.27, 61.67, 61.36, 55.95, 49.97, 39.19, 33.44, 32.77, 31.13, 27.46, 24.44, 20.44, 14.45, 14.41 ppm.
[23] See for example: R. Mook, P. M. Sher, *Org. Synth. Coll. Vol. VIII*, **1993**, 381 – 386.
[24] The participation of an ester group in cycloisomerizations has already been proposed: L. A. Goj, A. Cisneros, W. Yang, R. A. Widenhoefer, *J. Organomet. Chem.* **2003**, *687*, 498 – 507.
[25] As we could anticipate, the Sn(IV) catalyst system was unselective for the cyclization of simple dialkyl diallylmalonates. The reaction led preferentially to a mixture of isomeric unsaturated five-membered-ring compounds.
[26] NMR data for **9b** : ^{1}H NMR (500 MHz, $CDCl_3$): $\delta = 5.08$ (1H, s), 4.11 (4H, q, $J = 7.3$ Hz), 2.55 (2H, s), 2.14 (2H, m), 1.67 (3H, s), 1.48 (2H, m), 1.18 (6H, t, $J = 7.4$ Hz), 0.93 ppm (6H, s); ^{13}C NMR (126 MHz, $CDCl_3$): $\delta = 172.38$ (2C), 136.44, 130.28, 61.56 (2C), 57.06, 44.98, 36.10, 35.94, 30.27 (2C), 29.96, 28.14, 14.39 ppm (2C); NOESY $\delta = 5.08$ ppm correlates with $\delta =$ 0.93 ppm.
[27] For transition-metal-catalyzed intramolecular hydroarylation of alkenes, see for example: S. W. Youn, S. J. Pastine, D. Sames, *Org. Lett.* **2004**, *6*, 581 – 584.
[28] These alkene arylation reactions will be developed in a separate research project.
[29] a) Reaction conditions: 5 mol% Tf_2NH, nitromethane, 2.5 h at 25 °C. b) Reaction conditions: 5 mol% Tf_2NH, nitromethane, 5 h at 101 °C.
[30] J. J. Eisch, P. O. Otieno, K. Mackenzie, B. W. Kotowicz, *ACS Symp. Ser.* **2002**, 822, 88 – 103, CAN 137:294994 (Group 13 Chemistry).
[31] H. Yamamoto, K. Futatsugi, *Angew. Chem.* **2005**, *117*, 1958 – 1977; *Angew. Chem. Int. Ed.* **2005**, *44*, 1924 – 1942.
[32] We do not observe any reaction of **1a** with either concentrated HCl or *p*-toluene sulfonic acid in dichloroethane (60 °C, 3 h).
[33] I. J. S. Fairlamb, S. Grant, A. C. Whitwood, J. Whitthall, A. S. Batsanov, J. C. Collings, *J. Organomet. Chem.* **2005**, *690*, 4462 – 4477.
[34] a) B. M. Trost, *Acc. Chem. Res.* **2002**, *35*, 695 – 705; b) B. M. Trost, *Angew. Chem.* **1995**, *107*, 285 – 307; *Angew. Chem. Int. Ed. Engl.* **1995**, *34*, 259 – 281; c) B. M. Trost, *Science* **1991**, *254*, 1471 – 1477.

 © 2006 Wiley-VCH Verlag GmbH & Co. KGaA, Weinheim

Homogeneous Catalysis

DOI: 10.1002/anie.200602386

Aqueous-Phase Hydroformylation of 1-Octene: Styrene Latices as Phase-Transfer Agents**

*Katharina Kunna, Christian Müller, Joachim Loos, and Dieter Vogt**

The Co- and Rh-catalyzed hydroformylation of olefins to aldehydes has become one of the most important commercial applications of homogeneous catalysis. However, one of the major problems is the catalyst recovery from the reaction mixture. A commercial solution was applied in 1984 with the RCH/RP process,[1] which is an aqueous-phase hydroformylation that converts propene to *n*-butyraldehyde (ca. 0.8 Mt a^{-1}) and isobutyraldehyde in the presence of $[HRh(CO)(tppts)_3]$ (see Scheme 3 for tppts). The modified rhodium catalyst is dissolved in the aqueous phase, and propene is significantly soluble in water. Thus, the catalyst is recovered without any significant loss by separation of the organic product layer from the aqueous phase. However, the process is limited to olefins with short alkyl chains since the solubilities of olefins in water decrease with increasing number of carbon atoms, and the hydroformylation is therefore limited by the rate of mass transfer. Thus, higher olefins ($> C_6$) are not suited for the RCH/RP process.

Several approaches have been proposed in the literature for the hydroformylation of higher olefins. Examples include anchoring rhodium catalysts to resins, polymeric supports, or denrimers;[1a,2] the use of ligands with amphiphilic properties;[3] or performing the reaction in the presence of cyclodextrins,[4] calix[4]arenes,[4] cosolvents,[5] (CTAB) micelles,[6] or in ionic liquids.[7]

We report herein on the use of microsuspensions (also called microemulsions) as phase-transfer agents in the hydroformylation of 1-octene. Microsuspensions or latices are thermodynamically stable dispersions of submicron polymer particles in water. Latices are synthesized by microemulsion polymerization of suitable monomers or mixtures of monomers dispersed in water in the presence of a surfactant.

[*] Dipl.-Chem. K. Kunna, Dr. C. Müller, Prof. Dr. D. Vogt
Schuit Institute for Inorganic Chemistry and Catalysis
Eindhoven University of Technology
P.O. Box 513, 5600 MB Eindhoven (The Netherlands)
Fax: (+31) 40-245-5054
E-mail: d.vogt@tue.nl

Dr. J. Loos
Laboratory of Polymer Technology and Material and Interface Chemistry
Eindhoven University of Technology
5600 MB Eindhoven (The Netherlands)

[**] Prof. Dr. A. van Herk (TU/e) is gratefully acknowledged for helpful discussions. We thank A. J. P. M. Staring for technical assistance and Umicore for a generous gift of $[Rh(acac)(CO)_2]$. The Dutch National Research School Combination Catalysis (NRSCC) is gratefully acknowledged for financial support.

 © 2006 Wiley-VCH Verlag GmbH & Co. KGaA, Weinheim

Conventional latices consist of a lipophilic core of organic polymers and a hydrophilic surfactant, which provides charge stabilization to the colloidal dispersion. The size of the particles ranges from 4 to 100 μm, and their shape depends on the composition and type of surfactant, giving structures such as spheres, rods, or disks. The latex particles are stabilized by the hydrophilic surfactant, while the lipophilic core can absorb organic compounds.

We expect that these amphiphilic properties provide the possibility to use latices as phase-transfer agents in a biphasic hydroformylation of higher olefins using the water-soluble catalyst $[HRh(CO)(tppts)_3]$. Thus, the polystyrene-based latices **1a–c**[8] were prepared by free-radical polymerization (Scheme 1). All latices are composed of the amphiphilic

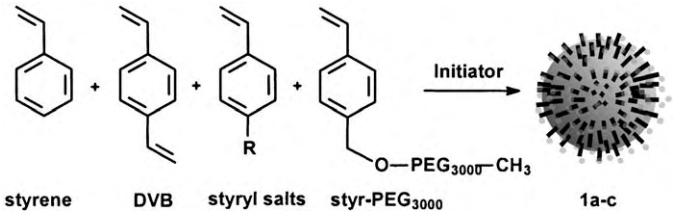

Scheme 1. Synthesis of polystyrene-based latices **1a** (R = H), **1b** (R = SO_3Na), and **1c** (R = $CH_2NMe_3BF_4$).

macromonomer styr-PEG_{3000} (polyethylene glycol) and the crosslinker DVB (divinylbenzene) as a stabilizing agent (Scheme 2). Produced in this way, the latices consist of a

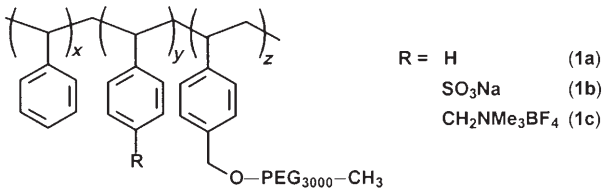

Scheme 2. The structures of the nonionic (**1a**), anionic (**1b**), and cationic (**1c**) latices (DVB part is omitted for clarity).

lipophilic core and a hydrophilic shell, and the only variation is the presence of different substituents R on the styryl groups. These specific structures are supposed to act as phase-transfer agents and transport the water-insoluble olefin into the water phase.

The hydrodynamic diameters (D_h) of the latex particles were calculated by means of transmission electron microscopy (TEM; Figure 1)[9] and dynamic light scattering (DLS).[10] The particle sizes that were measured with TEM were smaller than those measured with DLS,[11] which is most likely a result of shrinkage of the particles during sample preparation (Table 1).

The ability of the latices to act as phase-transfer agents was further investigated by means of partitioning experiments. In all cases a significant solubility of the organic compounds in the microsuspension was observed, while the latices preferably interacted with 1-octene instead of nonanal by a factor of 2.5.[12]

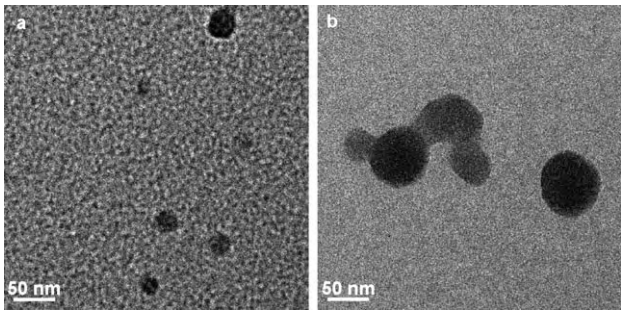

Figure 1. TEM images of latices **1a** (a) and **1b** (b).

Table 1: Diameters of the latex particles **1a–c**.

Sample	D_h [nm] (TEM)	D_h [nm] (DLS)[a]
1a	25 ± 3	302
1b	78 ± 2	273
1c	43 ± 5	218

[a] Measured at 25 °C.

Aqueous-phase hydroformylation experiments were carried out using the water-soluble catalyst system tppts/$[Rh(acac)(CO)_2]$ (Scheme 3; acac = acetylacetonate) and the

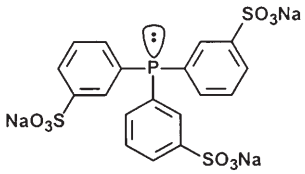

Scheme 3. The ligand tppts.

latices **1a–c** as phase-transfer agents. To gain insight into the kinetics of the hydroformylation reaction, gas uptake of CO/H_2 was measured automatically during the course of the reactions (Figure 2). Notably, the gas-uptake curves represent the conversion of 1-octene into aldehydes as no hydrogena-

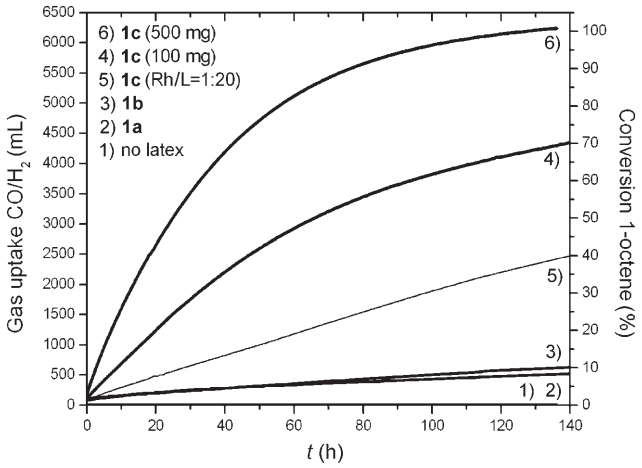

Figure 2. Gas uptake of CO/H_2 and conversion of 1-octene in the Rh(tppts)-catalyzed aqueous-phase hydroformylation of 1-octene.

 © 2006 Wiley-VCH Verlag GmbH & Co. KGaA, Weinheim

tion products (octane, alcohols) were observed as by-products. From the gas-uptake curves it is obvious that in all cases catalytic activity was observed in the presence of latex particles but that the different styryl salts had a dramatic influence on the conversion of 1-octene.

The organic phase was further analyzed by means of gas chromatography. The obtained yields of aldehydes are somewhat lower compared to the theoretical ones, owing to their solubility in the microsuspension. The results are summarized in Table 2. In the absence of any latex particles, the hydroformylation of 1-octene with CO/H_2 (1:1) in water using tppts/$[Rh(acac)(CO)_2]$ at 80 °C and 20 bar pressure showed no conversion at all (Table 2, entry 1). The addition of **1a** to the reaction mixture increased the conversion of 1-octene to 9% during the 140-hour reaction time (Table 2, entry 2), and addition of **1b** increased conversion to 11% (Table 2, entry 3). Interestingly, when the same reaction was carried out using **1c** as the phase-transfer agent (Table 2, entry 4), the conversion of 1-octene increased to 70%. By using a higher amount of latex as phase-transfer agent, the conversion of 1-octene increased to 100% with an observed turnover frequency of 150 h^{-1} (Table 2, entry 6). These results nicely demonstrate the mass-transfer limitation of the aqueous-phase hydroformylation of 1-octene.

Table 2: Rhodium-catalyzed aqueous-phase hydroformylation of 1-octene.[a]

Entry	Ligand + additive	Conversion [%][b]	Yield [%][c]	l/b[d]
1	tppts	–	–	–
2	tppts + **1a**	9.0	4.5	1.9
3	tppts + **1b**	11	7.38	2.0
4	tppts + **1c**	70	49	3.4
5	tppts + **1c**[e]	44	35	5.1
6	tppts + **1c**[f]	99	90	2.9

[a] Reaction conditions: 1-octene (150 mmol), tppts (0.21 mmol), [Rh(acac)(CO)$_2$] (0.035 mmol), water/organic phase 1:2.3, S/P/Rh 5000:6:1, latex (100 mg solid content), dodecane external standard (15 mmol), CO/H_2 1:1, $p = 20$ bar, $T = 80$ °C, $t = 140$ h, stirring rate 600 rpm. [b] Determined by gas uptake (see also Figure 2). [c] Determined by GC analysis; corresponds to yield of aldehyde in the organic phase. [d] Ratio linear/branched product. [e] tppts (0.71 mmol), Rh/L 1:20. [f] Latex (500 mg solid content).

The strikingly better performance of the ammonium-modified latex particle **1c** may be explained by a preferred association of the sulfonated catalyst complex with the ammonium groups of these latex particles, thereby associating the catalyst with the phase-transfer agent and thus enhancing the hydroformylation reaction.[6] This association might be described as a combination of electrostatic, van der Waals, and hydrophobic interactions. In fact, remarkable stable complexes of cationic ammonium substrates and polysulfonated host molecules have been observed before and are well documented in the literature.[13]

Further investigation of the product mixture revealed an l/b ratio of about 2, as expected for monodentate PR_3/Rh systems. To increase the linearity, the L/Rh ratio was increased from 6:1 to 20:1. In this way an l/b ratio of about 5 was obtained, along with a decrease in activity to 44% (Table 2, entry 5).

In summary, we investigated the possibility of polystyrene-based latices to act as phase-transfer agents in the aqueous-phase hydroformylation of 1-octene. It was thereby observed that the substituent R of the styryl salts has a significant influence on the conversion of 1-octene. Consequently these catalytic systems provide new options in the field of continuous aqueous organometallic catalysis. Further investigations on the use of higher olefins ($> C_8$) and on variations of both ligand and latex particles are currently being carried out.

Experimental Section

The ligand tppts and 1-octene were purchased from Aldrich and purified by flash chromatography (Al_2O_3); the latter was distilled over CaH_2 and degassed. The polystyrene-based latices were synthesized by emulsion polymerization of styrene as described below.

General preparation of polystyrene-based latices **1a–c**:[8] A solution of the internal styrene salt[14] (12 mmol) in degassed and deionized water (80 mL) was placed into an autoclave equipped with a mechanical stirrer. The solution was heated to 80 °C and stirred at 100 rpm. After the temperature was reached, styrene (49 mmol), divinylbenzene (1.85 mmol), and the initiator[15] (0.48 mmol) were added. The stirring rate was increased to 300 rpm. After 10 minutes the mixture became milky, indicating formation of the microsuspension. The macromonomer functional PEG_{3000}[16] (1.23 mmol) in water (20 mL) was added and the suspension was stirred for 4 h. During this process several samples were taken to measure the solid contents and consequently to monitor the conversion. Finally, the latex was cooled to room temperature and stored at 4 °C. The latices were purified by dialysis over 3–4 days by using a membrane with a pore size of 25–30 Å. In case of bigger particles, centrifugation was performed. The particles were analyzed by means of TEM and DLS.

General procedure for the aqueous-phase hydroformylation of 1-octene: The reactor was charged with water (11 mL), [Rh(acac)(CO)$_2$] (0.0356 mmol), tppts (0.21 mmol)[17], and latex (100 mg, 2 mL), giving a Rh/tppts ratio of 1:6. The catalyst was preformed at 0 °C and 20 bar CO/H_2 for 3 h at 600 rpm. Subsequently, the substrate 1-octene (150 mmol, Rh/S 1:5000) was added by a dropping funnel, and the conversion was measured by gas uptake of CO/H_2.[18] After 140 h the reaction was stopped by cooling the reactor to room temperature and venting. The organic layer was analyzed by gas chromatography on a PONA column (length 50 m, $d = 0.2$ mm, film 0.5 μm, J&W Scientific).

Received: June 14, 2006
Published online: October 9, 2006

Keywords: biphasic catalysis · hydroformylation · latices · microemulsion · polystyrene

[1] a) *Multiphase Homogeneous Catalysis* (Eds.: B. Cornils, W. A. Hermann, I. T. Horváth, W. Leitner, S. Mecking, H. Olivier-Bourbigou, D. Vogt), Wiley-VCH, Weinheim, **2005**, p. 166; b) P. W. N. M. van Leeuwen in *Homogeneous Catalysis—Understanding the Art* (Ed.: P. W. N. M. van Leeuwen), Kluwer, Amsterdam, **2004**; c) C. Claver, P. W. N. M. van Leeuwen in *Rhodium Catalyzed Hydroformylation* (Eds.: P. W. N. M. van Leeuwen, C. Claver), Kluwer, Amsterdam, **2000**.

 © 2006 Wiley-VCH Verlag GmbH & Co. KGaA, Weinheim

[2] T. Jongsma, H. Van Aert, M. Fossen, G. Challa, P. W. N. M. van Leeuwen, *J. Mol. Catal.* **1993**, *83*, 37 – 50.
[3] a) B. E. Hanson, H. Ding, C. W. Kohlpaintner, *Catal. Today* **1998**, *42(4)*, 421 – 429; b) B. Fell, G. Papadogianakis, *J. Mol. Catal.* **1991**, *66*, 143 – 154.
[4] S. Shimizu, S. Shirakawa, Y. Sasaki, C. Hirai, *Angew. Chem.* **2000**, *112*, 1313 – 1315; *Angew. Chem. Int. Ed.* **2000**, *39*, 1256 – 1259.
[5] P. Purwanto, H. Delmas, *Catal. Today* **1995**, *24*, 135 – 140.
[6] A. Rijsager, B. E. Hanson, *J. Mol. Catal. A* **2002**, *189*, 195 – 202.
[7] P. Wasserscheid, W. Keim, *Angew. Chem.* **2000**, *112*, 3926 – 3945; *Angew. Chem.* **2000**, *39*, 3772 – 3789.
[8] R. Sablong, J. I. van der Vlugt, R. Thomann, S. Mecking, D. Vogt, *Adv. Synth. Catal.* **2005**, *347*, 633 – 636.
[9] TEM experiments were performed on a Fei Tecnai 20 after deposition and drying a droplet of the latex dispersion on a carbon-coated copper grid.
[10] DLS experiments were performed on a Malvern 4700 DLS Particle-Size Analyzer.
[11] C. Yi, Z. Zu, *J. Appl. Polym. Sci.* **2005**, *96*, 824 – 828.
[12] A mixture of 1-octene and *n*-nonanal was treated with an aqueous latex suspension under hydroformylation conditions, and the distribution between the phases was determined by GC analysis (external standard: dodecane). Furthermore, the stability of the microsuspension was tested at different temperatures and stirring rates. Optimal conditions without any significant coagulation were found at 80 °C and 600 rpm.
[13] See, for example: C. Bonal, Y. Israëli, J. Morel, N. Morel-Desrosiers, *J. Chem. Soc. Perkin Trans. 2* **2001**, 1075 – 1078.
[14] **1a**: no styryl salt; **1b**: sodium 4-vinylbenzylsulfonate; **1c**: 4-vinylbenzyltrimethylammonium tetrafluoroborate.
[15] **1a**: VA-086 (2,2′-azobis[2-methyl-*N*-(2-hydroxyethyl)]propionamide); **1b**,**c**: V-50 (2,2′-azobis(2-methylpropionamide) dihydrochloride).
[16] 4-Vinylbenzylstyrene PEG_{3000} was synthesized according to: K. Ito, S. Yokoyama, F. Arakawa, Y. Yukawa, T. Iwashita, Y. Yamasaki, *Polym. Bull.* **1986**, *16*, 337 – 344.
[17] 0.71 mmol tppts were used in Table 2, entry 5.
[18] Calibration of CO/H_2 [mL] was performed by hydroformylation of 1-octene using Sixantphos/[$Rh(acac)(CO)_2$] catalyst in toluene.

 © 2006 Wiley-VCH Verlag GmbH & Co. KGaA, Weinheim

Shielding Tensors of Benzene

DOI: 10.1002/anie.200601557

Proton Magnetic Shielding Tensors in Benzene—From the Individual Molecule to the Crystal**

Thomas Heine, Clémence Corminboeuf, Gisbert Grossmann, and Ulrich Haeberlen*

It may be surprising that in 2006, almost 200 years after the discovery of benzene, the proton shielding tensor in the solid phase of this important compound is still unknown. There is interest in computing this quantity for three reasons. First, benzene is *the* prototype of an aromatic system. Second, its experimental determination, which requires a single-crystal sample and a measurement temperature below 40 K,[1] is presently close to impossible. An early line-narrowing multiple-pulse NMR experiment using a powder sample in the year 1977 did not lead to definitive conclusions.[2] Third, the individual molecule proton shielding tensors are, effectively, not measurable quantities because in both single-crystal and powder samples the proton nuclear magnetic shielding tensors, and particularly their anisotropy, are strongly affected by the surrounding molecules. For all nuclei other than hydrogen this influence, based on aromatic ring currents, is usually negligible.[3]

The X-ray structure of benzene[4] possesses three crystallographically distinct protons. A consequence is that there are three different proton shielding tensors instead of only one. Our computations show that the differences between the three tensors are significant enough to render illusionary any detailed interpretation of a proton NMR powder spectrum. If calculated proton shielding tensors are ever to be compared with experimental results, the calculations must include the environment of the molecule considered. Herein, we show that this can be done relatively easily for van der Waals

[*] Dr. T. Heine, Prof. Dr. G. Grossmann
Fachbereich Chemie
Technische Universität Dresden
01062 Dresden (Germany)
Fax: (+49) 351-463-35953
E-mail: thomas.heine@chemie.tu-dresden.de
Homepage: http://theory.chm.tu-dresden.de/~theine
Dr. C. Corminboeuf[+]
Département de chimie physique
Université de Genève
1211 Genève 4 (Switzerland)
Prof. Dr. U. Haeberlen
Max-Planck-Institut für Medizinische Forschung
Jahnstrasse 29, 69120 Heidelberg (Germany)
[+] Current address:
Center for Computational Chemistry
University of Georgia
Athens, Georgia 30602-2556 (USA)

[**] We thank Prof. G. Seifert for continuous support.

Supporting information for this article is available on the WWW under http://www.angewandte.org or from the author.

WILEY InterScience DISCOVER SOMETHING GREAT
© 2006 Wiley-VCH Verlag GmbH & Co. KGaA, Weinheim

crystals and that this spherically shaped environment must be extended to a radius of at least 20 Å. In an analogous way, we have recently investigated the ^{1}H NMR shielding tensors of biphenyl,[1] which is a close relative to benzene. For biphenyl, our theoretical results could be demonstrated to agree within 0.5 ppm or better with the values obtained from direct multiple-pulse experiments. We are confident that the computations herein also reflect reality with the same level of accuracy.

To assess the ^{1}H NMR shielding tensors in benzene, clusters of spherical shape were constructed around the center

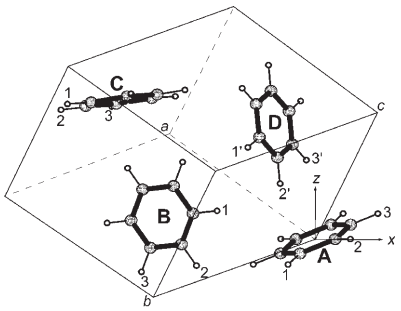

Figure 1. Unit cell of benzene, transformed to the position and orientation of ring **A** as given in Figure 3. The labelling of the protons is indicated. The rings **A**, **B**, and **D** are shown in the lattice position 0,0,0 whereas the ring **C** is in the 1,0,0 cell. The molecules occupy sites with inversion symmetry, thus resulting in identical shielding tensors of primed and unprimed hydrogens. Further details are given in Figures S1 and S2 and Tables S1 and S2.

of molecule **A** (Figure 1). The geometry of the individual molecules was optimized,[5–7] while the positions and orientations of the molecules within the unit cell were taken from the X-ray structure.[4a] Only the intermolecular interactions within the first neighboring shells show a sizeable effect on the electronic properties. On the other hand, the magnetic field associated with the benzene ring current results in a long-range shielding cone around the molecular C_6 axis, which has a considerable effect on the hydrogen nuclei of the surrounding molecules.[8] As illustrated in Figure 1, the H2′ site of molecule **D** is located directly in the shielding cone of molecule **A**, and a strong shift of its shielding to higher values is expected (see also Table S2).

The induced magnetic field at the position of a nucleus $\vec{r} = \vec{R}$ [$\vec{B}_{\mathrm{ind}}(\vec{R})$] is related to the applied homogeneous field $\vec{B}_{\mathrm{ext}}$ through the shielding tensor $\sigma_{\alpha\beta}$ [Eq. (1)]. Equation (1) is

$$(\vec{B}_{\mathrm{ind}}(\vec{R}))_\alpha = -\sum_{\beta=1}^{3} \sigma_{\alpha\beta}(\vec{R})\,(\vec{B}_{\mathrm{ext}})_\beta \qquad (1)$$

not restricted to nuclear positions $\vec{R}$, but holds at any position $\vec{r}$ in space.[8a,d,f] In the case of phenyl rings, $\vec{B}_{\mathrm{ind}}(\vec{r})$ is not negligible even at distances of 20 Å.[1,8c,e]

A direct calculation of $\sigma_{\alpha\beta}$ for a benzene cluster of this size, with 293 molecules and about 58000 basis functions, is not feasible with our present computational facilities. Therefore, we applied the following approximation to account for the long-range interactions. First, we calculated the shielding tensors of the protons of the central molecule in a cluster containing 17 benzene molecules, thereby encompassing all molecules in a sphere of 7.5-Å radius (Figure S2). As the electronic interactions between the central molecule and those of the second neighboring shell and beyond are negligible, we took into account the long-range contributions of the remaining molecules of the crystal by using the superposition scheme given in Equations (2) and (3). The

$$\vec{B}_{ind} = \underbrace{\vec{B}^0_{ind}}_{\text{short range}} + \underbrace{\sum_i \vec{B}^i_{ind}}_{\text{long range}} \qquad (2)$$

$$\sigma_{\alpha\beta} = \underbrace{\sigma^0_{\alpha\beta}}_{20-30\,\text{ppm}} + \underbrace{\sum_i \sigma^i_{\alpha\beta}}_{<0.3\,\text{ppm}} + \underbrace{O\left(\frac{\left|\vec{B}^{i\neq 0}_{ind}\right|}{\left|\vec{B}_{ext}\right|}\right)}_{\approx 10^{-6}\,\text{ppm}} \qquad (3)$$

index i runs over all individual molecules of the sphere except those which are included in the short-range region. In Equation (3), the intrinsic error of this approximation is negligible.

This approach has been tested thoroughly for clusters of biphenyl by direct computation and comparison with experiment.[1] A similar approach has been followed by Pecul and Sadlej for C_2H_2.[9] It is important to note that this approximation holds only if all neighbors that influence the electronic structure of the central molecule are explicitly included in the short-range term (see Table S3). These influences can arise from through-bond interactions, as laid out by Caramori et al.[10] (see the Supporting Information, particularly Table S4), but also from through-space electrostatic interactions (Martin et al.[11]). A further source of error stems from the interactions between individual ring currents, potentially accounting for errors of up to 5% *if a short-range domain that is too small is chosen*. In detail, for a single benzene molecule in the short-range region of a cluster containing 17 benzene molecules, we found a maximum difference of 1.15 ppm compared to the full calculation. This error is reduced to 0.65 ppm if the four next neighbors are included in the explicit calculation (Table S3). To avoid this source of error, we chose a rather large radius of 7.5 Å for the short-range environment (Table S5).

We calculated the individual contributions to the shielding tensor according to Equations (1) and (2) by using the IGLO method[12] within density functional perturbation theory.[13] In detail, we applied a gradient-corrected exchange correlation potential[14] and the IGLO-III basis set[12b] and employed the deMon[15] and deMon-NMR[13b] computer programs. This choice was found to yield results that agree satisfactorily with computations employing the more common GIAO method at the DFT and MP2 levels (Table S6).[16] Spherical clusters of increasing radii $R = 0 \ldots 72$ Å were constructed. They include all benzene molecules with an intercenter distance of $r_{cc} \leq R$ to the molecule at the origin and contain 1 ($R = 0$), 5 ($R =$ 5 Å), 17 ($R = 7.5$ Å), 293 ($R = 20$ Å), 2277 ($R = 40$ Å), and 13445 ($R = 72$ Å) benzene rings, respectively. It should be noted that the treatment differs for $r_{cc} \leq 7.5$ Å and $r_{cc} > 7.5$ Å; see Equations (2) and (3).

 © 2006 Wiley-VCH Verlag GmbH & Co. KGaA, Weinheim

In the isolated molecule, the three protons are equivalent and have identical shieldings σ_M; the calculated isotropic value is 23.53 ppm and the principal components σ_{11}, σ_{22}, σ_{33} are 20.67, 23.45, and 26.48 ppm, respectively. These values are expected to be overestimated by 0.05–0.60 ppm owing to inherent errors, that is, because of the choice of Gaussian-type basis functions, incompleteness of basis sets, errors in the IGLO DFT methods, and neglect of rovibrational corrections. This estimate was obtained by comparing experimental ^{1}H NMR chemical shielding constants of small molecules in the gas phase (H_2O, CH_4, C_2H_2, and C_2H_4)[17] with calculated values using the computational parameters of the present study.

The same quantities for a cluster containing 13445 molecules ($R = 72$ Å) are given in Table 1. The crystal environment provides an additional contribution to the isotropic shielding. This contribution ranges from 0.10 ppm for H1 up to 1.80 ppm for H2. The three shifts span an overall range of 1.70 ppm, which is more than 15% of the whole NMR scale for protons in organic molecules. As expected, a particularly strong influence of the crystal is observed for H2 because of the special location of a neighbor molecule. The shielding contribution of the next neighbor to H2 is as large as 2.16 ppm, which is even larger than that of the whole crystal. These numerical values are in accordance with the ab initio calculations by Jusélius and Sundholm for the ring current of benzene.[8e] Intermolecular contributions of similar magnitude to ^{1}H NMR chemical shifts have previously been observed for hexabenzocoronene.[18]

Table 1: Isotropic shielding σ_{iso} and principal shielding components σ_{11}, σ_{22}, σ_{33} of the distinct protons H1, H2, and H3 in a spherical cluster of benzene with $R = 72$ Å; see also Table S5.

	H1 [ppm]	H2 [ppm]	H3 [ppm]
σ_{iso}	23.63	25.33	23.76
σ_{11}	21.03	20.67	19.97
σ_{22}	22.77	24.34	22.96
σ_{33}	27.08	30.99	28.35

As expected from previous single-molecule calculations,[16c] the direction perpendicular to the plane is the least shielded (20.67 ppm). In contrast to the gas-phase results, the C–H bond is identified as the intermediate principal axis of proton shielding (23.45 ppm). The influence of the crystal environment becomes particularly spectacular when shielding *tensors* are compared (Tables 1 and S5). The strongest influence of the crystal was found for σ_{33} of H2, which is shielded by an additional amount of 4.51 ppm in comparison to the single molecule. The span of the principal components σ_{33}–σ_{11} changes from 5.81 ppm in the isolated benzene molecule to 6.05 ppm, 10.32, and 8.38 ppm in the crystal environment for H1, H2, and H3, respectively. Again, the influence is largest for H2.

Figure 2 demonstrates that a benzene cluster with a radius of 20 Å is sufficient to properly account for the intermolecular shielding contributions. The isotropic values (solid lines) show a slightly better convergence than the root-mean-square distances of the icosohedral components[19] (broken lines) that are defined by Equation (4).

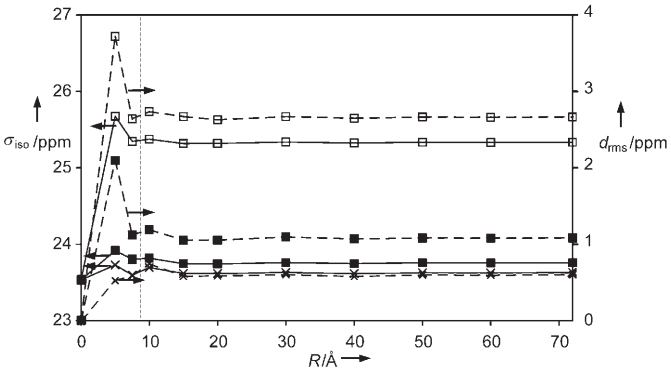

Figure 2. Isotropic shieldings σ_{iso} (solid lines) and root-mean-square distances d_{rms} (dashed lines) of the icosahedral tensor components [see Eq. (4)] as a function of the cluster radius R for the three distinct hydrogen atoms in solid benzene: H1 (×), H2 (□), and H3 (■). The arrows indicate which scale applies. All values to the left of the vertical dotted line correspond to full quantum chemical calculations. See also Table S7 and Figures S4–S7.

$$d_{rms} = \sqrt{\sum_{i=1}^{6} \frac{\sigma_{i,R} - \sigma_{i,R=0}}{6}} \qquad (4)$$

Figure 3 shows the change in magnitude and orientation of the shielding tensors that result from the influence of the intermolecular contributions in the pictorial representation of tensors from Radeglia,[20] where the shielding tensor is drawn as an ovaloid. We have represented the protons H1, H2, and H3 in equivalent space positions for all ovaloids. In the case of the isolated molecule, the ovaloids for all protons have the same shape (top row of Figure 3). The very different magnitude and orientation of the intermolecular contributions for the three protons are shown in the center row of this figure. In the bottom row, the shielding tensors of the three protons in the crystal are depicted and represent the sum of the upper two rows. The shape and axis directions are clearly different from each other and from the tensor of the isolated molecule. The most remarkable changes are observed for H2. A consequence of these findings is that low-temperature spectra from samples of benzene powder will inevitably reflect the superposition of the powder line shapes from three significantly different tensors.

In conclusion, the benzene proton shielding tensors have been evaluated for the first time in their crystal environment. We demonstrated that in benzene the intermolecular contributions are an essential part of the proton shielding. The isotropic shieldings of the three distinct protons are modified by as much as 1.7 ppm by the crystal environment and are increased on average by 0.71 ppm. The anisotropy of the shielding tensor is increased from 5.81 to 10.32 ppm for H2. The H2 site is subject to the strongest intermolecular interaction as it is located directly in the shielding cone of a neighboring benzene molecule. Its principal component σ_{33} is shifted by an additional amount of 4.51 ppm with a dominat-

 © 2006 Wiley-VCH Verlag GmbH & Co. KGaA, Weinheim

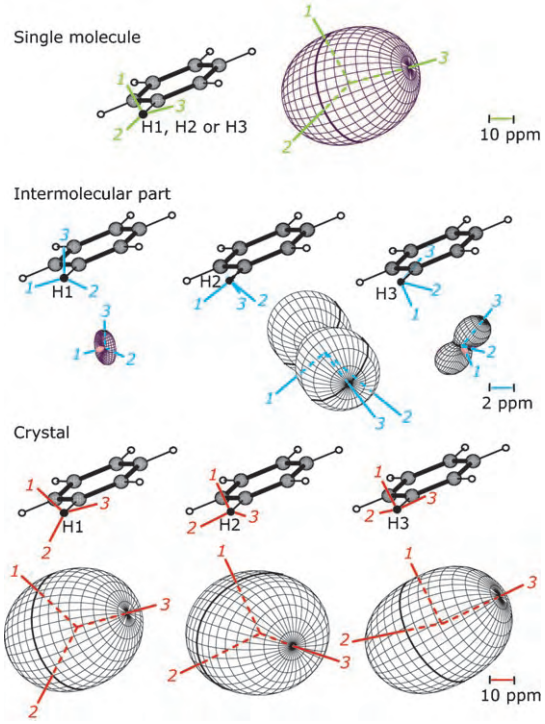

Figure 3. Ovaloid representation[20] of the proton nuclear shielding tensors H1, H2, and H3 of benzene. The principal components of shielding tensors are proportional to the lengths of the principal axes of the ovaloids shown. Red lines indicate negative shielding values; *1*, *2*, and *3* indicate the least, intermediate, and most shielded principal axes, respectively.

ing contribution from the direct neighbor. This observation is in line with a former calculation of the induced magnetic field around a benzene molecule.[8c,e]

The results of this work are in line with Wüthrich's suggestion of employing ^{1}H NMR chemical shifts of proteins to determine their conformation, as well as with developments of Brown and Spiess on the dynamics and structure of polymers.[21] We expect significant contributions to proton NMR data in biological molecules containing aromatic rings, such as the side chains of histidine and tryptophan. In a forthcoming paper we will discuss in more detail the inclusion of the intermolecular effects, both by straight quantum chemical calculation and by employing a semiempirical model.[22]

Received: April 20, 2006
Revised: July 31, 2006
Published online: September 20, 2006

Keywords: benzene · density functional calculations · intermolecular shielding · NMR spectroscopy · shielding tensors

[1] F. Schönborn, H. Schmitt, H. Zimmermann, U. Haeberlen, C. Corminboeuf, G. Grossmann, T. Heine, *J. Magn. Reson.* **2005**, *175*, 52.
[2] L. M. Ryan, R. C. Wilson, B. C. Gerstein, *J. Chem. Phys.* **1977**, *67*, 4310.
[3] D. Sitkoff, D. A. Case, *Prog. Nucl. Magn. Reson. Spectrosc.* **1998**, *32*, 165.
[4] a) V. M. Kozhin, *Zh. Fiz. Khim.* **1954**, *28*, 566; b) E. G. Cox, D. W. J. Cruickshank, J. A. S. Smith, *Proc. R. Soc. London Ser. A* **1958**, *247*, 1.
[5] The individual molecule has been optimized at the B3LYP/6-311 + G** level as implemented in Gaussian 03 (reference [7]).
[6] a) A. D. Becke, *J. Chem. Phys.* **1993**, *98*, 5648; b) C. Lee, W. Yang, R. G. Parr, *Phys. Rev. B* **1988**, *37*, 785; c) P. J. Stephens, F. J. Devlin, C. F. Chabalowski, M. J. Frisch, *J. Phys. Chem.* **1994**, *98*, 11623; d) R. Krishnan, J. S. Binkley, R. Seeger, J. A. Pople, *J. Chem. Phys.* **1980**, *72*, 650; e) T. Clark, J. Chandrasekhar, P. von R. Schleyer, *J. Comput. Chem.* **1983**, *4*, 294.
[7] Gaussian 03 (Revision B.03): M. J. Frisch et al., see the Supporting Information.
[8] a) C. E. Johnson, F. A. Bovey, *J. Chem. Phys.* **1958**, *29*, 1012; b) S. Klod, E. Kleinpeter, *J. Chem. Soc. Perkin Trans. 2* **2001**, 1893; c) G. Merino, T. Heine, G. Seifert, *Chem. Eur. J.* **2004**, *10*, 4367; d) T. Heine, C. Corminboeuf, G. Seifert, *Chem. Rev.* **2005**, *105*, 3889; e) J. Jusélius, D. Sundholm, *Phys. Chem. Chem. Phys.* **1999**, *1*, 3429; f) Z. Chen, T. Heine, P. von R. Schleyer, D. Sundholm in *Calculation of NMR and EPR Parameters: Theory and Applications* (Eds.: M. Kaupp, M. Bühl, V. G. Malkin), Wiley-VCH, Weinheim, **2004**, pp. 395–408.
[9] M. Pecul, J. Sadlej, *Chem. Phys.* **1999**, *248*, 27.
[10] G. F. Caramori, S. E. Galembeck, K. K. Laali, *J. Org. Chem.* **2005**, *70*, 3242.
[11] N. H. Martin, J. D. Brown, K. H. Nance, H. F. Schaefer, P. von R. Schleyer, Z. X. Wang, H. L. Woodcock, *Org. Lett.* **2001**, *3*, 3823.
[12] a) W. Kutzelnigg, *Isr. J. Chem.* **1980**, *19*, 193; b) W. Kutzelnigg, U. Fleischer, M. Schindler in *NMR Basic Principles and Progress*, *Vol. 23* (Eds.: P. Diehl, E. Fluck, H. Günther, R. Kosfeld, J. Seelig), Springer, Heidelberg, **1990**, pp. 165–262.
[13] a) W. Bieger, G. Seifert, H. Eschrig, G. Grossmann, *Chem. Phys. Lett.* **1985**, *115*, 275; b) V. G. Malkin, O. L. Malkina, D. R. Salahub, *Chem. Phys. Lett.* **1993**, *204*, 80.
[14] J. P. Perdew, K. Burke, M. Ernzerhof, *Phys. Rev. Lett.* **1996**, *77*, 3865.
[15] deMon: A. M. Köster, G. Geudtner, A. Goursot, T. Heine, A. Vela, S. Patchkovskii, D. R. Salahub, NRC, Canada, **2002**.
[16] a) R. Ditchfield, *Mol. Phys.* **1974**, *27*, 789; b) J. Gauss, *Chem. Phys. Lett.* **1992**, *191*, 614; c) K. Wolinski, J. F. Hinton, P. Pulay, *J. Am. Chem. Soc.* **1990**, *112*, 8251; d) *Calculation of NMR and EPR Parameters: Theory and Applications* (Eds.: M. Kaupp, M. Bühl, V. G. Malkin), Wiley-VCH, Weinheim, **2004**.
[17] a) D. K. Hindermann, C. D. Cornwell, *J. Chem. Phys.* **1968**, *48*, 4148; b) L. Petrakis, C. H. Sederholm, *J. Chem. Phys.* **1961**, *35*, 1174.
[18] C. Ochsenfeld, S. P. Brown, I. Schnell, J. Gauss, H. W. Spiess, *J. Am. Chem. Soc.* **2001**, *123*, 2597.
[19] D. W. Alderman, M. H. Sherwood, D. M. Grant, *J. Magn. Reson. Ser. A* **1993**, *101*, 188.
[20] R. Radeglia, *Solid State Nucl. Magn. Reson.* **1995**, *4*, 317.
[21] a) K. Wüthrich, *Angew. Chem.* **2003**, *115*, 3462–3486; *Angew. Chem. Int. Ed.* **2003**, *42*, 3340–3363; b) S. P. Brown, H. W. Spiess, *Chem. Rev.* **2001**, *101*, 4125.
[22] a) K. Osapay, D. A. Case, *J. Am. Chem. Soc.* **1991**, *113*, 9436; b) S. S. Wijmenga, M. Kruithof, C. W. Hilbers, *J. Biomol. NMR* **1997**, *10*, 337.

 © 2006 Wiley-VCH Verlag GmbH & Co. KGaA, Weinheim

Rotaxanes

DOI: 10.1002/anie.200602002

Bridging Rotaxanes' Wheels—Cyclochiral Bonnanes**

*Motkuri Radha Kishan, Amir Parham, Frauke Schelhase, Albena Yoneva, Gabriele Silva, Xiaoming Chen, Yoshio Okamoto, and Fritz Vögtle**

Dedicated to Professor Heinz A. Staab on the occasion of his 80th birthday

The creation of molecules with exotic architectures and useful functions is an area that continues to stimulate the imagination of synthetic chemists.[1] To this end, rotaxanes have gained interest in recent years particularly because of their demonstrated potential design for nanomachines, bistable switches, molecular motors, and molecular vehicles.[2] Although considerable progress has been made in the synthesis of rotaxanes,[3] chemical reactions on rotaxanes themselves have so far not been extensively examined, possibly as a result of the limited availability of functional groups in the earlier rotaxane types synthesized by the groups of Lüttringhaus and Schill,[4] Sauvage,[5] Stoddart,[6] and others.[7] However, newer rotaxanes[8,9] in which carbonamide or sulfonamide groups have been purposefully introduced in the wheel or axle open the conceivable employment of rotaxanes for further preparative chemistry, including our long-time goal of covalently bonding two wheels of a higher [*n*]rotaxane.

By applying our efficient hydrogen-bond-templated threading method,[10] we have achieved the first successful synthesis of the amide-based diastereomeric [3]rotaxanes[11] and [4]rotaxanes[12] which contain two and three achiral wheels as well as the first bridging of two sulfonamide wheels by a long-chain tether. This bridging yields a new cyclochiral architecture,[13] which we would like to name "bonnane",[14] the simplest member of a new interlocked species with both mechanical and covalent bonding elements based on architectural features of rotaxanes. The higher acidity of the sulfonamide group compared to the carbonamide protons in the wheel permits a selective deprotonation and then an alkylation for attaching a tether between the two wheels. This tether leads to an added complexity of rotaxanes and offers a way towards new functionality owing to the tunable intramolecular nanometric movements of such bonnanes. Like in the [1]rotaxane series,[15] bonnanes are attractive candidates for studying structure/chirality relations in large molecules that allow correlated nanoscale translational and rotational movements. We had already coined the name "bonnane" some time ago;[13,16] at that time, we had carried out the synthesis on a milligram scale and proven the existence of traces of bonnane **11A** by mass spectrometry. But its tedious synthetic procedure, isolation in pure form, and further enantioseparation could not be completed, mainly because the earlier chromatographic chiral stationary phases (CSP) were not efficient enough. Only after the appearance of a new generation of Chiralpak IA[18] (immobilized CSP) stationary phases, we were able to perform the enantioseparation owing to the favorable solubility and mobility properties in lipophilic mobile phases.

The synthesis of the intermediate rotaxanes was successfully carried out on a preparative scale by the reaction of stilbene diacid dichloride **3** with the (elongated) stopper building block **2** in the presence of the sulfonamide wheel **1** in dry chloroform at −3 °C in an inert atmosphere, whereby a mixture of the [2]rotaxane **5** (55 mg, 6.4 %), [3]rotaxane **6** (51 mg, 4.0 %), [4]rotaxane **7** (20 mg, 1.2 %), and axle **4** (60 mg, 13.0 %) resulted (Scheme 1). After careful and repetitive column chromatography (SiO_2, 63–100 mesh), the excess unreacted wheel **1** and stopper **2** could be recovered by using an eluent mixture of dichloromethane/*n*-hexane/ethyl acetate/acetone (9:7:2:1). For further separation of rotaxanes **5**–**7** we used either a mixture of dichloromethane/*n*-hexane/ethyl acetate/ethanol (9:7:2:0.5) or tetrahydrofuran/*n*-hexane/ethanol (9.5:7:0.5).

For bridging the wheels of the [3]rotaxane **6**, we considered three types of linkers: 1,10-diiododecane (**8**) with an aliphatic chain, the more conformationally rigid dibromide bis(4-bromomethylphenyl)methane (**9**), and the functional glycol ether 1,2-bis(2-iodoethoxy)ethane (**10**). Thus [3]rotaxane **6** was then subjected to the coupling of the two sulfonamide wheels in DMF in the presence of K_2CO_3 to yield the corresponding cyclochiral[13] bonnanes **11A**–**C**[17] with remarkably high yields of 65–90 % (Scheme 2) after column chromatography. The high yields are a result of the restricted mobility of the wheel's reaction centers and their confined arrangement on one and the same axle. Because of high dilution of the reaction mixture, not even traces of dimer formation were detected (MALDI-TOF).

The new rotaxanes **5**–**7** and bonnanes **11A**–**C**[17] were thoroughly characterized by MALDI-TOF and NMR spectroscopy (see the Experimental Section). The ^{1}H NMR spectra of bonnanes **11A** and **11B** in [D_7]DMF show the

[*] Dr. M. Radha Kishan, Dr. A. Parham, Dr. F. Schelhase, A. Yoneva, G. Silva, Prof. Dr. F. Vögtle
Kekulé-Institut für Organische Chemie und Biochemie
Universität Bonn
Gerhard-Domagk-Strasse 1, 53121 Bonn (Germany)
Fax: (+49) 228-735-662
E-mail: voegtle@uni-bonn.de
Homepage: http:/www.chemie.uni-bonn.de/oc/ak_vo/
Dr. X. Chen, Prof. Y. Okamoto
EcoTopia Science Institute
Nagoya University
Furo-cho, Chikusa-ku, Nagoya 464-8603 (Japan)

[**] Financial assistance from the EC Program CERC3 ("Topological Chiral Hybrids", from 2000 to 2004) and by the Deutsche Forschungsgemeinschaft (Sonderforschungsbereich 624, "Templates") is gratefully acknowledged. M.R.K. thanks the Alexander von Humboldt Foundation for a fellowship. We also thank Dr. J. Brüggemann and Dr. R. G. Henkel for recording MALDI-TOF mass spectra as well as Dr. J. van Heijst (Universität Bonn) and Dr. Oleg Lukin (ETH Zürich) for valuable discussions.

Supporting information for this article is available on the WWW under http://www.angewandte.org or from the author.

 InterScience © 2006 Wiley-VCH Verlag GmbH & Co. KGaA, Weinheim

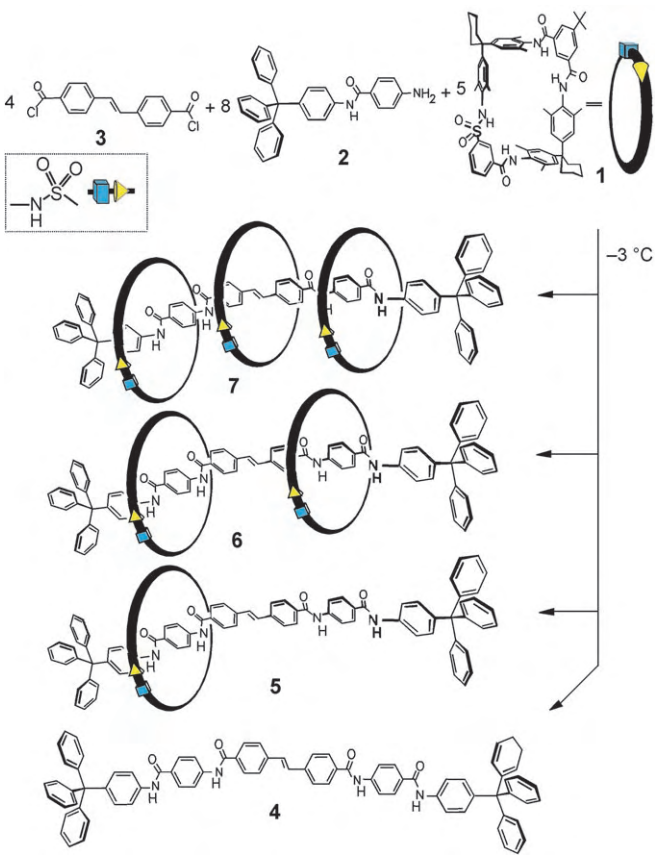

Scheme 1. Synthesis of [2]rotaxane **5** (6.4%), diastereomeric [3]rotaxane **6** (4.0%), and [4]rotaxane **7** (1.2%), along with free axle **4** (13.0%).

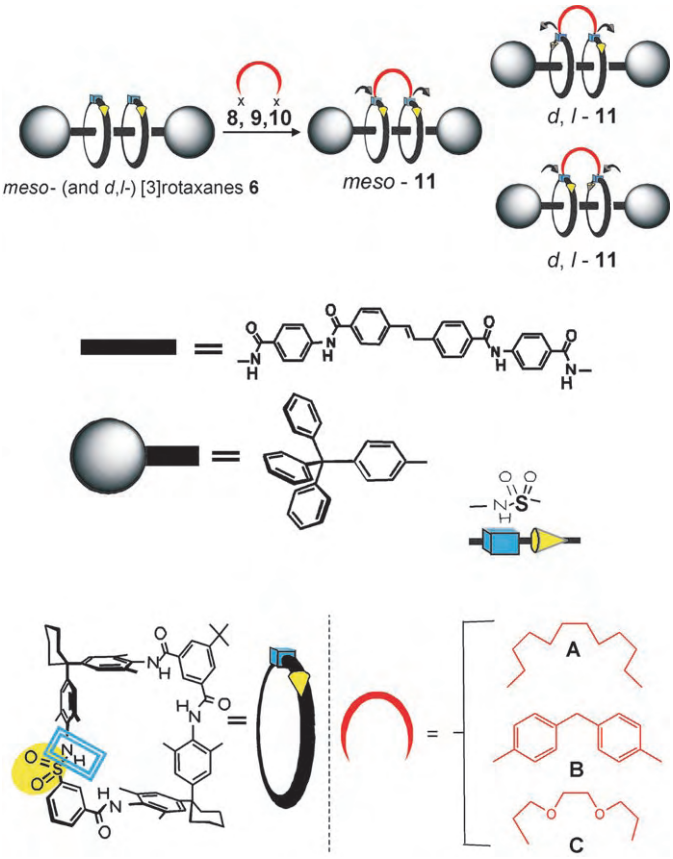

Scheme 2. Synthesis of bonnanes as a pair of cyclochiral enantiomers (*d*,*l*-**11**) and as *meso*-**11**.

amide signal pattern that is typical for the rotaxanes reported by us.[8]

As there is only one wheel in [2]rotaxane **5**, there is no possibility of stereoisomerism. But [3]- and [4]rotaxanes **6** and **7** with two or three wheels on an achiral axle result in cyclochirality.[13] In [3]rotaxane **6** a pair of enantiomers and a *meso* form exist, whereas in [4]rotaxane **7** a pair of enantiomers and a pair of *meso* forms are present. For comparison with the bonnane, we have also examined the hitherto unknown chiral separation of [3]rotaxane **6** by HPLC by using a commercial analytical chiral column (Chiralpak AD), and the corresponding CD spectra of the *d*,*l* enantiomers are shown in Figure 1.

Our initial efforts for the enantioseparation of bonnanes **11A** and **11B** under analogous conditions however yielded no chiral separation. Yet our recent efforts with the chiral stationary phase (CSP) Chiralpak IA[18] resulted in the successful chiral separation of bonnane **11A**. Its HPLC separation with *n*-hexane/ethanol/dichloromethane (75:20:5) with CD detection of the corresponding *d*,*l* enantiomers and UV detection of the *meso* form is shown in the Supporting Information. The CD spectra of the separated enantiomers give mirror-symmetrical Cotton effects (Figure 2), which confirm the purity of the enantiomers and by UV detection of the CD-inactive *meso* form. For further confirmation of the purity of the enantiomers, we then subjected the separated

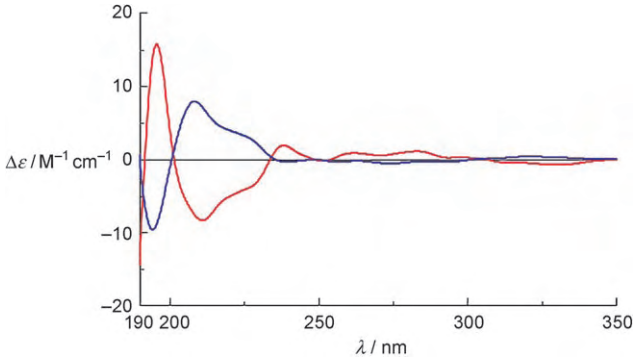

Figure 1. CD spectra of the cyclochiral enantiomers of [3]rotaxane **6**. Solvent: *n*-hexane/ethanol (80:20).

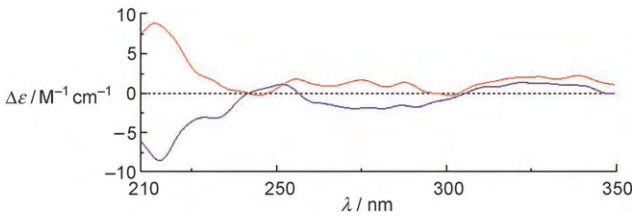

Figure 2. CD spectra of the enriched cyclochiral enantiomers of bonnane **11A**. Solvent: *n*-hexane/ethanol (80:20). The curves are impaired by incomplete HPLC separation and low solubility in UV-transparent solvents.

© 2006 Wiley-VCH Verlag GmbH & Co. KGaA, Weinheim

fractions to HPLC with the same eluent system and correlated them with the bonnane mixture **11A**, as shown in Figure 3.

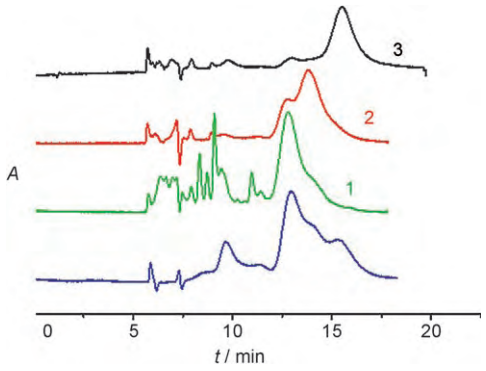

Figure 3. HPLC chromatogram of bonnane **11A** (blue) with the separated fractions of *meso* form (curve 1, green) *d*,*l* enantiomers [curves 2 (red) and 3 (black)]. Impurities (between 5 and 10 minutes) could easily be removed. Column: Chiralpak IA; eluent: *n*-hexane/ethanol/dichloromethane (80:20:4), flow rate = 0.5 mL min^{-1}, UV absorbance at $\lambda = 312$ nm.

The circular dichroism of the bonnane **11A** (Figure 2) clearly shows the enantiomers, for which the (cyclo)chirality stems from the orientation of the wheels on the axle as defined by the clockwise or counterclockwise sequence of the sulfonamide group relative to the amide groups. If the orientation is in the same direction, *meso*-**11** is obtained, and opposing directions of the wheels lead to *d*- and *l*-**11**. We expected the stereoisomers formed to be near the statistical ratio of *meso*/*d*/*l* = 2:1:1.

The wheels in [3]rotaxane are free to rotate separately on the axle, and as a result the chirality is pronounced, as earlier observed for catananes, pretzelanes, [1]rotaxanes, and trefoil knots of the amide type.[13,15] But in the bonnane, the bridge between the wheels leads to a certain fixation and correlation of wheel movement, which results in detectable, though not drastic, effects with regard to circular dichroism (Figures 1 and 2).

The successful synthesis of amide-based cyclodiastereomeric rotaxanes (*d*,*l*, *meso*) and then bonnanes leads to novel cyclochiral nanoarchitectures which might be useful on the long synthetic road to molecular devices. The fascinating action of the many existing natural molecular machines can be the source of future inspiration to assemble nanosized molecules based on rotaxanes/bonnanes bearing coupled elements that can undergo nanoscale yet controlled (translational, rotational) movements on an axle.

Among our future projects in this direction are "open bonnanes" **12** (see the Supporting Information), in which the sulfonamide group is linked to dendrons of various generation or to condensed arene moieties such that luminescence effects depending on the number of wheels on the axle can be determined. Bonnanes are expected to expand the field of nanometric molecular motors in which the rotary motion is controlled by tethering or clamping and highlight the significance of interlocked and more complex structures and devices in chemistry.

Experimental Section

The preparation and purification of rotaxanes **4**–**7** are described in the Supporting Information.

Synthesis of bonnanes **11A** and **11B**: Compound **8** (3.9 mg, 0.01 mmol) was dissolved in dry DMF (70 mL) and added dropwise at room temperature to a suspension of [3]rotaxane **6** (38 mg, 0.01 mmol) and K_2CO_3 (2.8 mg, 0.02 mmol) in dry DMF (70 mL). The solution was stirred at room temperature for 4 days. After adding $CHCl_3$ (100 mL), the solution was extracted three times with water (50 mL). The organic phase was separated and dried in vacuo and was then purified by column chromatography (SiO_2, 63–100 mesh; eluent: tetrahydrofuran/*n*-hexane/ethanol = 9.5:7:0.5) to yield bonnane **11A** (26 mg, 65%). Similarly, **9** (2.5 mg, 0.01 mmol) was added to **6** to yield the corresponding bonnane **11B** (20 mg, 90%). The spectroscopic results of the synthesized rotaxanes and bonnanes are given in the Supporting Information.

Received: May 19, 2006
Revised: July 17, 2006
Published online: October 9, 2006

Keywords: chirality · chromatography · enantiomer separation · rotaxanes · template synthesis

[1] H. Hopf, *Classics in Hydrocarbon Chemistry—Synthesis, Concept, Perspectives*, Wiley-VCH, Weinheim, **2000**.

[2] Recent contributions: a) C. A. Schalley, K. Beizai, F. Vögtle, *Acc. Chem. Res.* **2001**, *34*, 465–476; b) V. Balzani, M. Clemente-León, A. Credi, B. Ferrer, M. Venturi, A. H. Flood, J. F. Stoddart, *Proc. Natl. Acad. Sci. USA* **2006**, *103*, 1178–1183; c) J.-P. Collin, V. Heitz, J.-P. Sauvage, *Top. Curr. Chem.* **2005**, *262*, 29–62; d) V. Balzani, A. Credi, M. Venturi, *Molecular Devices and Machines*, Wiley-VCH, Weinheim, **2003**; e) E. R. Kay, D. A. Leigh, *Nature* **2006**, *440*, 286–287; f) T. R. Kelly, *Top. Curr. Chem.* **2005**, *262*; g) L. De Cola, *Top. Curr. Chem.* **2005**, *257*; h) H. Tian, Q. C. Wang, *Chem. Soc. Rev.* **2006**, *35*, 361–374; i) E. Mahan, H. W. Gibson in *Cyclc Polymers*, 2nd ed. (Ed.: J. A. Semlyen), Kluwer Publishers, Dordrecht, **2000**, pp. 415–560; j) T. J. Hubin, D. H. Busch, *Coord. Chem. Rev.* **2000**, *200–202*, 5–52; k) T. Takata, N. Kihara, *Rev. Heteroat. Chem.* **2000**, *22*, 197–218; l) I. G. Panova, I. N. Topchieva, *Russ. Chem. Rev.* **2001**, *70*, 23–44; m) K. Kim, *Chem. Soc. Rev.* **2002**, *31*, 96–107; n) T. Felder, C. A. Schalley, *Highlights Bioorg. Chem.* **2004**, 526–539; o) A. H. Flood, R. J. A. Ramirez, W.-Q. Deng, R. P. Muller, W. A. Goddard III, J. F. Stoddart, *Aust. J. Chem.* **2004**, *57*, 301–322; p) F. Huang, H. W. Gibson, *Prog. Polym. Sci.* **2005**, *30*, 982–1018.

[3] Synthesis of rotaxanes: a) C. Heim, D. Udelhofen, F. Vögtle in *Molecular Catenanes, Rotaxanes and Knots. A Journey Through the World of Molecular Topology* (Eds.: J.-P. Sauvage, C. Dietrich-Buchecker), Wiley-VCH, Weinheim, **1999**, pp. 177–222; b) C. Seel, F. Vögtle, *Chem. Eur. J.* **2000**, *6*, 21–24; c) A. Werner, G. Lutz, W. G. Ulrich, B. Karin, *Chem. Eur. J.* **2004**, *10*, 3562–3568; d) N. Kameta, K. Hiratani, Y. Nagawa, *Chem. Commun.* **2004**, 466–467; e) S.-H. Chiu, A. M. Elizarov, P. T. Glink, J. F. Stoddart, *Org. Lett.* **2002**, *4*, 3561–3564; f) F. Vögtle, T. Dünnwald, T. Schmidt, *Acc. Chem. Res.* **1996**, *29*, 451–460; g) K. Srinivasan, P. Rajakumar, *Synthesis* **2005**, *16*, 2772–2776; h) C. A. Schalley, T. Weilandt, J. Brüggemann, F. Vögtle, *Top. Curr. Chem.* **2004**, 248, 141–2000.

[4] a) G. Schill, A. Lüttringhaus, *Angew. Chem.* **1964**, *76*, 567–568; *Angew. Chem. Int. Ed. Engl.* **1964**, *3*, 546–547; b) G. Schill, *Catenanes, Rotaxanes and Knots*, *Organic Chemistry*, *Vol. 22*, Academic Press, New York, **1971**.

 © 2006 Wiley-VCH Verlag GmbH & Co. KGaA, Weinheim

[5] a) M. C. Jimenez, C. Dietrich-Buchecker, J.-P. Sauvage, *Angew. Chem.* **2000**, *112*, 3422 – 3425; *Angew. Chem. Int. Ed.* **2000**, *39*, 3284 – 3287; b) T. Kraus, M. Budesinsky, J. Cvacka, J.-P. Sauvage, *Angew. Chem.* **2006**, *118*, 264 – 267; *Angew. Chem. Int. Ed.* **2006**, *45*, 258 – 261; c) M. Anderson, M. Linke, J.-C. Chambron, J. Davissson, V. Heitz, L. Hammarström, J.-P. Sauvage, *J. Am. Chem. Soc.* **2002**, *124*, 4347 – 4362.

[6] a) H.-R. Tseng, S. A. Vignon, J. F. Stoddart, *Angew. Chem.* **2003**, *115*, 1529 – 1533; *Angew. Chem. Int. Ed.* **2003**, *42*, 1491 – 1495; b) T. Iijima, S. A. Vignon, H.-R. Tseng, T. Jarrosson, J. K. M. Sanders, F. Marchioni, M. Venturi, E. Apostoli, V. Balzani, J. F. Stoddart, *Chem. Eur. J.* **2004**, *10*, 6375 – 6392.

[7] a) A. F. M. Kilbinger, S. J. Cantrill, A. W. Waltman, M. W. Day, R. H. Grubbs, *Angew. Chem.* **2003**, *115*, 3403 – 3407; *Angew. Chem. Int. Ed.* **2003**, *42*, 3281 – 3285; b) D. W. Zehnder II, D. B. Smithrud, *Org. Lett.* **2001**, *3*, 2485 – 2487; c) R. Shukla, M. J. Deetz, B. D. Smith, *Chem. Commun.* **2000**, 2397 – 2398; d) E. Lee, J. Kim, J. Heo, D. Whang, K. Kim, *Angew. Chem.* **2001**, *113*, 413 – 416; *Angew. Chem. Int. Ed.* **2001**, *40*, 399 – 402; e) C. A. Hunter, C. M. R. Low, M. J. Packer, S. E. Spey, J. G. Vinter, M. O. Vysotsky, C. Zonta, *Angew. Chem.* **2001**, *113*, 2750 – 2754; *Angew. Chem. Int. Ed.* **2001**, *40*, 2678 – 2682; f) C. G. Gong, T. E. Glass, H. W. Gibson, *Macromolecules* **1998**, *31*, 308 – 313; g) M. R. Sambrook, P. D. Beer, M. D. Lankshear, R. F. Ludlow, J. A. Wisner, *Org. Biomol. Chem.* **2006**, *4*, 1529 – 1538; h) F. Cacialli, J. S. Wilson, J. J. Michels, C. Daniel, C. Silva, R. H. Friend, N. Severin, P. Samori, J. P. Rabe, M. J. O'Connell, P. N. Taylor, H. L. Anderson, *Nat. Mater.* **2002**, *1*, 160 – 164; i) C. Wu, P. R. Lecavalier, Y. X. Shen, H. W. Gibson, *Chem. Mater.* **1991**, *3*, 569 – 572.

[8] a) A. H. Parham, R. Schmieder, F. Vögtle, *Synlett* **1999**, *12*, 1887 – 1890; b) T. Dünnwald, A. H. Parham, F. Vögtle, *Synthesis* **1998**, *3*, 339 – 348; c) O. Lukin, T. Kubota, Y. Okamoto, F. Schelhase, A. Yoneva, W. M. Müller, U. Müller, F. Vögtle, *Angew. Chem.* **2003**, *115*, 4681 – 4684; *Angew. Chem. Int. Ed.* **2003**, *42*, 4252 – 4845.

[9] a) C. A. Schalley, W. Reckien, S. Peyerimhoff, B. Baytekin, F. Vögtle, *Chem. Eur. J.* **2004**, *10*, 4777 – 4789; b) G. M. Hübner, J. Gläser, C. Seel, F. Vögtle, *Angew. Chem.* **1999**, *111*, 395 – 398; *Angew. Chem. Int. Ed.* **1999**, *38*, 383 – 386.

[10] C. Seel, A. H. Parham, O. Safarowsky, G. M. Hübner, F. Vögtle, *J. Org. Chem.* **1999**, *64*, 7236 – 7242.

[11] a) F. Vögtle, T. Dünnwald, M. Händel, R. Jäger, S. Meier, G. Harder, *Chem. Eur. J.* **1996**, *2*, 640 – 643; b) R. Schmieder, G. Hübner, C. Seel, F. Vögtle, *Angew. Chem.* **1999**, *111*, 3741 – 3743; *Angew. Chem. Int. Ed.* **1999**, *38*, 3528 – 3530; c) Y. Nagawa, J. Suga, K. Hiratani, E. Koyama, M. Kanesato, *Chem. Commun.* **2005**, 749 – 751; d) S. Anderson, H. L. Anderson, *Angew. Chem.* **1996**, *108*, 2075 – 2078; *Angew. Chem. Int. Ed. Engl.* **1996**, *35*, 1956 – 1959.

[12] a) F. Vögtle, M. Händel, S. Meier, S. Ottens-Hildebrandt, F. Ott, T. Schmidt, *Liebigs Ann.* **1995**, 739 – 743; b) D. Tuncel, J. H. G. Steinke, *Chem. Commun.* **2002**, 496 – 497.

[13] O. Lukin, F. Vögtle, *Angew. Chem.* **2005**, *117*, 1480 – 1501; *Angew. Chem. Int. Ed.* **2005**, *44*, 1456 – 1477.

[14] The name "bonnane" is used here in acknowledgement of the city Bonn, the former capital of Germany and location of the Kekulé Institute. The bridge between the wheels symbolizes Bonn as a "bridge capital" during the period 1949 – 1999. A short classification system for bonnane structures that can form the foundation for a more detailed nomenclature of specific compounds on the basis of the rules by Vögtle et al.[16] for naming rotaxanes is given in the Supporting Information.

[15] a) C. Reuter, A. Mohry, A. Sobanski, F. Vögtle, *Chem. Eur. J.* **2000**, *6*, 1674 – 1682; b) C. Yamamoto, Y. Okamoto, T. Schmidt, R. Jäger, F. Vögtle, *J. Am. Chem. Soc.* **1997**, *119*, 10547 – 10548.

[16] O. Safarowsky, B. Windisch, A. Mohry, F. Vögtle, *J. Prakt. Chem.* **2000**, *342*, 437 – 444.

[17] We also synthesized the bis(ethylene glycol)-bridged bonnane **11C**, but the purification proved to be difficult owing to lower solubility of the compound.

[18] T. Zhang, C. Kientzy, P. Franco, A. Ohnishi, Y. Kagamihara, H. Kurosawa, *J. Chromatogr. A* **2005**, *1075*, 65 – 75.

 © 2006 Wiley-VCH Verlag GmbH & Co. KGaA, Weinheim

Cover Picture

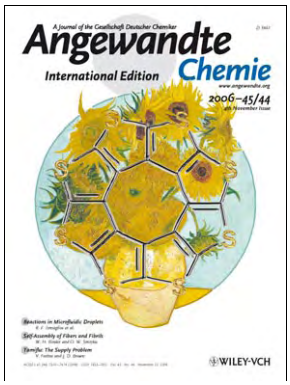

Konstantin Yu. Chernichenko, Viktor V. Sumerin, Roman V. Shpanchenko, Elizabeth S. Balenkova, and Valentine G. Nenajdenko*

The bloom of a sunflower
is used to describe the highly symmetric planar structure of octathio[8]circulene, whose trivial name "sulflower" derives from sulfur and flower (see cover picture). In their Communication on page 7367 ff., V. G. Nenajdenko and co-workers describe the synthesis and characterization of sulflower, a molecule that can be considered as a new form of carbon sulfide and as an oligothiophene, that is, as both inorganic and organic. (Background picture: "Sunflowers" by Vincent van Gogh. Copyright: Neue Pinakothek, Munich.)

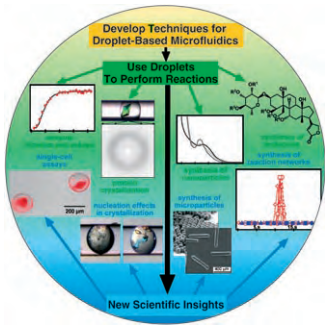

Microfluidics
Droplet-based microfluidics enables high-throughput applications, such as the optimization of reaction conditions or the analysis of complex biological processes. Current developments in this field are discussed by R. F. Ismagilov and co-workers in their Review on page 7336 ff.

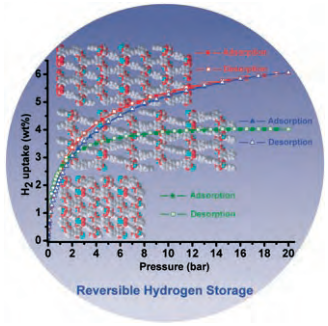

Metal–Organic Frameworks
In their Communication on page 7358 ff., N. R. Champness, P. Hubberstey, M. Schröder, and co-workers compare the H_2 sorption of a series of metal–organic frameworks. Those with smaller pores adsorb higher densities of H_2, whereas those with larger pores have higher maximum H_2 storage capacities.

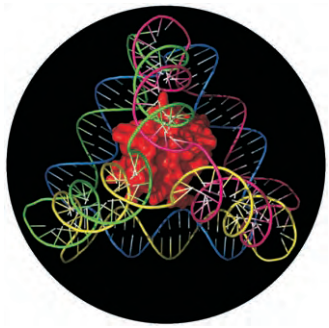

DNA Structures
A. J. Turberfield and co-workers have incarcerated cytochrome *c*: single molecules of the protein are trapped in rigid tetrahedral DNA cages, which can also accommodate larger globular proteins. These results are discussed in the Communication on page 7414 ff.

Contents

The following Communications have been judged by at least two referees to be "very important papers" and will be published online at www.angewandte.org soon:

A. Corma, M. Renz**
A General Method for the Preparation of Ethers Using Water-Resistant Solid Lewis Acids

K. Banert, Y.-H. Joo, T. Rüffer, B. Walfort, H. Lang*
The Exciting Chemistry of Tetraazidomethane

B. V. Popp, J. E. Wendlandt, C. R. Landis, S. S. Stahl**
Reaction of Molecular Oxygen with an NHC-Coordinated Pd^0 Complex: Computational Insights and Experimental Implications

R. Martinez, R. Chevalier, S. Darses, J.-P. Genet**
A Versatile Ruthenium Catalyst for C–C Bond Formation through C–H Bond Activation

*H. Nuss, M. Jansen**
$Cs_5([12]crown\text{-}4)_2(O_3)_5$: The First Supramolecular Ozonide Compound Containing $^1{}_\infty\{Cs_8(O_3)_{10}\}^2$ Rods

F. Camerel, R. Ziessel, B. Donnio, C. Bourgogne, D. Guillon, M. Schmutz, C. Iacovita, J.-P. Bucher*
Formation of Gels and Liquid Crystals Induced by Pt···Pt Interactions in Luminescent σ-Alkynyl Platinum(II) Terpyridine Complexes

News

Microfluidics: E. Delamarche honored ——— **7320**

Biophysical Chemistry: Awards to T. Fiebig and H.-A. Wagenknecht ——— **7320**

Books

Organic Photovoltaics — Sam-Shajing Sun, Niyazi Serdar Sariciftci — *reviewed by N. Robertson* ——— **7321**

Chemical Micro Process Engineering — Volker Hessel, Holger Löwe, Andreas Müller, Gunther Kolb — *reviewed by C. de Bellefon* ——— **7321**

Highlights

Alzheimer's Disease

W. H. Binder,* O. W. Smrzka **7324 – 7328**

Self-Assembly of Fibers and Fibrils

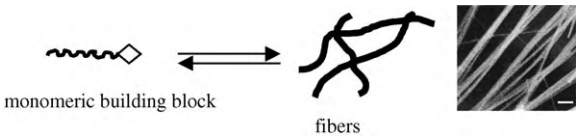

Too much fiber? Protein fibers play an important role in cellular processes, but are also involved in protein-folding diseases, such as Alzheimer's disease. Modern screening and validation models allow the investigation of the aggregation and deaggregation kinetics of protein fibers (see scheme). These studies can serve as a starting point for the development of new therapeutic strategies.

Antiviral Agents

V. Farina,* J. D. Brown* ——— **7330 – 7334**

Tamiflu: The Supply Problem

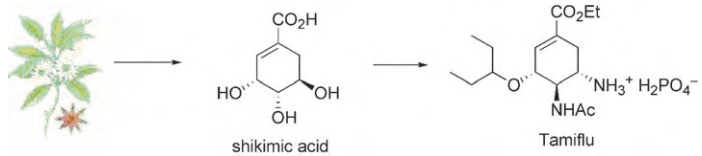

Taming of the flu: Shikimic and quinic acids are the established starting materials for Tamiflu, a viral neuraminidase inhibitor that is considered by many as the first-line treatment against a possible H5N1 (bird flu) pandemic. Several syntheses have been described recently that circumvent the use of these natural products. These, or related approaches, may provide an alternative practical approach to this important drug.

WILEY InterScience DISCOVER SOMETHING GREAT
© 2006 Wiley-VCH Verlag GmbH & Co. KGaA, Weinheim

Reviews

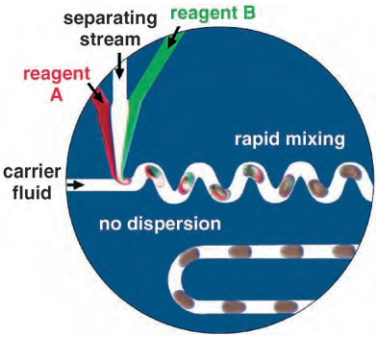

Reactions that go with the flow: Many applications in chemical research require multiple reactions to be performed in parallel and in series. Microfluidic droplets can be used as chemical microreactors for performing many reactions on small scale (see picture). New techniques in droplet-based microfluidics and their applications (e.g., for analysis of complex biological processes or optimization of reaction conditions) are discussed.

Droplet-Based Microfluidics

H. Song, D. L. Chen, R. F. Ismagilov* ——— **7336 – 7356**

Reactions in Droplets in Microfluidic Channels

Communications

First-class accommodation: A series of coordination frameworks with different pore sizes (see structure of one; Cu blue, C gray, H white, O red) are prepared from Cu^{II} ions and carboxylate ligands of various lengths. Comparison of their sorption properties reveals that smaller pores allow higher densities of adsorbed H_2, whereas larger pores allow higher maximum H_2 storage capacities.

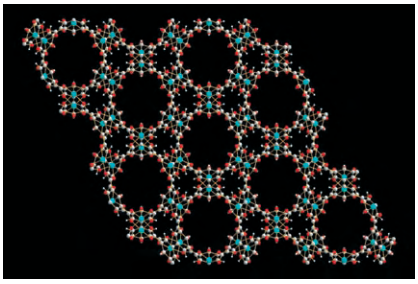

Hydrogen Storage

X. Lin, J. Jia, X. B. Zhao, K. M. Thomas, A. J. Blake, G. S. Walker, N. R. Champness,* P. Hubberstey,* M. Schröder* ——— **7358 – 7364**

High H_2 Adsorption by Coordination-Framework Materials

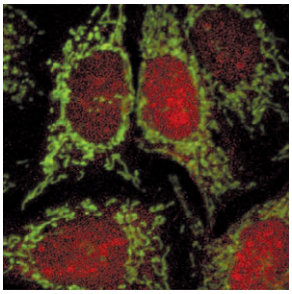

Playing tag: Noncanonical amino acid tagging enables the selective fluorescent visualization of newly synthesized proteins in mammalian cells (see the picture). Susceptibility to tagging is determined by the spatial and temporal character of the protein synthesis, thus providing a complement to methods which identify relevant members of the proteome.

Fluorescent Probes

K. E. Beatty, J. C. Liu, F. Xie, D. C. Dieterich, E. M. Schuman, Q. Wang, D. A. Tirrell* ——— **7364 – 7367**

Fluorescence Visualization of Newly Synthesized Proteins in Mammalian Cells

For the USA and Canada:
ANGEWANDTE CHEMIE International Edition (ISSN 1433-7851) is published weekly by Wiley-VCH PO Box 191161, D 69451 Weinheim, Germany. Air freight and mailing in the USA by Publications Expediting Inc. 200 Meacham Ave., Elmont, NY 11003. Periodicals postage paid at Jamaica NY 11431. US POSTMASTER: send address changes to *Angewandte Chemie*, Wiley-VCH, 111 River Street, Hoboken, NJ 07030. Annual subscription price for institutions: US$ 5685/5168 (valid for print and electronic / print or electronic delivery); for individuals who are personal members of a national chemical society prices are available on request. Postage and handling charges included. All prices are subject to local VAT/sales tax.

© 2006 Wiley-VCH Verlag GmbH & Co. KGaA, Weinheim

The best in chemistry –

for more than a hundred years

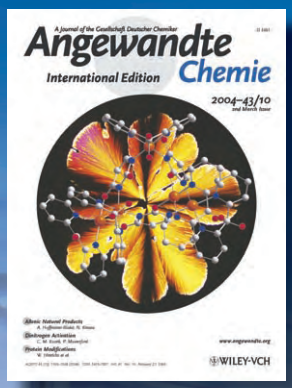

A Journal of the Gesellschaft Deutscher Chemiker

Angewandte
International Edition **Chemie**

www.angewandte.org

1888: ***The beginning of a success story***

Constant Innovations

1962: First issue of the International Edition
1976: Graphical abstracts
1979: Cover pictures
1988: Centenary of Angewandte
1989: Routine use of color
1991: New section: Highlights
1992: Computerized editorial tracking system
1995: Internet service for readers
1998: Regular press service; full-text online
2000: New section: Essays; EarlyView: Communications available online ahead of the printed version
2001: New section: Minireviews
2002: Online submission of manuscripts
2003: Weekly publication; new section: News; new layout
2004: Backfiles (1962-1997); ManuscriptXpress: Online system for authors and referees

Angewandte's advisors...

Ryoji Noyori
Nagoya University and RIKEN (Tokyo)

»***Angewandte Chemie*** *is the best scientific arena for both players and audience. This international journal has taken a leading role in raising the potential of chemistry to the current high standard.*«

Angewandte Chemie International Edition *is a journal of the German Chemical Society (GDCh)*

GDCh

WILEY InterScience® DISCOVER SOMETHING GREAT

WILEY-VCH

1187404_gu

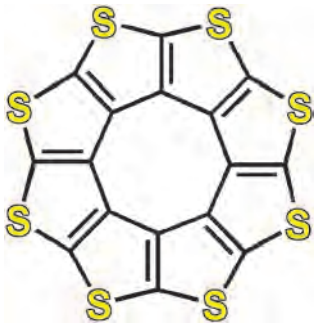

A sunny outlook: As the first fully heterocyclic circulene, sulflower opens the way to an unprecedented class of compounds that are both organic and inorganic. Sulflower is an oligothiophene as well as a new form of carbon sulfide that resembles a flower (see picture) and was synthesized in a short and effective approach.

Sulfur Heterocycles

K. Y. Chernichenko, V. V. Sumerin, R. V. Shpanchenko, E. S. Balenkova, V. G. Nenajdenko* _____ **7367 – 7370**

"Sulflower": A New Form of Carbon Sulfide

A new approach to stabilization of ZnO nanocrystals by ionic-liquid components, which endow the nanocrystals with high thermal stability and good fluidity, is demonstrated. The ionic-liquid/ZnO composites exhibit tunable photoluminescence (see picture) with a high quantum yield.

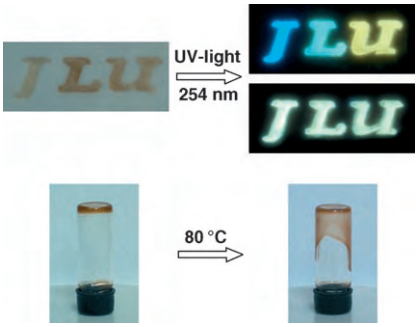

ZnO Nanocrystals

D. P. Liu, G. D. Li, Y. Su, J. S. Chen* _____ **7370 – 7373**

Highly Luminescent ZnO Nanocrystals Stabilized by Ionic-Liquid Components

---

Unbalanced surface stresses, induced in stereocomplex crystals formed by blends of two enantiomeric polylactide diblock copolymers by the presence of immiscible blocks of different lengths, result in lamella curving and formation of onion-like multilamellar structures (see picture for schematic structure and a TEM image).

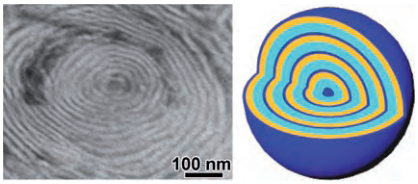

Lamellar Materials

L. Sun, L. Zhu,* L. Rong, B. S. Hsiao _____ **7373 – 7376**

Tailor-Made Onionlike Stereocomplex Crystals in Incompatible, Enantiomeric, Polylactide-Containing Block Copolymer Blends

---

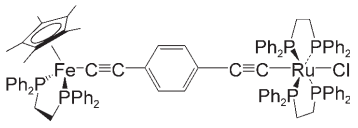

Successive oxidation processes in a heterobimetallic iron–ruthenium complex (see picture) "switch" the optical transitions at long wavelengths, and these linear electrochromic effects are accompanied by changes in the nonlinear optical properties of the complex.

Nonlinear Optics

M. Samoc,* N. Gauthier, M. P. Cifuentes, F. Paul,* C. Lapinte, M. G. Humphrey* _____ **7376 – 7379**

Electrochemical Switching of the Cubic Nonlinear Optical Properties of an Aryldiethynyl-Linked Heterobimetallic Complex between Three Distinct States

© 2006 Wiley-VCH Verlag GmbH & Co. KGaA, Weinheim

Contents

Molecular Wheels

P. King, T. C. Stamatatos, K. A. Abboud, G. Christou* ——— **7379 – 7383**

Reversible Size Modification of Iron and Gallium Molecular Wheels: A Ga_{10} "Gallic Wheel" and Large Ga_{18} and Fe_{18} Wheels

Wheelin' and dealin': The M_{10} molecular wheels $[M_{10}(OMe)_{20}(O_2CR)_{10}]$ (M = Ga, R = Me; M = Fe, R = Ph) were modified to M_{18} wheels in a nontemplate synthesis upon incorporation of a diolate ligand (see space-filling model of $[Ga_{18}(pd)_{12}(pdH)_{12}(O_2CMe)_6(NO_3)_6]^{6+}$; Ga yellow, O red, N blue, C gray; pdH_2 = 1,3-propanediol). Remarkably, dissolution in MeOH converts both M_{18} wheels back into the M_{10} wheels.

DNA Structures

Y. Weizmann, M. K. Beissenhirtz, Z. Cheglakov, R. Nowarski, M. Kotler, I. Willner* ——— **7384 – 7388**

A Virus Spotlighted by an Autonomous DNA Machine

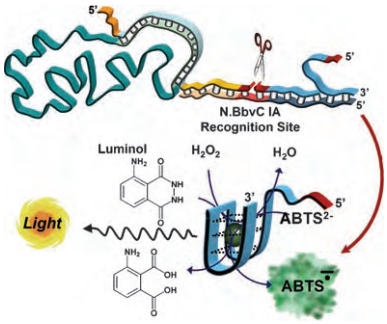

Highly sensitive: Analysis of viral DNA (M13 phage) is possible by using a DNA-based machine that is fueled by dNTPs and synthesizes DNAzyme reporter units. The DNAzymes mimic peroxidase and lead to a colorimetric or chemiluminescent readout of the analyzed DNA.

Conformation Analysis

V. M. Sánchez-Pedregal, K. Kubicek, J. Meiler, I. Lyothier, I. Paterson, T. Carlomagno* ——— **7388 – 7394**

The Tubulin-Bound Conformation of Discodermolide Derived by NMR Studies in Solution Supports a Common Pharmacophore Model for Epothilone and Discodermolide

Bound to have similarities: Although the overall shape of discodermolide bound to tubulin resembles the structure of the free ligand, the precise conformation and orientation of the lactone ring are different. A partially overlapping pharmacophore model supported by protein-mediated interligand NOE signals (see picture) is proposed to explain the similar (but not fully equivalent) biological activity of discodermolide and epothilone A.

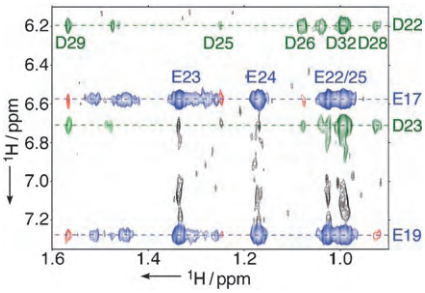

Iron Imido Complexes

E. J. Klinker, T. A. Jackson, M. P. Jensen, A. Stubna, G. Juhász, E. L. Bominaar, E. Münck,* L. Que, Jr.* ——— **7394 – 7397**

A Tosylimido Analogue of a Nonheme Oxoiron(IV) Complex

High-valent versatility: N4Py is a versatile pentadentate ligand demonstrated to stabilize both high-valent oxo and imido compounds. The $[Fe^{IV}(NTs)(N4Py)]^{2+}$ complex (see DFT-optimized structure) has been characterized spectroscopically and formulated as having an $S = 1$ iron(IV) center with an Fe=N bond (1.73 Å) that is longer than the Fe=O bond of its oxo analogue (1.65 Å).

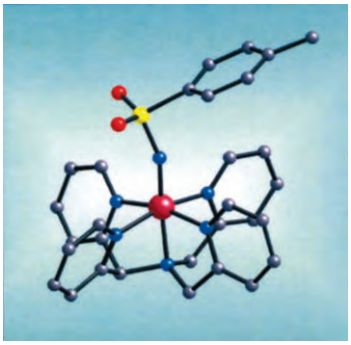

© 2006 Wiley-VCH Verlag GmbH & Co. KGaA, Weinheim

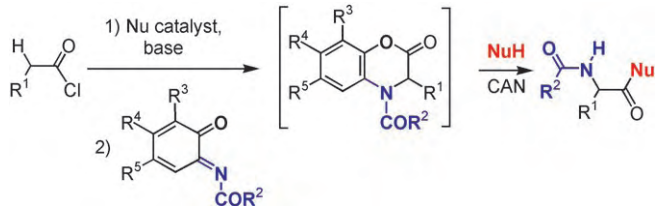

Cycloaddition of *o*-benzoquinone imides with chiral ketene enolates derived from cinchona alkaloid catalysts is the basis of a catalytic asymmetric synthesis of 1,4-benzoxazinones and 1,4-benzoxazines. The resulting cycloadducts can be derivatized in situ to provide α-amino acid products in good-to-excellent yields with very high enantioselectivities (see scheme; CAN = ceric ammonium nitrate, Nu = nucleophile).

Amino Acids

J. Wolfer, T. Bekele, C. J. Abraham, C. Dogo-Isonagie, T. Lectka* **7398 – 7400**

Catalytic, Asymmetric Synthesis of 1,4-Benzoxazinones: A Remarkably Enantioselective Route to α-Amino Acid Derivatives from *o*-Benzoquinone Imides

Giving it a tri: Ternary complexes formed from a macrocyclic host (*p*-sulfonatocalix[4]arene), an organic guest (2,3-diazabicyclo[2.2.2]oct-2-ene), and transition-metal ions (see picture) result in a host-assisted formation of a metal–ligand bond. The system displays a very high selectivity as a result of triple supramolecular recognition involving Coulombic interactions, hydrophobic guest binding, and weak metal–ligand interactions.

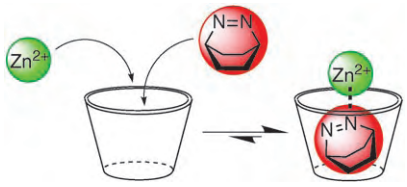

Supramolecular Chemistry

H. Bakirci, A. L. Koner, M. H. Dickman, U. Kortz, W. M. Nau* **7400 – 7404**

Dynamically Self-Assembling Metalloenzyme Models Based on Calixarenes

Surface value: Scanning tunneling microscopy reveals that aryl–carbonyl assemblies form through C–H···O interactions on a Pt(111) surface (see picture). The strong hydrogen bonding is activated by the chemisorption-induced polarization of the arene and is tunable by substitution on the aromatic ring. These findings are relevant to stereoselective heterogeneous and homogeneous catalysis.

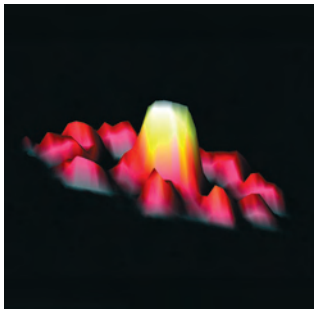

Asymmetric Catalysis

S. Lavoie, G. Mahieu, P. H. McBreen* **7404 – 7407**

Chemisorption-Induced Double Hydrogen Bonding, Self-Assembly, and Stereoselection

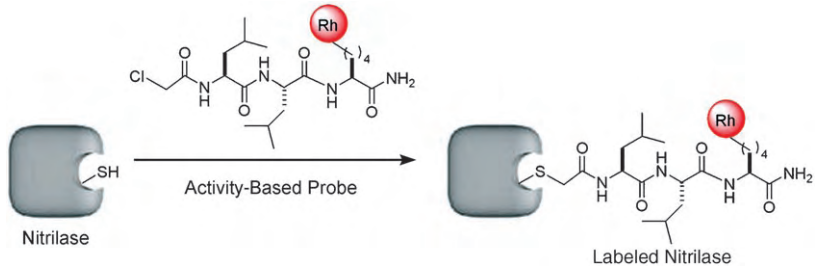

Up and at it: A set of activity-based proteomics probes containing a dipeptide α-chloroacetamide scaffold that targets the nitrilase family of enzymes is described. One member of the nitrilase class, ureidopropionase-β, was found to react selectively with a single probe that mimics the enzyme's endogenous substrate *N*-carbamoyl β-alanine.

Activity-Based Proteomics

K. T. Barglow, B. F. Cravatt* **7408 – 7411**

Substrate Mimicry in an Activity-Based Probe That Targets the Nitrilase Family of Enzymes

© 2006 Wiley-VCH Verlag GmbH & Co. KGaA, Weinheim

Contents

Coordination Frameworks

X.-L. Wang, C. Qin, E.-B. Wang*
Z.-M. Su,* Y.-G. Li, L. Xu ____ **7411 – 7414**

Self-Assembly of Nanometer-Scale $[Cu_{24}I_{10}L_{12}]^{14+}$ Cages and Ball-Shaped Keggin Clusters into a (4,12)-Connected 3D Framework with Photoluminescent and Electrochemical Properties

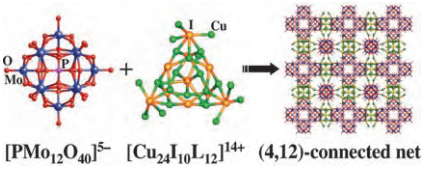

Bridging two traditional but distinct research areas—polyoxometalate chemistry and cuprous halide clusters—the (4,12)-connected 3D framework $(NH_4)[Cu_{24}I_{10}L_{12}][PMo^{V}_{2}Mo^{VI}_{10}O_{40}]_3$ has been built by covalent linkage of nanoscale Keggin anions and $[Cu_{24}I_{10}L_{12}]^{14+}$ clusters (see picture; L is a multidentate N-heterocyclic ligand); it exhibits remarkable photoluminescent and electrochemical properties.

DNA Structures

C. M. Erben, R. P. Goodman,
A. J. Turberfield* ____ **7414 – 7417**

Single-Molecule Protein Encapsulation in a Rigid DNA Cage

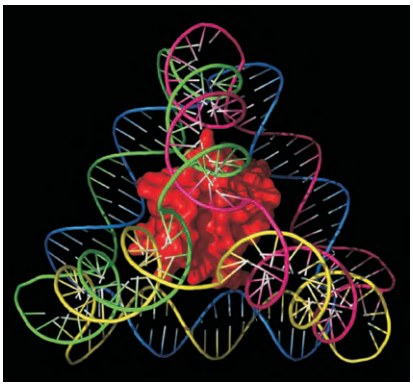

Behind bars: A single molecule of the protein cytochrome *c* has been incarcerated within a rigid tetrahedral DNA cage (see picture). The central cavity is estimated to be large enough to accommodate a sphere of approximately 2.6 nm in radius, such as a 60-kDa globular protein (M_r of cytochrome *c*: 12.4 kDa). The finding demonstrates the potential of DNA containers as a new kind of drug-delivery system.

Sialic Acid Synthesis

Z. Hong, L. Liu, C.-C. Hsu,
C.-H. Wong* ____ **7417 – 7421**

Three-Step Synthesis of Sialic Acids and Derivatives

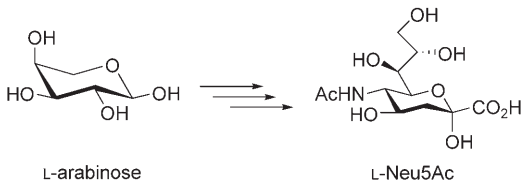

Flexible yet efficient: Sialic acids such as L-*N*-acetylneuraminic acid (see picture) can be synthesized in only three steps by 1) vinylation of an aldose through a modified Petasis coupling reaction, 2) 1,3-dipolar cycloaddition with a nitrone to construct an isoxazolidine ring, and 3) base-catalyzed β elimination/ring opening of the isoxazolidine to generate a γ-hydroxy-α-keto acid.

Carbido Complexes

S. R. Caskey, M. H. Stewart,
M. J. A. Johnson,*
J. W. Kampf ____ **7422 – 7424**

Carbon–Carbon Bond Formation at a Neutral Terminal Carbido Ligand: Generation of Cyclopropenylidene and Vinylidene Complexes

A C_1 source, the carbido complex $[Ru(C)(PCy_3)_2Cl_2]$ (**1**) adds cleanly to dimethylacetylene dicarboxylate (DMAD), affording the cyclopropenylidene complex **2** (red O, green Cl, yellow P, gray C). This product is surprising given the instability of its *trans*-cyclopropylidene analogue. HX reagents effect 1,1-addition and ring opening, forming vinylidene complexes such as **3** which catalyze the ring-opening metathesis polymerization of norbornene.

© 2006 Wiley-VCH Verlag GmbH & Co. KGaA, Weinheim

To cap it off: A high-spin cyanide-bridged Ni_9W_6 cluster ($S = 12$) shows ferromagnetic coupling between Ni^{II} (green) and W^{V} (purple) ions within the molecule. The surface was modified by substituting the solvent molecules on the surface of the cluster with 2,2′-bipyridine to afford an air-stable Ni_9W_6 cluster with single-molecule magnetism.

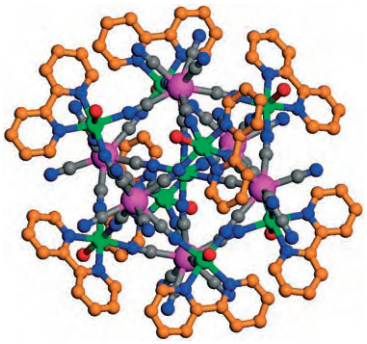

Single-Molecule Magnets

J. H. Lim, J. H. Yoon, H. C. Kim, C. S. Hong* ——— 7424 – 7426

Surface Modification of a Six-Capped Body-Centered Cube Ni_9W_6 Cluster: Structure and Single-Molecule Magnetism

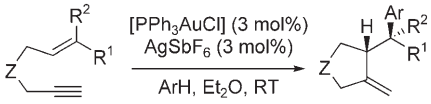

A golden tandem reaction: The $[PPh_3AuCl]/AgSbF_6$ catalytic system promotes a tandem reaction composed of a Friedel–Crafts-type addition of electron-rich aromatic and heteroaromatic derivatives to unactivated alkenes and a carbocyclization (see scheme; $Z = C(CO_2Me)_2$, $C(SO_2Ph)_2$, O, NTs). The reaction is compatible with various functional groups on the enynes and nucleophiles, and proceeds rapidly at room temperature.

C–H Activation

P. Y. Toullec, E. Genin, L. Leseurre, J.-P. Genêt,* V. Michelet* ——— 7427 – 7430

Room-Temperature Au^{I}-Catalyzed C–C Bond Formation through a Tandem Friedel–Crafts-Type Addition/Carbocyclization Reaction

Going retro: Controlled-potential electrolysis (CPE) is employed as a synthetic tool in the selective removal of addends from fullerene adducts. Reductive CPE has been extensively used in the retro-cyclopropanation of fullerenes without affecting pyrrolidine addends also present. Now oxidative CPE for the selective removal of pyrrolidine addends in the presence of methano adducts is reported (see scheme).

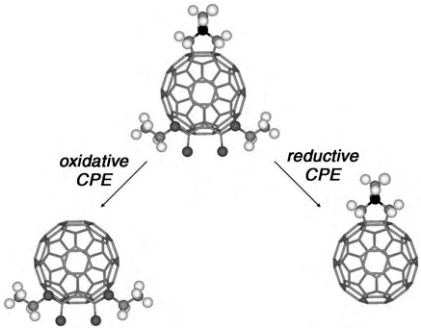

Fullerenes

O. Lukoyanova, C. M. Cardona, M. Altable, S. Filippone, Á. Martín Domenech, N. Martín,* L. Echegoyen* ——— 7430 – 7433

Selective Electrochemical Retro-Cycloaddition Reaction of Pyrrolidinofullerenes

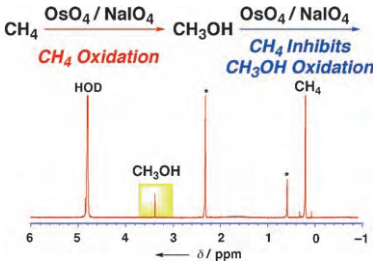

Cast in a new role: Aqueous solutions of OsO_4 and $NaIO_4$ oxidize methane to methanol under very mild conditions (see scheme). The generated methanol is preserved over 5 days at 50 °C, although it is more readily oxidized than methane in separate experiments. Remarkably, methanol oxidation by aqueous OsO_4/$NaIO_4$ is inhibited by the presence of methane.

Methane and Methanol Oxidation

T. Osako, E. J. Watson, A. Dehestani, B. C. Bales, J. M. Mayer* ——— 7433 – 7436

Methane Oxidation by Aqueous Osmium Tetroxide and Sodium Periodate: Inhibition of Methanol Oxidation by Methane

© 2006 Wiley-VCH Verlag GmbH & Co. KGaA, Weinheim

Contents

Glycosylation

J. Y Baek, T. J. Choi, H. B. Jeon, K. S. Kim* ——— **7436 – 7440**

A Highly Reactive and Stereoselective β-Mannopyranosylation System: Mannosyl 4-Pentenoate/PhSeOTf

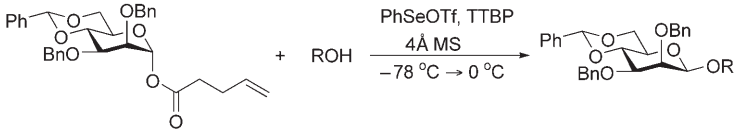

Controlled linkage: PhSeOTf-promoted glycosylations of a variety of acceptor alcohols with 4,6-*O*-benzylidene-2,3-di-*O*-benzylmannopyranosyl pentenoate afford β-mannopyranosides in high yields and with excellent stereoselectivity (see scheme). This method is even better than other known methods for the mannosylation of simple reactive primary alcohols. Tf = trifluoromethanesulfonyl, TTBP = 2,4,6-tri-*tert*-butylpyrimidine.

Surface Chemistry

O. Azzaroni, B. Trappmann, P. van Rijn, F. Zhou, B. Kong, W. T. S. Huck* ——— **7440 – 7443**

Mechanically Induced Generation of Counterions Inside Surface-Grafted Charged Macromolecular Films: Towards Enhanced Mechanotransduction in Artificial Systems

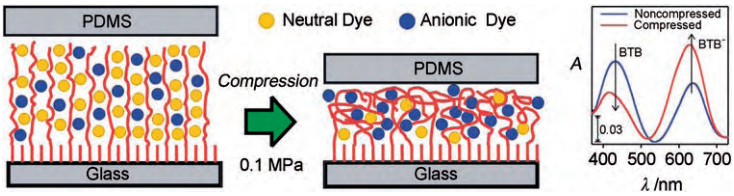

Brushing up on films: A simple model, based on strong ion-pairing interactions of a dye probe (bromothymol blue, BTB) within surface-grafted charged polyelectrolyte brushes, provides evidence that physical forces can be easily mechanotransducted into chemical signals (see picture, PDMS = poly(dimethylsiloxane)). The application of a mechanical force results in a shift of the equilibrium for BTB, which can be monitored by UV/Vis spectroscopy.

Block Copolymers

T. Azzam, A. Eisenberg* ——— **7443 – 7447**

Control of Vesicular Morphologies through Hydrophobic Block Length

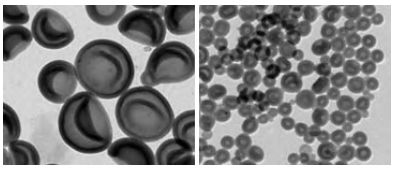

About the size of it: A series of polystyrene-*block*-poly(acrylic acid) (PS-b-PAA) block copolymers were developed in which the length of the PAA block was kept constant and the length of the PS block was varied. This allowed a study of the effect of the PAA/PS block ratio on the vesicle sizes as well as on the wall thicknesses.

P-Substituted Carbenes

S. Marrot, T. Kato,* F. P. Cossío, H. Gornitzka, A. Baceiredo* **7447 – 7450**

Cyclic Carbodiphosphorane–Diphosphinocarbene Thermal Interconversion

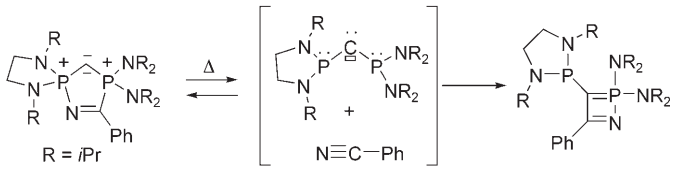

Unusual thermal ring contraction of five-membered cyclic azacarbodiphosphorane into a four-membered 1,2λ⁵-azaphosphete was observed (see scheme). Experimental and computational results indicate that the ring contraction results from a remarkable interconversion between two different types of divalent carbon species (dianionic and carbene): carbodiphosphorane and diphosphinocarbene.

© 2006 Wiley-VCH Verlag GmbH & Co. KGaA, Weinheim

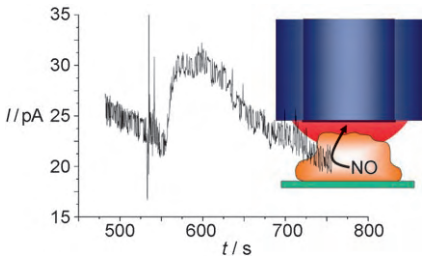

Pin point: Accurate positioning of highly sensitive and selective NO microsensors by using a shear-force-dependent constant-distance mode of SECM allows reproducible detection of stimulated NO release from adherently growing endothelial cells. The picture shows the diffusion profile of NO after stimulation of a cell (right) and the amperometric current trace of a microsensor positioned over a cell (left).

NO Microsensors

S. Isik, W. Schuhmann* ___ **7451 – 7454**

Detection of Nitric Oxide Release from Single Cells by Using Constant-Distance-Mode Scanning Electrochemical Microscopy

---

A good imitation: Aryl-1-indanyl ketones are found to be highly efficient, reversible, cell-penetrating inhibitors of the human peptidyl prolyl *cis/trans* isomerase Pin1. Owing to their structure **1**, they are assumed to mimic the transition state **2** of the enzymatically catalyzed rotation about the imidic peptide bond preceding a proline residue.

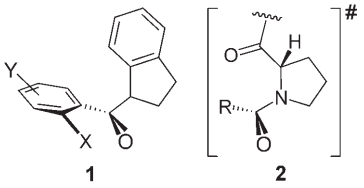

Enzyme Inhibitors

S. Daum, F. Erdmann, G. Fischer, B. Féaux de Lacroix, A. Hessamian-Alinejad, S. Houben, W. Frank, M. Braun* ___ **7454 – 7458**

Aryl Indanyl Ketones: Efficient Inhibitors of the Human Peptidyl Prolyl *cis/trans* Isomerase Pin1

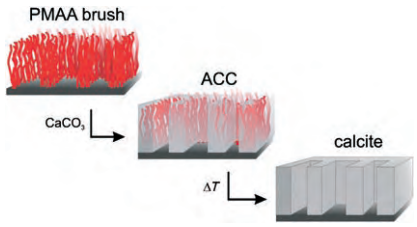

How to get into films: Micropatterned poly(methacrylic acid) (PMAA) brushes are used as an ionotropic matrix for the fabrication of microstructured calcite thin films. The calcite films are an exact 3D replica of the PMAA brush matrix (see Scheme; ACC = amorphous $CaCO_3$ phase).

Biomimetic Thin Films

S. Tugulu, M. Harms, M. Fricke, D. Volkmer,* H.-A. Klok* ___ **7458 – 7461**

Polymer Brushes as Ionotropic Matrices for the Directed Fabrication of Microstructured Calcite Thin Films

---

I see red, I see red, I see red: Optically switchable compounds were synthesized whose visible fluorescence can be quenched down to 6% with light at 360–400 nm and then restored with red light from a diode laser. The molecular switch offers potential applications in data storage and far-field microscopy with spatial resolution far below the diffraction limit.

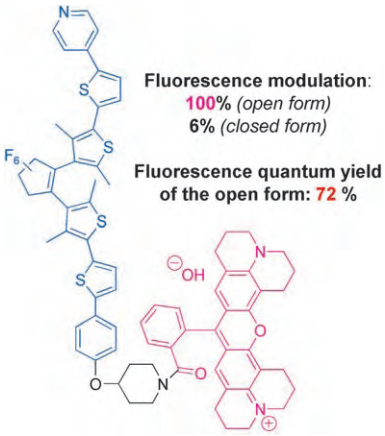

Molecular Switches

M. Bossi, V. Belov, S. Polyakova, S. W. Hell* ___ **7462 – 7465**

Reversible Red Fluorescent Molecular Switches

© 2006 Wiley-VCH Verlag GmbH & Co. KGaA, Weinheim

Contents

Intermetallic Compounds

M.-H. Whangbo,* C. Lee, J. Köhler* ——— **7465 – 7469**

Transition-Metal Anions in Solids and Their Implications on Bonding

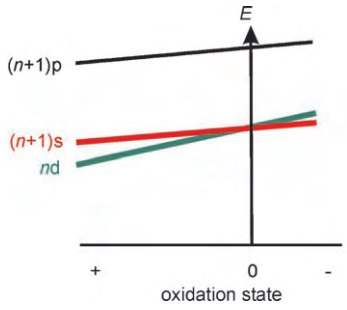

A negative disposition: Electronic-band-structure calculations reveal that in La_2M_2In (M = Pt, Cu) the transition-metal atoms can be regarded as anions with fully occupied *nd* orbitals and bonding characters similar to that of the Ge^{3-} ions in La_2Ge_2In. The orbital sequence in La_2M_2In is $(n+1)s < nd < (n+1)p$, as a result of the low oxidation states of the transition metals (see graph).

Supporting information available on the WWW (see article for access details).

A video clip is available as Supporting Information on the WWW (see article for access details).

WILEY InterScience® DISCOVER SOMETHING GREAT

"**Hot Papers**" are chosen by the Editors for their importance in a rapidly evolving field of high current interest. A preview with the graphical abstracts of these articles can be found on the *Angewandte Chemie* homepage in Wiley InterScience at www.angewandte.org.

All articles in *Angewandte Chemie* are published online several weeks ahead of print. They are found under the "**EarlyView**" link on the journal's homepage in Wiley InterScience.

Service

Keywords ——— *7471*

Authors ——— *7472*

Preview ——— *7473*

For more information on Chemistry—An Asian Journal see www.chemasianj.org

RSS Feed

Journal content prior to publication in an issue can be found online on our **Early View** page at www.angewandte.org. Stay updated on the latest journal content by registering for our **free e-mail alerts** at http://interscience.wiley.com/alerts.

Keep up with the latest research with our **RSS feed**, which provides the titles, authors, and the Digital Object Identifiers (DOIs) of Early View articles, including links to the full texts. RSS ("Really Simple Syndication") is an XML-based format for sharing and distributing web content. To receive the RSS feed, just click on the orange feed icon at www.angewandte.org, and visit http://interscience.wiley.com/rss for more information.

© 2006 Wiley-VCH Verlag GmbH & Co. KGaA, Weinheim

Awarded...

E. Delamarche receives Werner Prize

Emmanuel Delamarche (IBM Zurich, Rüschlikon) received the Swiss Chemical Society (SCS) Werner Prize for excellent research by young scientists in Switzerland. The award is named in honor of Alfred Werner (1866–1919), who was awarded the 1913 Nobel Prize in Chemistry for his work on the chemical bonding of complexes. Delamarche lectured at the Fall Meeting of the SCS on October 13 in Zurich on the topic of microcontact processing for microtechnology and biology. He recently published a Review in *Advanced Materials* on the use of microfluidics for the processing of surfaces and the miniaturization of biological assays.[1a] In 2003, his work on self-assembled microarrays of attoliter molecular vessels featured on the cover of *Angewandte Chemie*.[1b]

E. Delamarche

Delamarche received a degree in supramolecular chemistry in 1992 from the University Paul Sabatier of Toulouse in France and his PhD in biochemistry in 1995 from the University of Zurich with Dr. B. Michel (IBM), Prof. H. Sigrist (University of Bern), and Prof. H. R. Bosshard (University of Zurich). His work at the IBM Zurich Research Laboratory focuses on the use of microtechnology for biological and medical analysis. This work involves the patterning of biological molecules by microprinting and the production of functional elements of microfluidics chips, for example, for use in immunoassays. In 2003, he was recognized by IBM as a "Master Inventor".

Gramaticakis–Neumann Prize to T. Fiebig and H.-A. Wagenknecht

Torsten Fiebig (Boston College, USA) and H.-A. Wagenknecht (Technical University Munich) received the Gramaticakis–Neumann Prize of the Swiss Chemical Society. Fiebig lectured at the Fall Meeting of the SCS on light-induced dynamics in DNA on the femtosecond timescale (DNA photonics) and Wagenknecht on photoinduced electron transfer in DNA and its application in fluorescent DNA analytics. They recently reported their combined spectroscopic and chemical investigations of the reductive electron transfer in DNA in *Angewandte Chemie*, [2a] as well as model studies for reductive electron transfer in DNA with pyrene-modified pyrimidine nucleosides in *ChemPhysChem*.[2b]

Fiebig studied at the University of Göttingen and received his PhD on the electron transfer in covalently bound bichromophores in 1996 from the Max Planck Institute for Biophysical Chemistry under the supervision of J. Troe. From 1997 to 2000, he undertook postdoctoral research at the California Institute of Technology (Pasadena, USA) in the group of A. Zewail (Nobel Prize in Chemistry 1999). He then led a research group at the Technical University Munich, where he finished his habilitation in 2004 on the femtosecond dynamics of multichromophoric systems. Since 2003, he has been an assistant professor at Boston College. His research group develops spectroscopic methods to investigate structural changes in biological molecules in real time.

T. Fiebig

The group of H.-A. Wagenknecht is involved in the synthesis and characterization of fluorescent sensors, DNA bases, DNA-binding peptides, and oligonucleotides to study the mechanisms and kinetics of charge-transfer reactions, the electronic properties of DNA, and the interactions of fluorescent sensors in DNA. Wagenknecht studied chemistry at the University of Freiburg and received his PhD in 1998 in the group of W.-D. Woggon at the University of Basel on enzyme models and intermediates of the chloroperoxidase cycle. He spent the following two years with J. K. Barton at the California Institute of Technology (Pasadena, USA). From 2000 to 2004, he led a research group at the Institute for Organic Chemistry at the TU Munich, where he completed his habilitation on charge transfer in DNA. In October 2006 he became a professor of organic chemistry at the University of Regensburg.

H.-A. Wagenknecht

[1] a) E. Delamarche, D. Juncker, H. Schmid, *Adv. Mater.* **2005**, *17*, 2911; b) D. Stamou, C. Duschl, E. Delamarche, H. Vogel, *Angew. Chem.* **2003**, *115*, 5783; *Angew. Chem. Int. Ed.* **2003**, *42*, 5580.

[2] a) P. Kaden, E. Mayer-Enthart, A. Trifonov, T. Fiebig, H.-A. Wagenknecht, *Angew. Chem.* **2005**, *117*, 1662; *Angew. Chem. Int. Ed.* **2005**, *44*, 1636; b) M. Raytchev, E. Mayer, N. Amann, H.-A. Wagenknecht, T. Fiebig, *ChemPhysChem* **2004**, *5*, 706.

DOI: 10.1002/anie.200603798

WILEY InterScience DISCOVER SOMETHING GREAT
© 2006 Wiley-VCH Verlag GmbH & Co. KGaA, Weinheim

Alzheimer's Disease

DOI: 10.1002/anie.200602001

Self-Assembly of Fibers and Fibrils**

Wolfgang H. Binder and Oskar W. Smrzka*

Keywords:
Alzheimer's disease · fibrous proteins · gelators · peptides · self-assembly

Aggregation and deaggregation are central phenomena in nature. In this context, the formation of fibers through self-assembly[1] is of particular interest, as common building principles are found in both living and nonliving systems.

Protein fibers are involved in intra- and extracellular functions, such as movement, cell deformation and division, and blood clotting.[2] However, protein fibers are also involved in a group of diseases that feature pathological changes in protein conformation.[3–7] A subset of these diseases are characterized by histological and biophysical changes associated with amyloid. In these cases, the disease (amyloidosis) results from the excessive accumulation of amyloid, which consists of amyloidogenic peptides.[3–5] One of the best-studied examples is the amyloid β-peptide (Aβ), a cleavage product of the amyloid precursor protein (APP),[6] which is causally implicated in Alzheimer's disease and other neurodegenerative disorders. Other examples include amylin (or islet amyloid polypeptide (IAPP)), which is associated with diabetes, and prion protein (PrP), which is associated with transmissible spongiform encephalopathies (including bovine spongiform encephalopathy (BSE), scrapie (in sheep), and Creutzfeld–Jakob disease (in humans)). As proposed by different models,[7] β sheets form within Aβ, and the peptide then assembles into fibrils, which subsequently aggregate into hierarchical assemblies. Hydrogen bonds and hydrophobic interactions between the peptide molecules are responsible for this assembly process. A consequence of the process is the formation of extracellular amyloid plaques composed of aggregated Aβ. Another characteristic of Alzheimer's disease is the intracellular assembly of filaments of tau proteins into paired helical filaments (PHFs).[7f,h,i]

Fibers and fibrils are generated from macromolecules or small molecules through self-assembly processes (Figure 1).[8] Organogelators are a class of small organic molecules designed to effect gelation at low concentrations, through fiber aggregation and crosslinking.[9] Important factors enabling efficient fiber assembly are 1) the control of fiber–solvent interactions through a proper balance between hydrophilic and hydrophobic groups within the molecule, 2) the prevention of crystalli-

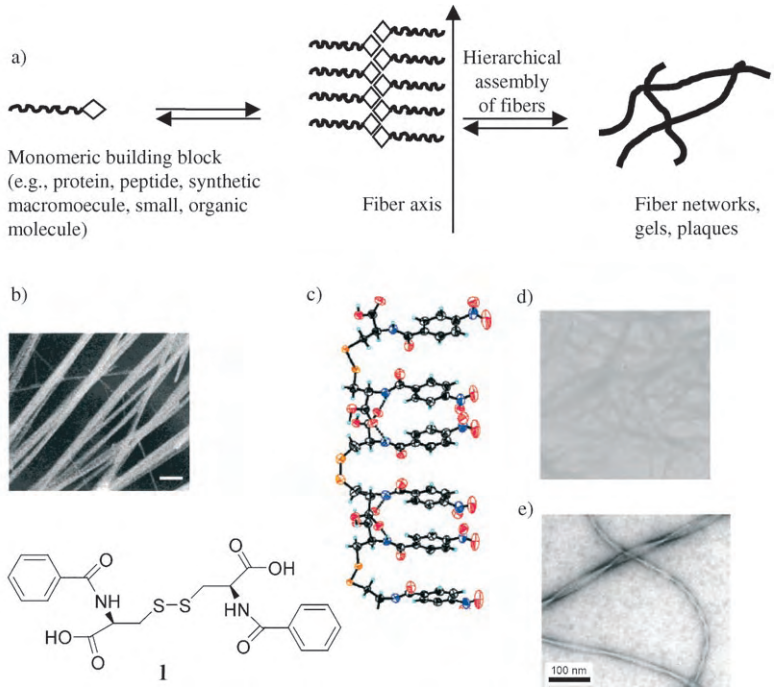

Figure 1. Self-assembly of fibers and fibrils. a) The principle of fiber formation by self-assembly: monomeric building blocks aggregate into fibers through specific intermolecular interactions and then form higher-order structures through hierarchical assembly. b) Fibrils assembled from a 3 mM solution of a low-molecular-weight gelator (**1**); scale bar is 1 μm; fibers have lengths of 50–300 nm. c) Model for the aggregation of **1** in (b); C black, H green, N blue, O red, S orange. d) TEM image of fibers assembled from dendrimers. e) TEM image of amyloid fibrils assembled from Aβ in vitro. Reproduced with permission, from references [9a,b] and [14].

[*] Prof. Dr. W. H. Binder
Vienna University of Technology
Institute of Applied Synthetic Chemistry
Getreidemarkt 9/163/MC, 1060 Vienna (Austria)
Fax: (+43) 1-58801-16299
E-mail: wbinder@mail.zserv.tuwien.ac.at
Dr. O. W. Smrzka
Children's Cancer Research Institute
St. Anna Kinderkrebsforschung
Kinderspitalgasse 6, 1090 Vienna (Austria)

[**] We kindly acknowledge the FWF of the Austrian Science Foundation for financial support (18740 B03).

InterScience
© 2006 Wiley-VCH Verlag GmbH & Co. KGaA, Weinheim

zation through anisotropic aggregation chemistry, and 3) the presence of fiber–fiber interactions leading to network formation.[9c] Many low-molecular-weight gelators that assemble into fibers in aqueous systems are therefore composed of an amide framework with hydrogen bridges and a hydrophobic exterior (*n*-alkyl or aromatic groups).[9a]

In this context, the following questions are important. How do such assembly processes take place, and how can they be controlled or even reversed? What are the differences between the aggregation of molecules with low molecular weights and the aggregation of proteins?

The aggregation of low-molecular-weight compounds into fibers and subsequently into entangled fiber networks usually takes place over several seconds or minutes in solution, hindering direct study of the self-assembly process.[10] Most current models are based on nucleation processes described by a modified Avrami model adapted from conventional crystallization processes.[11] The larger the difference $T_g - T$ between the gelation temperature T_g and the incubation temperature T, the higher the number of initial nucleating centers, which results in a faster gelation with more branched and entangled fibers.[11c] Moreover, the gelation time t_g is related to the nucleation rate J by $t_g \approx J^{-1}$.[12] Thus, a lag time for gelation on the order of minutes or even hours results, depending on the concentration of nucleation centers in solution. Therefore, the nucleation process can be controlled by the degree of supersaturation $\sigma(T)$,[11b] which is defined as $\sigma(T) = (X - X_{eq}(T))/X_{eq}(T)$, where X and $X_{eq}(T)$ are the actual and equilibrium molar fractions of solute in solution at a given temperature T. Recently, a correlation between the degree of supersaturation and the degree of branching within fibrillar networks was reported.[13] A low-molecular-weight gelator (**2**) in propylene glycol was investigated using direct light microscopy (Figure 2). A higher supersaturation (achieved through a higher cooling rate) leads to a distinct increase in branching in the formation of fibrillar or spherulitic networks.

In the case of Aβ, the major plaque-forming agent in Alzheimer's disease, the situation is different, as temperature does not directly affect the fiber-aggregation process. The basic structure of amyloid is characterized by straight, unbranched fibrils of 7–12 nm in diameter and of indeterminate length (Figure 3), which are often arranged in a spherulitic network.[14,7] Combined structural investigations of peptide fragments with solid-state NMR spectroscopy, transmission electron microscopy (TEM), image reconstruction analysis, and X-ray diffraction revealed the presence of a cross unit consisting of β sheets (residues 12–24 and 30–40) held together in a double layer by hydrogen bonds.[7j] It has been proposed that hydrophobic interactions and π–π stacking between phenylalanine residues also contribute to the formation of the fibrillar structures.[7e] Moreover, recent studies suggest that tyrosine–tyrosine interactions play an important role in the assembly process.[7i]

A Congo red (CR) binding assay and an assay using the fluorescent dye thioflavine T (ThT), which specifically binds to cross units, enable the detection of amyloid deposits and the in vitro monitoring of the aggregation process. Both binding assays rely on hydrophobic aromatic π-stacking interactions, and the CR assay additionally relies on electrostatic interactions between sulfonate moieties and positively charged amino acids of Aβ.[15]

The details of the aggregation process are still unknown. In the case of Aβ formation in Alzheimer's disease, aggregation occurs in a stochastic manner and involves nucleation steps[16] based on the misfolding of Aβ (Figure 4).[17] Short peptide sequences have been proposed as nucleation sites in this process.[7i] Above a certain protein concentration, there is a lag phase in fibril formation, which can be shortened if a preformed nucleus is present in the supersaturated solution. Thus, the lag time can be reduced from several days to less than one hour by sonicating, and thereby partially destroying fibrils,

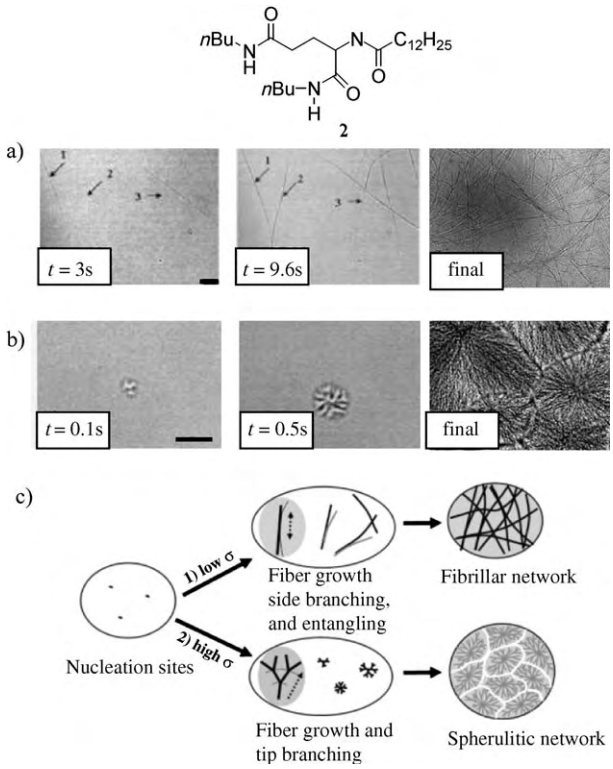

Figure 2. Kinetics of fiber assembly from supersaturated solutions of **2** (obtained by cooling saturated solutions below the gelation temperature T_g). The assembly process was monitored by light microscopy. a) Evolution of a fibrillar network at low supersaturation σ; scale bar is 20 μm; three nucleation points are indicated. b) Evolution of a spherulitic network at higher supersaturation (obtained by faster cooling); scale bar is 50 μm. c) Model for the aggregation of **2** into either fibrillar or spherulitic networks by nucleation and subsequent hierarchical assembly. Reproduced with permission, from reference [13].

© 2006 Wiley-VCH Verlag GmbH & Co. KGaA, Weinheim

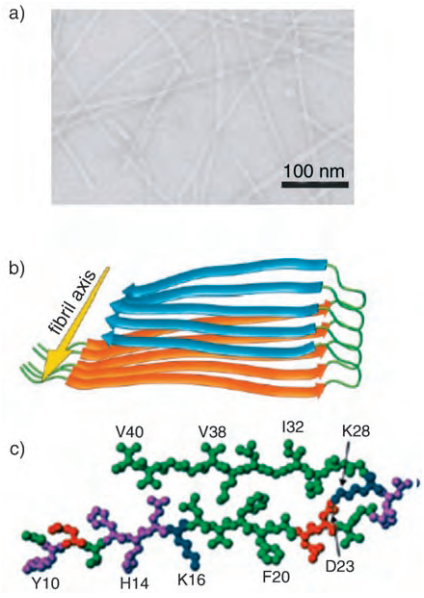

Figure 3. Structure of $A\beta_{1-40}$ fibrils. a) TEM image of negatively stained amyloid fibrils, which are long and unbranched. b) Model of the structure of $A\beta_{1-40}$ fibrils based on solid-state NMR spectroscopy, which incorporates the cross units typical of amyloid fibrils. Within the five-molecule layer shown, the parallel β sheets formed by residues 12–24 are represented as orange ribbons, and those formed by residues 30–40 are represented as blue ribbons. c) Model of the cross section of an $A\beta_{1-40}$ fibril based on scanning electron microscopy (SEM), showing the interface between two β sheets; hydrophobic green, polar magenta, positive blue, negative red. Reproduced with permission, from references [7c,d].

which can then serve as nucleation points in vitro.[18]

In the aggregation process, small beadlike structures (prefibrillar aggregates) are generated first,[18c] and these subsequently assemble into more distinct morphologies (protofilaments, protofibrils). As demonstrated recently by solid-state NMR spectroscopy on $A\beta_{10-40}$ fragments, the final state of the fibrils (morphology and degree of hydration) does not depend on the amino acids in positions 1–9.[18d] The fibril-forming process was also recently investigated by light microscopy; in this study, the assembly of fibers into spherulitic networks was monitored directly, and a strong similarity to the growth of low-molecular-weight gels was demonstrated (see above).[18b]

Starting from the natively unfolded protein in vivo, genetic and extracellular factors can lead to misfolding, which can cause the protein to aggregate into oligomers, and subsequently into protofibrils and mature fibrils. Heat shock proteins (Hsp; chaperones) can guide the folding process and, thus, prevent aggregation.[17e,f] Additionally, ubiquitinylation (the attachment of ubiquitin (Ub)) can mark misfolded proteins for destruction inside a proteasome complex, thus, preventing their accumulation. Whereas in vitro a minimum concentration of misfolded protein precursor of 20–80 μM for $A\beta_{1-40}$ or approximately 100 μM for $A\beta_{1-42}$ is required to achieve fibril nucleation,[19a,b] in vivo the minimum concentration of Aβ in the blood or cerebrospinal fluid is at least three orders of magnitude lower (in the nanomolar range). The large difference between the minimum in vitro and in vivo concentrations has not yet been explained; however, lipid–protein interactions are a possible reason for the increased local accumulation of Aβ in vivo.[19c] According to another hypothesis, oligomeric species (for example, micellar aggregates of Aβ) may be the actual cause of neuronal toxicity in vivo.[19d]

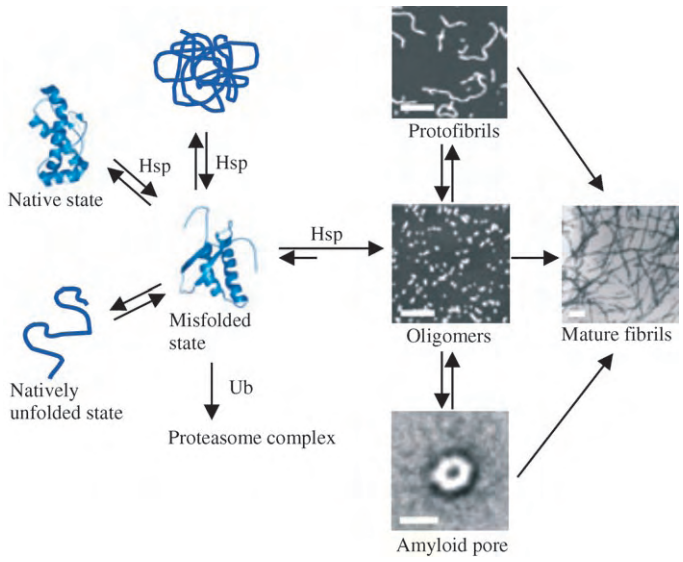

Figure 4. Factors influencing the folding and subsequent aggregation of Aβ in vivo. Starting from a natively unfolded state of Aβ, a population of misfolded protein is generated. Pathways involving heat shock proteins (Hsp) or ubiquitin (Ub) can reduce the amount of misfolded protein. The misfolded protein can assemble into oligomers and, subsequently, into protofibrils and fibrils. Reproduced with permission, from reference [17a].

An important prerequisite for studying the assembly process of Aβ is the existence of assays allowing the aggregation to be monitored in vitro and in vivo. Such assays can be used for aggregation-inhibitor screening or for validation. The feasibility of these assays has been demonstrated for Aβ,[20b–f] and for other filament-forming proteins and peptides,[20a,g] through the use of physicochemical[20e–g] or even biological/genetic detection systems (such as those used in an antiprion screen[20a]). Several methods have been tested for in vitro assays: fluorescence analysis (by CR and ThT binding), surface plasmon resonance spectroscopy,[21] density gradient centrifugation, and fluorescence correlation spectroscopy.[22]

In a recent paper, a molecular scaffold with four $A\beta_{16-37}Y_{20}K_{22}K_{24}$ segments (in which Phe20 was mutated to Tyr, and Glu22 and Val24 were mutated to Lys) was described (Figure 5).[20d] This model system was able to assemble into protofibrils without the lag phase typically observed for native Aβ, enabling the study of the early stages of aggregation.

Another facet in the study of fibril formation is the early detection of amyloid in the brain, which is important for an early start of treatment, as well as for a better understanding of the in vivo assembly process. Recently, promising techniques in positron-emission tomography (PET)[23a] and near infrared spectroscopy,[23b] which utilize selectively enriched marker molecules have been developed.

Numerous studies on the identification of possible inhibitors for Aβ aggre-

 © 2006 Wiley-VCH Verlag GmbH & Co. KGaA, Weinheim

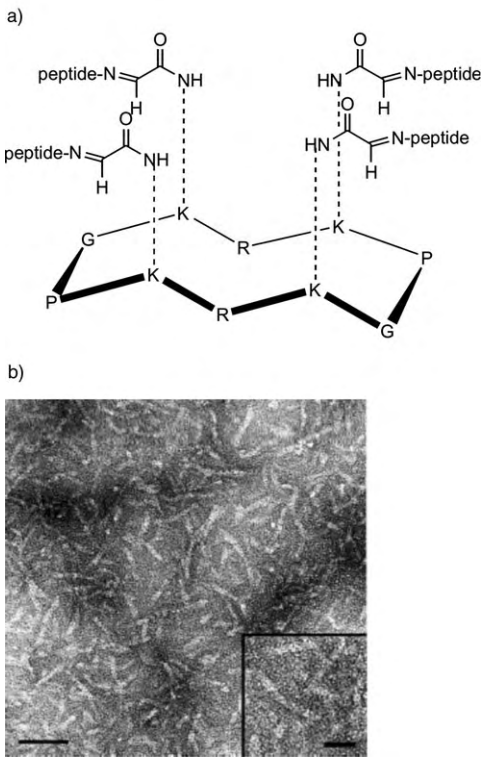

Figure 5. Protofibril assembly by a template approach. a) Four identical peptides (peptide = $A\beta_{16-37}Y_{20}K_{22}K_{24}$) are fixed on a cyclic peptide backbone. b) TEM image of the protofibrils formed from the peptide template; scale bar is 50 nm. Inset: magnified image; scale bar is 20 nm. Reproduced with permission, from reference [20d].

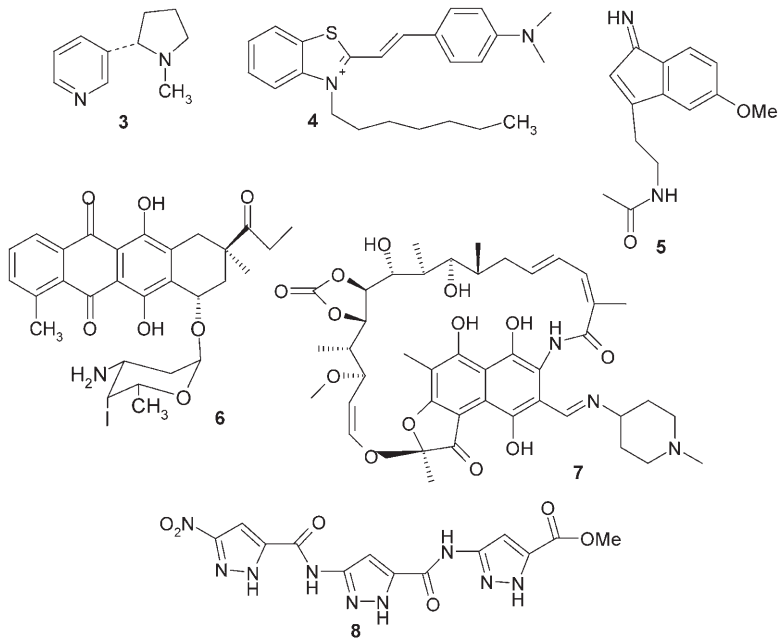

Scheme 1. Inhibitors of fibril formation by Aβ: nicotine (**3**), a benzothiazole (**4**), a melatonin (**5**), an anthracycline (**6**), a rifamycin (**7**), a "trimeric" 3-aminopyrazole (**8**).

gation have been performed.[24] Inhibiting fibril and, ultimately, plaque formation in vivo is very difficult. Thus, a number of small organic molecules that inhibit this aggregation process in vitro have been identified (Scheme 1). However, since the interacting interface between Aβ molecules is large, a plethora of binding sites are present, which leads to an ill-defined model for the structure–activity relationship (SAR) and a relatively low inhibition efficiency. The use of proteins (for example, the use of butyrylcholinesterase[25a] or immunotherapeutic strategies[25b]) and peptides for inhibition is more successful: a number of active peptides (for example, with the sequence KLVFF)[14b] able to block the aggregation process have been identified.[14] A disadvantage is that the clinical administration of large peptides is difficult, particularly because of their poor ability to cross the blood–brain barrier.

A new approach is the development of β-sheet mimetics consisting of either 3-aminopyrazoles[22] or of peptides containing 3-aminopyrazole motifs.[26] By utilizing the distinct hydrogen-bonding motif (donor–acceptor–donor) of the 3-aminopyrazole unit, a binding of Aβ fragments in the micromolar range could be achieved. Systems based on the simultaneous interaction of two peptides with a specific low-molecular-weight compound (that is, peptide–ligand–peptide) are ideal for inhibition. In such a system, the low-molecular-weight compound (ligand) consists of a small organic moiety with an affinity for Aβ (such as CR) and a component with an affinity for another protein (such as the synthetic ligand for FK_{506}-binding protein (SLF)). The steric demand of the second protein blocks the aggregation of Aβ. This approach has already delivered excellent results: a fivefold increase in efficiency over that of the ligand alone was achieved in vitro.[27]

The formation of fibers and fibrils is an important process in living and nonliving systems. In both instances, nucleation is often guided by specific events, which determine the assembly kinetics and the final morphology. New in vitro and in vivo screening and validation models allowing the study of aggregation/deaggregation kinetics in various protein-folding diseases are becoming available. These models form the basis for drug-screening and validation assays. In particular, the understanding of fibril formation in Alzheimer's disease is a major driving force in the development novel therapeutic strategies.

Published online: October 20, 2006

[1] S. Zhang, *Nat. Biotechnol.* **2003**, *21*, 1171–1178.
[2] a) T. Scheibel, *Curr. Opin. Biotechnol.* **2005**, *16*, 427–433; b) L. A. Smith, P. X. Ma, *Colloids Surf. B* **2004**, *39*, 125–131.
[3] a) D. J. Selkoe, *Nature* **2003**, *426*, 900–904; b) C. A. Ross, M. A. Poirier, *Nat. Med.* **2004**, S10–S17.
[4] J. Johansson, *FEBS J.* **2005**, *272*, 5941, special series on Alzheimer's disease.
[5] a) J.-C. Rochet, P. T. Lansbury, Jr., *Curr. Opin. Struct. Biol.* **2000**, *10*, 60–68; b) C. Lee, M.-H. Yu, *J. Biochem. Mol. Biol.* **2005**, *38*, 275–280.
[6] M. Citron, *Nat. Rev.* **2004**, *5*, 677–685.
[7] a) O. S. Makin, E. Atkins, P. Sikorski, J. Johansson, L. C. Serpell, *Proc. Natl. Acad. Sci. USA* **2005**, *102*, 315–320; b) R. Tycko, *Curr. Opin. Struct. Biol.* **2004**, *14*, 96–103; c) O. S. Makin, L. C. Serpell, *FEBS J.* **2005**, *272*, 5950–5961; d) A. T. Petkova, Y. Ishii, J. J. Balbach,

 © 2006 Wiley-VCH Verlag GmbH & Co. KGaA, Weinheim

O. N. Antzutkin, R. D. Leapman, F. Delaglio, R. Tycko, *Proc. Natl. Acad. Sci. USA* **2002**, *99*, 16742 – 16747; e) R. Azriel, E. Gazit, *J. Biol. Chem.* **2001**, *276*, 34156 – 34161; f) F. A. R. Quijano, D. Morrow, B. M. Wise, F. L. Brancia, W. J. Goux, *Biochemistry* **2006**, *45*, 4638 – 4652; g) J.-P. Guo, T. Arai, J. Miklossy, P. L. McGeer, *Proc. Natl. Acad. Sci. USA* **2006**, *103*, 1953 – 1958; h) S. Bieler, L. Estrada, R. Lagos, M. Baeza, J. Castilla, C. Soto, *J. Biol. Chem.* **2005**, *280*, 26880 – 26885; i) H. Inouye, S. Deepak, W. Goux, D. A. Kirschner, *Biophys. J.* **2006**, *90*, 1774 – 1789; j) M. J. Thompson, S. A. Sievers, J. Karanicolas, M. I. Ivanova, D. Baker, D. Eisenberg, *Proc. Natl. Acad. Sci. USA* **2006**, *103*, 4074.

[8] N. M. Sangeetha, U. Maitra, *Chem. Soc. Rev.* **2005**, *34*, 821 – 836.

[9] a) F. M. Menger, K. L. Caran, *J. Am. Chem. Soc.* **2000**, *122*, 11679 – 11691, and references therein; b) K. J. C. van Bommel, C. van der Pol, I. Muizbelt, A. Friggeri, A. Heeres, A. Meetsma, B. L. Feringa, J. van Esch, *Angew. Chem.* **2004**, *116*, 1695; *Angew. Chem. Int. Ed.* **2004**, *43*, 1663 – 1667; representative reviews: c) M. de Loos, B. L. Feringa, J. H. van Esch, *Eur. J. Org. Chem.* **2005**, 3615 – 3631; d) A. R. Hirst, D. K. Smith, *Chem. Eur. J.* **2005**, *11*, 5496 – 5508; e) P. Terech, R. G. Weiss, *Chem. Rev.* **1997**, *97*, 3133 – 3159; f) D. J. Abdallah, R. G. Weiss, *Adv. Mater.* **2000**, *12*, 1237 – 1247.

[10] Attempts at direct observation by cryo-TEM: L. A. Estroff, L. Leiserowitz, L. Addadi, S. Weiner, A. D. Hamilton, *Adv. Mater.* **2003**, *15*, 38 – 42; by fluorescence: S. Mukhopadyay, U. Maitra, Ira, G. Krishnamoorthy, J. Schmidt, Y. Talmon, *J. Am. Chem. Soc.* **2004**, *126*, 15905 – 15914; for a recent example of supramolecular fiber association and direct observation by CD spectroscopy see: P. Jonkheijm, P. van der Schoot, A. P. H. J. Schenning, E. W. Meijer, *Science* **2006**, *313*, 80 – 83.

[11] a) M. Avrami, *J. Chem. Phys.* **1940**, *8*, 212 – 224; application to gels: b) J.-L. Li, X.-Y. Liu, R.-Y. Wang, J.-Y. Xiong, *J. Phys. Chem. B* **2005**, *109*, 24231 – 24235; c) X. Huang, P. Terech, S. R. Raghavan, R. G. Weiss, *J. Am. Chem. Soc.* **2005**, *127*, 4336 – 4344.

[12] X. Y. Liu, P. D. Sawant, *Adv. Mater.* **2002**, *14*, 421 – 426.

[13] R. Wang, X.-Y. Liu, J. Xiong, J. Li, *J. Phys. Chem. B* **2006**, *110*, 7275 – 7280.

[14] Recent publications: a) M. Necula, C. N. Chirita, J. Kuret, *Biochemistry* **2005**, *44*, 10227 – 10237; b) E. Gazit, *FEBS J.* **2005**, *272*, 5971 – 5978; c) T. D. Gibson, R. M. Murphy, *Biochemistry* **2005**, *44*, 8898 – 8907.

[15] a) H. Levine III, *Amyloid* **1995**, *2*, 1 – 6; b) R. Khurana, V. N. Uversky, L. Nielsen, A. L. Fink, *J. Biol. Chem.* **2001**, *276*, 22715 – 22721.

[16] a) H. Inouye, D. A. Krischner, *J. Struct. Biol.* **2000**, *130*, 123 – 129; b) J. van Gestel, S. W. de Leeuw, *Biophys. J.* **2006**, 90, 3134 – 3145.

[17] a) T. R. Jahn, S. E. Radford, *FEBS J.* **2005**, *272*, 5962 – 5970; b) A. Melquiond, G. Boucher, N. Mousseau, P. Derreumaux, *J. Chem. Phys.* **2005**, *122*, 174904; c) D. Thiruumalai, D. K. Klimov, R. I. Dima, *Curr. Opin. Struct. Biol.* **2003**, *13*, 146 – 159; d) P. Westermark, *FEBS J.* **2005**, *272*, 5942 – 5949; e) S. Lee, F. T. F. Tsai, *J. Biochem. Mol. Biol.* **2005**, *38*, 259 – 265; f) R. Carotta, M. Manno, D. Bulone, V. Martorana, P. L. S. Biagio, *J. Biol. Chem.* **2005**, *280*, 30001 – 30008.

[18] a) P. Friedhoff, M. von Bergen, E.-M. Mandelkow, P. Davies, E. Mandelkow, *Proc. Natl. Acad. Sci. USA* **1998**, *95*, 15712 – 15717; b) S. S. Rogers, M. R. H. Krebs, E. H. C. Bromley, E. van der Linden, A. M. Donald, *Biophys. J.* **2006**, *90*, 1043 – 1054; c) C. M. Dobson, *Nature* **2003**, *426*, 884; d) A. K. Paravastu, A. T. Petkova, R. Tycko, *Biophys. J.* **2006**, *90*, 4618 – 4629.

[19] a) J. D. Harper, P. T. Lansbury, Jr., *Annu. Rev. Biochem.* **1997**, *66*, 385 – 407; b) F. Chiti, P. Webster, N. Taddei, A. Clark, M. Stefani, G. Ramponi, C. M. Dobson, *Proc. Natl. Acad. Sci. USA* **1999**, *96*, 3590 – 3594; c) Review: G. P. Gorbenko, P. K. J. Kinnunen, *Chem. Phys. Lipids* **2006**, *141*, 72 – 82; d) R. Kayed, E. Head, J. L. Thompson, T. M. McIntire, S. C. Milton, C. W. Cotman, C. G. Glabe, *Science* **2003**, *300*, 486.

[20] a) D. Triboulliard, S. Bach, F. Gug, N. Desban, V. Beringue, T. Andrieu, D. Dormont, H. Galons, H. Laude, D. Vilette, M. Blondell, *Biotechnol. J.* **2006**, *1*, 58 – 67; b) P. Makshi, Y.-F. Liao, J. Gao, J. Ni, R. Stein, L.-A. Yeh, M. S. Wolfe, *J. Biomol. Screening* **2005**, *10*, 1 – 12; c) L. Söderberg, C. Dahlqvist, H. Kakuyama, J. Thyberg, A. Ito, B. Winblad, J. Näslund, L. O. Tjernberg, *FEBS J.* **2005**, *272*, 2231 – 2236; d) G. T. Dolphin, P. Dumy, J. Garcia, *Angew. Chem.* **2006**, *118*, 2765 – 2768; *Angew. Chem. Int. Ed.* **2006**, *45*, 2699 – 2702; e) S. Akikusa, K. I. Watanabe, E. Horikawa, K. Nakamura, M. Kodaka, H. Okuno, T. Konakahara, *J. Pept. Res.* **2003**, *61*, 1 – 6; f) X. Cheng, R. B. van Breemen, *Anal. Chem.* **2005**, *77*, 7012 – 7015; g) M. Pickhardt, *J. Biol. Chem.* **2005**, *280*, 3628 – 3635.

[21] C. W. Cairo, A. Strzelec, R. M. Murphy, L. L. Kiessling, *Biochemistry* **2002**, *41*, 8620 – 8629.

[22] P. Rzepecki, L. Nagel-Steger, S. Feuerstein, U. Linne, O. Molt, R. Zadmard, K. Aschermann, M. Wehner, T. Schrader, D. Riesner, *J. Biol. Chem.* **2004**, *279*, 47497 – 47505.

[23] a) S. T. DeKosky, K. Marek, *Science* **2003**, *302*, 830 – 834; b) E. E. Nesterov, J. Koch, B. T. Hyman, W. E. Klunk, B. J. Bacskai, T. M. Swager, *Angew. Chem.* **2005**, *117*, 5588 – 5592; *Angew. Chem. Int. Ed.* **2005**, *44*, 5452 – 5456.

[24] H. LeVine, *Curr. Med. Chem.* **2002**, *9*, 1121 – 1133.

[25] a) S. Diamant, E. Podoly, A. Friedler, H. Ligumsky, O. Livnah, H. Soreq, *Proc. Natl. Acad. Sci. USA* **2006**, *103*, 8628 – 8633; b) H. L. Weiner, D. Frenkel, *Nat. Rev. Immunol.* **2006**, *6*, 404 – 416.

[26] P. Rzepecki, T. Schrader, *J. Am. Chem. Soc.* **2005**, *127*, 3016 – 3025.

[27] M. Bose, J. E. Gestwicki, V. Devasthali, G. R. Crabtree, I. A. Greaf, *Biochem. Soc. Trans.* **2005**, *33*, 543 – 547.

 © 2006 Wiley-VCH Verlag GmbH & Co. KGaA, Weinheim

Antiviral Agents

DOI: 10.1002/anie.200602623

Tamiflu: The Supply Problem

Vittorio Farina and Jack D. Brown**

Keywords:
antiviral agents · inhibitors · quinic acid · shikimic acid · synthetic methods

The influenza pandemic of 1918 (the Spanish flu) is estimated to have killed between 20 and 40 million people worldwide;[1] that is, more than the World War that preceded it. The 1957 (Asian) and 1968 (Hong Kong) epidemics wreaked less havoc, but shared some basic features with the Spanish flu: they were caused by recombinant viruses of avian origin, the products of a reassortment between known human viruses and/or bird viruses. The recurrence of these outbreaks leaves little doubt about the future emergence of new influenza strains, against which humans will have no immunity. A major flu pandemic will eventually strike again. The important questions are when, and how will we deal with it.

The avian H5N1 influenza, which originated in poultry in Hong Kong in 1997, has already infected over 100 humans and shown a lethality rate of over 50%. The isolated virus is purely avian in origin, that is, it is not a reassortant and does not spread from human to human. However, there is mounting fear that a mutated form of this virus may lead to a new pandemic. Perhaps less appreciated is the fact that each year, despite widespread immunizations, influenza kills 20000–40000 Americans. These epidemics cost the US economy about $12 billion per year in healthcare expenses and productivity losses.[2]

There is considerable political debate regarding the preparedness of the US and other countries to combat a possible pandemic of the type experienced in 1918.[3] With respect to a century ago medicine has made some progress against this disease, and it is widely believed that adequate weapons currently exist to combat the next flu outbreak or at least lessen its blow, given sufficient financial resources.

The influenza A, B, and C viruses are RNA viruses. The type A virus is classified according to subtypes based on the structure of the two surface proteins, haemagglutinin (H) and neuraminidase (NA). The influenza A virus, in addition, contains the M2 protein, a proton channel. This protein is not present in type B and C viruses.[4]

Immunization is traditionally an effective approach to fight flu epidemics. However, the protective efficacy of these vaccines is 70–90% in healthy individuals under 65 years of age, and drops further when dealing with older patients.[5] In addition, the antigenic drift caused by error-prone RNA replication requires continuous updates of vaccines. While immunization remains an important approach to prevent influenza, small-molecule antiviral agents represent a novel opportunity for effective prevention and therapy of flu.

Inhibitors of the M2 proton pump have been known for decades, but widespread use of amantadine and rimantadine, the two marketed, clinically effective inhibitors, has been thwarted by the emergence of drug resistance and by toxic side effects. In addition, applicability to influenza A only is a serious limitation.[6] In contrast, neuraminidase is an essential enzyme for viral replication in all three classes. NA catalyzes the cleavage of sialic acid residues from glycoproteins and liberates the budding virion from the infected cell, inhibiting entrapment and self-aggregation. The enzyme is a tetramer made up of identical subunits, and its X-ray crystal structure has been solved, as has the structure of its complex with sialic acid.[7] The active site is highly conserved across all influenza A and B virus strains, thus suggesting NA as a target for the development of broad-spectrum influenza antibiotics. Structural data have allowed the rational design of potent inhibitors.[2] Two of these inhibitors have reached the market, namely, zanamivir (GSK's Relenza (**1**)) in July 1999, and oseltamivir phosphate (Gilead's Tamiflu (**2**), also marketed by Roche) in October 1999.

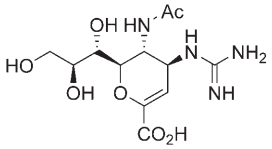

1

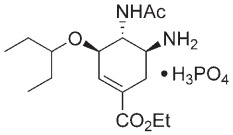

2

Zanamivir has low bioavailability and is administered by inhalation, which can cause problems in patients with underlying respiratory disease. In contrast, oseltamivir phosphate is administered as capsules and has very high bioavailability. Its ester function is

[*] Dr. V. Farina
Department of Chemical Development
Boehringer Ingelheim Pharmaceuticals
900 Ridgebury Rd
Ridgefield CT 06877 (USA)
Fax: (+1) 203-791-6130
E-mail:
farinav@rdg.boehringer-ingelheim.com
Dr. J. D. Brown
Department of Development
Boehringer Ingelheim Chemicals
2820 North Normandy Drive
Petersburg VA 23805–9372 (USA)
Fax: (+1) 804-698-7214
E-mail: jbrown@bichem.com

InterScience
© 2006 Wiley-VCH Verlag GmbH & Co. KGaA, Weinheim

cleaved in vivo, and oseltamivir must therefore be considered a prodrug. Both inhibitors are active in vitro against all known influenza strains, including the H5N1 avian strain. Because the amino acid residues at the enzyme active site are highly conserved, there is hope that these inhibitors may be active against an influenza pandemic, regardless of the particular viral strain.[8] Indeed, whereas resistance to NA inhibitors has been engineered by multiple virus passages in vitro, preliminary information shows that all these mutants are either poorly stable or display reduced infectivity in animal models.[9]

Notably, oseltamivir phosphate has been shown to be effective in the *prevention* of influenza infection. Its drawback, shared with zanamivir, is that it must be administered to influenza patients no later than 36–48 h after the manifestation of the symptoms in order to be effective.[10] This has led to public demand for stockpiles of Tamiflu, both as a reasonable frontline therapy against a possible flu pandemic and as a preventive agent, in conjunction with convenient diagnostic kits, which are under development.[3] In response to worldwide demand, Roche has been pressured to ease patent restrictions on Tamiflu to help meet the huge backlog of orders, and has pledged, through the recruitment of manufacturing partners, to increase output to 300 million treatments per year.[11] Each treatment (75 mg capsules, 5-day course) costs $80–90.

One of the factors limiting the large-scale production of the drug is the scarcity of the synthetic precursors, which are extracted from plants. Shikimic acid (**3**) and quinic acid (**4**) are intermediates in the biosynthesis of essential aromatic amino acids. In plants, these compounds are also precursors to lignins and phenols[12] and they accumulate to some extent, especially in gymnosperms and woody dicotyledons. Shikimic acid is present in concentrations of up to 0.16 mg g^{-1} fresh weight, and quinic acid is also a widespread and relatively abundant component.

The most important source of shikimic acid is in the family of *Illicium* (a small tree or shrub of known herbal value). Shikimic acid was first isolated from a member of this family (*I. religiosum*) in 1885.[13] Star anise (*I. verum*), found in four provinces of Southern China, is a rich natural source for shikimic acid, with 30 kg of dried plant required to produce 1 kg of shikimic acid.[14] To realize the plan by the US government to store 300 million doses of Tamiflu, 23 tons of bulk drug substance would be required (assuming a yield of 35% from shikimic acid to oseltamivir phosphate and a dose of 75 mg), equivalent to about 840 tons of star anise.[14] The needs for the US alone clearly require an alternative source of shikimic acid. This was partially addressed by Frost and co-workers at Michigan State University. They were able to genetically modify *E. coli* to produce shikimic acid by recombinant microbial biocatalysis.[15] Currently, the fermentation approach supplies approximately 30% of the present requirements.[14]

The increasing demand for oseltamivir phosphate has placed further pressure on Roche and the chemical community in general to increase the supply of shikimic and quinic acids through improved isolation, fermentation, or synthesis, and also to develop new routes to the drug that do not involve complex natural products as precursors, but rather cheap and widely available commodity chemicals. The current manufacturing process to **2** is shown in Scheme 1. The synthesis proceeds through intermediate **5**, which is regioselectively reduced to epoxide **6**.[16] Several approaches have been developed for the introduction of the N-based substituents, initially involving the use of hazardous azide-based reagents. Aziridines such as **7** have been obligatory intermediates. The dependence on using azide chemistry to convert epoxide **6** into oseltamivir phosphate was considered a weakness in the first-generation manufacturing process.

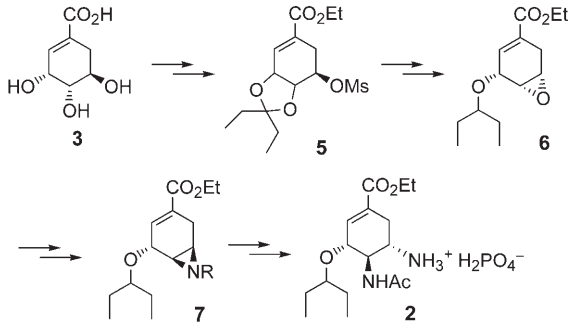

Scheme 1. Key intermediates to oseltamivir phosphate from shikimic acid. Ms = methanesulfonyl.

Scientists at Roche tried to address this problem by developing several routes to **2** by using epoxide **6** as the starting point, together with non-azide N-based nucleophiles.[17] These routes have been reviewed.[18] The elimination of shikimic or quinic acids as raw materials has proved to be more challenging, and several attempts have been described in the patent literature.[19,20] The first one (Scheme 2) employed the Diels–Alder reaction of furan and ethyl acrylate as the starting point. This reaction resulted in a 9:1 mixture of *exo*/*endo* adducts. The racemic adduct **8** was

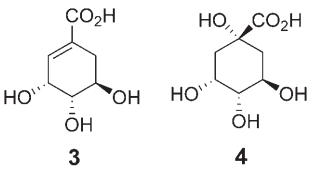

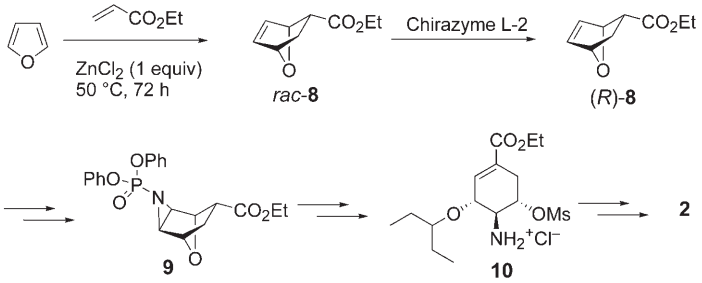

Scheme 2. Approach to oseltamivir by a Diels–Alder reaction followed by enzymatic resolution.

© 2006 Wiley-VCH Verlag GmbH & Co. KGaA, Weinheim

resolved by using an esterase. The double bond resulting from the cycloaddition was functionalized by using a phosphoryl azide to give two regioisomeric [3+2] *exo* products. The two *exo*-triazoles were thermally decomposed to give aziridine **9**, which following transesterification with ethanol and base elimination gave **10**, a key precursor to **2**.[18]

Although this process eliminated the use of shikimic and quinic acids, it suffered from several impractical steps that required high dilution, which in turn can seriously affect the production output. In addition, the yield of the enzymatic resolution step is quite low (20%).

In another approach, also reported by scientists at Roche, a very inexpensive starting material, 1,6-dimethoxyphenol (**11**), is used (Scheme 3). The process was inspired by the recognition of the hidden C_2 symmetry in **2**. After introduction of the 3-pentyl ether, bromination and a double ethoxycarbonylation reaction gave diester **12**. Ru-catalyzed hydrogenation gave an all-*cis* diether, in which the ether functions were removed by using in situ generated trimethylsilyl iodide. The product from this reaction was the dihydroxy diester **13**, which was desymmetrized by using inexpensive pig-liver esterase to give **14** in very high yield (96%) and enantiomeric excess (96–98% *ee*). This intermediate, **14**, was subjected to a Yamada–Curtius degradation using diphenylphosphoryl azide, leading to oxazolidinone **12**. Further elaboration, using NaN_3 as nucleophile, gave the desired intermediate azide **16**, which was transformed into **2** in four additional steps in good overall yield (30%).

This approach (Scheme 3) avoids the use of either quinic or shikimic acids and compares favorably with the manufacturing process; its drawback is that it still uses sodium azide late in the process, which is undesirable from a reaction safety standpoint.

More recently, the Tamiflu supply issue has piqued the attention of academic chemists, and some new approaches have been reported. Corey and co-workers recently reported an interesting approach employing 1,3-butadiene and trifluoroethyl acrylate as raw materials.[21] The approach features a highly enantioselective and high-yielding cycloaddition promoted by a catalytic amount of oxazaborolidine **17** (Scheme 4). The cycloaddition was followed by amidation, iodo-lactamization, and protection to yield **19**, dehydrohalogenation of which followed by allylic bromination yielded **21**. Base-promoted dehydrohalogenation gave **22**, and its regio- and stereoselective bromo-amidation yielded **23**. Sequential dehydrohalogenation gave an intermediate aziridine, which was regioselectively opened with 2-pentanol to furnish **24**. Deprotection of **24** yielded oseltamivir phosphate in 11 chemical steps and about 30% overall yield.

Shibasaki and co-workers also reported an enantioselective approach to oseltamivir by using another cheap and widely available raw material, 1,4-cyclohexadiene (Scheme 5).[22] Thus, opening of acylaziridine **25** with trimethylsilylazide under the catalysis of Y^{III} and chiral ligand **26** yielded **27** with 91% *ee*. This enantioselectivity could be further upgraded by crystallization. Functional manipulations gave **28**, which was oxidized (allylic) in two steps using selenium dioxide and Dess–Martin periodinane to give **29**. Ni-catalyzed cyanation yielded **30**, which was stereoselectively reduced to **31**. The crucial ether bond was formed by a Mitsunobu reaction, and then standard manipulations yielded oseltamivir in 17 steps and an overall yield of 1%.

Cong and Yao also reported a synthesis of the active pharmaceutical ingredient by using a cheap and widely available chiral raw material, L-serine.[23] The synthesis (Scheme 6) is based on a ring-closing metathesis reaction, catalyzed by second-generation Ru carbene species **37**, to form the key cyclohexene core in **38**. Unfortunately, formation of **36** is poorly diastereoselective (3:1) and

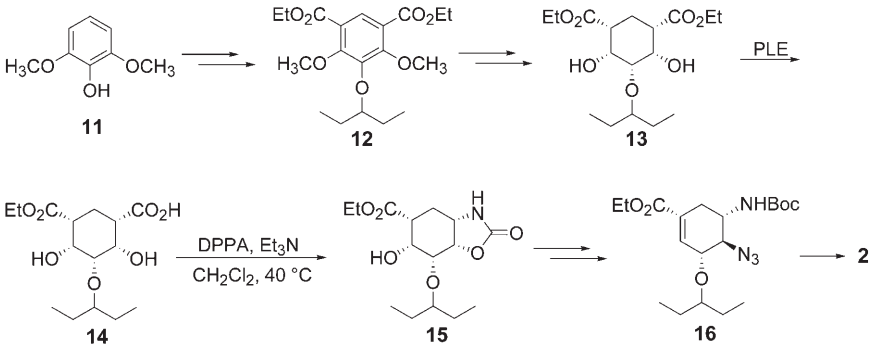

Scheme 3. Desymmetrization approach to oseltamivir. PLE = pig-liver esterase, DPPA = diphenylphosphoryl azide, Boc = *tert*-butyloxycarbonyl.

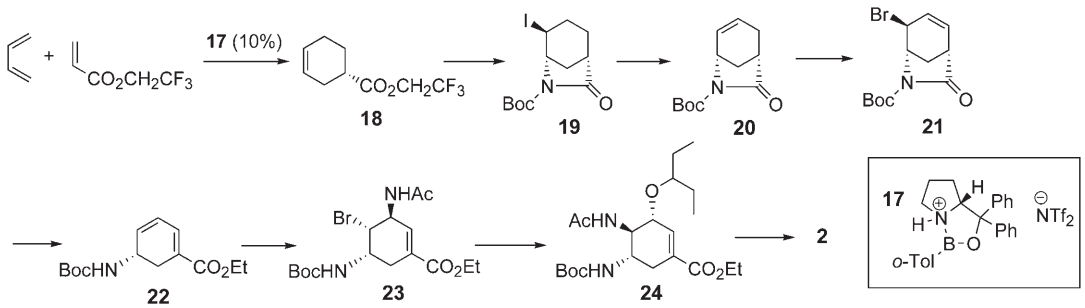

Scheme 4. Corey and co-worker's approach.[21] Tf = trifluoromethanesulfonyl, Tol = tolyl.

 © 2006 Wiley-VCH Verlag GmbH & Co. KGaA, Weinheim

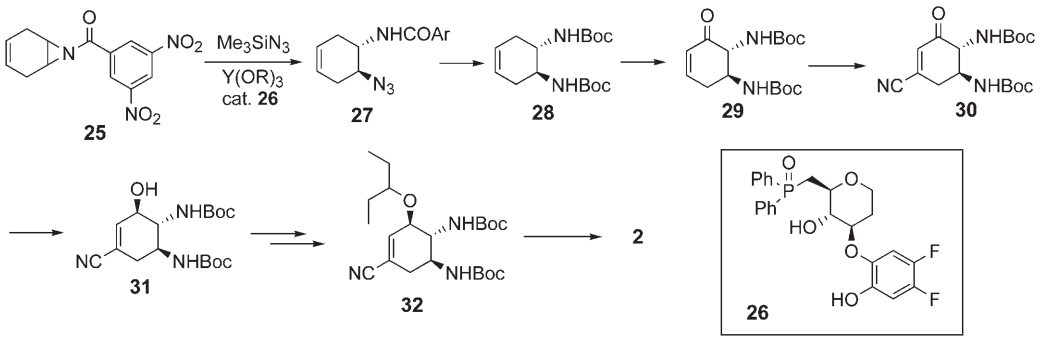

Scheme 5. Shibasaki and co-worker's approach.[22]

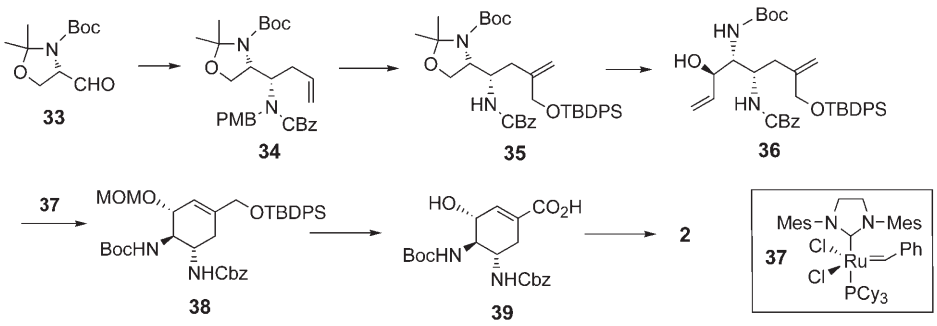

Scheme 6. Cong and Yao's approach.[23] PMB = *p*-methoxybenzyl, CBz = carbobenzyloxy, TBPS = *tert*-butyldiphenylsilyl, MOM = methoxymethyl, Mes = 2,4,6-trimethylphenyl, Cy = cyclohexyl.

this may be a serious drawback from the viewpoint of efficiency. Finally, standard manipulations completed the synthesis of **2** in a total of 18 steps and 16.5% overall yield from known intermediate **34**.

Of the three new approaches, that of Corey and co-workers is clearly the most concise and the one that affords the highest overall yield. Their synthesis is the one that best minimizes the use of steps that are considered inefficient and wasteful from the standpoint of a manufacturing process, such as protection–deprotections and functional group oxidation-state adjustments. Only 2 out of 11 steps fall in this category. The other syntheses are less efficient; that of Shibasaki and co-workers, for example, features 9 of these operations out of 17 steps. On the other hand, this means that the approach has much room for improvement in terms of streamlining, and cannot be ruled out as a practical route.

In general, it is very difficult to evaluate academic syntheses from the standpoint of potential as a manufacturing process because they have not been developed; that is, they use academic-style unit operations (too many purifications, use of chromatography, and solvents that must be avoided in a plant setting) and their safety has not been assessed. The approach of Corey and co-workers is azide-free, which certainly makes it most attractive from a safety standpoint, but careful analysis on the rest of the process could identify weaknesses that require attention. Ultimately, only a careful cost analysis on a fully developed, safe industrial process can determine whether these approaches could be competitive with the current manufacturing process of Roche, or simply afford the target at a viable cost.

However, these recent efforts demonstrate that the scarcity of quinic and shikimic acids is unlikely to be a major obstacle to the large-scale production of oseltamivir. To complement aggressive sourcing strategies and fermentation methods, three groups of creative organic chemists have already identified diverse strategies that employ, as raw materials, either cheap chiral-pool synthons or commodity chemicals in conjunction with chiral catalysts. These new chemistries complement the two approaches developed by chemists at Roche (illustrated in Schemes 1 and 2). It is very likely, therefore, that these or other simple, enantioselective approaches to **2** could be developed within a few years (or less) and used to complement the current output of oseltamivir, provided that adequate financial resources could be made available.

The Tamiflu supply problem, from a scientific standpoint, can be solved in a number of ways. Any potentially disastrous shortfall of this important drug is more likely to result from shortsighted health policies or legal entanglements than from lack of practical scientific avenues.

Published online: October 19, 2006

[1] J. K. Taubenberger, A. H. Reid, T. G. Fanning, *Virology* **2000**, *274*, 241.
[2] G. T. Wang, *Expert Opin. Ther. Pat.* **2002**, *12*, 845; K. Klumpp, *Expert Opin. Ther. Pat.* **2004**, *14*, 1153.
[3] G. Laver, E. Garman, *Science* **2001**, *293*, 1776.
[4] http://www.cdc.gov/flu/about/fluviruses.htm.
[5] J. L. McKimm-Breschkin, *Expert Opin. Pharmacother.* **2002**, *3*, 103.

 © 2006 Wiley-VCH Verlag GmbH & Co. KGaA, Weinheim

[6] J. S. Oxford, S. Bossuyt, S. Balasingam, A. Mann, P. Novelli, R. Lambkin, *Clin. Microbiol. Infect.* **2003**, *9*, 1.
[7] P. M. Colman, J. N. Varghese, W. G. Laver, *Nature* **1983**, *303*, 41; J. N. Varghese, J. L. McKimm-Breschkin, J. B. Caldwell, *Proteins Struct. Funct. Genet.* **1992**, *14*, 327.
[8] P. Ward, I. Small, J. Smith, P. Suter, R. Dutkowski, *J. Antimicrob. Chemother.* **2005**, *55*(Suppl.S1), 5.
[9] J. Carr, J. Ives, L. Kelly, R. Lambkin, J. Oxford, D. Mendel, L. Tai, N. Roberts, *Antiviral Res.* **2002**, *54*, 79; M. L. Herlocher, J. Carr, J. Ives, S. Elias, R. Truscon, N. Roberts, A. S. Monto, *Antiviral Res.* **2002**, *54*, 99; J. A. L. Ives, J. A. Carr, D. B. Mendel, C. Y. Tai, R. Lambkin, L. Kelly, J. S. Oxford, F. H. Hayden, N. A. Roberts, *Antiviral Res.* **2002**, *55*, 307; H. C. Jackson, N. Roberts, Z. M. Wange, R. Belshe, *Clin. Drug Invest.* **2000**, *20*, 447.
[10] A. Graul, P. A. Leeson, J. Castañer, *Drugs Future* **1999**, *24*, 1189.
[11] See, for example: *Nature* **2006**, *5*, 10 (News and Analysis).
[12] A. Boudet, *Phytochemistry* **1973**, *12*, 363; B. Möller, K. Herrmann, *Phytochemistry* **1983**, *22*, 477.
[13] S. Jiang, G. Singh, *Tetrahedron* **1998**, *54*, 4697; this review also describes approaches to shikimic acid by total chemical synthesis.
[14] G. Flores, *The Scientist*, Published online: January 4, **2006**.
[15] K. M. Draths, D. R. Knop, J. W. Frost, *J. Am. Chem. Soc.* **1999**, *121*, 1603; J. Frost, WO 2005/030949A1, **2005**, and preceding patents.
[16] M. Federspiel, R. Fischer, M. Hennig, H.-J. Mair, T. Oberhauser, G. Rimmler, T. Albiez, J. Bruhin, H. Estermann, C. Gandert, V. Göckel, S. Götzö, U. Hoffmann, G. Huber, G. Janatsch, S. Lauper, O. Röckel-Stäbler, R. Trussardi, A. G. Zwahlen, *Org. Process Res. Dev.* **1999**, *3*, 266.
[17] M. Karpf, R. Trussardi, *J. Org. Chem.* **2001**, *66*, 2044; P. J. Harrington, J. D. Brown, T. Foderaro, R. C. Hughes, *Org. Process Res. Dev.* **2004**, *8*, 86.
[18] S. Abrecht, P. Harrington, H. Iding, M. Karpf, R. Trussardi, B. Wirz, U. Zutter, *Chimia* **2004**, *58*, 621.
[19] S. Abrecht, M. Karpf, R. Trussardi, B. Wirz, US Patent 6,403,824, **2002**.
[20] H. Iding, B. Wirz, U. Zutter, US Patent 6,518,048, **2003**.
[21] Y.-Y. Yeung, S. Hong, E. J. Corey, *J. Am. Chem. Soc.* **2006**, *128*, 6310.
[22] Y. Fukuta, T. Mita, N. Fukuda, M. Kanai, M. Shibasaki, *J. Am. Chem. Soc.* **2006**, *128*, 6312.
[23] X. Cong, Z.-J. Yao, *J. Org. Chem.* **2006**, *71*, 5368.

 © 2006 Wiley-VCH Verlag GmbH & Co. KGaA, Weinheim

Droplet-Based Microfluidics

DOI: 10.1002/anie.200601554

Reactions in Droplets in Microfluidic Channels

*Helen Song, Delai L. Chen, and Rustem F. Ismagilov**

Keywords:
analytical systems · interfaces · microfluidics · microreactors · plugs

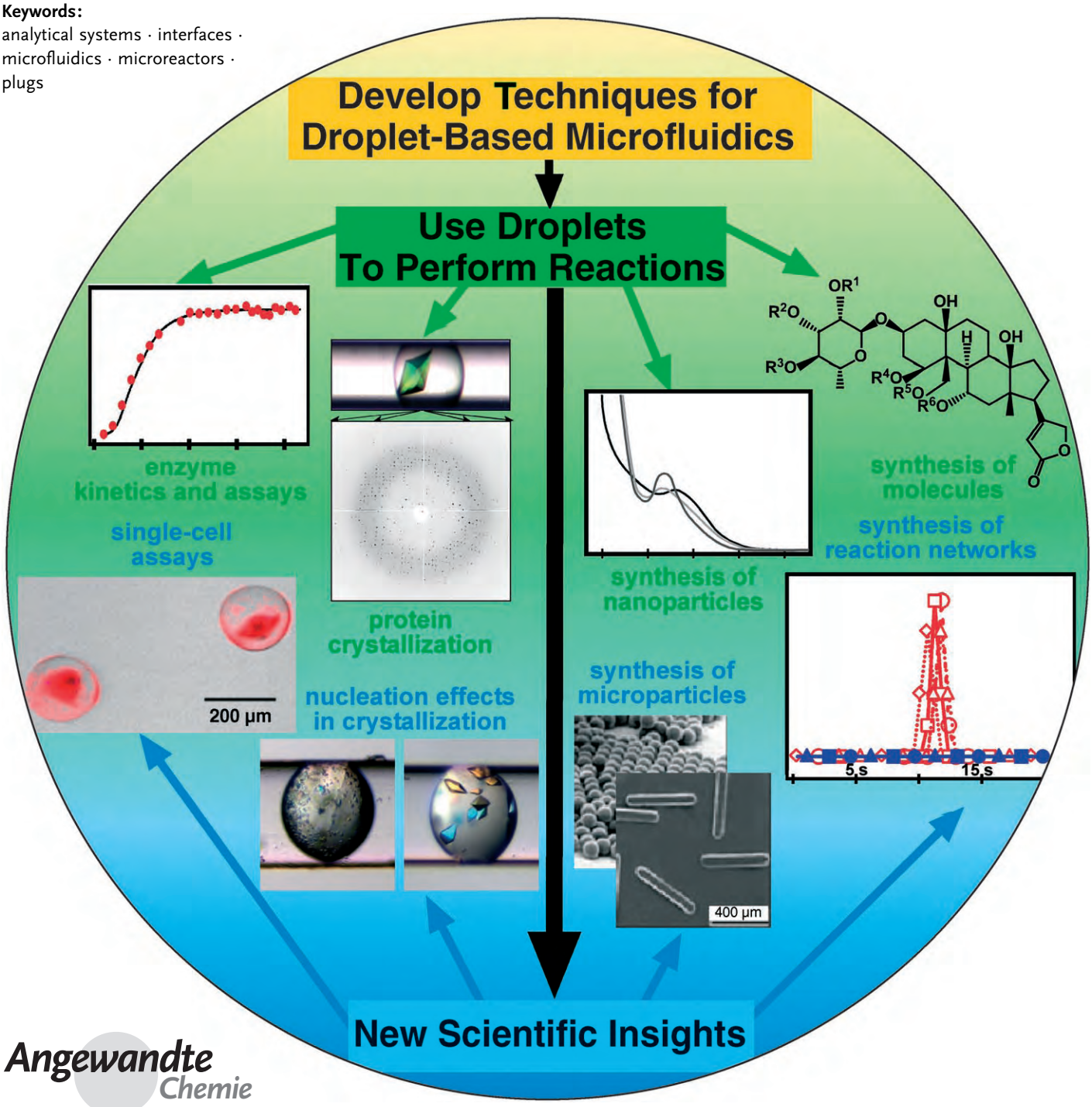

© 2006 Wiley-VCH Verlag GmbH & Co. KGaA, Weinheim

Fundamental and applied research in chemistry and biology benefits from opportunities provided by droplet-based microfluidic systems. These systems enable the miniaturization of reactions by compartmentalizing reactions in droplets of femoliter to microliter volumes. Compartmentalization in droplets provides rapid mixing of reagents, control of the timing of reactions on timescales from milliseconds to months, control of interfacial properties, and the ability to synthesize and transport solid reagents and products. Droplet-based microfluidics can help to enhance and accelerate chemical and biochemical screening, protein crystallization, enzymatic kinetics, and assays. Moreover, the control provided by droplets in microfluidic devices can lead to new scientific methods and insights.

From the Contents

1. Introduction: Reactions in Droplets 7337
2. Criteria for Performing Reactions in Droplets 7340
3. Applications of Droplet-Based Microfluidics 7345
4. Conclusions and Outlook 7352

1. Introduction: Reactions in Droplets

This Review discusses the use of droplets in microfluidic channels as chemical microreactors for performing many reactions on a small scale (Figure 1).[1] Microreactors in general[2] and bulk micellar systems[3] have been covered in recent review articles in *Angewandte Chemie* and thus will not be covered herein. We describe new techniques that have been developed to perform chemical reactions within droplets and reactions that have been studied by using droplets. We also discuss how droplet-based microfluidics can lead to new scientific methods and insights.

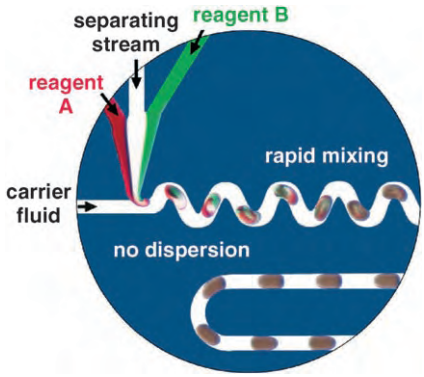

Figure 1. Droplets formed within microfluidic channels can serve as microreactors. In this example, the reactions are performed within aqueous droplets, which contain reagent A, reagent B, and a separating stream containing buffer. The droplets are encapsulated by a layer of a fluorinated carrier fluid and transported through the microchannels. Reprinted from reference [1].

1.1. Reaction Control for High Throughput

A number of applications require multiple reactions to be performed in parallel, for example, drug discovery, gene-expression analysis, and high-throughput assays. For these applications, it is only feasible to perform reactions on a microscale, because reagents can be expensive or only available in limited amounts. In other applications, multiple reactions need to be carried out to characterize stochastic processes, such as the nucleation of crystals.

Microfluidics can be used to handle small volumes of liquid and is a promising method to form microreactors.[2,4,5] Benefits from miniaturization include low consumption of reagents and high-throughput fabrication of devices. For example, soft lithography with poly(dimethylsiloxane) (PDMS) can be used for the rapid and inexpensive fabrication[6,7] and modification[8–10] of devices.

1.2. Parallel or Serial Compartmentalization of Multiple Reactions

To perform many reactions in high throughput, each reaction condition must be uniquely addressable or indexed. The reactions can be indexed if each reaction condition is compartmentalized either in parallel or in series[11] (Figure 2). Reaction conditions can be compartmentalized in parallel by using a well plate (Figure 2a). The final result of the reaction is indexed as a function of the spatial location of the well.[12–14] Reaction conditions can also be compartmentalized in series as in flow injection analysis (Figure 2b). The final result of the reaction is indexed as a function of the elution time. Chemical indexing in combinatorial chemistry has also been achieved by using molecular tags,[15] labeled beads,[16,17] and encoded particles.[18,19]

[*] H. Song, D. L. Chen, Prof. Dr. R. F. Ismagilov
Department of Chemistry and Institute for Biophysical Dynamics
The University of Chicago
5735 South Ellis Avenue, Chicago, IL 60637 (USA)
Fax: (+1) 773-702-0805
E-mail: r-ismagilov@uchicago.edu
Homepage: http://ismagilovlab.uchicago.edu/

Supporting information (three movies showing droplets forming and mixing in microfluidic channels, and a movie of the mixing of modeling clay by chaotic advection) for this article is available on the WWW under http://www.angewandte.org or from the author.

© 2006 Wiley-VCH Verlag GmbH & Co. KGaA, Weinheim

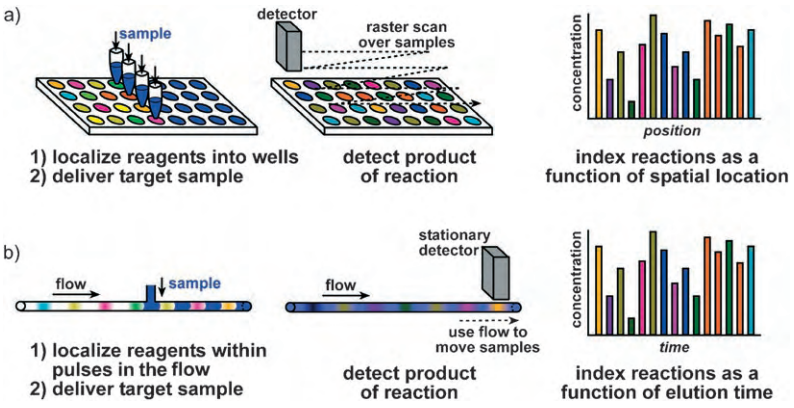

Figure 2. Comparison of reactions compartmentalized in parallel and in series. a) Parallel reactions performed by using well plates: The reagents are localized within wells, and the target sample is delivered to the well through a multipipettor. The reaction products are detected by scanning over the samples, and each reaction is indexed as a function of the spatial location of each well. b) Serial reactions performed by using flow. Reactions are localized within pulses and separated by a buffer solution between each reagent. These pulses are transported through the reaction tube by the flow, and the target sample is delivered to the reagents. The pulses are transported by the flow past a stationary detector to analyze the reaction products. Each reaction is indexed as a function of the elution time.

1.3. Control of the Compartmentalization

For performing reactions in parallel, the handling of the fluid and evaporation within the compartments needs to be controlled. PDMS devices with enclosed chambers and valves allow many reactions to be performed by multiplexing methods.[20–23] This system has been applied to protein crystallization,[24–26] bacterial chemostats,[27] and the synthesis of radiolabeled probes.[22] The valves used to handle fluids require multilayer fabrication. As PDMS is permeable to the vapor of organic and aqueous solutions, eliminating evaporation through PDMS requires special measures (although this permeability was controlled and used as an advantage in some applications,[28] such as the filling of dead-end channels).[25]

For reactions performed in series in a single-phase flow, dispersion can lead to cross-contamination of reaction conditions and dilution of samples. Pressure-driven flow of a single-phase solution through a microchannel is laminar and displays a parabolic velocity profile.[29,30] As a result of the parabolic flow profile, the reagents in solution are transported at a range of velocities in the microchannel. Taylor dispersion describes the transport and broadening of a pulse of a solute within a solution that is flowing through a tube.[29,30] As a result of dispersion, localization of the reaction and accurate control of the reaction time is difficult. Cross-contamination can occur between pulses of different reagents that are traveling through the same tube. Furthermore, reagents are in direct contact with the solid microchannel wall, so the surface chemistry of the wall must be controlled. The control of surface chemistry is especially critical for devices that use electroosmotic flow to solve the problem of Taylor dispersion.[31,32] Dilution of the sample solution can occur through diffusion within a single-phase flow, especially with prolonged incubation times. This broadening of the sample pulse occurs regardless of whether the flow is driven by pressure or electroosmotic forces.

1.4. Compartmentalization in Nanoliter-Sized Droplets

Nanoliter-sized droplets can serve as compartments for reactions. Multiple reactions can be performed by varying the reaction conditions within each droplet. The problems of evaporation, complicated fluid handling, dispersion, and diffusion can be overcome by using multiphase flows of immiscible liquids to form droplets in microfluidic channels (Figure 1).[1] Evaporation can be controlled for long-term incubation experiments by transporting droplets into glass capillaries.[33,34] Complicated fluid handling is minimized, as uniformly sized droplets form spontaneously in a cross-stream flow of two immiscible liquids.[1,35–39] The flow of fluids within the microchannels can be used to manipulate droplets and arrays of droplets in a controlled manner.[1,37,38,40–42] Dispersion due to convection and diffusion is eliminated because the reagents are encapsulated within droplets. Furthermore, surface chemistry can be easily controlled at the liquid–liquid interface between the immiscible phases of the reagent fluid and the carrier fluid.[43] Mixing within droplets can be achieved by chaotic advection.[1,37,40,44,45]

To obtain compartments that do not move (as analogues of well plates), droplets can be transported into capillaries and incubated for up to one year. To obtain compartments that move (as analogues of flow injection analysis), flow can be used to transport droplets continuously through the

Helen Song received her BSc and MSc degrees in chemistry at the University of Chicago. She started her work in developing techniques for droplet-based microfluidics and using this method to study enzyme kinetics at the University of Chicago in 2002 under the supervision of Prof. Rustem Ismagilov. She successfully defended her PhD thesis in 2005.

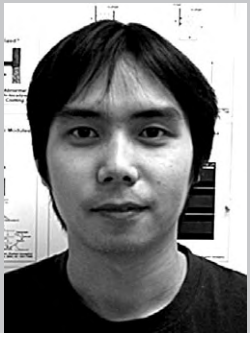

Delai Chen received his BSc in chemistry at Peking University and his MSc in chemistry at the University of Chicago. He started his work on using droplet-based microfluidics to study stochastic processes in protein crystallization and to optimize conditions in organic reactions at the University of Chicago in 2004 under the supervision of Prof. Rustem Ismagilov.

 © 2006 Wiley-VCH Verlag GmbH & Co. KGaA, Weinheim

microchannel in the device. By using droplets, it is possible both to compartmentalize reactions and control the reaction time accurately.

1.5. Scope of the Review

In this Review, we discuss reactions that occur within segmented flows in a microfluidic system. Segmented flows are composed of at least two immiscible phases: one dispersed phase and one continuous phase. The droplet consists of the dispersed phase, and the continuous phase encapsulates the droplet and preferentially wets or coats the surface of the microchannel.

For this Review, we differentiate between two types of segmented flows on the basis of the phase in which the reaction takes place. In the first type, discrete liquid droplets are encapsulated by a carrier fluid that wets the microchannel (Figure 3a).[1] These droplets, termed "plugs" herein, form the dispersed phase in which the reactions occur. Systems that use plugs differ from segmented-flow injection analysis in that reagents in plugs do not come into contact with the microchannel wall and are transported without dispersion. In the second type of segmented flow, liquid "slugs" are separated by discrete gas bubbles (Figure 3b).[46–51] In this case, reactions occur within the slugs that form the continuous phase; reagents are exposed to the walls of the channels and some dispersion occurs. This second system is similar to segmented-flow injection analysis.[52–56] For the remainder of the Review, the terms "plugs" and "slugs" are used to differentiate these two types of segmented flows.

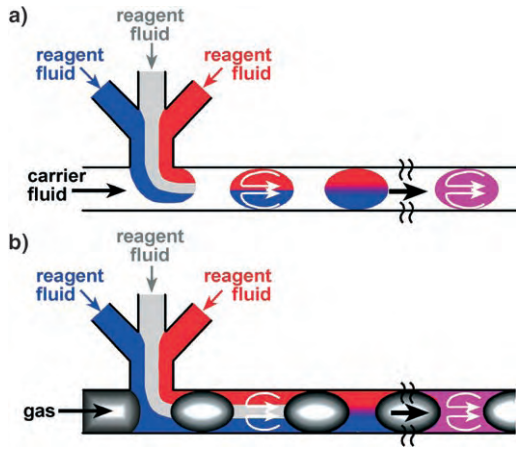

Figure 3. Reactions can be studied in two types of segmented flows in microfluidic channels. a) Discrete liquid plugs are encapsulated by an immiscible continuous phase (for example, a fluorocarbon-based carrier fluid). Reactions occur within the dispersed phase (within the plugs). Owing to the surface properties of the microchannel walls, these walls are preferentially wet by the continuous phase. b) Aqueous slugs are separated by another immiscible phase (for example, discrete gas bubbles). Reactions occur within the continuous phase (i.e., within the slugs).

Rustem Ismagilov received his PhD in 1998 at University of Wisconsin, Madison under the direction of Prof. Stephen F. Nelsen and was a postdoctoral fellow with Professor George M. Whitesides at Harvard University. He began his independent career at the University of Chicago in 2001 and was promoted to Associate Professor in 2005. His current research involves using microfluidics to control complex chemical and biological systems in space and time.

We do not cover reactions in bulk systems that use multiple immiscible phases to form micelles, emulsions, and droplets. Emulsions take advantage of only some of the spatial control available by compartmentalization. Extensive review articles cover reactions in micelles,[3] colloids,[57,58] miniemulsions,[59] and multilayer microcapsules.[60] Emulsions and vesicles have been used for in vitro compartmentalization,[61,62] and vesicle reactors can also act as synthetic cells.[63–65] Emulsions formed by microfluidics[66–68] have been used to synthesize permeable colloids[69] and to fabricate monodisperse capsules by using steady coaxial jets.[70]

The area of "digital microfluidics", in which droplets are manipulated by an array of electrodes[71–75] ("active control") rather than through a continuous flow ("passive control"), is also not covered. The principles of electrowetting-based actuation and the automation of this technique have been reviewed.[76–78] Digital microfluidic devices have been used for analyzing proteins and peptides with matrix-assisted laser desorption/ionization mass-spectrometry (MALDI MS),[79,80] performing PCR with optical detection,[81] measuring glucose concentration in droplets with optical detection,[82] performing a luciferase-based assay,[83] and synthesizing anisotropic particles.[84]

Microfluidic systems that use multiphase flow but do not report reactions will not be discussed in detail. We define reactions broadly and include the interconversion of chemical species[85] and phase transitions, such as crystallization and the formation of particles. Methods of forming and manipulating droplets are being continuously developed to take advantage of novel physical principles, such as electrowetting,[86–88] magnetic fields,[89,90] optically induced Marangoni effects,[91,92] acoustic waves,[93] and surface chemistry.[94,95] Recent innovations on the generation of gas bubbles in microfluidic devices include the use of segmented flow in microchannels as multiphase monolith reactors,[96] the formation of monodisperse gas bubbles by flow focusing,[97,98] the study of nonlinear dynamics of a flow-focusing bubble generator,[99] and characterization of the transport of bubbles in square channels.[100]

The flow of immiscible fluids within microchannels may result in continuous laminar flow rather than the formation of droplets.[101] These continuous-laminar-flow systems, though suitable for conducting chemical reactions and bioassays,[102–104] as well as for patterning and microfabrication within microchannels,[105,106] are not discussed herein.

This Review summarizes recent developments in the use of droplets in microfluidics as chemical reactors for many reactions. We introduce techniques for conducting reactions and discuss examples of reactions in droplet-based microfluidic systems. Furthermore, we examine how microfluidics can open up new research areas.

 © 2006 Wiley-VCH Verlag GmbH & Co. KGaA, Weinheim

2. Criteria for Performing Reactions in Droplets

To perform reactions within microfluidic devices, at least two criteria should be met. First, the microfluidic tool should be able to perform typical procedures that are conducted for reactions on the macroscale. These procedures include the controlled addition of reagents to a reaction mixture, the thorough mixing of reagents, control of the reaction time, the combining and splitting of reaction mixtures for multiple-step reactions, and analysis over the course of a reaction. Second, the microfluidic tool should provide a characteristic advantage, for example, the ability to perform more reactions under more reaction conditions. As with any high-throughput screening technique, there must be a method for organizing and indexing each reaction condition. Likewise, there must be an efficient method for assaying many different conditions and also for optimizing a particular condition. These methods should be scalable, straightforward, and simple. In this section, we discuss techniques that were developed for droplet-based microfluidics to fulfill the two criteria described above.

2.1. Formation of Droplets within Microfluidic Channels

Droplet formation in two-phase systems has been extensively studied for both liquid–liquid flows[107–109] and gas–liquid flows.[110] Although many methods are available for making bulk emulsions, droplets in microfluidic channels have been generated mostly by two techniques: T junctions[1,35–39] and flow-focusing.[36,97,98,111–115] In T junctions, the disperse phase and the continuous phase are injected from two branches of the "T". Droplets of the disperse phase are produced as a result of the shear force and interfacial tension at the fluid–fluid interface (Figure 4; see also Figure 1). The

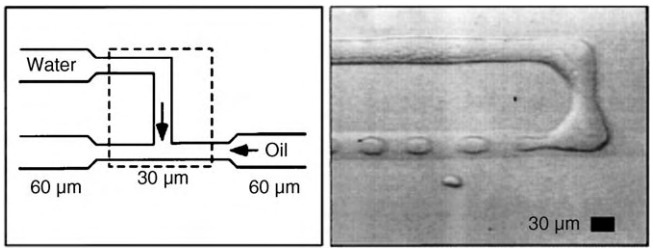

Figure 4. Formation of droplets within a T junction of a microfluidic device.[35] In this case, the oil is a mixture of hydrocarbon and the surfactant Span80, and the channels are made of polymerized acrylated urethane. Reprinted with permission from reference [35]. Copyright 2001 American Physical Society.

phase that has lower interfacial tension with the channel wall is the continuous phase.[37] To generate droplets in a flow-focusing configuration, the continuous phase is injected through two outside channels and the disperse phase is injected through a central channel into a narrow orifice (Figure 5).[111] This geometry is only slightly more difficult to implement than a T junction and may facilitate the formation of droplets, especially small or viscous droplets.[45,97,111,115–117]

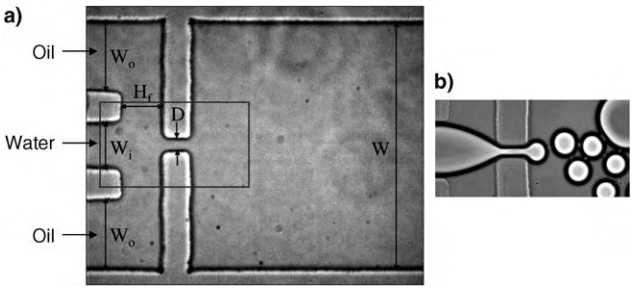

Figure 5. Formation of droplets by flow-focusing.[111] Modified from reference [111]. a) A schematic of the device. The rectangle outlines the field of view in (b). Copyright 2003 American Institute of Physics.

For both methods, surfactants are often added to the continuous phase to stabilize the fluid–fluid interfaces of the droplets.[1,35,111] The conditions under which monodisperse droplets form have been well documented.[96,118–123] The droplets are not useful as general microreactors, however, unless methods of introducing reagents into the droplets are also developed, as is discussed below.

2.2. Introduction of Reagents into Droplets

Different techniques have been developed to introduce reagents into droplets for different droplet-based microfluidic applications. For high-throughput screenings, one target sample must be tested against a large number of different reaction conditions. Each reaction condition may be composed of different reagents or a different combination of a set of reagents. For measuring kinetics or optimizing reaction conditions, only a few reagents need to be incorporated within the droplet, but the concentration of these reagents are varied. For multiple-step reactions, the addition of a reagent should occur at a specific time during the course of the reaction. Each of these applications requires a different method for introducing the reagents.

2.2.1. Cartridge Technique

For screening a large number of reaction conditions against one target sample, preformed cartridges can be produced to store an array of plugs (Figure 6a,b).[42] Each plug contains a different reaction condition of different reagents. For example, an array of 48 plugs was formed in which each plug contained 15 nL of a different reagent.[42] The target sample can be introduced into the preformed plugs by using a microchannel T junction (Figure 6c). Reagent cartridges can be stored inside sealed capillaries for months without evaporation or exposure to the ambient environment.[42]

Reagent cartridges can be used for applications that require parallel screening of one target sample against many different reagents or reaction conditions. By using a repeated splitting device, 16 reagent cartridges (each containing approximately 20-nL plugs) were formed in parallel by splitting one array containing large droplets (ca. 320 nL).[125] Such parallel preparation of reagent cartridges accelerates

 © 2006 Wiley-VCH Verlag GmbH & Co. KGaA, Weinheim

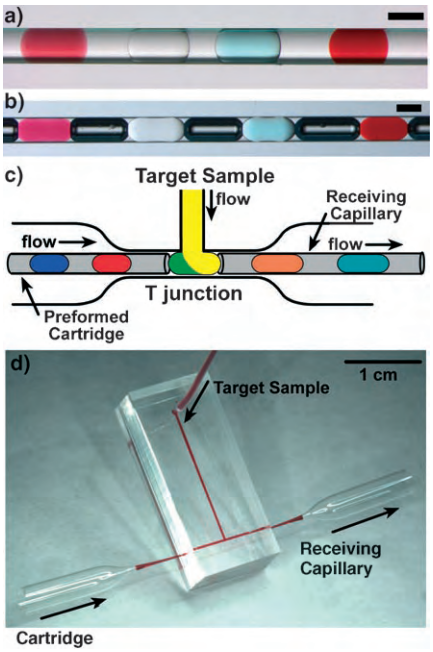

Figure 6. Preformed cartridges of plugs enable the combination of a large number of reagents with a sample in sub-microliter volumes.[42,124] a,b) Four different reagents stored as an array of plugs in a capillary. The plugs are separated by a fluorocarbon carrier fluid, as well as air bubbles (in b), to prevent cross-communication between the plugs. Scale bars: 200 μm. c) Merging of plugs from a preformed cartridge with a target sample stream through a T junction. The resulting array of plugs is transferred into a receiving capillary and the trials are collected. d) Photograph of the T junction. Reprinted from reference[42] (a,b) and with permission from Elsevier from reference [124] (c,d).

high-throughput screening. Reagent cartridges have already been used in a range of applications: screening of protein crystallization conditions and in enzyme assays,[42] screening of the reaction conditions for an organic reaction,[126] and for immunoassays (using a liquid–air two-phase cartridge).[127]

2.2.2. *Variation of Reagent Concentrations*

For some reactions, rate constants or optimal reaction conditions are determined by varying the concentrations of several reagents. In one case, laminar flow was used to dilute two reagents within plugs on a chip.[44] The plugs were formed by using two streams of reagents with a buffer stream in the middle to prevent premature mixing of the two reagent streams (Figure 7). Varying the relative flow rates of the three aqueous streams varies the concentration of the reagents within the plug (Figure 7c). For example, a higher flow rate of the stream containing reagent A (green stream, 45 $nL\,s^{-1}$) results in a larger proportion of the green reagent in the plug (Figure 7c, left).

This technique was also used to obtain an array of plugs, whereby each plug contained a unique composition of four reagents.[128] The composition of reagents within each plug was determined by the relative flow rates of the reagent streams, which were controlled by a computer. This capability

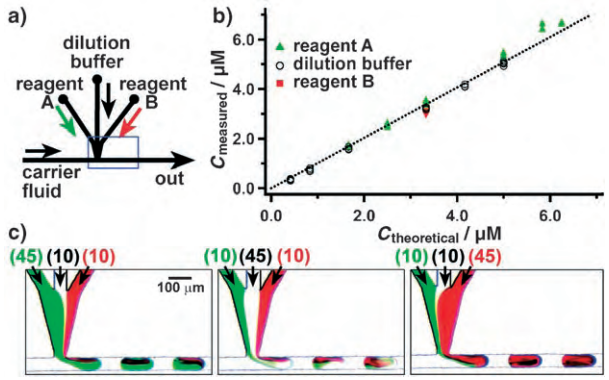

Figure 7. Controlling the concentrations of reagents within plugs by on-chip dilution.[44] a) Experimental setup; the blue rectangle shows the field of view for microphotographs shown in (c). b) A graph quantifying the on-chip dilution method. The concentrations measured from the fluorescence intensity of plugs traveling through the microchannel are plotted as a function of theoretical concentration calculated from the flow rates of the streams containing reagent A, the dilution buffer, and reagent B. c) The concentrations of the reagents were controlled by the relative flow rates of the reagent streams (values in parentheses, in $nL\,s^{-1}$). Reprinted with permission from reference [44]. Copyright 2003 American Chemical Society.

allows rapid switching of reaction conditions without stopping the experiment or wasting valuable reagents. This approach is not limited to the geometries shown in Figure 7; it is also compatible with "flow focusing" (Figure 5) for forming droplets with controlled concentrations of reagents.

2.2.3. *Direct Injection of Reagents into Droplets*

For multiple-step reactions, a reaction mixture is allowed to react for a certain time and then another reagent is added to the mixture. In droplet-based microfluidics, the first step of the reaction can be contained within a plug that is transported within the microchannel. Then, a reagent for the second step of the reaction can be injected into the plug through a side channel further along the microchannel network.

A reagent flowing through a side channel can be injected directly into droplets through a T junction (as shown in Figure 6 for the injection of a target sample into an array of plugs). However, if the T junction is preferentially wetted by the carrier fluid (e.g., with a hydrophobic junction and aqueous reagents), then the injection of the reagent into a plug is favorable only at low values of the capillary number ($Ca \approx 0.01$).[129,130] At higher values of Ca (for example, at higher flow rates), the injection can be accomplished by mechanical agitation of the PDMS channel.[129]

Another injection method was developed with a side channel that is preferentially wetted by the reagent fluid (e.g., with a hydrophilic channel and aqueous reagents; Figure 8a).[131,132] As a droplet is formed from the injection of reagent fluid from a side channel into the main channel, wetting of the side channel prevents this droplet from breaking off until a plug passes by the side channel, and this droplet is injected into the plug.[131] With this injection method, the volume of the reagent injected into the plug increases linearly with the flow rate of the reagent stream in

 © 2006 Wiley-VCH Verlag GmbH & Co. KGaA, Weinheim

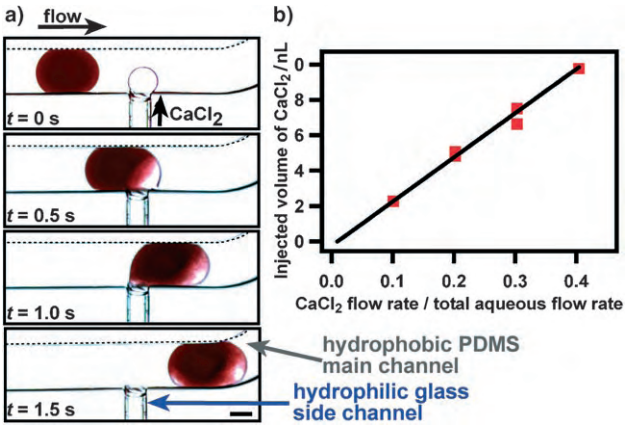

Figure 8. Injection of a $CaCl_2$ solution into a plug (blood) through a hydrophilic side channel.[132] a) Time-lapse microphotographs of the injection process. b) The injection volume is controlled by the flow rate ($\mu L\,min^{-1}$) of the $CaCl_2$ stream. Each data point on the graph denotes measurements for 10 plugs ($y = 24.947x - 0.2312$, $R^2 = 0.9849$). Reprinted with permission from reference [132]. Copyright 2006 American Chemical Society.

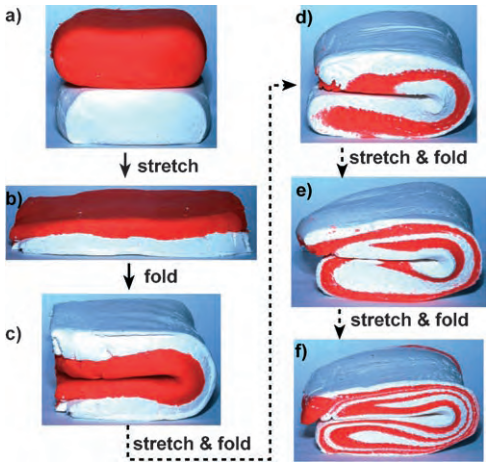

Figure 9. Model for the mixing of two reagents by chaotic advection at low values of the Reynolds number; photographs of two layers of modeling clay being stretched and folded. Images are courtesy of Joshua D. Tice.

the side channel (Figure 8b).[132] Cross-contamination between plugs at the T junction was quantified by fluorescence measurements and found to be minimal.[131]

For gas–liquid slugs, the reagents need to be injected into the continuous phase, as reactions occur within this phase. Such injection is easy, as this continuous phase is always in contact with the microchannel wall. However, contamination between slugs can result, especially in rectangular microchannels. The merging of a tracer dye into the continuous phase was demonstrated for slugs within microchannels.[48]

2.3. Controlling Mixing by Chaotic Advection

The control of mixing is important for reactions and autocatalytic processes.[133,134] Rapid mixing of reagents is necessary to determine the starting time of a reaction accurately. Droplet-based microfluidics allows rapid mixing and the extent of mixing can be quantified.[1,40,135] It has been reported that for a single-phase microfluidic flow, a reagent can be mixed by hydrodynamic focusing with a large excess of a second reagent with mixing times of only 10 μs.[136] The mixing was sufficiently rapid that the time resolution of kinetic measurements was limited by dispersion and not by mixing. Chaotic advection in a staggered herringbone mixer[137] was used to achieve complete mixing of two reagents in milliseconds and to reduce dispersion. This idea of chaotic advection (see Figure 9 and a movie in the Supporting Information) was implemented with droplets.[1,40,46] Chaotic advection[137–139] relies on repeated folding and stretching of the two fluids to achieve layers of fluids (striations) that become exponentially thinner and thinner (Figure 9) until mixing by diffusion becomes rapid. Mixing in droplets by chaotic advection can be achieved in sub-millisecond times[40] without dispersion and is especially useful when both mixing on a short timescale and dispersion over a longer timescale need to be controlled.

Droplets traveling through a microchannel experience internal recirculation, which has been used to enhance mixing in plugs[37,140–143] and slugs.[46,50,144–146] In straight channels, two symmetric vortices form on the left and right halves of a plug (in the direction of plug movement, Figure 3). The mixing occurs by convection within each half and mainly by diffusion between the two halves of the plug. In winding channels (Figure 10), the interface between the two halves of the plug

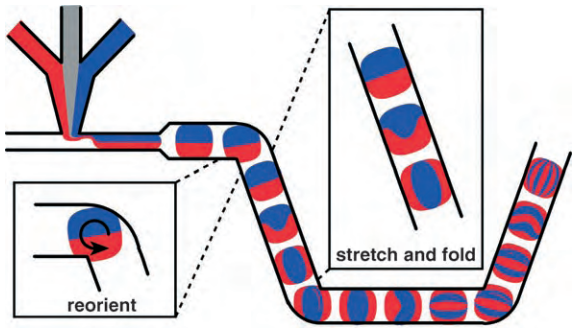

Figure 10. Mixing by chaotic advection in a plug moving through a winding channel. The interfaces between the red and blue fluids are reoriented, stretched, and folded as the plug moves through the corners and straight sections of the channel. Reprinted with permission from reference [40]. Copyright 2003 American Institute of Physics.

is reoriented from the direction of plug movement and is stretched and folded by recirculations (Figure 10). This technique greatly enhances mixing (see two movies in the Supporting Information for a comparison of mixing in straight and winding channels).

The extent of mixing is dependent on the number of winding turns and can be quantified by analyzing fluorescence images (Figure 11b). By using a "bumpy" mixer (Figure 12) to generate oscillating shear within plugs, even viscous biological samples containing high concentrations of bovine serum albumin or hemoglobin can be mixed within milliseconds.[45] The striations (Figure 12c) observed in this mixer

 © 2006 Wiley-VCH Verlag GmbH & Co. KGaA, Weinheim

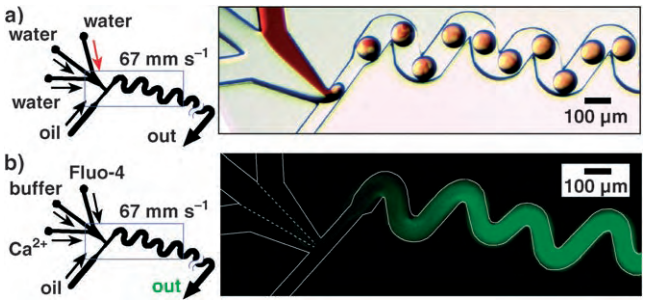

Figure 11. Rapid mixing in droplets by chaotic advection.[40] Left: Schematics of the microfluidic network. Right: a) Bright-field and b) fluorescence microscopy images of plugs moving through winding channels. The observed fluorescence is a time average of the fluorescence of many plugs passing through the field of view throughout the 2-s exposure time. The mixing was quantified by using the fluorogenic substrate Fluo-4, whose fluorescence increases upon binding to Ca^{2+}. Figure reprinted with permission from reference [40]. Copyright 2003 American Institute of Physics.

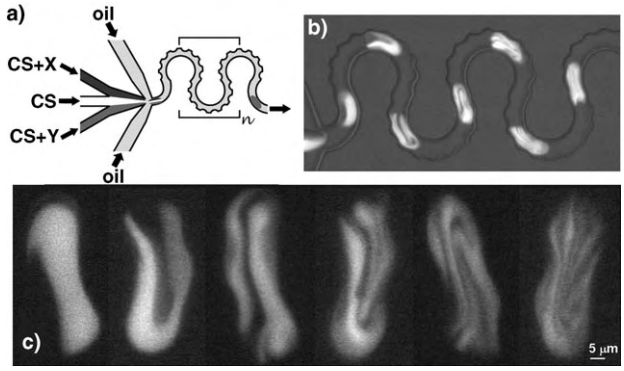

Figure 12. Mixing of viscous solutions in plugs with a bumpy mixer.[45] a) Schematic of the bumpy serpentine mixer; CS: crowded solutions, X and Y: reagents. b) Mixing of plugs containing bovine serum albumin (BSA, 200 mg mL^{-1}) and a calcein dye. c) Images of the striations observed inside the plugs during mixing of a hemoglobin solution (300 mg mL^{-1}) with a BSA solution (260 mg mL^{-1} with 5 mM calcein). Figure reprinted with permission from reference [45]. Copyright 2006 American Chemical Society.

are astonishingly similar to those expected for chaotic advection (Figure 9, Figure 10).

2.4. Control of the Interfacial Chemistry

In microfluidics, surface effects are important because of the high surface-area-to-volume ratio. Surface effects can appear at the interface between the solid microchannel wall and the fluid (solid–liquid) or between the two immiscible fluids in the microchannel (liquid–liquid). For a molecule within a droplet, interactions at the liquid–liquid interface become especially important as the dimension of the droplet approaches Γ_{max}/C_0, in which Γ_{max} (mol m^{-2}) is the maximum surface coverage of the interface that can be achieved at saturating concentrations of the molecule and C_0 (mol m^{-3}) is the initial concentration of the molecule. A recent review article illustrates how interfaces between fluids and interactions in fluids can be controlled by microfluidics.[119] These interactions can be used to concentrate solutes within the droplets,[147] to maximize efficiency of a catalyst embedded on the surface of a microchannel,[104] and to synthesize coated particles by interfacial reactions.[112,117] A high surface-area-to-volume ratio ensures rapid heat transfer between plugs and the carrier fluid and allows rapid switching between different temperatures. This rapid switching is essential for DNA amplification,[148] in vitro protein expression in plugs,[149] and DNA analysis.[51]

Interactions at solid–liquid and liquid–liquid interfaces in a microchannel can be advantageous for certain applications yet detrimental for others. Therefore, these interactions need to be controlled. For plugs, the reaction occurs within the dispersed phase, which does not come in contact with the solid microchannel wall but is encapsulated by a layer of the carrier fluid. Therefore, reactions within plugs will be affected by the surface chemistry at the liquid–liquid interface. For slugs, the reaction occurs within the continuous phase, which is in contact with both the solid microchannel and the dispersed phase. Therefore, reactions within slugs will be affected by the surface chemistry at both the solid–liquid and liquid–gas interfaces.

To form plugs in microchannels, the surface of channels should be treated to ensure that the carrier fluid (and not the aqueous phase) preferentially wets the channel wall. The surface tension between the aqueous phase and the carrier fluid should be lower than the surface tension between the aqueous phase and the channel wall. Surfactants can be used within the carrier fluid to lower the surface tension between the aqueous phase and the carrier fluid. However, this surface tension should not be lowered too far as the capillary number Ca of the flow must be low to favor the formation of plugs;[38] the capillary number is defined as $Ca = \mu U/\gamma$, in which μ (kg m^{-1} s^{-1}) is the viscosity of the fluid, U (m s^{-1}) is the flow rate and γ (N m^{-1}) is the interfacial tension between the aqueous phase and the carrier fluid.

Perfluorinated liquids are optimal carrier fluids for the formation of plugs. They are considered to be chemically and biologically inert and have been used as blood substitutes,[150] for liquid ventilation of fetuses,[151] for diagnostic ultrasound imaging,[152] for cell cultures,[153,154] and in drug delivery.[155] Many types of fluorocarbons and fluorinated surfactants are commercially available (however, recent evidence shows that some fluorinated surfactants may accumulate in tissues,[156,157] and therefore such surfactants should be handled with care). Also, fluorocarbons and fluorinated surfactants provide an orthogonal chemistry to reactions conducted in organic phases.[158]

Fluorinated surfactants can be used to control the surface chemistry at the liquid–liquid interface between the aqueous phase and the fluorinated phase,[43] in a similar manner to how hydrocarbon surfactants are used to block adsorption at the interface between aqueous and hydrocarbon phases.[159–161] Fluorinated surfactants are insoluble in the aqueous phase and arrange themselves at the interface between the aqueous and fluorous phases. Plugs are encapsulated in a thin layer of carrier fluid, so different surface properties can be obtained by simply changing the surfactant in the fluorous carrier fluid

 © 2006 Wiley-VCH Verlag GmbH & Co. KGaA, Weinheim

without requiring functionalization of the microchannel wall. The adsorption of fibrinogen within a plug was controlled by using this method (Figure 13). A surfactant with a carboxylic acid group resulted in adsorption (Figure 13a), whereas a surfactant with an oligoethylene glycol group prevented adsorption (Figure 13b).

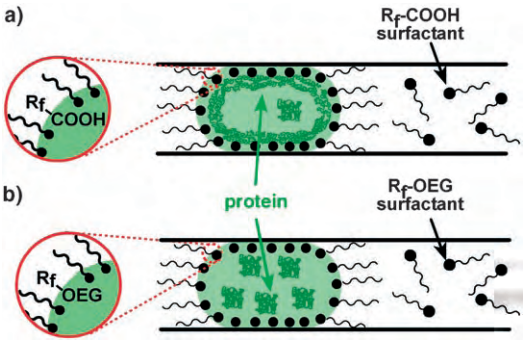

Figure 13. Control of the surface behavior of plugs with surfactants at the interface between the aqueous and fluorous phases. a) A COOH surfactant with a fluorinated side chain (R_f) provides a non-inert interface that is prone to protein adsorption. b) A surfactant with a fluorinated side chain and a polar oligoethyleneglycol (OEG) head group provides an inert, biocompatible interface. Reprinted with permission from reference [43]. Copyright 2005 American Chemical Society.

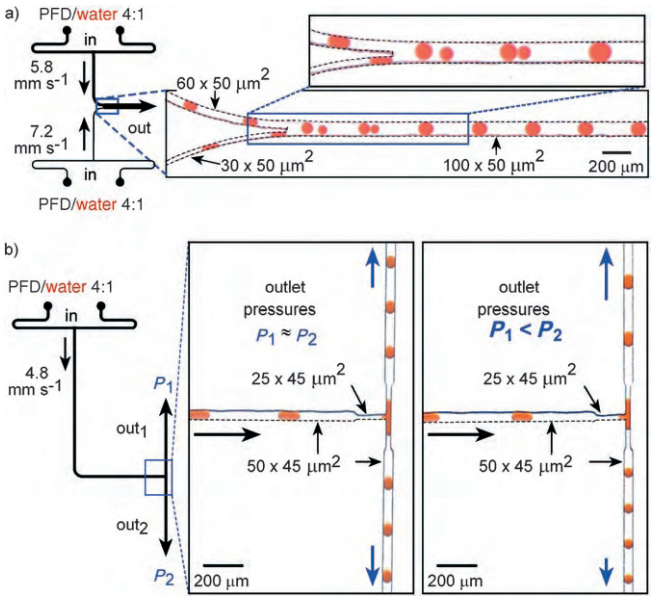

Figure 14. Merging and splitting of droplets in microchannels.[1] Left: Schematic of the microfluidic network. Right: Microphotographs of plugs traveling through the microchannel. a) Spontaneous merging of pairs of plugs into single plugs in the main microchannel. b) Spontaneous splitting of plugs at the branching point in a microchannel. When the outlet pressures are equal, a stream of plugs splits into plugs of approximately half the volume of the initial plugs (middle). When the outlet pressures are different, asymmetric splitting of plugs is observed (right). Perfluorodecalin (PFD) serves as the carrier fluid. Reprinted from reference [1].

2.5. Combining and Splitting Reactions

To perform a multiple-step reaction, reaction mixtures must be combined and split in a controlled manner. By using droplet-based microfluidics, a range of interactions between reactions can be controlled in time.[1] Reactions can be combined by merging two droplets, and reactions can be split by splitting one droplet into two smaller droplets (Figure 14).[1,162]

Various methods have been developed for merging and splitting droplets. To combine two parallel reactions, two sets of droplets can be formed in two parallel microchannels that converge into one main channel. The two sets of droplets will merge within the main channel if the frequency is matched between the two droplets and the droplets are of different sizes (Figure 14a).[1] The merging of several smaller droplets with a single larger droplet[163] and of two droplets of the same size has also been shown.[164] The splitting of droplets in a constricted T junction (Figure 14b)[1,125] and at isolated obstacles has also been studied.[165]

Numerous studies have investigated how droplets can be manipulated and controlled within microchannels;[166] examples include the sorting of droplets with dielectrophoretic forces,[167] the control of droplet volume, chemical concentrations, and sorting of droplets,[168] as well as numerical studies on the deformation, breakup, and coalescence of droplets.[110,130,169] A method was developed recently that uses electric forces to combine and split droplets in microchannels. In this method, two streams of droplets are produced, and opposite charges are applied to the interfaces of aqueous and carrier fluid (Figure 15); the two streams are synchronized and combine completely in a 1:1 ratio upon confluence.[170a] Neutral droplets could be recharged by splitting each droplet into two droplets of opposite charge.[170a] Charged droplets were also sorted by means of electric interactions.[170a] Another method used alternating current field to control the coalescence of plugs.[170b] These techniques should be useful for developing automated, droplet-based microfluidic platforms.

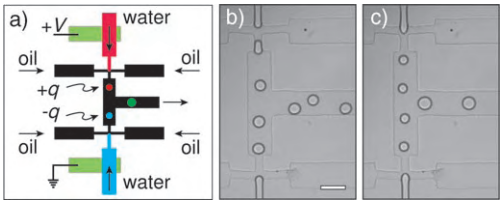

Figure 15. Coalescence of drops by means of electric forces.[170a] a) Drops with opposite signs of electrostatic charge could be generated by applying a voltage across the two aqueous streams. b) In the absence of an electric field, the frequency and timing of drop formation at the two nozzles are independent even at identical infusion rates. In the presence of surfactant, the drops did not coalescence upon confluence of the two streams (scale bar: 100 µm). c) With an applied voltage of 200 V (separation of the nozzles: 500 µm), the drops broke off from the two nozzles simultaneously and coalesced upon confluence. Reprinted with minor modification from reference [170a].

 © 2006 Wiley-VCH Verlag GmbH & Co. KGaA, Weinheim

2.6. Indexing Reaction Conditions by Means of Droplet Pairs

Indexing of droplets is important when many droplets, each containing different reactants, are involved. One possibility is to add reporter dyes at concentrations that are correlated with those of the reagents in the droplet. To avoid possible interference of the reaction by the reporter dyes, pairs of droplets can be produced, one in which the reaction is performed and the other for carrying the information (Figure 16).[33,41] Information about the reaction conditions

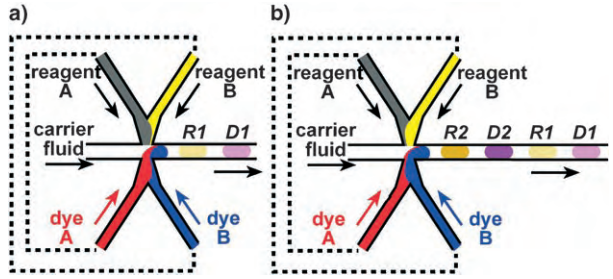

Figure 16. The concentrations within the droplets can be indexed by producing alternating droplets within the microchannels.[41] Pairs of droplets *R* and *D* are formed; droplet *R* contains the reagents, and droplet *D* contains dyes for indexing. The flow rates of reagent A and dye A and of reagent B and dye B are correlated (indicated by the dashed lines). a) The concentrations of reagents A and B in *R1* are correlated with the concentrations of dyes A and B, respectively, in *D1*, so that the concentrations of dyes A and B in *D1* can be used to index the concentrations of reagents A and B in *R1*. b) An array of alternating droplets. Reprinted with permission from reference [41] with minor modifications. Copyright 2004 American Chemical Society.

can be spatially organized with these pairs of droplets—one droplet contains the reaction mixture, the other contains dyes whose ratiometric intensity reports the ratio of reagents within the first droplet.[33,41]

Droplets within microchannels can be generated with alternating compositions (XYXY…). A pair of droplets consists of a droplet of composition "X" and a droplet of composition "Y". The formation of alternating droplets in microchannels was characterized as a function of the capillary number and the flow rates of the aqueous and carrier-fluid streams.[41] A movie of alternating droplets forming in a microchannel can be found in the Supporting Information.

2.7. Analysis of Droplet Contents

There are two methods of analyzing the composition of the reaction mixture and the progress of the reaction within droplets: either each droplet can be analyzed individually or a single measurement can be made of many droplets.

Analysis of the contents of a single droplet requires the handling of a small volume of sample (typically from femtoliters to microliters). Fluorescence is used most often for analysis within microfluidic devices, in which case the contents of a single droplet are detected by using a fluorogenic substrate. Electrophoresis has been used in integrated microfluidic devices.[51] Recently, MALDI-MS was used for semiquantitative characterization of deacetylation reactions in nanoliter-sized plugs.[126] Also, microcoil NMR spectroscopy can be used to analyze small samples.[171] X-ray diffraction has also been used to analyze single protein crystals within a plug.[34]

Measurements on multiple droplets can be made either outside or within the microfluidic device. For external analysis, droplets can be collected into vials until there is sufficient volume for analysis. This method is typically used for nanoparticle synthesis, the characterization of which requires absorbance measurements, SEM, and similar methods. For on-chip analysis, time-resolved measurements can be obtained from a single spatially resolved fluorescence microphotograph (such as that in Figure 11 b).[1,44] The fluorescence intensity is linearly related to the formation of the cleavage product. As dispersion is absent, the amount of product formed at time t can be determined by measuring the fluorescence intensity within the microchannel at distance d (Figure 17). Kinetics can be measured with this method on a millisecond timescale with nanoliter volumes of reagents.[44]

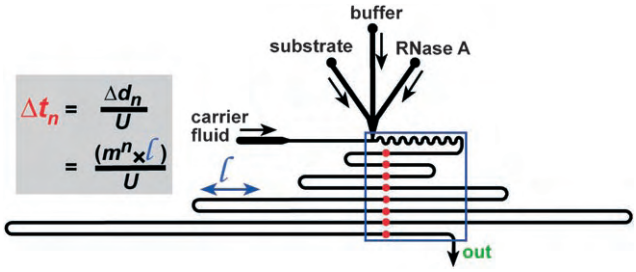

Figure 17. Kinetic measurements by analysis of a single microphotograph of droplets traveling through a microchannel.[44] The red points indicate time points t_n, and the blue rectangle outlines the field of view for the fluorescence microphotograph. The reaction being measured within the droplets should result in a change in fluorescence (as in Figure 11 b). The time course of the reaction can be obtained by measuring the fluorescence intensity at each position (red circles) within the microphotograph. The equation shown enables the time difference between each point to be determined; Δt_n [s] is the time interval between $n=1$ to 8 (for each row of microchannel in the field of view), $m=1.5$, $l=0.9$ mm, $U=106$ mm s^{-1}. Reprinted with permission from reference [44]. Copyright 2003 American Chemical Society.

3. Applications of Droplet-Based Microfluidics

The techniques described above have been applied to many different types of reactions, performed in parallel as well as in series. We divide these reactions into five categories: 1) enzyme kinetics, enzyme assays, and DNA analysis; 2) protein crystallization; 3) synthesis of molecules; 4) synthesis of nanoparticles, microparticles, and colloidal assemblies; 5) synthesis of reaction networks.

3.1. Enzyme Kinetics, Enzyme Assays, and DNA Analysis

3.1.1. Enzyme Kinetics within Droplets

The rapid mixing (Section 2.3), the biocompatible interfacial chemistry (Section 2.4), and the absence of dispersion

 © 2006 Wiley-VCH Verlag GmbH & Co. KGaA, Weinheim

make droplet-based microfluidics the method of choice to measure single-turnover kinetics of the enzyme ribonuclease A (RNase A) with millisecond resolution (Figure 18).[44]

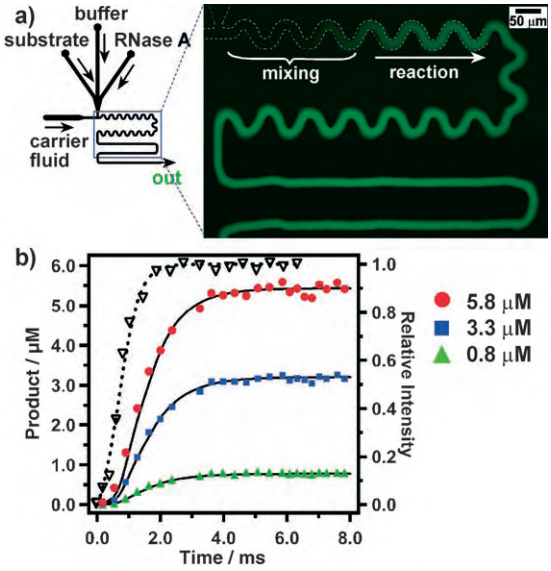

Figure 18. Kinetic analysis on a millisecond timescale of the turnover of RNase A in plugs.[44] a) Left: Experimental setup. Right: Fluorescence microphotograph (false-colored) that shows the time-averaged (exposure time 2 s) intensity of aqueous plugs and carrier fluid moving through the microchannel. b) Graph of the experimental kinetic data for three substrate concentrations at 0.8 (▲), 3.3 (■), and 5.8 μM (●); the data is obtained from analysis of images such as that in (a). Also shown is a mixing curve (right axis, ▽) for a Fluo-4/Ca^{2+} system in the same microfluidic device. The solid lines are fits of the reaction progress including explicit treatment of mixing. Reprinted with permission from reference [44]. Copyright 2003 American Chemical Society.

By using on-chip dilution (Section 2.2.2), serial measurements of the kinetics of RNase A turnover were performed for three substrate concentrations (Figure 18b). A kinetic trace is obtained from a time-averaged image of the fluorescence intensity (Section 2.7); each kinetic trace required approximately 66 nL of sample. The conversion of alkaline phosphatase was also studied within plugs on a millisecond timescale.[43] The activity of luciferase within droplets of viscous solutions could be studied with millisecond resolution by using the "bumpy mixer" (Figure 12a).[45] Control of dispersion enables plugs to be used to perform enzymatic reactions on slower timescales (from seconds to hours). A multiple-step assay to measure the clotting time of blood was adapted to the droplet-based microfluidic system, which allowed fibrin clots within the droplets to be transported through the channel without contacting or contaminating the channel walls.[132] By using a preformed cartridge containing plugs of various enzymes (Section 2.2.1) and by merging these plugs with a stream of a substrate (Figure 6), enzymes could be screened to identify an enzyme with desired reactivity.[42]

Microreactors for in vitro protein expression are useful for directed evolution of proteins, because the genes and substrate for the protein can be contained in the same microreactor to express the protein and probe its function simultaneously.[61,149] In a microfluidic device, droplets of subpicoliter volume were formed from two aqueous streams (Section 2.2.2) containing the components for GFP expression (GFP-encoding vector, RNA polymerase, amino acids, nucleotides, and ATP; GFP = green fluorescent protein).[149] After incubation of the droplets at 37 °C, the expression of GFP was confirmed by high-sensitivity epifluorescence microscopy (Figure 19).[149] This method, which allows easy control of the concentrations of a large number of droplets (Section 2.2.2), demonstrates the potential application of droplet-based microfluidic channels for the directed evolution of proteins.

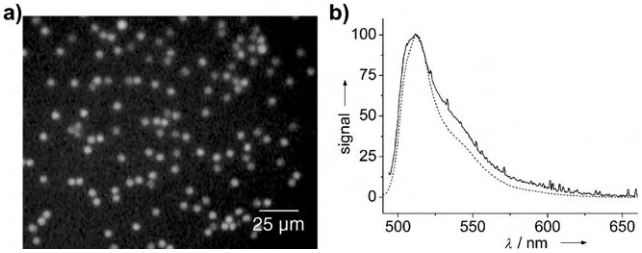

Figure 19. In vitro translation of GFP within droplets.[149] a) Fluorescence microphotograph of the droplets after GFP expression. The droplets were collected in a microfabricated well. b) Fluorescence spectrum of GFP; dashed line: commercially obtained protein in aqueous solution, solid line: individual droplet after in vitro expression. Reprinted from reference [149].

3.1.2. *Encapsulation of Macromolecules and Cells in Droplets*

Cell cultivation can be highly parallelized with droplet-based microfluidics, as has been demonstrated for *C. elegans* embryos[172] and microbial cells.[162,173,174] By confining a cell within a droplet, dilution is minimized, and the small amounts of molecules released by the cell can be more easily detected.

Single-cell enzymatic assays have been achieved by encapsulating single cells inside droplets.[175] A single droplet of controlled femtoliter volume could be generated by using specially designed T channels. Before the formation of the droplet, a single cell was selected from the aqueous solution and moved by optical trapping to the interface between the aqueous phase and the carrier fluid.[175] The cell was encapsulated in the resulting droplet. Similar selective encapsulation has been demonstrated for polystyrene beads, single cells, and single mitochondria.[175] In one example, a single mast cell was encapsulated in a droplet containing a fluorogenic substrate outside the cell (Figure 20a). Before

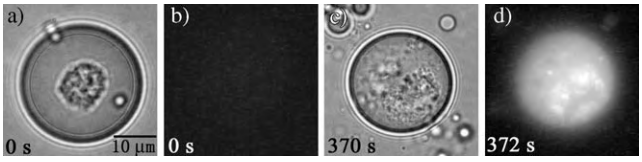

Figure 20. An enzymatic assay for a single mast cell within a droplet.[175] a, c) Brightfield images; b, d) fluorescence images. Reprinted with permission from reference [175]. Copyright 2005 American Chemical Society.

 © 2006 Wiley-VCH Verlag GmbH & Co. KGaA, Weinheim

photolysis of the cell, the droplet appeared dark under the fluorescence microscope (Figure 20b). After photolysis of the cell (Figure 20c), the intracellular enzyme β-galactosidase was released and cleaved the fluorogenic substrate, and thus the droplet became fluorescent (Figure 20d).[175] In a microfluidic device with integrated heaters and coolers, slugs were used for cells lysis and for detection of the transient responses of the MAPK signaling pathway.[176]

Recently, microfluidic droplets were also used to generate lipid vesicles encapsulating biological macromolecules or cells. Aqueous droplets were first generated by using oleic acid containing phospholipids as the carrier fluid (continuous phase).[177] This water–lipid emulsion was subsequently injected into an $EtOH/H_2O$ mixture to extract the oleic acid, and the phospholipids rearranged to form vesicles.[177] Encapsulation of biological molecules or cells was achieved by using an aqueous solution containing the encapsulation targets to generate the initial droplets (Figure 21).[177] Cells encapsulated in vesicles with this method remained viable for 2 hours.[177] This approach is a single-step process and does not require toxic solvents.[177]

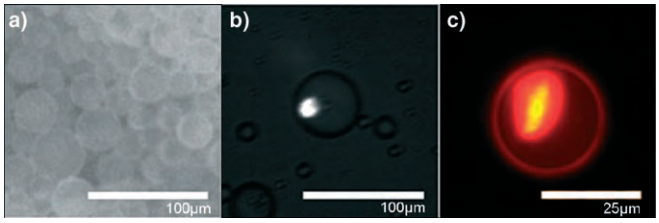

Figure 21. Fluorescence microscopy of a) GFP encapsulated in DOPC vesicles; b) a single Hela cervical carcinoma cell (diameter 10 μm) encapsulated in a DOPC vesicle; c) MCF7 breast cancer cell encapsulated in a DMPC vesicle. Reprinted from reference [177]. Copyright 2006 American Chemical Society. DOPC = dioleoylphosphatidylcholine, DMPC = dimyristoylphosphatidylcholine.

3.1.3. DNA Analysis

The use of slugs as microreactors was nicely illustrated by an integrated DNA analyzer.[51] This device measures and handles nanoliter volumes of solutions in slugs. A hydrophilic microchannel with a hydrophobic patch on its surface is filled by capillary action with an aqueous solution (of the sample or reagent) until the solution reached the hydrophobic patch (Figure 22).[51,178] An air bubble is then generated by pressure to split off a liquid slug of nanoliter volume and to move it through the channel (Figure 22). The sample and reagent slugs are subsequently combined and heated in the reaction chamber. When the reaction is finished, the slug is moved by pressure to an electrophoresis channel for on-chip separation and detection. Polymerase chain reaction of DNA has also been performed in continuous flows of slugs[148a,b] and plugs.[148c]

3.2. Protein Crystallization with Droplet-Based Microfluidics

Growing high-quality crystals is an important step in solving protein structures by X-ray crystallography. Crystals

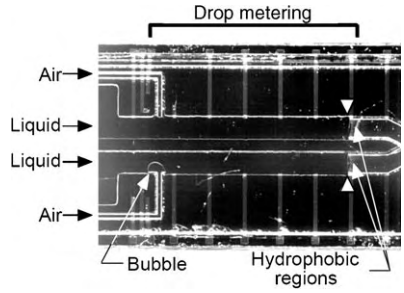

Figure 22. Optical microphotograph of the liquid-injection part of an integrated DNA analyzer. Reprinted from reference [51]. Copyright 1998 AAAS.

are typically grown by using the microbatch method or the vapor-diffusion method. In microbatch methods, a microliter-sized drop containing precipitants and the protein sample is incubated under a layer of oil. In vapor-diffusion methods, a microliter-sized drop containing precipitants and the protein sample is placed next to a reservoir containing a high concentration of desiccant. In this method, water evaporates from the drop into the reservoir, which increases the concentration of the supersaturated solution within drop and promotes the nucleation and growth of crystals.

Protein samples are usually available in only limited amounts. Therefore, strategies have been developed to miniaturize these processes by using either robotics[179,180] or microvalve-based microfluidics.[24–26] Droplet-based microfluidics allows the use of nanoliter-sized droplets, so a thousand crystallization trials can be set up with approximately 10 μL of protein sample. In this section, we discuss how droplets can be used to conduct both microbatch and vapor-diffusion methods of crystallization, to perform on-chip X-ray diffraction, and to study the effect of mixing on the nucleation and growth of protein crystals.

3.2.1. Protein Crystallization by Sparse-Matrix and Gradient Screening

The growth of crystals of a protein with the microbatch method usually involves two steps. First, a large number of crystallization reagents (a particular combination of buffer, precipitants, and polymer solution) are tested with the protein to identify the appropriate combinations of reagents that produce protein crystals (sparse-matrix screening). Then, the concentration of each reagent in the combination is finely screened to grow crystals of diffraction quality (gradient screening).

Sparse-matrix screening was performed with droplet-based microfluidics by introducing the protein sample into a preformed cartridge containing an array of crystallization reagents (Section 2.2.1).[42] The plugs in the cartridge were combined with a stream of thaumatin protein through a T junction, transported into a glass capillary, sealed, and finally incubated to allow crystals to grow. These trials could be stored in glass capillaries for more than half a year without evaporation.[42] Protein crystals grown in the capillaries were detected with a bright-field microscope equipped with a polarizer.

© 2006 Wiley-VCH Verlag GmbH & Co. KGaA, Weinheim

Gradient screening was performed by using a computer program to control the flow rates of the reagents to produce an array of droplets (Figure 23).[128] The concentrations of the reagents were varied by changing the flow rates of the reagents (Section 2.2.2). After setting up the gradient screen, the flow of reagents was stopped and the array of droplets was incubated to determine the appropriate crystallization conditions for the protein.

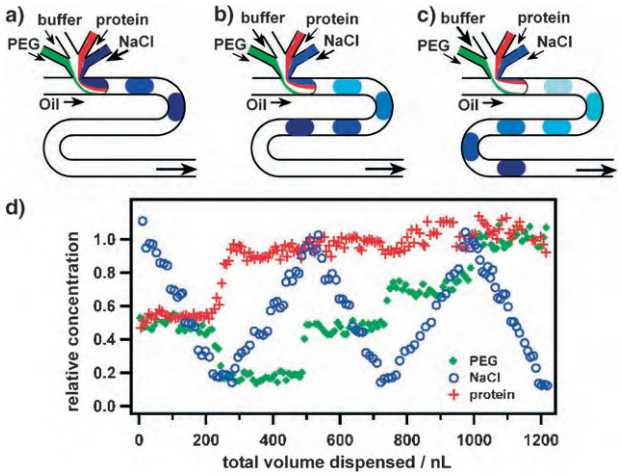

Figure 23. Gradient screening of protein crystallization conditions in droplets.[128] a–c) The concentrations of the crystallizing reagents (PEG, buffer, protein, and NaCl) are varied by varying the relative flow rates of the reagents. d) Experimental characterization of the gradient screen. Two droplets with volume of 7.5 nL were formed each second; each data point represents one droplet. Reprinted with permission from reference [128]. Copyright 2003 American Chemical Society.

3.2.2. *Protein Crystallization by Vapor Diffusion*

In the vapor-diffusion method of crystallization, the diffusion of water vapor from a drop containing the crystallization reagents is accelerated by a reservoir containing a solution of a desiccant (e.g., a concentrated salt solution). To implement this method in droplet-based microfluidics, pairs of alternating plugs (Section 2.6) were formed in which one droplet contained a mixture of protein and precipitant, and the other droplet contained a concentrated salt solution (Figure 24).[34] To allow water to transfer between plugs, a water-permeable carrier fluid was used to form the plugs.

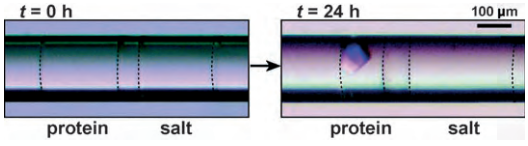

Figure 24. Protein crystallization by the vapor-diffusion method by using alternating droplets.[34] Microphotographs of a pair of alternating droplets at 0 h (left) and at 24 h (right) after the droplets were transported into the capillary. A crystal formed within the droplet of the protein solution after the volume of the droplet decreased by 50%. Dashed lines indicate the interfaces between the aqueous droplets and the carrier fluid. Reprinted from reference [34].

3.2.3. *Protein Structure Determination by On-Chip X-ray Diffraction and In Situ Structure Solution*

Before X-ray diffraction data can be obtained, the crystals must be transferred from the mother liquor, soaked with cryoprotectant, frozen, and finally mounted onto an X-ray diffractometer. Handling these crystals is often not trivial. By growing crystals in plugs inside X-ray-transparent capillaries, the diffraction pattern of a thaumatin crystal was obtained directly (Figure 25).[34]

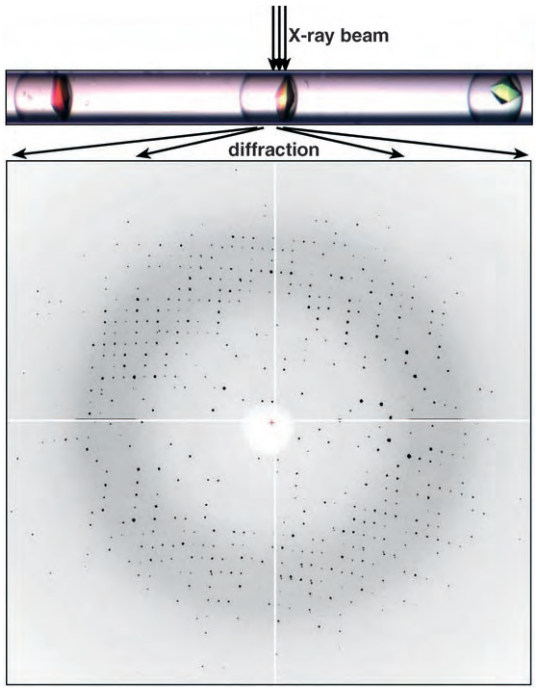

Figure 25. On-chip X-ray diffraction of thaumatin crystals within a capillary.[34] Reprinted from reference [34].

As crystals are easily damaged by X-ray radiation, it is difficult to obtain a complete set of data from one crystal without freezing the crystal. By growing multiple crystals in a capillary and merging the data from each crystal, a complete data set was obtained. This concept of "in situ structure solution"[181] has been demonstrated for model proteins within plugs.[182] It will be important to establish whether this method can be used as a general approach for determining the structure of a broad range of proteins.

3.2.4. *Influence of Mixing on Protein Crystallization*

Mixing has been presumed to be a cause of inconsistencies in batch crystallization. In typical benchtop procedures, mixing is not well controlled, and the effect of mixing is difficult to study with conventional pipetting methods. As mixing can be controlled within plugs (Section 2.3), the effect of mixing on the nucleation of protein crystals within plugs can be studied (Figure 26).[183] The rate of nucleation increases rapidly (exponential squared) with increasing concentration above supersaturation (related to the concentra-

 © 2006 Wiley-VCH Verlag GmbH & Co. KGaA, Weinheim

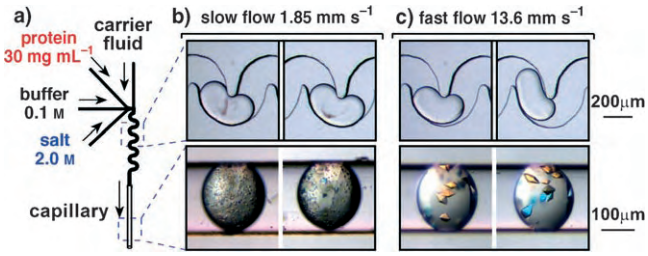

Figure 26. Study of the influence of mixing on the nucleation of protein crystals by using droplets.[183] a) Experimental setup. b) At a low flow rate, precipitation was observed (top image); precipitate and microcrystals grew within the plugs (bottom image). c) At a higher flow rate, fewer and larger crystals were observed (bottom image). Reprinted with permission from reference [183]. Copyright 2005 American Chemical Society.

tions of the protein and the precipitant). Because precipitants (often small molecules or salts) may diffuse faster than the protein, the solution at the interface between the solutions of the protein and the precipitant is more supersaturated than the solution after mixing. Mixing was used to control the lifetime of the interface between the solutions of protein and salt in plugs. If mixing was slow, then the lifetime of the interface was long and excessive nucleation resulted (Figure 26b). If mixing was fast, then the lifetime was short and fewer nucleation events resulted (Figure 26c).

3.3. Syntheses in Droplets

3.3.1. Synthesis of Organic Molecules in Droplets

Organic reactions have been performed in microfluidic plugs and slugs to exploit the advantages of miniaturization as well as facile heat and mass transfer. Examples of single-step reactions that have been performed within plugs include the nitration of benzene,[184–186] the extraction of acid from kerosene,[187] the fluorination of aromatics,[49] the bromination of alkenes,[188] and precipitate-forming reactions.[189] Monomeric and novolak azo dyes were formed within plugs in a two-step reaction.[47] The hybridization efficiency on DNA microarrays was improved by segmenting the samples into slugs.[190]

Mass transport is crucial for heterogeneous reactions that occur between multiple phases. In droplet-based microfluidics, effective and well-controlled mass transport between phases can be achieved[96] thanks to the reproducible flow patterns. This enables droplet-based microfluidics to be used as a tool for investigating the effect of mass transport on heterogeneous reactions. One example of this application is the catalytic hydrogenation of unsaturated aldehydes, in which three phases were involved: the aqueous phase contained the [Ru^{II}(tppts)] catalyst (tppts = triphenylphosphane trisulfonate), the organic phase contained the unsaturated aldehyde, and the gas phase was composed of H_2. The reaction was conducted in capillaries by forming alternating (Section 2.6) aqueous droplets and H_2 bubbles in an organic solvent, which served as the carrier fluid (Figure 27).[191] The mass transfer between phases was controlled by the flow rates

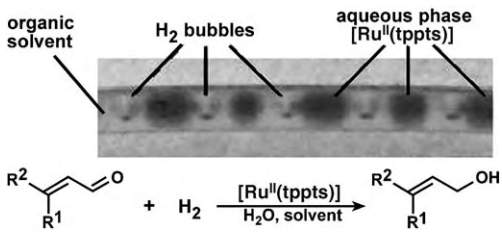

Figure 27. Catalytic multiphase reaction for the hydrogenation of unsaturated aldehydes performed by using alternating droplets.[191] Photograph of a capillary (diameter 750 μm) containing alternating H_2 bubbles and aqueous droplets. The continuous phase is an organic solvent (either toluene or hexane) that contains the unsaturated aldehyde. Figure reprinted from reference [191].

and the diameter of capillary. This study suggested that the mass transport is the rate-determining factor of the reaction.[191]

Minimization of the reagent consumption is an important factor for optimizing reactions of precious substrates. The consumption of substrates per reaction can be decreased to nanoliter volumes by conducting these reactions in plugs. A preformed cartridge (Section 2.2.1) containing different reaction conditions (Figure 28) was used to optimize an organic reaction,[126] and the plugs from the cartridge were merged (Section 2.2.3) with a stream of the substrate solution. In the selective deacetylation of the substrate hexaacetyl ouabain (Ac_6-OUA), less than 1 μg of Ac_6-OUA was required for each reaction. In contrast to screening in microtiter plates, this plug-based method requires only two syringe pumps for flow control. Evaporation is also eliminated. MALDI-MS was used as a semiquantitative detection method to analyze the reaction in the nanoliter-sized droplets (Figure 28b).[126]

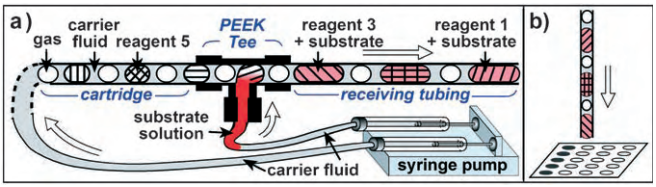

Figure 28. Testing of the conditions of organic reactions in plugs with subsequent analysis by MALDI-MS.[126] a) Setup for serial merging of the reagent plugs with a stream of substrate solution. "PEEK Tee" is a commercially available T junction. b) The reaction plugs are deposited on a MALDI plate for analysis. Figure reprinted from reference [126]. Copyright 2006 American Chemical Society.

3.3.2. Synthesis of Monodisperse Nanoparticles

In addition to kinetic measurements, the synthesis of monodisperse polymers and particles also requires accurate control of the reaction time. Compartmentalization and rapid mixing (Section 2.3) result in a defined starting point of reactions and a narrow distribution of residence times. This control of mixing enabled, for example, the synthesis of silica gel particles of uniform size within liquid slugs.[192] The size of the nanoparticles was controlled by varying the flow rate and therefore the residence time (Figure 29).[48,129,192] The repro-

 © 2006 Wiley-VCH Verlag GmbH & Co. KGaA, Weinheim

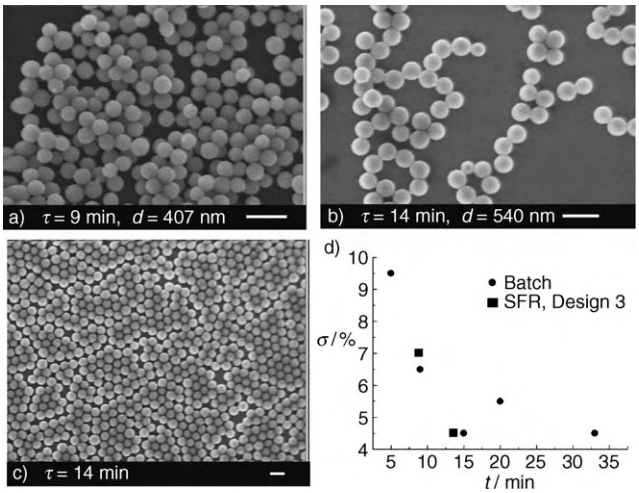

Figure 29. Synthesis of monodisperse particles of silica gel with a segmented-flow reactor (SFR).[192] Various residence times τ resulted in silica particles with different average diameters d_{avg}. SEM microphotographs are shown for a) $\tau = 9$ min, $d_{avg} = 407$ nm, and b) $\tau = 14$ min, $d_{avg} = 540$ nm. c) Low-magnification SEM image of sample shown in (b). d) Standard deviation of the mean diameter σ versus τ for particles formed by using an SFR or a batch reactor. Reprinted with permission from reference [192]. Copyright 2004 American Chemical Society.

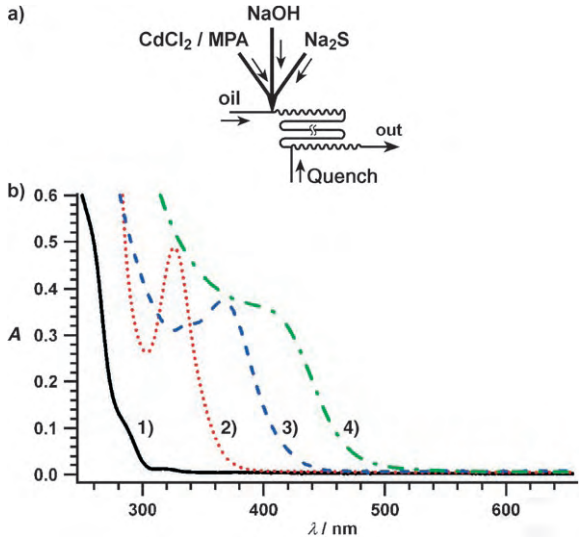

Figure 30. Multiple-step synthesis of nanoparticles in droplets on a millisecond timescale.[129] a) Experimental setup. b) UV/Vis spectra of four types of CdS nanoparticles; reaction conditions: 1) $CdCl_2/Na_2S$ 20:1, quench with methylpropionic acid (MPA) (black); 2) $CdCl_2/Na_2S$ 10:1, quench with MPA (red); 3) $CdCl_2/Na_2S$ 1:1, quench with Na_2S (blue). 4) CdS/CdSe core–shell nanoparticle, synthesized using $CdCl_2/Na_2S$ 1:1 with Na_2Se quenching (green). Reprinted with permission from reference [129]. Copyright 2004 The Royal Society of Chemistry.

ducible synthesis of CdSe nanocrystals at elevated temperatures was achieved within both slugs[116a] and plugs[116b] in microfluidic devices.

A multiple-step synthesis of CdS and CdS/CdSe core–shell nanoparticles was demonstrated within plugs in a PDMS device. By using a merging junction (Section 2.2.3) to deliver a quenching reagent, the nanoparticles were more monodisperse than those produced without the quenching step (Figure 30).[129] The quenching step also allowed core–shell particles to be synthesized.

3.3.3. *Synthesis of Microparticles with Controlled Morphology*

Microparticles with uniform morphology are important in drug delivery, electrooptic devices, and catalysis.[193] Most methods for the synthesis of these particles[117,194] are either expensive or specific to only a particular type of material with controlled morphology.[195] As droplets produced in microfluidic devices are uniform in size and shape, they can be used to study the self-assembly of gel emulsions[196] and colloidal particles into three-dimensional[197] and periodic two-dimensional[198] structures. Trapping these uniform droplets by either interfacial polymerization or bulk solidification is a practical alternative to the existing methods for synthesis of particles with micrometer dimensions.

Uniform capsules (Figure 31 a) were synthesized by forming droplets with an axially symmetric flow-focusing device, in which the dispersed phase was an aqueous solution of 1,6-hexanediamine and the continuous phase was hexadecane with adipoyl chloride.[117] Polymerization of 1,6-hexanediamine and adipoyl chloride at the interface between the aqueous and the hexadecane phase generated a semipermeable membrane (Figure 31 c) of nylon-6,6 coating the

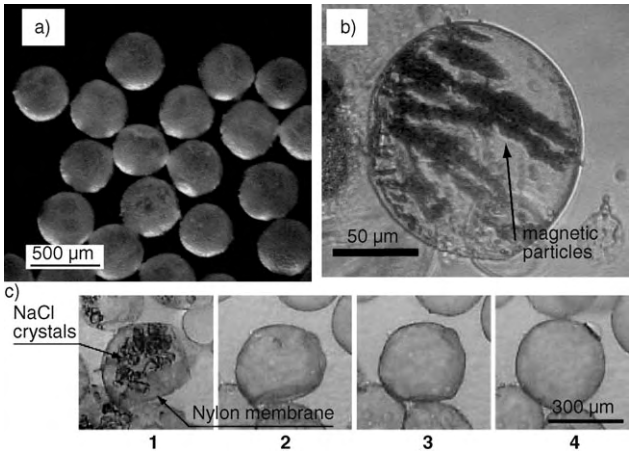

Figure 31. Nylon-coated aqueous droplets generated by interfacial polymerization at the liquid–liquid interface of droplets.[117] Top: a) Capsules with narrow size distribution formed with an axially symmetric flow focusing device. b) Capsules containing magnetic particles that align in an induced magnetic field. c) Capsules containing NaCl were dehydrated by adding ethanol (frame 1). As ethanol was exchanged for water, the membrane swelled over time (frames 2–4). After 30 s, the capsules were fully swelled (frame 4). Reprinted from reference [117].

aqueous droplets.[117] The diameter of the capsules could be controlled by adjusting the flow rates of the dispersed and continuous phases. It is possible to introduce novel functionality by adding micro- or nanoparticles to the dispersed phase. For example, by incorporating superparamagnetic iron oxide

 © 2006 Wiley-VCH Verlag GmbH & Co. KGaA, Weinheim

nanoparticles into the aqueous solution, the resulting capsules can be manipulated under a magnetic field (Figure 31 b).[117] Semipermeable polyamide capsules have been synthesized by means of a droplet-generating device, which was produced without microfabrication methods.[112] Capsules have been formed by encapsulating yeast cells inside droplets and polymerizing the outer shell of the droplet.[199]

Solid particles with controlled shape can be fabricated in two steps by first generating uniform droplets of the desired shape in a microfluidic device and then solidifying the content of the droplet. As the morphology of droplets is determined only by the physical properties of the fluids and operating conditions (device geometry and flow rates), this method is a general way to synthesize particles of a variety of materials with dimensions on the micrometer scale. By increasing the flow rate of the dispersed phase, the volume of the droplet is increased, and the shape of the droplet changes from spheres into nonspherical shapes that touch the walls of the microchannel. The droplets could be solidified by photoinduced polymerization, thermally induced gelation, or through a liquid–solid phase transition. Monodisperse particles with a range of morphologies (spherical, cylindrical, and rod-shaped) were synthesized by various methods of solidification with this method (Figure 32).[194] With similar or modified

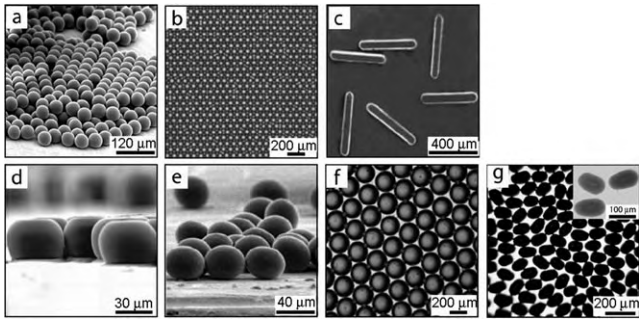

Figure 32. Monodisperse particles with controlled shape and sizes generated in droplets.[194] a) Polymer microspheres, b) a crystal of polymer microspheres, c) polymer rods, d) polymer disks, e) polymer ellipsoids, f) agarose disks, and g) bismuth alloy ellipsoids. Reprinted from reference [194].

methods, monodisperse polymer particles were synthesized with different functionalities, including nonspherical particles,[200] molecularly imprinted polymer beads,[201] particles with novel core–shell structures,[195] particles containing immobilized biocatalyst,[202] bicolor beads,[203,204] and particles of biodegradable microgels.[205]

Double emulsions are droplets that contain smaller droplets within them. Their potential applications range from food science to pharmaceutics.[206] Monodisperse double emulsions and core–shell structures of various sizes and internal composition have been fabricated by means of droplet-based microfluidics.[206–208] By using a flow of alternating droplets (Section 2.6), double emulsions containing two droplets of different composition were formed (Figure 33).

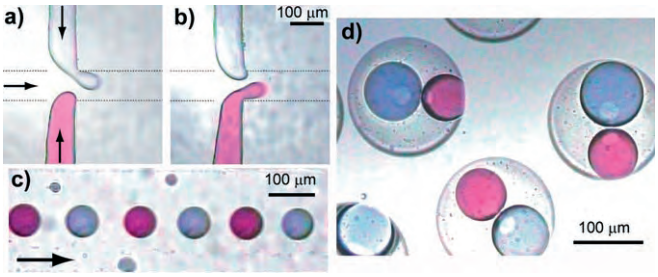

Figure 33. Formation of double emulsions by encapsulation of alternating droplets.[206] Alternating red and blue droplets were formed (a, b) and transported through the microchannel (c) to another droplet-forming region. Double emulsions that contained one red and one blue droplet were formed (d). Reprinted with permission from reference [206]. Copyright 2004 American Chemical Society.

3.4. Synthesis of Functional Reaction Networks

A number of biological functions (e.g., self-regulation, energy conversion, and amplification) are performed by networks of interacting enzymatic reactions. Such functional networks of chemical reactions are nonequilibrium systems, and synthesizing them is an exciting challenge for chemists. Microfluidic droplets provide an opportunity to maintain reactions away from equilibrium by using fluid flow to supply reagents and remove products. Reactions can also be controlled so that they occur "at the right place and the right time".

A reaction network that displays signal amplification with a threshold response has been synthesized by using plugs to compartmentalize an autocatalytic reaction and to control the interactions between reactions. The oxidation of a Co^{3+} complex by $KHSO_5$ produces Co^{2+} ions, which catalyze the reaction and therefore their own production (Figure 34 a).[163] Oxidation of the ligand leads to dissociation of the complex and liberation of the unstable Co^{3+} ion, which is subsequently reduced by the by-products of the ligand oxidation reaction. Without Co^{2+} ions, the reaction proceeds at a very low initial rate, but this reaction mixture is far from equilibrium and unstable. Because the reaction is autocatalytic, once the concentration of Co^{2+} accumulates to a certain level, the reaction accelerates rapidly and is complete within a short period of time. Thus, the transition time required for all of the Co^{3+} complex to be converted into Co^{2+} ions decreases with increasing initial Co^{2+} concentration.

The network was designed with two stages in tandem; Co^{2+} ions act as both the input and the output (Figure 34 b).[163] In the first stage, the input solution containing Co^{2+} ions is combined with streams containing the Co^{3+} complex and a solution of $KHSO_5$ to form small plugs (Figure 34 b, left microphotograph). These plugs are transported through a small microchannel over a defined period of time to the junction with a second, larger channel, where additional streams containing solutions of Co^{3+} complex and $KHSO_5$ are introduced to form large plugs. Several small plugs from the first channel are merged with a large plug from the second channel at the junction (Section 2.5). The second stage of the reaction is monitored as the large plugs flowed

© 2006 Wiley-VCH Verlag GmbH & Co. KGaA, Weinheim

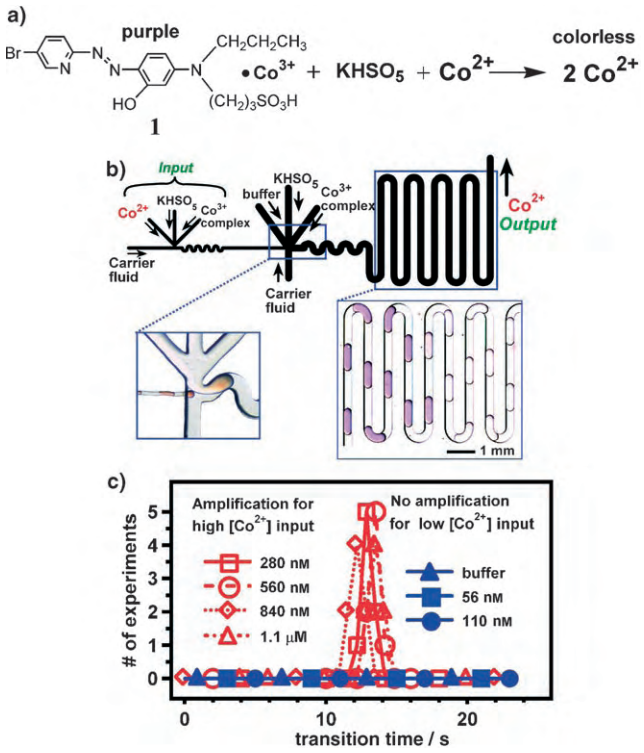

Figure 34. Signal amplification with a reaction network that relies on a droplet-based microfluidic system.[163] a) Autocatalytic formation of the Co^{3+} complex **1**. b) Schematic of the microfluidic device for two-stage amplification. The first stage of the reaction takes place in the thinner channels. The second stage takes place in the thicker channels. Left: Microphotograph of the merging junction, where small droplets of a red solution merge with larger ones. Right: Microphotograph of plugs containing the autocatalytic reaction mixture; the abrupt color transition corresponds to the conversion of the purple Co^{3+} complex (**1**) into colorless Co^{2+} ions. c) Below a threshold initial concentration of Co^{2+} (110 nM and below), there is not enough time for formation of Co^{2+} within the plug in the small channels by the reaction in the first stage. Therefore, the input concentration of Co^{2+} is not amplified in the first stage and is further reduced upon merging and dilution. In this case, no response is observed in the second stage (blue symbols). Above a threshold initial concentration of Co^{2+} (280 nM and above), the reaction in the small droplets of the first stage takes place to produce enough Co^{2+} ions to trigger the reaction in the second stage, and a response is observed (red symbols). Reprinted with permission from reference [163]. Copyright 2004 American Chemical Society.

through the second channel (Figure 34b, right microphotograph). The flow rate and the length of the first channel determines the time between formation of the small plugs and injection into the large plugs. This reaction network shows a threshold response to the input Co^{2+} concentration: only input Co^{2+} concentration above a threshold value is amplified (Figure 34c).[163]

This network mimicks biochemical networks[163] that perform amplification in vision and signal transduction. The fundamental principles are similar to those of biochemical networks: 1) a metastable, kinetically trapped state; 2) a threshold response that stabilizes this nonequilibrium state so long as the input concentration of autocatalyst is below the threshold level, thus ensuring that the network is stable to noise; 3) multiple stages of amplification to increase the overall amplification. Droplet-based microfluidics was essential in the development of this system, as it provided the influx of reagents to implement the first principle, and provided the time control to implement the second and third principles. This network may find practical applications in the detection of autocatalytic species and the control of nucleation in protein crystallization.

4. Conclusions and Outlook

To perform chemical reactions in droplets, a set of basic techniques has been developed to introduce, mix, and transport reagents, control the interfacial chemistry of droplets, and analyze the reactions. On the basis of these techniques, miniaturization of many types of reactions has been demonstrated, including enzymatic assays, protein crystallization, as well as organic and particle syntheses. Some unique properties of droplets, such as their controllable morphology, were used to synthesize particles.

Challenges remain for the further improvement of the capabilities of droplet-based microfluidics, both in the construction of devices as well as the control of fluids. Some of these challenges are general for microfluidics. Examples include the development of new materials for fabricating devices with desired properties, techniques for surface patterning, analytical tools with higher sensitivity and accuracy, and integrated microfluidic platforms. Other challenges are specific to droplets, for example, the automated control of the movement of many droplets.

Current progress is being made in methods for the active control of droplets by means of electrowetting on dielectric (EWOD),[71–74] dielectrophoretic,[167] and electric forces.[170] "Liquid teflon" is one example of a new material for microfluidics.[209] These developments will lead to further applications. In particular, new analytical methods with high resolution in both space and time will be critical for studying reactions and reaction networks.[210]

The basic properties of droplets have been well understood for a number of years, but the behavior of droplets can rapidly become complicated.[35,99,211] Research is being undertaken to understand these phenomena better.[143,163,183,212] New technologies based on droplets will also benefit many areas of science. The synthesis of functional reaction networks[163] and investigation of the influence of mixing on nucleation of protein crystals[183] are the examples discussed herein. These and numerous other examples—such as the analysis of the pressure changes as different cells pass through microfluidic channels,[212,213] the formation of nonspherical bubbles by using "colloidal armor",[214] and understanding the nonlinear dynamics in a bubble generator[99]—suggest that technologies based on droplets in microchannels will continue to lead to scientific advances.

Addendum (October 16, 2006)

Performing reactions in droplets in microchannels has become increasingly established as a standard part of micro-

 © 2006 Wiley-VCH Verlag GmbH & Co. KGaA, Weinheim

fluidics,[215–217] and during the time since submission of this Review over a dozen papers have been published. These publications cover new techniques and devices such as the formation of droplets,[218–221] regulation of droplet traffic,[222] merging of droplets,[223,224] a microfluidic viscometer[225] and interfacial tensiometer,[226] and analysis of droplets with Raman spectroscopy.[227,228] New applications range from the synthesis of microparticles[229–231] and capsules,[232–234] the rate enhancement of reactions,[235] to the control of nucleation and growth of protein crystals.[236] Basic studies to understand the pressure drop in droplet flow[237] and the physics in formation[238] and organization[239] of bubbles were also reported during this period.

The research in our laboratory has been supported by the NIH (National Institute for Biomedical Imaging and Bioengineering R01 EB001903 and the National Institute of General Medical Sciences R01 GM075827), the Beckman Young Investigator Program, and by the DuPont Young Professor Award. We thank Joshua D. Tice for the images in Figure 9 and all members of our research group for their work described herein. We thank our colleagues in the field of droplet-based microfluidics for providing figures and for valuable suggestions.

Received: April 19, 2006
Revised: July 4, 2006

[1] H. Song, J. D. Tice, R. F. Ismagilov, *Angew. Chem.* **2003**, *115*, 792 – 796; *Angew. Chem. Int. Ed.* **2003**, *42*, 768 – 772.
[2] K. Jähnisch, V. Hessel, H. Löwe, M. Baerns, *Angew. Chem.* **2004**, *116*, 410 – 451; *Angew. Chem. Int. Ed.* **2004**, *43*, 406 – 446.
[3] T. Dwars, E. Paetzold, G. Oehme, *Angew. Chem.* **2005**, *117*, 7338 – 7364; *Angew. Chem. Int. Ed.* **2005**, *44*, 7174 – 7199.
[4] P. Watts, S. J. Haswell, *Chem. Soc. Rev.* **2005**, *34*, 235 – 246.
[5] P. Watts, S. J. Haswell, *Curr. Opin. Chem. Biol.* **2003**, *7*, 380 – 387.
[6] Y. N. Xia, G. M. Whitesides, *Annu. Rev. Mater. Sci.* **1998**, *28*, 153 – 184.
[7] B. Xu, F. Arias, S. T. Brittain, X. M. Zhao, B. Grzybowski, S. Torquato, G. M. Whitesides, *Adv. Mater.* **1999**, *11*, 1186 – 1189.
[8] D. C. Duffy, J. C. McDonald, O. J. A. Schueller, G. M. Whitesides, *Anal. Chem.* **1998**, *70*, 4974 – 4984.
[9] J. C. McDonald, D. C. Duffy, J. R. Anderson, D. T. Chiu, H. K. Wu, O. J. A. Schueller, G. M. Whitesides, *Electrophoresis* **2000**, *21*, 27 – 40.
[10] J. C. McDonald, G. M. Whitesides, *Acc. Chem. Res.* **2002**, *35*, 491 – 499.
[11] P. S. Dittrich, A. Manz, *Nat. Rev. Drug Discovery* **2006**, *5*, 210 – 218.
[12] M. F. Templin, D. Stoll, M. Schrenk, P. C. Traub, C. F. Vohringer, T. O. Joos, *Trends Biotechnol.* **2002**, *20*, 160 – 166.
[13] M. C. Pirrung, *Chem. Rev.* **1997**, *97*, 473 – 488.
[14] P. O. Brown, D. Botstein, *Nat. Genet.* **1999**, *21*, 33 – 37.
[15] M. H. J. Ohlmeyer, R. N. Swanson, L. W. Dillard, J. C. Reader, G. Asouline, R. Kobayashi, M. Wigler, W. C. Still, *Proc. Natl. Acad. Sci. USA* **1993**, *90*, 10922 – 10926.
[16] K. S. Lam, M. Lebl, V. Krchnak, *Chem. Rev.* **1997**, *97*, 411 – 448.
[17] F. Guillier, D. Orain, M. Bradley, *Chem. Rev.* **2000**, *100*, 2091 – 2157.
[18] K. Braeckmans, S. C. De Smedt, M. Leblans, R. Pauwels, J. Demeester, *Nat. Rev. Drug Discovery* **2002**, *1*, 447 – 456.
[19] N. H. Finkel, X. H. Lou, C. Y. Wang, L. He, *Anal. Chem.* **2004**, *76*, 353A – 359A.
[20] T. Thorsen, S. J. Maerkl, S. R. Quake, *Science* **2002**, *298*, 580 – 584.
[21] J. W. Hong, S. R. Quake, *Nat. Biotechnol.* **2003**, *21*, 1179 – 1183.
[22] C. C. Lee, G. D. Sui, A. Elizarov, C. Y. J. Shu, Y. S. Shin, A. N. Dooley, J. Huang, A. Daridon, P. Wyatt, D. Stout, H. C. Kolb, O. N. Witte, N. Satyamurthy, J. R. Heath, M. E. Phelps, S. R. Quake, H. R. Tseng, *Science* **2005**, *310*, 1793 – 1796.
[23] J. S. Marcus, W. F. Anderson, S. R. Quake, *Anal. Chem.* **2006**, *78*, 956 – 958.
[24] C. L. Hansen, M. O. A. Sommer, S. R. Quake, *Proc. Natl. Acad. Sci. USA* **2004**, *101*, 14431 – 14436.
[25] C. L. Hansen, E. Skordalakes, J. M. Berger, S. R. Quake, *Proc. Natl. Acad. Sci. USA* **2002**, *99*, 16531 – 16536.
[26] C. L. Hansen, S. Classen, J. M. Berger, S. R. Quake, *J. Am. Chem. Soc.* **2006**, *128*, 3142 – 3143.
[27] F. K. Balagadde, L. C. You, C. L. Hansen, F. H. Arnold, S. R. Quake, *Science* **2005**, *309*, 137 – 140.
[28] G. C. Randall, P. S. Doyle, *Proc. Natl. Acad. Sci. USA* **2005**, *102*, 10813 – 10818.
[29] R. B. Bird, W. E. Stewart, E. N. Lightfoot, *Transport Phenomena*, Wiley, New York, **2002**.
[30] G. I. Taylor, *Proc. R. Soc. London Ser. A* **1953**, *219*, 186 – 203.
[31] V. Dolnik, *Electrophoresis* **2004**, *25*, 3589 – 3601.
[32] D. Belder, M. Ludwig, *Electrophoresis* **2003**, *24*, 3595 – 3606.
[33] B. Zheng, J. D. Tice, R. F. Ismagilov, *Adv. Mater.* **2004**, *16*, 1365 – 1368.
[34] B. Zheng, J. D. Tice, L. S. Roach, R. F. Ismagilov, *Angew. Chem.* **2004**, *116*, 2562 – 2565; *Angew. Chem. Int. Ed.* **2004**, *43*, 2508 – 2511.
[35] T. Thorsen, R. W. Roberts, F. H. Arnold, S. R. Quake, *Phys. Rev. Lett.* **2001**, *86*, 4163 – 4166.
[36] T. Nisisako, T. Torii, T. Higuchi, *Lab Chip* **2002**, *2*, 24 – 26.
[37] J. D. Tice, H. Song, A. D. Lyon, R. F. Ismagilov, *Langmuir* **2003**, *19*, 9127 – 9133.
[38] J. D. Tice, A. D. Lyon, R. F. Ismagilov, *Anal. Chim. Acta* **2004**, *507*, 73 – 77.
[39] H. J. Liu, M. Nakajima, T. Kimura, *J. Am. Oil Chem. Soc.* **2004**, *81*, 705 – 711.
[40] H. Song, M. R. Bringer, J. D. Tice, C. J. Gerdts, R. F. Ismagilov, *Appl. Phys. Lett.* **2003**, *83*, 4664 – 4666.
[41] B. Zheng, J. D. Tice, R. F. Ismagilov, *Anal. Chem.* **2004**, *76*, 4977 – 4982.
[42] B. Zheng, R. F. Ismagilov, *Angew. Chem.* **2005**, *117*, 2576 – 2579; *Angew. Chem. Int. Ed.* **2005**, *44*, 2520 – 2523.
[43] L. S. Roach, H. Song, R. F. Ismagilov, *Anal. Chem.* **2005**, *77*, 785 – 796.
[44] H. Song, R. F. Ismagilov, *J. Am. Chem. Soc.* **2003**, *125*, 14613 – 14619.
[45] A. Liau, R. Kamik, A. Majumdar, J. H. D. Cate, *Anal. Chem.* **2005**, *77*, 7618 – 7625.
[46] A. Günther, M. Jhunjhunwala, M. Thalmann, M. A. Schmidt, K. F. Jensen, *Langmuir* **2005**, *21*, 1547 – 1555.
[47] P. M. Günther, F. Möller, T. Henkel, J. M. Köhler, G. A. Groß, *Chem. Eng. Technol.* **2005**, *28*, 520 – 527.
[48] A. Günther, S. A. Khan, M. Thalmann, F. Trachsel, K. F. Jensen, *Lab Chip* **2004**, *4*, 278 – 286.
[49] N. de Mas, A. Günther, M. A. Schmidt, K. F. Jensen, *Ind. Eng. Chem. Res.* **2003**, *42*, 698 – 710.
[50] K. Hosokawa, T. Fujii, I. Endo, *Anal. Chem.* **1999**, *71*, 4781 – 4785.
[51] M. A. Burns, B. N. Johnson, S. N. Brahmasandra, K. Handique, J. R. Webster, M. Krishnan, T. S. Sammarco, P. M. Man, D. Jones, D. Heldsinger, C. H. Mastrangelo, D. T. Burke, *Science* **1998**, *282*, 484 – 487.

 © 2006 Wiley-VCH Verlag GmbH & Co. KGaA, Weinheim

[52] C. J. Patton, S. R. Crouch, *Anal. Chim. Acta* **1986**, *179*, 189 – 201.
[53] K. K. Stewart, *Anal. Chem.* **1983**, *55*, A931 – A934.
[54] B. Rocks, C. Riley, *Clin. Chem.* **1982**, *28*, 409 – 421.
[55] K. K. Stewart, *Talanta* **1981**, *28*, 789 – 797.
[56] L. T. Skeggs, H. Hochstrasser, *Clin. Chem.* **1964**, *10*, 918 – 936.
[57] M. P. Pileni, *Adv. Colloid Interface Sci.* **1993**, *46*, 139 – 163.
[58] "Microemulsion polymerizations and reactions": P. Y. Chow, L. M. Gan in *Polymer Particles*, *Vol. 175*, Springer, Berlin, **2005**, pp. 257 – 298.
[59] "Miniemulsions for nanoparticle synthesis": K. Landfester in *Colloid Chemistry II*, *Vol. 227*, Springer, Berlin, **2003**, pp. 75 – 123.
[60] C. S. Peyratout, L. Dähne, *Angew. Chem.* **2004**, *116*, 3850 – 3872; *Angew. Chem. Int. Ed.* **2004**, *43*, 3762 – 3783.
[61] A. Aharoni, A. D. Griffiths, D. S. Tawfik, *Curr. Opin. Chem. Biol.* **2005**, *9*, 210 – 216.
[62] K. Bernath, M. T. Hai, E. Mastrobattista, A. D. Griffiths, S. Magdassi, D. S. Tawfik, *Anal. Biochem.* **2004**, *325*, 151 – 157.
[63] M. S. Long, C. D. Jones, M. R. Helfrich, L. K. Mangeney-Slavin, C. D. Keating, *Proc. Natl. Acad. Sci. USA* **2005**, *102*, 5920 – 5925.
[64] V. Noireaux, A. Libchaber, *Proc. Natl. Acad. Sci. USA* **2004**, *101*, 17669 – 17674.
[65] D. T. Chiu, C. F. Wilson, F. Ryttsen, A. Stromberg, C. Farre, A. Karlsson, S. Nordholm, A. Gaggar, B. P. Modi, A. Moscho, R. A. Garza-Lopez, O. Orwar, R. N. Zare, *Science* **1999**, *283*, 1892 – 1895.
[66] S. Sugiura, N. Kumazawa, S. Iwamoto, T. Oda, M. Satake, M. Nakajima, *Kagaku Kogaku Ronbunshu* **2004**, *30*, 129 – 134.
[67] S. Sugiura, M. Nakajima, M. Seki, *Ind. Eng. Chem. Res.* **2002**, *41*, 4043 – 4047.
[68] S. Sugiura, M. Nakajima, J. H. Tong, H. Nabetani, M. Seki, *J. Colloid Interface Sci.* **2000**, *227*, 95 – 103.
[69] A. D. Dinsmore, M. F. Hsu, M. G. Nikolaides, M. Marquez, A. R. Bausch, D. A. Weitz, *Science* **2002**, *298*, 1006 – 1009.
[70] I. G. Loscertales, A. Barrero, I. Guerrero, R. Cortijo, M. Marquez, A. M. Ganan-Calvo, *Science* **2002**, *295*, 1695 – 1698.
[71] M. G. Pollack, A. D. Shenderov, R. B. Fair, *Lab Chip* **2002**, *2*, 96 – 101.
[72] M. G. Pollack, R. B. Fair, A. D. Shenderov, *Appl. Phys. Lett.* **2000**, *77*, 1725 – 1726.
[73] S. K. Cho, H. J. Moon, C. J. Kim, *J. Microelectromech. Syst.* **2003**, *12*, 70 – 80.
[74] J. Lee, H. Moon, J. Fowler, T. Schoellhammer, C. J. Kim, *Sens. Actuators A* **2002**, *95*, 259 – 268.
[75] O. D. Velev, B. G. Prevo, K. H. Bhatt, *Nature* **2003**, *426*, 515 – 516.
[76] F. Mugele, J. C. Baret, *J. Phys. Condens. Matter* **2005**, *17*, R705 – R774.
[77] H. Ding, K. Chakrabarty, R. B. Fair, *IEEE Trans. Comput-Aided Des. Integr. Circuits Syst.* **2001**, *20*, 1463 – 1468.
[78] T. H. Zhang, K. Chakrabarty, R. B. Fair, *IEEE Trans. Comput-Aided Des. Integr. Circuits Syst.* **2004**, *23*, 843 – 858.
[79] A. R. Wheeler, H. Moon, C. J. Kim, J. A. Loo, R. L. Garrell, *Anal. Chem.* **2004**, *76*, 4833 – 4838.
[80] A. R. Wheeler, H. Moon, C. A. Bird, R. R. O. Loo, C. J. Kim, J. A. Loo, R. L. Garrell, *Anal. Chem.* **2005**, *77*, 534 – 540.
[81] Z. Guttenberg, H. Müller, H. Habermüller, A. Geisbauer, J. Pipper, J. Felbel, M. Kielpinski, J. Scriba, A. Wixforth, *Lab Chip* **2005**, *5*, 308 – 317.
[82] V. Srinivasan, V. K. Pamula, R. B. Fair, *Anal. Chim. Acta* **2004**, *507*, 145 – 150.
[83] T. Taniguchi, T. Torii, T. Higuchi, *Lab Chip* **2002**, *2*, 19 – 23.
[84] J. R. Millman, K. H. Bhatt, B. G. Prevo, O. D. Velev, *Nat. Mater.* **2005**, *4*, 98 – 102.
[85] A. D. McNaught, A. Wilkinson, *Compendium of Chemical Terminology: IUPAC Recommendations*, 2nd ed., Blackwell, Malden, **1997**.
[86] J. S. Kuo, P. Spicar-Mihalic, I. Rodriguez, D. T. Chiu, *Langmuir* **2003**, *19*, 250 – 255.
[87] H. Moon, S. K. Cho, R. L. Garrell, C. J. Kim, *J. Appl. Phys.* **2002**, *92*, 4080 – 4087.
[88] M. Y. He, J. S. Kuo, D. T. Chiu, *Appl. Phys. Lett.* **2005**, *87*, 031916.
[89] N. Pekas, M. D. Porter, M. Tondra, A. Popple, A. Jander, *Appl. Phys. Lett.* **2004**, *85*, 4783 – 4785.
[90] I. F. Lyuksyutov, D. G. Naugle, K. D. D. Rathnayaka, *Appl. Phys. Lett.* **2004**, *85*, 1817 – 1819.
[91] K. T. Kotz, K. A. Noble, G. W. Faris, *Appl. Phys. Lett.* **2004**, *85*, 2658 – 2660.
[92] N. Garnier, R. O. Grigoriev, M. F. Schatz, *Phys. Rev. Lett.* **2003**, *91*, 054501.
[93] S. Daniel, M. K. Chaudhury, P. G. de Gennes, *Langmuir* **2005**, *21*, 4240 – 4248.
[94] P. Aussillous, D. Quere, *Nature* **2001**, *411*, 924 – 927.
[95] M. Fialkowski, A. Bitner, B. A. Grzybowski, *Nat. Mater.* **2005**, *4*, 93 – 97.
[96] M. T. Kreutzer, F. Kapteijn, J. A. Moulijn, J. J. Heiszwolf, *Chem. Eng. Sci.* **2005**, *60*, 5895 – 5916.
[97] A. M. Ganan-Calvo, J. M. Gordillo, *Phys. Rev. Lett.* **2001**, *87*, 274501.
[98] P. Garstecki, I. Gitlin, W. DiLuzio, G. M. Whitesides, E. Kumacheva, H. A. Stone, *Appl. Phys. Lett.* **2004**, *85*, 2649 – 2651.
[99] P. Garstecki, M. J. Fuerstman, G. M. Whitesides, *Phys. Rev. Lett.* **2005**, *94*, 234502.
[100] T. Cubaud, C. M. Ho, *Phys. Fluids* **2004**, *16*, 4575 – 4585.
[101] P. Guillot, A. Colin, *Phys. Rev. E* **2005**, *72*, 066301.
[102] M. Tokeshi, T. Minagawa, K. Uchiyama, A. Hibara, K. Sato, H. Hisamoto, T. Kitamori, *Anal. Chem.* **2002**, *74*, 1565 – 1571.
[103] M. Goto, K. Sato, A. Murakami, M. Tokeshi, T. Kitamori, *Anal. Chem.* **2005**, *77*, 2125 – 2131.
[104] J. Kobayashi, Y. Mori, K. Okamoto, R. Akiyama, M. Ueno, T. Kitamori, S. Kobayashi, *Science* **2004**, *304*, 1305 – 1308.
[105] B. Zhao, J. S. Moore, D. J. Beebe, *Science* **2001**, *291*, 1023 – 1026.
[106] P. J. A. Kenis, R. F. Ismagilov, G. M. Whitesides, *Science* **1999**, *285*, 83 – 85.
[107] G. I. Taylor, *Proc. R. Soc. London Ser. A* **1934**, *146*, 501 – 523.
[108] G. I. Taylor, *J. Fluid Mech.* **1961**, *10*, 161 – 165.
[109] F. P. Bretherton, *J. Fluid Mech.* **1961**, *10*, 166 – 188.
[110] R. E. Thiers, A. H. Reed, K. Delander, *Clin. Chem.* **1971**, *17*, 42 – 48.
[111] S. L. Anna, N. Bontoux, H. A. Stone, *Appl. Phys. Lett.* **2003**, *82*, 364 – 366.
[112] E. Quevedo, J. Steinbacher, D. T. McQuade, *J. Am. Chem. Soc.* **2005**, *127*, 10498 – 10499.
[113] R. Dreyfus, P. Tabeling, H. Willaime, *Phys. Rev. Lett.* **2003**, *90*, 144505.
[114] Q. Y. Xu, M. Nakajima, *Appl. Phys. Lett.* **2004**, *85*, 3726 – 3728.
[115] T. Ward, M. Faivre, M. Abkarian, H. A. Stone, *Electrophoresis* **2005**, *26*, 3716 – 3724.
[116] a) B. K. H. Yen, A. Günther, M. A. Schmidt, K. F. Jensen, M. G. Bawendi, *Angew. Chem.* **2005**, *117*, 5583 – 5587; *Angew. Chem. Int. Ed.* **2005**, *44*, 5447 – 5451; b) E. M. Chan, A. P. Alivisatos, R. A. Mathies, *J. Am. Chem. Soc.* **2005**, *127*, 13854 – 13861.
[117] S. Takeuchi, P. Garstecki, D. B. Weibel, G. M. Whitesides, *Adv. Mater.* **2005**, *17*, 1067 – 1072.
[118] H. A. Stone, A. D. Stroock, A. Ajdari, *Annu. Rev. Fluid Mech.* **2004**, *36*, 381 – 411.
[119] J. Atencia, D. J. Beebe, *Nature* **2005**, *437*, 648 – 655.
[120] M. Joanicot, A. Ajdari, *Science* **2005**, *309*, 887 – 888.

 © 2006 Wiley-VCH Verlag GmbH & Co. KGaA, Weinheim

[121] T. M. Squires, S. R. Quake, *Rev. Mod. Phys.* **2005**, *77*, 977 – 1026.
[122] L. Kiwi-Minsker, A. Renken, *Catal. Today* **2005**, *110*, 2 – 14.
[123] P. Garstecki, M. J. Fuerstman, H. A. Stone, G. M. Whitesides, *Lab Chip* **2006**, *6*, 437 – 446.
[124] B. Zheng, C. J. Gerdts, R. F. Ismagilov, *Curr. Opin. Struct. Biol.* **2005**, *15*, 548 – 555.
[125] D. N. Adamson, D. Mustafi, J. X. J. Zhang, B. Zheng, R. F. Ismagilov, *Lab Chip* **2006**, *6*, 1178 – 1186.
[126] T. Hatakeyama, D. L. Chen, R. F. Ismagilov, *J. Am. Chem. Soc.* **2006**, *128*, 2518 – 2519.
[127] V. Linder, S. K. Sia, G. M. Whitesides, *Anal. Chem.* **2005**, *77*, 64 – 71.
[128] B. Zheng, L. S. Roach, R. F. Ismagilov, *J. Am. Chem. Soc.* **2003**, *125*, 11170 – 11171.
[129] I. Shestopalov, J. D. Tice, R. F. Ismagilov, *Lab Chip* **2004**, *4*, 316 – 321.
[130] T. Henkel, T. Bermig, M. Kielpinski, A. Grodrian, J. Metze, J. M. Köhler, *Chem. Eng. J.* **2004**, *101*, 439 – 445.
[131] L. Li, J. Boedicker, R. F. Ismagilov, **2006**, unpublished results.
[132] H. Song, H.-W. Li, M. S. Munson, T. G. van Ha, R. F. Ismagilov, *Anal. Chem.* **2006**, 78, 4839 – 4849.
[133] I. R. Epstein, *Nature* **1995**, *374*, 321 – 327.
[134] J. M. Ottino, S. Wiggins, *Science* **2004**, *305*, 485 – 486.
[135] M. R. Bringer, C. J. Gerdts, H. Song, J. D. Tice, R. F. Ismagilov, *Philos. Trans. R. Soc. London Ser. A* **2004**, *362*, 1087 – 1104.
[136] J. B. Knight, A. Vishwanath, J. P. Brody, R. H. Austin, *Phys. Rev. Lett.* **1998**, *80*, 3863 – 3866.
[137] A. D. Stroock, S. K. W. Dertinger, A. Ajdari, I. Mezic, H. A. Stone, G. M. Whitesides, *Science* **2002**, *295*, 647 – 651.
[138] J. M. Ottino, *The Kinematics of Mixing: Stretching, Chaos, and Transport*, Cambridge University Press, Cambridge, **1989**.
[139] H. Aref, *J. Fluid Mech.* **1984**, *143*, 1 – 21.
[140] K. Handique, M. A. Burns, *J. Micromech. Microeng.* **2001**, *11*, 548 – 554.
[141] M. N. Kashid, I. Gerlach, S. Goetz, J. Franzke, J. F. Acker, F. Platte, D. W. Agar, S. Turek, *Ind. Eng. Chem. Res.* **2005**, *44*, 5003 – 5010.
[142] R. O. Grigoriev, *Phys. Fluids* **2005**, *17*, 033601.
[143] M. Muradoglu, H. A. Stone, *Phys. Fluids* **2005**, *17*, 073305.
[144] P. Garstecki, M. A. Fischbach, G. M. Whitesides, *Appl. Phys. Lett.* **2005**, *86*, 244108.
[145] W. Salman, P. Angeli, A. Gavriilidis, *Chem. Eng. Technol.* **2005**, *28*, 509 – 514.
[146] P. Garstecki, M. J. Fuerstman, M. A. Fischbach, S. K. Sia, G. M. Whitesides, *Lab Chip* **2006**, *6*, 207 – 212.
[147] M. Y. He, C. H. Sun, D. T. Chiu, *Anal. Chem.* **2004**, *76*, 1222 – 1227.
[148] a) M. Curcio, J. Roeraade, *Anal. Chem.* **2003**, *75*, 1 – 7; b) N. Park, S. Kim, J. H. Hahn, *Anal. Chem.* **2003**, *75*, 6029 – 6033; c) K. D. Dorfman, M. Chabert, J. H. Codarbox, G. Rousseau, P. de Cremoux, J. L. Viovy, *Anal. Chem.* **2005**, *77*, 3700 – 3704.
[149] P. S. Dittrich, M. Jahnz, P. Schwille, *ChemBioChem* **2005**, *6*, 811 – 814.
[150] J. E. Squires, *Science* **2002**, *295*, 1002 – 1005.
[151] C. L. Leach, J. S. Greenspan, S. D. Rubenstein, T. H. Shaffer, M. R. Wolfson, J. C. Jackson, R. DeLemos, B. P. Fuhrman, *N. Engl. J. Med.* **1996**, *335*, 761 – 767.
[152] E. G. Schutt, D. H. Klein, R. M. Mattrey, J. G. Riess, *Angew. Chem.* **2003**, *115*, 3336 – 3355; *Angew. Chem. Int. Ed.* **2003**, *42*, 3218 – 3235.
[153] I. Giaever, C. R. Keese, *Proc. Natl. Acad. Sci. USA* **1983**, *80*, 219 – 222.
[154] C. R. Keese, I. Giaever, *Science* **1983**, *219*, 1448 – 1449.
[155] J. G. Riess, M. P. Krafft, *Biomaterials* **1998**, *19*, 1529 – 1539.
[156] P. M. Hinderliter, M. P. DeLorme, G. L. Kennedy, *Toxicology* **2006**, *222*, 80 – 85.
[157] M. K. So, N. Yamashita, S. Taniyasu, Q. T. Jiang, J. P. Giesy, K. Chen, P. K. S. Lam, *Environ. Sci. Technol.* **2006**, *40*, 2924 – 2929.
[158] J. A. Gladysz, D. P. Curran, *Tetrahedron* **2002**, *58*, 3823 – 3825.
[159] E. Dickinson, *ACS Symp. Ser.* **1991**, *448*, 114 – 129.
[160] S. E. Euston, H. Singh, P. A. Munro, D. G. Dalgleish, *J. Food Sci.* **1995**, *60*, 1124 – 1131.
[161] J. M. Girardet, G. Humbert, N. Creusot, V. Chardot, S. Campagna, J. L. Courthaudon, J. L. Gaillard, *J. Colloid Interface Sci.* **2001**, *243*, 515 – 522.
[162] J. M. Köhler, T. Henkel, A. Grodrian, T. Kirner, M. Roth, K. Martin, J. Metze, *Chem. Eng. J.* **2004**, *101*, 201 – 216.
[163] C. J. Gerdts, D. E. Sharoyan, R. F. Ismagilov, *J. Am. Chem. Soc.* **2004**, *126*, 6327 – 6331.
[164] L. H. Hung, K. M. Choi, W. Y. Tseng, Y. C. Tan, K. J. Shea, A. P. Lee, *Lab Chip* **2006**, *6*, 174 – 178.
[165] D. R. Link, S. L. Anna, D. A. Weitz, H. A. Stone, *Phys. Rev. Lett.* **2004**, *92*, 054503.
[166] W. Engl, M. Roche, A. Colin, P. Panizza, A. Ajdari, *Phys. Rev. Lett.* **2005**, *95*, 208304.
[167] K. Ahn, C. Kerbage, T. P. Hunt, R. M. Westervelt, D. R. Link, D. A. Weitz, *Appl. Phys. Lett.* **2006**, *88*, 024104.
[168] Y. C. Tan, J. S. Fisher, A. I. Lee, V. Cristini, A. P. Lee, *Lab Chip* **2004**, *4*, 292 – 298.
[169] V. Cristini, Y. C. Tan, *Lab Chip* **2004**, *4*, 257 – 264.
[170] a) D. R. Link, E. Grasland-Mongrain, A. Duri, F. Sarrazin, Z. D. Cheng, G. Cristobal, M. Marquez, D. A. Weitz, *Angew. Chem.* **2006**, *118*, 2618 – 2622; *Angew. Chem. Int. Ed.* **2006**, *45*, 2556 – 2560; b) M. Chabert, K. D. Dorfman, J. L. Viovy, *Electrophoresis* **2005**, *26*, 3706 – 3715.
[171] R. A. Kautz, W. K. Goetzinger, B. L. Karger, *J. Comb. Chem.* **2005**, *7*, 14 – 20.
[172] J. M. Köhler, T. Henkel, *Appl. Microbiol. Biotechnol.* **2005**, *69*, 113 – 125.
[173] K. Martin, T. Henkel, V. Baier, A. Grodrian, T. Schön, M. Roth, J. M. Köhler, J. Metze, *Lab Chip* **2003**, *3*, 202 – 207.
[174] A. Grodrian, J. Metze, T. Henkel, K. Martin, M. Roth, J. M. Köhler, *Biosens. Bioelectron.* **2004**, *19*, 1421 – 1428.
[175] M. Y. He, J. S. Edgar, G. D. M. Jeffries, R. M. Lorenz, J. P. Shelby, D. T. Chiu, *Anal. Chem.* **2005**, *77*, 1539 – 1544.
[176] J. El-Ali, S. Gaudet, A. Günther, P. K. Sorger, K. F. Jensen, *Anal. Chem.* **2005**, *77*, 3629 – 3636.
[177] Y.-C. Tan, K. Hettiarachchi, M. Siu, Y.-R. Pan, A. P. Lee, *J. Am. Chem. Soc.* **2006**, *128*, 5656 – 5658.
[178] K. Handique, D. T. Burke, C. H. Mastrangelo, M. A. Burns, *Anal. Chem.* **2000**, *72*, 4100 – 4109.
[179] "Robotics for automated crystal formation and analysis": M. Weselak, M. G. Patch, T. L. Selby, G. Knebel, R. C. Stevens in *Macromolecular Crystallography Pt C*, *Vol. 368*, Academic Press, San Diego, **2003**, pp. 45 – 76.
[180] R. C. Stevens, *Curr. Opin. Struct. Biol.* **2000**, *10*, 558 – 563.
[181] A. McPherson, *J. Appl. Crystallogr.* **2000**, *33*, 397 – 400.
[182] M. K. Yadav, C. J. Gerdts, R. Sanishvili, W. W. Smith, L. S. Roach, R. F. Ismagilov, P. Kuhn, R. C. Stevens, *J. Appl. Crystallogr.* **2005**, *38*, 900 – 905.
[183] D. L. Chen, C. J. Gerdts, R. F. Ismagilov, *J. Am. Chem. Soc.* **2005**, *127*, 9672 – 9673.
[184] J. R. Burns, C. Ramshaw, *Chem. Eng. Res. Des.* **1999**, *77*, 206 – 211.
[185] J. R. Burns, C. Ramshaw, *Chem. Eng. Commun.* **2002**, *189*, 1611 – 1628.
[186] G. Dummann, U. Quittmann, L. Groschel, D. W. Agar, O. Worz, K. Morgenschweis, *Catal. Today* **2003**, *79*, 433 – 439.
[187] J. R. Burns, C. Ramshaw, *Lab Chip* **2001**, *1*, 10 – 15.
[188] Z. T. Cygan, J. T. Cabral, K. L. Beers, E. J. Amis, *Langmuir* **2005**, *21*, 3629 – 3634.

 © 2006 Wiley-VCH Verlag GmbH & Co. KGaA, Weinheim

[189] S. L. Poe, M. A. Cummings, M. R. Haaf, D. T. McQuade, *Angew. Chem.* **2006**, *118*, 1574 – 1578; *Angew. Chem. Int. Ed.* **2006**, *45*, 1544 – 1548.
[190] C. W. Wei, J. Y. Cheng, C. T. Huang, M. H. Yen, T. H. Young, *Nucleic Acids Res.* **2005**, *33*, e78.
[191] Y. Onal, M. Lucas, P. Claus, *Chem. Eng. Technol.* **2005**, *28*, 972 – 978.
[192] S. A. Khan, A. Günther, M. A. Schmidt, K. F. Jensen, *Langmuir* **2004**, *20*, 8604 – 8611.
[193] "Generation, characterization, and modeling of polymer micro- and nano-particles": J. U. Otaigbe, M. D. Barnes, K. Fukui, B. G. Sumpter, D. W. Noid in *Polymer Physics and Engineering*, *Vol. 154*, Springer, Berlin, **2001**, pp. 1 – 86.
[194] a) S. Q. Xu, Z. H. Nie, M. Seo, P. Lewis, E. Kumacheva, H. A. Stone, P. Garstecki, D. B. Weibel, I. Gitlin, G. M. Whitesides, *Angew. Chem.* **2005**, *117*, 734 – 738; *Angew. Chem. Int. Ed.* **2005**, *44*, 724 – 728; Erratum: S. Q. Xu, Z. H. Nie, M. Seo, P. Lewis, E. Kumacheva, H. A. Stone, P. Garstecki, D. B. Weibel, I. Gitlin, G. M. Whitesides, *Angew. Chem.* **2005**, *117*, 3865; *Angew. Chem. Int. Ed.* **2005**, *44*, 3799; b) S. H. Cho, J. B. Jun, J. H. Ryu, K. D. Suh, *Colloid Surf. A* **2005**, *254*, 1 – 7.
[195] Z. H. Nie, S. Q. Xu, M. Seo, P. C. Lewis, E. Kumacheva, *J. Am. Chem. Soc.* **2005**, *127*, 8058 – 8063.
[196] C. Priest, S. Herminghaus, R. Seemann, *Appl. Phys. Lett.* **2006**, *88*, 024106.
[197] G. R. Yi, T. Thorsen, V. N. Manoharan, M. J. Hwang, S. J. Jeon, D. J. Pine, S. R. Quake, S. M. Yang, *Adv. Mater.* **2003**, *15*, 1300 – 1304.
[198] M. Seo, Z. H. Nie, S. Q. Xu, P. C. Lewis, E. Kumacheva, *Langmuir* **2005**, *21*, 4773 – 4775.
[199] H. J. Oh, S. H. Kim, J. Y. Baek, G. H. Seong, S. H. Lee, *J. Micromech. Microeng.* **2006**, *16*, 285 – 291.
[200] D. Dendukuri, K. Tsoi, T. A. Hatton, P. S. Doyle, *Langmuir* **2005**, *21*, 2113 – 2116.
[201] M. Zourob, S. Mohr, A. G. Mayes, A. Macaskill, N. Perez-Moral, P. R. Fielden, N. J. Goddard, *Lab Chip* **2006**, *6*, 296 – 301.
[202] W. J. Jeong, J. Y. Kim, J. Choo, E. K. Lee, C. S. Han, D. J. Beebe, G. H. Seong, S. H. Lee, *Langmuir* **2005**, *21*, 3738 – 3741.
[203] T. Nisisako, T. Torii, T. Higuchi, *Chem. Eng. J.* **2004**, *101*, 23 – 29.
[204] T. Nisisako, T. Torii, T. Takahashi, Y. Takizawa, *Adv. Mater.* **2006**, *18*, 1152 – 1156.
[205] B. G. De Geest, J. P. Urbanski, T. Thorsen, J. Demeester, S. C. De Smedt, *Langmuir* **2005**, *21*, 10275 – 10279.
[206] S. Okushima, T. Nisisako, T. Torii, T. Higuchi, *Langmuir* **2004**, *20*, 9905 – 9908.
[207] A. S. Utada, E. Lorenceau, D. R. Link, P. D. Kaplan, H. A. Stone, D. A. Weitz, *Science* **2005**, *308*, 537 – 541.
[208] E. Lorenceau, A. S. Utada, D. R. Link, G. Cristobal, M. Joanicot, D. A. Weitz, *Langmuir* **2005**, *21*, 9183 – 9186.
[209] J. P. Rolland, R. M. Van Dam, D. A. Schorzman, S. R. Quake, J. M. DeSimone, *J. Am. Chem. Soc.* **2004**, *126*, 8349 – 8349.
[210] N. Damean, S. K. Sia, V. Linder, M. Narovlyansky, G. M. Whitesides, *Proc. Natl. Acad. Sci. USA* **2005**, *102*, 10035 – 10039.
[211] P. Garstecki, M. J. Fuerstman, G. M. Whitesides, *Nat. Phys.* **2005**, *1*, 168 – 171.
[212] M. Abkarian, M. Faivre, H. A. Stone, *Proc. Natl. Acad. Sci. USA* **2006**, *103*, 538 – 542.
[213] C. Queguiner, D. Barthes-Biesel, *J. Fluid Mech.* **1997**, *348*, 349 – 376.
[214] A. B. Subramaniam, M. Abkarian, L. Mahadevan, H. A. Stone, *Nature* **2005**, *438*, 930 – 930.
[215] G. M. Whitesides, *Nature* **2006**, *442*, 368 – 373.
[216] A. J. deMello, *Nature* **2006**, *442*, 394 – 402.
[217] J. El-Ali, P. K. Sorger, K. F. Jensen, *Nature* **2006**, 442, 403 – 411.
[218] J. H. Xu, S. W. Li, J. Tan, Y. J. Wang, G. S. Luo, *Langmuir* **2006**, *22*, 7943 – 7946.
[219] R. M. Lorenz, J. S. Edgar, G. D. M. Jeffries, D. T. Chiu, *Anal. Chem.* **2006**, *78*, 6433 – 6439.
[220] O. Ozen, N. Aubry, D. T. Papageorgiou, P. G. Petropoulos, *Phys. Rev. Lett.* **2006**, *96*, 144501.
[221] V. Barbier, M. Tatoulian, H. Li, F. Arefi-Khonsari, A. Ajdari, P. Tabeling, *Langmuir* **2006**, *22*, 5230 – 5232.
[222] G. Cristobal, J. P. Benoit, M. Joanicot, A. Ajdari, *Appl. Phys. Lett.* **2006**, *89*, 034104.
[223] W. H. Tan, S. Takeuchi, *Lab Chip* **2006**, *6*, 757 – 763.
[224] K. Ahn, J. Agresti, H. Chong, M. Marquez, D. A. Weitz, *Appl. Phys. Lett.* **2006**, *88*, 264105.
[225] N. Srivastava, M. A. Burns, *Lab Chip* **2006**, *6*, 744 – 751.
[226] J. T. Cabral, S. D. Hudson, *Lab Chip* **2006**, *6*, 427 – 436.
[227] G. Cristobal, L. Arbouet, F. Sarrazin, D. Talaga, J. L. Bruneel, M. Joanicot, L. Servant, *Lab Chip* **2006**, *6*, 1140 – 1146.
[228] S. E. Barnes, Z. T. Cygan, J. K. Yates, K. L. Beers, E. J. Amis, *Analyst* **2006**, *131*, 1027 – 1033.
[229] K. S. Huang, T. H. Lai, Y. C. Lin, *Lab Chip* **2006**, *6*, 954 – 957.
[230] Z. H. Nie, W. Li, M. Seo, S. Q. Xu, E. Kumacheva, *J. Am. Chem. Soc.* **2006**, *128*, 9408 – 9412.
[231] R. F. Shepherd, J. C. Conrad, S. K. Rhodes, D. R. Link, M. Marquez, D. A. Weitz, J. A. Lewis, *Langmuir* **2006**, *22*, 8618 – 8622.
[232] H. Zhang, E. Tumarkin, R. Peerani, Z. Nie, R. M. A. Sullan, G. C. Walker, E. Kumacheva, *J. Am. Chem. Soc.* **2006**, *128*, 12205 – 12210.
[233] J. L. Steinbacher, R. W. Y. Moy, K. E. Price, M. A. Cummings, C. Roychowdhury, J. J. Buffy, W. L. Olbricht, M. Haaf, D. T. McQuade, *J. Am. Chem. Soc.* **2006**, *128*, 9442 – 9447.
[234] S. Abraham, E. H. Jeong, T. Arakawa, S. Shoji, K. C. Kim, I. Kim, J. S. Go, *Lab Chip* **2006**, *6*, 752 – 756.
[235] B. Ahmed, D. Barrow, T. Wirth, *Adv. Synth. Catal.* **2006**, *348*, 1043 – 1048.
[236] C. J. Gerdts, V. Tereshko, M. K. Yadav, I. Dementieva, F. Collart, A. Joachimiak, R. C. Stevens, P. Kuhn, A. Kossiakoff, R. F. Ismagilov, *Angew. Chem.* DOI:10.1002/ange.200602946; *Angew. Chem. Int. Ed.* DOI:10.1002/anie.200602946.
[237] B. J. Adzima, S. S. Velankar, *J. Micromech. Microeng.* **2006**, *16*, 1504 – 1510.
[238] M. J. Jensen, H. A. Stone, H. Bruus, *Phys. Fluids* **2006**, *18*, 077103.
[239] P. Garstecki, G. M. Whitesides, *Phys. Rev. Lett.* **2006**, *97*, 024503.

 © 2006 Wiley-VCH Verlag GmbH & Co. KGaA, Weinheim

Hydrogen Storage

DOI: 10.1002/anie.200601991

High H_2 Adsorption by Coordination-Framework Materials**

Xiang Lin, Junhua Jia, Xuebo Zhao, K. Mark Thomas, Alexander J. Blake, Gavin S. Walker, Neil R. Champness, Peter Hubberstey,* and Martin Schröder**

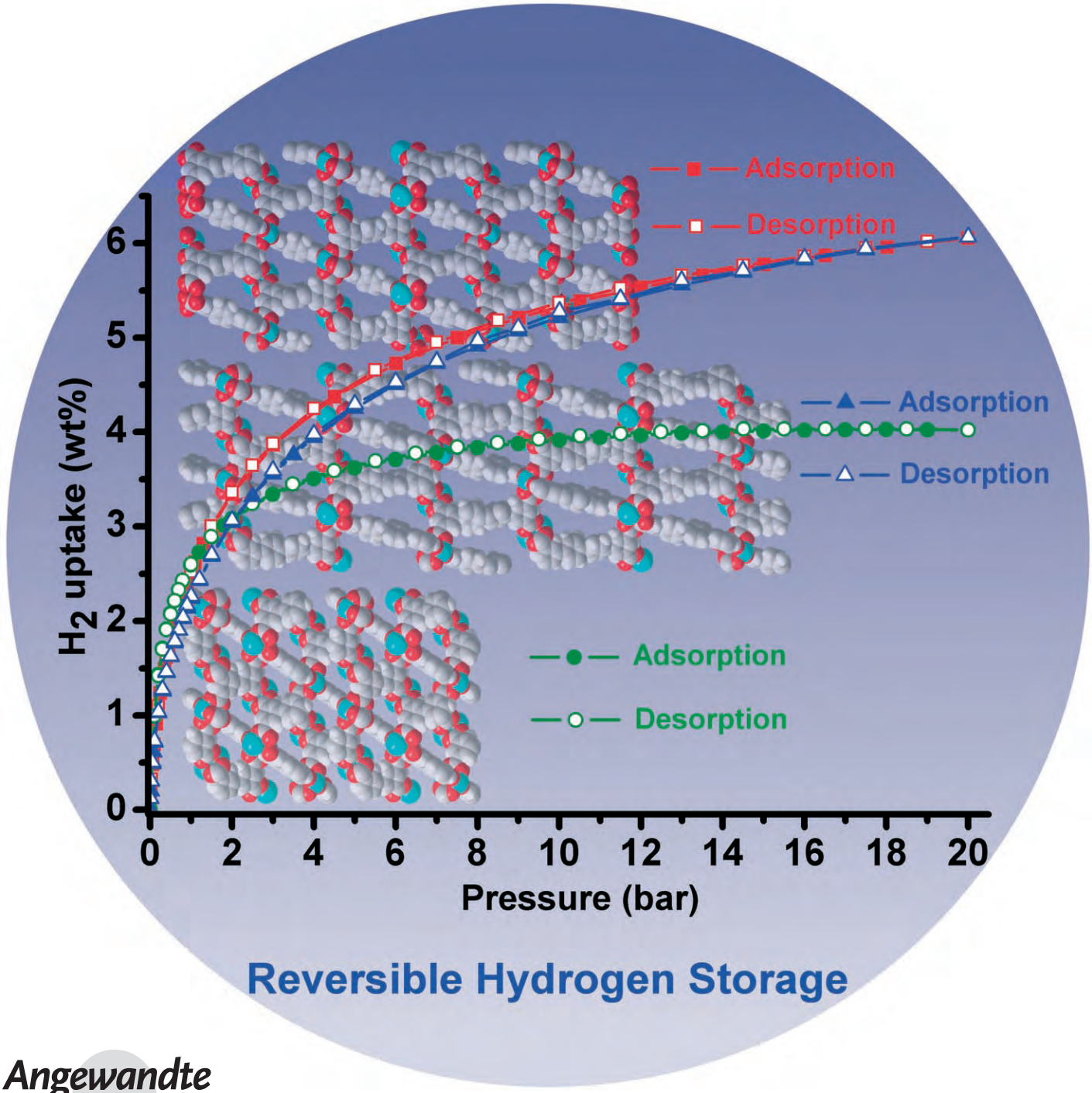

WILEY InterScience DISCOVER SOMETHING GREAT

© 2006 Wiley-VCH Verlag GmbH & Co. KGaA, Weinheim

The storage of H_2 in a safe and compact form represents a significant current challenge,[1] and there is wide-ranging interest in materials that can store and release H_2 with fast kinetics and high reversibility over multiple cycles.[2] Porous coordination frameworks have become competitors to other porous materials, such as zeolites[3] and carbon materials (for example, activated carbon or nanotubes),[4] with recent studies confirming that these frameworks can store considerable quantities of H_2 at 78 K.[5–11] Most studies of H_2 adsorption in coordination frameworks focus on the low-pressure region (0–1 bar) and, therefore, do not fully address the relationship between porosity and storage capacity. Although recent high-pressure volumetric measurements on some coordination frameworks revealed a correlation between maximum uptake and surface area,[9] the study involved several coordination frameworks with different structure types, and the influence of pore size and shape on guest adsorption was not investigated systematically. Herein, we report the structures of three close structural analogues, along with studies of high-pressure H_2 adsorption by these materials, to establish a route to higher H_2 storage capacity.

In coordination frameworks, the metal cations and carboxylate ligands can form a range of multinuclear nodes with predefined geometries (for example, the binuclear paddle-wheel units $\{Zn_2(O_2CR)_4\}$[12] and $\{Cu_2(O_2CR)_4\}$[5,10,13] (4-connected), the trinuclear units $\{Ni_3O(O_2CR)_6\}$, $\{Fe_3O(O_2CR)_6\}$,[6,14] and $\{Cr_3O(O_2CR)_6\}$[11] (6-connected), and the tetranuclear unit $\{Zn_4O(O_2CR)_6\}$[7,15] (6-connected)), which are largely dependent upon the metal cation and the reaction stoichiometry. The three coordination-framework materials in this study are based on biphenyl, terphenyl, and quaterphenyl tetracarboxylic acids. By varying the length of the organic backbone of these ligands, we obtain the desired structural analogues, in terms of framework composition and topology, and thereby investigate the correlation of pore size with gas-adsorption behavior.

Biphenyl-3,3′,5,5′-tetracarboxylic acid (H_4L^1; Figure 1) was synthesized by the oxidation of 3,3′,5,5′-tetramethylbiphenyl with $KMnO_4$. Terphenyl-3,3″,5,5″-tetracarboxylic acid (H_4L^2; Figure 1) and quaterphenyl-3,3‴,5,5‴-tetracarboxylic acid (H_4L^3; Figure 1) were synthesized by the Suzuki coupling of diethylisophthalate-5-boronic acid and dibromobenzene (for H_4L^2) or dibromobiphenyl (for H_4L^3). Solvothermal reaction of H_4L^1, H_4L^2, or H_4L^3 with $Cu(NO_3)_2{\cdot}2.5\,H_2O$ in a slightly acidified mixture of DMF/1,4-dioxane/H_2O afforded the solvated framework compounds $[Cu_2(L^1)(H_2O)_2]$ (**1**), $[Cu_2(L^2)(H_2O)_2]$ (**2**), and $[Cu_2(L^3)(H_2O)_2]$ (**3**), respectively (Figure 1). Acidic reaction solutions are necessary to obtain crystalline products; aqueous HCl is the most effective acid for this purpose. We were unable to reproduce the preparation of **1** in pure crystalline form by following the reported procedure,[5] but with our experimental procedures, the complex can be synthesized in good yield, in a highly crystalline form.

Crystal-structure determinations for **1**–**3** confirm that all three compounds have the same framework topology. Each Cu^{II} ion is coordinated by five O atoms in a square pyramidal geometry. Pairs of Cu^{II} centers are bridged by four carboxylate groups, forming $\{Cu_2(O_2CR)_4\}$ paddle-wheel units (Figure 2). One H_2O molecule binds to each metal centre along the paddle-wheel axis. Each $\{Cu_2(O_2CR)_4\}$ paddle wheel is linked to four biphenyl, terphenyl, or quaterphenyl connectors (and vice versa; Figure 2), to give frameworks with NbO-type topologies.

Views of the structures of **1**–**3** along the *c* axes reveal hexagonal channels that run through the frameworks (Figure 1). The diameters of the channels are predefined by the geometry of the $\{Cu_2(O_2CR)_4\}$ units and the span of the dicarboxylato moieties of the isophthalate groups on each terminus of the bridging ligands. Therefore, the diameters of the channels are the same in all three structures, approximately 5.0 Å. These channels are interconnected through triangular windows, which can be seen in views of the structures along the *a* or *b* axes (Figure 1). Because of the variation in ligand length, the size of the triangular windows expands on going from **1**–**3**. While it is difficult to derive reliable estimates of pore size from the crystal structures, pore size distributions (PSDs) derived from the N_2 isotherms of the desolvated materials at 78 K suggest that the pore size increases from **1**–**3** (Table 1). The solvent molecules in the as-prepared crystals are disordered within the pores; their contributions to the X-ray diffraction patterns were estimated by using PLATON/SQUEEZE.[16] By using PLATON/SOLV,[16] the accessible voids in the desolvated structures of **1**, **2**, and **3** were estimated to correspond to 63.3, 70.4, and 75.5 % of the total volumes, respectively (Table 1). Powder X-ray diffraction (PXRD) was used to confirm the phase purity and to examine the crystallinity of bulk samples. Thermal gravimetric analysis (TGA) was used to verify the ratio of Cu/L in the desolvated compounds (see Supporting Information).

The free solvent molecules in the Cu^{II} complexes can be readily exchanged for other organic solvents (for example, acetone) or removed by heating at 100 °C, either under a flow

[*] Dr. X. Lin, J. Jia, Dr. A. J. Blake, Prof. Dr. N. R. Champness, Dr. P. Hubberstey, Prof. Dr. M. Schröder
School of Chemistry
University of Nottingham
University Park, NG72RD (UK)
Fax: (+44) 115-951-3563
E-mail: Neil.Champness@nottingham.ac.uk
Peter.Hubberstey@nottingham.ac.uk
m.schroder@nottingham.ac.uk
Dr. G. S. Walker
School of Mechanical Materials & Manufacturing Engineering
University of Nottingham
University Park, NG72RD (UK)
Dr. X. B. Zhao, Prof. Dr. K. M. Thomas
Northern Carbon Research Laboratories
Department of Chemistry
University of Newcastle upon Tyne
Newcastle upon Tyne, NE1 7RU (UK)

[**] We thank the EPSRC (UKSHEC) for support, and the CVCP and the University of Nottingham for funding (to J.J.). M.S. gratefully acknowledges the receipt of a Royal Society Wolfson Merit Award and a Royal Society Leverhulme Trust Senior Research Fellowship.

Supporting information for this article is available on the WWW under http://www.angewandte.org or from the author.

 © 2006 Wiley-VCH Verlag GmbH & Co. KGaA, Weinheim

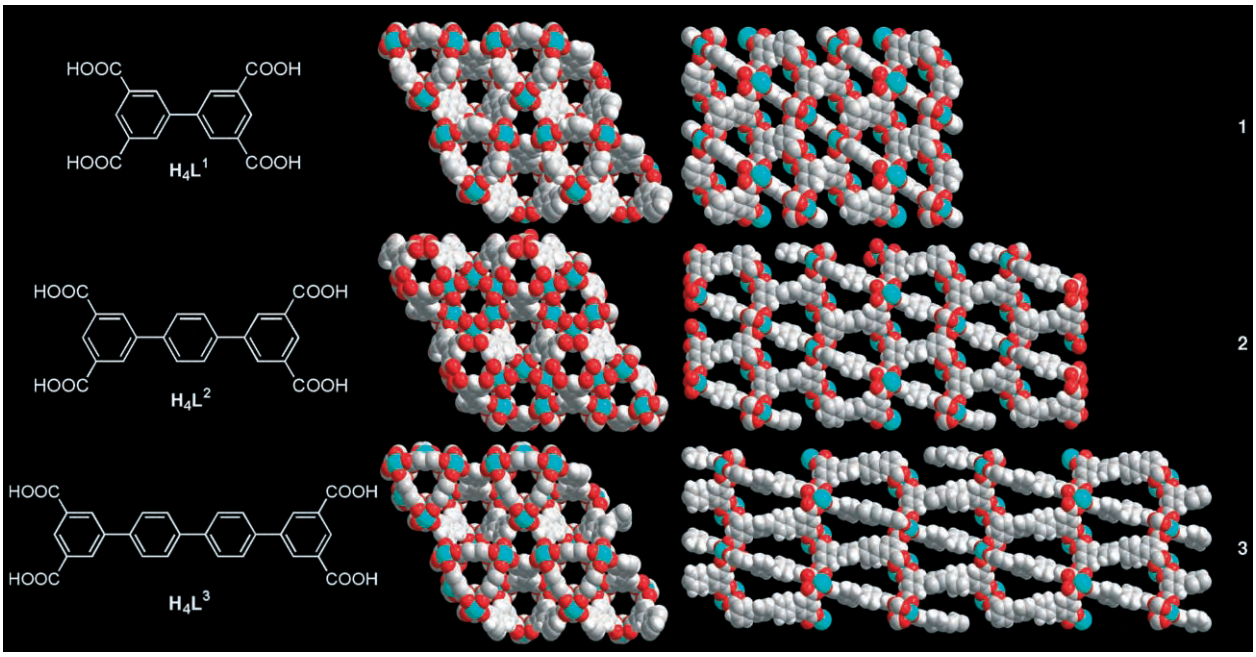

Figure 1. Acidic forms H_4L^1, H_4L^2, and H_4L^3 (left) of the ligands in **1**–**3**. Space-filling representations of **1**–**3** viewed along the *c* axes (middle) and along the *a* axes (right) of the structures; Cu blue, C gray, H white, O red; disordered solvent molecules omitted.

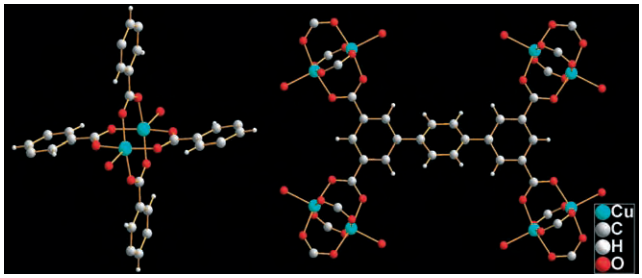

Figure 2. The 4-connected $\{Cu_2(O_2CR)_4\}$ paddle-wheel unit (left) and the 4-connected L^2 ligand (right) of **2**.

of N_2 gas or under vacuum. Compounds **1**–**3** show very similar thermal behavior, as determined by TGA. The as-synthesized blue-green crystalline samples lose solvent rapidly over 25–120 °C, resulting in a deep purple-blue crystalline material. A plateau is observed from 120–300 °C in the TGA profiles, indicating no further weight loss, and above 300 °C the complexes start to decompose rapidly to produce CuO. The desolvated samples of **1**–**3** are stable in a dry environment, and the structural integrity of the framework is retained in each case, as verified by PXRD. However, once in contact with moisture, their color rapidly reverts to blue-green, and the samples lose crystallinity and porosity.

To study the sorption isotherms of the evacuated frameworks, the acetone-exchanged samples were degassed at 100 °C and 10^{-10} bar for 16 h to give fully desolvated **1**–**3**. The isotherms for N_2, H_2, and D_2 sorption were measured at 78 K.

The N_2 sorption isotherms for **1**–**3** show typical type-I adsorption behavior, confirming the retention of the microporous structures after the removal of solvent from the crystalline samples (Figure 3a). The BET surface areas for desolvated **1**–**3** were estimated as 1670, 2247, and 2932 $m^2 g^{-1}$, respectively (Table 1). These high surface areas do not represent "true" surface areas, since there are contributions from pore-filling effects. However, BET surface areas do give an indication of the adsorption capacities of porous materials.[17] The pore sizes determined by applying a Dubinin–Astakhov analysis to the sorption data are narrowly distributed around 6.5, 7.3, and 8.3 Å for desolvated **1**, **2**, and **3**, respectively (Table 1). The pore volumes calculated from the maximum amount of N_2 adsorbed are 0.680, 0.886, and 1.138 $cm^3 g^{-1}$ for desolvated **1**, **2** and **3**, respectively (Table 1). These data clearly show that using longer ligands can produce more porous materials with higher adsorption capacities.

Table 1: Physical characteristics and sorption properties of **1**–**3**.

	N_2 uptake (1 bar) [$cm^3 g^{-1}$]	BET area [$m^2 g^{-1}$]	Calcd density[a] [$g cm^{-3}$]	Expt density[b] [$g cm^{-3}$]	Accessible voids[a] [%]	Pore volume[a] [$cm^3 g^{-1}$]	Pore volume (N_2)[c] [$cm^3 g^{-1}$]	Pore size (N_2)[c] [Å]	H_2 uptake (1/20 bar) [wt%]	Max H_2 uptake[d] [wt%]	Adsorbed H_2 density (20 bar/max) [$g cm^{-3}$]	Max H_2 uptake [$g L^{-1}$]
1	448	1670	0.927	1.75	63.3	0.683	0.680	6.5	2.59/4.02	4.20	0.0591/0.0615	38.9
2	573	2247	0.650	1.67	70.4	1.083	0.886	7.3	2.52/6.06	6.70	0.0560/0.0619	43.6
3	736	2932	0.587	1.60	75.5	1.284	1.138	8.3	2.24/6.07	7.01	0.0472/0.0546	41.1

[a] Calculated using PLATON/SOLV;[16] [b] determined from He sorption isotherms at 273 K; [c] determined from N_2 sorption isotherms at 78 K; [d] determined from Langmuir plots.

© 2006 Wiley-VCH Verlag GmbH & Co. KGaA, Weinheim

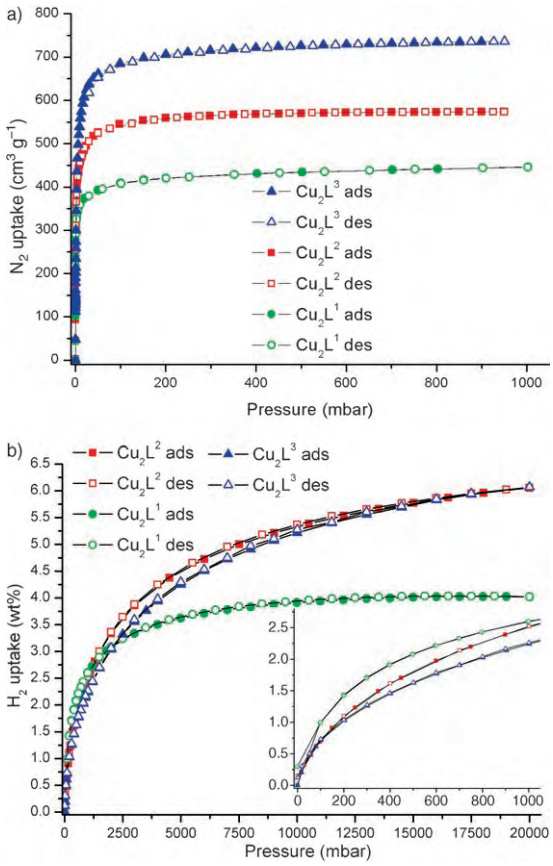

Figure 3. a) N_2 and b) H_2 sorption isotherms measured for desolvated **1**–**3** at 78 K; the inset in (b) is an enlargement of the low-pressure region of the H_2 isotherms; ads = adsorption, des = desorption

Gravimetric H_2 sorption isotherms were recorded from 0–20 bar at 78 K (Figure 3b). All data were rigorously corrected for the buoyancy of the system, samples, and adsorbates. The sample densities used in the buoyancy corrections were determined from He displacement isotherms (up to 20 bar) measured at 273 K. The H_2 sorption isotherms of desolvated **1**–**3** show good reversibility and an absence of hysteresis. Kinetic data for H_2 adsorption confirm that equilibrium is achieved rapidly, within approximately 3 min of an isotherm pressure step. These data are consistent with typical H_2 adsorption and exclude any significant effects due to the presence of impurities. Importantly, D_2 sorption isotherms were measured to verify that the observed H_2 adsorption is due to H_2, rather than other impurities (see Supporting Information). We obtained values of 1.05–1.20 for the molar ratio of adsorbed D_2/H_2 over 0.1–9.0 bar at 78 K, which are comparable to the values obtained for porous carbon materials at 78 K (1.06–1.10);[18,19] values of approximately 1.16 have been observed for zeolite NaA.[20]

The H_2 sorption isotherm of desolvated **1** reveals an uptake of 2.59 wt% at 1 bar, which is slightly higher than the reported value (2.47 wt%), although the BET surface area of desolvated **1** determined from the N_2 sorption isotherm is lower than the reported value.[5] Desolvated **2** adsorbs 2.52 wt% H_2 at 1 bar. This uptake is similar to that observed for **1**, but in the low-pressure region (0–800 mbar), the H_2 adsorption of **2** is significantly lower than that of **1**. Desolvated **3** has the lowest H_2 adsorption at 1 bar, 2.24 wt%, despite having the largest pore size. At low H_2 pressures, the H_2 adsorption is still far from saturation for desolvated **1**–**3**, indicating that their H_2 storage capacity is dominated by the affinity between H_2 molecules and the frameworks. Given that **1**–**3** all have the same NbO topology and have chemically very similar internal surfaces comprising binuclear Cu–carboxylate nodes and aryl groups, the implication of our adsorption results is that a smaller pore size leads to a higher affinity for H_2 adsorption. Interestingly, the frameworks of **1**–**3**, which contain binuclear Cu nodes, show significantly higher H_2 uptakes than related frameworks based on Zn or Fe nodes.[6,7,14,15]

When the H_2 pressure is increased, desolvated **1** adsorbs additional H_2 gas, until saturation is nearly reached at 10 bar; above this pressure, **1** has very little potential to adsorb more H_2. The highest adsorption of H_2 by **1**, 4.02 wt%, was recorded at 20 bar. The adsorption data above 2 bar can be fitted to the Langmuir equation, from which a maximum adsorption of 4.20 wt% is predicted for **1** (Table 1). Compound **2** incorporates a longer organic ligand than **1**, resulting in a larger pore volume and, correspondingly, a higher surface area. Thus, **2** has a greater potential for H_2 adsorption at higher pressures. At 1.2 bar, the adsorption of H_2 by **2** begins to exceed that observed for **1**, and at 20 bar, **2** adsorbs a remarkable 6.06 wt% of H_2. Thus, although **1** has the highest affinity for H_2, its small pore volume imposes an upper limit on its absorption of the gas.

Compound **3** incorporates the longest organic ligand and has the largest pore volume and surface area of the three compounds. Although it has the lowest uptake at 1 bar, 2.24 wt%, it also shows good potential to store H_2. At 2.5 bar, its uptake exceeds that observed for **1**, and at 20 bar, it has an uptake of 6.07 wt% H_2, which is comparable to that observed for **2**. It can be anticipated that higher H_2 adsorption would be observed at pressures higher than 20 bar. Fitting the high-pressure region of the H_2 isotherms of **2** and **3** to the Langmuir equation gives maximum adsorptions of 6.70 wt% and 7.01 wt% H_2, respectively (Table 1).

The three compounds not only have excellent gravimetric H_2 storage capacities, but also have volumetric storage capacities that are the highest yet reported for coordination frameworks (Table 1). Significantly, the value of 43.6 $g\,L^{-1}$ observed for **2** is very close to the 2010 U.S. Department of Energy (DOE) target of 45 $g\,L^{-1}$.[21] The data in Table 1 indicate that the crystallographic pore volume has the closest correlation with the maximum theoretical H_2 uptake for **1** and **2**. Thus, for desolvated **1**–**3**, the ratios of the crystallographic pore volumes are 1:1.59:1.88, respectively, and the ratios for the N_2 pore volumes are 1:1.30:1.67, respectively. The maximum theoretical H_2 uptake obtained from Langmuir isotherms for **1**–**3** are 1:1.60:1.67, respectively (Table 1). From **1** to **2**, the proportional increase in the maximum possible H_2 uptake is larger than that in pore volume, presumably because of a more optimal pore geometry in **2**. However, the proportional increase in the maximum H_2 uptake from **2** to **3** is less than that in pore volume, reflecting the comparatively lower affinity between H_2 molecules and the pores of **3**.

 © 2006 Wiley-VCH Verlag GmbH & Co. KGaA, Weinheim

Given that the density of liquid H_2 is 0.0708 g cm^{-3} at 20 K,[22] the densities for adsorbed H_2 calculated herein (Table 1) suggest that H_2 is highly compressed within the pores of **1**–**3**. The densities are similar to the values reported for H_2 adsorption on porous carbon materials (0.05–0.06 g cm^{-3}).[19] However, the carbon materials have a large PSD, whereas in crystalline metal–organic frameworks, the pores sizes are generally well-defined. The H_2 uptake and adsorbed H_2 density under low-pressure conditions decrease with increasing pore size from **1**–**3** (determined by ligand length), while the maximum amount of H_2 adsorbed increases while the maximum adsorbate density decreases with increasing pore size. These effects are related to the enhancement of adsorption in smaller pores at low pressures due to the overlap of the potential energy fields of the pore walls. The contrasting trends of increasing maximum H_2 uptake and decreasing adsorbed H_2 density with increasing pore size suggest that an optimum pore size exists. Therefore, a strategy of only increasing pore volume may not give the optimum material.

Férey and co-workers have synthesized $[Cr_3F(H_2O)_2(bdc)_3]\cdot n\,H_2O$ ($n \approx 25$; bdc = benzene-1,4-dicarboxylate), which has a cubic zeotype structure with a very large cell volume (ca. 702 000 Å^3) and containing a hierarchy of large pores.[23] The material has an N_2 pore volume of 2.0(1) cm^3 g^{-1} and a Langmuir surface area of approximately 5900 m^2 g^{-1}. Interestingly, H_2 adsorption studies on this material demonstrated that it adsorbs 4.5 wt % H_2 at 77 K and 3 MPa, with the density of the adsorbed H_2 being lower than in **1**–**3**. However, higher-pressure data are required to identify the maximum density of adsorbed H_2 for this material. Also, one could argue that the maximum possible density of H_2 within a porous framework is that of solid H_2, which is 0.077 g cm^{-3} at the triple point (13.8 K).[22] This density might be more appropriate for comparison with the densities of H_2 adsorbed at very low temperatures, while the liquid density is probably a better model for experiments at 78 K.

In summary, the sorption isotherms for desolvated **1**–**3** do not provide any evidence of adsorption of H_2 on different types of sites within the frameworks, but confirm that H_2 adsorption is controlled by the available pore volume, with a proportional decrease in adsorbate density with increasing pore size (Table 1). The adsorption of supercritical H_2 is limited by its low interaction energy with adsorbent surfaces, and this interaction potential can be enhanced in nanosized pores by overlap of the potential fields from both sides of the pore.[24] There is, thus, an intrinsic conflict between the large pore volume required to enhance H_2 storage capacity and the resulting decrease in the strength of the interaction in larger pores. Open metal centers are potentially significant, in that they are part of the porous structure, but have the disadvantage that they will adsorb H_2 impurities, such as H_2O. The sorption isotherms of **1**–**3** are reversible, and there is no evidence for chemisorption of H_2. There are also no steps in the isotherms that might be indicative of either adsorption on different sites or, alternatively, structural changes in the flexible framework during adsorption. We conclude that increasing the pore volume is not the only factor to be considered in the design of H_2-storage materials, because the adsorbed H_2 density may decrease with increasing pore size, as demonstrated by the series of compounds reported herein (Table 1).

Given that four coordination frameworks (**2**, **3**, MOF-177,[9] and IRMOF-20[9]) have now achieved (at 78 K and pressures below 80 bar) the 6 wt % H_2 gravimetric storage capacity of the 2010 DOE guidelines,[21] and that the volumetric capacity of **2** is also very close to the 2010 DOE target of 45 g L^{-1}, it is reasonable to anticipate the discovery of new materials with enhanced H_2 storage. We are currently investigating the challenge of synthesizing new coordination frameworks for higher H_2 storage capacity by searching for new metal building blocks, by determining the optimum compromise between large total pore volume and small pore size, and by optimizing the framework topology for H_2 adsorption.

Experimental Section

H_4L^2 and H_4L^3: The ligands H_4L^2 and H_4L^3 were synthesized using similar experimental procedures. The synthesis of H_4L^2 is described herein. Dibromobenzene (0.234 g, 1 mmol), diethylisophthalate-5-boronic acid (0.64 g, 2.4 mmol), and K_3PO_4 (2.10 g, 10 mmol) were mixed in 1,4-dioxane (30 mL), and the mixture was de-aerated using N_2. $Pd(PPh_3)_4$ (0.05 g, 0.043 mmol) was added to the stirred reaction mixture, and the mixture was then heated at 80 °C for 3 days under an N_2 atmosphere. The resultant mixture was evaporated to dryness, extracted into $CHCl_3$, and then dried over $MgSO_4$. The solution was evaporated to dryness, and the residue was briefly washed with EtOH (10 mL). The resulting crude product (mainly tetraethyl esters of the target ligand) was hydrolyzed by heating in aqueous NaOH (2 M) under reflux, followed by acidification with aqueous HCl (37 %), affording H_4L^2 (yield: 0.28 g, 65 %). ^{1}H NMR ([D$_6$]DMSO, 300 MHz): H_4L^2: $\delta = 8.48$ (t, $J = 1.6$ Hz, 1H), 8.44 (d, $J = 2.1$ Hz, 2H), 7.91 ppm (s, 2H); H_4L^3: 8.48 (t, 1H), 8.45 (d, $J = 1.5$ Hz, 2H), 7.90 ppm (dd, $J = 1.1$ Hz 4H). Elemental analysis (%) calcd for H_4L^2 ($C_{22}O_8H_{14}$): C 65.03, H 3.47; found: C 64.87, H 3.59; calcd for H_4L^3 ($C_{28}O_8H_{18}$): C 69.71, H 3.76; found: C 69.59, H 3.90.

1–**3**: The same experimental procedure was employed in the syntheses of **1**–**3**. The synthesis of **2** is described herein. H_4L^2 (0.05 g, 0.12 mmol) and $Cu(NO_3)_2\cdot 2.5\,H_2O$ (0.1 g, 0.43 mmol) were mixed and dispersed in DMF/1,4-dioxane/H_2O (2:1:1 v/v/v, 15 mL). The resulting blue-green slurry turned clear upon addition of 2 drops of aqueous HCl (37 %). The solution was gradually heated to 80 °C over a period of 12 h, and kept at this temperature for 3 days. The blue crystalline product was separated by filtration when the solution was still warm (50 °C), washed sequentially by DMF/H_2O (1:2 v/v) and DMF, and then dried briefly in air (yield: 0.082 g, 75.8 %). Elemental analysis (%) calcd for **2** ($C_{36.50}H_{46.5}Cu_2N_{1.5}O_{17.5}$): C 47.99, H 5.13, N 2.30; found C 48.52, H 5.03, N 2.07; calcd for **3** ($C_{42.5}H_{54.5}Cu_2N_{1.5}O_{19.5}$): C 49.78, H 5.36, N 2.05; found C 49.60, H 4.56, N 1.58. The volatility of the co-crystallized solvents in the samples contributes to the discrepancy in the elemental analyses. The weight ratio of $[Cu_2(L)]/2\,CuO$ for desolvated samples ($[Cu_2(L)]$) was determined by TGA: calcd for **1**: 2.8365; found: 2.7630; calcd for **2**: 3.4528; found: 3.4760; calcd for **3**: 3.9308; found: 3.7299. IR (KBr): for **2**: $\tilde{\nu} = 1736$ (m), 1618 (vs), 1566 (vs), 1451 (s), 1406 (vs), 1384 (vs), 1303 (m), 1261 (m), 1111 (w), 1080 (w), 838 (m), 772 (m), 729 cm^{-1} (m); for **3**: $\tilde{\nu} = 1716$ (m), 1616 (s), 1558 (s), 1505 (s), 1442 (s), 1384 (vs), 1261 (w), 1020 (w), 824 (w), 767 (m), 730 (m), 669 (m), 630 cm^{-1} (w).

Crystal-structure determinations: intensity data for **2** and **3** were collected at 150(2) K on a Bruker SMART APEX CCD area-detector diffractometer using graphite-monochromated $Mo_{K\alpha}$ radiation. The structures were solved by direct methods and subsequent difference Fourier syntheses, and refined using the SHELXTL software package. The H atoms on the ligands were placed in idealized positions and refined using a riding model. The H atoms of the coordinated H_2O

 © 2006 Wiley-VCH Verlag GmbH & Co. KGaA, Weinheim

molecules could not be located, but are included in the formulae. The unit cell includes a large region of disordered solvent molecules, which could not be modeled as discrete atomic sites. We employed PLATON/SQUEEZE[16] to calculate the diffraction contribution of the solvent molecules and, thereby, to produce a set of solvent-free diffraction intensities. The final formulae were calculated from the SQUEEZE results combined with the elemental analyses. **2**: $[Cu_2(C_{22}H_{10}O_8)(H_2O)_2]\cdot 1.5(C_3H_7NO)\cdot 2.5(C_4H_8O_2)\cdot H_2O$, $M_r = 913.3$, blue-green block, $0.07 \times 0.24 \times 0.26$ mm, trigonal, $R\bar{3}m$, $a = 18.629(1)$, $c = 38.492(2)$ Å, $V = 11569(2)$ Å^3, $Z = 9$, $\rho_{calcd} = 1.180$ g cm^{-3}, $\mu = 0.887$ mm^{-1}, $F(000) = 4266$, 23387 reflections, 3244 unique, $R_{int} = 0.055$, $R_1 = 0.0353$, $wR_2 = 0.0947$, GOF = 0.949, max/min residual electron density = 0.72/−0.24 e Å^{-3}. **3**: $[Cu_2(C_{28}H_8O_{14})(H_2O)_2]\cdot 1.5(C_3H_7NO)\cdot 2.5(C_4H_8O_2)\cdot 3H_2O$, $M_r = 1025.5$, blue-green block, $0.14 \times 0.15 \times 0.40$ mm, trigonal, $R\bar{3}m$, $a = 18.434(1)$, $c = 52.364(3)$ Å, $V = 15409(2)$ Å^3, $Z = 9$, $\rho_{calcd} = 0.995$ g cm^{-3}, $\mu = 0.674$ mm^{-1}, $F(000) = 4806$, 93972 reflections, 4319 unique, $R_{int} = 0.051$, $R_1 = 0.0393$, $wR_2 = 0.1073$, GOF = 0.871, max/min residual electron density = 0.45/−0.25 e Å^{-3}. CCDC-606908 (**2**) and CCDC-606909 (**3**) contain the supplementary crystallographic data for this paper. These data can be obtained free of charge from The Cambridge Crystallographic Data Centre via www.ccdc.cam.ac.uk/data_request/cif.

Sorption isotherms: N_2, H_2, and D_2 sorption isotherms were measured using a Hiden Isochema Intelligent Gravimetric Analyser (IGA-003), which is an ultra-high-vacuum, clean instrument with a diaphragm and turbo pumping system. H_2 and D_2 were purified by using calcium aluminosilicate and activated carbon adsorbents to remove trace amounts of H_2O and other impurities. The measurement protocols used were validated by the complete desorption of H_2 and the comparison of results from porous carbon samples on two different instruments.

The Supporting Information includes additional views of the crystal structures, PXRD patterns, TGA profiles, PSD analyses, detailed H_2 and D_2 sorption isotherms, Langmuir fitting analyses, and further experimental details.

Received: May 18, 2006
Revised: June 23, 2006
Published online: August 23, 2006

Keywords: adsorption · copper · hydrogen storage · metal–organic frameworks · microporous materials

[1] L. Schlapbach, *MRS Bull.* **2002**, *27*, 675 – 676.
[2] M. G. Nijkamp, J. E. M. J. Raaymakers, A. J. van Dillen, K. P. de Jong, *Appl. Phys. A* **2001**, *72*, 619 – 623.
[3] H. W. Langmi, A. Walton, M. M. Al-Mamouri, S. R. Johnson, D. Book, J. D. Speight, P. P. Edwards, I. Gameson, P. A. Anderson, I. R. Harris, *J. Alloys Compd.* **2003**, *356–357*, 710 – 715; A. Zecchina, S. Bordiga, J. G. Vitillo, G. Ricchiardi, C. Lamberti, G. Spoto, M. Bjorgen, K. P. Lillerud, *J. Am. Chem. Soc.* **2005**, *127*, 6361 – 6366; J. Eckert, J. M. Nicol, J. Howard, F. R. Trouw, *J. Phys. Chem.* **1996**, *100*, 10646 – 10651.
[4] B. Panella, M. Hirscher, S. Roth, *Carbon* **2005**, *43*, 2209 – 2214; H. G. Schimmel, G. J. Kearley, M. G. Nijkamp, C. T. Visser, K. P. de Jong, F. M. Mulder, *Chem. Eur. J.* **2003**, *9*, 4764 – 4770; G. Gundiah, A. Govindaraj, N. Rajalakshmi, K. S. Dhathathreyan, C. N. R. Rao, *J. Mater. Chem.* **2003**, *13*, 209 – 213; M. Becher, M. Haluska, M. Hirscher, A. Quintel, V. Skakalova, U. Dettlaff-Weglikovska, X. Chen, M. Hulman, Y. Choi, S. Roth, V. Meregalli, M. Parrinello, R. Strobel, L. Jorissen, M. M. Kappes, J. Fink, A. Zuttel, I. Stepanek, P. Bernier, *C. R. Phys.* **2003**, *4*, 1055 – 1062; A. Zuttel, P. Sudan, P. Mauron, T. Kiyobayashi, C. Emmenegger, L. Schlapbach, *Int. J. Hydrogen Energy* **2001**, *26*, 203 – 212; M. S. Dresselhaus, K. A. Williams, P. C. Eklund, *MRS Bull.* **1999**, *24*, 45 – 50; M. Rzepka, P. Lamp, M. A. de la Casa-Lillo, *J. Phys. Chem. B* **1998**, *102*, 10894 – 10898; A. C. Dillon, K. M. Jones, T. A. Bekkedahl, C. H. Kiang, D. S. Bethune, M. J. Heben, *Nature* **1997**, *386*, 377 – 379; Y. Gogotsi, R. K. Dash, G. Yushin, T. Yildirim, G. Laudisio, J. E. Fischer, *J. Am. Chem. Soc.* **2005**, *127*, 16006 – 16007.
[5] B. Chen, N. W. Ockwig, A. R. Millward, D. S. Contreras, O. M. Yaghi, *Angew. Chem.* **2005**, *117*, 4823 – 4827; *Angew. Chem. Int. Ed.* **2005**, *44*, 4745 – 4749. $[Cu_2(L^1)(H_2O)_2]$ (**1**) has also been termed MOF-505.
[6] A. C. Sudik, A. R. Millward, N. W. Ockwig, A. P. Côté, J. Kim, O. M. Yaghi, *J. Am. Chem. Soc.* **2005**, *127*, 7110 – 7118.
[7] J. L. C. Rowsell, A. R. Millward, K. S. Park, O. M. Yaghi, *J. Am. Chem. Soc.* **2004**, *126*, 5666 – 5667.
[8] N. L. Rosi, J. Eckert, M. Eddaoudi, D. T. Vodak, J. Kim, M. O'Keeffe, O. M. Yaghi, *Science* **2003**, *300*, 1127 – 1130; J. L. C. Rowsell, J. Eckert, O. M. Yaghi, *J. Am. Chem. Soc.* **2005**, *127*, 14904 – 14910; S. S. Kaye, J. R. Long, *J. Am. Chem. Soc.* **2005**, *127*, 6506 – 6507; J. L. C. Rowsell, O. M. Yaghi, *J. Am. Chem. Soc.* **2006**, *128*, 1304 – 1315; B. Kesanli, Y. Cui, M. R. Smith, E. W. Bittner, B. C. Brockrath, W. Lin, *Angew. Chem.* **2005**, *117*, 74 – 77; *Angew. Chem. Int. Ed.* **2005**, *44*, 72 – 75.
[9] A. G. Wong-Foy, A. J. Matzger, O. M. Yaghi, *J. Am. Chem. Soc.* **2006**, *128*, 3494 – 3495.
[10] D. Sun, S. Ma, Y. Ke, D. J. Collins, H.-C. Zhou, *J. Am. Chem. Soc.* **2006**, *128*, 3896 – 3897.
[11] A. Vimont, J. M. Goupil, J. C. Lavalley, M. Daturi, S. Surblé, C. Serre, F. Millange, G. Férey, N. Audebrand, *J. Am. Chem. Soc.* **2006**, *128*, 3218 – 3227; S. Surblé, C. Serre, C. Mellot-Draznieks, F. Millange, G. Férey, *Chem. Commun.* **2006**, 284 – 286.
[12] M. E. Braun, C. D. Steffek, J. Kim, P. G. Rasmussen, O. M. Yaghi, *Chem. Commun.* **2001**, 2532 – 2533; M. Eddaoudi, H. Li, O. M. Yaghi, *J. Am. Chem. Soc.* **2000**, *122*, 1391 – 1397.
[13] S. S. Y. Chui, S. M. F. Lo, J. P. H. Charmant, A. G. Orpen, I. D. Williams, *Science* **1999**, *283*, 1148 – 1150.
[14] A. C. Sudik, A. P. Côté, O. M. Yaghi, *Inorg. Chem.* **2005**, *44*, 2998 – 3000.
[15] M. Eddaoudi, J. Kim, N. Rosi, D. Vodak, J. Wachter, M. O'Keeffe, O. M. Yaghi, *Science* **2002**, *295*, 469 – 472.
[16] A. L. Spek, *J. Appl. Crystallogr.* **2003**, *36*, 7 – 13; A. L. Spek, PLATON, A Multipurpose Crystallographic Tool, Utrecht University, The Netherlands, **2006**; available via http://www.cryst.chem.uu.nl/platon (for Unix) and http://www.chem.gla.ac.uk/~louis/software/platon/ (for MS Windows).
[17] J. F. Byrne, H. Marsh in *Porosity in Carbons: Characterization and Applications* (Ed.: J. W. Patrick), Edward Arnold, London, **1995**, pp. 1 – 48; B. H. Davis, K. S. W. Sing in *Handbook of Porous Solids* (Eds.: F. Schüth, K. S. W. Sing, J. Weitkamp), Wiley-VCH, Weinheim, **2002**, Vol. 1, pp. 3 – 23.
[18] X. B. Zhao, B. Xiao, A. J. Fletcher, K. M. Thomas, *J. Phys. Chem. B* **2005**, *109*, 8880 – 8888; H. Tanaka, H. Kanoh, M. Yudasaka, S. Iijima, K. Kaneko, *J. Am. Chem. Soc.* **2005**, *127*, 7511 – 7516; R. Yaris, J. R. Sams, Jr., *J. Chem. Phys.* **1962**, *37*, 571 – 576; W. van Dingenen, A. van Itterbeek, *Physica* **1939**, *6*, 49 – 58.
[19] X. B. Zhao, S. Villar-Rodil, A. J. Fletcher, K. M. Thomas, *J. Phys. Chem. B* **2006**, *110*, 9947 – 9955.
[20] F. Stephanie-Victoire, A. M. Goulay, E. C. de Lara, *Langmuir* **1998**, *14*, 7255 – 7259.
[21] *Hydrogen, Fuel Cells & Infrastructure Technologies Program: Multi-Year Research, Development and Demonstration Plan*, U.S. Department of Energy, **2005**, http://www.eere.energy.gov/hydrogenandfuelcells/mypp/; *Basic Research Needs for the Hydrogen Economy*, report of the Basic Energy Sciences Workshop on Hydrogen Production, Storage, and Use, U.S. Department of Energy, **2004**, http://www.sc.doe.gov/bes/; E. Tzimas, C. Filiou, S. D. Peteves, J.-B. Veryret, *Hydrogen Storage: State-of-the-Art and Future Perspective*, European Commision, Institute for Energy, **2003**, http://ie.jrc.cec.eu.int/publications/scientific_publications/2003/P2003-181=EUR20995EN.pdf.

 © 2006 Wiley-VCH Verlag GmbH & Co. KGaA, Weinheim

[22] *CRC Handbook of Chemistry and Physics*, 74th ed., CRC, Boca Ratan, **1993**.
[23] G. Férey, C. Mellot-Draznieks, C. Serre, F. Millange, J. Dutour, S. Surblé, I. Margiolaki, *Science* **2005**, *309*, 2040 – 2042; Correction: G. Férey, C. Mellot-Draznieks, C. Serre, F. Millange, J. Dutour, S. Surblé, I. Margiolaki, *Science* **2005**, *310*, 1119
[24] X. Zhao, B. Xiao, A. J. Fletcher, K. M. Thomas, D. Bradshaw, M. J. Rosseinsky, *Science* **2004**, *306*, 1012 – 1015; H. Chun, D. N. Dybtsev, H. Kim, K. Kim, *Chem. Eur. J.* **2005**, *11*, 3521 – 3529; B. Kesanli, Y. Cui, M. R. Smith, E. W. Bittner, B. C. Brockrath, W. Lin, *Angew. Chem.* **2005**, *117*, 74 – 77; *Angew. Chem. Int. Ed.* **2005**, *44*, 72 – 75.

 © 2006 Wiley-VCH Verlag GmbH & Co. KGaA, Weinheim

Fluorescent Probes

DOI: 10.1002/anie.200602114

Fluorescence Visualization of Newly Synthesized Proteins in Mammalian Cells**

*Kimberly E. Beatty, Julie C. Liu, Fang Xie, Daniela C. Dieterich, Erin M. Schuman, Qian Wang, and David A. Tirrell**

Modern proteomic methods enable efficient identification of the hundreds or thousands of proteins present in whole cells or in isolated organelles.[1] However, a thorough understanding of the proteome requires insight into protein localization as well as protein identity. Recently, visualization of newly synthesized proteins in bacterial cells was demonstrated through co-translational introduction of an alkynyl amino acid followed by selective Cu^{I}-catalyzed ligation of the alkynyl side chain to the fluorogenic dye 3-azido-7-hydroxycoumarin.[2] Here we report that selective fluorescence labeling and imaging of newly synthesized proteins can be accomplished in a diverse set of mammalian cells.

Fluorescence microscopy provides the most convenient means of visualizing cellular proteins. Protein tagging with green fluorescent protein (GFP) or with tetracysteine motifs has provided powerful tools for tracking individual proteins in intact cells.[3] However, a more global analysis of protein synthesis and transport requires a different approach: as the identities of the proteins of interest may not be known a priori, a labeling strategy without genetic manipulation is needed.

Co-translational incorporation of noncanonical amino acids provides a solution to this problem.[4] Recently, bioorthogonal noncanonical amino acid tagging (BONCAT) demonstrated the unbiased and selective enrichment and identification of newly synthesized proteins in a mammalian cell line.[5] Susceptibility to amino acid tagging is determined not by the identity of the protein, but rather by the spatial and temporal character of its synthesis, and proper design of the noncanonical side chain enables facile labeling with fluorescent probes through selective transformations such as the Staudinger or azide–alkyne ligations.[2,6–8] Azides and alkynes are essentially absent from mammalian cells, which makes the azide–alkyne ligation very selective, and the reaction rate can be enhanced by Cu^{I} catalysis or by ring strain.[9]

Here we describe the use of homopropargylglycine (Hpg) for tagging and fluorescence visualization of newly synthesized mammalian proteins. Protein tagging with Hpg is operationally similar to conventional pulse-labeling with ^{35}S-methionine; the absence of Met synthesis in mammalian cells and the promiscuity of the methionyl-tRNA synthetase make it straightforward to incorporate Hpg into mammalian proteins in competition with Met.[10] After incorporation, Hpg is susceptible to labeling with the membrane-permeant fluorogenic dye 3-azido-7-hydroxycoumarin for in situ imaging (Figure 1).[11]

Initial experiments were performed with mouse embryonic fibroblasts that express a mitochondrially targeted GFP (MEF-mitoGFP).[12] Cells were grown to confluence before passage into serum-free medium lacking Met (SFM). After incubation to deplete any residual Met, cultures were supplemented with 1 mM Met or Hpg for a 4 h pulse.

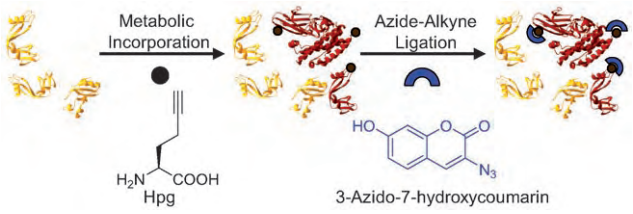

Figure 1. Bioorthogonal labeling of newly synthesized proteins for fluorescence visualization in mammalian cells.

[*] K. E. Beatty,[+] Dr. J. C. Liu,[+] Prof. D. A. Tirrell
Division of Chemistry and Chemical Engineering
California Institute of Technology
1200 E. California Blvd., Pasadena, CA 91125 (USA)
Fax: (+1) 626-568-8824
E-mail: tirrell@caltech.edu
F. Xie, Prof. Q. Wang
Department of Chemistry and Biochemistry
University of South Carolina
631 Sumter St., Columbia, SC 29208 (USA)
Dr. D. C. Dieterich, Prof. E. M. Schuman
Howard Hughes Medical Institute and Division of Biology
California Institute of Technology
1200 E. California Blvd., Pasadena, CA 91125 (USA)
[+] These authors contributed equally.

[**] We thank Scott Fraser, Chris Waters, and the Beckman Imaging Center for advice on microscopy, and Rochelle Diamond, Stephanie Adams, and the Caltech Flow Cytometry Facility for assistance with flow cytometry. We thank Anand Asthagiri, Chase Beisel, David Chan, Scott Detmer, Nicholas Graham, Melissa Pope, and Christina Smolke for cell lines and reagents. James Van Deventer made helpful comments on the manuscript. This work was supported by a Fannie and John Hertz Foundation Fellowship (to K.E.B.), a Whitaker Foundation Graduate Fellowship (to J.C.L.), a postdoctoral fellowship from the German Academy for Natural Scientists Leopoldina (BMBF-LPD9901/8-95 to D.C.D.), an NSF-NER grant (to Q.W.), NIH grant GM62523 (to D.A.T.), and the Beckman Institute at Caltech. E.M.S. is an Investigator of the Howard Hughes Medical Institute.

Supporting information for this article (including detailed experimental protocals) is available on the WWW under http://www.angewandte.org or from the author.

WILEY InterScience DISCOVER SOMETHING GREAT
© 2006 Wiley-VCH Verlag GmbH & Co. KGaA, Weinheim

Incorporation of Hpg into proteins did not appear to affect cell viability; staining with propidium iodide demonstrated that viability was similar when cells were pulse-labeled either with Met or with Hpg for 4 h (data not shown). During a 2 h chase, cells were incubated in SFM containing 1 mM Met. The cells were washed, fixed, and blocked before reaction with 200 μM $CuSO_4$, 400 μM triscarboxyethylphosphine (TCEP), 200 μM tris((1-benzyl-1*H*-1,2,3-triazol-4-yl)methyl)amine (triazole ligand), and 25 μM 3-azido-7-hydroxycoumarin.[8] The cells were treated overnight at room temperature in the dark and then washed before visualization.

Individual cells were examined by confocal microscopy and flow cytometry. Microscopy observations using differential interference contrast (DIC) delineated the cells, and GFP fluorescence confirmed that the mitochondria had the proper morphology (Figure 2a). Images of coumarin fluorescence were acquired with identical acquisition settings for cells labeled either with Hpg or with Met (Figure 2a, third column). Bright coumarin fluorescence was observed only for cells exposed to Hpg during the pulse. As a control, one of two inhibitors of protein synthesis, cycloheximide or anisomycin, was added to the medium 30 minutes prior to pulse-labeling with 1 mM Hpg. Cells labeled in this medium exhibited levels of coumarin fluorescence comparable to the background levels observed for Met-labeled cells (Figure 2a, bottom panels). The inhibitor control samples maintained low levels of fluorescence even when imaged by taking a sum of four coumarin scans (Figure 2a, inset). Flow cytometry was used to quantitate the fluorescence enhancement; cells treated with 1 mM Hpg were characterized by mean fluorescence that was 18-fold higher than that of cells pulse-labeled with Met (Figure 2b). Addition of cycloheximide or anisomycin to cells prior to addition of 1 mM Hpg reduced the mean fluorescence to the level observed for the Met control. Both microscopy and flow cytometry indicate that fluorescence labeling is highly selective for newly synthesized proteins that contain Hpg.

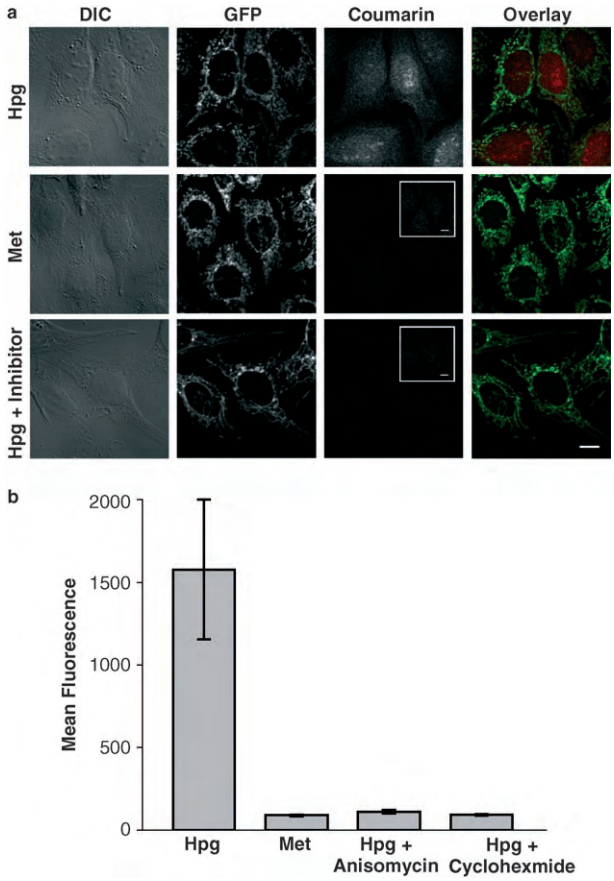

Figure 2. Fluorescence labeling of proteins in MEF-mitoGFP. a) Imaging of MEF-mitoGFP cells pulse-labeled in media containing 1 mM Hpg (top), 1 mM Met (middle), and 1 mM Hpg + 50 μM cycloheximide (bottom). The differential interference contrast (DIC) images are shown in the first column. Each set of images was obtained with identical conditions to capture either GFP (second column) or coumarin (third column) fluorescence. The insets for the coumarin fluorescence represent the sum of four scans. The final overlay contains the superposition of the GFP (green) and coumarin (red) images. Scale bars represent 10 μm. b) Mean fluorescence of cells obtained from flow cytometry. Each column represents three samples with 10000 events collected for each sample. Error bars represent one standard deviation.

Understanding the dependence of the observed fluorescence on Hpg concentration and on the Hpg/Met ratio should be useful for applications in which one wishes to control the extent of labeling. The optimal Hpg concentration was established by flow cytometry. The mean fluorescence increased twofold when the Hpg concentration was raised from 0.1 to 0.5 mM. There was no further enhancement in the range 0.5 to 2.0 mM Hpg, although there was some variability in the fluorescence levels at 0.5 mM. To ensure consistent fluorescence labeling, we used 1 mM Hpg for pulse-labeling. Reducing the Hpg/Met ratio in the medium from 1000:1 to 100:1 caused a decrease in the mean fluorescence (Figure 3a). Previous in vitro studies have shown that the specificity constant k_{cat}/K_m is reduced approximately 500-fold for Hpg relative to Met (for activation by the methionyl-tRNA synthetase derived from *E. coli*).[10] In accord with those studies, we find that coumarin fluorescence could be discerned by confocal microscopy when the Hpg/Met ratio was 500:1, but not at a ratio of 100:1.

To define the temporal resolution of the method, we examined pulse lengths ranging from 15 minutes to 6 hours. Flow cytometry showed that a 15-minute pulse with no chase yielded a fivefold enhancement in the mean fluorescence relative to Met controls. The mean fluorescence increased as the pulse length was extended to 4 hours but did not increase further at 6 hours.

The concentration of the $CuSO_4$ catalyst was varied from 50 to 200 μM (Figure 2b). The mean fluorescence at 50 μM $CuSO_4$ was comparable to that of cells treated only with Met. The mean fluorescence increased as the copper concentration was increased in this range. Copper concentrations of 250–500 μM resulted in only modest further enhancement of the fluorescence intensity.

The imaging strategy described here can be extended easily to a wide variety of cell types (Figure 4). Newly synthesized proteins in both transfected (MEF-mitoGFP, CHO-α_5GFP) and nontransfected (MCF-10A, HUVEC) cells can be visualized when the cells are pulse-labeled with Hpg. The method works well on different cell types (fibroblasts,

 © 2006 Wiley-VCH Verlag GmbH & Co. KGaA, Weinheim

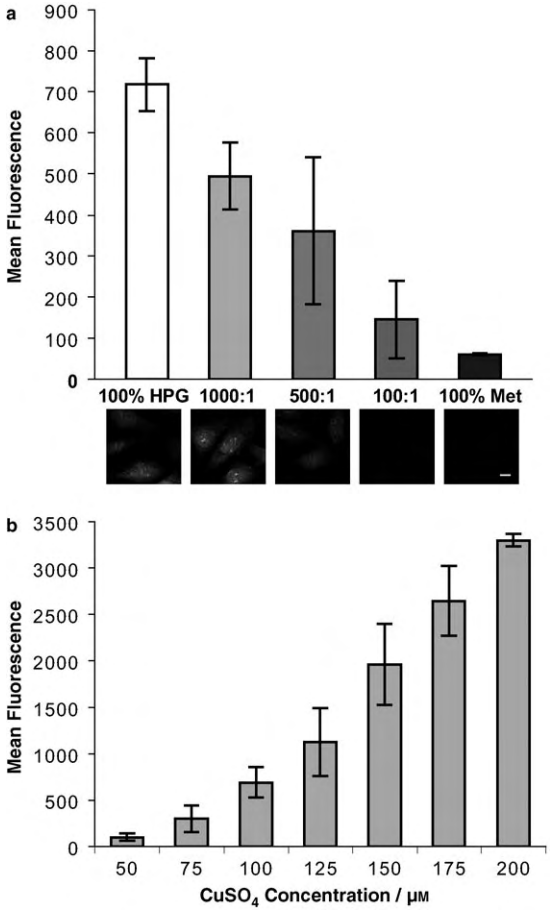

Figure 3. Flow cytometric analysis of pulse-labeling and dye-labeling conditions. a) Fluorescence of cells pulse-labeled with various Hpg/Met ratios. All Hpg-treated samples contained 1 mM Hpg, and the 100% Met sample contained 1 mM Met. Mean fluorescence was determined by flow cytometry. The same acquisition settings were used for all samples in the corresponding coumarin images . The scale bar represents 10 μm. b) Mean fluorescence of cells treated with various concentrations of $CuSO_4$. Each column represents three flow-cytometry samples with 10000 events collected for each sample. Error bars represent one standard deviation.

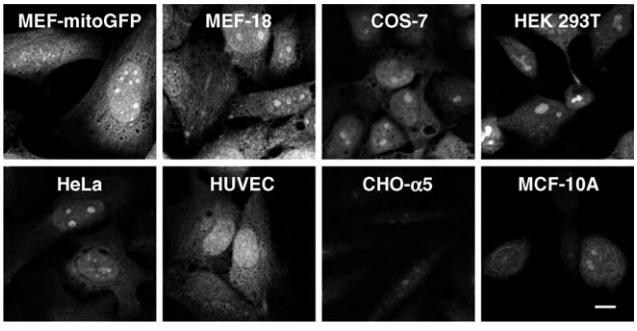

Figure 4. Coumarin labeling of newly synthesized proteins in a wide variety of cell types. The scale bar represents 10 μm.

endothelial and epithelial cells) and on cells derived from numerous species (human, mouse, monkey, hamster).

In many of the cell types examined here, the most intense coumarin fluorescence appeared to be localized in nucleolar structures (Figure 4). When HeLa and HEK 293T cells were stained with an antinucleolar antibody, the areas of brightest coumarin fluorescence co-localized with the antibody (Figure 5). Nucleoli, sites of ribosomal biogenesis, are pro-

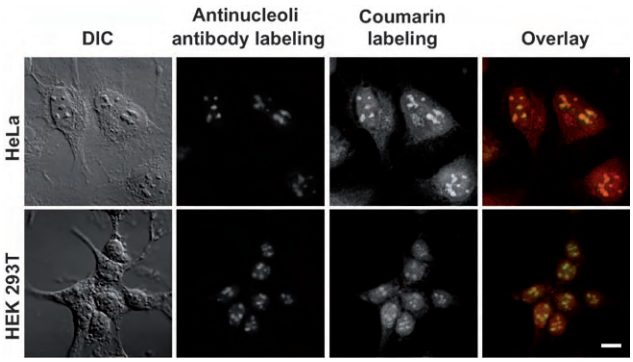

Figure 5. Fluorescence micrographs of nucleolar and coumarin labeling in HeLa and HEK 293T cells. Nucleoli are clearly visible in the DIC image (first column) and were labeled with an antinucleolar antibody and detected with a Cy2-conjugated antibody (second column). Coumarin labeling shows intense fluorescence at the nucleoli (third column). The overlay combines the antibody (green) and coumarin (red) labeling. The scale bar represents 10 μm.

tein-rich (> 80 % protein) and are the most dense part of the cell.[13] They exchange proteins rapidly; dynamic analysis of HeLa nucleoli indicated that proteomic changes are observed in less than two hours.[14] Furthermore, a recent proteomics study of HEK 293 cells identified nucleolin and nucleophosmin (B23), major nucleolar proteins, as being synthesized during a two-hour pulse with azidohomoalanine.[5,15] Evidence that there is rapid nucleolar assembly and protein turnover is consistent with our observation that a subset of newly synthesized proteins localize in nucleoli during a four-hour window.[16]

Noncanonical amino acid tagging offers a facile means of labeling newly synthesized proteins in mammalian cells. Since labeling is determined solely by the timing (and in principle by the location) of the Hpg pulse, it is possible to visualize proteins of unknown sequence, structure, or function. We suggest that this method will be useful for elucidating complex processes involving spatially localized protein translation, for example, the hypothesis that synaptic plasticity is modulated by translation localized in dendrites.[17] Moreover, other noncanonical amino acids can be metabolically incorporated and modified by the azide–alkyne or Staudinger ligations.[2,7,18] Multicolor analysis should be possible by using multiple dyes to visualize subsets of the proteome expressed during sequential pulses.

Received: May 26, 2006
Revised: August 1, 2006
Published online: October 11, 2006

Keywords: alkynes · azides · fluorescent probes · protein modifications · proteomics

 © 2006 Wiley-VCH Verlag GmbH & Co. KGaA, Weinheim

[1] a) M. Hamdan, P. Righetti, *Proteomics Today: Protein Assessment and Biomarkers Using Mass Spectrometry, 2D Electrophoresis, and Microarray Technology*, Wiley, Hoboken, **2005**; b) D. E. Warnock, E. Fahy, S. W. Taylor, *Mass Spectrom. Rev.* **2004**, *23*, 259.

[2] K. E. Beatty, F. Xie, Q. Wang, D. A. Tirrell, *J. Am. Chem. Soc.* **2005**, *127*, 14150.

[3] a) R. Y. Tsien, *Annu. Rev. Biochem.* **1998**, *67*, 509; b) B. A. Griffin, S. R. Adams, R. Y. Tsien, *Science* **1998**, *281*, 269; c) B. N. G. Giepmans, S. R. Adams, M. H. Ellisman, R. Y. Tsien, *Science* **2006**, *312*, 217.

[4] a) S. W. Botchway, I. Barba, R. Jordan, R. Harmston, P. M. Haggie, S. P. William, A. M. Fulton, A. W. Parker, K. M. Brindle, *Biochem. J.* **2005**, *390*, 787; b) A. J. Link, M. L. Mock, D. A. Tirrell, *Curr. Opin. Biotechnol.* **2003**, *14*, 603; c) L. Wang, P. G. Schultz, *Angew. Chem.* ***2005***, *117*, 34; *Angew. Chem. Int. Ed.* **2005**, *44*, 34; d) N. Budisa, *Angew. Chem.* **2004**, *116*, 6586; *Angew. Chem. Int. Ed.* **2004**, *43*, 6426; e) T. L. Hendrickson, V. de Crecy-Lagard, P. Schimmel, *Annu. Rev. Biochem.* **2004**, *73*, 147.

[5] D. C. Dieterich, A. J. Link, J. Graumann, D. A. Tirrell, E. M. Schuman, *Proc. Natl. Acad. Sci. USA* **2006**, *103*, 9482.

[6] a) J. A. Prescher, C. R. Bertozzi, *Nat. Chem. Biol.* **2005**, *1*, 13; b) P. F. van Swieten, M. A. Leeuwenburgh, B. M. Kessler, H. S. Overkleeft, *Org. Biomol. Chem.* **2005**, *3*, 20; c) A. J. Link, D. A. Tirrell, *J. Am. Chem. Soc.* **2003**, *125*, 11164; d) A. E. Speers, B. F. Cravatt, *Chem. Biol.* **2004**, *11*, 535.

[7] a) G. A. Lemieux, C. L. de Graffenried, C. R. Bertozzi, *J. Am. Chem. Soc.* **2003**, *125*, 4708; b) M. L. Tsao, F. Tian, P. G. Schultz, *ChemBioChem* **2005**, *6*, 2147; c) A. Deiters, P. G. Schultz, *Bioorg. Med. Chem. Lett.* **2005**, *15*, 1521.

[8] Q. Wang, T. R. Chan, R. Hilgraf, V. V. Fokin, K. B. Sharpless, M. G. Finn, *J. Am. Chem. Soc.* **2003**, *125*, 3192.

[9] a) V. V. Rostovtsev, L. G. Green, V. V. Fokin, K. B. Sharpless, *Angew. Chem.* **2002**, *114*, 2708; *Angew. Chem. Int. Ed.* **2002**, *41*, 2596; b) C. W. Tornoe, C. Christensen, M. Meldal, *J. Org. Chem.* **2002**, *67*, 3057; c) N. J. Agard, J. A. Prescher, C. R. Bertozzi, *J. Am. Chem. Soc.* **2004**, *126*, 15046.

[10] a) J. C. M. van Hest, K. L. Kiick, D. A. Tirrell, *J. Am. Chem. Soc.* **2000**, *122*, 1282; b) K. L. Kiick, R. Weberskirch, D. A. Tirrell, *FEBS Lett.* **2001**, *502*, 25.

[11] K. Sivakumar, F. Xie, B. M. Cash, S. Long, H. N. Barnhill, Q. Wang, *Org. Lett.* **2004**, *6*, 4603.

[12] H. C. Chen, A. Chomyn, D. C. Chan, *J. Biol. Chem.* **2005**, *280*, 26185.

[13] a) W. S. Vincent, *Int. Rev. Cytol.* **1955**, *4*, 269; b) M. Birnstiel, *Annu. Rev. Plant Physiol.* **1967**, *18*, 25.

[14] a) R. D. Phair, T. Misteli, *Nature* **2000**, *404*, 604; b) J. S. Andersen, Y. W. Lam, A. K. L. Leung, S.-E. Ong, C. E. Lyon, A. I. Lamond, M. Mann, *Nature* **2005**, *433*, 77.

[15] Azidohomoalanine (Aha), like Hpg, is a methionine surrogate. The rates of activation of Aha and Hpg by the *E. coli* methionyl-tRNA synthetase are nearly identical (see Ref. [18]). Polyacrylamide gel electrophoresis reveals no significant differences in the patterns of protein synthesis in mammalian cells treated with methionine or with Aha (see Ref. [5]).

[16] a) O. V. Zatsepina, O. A. Dudnic, Y. S. Chentsov, M. Thiry, H. Spring, M. F. Trendelenburg, *Exp. Cell Res.* **1997**, *233*, 155; b) F. Yu, P. Feigelson, *Proc. Natl. Acad. Sci. USA* **1972**, *69*, 2833.

[17] O. Steward, E. M. Schuman, *Neuron* **2003**, *40*, 347.

[18] K. L. Kiick, E. Saxon, D. A. Tirrell, C. R. Bertozzi, *Proc. Natl. Acad. Sci. USA* **2002**, *99*, 19.

 © 2006 Wiley-VCH Verlag GmbH & Co. KGaA, Weinheim

Sulfur Heterocycles

DOI: 10.1002/anie.200602190

"Sulflower": A New Form of Carbon Sulfide**

*Konstantin Yu. Chernichenko, Viktor V. Sumerin, Roman V. Shpanchenko, Elizabeth S. Balenkova, and Valentine G. Nenajdenko**

Besides the many aesthetic aspects of chemistry,[1] such as molecular complexity,[2] self-organization, and nonlinear dynamics, the sheer beauty and elegance of molecular structures has always played an important role in the development of chemistry.[3] A classic example is buckminsterfullerene, a molecule whose name is dedicated to a great architect. Starting from the idea of an elegant highly symmetrical C_{60} structure and its theoretical analysis, fullerene chemistry now lies in the mainstream of contemporary science.[4] The rapid growth of modern nanoscience and materials science has stemmed to an extent from the discovery of fullerenes.[5] Herein, we describe the investigation of a first representative of the new class of highly symmetric molecules with unusual electronic properties, namely the octathio[8]circulene (**1**)—the first fully heterocyclic circulene.[6] This molecule, which we have named "sulflower" (from sulfur and flower) has several remarkable features: It is both organic and inorganic as it has a belt of eight annulated thiophenic cycles and contains no hydrogen atoms. Its molecular formula $C_{16}S_8$ (or simply $(C_2S)_8$) allows one to classify it as a novel form of carbon sulfide. Its highly symmetric planar structure resembles the bloom of a sunflower or an eight-pointed star (Figure 1).

Several binary carbon–sulfur compounds are known besides CS_2 and its polymeric form, such as C_3S_2, C_3S_8, C_4S_6, C_5S_7, C_6S_8, C_6S_{10}, C_6S_{12}, C_8S_8, and C_9S_9.[7] The hypothetical polymer $(-C{=}C-S-)_n$ is also an isomeric form of C_2S and some lower representatives of this have been synthesized.[8] Annulated oligothiophenes represent another form of carbon sulfide with the formula $(C_2S)_n$. There are two types of thiophenic ring annulation, namely 2,3-*b* and 3,2-*b*, that allow the formation of oligomeric annulated structures. Combination of these annulation types gives essentially an infinite

[*] K. Y. Chernichenko, V. V. Sumerin, Dr. R. V. Shpanchenko, Prof. Dr. E. S. Balenkova, Prof. Dr. V. G. Nenajdenko
Department of Chemistry
Moscow State University
Leninskiye Gory, 119992 Moscow (Russia)
Fax: (+7) 495-932-8846
E-mail: nen@acylium.chem.msu.ru

[**] We thank D. Denisenko and Dr. D. Gribkov for the development of alternative routes to sulflower, Dr. A. Krasovskiy for HRMS spectra, Dr. D. Tyurin for quantum chemical calculations, Bruker Spectrospin for solid-state ^{13}C NMR spectra, Dr. A. Abakumov for help with XRPD, Prof. I. Alabugin for valuable remarks, and the Russian Foundation for Basic Research for financial support.

Supporting information for this article is available on the WWW under http://www.angewandte.org or from the author.

© 2006 Wiley-VCH Verlag GmbH & Co. KGaA, Weinheim

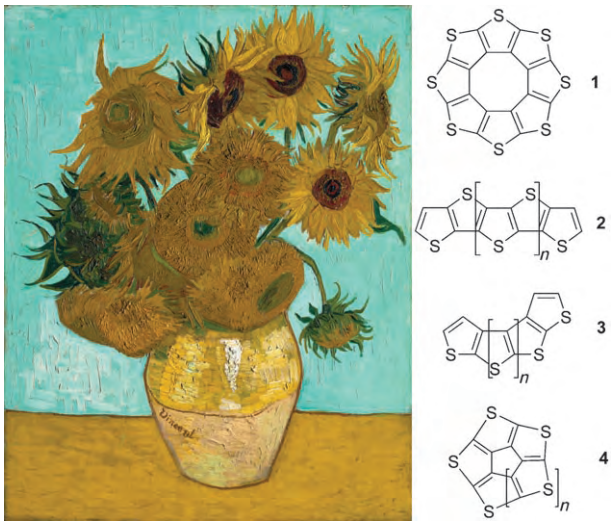

Figure 1. Left: "Sunflowers" by Vincent van Gogh (Copyright, Neue Pinakothek, Munich). Right: Types of annulated oligothiophenes: sulflower (**1**), linear **2**, helical **3**, and circulenic **4**.

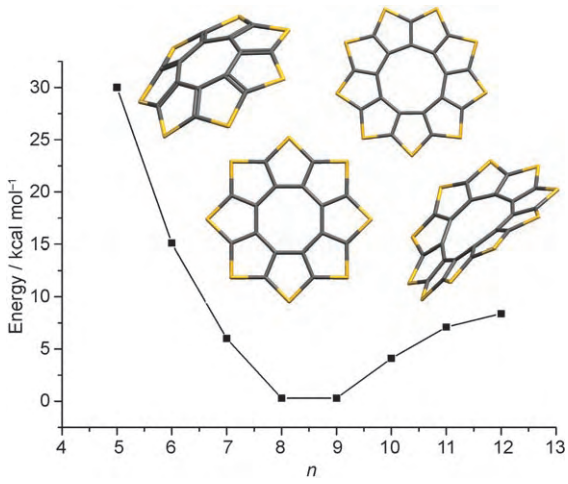

Figure 2. Calculated strain and geometries for fully thiophenic circulenes (n = number of thiophene rings). S yellow, C gray.

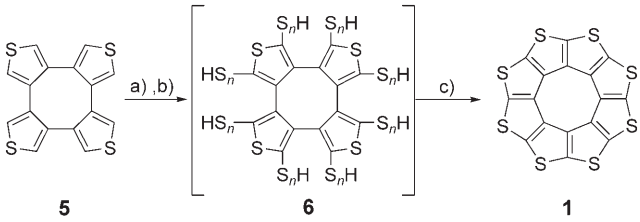

Scheme 1. Synthesis of circulene **1** from tetrathiophene **5** via polythiole **6** (n = 1). Reagents and conditions: a) LDA (16 equiv), sulfur (16 equiv), room temperature, 24 h; b) aq. HCl; c) vacuum pyrolysis.

variety of annulated oligothiophene forms, while the most interesting are structures with regular annulation, such as linear oligothiophene **2** and helical oligothiophene **3** (Figure 1). Examples of these classes have been successfully synthesized recently.[9] Frameworks **2** and **3** reach the empirical formula C_2S when $n \rightarrow \infty$, that is, in the case of a polymer, thus giving rise to a new form of carbon sulfide. A helical structure could be closed to give a macrocycle, thus forming the circulene **3**, which consists of thiophenyl rings with an empirical formula C_2S for any number of rings.

Initially, we used quantum chemical calculations to estimate the stability of thiophenyl circulenes and to choose the most promising candidate for synthetic preparation. According to the calculations, the strain is minimized in the flat, fully thiophenyl circulenes that contain eight or nine thiophene rings (**4**, $n = 4, 5$; Figure 1). To cope with the strain, lower members distort into crown-shaped structures analogous to the previously synthesized corannulene and trithiacoronene,[10] while circulenes, which contain larger number of units, create corrugated structures as was predicted[11] and confirmed by the structure of [7]circulene.[12] All calculated structures are highly symmetric, with circulenes that contain up to nine rings exhibiting an n-fold symmetry axis (n is the number of rings; Figure 2).

Of the two almost unstrained circulenes, the octathio[8]-circulene **1** was chosen as a synthetic target. For a long time, highly annulated oligothiophenes remained practically unexplored because of the lack of suitable synthetic methodology. Although significant progress in this area has been made in the last two years,[13] the nontrivial structure of sulflower presented a unique challenge which required the development of a new synthetic strategy that proved to be quite effective, simple, and straightforward. We chose tetrathiophene **5** as the most perspective precursor to **1** and envisioned that effective introduction of sulfur could be achieved through the lithium salts of **5** (Scheme 1). The essential innovation in our approach involved simultaneous treatment of **5** with an excess of lithium diisopropylamide and sulfur. This technique resulted in complete sulfurization of free thiophene sites and efficient formation of an intermediate polythiolate, which was then converted into polythiol **6** by acidification with HCl.[14] Subsequent vacuum pyrolysis of the crude polythiol led to elimination of the excess of sulfur through H_2S and elemental sulfur. The target circulene **1** was obtained in overall 80% yield starting from **5**, which itself is easily attained in 70% yield starting from commercially available 3,4-dibromothiophene.[15] Thus, we have developed an extremely short and effective approach to this complicated and aesthetic molecular architecture.

Sulflower (**1**) was isolated as a dark red powder that is insoluble in common organic solvents. Elemental analysis and high-resolution mass spectrometry (HRMS) revealed a perfect agreement of analytical data for **1** with the calculated values. In particular, the molecular ion multiplet at m/z 448 in the mass spectrum showed the same relative intensities and m/z ratios as those predicted. The high symmetry of sulflower was confirmed by both solid-state magic-angle spinning (MAS) ^{13}C NMR experiments, which revealed two signals at $\delta = 125$ and 138 ppm, and IR spectroscopy, which showed very weak absorption (the average absorbance was less than 0.05, while maximal adsorbance of highest peaks was less than 0.2). Intense peaks at 499, 724, and 947 cm^{-1} are characteristic for C–S bonds in annulated oligothiophenes.[16]

 © 2006 Wiley-VCH Verlag GmbH & Co. KGaA, Weinheim

The final proof of the structure was obtained by X-ray diffraction measurements. Although good-quality single crystals of circulene **1** were not accessible, the X-ray powder diffraction data were successfully used for the final solution and refinement of the structure.[17] The results of structure refinement revealed a very good agreement between the calculated and experimental data. The sulflower molecule was found to be flat, with the average bond lengths and angles close to those values for the calculated model. Despite its high symmetry, sulflower crystallizes in a non-centrosymmetric $P2_1$ space group. The packing of the C_2S molecules in the unit cell is shown in Figure 3. Along the *c* axis, the molecules are

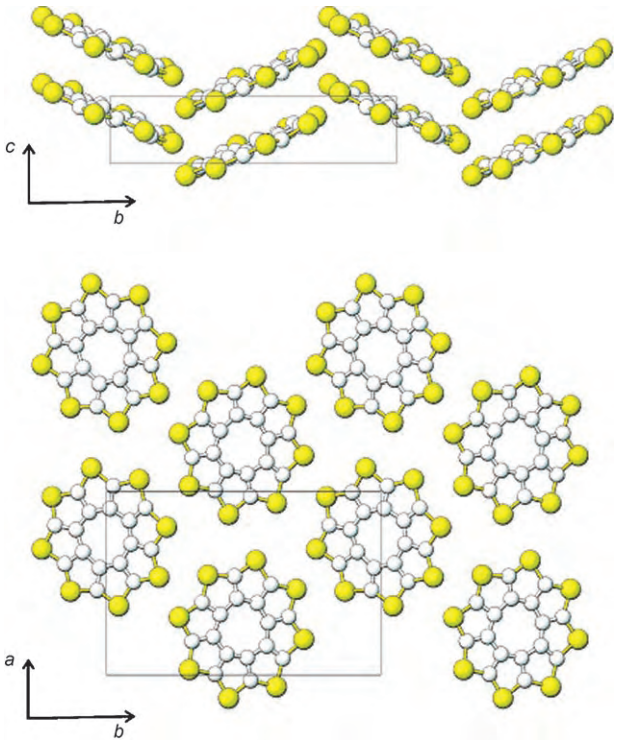

Figure 3. Packing of sulflower (**1**) molecules in the unit cell. S yellow, C white.

situated one under another and separated by about 3.9 Å to result in infinite columns. Inside the columns, molecules are tilted and form the corrugated layers perpendicular to the *c* axis. The angle between the molecules in adjacent columns is close to 131°. The separation between the sulfur atoms in the neighboring molecules is very small ($\approx$3.25 Å) and close to that for two neighboring atoms inside the molecule. A reduction in the electrostatic repulsion between sulfur atoms is achieved by the mutual orientation of the molecules where three closest sulfur atoms form an almost regular triangle. One should bear in mind that the precise interatomic distances cannot be obtained from the X-ray powder diffraction technique and that further structural investigations (e.g. neutron diffraction) are needed.

Organosulfur compounds display important electronic properties.[18] For example, tetrathiafulvalenes and π-conjugated oligothiophenes are extensively used in light-emitting devices,[19] thin-film transistors,[20] and other applications.[21] The extremely close packing of the sulflower molecules in the solid state suggests strong intermolecular interactions both within layers and between adjacent layers. Although such interactions should be favorable for the future use of sulflower as an electron donor in materials science applications, they also result in its insolubility in common solvents and complicate the preparation of thin-film materials based on sulflower. This latter complication forced us to seek other methods to prepare a more soluble form of this molecule. Sulflower dissolves in triflic acid (CF_3SO_3H) with the formation of deep purple solutions. ESR investigations revealed the presence of a paramagnetic species that displays a broad singlet in the ESR spectrum (*g* factor: 2.008), which most likely corresponds to the radical cation of sulflower. Solubility of sulflower in the form of the radical cation should allow the preparation of thin films thereof. Another possibility to prepare thin films is by vacuum sublimation owing to the high thermal stability of **1**.

In summary, sulflower is the first representative of a novel class of heterocyclic circulenes. This study illustrated the high stability of these structures and the development of an efficient synthetic methodology, which should be applicable to the new families of Se-, Te-, N-, and P-containing heterocyclic circulenes. Variation of the heteroatoms should allow the preparation of novel materials with diverse electronic properties. We have already succeeded in the preparation of a mixed thiophene-selenophene circulene, $C_{16}S_4Se_4$ (data not shown). Further research is underway.

Experimental Section

Starting material tetrathiophene **5** was prepared according to a described procedure.[15] Reagents were purchased from Acros Organics or Sigma-Aldrich.

Preparation of **1**: Diisopropylamine (9.9 mL, 70 mmol) was added to a suspension of tetrathiophene **5** (0.985 g, 3 mmol) in diethyl ether (150 mL) in a 250-mL three-necked flask flashed with argon, and the mixture was cooled to −20 °C. A solution of *n*-butyllithium in hexanes (23.2 mL of 2.5 M solution, 58 mmol) was added, and the mixture was allowed to warm to about 0 °C and then stirred at this temperature for 30 min. Powdered sulfur (1.530 g, 48 mmol) was then added, and the reaction was stirred for 24 h at room temperature. Water (100 mL) was added, and the mixture was stirred for 30 min. The aqueous layer was separated, washed with diethyl ether (50 mL), and acidified with 5 N HCl. The resulting precipitate was filtered, thoroughly washed with water, and dried in air on the filter and then under vacuum to give a solid (2.25 g). Vacuum pyrolysis was carried out at a dynamic vacuum of 0.04–0.05 torr, with the sample of polythiole placed in the sealed end of a silica or pyrex tube and plugged with glass wool. Heating was carried out by using a flame or tube furnace. The excess of sulfur began to sublime at temperatures above 150 °C, while circulene **1** sublimes in the temperature range 450–530 °C. The tube fragment containing the sublimed circulene **1** was cut off, and the product was purified by repeated vacuum sublimation to give pure sulflower (1.070 g).

Received: June 1, 2006
Published online: September 26, 2006

Keywords: annulation · oligothiophenes · polycycles · sulfur heterocycles · X-ray diffraction

 © 2006 Wiley-VCH Verlag GmbH & Co. KGaA, Weinheim

[1] R. Hoffmann, *HYLE – International Journal for Philosophy of Chemistry* **2003**, *9*, 7–10; see http://www.hyle.org/journal/issues/9-1/hoffmann.htm.
[2] G. M. Whitesides, R. F. Ismagilov, *Science* **1999**, *284*, 89–92.
[3] P. Laszlo, *HYLE – International Journal for Philosophy of Chemistry* **2003**, *9*, 11–32; see http://www.hyle.org/journal/issues/9-1/laszlo.htm.
[4] H. W. Kroto, J. R. Heath, S. C. O'Brien, R. F. Curl, R. E. Smalley, *Nature* **1985**, *318*, 162–163.
[5] A. Hirsch, M. Brettreich, *Fullerenes: Chemistry and Reactions*, Wiley-VCH, Weinheim, **2005**.
[6] Circulenes are a rare class of polycyclic aromatic compounds built from arenes annulated in a macrocycle. [6]Circulene (coronene) is the next step from benzene to graphite, while [5]circulene (corannulene) is the bottom part of C_{60}. To date, only benzenoid and mixed circulenes built from benzene and heterocyclic rings are known.
[7] See Supporting Information for more references about these carbon sulfide forms.
[8] A. W. M. Lee, A. B. W. Yeung, M. S. M. Yuen, H. Zhang, X. Zhao, W. Y. Wong, *Chem. Commun.* **2000**, 75–76.
[9] a) A. Rajca, M. Miyasaka, M. Pink, H. Wang, S. Rajca, *J. Am. Chem. Soc.* **2004**, *126*, 15211–15222, and references therein; b) A. Rajca, H. Wang, M. Pink, S. Rajca, *Angew. Chem.* **2000**, *112*, 4655–4657; *Angew. Chem. Int. Ed.* **2000**, *39*, 4481–4483.
[10] K. Imamura, K. Takimiya, Y. Aso, T. Otsubo, *Chem. Commun.* **1999**, 1859–1860.
[11] J. H. Dopper, H. Wynberg, *J. Org. Chem.* **1975**, *40*, 1957–1966.
[12] K. Yamamoto, T. Harada, M. Nakazaki, T. Naka, Y. Kai, S. Harada, N. Kasai, *J. Am. Chem. Soc.* **1983**, *105*, 7171–7172.
[13] a) V. G. Nenajdenko, V. V. Sumerin, K. Yu. Chernichenko, E. S. Balenkova, *Org. Lett.* **2004**, *6*, 3437–3439; b) T. Okamoto, K. Kudoh, A. Wakamiya, S. Yamaguchi, *Org. Lett.* **2005**, *7*, 5301–5304; c) K. Oyaizu, T. Iwasaki, Y. Tsukahara, E. Tsuchida, *Macromolecules* **2004**, *37*, 1257–1270; d) T. Iwasaki, Y. Kohinata, H. Nishide, *Org. Lett.* **2005**, *7*, 755–758.
[14] Polythiole **6** was not carefully identified because it was not required during the course of our work. For more information on its possible structure, see: W. Schroth, E. Hintzsche, H. Jordan, T. Jende, R. Spitzner, I. Thondorf, *Tetrahedron* **1997**, *53*, 7509–7528.
[15] Z. Zhou, T. Yamamoto, *J. Organomet. Chem.* **1991**, *414*, 119–127; for the preparation of **5**, see also: S. M. H. Humayun, M. Miura, S. Sasaki, G. Harada, Y. Kuwatani, M. Yoshida, M. Iyoda, *Heterocycles* **2000**, *52*, 761–774.
[16] R. M. Osuna, R. P. Ortiz, M. C. R. Delgado, V. G. Nenajdenko, V. V. Sumerin, E. S. Balenkova, V. Hernández, J. T. L. Navarrete, *J. Phys. Chem. B* **2006**, in press.
[17] See Supporting Information for details of XRPD experiments. Crystal data for **1**: Dark red powder; $C_{16}S_8$, monoclinic, $P2_1$, $a=11.15402(18)$ Å, $b=16.5628(3)$ Å, $c=3.90742(4)$ Å, $\beta=94.180(1)°$, $V=719.94(2)$ Å^3, $Z=16$, $Cu_{K\alpha1}$ radiation, $\lambda=1.5406$ Å, $D_{calcd}=2.070$ g cm^{-3}, $\mu=1.233$ mm^{-1}, $T=293(2)$ K. CCDC 609788 contains the supplementary crystallographic data for this paper. These data can be obtained free of charge from The Cambridge Crystallographic Data Centre via www.ccdc.cam.ac.uk/data_request/cif.
[18] M. Gingras, J.-M. Raimundo, Y. M. Chabre, *Angew. Chem.* **2006**, *118*, 1718–1745; *Angew. Chem. Int. Ed.* **2006**, *45*, 1686–1712.
[19] I. Perepichka, D. Perepichka, H. Meng, F. Wudl, *Adv. Mater.* **2005**, *17*, 2281–2305.
[20] Y. Sun, Y. Liu, D. Zhu, *J. Mater. Chem.* **2005**, *15*, 53–65.
[21] G. Barbarella, M. Melucci, G. Sotgiu, *Adv. Mater.* **2005**, *17*, 1581–1593.

 © 2006 Wiley-VCH Verlag GmbH & Co. KGaA, Weinheim

ZnO Nanocrystals

DOI: 10.1002/anie.200602429

Highly Luminescent ZnO Nanocrystals Stabilized by Ionic-Liquid Components**

*Da-Peng Liu, Guo-Dong Li, Yan Su, and Jie-Sheng Chen**

In the past two decades considerable efforts have been concentrated on the use of II–VI semiconductor nanocrystals (NCs) as luminescent materials.[1] Owing to quantum-confinement effects, the optical properties of these nanocrystals (quantum dots) can be tuned by varying the crystal size.[2] Efficient red- or green-light emitters have been prepared containing zinc (cadmium) sulfide (selenide) II–VI NCs,[3] whereas the preparation of blue-emitting NCs of these compounds has not been as successful.[4] In addition, the involvement of Cd, S, and Se in these luminescent systems may cause toxicity and pollution problems, and sulfides or selenides are intrinsically less-resistant to oxidation by the O_2 in air.

As one of the group of II–VI semiconductors, ZnO has attracted increasing attention recently because it is nontoxic, less expensive, and chemically stable towards air. However, its nanoscale crystals tend to aggregate or to undergo Ostwald ripening[5] because of their high surface energy. To stabilize NCs, appropriate surface modifications are usually necessary.[6] We have reported a facile sol–gel approach for the preparation of PEGME-modified (PEGME = poly(ethylene glycol) methyl ether) ZnO NCs with size-dependent photoluminescence (PL) and a high quantum yield (QY) of about 30% at room temperature.[7] These ZnO NCs are stable in solution, but they still undergo Ostwald ripening upon thermal treatment or aging without the protection of LiOH in the solvent-free state. Xia and co-workers recently also obtained a polymer-stabilized nano-ZnO with remarkable blue PL.[8] However, only blue-emission was observed for this luminescent system and the origin of the emission was not very clear.

Further stabilization of the NCs can be achieved if they are protected by charged species, such as alkyl ammonium cations, because the charges repel each other, thereby more effectively preventing the particles from undergoing aggregation or Ostwald ripening.[9,10] In addition, the alkyl chains of

[*] D. P. Liu, G. D. Li, Y. Su, Prof. J. S. Chen
State Key Laboratory of Inorganic Synthesis and Preparative Chemistry
College of Chemistry
Jilin University
Changchun 130012 (P.R. China)
Fax: (+86) 431-516-8624
E-mail: chemcj@jlu.edu.cn

[**] This work was supported by the National Natural Science Foundation of China.

Supporting Information for this article is available on the WWW under http://www.angewandte.org or from the author.

WILEY InterScience DISCOVER SOMETHING GREAT
© 2006 Wiley-VCH Verlag GmbH & Co. KGaA, Weinheim

the protecting cations make the NCs more dispersible in organic solvents, which can be used to extract the NCs from the aqueous phase so as to achieve phase transfer easily.[9–11] Furthermore, upon ion-exchange with suitable counterions,[12,13] the NC-containing composite may behave as a liquid-like organic salt, usually dubbed an ionic liquid (IL) if it has a melting point below 100 °C.[14] Therefore, it is possible to enhance the processability and other physicochemical properties of NCs by modification with IL components.[12,13] Nevertheless, in all the reported work the IL-component modification was performed after the NCs were formed, and, as a result, the NC particle size and related physicochemical properties could not be tuned. Giannelis and co-workers, for example, have used positively charged organosilanes to modify the surface of ZnO NCs preformed from zinc acetate, and only a yellow-emitting (in the visible region) IL-ZnO composite with a modest QY was obtained.[13b]

Herein we describe a new approach for preparation of ZnO NCs stabilized by IL components. In this approach, the IL-ZnO nanocrystal composite is formed directly from an IL salt containing Zn^{II} cations (see Scheme 1), and the ZnO NC

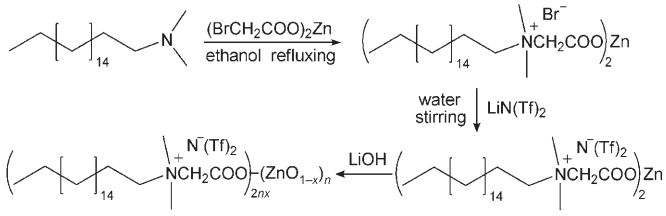

Scheme 1. Synthesis of IL-ZnO NC composites. Tf = trifluoromethanesulfonyl.

size, and consequently the photoluminescent properties of the NCs, can be tuned by varying the reaction conditions. The nanomaterials emit blue to yellow light efficiently both in the solvated and in the solvent-free states. Furthermore, the photoluminescent QY of the IL-ZnO materials reaches as high as 45% in solvent, and the PL spectrum of the solvent-free IL-ZnO is stable even when the sample is heated at 80 °C.

Three typical IL-ZnO samples (IL-ZnO-A, IL-ZnO-B, and IL-ZnO-C) were prepared with [LiOH]/[Zn] ratios in the reaction mixture of 3.5, 1.4, and 1.0, respectively (see Experimental Section). Figure 1 shows high-resolution transmission electron microscope (HRTEM) images of samples

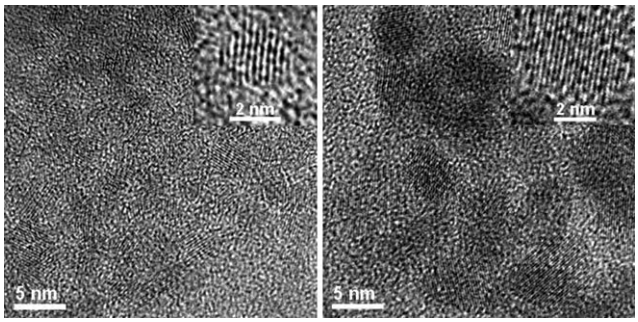

Figure 1. HRTEM images of IL-ZnO-B (left) and IL-ZnO-C (right) nanocrystals. Insets: enlarged images.

IL-ZnO-B and IL-ZnO-C. It can be seen that the IL-ZnO NCs are uniform and monodisperse with a diameter of about 2.5 nm for IL-ZnO-B and 4.0 nm for IL-ZnO-C; these NCs all have a wurtzite structure.[15] HRTEM images could not be obtained of the smaller IL-ZnO NCs because these composite particles always move fast under the intense electron beams.[7] IR spectroscopy indicates that the alkyl ammonium molecules are bonded to the surface of the ZnO NC cores through their carboxylate groups, and thermogravimetric and differential thermal analysis (TG-DTA) shows that the decomposition temperature of the IL-ZnO composites is above 250 °C. A calcination temperature of 600 °C results in a residue of 16.5 wt% ZnO (see Supporting Information).

Figure 2 displays the differential scanning calorimetry (DSC) curves, which show the phase-transition process of the

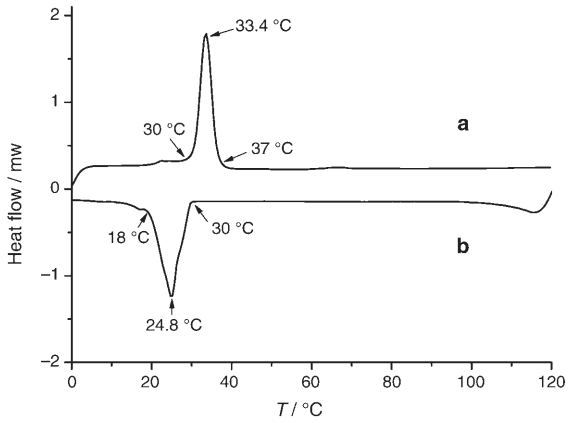

Figure 2. DSC curves for IL-ZnO-C: a) heating and b) cooling.

IL-ZnO composite. An endothermic peak appears at 33.4 °C in the heating curve (curve a) whereas an exothermic one is observed at 24.8 °C in the cooling curve (curve b). Both the heating and cooling curves show an onset of about 30 °C, which corresponds to the phase-transition temperature of the IL-ZnO system. No other phase transition is observed for the IL-ZnO sample in the temperature range of the DSC measurement.

The PL spectra (Figure 3) show that the emission peaks of IL-ZnO-A, -B, and -C in chloroform are located at 425, 461,

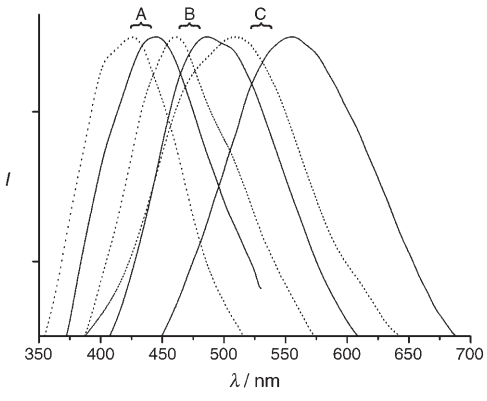

Figure 3. Normalized PL emission spectra of IL-ZnO-A, -B, and -C in the solvated state (dotted lines) and in the solvent-free state after thermal treatment at 80 °C for one week (solid lines).

 © 2006 Wiley-VCH Verlag GmbH & Co. KGaA, Weinheim

and 510 nm, corresponding to purplish-blue, bluish-green, and greenish-yellow colors, respectively. The photoluminescent QYs of the materials dispersed in solvent are about 43, 45, and 41 %, respectively. After removal of the solvent under vacuum at 80 °C, the respective IL-ZnO NC samples emit blue, green, and yellow light when excited with UV radiation. Interestingly, the emission peaks of the solvent-free samples shift to 445, 495, and 555 nm, respectively (Figure 3). Nevertheless, when the solvent-free samples are re-dispersed in chloroform, the emission peaks shift back to the positions corresponding to those of the original solvated samples. This phenomenon suggests that the emission-peak shift arises from a solvent effect but not from the particle-size variation in the solvation–desolvation process. The PL spectra of the solvent-free samples remain almost unchanged after aging at 80 °C for at least one week, thus indicating that the ZnO NCs in these samples undergo no aggregation or Ostwald ripening under these conditions.

To demonstrate the light emission of the IL-ZnO NC materials further, the three solvent-free samples were each loaded in a mould with three letter-shaped grooves and illuminated with a UV lamp ($\lambda = 254$ nm). Upon UV excitation, the three letters emit blue, green, and yellow light (Figure 4, top right), respectively, in accordance with the corresponding emission spectra presented in Figure 3. Note that when the three solvent-free samples (IL-ZnO-A, -B, and -C) are mixed together in a weight ratio of approximately 1:1:1, the resulting material emits bright white light (Figure 4, middle right) with CIE (Commision Internationale de L'Eclairage) coordinates of (0.28, 0.32). This result means that by adjusting the ZnO nanocrystal size and simple mixing of the differently sized IL-ZnO NC samples, white-light emission is easily achieved. Furthermore, the IL-ZnO composite clearly shows its liquid-like features after heating. Although a phase-transition temperature of around 30 °C is observed, the composite material is still rather viscous at this temperature. However, heating to 80 °C renders the IL-ZnO sample fluid (Figure 4, bottom part). This fluidity of the IL-ZnO composite implies that the material should be highly processable upon mild thermal treatment.

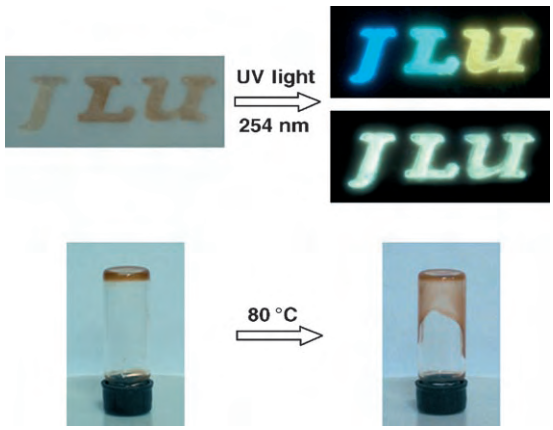

Figure 4. Photographs of IL-ZnO showing the tunable PL (upper part; see text for details) and the fluidity (lower part) of the samples.

The PL of ZnO NCs in the visible region arises from transitions involving trapped levels[15,16] and that oxygen vacancies play an important role in the formation of these trapped levels. When excited electrons in the conduction band of the NCs combine with the holes in the trapped levels, or alternatively when the electrons in the trapped levels combine with the holes in the valence band, emissions occur. The energy gaps between the conduction band and the trapped levels and those between the trapped levels and the valence band are proportional to the band gap of the NCs, therefore it is not surprising that the emission of ZnO NCs shifts to higher frequency as the NC size decreases because of quantum confinement effects. On the other hand, as the particle size of the ZnO NCs is rather small, the surface area of the NCs is distinctly larger than that of bulk ZnO crystals. This high surface area is conducive to the formation of a high concentration of oxygen vacancies, and consequently a high concentration of trapped levels in the NCs.[17] This situation explains why the photoluminescent QYs of the IL-ZnO composite materials are remarkably high. The notable thermal stability of the IL-ZnO composite materials is sustained by the electrostatic repulsion between the nanoparticles. The cationic components of the IL are bound to the ZnO NC cores through the carboxylate moieties (see Supporting Information), and the positive charges of the cationic species are balanced by the $[N(Tf)_2]^-$ counterions. The ZnO NCs protected by the positively charged species and separated by the counterions are not able to come into contact with one another, even after thermal treatment, to form aggregates or to undergo Ostwald ripening because of this electrostatic repulsion (see the schemes in the Supporting Information).

In conclusion, we have demonstrated a new route for the stabilization of ZnO NCs that show tunable photoluminescence. Their excellent photoluminescence, high thermal stability, and good processability in both the solvated and solvent-free state make these composites highly applicable as new luminescent materials.

Experimental Section

Zinc bromoacetate: Excess $Zn(OH)_2$, which was freshly precipitated from an aqueous solution of $ZnCl_2$ by addition of NaOH, was mixed with an aqueous solution of 10 mmol of bromoacetic acid and the mixture was heated at 70 °C with vigorous stirring until the pH value of the system reached about 6.0. The residual $Zn(OH)_2$ was then removed by filtration and the filtrate was concentrated on a rotary evaporator. The resulting solid was dried in a vacuum oven at 100 °C.

N,*N*-dimethyloctadecylammonium bromide acetate zinc salt (C_{18}-Zn): *N*,*N*-dimethyloctadecylamine (Aldrich; 10 mmol) and zinc bromoacetate (5 mmol) were dissolved in absolute ethanol (50 mL) and the vigorously stirred solution was heated under reflux for 24 h in a 100-mL round-bottomed flask. The solution was then concentrated on a rotary evaporator to about 4 mL. This solution was cooled to −12 °C and anhydrous diethyl ether (20 mL) was added to precipitate C_{18}-Zn as a white solid (3 mmol, 2.81 g), which was isolated by filtration and washed with anhydrous diethyl ether. To remove the residual zinc bromoacetate from the product completely, the solid was redissolved in chloroform, filtered, and dried by evaporation. ^{1}H NMR ($CDCl_3$, TMS): $\delta = 4.15$ (s, 2H), 3.59 (t, $J = 7.0$ Hz, 2H), 3.35 (s, 6H), 1.72 (s, 2H), 1.33–1.28 (m, 6H), 1.26 (s, 24H), 0.89 ppm (t, $J = 7.0$ Hz, 3H).

 © 2006 Wiley-VCH Verlag GmbH & Co. KGaA, Weinheim

N,*N*-dimethyloctadecylammonium bis((trifluoromethyl)sulfonyl)amide acetate zinc salt (IL-Zn): An aqueous solution (50 mL) of C_{18}-Zn (1 mmol) and an aqueous solution (50 mL) of lithium bis((trifluoromethyl)sulfonyl)amide ($LiN(Tf)_2$) (Fluka, 2 mmol) were mixed and heated at 70 °C for several minutes whilst stirring until the solution turned turbid. Chloroform (50 mL) was then added to the hot mixture to extract the reaction product. The extract was concentrated on a rotary evaporator and dried in vacuo at 70 °C to give 0.97 mmol of IL-Zn.

IL-ZnO: IL-Zn (1 mmol) was treated with LiOH in ethanol at room temperature. The [LiOH]/[Zn] molar ratio in the reaction system was controlled to be 3.5, 1.4, and 1.0, respectively for IL-ZnO-A, -B, -C. The resulting solution was evaporated to dryness on a rotary evaporator and the obtained solid product was re-dissolved in 20 mL of chloroform to form a stable 0.02 M colloidal solution.

Characterization: ^{1}H NMR spectra (with tetramethylsilane as reference) were recorded with a Bruker Ultrashield 500 MHz NMR spectrometer and the IR spectra were recorded with a Bruker IFS 66v/S FTIR spectrometer equipped with a DGTS detector. A Perkin–Elmer LS 55 luminescence spectrometer was used to obtain the photoluminescence spectra for the IL-ZnO materials both in their solvated and solvent-free states. The HRTEM images were recorded with a JEOL JEM-3010 transmission electron microscope operating at 300 kV. The thermogravimetric and differential thermal analysis (TG-DTA) curves were recorded with a Perkin–Elmer Pyris Diamond TG/DTA thermal analyzer at a temperature-increase rate of 20 °C min^{-1} under nitrogen. The DSC measurements were performed with a Netzsch DSC 204 calorimeter at a scanning rate of 10 °C min^{-1}.

For evaluation of the fluorescence QYs of the IL-ZnO materials, quinine sulfate in 0.5 M sulfuric acid was used as the reference for the sample emitting blue light while rhodamine 6G in ethanol was used for those emitting green and yellow light.[7]

Received: June 16, 2006
Published online: October 9, 2006

Keywords: ionic liquids · nanocrystals · photoluminescence · quantum yield · zinc

[1] a) V. L. Colvin, M. C. Schlamp, A. P. Alivisatos, *Nature* **1994**, *370*, 354; b) W. C. W. Chan, S. Nie, *Science* **1998**, *281*, 2016; c) S. Coe, W. K. Woo, M. Bawendi, V. Bulovic, *Nature* **2002**, *420*, 800.
[2] a) A. P. Alivisatos, *Science* **1996**, *271*, 933; b) B. O. Dabbousi, J. Rodriguez-Viejo, F. V. Mikulec, J. R. Heine, H. Mattoussi, R. Ober, K. F. Jensen, M. G. Bawendi, *J. Phys. Chem. B* **1997**, *101*, 9463; c) A. Pan, H. Yang, R. Liu, R. Yu, B. Zou, Z. Wang, *J. Am. Chem. Soc.* **2005**, *127*, 15692.
[3] a) L. Qu, Z. Peng, X. Peng, *Nano Lett.* **2001**, *1*, 333; b) X. Zhong, R. Xie, Y. Zhang, T. Basché, W. Knoll, *Chem. Mater.* **2005**, *17*, 4038.
[4] a) L. Spanhel, M. Haase, H. Weller, A. Henglein, *J. Am. Chem. Soc.* **1987**, *109*, 5649; b) C. B. Murray, D. J. Norris, M. G. Bawendi, *J. Am. Chem. Soc.* **1993**, *115*, 8706; c) M. A. Hines, P. Guyot-Sionnest, *J. Phys. Chem. B* **1998**, *102*, 3655; d) J. S. Steckel, J. P. Zimmer, S. Coe-Sullivan, N. E. Stott, V. Bulović, M. G. Bawendi, *Angew. Chem.* **2004**, *116*, 2206; *Angew. Chem. Int. Ed.* **2004**, *43*, 2154.
[5] W. Z. Ostwald, *Phys. Chem.* **1901**, *37*, 385.
[6] A. Henglein, *Chem. Rev.* **1989**, *89*, 1861.
[7] H. M. Xiong, D. P. Liu, Y. Y. Xia, J. S. Chen, *Chem. Mater.* **2005**, *17*, 3062.
[8] H. M. Xiong, Z. D. Wang, Y. Y. Xia, *Adv. Mater.* **2006**, *18*, 748.
[9] D. G. Kurth, P. Lehmann, C. Lesser, *Chem. Commun.* **2000**, 949.
[10] a) H. Zhang, Z. Cui, Y. Wang, K. Zhang, X. Ji, C. Lü, B. Yang, M. Gao, *Adv. Mater.* **2003**, *15*, 777; b) H. Zhang, C. Wang, M. Li, J. Zhang, G. Lu, B. Yang, *Adv. Mater.* **2005**, *17*, 853.
[11] a) T. Nakashima, T. Kawai, *Chem. Commun.* **2005**, 1643; b) T. Nakashima, T. Sakakibara, T. Kawai, *Chem. Lett.* **2005**, *34*, 1410.
[12] a) V. Mévellec, B. Leger, M. Mauduit, A. Roucoux, *Chem. Commun.* **2005**, 2838; b) M. Antonietti, D. Kuang, B. Smarsly, Y. Zhou, *Angew. Chem.* **2004**, *116*, 5096; *Angew. Chem. Int. Ed.* **2004**, *43*, 4988; c) J. Dupont, G. S. Fonseca, A. P. Umpierre, P. F. P. Fichtner, S. R. Teixeira, *J. Am. Chem. Soc.* **2002**, *124*, 4228.
[13] a) A. B. Bourlinos, R. Herrera, N. Chalkias, D. D. Jiang, Q. Zhang, L. A. Archer, E. P. Giannelis, *Adv. Mater.* **2005**, *17*, 234; b) A. B. Bourlinos, A. Stassinopoulos, D. Anglos, R. Herrera, S. H. Anastasiadis, D. Petridis, E. P. Giannelis, *Small* **2006**, *2*, 513.
[14] P. Wasserscheid, W. Keim, *Angew. Chem.* **2000**, *112*, 3926; *Angew. Chem. Int. Ed.* **2000**, *39*, 3772.
[15] A. Wood, M. Giersig, M. Hilgendorff, A. Vilas-Campos, L. M. Liz-Marzán, P. Mulvaney, *Aust. J. Chem.* **2003**, *56*, 1051.
[16] a) K. Vanheusden, W. L. Warren, J. A. Voigt, C. H. Seager, D. R. Tallant, *Appl. Phys. Lett.* **1995**, *67*, 1280; b) K. Vanheusden, W. L. Warren, C. H. Seager, D. R. Tallant, J. A. Voigt, B. E. Gnade, *J. Appl. Phys.* **1996**, *79*, 7983; c) A. van Dijken, E. A. Meulenkamp, D. Vanmaekelbergh, A. Meijerink, *J. Phys. Chem. B* **2000**, *104*, 1715.
[17] A. van Dijken, J. Makkinje, A. Meijerink, *J. Lumin.* **2001**, *32*, 323.

 © 2006 Wiley-VCH Verlag GmbH & Co. KGaA, Weinheim

Lamellar Materials

DOI: 10.1002/anie.200602541

Tailor-Made Onionlike Stereocomplex Crystals in Incompatible, Enantiomeric, Polylactide-Containing Block Copolymer Blends**

Lu Sun, Lei Zhu, Lixia Rong, and Benjamin S. Hsiao*

Self-assembled soft materials having curved lamellar structures include uni- and multilamellar vesicles (MLVs) and scrolled or curled tubules.[1] Due to their potential applications as chemical and biological microreactors, MLVs (or onions) have received much attention.[2] In concentrated

[*] L. Sun, Prof. L. Zhu
Polymer Program, Institute of Materials Science and
Department of Chemical, Materials, and Biomolecular Engineering
University of Connecticut
Storrs, CT 06269-3136 (USA)
Fax: (+1) 860-486-4745
E-mail: lei.zhu@uconn.edu
Homepage: http://www.ims.uconn.edu/~lzhu
Dr. L. Rong, Prof. B. S. Hsiao
Department of Chemistry
State University of New York at Stony Brook
Stony Brook, NY 11794-3400 (USA)

[**] This work was supported by ACS PRF (41918-G7) and NSF CAREER Award DMR-0348724. The synchrotron X-ray experiments were carried out at the National Synchrotron Light Source in Brookhaven National Laboratory, supported by DoE.

Supporting information for this article is available on the WWW under http://www.angewandte.org or from the author.

© 2006 Wiley-VCH Verlag GmbH & Co. KGaA, Weinheim
InterScience

solutions of surfactants, monodisperse and closely packed onion phases were obtained under mechanical shear.[3] Occasionally, onionlike vesicles could be formed spontaneously, for example, cosurfactants were used to induce onion phases.[4] Multilamellar vesicles were also induced without shear by electrostatic interactions between cationic and anionic surfactants[5] or anionic macromolecules such as DNA.[6] The detailed formation mechanism for these surfactant onions is still under investigation.[7] Besides these lyotropic systems, thermotropic liquid crystals can also form onion defects in focal conic domains with positive Gaussian curvature.[8] The onionlike morphology was also predicted and reported in homopolymer/copolymer[9] and copolymer/copolymer[10] blends, where thermodynamic equilibrium played an important role. Contrary to the "soft" nature of the above materials, crystals cannot readily exhibit onionlike morphology due to their high bending moduli and symmetric structures. Indeed, in semicrystalline polymers only twisted and scrolled crystals with open structures have been reported.[11] Unbalanced stresses at folding surfaces were believed to be the origin of lamellar crystal curving. Direct evidence of this mechanical origin is still lacking.

Understanding or controlling lamellar curvature is thus an important research topic in the fields of biophysics and polymer science. In this study, we have designed a novel approach to tailor-make onionlike polymer crystals using the concept of unbalanced surface stresses. Crystalline stereocomplexes were obtained from enantiomeric polylactide (PLA) block copolymer blends, namely, poly(ethylene oxide)-*b*-poly(L-lactide) (PEO-*b*-PLLA) and poly(ethylene-*co*-1-butene)-*b*-poly(D-lactide) (PEB-*b*-PDLA). By biasing the PEO and PEB molecular weights (or volumes) to be unsymmetric, unbalanced stresses are generated on crystal basal planes and thus lamella curving is induced.

Three well-defined enantiomeric PLA block copolymer samples—two PEO-*b*-PLLA and a PEB-*b*-PDLA—were synthesized by controlled ring-opening polymerization of L- and D-lactides from monohydroxyl-terminated PEO-OH and PEB-OH prepolymers, respectively.[12] The number-average molecular weights M_n (k denotes thousands) and polydispersity indices (PDI) of these block copolymers were determined by ^{1}H NMR spectroscopy and size-exclusion chromatography (SEC): PEO-*b*-PLLA (5k–5.1k), PDI = 1.14; PEO-*b*-PLLA (2k–5.4k), PDI = 1.12; and PEB-*b*-PDLA (4.2k–5.4k), PDI = 1.09. Two stereocomplex samples were obtained by equimolar blending of PEB-*b*-PDLA (4.2k–5.4k) with PEO-*b*-PLLA (2k–5.4k) and PEO-*b*-PLLA (5k–5.1k), respectively, by using chloroform as a good solvent. They are denoted as SC5k-EO2k and SC5k-EO5k, respectively. The solution-cast samples were heated to 250 °C and held there for 15 min to melt stereocomplex crystals (melting temperatures ca. 195 °C), and stereocomplexes were crystallized by cooling at 1 °C min^{-1} under a dry N_2 atmosphere to room temperature.

Quantitative yields of stereocomplex crystals were confirmed by wide-angle X-ray diffraction (WAXD, Figure 1B). Trigonal[13a] reflections for PLA stereocomplex (SC) crystals, $(110)_{SC}$, $(300)_{SC}$, $(220)_{SC}$, were seen at 8.4, 14.5, 16.9 nm^{-1} for both blends. No orthorhombic[13b] PLLA or PDLA crystal

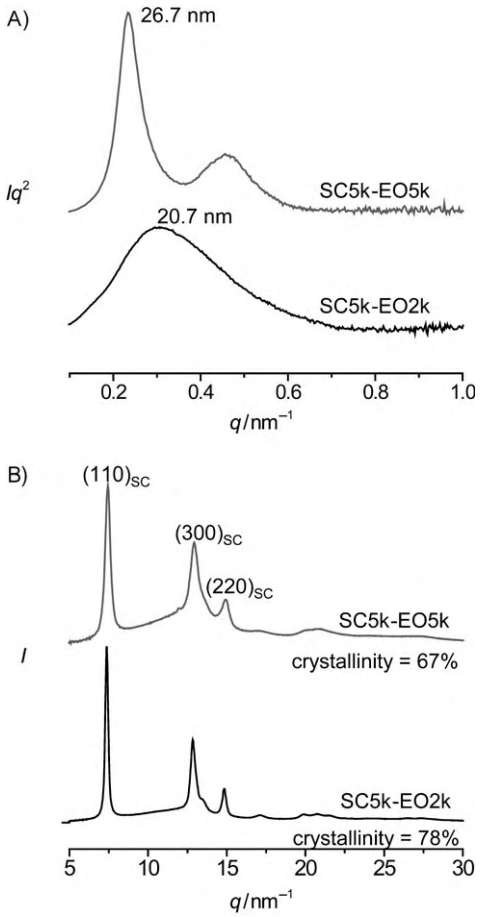

Figure 1. A) Small-angle X-ray scattering and B) wide-angle X-ray diffraction profiles for SC5k-EO5k and SC5k-EO2k at 50 °C. Curves are offset for clarity.

reflections were observed (e.g., the strong and overlapped $(110)_{LA}/(200)_{LA}$ reflections at 12.1 nm^{-1} were missing; LA = lactide). After peak deconvolution in Figure 1B and normalization to the PLA weight percentages, the stereocomplex crystallinities for SC5k-EO5k and SC5k-EO2k were calculated to be 67 and 78 wt %, respectively.

Lamellar morphology of these stereocomplexes was studied by small-angle X-ray scattering (SAXS, Figure 1A). SC5k-EO5k demonstrated the typical lamellar morphology with first- and second-order reflections at 0.23 and 0.46 nm^{-1}, respectively. The overall spacing was 26.7 nm. In contrast, a broader reflection with an average spacing of 20.7 nm was seen for SC5k-EO2k.

The difference in the SAXS profiles of SC5k-EO5k and SC5k-EO2k suggested different lamellar organizations inside the samples. Figure 2A shows a typical transmission electron microscopy (TEM) image for SC5k-EO5k. Flat lamellar morphology with bright layers corresponding to PEB and stereocomplex crystals and dark layers corresponding to PEO and amorphous PLA was seen. This is because PEB and stereocomplex crystals resisted staining with RuO_4, but PEO and amorphous PLA did not.[12]

By decreasing the M_n of PEO from 5000 to 2000, the volume balance between PEB and PEO blocks was broken.

 © 2006 Wiley-VCH Verlag GmbH & Co. KGaA, Weinheim

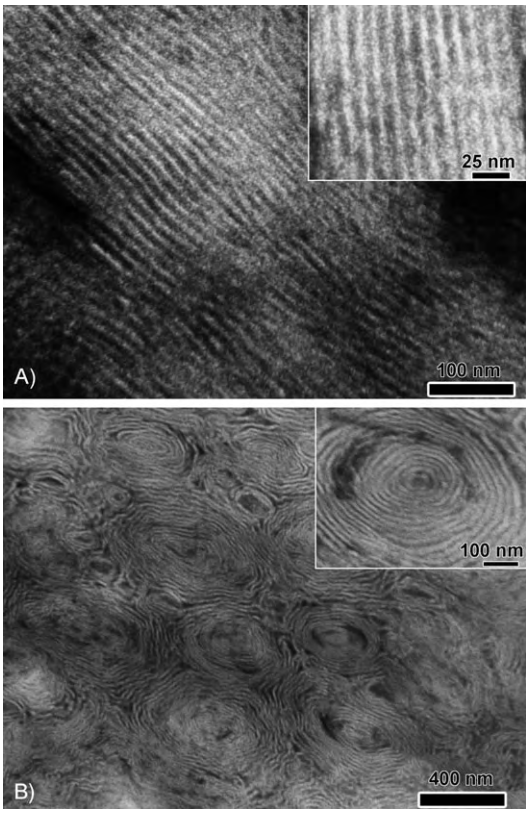

Figure 2. Bright-field TEM images of A) SC5k-EO5k and B) SC5k-EO2k crystallized from the melt during cooling at 1 °C min^{-1}.

Figure 2 B shows the typical morphology of SC5k-EO2k. Intriguingly, concentric microdomains were seen throughout the sample. We concluded that onion crystals, instead of scrolled lamellar crystals,[11] were obtained. A closer view of the onion structure is shown in the inset of Figure 2 B. The central dark microdomain represents amorphous PEO and PLAs (the sectioning happened to cut through the center of the onion). The lamellar stacking near the center seemed tighter than that at the periphery. Again, the bright layers are PEB and crystalline stereocomplexes, and the dark layers amorphous PEO and PLAs. The overall diameter and shape of the onions seemed to be variable. However, since the sample was sectioned (ca. 70 nm) at various portions of the onions, the actual onion sizes were not equal to those observed in TEM, and will be studied in the future by small-angle light scattering. The slightly elliptical shape of the onions may result from film compression during cutting.

Based on the above results, we propose a possible molecular model for the onionlike stereocomplex crystals (Figure 3). Curved PEB, PLA stereocomplex, and PEO-rich microdomains arrange into a noncentrosymmetric multilamellar structure in which PEB and PEO are always at the outside and the inside of a curved PLA stereocomplex lamellar crystal, respectively. This is reminiscent of the noncentrosymmetric scrolled crystals of chrysotile asbestos.[11] We performed a quantitative thickness analysis of the PEO-rich, PEB, and PLA stereocomplex layers for both samples using the thicknesses of the dark and bright layers in the TEM images (Figure 2). Detailed calculations are described in the

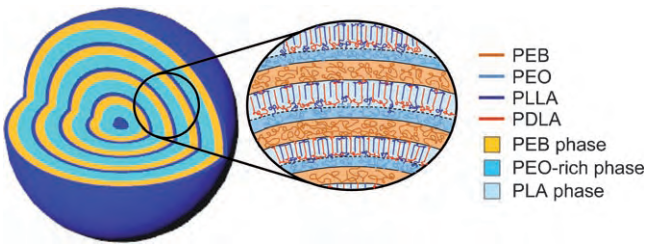

Figure 3. Molecular schemes of a SC5k-EO2k onionlike crystal with a curved noncentrosymmetric lamellar structure.

Supporting Information. The respective thicknesses of the PEO-rich, PEB, and PLA stereocomplex microdomains were 7.02, 9.18, and 4.50 nm for SC5k-EO2k, and 10.85, 7.22, and 8.66 nm for SC5k-EO5k. Since differential scanning calorimetry showed similar melting temperatures (193 °C for SC5k-EO2k and 199 °C for SC5k-EO5k), the thicknesses of the stereocomplex-crystal lamellae in both samples should be similar. It is reasonable to assume that SC5k-EO2k has a noncentrosymmetric structure with a single layer of PLA stereocomplex crystal (thickness ca. 4.5 nm), whereas SC5k-EO5k has a centrosymmetric structure with two layers of PLA stereocomplex crystals, each about 4.3 nm thick, within a long period. Note that the immiscible PEO-rich and PEB layers thus have direct contact, as shown in Figure 3. We speculate that the energy penalty from direct contacts between PEB and PEO could be compensated by lamella bending induced by unbalanced surface stresses. Experimental studies are currently underway to further prove this noncentrosymmetric structure.

Before stereocomplex growth, a honeycomb rather than onion structure was seen in molten SC5k-EO2k at 205 °C.[12] We speculate that formation of the onion structure is closely related to the crystallization process. During crystal growth, screw dislocations might often occur, and they could force a PLA stereocomplex crystal (PEB and PEO at each side of a PLA crystal) to stack into a noncentrosymmetric structure. Detailed stereocomplex crystallization pathways are currently under study.

The maximum and minimum curvature in the onion crystals should be determined by the bending rigidity of stereocomplex crystals, similar to the situation in chrysotile asbestos.[11] From the TEM image in Figure 2 B, the inner and outer onion diameters are 40–50 and 500–700 nm, respectively.

In conclusion, using SAXS and TEM techniques we compared crystalline morphologies in stereocomplexes SC5k-EO5k and SC5k-EO2k. In SC5k-EO5k, PEO and PEB have similar molecular weights (or volumes), and flat lamellar crystals were obtained. In contrast, since PEO had a much smaller molecular weight (or volume) than PEB in SC5k-EO2k, unbalanced surface stresses from the stretching of PEB brushes induced onionlike crystals.

Experimental Section

Model PEO-*b*-PLLA and PEB-*b*-PDLA diblock copolymers were prepared by controlled ring-opening polymerization of L- and D-

 © 2006 Wiley-VCH Verlag GmbH & Co. KGaA, Weinheim

lactides from PEO-OH ($M_n = 2000\ g\,mol^{-1}$ with PDI = 1.07 and $M_n = 5000\ g\,mol^{-1}$ with PDI = 1.08, Aldrich) and PEB-OH ($M_n = 4200\ g\,mol^{-1}$, 67% ethylene and 33% 1-butene, PDI = 1.06, Aldrich), respectively, in toluene with 0.5 equiv $AlEt_3$ as catalyst.[12] PLA molecular weight was controlled by conversion and determined by ^1H NMR spectroscopy on a Bruker DMX 500 spectrometer. To remove unconverted monomers and impurities, crude products were dissolved in chloroform and precipitated in hexanes for PEO-*b*-PLLA (in methanol for PEB-*b*-PDLA). PEO-*b*-PLLA was further washed with methanol (PEB-*b*-PDLA with hexane) twice to remove unconverted PEO-OH (PEB-OH) homopolymer. The PDIs for all samples were determined by SEC with THF as solvent and polystyrene as standard on a Viscotek GPCmax system. To prepare the stereocomplex, PEO-*b*-PLLA (2k–5.4k) and PEO-*b*-PLLA (5k–5.1k) were blended with PEB-*b*-PDLA (4.2k–5.4k) in chloroform at a concentration of 10 wt%. After drying in a vacuum oven at 50 °C for 3 d, stereocomplexes were stored in a desiccator. SAXS and WAXD experiments were performed at the X27C beamline in the National Synchrotron Light Source, Brookhaven National Laboratory. The wavelength of the X-ray beam was 0.137 nm. TEM experiments were performed on a Philips EM300 at an accelerating voltage of 80 kV. Thin sections with a thicknesses of about 75 nm were obtained by using a Leica Ultracut UCT microtome equipped with a diamond knife at −30 °C. Thin sections were collected on 400-mesh TEM grids, freeze-dried, and stained in RuO_4 vapor at room temperature for 30–60 min.

Received: June 25, 2006
Revised: August 9, 2006
Published online: October 13, 2006

Keywords: block copolymers · crystal engineering · phase transitions · self-assembly · stereocomplexes

[1] a) M.-E. Meyre, C. Faure, *Recent Res. Dev. Phys. Chem.* **2004**, *7*, 321–338; b) S. Zhang, D. M. Marini, W. Hwang, S. Santoso, *Curr. Opin. Chem. Biol.* **2002**, *6*, 865–871; c) J. M. Schnur, *Science* **1993**, *262*, 1669–1676.

[2] a) F. Gauffre, D. Roux, *Langmuir* **1999**, *15*, 3738–3747; b) O. Regev, R. Backov, C. Faure, *Chem. Mater.* **2004**, *16*, 5280–5285; c) P. Chenevier, L. Bourel-Bonnet, D. Roux, *J. Am. Chem. Soc.* **2003**, *125*, 16261–16270.

[3] a) P. Sierro, D. Roux, *Phys. Rev. Lett.* **1997**, *78*, 1496–1499; b) P. Versluis, J. C. van de Pas, J. Mellema, *Langmuir* **2001**, *17*, 4825–4835; c) C. Oliviero, L. Coppola, R. Gianferri, I. Nicotera, U. Olsson, *Colloids Surf. A* **2003**, *228*, 85–90.

[4] a) H. Hoffmann, U. Munker, C. Thunig, M. Valiente, *J. Colloid Interface Sci.* **1994**, *163*, 217–228; b) J. Oerdisse, C. Couve, J. Appell, J. F. Berret, C. Ligoure, G. Porte, *Langmuir* **1996**, *12*, 1212–1218.

[5] a) J. Hao, H. Hoffmann, K. Horbaschek, *J. Phys. Chem. B* **2000**, *104*, 10144–10153; b) A. Song, S. Dong, X. Jia, J. Hao, W. Liu, T. Liu, *Angew. Chem.* **2005**, *117*, 4086–4089; *Angew. Chem. Int. Ed.* **2005**, *44*, 4018–4021.

[6] a) B. J. Battersby, R. Grimm, S. Huebner, G. Cevc, *Biochim. Biophys. Acta* **1998**, *1372*, 379–383; b) S. Hubner, B. J. Battersby, R. Grimm, G. Cevc, *Biophys. J.* **1999**, *76*, 3158–3166.

[7] L. Ramos, D. Roux, P. D. Olmsted, M. E. Cates, *Europhys. Lett.* **2004**, *66*, 888–894.

[8] a) P. Boltenhagen, O. D. Lavrentovich, M. Kléman, *Phys. Rev. A* **1992**, *46*, R1743–R1746; b) M. C. Choi, T. Pfohl, Z. Wen, Y. Li, M. W. Kim, J. N. Israelachvili, C. R. Safinya, *Proc. Natl. Acad. Sci. USA* **2004**, *101*, 17340–17344.

[9] a) K. M. Hong, J. Noolandi, *Macromolecules* **1983**, *16*, 1083–1093; b) S. Koizumi, H. Hasegawa, T. Hashimoto, *Macromolecules* **1994**, *27*, 6532–6540.

[10] J.-J. Zhang, G. Jin, Y. Ma, *J. Phys. Condens. Matter* **2006**, *18*, 837–845.

[11] B. Lotz, S. Z. D. Cheng, *Polymer* **2005**, *46*, 577–610, and references therein.

[12] L. Sun, J. E. Ginorio, L. Zhu, I. Sics, L. Rong, B. S. Hsiao, *Macromolecules*, submitted.

[13] a) L. Cartier, T. Okihara, B. Lotz, *Macromolecules* **1997**, *30*, 6313–6322; b) L. Cartier, T. Okihara, Y. Ikada, H. Tsuji, J. Puiggali, B. Lotz, *Polymer* **2000**, *41*, 8909–8919.

 © 2006 Wiley-VCH Verlag GmbH & Co. KGaA, Weinheim

Nonlinear Optics

DOI: 10.1002/anie.200602684

Electrochemical Switching of the Cubic Nonlinear Optical Properties of an Aryldiethynyl-Linked Heterobimetallic Complex between Three Distinct States**

Marek Samoc, Nicolas Gauthier, Marie P. Cifuentes, Frédéric Paul,* Claude Lapinte, and Mark G. Humphrey**

Materials with nonlinear optical (NLO) properties are required in emerging photonics-based technologies for various applications, including processing of optical signals, optical data storage, nanophotonics, and biophotonics.[1–3]

[*] Dr. M. Samoc
Laser Physics Centre
Research School of Physical Sciences and Engineering
Australian National University
Canberra, ACT 0200 (Australia)
Fax: (+61) 2-6125-0029
E-mail: marek.samoc@.anu.edu.au

N. Gauthier, Dr. F. Paul, Dr. C. Lapinte
Sciences Chimiques de Rennes
UMR CNRS 6226
Université de Rennes 1
Campus de Beaulieu, 35042 Rennes Cedex (France)
Fax: (+33) 2-2323-5637
E-mail: frederic.paul@univ-rennes1.fr

Dr. M. P. Cifuentes, Prof. M. G. Humphrey
Department of Chemistry
Australian National University
Canberra, ACT 0200 (Australia)
Fax: (+61) 2-6125-0760
E-mail: mark.humphrey@anu.edu.au

[**] We thank the Australian Research Council (ARC) and the CNRS for financial support. This project is supported by the International Science Linkages Programme established under the Australian Government's innovation statement, Backing Australia's Ability. F.P. and N.G. thank Region Bretagne for financial support. M.G.H. thanks Johnson Matthey Technology Centre for the generous loan of ruthenium salts. M.G.H. is an ARC Australian Professorial Fellow and M.P.C. is an ARC Australian Research Fellow.

Supporting information for this article is available on the WWW under http://www.angewandte.org or from the author.

WILEY InterScience DISCOVER SOMETHING GREAT
© 2006 Wiley-VCH Verlag GmbH & Co. KGaA, Weinheim

Although the focus was initially on the preparation of compounds with large nonlinearities, there has been significant recent interest in the reversible switching or modulation of NLO properties.[4–13] Switching of NLO properties has been achieved by protonation/deprotonation, oxidation/reduction, and photoisomerization sequences, but cubic NLO switchable systems have thus far been restricted to two NLO "states".[14] The coupling of two different ligated metal centers with well-separated redox potentials and distinct linear optical properties by an appropriate molecular linker could in principal permit switching between three redox states and, potentially, afford up to three linear-optical and NLO states. We report herein linear and nonlinear electrochromism of a mixed iron–ruthenium complex along with switching its NLO properties at more than one wavelength and between three distinct cubic NLO states.

The complex chosen for the current study (**1**) was prepared by an extension of standard procedures.[15] We

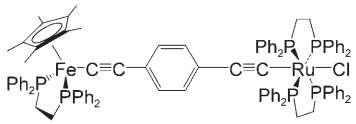

1

have previously shown that the NLO properties of homometallic iron or ruthenium alkynyl complexes can be conveniently switched electrochemically through the reversible M^{II}/M^{III} couples.[7,9,10,12,13] The Fe^{II}/Fe^{III} and Ru^{II}/Ru^{III} couples are far removed from one another, and, under electrochemical control, one can access the Fe^{II}/Ru^{II}, Fe^{III}/Ru^{II}, or Fe^{III}/Ru^{III} states (**1**, $\mathbf{1}^+$, and $\mathbf{1}^{2+}$, respectively) by applying a potential of −0.6, 0, or +0.8 V (vs. Ag/AgCl).

The UV/Vis/NIR spectra of **1**, $\mathbf{1}^+$, and $\mathbf{1}^{2+}$ in CH_2Cl_2 are shown in Figure 1. Complex **1** is essentially transparent at wavelengths longer than 600 nm; oxidation to $\mathbf{1}^+$ affords an optical spectrum with a broad band centered at 1124 nm, and further oxidation to $\mathbf{1}^{2+}$ results in a decrease in intensity of this band and the appearance of strong bands centered at 706 and 914 nm. Cycling between the three oxidation states of the

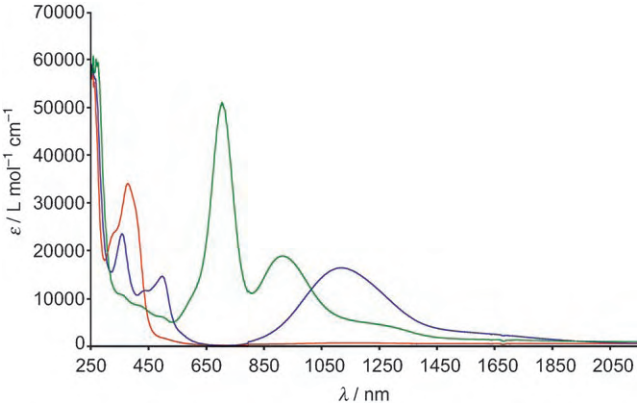

Figure 1. UV/Vis/NIR spectra of **1** (red trace), $\mathbf{1}^+$ (blue trace), and $\mathbf{1}^{2+}$ (green trace) in CH_2Cl_2.

complex in solution in an optically transparent thin-layer electrochemical (OTTLE) cell can be achieved by applying the appropriate potentials; isosbestic points are observed in the UV/Vis/NIR spectra, which is consistent with fully reversible electrochemical conversions between the three forms.

A change in linear optical properties can be accompanied by a change in nonlinear properties, so the possibility of NLO switching was examined for solutions of the complex in CH_2Cl_2 in a specially modified OTTLE cell[7] at 790 and 1200 nm, wavelengths at which the $\mathbf{1}^{2+}$ and $\mathbf{1}^+$ forms, respectively, possess strong linear optical absorption, and which are therefore candidate wavelengths for NLO switching. The third-order NLO properties were assessed by a combination of open- and closed-aperture *Z*-scan experiments.

The effect of applied potential on the open-aperture signal (from which the imaginary component of the nonlinearity is available) is shown in Figures 2 and 3. Cation $\mathbf{1}^+$

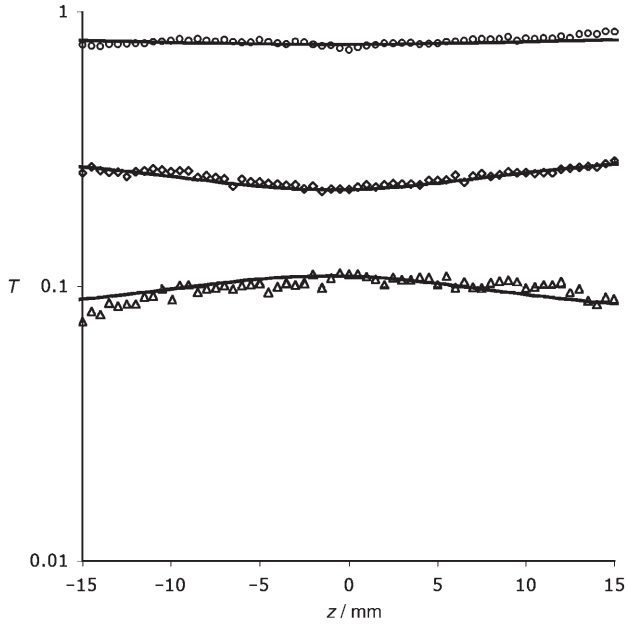

Figure 2. Open-aperture scans at 790 nm at an applied potential of 0 V (diamonds, $\mathbf{1}^+$), −0.6 V (circles, **1**), and +0.8 V (triangles, $\mathbf{1}^{2+}$). Lines denote theoretically computed *Z*-scans. The complex is a two-photon absorber at 0 V, shows almost no nonlinear absorption at the negative potential, and is a saturable absorber at the positive potential. *T* = open-aperture transmittance.

was found to be an efficient two-photon absorber at 790 nm. Scans in which the potential applied to the working electrode was negative indicated that the neutral form **1** exhibits a negligible nonlinear absorption and that the doubly oxidized form $\mathbf{1}^{2+}$, obtained by switching to positive potential, is a one-photon absorber and a saturable absorber at 790 nm. These changes of the imaginary part of the third-order polarizability γ were also accompanied by changes in the real part of the hyperpolarizability that were assessed by closed-aperture *Z*-scan, but it could only be established that the real part of γ for $\mathbf{1}^+$ is negative and that the real part of γ for **1** and $\mathbf{1}^{2+}$ could not

 © 2006 Wiley-VCH Verlag GmbH & Co. KGaA, Weinheim

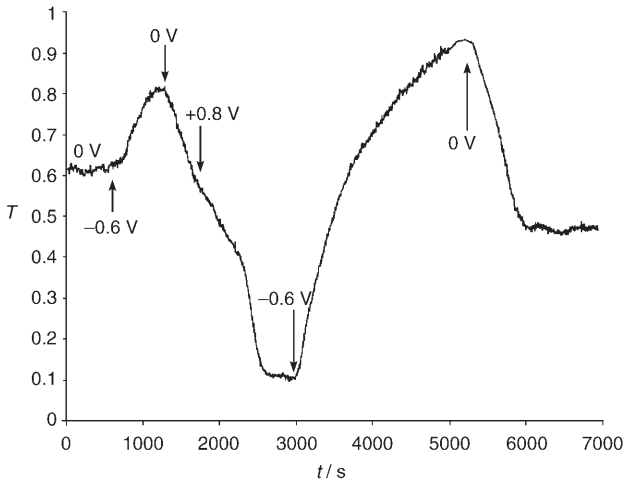

Figure 3. The $z=0$ open-aperture Z-scan signal at 790 nm as a function of time and potential. Arrows show application of the electrochemical potentials.

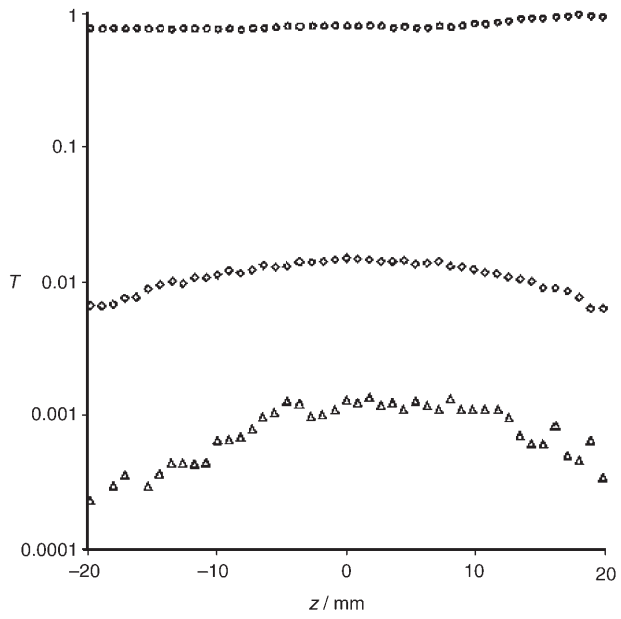

Figure 4. Open-aperture Z-scans at 1200 nm (0 V: diamonds, −0.6 V: circles, +0.8 V: triangles). The presence of maxima in scans at 0 and +0.8 V indicates saturable absorption.

be reliably determined. Table 1 summarizes the data at 790 nm.

Table 1: Experimental cubic nonlinear optical response parameters.

Cmpd[a]	γ_{real}[b]	γ_{imag}[b]	$\lvert\gamma\rvert$[b]	σ_2[c]
1	<100	<100	ca. 0	ca. 0
$\mathbf{1}^{+}$	-450 ± 100	1600 ± 200	1700 ± 250	420 ± 50
$\mathbf{1}^{2+}$	<300	-970 ± 200	1000 ± 300	-250 ± 50

[a] Conditions: measurements were carried out in CH_2Cl_2 at 790 nm; values are referenced to the nonlinear refractive index of silica $n_2=3\times10^{-16}$ cm^2 W^{-1}. [b] 10^{-36} esu. [c] 10^{-50} cm^4 s (=Goeppert–Mayer unit).

Measurements carried out at 1200 nm reveal behavior that differs from that at 790 nm (Table 2), and the open-aperture traces are displayed in Figure 4. The magnitudes of the parameters for the nonlinear effects at 1200 nm cannot be readily determined quantitatively because the open-aperture scans cannot be accurately fitted with the approximation that was used at 790 nm, namely, that absorption saturation is a negative analogue of two-photon absorption (i.e., the absorption coefficient is approximated as $\alpha=\alpha_0-\beta I$, whereby I is the intensity and β is the nonlinear absorption coefficient). This approximation is known to fail in the case of strong absorption-saturation effects.[16]

Table 2: Nonlinear absorption behavior of **1**, $\mathbf{1}^{+}$, and $\mathbf{1}^{2+}$ at 790 and 1200 nm.

Cmpd	790 nm	1200 nm
1	negligible	negligible
$\mathbf{1}^{+}$	two-photon absorber	saturable absorber
$\mathbf{1}^{2+}$	saturable absorber	saturable absorber

In conclusion, oxidation processes in this heterobimetallic complex "switch on" optical transitions at long wavelength, and these linear electrochromic effects are accompanied by modifications in the NLO properties. To the best of our knowledge, the effect observed at 790 nm constitutes the first example of cubic NLO switching between three states (nonlinearity "off", and two forms of nonlinearity "on", namely, two-photon absorber and saturable absorber, which correspond to differences in sign of the imaginary component of the third-order nonlinearity). The switching phenomenon is not restricted to this wavelength range; a system corresponding to nonlinearity "off" in the neutral complex and "on" in the oxidized forms is observed at the longer wavelength.

Experimental Section

Complex **1** was prepared by standard procedures.[15] Third-order nonlinearities of **1**, $\mathbf{1}^{+}$, and $\mathbf{1}^{2+}$ were investigated by Z-scan measurements at 790 and 1200 nm. Complex **1** was examined in an OTTLE cell by using a laser system with a Clark-MXR regenerative amplifier pumping a light-conversion TOPAS optical parametric amplifier. The measurements at 790 nm were performed with the doubled idler from the TOPAS and the measurements at 1200 nm used the signal from the TOPAS. The repetition rate of the regenerative amplifier was set to 82 Hz to reduce problems with thermal nonlinearity and the possibility of material photodecomposition. The pulse duration was about 150 fs. The Z-scan system used a focused spot with $w_0=65$ μm at 790 nm and $w_0=80$ μm at 1200 nm, as was found from numerical fitting of closed-aperture scans for fused silica samples. Measurements on silica also served for calibration of the light intensities and therefore magnitudes of the nonlinearities. It was assumed that the nonlinear index of silica was $n_2=3\times10^{-16}$ cm^2 W^{-1}.

Solutions of **1** (concentration = 0.896 % w/w for measurements at 790 nm and 0.9 % w/w for measurements at 1200 nm) in dichloromethane were placed in a glass (0.5-mm path length) electrochemical cell equipped with a large-area platinum working electrode with a 1.5-mm-diameter round hole. The Z-scan experiments were carried out

 © 2006 Wiley-VCH Verlag GmbH & Co. KGaA, Weinheim

by passing the focused beam through that hole. Electrochemically induced linear and nonlinear optical property changes were investigated either by recording the transmission through the hole at a fixed position of the electrochemical cell (see Figure 3) or by performing scans in which the z coordinate (i.e., the distance of the sample from the focal plane of the lens) was scanned between $z = -20$ and 20 mm (see Figure 2 for open-aperture scans).

Received: July 5, 2006
Published online: October 11, 2006

Keywords: alkynyl ligands · electrochemistry · molecular switches · nonlinear optics

[1] J. L. Brédas, C. Adant, P. Tackx, A. Persoons, *Chem. Rev.* **1994**, *94*, 243.
[2] P. N. Prasad, *Introduction to Biophotonics*, Wiley, New York, **2003**.
[3] P. N. Prasad, *Nanophotonics*, Wiley, New York, **2004**.
[4] B. J. Coe, *Chem. Eur. J.* **1999**, *5*, 2464.
[5] J. A. Delaire, K. Nakatani, *Chem. Rev.* **2000**, *100*, 1817.
[6] T. Weyland, I. Ledoux, S. Brasselet, J. Zyss, C. Lapinte, *Organometallics* **2000**, *19*, 5235.
[7] M. P. Cifuentes, C. E. Powell, M. G. Humphrey, G. A. Heath, M. Samoc, B. Luther-Davies, *J. Phys. Chem. A* **2001**, *105*, 9625.
[8] M. Malaun, R. L. Paul, J. C. Jeffery, J. A. McCleverty, M. D. Ward, I. Asselberghs, K. Clays, A. Persoons, *Chem. Commun.* **2001**, 49.
[9] C. E. Powell, M. P. Cifuentes, J. P. Morrall, R. Stranger, M. G. Humphrey, M. Samoc, B. Luther-Davies, G. A. Heath, *J. Am. Chem. Soc.* **2003**, *125*, 602.
[10] C. E. Powell, M. G. Humphrey, M. P. Cifuentes, J. P. Morrall, M. Samoc, B. Luther-Davies, *J. Phys. Chem. A* **2003**, *107*, 11264.
[11] I. Asselberghs, K. Clays, A. Persoons, A. M. McDonagh, M. D. Ward, J. A. McCleverty, *Chem. Phys. Lett.* **2003**, *368*, 408.
[12] F. Paul, K. Costuas, I. Ledoux, S. Deveau, J. Zyss, J.-F. Halet, C. Lapinte, *Organometallics* **2002**, *21*, 5229.
[13] M. P. Cifuentes, M. G. Humphrey, J. P. Morrall, M. Samoc, F. Paul, T. Roisnel, C. Lapinte, *Organometallics* **2005**, *24*, 4280.
[14] Switching quadratic NLO properties between three states has recently been demonstrated: C. Sporer, I. Ratera, D. Ruiz-Molina, Y. Zhao, J. Vidal-Gancedo, K. Wurst, P. Jaitner, K. Clays, A. Persoons, C. Rovira, J. Veciana, *Angew. Chem.* **2004**, *116*, 5378; *Angew. Chem. Int. Ed.* **2004**, *43*, 5266.
[15] N. Gauthier, D. Touchard, S. Rigaut, C. Olivier, M. P. Cifuentes, F. Paul, C. Lapinte, M. G. Humphrey, M. Samoc, unpublished results. Complete synthesis and characterization details for **1** are given in the Supporting Information.
[16] M. Samoc, A. Samoc, B. Luther-Davies, H. Reisch, U. Scherf, *Opt. Lett.* **1998**, *23*,1295.

 © 2006 Wiley-VCH Verlag GmbH & Co. KGaA, Weinheim

Molecular Wheels

DOI: 10.1002/anie.200602743

Reversible Size Modification of Iron and Gallium Molecular Wheels: A Ga_{10} "Gallic Wheel" and Large Ga_{18} and Fe_{18} Wheels**

*Philippa King, Theocharis C. Stamatatos, Khalil A. Abboud, and George Christou**

Complexes of high nuclearity, symmetry, and architectural beauty have long fascinated chemists, owing both to their aesthetically pleasing nature and to their often interesting properties. A particularly intriguing type within this class is the single-strand molecular wheel, whose prototype [{Fe-$(OMe)_2(O_2CCH_2Cl)\}_{10}$] was dubbed the "ferric wheel"[1] and was also later reported with other carboxylates.[2] Many other Fe_x wheels have since been reported and now comprise the largest family of known molecular wheels.[3] There are, however, other examples composed of Co,[4] Cr,[2c,5] Cu,[6] Dy,[7] Mo,[8] Mn,[9] Ni[10] and V metal centers.[11]

Molecular wheels almost always contain an even number of metal ions, with nuclearities including 6,[3a,c] 8,[2e,3h,11a] 10,[2c,7] 12,[3g,6b,9d,10c] 16,[9c] 18,[12] 24,[10b] and 84;[9b] there are only a very few odd-membered wheels.[11b,13] Most even-membered wheels are antiferromagnetic with $S=0$ ground states,[2a,6b,14] and represent ideal model systems for the study of one-dimensional magnetism, magnetic anisotropy,[15] and quantum effects such as coherent tunneling of the Néel vector.[16] However, there are also many wheels with large S values, such as Ni_{12},[10c] Mn_{12},[9d] and Mn_{16} species,[9c] that are also single-molecule magnets (SMMs). Antiferromagnetic odd-membered wheels represent a simple system for studying spin frustration.[17] Multiple-strand, torus-shaped wheels are also known, such as Mn_{84},[9b] Mo_{154},[8] and Mo_{176} species.[8]

We have recently become interested in developing new synthetic routes to molecular wheels, but also in developing some level of control of the metal nuclearity (that is, the wheel size) for a given ligand type. Almost all wheel compounds were originally prepared serendipitously, but methods of deliberately altering the wheel size after the initial synthesis are very few and all based on a template approach. Saalfrank et al. elegantly showed that the size of certain Fe_x wheels could be controlled by the central Group 1 metal ion template around which the wheel forms, thus giving $\{Fe_6M\}$ for $M=Li^+$ or Na^+, but $\{Fe_8M\}$ for $M=Cs^+$.[18] Similarly, Winpenny, Timco, and co-workers found that the organic amine template controls the nuclearity of the M_x ($x=$ 8–10) homo- or heterometallic wheels.[19] Because almost all

[*] Dr. P. King, T. C. Stamatatos, Dr. K. A. Abboud, Prof. Dr. G. Christou
Department of Chemistry
University of Florida
Gainesville, FL 32611-7200 (USA)
Fax: (+1) 352-392-8757
E-mail: christou@chem.ufl.edu

[**] This work was supported by the National Science Foundation.

© 2006 Wiley-VCH Verlag GmbH & Co. KGaA, Weinheim

single-strand wheels are of nuclearity 12 or less and because a template approach is much less feasible for larger wheels (since it requires a correspondingly larger template), we have sought alternative means of modifying the wheel size. We report herein a) the first gallium(III) molecular wheels and b) a nontemplate route for reversibly interconverting the Ga and Fe wheel size between M_{10} and M_{18}. Result (b) arises from use of 1,3-propanediolate, a ligand type with little previous employment in metal chemistry.[20]

We suspected the Ga^{III} analogue of the "ferric wheel" should be accessible, and sought it from the reaction of $Ga(NO_3)_3$ with NaO_2CMe in a 1:1 ratio in MeOH. Diffusion of Et_2O into the resulting solution yielded colorless crystals of $[\{Ga(OMe)_2(O_2CMe)\}_{10}]\cdot x\,MeOH$ (**1**$\cdot x\,$MeOH) in 26% yield. The crystal structure of **1** (Figure 1)[21a] confirms the desired

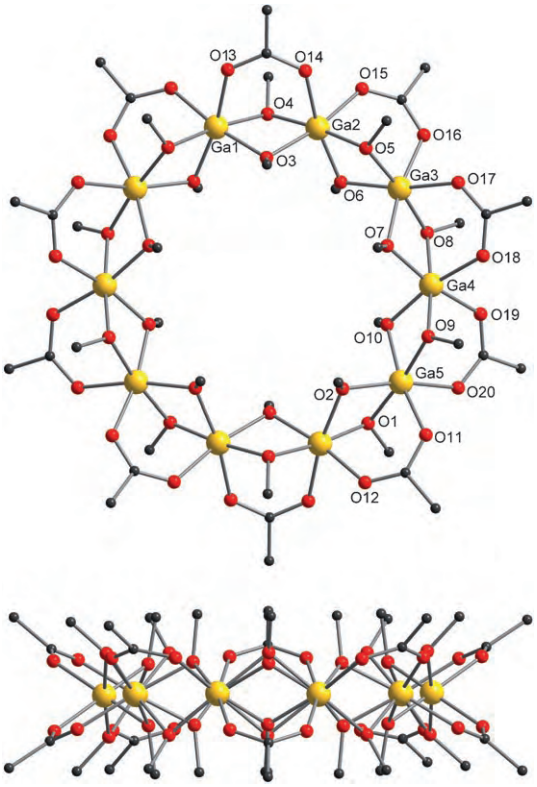

Figure 1. Top: Molecular structure of **1**. Bottom: Side view of **1** emphasizing the wheel planarity and O/Ga/O layered structure (Ga yellow, O red, C gray). Hydrogen atoms have been omitted for clarity.

"gallic wheel", which consists of ten Ga^{III} ions of near-octahedral geometry with each Ga_2 pair bridged by one $MeCO_2^-$ ligand and two MeO^- groups, thus isostructural with the "ferric wheels". The side view in Figure 1 shows the planar Ga_{10} unit sandwiched between two layers of O atoms.

We then undertook the challenge of altering the wheel size in a nontemplate manner. Figure 1 shows that the methoxide locations would allow a bulkier alkoxide ligand to be accommodated without requiring wheel expansion. We thus reasoned instead that if adjacent MeO^- groups were linked within a diolate group, this might affect the ring curvature and yield a bigger wheel. A smaller wheel seemed unlikely in view of the resulting steric congestion in the central hole. Of course, the extra restrictions imposed by the diolate group could instead lead to a nonwheel product, as nothing is guaranteed in synthetic chemistry. Nevertheless, we chose 1,3-propanediol (pdH_2) as the diol, and carried out the 1:1 reaction of $Ga(NO_3)_3$ with NaO_2CMe in pdH_2/MeCN, followed by diffusion of Et_2O into the resulting solution. Colorless crystals slowly grew to give the wheel complex $[Ga_{18}(pd)_{12}(pdH)_{12}(O_2CMe)_6(NO_3)_6](NO_3)_6\cdot x\,MeCN$ (**2**$\cdot x\,$MeCN) in 35% yield. The centrosymmetric cation of **2** (Figure 2)[21b] comprises 18 Ga^{III} ions linked through acetate, pd^{2-}, and pdH^- bridges to form a puckered wheel, which can be conveniently described as a hexagon of $\{Ga_3(pd)_2(NO_3)\}$ units (Ga9-Ga1-Ga2, Ga3-Ga4-Ga5, etc.) linked at each vertex by an acetate group and two pdH^- groups (Figure 2, bottom); the latter groups each bridge separate Ga_3 units with their deprotonated O atom and bind terminally with their protonated OH group. The central Ga ion (Ga1, Ga4, Ga7) of each

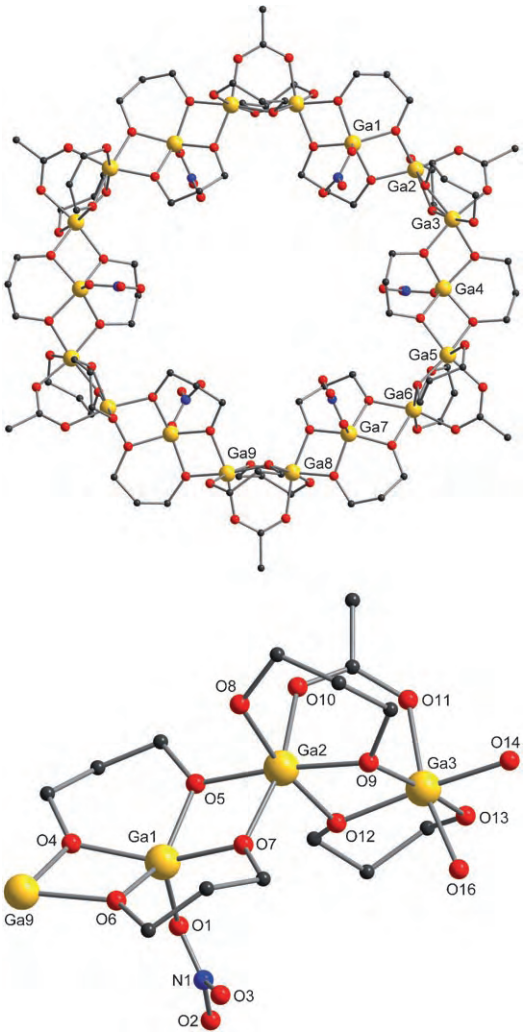

Figure 2. Top: Molecular structure of the cation of **2**. Bottom: Enlarged view of a trinuclear $\{Ga_3(pd)_2(NO_3)\}$ unit (Ga9/Ga1/Ga2) and the means of attachment to Ga3 of an adjacent unit(Ga yellow, O red, N blue, C gray). Hydrogen atoms have been omitted for clarity.

 © 2006 Wiley-VCH Verlag GmbH & Co. KGaA, Weinheim

near-linear Ga_3 unit (Ga-Ga-Ga 146.81–153.39°) exhibits square-pyramidal geometry, whereas the others have octahedral geometry. The pd^{2-} groups within each Ga_3 unit doubly bridge with each O atom, as seen previously in a Ga-Fe-Ga complex.[19b] Thus, although each pd^{2-} group did not merely replace two MeO^- groups of $[\{Ga(OMe)_2(O_2CMe)\}_{10}]$ (**1**) to give a larger $[\{Ga(pd)(O_2CMe)\}_x]$ wheel ($x > 10$), its restrictive diolate nature nevertheless did as we had hoped, but in a different way, and gave a large $[Ga_x(pd)_{2x/3}(pdH)_{2x/3}(O_2CMe)_{x/3}(NO_3)_{x/3}]_x^{6+}$ ($x = 18$) wheel.

Since pdH_2 gave a Ga_{18} wheel instead of Ga_{10}, we investigated whether it would similarly give an Fe_{18} wheel rather than Fe_{10}. Various carboxylates were explored, and benzoate gave the most crystalline product. Thus, the 1:1 reaction of $Fe(NO_3)_3 \cdot 9H_2O$ with NaO_2CPh in pdH_2/MeCN and subsequent diffusion of Et_2O into the yellow solution yielded yellow crystals of $[Fe_{18}(pd)_{12}(pdH)_{12}(O_2CPh)_6(NO_3)_6](NO_3)_6 \cdot x\,MeCN$ (**3**·*x* MeCN) in 87% yield. The cation of **3**[21c] is isostructural with **2**, except for the carboxylate identity (Figure 3). The cation of **3** thus joins $[Fe_{18}(OH)_6(OMe)_{24}(xdk)_6(O_2CMe)_{12}]$[12] (xdk = *m*-xylenediamine bis(Kemp's triacid imide) dianion) as the largest Fe^{III} wheels to date.

Wheels **1**–**3** are shown as space-filling representations in Figure 4. The Ga_{10} wheel **1** has a diameter of 16.7 Å, with a central hole of diameter 8.1 Å. The Ga_{18} wheel **2** is larger, with a diameter of 23.7 Å and a central hole of diameter 10.4 Å. The Fe_{18} wheel **3** is larger than **2** owing to the different carboxylate groups and has a diameter of 29.9 Å, but the central hole is very similar to that of **2** with a diameter of 10.7 Å. In all three complexes, there is no residual electron density in the central hole, and the wheels stack to form tubular channels.

We conclude that the M_{10} versus M_{18} wheel size is a result of the differing nature of MeO^- versus diolate bridges. In support of this conclusion, we successfully converted the M_{18} wheels into M_{10} by dissolution of **3** in MeOH; yellow needles slowly formed that were identified by elemental analysis and X-ray crystallography as $[Fe_{10}(OMe)_{20}(O_2CPh)_{10}]$ (**4**) in

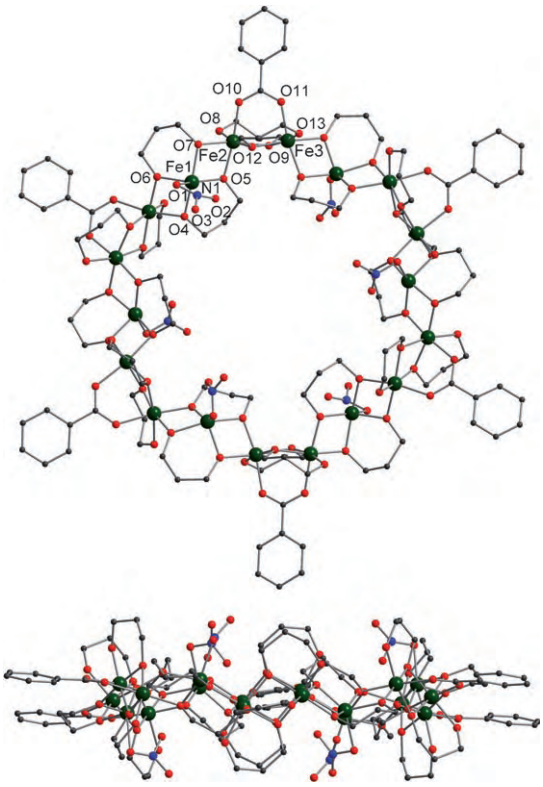

Figure 3. Top: Molecular structure of the cation of **3**. Bottom: Side view emphasizing the puckering (Fe green, O red, N blue, C gray). Hydrogen atoms have been omitted for clarity.

greater than 90% yield. Similar treatment of **2** gave white crystals of **1**. Thus, replacement of the pd^{2-} and pdH^- groups with MeO^- converts M_{18} wheels into M_{10}, consistent with this being the preferred size with methoxide. Similarly, dissolution of the Fe_{10} wheel in pdH_2/MeCN/$NaNO_3$ led to subsequent isolation of the corresponding Fe_{18} wheel in about 20% yield, but the product was contaminated with white solids. A cleaner conversion was achieved by addition of soluble $Fe(NO_3)_3$ to the Fe_{10} wheel in pdH_2/MeCN, which increased the yield of

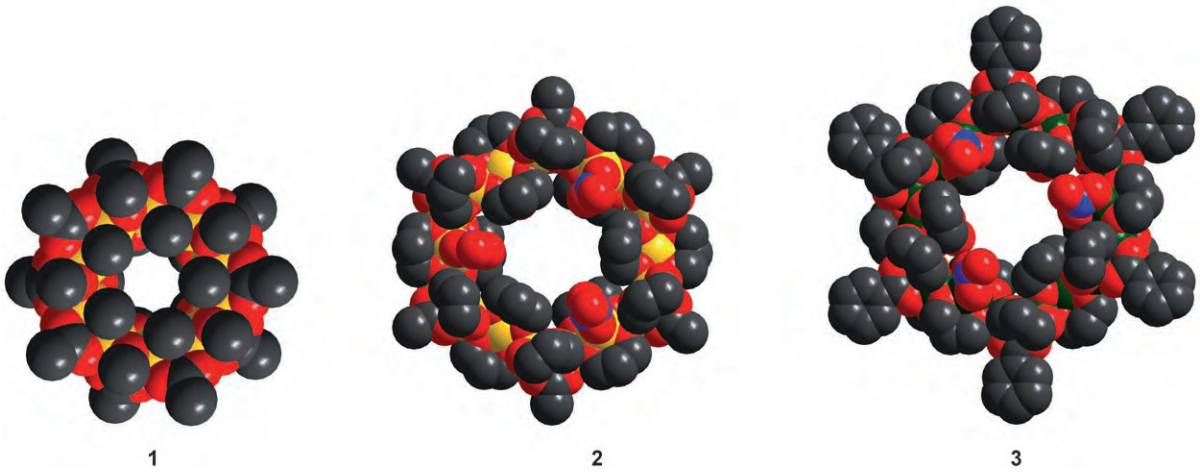

Figure 4. Comparison of the space-filling representations of compounds **1**, **2**, and **3** showing the differing interior cavity diameters (Ga yellow, O red, N blue, C gray, Fe green).

© 2006 Wiley-VCH Verlag GmbH & Co. KGaA, Weinheim

the Fe_{18} wheel to 40%, presumably by helping sequester the carboxylate groups. The conclusion is again that the pd^{2-} group gives a larger wheel than methoxide.

Magnetic susceptibility (χ_M) measurements were performed on a vacuum-dried, polycrystalline sample of **3** in the 5.0–300 K range and in a 0.1 T magnetic field. The value of $\chi_M T$ decreases steadily with decreasing temperature from 29.22 $cm^3 mol^{-1} K$ at 300 K to 0.90 $cm^3 mol^{-1} K$ at 5.0 K (Figure 5). This trend indicates an $S = 0$ ground state, as expected for antiferromagnetic interactions between an even number of high-spin ($S = 5/2$) Fe^{III} ions.[2a,e,14]

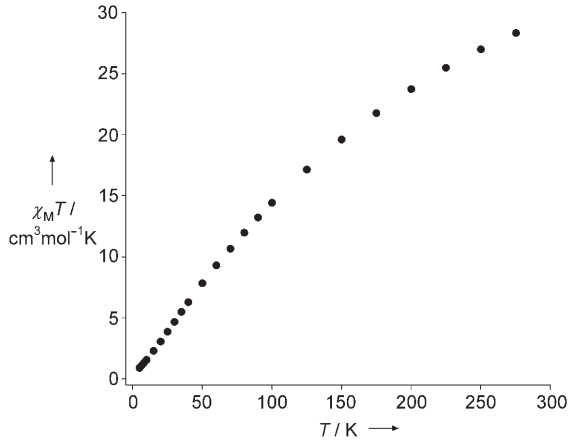

Figure 5. Plot of $\chi_M T$ versus T for complex **3**.

In conclusion, the first gallium wheels have been prepared, together with a nontemplate method for increasing the size of both Ga_{10} and Fe_{10} wheels. This procedure keeps the central cavity empty, imparting tubular channels to the crystal. The "gallic wheel" **1** is isostructural with the "ferric wheel",[1] and Ga_{18} and Fe_{18} are also isostructural, thus consistent with the similar chemistry of Fe^{III} and Ga^{III}. Moreover, M_{10} and M_{18} can be interconverted by alkoxide substitution. This work is currently being extended to other diols, such as 1,2-ethanediol and 1,4-butanediol.

Experimental Section

1: $Ga(NO_3)_3 \cdot x H_2O$ (0.051 g, 0.20 mmol) was added to a stirred solution of sodium acetate (0.016 g, 0.20 mmol) in MeOH (10 mL). The colorless solution was stirred for 10 min further and filtered, and the filtrate was layered with Et_2O. After one day, colorless crystals of $[Ga_{10}(OMe)_{20}(O_2CMe)_{10}] \cdot x$ MeOH were collected by filtration, washed with MeOH, and dried in vacuo. Yield: 26%. Elemental analysis (%) calcd for **1**: C 25.18, H 4.75; found: C 24.97, H 4.61. Selected IR data (KBr): $\tilde{\nu} = 3440$(w), 2940(m), 2833(s), 1633(m), 1551(s), 1452(s), 1384(s), 1052(m), 682(s), 621(s), 548(s), 507(s), 474(s), 425 cm^{-1} (s).

2: $Ga(NO_3)_3 \cdot x H_2O$ (0.051 g, 0.20 mmol) was added to a stirred solution of sodium acetate (0.016 g, 0.20 mmol) in pdH_2/MeCN (3 mL/20 mL). The solution was stirred for 10 min further and filtered, and the filtrate was layered with Et_2O. After one day, colorless crystals of $[Ga_{18}(O_2CMe)_6(pd)_{12}(pdH)_{12}(NO_3)_6](NO_3)_6 \cdot 12$ MeCN were collected by filtration, washed with MeCN, and dried in vacuo. Yield: 35%. The dried material is hygroscopic and was analyzed as $2 \cdot 6NO_3 \cdot 8H_2O$. Elemental analysis (%) calcd for $2 \cdot 6NO_3 \cdot 8H_2O$: C 23.53, H 4.47, N 3.92; found: C 23.37, H 4.27, N 3.75. Selected IR data (KBr): $\tilde{\nu} = 3391$(w), 2950(m), 2890(m), 1656(m), 1559(s), 1384(m), 1180(s), 1059(m), 979(s), 937(m), 825(s), 684(s), 527 cm^{-1} (w).

3: $Fe(NO_3)_3 \cdot 9H_2O$ (0.081 g, 0.20 mmol) was added to a stirred solution of sodium benzoate (0.029 g, 0.20 mmol) in pdH_2/MeCN (3 mL/20 mL). The yellow solution was stirred for 10 min further and filtered, and the filtrate was layered with Et_2O. After one day, yellow crystals of $[Fe_{18}(O_2CPh)_6(pd)_{12}(pdH)_{12}(NO_3)_6](NO_3)_6 \cdot 48$ MeCN had formed and were collected by filtration, washed with MeCN, and dried in vacuo. Yield: 87%. The dried material is hygroscopic and was analyzed as $3 \cdot 6NO_3 \cdot 10H_2O$. Elemental analysis (%) calcd for $3 \cdot 6NO_3 \cdot 10H_2O$: C 30.80, H 4.67, N 3.78; found: C 30.62, H 4.42, N 3.59. Selected IR data (KBr): $\tilde{\nu} = 3380$(w), 2944(m), 2864(m), 1647(m), 1592(s), 1527(s), 1493(s), 1404(s), 1384(s), 1352(s), 1177(s), 1122(s), 1050(s), 974(s), 936(m), 822(s), 722(s), 679(s), 538(m), 476 cm^{-1} (m).

Received: July 10, 2006
Published online: October 18, 2006

Keywords: gallium · iron · molecular wheels · propanediol · structure elucidation

[1] K. L. Taft, S. J. Lippard, *J. Am. Chem. Soc.* **1990**, *112*, 9629.
[2] a) K. L. Taft, C. D. Delfs, G. C. Papaefthymiou, S. Foner, D. Gatteschi, S. J. Lippard, *J. Am. Chem. Soc.* **1994**, *116*, 823; b) C. Benelli, S. Parsons, G. A. Solan, R. E. P. Winpenny, *Angew. Chem.* **1996**, *108*, 1967; *Angew. Chem. Int. Ed. Engl.* **1996**, *35*, 1825; c) E. J. L. McInnes, C. Anson, A. K. Powell, A. J. Thomson, S. Poussereau, R. Sessoli, *Chem. Commun.* **2001**, 89; d) M. Helliwell, A. A. Smith, S. J. Teat, R. E. P. Winpenny, *Inorg. Chim. Acta* **2003**, 49; e) C. Cañada-Vilalta, M. Pink, G. Christou, *Chem. Commun.* **2003**, 1240.
[3] a) G. L. Abbati, A. Cornia, A. C. Fabretti, W. Malavasi, L. Schenetti, A. Caneschi, D. Gatteschi, *Inorg. Chem.* **1997**, *36*, 6443; b) M. Frey, S. G. Harris, J. M. Holmes, D. A. Nation, S. Parsons, P. A. Tasker, S. J. Teat, R. E. P. Winpenny, *Angew. Chem.* **1998**, *110*, 3436; *Angew. Chem. Int. Ed.* **1998**, *37*, 3246; c) O. Waldmann, J. Schülein, R. Koch, P. Müller, I. Bernt, R. W. Saalfrank, H. P. Andres, H. U. Guldel, P. Allenspach, *Inorg. Chem.* **1999**, *38*, 5879; d) R. W. Saalfrank, I. Bernt, M. M. Chowdhry, F. Hampel, G. B. N. Vaughan, *Chem. Eur. J.* **2001**, *7*, 2765; e) O. Waldmann, R. Koch, S. Schromm, J. Schülein, P. Müller, I. Bernt, R. W. Saalfrank, F. Hampel, E. Balthes, *Inorg. Chem.* **2001**, *40*, 2986; f) H. Kooijman, A. L. Spek, E. Bouwman, F. Micciche, S. T. Warzeska, J. Reedijk, *Acta Crystallogr. Sect. E* **2002**, *58*, m93; g) L. F. Jones, A. Batsanov, E. K. Brechin, D. Collison, M. Helliwell, T. Mallah, E. J. L. McInnes, S. Piligkos, *Angew. Chem.* **2002**, *114*, 4494; *Angew. Chem. Int. Ed.* **2002**, *41*, 4318; h) A.-A. H. Abu-Nawwas, J. Cano, P. Christian, T. Mallah, G. Rajaraman, S. J. Teat, R. E. P. Winpenny, Y. Yukawa, *Chem. Commun.* **2004**, 314; i) S. Lin, S-X. Liu, Z. Chen, B.-Z. Lin, S. Gao, *Inorg. Chem.* **2004**, *43*, 2222.
[4] a) J. K. Beattie, T. W. Hambley, J. A. Klepetko, A. F. Masters, P. Turner, *Chem. Commun.* **1998**, 45; b) E. K. Brechin, O. Cador, A. Caneschi, C. Cadiou, S. G. Harris, S. Parsons, M. Vonci, R. E. P. Winpenny, *Chem. Commun.* **2002**, 1860.
[5] a) N. V. Gerbeleu, Y. T. Struchkov, G. A. Timko, A. S. Batsanov, K. M. Indrichan, G. A. Popovic, *Dokl. Chem.* **1991**, *313*, 232; b) I. M. Atkinson, C. Benelli, M. Murrie, S. Parsons, R. E. P. Winpenny, *Chem. Commun.* **1999**, 285; c) M. Eschel, A. Bino, I. Felner, D. C. Johnston, M. Luban, L. L. Miller, *Inorg. Chem.* **2000**, *39*, 1376; d) J. Van Slageren, R. Sessoli, D. Gatteschi, A. A. Smith, M. Helliwell, R. E. P. Winpenny, A. Cornia, A. L. Barra, A. G. M. Jansen, E. Rentschler, G. A. Timco, *Chem. Eur. J.* **2002**,

 © 2006 Wiley-VCH Verlag GmbH & Co. KGaA, Weinheim

8, 277; e) J. Overgaard, B. B. Iversen, S. P. Palii, G. A. Timco, N. V. Gerbeleu, F. K. Larsen, *Chem. Eur. J.* **2002**, *8*, 2775; f) P. Christian, G. Rajaraman, A. Harrison, J. J. W. McDouall, J. T. Raftery, R. E. P. Winpenny, *Dalton Trans.* **2004**, 1511.

[6] a) E. Rentschler, D. Gatteschi, A. Cornia, A. C. Fabretti, A.-L. Barra, O. I. Shchegolikhina, A. A. Zhdanov, *Inorg. Chem.* **1996**, *35*, 4427; b) G. Mezei, P. Baran, R. G. Raptis, *Angew. Chem.* **2004**, *116*, 584; *Angew. Chem. Int. Ed.* **2004**, *43*, 573.

[7] L. G. Westin, M. Kritikos, A. Caneschi, *Chem. Commun.* **2003**, 1012.

[8] a) A. Müller, E. Krickemeyer, J. Meyer, H. Bögge, F. Peters, W. Plass, E. Diemann, S. Dillinger, F. Nonnenbruch, M. Randerath, C. Menke, *Angew. Chem.* **1995**, *107*, 2293; *Angew. Chem. Int. Ed. Engl.* **1995**, *34*, 2122; b) A. Müller, E. Krickemeyer, H. Bögge, M. Schmidtmann, C. Beugholt, P. Kögerler, C. Lu, *Angew. Chem.* **1998**, *110*, 1278; *Angew. Chem. Int. Ed.* **1998**, *37*, 1220; c) B. Salignac, S. Riedel, A. Dolbecq, F. Sécheresse, E. Cadot, *J. Am. Chem. Soc.* **2000**, *122*, 10381; d) A. Müller, C. Serain. *Acc. Chem. Res.* **2000**, *33*, 2.

[9] a) G. L. Abbati, A. Cornia, A. C. Fabretti, A. Caneschi, D. Gatteschi, *Inorg. Chem.* **1998**, *37*, 1430; b) A. J. Tasiopoulos, A. Vinslava, W. Wernsdorfer, K. A. Abboud, G. Christou, *Angew. Chem.* **2004**, *116*, 2169; *Angew. Chem. Int. Ed.* **2004**, *43*, 2117; c) M. Murugesu, W. Wernsdorfer, K. A. Abboud, G. Christou, *Angew. Chem.* **2005**, *117*, 914; *Angew. Chem. Int. Ed.* **2005**, *44*, 892; d) D. Foguet-Albiol, T. A. O'Brien, W. Wernsdorfer, B. Moulton, M. J. Zaworotko, K. A. Abboud, G. Christou, *Angew. Chem.* **2005**, *117*, 919; *Angew. Chem. Int. Ed.* **2005**, *44*, 897; e) E. M. Rumberger, S. J. Shah, C. C. Beedle, L. N. Zakharov, A. L. Rheingold, D. N. Hendrickson, *Inorg. Chem.* **2005**, *44*, 2742.

[10] a) A. J. Blake, C. M. Grant, S. Parsons, J. M. Rawson, R. E. P. Winpenny, *Chem. Commun.* **1994**, 2363; b) A. L. Dearden, S. Parsons, R. E. P. Winpenny, *Angew. Chem.* **2001**, *113*, 155; *Angew. Chem. Int. Ed.* **2001**, *40*, 151; c) C. Cadiou, M. Murrie, C. Paulsen, V. Villar, W. Wernsdorfer, R. E. P. Winpenny, *Chem. Commun.* **2001**, 2666; d) H. Andres, R. Basler, A. J. Blake, C. Cadiou, G. Chaboussant, C. M. Grant, H.-U. Güdel, M. Murrie, S. Parsons, C. Paulsen, F. Semadini, V. Villar, W. Wernsdorfer, R. E. P. Winpenny, *Chem. Eur. J.* **2002**, *8*, 4867.

[11] a) H. Kumagai, S. Kitagawa, *Chem. Lett.* **1996**, 471; b) Y. Chen, Q. Liu, Y. Deng, H. Zhu, C. Chen, H. Fan, D. Liao, E. Gao, *Inorg. Chem.*, **2001**, *40*, 3723.

[12] S. P. Watton, P. Fuhrmann, L. E. Pence, A. Caneschi, A. Cornia, G. L. Abbati, S. J. Lippard, *Angew. Chem.* **1997**, *109*, 2917; *Angew. Chem. Int. Ed. Engl.* **1997**, *36*, 2774.

[13] a) C. S. Campos-Fernádez, R. Clérac, J. M. Koomen, D. H. Russell, K. R. Dunbar, *J. Am. Chem. Soc.* **2001**, *123*, 773; b) O. Cador, D. Gatteschi, R. Sessoli, F. K. Larsen, J. Overgaard, A.-L. Barra, S. J. Teat, G. A. Timco, R. E. P. Winpenny, *Angew. Chem.* **2004**, *116*, 5308; *Angew. Chem. Int. Ed.* **2004**, *43*, 5196.

[14] B. Normand, X. Wang, X. Zotos, D. Loss, *Phys. Rev. B* **2001**, 63, 184409.

[15] a) A. Cornia, A. G. M. Jansen, M. Affronte, G. L. Abbati, D. Gatteschi, *Angew. Chem.* **1999**, *111*, 2409; *Angew. Chem. Int. Ed.* **1999**, *38*, 2264; b) A. Cornia, A. G. M. Jansen, M. Affronte, *Phys. Rev. B* **1999**, *60*, 12177.

[16] a) A. Chiolero, D. Loss, *Phys. Rev. Lett.* **1998**, *80*, 169; b) F. Meier, D. Loss, *Phys. Rev. B* **2001**, *64*, 224411; c) F. Meier, D. Loss, *Phys. Rev. Lett.* **2001**, *86*, 5373.

[17] O. Cador, D. Gatteschi, R. Sessoli, A.-L. Barra, G. A. Timco, R. E. P. Winpenny, *J. Magn. Magn. Mater.* **2005**, *290*, 55.

[18] R. W. Saalfrank, I. Bernt, E. Uller, F. Hampel, *Angew. Chem.* **1997**, *109*, 2596; *Angew. Chem. Int. Ed. Engl.* **1997**, *36*, 2482.

[19] a) G. A. Timco, A. S. Batsanov, F. K. Larsen, C. A. Muryn, J. Overgaard, S. J. Teate, R. E. P. Winpenny, *Chem. Commun.* **2005**, 3649; b) R. H. Laye, F. K. Larsen, J. Overgaard, C. A. Muryn, E. J. L. McInnes, E. Rentschler, V. Sanchez, H. U. Güdel, O. Waldmann, G. A. Timco, R. E. P. Winpenny, *Chem. Commun.* **2005**, 1125.

[20] a) C. N. McMahon, S. J. Obrey, A. Keys, S. G. Bott, A. R. Barron, *Dalton Trans.* **2000**, 2151; b) S. J. Obrey, S. G. Bott, A. R. Barron, *Inorg. Chem.* **2002**, *41*, 571.

[21] a) Crystal structure data for **1**·*x*MeOH: $C_{40}H_{90}Ga_{10}O_{40}$ (without MeOH), $M_r = 1908.32$, monoclinic, space group $P2_1/n$, $a = 17.440(2)$, $b = 15.812(2)$, $c = 26.090(3)$ Å, $\beta = 99.000(3)°$, $V = 7106(16)$ Å^3, $T = 173$ K, $Z = 4$, $\rho_{calcd} = 1.784$ g cm^{-3}, 46564 reflections collected, 16196 unique ($R_{int} = 0.0929$), $R1 = 0.0435$, w$R2 = 0.1085$, using 16196 reflections with $I > 2\sigma(I)$. The asymmetric unit consists of two half wheels and partial MeOH molecules above and below the plane of each. The latter represents a small fraction which could not be properly modeled or removed using the program SQUEEZE, a part of the PLATON package (PLATON: A. L. Spek, *Acta Crystallogr. Sect. A* **1990**, *46*, 1–34) of crystallographic software, owing to the proximity to the wheel. b) Crystal structure data for **2**·*x*MeCN: $C_{114}H_{218}Ga_{18}N_{12}O_{96}$, $M_r = 4716.08$ (without MeCN), monoclinic, space group $P2_1/c$, $a = 17.8400(11)$, $b = 29.6264(19)$, $c = 18.4009(12)$ Å, $\beta = 103.615(2)°$, $V = 9452(1)$ Å^3, $T = 173$ K, $Z = 2$, $\rho_{calcd} = 1.657$ g cm^{-3}, 39439 reflections collected, 12350 unique ($R_{int} = 0.1205$), $R1 = 0.0529$, w$R2 = 0.1003$, using 12350 reflections with $I > 2\sigma(I)$. The asymmetric unit consists of half of the Ga_{18} wheel, three nitrate anions, and approximately 6 MeCN molecules of crystallization. The latter were disordered and could not be modeled properly, thus the program SQUEEZE was used to calculate the area of solvent disorder and remove its contribution to the overall intensity data. The six pdH$^-$ hydroxyl protons of the asymmetric unit were located from a difference Fourier map and refined as riding on their parent O atoms. c) Crystal structure data for **3**·*x*MeCN: $C_{212}H_{342}Fe_{18}N_{60}O_{96}$, $M_r = 6272.76$ (without MeCN), rhombohedral, space group $R\bar{3}$, $a = 32.5526(19)$, $c = 20.503(2)$ Å, $\beta = 120°$, $V = 18816(3)$ Å^3, $T = 173$ K, $Z = 3$, $\rho_{calcd} = 1.661$ g cm^{-3}, 55780 reflections collected, 9578 unique ($R_{int} = 0.1061$), $R1 = 0.0469$, w$R2 = 0.1165$, using 9578 reflections with $I > 2\sigma(I)$. The asymmetric unit consists of one-sixth of the Fe_{18} wheel (lying on S_6 symmetry axes), one nitrate anion and approximately 8 MeCN molecules of crystallization. The latter were disordered and could not be modeled properly, thus the program SQUEEZE was used to calculate the area of solvent disorder and remove its contribution to the overall intensity data. CCDC-609458–609460 contain the supplementary crystallographic data for this paper. These data can be obtained free of charge from The Cambridge Crystallographic Data Centre via www.ccdc.cam.ac.uk/data_request/cif.

 © 2006 Wiley-VCH Verlag GmbH & Co. KGaA, Weinheim

DNA Structures

DOI: 10.1002/anie.200602754

A Virus Spotlighted by an Autonomous DNA Machine**

*Yossi Weizmann, Moritz K. Beissenhirtz, Zoya Cheglakov, Roni Nowarski, Moshe Kotler, and Itamar Willner**

We report on an autonomous DNA-based machine that amplifies the detection of M13 phage single-stranded (ss) DNA. The machine is unique in that it makes use of both the genetic and catalytic properties of DNA. Upon recognition of the input viral DNA, the machine is activated and synthesizes a peroxidase-mimicking DNAzyme, which, in turn, generates colorimetric or chemiluminescence readout signals. Multiple rounds of isothermal strand replication, which lead to strand displacement and activation of the DNAzyme moiety, constitute two consecutive levels of signal amplification for this novel detection paradigm that rivals PCR for sensitivity.

Amplification is a fundamental element in bioanalysis. Enzymes,[1] DNAzymes,[2] and lately, nanoparticles[3] or nanocontainers[4] are widely employed for the sensitive detection of biorecognition events. Within these efforts, the amplified and sensitive detection of DNA is particularly challenging and directed to the analysis of pathogens, the detection of genetic disorders, and for forensic applications.[5] PCR provides a general protocol for the amplified detection of DNA. Although the PCR method is time consuming and not free of limitations, it provides the most versatile method to detect minute amounts of DNA. The design of alternative approaches for the sensitive detection of DNA is in continuous demand. Substantial research efforts have been directed lately to the development of DNA-based machines.[6] A DNA-based machine that cleaves RNA by a DNAzyme,[7] DNA-based tweezers,[8,9] autonomous DNA walkers on prearchitectured tracks,[10–13] and signal-triggered switchable structural transformations between duplex DNA and G-quadruplex configurations[14] were reported. The use of the DNA machines as computing systems[15–17] or as sensor systems[18,19] was discussed. Herein we report on an isothermic autonomous DNA machine for the generation of DNAzyme labels. We demonstrate activation of the DNA machine by the analyzed DNA, which allows it to self-detect. The resulting synthesized DNAzyme acts as a peroxidase-mimicking enzyme and as an amplifying label for the analysis of the target DNA. The machine employs colorimetric or chemiluminescent readout signals for the detection of the target DNA. The paradigm developed in the present study represents an approach that might complement or substitute the PCR method. In contrast with the PCR and real-time-PCR (RT-PCR) methods that require thermal replication cycles, costly optical labels, and dedicated instrumentation, the procedure developed by us proceeds isothermally, reaches a sensitivity limit of 10^{-14} M, is cost-effective, and can be visually imaged. The uniqueness of the new paradigm is the amplification of the analyzed DNA by two consecutive steps: the autonomous synthesis and displacement of a nucleic acid that is generated by a biomolecular machine on a DNA template, and the self assembly of the displaced strand into a biocatalytic DNAzyme label that enables the colorimetric or chemiluminescent imaging of the reaction.

The specific DNAzyme synthesized in the present study is a G-quadruplex nucleic acid structure, which intercalates hemin and mimics peroxidase activity.[20,21] In a series of recent studies, we have reported that the hemin/G-quadruplex complex catalyzes the generation of chemiluminescence, in the presence of luminol/H_2O_2, and that it biocatalyzes the oxidation of 2,2′-azino-bis(3-ethylbenzothiazoline-6-sulfonic acid) ($ABTS^{2-}$) by H_2O_2. These biocatalytic reactions were used to develop different DNA-detection assays.[22]

The autonomous synthesis of the DNAzyme is depicted in Figure 1. The template **1**, consisting of three regions, is used as the "track" on which the autonomous synthesis of the DNAzyme is activated. Region I (orange) is complementary to the primer. The segment II (red) is complementary to a nucleic acid that, upon hybridization, yields a double strand that binds the N.BbvC IA nicking endonuclease. Segment III (green) is complementary to the DNAzyme that is synthesized by the machine. Upon the hybridization of the primer **2**, and in the presence of exonuclease-free Klenow (Klenow fragment, exo-) polymerase and the nucleotide mixture (deoxynucleotide triphosphate (dNTPs) act as fuel), the machine is activated. The polymerase-induced reaction replicates the template. Replication of the template, however, yields the double-stranded domain that associates N.BbvC IA and results in the nicking (scission) of the replicated single strand at the marked position. The cleavage of the single strand generates a new site for the initiation of replication. Thus, the polymerase completes the replication of the DNAzyme, and the reactivated replication at the scission site displaces the already synthesized DNAzyme. Subsequently, in the presence of hemin, the autonomous synthesis of the G-quadruplex DNAzyme structure is activated. The DNAzyme catalyzes the oxidation of $ABTS^{2-}$ by H_2O_2 or stimulates the generation of chemiluminescence in the presence of luminol/H_2O_2.

Figure 2 A shows the rate of $ABTS^{2-}$ oxidation by H_2O_2 in the presence of the DNAzymes, which were generated within 5 min by using different concentrations of the template DNA **1**. As the concentration of the template increases, the formation of oxidized $ABTS^{2-}$ is enhanced, implying an

[*] Y. Weizmann, Dr. M. K. Beissenhirtz, Z. Cheglakov, Prof. I. Willner
Institute of Chemistry
The Farkas Center for Light-Induced Processes
The Hebrew University of Jerusalem
Jerusalem 91904 (Israel)
Fax: (+972) 2-6527-715
E-mail: willnea@vms.huji.ac.il
R. Nowarski, Prof. M. Kotler
Department of Experimental Pathology
The Hebrew University–Hadassah Medical School
Jerusalem 91120 (Israel)

[**] This research is supported by the Israel Ministry of Science and by the Minerva Foundation (Moritz K. Beissenhirtz).

 InterScience © 2006 Wiley-VCH Verlag GmbH & Co. KGaA, Weinheim

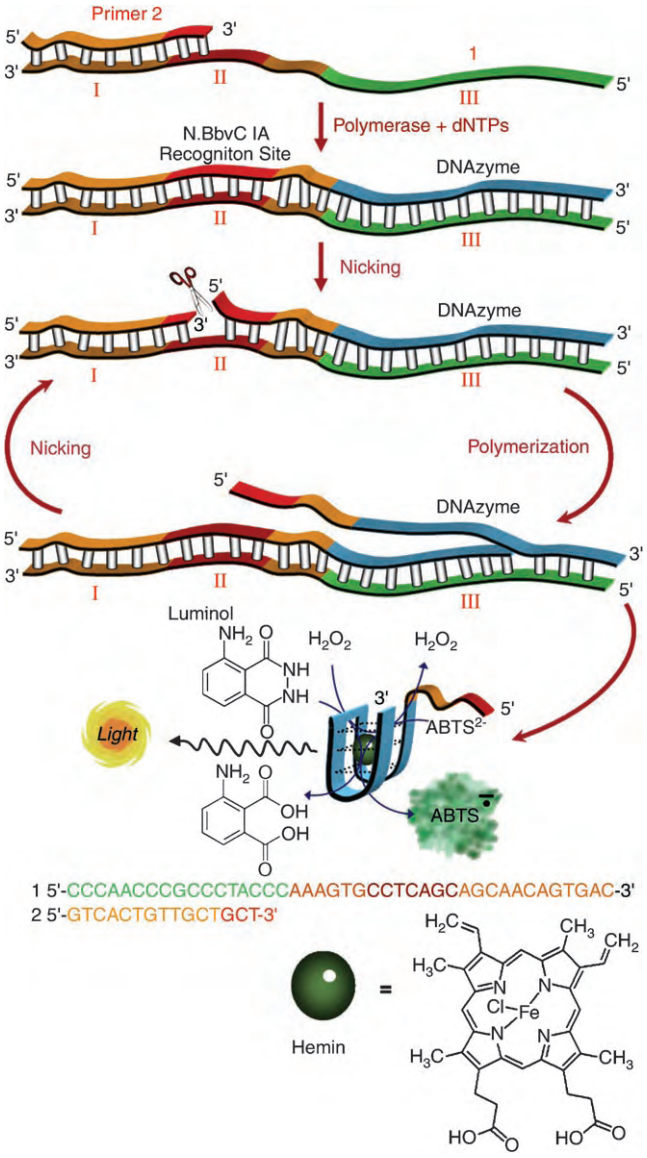

Figure 1. Primer-induced autonomous synthesis of DNAzyme units on template DNA by using polymerase/dNTPs and a nicking enzyme as the biocatalyst.

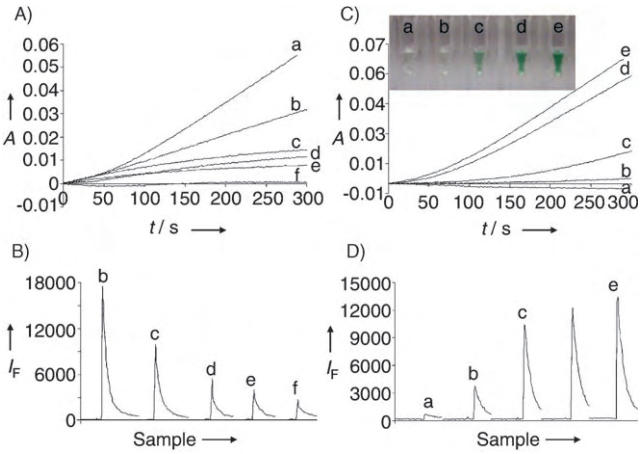

Figure 2. A) Absorbance changes and B) chemiluminescence intensities observed upon the oxidation of $ABTS^{2-}$ by H_2O_2, or the light emission by luminol/H_2O_2 by the DNA-based machine as depicted in Figure 1. Different concentrations of the template **1** were used: a) 1×10^{-6} M, b) 1×10^{-8} M, c) 1×10^{-10} M, d) 1×10^{-12} M, e) 1×10^{-14} M, and f) analysis of the foreign calf-thymus ssDNA (1×10^{-8} M). C) Absorbance changes and D) chemiluminesence intensities observed upon the oxidation of $ABTS^{2-}$ by H_2O_2 or light emission by luminol/H_2O_2 and the DNAzyme synthesized by the DNA-based machine at different time intervals and at the fixed concentrations of **1** (1×10^{-6} M) and **2** (1×10^{-6} M): a) 0 min, b) 10 min, c) 30 min, d) 60 min, e) 90 min. For the absorbance studies, the system included $ABTS^{2-}$ (1.8×10^{-4} M), H_2O_2 (4.4×10^{-5} M), and hemin (4×10^{-7} M). For the chemiluminescence studies, the system included luminol (1×10^{-9} M), H_2O_2 (3×10^{-2} M), and hemin (5×10^{-4} M). Each of the systems were analyzed in a separate vial with a total volume of 50 μL consisting of a buffer solution (NaCl (50 mM), Tris-HCl (10 mM), $MgCl_2$ (10 mM), and dithiothreitol (1 mM); pH 7.9), polymerase (0.4 units), dNTPs (0.2 mM), and N.BbvC IA (0.5 units). The reactions in the respective vials were performed at 37 °C for the specified time intervals and blocked by cooling to 4 °C. The respective colorimetric or chemiluminescence developing solutions consisting of HEPES buffer solution (25 mM), pH 7.4 for the $ABTS^{2-}/H_2O_2$ color test, and pH 9.0 for the luminol/H_2O_2 chemiluminescence assay. KCl (20 mM), NaCl (200 mM), and the respective $ABTS^{2-}/H_2O_2$ or luminol/H_2O_2 substrates were added to the vials to yield a total volume of 200 μL. Absorbance spectra were recorded at $\lambda = 415$ nm. Chemiluminescence was monitored at $\lambda_{em} = 420$ nm. The inset of Figure 2C shows the visual time-dependent color changes upon the oxidation of $ABTS^{2-}$ by the DNAzyme synthesized by the machine. Detailed description of the experimental conditions are provided in the Experimental Section. I_F = fluorescence intensity.

increased content of the generated DNAzyme. Control experiments indicate that oxidation of $ABTS^{2-}$ by H_2O_2 does not occur in the absence of hemin or in the presence of hemin without the generation of the nucleic acid sequence that generates the DNAzyme. Furthermore, exclusion of either the nicking endonuclease, the polymerase, or the dNTPs mixture prohibits the biocatalytic oxidation of $ABTS^{2-}$. Thus, the cooperative polymerization by polymerase, and scission by the nicking enzyme, is essential to self-assemble the DNAzyme in the presence of hemin. The operation of the biomolecular machine was determined by chemiluminescence signals (see Figure 1). The DNAzyme catalyzes the generation of chemiluminescence in the presence of luminol/H_2O_2. Figure 2B shows the chemiluminescence intensities generated by the DNAzymes formed by the biomolecular machine after a time interval of 90 min, in the presence of variable concentrations of the template **1**. The chemiluminescence intensities are enhanced as the concentration of the template is increased, indicating that the contents of the synthesized DNAzymes increase with the template concentration. As before, the different control experiments indicate that all of the components included in the system are essential to drive the synthesis and self-assembly of the DNAzymes. Figure 2C shows the rate of oxidation of $ABTS^{2-}$ by H_2O_2 in the presence of DNAzyme units generated by the biomolecular machine, with a constant concentration of the template **1** (1×10^{-6} M), and at different time intervals. The rate of $ABTS^{2-}$ oxidation is enhanced as the time interval for the formation of the DNAzymes is prolonged. Figure 2D shows the light intensities generated by

 © 2006 Wiley-VCH Verlag GmbH & Co. KGaA, Weinheim

DNAzymes formed in the presence of a fixed concentration of the template **1** (1×10^{-6} M) and at different time intervals of the machine operation. As the operation of the biomolecular machine is prolonged, the emitted light intensities are higher, indicating increased contents of the DNAzyme.

The autonomous synthesis of the DNAzyme units, through the operation of the DNA machine, is further confirmed by electrophoretic experiments. Figure 3 depicts

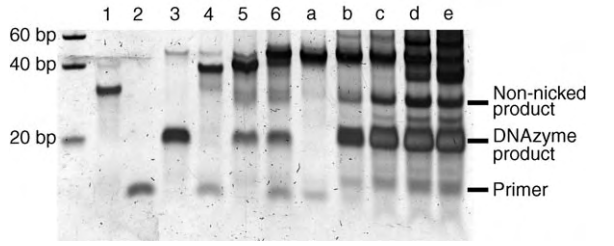

Figure 3. Nondenaturating PAGE analysis of the DNAzyme synthesized by the DNA machine according to Figure 1. 1) Template **1** only, 2) primer **2** only, 3) product (5′-TGAGGCACTTTGGGTAGGG CGGGTTGGG-3′) only, 4) template **1** + primer **2**, 5) template **1** + product, 6) template **1** + primer **2** + product. a)–e) Products generated by the DNA machine at different time intervals, a) $t=0$, b) $t=10$, c) $t=30$, d) $t=60$, and e) $t=90$ minutes. Experimental conditions for the DNA machine operation are as outlined in Figure 2C and D and the details given in the Experimental Section.

the electrophoresis results upon analyzing the model primer DNA **2**, which correspond to the synthesis of the DNAzymes by the DNA machine. Runs a) to e) show the resulting nucleic acid bands generated at different time intervals by the machine. As the operation of the machine is prolonged, the content of the DNAzyme product increases as expected (note that at $t=0$ min no DNAzyme is present). Furthermore, a new band that corresponds in size to the original template is intensified as the operation of the DNA machine is prolonged. This band is attributed to the non-nicked nucleic acid product that is dissociated from the double strand by a thermal treatment prior to electrophoresis (the heat treatment deactivates the enzymes and allows the imaging of the system at a defined time interval). Note that the formation of the double strand between the non-nicked product and the template is inhibited by the competitive association of the excess of DNAzyme to the template. The application of the DNA machine for the amplified analysis of real DNA samples requires the use of an intermediate nucleic acid hairpin structure that is opened by the analyte DNA. The opened stem activates the machine, as depicted in Figure 4. This is exemplified with the analysis of M13 phage ssDNA by using a hairpin probe, and the resulting hybrid triggers the autonomous synthesis of the DNAzyme units. The hairpin structure **3** includes, in the single-stranded loop, the recognition sequence for hybridization with the M13 phage DNA analyte **4**, and upon hybridization with **4**, **3** is opened. The template of the machine **5** includes the domain I, which is complementary to the single-strand nucleic acid of the stem of **3**, and is released upon hybridization with M13 phage DNA. The region II, upon formation of the respective duplex, yields the nicking

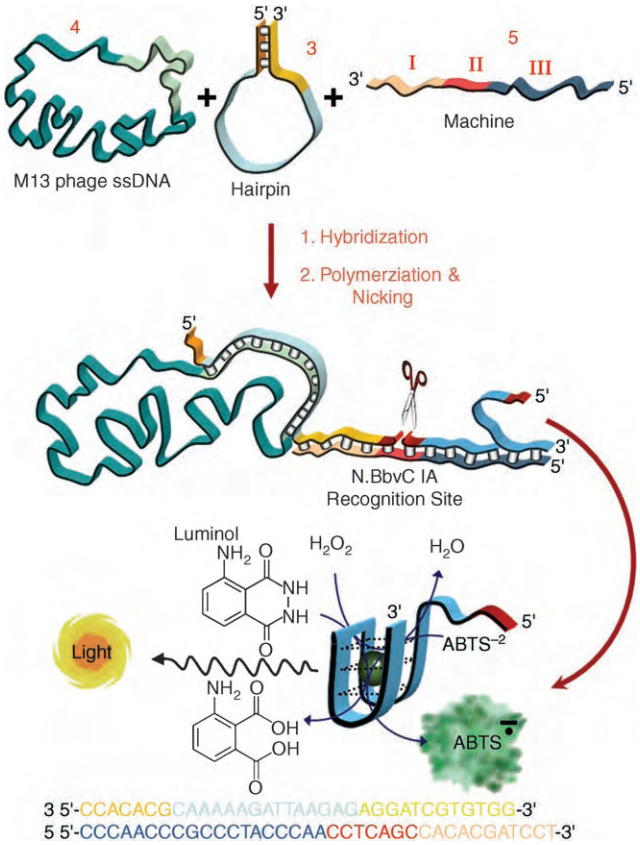

Figure 4. Analysis of M13 phage ssDNA by the hairpin **3** and the DNA-based machine by using template **5**.

site for N.BbvC IA, and the region III is complementary to the DNAzyme sequence. The hybridization of M13 phage DNA with **3** results in the binding of the open hairpin structure to the template **5**. This activates, in the presence of the nucleotide mixture, dNTPs, the polymerase, and the nicking enzyme N.BbvC IA, the autonomous operation of the machine and the synthesis of the DNAzyme. Figure 5 A shows the rate of $ABTS^{2-}$ oxidation by the hemin-functionalized DNAzyme synthesized by the template **5**, upon analyzing different concentrations of M13 phage DNA. The control experiment, in which calf thymus DNA (1×10^{-8} M) is examined by the DNA template, does not lead to any DNAzyme formation and yields a trace oxidation of $ABTS^{2-}$ (Figure 5 A, curve e). Also, in the absence of the M13 phage DNA, or upon exclusion of the hairpin **3**, no oxidation of $ABTS^{2-}$ occurs. A further control experiment revealed that the DNA machine was not triggered by the hairpin **3** in the absence of M13 phage ssDNA. The seven-base stem structure prevents the thermal opening of the hairpin and the non-specific activation of the machine. As the concentration of the analyte decreases, the rate of $ABTS^{2-}$ oxidation decreases, implying that less DNAzyme is synthesized by the machine. The control experiments reveal that the analysis of M13 phage DNA is specific and that the analyte can be detected with a sensitivity limit of 1×10^{-14} M with a signal-to-noise ratio of 2.8. Furthermore, the two readout methods reveal comparable sensitivities. Although the colorimetric assay

 © 2006 Wiley-VCH Verlag GmbH & Co. KGaA, Weinheim

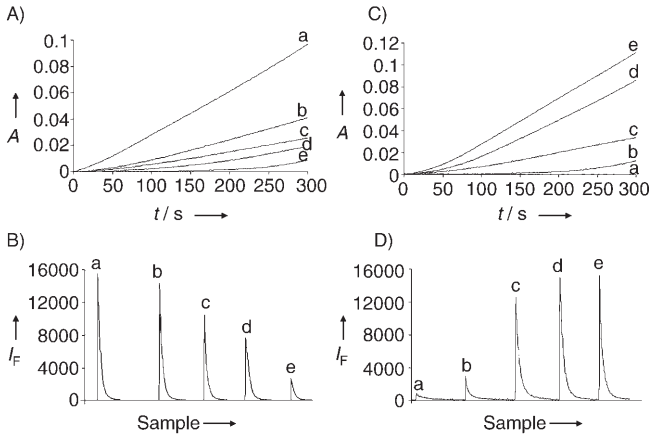

Figure 5. A) Absorbance changes and B) chemiluminescence intensities upon the oxidation of $ABTS^{2-}$ by H_2O_2 or the light emission by luminol/H_2O_2 by the DNA-based machine depicted in Figure 4. Different concentrations of M13 phage ssDNA **4** were analyzed: a) 1×10^{-9} M, b) 1×10^{-11} M, c) 1×10^{-12} M, d) 1×10^{-14} M, and e) analysis of the foreign calf-thymus ssDNA, 1×10^{-8} M. In all systems, fixed concentrations of the hairpin **3** (1×10^{-6} M) and the template **5** (1×10^{-6} M) were employed. Polymerase (0.4 units), dNTPs (0.2 mM), and N.BbvC IA (0.5 units) were included in all of the systems. C) Absorbance changes and D) chemiluminesence intensities upon analyzing M13 phage ssDNA (1×10^{-9} M) by the DNA-based machine at different time intervals and fixed concentrations of **3** (1×10^{-6} M) and **5** (1×10^{-6} M): a) 0 min, b) 10 min, c) 30 min, d) 60 min, and e) 90 min. For the absorbance studies, $ABTS^{2-}$ (1.8×10^{-4} M), H_2O_2 (4.4×10^{-5} M), and hemin (4×10^{-7} M) were included in the system. For the chemiluminescence studies, luminol (1×10^{-9} M), H_2O_2 (3×10^{-2} M), and hemin (5×10^{-4} M) were included in the system. The different measurements were performed in separate vials according to the details provided in the caption of Figure 2. Absorbance spectra were recorded at $\lambda = 415$ nm. Chemiluminescence was monitored at $\lambda_{em} = 420$ nm. Detailed description of the experimental conditions is provided in the Experimental Section.

yields more pronounced signals, the time interval needed to generate the colour response (approximately 250 sec) is an accompanying disadvantage. The chemiluminescence signal is instantaneous, but its translation to a quantitative assay of the analyzed DNA is less accurate. The analysis of the M13 phage ssDNA was also determined by the DNAzyme-generated chemiluminescence, Figure 5B. The generated chemiluminescence decreases in its intensity as the concentration of M13 phage DNA is lowered, and foreign DNA leads to a trace chemiluminescence. Figure 5C shows the rate of $ABTS^{2-}$ oxidation by the DNAzyme and upon analyzing a fixed M13 phage DNA concentration of 1×10^{-9} M. As the time interval for operating the machine is prolonged, the rate of $ABTS^{2-}$ oxidation is enhanced, indicating that the content of synthesized DNAzyme increases with the operating time of the machine. Also, upon analyzing a fixed concentration of M13 phage DNA, the chemiluminescence is intensified as the operation time of the DNA machine is prolonged (see Figure 5D).

In conclusion, the present study has introduced a new paradigm for the sensitive analysis of DNA by using a DNA-based machine that consists of a DNA template, polymerization/nicking enzymes, and strand displacement of the synthesized DNAzyme. The strand displacement and the formation of the DNAzyme represent two consecutive amplification steps in the analytical procedure. Furthermore, we demonstrate that the operation of the DNA machine is triggered by the opening of a predesigned hairpin nucleic acid by the analyte DNA. We also show that the colorimetric or chemiluminescence signals allow the readout of the DNA machine function and operation. The isothermal and rapid (approximately 90 min) analysis of the target DNA, together with the quantitative detection of the analyte, demonstrate the appealing bioanalytical features of the method. This study has substantially broader perspectives for the future development of DNA-based machines, for example, the displaced DNA may be used as a promoter for the aggregation of Au nanoparticles, thus enabling the optical imaging of the analyte through the operation of the machine. Alternatively, the parallel use of several DNA machines may lead to the displacement of nucleic acid barcodes that are analyzed on an array of electrodes (e.g. by electrochemical impedance spectroscopy).

Experimental Section

Materials: Oligonucleotides **1**, **2**, **3**, **5**, the product (5′-TGAGGCACTTTGGGTAGGGCGGGTTGGG-3′; Genosys, Sigma), the deoxynucleotide solution mixture (dNTPs) in NEB buffer solution (NaCl (50 mM), (hydroxymethyl)aminomethane hydrochloride (Tris-HCl; 10 mM), $MgCl_2$ (10 mM), dithiothreitol (1 mM); pH 7.9), the N.BbvC IA endonuclease (New England BioLabs, Inc.), M13 mp18(+) strand DNA, and polymerase Klenow fragment exo- (Amersham Biosciences Corp), and hemin (Frontier Scientific, Inc.) were used without any further purification. A hemin stock solution was prepared in dimethyl sulfoxide (DMSO) and stored in the dark at −20 °C. The single-stranded calf-thymus DNA, luminol, and H_2O_2 were purchased from Sigma.

Colorimetric measurements assay: The experiment was performed in a solution consisting of the products; hemin (4×10^{-7} M), H_2O_2 (4.4×10^{-5} M), and $ABTS^{2-}$ (1.82×10^{-4} M) all in a buffer solution consisting of 2-[4-(2-hydroxyethyl)-1-piperazininyl]ethanesulfonic acid) (HEPES; 25 mM), KCl (20 mM), and NaCl (200 mM); pH 7.4 and at 25 °C. Absorbance changes at 415 nm were followed to characterize the rate of oxidation of $ABTS^{2-}$.

Chemiluminescence measurements: Light-emission experiments were performed by using a photon-counting spectrometer (Edinburgh Instruments, FLS 920) equipped with a cooled photomultiplier detection system, which was connected to a computer (F900 v.6.3 software). Measurements were made in a cuvette that included a buffer solution consisting of HEPES (25 mM), KCl (20 mM), and NaCl (200 mM); pH 9.0 and hemin (1×10^{-9} M), luminol (0.5 mM), and H_2O_2 (30 mM). The light emission was monitored at $\lambda_{em} = 420$ nm.

Received: July 11, 2006
Revised: August 22, 2006
Published online: October 11, 2006

Keywords: biosensors · chemiluminescence · DNA structures · DNAzymes · enzymes

[1] D. J. Caruana, A. Heller, *J. Am. Chem. Soc.* **1999**, *121*, 769–774.
[2] Y. Xiao, V. Pavlov, T. Niazov, A. Dishon, M. Kotler, I. Willner, *J. Am. Chem. Soc.* **2004**, *126*, 7430–7431.

 © 2006 Wiley-VCH Verlag GmbH & Co. KGaA, Weinheim

[3] J. Wang, G. Liu, A. Merkoçi, *J. Am. Chem. Soc.* **2003**, *125*, 3214 – 3215.
[4] J. Wang, O. Rincon, R. Polsky, E. Dominguez, *Electrochem. Commun.* **2003**, *5*, 83 – 86
[5] J. J. Gooding, *Electroanalysis* **2002**, *14*, 1149 – 1156.
[6] a) F. C. Simmel, W. U. Dittmer, *Small* **2005**, *1*, 284 – 299; b) M. K. Beissenhirtz, I. Willner, *Org. Biolmol. Chem.* **2006**, *4*, 3392 – 3401.
[7] J. Liu, Y. Lu, *J. Am. Chem. Soc.* **2003**, *125*, 6642 – 6643.
[8] B. Yurke, A. J. Turberfield, A. P. Mills Jr., F. C. Simmel, J. L. Neumann, *Nature* **2000**, *406*, 605 – 608.
[9] Y. Chen, M. Wang, C. Mao, *Angew. Chem.* **2004**, *116*, 3638 – 3641; *Angew. Chem. Int. Ed.* **2004**, *43*, 3554 – 3557.
[10] J.-S. Shin, N. A. Pierce, *J. Am. Chem. Soc.* **2004**, *126*, 10834 – 10835.
[11] W. B. Sherman, N. C. Seeman, *Nano Lett.* **2004**, *4*, 1203 – 1207.
[12] P. Yin, H. Yan, X. G. Daniell, A. J. Turberfield, J. H. Reif, *Angew. Chem.* **2004**, *116*, 5014 – 5019; *Angew. Chem. Int. Ed.* **2004**, *43*, 4906 – 4911.
[13] J. Bath, S. J. Green, A. J. Turberfield, *Angew. Chem.* **2005**, *117*, 4432 – 4435; *Angew. Chem. Int. Ed.* **2005**, *44*, 4358 – 4361.
[14] P. Alberti, J.-L. Mergny, *Proc. Natl. Acad. Sci. USA* **2003**, *100*, 1569 – 1573.
[15] Y. Benenson, B. Gil, U. Ben-Dor, R. Adar, E. Shapiro, *Nature* **2004**, *429*, 423 – 429.
[16] Y. Benenson, R. Adar, T. Paz-Elizur, Z. Livneh, E. Shapiro, *Proc. Natl. Acad. Sci. USA* **2003**, *100*, 2191 – 2196.
[17] M. N. Stojanovic, D. Stefanovic, *Nat. Biotechnol.* **2003**, *21*, 1069 – 1074.
[18] Y. Weizmann, Z. Cheglakov, V. Pavlov, I. Willner, *Angew. Chem.* **2006**, *118*, 2296 – 2300; *Angew. Chem. Int. Ed.* **2006**, *45*, 2238 – 2242.
[19] S. Beyer, F. C. Simmel, *Nucleic Acids Res.* **2006**, *34*, 1581 – 1587.
[20] P. Travascio, P. K. Witting, A. G. Mauk, D. Sen, *J. Am. Chem. Soc.* **2001**, *123*, 1337 – 1348.
[21] P. Travascio, Y. Li, D. Sen, *Chem. Biol.* **1998**, *5*, 505 – 517.
[22] a) T. Niazov, V. Pavlov, Y. Xiao, R. Gill, I. Willner, *Nano Lett.* **2004**, *4*, 1683 – 1687; b) z. Cheglakov, Y. Weizmann, M. K. Beissenhirz, I. Willner, *Chem. Comm.* **2006**, 3205 – 3207.

 © 2006 Wiley-VCH Verlag GmbH & Co. KGaA, Weinheim

Conformation Analysis

DOI: 10.1002/anie.200602793

The Tubulin-Bound Conformation of Discodermolide Derived by NMR Studies in Solution Supports a Common Pharmacophore Model for Epothilone and Discodermolide**

*Víctor M. Sánchez-Pedregal, Karel Kubicek, Jens Meiler, Isabelle Lyothier, Ian Paterson, and Teresa Carlomagno**

Discodermolide (DDM) is an antimitotic polyketide, isolated from a deep-sea sponge, that displays potent cytotoxic activity against a number of human tumor cell lines.[1–3] In a similar manner to taxol and epothilone (EPO), DDM suppresses normal microtubule (MT) dynamics and disrupts the formation of mitotic spindles, thus leading to apoptosis.[4–6] DDM binds to tubulin more strongly than taxol, is more efficient in promoting tubulin polymerization, and is active also in taxol-resistant ovarian and colon carcinoma cells.[1] These properties have triggered strong interest in DDM as a lead structure for the development of a novel cancer chemotherapeutic agent. Competition experiments with radiolabeled taxol show that DDM displaces taxol from tubulin, thereby suggesting an overlapping binding site for the two drugs.[7] However, an allosteric mechanism as a basis for the competitive binding of taxol and DDM to tubulin cannot be ruled out.

The taxol binding site of tubulin can accommodate a variety of ligands, including epothilones, dictyostatin, and

[*] Dr. V. M. Sánchez-Pedregal,[+] Dr. K. Kubicek, Dr. T. Carlomagno
Abteilung NMR-basierte Strukturbiologie
Max-Planck-Institut für biophysikalische Chemie
Am Fassberg 11, 37077 Göttingen (Germany)
Fax: (+49) 551-201-2202
E-mail: taco@nmr.mpibpc.mpg.de

Prof. J. Meiler
Center for Structural Biology
Vanderbilt University
654 21st Ave South, BIOSCI/MRBIII, Nashville, TN 37212 (USA)

Dr. I. Lyothier, Prof. I. Paterson
Department of Chemistry
University of Cambridge
Lensfield Road, Cambridge, CB21EW (UK)

[+] Present address: Facultad de Química
Dpto. Química Orgánica
Universidad de Santiago de Compostela
Campus Universitario Sur, s/n
15782 Santiago de Compostela (Spain)

[**] This work was supported by the Max-Planck-Gesellschaft, the Volkswagen-Stiftung (Grant no. I/80 798 to T.C.), by the European Union (Marie Curie fellowship to V.M.S.-P.), and by the DAAD (Postdoctoral fellowship PKZ A/06/04203 to K.K). We thank Christian Griesinger for critical reading of this manuscript and useful discussions, Marcel Reese for support, and Holger Stark for the electron microscopy studies. I.P. thanks Novartis Pharma AG for financial support.

Supporting information for this article is available on the WWW under http://www.angewandte.org or from the author.

WILEY InterScience DISCOVER SOMETHING GREAT
© 2006 Wiley-VCH Verlag GmbH & Co. KGaA, Weinheim

DDM, as well as others that share the MT-stabilizing activity of taxol while having very different chemical structures[8] (Scheme 1). Despite the availability of an impressive amount of structure–activity data, as well as modeling and

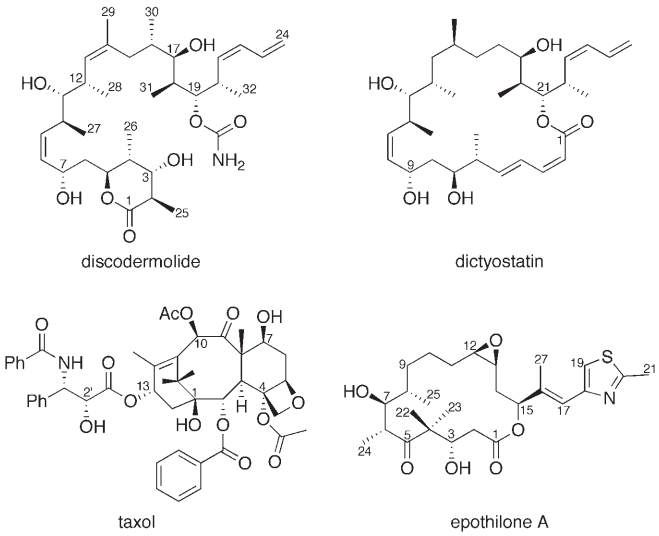

Scheme 1. Structures of discodermolide, dictyostatin, taxol, and epothilone A.

structural studies,[9] an explanation of how different classes of structurally unrelated molecules exert a similar effect on MT dynamics is still lacking. Direct structural information on the interaction of these natural products with tubulin is limited to the complexes of tubulin either with taxol or epothilone A (EPO-A), as determined by electron diffraction studies of Zn-stabilized two-dimensional sheets of tubulin.[10,11] In addition, we have determined the first tubulin-bound conformation of EPO-A in the solution state by NMR spectroscopy[12] by using a combination of transferred NOE (tr-NOE) and transferred cross-correlated relaxation data.[13] As for DDM, the free conformation of the molecule has been determined in solution by NMR spectroscopy[14,15] and in the solid state by X-ray diffraction,[16] while its tubulin-bound structure has remained elusive.

Herein, we derive for the first time the bioactive, tubulin-bound conformation of DDM in solution by NMR structural analysis. Additionally, we apply the recently developed INPHARMA technique,[17] which is based on the observation of protein-mediated interligand NOE signals, to prove that DDM does indeed bind to the taxane binding pocket and this, in turn, enables a common pharmacophore model for EPO and DDM to be constructed.

NOESY spectra of tubulin-free DDM show weak cross-peaks, as expected for a small molecule tumbling rapidly in solution. In contrast, the NOESY spectra of a solution of 500 μM DDM in the presence of 10 μM tubulin show intense cross-peaks (tr-NOE), thus indicating that DDM binds to soluble tubulin with $k_{off} > 100$ Hz, as previously shown for EPO-A.[12] The NMR sample is devoid of GTP and Mg^{2+} ions and contains instead 1.5 mM Ca^{2+} ions, which prevents complete polymerization of tubulin upon addition of DDM.[18] Under these conditions DDM promotes polymerization of tubulin to form "microtubule sheets" or "open microtubules" (see the Supporting Information), which have been previously observed in MT preparations stabilized by EPO or taxol[19] and by GMPCPP at low temperature.[20] While it is known that DDM binds much tighter to MTs than to soluble tubulin, our data demonstrate that the weaker binding of DDM to soluble tubulin is functionally relevant as it triggers formation of ordered tubulin polymers, even in the presence of Ca^{2+} ions. Once the polymers are formed (see the Supporting Information), they precipitate out of solution in a few hours and do not contribute to the NMR signal. Our structural data correspond to DDM bound to soluble tubulin, namely to the first step in the chain of conformational change events that lead to the drug-induced formation of MTs. The binding constant of DDM to tubulin is larger than that of EPO-A, as derived by comparison of the intensity of tr-NOE signals at a short mixing time. The relative affinity of the different MT-stabilizing agents for soluble tubulin follows the same order as for their binding to preformed MTs,[21] further confirming the biological relevance of the interaction of the ligands with tubulin before polymerization.

A total of 201 nonredundant tr-NOE peaks were identified in the NOESY spectra and were used as restraints in the structure calculation. The complete relaxation matrix approach was used to calculate the structure of tubulin-bound DDM.[22] This method minimizes the difference between the computed and the experimental 2D NOE intensities while accounting for spin diffusion effects.

The structure calculations converged to a unique family comprising the 12 lowest energy conformers (Figure 1 A). The overall shape of the tubulin-bound DDM resembles that of free DDM in the solid state (Figure 1 B). In contrast, free DDM exists in DMSO solution as a family of over 10 different conformations,[15] none of which is as compact as that observed in the X-ray structure.[16]

While most natural products binding to tubulin in the taxane binding site can be roughly described as a combination of a central cyclic core and a side-chain tail,[23] DDM is a potentially more flexible linear molecule that does not fit into this body–tail description. However, our study demonstrates that, when bound to tubulin, the main carbon chain of DDM folds in a right-handed helical twist, thereby forming a central core that mimics the rigid cyclic skeleton of taxol or EPO. Such a fold was proposed in a computational DFT study conducted in the gas phase,[24] in which DDM was assumed to fit the body–tail structural motif by folding in the compact globular X-ray conformation.

The similarity between the tubulin-bound conformation of DDM and the X-ray structure provides a rationale for the potent biological activity of the marine natural product dictyostatin, a 22-membered macrocyclic lactone which is structurally and biogenetically related to DDM. Dictyostatin competes with the taxanes for tubulin binding and has an analogous effect on MT dynamics, which suggests that it interacts with tubulin in a similar way as DDM.[25] Not surprisingly, the tubulin-bound conformation of DDM derived here is closely related to the solution structure of dictyostatin in water (Figure 2), which supports a common

 © 2006 Wiley-VCH Verlag GmbH & Co. KGaA, Weinheim

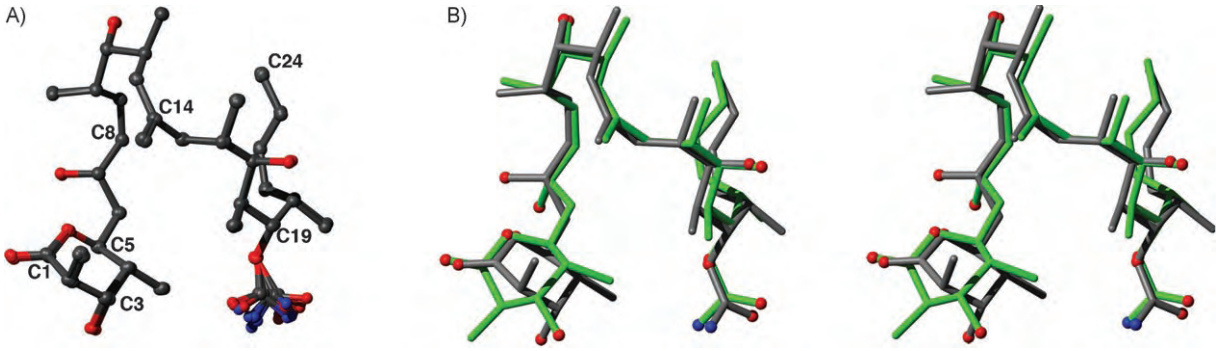

Figure 1. A) Superposition of the 12 lowest energy structures of DDM derived from NMR data (C gray, O red, N blue). The NMR-derived structure is well defined with a heavy-atom rmsd of 0.26 Å. B) Stereoview of the overlaid tubulin-bound (NMR-derived, in gray) and free (X-ray derived, in green)[16] conformations of discodermolide. Heteroatoms are displayed as spheres: O in red and N in blue. The two conformations are quite similar except for the lactone moiety. All figures were prepared with the program Molmol.[37]

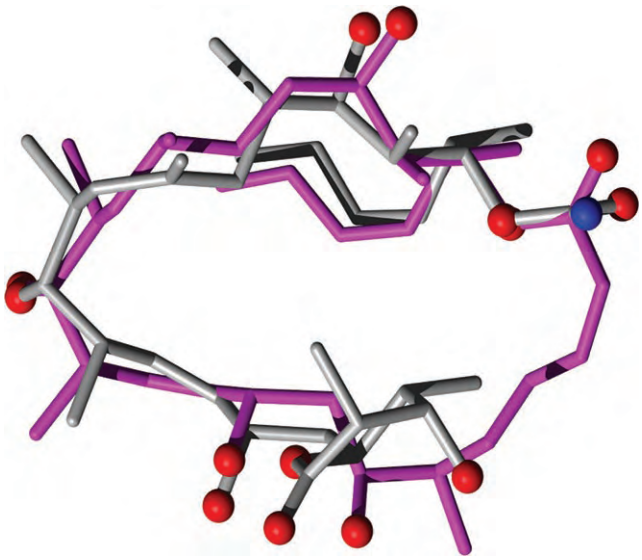

Figure 2. Overlay of the tubulin-bound (NMR-derived, in gray) conformation of discodermolide and the solution conformation of free dictyostatin (in magenta).[25] Heteroatoms are displayed as spheres: O red and N blue.

mechanism for the MT-stabilizing activity of the two compounds.

The presence of strong structural requirements for the stability of the tubulin-bound compact helical conformation of DDM in the C6–C16 region is confirmed by the structure–activity relationship (SAR) data, which show that modifications in this segment are usually detrimental for activity. In particular, constraint of the C9–C13 section in a cyclopentane ring,[26] saturation,[27] or a change in the geometry of the C8–C9 or the C13–C14 double bonds from *Z* to *E*,[7,28] or inversion of the C16 configuration[29] severely affect the capacity of DDM to stabilize MTs.

The δ-lactone ring adopts a twisted-boat conformation in the solid-state structure, where all the substituents show a pseudoequatorial orientation that minimizes their nonbonding interactions. In contrast, the tubulin-bound conformation of the lactone is closer to a flattened chair, with two substituents (2-Me and 3-OH) in an axial position and the other two (4-Me and the C5 main chain) adopting an equatorial position (Figure 1). The structural analysis of free DDM in DMSO solution shows both the boat and the chair conformations. Moreover, the torsion angles around the C5–C6 and C6–C7 bonds in the tubulin-bound structure differ from those in the X-ray structure by −43° and +19°, respectively. The conformational change occurring upon binding tubulin brings about a displacement of the position of the methyl group at C2 by 3.6 Å, while the position of the carbonyl group at C1 remains almost unvaried.

Several SAR studies show that the precise structural details of the lactone segment influence the activity only moderately. For example, simplification of the lactone ring (for example, by removal or inversion of the configuration at either one, two, or three of the substituents on C2–C4, or by reducing the size of the ring) leads to compounds with similar potency as the parent DDM (within one order of magnitude), thus indicating that the 3-hydroxy and the 2- and 4-methyl substituents do not play a critical role in determining DDM cytotoxicity.[27,30] However, the change in the conformation of the lactone observed upon tubulin binding places the methyl group at C2 close to the hydrophobic central body of DDM and is likely to be dictated by the need to optimize the contacts of the ligand with the hydrophobic floor of the protein binding pocket. Additionally, the significance of the configuration of butyrolactone analogues at C4[30] and the conspicuous loss in activity (one to three orders of magnitude) of DDM analogues in which the conformationally constrained lactone moiety has been replaced by diverse flexible esters or by substituted phenyl rings[31,32] underlie the relevance of the carbonyl group at C1 for activity. In agreement with this SAR data, the carbonyl group at C1 points away from the hydrophobic DDM skeleton, where it is readily available for contacts with hydrophilic protein side chains.

The one-dimensional ^{1}H and NOESY spectra showed that the δ-lactone ring of DDM opens up slowly by hydrolysis in the buffer. Comparison of the intensities of cross- and diagonal peaks reveals that the NOE rates of hydrolyzed DDM are only 15% of the NOE rates of intact DDM, thus indicating that binding of hydrolyzed DDM to tubulin is much weaker. This finding is in good agreement with activity data

 © 2006 Wiley-VCH Verlag GmbH & Co. KGaA, Weinheim

showing that the potency of DDM decreases approximately by a factor of six upon opening of the lactone.[27]

We have recently developed a new methodology, called INPHARMA, which is based on the observation of protein-mediated interligand NOE signals and allows the definition of the relative binding mode of two ligands binding to a common target in a mutually exclusive manner.[17] Briefly, during the mixing time of a NOESY experiment, acquired on a mixture of two competitive ligands A and B and a receptor protein T, the binding pocket of T is occupied by either of the two ligands A and B. Spin-diffusion through protons of the receptor generates a set of intermolecular cross-peaks between those protons of ligands A and B that are close to a common receptor site in the TA and TB complexes. A number of such intermolecular NOE signals define the relative orientation of the two ligands.

We have now applied the INPHARMA methodology to a mixture of tubulin (12 μM), epothilone (500 μM), and discodermolide (70 μM) with the goal of determining a common pharmacophore for the two drugs. A number of interligand NOE signals are observed between the two ligands (Figure 3A). Such NOE signals are not observed in the absence of the protein, thus confirming that they do not originate from the transient aggregation of the two ligands. Simultaneous binding of the two ligands to the protein can be excluded on the basis of biochemical data, thereby indicating that both DDM and EPO compete with taxol for tubulin binding.[1] The presence of protein-mediated interligand NOE signals verifies that DDM and EPO-A bind to the same binding pocket on tubulin, thus excluding an allosteric mechanism for the competitive binding of the two drugs. A summary of the observed interligand NOE signals is given in Figure 3B.

The higher affinity of DDM for tubulin meant that we had to use a very low concentration of DDM (70 μM), with the consequence that the interligand NOE signals are rather weak and can be observed mostly for the intense resonances of the methyl groups. The extensive overlap of the resonances of EPO-A and DDM between $\delta = 1$ and 2.5 ppm does not permit interpretation of the interligand NOE signals in this region. Me25, Me28, and Me29 of DDM (Scheme 1 and Figure 3B) show the strongest interligand NOE signals to both the side chain and ring protons of EPO, which indicates that these methyl groups are in contact with the protein surface. No interligand NOE signals can be evaluated for Me29 and Me32 of DDM because of the overlap with signals from Me25 and Me22 of EPO-A (Scheme 1).

As noted previously,[17] these protein-mediated interligand NOE signals can be quantitatively interpreted to discriminate between pairs of docking modes of the two ligands. However, the low intensity of the interligand NOE signals observed for the mixture of DDM and EPO-A in the presence of tubulin deterred us from a quantitative interpretation of the data. Instead, we assume that a partially overlapping pharmacophore exists for EPO-A and DDM, and we propose such a pharmacophore model guided by the qualitative interpretation of the interligand NOE signals and by the SAR data available for the two compounds. The presence of interligand NOE signals between one proton of DDM and one proton of EPO-A is interpreted as evidence

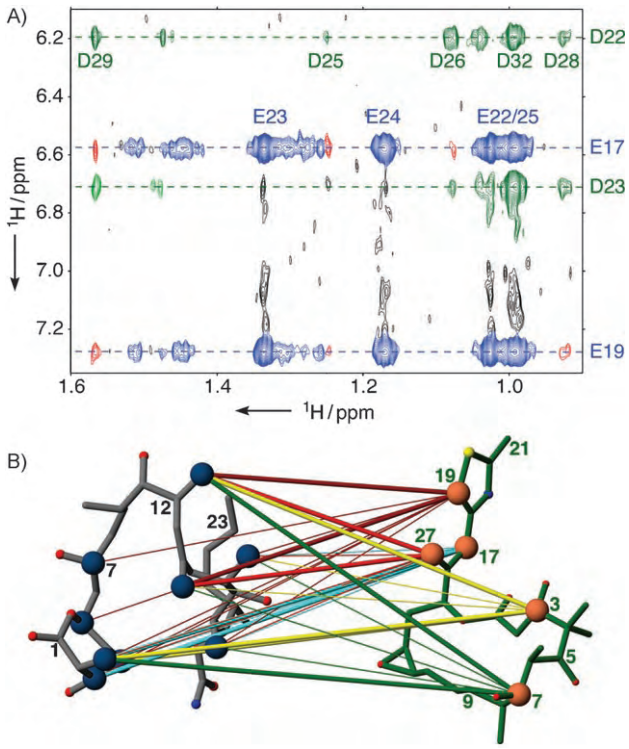

Figure 3. A) NOESY spectrum of the mixture DDM (70 μM), EPO-A (500 μM), and tubulin (12 μM) for the measurement of the INPHARMA NOE signals between the two ligands. The mixing time was 300 ms. Green and blue peaks represent intraligand transfer-NOE signals of DDM (labeled with D) and EPO-A (labeled with E), respectively, while the red peaks are the protein-mediated, interligand NOE signals (INPHARMA NOE signals). B) Schematic representation of the interligand NOE signals observed between DDM and EPO-A. The carbon atoms carrying the protons that show interligand NOE signals between DDM and EPO-A in the presence of tubulin are represented as spheres (blue for DDM and orange for EPO-A). Lines connect the sites of the two molecules that show an interligand NOE signal. Thick and thin lines represent strong and weak interligand NOE signals, respectively. Interligand NOE signals to the protons H3, H7, H17, H19, and H27 of EPO-A are represented by yellow, green, blue, brown, and red lines, respectively.

that these two protons occupy close sites in their complexes with the protein. Additionally, our common pharmacophore model tries to match the regions of both DDM and EPO-A identified to be essential for the interaction with tubulin and to reproduce the position of H-bond acceptors/donors and of hydrophobic elements in the two molecules. However, we also consider that the different morphology of the microtubules obtained in the presence of DDM and EPO suggests nonfully overlapping pharmacophores for the two drugs.[1]

Similar to EPO, DDM has a disc shape with dimensions $11 \times 10 \times 4.5$ Å (Figure 4A,B). The functional groups that are potentially involved in H bonds or in electrostatic interactions with the protein are concentrated on two edges of the disc, namely at the C1–C11 and at the C17–C19 regions (Figure 4A). Similarly, the partially charged groups of EPO are concentrated on the N-C1-C5 side and at C7.[12] The interligand NOE data suggest that the thiazole side chain and the C1–C3 region of the macrolide ring of EPO-A are

 © 2006 Wiley-VCH Verlag GmbH & Co. KGaA, Weinheim

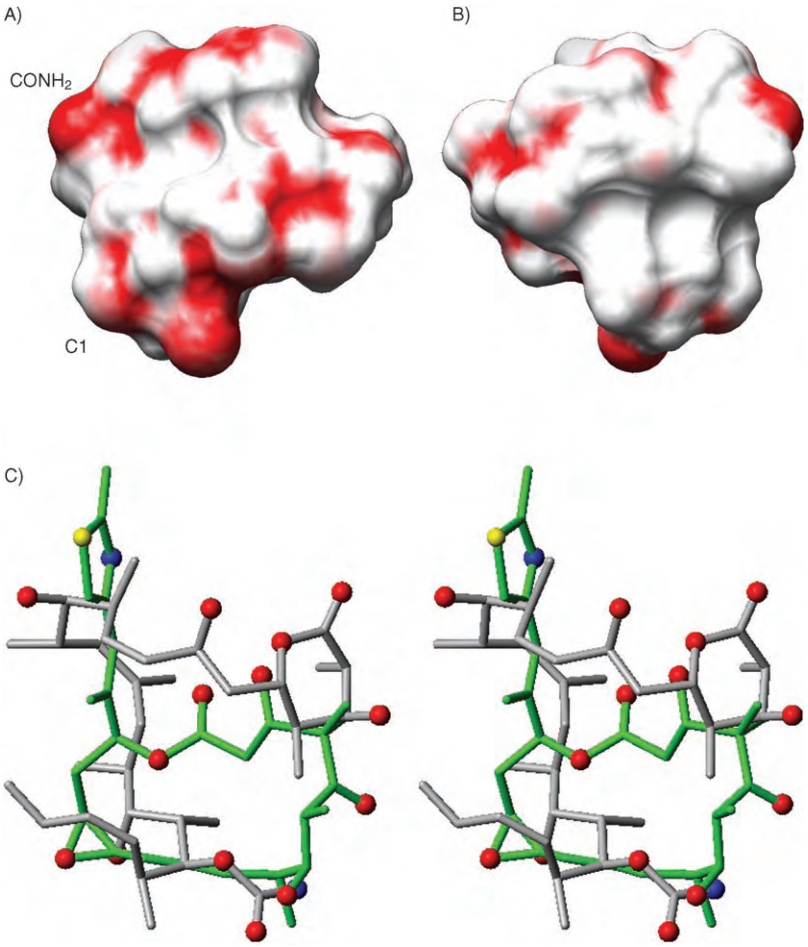

Figure 4. A) DDM, in a space-filling representation, has the form of a disc. The upper and lower edges present a high concentration of oxygen atoms (in red), while the flat sides of the disc are highly hydrophobic. B) Same as in (A) but turned 180° around the vertical axis. C) Stereoview of the common pharmacophore model for epothilone A (in green) and discodermolide (in gray) derived from INPHARMA NMR and literature SAR data. Heteroatoms are displayed as spheres: O red, S yellow, and N blue. In this model the C20–C24 tail of DDM is on the same side as the section C10–C13 of EPO-A, the carbamate group and the lactone ring occupy similar positions as the 7-OH group and C3–C4 unit of EPO-A, respectively, while the C8–C15 segment of DDM corresponds to the C15–C18 region of the side chain of EPO-A.

situated on the same side as the C1–C11 region of DDM, as we observe the strongest interligand NOE signals between Me25, Me28, and Me29 of DDM and H3, H19, and Me27 of EPO-A, while the interligand NOE signals of the same protons of EPO-A with Me30 and Me31 of DDM are weaker. Therefore, in our pharmacophore model the oxygen-rich C1–C11 region of DDM overlaps with the N-C1-C5 section of EPO-A (Figure 4C). The lactone ring of DDM, which is rich in hydrophilic groups, overlaps with the C3–C4 unit of EPO-A, with the O1 oxygen atom of DDM occupying a position close to the 3-OH group of EPO-A. The relevance of a hydrogen-bond acceptor in this region is supported by SAR data for both the carbonyl group at C1 of DDM and the 3-OH group of EPO.[33]

In our pharmacophore model for DDM and EPO-A (Figure 4C), the C15–C18 portion of the side chain of EPO-A overlaps with the C8–C15 segment of DDM, which contains the sharp turn in the extended backbone and the two double bonds at C8–C9 and C13–C14. Both regions feature sites of unsaturation and can interact favorably with hydrophobic regions on the protein. However, DDM does not extend as far as EPO-A and lacks an aromatic ring. Fundamental differences in the interaction of the two ligands with the protein are anticipated in this region, which in the EPO-A/tubulin complex involves the key residue H227 of the tubulin helix H7.[11] These differences could account for the different morphology of the tubulin polymers stabilized by DDM and EPO.

The second hydroxy group in the macrolide ring of EPO-A, attached at C7, overlaps with the carbamate side chain of DDM (Figure 4C). It has been suggested that the 7-OH group of EPO is involved in contacts with tubulin side chains, as inversion of the configuration at C7 results in a considerable loss of potency.[33] Similarly, DDM analogues lacking the carbamate moiety at C19 have reduced MT-stabilizing activity, while most of the activity can be recovered by introduction of a carbamate group at C17 or an acetyl group at C19.[31] These data suggest that the presence of an H-bond acceptor is essential at similar positions in DDM and EPO.

Finally, the hydrophobic C20–C24 tail of DDM is situated on the same side as the C10–C13 hydrophobic section of EPO-A, but does not fully overlap with it. In our common pharmacophore model for DDM and EPO, the C20–C24 tail of DDM propagates from the C10–C11 bond of EPO towards the protein. Analogously to the C10–C13 segment in EPO-A, SAR data support the contact of the C20–C24 tail of DDM with a hydrophobic cleft of the tubulin binding pocket. In fact, substitution of the whole moiety with a number of lipophilic groups or reduction of one or both double bonds of the diene side chain is well tolerated,[34] while shortening of the segment to an isopropyl group or complete deletion has a detrimental effect on potency.[28] Similarly, the C10–C13 segment of EPO cannot be shortened without hampering the activity, while hydrophobic substituents on C12 even increase the potency. A previously proposed pharmacophore model suggests instead that the C20–C24 tail of DDM corresponds to the side chain of EPO-A.[35] This model, however, does not explain very well the intermolecular NOE signals observed between the side chain of EPO-A and the methyl groups of the C1–C11 stretch of DDM.

Two highly hydrophobic pockets are found in the taxane binding site of tubulin that could host the C20–C24 tail of DDM (see the Supporting Information): the first comprising A206, L207, and I210 of helix H6 as well as L228 of helix H7 (see the Supporting Information), and the second comprising the F270–P272 section of the M loop as well as A231 and G235 of helix H7 (see the Supporting Information). However, unlike taxol, DDM conserves full activity on cell lines presenting the F270V and A364T mutations,[1] which allows us to exclude the possibility that DDM closely interacts with the second pocket and to propose that the C20–C24 side chain

 © 2006 Wiley-VCH Verlag GmbH & Co. KGaA, Weinheim

penetrates the hydrophobic cleft formed by the H6 helix and the N-terminal part of the H7 helix. EPO does not occupy this pocket,[11] while taxol places the C2 benzoyl side chain in it. Such structural differences could be partially responsible for the different morphology of MTs formed in the presence of EPO or DDM.

In conclusion, we have determined the bioactive conformation of DDM in solution from NMR tr-NOE data and found that DDM binds to tubulin in a compact globular shape. This result supports the existence of common structural requirements for the diverse natural products binding to the taxane binding pocket, with the bioactive structural motif being centered on a compact core.

With the help of both protein-mediated interligand NOE signals between DDM and EPO and the SAR data available for the two drugs, we propose a common pharmacophore model in which the C20–C24 segment of DDM does not overlap with the thiazole side chain of EPO. Similarities and differences in the pharmacophore of the two drugs may provide a rationale for the analogous but not fully equivalent biological activity of the two natural products.

Experimental Section

Tubulin preparation: Tubulin extracted from bovine brain was purchased from Cytoskeleton Inc. (Denver, CO, USA). Tubulin solution (66 μL) were diluted in buffer (350 μL, aqueous solution containing 1.5 mM phosphate, 1.5 mM calcium, and sodium at pH 7.0) and dialyzed twice with buffer (2 × 1.5 L) at 4 °C. The solution was dialyzed further with D_2O buffer (2 × 15 mL) to exchange H_2O for D_2O.

Sample preparation: DDM was first dissolved in [D_6]DMSO (25 μL) and then added to the tubulin solution to give a volume of 500 μL containing 5% v/v [D_6]DMSO with the desired amount of ligand (0.5 mM). A final concentration of tubulin of 10 μM is estimated. 5% [D_6]DMSO was used as cosolvent to increase the DDM solubility. In our experience, this small amount of DMSO does not affect either the observation or the size of tr-NOE of other tubulin ligands, such as EPO-A or taxol.

NMR spectroscopy: NMR experiments were measured on a Bruker 800 MHz spectrometer. Resonances of DDM were assigned from COSY, TOCSY, HSQC, and HMBC spectra. A series of NOESY experiments was recorded at 25 °C with mixing times of 20, 40, 60, 80, 150, and 200 ms on the two samples tubulin–DDM and free-DDM. Processed spectra were analyzed with FELIX (Accelrys Software Inc., CA, USA).

Structure calculation: Structures were calculated with XPLOR-NIH 2.13[36] using restrained simulated annealing (SA) from a single extended starting template. NOE signals were used in the full relaxation matrix approach. Protocol details are provided in the Supporting Information.

Interligand NOE signals: Protein-mediated interligand NOE signals between EPO-A and DDM were observed in a NOESY spectrum acquired at 900 MHz on a sample containing 12 μM tubulin, 500 μM EPO-A, and 70 μM DDM in a D_2O/DMSO (95/5) solution. The mixing time was 300 ms.

Received: July 13, 2006
Published online: October 12, 2006

Keywords: conformation analysis · discodermolide · NMR spectroscopy · structure–activity relationships · tubulin

[1] R. J. Kowalski, P. Giannakakou, S. P. Gunasekera, R. E. Longley, B. W. Day, E. Hamel, *Mol. Pharmacol.* **1997**, *52*, 613 – 622.
[2] S. Kar, G. J. Florence, I. Paterson, L. A. Amos, *FEBS Lett.* **2003**, *539*, 34 – 36.
[3] G. S. Huang, L. Lopez-Barcons, B. S. Freeze, A. B. Smith, G. L. Goldberg, S. B. Horwitz, H. M. McDaid, *Clin. Cancer Res.* **2006**, *12*, 298 – 304.
[4] D. M. Bollag, *Expert Opin. Invest. Drugs* **1997**, *6*, 867 – 873.
[5] E. Hamel, *Med. Res. Rev.* **1996**, *16*, 207 – 231.
[6] J. Verweij, M. Clavel, B. Chevalier, *Ann. Onc.* **1994**, *5*, 495 – 505.
[7] L. A. Martello, M. J. LaMarche, L. F. He, T. J. Beauchamp, A. B. Smith, S. B. Horwitz, *Chem. Biol.* **2001**, *8*, 843 – 855.
[8] K. H. Altmann, *Curr. Opin. Chem. Biol.* **2001**, *5*, 424 – 431.
[9] J. Jimenez-Barbero, F. Amat-Guerri, J. P. Snyder, *Curr. Med. Chem.: Anti-Cancer Agents* **2002**, *2*, 91 – 122.
[10] E. Nogales, S. G. Wolf, K. H. Downing, *Nature* **1998**, *393*, 191 – 191.
[11] J. H. Nettles, H. L. Li, B. Cornett, J. M. Krahn, J. P. Snyder, K. H. Downing, *Science* **2004**, *305*, 866 – 869.
[12] T. Carlomagno, M. J. J. Blommers, J. Meiler, W. Jahnke, T. Schupp, F. Petersen, D. Schinzer, K. H. Altmann, C. Griesinger, *Angew. Chem.* **2003**, *115*, 2619 – 2621; *Angew. Chem. Int. Ed.* **2003**, *42*, 2511 – 2515.
[13] T. Carlomagno, V. M. Sanchez, M. J. J. Blommers, C. Griesinger, *Angew. Chem.* **2003**, *115*, 2615 – 2519; *Angew. Chem. Int. Ed.* **2003**, *42*, 2515 – 2517.
[14] A. B. Smith, M. J. LaMarche, M. Falcone-Hindley, *Org. Lett.* **2001**, *3*, 695 – 698.
[15] E. Monteagudo, D. O. Cicero, B. Cornett, D. C. Myles, J. P. Snyder, *J. Am. Chem. Soc.* **2001**, *123*, 6929 – 6930.
[16] S. P. Gunasekera, M. Gunasekera, R. E. Longley, *J. Org. Chem.* **1990**, *55*, 4912 – 4915.
[17] V. M. Sanchez-Pedregal, M. Reese, J. Meiler, M. J. J. Blommers, C. Griesinger, T. Carlomagno, *Angew. Chem.* **2005**, *117*, 4244 – 4247; *Angew. Chem. Int. Ed.* **2005**, *44*, 4172 – 4175.
[18] F. Solomon, *Biochemistry* **1977**, *16*, 358 – 363.
[19] J. F. Diaz, J. M. Andreu, *Biochemistry* **1993**, *32*, 2747 – 2755.
[20] H. W. Wang, E. Nogales, *Nature* **2005**, *435*, 911 – 915.
[21] R. M. Buey, I. Barasoain, E. Jackson, A. Meyer, P. Giannakakou, I. Paterson, S. Mooberry, J. M. Andreu, J. F. Diaz, *Chem. Biol.* **2005**, *12*, 1269 – 1279.
[22] F. Ni, *Prog. Nucl. Magn. Reson. Spectrosc.* **1994**, *26*, 517 – 606.
[23] L. F. He, G. A. Orr, S. B. Horwitz, *Drug Discovery Today* **2001**, *6*, 1153 – 1164.
[24] P. Ballone, M. Marchi, *J. Phys. Chem. A* **1999**, *103*, 3097 – 3102.
[25] I. Paterson, R. Britton, O. Delgado, A. Meyer, K. G. Poullennec, *Angew. Chem.* **2004**, *116*, 4729 – 4733; *Angew. Chem. Int. Ed.* **2004**, *43*, 4629 – 4633.
[26] S. P. Gunasekera, S. J. Mickel, R. Daeffler, D. Niederer, A. E. Wright, P. Linley, T. Pitts, *J. Nat. Prod.* **2004**, *67*, 749 – 756.
[27] S. P. Gunasekera, G. K. Paul, R. E. Longley, R. A. Isbrucker, S. A. Pomponi, *J. Nat. Prod.* **2002**, *65*, 1643 – 1648.
[28] N. Choy, Y. S. Shin, P. Q. Nguyen, D. P. Curran, R. Balachandran, C. Madiraju, B. W. Day, *J. Med. Chem.* **2003**, *46*, 2846 – 2864.
[29] D. T. Hung, J. B. Nerenberg, S. L. Schreiber, *J. Am. Chem. Soc.* **1996**, *118*, 11 054 – 11 080.
[30] S. J. Shaw, K. F. Sundermann, M. A. Burlingame, D. C. Myles, B. S. Freeze, M. Xian, I. Brouard, A. B. Smith, *J. Am. Chem. Soc.* **2005**, *127*, 6532 – 6533.
[31] J. M. Minguez, S. Y. Kim, K. A. Giuliano, R. Balachandran, C. Madiraju, B. W. Day, D. P. Curran, *Bioorg. Med. Chem.* **2003**, *11*, 3335 – 3357.
[32] A. B. Smith, S. B. Freeze, M. J. LaMarche, T. Hirose, I. Brouard, M. Xian, K. F. Sundermann, S. J. Shaw, M. A. Burlingame, S. B. Horwitz, D. C. Myles, *Org. Lett.* **2005**, *7*, 315 – 318.

 © 2006 Wiley-VCH Verlag GmbH & Co. KGaA, Weinheim

[33] K. C. Nicolaou, F. Roschangar, D. Vourloumis, *Angew. Chem.* **1998**, *110*, 2120 – 2153; *Angew. Chem. Int. Ed.* **1998**, *37*, 2015 – 2045.
[34] A. B. Smith, M. Xian, *Org. Lett.* **2005**, *7*, 5229 – 5232.
[35] I. Ojima, S. Chakravarty, T. Inoue, S. N. Lin, L. F. He, S. B. Horwitz, S. D. Kuduk, S. J. Danishefsky, *Proc. Natl. Acad. Sci. USA* **1999**, *96*, 4256 – 4261.
[36] C. D. Schwieters, J. J. Kuszewski, N. Tjandra, G. M. Clore, *J. Magn. Reson.* **2003**, *160*, 65 – 73.
[37] R. Koradi, M. Billeter, K. Wüthrich, *J. Mol. Graphics* **1996**, *14*, 51 – 55.

 © 2006 Wiley-VCH Verlag GmbH & Co. KGaA, Weinheim

Iron Imido Complexes

DOI: 10.1002/anie.200602799

A Tosylimido Analogue of a Nonheme Oxoiron(IV) Complex**

Eric J. Klinker, Timothy A. Jackson, Michael P. Jensen, Audria Stubna, Gergely Juhász, Emile L. Bominaar, Eckard Münck, and Lawrence Que, Jr.**

High-valent nonheme iron complexes play key roles as intermediates in biology and catalysis.[1–3] Examples of oxoiron(IV) centers in nonheme ligand environments have been characterized in both enzymes[4,5] and model systems[6] and have been shown to participate in the hydroxylation of C–H bonds.[7,8] The analogous imidoiron(IV) unit should be capable of isolobal amination reactions and has been implicated in such iron-catalyzed reactions;[9] it is also proposed to be an intermediate in the formation of an isolated amidoiron(III) complex.[10] The only two structurally characterized examples of an imidoiron(IV) unit show this group in a tetrahedral geometry supported by a tridentate pyrazolyl/bis(phosphino)borate ligand[11] or as part of a novel $\{Fe^{III}{}_3Fe^{IV}(NR)_4\}$ cubane cluster.[12] In this paper, we report the generation and characterization of the tosylimidoiron(IV) analogue of the well-characterized oxoiron(IV) complex $[Fe^{IV}(O)(N4Py)]^{2+}$ (N4Py = *N*,*N*-bis(2-pyridylmethyl)bis(2-pyridyl)methylamine).[13] This first example of a pair of complexes with a ligand that can support both an oxo- and imidoiron(IV) unit provides a unique opportunity for a comparative study.

The oxoiron(IV) complex $[Fe^{IV}(O)(N4Py)]^{2+}$ (**1**) can be readily generated in high yield by oxygen-atom transfer from solid iodosylbenzene (PhIO) to $[Fe^{II}(NCMe)(N4Py)]^{2+}$ in MeCN.[8] In an analogous manner, the tosylimidoiron(IV) complex $[Fe^{IV}(NTs)(N4Py)]^{2+}$ (**2**) was prepared by treating the iron(II) precursor in MeCN with solid mesityl-*N*-tosylimidoiodinane (MsINTs; Ms = 2,4,6-$Me_3C_6H_2$, Ts = tosyl) at room temperature. Within minutes of the addition, the orange solution of the iron(II) starting material faded to a gold color. Complex **2** exhibits a visible spectrum (Figure 1) with an intense band at $\lambda = 445$ nm ($\varepsilon = 2700\,M^{-1}cm^{-1}$) and a much weaker and broader feature at $\lambda = 660$ nm ($\varepsilon = 250\,M^{-1}cm^{-1}$, Figure 1 inset). The latter may correspond to the band at $\lambda =$ 695 nm ($\varepsilon = 400\,M^{-1}cm^{-1}$, Figure 1 inset) observed for **1** that arises from ligand-field transitions characteristic of an $S = 1$ oxoiron(IV) center.[14] Complex **2** has a Mössbauer spectrum at 4.2 K that consists of a doublet with a quadrupole splitting of 0.93 $mm\,s^{-1}$ and an isomer shift of 0.02 $mm\,s^{-1}$, parameters that fall within the range of those found for nonheme oxoiron(IV) complexes.[2] It gives rise to a high-resolution electrospray mass spectrum with a major ion species at *m*/*z* 741.0860 that corresponds to $[\{Fe^{IV}(NTs)(N4Py)\}(SO_3CF_3)]^+$ (*m*/*z* calculated 741.0859).

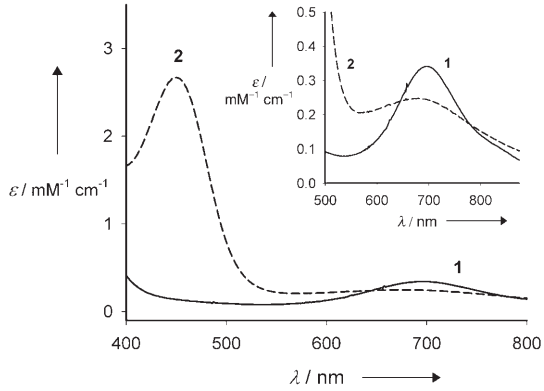

Figure 1. Visible spectra of $[Fe^{IV}(X)(N4Py)]^{2+}$ in MeCN (X = O, **1**; X = NTs, **2**). Inset: Vertically expanded lower-energy region.

The ^1H NMR spectrum of **2** (Figure 2) is similar to, but distinct from, that of **1**. Like **1**, complex **2** exhibits two equally intense sets of paramagnetically shifted pyridine ring protons, indicating the presence of an effective mirror plane of symmetry on the NMR time scale. The pyridine protons display a unique shift pattern arising from the $S = 1$ iron(IV) center[13] in which one pyridine β-proton signal is downfield-shifted to about $\delta = 45$ ppm, the other β-proton signal is upfield-shifted to about $\delta = -15$ ppm, and the γ-proton peak is downfield-shifted to about $\delta = 18$ ppm. The ^1H NMR spectrum of **2** also shows the presence of a small amount of **1**; the latter arises from trace water in the solvent that

[*] Dr. A. Stubna, Dr. G. Juhász, Prof. Dr. E. L. Bominaar, Prof. Dr. E. Münck
Department of Chemistry
Carnegie Mellon University
Pittsburgh, PA 15213 (USA)
Fax: (+1) 412-268-1061
E-mail: emunck@cmu.edu
E. J. Klinker, Dr. T. A. Jackson, Dr. M. P. Jensen, Prof. Dr. L. Que, Jr.
Department of Chemistry and
Center for Metals in Biocatalysis
University of Minnesota
Minneapolis, MN 55455 (USA)
Fax: (+1) 612-624-7029
E-mail: que@chem.umn.edu

[**] Supported by NIH grants GM-33162 (L.Q.) and GM-22701 (E.M.), an NIH postdoctoral fellowship to T.A.J., and an NSF graduate research fellowship to A.S. XAS data were collected at the Stanford Synchrotron Radiation Laboratory (SSRL), which is supported by the US Department of Energy and the National Institutes of Health.

Supporting information for this article is available on the WWW under http://www.angewandte.org or from the author.

InterScience
© 2006 Wiley-VCH Verlag GmbH & Co. KGaA, Weinheim

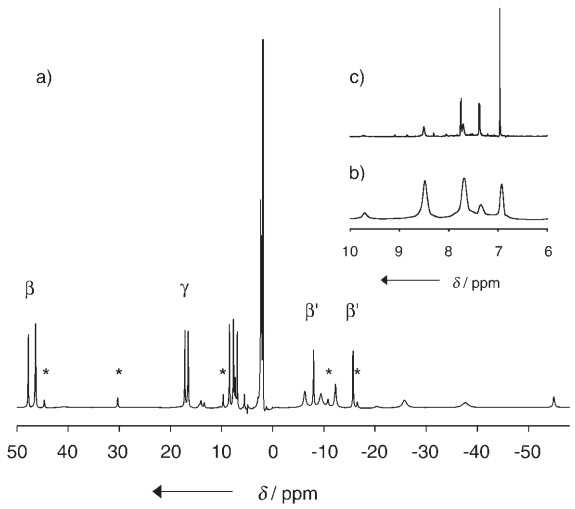

Figure 2. ^{1}H NMR spectrum of **2** in CD_3CN. Peaks assigned to a minor impurity of **1** are marked by (*). Insets show the $\delta = 6$–10 ppm region for **2** under conditions to enhance paramagnetically shifted protons (b) and under normal ^{1}H NMR conditions (c).

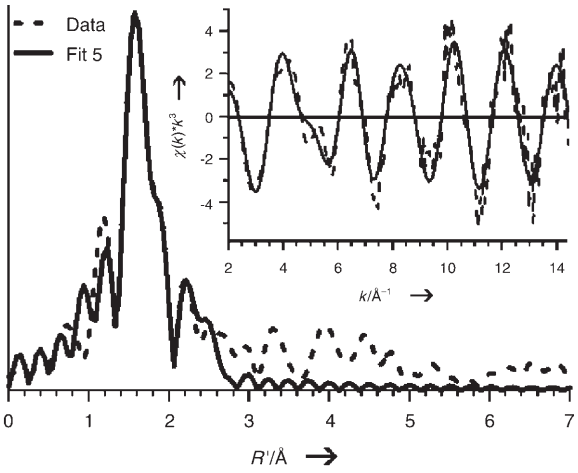

Figure 3. Fourier transform of the Fe K-edge EXAFS data and EXAFS spectrum (inset) of $[Fe^{IV}(NTs)(N4Py)]^{2+}$. Experimental data are shown in dashed lines and fits in solid lines. See the Supporting Information for EXAFS and Fourier transform range.

hydrolyzes part of the MsINTs oxidant to MsIO (**2** is not converted into **1** by the addition of trace water). The tosyl aromatic protons are observed at $\delta = 8.50$ and 7.71 ppm (Figure 2b), with integrations that match the values found for the pyridine proton peaks of **2**. With ^{1}H NMR parameters used for diamagnetic compounds, these tosyl resonances become obscured by peaks at $\delta = 7.75$ and 7.37 ppm (Figure 2c) corresponding to the protons of free tosylamide. The integrations of these peaks relative to that of the aromatic protons of the iodomesitylene by-product ($\delta = 6.95$ ppm) reveal an amount of free tosylamide (20%) that corresponds well to the amount of **1** present in the sample (15%). These data further support the formulation of **2** as $[Fe^{IV}(NTs)(N4Py)]^{2+}$.

Fe K-edge X-ray absorption spectroscopy (XAS) provides additional insight into the geometric and electronic structure of **2**. Complexes **1** and **2** exhibit 1s→3d transitions at about 7114 eV with areas of 25 and 18 units, respectively (Supporting Information).[15] As discussed previously, the relatively large value observed for **1** is a result of the short Fe–O bond length of 1.64 Å;[15] consequently, the pre-edge area of 18 suggests a smaller degree of distortion for the iron center of **2**, namely, a relatively long Fe–NTs bond. Indeed, a similar value was recently observed for the thiolate-ligated oxo-iron(IV) complex $[Fe^{IV}(O)(tmcs)]^+$ (tmcs = monoanion of 1-mercaptoethyl-4,8,11-trimethyl-1,4,8,11-tetraazacyclotetradecane), which, on the basis of an EXAFS analysis, exhibits a somewhat longer Fe–O bond (1.70 Å).[16]

An analysis of the EXAFS data obtained for **2** provides metric details of the iron coordination environment. In Figure 3 are displayed the *R*′-space and *k*-space EXAFS spectra of **2** along with the best fit to these data (see the Supporting Information for fitting details). The EXAFS data for **2** are well fit with three shells consisting of one N scatterer at 1.73 Å, five N scatterers at 1.97 Å, and six C scatterers at 2.87 Å. The latter two shells can be associated respectively with N and C atoms of the N4Py ligand, as observed in the X-ray crystal structure of **1**. The single scatterer at 1.73 Å is thus attributed to the N atom of the NTs ligand.

Notably, the Fe–N bond length found for **2** (1.73 Å) is significantly longer than the bond lengths observed crystallographically for the Fe–O bond in **1**[13] and for the Fe–N bonds of two other iron(IV) imido complexes (ca. 1.65 Å).[11,12] Relative to the latter two complexes, the longer bond in **2** can be rationalized by the difference in the coordination numbers of the iron(IV) centers. The previously characterized complexes have a tetrahedral geometry about the iron center with a strong trigonal distortion for which the π-antibonding molecular orbitals (MOs) associated with the imido ligand are unoccupied.[3] These complexes thus have a formal Fe≡NR triple bond and a collinear Fe-N-R unit.[3,11,12] In contrast, the corresponding MOs for octahedral **2** are singly occupied, thus giving rise to an Fe=N double bond instead. This experimental result is supported by a DFT geometry-optimized structure for **2** (Figure 4a and the Supporting Information), which is constrained to have C_s symmetry to be consistent with the NMR results and displays a Fe–NTs bond length of 1.75 Å.

The effects of the different Fe=X units in **1** and **2** on their ground-state electronic structures were revealed by high-field Mössbauer analysis; the experimental results were complemented by DFT calculations that were based on the geometry-optimized structures for **1** and **2** (see the Supporting Information). Variable-temperature Mössbauer spectra for **1** and **2** in acetonitrile were obtained in applied magnetic fields of up to 8.0 T; spectra of each compound at 4.2 K are shown in Figure 5. The spectra were simulated by using the $S = 1$ spin Hamiltonian of Equation (1), in which all symbols have their conventional meanings.[17]

$$H = D(S_z^2 - {}^2/_3) + E(S_x^2 - S_y^2) + \beta \mathbf{B}\,\mathbf{g}\,\mathbf{S} + \mathbf{S}\,\mathbf{A}\,\mathbf{I} - g_n\beta_n\,\mathbf{I}\,\mathbf{B} + H_Q$$
$$H_Q = \frac{e\,Q\,V_{zz}}{12}\left[3\,I_z^2 - \frac{15}{4} + \eta(I_x^2 - I_y^2)\right] \quad (1)$$

Analysis of the spectra of **1** shows that the magnetic hyperfine tensor, **A**, and the zero-field splitting (ZFS) tensor

 © 2006 Wiley-VCH Verlag GmbH & Co. KGaA, Weinheim

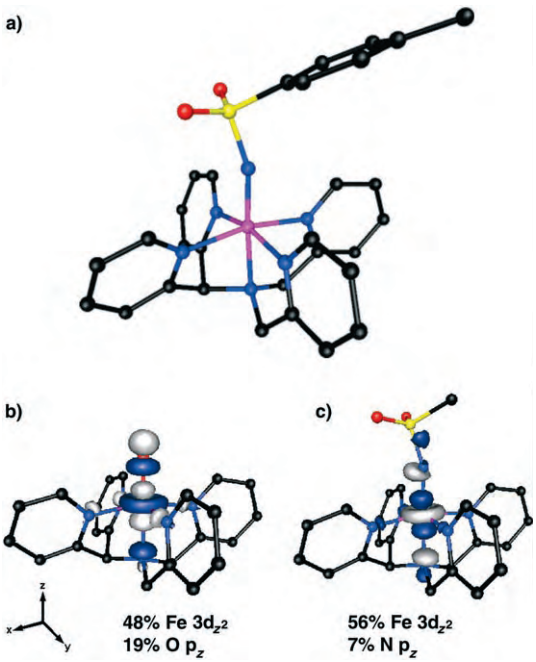

Figure 4. Molecular structure of $[Fe^{IV}(NTs)(N4Py)]^{2+}$ based on DFT geometry optimization (a), and contour plots of the Fe $3d_{z^2}$-based MOs of $[Fe^{IV}(O)(N4Py)]^{2+}$ (b) and $[Fe^{IV}(NTs)(N4Py)]^{2+}$ (c) based on DFT computations. Fe purple, C black, N blue, O red, S yellow. The contributions to the MOs from the Fe $3d_{z^2}$ and oxo O and imido N 2p orbitals are displayed. For clarity in (c), the tolyl ring is not shown.

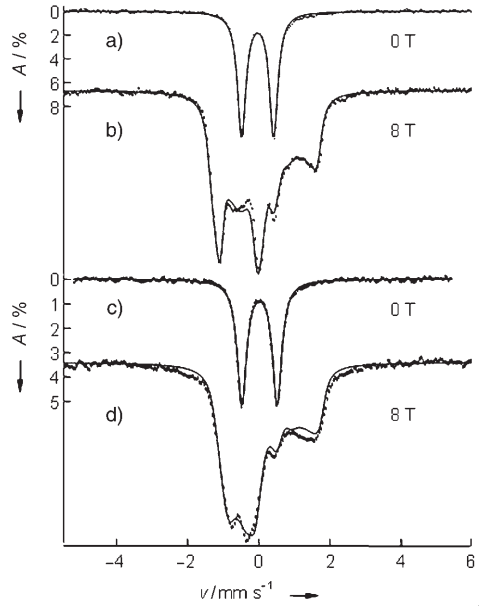

Figure 5. Mössbauer spectra of **1** (a, b) and **2** (c, d) in CH_3CN at 4.2 K. Spectra in (a) and (c) were obtained in zero field while those in (b) and (d) were obtained in a magnetic field of 8.0 T applied parallel to the observed γ rays. The solid lines are spectral simulations based on the $S=1$ Hamiltonian of Equation (1) using the parameters in Table 1 and in Table S2 of the Supporting Information. Both **1** and **2** contained minor contaminants; for clarity, their contributions were removed from the spectra. A complete set of data, spectral simulations, and information about the contaminants are given in the Supporting Information.

are both axial (that is, $A_x = A_y$ and $E/D = 0$) and that A_z lies along the symmetry axis of the ZFS tensor (Table 1). DFT computations for **1** also yield an axial **A** tensor, with A_z aligned within 10° of the Fe–O bond. Our combined DFT/crystal-field studies of previous complexes[14,16,18] and **1** suggest that the z axis of the ZFS tensor and therefore of Equation (1) is along the Fe–O vector.

Table 1: Properties of $[Fe^{IV}(NTs)(N4Py)]^{2+}$ (**2**) and $[Fe^{IV}(O)(N4Py)]^{2+}$ (**1**) complexes.[a]

	$[Fe^{IV}(NTs)(N4Py)]^{2+}$	$[Fe^{IV}(O)(N4Py)]^{2+}$
$t_{1/2}$ at 25 °C [h]	3 h	60 h
r(Fe–N/O) [Å]	1.73 (1.75)	1.64[b] (1.65)
	1.97 (2.01)	1.96 (2.01)
λ_{max} [nm] {ε [$M^{-1}cm^{-1}$]}	445 {2700}	
	660 {250}	695 {400}
δ [mm s^{-1}]	0.02 (0.13[c])	−0.04 (0.03[c])
ΔE_Q [mm s^{-1}]	+0.98 (1.13)	+0.93 (1.03)
η	−0.7 (−1.2)	$0<\eta<0.5$ (0.01)
D [cm^{-1}]	29	22
E/D	0.23	0
$A_x/g_n\beta$ [T][d,e]	−20 (−20.5)	−21 (−20.3)
$A_y/g_n\beta_n$ [T][d,e]	−21 (−18.3)	−21 (−20.8)
$A_z/g_n\beta_n$ [T][d,e]	−3 (−5)	−5 (−4.1)
E_o [eV]	7123.8	7123.7[f]
$E_{pre\text{-}edge}$ [eV]	7113.9	7114.3[f]
pre-edge area	18	25[f]

[a] Values in parentheses derived from DFT calculations (see the Supporting Information for details). [b] Obtained by X-ray crystallography; see reference [13]. [c] For the N4Py ligand, for reasons not yet understood, our computations yield δ values noticeably larger than those observed experimentally. Rotation of the tosyl group around the Fe–N bond, followed by geometry optimization, changed the δ value by less than 0.02 mm s^{-1}. [d] Final A values were obtained by adding the calculated spin–dipolar contribution to the experimental value $A_{iso} = (A_x + A_y + A_z)/3$. We used this procedure because DFT A_{iso} values generally are in poor agreement with experimental data. The z axes of the electric-field gradient tensor and the spin–dipolar part of **A** are coincident within 5° with the Fe–NTs bond axis. [e] At 4.2 K the internal field $B_{int} \approx \{g_\perp A_\perp S(S+1)/D\}\beta B/g_n\beta_n$ and thus the product $g_\perp A_\perp$, rather than $A_\perp$, is determined, thereby illustrating the point for axial symmetry. In our simulations we have fixed $g_\perp = 2$. The real $A_\perp$ value may be slightly smaller but probably not by more than 10%. As an example, the correction is about 1% for $[Fe^{IV}(O)(tmcs)]^+$ as calculated by time-dependent DFT.[16] [f] From reference [15].

The applied-field Mössbauer spectra of **2** are quite distinct from those of **1** (Figure 5b,d). These differences arise from a substantial anisotropy of the magnetic hyperfine field ($\mathbf{B}_{int} = -\langle \mathbf{S} \rangle \mathbf{A}/g_n\beta_n$) in the xy plane of **2** (for example, 3.3 T in the spectrum of Figure 5d). This anisotropy can be caused by a rhombic ZFS tensor ($E/D \neq 0$) and/or by a rhombic **A** tensor ($A_x \neq A_y$). Although the Mössbauer data do not allow us to determine these three parameters independently, the expression $A_\perp = (A_x + A_y)/2$ is nearly independent of the E/D value used to fit the spectra. For C_s symmetry, implied by the ^{1}H NMR spectrum of **2** (Figure 2), the anisotropy of **A** is determined by the spin–dipolar contribution, $\mathbf{A}_{S\text{-}D}$. As DFT calculations on **2** yield a nearly axial $\mathbf{A}_{S\text{-}D}$, ($A_{jj}/g_n\beta_n = -3.5, -5, +8.5$ T for $j = x$, y, and z, respectively), we conclude that the magnetic anisotropy of **2** is a result of a finite E/D value of

 © 2006 Wiley-VCH Verlag GmbH & Co. KGaA, Weinheim

0.23, determined by fitting the Mössbauer spectra of **2** with a nearly axial **A** tensor. For **2** we found that $A_\perp/g_n\beta_n$ is about −20.5 T if $S=1$ is assumed, a value which fits well in the range −20 T to −23 T observed for $S=1$ complexes.[6,16,19] In contrast, fitting the spectra of **2** under assumption of an $S=2$ ground state yielded $A_\perp/g_n\beta_n \approx -6.5$ T, which, in magnitude, is substantially below $-A_\perp/g_n\beta_n = 16$–20 T observed for $S=2$ Fe^{IV} species.[4,20]

Nonheme oxoiron(IV) complexes exhibit large D values, which arise from spin–orbit coupling of the $S=1$ ground state with low-lying $S=2$ excited states.[16,18] Importantly, this coupling modifies the D value but affects the **g** and **A** tensors of Equation (1) in a minor way at most. Spin–orbit coupling with low-lying $S=1$ excited states would give rise to substantially smaller $A_\perp/g_n\beta_n$ values owing to partial unquenching of the orbital angular momentum and give a positive contribution to **A**.[21] Because this is not the case for **1** and **2**, we conclude that spin–orbit coupling of the ground state with low-lying $S=2$ and/or $S=0$ excited states is responsible for the large D value, as shown in the Supporting Information.

The DFT calculations also shed light on the dominant bonding interactions that determine the differing Fe=X bond lengths of **1** and **2**. For both systems, a $(3d_{xy})^2(3d_{xz})^1(3d_{yz})^1$ electronic configuration is observed, thus consistent with formal Fe=O and Fe=NR bonds. As evidenced by the almost equal mixture of Fe 3d and oxo O 2p or imido N 2p character in the Fe $3d_{xz}$- and $3d_{yz}$-based MOs, both complexes exhibit strong Fe=X π bonds. However, differences between **1** and **2** are apparent in the Fe $3d_{z^2}$-based MOs. For **1**, a strong σ-antibonding interaction between the $3d_{z^2}$ orbital and the O p_z orbital (Figure 4a) splits the spin-up Fe $3d_{x^2-y^2}$- and $3d_{z^2}$-based MOs by roughly 0.6 eV (Supporting Information). In contrast, the corresponding MOs of **2** are nearly degenerate (split by only about 0.05 eV). This is a result of a less favorable interaction between the Fe $3d_{z^2}$ and the N p_z-like orbital of the tosylimido ligand (Figure 4c), the latter of which is stabilized relative to the corresponding N $2p_y$ and $2p_x$ orbitals owing to the N–S bonding interaction. Thus, these DFT studies reveal that, despite the fact that both **2** and **1** contain formal Fe=N and Fe=O bonds, respectively, the Fe–O σ interaction of **1** is significantly stronger than the corresponding Fe–NTs interaction in **2**, which accounts in part for the relatively long Fe–NTs bond length of 1.73 Å.

The longer Fe–N bond of **2** suggests that the tosylimido group may not be able to stabilize the iron(IV) center as well as the oxo ligand in **1**. Indeed, **2** has a half-life of three hours for self-decay at room temperature, which is a factor of 20 shorter than that of **1**. This difference is also consistent with the faster transfer of NTs from PhINTs (versus PhIO) to the pendant phenyl group of $[Fe^{II}(6\text{-Ph-tpa})]^{2+}$ (tpa = tris(2-pyridylmethyl)amine).[9a] Further studies are clearly warranted to understand the relative oxidative abilities of Fe^{IV}=O and Fe^{IV}=NR units and to place them within the greater context of recently reported high-valent nitridoiron complexes.[22]

Received: July 13, 2006
Published online: October 13, 2006

Keywords: bioinorganic chemistry · density functional calculations · imido ligands · iron · Mössbauer spectroscopy

[1] M. Costas, M. P. Mehn, M. P. Jensen, L. Que, Jr., *Chem. Rev.* **2004**, *104*, 939.
[2] X. Shan, L. Que, Jr., *J. Inorg. Biochem.* **2006**, *100*, 421.
[3] M. P. Mehn, J. C. Peters, *J. Inorg. Biochem.* **2006**, *100*, 634.
[4] J. C. Price, E. W. Barr, B. Tirupati, J. M. Bollinger, Jr., C. Krebs, *Biochemistry* **2003**, *42*, 7497.
[5] D. A. Proshlyakov, T. F. Henshaw, G. R. Monterosso, M. J. Ryle, R. P. Hausinger, *J. Am. Chem. Soc.* **2004**, *126*, 1022; P. J. Riggs-Gelasco, J. C. Price, R. B. Guyer, J. H. Brehm, E. W. Barr, J. M. Bollinger, Jr., C. Krebs, *J. Am. Chem. Soc.* **2004**, *126*, 8108.
[6] J.-U. Rohde, J.-H. In, M.-H. Lim, W. W. Brennessel, M. R. Bukowski, A. Stubna, E. Münck, W. Nam, L. Que, Jr., *Science* **2003**, *229*, 1037; M. H. Lim, J.-U. Rohde, A. Stubna, M. R. Bukowski, M. Costas, R. Y. N. Ho, E. Münck, W. Nam, L. Que, Jr., *Proc. Natl. Acad. Sci. USA* **2003**, *100*, 3665.
[7] J. C. Price, E. W. Barr, T. E. Glass, C. Krebs, J. M. Bollinger, Jr., *J. Am. Chem. Soc.* **2003**, *125*, 13008.
[8] J. Kaizer, E. J. Klinker, N. Y. Oh, J.-U. Rohde, W. J. Song, A. Stubna, J. Kim, E. Münck, W. Nam, L. Que, Jr., *J. Am. Chem. Soc.* **2004**, *126*, 472.
[9] M. P. Jensen, M. P. Mehn, L. Que, Jr., *Angew. Chem.* **2003**, *115*, 3940; *Angew. Chem. Int. Ed.* **2003**, *42*, 4357; F. Avenier, J.-M. Latour, *Chem. Commun.* **2004**, 1544.
[10] R. L. Lucas, D. R. Powell, A. S. Borovik, *J. Am. Chem. Soc.* **2005**, *127*, 11596.
[11] C. M. Thomas, N. P. Mankad, J. C. Peters, *J. Am. Chem. Soc.* **2006**, *128*, 4956.
[12] A. K. Verma, T. N. Nazif, C. Achim, S. C. Lee, *J. Am. Chem. Soc.* **2000**, *122*, 11013.
[13] E. J. Klinker, J. Kaizer, W. W. Brennessel, N. L. Woodrum, C. J. Cramer, L. Que, Jr., *Angew. Chem.* **2005**, *117*, 3756; *Angew. Chem. Int. Ed.* **2005**, *44*, 3690.
[14] A. Decker, J.-U. Rohde, L. Que, Jr., E. I. Solomon, *J. Am. Chem. Soc.* **2004**, *126*, 5378.
[15] J.-U. Rohde, S. Torelli, X. Shan, M. H. Lim, E. J. Klinker, J. Kaizer, K. Chen, W. Nam, L. Que, Jr., *J. Am. Chem. Soc.* **2004**, *126*, 16750.
[16] M. R. Bukowski, K. D. Koehntop, A. Stubna, E. L. Bominaar, J. A. Halfen, E. Münck, W. Nam, L. Que, Jr., *Science* **2005**, *310*, 1000.
[17] E. Münck in *Physical Methods in Bioinorganic Chemistry. Spectroscopy and Magnetism* (Ed.: L. Que, Jr.), University Science Books, Sausalito, CA, **2000**, p. 287.
[18] J. C. Schoneboom, F. Neese, W. Thiel, *J. Am. Chem. Soc.* **2005**, *127*, 5840.
[19] C. V. Sastri, M. J. Park, T. Ohta, T. A. Jackson, A. Stubna, M. S. Seo, J. Lee, J. Kim, T. Kitagawa, E. Münck, L. Que, Jr., W. Nam, *J. Am. Chem. Soc.* **2005**, *127*, 12494; J. Bautz, M. R. Bukowski, M. Kerscher, A. Stubna, P. Comba, A. Lienke, E. Münck, L. Que, Jr., *Angew. Chem.* **2006**, *118*, 5810; *Angew. Chem. Int. Ed.* **2006**, *45*, 5681.
[20] K. L. Kostka, B. G. Fox, M. P. Hendrich, T. J. Collins, C. E. F. Richard, L. J. Wright, E. Münck, *J. Am. Chem. Soc.* **1993**, *115*, 6746; O. Pestovsky, S. Stoian, E. Bominaar, X. Shan, E. Münck, L. Que, Jr., A. Bakac, *Angew. Chem.* **2005**, *117*, 7031; *Angew. Chem. Int. Ed.* **2005**, *44*, 6871.
[21] W. T. Oosterhuis, G. Lang, *J. Chem. Phys.* **1973**, *58*, 4757.
[22] T. A. Betley, J. C. Peters, *J. Am. Chem. Soc.* **2004**, *126*, 6252; N. Aliaga-Alcalde, S. DeBeer George, B. Mienert, E. Bill, K. Wieghardt, F. Neese, *Angew. Chem.* **2005**, *117*, 2968; *Angew. Chem. Int. Ed.* **2005**, *44*, 2908; J. F. Berry, E. Bill, E. Bothe, S. D. George, B. Mienert, F. Neese, K. Wieghardt, *Science* **2006**, *312*, 1937.

 © 2006 Wiley-VCH Verlag GmbH & Co. KGaA, Weinheim

Amino Acids

DOI: 10.1002/anie.200602801

Catalytic, Asymmetric Synthesis of 1,4-Benzoxazinones: A Remarkably Enantioselective Route to α-Amino Acid Derivatives from *o*-Benzoquinone Imides**

*Jamison Wolfer, Tefsit Bekele, Ciby J. Abraham, Cajetan Dogo-Isonagie, and Thomas Lectka**

Molecules that serve as versatile branch points for the synthesis of pharmaceutically or biologically active products, besides being of interest in their own right, are especially valuable targets for asymmetric catalysis. The 1,4-benzoxazinone[1] and 1,4-benzoxazine[2] systems are intriguing because they are present in clinically significant pharmaceuticals and other biologically active molecules. On the basis of previous success in the preparation of α-oxygenated carboxylic acid derivatives from benzodioxinones,[3] we speculated that chiral 1,4-benzoxazinone intermediates could also serve as flexible precursors for the efficient synthesis of highly enantiomerically enriched α-amino acids and related derivatives.[4] Herein, we present the first catalytic, asymmetric synthesis of 1,4-benzoxazinones that relies on the highly enantioselective [4+2] cycloaddition of *o*-benzoquinone imides with chiral ketene enolates (derived from acid chlorides and cinchona alkaloid[5] catalysts; Scheme 1). These cycloadducts can be

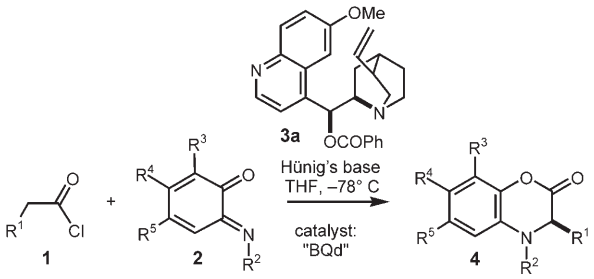

Scheme 1. Synthesis of 1,4-benzoxazinones.

functionalized in situ to provide 1,4-benzoxazines and α-amino acid derivatives in good-to-excellent yields and with virtual enantiopurity, only rivaled by that of enzymatic amino acid synthesis. As a testament to the flexibility of this methodology, a variety of substituents and *N*-acyl groups can be incorporated into the products.

We also highlight the synthesis of several biologically significant α-amino acid derivatives (e.g., α-fluoro,[6] β,γ-alkynyl,[7] and β,γ-alkenyl species) whose optically pure synthesis has not been solved by asymmetric catalysis and that are very difficult to prepare by using other methods.[8] For example, α-fluoro α-amino acid derivatives are of great value in the preparation of peptidomimetics and transition-state analogues of peptide-containing therapeutic agents.[9] Similarly, β,γ-alkynyl and β,γ-alkenyl α-amino acid derivatives display analogous activity, postulated to be caused by conformational constraint.[7]

We have had an interest in the catalytic, enantioselective reactions of α-imino esters, chemistry which provides a variety of useful products (β-lactams and α- or β-amino acids) with high enantioselectivity upon alkylation at the carbon atom.[10] Although we noted that *o*-benzoquinone imides share structural similarity to α-imino esters, they prefer to alkylate at the nitrogen atom instead, thus providing products in which the aromaticity is restored.[11] An approach employing chiral ketene enolates provides three points of modification: the quinone core, the N substituent, and the acid chloride. We noted that electron-withdrawing *N*-acyl groups should increase the reactivity of the quinone unit towards cycloaddition, besides serving as protecting groups that can subsequently be removed. Initially, we examined several N-acylated quinone imides[12] and chose experimental conditions that worked well for the asymmetric cycloaddition of ketene enolates and *o*-quinones.[3] We found that by employing 4-methylvaleryl chloride **1a** ($R^1 = i$Bu), imide **2a** ($R^2 = p$-NO_2PhCO, R^3 = H, $R^4 = R^5$ = Cl), 10 mol% benzoylquinidine (**3a**; BQd), and Hünig's base in THF at −78 °C, we formed cycloadduct **4a** in 65% yield with over 99% *ee* (Scheme 2).[13] Several other 1,4-benzoxazinones were synthesized from different quinone imides and acid chlorides to provide products in good yield with uniformly excellent enantiomeric excess.[14] One reaction of special interest would be the conversion of chiral 1,4-benzoxazinones into 1,4-benzoxazines, skeleta that are present in biologically relevant molecules, such as levofloxacin.[15] For example, benzoxazinone **4l** reacts smoothly with $BH_3{\cdot}SMe_2$[16] to provide the corresponding benzoxazine **7l** in 68% yield and with full preservation of the enantiomeric excess.

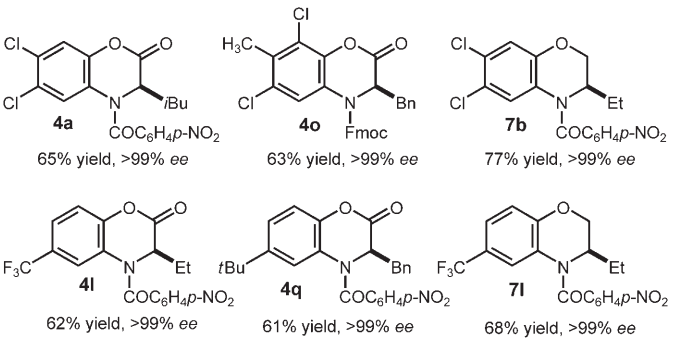

Scheme 2. Chiral 1,4-benzoxazinone and 1,4-benzoxazine products. Fmoc = 9-fluorenylmethoxycarbonyl, Bn = benzyl.

[*] J. Wolfer, T. Bekele, C. J. Abraham, C. Dogo-Isonagie, Prof. T. Lectka
Department of Chemistry
Johns Hopkins University
3400 North Charles Street, Baltimore, MD 21218 (USA)
Fax: (+1) 410-516-7044
E-mail: lectka@jhu.edu

[**] T.L. thanks the NIH (GM064559); the Sloan, Guggenheim, and Dreyfus Foundations; and Merck & Co. for support.

Supporting information for this article is available on the WWW under http://www.angewandte.org or from the author.

InterScience
© 2006 Wiley-VCH Verlag GmbH & Co. KGaA, Weinheim

We discovered that cycloadduct **4a** undergoes rapid ring-opening methanolysis to afford ester **5a**, thus indicating that in situ transformation to α-amino acid derivatives by various nucleophiles would occur. Thus, we sought to convert the cycloadducts directly into the α-amino acids in one pot (Scheme 3).[17]

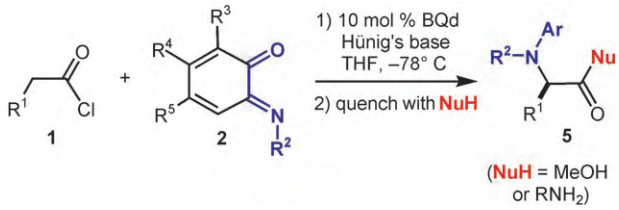

Scheme 3. One-pot amino acid synthesis.

We chose *o*-benzoquinone imides derived from halogenated *o*-aminophenols as templates for α-amino acid synthesis for a variety of reasons—the starting materials are inexpensive and the electron-withdrawing groups in the 3- and 4-positions block undesired reactivity at the quinone ring and enhance the overall reactivity of the system.[18] Following the cycloaddition (ca. 5 h at −78 °C), MeOH was added to the reaction mixture, which was then warmed to room temperature to produce products **5** in high yield. Having chosen $R^2 = p\text{-}NO_2PhCO$ as the group that performed the best overall, we then screened a variety of R^1 substituents and cores, (Table 1, entries 1—13 and 16). In each case, the reaction occurred in good yield and with excellent enantiomeric excess.

Most notably, we accomplished the synthesis of three biologically significant derivatives—β,γ-alkynyl acid **5g**, β,γ-alkenyl acid **5h**, and α-fluoro acid **5p** (Table 1, entries 7, 8, and 16, respectively)—all in good yield and with excellent enantiomeric excess. To our knowledge, α-fluoro α-amino acid derivatives have not heretofore been addressed by asymmetric catalysis.[6]

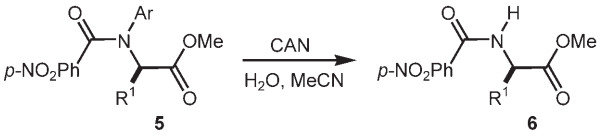

(1)

Finally, oxidation by using ceric ammonium nitrate (CAN)[19] removes the aryl group in good yield under mild conditions [Eq. (1)]; for example, see Table 2, entries 1

Table 2: Deprotection using CAN.

Entry	R^2	R^1	Product		*ee* [%]	Yield[a] [%]
1	Fmoc	Bn		**6o**	>99	71
2	*p*-NO_2PhCO	Bn	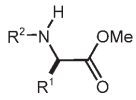	**6d**	>99	71
3	*p*-NO_2PhCO	Bn		**6d**	>99	64
4	*p*-NO_2PhCO	Ph		**6e**	>99	58
5	*p*-NO_2PhCO	$PhOCH_2$		**6f**	>99	72
6	*p*-NO_2PhCO	PhCH=CH		**6h**	>99	74

[a] Reactions run with **5** (0.55 mmol) and CAN (1.65 mmol) in water/MeCN (1:3) at 0 °C. Yield after column chromatography.

Table 1: Synthesis of α-amino acid derivatives.

Entry	R^2	R^1	Product[a]		*ee* [%]	Yield [%]
1[b]	*p*-NO_2PhCO	*i*Bu		**5a**	>99	73
2[b]	*p*-NO_2PhCO	Et		**5b**	>99	62
3[b]	*p*-NO_2PhCO	Me		**5c**	>99	69
4[b]	*p*-NO_2PhCO	Bn		**5d**	>99	63
5[b]	*p*-NO_2PhCO	Ph		**5e**	>99	66
6[b]	*p*-NO_2PhCO	$PhOCH_2$	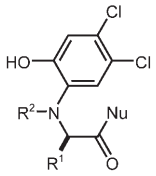	**5f**	>99	72
7[b]	*p*-NO_2PhCO	$CH_3CH_2C{\equiv}C$		**5g**	>99	59
8[b]	*p*-NO_2PhCO	PhCH=CH		**5h**	>99	61
9[c]	*p*-NO_2PhCO	$PhOCH_2$		**5i**	>99	71
10[d]	*p*-NO_2PhCO	Et		**5j**	>99	90
11[b]	*p*-NO_2PhCO	Bn		**5k**	>99	83
12[b]	*p*-NO_2PhCO	Et	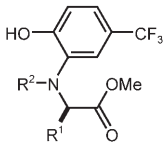	**5l**	>99	71
13[b]	*p*-NO_2PhCO	*i*Bu		**5m**	>99	73
14[e]	Fmoc	Et		**5n**	>99	59
15[e]	Fmoc	Bn		**5o**	>99	62
16[b]	*p*-NO_2PhCO	F	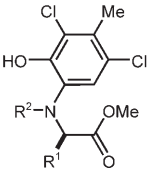	**5p**	>99	60

[a] Nu = OMe for all entries, except entry 9 (Nu = NH_2) and entry 10 (Nu = BnNH). [b] Reactions run with catalyst (10 mol %), Hünig's base (0.55 mmol), acid chloride (0.55 mmol), and quinone imide (0.55 mmol) at −78 °C followed by addition of MeOH and overnight stirring. Yield for cycloaddition and methanolysis. [c] Reaction quenched with NH_4OH to yield amide **5i**. [d] Reaction quenched with benzylamine in THF to yield **5j**. [e] Quinone imide formed in situ at −78 °C; yield for both steps.

(conversion of **5o** into **6o**), 2 (**5k** into **6d**), 3 (**5d** into **6d**), 4 (**5e** into **6e**), 5 (**5f** into **6f**), and 6 (**5h** into **6h**).

We then screened other quinone imides in which the *N*-acyl group was varied (Table 1, entries 14 and 15). In particular, we were interested in highlighting a signature protecting group important in peptide synthesis, such as 9-fluorenylmethyl carbamate (Fmoc).[20] For example, when $R^1 = Bn$ and $R^2 = Fmoc$, the reaction occurs smoothly in THF at −78 °C to form product **5o** in 62 % yield with greater than 99 % *ee*. The Fmoc group was then removed by piperidine to afford **8** in high yield (92 %) followed by deprotection with CAN to give **9** in good yield and without loss of optical activity (Scheme 4).[20]

In conclusion, we have illustrated the first highly enantioselective synthesis of 1,4-benzoxazinones and 1,4-benzoxazines. These products are readily con-

 © 2006 Wiley-VCH Verlag GmbH & Co. KGaA, Weinheim

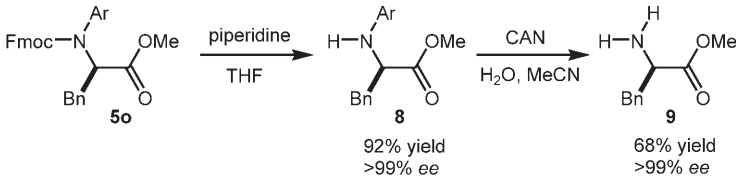

Scheme 4. Synthesis of N-deprotected α-amino esters.

verted into virtually optically pure α-amino acid esters. This study compares very favorably with other chiral α-amino acid syntheses because of the remarkably high enantioselectivities obtained and as it provides access important classes of chiral compounds that are otherwise difficult to synthesize.

Experimental Section

General procedure: A solution of the quinone imide (0.12 mmol) in THF (2 mL) was added to a reaction flask containing an acid chloride (0.12 mmol), Hünig's base (0.12 mmol), and BQd (**3a**; 0.012 mmol) at −78 °C. After stirring for 6 h, the reaction was concentrated in vacuo and the crude residue was purified by column chromatography. Additional procedures and characterization data are presented in the Supporting Information.

Received: July 14, 2006
Published online: October 12, 2006

Keywords: amino acids · asymmetric catalysis · benzoxazines · benzoxazinones · cycloaddition

[1] Benzoxazinones are known as antitumor agents and protease inhibitors: a) S. K. Sengupta, D. H. Trites, M. S. Madhavarao, W. R. Beltz, *J. Med. Chem.* **1979**, *22*, 797; b) R. L. Jarvest, S. C. Connor, J. G. Gorniak, L. J. Jennings, H. T. Serafinowska, A. West, *Bioorg. Med. Chem. Lett.* **1997**, *7*, 1733; c) F. Bihel, J.-L. Kraus, *Org. Biomol. Chem.* **2003**, *1*, 793.

[2] Benzoxazines are active as antioxidative neuroprotectants and antibiotics: a) M. Largeron, B. Lockhart, B. Pfeiffer, M.-B. Fleury, *J. Med. Chem.* **1999**, *42*, 5043; b) Y.-G. Zhou, P.-Y. Yang, X.-W. Han, *J. Org. Chem.* **2005**, *70*, 1679; c) J. Ilas, P. S. Anderluh, M. S. Delenc, D. Kikelj, *Tetrahedron* **2005**, *61*, 7325.

[3] T. Bekele, M. H. Shah, J. Wolfer, C. J. Abraham, A. Weatherwax, T. Lectka, *J. Am. Chem. Soc.* **2006**, *128*, 1810.

[4] For recent examples of asymmetric α-amino acid synthesis, see: a) T. Abellan, R. Chinchilla, N. Galindo, G. Guillena, C. Najera, J. M. Sansano, *Eur. J. Org. Chem.* **2000**, 2689; b) J. Kobayashi, M. Nakamura, Y. Mori, Y. Yamashita, S. Kobayashi, *J. Am. Chem. Soc.* **2004**, *126*, 9192; c) T. Belser, M. Stohr, A. Pfaltz, *J. Am. Chem. Soc.* **2005**, *127*, 8720.

[5] K. Kacprzak, J. Gawronski, *Synthesis* **2001**, *7*, 961.

[6] a) D. P. Huber, K. Stanek, A. Togni, *Tetrahedron: Asymmetry* **2006**, *17*, 658; b) B. Mohar, J. Baudoux, J.-C. Plaquevent, D. Cahard, *Angew. Chem.* **2001**, *113*, 4666; *Angew. Chem. Int. Ed.* **2001**, *40*, 4214.

[7] P. Meffre, F. Le Goffic, *Amino Acids* **1996**, *11*, 313.

[8] Presumably, these amino acids are not very amenable to synthesis through asymmetric hydrogenation (that is, **5g** and **5h** by virtue of their unsaturation), through the chiral phase-transfer synthesis (that is, **5g** and **5h** as no suitable S_N2 substrates exist), or the Strecker reaction (that is, the conditions for the hydrolysis of the nitrile group can be harsh for **5g**, **5h**, and **5p**).

[9] V. P. Kukhar in *Fluorine-Containing Amino Acids, Synthesis and Properties* (Ed.: V. A. Soloshonok), Wiley, Chichester, **1995**.

[10] a) D. Ferraris, B. Young, T. Dudding, T. Lectka, *J. Am. Chem. Soc.* **1998**, *120*, 4548; b) A. E. Taggi, A. M. Hafez, H. Wack, B. Young, W. J. Drury III, T. Lectka, *J. Am. Chem. Soc.* **2000**, *122*, 7831.

[11] For a detailed study of *o*-quinone imide cycloadditions: K. C. Nicolaou, K. Sugita, P. S. Baran, Y.-L. Zhong, *J. Am. Chem. Soc.* **2002**, *124*, 2221.

[12] In some cases, the quinone imides were isolated, in other cases, they were generated in situ by simple $Pb(OAc)_4$ oxidation.

[13] The opposite *S* enantiomer products can be made in comparable selectivity with benzoylquinine (BQ, **3b**) as the catalyst.

[14] Absolute configurations were determined by correlation to several known α-amino acid derivatives; the sense of induction observed was consistent with that obtained in other cinchona alkaloid catalyzed reactions (see Reference [10]).

[15] K. F. Croom, K. L. Goa, *Drugs* **2003**, *63*, 2769.

[16] P. Verma, S. Singh, D. K. Dikshit, R. Suprabhat, *Synthesis* **1987**, *1*, 68.

[17] Reactions were quenched with a THF solution of the desired nucleophile at room temperature.

[18] R. Adams, J. M. Stewart, *J. Am. Chem. Soc.* **1952**, *74*, 5876.

[19] For an example of dearylation by using CAN, see: S. Kobayashi, J. Kobayashi, H. Ishiani, M. Ueno, *Chem. Eur. J.* **2002**, *8*, 4185.

[20] For a review, see: L. A. Carpino, *Acc. Chem. Res.* **1987**, *20*, 401.

 © 2006 Wiley-VCH Verlag GmbH & Co. KGaA, Weinheim

Supramolecular Chemistry

DOI: 10.1002/anie.200602999

Dynamically Self-Assembling Metalloenzyme Models Based on Calixarenes**

*Hüseyin Bakirci, Apurba L. Koner, Michael H. Dickman, Ulrich Kortz, and Werner M. Nau**

Macrocyclic host molecules have long been recognized as attractive models for enzymes.[1] When transition metals are coordinated in proximity to the hydrophobic cavities, the macrocycles resemble metalloenzymes in their structure and function. One approach, which has been pioneered by Breslow and co-workers for cyclodextrins,[2] and later extended to calixarenes,[3–6] involves the design of host

[*] Dr. H. Bakirci, A. L. Koner, Dr. M. H. Dickman, Prof. Dr. U. Kortz, Prof. Dr. W. M. Nau
School of Engineering and Science
International University Bremen
Campus Ring 1, 28759 Bremen (Germany)
Fax: (+49) 421-200-3229
E-mail: w.nau@iu-bremen.de
Homepage: http://www.iu-bremen.de/schools/ses/wnau/

[**] This work was supported within the graduate program "Nanomolecular Science" of the International University Bremen.

Supporting information for this article is available on the WWW under http://www.angewandte.org or from the author.

 WILEY InterScience DISCOVER SOMETHING GREAT

© 2006 Wiley-VCH Verlag GmbH & Co. KGaA, Weinheim

molecules with covalently attached nitrogen ligands, which can be subsequently coordinated with transition metals to form sophisticated metalloenzyme mimics. The second principal approach, in which metalloenzyme models were studied from a structural point of view in the solid state, was explored by Atwood and co-workers[7,8] using *p*-sulfonatocalix[4]arene (CX4) as the host,[9] pyridine or pyridine-*N*-oxide as the guest, and the presence of metal ions. Herein, we present a simple supramolecular approach to metalloenzyme models in aqueous solution, which is based on the dynamic self-assembly between macrocyclic hosts with cation receptor properties, organic guests, and metal ions (Figure 1). In the resulting ternary complex, the guest is held in place by hydrophobic interactions with the host, while the metal ion experiences attractive Coulombic interactions with the negative charges positioned at the portal of the macrocycle.

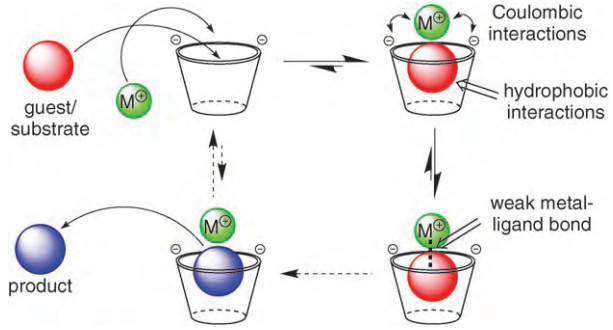

Figure 1. Dynamically self-assembling metalloenzyme model.

If the guest functions as a weak ligand, the host can assist the formation of a metal–ligand bond with the guest, which in turn reinforces the ternary complex and results in a positive cooperativity. Finally, if the guest possesses a functional group to allow a chemical reaction to occur, the catalytic activity of the coordinating metal may be probed. We now demonstrate the structural viability of the dynamic self-assembly approach (solid arrows in Figure 1) as well as thermodynamic and selectivity aspects by employing calixarenes (namely CX4) as hosts.

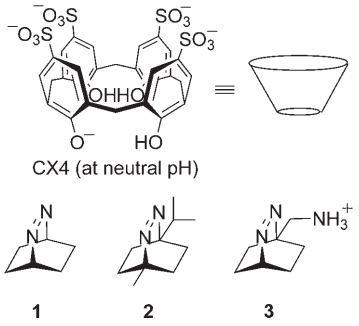

Close inspection of Figure 1 reveals that the proper choice of the guest is quintessential. The guest should be sufficiently large to maximize hydrophobic interactions, but sufficiently small to allow the docking of cations to the upper rim of the host. It should possess functional groups to enable (weak) metal–ligand interactions and to allow chemical reactions and catalytic effects to be probed. We identified bicyclic azoalkanes, in particular 2,3-diazabicyclo[2.2.2]oct-2-ene (**1**), as ideal guest molecules. Among neutral guests, **1** has the highest binding constant with CX4 ($K \approx 1000\,\text{M}^{-1}$),[10] and its small spherical shape facilitates the concomitant binding of cations. Compared to common nitrogen ligands, bicyclic azoalkanes are weak ligands,[11] which is nicely reflected in their weak basicity ($pK_a \approx 0.5$ for **1**).[12] Most importantly, the complexation of **1** by the host and subsequent ligation of the metal can be conveniently monitored by optical spectroscopy, because **1** shows strong fluorescence in water[13] and has a weak but distinct near-UV absorption which displays characteristic shifts in different host environments[14] and upon complexation (protonation).[12]

Addition of CX4 to a solution of **1** at neutral pH[15] led to the formation of the 1:1 complex with a UV absorption maximum at 366 nm (solid lines in Figure 2).[10,16] Upon

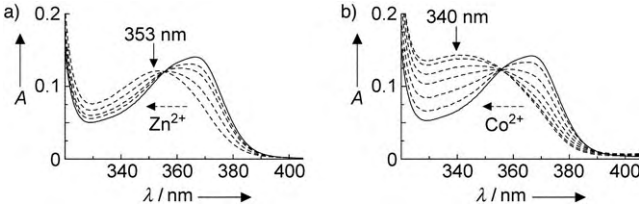

Figure 2. Changes in the UV spectra of **1** (2 mM) with CX4 (4 mM) in water at pH 7.0 (solid lines) upon addition (up to 10 mM) of a) Zn^{2+} and b) Co^{2+} ions (dotted lines).

addition of transition metals (e.g., Zn^{2+}, Co^{2+}, Mn^{2+}), a hypsochromic shift was observed (Figure 2), which signals the formation of a ternary complex in which the azo group functions as a monodentate ligand.[16] Control experiments revealed that the addition of the same metal ions (up to 20 mM) to aqueous solutions of **1** did not give rise to a significant shift in the UV spectrum, which reveals that the azo–metal complex has a very low binding constant ($K < 5\,\text{M}^{-1}$) in solution.[11] Only in the presence of the macrocyclic host will the guest and metal form the desired complex, that is, the host assists or "templates" the formation of the metal–ligand bond. In essence, the host brings two species together, like an enzyme does with a substrate and a catalytic center, to form a metal–ligand complex, which in the absence of host is not present in significant amounts because of low bimolecular affinity.[17]

Independent evidence for the formation of the ternary complex in the presence of Zn^{2+} ions comes from ^{1}H NMR studies. The formation of the inclusion complex between **1** (2 mM) and CX4 (4 mM) was established through intermolecular ROESY cross-peaks and the characteristic up-field shifts of the guest protons[10] which arise from the shielding effect of the CX4 aryl groups. Upon addition of Zn^{2+} ions (20 mM), the ROESY cross-peaks were retained and, more importantly, an extra up-field shift was observed (by ca. 0.3 ppm, Figure 3). This is consistent with the pictorial representation of the metal ion as a lid, which presses the guest somewhat more

 © 2006 Wiley-VCH Verlag GmbH & Co. KGaA, Weinheim

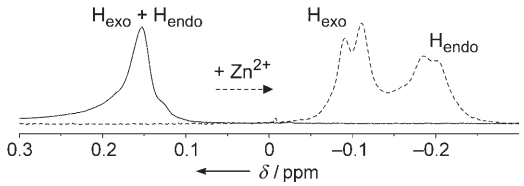

Figure 3. Shift in the ^{1}H NMR spectrum of **1** (2 mM) in the presence of CX4 (4 mM) in D_2O at pD 7.4 (solid line) upon addition of 20 mM Zn^{2+} ions (dotted line).

tightly into the cavity (Figure 4). Interestingly, when the bridgehead-alkylated derivative **2** (2 mM) was studied in the presence of CX4 (4 mM, $K = 480\,M^{-1}$),[10] the NMR shift upon

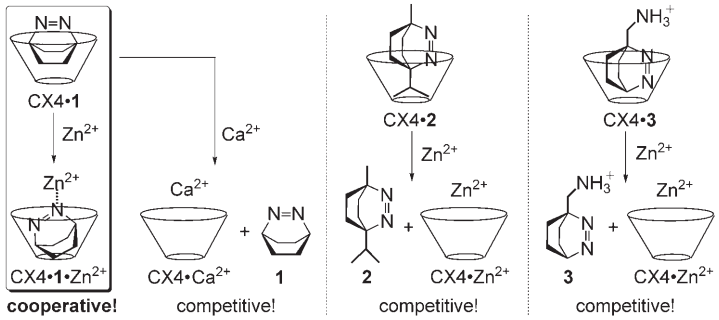

Figure 4. Interplay between cooperative and competitive binding.

addition of Zn^{2+} ions (20 mM) to the preformed complex was opposite (down-field by ca. 0.4 ppm), which signals a competitive binding, that is, the docking of the metal ion results in a steric interference with the bound guest, and the proper metal–ligand bond geometry can no longer be attained. Moreover, when Ca^{2+} ions (20 mM) were added to the CX4·**1** complex, a similar down-field shift (by ca. 0.3 ppm) was observed. This observation reveals that **1** is again released as a result of competitive binding,[18] because the ternary complex with the oxophilic Ca^{2+} ion is not stabilized by an additional metal–ligand bond as is formed with transition metals, and steric hindrance comes into play instead.

The fluorescence of **1**, which is high in water, decreases upon complexation by CX4[16] as a result of exciplex-induced quenching by the electron-rich aryl groups of the surrounding host. When Zn^{2+} ions (which do not quench the fluorescence of free **1**) were added to the preformed host–guest complex, the fluorescence of **1** was further decreased, but reached a plateau at an intermediate metal-ion concentration (Figure 5a). This observation signals the formation of the ternary complex, in which the fluorescence intensity is modulated due to altered photophysical properties of the complexed chromophore. For comparison, when zinc ions were added to the CX4 complex of the 1-ammoniomethyl derivative **3** (Figure 5b), which is stabilized by the additional positive charge ($K = 60\,000\,M^{-1}$ at pH 7.0), the fluorescence increased, because the binding is again competitive and leads to release of the guest. For **3**, this is primarily due to charge repulsion between the ammonium group and the zinc ions. A similar

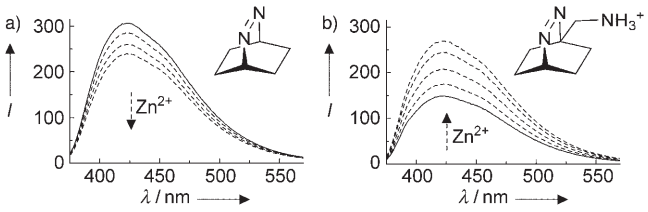

Figure 5. Changes in the fluorescence spectra at pH 7.0 (solid lines) upon addition of Zn^{2+} ions (up to 10 mM; dotted lines) to: a) azoalkane **1** (1 mM) with CX4 (1.6 mM) and b) azoalkane **3** (1 mM) with CX4 (0.5 mM).

fluorescence recovery arising from competitive binding was found for **2**.

As can be seen, a fascinating interplay between cooperative binding (formation of ternary complex) and competitive binding (release of guest) occurs. As depicted in Figure 4, the formation of the ternary complex (the metalloenzyme model) occurs only if 1) metal and guest binding do not clash because of steric or electrostatic factors, 2) a transition-metal ion is employed, and 3) the proper geometry for formation of the metal–ligand bond can be attained. A very high selectivity results, with only the parent **1** forming the desired ternary complex; even slight variations, such as the alkylation in **2** or the introduction of an ammonium group in **3**, suppress its formation. This result is in sharp contrast to the generally accepted very poor selectivity of CX4 towards guest binding, which has led Rebek and co-workers to correctly conclude that such simple hosts can recognize little more than a positive charge.[19] Our results show that an otherwise unselective host can be twisted into a highly selective one simply by exploiting additional supramolecular interactions.

The dramatic increase in the selectivity of the ternary complex is made possible by a "triple recognition". In other words, three supramolecular interactions act in concert (Figure 1). This expands the concept of Tabushi et al., who emphasized the need for a double recognition of the guest in metalloenzymes (hydrophobic and metal–ligand interactions);[20] the present metalloenzyme models incorporate additionally weak Coulombic interactions between the metal and the host, which allows for a rapid exchange in a dynamic supramolecular assembly. For comparison, the metal in the previously designed metalloenzyme mimics[1–6] was tightly incorporated into the host through interaction with covalently attached nitrogen ligands.

Circumstantial evidence for the ternary complexes implicated in solution comes also from the crystal structures of the zinc and cobalt complexes, which are isostructural (Figure 6 and see the Supporting Information).[15] Note that **1** is immersed with its hydrophobic portion in the CX4 cone, while it serves at the same time as a monodentate σ-donor ligand in the first coordination sphere.

Besides the structural aspects, the binding constants are also very relevant because a rapid dynamic equilibrium applies in solution (Figure 7). The binding constant of Zn^{2+} ions with CX4 was determined as $2000 \pm 200\,M^{-1}$ at neutral pH (K_1) by analyzing the fluorescence recovery of **2** and **3** upon addition of zinc ions (see above). This value is comparable to that obtained with the similarly large

 © 2006 Wiley-VCH Verlag GmbH & Co. KGaA, Weinheim

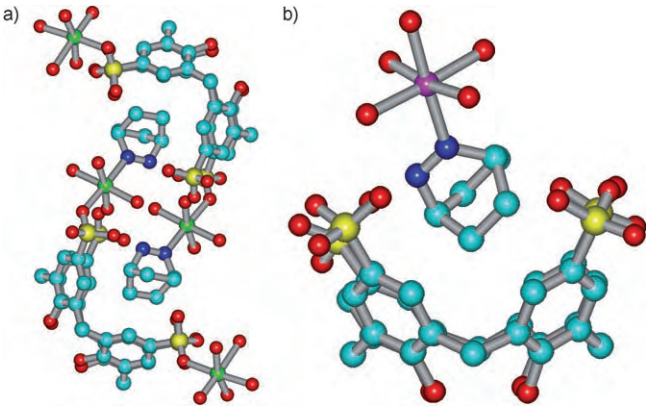

Figure 6. Crystal structures of the complexes formed between CX4, **1**, and transition-metal ions: a) the mutually encapsulating, binuclear repeat unit (with Zn^{2+} ions, green) and b) view of ternary complex (with Co^{2+} ions, magenta; C turquoise, N blue, O red, S yellow).

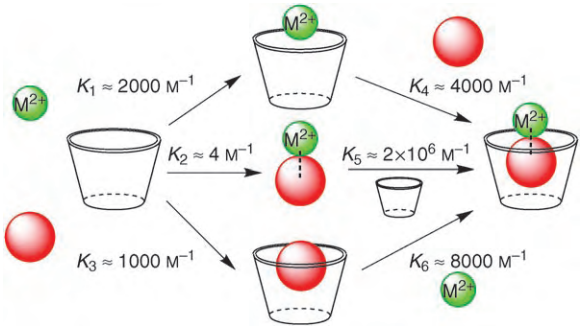

Figure 7. Binding constants in ternary complexes.

Mg^{2+} ions.[18] The binding constant of **1** in the absence of metal ions amounts to $1000\,M^{-1}$ (K_3).[10,12,16] By titrating CX4 into a solution of **1** (2 mM) in the presence of an excess of Zn^{2+} ions (20 mM, this direct UV titration is possible because free **1** has no sizable affinity to Zn^{2+} ions, while CX4 is virtually quantitatively complexed at this concentration of Zn^{2+} ions), a binding constant of $4000 \pm 500\,M^{-1}$ was determined, which corresponds to the apparent binding constant of **1** to the CX4·Zn^{2+} complex (K_4). From these three binding constants, the remaining ones can be calculated (K_6) or estimated (K_2, K_5). The increased binding in the presence of Zn^{2+} ions (factor of 4, K_4/K_3) reflects the positive cooperativity of the binding (synergistic effect). This value is consistent with the low binding constant between Zn^{2+} ions and uncomplexed **1** in aqueous solution (see above), although the values could also differ slightly because of different coordination spheres of zinc ions in water and when complexed to CX4.

The increase in the binding constants in the presence of the metal ion (K_4 versus K_3) as a result of the additional metal–ligand interaction may also be of interest for other areas where the modulation of guest binding constants is of interest, for example in sensor applications. A specific example is shown in Figure 8a for the fluorescence regeneration of **1** from its CX4 complex upon addition of acetylcholine as analyte.[16] As can be seen, the sensitivity of this fully

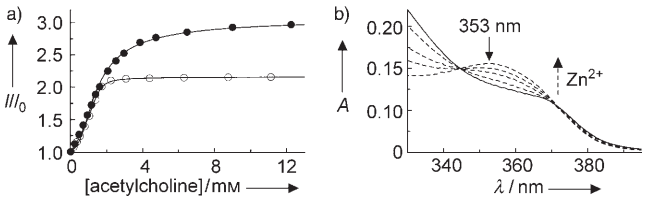

Figure 8. a) Fluorescence recovery of **1** (1 mM) with CX4 (1.6 mM) at pH 7.0 in the absence (open circles) and presence (filled circles) of 10 mM Zn^{2+} ions upon addition of acetylcholine (for the displacement assay principle, see Ref. [16]). b) Changes in the UV spectra of **1** (2 mM) with CX4 (4 mM) in water at pH 2.0 (solid line) upon addition of Zn^{2+} ions (up to 10 mM; dotted lines).

water-soluble sensor system can be significantly enhanced by the addition of 10 mM zinc ions, thus expanding both the overall sensitivity (increase in fluorescence) as well as the accessible range for the sensing of this neurotransmitter.

Let us finally bridge the gap to metalloenzymes. One of the prime assets of Zn^{2+} ions in hydrolytic metalloenyzmes is their ability to deprotonate ligands or water molecules in the course of metal–ligand bond formation.[21] This function could be nicely demonstrated in our self-assembling models as well. At lower pH values, for example, at pH 2, the guest is protonated in the CX4 complex (CX4·$\mathbf{1}H^+$),[12,15] such that the UV absorption of **1** is shifted to the far UV region (Figure 8b, solid line).[16] Upon addition of Zn^{2+} ions, a new band emerges at 353 nm, which corresponds precisely to the absorption of the ternary complex (CX4·**1**·Zn^{2+}, see Figure 2a). In this particular case, Zn^{2+} ions do not destabilize the complex of the cationic guest (as found for **3**), but rather deprotonate the guest by forming the metal–ligand bond [Equation (1)]. In

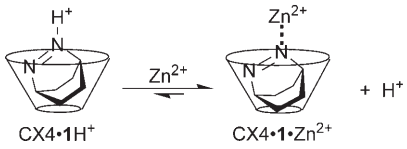

(1)

other words, the docking of the zinc ion to the calixarene causes a shift in the pK_a value of the hydrophobically bound guest, thus showing a remote resemblance to its biological activity.

In summary, we have employed a dynamic self-assembly of a simple macrocycle, metal ions, and a rationally selected guest molecule to construct interesting structural metalloenzyme models in aqueous solution. Conceptually, the phenomenon of host-assisted metal–ligand bond formation stands out, as well as the high selectivity for the formation of a ternary complex. This strategy results in an interesting interplay between cooperative and competitive binding arising from a triple supramolecular recognition motif. With the valid proof of concept in hand, functional aspects (dashed arrows in Figure 1) need to be investigated next.

Received: July 25, 2006
Revised: September 4, 2006
Published online: October 11, 2006

 © 2006 Wiley-VCH Verlag GmbH & Co. KGaA, Weinheim

Keywords: calixarenes · metalloenzyme models · molecular recognition · self-assembly · supramolecular chemistry

[1] *Artificial Enzymes* (Ed.: R. Breslow), Wiley-VCH, Weinheim, **2005**.
[2] R. Breslow, S. D. Dong, *Chem. Rev.* **1998**, *98*, 1997 – 2011.
[3] C. D. Gutsche, *Calixarenes Revisited*, Royal Society of Chemistry, Cambridge, **1998**.
[4] P. Molenveld, J. F. J. Engbersen, D. N. Reinhoudt, *Chem. Soc. Rev.* **2000**, *29*, 75 – 86.
[5] F. Sansone, M. Segura, R. Ungaro in *Calixarenes 2001* (Eds.: Z. Asfari, V. Böhmer, J. Harrowfield, J. Vicens), Kluwer, Dordrecht, **2001**, pp. 496 – 512.
[6] G. Izzet, B. Douziech, T. Prange, A. Tomas, I. Jabin, Y. Le Mest, O. Reinaud, *Proc. Natl. Acad. Sci. USA* **2005**, *102*, 6831 – 6836.
[7] J. L. Atwood, G. W. Orr, K. D. Robinson, F. Hamada, *Supramol. Chem.* **1993**, *2*, 309 – 317.
[8] G. W. Orr, L. J. Barbour, J. L. Atwood, *Science* **1999**, *285*, 1049 – 1052.
[9] S. Shinkai, K. Araki, T. Matsuda, N. Nishiyama, H. Ikeda, I. Takasu, M. Iwamoto, *J. Am. Chem. Soc.* **1990**, *112*, 9053 – 9058.
[10] H. Bakirci, A. L. Koner, W. M. Nau, *J. Org. Chem.* **2005**, *70*, 9960 – 9966.
[11] S. C. Blackstock, J. K. Kochi, *J. Am. Chem. Soc.* **1987**, *109*, 2484 – 2496.
[12] H. Bakirci, A. L. Koner, T. Schwarzlose, W. M. Nau, *Chem. Eur. J.* **2006**, *12*, 4799 – 4807.
[13] X. Zhang, G. Gramlich, X. Wang, W. M. Nau, *J. Am. Chem. Soc.* **2002**, *124*, 254 – 263.
[14] C. Márquez, W. M. Nau, *Angew. Chem.* **2001**, *113*, 4515 – 4518; *Angew. Chem. Int. Ed.* **2001**, *40*, 4387 – 4390.
[15] CX4 exists as a pentaanion at neutral pH and as a tetraanion with all phenolic hydroxy groups protonated at strongly acidic pH values, for example, at pH 2, see Ref. [12]. The formation of the ternary complexes occurs independently of this protonation equilibrium, as demonstrated by UV, NMR, and fluorescence studies at both pH 7 and pH 2 (see the Supporting Information). The crystals were also grown from acidic solution, where the CX4 tetraanion forms the corresponding ternary complex.
[16] H. Bakirci, W. M. Nau, *Adv. Funct. Mater.* **2006**, *16*, 237 – 242.
[17] This is conceptually important, because if the guest would already form a stable transition-metal complex in the absence of host, a supramolecular self-assembly to a metalloenzyme model would no longer apply. Instead, one is dealing with host–guest complexes, in which transition-metal complexes serve as guests; the latter were previously documented, for example, for cyclodextrins; see D. R. Alston, A. M. Z. Slawin, J. F. Stoddart, D. J. Williams, *Angew. Chem.* **1985**, *97*, 771 – 772; *Angew. Chem. Int. Ed. Engl.* **1985**, *24*, 786 – 787.
[18] H. Bakirci, A. L. Koner, W. M. Nau, *Chem. Commun.* **2005**, 5411 – 5413.
[19] P. Ballester, A. Shivanyuk, A. R. Far, J. Rebek, Jr., *J. Am. Chem. Soc.* **2002**, *124*, 14014 – 14016.
[20] I. Tabushi, N. Shimizu, T. Sugimoto, M. Shiozuka, K. Yamamura, *J. Am. Chem. Soc.* **1977**, *99*, 7100 – 7102.
[21] G. Parkin, *Chem. Rev.* **2004**, *104*, 699 – 767.

 © 2006 Wiley-VCH Verlag GmbH & Co. KGaA, Weinheim

Asymmetric Catalysis

DOI: 10.1002/anie.200603103

Chemisorption-Induced Double Hydrogen Bonding, Self-Assembly, and Stereoselection**

*Stéphane Lavoie, Gautier Mahieu, and Peter H. McBreen**

By carefully choosing molecular components, it is possible to design supramolecular assemblies on metal surfaces for a variety of applications ranging from templating to asymmetric catalysis.[1–3] The choice of molecular building blocks is based on the fundamental chemical concept of functional groups; hydrogen-bond donor–acceptor pairs have proven exceptionally useful for self-assembly.[4–6] Hence, it is crucial to recognize that associative chemisorption can generate hydrogen-bond donor functionality in molecules for which hydrogen bonding is negligible in the gas or solution-phase.[7,8]

Herein, we report that nonsubstituted arenes form strong C–H···O hydrogen bonds to co-adsorbed esters and ketoesters on Pt(111) surfaces. Scanning tunneling microscopy (STM) imaging is used to isolate well-defined aryl–carbonyl assemblies at 150–300 K and to identify the interaction that binds them as double hydrogen bonding. In this way, chemisorption-activated arenes are found to combine two powerful properties for 2D self-assembly: planarity and double hydrogen bonding. Furthermore, the direct observation of aryl–carbonyl C–H···O interactions supports a new mechanism for the stereoselective hydrogenation of ketoesters on cinchona-modified platinum.[7] In turn, the observation also suggests that aryl C–H···X bonding, where X is a hydrogen-bond acceptor, should be explicitly considered in the design of metal–arene chiral catalysts.

STM images of a single chemisorbed pyrene molecule surrounded by 10 molecules of ethyl formate, one for each aryl C–H bond, are shown in Figure 1 A,B. These crownlike structures are observed over the entire Pt(111) surface (Figure 1 D). Pyrene is imaged as an oval-shaped protrusion with a long and a short axis, in keeping with its molecular structure. The long axis is collinear with two C–H bonds, whereas the short axis lies between C–H bonds (Figure 1 C). The docking of ethyl formate to pyrene occurs along the short axis, but not along the long axis (Figure 1 A), revealing that each interadsorbate interaction involves a pair of adjacent C–

[*] Dr. S. Lavoie, Dr. G. Mahieu, Dr. P. H. McBreen
Département de chimie
Université Laval
Québec, QC G1K 7P4 (Canada)
Fax: (+1) 418-656-7916
E-mail: peter.mcbreen@chm.ulaval.ca

[**] We acknowledge research support from the Natural Sciences and Engineering Research Council (NSERC) of Canada, the Canadian Foundation for Innovation, and the Fonds québécois de la recherche sur la nature et les technologies. S.L. acknowledges the receipt of an NSERC doctoral scholarship. The figures were prepared with the help of Marc-André Laliberté.

© 2006 Wiley-VCH Verlag GmbH & Co. KGaA, Weinheim

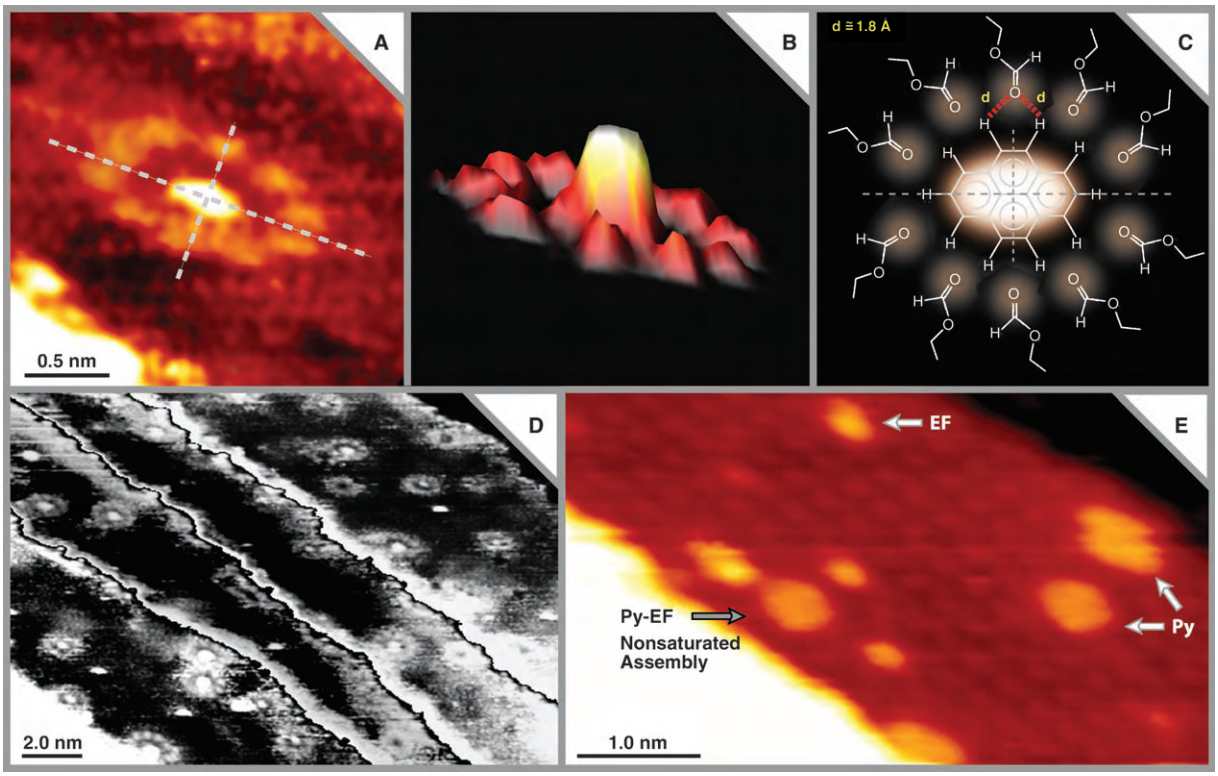

Figure 1. STM images of pyrene (Py) and ethyl formate (EF) co-adsorbed on a Pt(111) surface at 150 K. A) and B) An assembly of 10 molecules of ethyl formate around a single pyrene molecule. C) Illustration of the assembly. D) Assemblies located on terraces over the entire surface. E) A nonsaturated assembly of three molecules of ethyl formate around a single pyrene molecule.

H bonds. The strong directionality of the interaction indicates that the aromatic molecule serves as a double hydrogen-bond donor to ethyl formate, forming one C–H···O bond per lone pair of electrons on the carbonyl oxygen atoms. Saturated complexes containing one carbonyl group per C–H bond are observed at low coverages of pyrene and moderate coverages of ethyl formate. The ethyl formate protrusions are not equally distant from the aromatic molecule in unsaturated assemblies (Figure 1E). The more well-defined structure of the saturated assemblies suggests a cooperative hydrogen-bonding process.

Aryl C–H···O bonding is known to play a role in self-assembly on noble-metal surfaces in cases where an aromatic donor is activated by an electron-withdrawing nitro or carboxylate group.[9–11] The carboxylate groups serve, in turn, as charge-bearing hydrogen-bond acceptors, and it is known that appropriately substituted aromatic molecules can form strong hydrogen bonds to anion acceptors.[12] In contrast, the interaction between pyrene and ethyl formate on the Pt(111) surface is due to the chemisorption-induced polarization of an otherwise non-activated aromatic molecule. Computational studies have shown that the chemisorption of aromatic molecules on Group VIII metals results in an unequal elongation of the C–C bonds, a movement of the hydrogen atoms out of the molecular plane by approximately 20°, an increased positive charge on the hydrogen atoms, and an increased negative charge on the carbon atoms.[13–15] These effects translate into enhanced acidity for the aromatic molecule, thereby, enabling C–H···O bonding to nonresonant carbonyl groups. A related phenomenon was reported by Ho and co-workers.[16,17] They found that O_2 molecules adsorbed on a Ag(111) surface serve as hydrogen-bond acceptors in interactions with co-adsorbed ethylene and acetylene molecules.

The hydrogen-bond lengths in the crownlike assemblies were deduced by averaging hundreds of peak-to-peak distances between pyrene and ethyl formate protrusions. The model illustrated in Figure 1C and reference distances determined from atomically resolved images of the Pt(111) surface (Figure 1E) were used to estimate the O···H distances as $d = (1.8 \pm 0.1)$ Å. For this distance estimation, the dimensions of gas-phase pyrene were used, with the exception that the C–H bonds were assumed to tilt away from the surface by 20°; adsorbate–metal distances were not taken into account; and the protrusions observed for ethyl formate were assumed to be centered over the carbonyl oxygen atom.

The strength and, hence, the number of C–H···O interactions may be tuned by substitution on the aromatic molecule. As shown in the STM images in Figure 2, ethyl formate preferentially assembles at one ring of methylnaphthalene molecules adsorbed on a Pt(111) surface. The images show two, three, or rarely four ethyl formate molecules located at one side of the substituted aromatic molecule, whereas nonsubstituted naphthalene molecules adsorbed on Pt(111) may be completely surrounded by ethyl formate molecules. The methyl group of the methylnaphthalene

 © 2006 Wiley-VCH Verlag GmbH & Co. KGaA, Weinheim

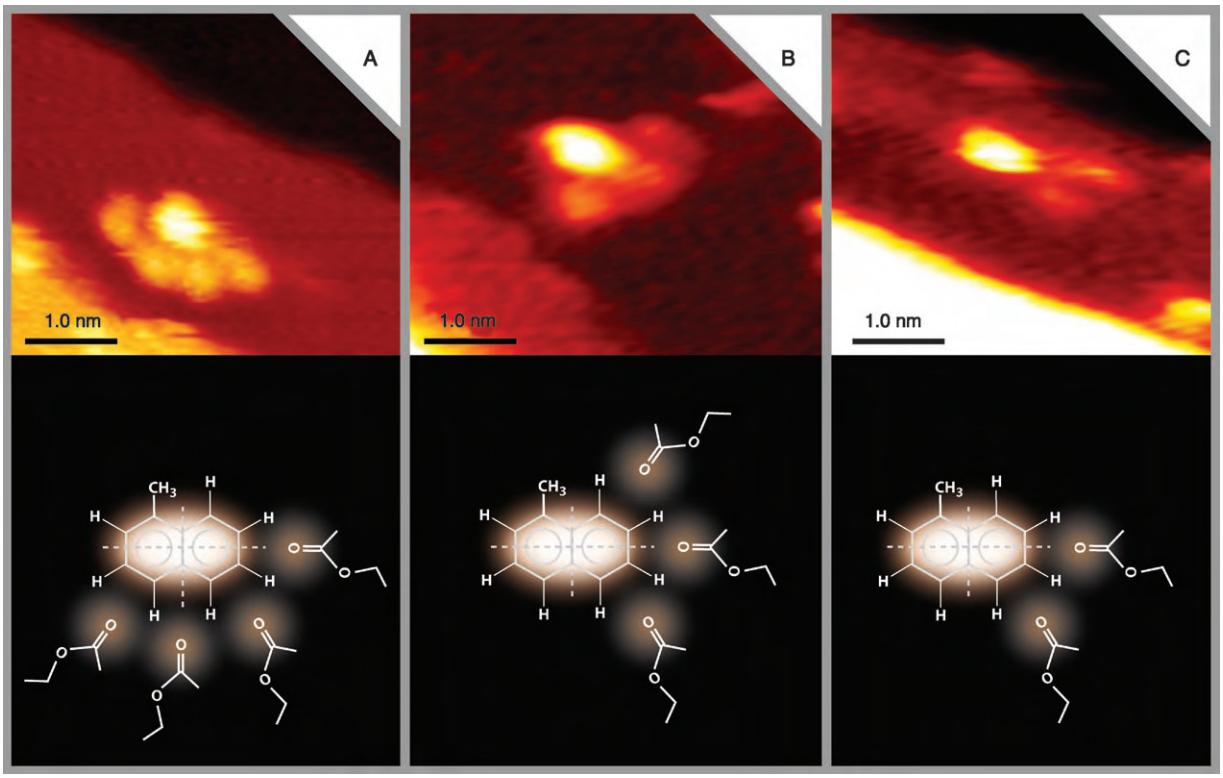

Figure 2. A)–C) STM images of methylnaphthalene and ethyl formate co-adsorbed on a Pt(111) surface at 150 K. The assemblies of ethyl formate and methylnaphthalene molecules are illustrated in the lower panels.

molecule weakens the interaction of one aromatic ring with the metal surface, leading to the effective activation of only the nonsubstituted ring.

Figure 3A displays an STM image (measured at room temperature) of an assembly of 10 molecules of methyl pyruvate around a single pyrene molecule on a Pt(111) surface. This manifestation of metal-activated C–H···O bonding is of particular relevance to the enantioselective hydrogenation of α-ketoesters on chirally modified platinum catalysts.[18,19] The reaction is performed at room temperature using a range of modifier–substrate pairs with the following characteristics.[7] All modifiers (for example, cinchonidine) are anchored to the platinum surface by a multiple-ring aromatic group and all have a conventional hydrogen-bonding group, which is held away from the surface. All substrates (for example, methyl pyruvate) contain both an activated prochiral ketocarbonyl and a second group capable of conventional hydrogen bonding. Hence, if platinum-activated aryl C–H···O bonding is taken into account, all modifier–substrate pairs can simultaneously form two distinct hydrogen-bonding interactions, as illustrated in Figure 3B. An energetic inequivalence of approximately 2–3 kcal mol^{-1} is required for the observed levels of enantioselection (ca. 95% *ee*). Hence, we assume that the strength of the double C–H···O bond is at least 2–3 kcal mol^{-1}. This hypothesis is consistent with calculations and experimental data showing that polarized aromatic molecules, such as tetrafluorobenzene, can form relatively strong C–H···O bonds.[20] The observation that the substituted ring of methylnaphthalene is not strongly activated towards C–H···O bonding is consistent with the fact that all effective modifiers for the Orito reaction contain multiple-ring aromatic groups.

The significance of metal-activated aryl–carbonyl C–H···O bonding extends to homogeneous chiral catalysis with planar-chiral and double hydrogen-bond donor catalysts. Planar-chiral catalysts are based on arene–metal complexes.[21] As with the activation of aromatic molecules on the platinum surface, the aromatic groups of the planar-chiral catalysts display enhanced acidity because of their activation by the metal.[22] It is instructive to consider the unexpected antiperiplanar conformation observed for formyl ligands in metal–cyclopentadiene complexes.[23] In the antiperiplanar geometry, the formyl oxygen atom points towards the arene ring, consistent with C–H···O bond formation to the metal-activated cyclopentadienyl group.[24] In contrast, the synperiplanar orientation, in which the carbonyl oxygen atom points away from the arene, is observed for the pentamethylcyclopentadienyl (Cp*) complex [Cp*Ru(CO)(PPhMe$_2$)HCO],[25] presumably because of the absence of aryl C–H bonds. Indeed, evidence for intermolecular C–H···O bonding is found in the crystal structures of metal–arene complexes.[26] Hence, our work indicates that a stereodirecting role for C–H···X bonding in planar-chiral catalysis should be considered. The ability to directly image aryl–carbonyl bonding is also important in the context of asymmetric catalysis activated by double hydrogen-bond donors.[27–29] Aromatic systems combine a high density of donor pairs with skeletal rigidity, well-defined planar shapes, and the opportunity to tune the C–H···X interaction through judicious substitution.

 © 2006 Wiley-VCH Verlag GmbH & Co. KGaA, Weinheim

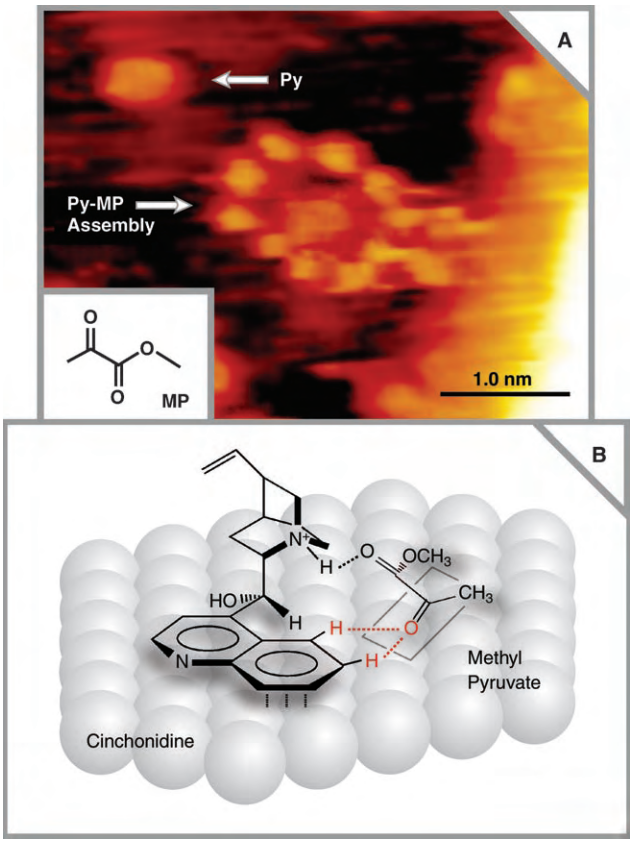

Figure 3. A) STM image of pyrene (Py) and methyl pyruvate (MP) co-adsorbed on a Pt(111) surface. Adsorption was carried out at 150 K and images were recorded at room temperature. B) Illustration of the role of aryl–carbonyl C–H···O bonding in the formation of a prochiral complex between cinchonidine and methyl pyruvate co-adsorbed on platinum.

In summary, we have shown that nonsubstituted aromatic molecules chemisorbed on a platinum surface form double C–H···O bonds to co-adsorbed esters and ketoesters. The hydrogen-bond strength is sufficient to form well-defined assemblies at 150–300 K and may be tuned by substitution on the aromatic molecule. The C–H···O interaction is key to understanding the asymmetric hydrogenation of α-ketoesters on cinchona-modified platinum catalysts and may also be relevant to catalysis by metal–arene complexes. We anticipate that double hydrogen bonding involving aromatic molecules will play an increasingly important role in the rational design of both chiral catalysts and 2D supramolecular structures.

Experimental Section

Variable-temperature STM measurements were carried out on clean polished Pt(111) surfaces under ultrahigh vacuum. A tunneling current of $I_t = 0.96$ nA and tunneling voltages of $V = -0.84$ to -0.99 V were used.

Received: August 1, 2006
Published online: October 11, 2006

Keywords: asymmetric catalysis · chemisorption · hydrogen bonds · scanning probe microscopy · self-assembly

[1] S. M. Barlow, R. Raval, *Surf. Sci. Rep.* **2003**, *50*, 201.
[2] J. V. Barth, G. Costantini, K. Kern, *Nature* **2005**, *437*, 671.
[3] R. Fasel, M. Parschau, K. H. Ernst, *Nature* **2006**, *439*, 449.
[4] Q. Chen, N. V. Richardson, *Nat. Mater.* **2003**, *2*, 324.
[5] L. J. Prins, F. De Jong, P. Timmerman, D. N. Reinhoudt, *Nature* **2000**, *408*, 181.
[6] K. G. Nath, O. Ivasenko, J. A. Miwa, H. Dang, J. D. Wuest, A. Nanci, D. F. Perepichka, F. Rosei, *J. Am. Chem. Soc.* **2006**, *128*, 4212.
[7] S. Lavoie, M.-A. Laliberté, I. Temprano, P. H. McBreen, *J. Am. Chem. Soc.* **2006**, *128*, 7588.
[8] S. Lavoie, P. H. McBreen, *J. Phys. Chem. B* **2005**, *109*, 11986.
[9] M. Bohringer, K. Morgenstern, W. D. Schneider, R. Berndt, F. Mauri, A. De Vita, R. Car, *Phys. Rev. Lett.* **1999**, *83*, 324.
[10] F. Vidal, E. Delvigne, S. Stepanow, N. Lin, J. V. Barth, K. Kern, *J. Am. Chem. Soc.* **2005**, *127*, 10101.
[11] S. Stepanow, N. Lin, F. Vidal, A. Landa, M. Ruben, J. V. Barth, K. Kern, *Nano Lett.* **2005**, *5*, 901.
[12] V. S. Bryantsev, B. P. Hay, *Org. Lett.* **2005**, *7*, 5031.
[13] C. Morin, D. Simon, P. Sautet, *J. Phys. Chem. B* **2004**, *108*, 12084.
[14] G. Held, W. Braun, H. R. Steinruck, S. Yamagishi, S. J. Jenkins, D. A. King, *Phys. Rev. Lett.* **2001**, *87*, 216102.
[15] Y. P. Tan, S. Khatua, S. J. Jenkins, J.-Q. Yu, J. B. Spencer, D. A. King, *Surf. Sci.* **2005**, *589*, 173.
[16] S. W. Gao, J. R. Hahn, W. Ho, *J. Chem. Phys.* **2003**, *119*, 6232.
[17] J. R. Hahn, W. Ho, *J. Phys. Chem. B* **2005**, *109*, 20350.
[18] Y. Orito, S. Imai, S. Niwa, *J. Chem. Soc. Jpn.* **1979**, *8*, 1118.
[19] C. J. Baddeley, *Top. Catal.* **2003**, *25*, 17.
[20] V. Venkatesan, A. Fujii, N. Mikami, *Chem. Phys. Lett.* **2005**, *409*, 57.
[21] G. C. Fu, *Acc. Chem. Res.* **2000**, *33*, 412.
[22] F. Mathey, A. Sevin, *Molecular Chemistry of the Transition Elements: An Introductory Course*, Wiley, New York, **1996**.
[23] S. Shambayati, W. E. Crowe, S. L. Schreiber, *Angew. Chem.* **1990**, *102*, 273; *Angew. Chem. Int. Ed. Engl.* **1990**, *29*, 256.
[24] W.-K. Wong, W. Tam, C. E. Strouse, J. A. Gladysz, *J. Chem. Soc. Chem. Commun.* **1979**, 530.
[25] G. O. Nelson, C. E. Sumner, *Organometallics* **1986**, *5*, 1983.
[26] D. Braga, F. Grepioni, *Acc. Chem. Res.* **2000**, *33*, 601.
[27] M. S. Taylor, E. N. Jacobsen, *Angew. Chem.* **2006**, *118*, 1550; *Angew. Chem. Int. Ed.* **2006**, *45*, 1520.
[28] P. M. Pihko, *Angew. Chem.* **2004**, *116*, 2110; *Angew. Chem. Int. Ed.* **2004**, *43*, 2062.
[29] Y. Huang, A. K. Unni, A. N. Thadani, V. H. Rawal, *Nature* **2003**, *424*, 146.

© 2006 Wiley-VCH Verlag GmbH & Co. KGaA, Weinheim

Activity-Based Proteomics

DOI: 10.1002/anie.200603187

Substrate Mimicry in an Activity-Based Probe That Targets the Nitrilase Family of Enzymes**

*Katherine T. Barglow and Benjamin F. Cravatt**

A principal goal of proteomics is to assign functions to each of the proteins encoded by prokaryotic and eukaryotic genomes.[1,2] A protein's function can be defined on multiple levels that reflect its coincident impact on biochemical, cellular, and physiological processes. Activity-based protein profiling (ABPP) is a functional proteomics method that utilizes active-site-directed chemical probes to characterize enzymes in native biological samples.[3–5] ABPP probes have proven useful for relating the activity state of enzymes to higher-order physiological and pathological processes, including cancer pathogenesis,[6–8] parasite invasiveness,[9] and obesity.[10] The extent to which these chemical tools might also offer insights into the structures of endogenous substrates of enzymes remains a pertinent, but largely unanswered question. Herein we show that profiling proteomes with a library of protein-reactive chemical probes can generate structure–activity data that are reflective of the natural substrates of enzymes. Thus, ABPP can facilitate the annotation of protein function at multiple levels.

Previous ABPP studies revealed markedly distinct proteome reactivity profiles for members of a library of rhodamine-tagged dipeptide α-chloroacetamide (α-CA) probes.[10] Some protein targets showed exclusive or preferential reactivity with a single α-CA, whereas others showed a more promiscuous profile, reacting with several members of the probe library. Among the more intriguing proteins that fell into the former class was a 44-kDa liver protein that exclusively reacted with Leu-Asp α-CA, where Leu and Asp represent R^2 and R^1, respectively (Figure 1a). We sought to further characterize the probe-labeling profile of this protein by testing its reactivity with an expanded library of α-CA probes in which either the R^1 or R^2 position was held constant as leucine and the complementary site varied with one of twenty amino acid side chains (Figure 1a). The 44-kDa protein was again found to react specifically with Leu-Asp α-CA, and showed negligible labeling with other probes including the structurally related Leu-Glu, Leu-Gln, and Asp-Leu α-CAs (Figure 1b and the Supporting Information).

The 44-kDa protein was enriched from mouse liver proteomes by labeling with a trifunctional Leu-Asp α-CA

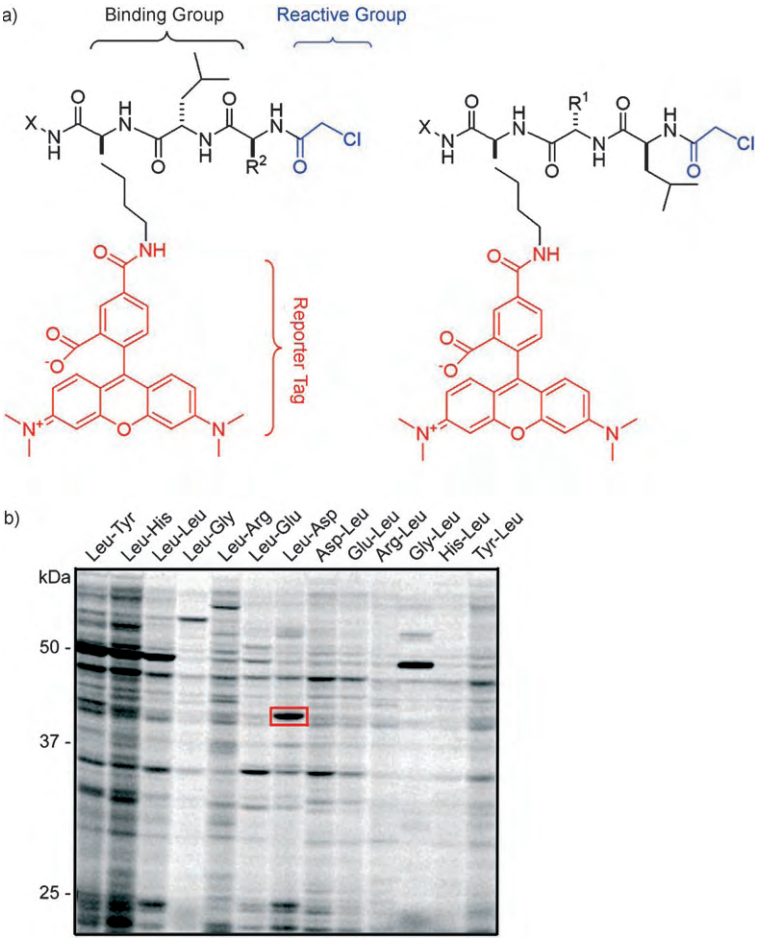

Figure 1. A library of dipeptide α-CA probes for ABPP. a) Structure of the dipeptide α-CA, where R^1 and R^2 are 15 different natural amino acids, phospho-serine, phospho-tyrosine, D-leucine, D-proline, or D-aspartate (see the Supporting Information for a complete summary of the dipeptide α-CA probes). For proteome screening, X = H; for protein identification, X = lysine-biotin. The α-CA reactive group and rhodamine tag are colored in blue and red, respectively. b) Proteome reactivity profiles for representative members of the α-CA probe library. Probes (20 μM) were allowed to react with mouse-liver proteome (2 mg protein mL^{-1}) for 1 h at room temperature and the reactions analyzed by SDS-PAGE and in-gel fluorescence scanning. A 44-kDa protein that reacted selectively with the Leu-Asp α-CA probe is highlighted by a red box. See the Supporting Information for comparison of the reactivity of this protein with Leu-Asp and Leu-Asn α-CA. Fluorescent gel images are shown in grayscale.

[*] K. T. Barglow, Prof. B. F. Cravatt
The Skaggs Institute for Chemical Biology and
Departments of Cell Biology and Chemistry
The Scripps Research Institute
10550 North Torrey Pines Road, La Jolla, CA 92037 (USA)
Fax: (+1) 858-784-8023
E-mail: cravatt@scripps.edu

[**] This research was supported by the NIH (CA087660), the Howard Hughes Medical Institute (predoctoral fellowship to K.T.B.), and the Skaggs Institute for Chemical Biology. We thank M. Patricelli (Activx Biosciences) for assistance with the identification of probe sites of labeling for nitrilase enzymes and the members of the Cravatt lab for helpful discussions and critical reading of the manuscript.

Supporting information for this article, which also contains details of the materials and methods, is available on the WWW under http://www.angewandte.org or from the author.

InterScience
© 2006 Wiley-VCH Verlag GmbH & Co. KGaA, Weinheim

probe coupled to both biotin and rhodamine, followed by avidin affinity chromatography and SDS-PAGE. Liquid chromatography (LC)–MS analysis of a trypsin digest of the gel-excised 44-kDa protein identified it as ureidopropionase-β (Upβ), a 43.9-kDa member of the nitrilase superfamily (see the Supporting Information). To confirm this identification, a cDNA (complementary DNA) encoding the full-length mouse Upβ (appended with a C-terminal myc epitope tag) was subcloned into the pcDNA3.1 expression vector and transiently transfected into COS-7 cells. A strong Leu-Asp α-CA-reactive 44-kDa protein was detected in Upβ-transfected cells, but not mock-transfected cells (Figure 2a, left). Like native liver Upβ, the recombinantly expressed form of this enzyme showed nearly exclusive labeling with Leu-Asp α-CA (Figure 2b).

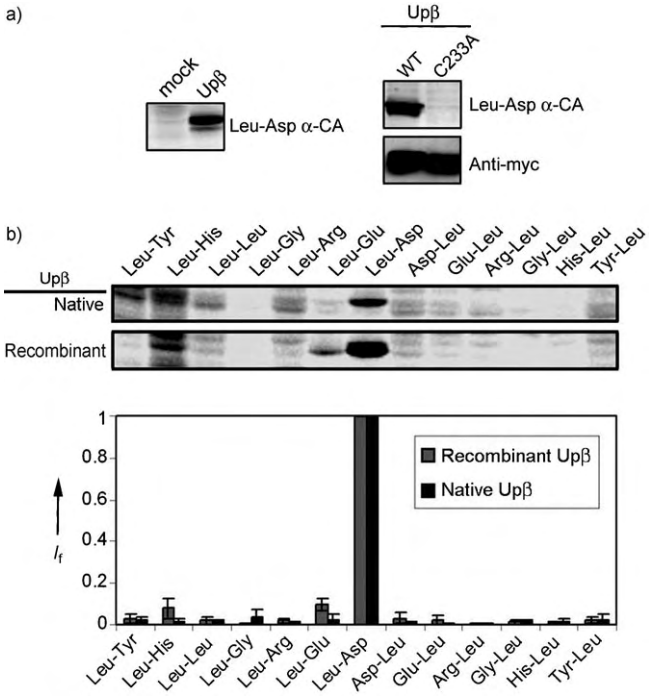

Figure 2. Identification and characterization of Upβ as a target of Leu-Asp α-CA. a) Left: Upβ-transfected, but not mock-transfected, COS-7 cells possess a 44-kDa protein that reacted with Leu-Asp α-CA; right: mutation of the cysteine nucleophile of Upβ to alanine (C233A) eliminated labeling by Leu-Asp α-CA. b) Native (liver) and recombinant (transfected COS-7) Upβ enzymes selectively reacted with Leu-Asp α-CA compared with other dipeptide α-CA probes. Note that low signals were also observed in the molecular-mass range of Upβ for the Leu-Tyr and Leu-His probes; however, these probes showed much higher overall background proteome reactivity (see Figure 1b), suggesting that these signals may be nonspecific. Top: fluorescent gel images shown in grayscale. Bottom: quantification of fluorescent signals. Data represent the average ± standard deviation for four independent experiments. I_f = relative fluorescence, WT = wild type.

The nitrilase family is a phylogenetically ancient class of enzymes with multiple mammalian members that utilize a conserved Cys-Lys-Glu catalytic triad to cleave C–N bonds, including nitriles, carbamates, ureas, and amides.[11,12] Upβ, in particular, catalyzes the hydrolysis of *N*-carbamoyl β-alanine (CarβAla) to β-alanine, which is a central step in the pyrimidine catabolic pathway.[13] Mutation of Upβ in humans leads to a buildup of CarβAla, which exerts neurotoxic effects resulting in severe neuropathology and movement disorders.[13] In considering possible explanations for the high selectivity displayed by Upβ for Leu-Asp α-CA, we noted a striking structural similarity between this probe and Upβ's endogenous substrate CarβAla (Figure 3). This structural relation suggested that Leu-Asp α-CA bound and labeled Upβ at the active site. This premise was confirmed by mapping the site of probe modification, which was identified by tandem MS analysis as cysteine 233, the catalytic nucleophile of Upβ (Table 1).[11] Mutation of this residue to alanine produced a Upβ variant (C233A) that was expressed at wild-type levels in transfected COS-7 cells but failed to react with Leu-Asp α-CA (Figure 2a, right).

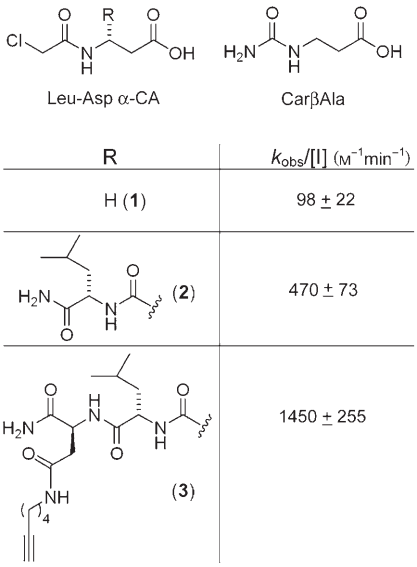

Figure 3. Leu-Asp α-CA is structurally similar to the natural Upβ substrate CarβAla. Top: structural comparison of Leu-Asp α-CA and CarβAla. Bottom: a comparison of the rates of inactivation of Upβ by analogues of Leu-Asp α-CA. The structure of the rhodamine-tagged Leu-Asp probe can be inferred from Figure 1.

Table 1: Sites of α-CA probe labeling for members of nitrilase family.

Enzyme	Labeled peptide[a]	Site of labeling[a]
Upβ	IAVNIC*YGR	C233
Nit1	VGLAIC*YDMRFPELSLK	C199

[a] Probe-labeled peptides and sites of labeling were determined by using an LC–MS platform for ABPP as described previously.[20,21] Proteomes were treated with an equimolar mixture of Leu-Asp, Leu-D-Asp, and D-Leu-D-Asp α-CA probes (20 μM of each probe).

Further evidence that Leu-Asp α-CA utilized substrate mimicry to achieve active-site modification of Upβ was sought by screening analogues of this probe for their ability to block enzyme labeling. Such competitive ABPP studies, when performed in a concentration- and time-dependent manner,

 © 2006 Wiley-VCH Verlag GmbH & Co. KGaA, Weinheim

can provide an estimate of the relative potency with which inhibitors target the active site of an enzyme.[14] An α-CA was designed that most closely resembled the Upβ substrate CarβAla, and this agent (**1**) was found to block probe labeling of Upβ with a $k_{obs}/[I]$ value of $98 \pm 22\,M^{-1}\,min^{-1}$ (I = competitive inhibitor, Figure 3). The addition of a leucine group (agent **2**) accelerated the rate of inactivation of Upβ, providing an agent that displayed a $k_{obs}/[I]$ value of $470 \pm 73\,M^{-1}\,min^{-1}$ (Figure 3). The introduction of a third amino acid derivative possessing an extended alkynyl side chain (agent **3**) further increased the rate of Upβ inactivation ($k_{obs}/[I] = 1450 \pm 255\,M^{-1}\,min^{-1}$, Figure 3) and enabled confirmation of covalent labeling of the enzyme by a click-chemistry reaction with an azide-rhodamine reporter group[15,16] (see the Supporting Information). These results indicate that an α-CA probe containing the core features of the CarβAla substrate is capable of covalently labeling the active site of Upβ, but that additional features of Leu-Asp α-CA further enhance this reaction.

Given that labeling of Upβ by Leu-Asp α-CA occurred on the enzyme's cysteine nucleophile, an essential catalytic residue conserved among all nitrilases,[11,12] we next tested whether α-CA probes might label other members of this enzyme family. Analysis of mouse-liver proteomes by using the MS-based platform ABPP-MudPIT (Multidimensional Protein Identification Technology)[17] identified nitrilase 2 (Nit2), along with Upβ, as specific targets of Leu-Asp α-CA (see the Supporting Information). Mouse nitrilase 1 (Nit1) was recombinantly expressed as a myc-tagged fusion protein in COS7 cells and treated with an expanded panel of α-CA probes that included agents where the chirality and order of the Leu-Asp dipeptide scaffold were systematically varied. Strong labeling was observed for Nit1 with several of the dipeptide α-CA probes (Figure 4 a and b), which contrasted with the more selective labeling pattern of Upβ (Figures 2b and 4b). Tandem MS analysis revealed that probe labeling of Nit1 occurred on the enzyme's cysteine nucleophile (C199; Table 1). These data indicate that dipeptide α-CAs serve as effective ABPP probes for multiple members of the nitrilase enzyme class.

In summary, we report the first example of active-site-directed proteomic probes that target the nitrilase family of enzymes. Nitrilases perform important functions in a wide range of organisms, including humans. For example, Upβ is a key component of the pyrimidine catabolic pathway, catalyzing the conversion of CarβAla to β-alanine.[13] This reaction appears to constitute the dedicated endogenous function of Upβ, as is reflected in the enzyme's restricted substrate selectivity, probe reactivity, and tissue distribution profiles (specific expression in liver; http://symatlas.gnf.org/SymAtlas/), as well as the metabolic defects that arise from its genetic mutation.[13] On the other hand, Nit1 is more ubiquitously expressed in mammalian tissues,[18] and the disruption of this enzyme leads to multiple phenotypes in mice, including accelerated cell growth and increased incidence of chemically induced tumors.[18] These physiological findings, coupled with the more promiscuous probe reactivity profile of Nit1, suggest that it may display a broader metabolic function than Upβ. Confirmation of this hypothesis will require identification of endogenous substrates for Nit1.

The additional finding that optimal probes for Upβ mimicked the structure of the enzyme's natural substrate has broader implications for enzyme annotation by using ABPP methods. Although other ABPP probes have been designed based on the substrate preferences of their target enzyme classes (e.g., negatively charged acyloxymethyl ketones for caspases[19]), our data with Upβ suggest provocatively that the relationships between enzymes and substrates can be "discovered" de novo by screening libraries of structurally diverse probes. By extension, we speculate that the probe-reactivity profiles of uncharacterized enzymes may also contain examples of substrate mimicry and, thus, provide insights into the endogenous biochemical functions of these proteins.

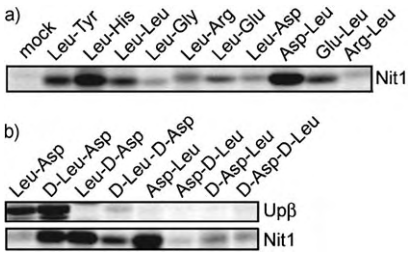

Figure 4. Identification and characterization of Nit1 as a target for dipeptide α-CA probes. a) Nit1-transfected, but not mock-transfected, COS7 cells possess a 35-kDa protein that reacted with several members of the α-CA probe library (mock-transfected proteome shown was allowed to react with Leu-Tyr α-CA). b) Comparison of the reactivity profiles of Upβ and Nit with a chiral library of Leu-Asp and Asp-Leu α-CA probes.

Received: August 5, 2006
Published online: October 11, 2006

Keywords: amino acids · biological activity · nitrilases · proteomics · screening

[1] P. C. Babbitt, *Curr. Opin. Chem. Biol.* **2003**, *7*, 230.
[2] A. Saghatelian, B. F. Cravatt, *Nat. Chem. Biol.* **2005**, *1*, 130.
[3] Y. Liu, M. P. Patricelli, B. F. Cravatt, *Proc. Natl. Acad. Sci. USA* **1999**, *96*, 14694.
[4] A. E. Speers, B. F. Cravatt, *ChemBioChem* **2004**, *5*, 41.
[5] A. B. Berger, P. M. Vitorino, M. Bogyo, *Am. J. Pharmacogenomics* **2004**, *4*, 371.
[6] N. Jessani, Y. Liu, M. Humphrey, B. F. Cravatt, *Proc. Natl. Acad. Sci. USA* **2002**, *99*, 10335.
[7] N. Jessani, M. Humphrey, W. H. McDonald, S. Niessen, K. Masuda, B. Gangadharan, J. R. Yates, 3rd, B. M. Mueller, B. F. Cravatt, *Proc. Natl. Acad. Sci. USA* **2004**, *101*, 13756.
[8] J. A. Joyce, A. Baruch, K. Chehade, N. Meyer-Morse, E. Giraudo, F. Y. Tsai, D. C. Greenbaum, J. H. Hager, M. Bogyo, D. Hanahan, *Cancer Cell* **2004**, *5*, 443.
[9] D. C. Greenbaum, A. Baruch, M. Grainger, Z. Bozdech, K. F. Medzihradszky, J. Engel, J. DeRisi, A. A. Holder, M. Bogyo, *Science* **2002**, *298*, 2002.
[10] K. T. Barglow, B. F. Cravatt, *Chem. Biol.* **2004**, *11*, 1523.
[11] P. Bork, E. V. Koonin, *Protein Sci.* **1994**, *3*, 1344.
[12] C. Brenner, *Curr. Opin. Struct. Biol.* **2002**, *12*, 775.

 © 2006 Wiley-VCH Verlag GmbH & Co. KGaA, Weinheim

[13] A. B. van Kuilenburg, R. Meinsma, E. Beke, B. Assmann, A. Ribes, I. Lorente, R. Busch, E. Mayatepek, N. G. Abeling, A. van Cruchten, A. E. Stroomer, H. van Lenthe, L. Zoetekouw, W. Kulik, G. F. Hoffmann, T. Voit, R. A. Wevers, F. Rutsch, A. H. van Gennip, *Hum. Mol. Genet.* **2004**, *13*, 2793.
[14] D. Leung, C. Hardouin, D. L. Boger, B. F. Cravatt, *Nat. Biotechnol.* **2003**, *21*, 687.
[15] A. E. Speers, G. C. Adam, B. F. Cravatt, *J. Am. Chem. Soc.* **2003**, *125*, 4686.
[16] A. E. Speers, B. F. Cravatt, *Chem. Biol.* **2004**, *11*, 535.
[17] N. Jessani, S. Niessen, B. Q. Wei, M. Nicolau, M. Humphrey, Y. Ji, W. Han, D. Y. Noh, J. R. Yates III, S. S. Jeffrey, B. F. Cravatt, *Nat. Methods* **2005**, *2*, 691.
[18] S. Semba, S. Y. Han, H. R. Qin, K. A. McCorkell, D. Iliopoulos, Y. Pekarsky, T. Druck, F. Trapasso, C. M. Croce, K. Huebner, *J. Biol. Chem.* **2006**, *281*, 28244.
[19] D. Kato, K. M. Boatright, A. B. Berger, T. Nazif, G. Blum, C. Ryan, K. Chehade, G. S. Salvensen, M. Bogyo, *Nat. Chem. Biol.* **2005**, *1*, 33.
[20] G. C. Adam, J. J. Burbaum, J. W. Kozarich, M. P. Patricelli, B. F. Cravatt, *J. Am. Chem. Soc.* **2004**, *126*, 1363.
[21] E. S. Okerberg, J. Wu, B. Zhang, B. Samii, K. Blackford, D. T. Winn, K. R. Shreder, J. J. Burbaum, M. P. Patricelli, *Proc. Natl. Acad. Sci. USA* **2005**, *102*, 4996.

 © 2006 Wiley-VCH Verlag GmbH & Co. KGaA, Weinheim

Coordination Frameworks

DOI: 10.1002/anie.200603250

Self-Assembly of Nanometer-Scale $[Cu_{24}I_{10}L_{12}]^{14+}$ Cages and Ball-Shaped Keggin Clusters into a (4,12)-Connected 3D Framework with Photoluminescent and Electrochemical Properties**

Xin-Long Wang, Chao Qin, En-Bo Wang, Zhong-Min Su,* Yang-Guang Li, and Lin Xu*

The design and construction of coordination polymers from preformed metal clusters,[1] such as metal carboxylate clusters[2] and chalcogenide supertetrahedral clusters,[3] to produce new materials with unique properties have been the focus of recent research interest. However, given the importance of cuprous iodide clusters in photochemistry and photophysics,[4] as well as their considerable variety of structural forms not encountered for other iodometalates,[5] it is surprising that relatively little progress has been made in using them as building blocks for the fabrication of multidimensional coordination frameworks.[6] On the other hand, polyoxometalates (POMs),[7,8] as a unique class of metal–oxide clusters, have many properties that make them attractive for applications in catalysis, biology, magnetism, optics, and medicine.[9] Impressive studies on linking of these well-defined metal–oxygen building blocks to generate giant discrete clusters and related extended structures have been performed.[10,11] However, up to now no reports have been made on the combination of these two interesting fields to prepare high-dimensional cluster-based compounds, although POM chemistry has touched an almost unprecedented number of other fields of chemistry.[9b] Such composite materials present the opportunity to generate high-dimensional nanoscopic assemblies from even larger multinanounits and also have vast potential for use in materials science by incorporation of their own physical and chemical properties.

Among the many different types of POMs, we chose the Keggin heteropolyanions, as they are the most widely recognized and thoroughly studied. Furthermore, we used the N-heterocyclic ligand 4-[3-(1*H*-1,2,4-triazol-1-yl)propyl]-4*H*-1,2,4-triazole (L, see the Supporting Information) for our synthetic strategy because 1) its clawlike donor atoms and bent coordination geometry offer the possibility of incorporating more metal atoms into high-nuclearity clusters, and 2) ligands containing a large number of N atoms could partially reduce Mo^{VI} to Mo^{V},[12] whereby the surface charge density of the polyanion is increased and the surface oxygen atoms are activated to facilitate formation of high-dimensional covalent networks. Herein we report the synthesis, structure, and luminescent and electrochemical properties of an unprecedented (4,12)-connected 3D network, namely, $(NH_4)[Cu_{24}I_{10}L_{12}][PMo^{V}_{2}Mo^{VI}_{10}O_{40}]_3$ (**1**), assembled by covalent connection of nanometer-scale $[Cu_{24}I_{10}L_{12}]^{14+}$ cages and ball-shaped Keggin anions.

Crystals of **1** were obtained by hydrothermal reaction of CuI, $H_3PMo_{12}O_{40}$, NH_4Cl, and L. Single-crystal X-ray analysis of **1**[13] showed the presence of two different nanocluster subunits (see the Supporting Information). One is the familiar Keggin cluster anion $[PMo^{V}_{2}Mo^{VI}_{10}O_{40}]^{5-}$ (ca. 10.5 Å in diameter), which consists of four internally edge sharing triads (Mo_3O_{13}) that share corners with each other and are disposed tetrahedrally around a central T_d atom (Figure 1c). Valence-sum calculations based on bond lengths established that the Mo centers are in $+5/+6$ oxidation states (see the Supporting Information). The assignment of the oxidation state is also consistent with the charge requirement of the anion and the UV/Vis spectrum.[14]

The other subunit is an unprecedented, highly symmetrical $[Cu_{24}I_{10}L_{12}]^{14+}$ cluster (Figure 1a) built up of a tetrahedral $Cu_{12}I_{10}N_{12}$ core and twelve supporting copper(I) atoms (Figure 1b). As shown in Figure 1d, the linking mode of the $Cu_{12}I_{10}N_{12}$ core is very similar to that of the Keggin ion, that is, four $Cu_3I_4N_3$ triad clusters that result from the association of three edge-sharing CuI_3N tetrahedra share corners to gen-

[*] Dr. X.-L. Wang, Dr. C. Qin, Prof. E.-B. Wang, Prof. Z.-M. Su, Dr. Y.-G. Li, Prof. L. Xu
Key Laboratory of Polyoxometalate Science of Ministry of Education
Institute of Polyoxometalate Chemistry
Department of Chemistry
Northeast Normal University
Changchun, Jilin, 130024 (China)
Fax: (+86) 431-509-8787
E-mail: wangenbo@public.cc.jl.cn
zmsu@nenu.edu.cn

[**] This work was financially supported by the National Natural Science Foundation of China (No. 20371011).

Supporting information for this article is available on the WWW under http://www.angewandte.org or from the author.

 © 2006 Wiley-VCH Verlag GmbH & Co. KGaA, Weinheim

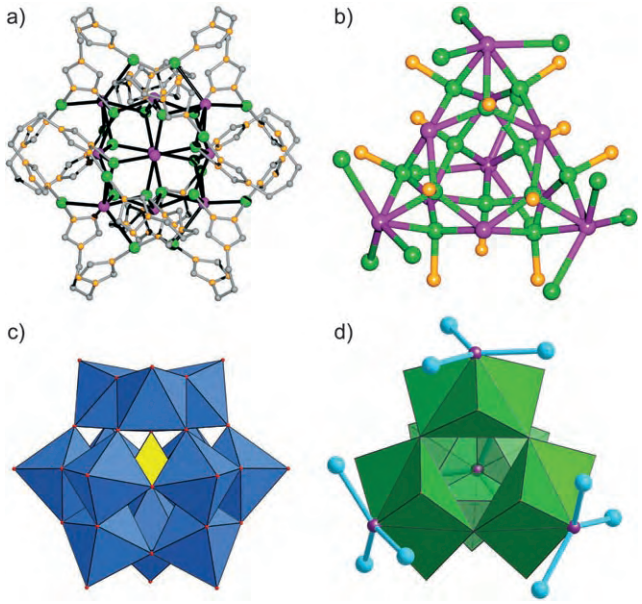

Figure 1. a) Ball-and-stick representation of the highly symmetrical $[Cu_{24}I_{10}L_{12}]^{14+}$ cluster. The basic $[Cu_{24}I_{10}N_{12}]^{14+}$ unit is highlighted by thick black bonds. Cu green, I purple, N orange, C gray. b) Ball-and-stick representation of the $Cu_{24}I_{10}N_{12}$ cluster with bridging ligands omitted for clarity. c) Polyhedral representation of Keggin-type $[PMo^{V}_{2}Mo^{VI}_{10}O_{40}]^{5-}$ cluster. Blue polyhedra MoO_6, yellow polyhedron PO_4. d) Polyhedral representation of the $Cu_{12}I_{10}N_{12}$ core with twelve supporting copper atoms shown as cyan balls.

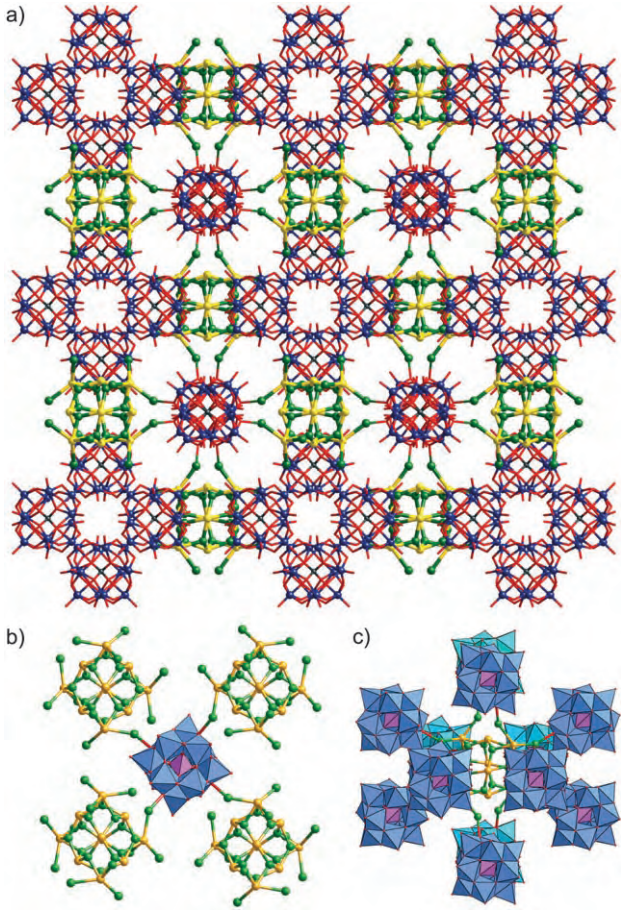

Figure 2. a) Ball-and-stick representation of the three-dimensional framework of **1**. b, c) Local connections of the two types of nanoclusters. Cu green, I yellow, Mo blue, P purple, O red. For clarity, ligands and isolated NH_4^+ ions are omitted.

erate the Cu_{12} core. All iodine atoms at the corners of the core are further bonded to three Cu atoms to give the novel $[Cu_{24}I_{10}L_{12}]^{14+}$ cluster. The arrangement of the central twelve Cu^I atoms can be approximated as a cuboctahedron with O_h symmetry, as found in the other two known species containing $Cu_{12}S_6$ clusters[15] (see the Supporting Information). Three adjacent Cu atoms that constitute a triad cluster form a perfect equilateral triangle with a Cu–Cu distance of 2.744(5) Å (Supporting Information). Such a short intermetallic distance, less than twice the van der Waals radius of Cu^I of 1.4 Å, implies strong Cu–Cu interactions. All the Cu^I centers and the inner six iodine atoms adopt tetrahedral coordination geometry, whereas the four remaining iodine atoms at the corners of the cluster have distorted octahedral geometry. The $[Cu_{24}I_{10}L_{12}]^{14+}$ cluster has a size of about 12.4 Å between corner metal sites and is the second largest iodocuprate(I) cluster made so far after the isolated cubic $[Cu_{36}I_{56}]^{20-}$ polyanion.[5b]

In coordination chemistry, it is quite rare that two different types of nanoclusters are directly assembled into crystalline solid-state materials.[16] Among the POM-based frameworks, we are aware of only two cases: $[\delta\text{-}Al_{13}O_4(OH)_{24}(H_2O)_{12}][XW_{12}O_{40}](OH)\cdot H_2O$ (X = H_2 or Co) in which $XW_{12}O_{40}^{6-}$ polyanions and $\delta\text{-}Al_{13}^{7+}$ polycations are packed alternately through intercluster hydrogen bonds and electrostatic interactions,[17] and a nanoring–nanosphere molecule with two K centers as hinge.[18] Compared to these species, the most important advance in **1** is the infinite and covalent assembly of the two types of nanoobjects. As illustrated in Figure 2, each $[Cu_{24}I_{10}L_{12}]^{14+}$ cluster is covalently bonded to twelve adjacent $[PMo_{12}O_{40}]^{5-}$ clusters via twelve peripheral copper atoms, and each $[PMo_{12}O_{40}]^{5-}$ cluster is connected with four $[Cu_{24}I_{10}L_{12}]^{14+}$ clusters via four μ_2-O atoms. Therefore, the overall 3D framework can be rationalized as a (4,12)-connected net with Schläfli symbol $(4^{30}\cdot6^{30}\cdot8^6)(4^6)_3$ by assigning the $[Cu_{24}I_{10}L_{12}]^{14+}$ cluster as a twelve-connected node and the $[PMo_{12}O_{40}]^{5-}$ cluster as a four-connected node (Figure 3 and Supporting Information).[19] The trigonal-icosahedral coordination of the twelve-connected $[Cu_{24}I_{10}L_{12}]^{14+}$ cluster in **1** (see the Supporting Information) makes it exceptional in that the only two comparable examples both adopt cuboctahedral coordination.[15b,20] Notably, the heterocyclic ligand does not, as one might expect, act as network linker, but rather templates the formation of the iodocuprate(I) cluster. Considering that nearly all iodocuprate(I) clusters have been prepared as isolated clusters, the twelve-connected $[Cu_{24}I_{10}L_{12}]^{14+}$ cluster present in **1** not only has the highest connectivity known to date, but is also the first cuprous iodide cluster extended to 3D architectures.

Compound **1** exhibits remarkably photoluminescent properties at ambient temperature. Two prominent emission peaks are observed at about 436 and 462 nm (excitation at 387 nm; see the Supporting Information). In accordance with the

 © 2006 Wiley-VCH Verlag GmbH & Co. KGaA, Weinheim

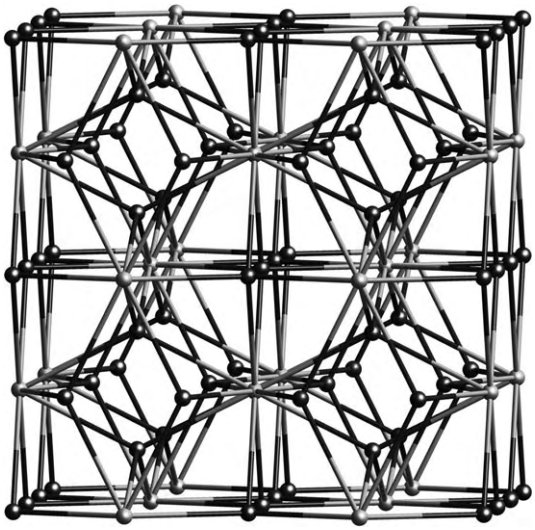

Figure 3. The (4,12)-connected $(4^{30}\cdot6^{30}\cdot8^{6})(4^{6})_3$ net. Dark gray: $[PMo_{12}O_{40}]^{5-}$ cluster; light gray: $[Cu_{24}I_{10}L_{12}]^{14+}$ cluster.

photoluminescent properties of cuprous halide clusters,[4] the two emissions may be attributed to a mixture of iodide-to-copper charge transfer and d–s transitions due to Cu–Cu interactions within the Cu_3 cluster.

The electrochemical behavior of **1**-modified carbon paste electrode (**1**-CPE) and its electrocatalytic reduction of nitrite were also studied (see the Supporting Information). Three well-defined redox couples can be observed in 1M aqueous H_2SO_4 solution at a scan rate of 20 $mV\,s^{-1}$. The approximate proportionality of the reduction peak current to the scan rate up to 500 $mV\,s^{-1}$ indicates that the redox process is surface-controlled.[21] Moreover, **1**-CPE is highly stable. When the potential range is maintained at +800 to −120 mV, the peak currents remain almost unchanged over 500 cycles. When **1**-CPE was stored at room temperature for two months, the current only decreased by 4% and could be renewed by squeezing a little carbon paste out of the tube. This is especially useful for electrocatalytic studies, since the catalytic activity is known to decrease when the electrode is fouled. The electroreduction of nitrite requires a large overpotential[22] and so no obvious response is observed in the range +700 to −200 mV on a bare carbon paste electrode in 1M H_2SO_4 containing 5 mM $NaNO_2$ (see the Supporting Information). However, **1**-CPE displays good electrocatalytic activity toward the reduction of nitrite. On addition of NO_2^-, the reduction peak currents increase and the corresponding oxidation peak currents decrease dramatically, and this suggests that nitrite is reduced. The results indicate that the three reduced species all have electrocatalytic activity for nitrite reduction. It was also noted that the third reduced species showed the best electrocatalytic activity, that is, the catalytic activity is enhanced with increasing extent of polyanion reduction.

In conclusion, a stable 3D covalent framework has been constructed by infinite assembly of two traditional but distinct nanoclusters. The novel nanoscale $[Cu_{24}I_{10}L_{12}]^{14+}$ cage building units and their covalent linkage with Keggin anions make this species an interesting solid-state rarity. More importantly, this framework generates a new kind of materials that combines the useful properties of the two clusters. Given the enormous structural diversity of POMs, this work opens new perspectives for the construction of fascinating multifunctional cluster-based networks. Work is continuing in this area.

Experimental Section

1: A mixture of CuI (95 mg, 0.5 mmol), $H_3PMo_{12}O_{40}$ (183 mg, 0.1 mmol), NH_4Cl (107 mg, 2 mmol), L (180 mg, 1 mmol), and water (10 mL) was sealed in a 20 mL teflon-lined autoclave and heated to 160 °C for 5 d. After slow cooling to room temperature, black crystals of **1** were obtained (yield: 139 mg, 40% based on Mo). Elemental analysis (%) calcd for $C_{84}H_{124}Cu_{24}I_{10}Mo_{36}N_{73}O_{120}P_3$: C 9.68, H 1.20, N 9.82, P 0.89, Mo 33.15, Cu 14.64; found: C 9.35, H 1.08, N 9.63, P 1.21, Mo 33.36, Cu 14.52. Materials and measurements are summarized in the Supporting Information.

Received: August 9, 2006

Keywords: cluster compounds · copper · molybdenum · N ligands · polyoxometalates

[1] a) A. K. Cheetham, G. Férey, T. Loiseau, *Angew. Chem.* **1999**, *111*, 3466; *Angew. Chem. Int. Ed.* **1999**, *38*, 3268; b) C. Janiak, *J. Chem. Soc. Dalton Trans.* **2003**, 2781; c) J. S. Seo, D. Whang, H. Lee, S. I. Jun, J. Oh, Y. J. Jeon, K. A. Kim, *Nature* **2000**, *404*, 982; d) A. Tripathi, T. Hughbanks, A. Clearfield, *J. Am. Chem. Soc.* **2003**, *125*, 10528; e) B. Kesanli, Y. Cui, M. R. Smith, E. W. Bittner, B. C. Bockrath, W. Lin, *Angew. Chem.* **2005**, *117*, 74; *Angew. Chem. Int. Ed.* **2005**, *44*, 72; f) M. B. Zhang, J. Zhang, S. T. Zheng, G. Y. Yang, *Angew. Chem.* **2005**, *117*, 1409; *Angew. Chem. Int. Ed.* **2005**, *44*, 1385.

[2] a) N. L. Rosi, J. Eckert, M. Eddaoudi, D. T. Vodak, J. Kim, M. O'Keeffe, O. M. Yaghi, *Science* **2003**, *300*, 1127; b) G. Férey, C. Mellot-Draznieks, C. Serre, F. Millange, J. Dutour, S. Surblé, I. Margiolaki, *Science* **2005**, *309*, 2040.

[3] P. Y. Feng, X. H. Bu, N. F. Zheng, *Acc. Chem. Res.* **2005**, *38*, 293.

[4] a) P. C. Ford, A. Vogler, *Acc. Chem. Res.* **1993**, *26*, 220; b) P. C. Ford, E. Cariati, J. Bourassa, *Chem. Rev.* **1999**, *99*, 3625.

[5] a) K. V. Domasevitch, J. A. Rusanova, O. Y. Vassilyeva, V. N. Kokozay, P. J. Squattrito, J. Sieler, P. R. Raithby, *J. Chem. Soc. Dalton Trans.* **1999**, 3087; b) H. Hartl, J. Fuchs, *Angew. Chem.* **1986**, *98*, 550; *Angew. Chem. Int. Ed. Engl.* **1986**, *25*, 569.

[6] a) H. W. Hou, Y. T. Fan, C. Du, Y. Zhu, W. L. Wang, X. Q. Xin, M. K. M. Low, W. Ji, H. G. Ang, *Chem. Commun.* **1999**, 647; b) N. R. Brooks, A. J. Blake, N. R. Champness, P. A. Cooke, P. Hubberstey, D. M. Proserpio, C. Wilson, M. Schröder, *J. Chem. Soc. Dalton Trans.* **2001**, 456.

[7] a) M. T. Pope, *Heteropoly and Isopoly Oxometalates*, Springer, Berlin, **1983**; b) C. L. Hill, *Chem. Rev.* **1998**, *98*, 1; c) K. Fukaya, T. Yamase, *Angew. Chem.* **2003**, *115*, 678; *Angew. Chem. Int. Ed.* **2003**, *42*, 654; d) C. D. Wu, C. Z. Lu, H. H. Zhuang, J. S. Huang, *J. Am. Chem. Soc.* **2002**, *124*, 3836; e) M. I. Khan, E. Yohannes, R. J. Doedens, *Angew. Chem.* **1999**, *111*, 1374; *Angew. Chem. Int. Ed.* **1999**, *38*, 1292.

[8] a) P. J. Hagrman, D. Hagrman, J. Zubieta, *Angew. Chem.* **1999**, *111*, 2798; *Angew. Chem. Int. Ed.* **1999**, *38*, 2638; b) E. Burkholder, J. Zubieta, *Chem. Commun.* **2001**, 2056.

[9] a) A. Müller, S. Q. N. Shah, H. Bögge, M. Schmidtmann, *Nature* **1999**, *397*, 48; b) P. Kögerler, L. Cronin, *Angew. Chem.* **2005**, *117*, 866; *Angew. Chem. Int. Ed.* **2005**, *44*, 844; c) L. Xu, M. Lu, B. B.

 © 2006 Wiley-VCH Verlag GmbH & Co. KGaA, Weinheim

Xu, Y. G. Wei, Z. H. Peng, D. R. Powell, *Angew. Chem.* **2002**, *114*, 4303; *Angew. Chem. Int. Ed.* **2002**, *41*, 4129.
[10] a) M. Sadakane, M. H. Dickman, M. Pope, *Angew. Chem.* **2000**, *112*, 3036; *Angew. Chem. Int. Ed.* **2000**, *39*, 2914; b) A. Müller, L. Toma, H. Bögge, C. Schäffer, A. Stammler, *Angew. Chem.* **2005**, *117*, 7935; *Angew. Chem. Int. Ed.* **2005**, *44*, 7757; c) A. Dolbecq, C. D. Peloux, A. L. Auberty, S. A. Mason, P. Barboux, J. Marrot, E. Cadot, F. Sécheresse, *Chem. Eur. J.* **2002**, *8*, 349.
[11] a) X. K. Fang, T. M. Anderson, C. L. Hill, *Angew. Chem.* **2005**, *117*, 3606; *Angew. Chem. Int. Ed.* **2005**, *44*, 3540; b) S. S. Mal, U. Kortz, *Angew. Chem.* **2005**, *117*, 3843; *Angew. Chem. Int. Ed.* **2005**, *44*, 3777.
[12] Y. Xu, J. Q. Xu, K. L. Zhang, Y. Zhang, X. Z. You, *Chem. Commun.* **2000**, 153.
[13] Crystal data of **1**: $C_{84}H_{124}Cu_{24}I_{10}Mo_{36}N_{73}O_{120}P_3$, $M_r = 10417.27$, cubic, space group $I\bar{4}3n$, $a = b = c = 22.4209(6)$ Å. $V = 11270.9(5)$ Å^3, $Z = 2$, $F(000) = 9764$. $\rho_{calcd} = 3.070$ g cm^{-3}, $R1$ ($wR2$) = 0.0395 (0.1081) and $S = 1.056$ for 3216 reflections with $I > 2\sigma(I)$. The data were collected at 273(2) K on a Rigaku R-AXIS RAPID IP diffractometer with monochromated $Mo_{K\alpha}$ radiation ($\lambda = 0.71073$ Å). The structure was solved by direct methods using SHELXS-97 and extended by Fourier techniques. CCDC 616371 contains the supplementary crystallographic data for this paper. These data can be obtained free of charge from The Cambridge Crystallographic Data Centre via www.ccdc.cam.ac.uk/data_request/cif.
[14] In the UV/Vis spectrum of **1**, the oxide-to-molybdenum charge-transfer adsorption maxima occur at 232 and 324 nm, and the characteristic combination d–d and intervalence charge transfer ($Mo^V \rightarrow Mo^{VI}$) absorption maximum is observed at around 750 nm. T. Yamase, *Chem. Rev.* **1998**, *98*, 307; O. Chen, C. L. Hill, *Inorg. Chem.* **1996**, *35*, 2403.
[15] a) R. V. Parish, Z. Salehi, R. G. Pritchard, *Angew. Chem.* **1997**, *109*, 276; *Angew. Chem. Int. Ed. Engl.* **1997**, *36*, 251; b) D. Li, T. Wu, X. P. Zhou, R. Zhou, X. C. Huang, *Angew. Chem.* **2005**, *117*, 4247; *Angew. Chem. Int. Ed.* **2005**, *44*, 4175.
[16] C. Wang, X. H. Bu, N. F. Zheng, P. Y. Feng, *J. Am. Chem. Soc.* **2002**, *124*, 10268.
[17] J. H. Son, Y.-U. Kwon, *Inorg. Chem.* **2003**, *42*, 4153.
[18] B. Botar, P. Kögerler, C. L. Hill, *J. Am. Chem. Soc.* **2006**, *128*, 5336.
[19] a) N. W. Ockwig, O. Delgado-Friedrichs, M. O'Keeffe, O. M. Yaghi, *Acc. Chem. Res.* **2005**, *38*, 176; b) S. R. Batten, R. Robson, *Angew. Chem.* **1998**, *110*, 1558; *Angew. Chem. Int. Ed.* **1998**, *37*, 1460.
[20] X. M. Zhang, R. H. Fang, H. S. Wu, *J. Am. Chem. Soc.* **2005**, *127*, 7670.
[21] L. Cheng, X. M. Zhang, X. D. Xi, S. J. Dong, *J. Electroanal. Chem.* **1996**, *407*, 97.
[22] B. Keita, L. Nadjo, *J. Electroanal. Chem.* **1987**, *227*, 77.

 © 2006 Wiley-VCH Verlag GmbH & Co. KGaA, Weinheim

DNA Structures

DOI: 10.1002/anie.200603392

Single-Molecule Protein Encapsulation in a Rigid DNA Cage**

*Christoph M. Erben, Russell P. Goodman, and Andrew J. Turberfield**

Herein, we demonstrate the encapsulation of a single molecule of cytochrome *c* within a rigid tetrahedral cage made of DNA. Encapsulation can be used to exert control over a guest molecule:[1] confinement within chaperone complexes promotes protein folding,[2] while synthetic cages have been used to stabilize reactive intermediates,[3] catalyze reactions,[4] and influence the conformation of peptides.[5] Containers on all scales down to the molecular level have been used to protect and target the delivery of drugs.[6] Capsules that could contain single proteins include multimeric fusion proteins,[7] viral capsids,[8] and DNA polyhedra.[9–11] DNA polyhedra are cagelike structures with edges formed from rigid double helices connected by branch junctions;[12] their dimensions are comparable to those of proteins and protein complexes. DNA tetrahedra are particularly attractive candidates for the encapsulation of other molecules: they can be made rapidly and in high yield by self-assembly, their braced architecture confers structural stability, and they can be opened by breaking bars of the cage.[11]

DNA tetrahedra were made by self-assembly of four oligonucleotides as described by Goodman et al.,[11a] and their structure is illustrated in Figure 1a. Each edge of a tetrahedron is a 20-base-pair double helix and is linked to the two edges that it meets at a vertex through unpaired single-nucleotide spacers: this double connection prevents rotation of the edge about its axis. The assembly process is stereoselective and forms the diastereomer that has the major grooves facing inwards at the vertices.[11a] Each oligonucleotide runs around one face. Four of the six edges of the tetrahedron contain nicks where the ends of an oligonucleotide meet: these nicks can be ligated or used as sites for chemical modification. We estimate that the central cavity of the tetrahedron could accommodate a sphere of radius of

[*] C. M. Erben, R. P. Goodman, Prof. A. J. Turberfield
Clarendon Laboratory
Department of Physics
University of Oxford
Parks Road, Oxford, OX1 3PU (UK)
Fax: (+44) 1865-272-400
E-mail: a.turberfield@physics.ox.ac.uk

[**] We thank Jonathan Bath for helpful discussions. This work was supported by the UK research councils BBSRC, EPSRC, MRC, and the MoD through the UK Bionanotechnology Interdisciplinary Research Collaboration, by the Rhodes Trust and the Oxford Life Sciences Interface Doctoral Training Centre.

Supporting information for this article is available on the WWW under http://www.angewandte.org or from the author.

WILEY InterScience DISCOVER SOMETHING GREAT
© 2006 Wiley-VCH Verlag GmbH & Co. KGaA, Weinheim

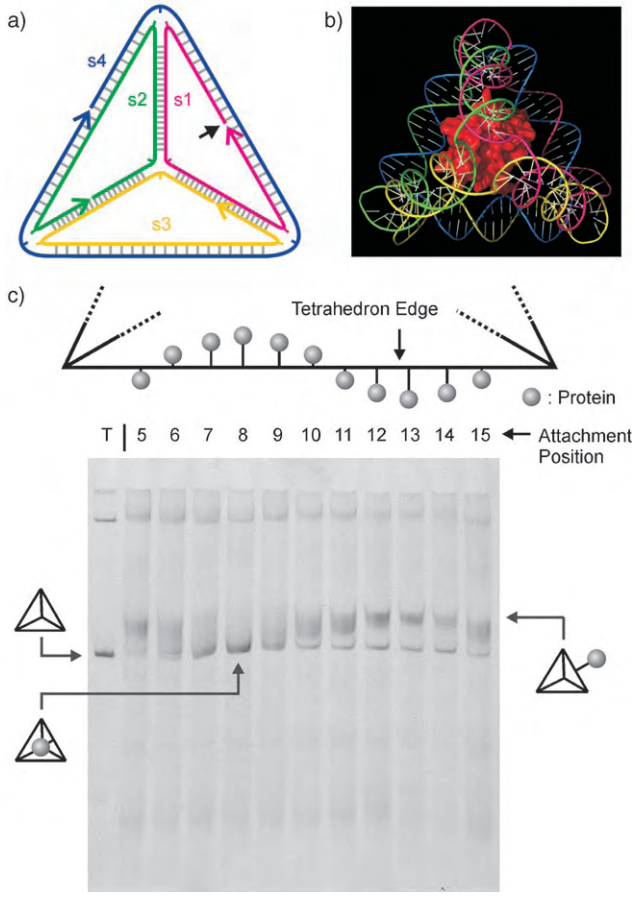

Figure 1. Positioning a protein within a DNA tetrahedron. a) Tetrahedron made from four oligonucleotides s1–s4. The black arrow indicates the protein attachment site at the 5′ end of s1. b) Molecular model which shows that cytochrome *c* can fit inside the tetrahedron. c) Native polyacrylamide gel showing the variation in electrophoretic mobility with the position of the attachment site. Control T: unmodified tetrahedron.

approximately 2.6 nm, corresponding to a globular protein with a molecular weight of roughly 60 kDa.[13] A model of the tetrahedron with a molecule of cytochrome *c* (12.4 kDa)[14] inside the cavity is shown in Figure 1b.

Horse-heart holo-cytochrome *c* was conjugated to the 5′ end of oligonucleotide s1 through a surface amine before assembly of the tetrahedron. This protein–DNA conjugate was then combined with oligonucleotides s2–s4 to form tetrahedra with the protein attached to one edge (see Experimental Section and Supporting Information). The position of the protein relative to the cage was controlled by altering the sequence of s1: when one nucleotide is transferred from the 3′ end of s1 to the 5′ end, then the attachment point of the protein—the nick in the edge formed by s1 and s4 where the ends of s1 meet—moves 0.34 nm along the double-helical edge of the tetrahedron and rotates clockwise by about 35° about its axis. As the edge is not free to rotate as a result of the double connection to neighboring edges, the attachment point of the protein on the edge determines the position of the protein relative to the tetrahedron cage. This makes it possible to choose whether the protein is held on the inside or on the outside of the tetrahedron. For the diastereomer that is selected by the assembly process,[11a] the attachment point is on the inside of the tetrahedron for conjugation at nucleotide 8 and on the outside at nucleotide 13 (counting in the 5′ to 3′ direction, with the unpaired nucleotide at the vertex as zero). The stereoselectivity of the synthesis[11a] is essential to the success of our strategy, as an attachment point that is on the inside of one diastereomer would be on the outside of the other.

Polyacrylamide gel electrophoresis (PAGE) was used to compare a group of 11 tetrahedra with cytochrome *c* conjugated at consecutive positions along one edge from the 5th to the 15th nucleotide (see Figure 1c). The control lane labeled "T" contains a tight band corresponding to a DNA tetrahedron without protein: this band is present in all other lanes (as a result of the presence of residual unconjugated oligonucleotides s1) and serves as a reference marker. A slower band corresponding to protein-conjugated tetrahedra is also visible; this band is broader, consistent with a distribution of conformations of the flexible DNA–protein linker. The mobility of the conjugate varies approximately sinusoidally with attachment position: the mobility difference between the conjugate and the unmodified tetrahedron is maximal for conjugation at nucleotide 13 and minimal for conjugation at nucleotide 8, that is, five bases further along the helix corresponding to approximately 180° rotation about the edge. When the protein is attached at nucleotide 8, the conjugate band is not separated from the nonconjugated control. The mobilities of the constructs with protein attachment at nucleotides 5 and 15, which are separated by one turn of the double helix, are approximately equal. This pattern is consistent with the expected helical trajectory of the attachment point along the edge.

To confirm this interpretation tetrahedron $T13^+$, with cytochrome *c* conjugated at nucleotide 13, the corresponding unmodified tetrahedron, $T13^-$ and $T8^+/T8^-$ (not resolved on non-denaturing gels), were purified on gel and analyzed on both non-denaturing and denaturing gels (Figure 2a and b). These tetrahedra differ from those shown in Figure 1c only in that the unmodified oligonucleotides s2–s4 had been ligated after assembly of the tetrahedron to form linked circles. Denaturation of $T13^-$ (band C) produces the expected fragments of unmodified tetrahedra: linked circles and single unmodified linear oligonucleotides (unligated s2–s4 or unmodified s1; see Supporting Information). Tetrahedron $T13^+$ (band B) contains one additional band corresponding to s1 conjugated to cytochrome *c*, thus confirming that this slow-migrating construct is the protein conjugate as identified above. Denaturing gel analysis of $T8^+/T8^-$ (band D) also reveals the presence of s1 conjugated to cytochrome *c*, thus confirming that $T8^+/T8^-$, which is unresolved from an empty tetrahedron on a non-denaturing gel, is not simply an empty tetrahedron but does contain the protein.

We conclude that when the protein is attached at nucleotide 13, it is positioned on the outside of the tetrahedron where it decreases the electrophoretic mobility of the construct. When it is attached at nucleotide 8, it has minimal effect on mobility as it is encapsulated within the tetrahedral cage.

© 2006 Wiley-VCH Verlag GmbH & Co. KGaA, Weinheim

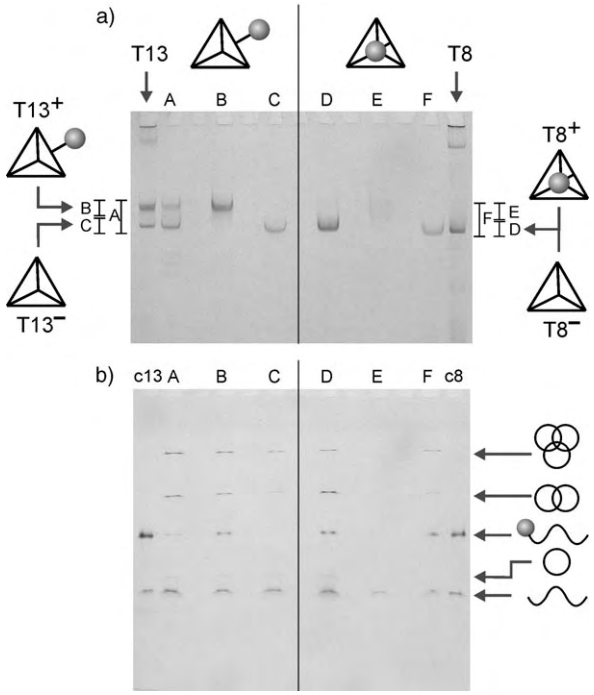

Figure 2. Analysis of protein–tetrahedron conjugates confirms the presence of the protein in $T8^+$ and $T13^+$. a) Native polyacrylamide gel showing constructs $T8^+$ and $T13^+$ with cytochrome *c* attached at the 8th and 13th nucleotides of one edge, that is, inside and outside the tetrahedron, respectively. Nonconjugated tetrahedra $T8^-$ and $T13^-$ are also present: $T8^+$ and $T8^-$ are not resolved. The outer lanes labeled T13 and T8 contain unpurified products of the synthesis; contents of lanes A–F were purified from the indicated regions of separate gels. b) Denaturing gel to analyze contents of gel-purified constructs. Controls c8, c13: cytochrome *c* conjugated to oligonucleotides s1 used to construct T8 and T13, respectively.

A DNA cage whose bars could be extended or broken might allow functional control of the encapsulated protein; for example, a cage that contains cytochrome *c* could control access by Apaf-1 (130 kDa), which forms a complex with cytochrome *c* to initiate an apoptotic protease cascade.[15] We have already demonstrated opening of the DNA tetrahedron cage by nucleases[11] and, through incorporation of a hairpin motif in one edge, by binding of a specific oligonucleotide sequence.[16] Conformation changes that could reveal the encapsulated protein could also be triggered by the following signals: binding of specific DNA[17] or RNA[18] sequences or, by incorporation of aptamer domains, proteins or small molecules;[19] changes in ionic concentrations[20] including pH;[21] ultraviolet[22] or radiofrequency radiation.[23] In contrast to conventional "caging" techniques that achieve functional control by means of photolabile protecting groups,[24] our strategy for geometric encapsulation does not require chemical modification or even knowledge of the active site: all that is necessary is a link between the encapsulated molecule and an oligonucleotide during assembly of the cage. Use of a DNA cage may also allow techniques for nonviral gene delivery[25] to be adapted to deliver the encapsulated molecule within a target cell.

In summary, we have demonstrated that a protein can be encapsulated within a DNA cage. Our assembly strategy requires control of the position of the attachment site on the cage; this was made possible by the rigid design and stereochemical purity of the DNA tetrahedron. Responsive DNA cages may allow functional control of proteins.

Experimental Section

All oligonucleotides were supplied by Integrated DNA Technologies Inc. (USA); see Supporting Information for sequences. Oligonucleotide s1 was synthesized with a C_6-amino modification at the 5′ end. Holo-cytochrome *c* from equine heart (Sigma) was conjugated to s1 by means of two heterobifunctional cross-linkers, sulfosuccinimidyl 4-(*N*-maleimidomethyl)cyclohexane-1-carboxylate (sulfo-SMCC) and *N*-succinimidyl 3-(2-pyridyldithio)propionate (SPDP; Pierce Biotechnology). Conjugates were gel-purified to remove proteins bound to more than one oligonucleotide. Tetrahedra were assembled by combining equal amounts of the s1–cytochrome *c* conjugate and oligonucleotides s2–s4 to a final concentration of 250 nM of each oligonucleotide in Tris buffer with 5 mM of divalent cations (either TM buffer: 10 mM Tris-HCl (pH 8), 5 mM $MgCl_2$; or TC buffer: 20 mM Tris-HCl (pH 8), 5 mM $CaCl_2$). The reaction mixture was maintained at 54 °C for 3 min then cooled to 4 °C over approximately 30 s. Tetrahedra can also be formed by incubation at room temperature, although the yield of the correctly self-assembled structure is reduced (see Supporting Information). When required, oligonucleotides s2–s4 were ligated by incubating assembled tetrahedra overnight with T4 DNA ligase (New England Biolabs) at room temperature. See Supporting Information for a detailed description of the experimental procedures used.

Received: August 18, 2006

Keywords: cytochrome *c* · DNA structures · host–guest systems · molecular devices · self-assembly

[1] J. C. Sherman, D. J. Cram, *J. Am. Chem. Soc.* **1989**, *111*, 4527–4528.
[2] F. U. Hartl, *Nature* **1996**, *381*, 571–580.
[3] D. J. Cram, M. E. Tanner, R. Thomas, *Angew. Chem.* **1991**, *103*, 1048–1051; *Angew. Chem. Int. Ed. Engl.* **1991**, *30*, 1024–1027.
[4] J. M. Kang, J. Rebek, *Nature* **1997**, *385*, 50–52.
[5] S. Tashiro, M. Tominaga, Y. Yamaguchi, K. Kato, M. Fujita, *Angew. Chem.* **2006**, *118*, 247–250; *Angew. Chem. Int. Ed.* **2006**, *45*, 241–244.
[6] D. A. LaVan, T. McGuire, R. Langer, *Nat. Biotechnol.* **2003**, *21*, 1184–1191.
[7] J. E. Padilla, C. Colovos, T. O. Yeates, *Proc. Natl. Acad. Sci. USA* **2001**, *98*, 2217–2221.
[8] F. P. Seebeck, K. J. Woycechowsky, W. Zhuang, J. P. Rabe, D. Hilvert, *J. Am. Chem. Soc.* **2006**, *128*, 4516–4517.
[9] a) J. H. Chen, N. C. Seeman, *Nature* **1991**, *350*, 631–633; b) Y. W. Zhang, N. C. Seeman, *J. Am. Chem. Soc.* **1994**, *116*, 1661–1669.
[10] W. M. Shih, J. D. Quispe, G. F. Joyce, *Nature* **2004**, *427*, 618–621.
[11] a) R. P. Goodman, I. A. T. Schaap, C. F. Tardin, C. M. Erben, R. M. Berry, C. F. Schmidt, A. J. Turberfield, *Science* **2005**, *310*, 1661–1665; b) R. P. Goodman, R. M. Berry, A. J. Turberfield, *Chem. Commun.* **2004**, 1372–1373.
[12] N. C. Seeman, *J. Theor. Biol.* **1982**, 99, 237–247.
[13] a) P. G. Squire, M. E. Himmel, *Arch. Biochem. Biophys.* **1979**, *196*, 165–177; b) K. Gekko, H. Noguchi, *J. Phys. Chem.* **1979**, *83*, 2706–2714.
[14] G. W. Bushnell, G. V. Louie, G. D. Brayer, *J. Mol. Biol.* **1990**, *214*, 585–595.

 © 2006 Wiley-VCH Verlag GmbH & Co. KGaA, Weinheim

[15] P. Li, D. Nijhawan, I. Budihardjo, S. M. Srinivasula, M. Ahmad, E. S. Alnemri, X. D. Wang, *Cell* **1997**, *91*, 479 – 489.
[16] R. P. Goodman, M. Heilemann, A. N. Kapanidis, A. J. Turberfield, unpublished results.
[17] B. Yurke, A. J. Turberfield, A. P. Mills, F. C. Simmel, J. L. Neumann, *Nature* **2000**, *406*, 605 – 608.
[18] Y. Benenson, B. Gil, U. Ben-Dor, R. Adar, E. Shapiro, *Nature* **2004**, *429*, 423 – 429.
[19] J. Tang, R. R. Breaker, *Chem. Biol.* **1997**, *4*, 453 – 459.
[20] C. D. Mao, W. Q. Sun, Z. Y. Shen, N. C. Seeman, *Nature* **1999**, *397*, 144 – 146.
[21] T. Liedl, F. C. Simmel, *Nano Lett.* **2005**, *5*, 1894 – 1898.
[22] P. Ordoukhanian, J. S. Taylor, *J. Am. Chem. Soc.* **1995**, *117*, 9570 – 9571.
[23] K. Hamad-Schifferli, J. J. Schwartz, A. T. Santos, S. G. Zhang, J. M. Jacobson, *Nature* **2002**, *415*, 152 – 155.
[24] a) K. Curley, D. S. Lawrence, *Curr. Opin. Chem. Biol.* **1999**, *3*, 84 – 88; b) G. Mayer, A. Heckel, *Angew. Chem.* **2006**, *118*, 5020 – 5042; *Angew. Chem. Int. Ed.* **2006**, *45*, 4900 – 4921.
[25] X. Gao, L. Huang, *Biochem. Biophys. Res. Commun.* **1991**, *179*, 280 – 285.

 © 2006 Wiley-VCH Verlag GmbH & Co. KGaA, Weinheim

Sialic Acid Synthesis

DOI: 10.1002/anie.200601555

Three-Step Synthesis of Sialic Acids and Derivatives**

*Zhangyong Hong, Lei Liu, Che-Chang Hsu, and Chi-Huey Wong**

Sialic acids are a family of monosaccharides of which more than 50 natural derivatives have been identified.[1] The most well-known member of the family is *N*-acetylneuraminic acid (Neu5Ac, **1**). Other important members include the 5-glycolylamido derivative Neu5Gc (**2**) and the non-aminated derivative KDN (**3**). These compounds represent one of the most important constituents of glycoconjugates in biological systems. They are involved in cell–cell recognition, blood coagulation, fertilization, and other biological events.[2] The peripheral positioning of sialic acids also instigates their participation in the pathogenesis of a variety of diseases including inflammatory disease, cancer metastasis, and virus infection. As a result, increasing attention has been paid recently to the utilization of sialic acids and analogues as probes or inhibitors in biological and medical research.[3] Some of the sialic acid analogues have even achieved commercial success, such as Relenza (**4**) and Tamiflu (**5**) for the treatment of influenza.[4] Further studies on the roles of sialic acids in biology as well as medicine are highly warranted. However, a challenge remaining in this area is the development of an efficient method for the synthesis of sialic acids and analogues with a high degree of flexibility in structural and stereochemical alteration.[5] In this context several de novo syntheses of sialic acids have been reported.[6–8] Most of these, however, are not cost effective because the synthetic routes are lengthy and the overall yields are low. Herein we describe our own advance in this direction, in which a novel and interesting route was successfully developed to synthesize sialic acids and derivatives from inexpensive starting materials with more satisfactory proficiency.

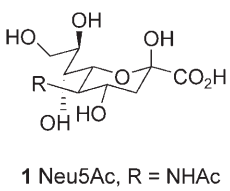

1 Neu5Ac, R = NHAc
2 Neu5Gc, R = NHGc
3 KDN, R = OH

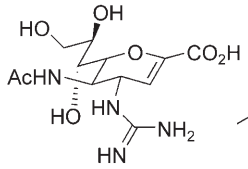

4 Relenza

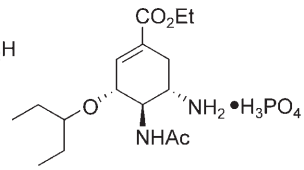

5 Tamiflu

We began our study with the synthesis of L-*N*-acetylneuraminic acid (**6**, L-Neu5Ac), which is the enantiomer of natural D-Neu5Ac (**1**). A potential application of the synthesis was to provide a sufficient quantity of L-Neu5Ac (**6**) for screening L peptides (by phage display) or D nucleic acids (by aptamer selection) that can bind L sugars.[9] To maximize the synthetic efficiency, we designed the retrosynthetic route shown in Scheme 1. The key steps in the synthesis include: 1) the simultaneous introduction of an amino group and a vinyl group to an aldose by means of the newly developed Petasis coupling reaction[10] and 2) the concise conversion of the vinyl group to a γ-hydroxy-α-keto acid moiety by means of a diastereoselective 1,3-dipolar cycloaddition reaction and subsequent ring opening. The scope of the proposed method was expected to be highly flexible, because by utilizing various types of aldoses (or polyhydroxy aldehydes) we would be able to obtain an unlimited number of sialic acid derivatives. At the same time, the efficiency of the method would be maximized if any protection and deprotection of the hydroxy groups could be strategically avoided.

The standard Petasis reaction is a three-component condensation of an α-hydroxy aldehyde, a primary or secondary amine, and a substituted vinyl boronic acid (or aryl boronic acid). However, our initial implementation of this reaction with an aldose was not successful until we realized that the unsubstituted vinyl boronic acid is an unstable compound that deteriorates rapidly.[11] In searching for a solution to this problem, we discovered that the commercially available dibutyl vinyl boronic acid ester could also be used in the Petasis coupling. An interesting

[*] Dr. Z. Hong, Dr. L. Liu, Dr. C.-C. Hsu, Prof. C.-H. Wong
Department of Chemistry and
The Skaggs Institute for Chemical Biology
The Scripps Research Institute
10550 North Torrey Pines Road, La Jolla, CA 92037 (USA)
Fax: (+1) 858-784-2409
E-mail: wong@scripps.edu

[**] This work was supported by the National Institutes of Health. We thank Dr. Lisa Whalen for proofreading the manuscript.

Supporting information for this article is available on the WWW under http://www.angewandte.org or from the author.

© 2006 Wiley-VCH Verlag GmbH & Co. KGaA, Weinheim

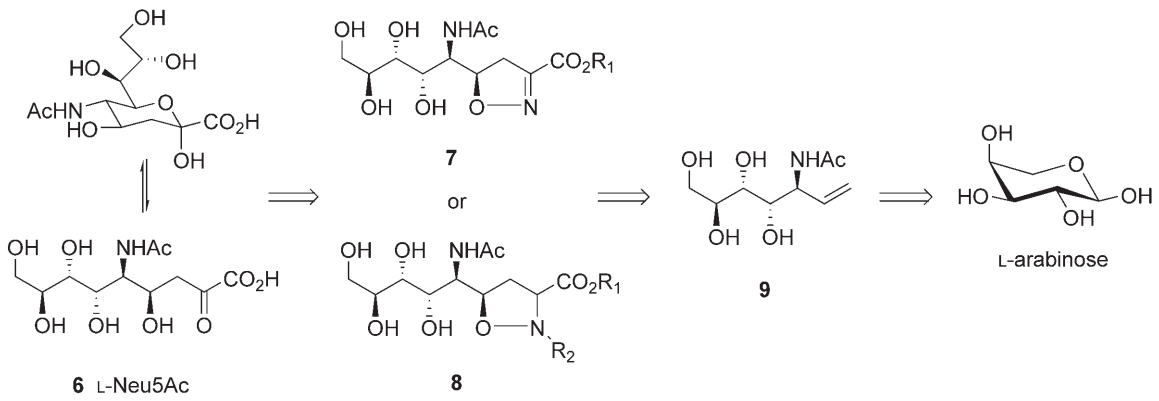

Scheme 1. Retrosynthesis of L-Neu5Ac (**6**).

aspect of this new finding was that water is necessary in the coupling of the boronic acid ester. This indicates that an in situ equilibrium between the boronic acid ester and boronic acid might occur under the reaction conditions (see Scheme 2). Owing to this exchange process, the coupling of dibutyl vinyl boronic acid ester had to be performed at a slightly higher reaction temperature (50 °C) and for a longer reaction time (72 h) in EtOH/H_2O (4:1) as compared to the standard conditions for the Petasis reaction (25 °C, 24 h, in pure EtOH).

Having solved the problem of incorporation of an unsubstituted vinyl group, we next successfully accomplished a one-pot synthesis of the key intermediate **9** (Scheme 2). In designing such a one-pot reaction, we confirmed through the NMR analysis of the crude reaction mixture that intermediate **11** was obtained as a nearly single diastereomer (> 99 % *de*). Rather than isolating compound **11**, we treated the reaction mixture with a catalytic amount of trifluoroacetic acid (TFA) and stirred the reaction overnight. After the bis(4-methoxyphenyl)methyl group had been successfully removed from the amino group, selective acetylation of the amino group was accomplished by treatment with Ac_2O/MeOH. At this stage we performed flash column chromatography to isolate compound **9**, which was obtained as a single diastereomer (> 99 % *de* as determined by ^1H and ^{13}C NMR analysis) in about 55 % yield as calculated from the starting material L-arabinose.[12]

With intermediate **9** in hand, we turned our attention to the next challenge—the conversion of the vinyl group in **9** into a γ-hydroxy-α-keto acid moiety. Our proposal was to accomplish this conversion by means of a tandem 1,3-dipolar cycloaddition and ring-opening reaction without any protection of the hydroxy groups. In our first attempt, we utilized a nitrile oxide ((*E*)-*N*-(2-ethoxy-2-oxoethylidene)methanamine oxide) as the dipole.[13] Unfortunately, although the 1,3-dipolar cycloaddition between this nitrile oxide and compound **9** proceeded smoothly to provide compound **7**, we could not selectively cleave the N–O bond in the dihydroisoxazole ring because of the presence of the C=N bond. Having failed with the nitrile oxide, we next tried to use

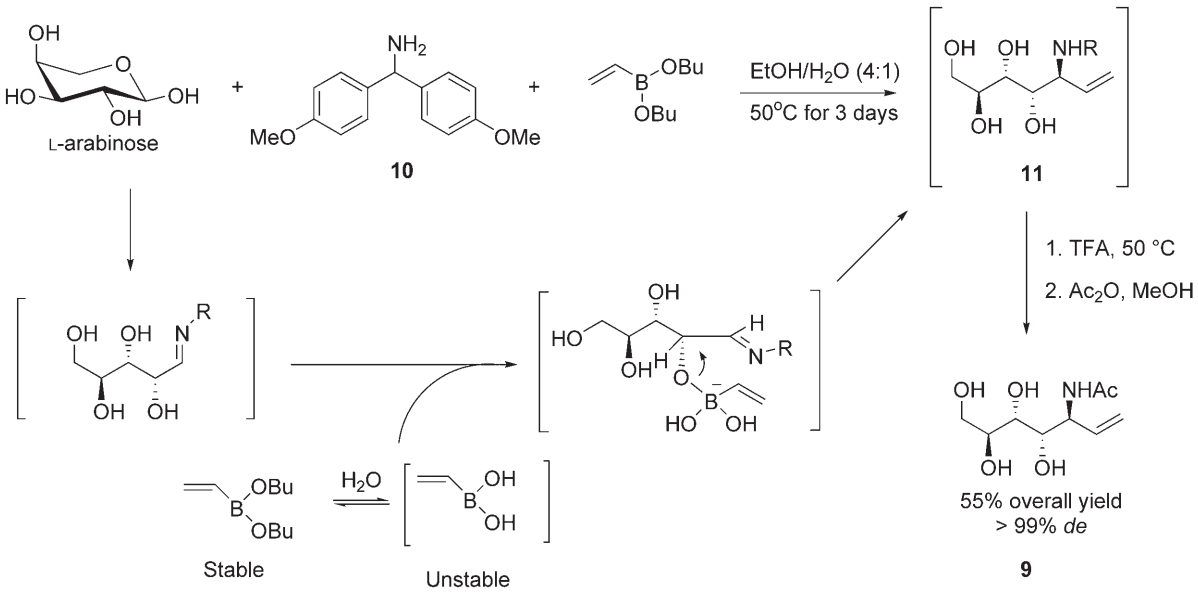

Scheme 2. One-pot synthesis of intermediate **9** and the possible mechanism of the boronic ester version of Petasis reaction. R = bis(4-methoxyphenyl)methyl.

 © 2006 Wiley-VCH Verlag GmbH & Co. KGaA, Weinheim

a nitrone in the 1,3-dipolar cycloaddition.[14] It is noteworthy that in the proposed product derived from a nitrone, the carbon atom at the α position relative to the acid group would not have the desired oxidation state (see Scheme 3). Without much literature precedence, we hypothesized that a base could be used to deprotonate the α-carbon and this might prompt the β elimination of oxygen from the nitrogen atom, affording the desired α-keto group. If this hypothesis were valid, we would obtain the γ-hydroxy-α-keto acid moiety from a vinyl group in an unprecedented way. To test our hypothesis, we carried out the 1,3-dipolar cycloaddition between compound **9** and the *N*-methyl nitrone **12** (Scheme 3). Without much difficulty, the desired product was successfully obtained in fairly good yields (>80%). Nevertheless, we were disappointed to observe a complex mixture of diastereomers in the product. Considerable attempts were carried out to improve the diastereoselectivity by changing the solvent (dioxane, MeOH, and EtOH), reaction temperature (from room temperature to 80°C), and the reactant concentration (from neat to 0.05 M). Unfortunately none of the conditions were satisfactory.

At this stage we went on to test the deprotonation/β-elimination hypothesis, because at least one of the chiral centers (i.e. the chiral center at the α position relative to the ester group) would disappear anyhow. Therefore, we treated the product mixture with NaOMe (0.05 M in MeOH) followed by an aqueous workup. The hypothesized reaction proceeded smoothly, affording L-Neu5Ac (and its 4-epimer) as the final products in 60% yield. (Note: the ester group was also hydrolyzed under the same reaction conditions.) ^{1}H and ^{13}C NMR analyses showed that the ratio between L-Neu5Ac and its 4-epimer was about 3:1, which resulted from the relatively poor diastereoselectivity in the 1,3-dipolar cycloaddition. To improve the diastereoselectivity, we tested different nitrones in the 1,3-dipolar addition. After some literature searching,[15] it came to our attention that the *N*-methyl nitrone **12** (Scheme 3) should exist as a mixture of *cis* and *trans* isomers. In contrast, when a bulky *tert*-butyl group is attached to the nitrogen atom, the resulting nitrone **15** should stay predominantly in the *cis* form. Taking these facts into consideration, we expected that improved diastereoselectivity could be attained by using the *N-tert*-butyl nitrone **15** in the 1,3-dipolar addition reaction.

To our satisfaction this hypothesis turned out to be correct. Thus, when the *N-tert*-butyl nitrone **15** was utilized, only two of the four possible isomers were produced in about 90% yield from the 1,3-dipolar cycloaddition. More importantly, these two isomers were found to have markedly different R_f values by TLC analysis (R_f(major) = 0.56 vs. R_f(minor) = 0.61 in 1:4 MeOH/CH_2Cl_2). Consequently it was fairly easy to separate the two isomers by standard flash column chromatography. NOE analyses of the purified products indicate that the major isomer is compound **16.**[16] Solvent, temperature, and reactant concentration were found to exert profound influences on the product ratio **16**/**17**. Under the optimal conditions (dioxane, 30°C, reactant concentration 0.05 M), the product ration was eventually optimized to be 10:1. Next, the purified compound **16** was subjected to the base-catalyzed β elimination, which successfully afforded L-Neu5Ac (**6**) in 60% yield. ^{1}H and ^{13}C NMR spectra of the synthetic L-Neu5Ac (**6**) were identical to the previously reported data for D-Neu5Ac.[17]

Thus, at this point we have successfully synthesized L-Neu5Ac from readily available L-arabinose. Starting from D-arabinose we also successfully synthesized D-Neu5Ac by the same three steps with an overall yield of 28%. It is important

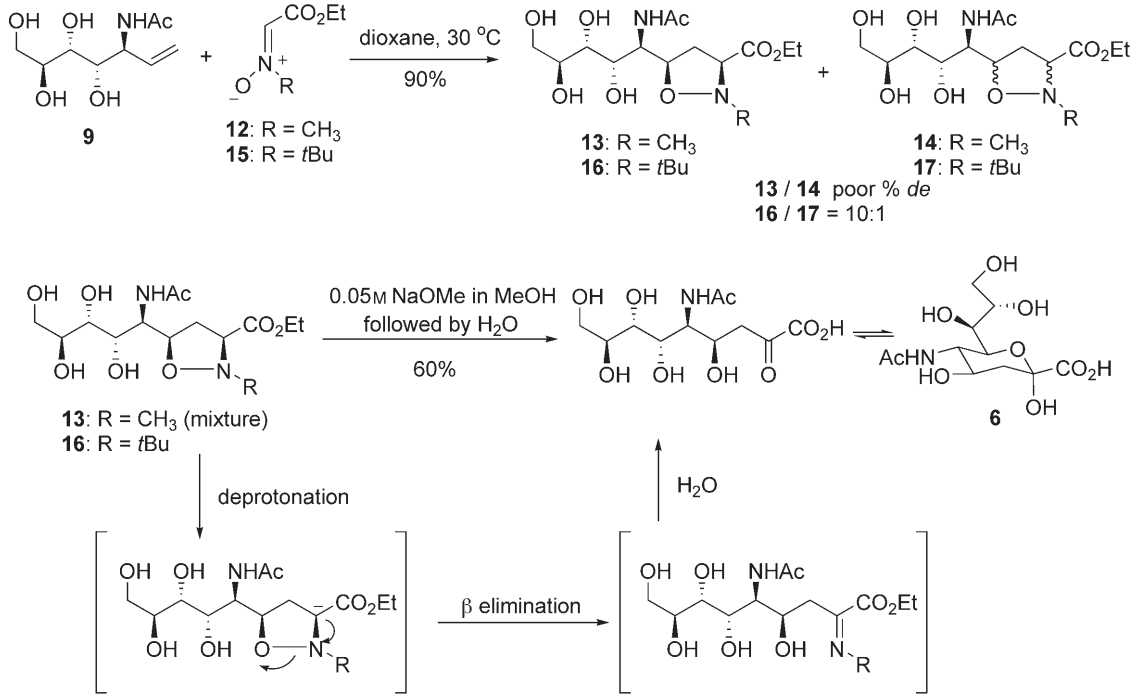

Scheme 3. Synthesis of L-Neu5Ac (**6**).

 © 2006 Wiley-VCH Verlag GmbH & Co. KGaA, Weinheim

to emphasize that the newly developed synthetic method is highly flexible for the synthesis of sialic acid analogues, because various aldose sugars (or polyhydroxy aldehydes) can be employed as the starting material. To demonstrate this, we describe further syntheses of some interesting sialic acid derivatives.

D-*N*-Glycolylneuraminic acid (**20**, D-Neu5Gc; Scheme 4): D-Neu5Gc is the hydroxylated derivative of D-Neu5Ac. It is produced in many non-human mammals, yet it typically is not detectable in humans.[18] It has been proposed that the presence of D-Neu5Gc on the cell surface in non-human primates may provide immunity to HIV infection in such species. Our synthesis of D-Neu5Gc began from commercially available D-arabinose. Using the aforementioned one-pot Petasis coupling we obtained compound **18** in 50% yield (>99% *de*), which was *N*-acylated by the activated ester of 2-acetoxyacetic acid (Scheme 4). Next, compound **18** was coupled with the *N*-*tert*-butyl nitrone **15** to afford compound **19** in 80% yield after separation from the undesired isomer (d.r. 12:1) by column chromatography. Finally, base-catalyzed β elimination and ester hydrolysis of **20** gave the target product in 55% yield. Thus, D-Neu5Gc was successfully

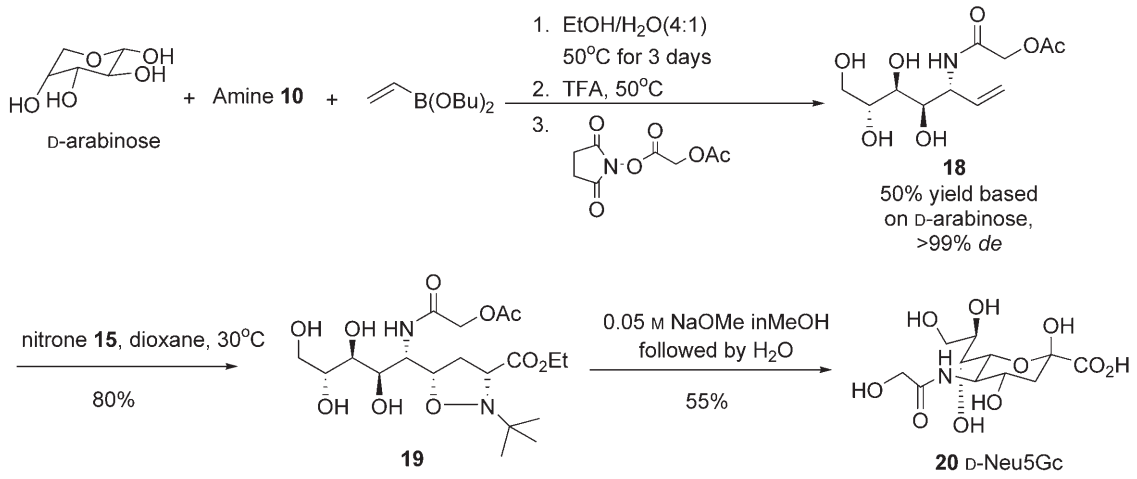

Scheme 4. Synthesis of D-Neu5Gc (**20**).

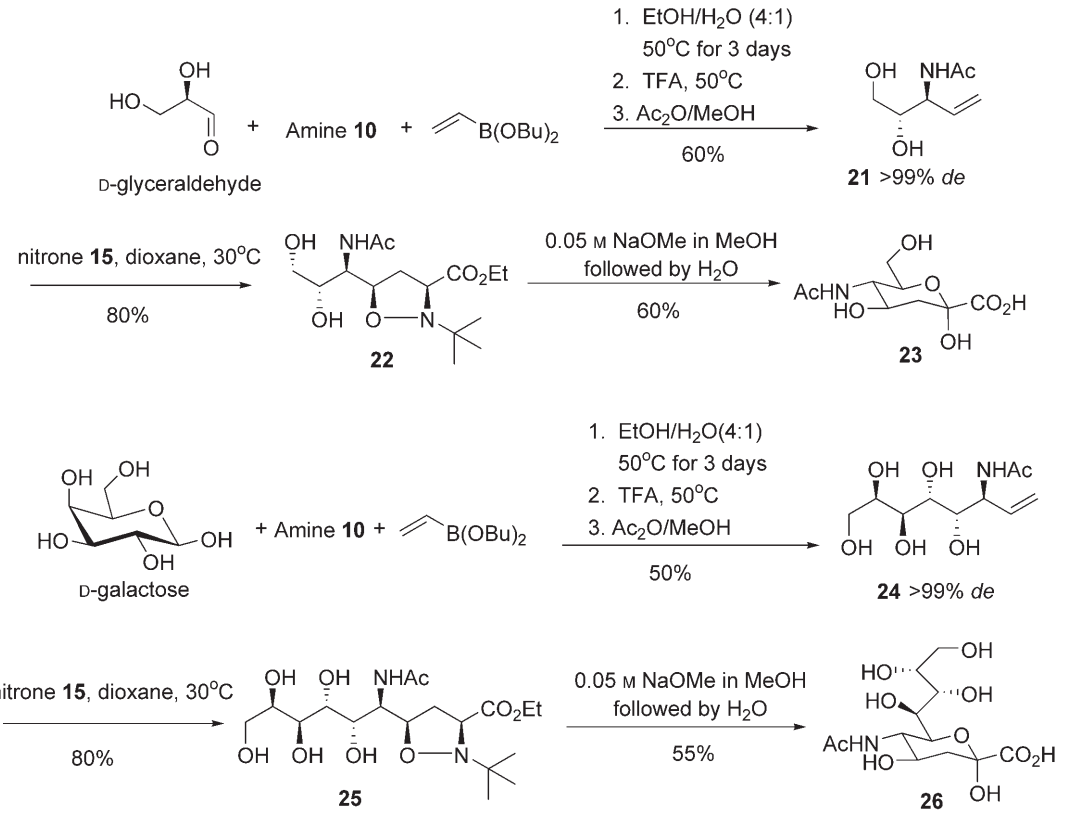

Scheme 5. Synthesis of truncated and elongated sialic acids.

 © 2006 Wiley-VCH Verlag GmbH & Co. KGaA, Weinheim

synthesized from readily available D-arabinose in three steps with an overall yield of 22%.

Truncated and elongated sialic acids: Some synthetic methods have been developed in the past for the preparation of 7-carbon analogues of sialic acids.[19] Herein, our own synthesis of the seven-carbon sialic acid analogue **23** was started from D-glyceraldehyde. Through the aforementioned "one-pot" Petasis coupling (60% yield, >99% *de*), 1,3-dipolar cycloaddition (80% yield, d.r. 8:1), and base-catalyzed β elimination and ester hydrolysis (60% yield), the target compound (**27**) was successfully obtained with an overall yield of 29% (Scheme 5). Similarly, we also synthesized the first ten-carbon analogue of sialic acid (**26**) in three steps from D-galactose with an overall yield of 22%.

In summary, in the present study we have developed a novel, efficient method for the synthesis of sialic acids and derivatives in only three steps from readily available starting materials. A boronic ester version of the Petasis coupling was developed, which facilitated the coupling of an unsubstituted vinyl group to an unprotected aldose. Next a highly diastereoselective 1,3-dipolar cycloaddition reaction was established that enabled the facile conversion of a vinyl group to an isoxazolidine ring carrying an ester group. Subsequently we discovered an unprecedented base-catalyzed ring-opening reaction for the direct conversion of the isoxazolidine to a γ-hydroxy-α-keto acid. All three reactions were completely compatible with the unprotected hydroxyl groups in carbohydrates. Armed with this novel approach, we successfully prepared several important, yet very expensive, sialic acid derivatives, including L-*N*-acetylneuraminic acid, D-*N*-glycolylneuraminic acid, a seven-carbon truncated analoguie, and a ten-carbon elongated analogue of sialic acid, in an economically competitive fashion.

Received: April 20, 2006
Revised: July 31, 2006
Published online: October 10, 2006

Keywords: cycloaddition · sialic acids · total synthesis

[1] a) T. Angata, A. Varki, *Chem. Rev.* **2002**, *102*, 439–469; b) A. Rosenberg, *Biology of Sialic Acids*, Plenum, New York, London, **1995**.

[2] *Essentials of Glycobiology* (Ed.: A. Varki, R. Cummings, J. Esko, H. Freeze, G. Hart, J. Marth), Cold Spring Harbor Laboratory Press, New York, **1999**.

[3] "N-Acetylneuraminic acid derivatives and mimetics as anti-influenza agents": R. Thomson, M. von Itzstein in *Carbohydrate-Based Drug Discovery* (Ed.: C.-H. Wong), Wiley-VCH, Weinheim, **2003**.

[4] a) M. von Itzstein, W. Y. Wu, G. B. Kok, M. S. Pegg, J. C. Dyason, B. Jin, P. T. Van, M. L. Smythe, H. F. White, S. W. Oliver, *Nature* **1993**, *363*, 418–423; b) C. U. Kim, W. Lew, M. A. Williams, H. Liu, L. Zhang, S. Swaminathan, N. Bischofberger, M. S. Chen, D. B. Mendel, C. Y. Tai, W. G. Laver, R. C. Stevens, *J. Am. Chem. Soc.* **1997**, *119*, 681–690; c) A. Moscona, *N. Engl. J. Med.* **2005**, *353*, 1363–1373.

[5] For recent reviews on the syntheses of sialic acids: a) L. S. Li, Y. L Wu, *Curr. Org. Chem.* **2003**, *7*, 447–475; b) M. J. Kiefel, M. von Itzstein, *Chem. Rev.* **2002**, *102*, 471–490; c) M. von Itzstein, R. J. Thompson, *Top. Curr. Chem.* **1997**, *186*, 119–170; d) M. P. DeNinno, *Synthesis* **1991**, 583–593.

[6] a) S. J. Danishefsky, M. P. DeNinno, S. H. Chen, *J. Am. Chem. Soc.* **1988**, *110*, 3929–3940; b) S. J. Danishefsky, W. H. Pearson, B. E. Segmuller, *J. Am. Chem. Soc.* **1985**, *107*, 1280–1285; c) S. H. Kang, H. W. Choi, J. S. Kim, J. H. Youn, *Chem. Commun.* **2000**, 227; d) E. A. Voight, C. Rein, S. D. Burke, *J. Org. Chem.* **2002**, *67*, 8489–8499; e) Dondoni, A. Marra, P. Merino, *J. Am. Chem. Soc.* **1994**, *116*, 3324–3336; f) A. Dondoni, A. Marra, A. Boscarato, *Chem. Eur. J.* **1999**, *5*, 3562–3572; g) T. Takahashi, H. Tsukamoto, M. Kurosaki, H. Yamada, *Synlett* **1997**, 1065–1066; h) M. Banwell, C. Desavi, K. Watson, *J. Chem. Soc. Perkin Trans. 1* **1998**, 2251–2252; i) L. S. Li, Y. L. Li, Y. Wu, *Org. Lett.* **2000**, *2*, 891–894; j) E. A. Voight, C. R. Rein, S. D. Burke, *Tetrahedron Lett.* **2001**, *42*, 8747–8749; k) K. G. Liu, S. Yan, Y. L. Wu, Z. J. Yao, *J. Org. Chem.* **2002**, *67*, 6758–6763.

[7] a) W. Fitz, M. J. Kim, W. J. Hennen, H. M. Sweers, C.-H. Wong, *J. Am. Chem. Soc.* **1988**, *110*, 6481–6486; b) C. Auge, S. David, C. Gautheron, *Tetrahedron Lett.* **1984**, *25*, 4663–4664; c) S. David, C. Auge, *Pure Appl. Chem.* **1987**, *59*, 1501–1508.

[8] a) T. H. Chan, M. C. Lee, *J. Org. Chem.* **1995**, *60*, 4228–4232; b) D. M. Gordon, G. M. Whitesides, *J. Org. Chem.* **1993**, *58*, 7937–7938; c) M. Warwel, W. Fessner, *Synlett* **2000**, 865–867; d) T. H. Chan, C. J. Li, *J. Chem. Soc. Chem. Commun.* **1992**, 747–748.

[9] a) I. A. Kozlov, S. Mao, Y. Xu, X. Huang, L. Lee, P. S. Sears, C. Gao, A. R. Coyle, K. D. Janda, C.-H. Wong, *ChemBioChem* **2001**, *2*, 741–746; b) C.-C. Hsu, Z.-Y. Hong, M. Wada, D. Franke, C.-H. Wong, *Proc. Natl. Acad. Sci. USA* **2005**, *102*, 9122.

[10] N. A. Petasis, I. A. Zavialov, *J. Am. Chem. Soc.* **1998**, *120*, 11798–11799.

[11] a) C. Morrill, R. H. Grubbs, *J. Org. Chem.* **2003**, *68*, 6031–6034; b) D. S. Matteson, *J. Am. Chem. Soc.* **1960**, *82*, 4228–4233.

[12] To further confirm its identity, we performed ozonolysis of compound **9** and successfully obtained L-ManNAc.

[13] a) K. V. Gothelf, K. A. Jorgensen, *Chem. Rev.* **1998**, *98*, 863–909; b) V. Jaeger, R. Schohe, *Tetrahedron* **1984**, *40*, 2199–2210; c) V. Jaeger, I. Mueller, *Tetrahedron* **1985**, *41*, 3519–3528.

[14] a) A. P. Kozikowski, *Acc. Chem. Res.* **1984**, *17*, 410–416; b) D. P. Curran, *J. Am. Chem. Soc.* **1983**, *105*, 5826–5833; c) P. Andreas, A. Vasella, *Helv. Chim. Acta* **1999**, *82*, 1044–1065; d) R. Huber, A. Vasella, *Helv. Chim. Acta* **1987**, *70*, 1461–1476; e) B. Bernet, E. Krawczyk, A. Vasella, *Helv. Chim. Acta* **1985**, *68*, 2299–2311.

[15] Y. Inouye, K. Takaya, H. Kakisawa, *Bull. Chem. Soc. Jpn.* **1983**, *56*, 3541–3542.

[16] In the ROESY NMR spectrum of compound **16**, there are strong H3α–H2 and H3α–H4 NOE correlations. A relatively weaker NOE correlation is also observed between H2 and H4. However, there is no NOE correlation between H3β and H2 (or between H3β and H4). These data suggest that compound **16** should be the 2*S*,4*R* isomer.

[17] a) E. S. Simon, M. D. Bednarski, G. M. Whitesides, *J. Am. Chem. Soc.* **1988**, *110*, 7159–7163; b) The optical rotation value for the synthetic L-Neu5Ac is $[\alpha]_D^{25} = +34.3°$ ($c = 0.5$ in H_2O); the literature value for D-Neu5Ac (Sigma) is $[\alpha]_D^{25} = -32 \pm 2°$.

[18] a) E. A. Muchmore, *Immun. Rev.* **2001**, *183*, 86; b) Y. N. Malykh, R. Schauer, L. Shaw, *Biochimie* **2001**, *83*, 623; c) A. Varki, *Biochimie* **2001**, *83*, 615.

[19] a) M. Warwel, W. D. Fessner, *Synlett* **2002**, 2104; b) M. Banwell, C. D. Savi, D. Hockless, K. Watson, *Chem. Commun.* **1998**, 645–646.

 © 2006 Wiley-VCH Verlag GmbH & Co. KGaA, Weinheim

Carbido Complexes

DOI: 10.1002/anie.200601652

Carbon–Carbon Bond Formation at a Neutral Terminal Carbido Ligand: Generation of Cyclopropenylidene and Vinylidene Complexes**

Stephen R. Caskey, Michael H. Stewart, Marc J. A. Johnson, and Jeff W. Kampf*

Olefin metathesis is an important tool for organic and polymer synthesis.[1] However, some key functional groups are not tolerated even by Ru-based catalysts.[2] We recently showed that vinyl esters can deactivate [Ru(CHPh)-$(PCy_3)_2Cl_2$] (**1**)[3] by quantitative formation of [Ru(C)-$(PCy_3)_2Cl_2$] (**2**)[4,5] A rare neutral terminal carbido complex,[4–7] **2** is surprisingly stable and has few reported reactions.[5–7] However, protonation of **2** by strong acid yields catalysts that rapidly initiate olefin metathesis.[7] Thus, **2** is both a precursor to and a decomposition product of olefin metathesis catalysts. We see **2** as a potential source of a C_1 fragment. Accordingly, we describe herein the first C–C bond-forming reaction of this unusual compound.

The terminal carbido ligand in **2** is a poor nucleophile, as shown by its failure to react with MeI, MeCOCl, and $PhCH_2Br$. Although **2** does not react with a variety of alkenes and alkynes (see the Supporting Information), it reacts cleanly with $MeO_2CC{\equiv}CCO_2Me$ (dimethyl acetylenedicarboxylate, DMAD) over 4 h in C_6H_6. A new blue-purple complex, **3**, is formed as the carbido signal for **2** (^{13}C NMR: $\delta = 471.8$ ppm) is replaced by a new signal at $\delta = 195.7$ ppm. The ^1H NMR spectrum evinces formation of a 1:1 adduct of **2** with DMAD. Formation of the cyclopropenylidene complex [Ru{=$CC_2(CO_2Me)_2$}$(PCy_3)_2Cl_2$] (Scheme 1) accounts for these observations. Several cyclopropenylidene complexes exist. Unlike **3**, however, the cyclopropenylidene units in these complexes are substituted by phenyl or electron-donating groups.[8–23] [Ru(C)(H_2IMes)$(PCy_3)Cl_2$] (**4**; H_2IMes = 4,5-dihydro-1,3-bis(mesityl)imidazol-2-ylidene) reacts similarly with DMAD, but the reaction is not clean since the product reacts further with DMAD before all of **4** has been consumed. However, **4** reacts more cleanly with $HC{\equiv}CCO_2Me$ (see the Supporting Information).

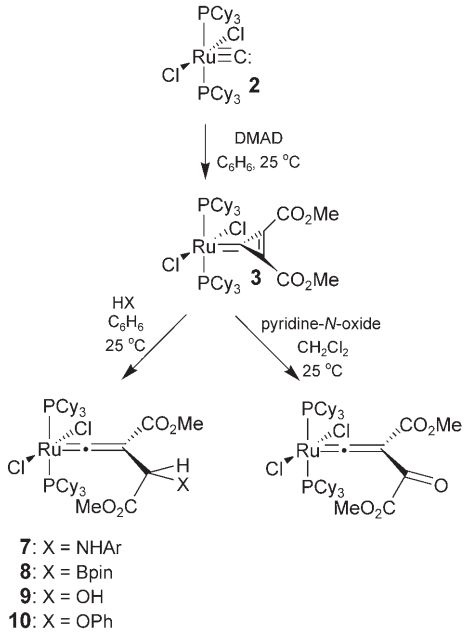

Scheme 1. Formation of **3** and ring-opening reactions. HBpin = pinacolborane, Ar = 3,5-$Me_2C_6H_3$.

Single-crystal X-ray diffraction confirmed the structure of **3**.[24] Figure 1 depicts a thermal ellipsoid plot of one of the two chemically equivalent but crystallographically independent molecules of **3** in the crystal. The data establish the expected connectivity in **3**, but the large uncertainty associated with the Ru=C bond length of 1.846(10) Å precludes comparison with those in related alkylidene complexes. The cyclopropenylidene ring lies in the Cl-Ru-Cl plane. The structure shows significant bond localization in the cyclopropenylidene fragment. These distances closely resemble those observed in free

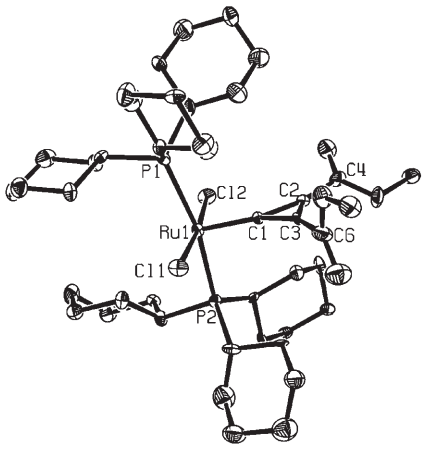

Figure 1. X-ray crystal structure of **3** (50% thermal ellipsoids). Selected bond lengths [Å] and angles [°]: Ru1-C1 1.846(10), Ru1-Cl1 2.389(3), Ru1-Cl2 2.402(3), Ru1-P1 2.407(3), Ru1-P2 2.390(3), C1-C2 1.410(13), C1-C3 1.425(14), C2-C3 1.300(14); C1-Ru1-Cl1 91.6(3); C1-Ru1-Cl2, 95.3(3), C1-Ru1-P1 97.0(3), C1-Ru1-P2 95.8(3), C2-C1-C3 54.6(7), C1-C2-C3 63.3(7), C1-C3-C2 62.1(7).

[*] S. R. Caskey, M. H. Stewart, Prof. M. J. A. Johnson, Dr. J. W. Kampf
Department of Chemistry
University of Michigan
930 North University Avenue
Ann Arbor, MI 48109-1055 (USA)
Fax: (+1) 734-647-4865
E-mail: mjaj@umich.edu

[**] This report is based upon work supported by the National Science Foundation under grant number CHE-0449459. We thank the Research Corporation, the University of Michigan, and the Camille and Henry Dreyfus Foundation for support. S.R.C. thanks the University of Michigan Chemistry Department for Margaret and Herman Sokol and Robert W. Parry Fellowships.

Supporting information for this article (including complete experimental details for new reactions) is available on the WWW under http://www.angewandte.org or from the author.

InterScience
© 2006 Wiley-VCH Verlag GmbH & Co. KGaA, Weinheim

$C_3(NiPr_2)_2$ (**5**)[25] and in other cyclopropenylidene complexes.[9,14–23]

The formation of **3** from **2** is interesting because the cyclopropylidene complex $[Ru\{=CC_2H_2(CO_2Me)_2\}(PCy_3)_2Cl_2]$ (**6**) is not observed as an intermediate when **2** is formed from **1** by reaction with Feist's ester.[4] Addition of 2 equivalents or less of PCy_3 to $[Ru\{=CC_2H_2(CO_2Me)_2\}(PPh_3)_2Cl_2]$ similarly yields **2**. In this case, too, **6** is not seen.[6]

The ^{13}C NMR shifts of the ring atoms in **3**, 195.7 and 162.2 ppm, closely resemble those observed for **5**[25] but less so other cyclopropenylidene complexes, for which some cyclopropenium character is often invoked.[14–23] Unlike **1**, **3** does not react appreciably with common olefins or alkynes, although under some conditions small amounts of **2** are formed, suggesting reversibility of the **2**→**3** transformation (see the Supporting Information). However, several reagents effect 1,1-addition of HX to the ring to form vinylidene complexes **7**–**10**; reaction with pyridine-*N*-oxide similarly yields **11** (Scheme 1). Cyclopropenium character could account for the observed reactivity, as all the reagents shown can act first as nucleophiles; however, there may be other explanations.

The structure of one vinylidene complex, $[Ru\{=C=C(CO_2Me)CH(NHAr)CO_2Me\}(PCy_3)_2Cl_2]$ (**7**, Ar = 3,5-$Me_2C_6H_3$), was determined by single-crystal X-ray diffraction.[26] The vinylidene unit is apical in square-pyramidal **7** (Figure 2).

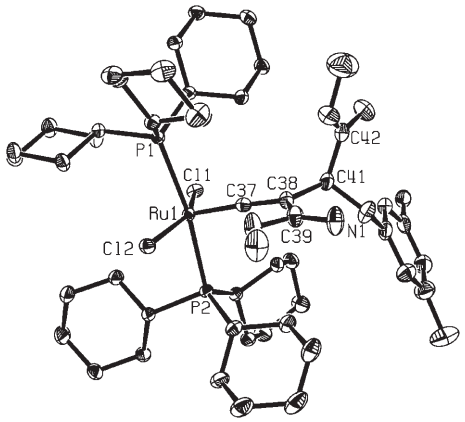

Figure 2. X-ray crystal structure of **7** (50% thermal ellipsoids). Selected bond lengths [Å] and angles [°]: Ru1-C37 1.7458(17), Ru1-Cl1 2.3441(4), Ru1-Cl2 2.3454(4), Ru1-P1 2.4405(4), Ru1-P2 2.4098(4), C37-C38 1.344(2); C37-Ru1-Cl1 105.16(5), C37-Ru1-Cl2 100.68(5), C37-Ru1-P1 95.78(5), C37-Ru1-P2 93.39(5), Ru1-C37-C38 176.16(14), C37-C38-C39 118.76(16), C37-C38-C41 121.94(16), C39-C38-C41 119.23(15).

Ruthenium vinylidenes are useful as catalysts and catalyst precursors for olefin metathesis, alkyne dimerization, and other reactions.[27,28] Like the "parent" vinylidene complex $[Ru(=C=CH_2)(PCy_3)_2Cl_2]$,[3] **7**–**11** do not catalyze the ring-closing metathesis of diethyl diallylmalonate, but they do polymerize norbornene.

In summary, terminal carbido complex **2** undergoes [2+1] addition with DMAD to yield the cyclopropenylidene complex **3**. Complex **4** reacts similarly with $HC{\equiv}CCO_2Me$ in the first C–C bond-forming reactions reported for neutral terminal carbido complexes. Protic reagents HX (X = OH, OPh, $NH(3,5\text{-}Me_2)C_6H_3$) as well as pinacolborane add in a 1,1 manner to one of the distal ring C atoms in **3**, forming vinylidene complexes **7**–**11** in high yield. We are currently exploring the reactivity of **7**–**11** as well as seeking a means of regenerating a metathesis-active alkylidene complex or the carbide complexes **2** and **4**.

Received: April 26, 2006
Revised: July 19, 2006
Published online: October 17, 2006

Keywords: carbides · cycloaddition · cyclopropenylidene ligands · ruthenium · vinylidene ligands

[1] R. H. Grubbs, *Handbook of Metathesis*, Wiley-VCH, Weinheim, **2003**.
[2] C. Morrill, R. H. Grubbs, *J. Org. Chem.* **2003**, *68*, 6031.
[3] P. Schwab, R. H. Grubbs, J. W. Ziller, *J. Am. Chem. Soc.* **1996**, *118*, 100.
[4] R. G. Carlson, M. A. Gile, J. A. Heppert, M. H. Mason, D. R. Powell, D. Vander Velde, J. M. Vilain, *J. Am. Chem. Soc.* **2002**, *124*, 1580.
[5] S. R. Caskey, M. H. Stewart, J. E. Kivela, J. R. Sootsman, M. J. A. Johnson, J. W. Kampf, *J. Am. Chem. Soc.* **2005**, *127*, 16750.
[6] A. Hejl, T. M. Trnka, M. W. Day, R. H. Grubbs, *Chem. Commun.* **2002**, 2524.
[7] P. E. Romero, W. E. Piers, R. McDonald, *Angew. Chem.* **2004**, *116*, 6287; *Angew. Chem. Int. Ed.* **2004**, *43*, 6161.
[8] K. Öfele, *Angew. Chem.* **1968**, *80*, 1032; *Angew. Chem. Int. Ed. Engl.* **1968**, *7*, 950.
[9] G. Huttner, S. Schelle, O. S. Mills, *Angew. Chem.* **1969**, *81*, 536; *Angew. Chem. Int. Ed. Engl.* **1969**, *8*, 515.
[10] K. Öfele, *J. Organomet. Chem.* **1970**, *22*, C9.
[11] C. W. Rees, E. V. Angerer, *J. Chem. Soc. Chem. Commun.* **1972**, 420.
[12] R. Gompper, E. Bartmann, *Angew. Chem.* **1978**, *90*, 490; *Angew. Chem. Int. Ed. Engl.* **1978**, *17*, 456.
[13] R. Weiss, C. Priesner, *Angew. Chem.* **1978**, *90*, 491; *Angew. Chem. Int. Ed. Engl.* **1978**, *17*, 457.
[14] R. D. Wilson, Y. Kamitori, H. Ogoshi, Z. I. Yoshida, J. A. Ibers, *J. Organomet. Chem.* **1979**, *173*, 199.
[15] U. Kirchgaessner, U. Schubert, *Organometallics* **1988**, *7*, 784.
[16] K. N. Juneau, L. S. Hegedus, F. W. Roepke, *J. Am. Chem. Soc.* **1989**, *111*, 4762.
[17] P. M. Fritz, J. Breimair, B. Wagner, W. Beck, *J. Organomet. Chem.* **1992**, *426*, 343.
[18] J. Schubert, S. Mock, U. Schubert, *Chem. Ber.* **1993**, *126*, 657.
[19] M. Tamm, A. Grzegorzewski, F. E. Hahn, *J. Organomet. Chem.* **1995**, *501*, 309.
[20] M. S. Morton, J. P. Selegue, A. Carrillo, *Organometallics* **1996**, *15*, 4664.
[21] M. Lutz, M. Haukka, T. A. Pakkanen, L. H. Gade, *Organometallics* **2001**, *20*, 2631.
[22] A. de Meijere, S. Müller, T. Labahn, *J. Organomet. Chem.* **2001**, *617*, 318.
[23] B. Fuss, M. Dede, B. Weibert, H. Fischer, *Organometallics* **2002**, *21*, 4425.
[24] Crystal data for **3**·1.5 CH_2Cl_2: $C_{44.50}H_{75}Cl_5O_4P_2Ru$, monoclinic, $P2_1/c$, $a = 11.926(2)$, $b = 18.555(3)$, $c = 45.638(8)$ Å, $\beta = 96.800(3)°$, $V = 10028(3)$ Å^3, $Z = 8$, $\rho_{calcd} = 1.344$ g cm^{-3}, $Mo_{K\alpha}$ radiation, $\lambda = 0.71073$ Å, $T = 123(2)$ K, 43778 measured reflec-

 © 2006 Wiley-VCH Verlag GmbH & Co. KGaA, Weinheim

tions, 8524 unique ($R_{int} = 0.1875$), 4942 reflections with $I_{net} > 2.0(I_{net})$, $\mu = 0.681\ mm^{-1}$, min/max transmission = 0.8758 and 0.9412, $R1$ ($I > 2\sigma$) = 0.0775, $wR2 = 0.1954$, GoF = 1.066, no. of parameters = 1056, final difference map within 1.008 and $-1.258\ e\ Å^{-3}$. CCDC-604841 (**3**·1.5 CH_2Cl_2) contains the supplementary crystallographic data for this paper. These data can be obtained free of charge from The Cambridge Crystallographic Data Centre via www.ccdc.cam.ac.uk/data_request/cif.

[25] V. Lavallo, Y. Canac, B. Donnadieu, W. W. Schoeller, G. Bertrand, *Science* **2006**, *312*, 722.

[26] Crystal data for **7**: $C_{51}H_{83}Cl_2NO_4P_2Ru$, monoclinic, $P2_1/c$, $a = 15.5355(8)$, $b = 18.9133(10)$, $c = 17.5169(9)$ Å, $\beta = 97.403(1)°$, $V = 5104.0(5)$ Å^3, $Z = 4$, $\rho_{calcd} = 1.312\ g\,cm^{-3}$, $Mo_{K\alpha}$ radiation, $\lambda = 0.71073$ Å, $T = 123(2)$ K, 101 108 measured reflections, 12 702 unique ($R_{int} = 0.0321$), 11 419 reflections with $I_{net} > 2.0(I_{net})$, $\mu = 0.518\ mm^{-1}$, min/max transmission = 0.8197 and 0.8602, $R1$ ($I > 2\sigma$) = 0.0295, $wR2 = 0.0740$, GoF = 1.059, no. of parameters = 554, final difference map within 0.885 and $-0.727\ e\ Å^{-3}$. CCDC-604842 (**7**) contains the supplementary crystallographic data for this paper. Data can be obtained as in Reference [24].

[27] C. Bruneau, P. H. Dixneuf, *Angew. Chem.* **2006**, *118*, 2232; *Angew. Chem. Int. Ed.* **2006**, *45*, 2176.

[28] H. Katayama, F. Ozawa, *Coord. Chem. Rev.* **2004**, *248*, 1703.

 © 2006 Wiley-VCH Verlag GmbH & Co. KGaA, Weinheim

Single-Molecule Magnets

DOI: 10.1002/anie.200601759

Surface Modification of a Six-Capped Body-Centered Cube Ni_9W_6 Cluster: Structure and Single-Molecule Magnetism**

*Jeong Hak Lim, Jung Hee Yoon, Hyoung Chan Kim, and Chang Seop Hong**

Research on single-molecule magnets (SMMs) has attracted intensive attention because of the intriguing physical properties associated with the quantum tunneling of magnetization effects and their potential applications in high-density information storage.[1] Since the slow magnetization relaxation in $[Mn_{12}O_{12}(CH_3COO)_{16}(H_2O)_4]$ (Mn12ac) was discovered, much effort has been made to fabricate metal–oxido clusters with the aim of generating properties analogous to those of the archetypical Mn_{12} cluster.[2,3] Recently, a giant Mn_{84} cluster with a diameter of around 4 nm that exhibits SMM behavior was characterized structurally and magnetically.[4] Despite the high nuclearity of the Mn_{84} supramolecular nanotube, its ground state (S) and energy barrier (U_{eff}) remain relatively small compared with the Mn12ac cluster.[4]

Alternatively, cyanides are frequently utilized for the construction of high-spin molecules because of their structural and magnetic predictability.[5] To attain SMMs with cyanides, it would be a rational approach to combine $[M(CN)_pL_q]^{n-}$ ($M = Fe^{III}$, Mn^{III}; L = polydentate ligand) or $[M'(CN)_xL_y]^{m-}$ ($M' = Mo^{III}$, Re^{II}) units as building blocks with magnetic anisotropy sources. In fact, when a metal ion with single-ion anisotropy is incorporated into a cluster, the magnetization at low temperatures relaxes slowly in some cases.[6,7] Given that U_{eff} is proportional to $S^2|D|$ for an integral spin state (D is the axial zero-field splitting parameter of a cluster), it is appropriate to seek high-spin clusters with negative values of D for the purpose of obtaining SMMs with increased values of U_{eff}. Sizable high-spin ground states were established in octacyanidometallate-based $M_9M'_6$ ($M = Mn^{II}$, Ni^{II}, Co^{II}; $M' = Mo^{V}$, W^{V}) clusters with spins up to $S = 51/2$.[8] In view of their high-spin ground states, the $M_9M'_6$ systems are good candidates for SMMs only if they have negative D values. For example, the judicial choice of the Co^{II} ion as an anisotropic source has led to unique examples of SMM behavior.[9] However, the disadvantage of $M_9M'_6$ analogues prepared to date is that they are air- and moisture-sensitive as a result of the facile loss of surface solvent molecules. In this context, we have attempted to achieve a stable analogue with SMM character by varying the typical molecular structures of the clusters. Herein we report the synthesis, structure, and magnetic properties of an air-stable Ni_9W_6 bimetallic complex whose surface is modified by 2,2′-bipyridine (bpy). Interestingly, the ligand substitution on the cluster surface breaks the overall molecular symmetry and as a result induces SMM characteristics.

The layering of $(Bu_4N)_3[W(CN)_8]$ in MeCN onto $[Ni(bpy)(H_2O)_4](SO_4)\cdot 2H_2O$ in water afforded yellow crystals of **1** in a yield of 8%. The IR spectrum shows that the characteristic CN vibrations of **1** are evident at 2183w and 2150w cm^{-1}, which are somewhat higher than those of the precursor $[W(CN)_8]^{3-}$ (2141w, 2130w, and 2123w (sh) cm^{-1}). This observation is essentially associated with CN groups acting as bridges in **1**.[10]

The molecular structure of **1** (Figure 1), analyzed by X-ray crystallography, can be described as an octahedral core consisting of a Ni center linked by CN groups to six peripheral W atoms and face-capped by eight Ni atoms. It is thus a body-centered cube of Ni atoms with each of the tetragonal faces capped with six W moieties. Four of the CN groups of $[W(CN)_8]^{3-}$ are connected to Ni atoms on the surface [mean Ni–W = 5.31(2) Å] and one to the central Ni ion [mean Ni–W = 5.35(2) Å]. Each peripheral Ni coordination sphere is

[*] J. H. Lim, J. H. Yoon, Prof. C. S. Hong
Department of Chemistry
Korea University
Seoul 136-701 (Korea)
Fax: (+82) 2-3290-3120
E-mail: cshong@korea.ac.kr
Dr. H. C. Kim
Systems Research Team
Research & Development Division
Nuclear Fusion Research Center
Daejeon 305-333 (Korea)

[**] This work was supported by Korea Research Foundation Grant funded by Korea Government (MOEHRD, Basic Research Promotion Fund) (KRF-2005-015-C00223) and CRM-KOSEF. C.S.H thanks an Operation Program on Shared Research Equipment of KBSI and MOST.

Supporting information for this article is available on the WWW under http://www.angewandte.org or from the author.

InterScience © 2006 Wiley-VCH Verlag GmbH & Co. KGaA, Weinheim

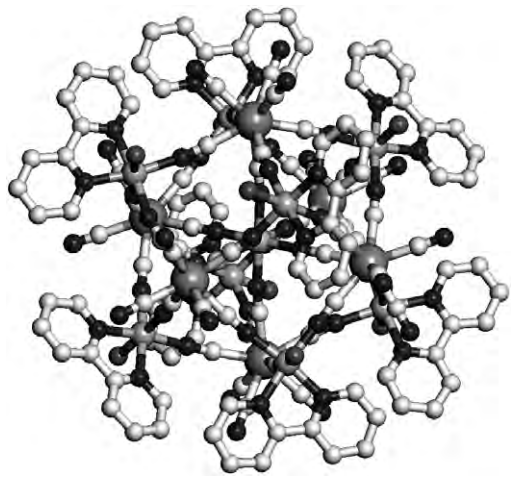

Figure 1. Molecular view of the Ni_9W_6 cluster. Progressively darker shades of gray represent C, Ni, W, O, and N, respectively.

also occupied by one water molecule and one bpy ligand, which is comparable with other $M_9M'_6$ clusters in which three coordination sites are filled by labile MeOH or EtOH molecules.[8,9] All the reported $M_9M'_6$ clusters tend to decompose upon exposure to air, so magnetic measurements were conducted cautiously in frozen solvent or liquid paraffin. The surface modification by the capping ligand bpy engenders the stability of sample in air as a result of the stronger binding affinity of bpy to the Ni center. Moreover, the coordination of bpy to the Ni ions on the molecular surface gives rise to an increase in the separation between clusters. The shortest distance between intercluster metal ions is 7.921 Å, which is significantly longer (by about 1 Å) than those within the $M_9M'_6$ clusters (see the Supporting Information).[8,9] The increased intercluster distance would preclude magnetic interactions between clusters and promote single-molecule magnetism.

The cryomagnetic properties were measured at $H=$ 1000 G and $T=1.8$–300 K (Figure 2). The $\chi_m T$ value of 15.11 $cm^3 K mol^{-1}$ at 300 K is slightly larger than the spin-only value (11.25 $cm^3 K mol^{-1}$) expected for nine noninteracting Ni ($S_{Ni}=1$) and six W ($S_W=1/2$) ions. As the temperature is lowered, $\chi_m T$ increases slowly and then abruptly reaches a maximum of 207.6 $cm^3 K mol^{-1}$ at 9 K. This behavior demonstrates the presence of ferromagnetic interactions among the magnetic centers. The sharp drop in $\chi_m T$ below the apex temperature can be attributed to zero-field splitting of a Ni^{II} ion. The magnetic interactions between nearest magnetic neighbors was assessed by employing the Curie–Weiss equation $[\chi_m = C/(T-\theta)]$, which gave values of $C=$ 12.2 $cm^3 K mol^{-1}$ and $\theta = 58.2$ K. The positive value of θ supports the hypothesis that ferromagnetic couplings between the spins of the Ni and W centers are mediated by the CN linkage.

The field-dependent magnetization (see the Supporting Information) reveals that the magnetization data at 1.8 K is saturated rapidly to 24.7 $N\beta$ at 7 T. The fast rise in magnetization in the low-field regime indicates the existence of a dominant ferromagnetic interaction, which is confirmed by the Brillouin curve with $g=2.06$ for the uncoupled spins of nine Ni^{II} and six W^{V} atoms. The $M(H)$ data at 1.8 K can be reproduced well with a Brillouin curve calculated with $S=12$ for each cluster, which shows that a ferromagnetic ground state exists with $S=12$. The ferromagnetic interactions between Ni^{II} and W^{V} through the CN bridges can be understood in terms of orbital considerations. The W 5d orbital forms π overlap with the CN bridge, whereas the Ni e_g orbitals are linked through σ bonds to the CN ligand.[10,11] Consequently, the corresponding magnetic orbitals are orthogonal to each other and ferromagnetic interactions result.[12]

The magnetizations were measured in the temperature range 1.8–4 K at several magnetic fields to probe the onset of zero-field splitting (see the Supporting Information). The reduced magnetization versus H/T plots do not superimpose, which suggests appreciable zero-field splitting. The ac magnetic susceptibility was collected at $H_{dc}=0$ G, $H_{ac}=5$ G, and with various frequencies to examine the magnetic nature further. The in-phase (χ'_m; see the Supporting Information) and out-of-phase (χ''_m; Figure 3) components are dependent on the oscillating frequency. The maxima (T_{max}) in $\chi'_m(T)$ shift toward higher temperature with increasing frequency (f). A quantity of the frequency-dependent shifts of T_{max}, defined as $\Delta T_{max}/[T_{max}\Delta(\log f)]$, was found to be 0.13, which is substan-

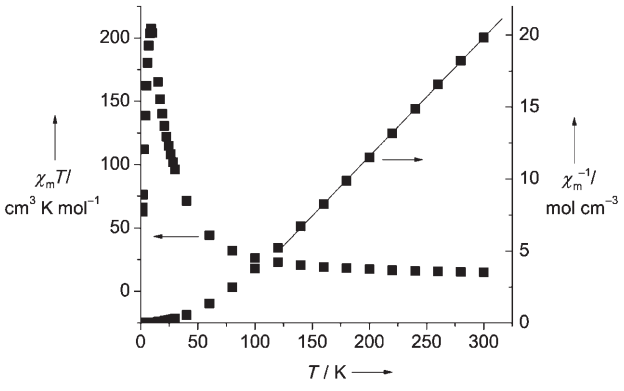

Figure 2. Plot of the temperature dependence of $\chi_m T$ and χ_m^{-1} with a fit to the Curie–Weiss equation (solid line).

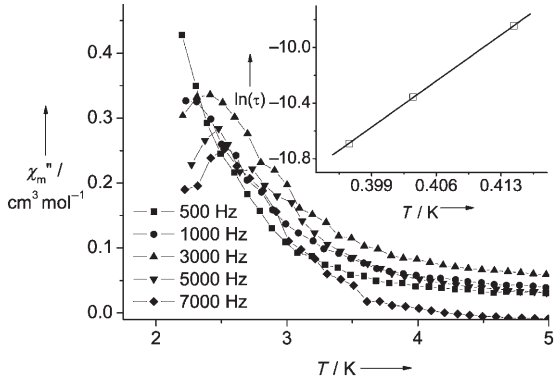

Figure 3. Plot of the out-of-phase term χ''_m versus temperature at the indicated oscillation frequencies. The solid line in the inset denotes a least-squares fit of the data to the Arrhenius equation.

 © 2006 Wiley-VCH Verlag GmbH & Co. KGaA, Weinheim

tially larger than those of canonical spin glasses.[13] The obtained quantity designates that the present compound behaves as a superparamagnet. The slow relaxation of the magnetization was evaluated by investigating the variation of the maxima in $\chi''_m(T)$ with the Arrhenius law [$\tau = \tau_0 \exp(U_{eff}/k_B T)$; τ_0 is the relaxation attempt frequency]. The least-squares fit gives parameters of $\tau_0 = 1.5 \times 10^{-13}$ s and $U_{eff} = 33.0\ cm^{-1}$, which are consistent with SMMs.[6,7,9] The zero-field parameter D is estimated to be approximately $-0.23\ cm^{-1}$, derived from the relationship $U_{eff} = S^2 |D| = 33.0\ cm^{-1}$, which is consistent with a Ni-based SMM.[14] This feature demonstrates that **1** exhibits SMM properties, which is surprising in that $Ni_9M'_6$ clusters show no χ''_m signal in zero dc field when the surface of the cluster is coordinated by MeOH molecules.[8c] The substitution of two MeOH molecules bound to each peripheral Ni coordination sphere with bpy lowers the molecular symmetry of the clusters, which is reflected in the change of crystal systems from a monoclinic ($C2/c$) to a triclinic space group ($P\bar{1}$). Hence, the surface modification plays a crucial role in reducing the structural symmetry and thus likely enhancing magnetic anisotropy, which eventually leads to such SMM behavior.

In summary, we have prepared an air-stable high-spin Ni_9W_6 cluster ($S = 12$) that displays ferromagnetic interactions between Ni^{II} and W^{V} ions bridged by CN groups. The symmetry-breaking ligand replacement with bpy into the spherical cluster gives rise to increased magnetic anisotropy and SMM behavior. This result shows that substitution of chelating ligands into symmetric entities should be an excellent strategy to facilitate structural anisotropy and thus magnetic anisotropy for SMMs with high spin-reversal energy barriers.

Experimental Section

In the dark $(Bu_4N)_3[W(CN)_8]$ (0.10 mmol) in MeCN was layered on top of $[Ni(bpy)(H_2O)_4]\cdot(SO_4)\cdot 2H_2O$[15] (0.15 mmol) in water. Yellow crystals of $[Ni\{Ni(bpy)(H_2O)\}_8\{W(CN)_8\}_6]\cdot 41H_2O$ suitable for X-ray crystallography grew after several days. The crystals were air-dried to yield $[Ni\{Ni(bpy)(H_2O)\}_8\{W(CN)_8\}_6]\cdot 23H_2O$ (**1**) in 8% yield. The chemical composition of **1** was checked by elemental and thermogravimetric analysis. Elemental analysis (%) calcd for $C_{128}H_{126}N_{64}Ni_9O_{31}W_6$: C 32.79, H 2.71, N, 19.12; found: C 32.42, H 2.47, N 18.72.

Elemental analyses were performed at the Elemental Analysis Service Center of Sogang University. Infrared spectra were obtained from KBr pellets with a Bomen MB-104 spectrometer. Magnetic susceptibility data for **1** were measured with MPMS-7 (dc data) and PPMS (ac data) susceptometers. Diamagnetic corrections were estimated from Pascal's tables.

Crystal data for **1**: $C_{128}H_{162}N_{64}Ni_9O_{49}W_6$, $M_r = 5012.71$, triclinic, space group $P\bar{1}$, $a = 18.3936(6)$, $b = 19.6124(6)$, $c = 30.4162(10)$ Å, $\alpha = 90.7410(10)$, $\beta = 105.5680(10)$, $\gamma = 113.6290(10)°$, $V = 9593.0(5)$ Å^3, $Z = 2$, $D_{calcd} = 1.735\ g\,cm^{-3}$, $\mu = 4.527\ mm^{-1}$, $T = 130$ K, 159090 reflections collected, 47147 unique ($R_{int} = 0.1204$), $R1 = 0.0542$, $wR2 = 0.0990$ [$I > 2\sigma(I)$]. CCDC-606405 contains the supplementary crystallographic data for this paper. These data can be obtained free of charge from The Cambridge Crystallographic Data Centre via www.ccdc.cam.ac.uk/data_request/cif.

Received: May 4, 2006
Revised: July 22, 2006
Published online: October 16, 2006

Keywords: cluster compounds · cyanides · magnetic properties · nickel · single-molecule studies

[1] D. Gatteschi, R. Sessoli, *Angew. Chem.* **2003**, *115*, 278–309; *Angew. Chem. Int. Ed.* **2003**, *42*, 268–297.
[2] R. Sessoli, D. Gatteschi, A. Caneschi, M. A. Novak, *Nature* **1993**, *365*, 141–143.
[3] a) M. Murugesu, M. Habrych, W. Wernsdorfer, K. A. Abboud, G. Christou, *J. Am. Chem. Soc.* **2004**, *126*, 4766–4767; b) A. J. Tasiopoulos, W. Wernsdorfer, B. Moulton, M. J. Zaworotko, G. Christou, *J. Am. Chem. Soc.* **2003**, *125*, 15274–15275.
[4] A. J. Tasiopoulos, A. Vinslava, W. Wernsdorfer, K. A. Abboud, G. Christou, *Angew. Chem.* **2004**, *116*, 2169–2173; *Angew. Chem. Int. Ed.* **2004**, *43*, 2117–2121.
[5] L. M. C. Beltran, J. R. Long, *Acc. Chem. Res.* **2005**, *38*, 325–334.
[6] a) C. P. Berlinguette, D. Vaughn, C. Cañada-Vilalta, J. R. Galán-Mascarós, K. R. Dunbar, *Angew. Chem.* **2003**, *115*, 1561–1564; *Angew. Chem. Int. Ed.* **2003**, *42*, 1523–1526; b) S. Wang, J.-L. Zuo, H.-C. Zhou, H. J. Choi, Y. Ke, J. R. Long, X.-Z. You, *Angew. Chem.* **2004**, *116*, 6066–6069; *Angew. Chem. Int. Ed.* **2004**, *43*, 5940–5943; c) D. Li, S. Parkin, G. Wang, G. T. Yee, A. V. Prosvirin, S. M. Holmes, *Inorg. Chem.* **2005**, *44*, 4903–4905.
[7] a) J. J. Sokol, A. G. Hee, J. R. Long, *J. Am. Chem. Soc.* **2002**, *124*, 7656–7657; b) E. J. Schelter, A. V. Prosvirin, K. R. Dunbar, *J. Am. Chem. Soc.* **2004**, *126*, 15004–15005.
[8] a) J. Larionova, H. Gross, M. Pilkington, H. Andres, H. Stoeckli-Evans, H. U. Güdel, S. Decurtins, *Angew. Chem.* **2000**, *112*, 1667–1672; *Angew. Chem. Int. Ed.* **2000**, *39*, 1605–1609; b) Z. J. Zhong, H. Seino, Y. Mizobe, M. Hidai, A. Fujishima, S. -i, Ohkoshi, K. Hashimoto, *J. Am. Chem. Soc.* **2000**, *122*, 2952–2953; c) F. Bonadio, M. Gross, H. Stoeckli-Evans, S. Decurtins, *Inorg. Chem.* **2002**, *41*, 5891–5896.
[9] Y. Song, P. Zhang, X.-M. Ren, X.-F. Shen, Y.-Z. Li, X.-Z. You, *J. Am. Chem. Soc.* **2005**, *127*, 3708–3709.
[10] a) J. H. Yoon, H. C. Kim, C. S. Hong, *Inorg. Chem.* **2005**, *44*, 7714–7716; b) Y. S. You, J. H. Yoon, J. H. Lim, H. C. Kim, C. S. Hong, *Inorg. Chem.* **2005**, *44*, 7063–7069; c) Y. S. You, D. Kim, Y. Do, S. J. Oh, C. S. Hong, *Inorg. Chem.* **2004**, *43*, 6899–6901.
[11] a) Y. Song, S.-i. Ohkoshi, Y. Arimoto, H. Seino, Y. Mizobe, K. Hashimoto, *Inorg. Chem.* **2003**, *42*, 1848–1856; b) L. F. Chibotaru, V. S. Mironov, A. Ceulemans, *Angew. Chem.* **2001**, *113*, 4561–4565; *Angew. Chem. Int. Ed.* **2001**, *40*, 4429–4433.
[12] O. Kahn, *Molecular Magnetism*, VCH, Weinheim, **1993**.
[13] J. A. Mydoshi, *Spin Glasses: An Experimental Introduction*, Taylor & Francis, London, **1993**.
[14] S. T. Ochsenbein, M. Murrie, E. Rusanov, H. Stoeckli-Evans, C. Sekine, H. U. Güdel, *Inorg. Chem.* **2002**, *41*, 5133–5140.
[15] P. C. Healy, J. M. Patrick, A. H. White, *Aust. J. Chem.* **1984**, *37*, 921–928.

 © 2006 Wiley-VCH Verlag GmbH & Co. KGaA, Weinheim

C–H Activation

DOI: 10.1002/anie.200601980

Room-Temperature Au^I-Catalyzed C–C Bond Formation through a Tandem Friedel–Crafts-Type Addition/Carbocyclization Reaction**

Patrick Yves Toullec, Emilie Genin, Lucie Leseurre, Jean-Pierre Genêt, and Véronique Michelet**

In the past ten years, significant research has been directed towards the development of catalytic reactions for the functionalization of C–H bonds.[1] These reactions represent an environmentally friendly and atom-economical concept when performed under mild conditions.[2] Several metals have been recognized as excellent candidates for the functionalization of aromatic or heteroaromatic C–H bonds.[1,3] As part of our ongoing program towards the development of catalytic tandem and atom-economical reactions,[4] we have been interested in the use of gold for such transformations. Kharash and Isbell were the first to show that Au^{III} could activate aromatic compounds at room temperature.[5] Following their seminal discovery, homogeneous gold catalysis was forsaken and interest only returned a few years ago.[6] The use of gold for C–H functionalization to create C–C bonds was recently realized in the presence of various electrophiles such as alkynes or activated alkenes.[1b,7] To our knowledge, few examples of additions to nonactivated alkenes have been described so far.[8] We anticipated that the unprecedented intermolecular addition of aromatic rings to unactivated alkenes may be feasible in the presence of a second electrophilic moiety such as an alkyne function. We describe herein our preliminary results concerning the novel and diastereoselective tandem gold-catalyzed carbocyclization reaction through Friedel–Crafts-type and cycloisomerization transformations.

Initial experiments were performed using enyne **1** and 1,3-dimethoxybenzene, and a selection of significant examples are shown in Table 1. When the reaction was attempted using

Table 1: [M]-catalyzed addition of 1,3-dimethoxybenzene to enyne **1**.[a]

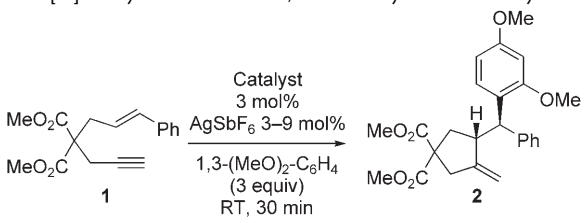

Entry	Catalyst	$AgSbF_6$ [mol%]	Solvent	Conv. (Yield) [%]
1	$AuCl_3$	9	Et_2O	-
2	$PtCl_2$	6	Et_2O	-
3	AuCl	3	Et_2O	17
4[b]	$AuCl_3/PPh_3$	9	Et_2O	100
5	$[PPh_3AuCl]$	3	Et_2O	100 (73)
6	$[PPh_3AuCl]$	3	CH_3CN	<10
7	$[PPh_3AuCl]$	3	CH_2Cl_2	100[c]

[a] General conditions: 3 equiv of 1,3-$(MeO)_2C_6H_4$, solvent (2.5 mol **1** L^{-1}) [b] 3 mol% PPh_3. [c] The internal isomerized alkene was detected in 10% yield.

$AuCl_3$, AuCl, $PtCl_2$, or $Sc(OTf)_3$ as the catalyst in diethyl ether at room temperature, no conversion was observed. However, the addition of silver salts, known to be halide-sequestering agents, induced appreciable activity in the case of the Au^I catalyst precursor (Table 1, entry 3). The combination of Au^I or Au^{III} precursors, additional phosphine ligands (such as triphenylphosphine), and silver salts provided the best results (Table 1, entries 4 and 5). The use of 3 mol% of the commercially available $[PPh_3AuCl]$ with 3 mol% of $AgSbF_6$ was found to be the best reproducible system, and the functionalized alkene **2** was isolated in 73% yield (Table 1, entry 5). The choice of the solvent influenced both the activity and the selectivity of the catalytic system. Acetonitrile inhibited the reaction (Table 1, entry 6), whereas dichloromethane (Table 1, entry 7) afforded the side product resulting from the internal isomerization of the alkene. The desired cyclic derivative **2** was detected as a unique stereoisomer (Table 1, entry 5).[10] The structure of **2** was fully characterized by NMR spectroscopy, and the stereochemistry of the reaction was unambiguously established by X-ray analysis of the related derivative **12** (Figure 1 and Table 2, entry 3).

It is noteworthy that the remarkable addition of the aromatic ring to the alkene is completely chemoselective. No traces of the product resulting from addition of the aromatic ring to the alkynyl moiety[7] were detected, and the presence of the electron-rich aromatic ring completely inhibits the well-documented cycloisomerization reactions.[9]

Interestingly, in the absence of a nucleophile, enyne **1** rapidly forms the well-known cyclized products **3** and **4**, which result from a metathesis-type reaction for **3** and a 6-*endo* cyclization for **4**, both in CH_2Cl_2[9] or in diethyl ether (Scheme 1).

The compatibility of the $[PPh_3AuCl]/AgSbF_6$ system with various enyne substrates and its efficiency in the presence of other nucleophiles were then examined (Table 2). The addition of 1,3-dimethoxybenzene and 1,3,5-trimethoxybenzene to substrates in which $Z = C(CO_2Me)_2$, $C(SO_2Ph)_2$, O, or

[*] Dr. P. Y. Toullec, E. Genin, L. Leseurre, Prof. J.-P. Genêt, Dr. V. Michelet
Laboratoire de Synthèse Sélective Organique et Produits Naturels, UMR 7573
Ecole Nationale Supérieure de Chimie de Paris
11, rue Pierre et Marie Curie
75231 Paris cedex 05 (France)
Fax: (+33) 1-4407-1062
E-mail: jean-pierre-genet@enscp.fr
veronique-michelet@enscp.fr

[**] This work was supported by the Centre National de la Recherche Scientifique (CNRS). E.G. is grateful to the Ministère de l'Education et de la Recherche for financial support (2003–2006). The authors thank L.-M. Chamoreau (UMR 7071, Laboratoire de Chimie Inorganique et Matériaux Moléculaires, Paris) for X-ray structure analysis.

Supporting information for this article is available on the WWW under http://www.angewandte.org or from the author.

© 2006 Wiley-VCH Verlag GmbH & Co. KGaA, Weinheim

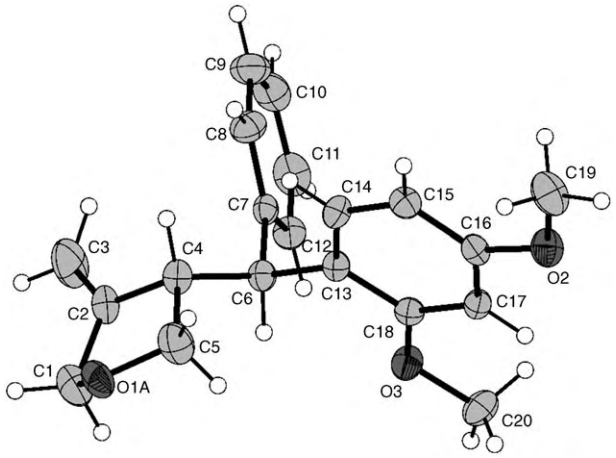

Figure 1. Molecular structure of alkene **12** with thermal ellipsoids set at the 30% probability level.

NTs (Ts = toluene-4-sulfonyl) afforded the desired alkenes **10**–**15** in good to excellent yields (Table 2, entries 1–6).

The bissulfone derivate **6** with a trisubstituted alkenyl side chain also reacted very cleanly and rapidly to give the corresponding alkene **15** in 72% yield (Table 2, entry 6). Nucleophilic aromatic halides proved to be compatible reaction partners, since the addition of 1-bromo-2,4-dimethoxybenzene to compound **7** led to the functionalized alkene **16** in 63% yield (Table 2, entry 7).

Electron-rich heteroaromatic derivatives have also been studied (Table 3). Indoles are found in many pharmaceuticals and have been described as nucleophiles in gold-catalyzed reactions to form C–C bonds.[3d,7h,r] Both methyl-substituted and nonsubstituted indoles were suitable nucleophiles for the tandem Friedel–Crafts-type addition and carbocyclization reactions. The corresponding *N*-methylindoles **17**–**20** were obtained in 47–99% yield (Table 3, entries 1–4). The addition of indoles was also possible for both carbon- and oxygen-tethered enynes, and led to the functionalized cyclic alkenes **21**–**23** in 43–99% yield (Table 3, entries 5–7). The regioselectivity in the C3 position was confirmed by comparison with other substituted derivatives.[7h,r] Pyrrole was also an excellent candidate for the tandem reaction, and the expected 2- and 3-substituted isomers **24a**,**b** and **25a**,**b** were isolated in overall yields of 58% and 90%, respectively (Table 3, entries 8 and 9).

On considering the mechanism, the first generally proposed step[6] is the formation of a cationic gold catalyst in the presence of the silver salt (Scheme 2). The complexation of the Lewis-acidic cationic gold catalyst to the alkyne function leads to intermediate **A**. The cyclization step may then occur directly through a concerted diastereoselective Friedel–Crafts-type addition/carbocyclization sequence leading to the vinylaurate intermediate **C**, or may proceed by stereoselective attack of the nucleophile on a transient carbenic species **B**, as proposed in several metal-catalyzed cycloisomerization reactions.[4e,8b,11] The final step would be the protodemetalation of the aurate intermediate. However, the actual reaction pathway cannot yet be confirmed. The process is completely stereoselective,[12] since the deuterated enyne

Table 2: Gold-catalyzed diastereoselective tandem addition/carbocyclization of aromatic derivatives to functionalized enynes.

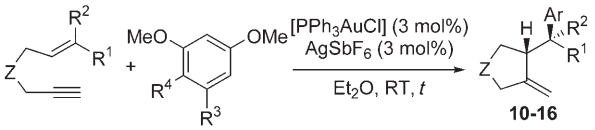

1: Z = $C(CO_2Me)_2$, R^1 = Ph, R^2 = H; **5**: Z = $C(SO_2Ph)_2$, R^1 = Ph, R^2 = H
6: Z = $C(SO_2Ph)_2$, R^1 = Me, R^2 = Me; **7**: Z = O, R^1 = 3,4-$(OCH_2O)C_6H_3$, R^2 = H
8: Z = O, R^1 = Ph, R^2 = H; **9**: Z = NTs, R^1 = Ph, R^2 = H
R^3 = H, OMe, R^4 = H, Br

Entry	Substr.	*t* [h]	Product		Yield[a] [%]
1	**5**	2	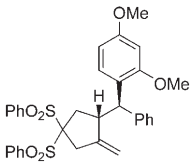	**10**	99
2	**7**	0.5	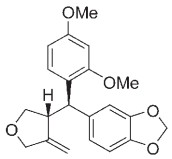	**11**	91
3	**8**	2.5	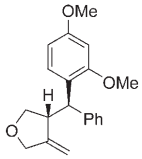	**12**	50
4	**9**	2.5	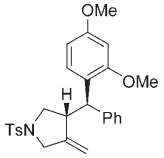	**13**	60
5	**1**	1	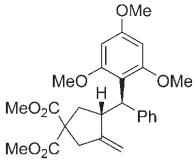	**14**	68
6	**6**	1	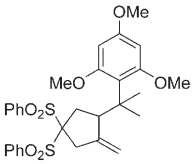	**15**	72
7	**7**	2.5	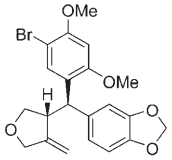	**16**	63

[a] Yield of isolated product.

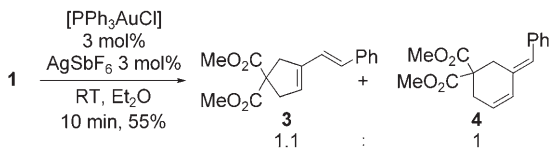

Scheme 1. Au-catalyzed cycloisomerization of enyne **1**.

 © 2006 Wiley-VCH Verlag GmbH & Co. KGaA, Weinheim

Table 3: Gold-catalyzed diastereoselective tandem addition/carbocyclization of heteroaromatic derivatives.

Entry	Substr.	*t* [h]	Product		Yield[a] [%]
1	**1**	0.5	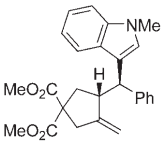	**17**	81
2	**5**	3.5	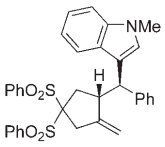	**18**	99
3	**6**	2	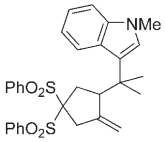	**19**	82
4	**9**	6	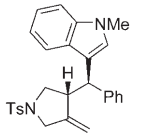	**20**	47[b]
5	**1**	2	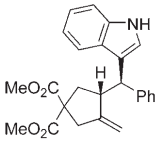	**21**	68
6	**7**	2.5	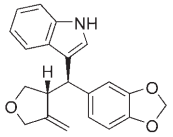	**22**	99
7	**7**	2.5	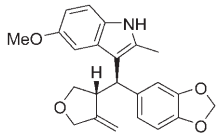	**23**	43
8	**1**	1	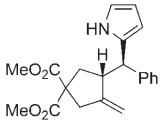	**24a**	47[c]
9	**5**	2	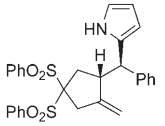	**25a**	80[d]

[a] Yield of isolated product. [b] 10 mol% catalyst, 40 °C. [c] The 3-pyrrole derivative **24b** was also isolated in 11% yield. [d] The 3-pyrrole derivative **25b** was also isolated in 10% yield.

$[D_1]$-**7** (>95% D)[4e] underwent a clean tandem reaction in the presence of $[PPh_3AuCl]/AgSbF_6$ (3 mol%) and three equivalents of 1,3,5-trimethoxybenzene to afford the deuterated alkene $[D_1]$-**26** (Scheme 2). The alkene (with >95% D determined from the ^1H NMR spectrum of the crude product) was isolated in 54% yield.

In summary, we have developed an efficient and atom-economical method for the synthesis of cyclic and functionalized carbo- and heterocycles. The $[PPh_3AuCl]/AgSbF_6$ catalytic system promoted a novel diastereoselective tandem Friedel–Crafts-type addition of electron-rich aromatic and heteroaromatic derivatives to unactivated alkenes, followed by a C–C bond cyclization reaction. The efficiency of this system allowed the reactions to be carried out at room temperature with short reaction times. The compatibility of the reaction conditions with a bromo-substituted nucleophile would allow further metal-catalyzed cross-coupling reactions. The development of an asymmetric version of this reaction and the extension of this methodology to other nucleophiles are currently under investigation in our laboratory.

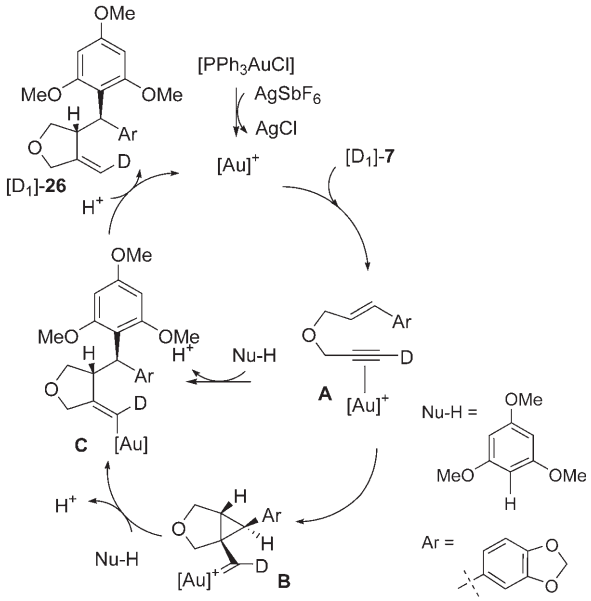

Scheme 2. Proposed mechanism and intermediates.

Received: May 18, 2006
Published online: October 11, 2006

Keywords: arenes · C–H activation · cyclization · gold · tandem reaction

[1] a) J. P. Collman, L. S. Hegedus, J. R. Norton, R. G. Finke, *Principles and Applications of Organotransition Metal Chemistry*, University Science Books, Mill Valley, CA, **1987**; b) A. S. Goldman, K. I. Goldberg, *ACS Symp. Ser.* **2004**, *885*, 1–43; c) C. Nevado, A. M. Echavarren, *Synthesis* **2005**, 167–182; d) G. Dyker, *Angew. Chem.* **1999**, *111*, 1698–1712; *Angew. Chem. Int. Ed.* **1999**, *38*, 1808–1822; e) V. Ritleng, C. Sirlin, M. Pfeffer, *Chem. Rev.* **2002**, *102*, 1731–1770; f) B. A. Arndtsen, R. G. Bergman, T. A. Modley, T. H. Peterson, *Acc. Chem. Res.* **1995**, *28*, 154–162.

[2] a) B. M. Trost, *Acc. Chem. Res.* **2002**, *35*, 695–705; b) P. N. Anastas, M. M. Kirchhoff, *Acc. Chem. Res.* **2002**, *35*, 686–694; c) B. M. Trost, D. F. Toste, A. B. Pinkerton, *Chem. Rev.* **2001**, *101*, 2067–2096; d) B. M. Trost, M. J. Krische, *Synlett* **1998**, 1–16; e) B. M. Trost, *Science* **1991**, *254*, 1471–1477.

[3] For representative examples, see : a) V. Mamane, P. Hannen, A. Fürstner, *Chem. Eur. J.* **2004**, *10*, 4556–4575; b) C. Nevado, A. M. Echavarren, *Chem. Eur. J.* **2005**, *11*, 3155–3164; c) N. Chatani, H. Inoue, T. Ikeda, S. Murai, *J. Org. Chem.* **2000**, *65*,

 © 2006 Wiley-VCH Verlag GmbH & Co. KGaA, Weinheim

4913 – 4918; d) A. S. K. Hashmi, R. Salathé, T. M. Frost, L. Schwarz, J.-H. Choi, *Appl. Catal. A* **2005**, *291*, 238 – 246.

[4] a) E. Genin, P. Y. Toullec, S. Antoniotti, C. Brancour, J.-P. Genêt, V. Michelet, *J. Am. Chem. Soc.* **2006**, *128*, 3112 – 3113; b) E. Genin, S. Antoniotti, V. Michelet, J.-P. Genêt, *Angew. Chem.* **2005**, *117*, 5029 – 5033; *Angew. Chem. Int. Ed.* **2005**, *44*, 4949 – 4953; c) S. Antoniotti, E. Genin, V. Michelet, J.-P. Genêt, *J. Am. Chem. Soc.* **2005**, *127*, 9976 – 9977; d) L. Charruault, V. Michelet, R. Taras, S. Gladiali, J.-P. Genêt, *Chem. Commun.* **2004**, 850 – 851; e) C. Nevado, L. Charruault, V. Michelet, C. Nieto-Oberhuber, M. P. Muñoz, M. Méndez, M.-N. Rager, J.-P. Genêt, A. M. Echavarren, *Eur. J. Org. Chem.* **2003**, 706 – 713; f) V. Michelet, L. Charruault, S. Gladiali, J.-P. Genêt, *Pure Appl. Chem.* **2006**, *78*, 397 – 407.

[5] M. S. Kharash, H. S. Isbell, *J. Am. Chem. Soc.* **1931**, *53*, 3053 – 3059.

[6] For representative reviews, see: a) S. Ma, S. Yu, Z. Gu, *Angew. Chem.* **2006**, *118*, 206 – 209; *Angew. Chem. Int. Ed.* **2006**, *45*, 200 – 203; b) A. S. K. Hashmi, *Angew. Chem.* **2005**, *117*, 7150 – 7154; *Angew. Chem. Int. Ed.* **2005**, *44*, 6990 – 6993; c) A. Höffmann-Röder, N. Krause, *Org. Biomol. Chem.* **2005**, *3*, 387 – 391; d) A. S. K. Hashmi, *Gold Bull.* **2004**, *37*, 51—65; e) A. Arcadi, S. Di Giuseppe, *Curr. Org. Chem.* **2004**, *8*, 795 – 812; f) G. Bianchi, A. Arcadi, *Targets Heterocycl. Syst.* **2004**, *8*, 82 – 119; g) A. S. K. Hashmi, *Gold Bull.* **2003**, *36*, 3 – 9; h) G. Dyker, *Angew. Chem.* **2000**, *112*, 4407 – 4409; *Angew. Chem. Int. Ed.* **2000**, *39*, 4237 – 4239.

[7] For recent examples of gold-catalyzed aromatic addition to alkyne and activated alkenes, see for alkynes: a) C. Ferrer, A. M. Echavarren, *Angew. Chem.* **2006**, *118*, 1123 – 1127; *Angew. Chem. Int. Ed.* **2006**, *45*, 1105 – 1109; b) Z. Shi, C. He, *J. Org. Chem.* **2004**, *69*, 3669 – 3671; c) M. T. Reetz, K. Sommer, *Eur. J. Org. Chem.* **2003**, 3485 – 3496; d) C. Nevado, A. M. Echavarren, *Chem. Eur. J.* **2005**, *11*, 3155 – 3164; e) A. S. K. Hashmi, M. C. Blanco, E. Kurpejovic, W. Frey, J. W. Bats, *Adv. Synth. Catal.* **2006**, *348*, 709 – 713; f) T. Shibata, R. Fujiwara, D. Takano, *Synlett* **2005**, 2062—2066; and for alkenes: g) A. Arcadi, M. Alfonsi, G. Bianchi, G. D'Anniballe, F. Marinelli, *Adv. Synth. Catal.* **2006**, *348*, 709 – 713; h) A. Arcadi, G. Bianchi, M. Chiarini, G. D'Anniballe, F. Marinelli, *Synlett* **2004**, 944 – 950; i) G. Dyker, E. Muth, A. S. K. Hashmi, L. Ding, *Adv. Synth. Catal.* **2003**, *345*, 1247 – 1252; j) A. S. K. Hashmi, L. Schwarzt, J.-H. Choi, T. M. Frost, *Angew. Chem.* **2000**, *112*, 2382 – 2385; *Angew. Chem. Int. Ed.* **2000**, *39*, 2285 – 2288; k) M. Alfonsi, A. Arcadi, G. Bianchi, F. Marinelli, A. Nardini, *Eur. J. Org. Chem.* **2006**, 2393 – 2402; For recent examples of gold-catalyzed aromatic addition to imines, alcohols, sulfonated or benzyl esters, and carbonyl derivatives, see: l) Z. Shi, C. He, *J. Am. Chem. Soc.* **2004**, *126*, 5964 – 5965; m) Y. Luo, C.-J. Li, *Chem. Commun.* **2004**, 1930 – 1931; n) K. Mertins, I. Iovel, J. Kischel, A. Zapf, M. Beller, *Adv. Synth. Catal.* **2006**, *348*, 691 – 695; o) A. S. K. Hashmi, L. Schwarz, P. Rubenbauer, M. C. Blanco *Adv. Synth. Catal.* **2006**, *348*, 705 – 708; p) C. Wei, Z. Li, C.-L. Li, *Synlett* **2004**, 1472 – 1483; For Au-catalyzed Claisen rearrangements, see: q) N. W. Reich, C.-G. Yang, Z. Shi, C. He, *Synlett* **2006**, 1472 – 1473; For a tandem C–C/C–O bond-forming reaction: r) T. Yao, X. Zhang, R. C. Larock, *J. Am. Chem. Soc.* **2004**, *126*, 11 164 – 11 165.

[8] a) J. Oxgaard, R. A. Periana, W. A. Goddard III, *J. Am. Chem. Soc.* **2004**, *126*, 11 658 – 11 665; b) C. Nieto-Oberhuber, S. Lopez, A. M. Echavarren, *J. Am. Chem. Soc.* **2005**, *127*, 6178 – 6179; c) M. Lail, C. M. Bell, D. Conner, T. R. Cundari, T. B. Gunnoe, J. L. Peterson, *Organometallics* **2004**, *23*, 5007 – 5020, and references therein.

[9] a) C. Nieto-Oberhuber, M. P. Muñoz, E. Buñuel, C. Nevado, D. J. Cardenas, A. M. Echavarren, *Angew. Chem.* **2004**, *116*, 2456 – 2460; *Angew. Chem. Int. Ed.* **2004**, *43*, 2402 – 2406; b) C. Nieto-Oberhuber, M. P. Muñoz, S. Lopez, E. Jimeñez-Nunez, C. Nevado, E. Herrero-Gomez, M. Raducan, A. M. Echavarren, *Chem. Eur. J.* **2006**, *12*, 1677 – 1693, and references therein; c) N. Mezailles, L. Ricard, F. Gagosz, *Org. Lett.* **2005**, *7*, 4133 – 4136.

[10] The diastereoselectivity was determined by ^{1}H NMR spectroscopy of the crude product mixture after elimination of the catalyst through a thin pad of silica.

[11] For recent reviews, see: a) A. M. Echavarren, C. Nevado, *Chem. Soc. Rev.* **2004**, *33*, 431 – 436; b) M. Méndez, V. Mamane, A. Fürstner, *Chemtracts: Org. Chem.* **2003**, *16*, 397 – 425; c) G. C. Lloyd-Jones, *Org. Biomol. Chem.* **2003**, *1*, 215 – 236.

[12] For another recent diastereoselecive addition to alkynes, see: A. S. K. Hashmi, J. P. Weyrauch, W. Frey, J. W. Bats, *Org. Lett.* **2004**, *6*, 4391 – 4394.

 © 2006 Wiley-VCH Verlag GmbH & Co. KGaA, Weinheim

Fullerenes

DOI: 10.1002/anie.200602431

Selective Electrochemical Retro-Cycloaddition Reaction of Pyrrolidinofullerenes**

Olena Lukoyanova, Claudia M. Cardona, Margarita Altable, Salvatore Filippone, Ángel Martín Domenech, Nazario Martín, and Luis Echegoyen**

Since the discovery of fullerenes, various methods for their functionalization have been developed and explored extensively.[1] Among the most widely employed derivatization reactions are Diels–Alder cycloadditions,[2] cyclopropanations,[3] and azomethine 1,3-dipolar cycloaddition reactions.[4] The cyclopropanation reaction,[3a] which forms a cyclopropano (methano) addend on the fullerene sphere, and the 1,3-

[*] M. Altable, Dr. S. Filippone, Dr. Á. Martín Domenech, Prof. Dr. N. Martín
Departamento de Química Orgánica
Facultad de Ciencias Químicas
Universidad Complutense de Madrid
Ciudad Universitaria s/n, 2840 Madrid (Spain)
Fax: (+34) 91-394-4103
E-mail: nazmar@quim.ucm.es

O. Lukoyanova, Dr. C. M. Cardona, Prof. Dr. L. Echegoyen
Department of Chemistry
Clemson University
219 Hunter Laboratories, Clemson, SC 29630-0973 (USA)
Fax: (+1) 864-656-6613
E-mail: luis@clemson.edu

[**] This work was financially supported by the US NSF (CHE-0509989), the MEC of Spain, and Comunidad de Madrid (Projects CTQ 2005-02609/BQU, MAT-02 12196-E, and P-PPQ-000225-0505). M.A. thanks the MEC for a research grant. This material is based upon work supported by Luna Innovations Incorporated and the Air Force Office of Scientific Research under Contract No. FA9550-05-C-0146. Any opinion, findings, and conclusions or recommendations expressed in this material are those of the authors and do not necessarily reflect the views of the Air Force Office of Scientific Research.

 WILEY InterScience DISCOVER SOMETHING GREAT © 2006 Wiley-VCH Verlag GmbH & Co. KGaA, Weinheim

dipolar cycloaddition reaction,[4a] which results in a pyrrolidine ring adduct, were first introduced in 1993. The products of these two reactions (methanofullerenes and pyrrolidinofullerenes) exhibit high thermal and chemical stability, whereas some Diels–Alder adducts are unstable upon heating and undergo thermal retro-cycloaddition reactions.[5] The instability of methano adducts under electrochemically reductive conditions was discovered in the late 1990s, and it has since been used as an effective method for retro-cyclopropanation reactions.[6] The di(alkoxycarbonyl)methano bridges can be efficiently removed from the carbon sphere by exhaustive controlled-potential electrolysis (CPE). This electrochemical retro-cyclopropanation reaction has been found to be of general applicability for different fullerenes and highly selective towards removal of cyclopropano addends in the presence of other types of addends.[7–8] Chemical reductive methods have also been employed for efficient retro-cyclopropanation reactions.[9]

Until recently, pyrrolidino[3,4:1,2][60]fullerenes (commonly known as fulleropyrrolidines) were believed to be the most stable adducts under various experimental conditions and were presumed not to undergo chemical, thermal, or reductive retro-cycloaddition reactions. However, some of us recently showed that the 1,3-dipolar cycloaddition reaction is thermally reversible.[10] The efficient removal of pyrrolidine rings from the various parent fullerenes occurred upon heating in the presence of a highly efficient dipolarophile.

The mechanism of the 1,3-dipolar retro-cycloaddition reaction is still not clear. Preliminary results suggested that both thermal cycloreversion and oxidative processes are possible mechanistic pathways. This latter possibility inspired us to probe the oxidative electrochemical properties of pyrrolidinofullerenes **1** and **2** further. Herein, we report the first efficient removal of pyrrolidine rings from fullerenes by electrochemical oxidation (Scheme 1).

N-Ethyl pyrrolidinofullerene **1** was synthesized according to previously established procedures for 1,3-dipolar additions.[4a] Controlled-potential electrolysis was employed for the electrochemical oxidation at an applied potential determined from cyclic-voltammetry (CV) experiments. The cyclic voltammogram of compound **1** in *o*-diclorobenzene (*o*-DCB) showed three reversible reduction waves, which correspond to the reduction of the fullerene core, and one irreversible oxidative wave (Figure 1). The irreversible wave was assigned

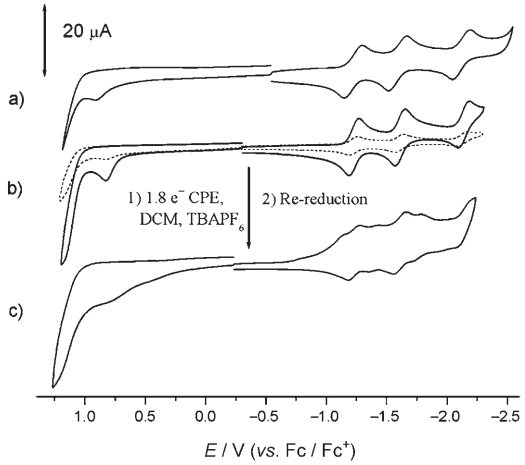

Figure 1. a) Cyclic voltammogram of **1** in 0.05 M $TBAPF_6$ *o*-DCB; scan rate 100 $mV s^{-1}$. b) Cyclic voltammogram of **1**, in 0.1 M $TBAPF_6$ DCM; scan rate 100 $mV s^{-1}$. Initially, **1** had low solubility in DCM (dotted line). Upon reductive electrolysis at the first reductive wave, and subsequent reoxidation, **1** was solubilized (solid line). c) Cyclic voltammogram after partial electrolysis of **1** in DCM.

to a pyrrolidine-based oxidation process, a strong suggestion of the instability of **1** upon electrochemical oxidation. Therefore, we electrolyzed **1** at a potential 100 mV more positive than this oxidation wave (1 V vs. the ferrocene/ferrocenium (Fc/Fc^+) couple). First, the electrolysis was conducted in *o*-DCB containing 0.05 M tetrabutylammonium hexafluorophosphate ($TBAPF_6$) with the exclusion of oxygen and light.[11] The electrolysis was stopped after charge corresponding to 1.8 electrons per molecule was transferred, and the solution was reduced at 0 V. The net charge that was transferred to the solution upon re-reduction corresponded to only 0.45 electrons per molecule. C_{60} could not be detected by CV during the electrolysis in *o*-DCB, probably because of blocking of the electrode surface as a result of the generation of by-products. The reaction mixture was purified by column chromatography (silica gel, CS_2), and C_{60} was obtained in 73% yield (Scheme 1). In a different experiment, the appearance of C_{60} during the course of the electrolysis in dichloromethane (DCM) could be detected directly by CV (Figure 1).

The applicability of the electrochemical retro-cycloaddition reaction to other fullerene species was further confirmed by the oxidative electrolysis of the *N*-ethyl pyrrolidinofullerene of $Sc_3N@C_{80}$ (**2**; Figure 2). Compound **2** was synthesized by a previously reported procedure,[12] and its cyclic voltammogram exhibited three reversible reduction waves and three irreversible oxidative waves (Figure 2a).[13] CPE was conducted at a potential of 0.45 V vs. Fc/Fc^+, which is 0.55 V lower than the potential required for the electrolysis of the C_{60}

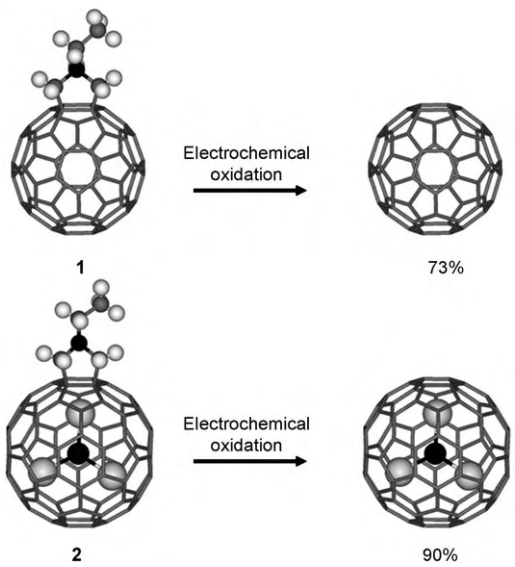

Scheme 1. Electrochemical retro-cycloaddition of *N*-ethyl pyrrolidino-[3,4:1,2][60]fullerene (**1**) and *N*-ethyl pyrrolidinofullerene $Sc_3N@C_{80}$ (**2**).

 © 2006 Wiley-VCH Verlag GmbH & Co. KGaA, Weinheim

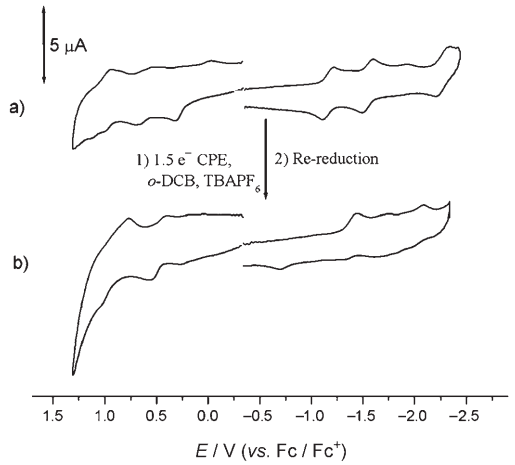

Figure 2. a) Cyclic voltammogram of **2** in 0.05 M $TBAPF_6$ *o*-DCB; scan rate 100 $mV s^{-1}$. b) Cyclic voltammogram after oxidative electrolysis of **2**.

derivative **1**. The voltammogram of **2** showed drastic changes after transfer of a charge corresponding to 1.5 electrons per molecule and re-reduction at zero potential. Comparison of the cyclic voltammogram of the new species in the solution with the previously reported cyclic voltammogram of $Sc_3N@C_{80}$[13] confirmed that the electrolysis was completed and the major product was $Sc_3N@C_{80}$ (90% yield, after purification by column chromatography).

The electrochemical retro-cycloaddition of compounds **1** and **2** led us to two important conclusions. First, for quantitative removal of the pyrrolidine group from the parent fullerene, the electrochemical oxidation must be performed at a potential corresponding exclusively to the oxidation of the pyrrolidine moiety but not oxidation of the fullerene cage. The higher yield obtained for the retro-cycloaddition of the *N*-ethyl pyrrolidino derivative of $Sc_3N@C_{80}$ is consistent with this finding, as the selective oxidation of the addend is more facile. Second, upon re-reduction of the electrolyzed solution at 0 V, the charge transferred corresponded to less that one electron per molecule. This observation indicated that upon completion of the electrochemical retro-cycloaddition, the parent fullerene was close to its neutral state. This result establishes a major difference from the electrochemical retro-cyclopropanation reaction, during which the fullerene species is reduced to give an anionic end state. These two findings suggest that the mechanism of the oxidative retro-cycloaddition mainly involves the pyrrolidine group with minimal involvement of the fullerene center.

To investigate the selectivity of this electrochemical oxidative retro-cycloaddition reaction, we synthesized the hybrid *e′* isomer bis adduct **3**, which contains both an *N*-methyl pyrrolidino and a bis(ethoxycarbonyl)methano addend (Scheme 2), and performed both electrolytic oxidation, to remove the pyrrolidine ring, and reduction, to remove the bis(ethoxycarbonyl)methano addend. The selective removal of the bis(ethoxycarbonyl)methano addend from a similar compound (*trans*-3 isomer) by electrochemical reduction proceeded with 63% yield.[8]

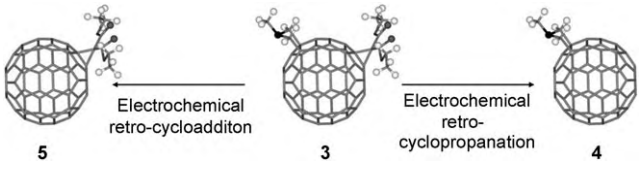

Scheme 2. Electrochemical retro-cycloaddition and retro-cyclopropanation of hybrid bis adduct **3** of C_{60}.

The reductive CPE of **3** was carried out in DCM at a potential 100 mV more negative than the second reduction peak potential (Figure 3a, downwards arrow) and yielded *N*-methyl pyrrolidinofullerene (**4**) as a major product (89%). This result demonstrates the instability of the cyclopropane ring and the stability of the pyrrolidine addend under reductive conditions and confirms the previously reported results for the *trans*-3 isomer.[8]

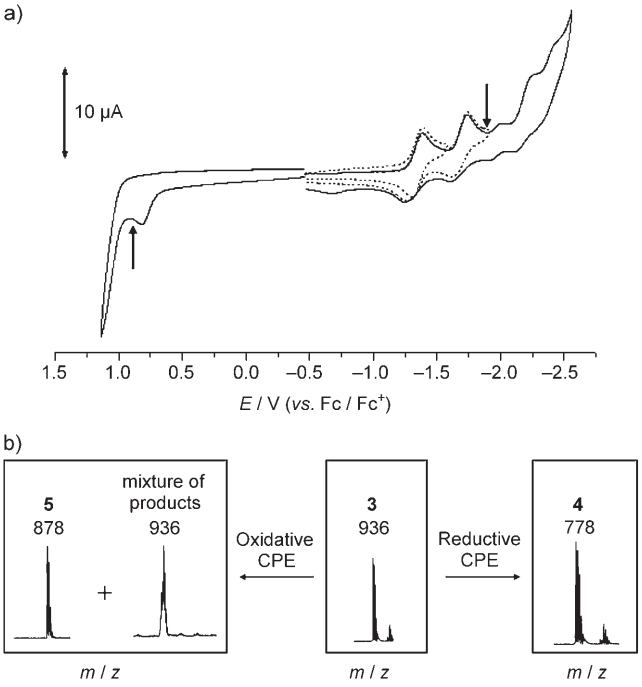

Figure 3. a) Cyclic voltammogram of **3** in 0.1 M $TBAPF_6$ in DCM; scan rate 100 $mV s^{-1}$. b) MALDI-TOF MS analysis of the products after electrolytic oxidation and reduction.

The oxidative CPE of **3** was performed in DCM by following the procedure established for compounds **1** and **2** (Figure 3a, oxidation potential shown by upwards arrow). Complete characterization (TLC, MALDI-TOF MS, and ^1H NMR spectroscopy) of the products revealed the presence of mainly two species.

The major product (60% yield) was identified as bis(ethoxycarbonyl)methanofullerene (**5**). The other species (30% yield) consisted of a mixture of several compounds with different retention factors (TLC) from **3** but with molecular-ion peaks (MALDI-MS) corresponding to the molecular weight of **3** (Figure 3b). We hypothesize that an isomerization reaction has occurred during electrolysis and the multiple compounds are isomeric mixed bis adducts. Most likely the

 © 2006 Wiley-VCH Verlag GmbH & Co. KGaA, Weinheim

pyrrolidine group has shuffled on the surface of the C_{60} sphere, in a similar manner to the previously observed "walk-on-the-sphere" rearrangement that occurs during the retro-cyclopropanation reaction.[14] This hypothesis is currently under investigation in our laboratory.

In summary, we propose electrochemical oxidative electrolysis as an alternative method to conduct thermal retro-cycloaddition reactions of fullerene derivatives. We have also shown, for the first time, the selective removal by electrochemical methods of targeted addends from a parent fullerene bearing the two most commonly used derivative groups (Scheme 2). The discovery of the retro-cyloaddition reaction creates new possibilities in protecting/deprotecting strategies for functionalization of fullerenes and also reveals the instability of the pyrrolidine addends under thermal and oxidative conditions. This latter fact represents potential difficulties for further applications of pyrrolidinofullerenes in the preparation of optoelectronic devices and should motivate the search for new, easily accessible, and more-stable functional groups.

Experimental Section

All CPE experiments were performed with a homemade cell under high vacuum with $TBAPF_6$ as supporting electrolyte, as previously described.[11]

Compounds **1**,[4a] **2**,[12] and *N*-methyl pyrrolidino[3,4:1,2][60]fullerene[4a] were synthesized according to literature procedures, and compound **3** as follows: DBU (17 μL, 0.12 mmol) was added to a solution of *N*-methyl pyrrolidino[3,4:1,2][60]fullerene[4] (50 mg, 0.06 mmol) and diethyl bromomalonate (10 μL, 0.06 mmol) in *o*-DCB. After 5 min the reaction mixture was subjected to column chromatography on silica with CH_2Cl_2. Compound **3** was isolated in 9% yield (5.5 mg). ^{1}H NMR spectroscopy (500 MHz, [D_8]toluene): $\delta = 4.06$ (q, $J = 10$ Hz, 4H), 3.68 (d, $J = 6.5$ Hz, 2H), 3.57 (d, $J = 6.5$ Hz, 2H). 2.42 ppm (s, 3H); MALDI-TOF MS (1,8,9-trihydroxyanthracene): m/z 936 [M^+].

Received: June 16, 2006
Published online: October 16, 2006

Keywords: azomethine ylides · cycloaddition · electrochemistry · fullerenes · retro reactions

[1] a) A. Hirsch, *The Chemistry of the Fullerene*, Thieme, Stuttgart, **1994**; b) A. Hirsch, M. Brettreich, *Fullerenes: Chemistry and Reactions*, Wiley-VCH, Weinheim, **2005**.

[2] N. Martín, J. L. Segura, F. Wudl in *Fullerenes: From Synthesis to Optoelectronic Properties* (Eds: D. M. Guldi, N. Martín), Kluwer Academic Publishers, Dordrech, **2002**, chap. 1, pp. 1–50.

[3] a) C. Bingel, *Chem. Ber.* **1993**, *126*, 1957–1959; b) A. Hirsch, I. Lamparth, H. R. Karfunkel, *Angew. Chem.* **1994**, *106*, 453–455; *Angew. Chem. Int. Ed. Engl.* **1994**, *33*, 437–438; c) C. Thilgen, A. Herrman, F. Diederich, *Angew. Chem.* **1997**, *109*, 2362–2374; *Angew. Chem. Int. Ed. Engl.* **1997**, *36*, 2268–2280; d) X. Champs, A. Hirsch, J. *Chem. Soc. Perkin Trans. 1* **1997**, 1595–1596.

[4] a) M. Maggini, G. Scorrano, M. Prato, *J. Am. Chem. Soc.* **1993**, *115*, 9798–9799; b) M. Prato, M. Maggini, *Acc. Chem. Res.* **1998**, *31*, 519–526; c) K. Kodratos, S. Bosi, T. Da Ros, A. Zambon, V. Lucchini, M. Prato, *J. Org. Chem.* **2001**, *66*, 2801–2808; d) N. Tagmatarchis, M. Prato, *Synlett* **2003**, 768–779.

[5] See, for example: M. A. Herranz, N. Martín, J. Ramey, D. M. Guldi, *Chem. Commun.* **2002**, 2968–2969.

[6] R. Kessinger, J. Crassous, A. Herman, M. Ruttimann, L. Echegoyen, F. Diederich, *Angew. Chem.* **1998**, *110*, 2022–2025; *Angew. Chem. Int. Ed.* **1998**, *37*, 1919–1922.

[7] a) N. S. Fender, B. Nuber, D. I. Schuster, S. R. Wilson, L. Echegoyen, *J. Chem. Soc. Perkin Trans. 2* **2000**, 1924–1928; b) C. Boudon, J.-P. Gisselbrecht, M. Cross, A. Herrmann, M. Ruttimann, J. Crassous, F. Cardullo, L. Echegoyen, F. Diederich, *J. Am. Chem. Soc.* **1998**, *120*, 7860–7868.

[8] R. Kessinger, N. S. Fender, L. E. Echegoyen, C. Thilgen. L. Echegoyen, F. Diederich, *Chem. Eur. J.* **2000**, *6*, 2184–2192.

[9] N. N. P. Moonen, C. Thilgen, L. Echegoyen, F. Diederich, *Chem. Commun.* **2000**, 335–336.

[10] N. Martín, M. Altable, S. Filippone, A. Martín-Domenech, L. Echegoyen, C. M. Cardona, *Angew. Chem.* **2006**, *118*, 116–120; *Angew. Chem. Int. Ed.* **2006**, *45*, 110–114.

[11] P. L. Boulas, Y. Zuo, L. Echegoyen, *Chem. Commun.* **1996**, 1547–1548.

[12] C. M. Cardona, A. Kitaygorodskiy, A. Ortiz, M. A. Herranz, L. Echegoyen, *J. Org. Chem.* **2005**, *70*, 5092–5097.

[13] B. Elliott, L. Yu, L. Echegoyen, *J. Am. Chem. Soc.* **2005**, *127*, 10885–10888.

[14] a) R. Kessinger, M. Gomez-Lopez, C. Boudon, J.-P. Gisselbrecht, M. Cross, L. Echegoyen, F. Diederich, *J. Am. Chem. Soc.* **1998**, *120*, 8545–8546; b) L. E. Echegoyen, F. D. Djojo, A. Hirsch, L. Echegoyen, *J. Org. Chem.* **2000**, *65*, 4994–5000.[2]

 © 2006 Wiley-VCH Verlag GmbH & Co. KGaA, Weinheim

Methane and Methanol Oxidation

DOI: 10.1002/anie.200602560

Methane Oxidation by Aqueous Osmium Tetroxide and Sodium Periodate: Inhibition of Methanol Oxidation by Methane**

*Takao Osako, Eric J. Watson, Ahmad Dehestani, Brian C. Bales, and James M. Mayer**

The direct oxidation of methane to methanol has long been one of the most important challenges in chemical reactivity.[1] Methane is the primary component of natural gas and is used both as a fuel and a feedstock. However, transportation and storage of methane are more demanding than for liquid

[*] Dr. T. Osako, Dr. E. J. Watson, Dr. A. Dehestani, Dr. B. C. Bales, Prof. Dr. J. M. Mayer
Department of Chemistry
University of Washington
Seattle, WA 98195-1700 (USA)
Fax: (+1) 206-685-8665
E-mail: mayer@chem.washington.edu

[**] This work was supported by the U.S. National Science Foundation (CHE-0204697 and CHE-0513023), the U.S. National Institutes of Health, and the Japan Society for the Promotion of Science (JSPS Postdoctoral Fellowship for Research Abroad to T.O.). We thank R. Morley for glassblowing.

Supporting information for this article is available on the WWW under http://www.angewandte.org or from the author.

© 2006 Wiley-VCH Verlag GmbH & Co. KGaA, Weinheim

methanol. Conversion of methane to methanol is difficult owing to the strong methane C–H bond (105 kcal mol^{-1})[2] and the ease of over-oxidation of methanol. Much effort has been devoted to this challenge, using both homogeneous and heterogeneous processes. Heterogeneous methane oxidation has been explored with many metal oxides, typically at high temperatures.[1,3] Studies of low-temperature, homogeneous methane oxidation have been inspired by the methane-oxidizing enzymes[4] and the discovery by Shilov et al. of the catalytic conversion of methane into CH_3OH and CH_3Cl with aqueous platinum salts.[5] Most of the enzymatic, biomimetic, and heterogeneous reactions are thought to follow free-radical pathways.[1,6,7] In contrast, the various Shilov-type systems utilizing soft heavy-metal ions are thought to have organometallic mechanisms initiated by methane binding to the metal.[8]

Herein, we describe a new approach to direct methane oxidation, using aqueous osmium tetroxide and sodium periodate (OsO_4/$NaIO_4$). Methanol overoxidation is still an issue in this system but remarkably methane inhibits the oxidation of methanol under these conditions. OsO_4 and RuO_4 could be the only two binary metal oxides whose reactivity with CH_4 has not been reported before, because their volatility and toxicity prevent heterogeneous, high-temperature studies. RuO_4 oxidizations of higher alkanes have been described[9] and we have reported OsO_4 oxidations of H_2[10] and higher alkanes (not methane) in basic aqueous solutions.[11]

Solutions of OsO_4 and $NaIO_4$ in D_2O react with CH_4 at 50 °C to give CH_3OH, $CH_2(OH)_2$, and CO_2 [Eq. (1)]. This

$$CH_4 \xrightarrow[D_2O \text{ at } 50\,^\circ C]{OsO_4/NaIO_4} CH_3OH + CH_2(OH)_2 + CO_2 \quad (1)$$

reaction—and all of the reactions described herein—used 50 mM concentrations of OsO_4 and $NaIO_4$ in D_2O in a flame-sealed NMR tube containing 9.5 atm of methane (12 mM[12]) at 50 °C.[13] The products were observed and quantified by ^{1}H NMR spectroscopy, referenced to a solution of C_6Me_6 in C_6D_6 in a sealed capillary in the NMR tube: $\delta = 3.38$ ppm, CH_3OH, 0.32 mM; $\delta = 4.85$ ppm, $CH_2(OH)_2$, 0.24 mM (Figure 1 A). Oxidation of $^{13}CH_4$ (99 % ^{13}C) under the standard conditions occurs similarly, with the $^{13}C\{^1H\}$ NMR spectrum showing $^{13}CH_3OH$, $^{13}CH_2(OH)_2$, and $^{13}CO_2$ at $\delta = 49$, 82, and 125 ppm, respectively (Figure 1 B). Monitoring by ^{1}H NMR spectroscopy showed that the methanol concentration reached 0.28 mM within 4 h of reaction and rose only slightly over the following 5 days (Figure 1 C). The final methanol concentration is only 0.6 % of the starting OsO_4 and $NaIO_4$ concentrations, and 2.7 % of the starting methane concentration. The reactions are carried out anaerobically, so Os^{VIII} and I^{VII} are the only oxidants present.[14] No methane oxidation products are detected by ^{1}H and ^{13}C NMR spectroscopy using aqueous $NaIO_4$ without OsO_4, or in OsO_4 without IO_4^-. The latter experiment was performed with phosphate buffer to set the pH to 4.3, the characteristic pH value of 50 mM periodate solutions. Thus, both OsO_4 and $NaIO_4$ are needed for the formation of methanol.

Mechanistically, methane oxidation is unlikely to involve hydroxyl radicals given the mild conditions ($OH^\bullet$ was ruled

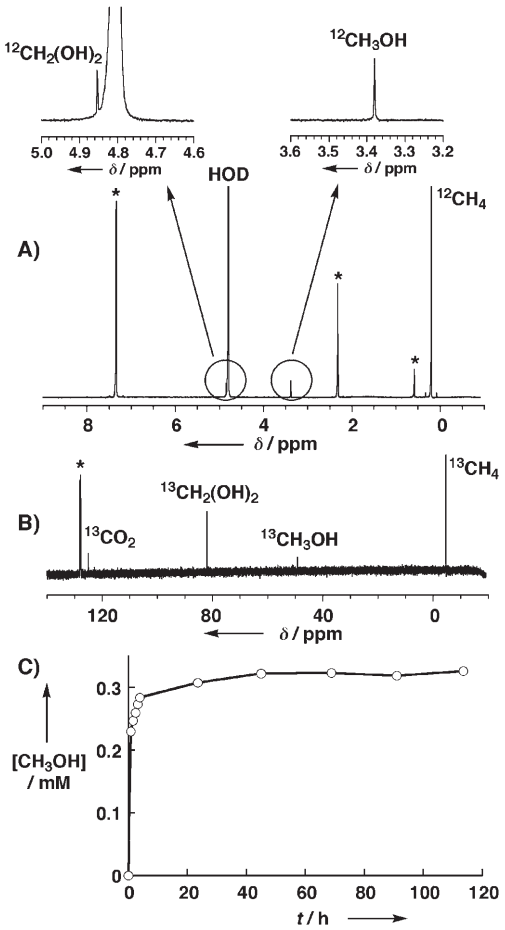

Figure 1. Oxidations of methane (9.5 atm) by OsO_4 and $NaIO_4$, both 50 mM in D_2O, at 50 °C. The asterisk peaks are due to the capillary standard (C_6Me_6 and H_2O in C_6D_6). A) ^{1}H NMR spectrum for $^{12}CH_4$ oxidation after 3 days. B) $^{13}C\{^1H\}$ NMR spectrum for $^{13}CH_4$ oxidation after 3 days. C) Time course for the oxidation of $^{12}CH_4$.

out in the higher-temperature, high-pH value oxidation of *iso*-butane based on the clean selectivity for oxidation of the tertiary C–H bond[11]). Methane coordination to osmium is also very unlikely given the limited affinity of OsO_4 for strong ligands, such as pyridine.[15] Perhaps the pathway involves [3+2] addition of a methane C–H bond to two oxo groups, as has been suggested in computational studies of CH_4 reactions with OsO_4 and RuO_4,[16] and in experimental and computational studies of OsO_4 and RuO_4 oxidations of H_2 and higher alkanes.[9–11,17]

The oxidation of methanol by OsO_4 and/or $NaIO_4$ has also been examined. There are a number of reports of alcohol oxidations by OsO_4 and by iodates, and IO_4^- has been used as the terminal oxidant in OsO_4-catalyzed reactions.[18] We find that 5 mM $^{13}CH_3OH$ is completely oxidized within 3 h at 50 °C by OsO_4/$NaIO_4$ under 9.5 atm of argon (Figure 2 C). In contrast, oxidation of $^{13}CH_3OH$ under the same conditions except with 9.5 atm $^{12}CH_4$ instead of Ar, proceeds much more slowly: most of the methanol still present after 5 days at 50 °C (Figure 2 A, B). Methanol oxidation is slowed by a factor of approximately 10^3 by 9.5 atm CH_4.

 © 2006 Wiley-VCH Verlag GmbH & Co. KGaA, Weinheim

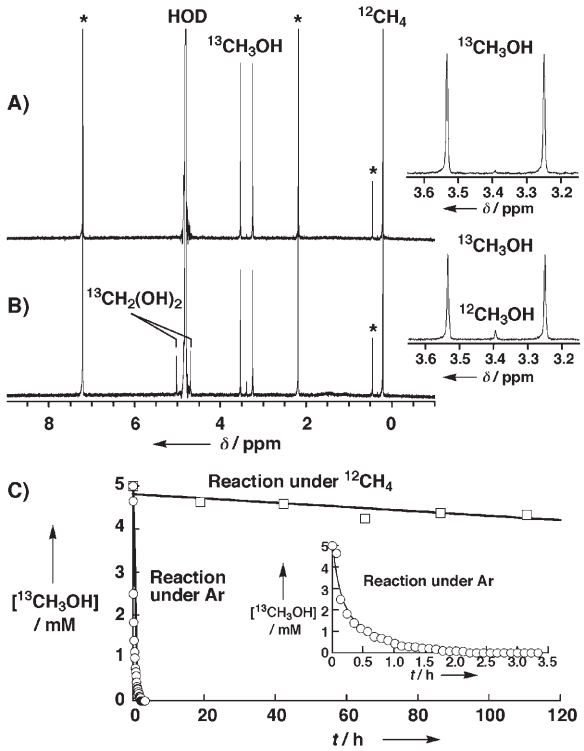

Figure 2. Oxidations of $^{13}CH_3OH$ (5 mM) by OsO_4 and $NaIO_4$, both 50 mM in D_2O, at 50 °C. The asterisk peaks are due to the capillary standard (C_6Me_6 and H_2O in C_6D_6). A,B) Under 9.5 atm $^{12}CH_4$: A) initial ^1H NMR spectrum, B) after 5 days. C) Time courses for the oxidations under 9.5 atm $^{12}CH_4$ (□) or 9.5 atm Ar (○). Inset: initial stage of the reaction under 9.5 atm Ar for 0–3.5 h.

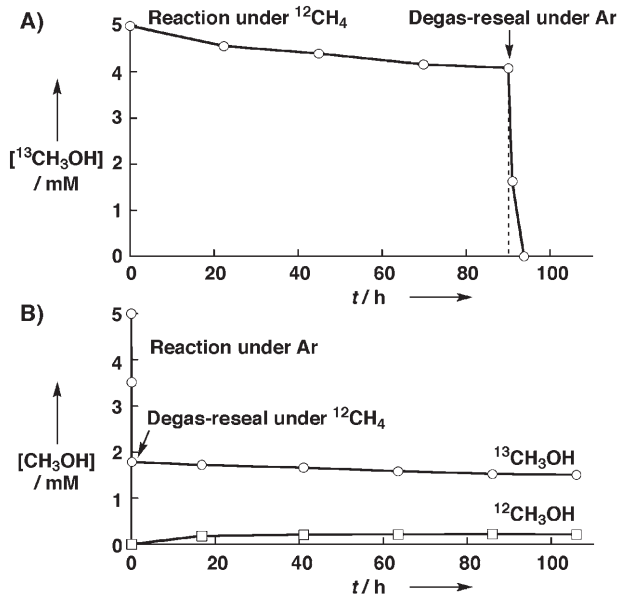

Figure 3. Time courses for the degas–reseal experiments at 50 °C (5 mM $^{13}CH_3OH$, 50 mM OsO_4, 50 mM $NaIO_4$ in D_2O). A) Reaction under 9.5 atm $^{12}CH_4$, which was then degassed and resealed under 9.5 atm Ar at the arrow/dotted line. B) Reaction under 9.5 atm Ar then 9.5 atm $^{12}CH_4$ at the arrow (10 min).

This very surprising inhibition by methane has been confirmed by two of the co-authors in a variety of experiments over more than a year. We have used $^{12}CH_4/^{13}CH_3OH$ and $^{13}CH_4/^{12}CH_3OH$, with different samples of OsO_4, periodate, and D_2O. The most dramatic observations come from degas–reseal experiments. A long medium-walled NMR tube was charged with 5.0 mM $^{13}CH_3OH$, OsO_4, and $NaIO_4$ in D_2O under our standard conditions. After three freeze-pump-thaw-degas cycles, $^{12}CH_4$ was added and the tube flame-sealed (all experiments carried out at 9.5 atm gas pressure[19]). After 4 days at 50 °C, only 18 % of the $^{13}CH_3OH$ had been consumed (Figure 3 A). The solution was then frozen, and the tube was cut open and returned to the vacuum line. The methane was removed with three freeze-pump-thaw cycles and replaced with argon, and the tube was re-sealed with a torch. Upon further heating of *the same solution*—having changed only the gas present—the methanol was consumed within 3 h. Figure 3 B shows the results of the complementary experiment: in the first stage under Ar, 64 % of the $^{13}CH_3OH$ is consumed after 10 min but after resealing under $^{12}CH_4$ the remaining $^{13}CH_3OH$ was preserved over 5 days and $^{12}CH_3OH$ was generated from $^{12}CH_4$.

Figure 3 A shows that the inhibition is caused by a material that is removed upon degassing. No inhibition is observed under argon in the presence of the volatile oxidation products CO or CO_2 (or formaldehyde or H_2). A degas–reseal experiment in which the initial methane was replaced with fresh methane showed no difference from a constant methane atmosphere. These experiments indicate that the inhibition is caused by methane, rather than products of methane oxidation.

Methanol oxidation by $OsO_4/NaIO_4$ is also inhibited by CD_4, but is not affected by 9.5 atm of Xe or Ar, 1 atm N_2, or 30 μL CCl_4. Preliminary experiments suggest that methanol oxidation at 50 °C is also inhibited by ethane and *iso*-butane but not by 30 μL of cyclohexane. Inhibition by methane is not observed in the presence of 500 mM phosphate buffer (maintaining the pH of 4.4 set by IO_4^- alone).

Under our standard conditions,[13] methanol oxidations by OsO_4 alone, or by $NaIO_4$ alone, are much slower than with the two oxidants together (36–43 % $^{13}CH_3OH$ consumed after 200 h versus completely consumed in 3 h). The presence of $^{12}CH_4$ does not affect $^{13}CH_3OH$ oxidation by OsO_4 alone and slows the oxidation by $NaIO_4$ by only a factor of about 4 (Supporting Information). Reactions of the separated oxidants are roughly as fast as observed for CH_4-inhibited $OsO_4/NaIO_4$. Thus an unusually active oxidant is formed from $OsO_4/NaIO_4$, consistent with the methane oxidation results. There is, however, no optical spectroscopic evidence for any interaction between OsO_4 and IO_4^-. It should be noted that under 9.5 atm CH_4, the methane concentration in D_2O is 9.5 ± 0.4 mM in all these solutions, varying only marginally with the other materials present in solution.

The inhibition of a reaction by a low concentration of methane is to our knowledge unprecedented. Methane is usually viewed as a very inert material. Under the conditions where inhibition is observed, only a small fraction of the OsO_4 and $NaIO_4$ are consumed, and there is no evidence from optical or NMR spectroscopy for any interaction of methane with any of the reagents. It is not clear whether the origin of this highly unusual inhibition is a chemical effect, inhibiting formation of the $OsO_4/NaIO_4$ active oxidant, or a physical

 © 2006 Wiley-VCH Verlag GmbH & Co. KGaA, Weinheim

effect related to unusual solvation in H_2O/CH_4 (perhaps related to H_2O/CH_4 clathrates[20]).

In conclusion, aqueous solutions of OsO_4 and $NaIO_4$ oxidize methane to give a small amount of methanol under very mild aqueous conditions: 50 °C, 9.5 atm CH_4. Further oxidation of methanol is competitive with methane oxidation. The presence of methane substantially inhibits the oxidation of methanol. Further studies are in progress to define the scope, kinetics, and mechanisms of both the methane oxidation and this unprecedented inhibition.

Received: June 27, 2006

Keywords: inhibition · methane · methanol · osmium · oxidation

[1] a) H. D. Gesser, N. R. Hunter in *Methane Conversion by Oxidative Processes* (Ed.: E. E. Wolf), Van Nostrand Reinhold, New York, **1992**, p. 403; b) M. G. Axelrod, A. M. Gaffney, R. Pitchai, J. A. Sofranko in *Natural Gas Conversion II*, Elsevier, Amsterdam, **1994**, p. 93; c) J. H. Lunsford, *Catal. Today* **2000**, *63*, 165; d) R. H. Crabtree, *Chem. Rev.* **1995**, *95*, 987.

[2] NIST Chemistry WebBook, http://webbook.nist.gov/chemistry/ National Institute of Standards and Technology, Gaithersburg MD, **2005**.

[3] a) H. D. Gesser, N. R. Hunter, C. B. Parkash, *Chem. Rev.* **1985**, *85*, 235; b) T. J. Hall, J. Hargreaves, G. J. Huncthing, R. W. Richard, W. Joyner, S. H. Taylor, *Fuel Process. Technol.* **1995**, *42*, 151; c) K. Tanaka, Y. Teng, T. Takemato, *Catal. Rev.* **2002**, *44*, 1.

[4] a) H. Zheng, J. D. Lipscomb, *Biochemistry* **2006**, *45*, 1685; b) M. H. Baik, M. Newcomb, R. A. Friesner, S. J. Lippard, *Chem. Rev.* **2003**, *103*, 2385; c) R. L. Lieberman, A. C. Rosenzweig, *Nature* **2005**, *434*, 177.

[5] a) N. F. Goldshleger, V. V. Eskova, A. E. Shilov, A. A. Shteinman, *Zh. Fiz. Khim.* **1972**, *46*, 1353; b) A. E. Shilov, G. B. Shul'pin, *Chem. Rev.* **1997**, *97*, 2897.

[6] see, for example, J. A. Labinger, *Catal. Lett.* **1988**, *1*, 371, and ref. [3c].

[7] a) *Biomimetic Oxidations Catalyzed by Transition Metal Complexes* (Ed.: B. Meunier), Imperial College Press, London **2000**; b) J. M. Mayer, E. A. Mader, J. P. Roth, J. R. Bryant, T. Matsuo, A. Dehestani, B. C. Bales, E. J. Watson, T. Osako, K. Valliant-Saunders, W. H. Lam, D. A. Hrovat, W. T. Bordon, E. R. Davidson, *J. Mol. Catal. A* **2006**, *251*, 24; c) Ref. [4a]; d) Ref. [4b] has an alternative view.

[8] a) *Activation and Functionalization of C–H Bonds* (Eds.: K. I. Goldberg, A. S. Goldman), American Chemical Society, Oxford University Press, Washington, DC, **2004**; b) R. A. Periana, O. Mironov, D. J. Taube, G. Bhalla, C. J. Jones, *Science* **2003**, *301*, 814; c) B. A. Arndtsen, R. G. Bergman, T. A. Mobley, T. H. Peterson, *Acc. Chem. Res.* **1995**. *28*, 154; d) J. S. Owen, J. A. Labinger, J. E. Bercaw, *J. Am. Chem. Soc.* **2006**, *128*, 2005.

[9] a) A. Tenaglia, E. Terranova, B. Waegell, *J. Org. Chem.* **1992**, *57*, 5523; b) A. Tenaglia, E. Terranova, B. Waegell, *J. Chem. Soc. Chem. Commun.* **1990**, 1344; c) A. Tenaglia, E. Terranova, B. Waegell, *Tetrahedron Lett.* **1989**, *30*, 5271; d) J. M. Bakke, A. E. Froehaug, *J. Phys. Org. Chem.* **1996**, *9*, 507; e) J. M. Bakke, A. E. Froehaug, *J. Phys. Org. Chem.* **1996**, *9*, 310.

[10] A. Dehestani, W. H. Lam, D. A. Hrovat, E. R. Davidson, W. T. Borden, J. M. Mayer, *J. Am. Chem. Soc.* **2005**, *127*, 3423.

[11] B. C. Bales, P. Brown, A. Dehestani, J. M. Mayer, *J. Am. Chem. Soc.* **2005**, *127*, 2832.

[12] Methane concentration calculated using: *IUPAC Solubility Data Series: Methane* (Eds.: H. L. Clever, C. L. Young), Pergamon, Oxford, **1987**.

[13] Typical procedure: A medium walled NMR tube was charged with 400 μL of a solution of OsO_4 (50 mM; Colonial Metal) and $NaIO_4$ (50 mM; Aldrich) in D_2O (Cambridge Isotope). After three cycles of freeze-pump thaw degassing, $^{12}CH_4$ (7.2 mL of 1 atm; 99.99 %, Matheson) at 25 °C was condensed into the tube with liquid N_2. The NMR tube was flame sealed to be 15 cm in length, shaken vigorously, and then placed in an oil bath at 50 °C.

[14] Other I^{VII} oxyanions are present in 50 mM aqueous $NaIO_4$ solutions: I. Kerezsi, G. Lente, I. Fábián, *Dalton Trans.* **2004**, 342.

[15] "Osmium": W. P. Griffith in *Comprehensive Coordination Chemistry*, *Vol. 4* (Ed.: G. Wilkinson), Pergamon, New York, **1987**, p. 519.

[16] a) W. H. Lam, A. Dehestani, D. A. Hrovat, E. R. Davidson, W. T. Borden, J. M. Mayer, unpublished results, **2004**; b) M. Drees, T. Strassner, *J. Org. Chem.* **2006**, *71*, 1755.

[17] J. P. Collman, L. M. Slaughter, T. A. Eberspacher, T. Strassner, J. I. Brauman, *Inorg. Chem.* **2001**, *40*, 6272.

[18] a) W. P. Griffith, M. Suriaatmaja, *Can. J. Chem.* **2001**, *79*, 598; b) A. M. Maione, A. Romeo, *Synthesis* **1984**, 955; c) B. Singh, A. K. Singh, M. B. Singh, A. P. Singh, *Tetrahedron* **1986**, *42*, 715; d) S. Singh, A. Gupta, A. K. Singh, *Transition Met. Chem.* **1998**, *23*, 277; e) G. A. Hiremath, P. L. Timanagoudar, R. B. Chougale, S. T. Nandibewoor, *J. Indian Chem. Soc.* **1998**, *75*, 363.

[19] The results are identical with 1 atm N_2 in place of 9.5 atm Ar.

[20] See a) S. F. Dec, K. E. Bowler, L. L. Stadterman, C. A. Koh, E. D. Sloan, Jr., *J. Am. Chem. Soc.* **2006**, *128*, 414; b) Z. Cao, J. W. Tester, K. A. Sparks, B. L. Trout, *J. Phys. Chem. B* **2001**, *105*, 10950.

 © 2006 Wiley-VCH Verlag GmbH & Co. KGaA, Weinheim

Glycosylation

DOI: 10.1002/anie.200602642

A Highly Reactive and Stereoselective β-Mannopyranosylation System: Mannosyl 4-Pentenoate/PhSeOTf**

*Ju Yuel Baek, Tae Jin Choi, Heung Bae Jeon, and Kwan Soo Kim**

Although many efficient methods for the stereoselective construction of glycosyl linkages are available,[1] the stereospecific formation of the 1,2-*cis*-β-D-mannopyranosyl linkage still poses a great challenge. Several diverse and innovative strategies for β-mannopyranosylation have been developed,[2] and recently, Crich and co-workers have made a significant

[*] J. Y. Baek, T. J. Choi, H. B. Jeon, Prof. Dr. K. S. Kim
Center for Bioactive Molecular Hybrids and
Department of Chemistry
Yonsei University
Seoul 120-749 (Korea)
Fax: (+82) 2-365-7608
E-mail: kwan@yonsei.ac.kr

[**] This work was supported by a grant from the Korea Science and Engineering Foundation through the Center for Bioactive Molecular Hybrids (CBMH).

Supporting information for this article is available on the WWW under http://www.angewandte.org or from the author.

WILEY InterScience DISCOVER SOMETHING GREAT
© 2006 Wiley-VCH Verlag GmbH & Co. KGaA, Weinheim

breakthrough in β-mannoside synthesis by employing 4,6-*O*-benzylidene-protected mannopyranosyl sulfoxides or thiomannopyranosides as glycosyl donors.[3] The effect of the 4,6-*O*-acetal group on the construction of β-mannosyl linkages was further confirmed with other mannosyl donors by us[4] and other workers.[5] Nevertheless, the effect of protecting groups at the 2-O and 3-O positions of the donor,[6] anomeric leaving groups, and acceptors on the stereoselectivity in this β-mannosylation of a 4,6-*O*-acetal-substituted sugar is not yet fully understood. More importantly, the β selectivity with certain glycosyl acceptors has never been satisfactory.[7] In the continuation of our effort to develop an efficient β-mannopyranosylation method, our attention focused on the use of 4,6-*O*-benzylidene mannosyl pentenoate **1** as a glycosyl donor in the presence of phenylselenyl triflate (PhSeOTf). Glycosyl pentenoates are not really new but have been reported as glycosyl donors with iodonium dicollidine perchlorate (IDCP) and *N*-iodosuccinimide/trifluoromethanesulfonic acid (NIS–TfOH) promoters by the research groups led by Kunz[8] and Fraser-Reid[9] independently. However, no detailed studies on the stereoselectivity and no application to oligosaccharide synthesis have been reported,[10] except that sialyl 4-pentenoate is reported to be inferior to 4-pentenyl sialoside as a glycosyl donor.[11] Herein we describe the use of **1** as the glycosyl donor and PhSeOTf as the promoter for the synthesis of β-mannopyranosides and the efficient construction of an oligosaccharide.

We envisioned that treatment of mannosyl pentenoate **1** with PhSeOTf in the presence of 2,4,6-tri-*tert*-butylpyrimidine (TTBP)[12] would induce the lactonization of **1** via selenonium ion **A** to generate γ-phenylselenylmethyl-γ-butyrolactone and oxocarbenium ion **B**, which might be in equilibrium with triflate **C** (Scheme 1). Subsequent reaction of **B** or **C** with a glycosyl acceptor would provide mannopyranoside **D**.

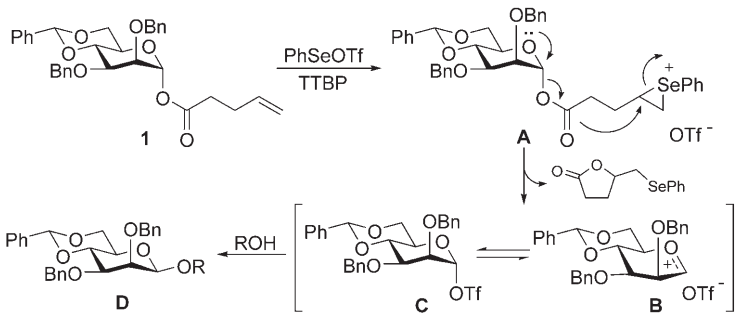

Scheme 1. Plausible mechanism of glycosylation with glycosyl pentenoate **1** as the donor and with PhSeOTf as a promoter. Bn = benzyl, Tf = trifluoromethanesulfonyl.

4,6-*O*-Benzylidene mannosyl pentenoate **1** ($\alpha/\beta = 10{:}1$) was readily prepared from the corresponding 1-hydroxy sugar **2**[5c] by simple treatment with commercially available 4-pentenoic acid in the presence of 1,3-diisopropylcarbodiimide (DIC) and a catalytic amount of 4-dimethylaminopyridine (DMAP) as shown in Scheme 2.

We initially examined the glycosylation of glycosyl acceptor **3** with pentenoate **1** and with various promoters (Table 1). The glycosylation with PhSeOTf at −78 °C to 0 °C afforded exclusively β-disaccharide **4** in 90 % yield (Table 1, entry 1). When PhSeBr was used, however, the

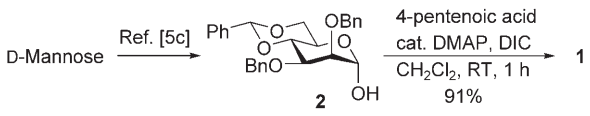

Scheme 2. Synthesis of 4,6-*O*-benzylidene mannosyl pentenoate **1**.

Table 1: Glycosylation with donor **1** using various promoters.

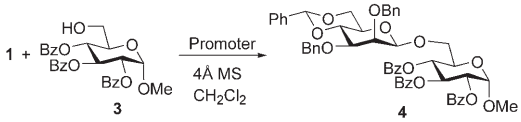

Entry	Promoter	Yield [%][a]	β/α[a]
1	PhSeOTf	90	β only
2	PhSeBr	0	–
3	IDCP	31	β only
4	NIS–TfOH	41	7:1[b]

[a] Determined after isolation of product. [b] Ratio was determined by ^{1}H NMR spectroscopy. Bz = benzoyl.

reaction did not proceed at all (Table 1, entry 2). The use of IDCP gave β-disaccharide **4** exclusively but only in 31 % yield (Table 1, entry 3), whereas the use of NIS–TfOH provided a mixture of β-disaccharide **4** and its α anomer in a 7:1 ratio and in 41 % yield (Table 1, entry 4). These results indicated that PhSeOTf is much more efficient and stereoselective than other known promoters for glycosylation when used in combination with **1**.

We also examined the glycosylation of **3** with 4-pentenyl 4,6-*O*- benzylidene mannoside **5** in order to compare the glycosyl 4-pentenoate with the well-known 4-pentenyl glycoside[13] as the glycosyl donor (Scheme 3). Reaction of pentenyl mannoside **5** and acceptor **3** in the presence of PhSeOTf, however, unexpectedly afforded a mixture of isomeric oxyselenides **6**, probably generated by addition of the alcohol **3** to the selenonium ion **A** (see Scheme 1).

We used mannosyl pentenoate **1** and PhSeOTf to examine glycosylations of a number of other glycosyl acceptors (Table 2). Glycosylation was carried out with 5 equiv of PhSeBr and AgOTf in the presence of 4-Å molecular sieves (MS) and TTBP at −78 °C in CH_2Cl_2. Glycosylation proceeded smoothly with 1.5 or 2 equiv of PhSeBr and AgOTf, but 5 equiv of the

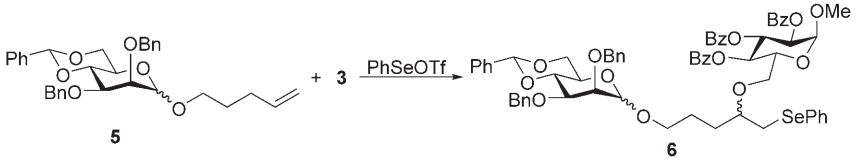

Scheme 3. Reaction of 4-pentenyl 4,6-*O*-benzylidene mannoside **5** as a donor with the acceptor **3**.

 © 2006 Wiley-VCH Verlag GmbH & Co. KGaA, Weinheim

Table 2: Glycosylations of various acceptors **7–16** with donor **1** in CH_2Cl_2.

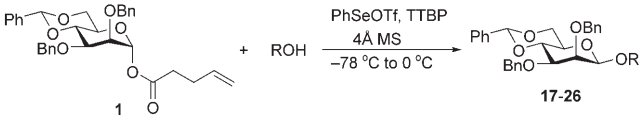

Entry	Glycosyl acceptor	Prod.	Yield [%][a,b]	β/α[a,b]
1	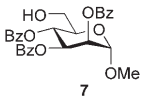 7	**17**	90 (87)	β only (β only)
2	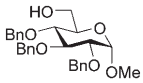 8	**18**	88 (89)	β only (β only)
3	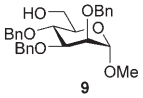 9	**19**	89 (87)	β only (β only)
4	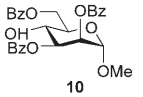 10	**20**	87 (87)	β only (β only)
5	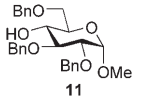 11	**21**	85 (85)	β only (β only)
6	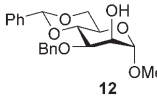 12	**22**	90 (89)	17:1 (4:1)
7	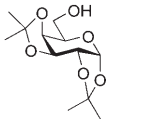 13	**23**	82 (85) 86[c] 88[d]	β only (β only) 5.6:1[c] 2.1:1[d]
8	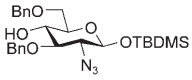 14	**24**	87	β only
9	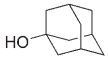 15	**25**	89 (88)	β only (β only)
10	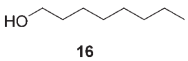 16	**26**	89 (89)	β only (β only)

[a] Determined after isolation of product. [b] Yields and ratios in parentheses are those from reactions in toluene as a solvent. [c] The result by Crich's sulfoxide method, see Ref. [3e]. [d] The result with 3-*O*-allyl-2-*O*-benzyl-4,6-*O*-benzylidene mannopyranosyl trichloroacetimidate by Schmidt's method, see Ref. [5a]. TBDMS = *tert*-butyldimethylsilyl.

promoters guarantees high yield and stereoselectivity even when the promoter deteriorates slightly or the generation of PhSeOTf is incomplete. Although the glycosylation of various acceptors with **1** was so efficient that the glycosyl donor was consumed within 20 min at −78 °C based on TLC, the reaction mixture was further warmed to 0 °C to ensure completion of the reaction. Glycosylations of primary alcohol acceptors **7–9** with **1** afforded exclusively β-disaccharides **17–19** in high yields (Table 2, entries 1–3). The complete conversion of acceptors **10** and **11** to give the corresponding β-disaccharides **20** and **21** was also easily achieved (Table 2, entries 4 and 5). However, glycosylation of **12** gave a mixture of α- and β-disaccharide **22** (β/α = 17:1) in 90 % yield (Table 2, entry 6). Interestingly, diacetone galactose **13**, mannosylation of which is known to be less stereoselective than that of other glycosyl acceptors under Crich's sulfoxide conditions[3e] and Schmidt's tricholoroacetimidate conditions,[5a] reacted with **1** under the present conditions to afford β-disaccharide **23** exclusively in 82 % yield (Table 2, entry 7). Glycosylations of azido sugar **14**, hindered tertiary alcohol **15**, and the simple primary alcohol 1-octanol (**16**) also afforded only β-mannopyranosides in high yields (Table 2, entries 8–10). Moreover, toluene was also found to be a good solvent in the present PhSeOTf-mediated mannosylation method; the results with toluene were almost same as those with CH_2Cl_2 (Table 2) unlike the sulfoxide method for β-mannopyranosylation.[3a] The stereochemistries at newly generated anomeric centers of unknown disaccharides **19**, **20**, and **24** were determined unequivocally on the basis of ^1H and ^{13}C NMR spectroscopic data, in particular the C1′,H1′ coupling constants: $^1J(C1',H1') = 159.4$ Hz in compound **19**, $^1J(C1',H1') = 160.0$ Hz in compound **20**, and $^1J(C1',H1') = 160.8$ Hz in compound **24**.

Like Seeberger et al. indicated,[5c] we observed that the mannosylation of more reactive primary alcohol acceptors showed poorer β stereoselectivity with known 4,6-*O*-benzylidene-substituted mannosyl donors. Therefore, we investigated the efficiency of the present mannosyl pentenoate/PhSeOTf method for the preparation of β-mannopyranoside **32** (which we needed to make a self-assembled β-mannoside monolayer on a gold surface) from primary alcohol **31** and compared the results with those from other mannosylation methods (Table 3). The glycosylation of **31** with the pentenoate donor **1** afforded β-mannopyranoside **32** exclusively in 87 % yield (Table 3, entry 1). While the glycosylation with the trichloroacetimidate donor **27** gave a mixture of α- and β-mannopyranoside **32** (β/α = 2:1, $^1J(C1'\text{-}H1') = 161.8$ Hz for β-mannoside and $^1J(C1'\text{-}H1') = 169.6$ Hz for α-mannoside) in 85 % yield (Table 3, entry 2), the use of 2′-carboxybenzyl glycoside **28**[4] as the mannosyl donor provided the undesired α anomer of **32** as the major product in good yield (Table 3, entry 3). On the other hand, glycosylations with thioglycoside **29** and with glycosyl sulfoxide **30** as glycosyl donors afforded a mixture of α- and β-mannopyranoside **32** (β/α = 1:2 for **29**, 11:1 for **30**) in yields of 70 % and 81 %, respectively (Table 3, entries 4 and 5). Accordingly, the present method appears to be more efficient than other known methods for the β-mannosylation of simple primary alcohols.

We applied this new glycosylation method to the synthesis of trisaccharide **36**, which has both α- and β-mannopyranosyl linkages, to show its effectiveness for oligosaccharide synthesis (Scheme 4). Mannosyl pentenoate donors **33** and **37** were readily prepared from D-mannose via the corresponding 1-hydroxy sugars (see the Supporting Information). Reaction of 4,6-*O*-benzylidene mannosyl donor **33** and acceptor **3** under the present glycosylation conditions using PhSeOTf afforded only β-disaccharide **34** in 85 % yield. Subsequent removal of the *p*-methoxybenzyl (PMB) group of **34** with 2,3-dichloro-5,6-dicyano-1,4-benzoquinone (DDQ) gave alcohol **35**. Glycosylation of the disaccharide **35** as an acceptor with benzoyl-protected mannosyl pentenoate **37** as a donor under

 © 2006 Wiley-VCH Verlag GmbH & Co. KGaA, Weinheim

Table 3: Glycosylation of acceptor **31** with various donors, **1**, and **27–30**.

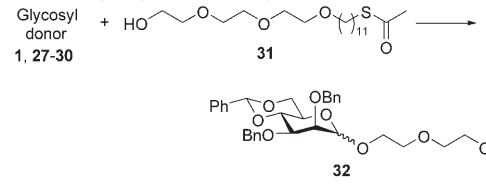

Entry	Glycosyl donor	Promoter	Yield [%][a]	β/α[a]	Reaction conditions
1	**1**	PhSeOTf TTBP	85	β only	Present work
2	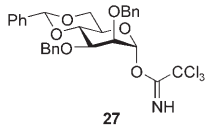 **27**	TMSOTf	87	2:1	Ref. [5a]
3	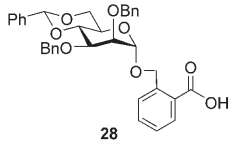 **28**	Tf_2O DTBMP[b]	91	1:6	Ref. [4]
4	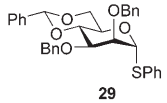 **29**	BSP[c] Tf_2O TTBP	70	1:2	Ref. [3g]
5	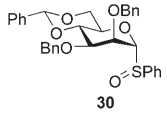 **30**	Tf_2O TTBP	81	11:1	Ref. [3b]

[a] Determined after isolation of product. [b] DTBMP = 2,6-di-*tert*-butyl-4-methylpyridine. [c] BSP = benzenesulfinylpiperidine. TMS = *tert*-butyldimethylsilyl.

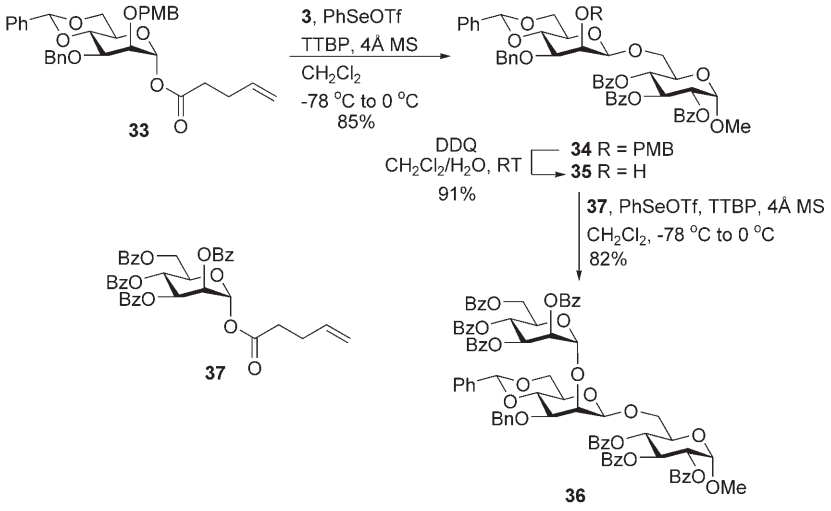

Scheme 4. Synthesis of trisaccharide **36**.

the same reaction conditions smoothly provided the diastereomerically pure α-trisaccharide **36** in 82% yield.

In conclusion, we have described a highly reactive and stereoselective procedure for the β-mannopyranosylation employing 4,6-*O*-benzylidene mannopyranosyl pentenoate **1** and PhSeOTf. This method for the β-mannopyranosylation was found to be comparable to and even better than other known methods for the mannosylation of the simple reactive primary alcohol. The versatility of the present methodology was readily demonstrated by the efficient synthesis of trisaccharide **36**, which has both α- and β-mannopyranosyl linkages, with perfect stereoselectivity in high yields.

Received: July 3, 2006
Revised: August 7, 2006
Published online: October 13, 2006

Keywords: β-mannopyranosylation · glycosides · glycosyl pentenoate · glycosylation · phenylselenyl triflate

[1] For selected reviews on glycosylation, see: a) R. R. Schmidt, *Angew. Chem.* **1986**, *98*, 213–236; *Angew. Chem. Int. Ed. Engl.* **1986**, *25*, 212–235; b) P. Sinaÿ, *Pure Appl. Chem.* **1991**, *63*, 519–528; c) K. Toshima, K. Tatsuta, *Chem. Rev.* **1993**, *93*, 1503–1531; d) G.-J. Boons, *Tetrahedron* **1996**, *52*, 1095–1121; e) B. G. Davis, *J. Chem. Soc. Perkin Trans. 1* **2000**, 2137–2160; f) A. V. Demchenko, *Lett. Org. Chem.* **2005**, *2*, 580–589.

[2] For selected reviews on β-mannosylation, see: a) H. Paulsen, *Angew. Chem.* **1982**, *94*, 184–201; *Angew. Chem. Int. Ed. Engl.* **1982**, *21*, 155–173; b) F. Barresi, O. Hindsgaul in *Modern Methods in Carbohydrate Synthesis* (Eds.: S. H. Khan, R. A. O'Neill), Harwood , Amsterdam, **1996**, pp. 251–276; c) V. Pozsgay in *Carbohydrates in Chemistry and Biology, Vol. 1* (Eds.: B. Ernst, G. W. Hart, P. Sinaÿ), Wiley-VCH, Weinheim, **2000**, pp. 319–343; d) J. J. Gridley, H. M. I. Osborn, *J. Chem. Soc. Perkin Trans. 1* **2000**, 1471–1491; e) A. V. Demchenko, *Synlett* **2003**, 1225–1240.

[3] a) D. Crich, S. Sun, *J. Org. Chem.* **1996**, *61*, 4506–4507; b) D. Crich, S. Sun, *J. Org. Chem.* **1997**, *62*, 1198–1199; c) D. Crich, S. Sun, *J. Am. Chem. Soc.* **1997**, *119*, 11217–11223; d) D. Crich, S. Sun, *J. Am. Chem. Soc.* **1998**, *120*, 435–436; e) D. Crich, S. Sun, *Tetrahedron* **1998**, *54*, 8321–8348; f) D. Crich, W. Cai, Z. Dai, *J. Org. Chem.* **2000**, *65*, 1291–1297; g) D. Crich, M. Smith, *J. Am. Chem. Soc.* **2001**, *123*, 9015–9020.

[4] K. S. Kim, J. H. Kim, Y. J. Lee, Y. J. Lee, J. Park, *J. Am. Chem. Soc.* **2001**, *123*, 8477–8481.

[5] a) R. Weingart, R. R. Schmidt, *Tetrahedron Lett.* **2000**, *41*, 8753–8758; b) S.-i. Tanaka, M. Takashina, H. Tokimoto, Y. Fujimoto, K. Tanaka, K. Fukase, *Synlett* **2005**, 2325–2328; c) J. D. C. Codée, L. H. Hossain, P. H. Seeberger, *Org. Lett.* **2005**, *7*, 3251–3254.

[6] a) A. A. H. Abdel-Rahman, E. Jonke, E. S. H. El Ashry, R. R. Schmidt, *Angew. Chem.* **2002**, *114*, 3100–3103; *Angew. Chem. Int. Ed.* **2002**, *41*, 2972–2974; b) D. Crich, P. Jayalath, *Org. Lett.* **2005**, *7*, 2277–2280; c) D. Crich, P. Jayalath, T. K. Hutton, *J. Org. Chem.* **2006**, *71*, 3064–3070.

[7] For examples, see: Refs. [3e,g,4,5a].

[8] H. Kunz, P. Wernig, M. Schultz, *Synlett* **1990**, 631–632.

[9] J. C. Lopez, B. Fraser-Reid, *J. Chem. Soc. Chem. Commun.* **1991**, 159–161.

[10] 3-*n*-Pentenoyl glycals were used for the synthesis of 2,3-unsaturated disaccharides: a) J. C. Lopez, B. Fraser-Reid, *J. Chem. Soc. Chem. Commun.* **1992**, 94–96; b) J. C. Lopez, A. M.

 © 2006 Wiley-VCH Verlag GmbH & Co. KGaA, Weinheim

Gomez, S. Valverde, B. Fraser-Reid, *J. Org. Chem.* **1995**, *60*, 3851 – 3858.
[11] K. Ikeda, J. Fukuyo, K. Sato, M. Sato, *Chem. Pharm. Bull.* **2005**, *53*, 1490 – 1493.
[12] D. Crich, M. Smith, Q. Tao, J. Picione, *Synthesis* **2001**, 323 – 326.
[13] For reviews, see: a) B. Fraser-Reid, U. E. Udodong, Z. Wu, H. Ottosson, J. R. Merritt, C. S. Rao, C. Roberts, R. Madsen, *Synlett* **1992**, 927 – 942; b) B. Fraser-Reid, R. Madsen in *Preparative Carbohydrate Chemistry* (Ed.: S. Hanessian), Marcel Dekker, New York, **1997**, pp. 339 – 356.

 © 2006 Wiley-VCH Verlag GmbH & Co. KGaA, Weinheim

Surface Chemistry

DOI: 10.1002/anie.200602666

Mechanically Induced Generation of Counterions Inside Surface-Grafted Charged Macromolecular Films: Towards Enhanced Mechanotransduction in Artificial Systems**

*Omar Azzaroni, Britta Trappmann, Patrick van Rijn, Feng Zhou, Bokyung Kong, and Wilhelm T. S. Huck**

Mechanical stresses modulate a variety of physiological functions, ranging from the detection of sound (hearing) to the growth of bone tissue. Physical forces or strains can activate mechanosensitive ion channels at the cell surface, alter the conformation of the extracellular matrix, or alter the function of tension-sensitive components of the cytoskeleton.[1] There is a significant research effort to discover how external mechanical forces regulate cell activity: from distortions of the cytoskeleton to the activation of gene expression and the synthesis of proteins.[2]

It is well-known that highly charged environments play an important role in the mechanical properties of biological tissues,[3,4] as is the case in articular cartilage where the compressive resistance is mainly due to electrostatic repulsive forces at the molecular level between highly charged chondroitin sulfate glycosaminoglycan chains.[5–8] The fundamental question central to the work reported here is if mechanical pathways can be exploited for manipulating chemical reactions[9,10] in confined environments and in particular how mechanical stresses can influence the chemical properties of thin polyelectrolyte films.

This initial study on model macromolecular systems to convert physical forces into chemical information aims to provide a design template for "smart" thin films whose response can be triggered by external mechanical stimuli.

Our thin polymer films consist of polyelectrolyte brushes, that is, charged polymers tethered at one end to the surface. At sufficiently high grafting densities in pure water the polymer chains are stretched away from the surface as a result of strong repulsion between the charges on the monomers. However, the addition of an electrolyte leads to screening of these charges and, as a consequence, to the collapse of the brushes.[11,12]

In seminal work, Klein and co-workers have shown that two surfaces coated with strong polyelectrolyte brushes exhibited significantly improved lubrication because of resistance of the brushes towards collapse.[13] The crucial observation we report here is that deliberate mechanical compression of strongly charged polyelectrolyte brushes in pure water should lead to a state where the microenvironment in the brush layer resembles the high ionic strength environment that would otherwise lead to collapse so as to minimize Coulombic repulsions between the charges on the brushes. To put this idea into practice we exploited the ionization of dye molecules immobilized inside polyelectrolyte brushes upon mechanical deformation of the surface-grafted polymer chains.

Polyelectrolyte brushes based on poly([2-methacroyloxy)ethyl]trimethylammonium chloride) (PMETAC; Figure 1) were synthesized using surface-initiated aqueous atom transfer radical polymerization (ATRP) from silane-initiator-modified glass slides following a previously reported procedure.[14–16] All the experimental details are described in the Supporting Information.

The brushes ($h \approx 20$ nm, "dry" thickness) were washed thoroughly with Milli-Q water to remove any excess salts, and subsequently placed in a 0.6 mM aqueous solution of bromothymol blue (BTB). BTB is known as a highly sensitive probe to monitor chemical and physical changes in biomembranes and proteins.[17] This dye changes its color at around pH 7, from a yellow (neutral form) to a blue (anionic form) state, which can be easily detected by UV/Vis spectroscopy.[18,19] Mechanical compression was accomplished by sandwiching the brush-coated glass slides between two slabs of cross-linked poly(dimethylsiloxane) (PDMS) and placing the assembly in a holder commonly used for IR experiments on liquids. Great care was taken to ensure that the brush-coated glass slides were never dried, since dehydration would inevitably lead to (irreversible) collapse of the brushes. The use of elastomeric PDMS is essential to ensure conformal contact with the brush surface and a homogeneous distribution of the load.[20,21] The screws on the cell were tightened to place the whole assembly under compression (up to approximately 0.1 MPa). Figure 2 shows the changes detected in the UV/Vis absorption spectra upon compression of the PMETAC/BTB assembly. The spectrum of BTB with no pressure applied shows the equilibrium population of both anionic and neutral species inside the hydrated (pH 7) brush.

[*] Dr. O. Azzaroni, B. Trappmann, P. van Rijn, Dr. F. Zhou, B. Kong, Dr. W. T. S. Huck
Melville Laboratory for Polymer Synthesis
Department of Chemistry
University of Cambridge
Lensfield Rd., Cambridge CB21EW (UK)
Fax: (+44) 1223-334-866
E-mail: wtsh2@cam.ac.uk

[**] Funding from a Studienstiftung des deutschen Volkes Scholarship (B.T.), a Marie Curie Research Fellowship (O.A.), and a DuPont Young Professor Award (W.T.S.H.) is acknowledged.

Supporting information for this article is available on the WWW under http://www.angewandte.org or from the author.

InterScience
© 2006 Wiley-VCH Verlag GmbH & Co. KGaA, Weinheim

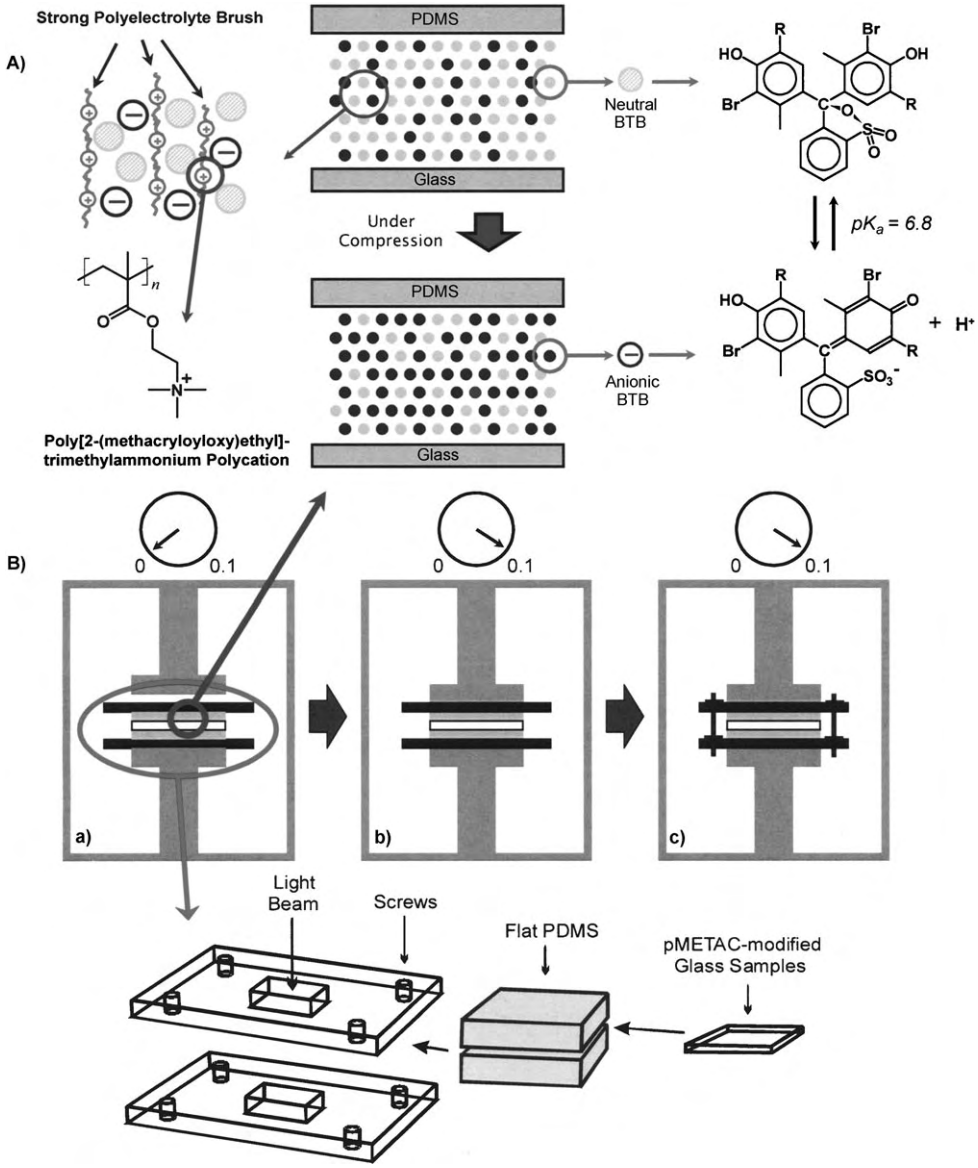

Figure 1. A) Simplified depiction of the variation in the population of neutral (light circles) and anionic (dark circles) bromothymol blue (BTB) species inside PMETAC brush films upon compression. Also depicted in the schematic representation are the chemical structures corresponding to the cationic polyelectrolyte brush (left) and the neutral and anionic form of the BTB dye (right). B) Schematic representation of the experimental setup used to compress the polyelectrolyte brushes. The IR cell containing the PDMS-sandwiched PMETAC-coated glass was introduced into a small laboratory press (a). The sandwiched glass slide was compressed at 0.1 MPa (b). Thereafter, the sandwiched experimental arrangement was fixed under compression using screws (c). The bottom part of the Figure depicts in detail the sandwiched glass slide introduced in the IR cell.

It should be noted that the strongly charged environment of the brush always leads to a certain additional ionization of BTB, partly as a result of the formation of a complex between the quaternary ammonium (QA*) groups and the sulfonate moieties in the dye molecules.[22]

However, a significant and easily detectable increase in the absorption at 625 nm (anionic form) was clearly observed when pressure was applied (Figure 2a). This change was accompanied by a decrease in the absorption at 430 nm (neutral form).

A similar trend upon compression is observed when starting from a different population distribution of anionic and neutral species (namely, placing the dye-loaded brushes in a solution at a different pH value). Compressing the BTB-loaded hydrated PMETAC brush at pH 4 again evidences the enhancement of the anionic form at 625 nm, together with a decrease in the absorption of the protonated dye at 430 nm (Figure 2b).

This increase in the absorption at 625 nm upon compression is clearly related to an increase in the population of anionic BTB dye molecules inside the brush layer. In strong polyelectrolyte brushes, the charges strongly repel each other in pure water and mechanical compression of such brushes would not be possible, since the repulsive Coulombic interactions cannot be easily overcome. In our case, with the dye added to the brush layer, the mechanical stresses effectively result in a pressure-induced Coulombic imbalance, and the excess of repulsive Coulombic interactions are rapidly compensated and effectively screened through an increase in the population of counterions resulting from dissociation of the dye (Figure 2). In other words, the presence of the dye molecules allows the brushes "an easy way out", and instead of resisting mechanical compression, the brushes can now collapse in response to mechanical stress. From a chemistry point of view, the mechanical stress combined with the nanoconfinement inside the brush layer affects the chemical equilibrium of the BTB inside the brush and as a consequence its pK_a value. In the absence of any pressure the equilibrium situation can be simply described as Equation (1).

$$\begin{array}{lcl} \mathrm{BTB} \rightarrow & \mathrm{BTB^-} + \mathrm{H^+} & K_a = \dfrac{[\mathrm{H^+}][\mathrm{BTB^-}]}{[\mathrm{BTB}]} = \dfrac{C^2\alpha^2}{C(1-\alpha)} \\ C(1-\alpha) & C\alpha \quad\quad C\alpha & \end{array} \tag{1}$$

© 2006 Wiley-VCH Verlag GmbH & Co. KGaA, Weinheim

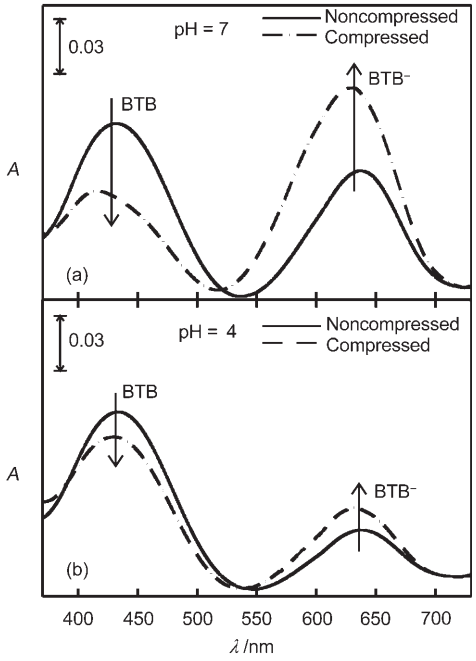

Figure 2. UV/Vis spectra corresponding to the compression experiments for BTB-loaded PMETAC brushes in a hydrated environment at different pH values: a) pH 7 and b) pH 4. Dotted and solid lines refer to spectra taken under compression and with no compression, respectively. The arrows indicate the direction of changes upon compression.

Here, K_a is the dissociation constant of the BTB dye, C is the formal concentration of the dye inside the brush, and α is the degree of dissociation at zero pressure. At 0.1 MPa the same equilibrium can be described as Equation (2),

$$\begin{array}{lcl} \mathrm{BTB} \rightarrow & \mathrm{BTB^-} + \mathrm{H^+} & K_a^{0.1\,\mathrm{MPa}} = \dfrac{[\mathrm{H^+}][\mathrm{BTB^-}]}{[\mathrm{BTB}]} = \dfrac{C^2\beta^2}{C(1-\beta)} \\ C(1-\beta) & C\beta \quad\quad C\beta & \end{array} \tag{2}$$

where $K_a^{0.1\,\mathrm{MPa}}$ and β are the dissociation constant and the degree of dissociation at 0.1 MPa, respectively.

Considering that a) the formal concentration (C) of the dye inside the brush remains the same, independent of pressure, and b) the concentration of the anionic dye species is approximately twice the original concentration upon compression, as derived from the change in the absorption of the anionic species at 625 nm (Figure 2a), $\beta \approx 2\alpha$ [Eq. (3)].

$$\frac{K_a}{K_a^{0.1\,\mathrm{MPa}}} = \frac{C^2\alpha^2}{C(1-\alpha)}\frac{C(1-\beta)}{C^2\beta^2} \approx \frac{C^2\alpha^2}{C(1-\alpha)}\frac{C(1-2\alpha)}{C^2(2\alpha^2)} \tag{3}$$

The UV/Vis spectra under zero pressure (Figure 2a) shows the distribution of species inside the brush under this condition. From the extinction coefficients (ε) of the neutral ($\varepsilon^N = 1.82\times10^4\,\mathrm{M^{-1}\,cm^{-1}}$) and anionic ($\varepsilon^A = 3.75\times10^4\,\mathrm{M^{-1}\,cm^{-1}}$) species in solution we estimated a α value of approximately 0.23. In this case Equation (3) becomes Equation (4).

$$K_a^{0.1\,\mathrm{MPa}} = 5.9\,K_a \tag{4}$$

Equation (4) can also be expressed in terms of pK_a values [Eq. (5)].

$$\begin{aligned} -\log K_a^{0.1\,\mathrm{MPa}} &= -\log(5.9\,K_a) = -[\log 5.9 + \log K_a] \\ &= \mathrm{p}K_{a_a}^{0.1\,\mathrm{MPa}} = \mathrm{p}K_a - \log 5.9 = \mathrm{p}K_a - 0.77 \end{aligned} \tag{5}$$

This equation shows that the compression of the brush was transducted in a shift in the pK_a value of about 0.77, as derived from the increase in the population of the anionic form of the BTB dye. Further confinement of the macromolecular layer promotes an increase in the electrostatic repulsion between the QA^+ moieties thus triggering the formation of new ion pairs to overcome the Coulombic unbalance.

The change in absorption upon compression is irreversible; once the brushes collapse, the dye molecules do not revert to their precompression equilibrium. To explore the origin of the irreversibility we studied the conformational changes (brush height, h) occurring in the polymer layer prior to and after compression by using atomic force microscopy (AFM). To estimate h under different conditions we have performed AFM measurements on patterned PMETAC brushes in water (Figure 3a). By combining AFM imaging

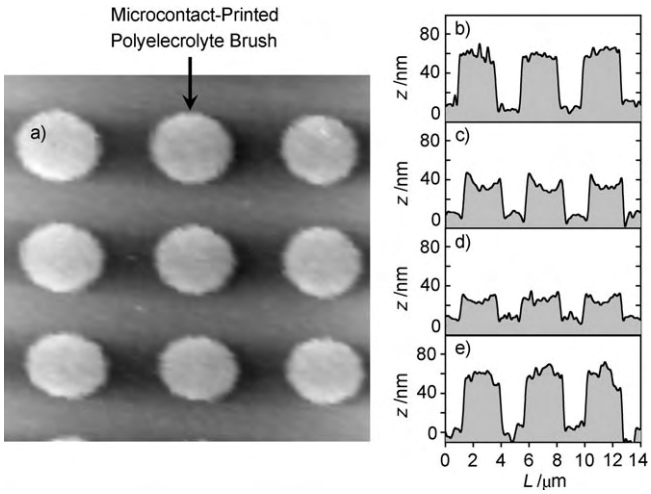

Figure 3. a) AFM image ($14\times14\ \mu m^2$) of patterned PMETAC brushes (dot shaped) on a gold substrate. Cross-sectional analyses derived from AFM imaging in water corresponding to: b) as-synthesized PMETAC brushes, c) BTB-loaded PMETAC brushes, d) BTB-loaded PMETAC brushes after compression, and e) as-synthesized PMETAC brushes after compression.

with patterned responsive brushes in liquids it is possible to obtain reliable information about the actual h value of the polymer brush in the liquid environment.[15,16] As expected, PMETAC when imaged in pure water shows an extended conformation ($h \approx 60$ nm) as a result of the strong repulsion between the like-charge monomers. Conversely, the dye-loaded PMETAC presents a less-extended conformation ($h \approx 45$ nm) when imaged under similar conditions. This fact is in agreement with the strong association (ion pairing) of the BTB dye with the cationic brush. After compressing the patterned samples, AFM of the samples in water revealed that

 © 2006 Wiley-VCH Verlag GmbH & Co. KGaA, Weinheim

the PMETAC brushes remain in a collapsed state ($h \approx 25$ nm). These results clearly support the irreversibility observed in the UV/Vis measurements. Deliberate compression triggers the formation of more ion pairs between the QA^+ moieties in the brushes and the SO_3^- groups of the dye. As previously reported in the literature, the formation of strong ion pairs is not easily reversed and the brushes remain in a strongly collapsed conformation.[15,23] This is the origin of the irreversibility observed in the system during the AFM and UV/Vis experiments. It must be noted that we carried out control experiments using PMETAC brushes without any dye. In these cases the brushes did revert to their original height after compression with a PDMS stamp (Figure 3e).

In conclusion, we have shown how mechanical forces can be channelled into shifting chemical equilibria by exploiting the properties of polyelectrolyte brushes. This approach is not limited to surfaces and could in principle be achieved in macroscopic systems, provided that nanoconfinement and compression of the polyelectrolytes can be ensured. This simple model, based on strong ion-pairing interactions of a dye probe within a surface-grafted charged macromolecular film, provides evidence that physical forces can be easily mechanotransducted into chemical signals. We believe that these results pave the way for the design of artificial (man-made) systems with mechanotransduction properties suitable for the fabrication of very sensitive and low-cost smart pressure-sensing devices involving simple read-out systems.

Received: July 5, 2006
Published online: October 10, 2006

Keywords: mechanochemistry · polycations · polymers · surface chemistry · thin films

[1] A. W. Orr, B. P. Helmke, B. R. Blackman, M. A. Schwartz, *Dev. Cell* **2006**, *10*, 11 – 20.
[2] C. J. Meyer, F. J. Alenghat, P. Rim, J. H.-J. Fong, B. Fabry, D. E. Ingber, *Nat. Cell Biol.* **2002**, *2*, 666 – 668.
[3] Y. Zhu, S. Granick, *Macromolecules* **2003**, *36*, 973 – 976.
[4] M. Benz, N. Chen, J. Israelachvili, *J. Biomed. Mater. Res. Part A* **2004**, *71*, 6 – 15.
[5] J. Moonsoo, A. J. Grodzinsky, *Macromolecules* **2001**, *34*, 8330 – 8339.
[6] J. Seog, D. Dean, A. H. K. Plaas, S. Wong-Palms, A. J. Grodzinsky, C. Ortiz, *Macromolecules* **2002**, *35*, 5601 – 5615.
[7] D. Dean, L. Han, C. Ortiz, A. J. Grodzinsky, *Macromolecules* **2005**, *38*, 4047 – 4049.
[8] J. Seog, D. Dean, B. Rolauffs, T. Wu, J. Genzer, A. H. K. Plaas, A. J. Grodzinsky, C. Ortiz, *J. Biomech. Eng.* **2005**, *38*, 1789 – 1797.
[9] M. K. Beyer, H. Clausen-Schaumann, *Chem. Rev.* **2005**, *105*, 2921 – 2948.
[10] J. M. J. Paulusse, R. P. Sijbesma, *Angew. Chem.* **2004**, *116*, 4560 – 4562; *Angew. Chem. Int. Ed.* **2004**, *43*, 4460 – 4462.
[11] J. Rühe, M. Ballauff, M. Biesalski, P. Dziezok, F. Grohn, D. Johannsmann, N. Houbenov, N. Hugenberg, R. Konradi, S. Minko, M. Motornov, R. R. Netz, M. Schmidt, C. Seidel, M. Stamm, T. Stephan, D. Usov, H. Zhang, *Adv. Polym. Sci.* **2004**, *165*, 79 – 150.
[12] Polymer Brushes: Synthesis, Characterization, Applications (Eds.: R. Advincula, W. J. Brittain, K. C. Caster, J. Rühe), Wiley, New York, **2004**.
[13] U. Raviv, S. Glasson, N. Kampf, J.-F. Gohy, R. Jerome, J. Klein, *Nature* **2003**, *425*, 163 – 165.
[14] V. L. Osborne, D. M. Jones, W. T. S. Huck, *Chem. Commun.* **2002**, 1838 – 1839.
[15] O. Azzaroni, S. E. Moya, T. Farhan, A. A. Brown, W. T. S. Huck, *Macromolecules* **2005**, *38*, 10192 – 10199.
[16] S. E. Moya, O. Azzaroni, T. Farhan, V. L. Osborne, W. T. S. Huck, *Angew. Chem.* **2005**, *117*, 4654 – 4657; *Angew. Chem. Int. Ed.* **2005**, *44*, 4578 – 4581.
[17] G. P. Gorbenko, *Biochim. Biophys. Acta* **1998**, *1370*, 107 – 118.
[18] P. M. Saikia, M. Bora, R. K. Dutta, *J. Colloid Interface Sci.* **2005**, *285*, 382 – 387.
[19] O. B. Miled, D. Grosso, C. Sanchez, J. Livage, *J. Phys. Chem. Solids* **2004**, *65*, 1751 – 1755.
[20] G. S. Ferguson, M. K. Chaudhury, G. B. Sigal, G. M. Whitesides, *Science* **1991**, *253*, 776 – 778.
[21] G. M. Grest, *Adv. Polym. Sci.* **1999**, *138*, 149 – 183.
[22] F. Quadrifoglio, V. Crescenzi, *J. Colloid Interface Sci.* **1971**, *35*, 447 – 459.
[23] M. Biesalski, D. Johannsmann, J. Rühe, *J. Chem. Phys.* **2004**, *120*, 8807 – 8814.

 © 2006 Wiley-VCH Verlag GmbH & Co. KGaA, Weinheim

Block Copolymers

DOI: 10.1002/anie.200602897

Control of Vesicular Morphologies through Hydrophobic Block Length**

*Tony Azzam and Adi Eisenberg**

Highly asymmetric amphiphilic block copolymers can self-assemble in selective solvents to form crew-cut aggregates of a wide range of morphologies, such as spherical micelles, rods, vesicles, and others.[1–4] In these aggregates, the long hydrophobic block forms either the core in micelles and rods, or the wall in bilayer structures, whereas the short hydrophilic block forms the corona. A number of research groups have studied block copolymer aggregates of various morphologies in the past.[5,6] Among these morphologies, vesicles and also liposomes made of phospholipids, are of great interest owing to their potential applications as encapsulation agents, particularly in the fields of biomedicine and drug delivery.[7] However, the stability of liposomes has been a concern owing to the high mobility of their lipidic components under

[*] T. Azzam, Prof. A. Eisenberg
Department of Chemistry
McGill University
801 Sherbrooke Street West, Montreal, PQ, H3A2K6 (Canada)
Fax: (+1) 514-398-3797
E-mail: adi.eisenberg@mcgill.ca

[**] We thank the Natural Science and Engineering Research Council of Canada (NSERC) for the support of this work.

Supporting information for this article is available on the WWW under http://www.angewandte.org or from the author.

© 2006 Wiley-VCH Verlag GmbH & Co. KGaA, Weinheim

physiological conditions; therefore, many efforts have been devoted to the stabilization of these structures by cross-linking or by the addition of polymeric stabilizers to the liposomes.[8] Polymeric vesicles, on the other hand, are robust structures and are very stable in aqueous solution.[6] These vesicles can be either equilibrium structures under certain conditions or, under others, kinetically trapped during preparation.[9]

To explore block copolymer vesicles for many potential applications, the control of vesicular characteristics, such as size, wall thickness, and inner volume, are of great importance. It is assumed that the parameters that control the morphologies of the aggregates, that is, core chain stretching, interfacial tension, and corona repulsion, are also responsible for the thermodynamic control of the vesicular architecture. Solution properties such as solvent composition, presence of additives (e.g. salts, acids, or bases) and water content were also shown to have a strong influence on vesicle size. For example, the addition of a base during the preparation of vesicles containing acrylic acid in the corona decreases the size of the vesicles owing to an increase in the electrostatic repulsion among the corona chains. The addition of acids or salts, on the other hand, increases the vesicle size owing to the screening of the electrostatic repulsion among the corona chains.[2,10,11]

Recently, the thermodynamic stabilization mechanism of diblock copolymer vesicles was elucidated.[12–14] It showed that the curvature in block copolymer vesicles is stabilized by preferential segregation of short hydrophilic blocks to the inside of the vesicles and the long blocks to the outside of the vesicle bilayer. The repulsion among the longer corona chains is greater than that among the shorter ones. Therefore, segregation of the hydrophilic blocks by length, which allows the formation of asymmetric lamellae, stabilizes the curvature of the vesicles.

The polystyrene-*block*-poly(acrylic acid) (PS-b-PAA) block copolymers, in all these studies, were synthesized by sequential anionic polymerization, as described elsewhere.[15,16] First, the PS block was prepared, followed by the addition of the *tert*-butylacrylate (*t*BA) monomer to form the PS-b-PtBA diblock copolymer. Finally, hydrolysis led to the corresponding amphiphilic diblock, PS-b-PAA. This method allows the formation of a PS block of a fixed length with varying PAA blocks. Although such block copolymers prepared by anionic polymerization are well defined with a polydispersity index (PI) of 1.1 or even lower, this method is technically challenging in that it is accompanied by the formation of homopolystyrene, which requires extensive purification.

Block copolymers needed for the exploration of the scaling relationships between the length of the acrylic acid block (in polymers containing a constant PS block length) and various vesicular parameters, such as size and wall thickness, are relatively easy to prepare by anionic polymerization, as described above. On the other hand, scaling relationships between the length of the styrene block (in polymers containing a PAA block of constant length) and various vesicular parameters have not been investigated systematically owing to the lack of appropriate synthetic methods for the preparation of such polymers. Herein we report on a new approach to the synthesis of block copolymers with a constant PAA block attached to PS blocks of various lengths as well as on trends in vesicle sizes and wall thicknesses as a function of the PS block length.

The PAA-b-PS block copolymers in this study were prepared by atom-transfer radical polymerization (ATRP).[17] Poly(*tert*-butyl acrylate) macroinitiators (PtBA-Br) with varying molecular weights and relatively low polydispersities ($PI < 1.18$) were prepared and used as precursors for the formation of PS blocks. By changing the [styrene]/[PtBA-Br] feed ratio, it was possible to synthesize well-defined block copolymers with a fixed PtBA block length and varying PS block lengths with relatively low PI values (see Supporting Information). Complete removal of the *tert*-butyl protecting groups of the PtBA block was accomplished by acid catalysis to obtain the corresponding amphiphilic blocks (see Supporting Information).[15]

It was shown, in a previous study, that vesicles made from PS_{310}-b-PAA_{28} copolymers in dioxane are relatively large and polydisperse (450 ± 160 nm). Increasing the THF content in the THF/dioxane solvent mixture results in the formation of smaller vesicles; further increase in the THF content leads to mixtures of vesicles and spheres, and finally, in pure THF, spheres are formed (Table 1).[4,11] On the basis of these

Table 1: Details of the morphologies obtained from various PAA-b-PS block copolymers.

Block copolymer[a]	PAA content [mol%][b]	Dominant morphology[c]	Average diameter [nm] in dioxane[d]		in dioxane/THF (3:1)[d]	
			TEM[e]	DLS[f]	TEM	DLS
PAA_{47}-b-PS_{670}	7	LCV	0.2–5 μm	ND	1–5 μm	ND
PAA_{47}-b-PS_{435}	9.8	V	340±150	450	290±120	420
PAA_{47}-b-PS_{370}	11.3	V	420±150	410	200±105	310
PAA_{47}-b-PS_{355}	11.7	V	300±120	300	150±75	395
PAA_{47}-b-PS_{310}	13.3	V	116±19	150	108±23	148
PAA_{47}-b-PS_{275}	14.6	V	94±16	130	100±20	140
PAA_{47}-b-PS_{250}	15.9	V	96±17	124	75±10	108
PAA_{47}-b-PS_{200}	19.3	M	20±2	45	20±2	45
PAA_{34}-b-PS_{325}	9.5	V	270±110	415	370±130	420
PAA_{34}-b-PS_{240}	12.5	V	180±85	280	135±60	185
PAA_{34}-b-PS_{190}	15.3	V	105±22	144	85±15	120

[a] Block copolymer composition (see Supporting Information). [b] Calculated by using the following equation: PAA [mol%] = $DP_{PtBA}/DP_{tot} \times 100$, where DP_{PtBA} is the average degree of polymerization of the PtBA block and DP_{tot} is the average total degree of polymerization of both blocks together. [c] Dominant morphology as observed by transmission electron microscopy (TEM). LCV = large compound vesicles, V = vesicles, and M = spherical micelles. [d] Solvent mixture used to dissolve the copolymers before self-assembly. [e] Average diameter of the vesicles/micelles determined by TEM in nm unless stated otherwise. [f] Average diameter of the vesicles/micelles determined by dynamic light scattering (DLS; see Supporting Information). ND = not determined.

 © 2006 Wiley-VCH Verlag GmbH & Co. KGaA, Weinheim

findings and to investigate the effect of the relative block lengths on vesicle sizes, all aggregates in this study were prepared in pure dioxane or in a dioxane/THF (3:1) mixture. Usually, large polydisperse vesicles are obtained under these conditions and, for the range of block lengths used in this study, no spherical or cylindrical micelles are seen (see Supporting Information).

Selective TEM images of the vesicles obtained from the PAA_{47}-b-PS_n series are shown in Figure 1. Large compound

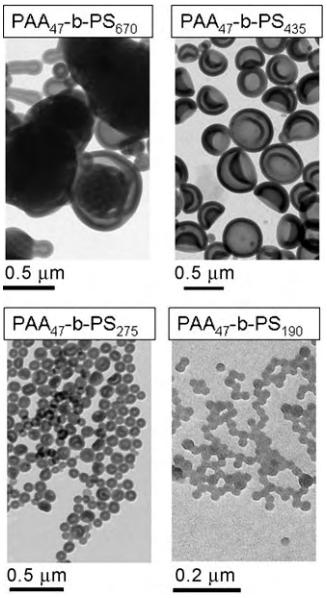

Figure 1. Selective TEM images of vesicles prepared from the PAA_{47}-b-PS_n block copolymer series. Vesicles were prepared from copolymer (1 wt%) in dioxane with a 50 wt% final water content (see Supporting Information). The full TEM images of all the PAA_{47}-b-PS_n block copolymers in the series can be found in the Supporting Information.

vesicles (LCVs) of an average size of 200 nm to a few microns were the predominant morphology of PAA_{47}-b-PS_{670}.[10,18] Vesicles made from PAA_{47}-b-PS_{435} (9.8 mol% PAA) and PAA_{47}-b-PS_{370} (11.3 mol% PAA) in dioxane were found to be large and polydisperse with an average diameter of 340 ± 150 nm and 420 ± 150 nm and a wall thickness of 42 ± 3 nm and 36 ± 4 nm, respectively. A shorter PS block, on the other hand (i.e. PAA_{47}-b-PS_{310}, 13.3 mol% PAA) resulted in a drastic decrease in vesicle size and a relatively narrow size distribution (116 ± 19 nm) and wall thickness (28 ± 2 nm). PAA_{47}-b-PS_{275} (14.6 mol% PAA) and PAA_{47}-b-PS_{248} (15.9 mol% PAA) also formed relatively small and narrowly dispersed vesicles with a diameter of 94 ± 16 and 96 ± 17 nm and a wall thickness of 27 ± 3 and 23 ± 2 nm, respectively. In contrast, when a relatively short PS block was used (PAA_{47}-b-PS_{200}, 19.3 mol% PAA), spherical micelles of 20 ± 2 nm average diameter were observed in the complete absence of vesicles. At a very short PS block length, the PAA coil dimensions become so large that packing into anything other than spherical micelles is not feasible.[1] A similar trend was observed when a shorter PAA block was involved (see Supporting Information). PAA_{34}-b-PS_{325} (9.5 mol% PAA) and PAA_{34}-b-PS_{240} (12.5 mol% PAA) yielded large and polydisperse vesicles of a diameter of 270 ± 110 nm and 177 ± 85 nm and a wall thickness of 39 ± 4 nm and 22 ± 2 nm, respectively. PAA_{34}-b-PS_{190} (15.3 mol% PAA), on the other hand, showed relatively small and narrowly dispersed vesicles with a 104 ± 22-nm diameter and a 20 ± 2-nm wall thickness. As can be clearly seen for both block copolymer series (PAA_{47}-b-PS_n and PAA_{34}-b-PS_n), vesicles made from copolymers with a PAA content of less than 12% showed a tendency to produce large and polydisperse vesicles, whereas those made from a PAA content of greater than 13% showed small and narrowly dispersed ones (see Table 1 and Supporting Information). The inverse relationship between size and polydispersity was explained by the fact that the interfacial area of vesicles of a small size is strongly size dependent, which induces a narrow size distribution. The interfacial area of large vesicles, on the other hand, is weakly size dependent and therefore a wide distribution in sizes is observed.[13] The inverse relationship between the hydrophilic block length and vesicle size was reported by Choucair et al. for PS-b-PAA diblock copolymers[11] and by Zhou and Yan for hyperbranched multiarm copolymers.[19] A similar trend in vesicle sizes was observed with dynamic light scattering (DLS) as shown in Table 1. However, as DLS is more sensitive to large aggregates, the sizes and polydispersity of vesicles obtained from TEM only were used for the statistical analysis.

A plot of the relationship between the average wall thickness of the vesicles made from the PAA_{47}-b-PS_n series versus the square root of the degree of polymerization of the styrene block ($\sqrt{N_{st}}$) is shown in Figure 2a. The average unperturbed (freely jointed) end-to-end distance ($l\sqrt{N}$) of a C–C polymer chain is equal to the length of one repeat unit ($l \approx 2.5$ Å) multiplied by the square root of the number of repeating units ($\sqrt{N}$). As can be clearly seen from Figure 2a, a linear fit ($r^2 = 0.986$) was obtained when $\sqrt{N_{st}}$ was plotted against the experimental average wall thickness ($d \pm \sigma$). Surprisingly, when N_{st} itself was plotted against the average wall thickness, a linear fit ($r^2 = 0.987$) was also obtained (Figure 2b). Although the unperturbed end-to-end distance (i.e. $l\sqrt{N_{st}}$) is more closely related to the experimental thickness of the vesicle walls multiplied by two (because they are bilayers), the results clearly show that the wall thickness, within the range of variables shown here, can also be related to the number of the repeat units. As the range of wall thicknesses in this study is narrow, it is impossible to distinguish, on a statistical basis, between the two plots of Figure 2a and b. Note that the quality of the fit in Figure 2 became poor when the values of the wall thicknesses of the PAA_{34}-b-PS_n series were combined with those for the PAA_{47}-b-PS_n series ($r^2 = 0.8$). The wall thickness of vesicles is clearly a function of both blocks (PS and PAA), and not only a function of the PS block length alone. A direct correlation with the PS block length is reasonable only when a constant PAA block is used (Figure 2a and b).

Zhang, Barlow, and Eisenberg showed empirically that the diameter of spherical micelles prepared from PS-b-PAA block copolymers could be correlated with $N_{st}^{0.4} N_{aa}^{-0.15}$, where N_{st} and N_{aa} are the degree of polymerization of styrene and acrylic acid blocks, respectively.[20,21] Figure 2c gives a plot of the average wall thickness (open circles) of all the vesicles

 © 2006 Wiley-VCH Verlag GmbH & Co. KGaA, Weinheim

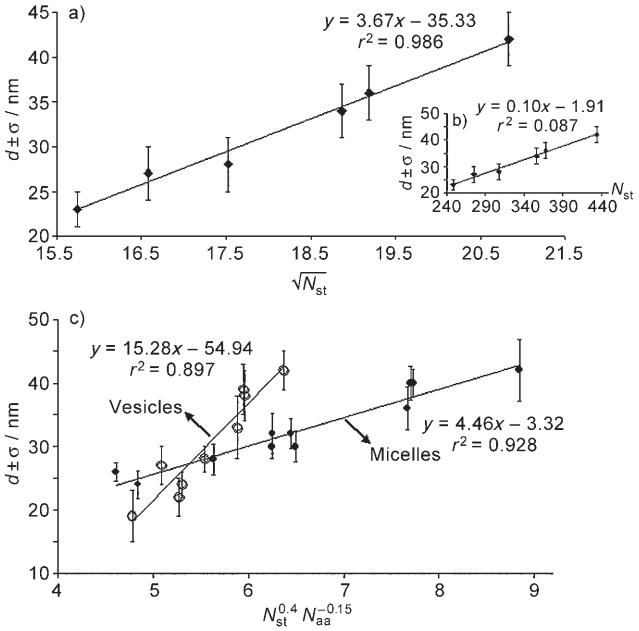

Figure 2. Average wall thickness of vesicles made from the PAA_{47}-b-PS_n block copolymer series versus a) the square root of the degree of polymerization of styrene ($\sqrt{N_{st}}$) and b) the degree of polymerization of styrene (N_{st}). The polymer concentration was fixed to 1 wt% in dioxane/THF (3:1 w/w) with a final water addition of 50 wt%. The average wall thickness was calculated from at least 300 measurements of each sample. c) Plot of average wall thickness of vesicles prepared from the PAA_{47}-b-PS_n and PAA_{34}-b-PS_n series (open circles) and the average diameter of micelles (filled circles) versus $N_{st}^{0.4}N_{aa}^{-0.15}$ for different block copolymers. N_{st} and N_{aa} are the degree of polymerization of styrene and acrylic acid, respectively, in a given block copolymer. In parts a and b, *d* represents the vesicle-wall thickness; in part c, *d* represents either the vesicle-wall thickness or the micelle diameter. σ represents the standard deviation. Linear fits to the data are given.

(from both the PAA_{47}-b-PS_n and PAA_{34}-b-PS_n series) versus $N_{st}^{0.4}N_{aa}^{-0.15}$ of the block copolymers. A plot showing the diameter of spherical micelles (filled circles) versus $N_{st}^{0.4}N_{aa}^{-0.15}$ is also incorporated in Figure 2c. The micelles of the broad range of sizes shown in Figure 2c were previously prepared and characterized from a wide range of PS-b-PAA diblock copolymers that were prepared by anionic polymerization.[20] As can be seen from Figure 2c, the wall thicknesses of the vesicles have a different slope compared with that obtained for the diameter of the micelles. Unlike the plot for micelles, however, the higher slope that was obtained for the vesicles indicates that the wall thickness is more sensitive to $N_{st}^{0.4}N_{aa}^{-0.15}$ and therefore minor changes in the PAA/PS block length ratio result in greater changes in the wall thickness than in the diameter of the spherical micelles. Notably, the $N_{st}^{0.4}N_{aa}^{-0.15}$ relation is empirical and was determined by trial and error to fit the diameter of micelles based on PS-b-PAA copolymer. Different power laws have been proposed for other micellar systems.[22] It is therefore not surprising that a different scaling relationship has also been found for vesicle wall thicknesses.[23]

In conclusion, vesicles are of great interest for potential applications in drug delivery, encapsulation, cosmetics, and many other areas. Small vesicles with a narrow size distribution can be targeted for applications that involve size limitations (e.g. membrane penetration), whereas large vesicles have an increased capacity for encapsulation. In this study, a facile approach to the synthesis of the series of PAA-b-PS block copolymers has been developed. The block copolymer series with a PAA block of a constant length and PS block of varying lengths enabled a systematic study of the effect of PAA/PS block ratio on the vesicle sizes as well as on the wall thicknesses. This new synthetic approach may be adapted for the synthesis of a wide range of amphiphilic block copolymers. Through this synthetic route, the hydrophilic block is controlled in size and polydispersity, whereas the hydrophobic block is varied. Although the size of vesicles can be manipulated by many parameters (solvent composition, concentration, water content, additives, etc.),[11–13,24] these variables are of great complexity and their effects are hard to understand. The present study shows an easy alternative for the preparation of PS-b-PAA amphiphilic block copolymers with the exclusive formation of vesicles in aqueous solution. This method can be extended to the preparation of other AB amphiphilic block copolymers in which the hydrophilic block is kept constant and the hydrophobic block length is varied systematically.

Received: July 19, 2006
Published online: October 10, 2006

Keywords: block copolymers · hydrophobic effect · polymerization · self-assembly · vesicles

[1] L. Zhang, A. Eisenberg, *Science* **1995**, *268*, 1728.
[2] L. Zhang, K. Yu, A. Eisenberg, *Science* **1996**, *272*, 1777.
[3] L. Zhang, C. Bartels, Y. Yu, H. Shen, A. Eisenberg, *Phys. Rev. Lett.* **1997**, *79*, 5034; G.-e. Yu, A. Eisenberg, *Macromolecules* **1998**, *31*, 5546; N. S. Cameron, M. K. Corbierre, A. Eisenberg, *Can. J. Chem.* **1999**, *77*, 1311; H. Shen, A. Eisenberg, *Angew. Chem.* **2000**, *112*, 3448; *Angew. Chem. Int. Ed.* **2000**, *39*, 3310; D. E. Discher, A. Eisenberg, *Science* **2002**, *297*, 967.
[4] Y. Yu, A. Eisenberg, *J. Am. Chem. Soc.* **1997**, *119*, 8383.
[5] J. C. M. van Hest, D. A. P. Delnoye, M. W. P. L. Baars, M. H. P. van Genderen, E. W. Meijer, *Science* **1995**, *268*, 1592; J. P. Spatz, S. Mössmer, M. Möller, *Angew. Chem.* **1996**, *108*, 1673; *Angew. Chem. Int. Ed. Engl.* **1996**, *35*, 1510; J. Ding, G. Liu, *Macromolecules* **1997**, *30*, 655; G. Liu, *Curr. Opin. Colloid Interface Sci.* **1998**, *3*, 200; J. Massey, K. N. Power, I. Manners, M. A. Winnik, *J. Am. Chem. Soc.* **1998**, *120*, 9533; S. A. Jenekhe, X. L. Chen, *Science* **1998**, *279*, 1903; J. J. L. M. Cornelissen, M. Fischer, N. A. J. M. Sommerdijk, R. J. M. Nolte, *Science* **1998**, *280*, 1427; F. Caruso, R. A. Caruso, H. Mohnwald, *Science* **1998**, *282*, 1111; A. Harada, K. Kataoka, *Science* **1999**, *283*, 65; K. Fischer, M. Gerle, M. Schmidt, *Polym. Mater. Sci. Eng.* **1999**, *80*, 133.
[6] B. M. Discher, Y.-Y. Won, D. S. Ege, J. C. M. Lee, F. S. Bates, D. E. Discher, D. A. Hammer, *Science* **1999**, *284*, 1143.
[7] M. Rosoff, *Vesicles* (Ed.: M. Rosoff), Marcel Dekker, New York, **1996**; N. M. Correa, Z. A. Schelly, *Langmuir* **1998**, *14*, 5802; A. V. Kabanov, T. K. Bronich, V. A. Kabanov, K. Yu, A. Eisenberg, *J. Am. Chem. Soc.* **1998**, *120*, 9941; H. B. Dastani, K. K. Singh, *Indian J. Pharm. Sci.* **1999**, *61*, 135; G. Gregoriadis, *Liposomes as Drug Carriers: Recent Trends and Progress* (Ed.: G. Gregoriadis), Wiley, Chichester, **1988**; B. M. Discher, D. A. Hammer, F. S. Bates, D. E. Discher, *Curr. Opin. Colloid Interface*

 © 2006 Wiley-VCH Verlag GmbH & Co. KGaA, Weinheim

Sci. **2000**, *5*, 125; M. Antonietti, S. Foerster, *Adv. Mater.* **2003**, *15*, 1323; S.-S. Feng, S. Chien, *Chem. Eng. Sci.* **2003**, *58*, 4087; E. Bourgeat-Lami, *Surfactant Sci. Ser.* **2003**, *115*, 189; P. Walde, *Encycl. Nanosci. Nanotechnol.* **2004**, *9*, 43; S. Takeoka, *Keio Univ. Int. Symp. Life Sci. Med.* **2005**, *13*, 35; S. Sofou, J. L. Thomas, *Handb. Nanostruct. Biomater. Their Appl. Nanobiotechnol.* **2005**, *2*, 437; H. A. E. Benson, *Curr. Drug Delivery* **2005**, *2*, 23; D. M. Vriezema, M. C. Aragones, J. A. A. W. Elemans, J. J. L. M. Cornelissen, A. E. Rowan, R. J. M. Nolte, *Chem. Rev.* **2005**, *105*, 1445.

[8] H. Ringsdorf, B. Schlarb, J. Venzmer, *Angew. Chem.* **1988**, *100*, 117; *Angew. Chem. Int. Ed. Engl.* **1988**, *27*, 113; W. Spevak, J. O. Nagy, D. H. Charych, M. E. Schaefer, J. H. Gilbert, M. D. Bednarski, *J. Am. Chem. Soc.* **1993**, *115*, 1146; M. Ladika, T. E. Fisk, W. W. Wu, S. D. Jons, *J. Am. Chem. Soc.* **1994**, *116*, 12093; D. H. Charych, J. O. Nagy, W. Spevak, M. D. Bednarski, *Science* **1993**, *261*, 585; J. Stavans, *Phys. A* **2002**, *306*, 368; A. A. Gabizon, *Cancer Invest.* **2001**, *19*, 424; A. A. Gabizon, *J. Drug Targeting* **2002**, *10*, 535; F. Martin, T. Huang, *Drugs Pharm. Sci.* **2003**, *126*, 689; F. J. Martin, T. Huang, *Drug Delivery Technol.* **2003**, *3*, 66; S. Zalipsky, N. Mullah, M. Qazen, *Methods Enzymol.* **2004**, *387*, 50.

[9] H. Shen, A. Eisenberg, *J. Phys. Chem. B* **1999**, *103*, 9473; H. Shen, A. Eisenberg, *Macromolecules* **2000**, *33*, 2561.

[10] L. Zhang, A. Eisenberg, *Macromolecules* **1996**, *29*, 8805.

[11] A. Choucair, C. Lavigueur, A. Eisenberg, *Langmuir* **2004**, *20*, 3894.

[12] L. Luo, A. Eisenberg, *J. Am. Chem. Soc.* **2001**, *123*, 1012.

[13] L. Luo, A. Eisenberg, *Langmuir* **2001**, *17*, 6804.

[14] L. Luo, A. Eisenberg, *Langmuir* **2002**, *18*, 1952.

[15] J. P. Hautekeer, S. K. Varshney, R. Fayt, C. Jacobs, R. Jerome, P. Teyssie, *Macromolecules* **1990**, *23*, 3893.

[16] X. F. Zhong, S. K. Varshney, A. Eisenberg, *Macromolecules* **1992**, *25*, 7160.

[17] J.-S. Wang, K. Matyjaszewski, *Macromolecules* **1995**, *28*, 7572; K. Matyjaszewski, M. Teodorescu, P. J. Miller, M. L. Peterson, *J. Polym. Sci. Part A* **2000**, *38*, 2440; S. C. Hong, H.-J. Paik, K. Matyjaszewski, *Macromolecules* **2001**, *34*, 5099; N. V. Tsarevsky, T. Sarbu, B. Goebelt, K. Matyjaszewski, *Macromolecules* **2002**, *35*, 6142; Y. Inoue, K. Matyjaszewski, *Macromolecules* **2004**, *37*, 4014; M. Li, N. M. Jahed, K. Min, K. Matyjaszewski, *Macromolecules* **2004**, *37*, 2434; J.-F. Lutz, K. Matyjaszewski, *J. Polym. Sci. Part A* **2005**, *43*, 897; K. Min, H. Gao, K. Matyjaszewski, *J. Am. Chem. Soc.* **2005**, *127*, 3825; Y. Zhang, I. S. Chung, J. Huang, K. Matyjaszewski, T. Pakula, *Macromol. Chem. Phys.* **2005**, *206*, 33.

[18] K. Yu, A. Eisenberg, *Macromolecules* **1998**, *31*, 3509.

[19] Y. Zhou, D. Yan, *Angew. Chem.* **2004**, *116*, 5004; *Angew. Chem. Int. Ed.* **2004**, *43*, 4896.

[20] L. Zhang, R. J. Barlow, A. Eisenberg, *Polym. Mater. Sci. Eng.* **1995**, *72*, 178.

[21] L. Zhang, R. J. Barlow, A. Eisenberg, *Macromolecules* **1995**, *28*, 6055.

[22] R. Nagarajan, K. Ganesh, *Macromolecules* **1989**, *22*, 4312; S. Foerster, M. Zisenis, E. Wenz, M. Antonietti, *J. Chem. Phys.* **1996**, *104*, 9956.

[23] G. Battaglia, A. J. Ryan, *J. Am. Chem. Soc.* **2005**, *127*, 8757; H. Bermudez, A. K. Brannan, D. A. Hammer, F. S. Bates, D. E. Discher, *Macromolecules* **2002**, *35*, 8203.

[24] A. Choucair, A. Eisenberg, *Eur. Phys. J. E* **2003**, *10*, 37.

 © 2006 Wiley-VCH Verlag GmbH & Co. KGaA, Weinheim

P-Substituted Carbenes

DOI: 10.1002/anie.200603151

Cyclic Carbodiphosphorane–Diphosphinocarbene Thermal Interconversion**

Sebastien Marrot, Tsuyoshi Kato, Fernando P. Cossío, Heinz Gornitzka, and Antoine Baceiredo**

Ring constraints that are caused by bending and twisting of the normally linear allene group engender substantial strain and resultant kinetic reactivity.[1] The small cyclic cumulenes are extremely short-lived intermediates, and their unique electronic properties and reactivities are of particular interest.[1–3] These highly strained cyclic allenes lie close in energy to corresponding aryl carbenes[4] or aryl nitrenes,[5] for which photochemical or thermal interconversions have been well-studied experimentally and computationally (Scheme 1).[4–7]

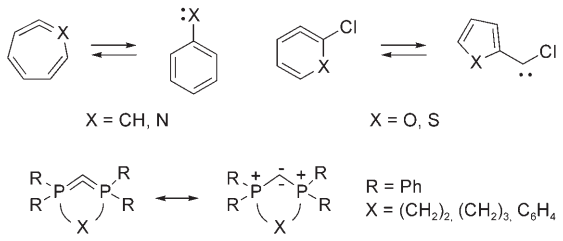

Scheme 1.

Cyclic carbodiphosphoranes can also be considered as heterocyclic allenes, but their ring strain should be much smaller owing to the polarized ylidic P–C double bonds.[8] Whereas the reduced ring size destabilizes these compounds, the critical ring size for stability seems to be five atoms.[9] Recently, we synthesized five-membered carbodiphosphorane **1a**, which exhibits unusual stability.[10] Herein, we report the unprecedented thermal ring contraction of the five-membered cyclic carbodiphosphorane **1a** into a four-π-electron four-membered 1,2λ^5-azaphosphete **2a** (Figure 1).[11] This rearrangement possibly takes place by an

[*] S. Marrot, Dr. T. Kato, Dr. H. Gornitzka, Dr. A. Baceiredo
Laboratoire Hétérochimie Fondamentale et Appliquée (UMR 5069)
Université Paul Sabatier
118, route de Narbonne, 31062 Toulouse Cedex 9 (France)
Fax: (+33) 5-6155-8204
E-mail: kato@chimie.ups-tlse.fr
baceired@chimie.ups-tlse.fr
Prof. F. P. Cossío
Departamento de Química Orgánica I
Universidad del País Vasco-Euskal Herriko Unibertsitatea
Facultad de Química
P.K. 1072, San Sebastián–Donostia (Spain)

[**] We are grateful to the CNRS for financial support of this work and to the FSE for a grant to S.M.

Supporting information for this article is available on the WWW under http://www.angewandte.org or from the author.

© 2006 Wiley-VCH Verlag GmbH & Co. KGaA, Weinheim

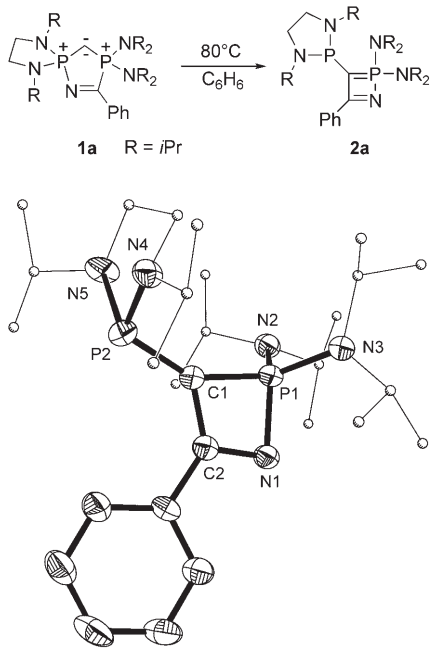

Figure 1. Ring contraction of **1a** and molecular structure of **2a**. Carbon atoms of substituents on the amino groups are simplified in the structure for clarity. Selected bond lengths [Å]: C1-C2 1.428(3), C2-N1 1.384(3), N1-P1 1.661(2), C1-P1 1.789(3). The mean deviation from the best C1-C2-N1-P1 plane is 0.005 Å.

interconversion between cyclic carbodiphosphorane **1a** and acyclic diphosphinocarbene **5a**.

The cyclic carbodiphosphorane **1a** transforms almost quantitatively and regioselectively to 1,2λ^5-azaphosphete **2a** when a solution of **1a** in benzene is heated at 80 °C for 60 hours. The ^{31}P and ^{13}C NMR spectroscopic data of **2a** are very similar to those of previously reported azaphosphetes.[11] This result is surprising because the thermal ring contraction of relatively small rings is quite rare.[12,13] It is important to note that the imine nitrogen atom in **2a** is now bonded to the bis(diisopropylamino)phosphino fragment, thus indicating that the ring contraction does not proceed by a simple P→C 1,2-migration of the imine carbon atom. The position of the nitrogen atom was spectroscopically confirmed by the chemical shift in the ^{31}P NMR spectrum ($\delta = 57.1$ ppm) and the large P,H coupling constant ($^3J_{PH} = 15$ Hz) typical for a tetravalent phosphorus atom.[14] The structure of **2a** was undoubtedly confirmed by a single-crystal X-ray diffraction analysis (Figure 1).[15]

In the course of careful analysis, we also observed a small amount (ca. 1 %) of *C*-phosphino phosphaalkene **3a** (^{31}P NMR: $\delta = 206.3$ and 105.3 ppm, $^2J_{PP} = 265$ Hz), which suggests the transient formation of diphosphinocarbene **5a** during the [3+2] retrocycloaddition (Scheme 2).[16]

To prove our hypothesis, diphosphinocarbene **5a** was generated from the corresponding diphosphinodiazomethane **4a** by thermolysis in toluene solution at 80 °C. As expected, in the absence of any trapping agent, phosphaalkene **3a** was isolated in nearly quantitative yield. In contrast, when the reaction was performed in the presence of benzonitrile (one equivalent), a mixture of **3a** (75 %), four-membered

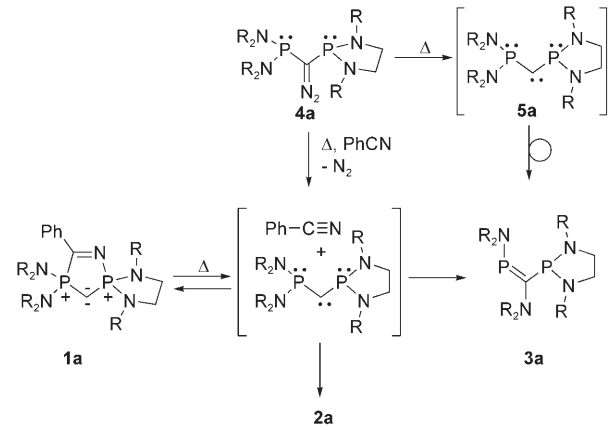

Scheme 2. Thermal interconversion between carbodiphosphorane **1a** and diphosphinocarbene **5a**.

heterocycle **2a** (20 %), and carbodiphosphorane **1a** (5 %) was obtained. As observed in the transformation of **1a**, only one regioisomer was detected for **2a**.[17] These observations are in agreement with the formation of carbene **5a** during the thermolysis of carbodiphosphorane **1a**, and their interconversion.

To confirm the transient formation of diphosphinocarbene **5a**, the thermal decomposition of **1a** was performed in the presence of one equivalent of *tert*-butyl isocyanide , which is known to react with phosphinocarbenes.[18] In this case, the reaction gave a mixture of the expected keteneimine **6a** (5 %) and four-membered ring **2a** (95 %; Scheme 3). In the presence of an excess of *tert*-butyl isocyanide, the reaction was not clean.

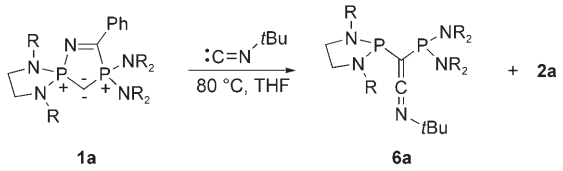

Scheme 3. Trapping reaction of diphosphinocarbene **5a** with *tert*-butyl isocyanide.

Density functional theory (DFT) calculations[19] were carried out to gain insight into the nature of the conversion of compound **1a** into **2a** (Scheme 1). Model compound **1b** (R = Me) was chosen to explore computationally its transformation into **2b**. The geometric and electronic properties of **1b** were calculated first. Our results indicate that **1b** exhibits the electronic properties that would be expected for an sp^2-hybridized singlet carbene possessing two additional electrons, as shown in Figure 2. In this figure it is shown that the usual frontier molecular orbitals of a singlet carbene become the HOMO−1 and HOMO in **1b**. Thus, the main atomic contributions to the HOMO−1 and HOMO in **1b** are similar to those of the carbon atom in the a_1-symmetric HOMO and b_2-symmetric LUMO of the sp^2-hybridized singlet methylene group, respectively. Moreover, the electrostatic potential that is projected onto the electron density of **1b** reveals a strong

 © 2006 Wiley-VCH Verlag GmbH & Co. KGaA, Weinheim

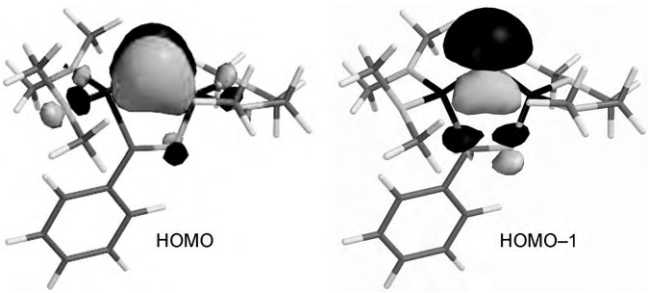

Figure 2. HOMO and HOMO−1 of **1b**.

negative potential around the central carbon atom of carbodiphosphorane **1**.

The reaction path that was found on the B3LYP/6-31 + G* potential-energy surface associated with the conversion of **1b** into **2b** is displayed in Figure 3. We have located the saddle point **TS1**, which is associated with a thermal [3+2] retrocycloaddition. This [3+2] retrocycloaddition step leads to one equivalent of benzonitrile and to carbene **5b** (R = Me). It is interesting to note that carbene **5b** and benzonitrile lie about 15 kcal mol^{-1} above **1b**, a result compatible with the observation of the formation of a small amount of **1a** when **5a** is allowed to react with one equivalent of PhCN (see above).

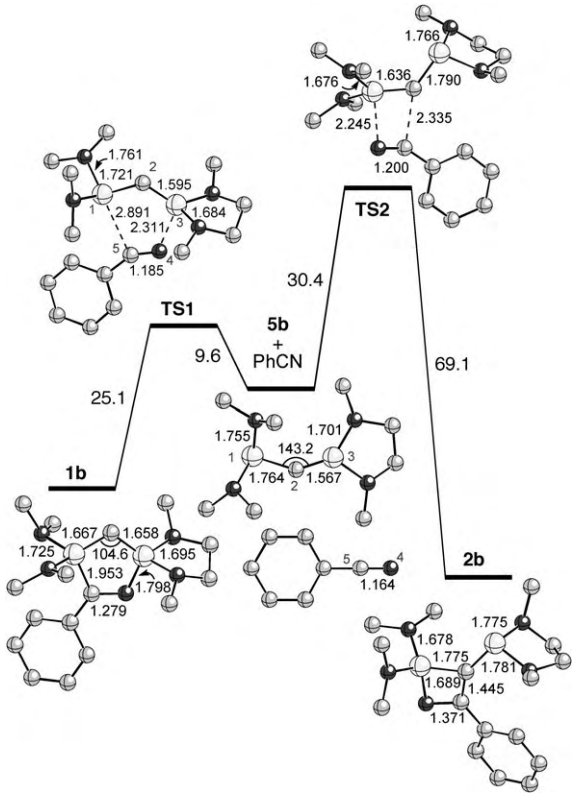

Figure 3. Chief geometric features of fully optimized (B3LYP/6-31 + G* level) structures involved in the conversion of **1b** into **2b**. Bond lengths and angles are given in Å and degrees, respectively. C gray, N black, P white. Hydrogen atoms have been omitted for clarity. Relative energies (B3LYP/6-31 + G* + ΔZPVE level) are given in kcal mol^{-1}.

Carbene **5b** can react in a formally [2+2] fashion via saddle point **TS2** to yield **2b**.[20] In this transition state, reactants interact in a suprafacial manner with a quite synchronous development of the C2−C5 and N4−P1 bonds. Natural bond orbital (NBO)[9] analysis of **TS2** reveals, however, a pseudopericyclic character for **TS2**, in which lone pairs, π bonds, and σ bonds interchange roles.[21]

In summary, our calculations are compatible with a retro-[3+2]/pseudo-[2+2] sequence in which carbenes of type **5** are involved, the whole process being exothermic by about 13 kcal mol^{-1}. As expected, the barrier in energy of the retro-[3+2] transformation is relatively small and even smaller than that of the subsequent cycloaddition. These theoretical results support our first hypothesis that the effect of high ring strain in **1** can be the driving force for this transformation to give a transient carbene **5**. Interestingly, the close energies between **1** and **5** and the small barrier also strongly support the unprecedented interconversion between two different types of divalent carbon species (dianionic and carbene): carbodiphosphorane **1a** and diphosphinocarbene **5a.** Further studies of the nature of this interconversion as well as the application of this new process for the preparation of original carbenes are in progress.

Experimental Section

Details of the experimental procedures are provided in the Supporting Information.

2a: White crystals. M.p. 71–73 °C; $^{31}P\{^1H\}$ NMR (C_6D_6, 81 MHz): $\delta = 57.1$, 76.3 ppm (AX system, $J_{PP} = 11.2$ Hz); ^{13}C NMR (C_6D_6, 75 MHz): $\delta = 22.2$ (d, $J_{CP} = 8.4$ Hz, CH_3), 22.7 (s, CH_3), 23.1 (d, $J_{CP} = 12.2$ Hz, CH_3), 23.6 (d, $J_{CP} = 2.4$ Hz, CH_3), 43.3 (d, $J_{CP} = 5.5$ Hz, NCH), 48.7 (d, $J_{CP} = 5.7$ Hz, NCH_2), 50.9 (d, $J_{CP} = 29.8$ Hz, NCH), 95.9 (dd, $J_{CP} = 40.0$ and 31.0 Hz, PCP), 127.6 (s, CH_{arom}), 130.0 (dd, $J_{PC} = 3.3$ and less than 1 Hz, CH_{arom}), 131.7 (dd, $J_{PC} = 3.3$ and less than 1 Hz, CH_{arom}), 137.8 (dd, $J_{CP} = 3.0$ and 49.8 Hz, C_{ipso}), 190.6 ppm (dd, $J_{CP} = 24.8$ and 33.2 Hz, C=N).

3a: Orange oil. $^{31}P\{^1H\}$ NMR (C_6D_6, 121 MHz): $\delta = 105.4$, 206.4 ppm (AX system, $J_{PP} = 264$ Hz); ^{13}C NMR (C_6D_6, 25 °C, 75 MHz): $\delta = 21.5$ (d, $J_{CP} = 6.8$ Hz, CH_3), 21.9 (d, $J_{CP} = 10.5$ Hz, CH_3), 24.1 (dd, $J_{CP} < 1$ Hz, CH_3), 24.1 (d, $J_{CP} = 7.6$ Hz, CH_3), 45.3 (dd, $J_{CP} = 3.2$ and 6.77 Hz, NCH_2), 46.7 (d, $J_{CP} = 5.1$ Hz, NCH), 50.0 (m, NCH), 168.1 ppm (d, $J_{CP} = 65.6$ and 82.6 Hz, PCP).

4a: Red oil. IR (THF): 2007 cm^{-1}; $^{31}P\{^1H\}$ NMR (C_6D_6, 121 MHz): $\delta = 53.2$, 106.2 ppm (AX system, $J_{PP} = 189$ Hz); ^{13}C NMR (C_6D_6, 75 MHz): $\delta = 22.3$ (dd, $J_{CP} = 8.6$ and less than 1 Hz, CH_3), 22.6 (dd, $J_{CP} = 8.6$ and 2.7 Hz, CH_3), 23.9 (d, $J_{CP} = 6.6$ Hz, CH_3), 24.6 (dd, $J_{CP} = 7.8$ and 2.64 Hz, CH_3), 46.4 (d, $J_{CP} = 7.9$ Hz, NCH_2), 47.7 (d, $J_{CP} = 12.2$ Hz, NCH), 48.6 ppm (d, $J_{CP} = 21.0$ Hz, NCH), signal for PCP was not observed.

6a: Orange oil. $^{31}P\{1H\}$ NMR (C_6D_6, 121 MHz): $\delta = 52.8$, 106.1 ppm (AX system, $J_{PP} = 249$ Hz); ^{13}C NMR (C_6D_6, 75 MHz): $\delta = 22.5$ (d, $J_{CP} = 11$ Hz, CH_3), 23.0 (dd, $J_{CP} = 2.8$ and 8.8 Hz, CH_3), 23.8 (d, $J_{CP} = 6.5$ Hz, CH_3), 24.8 (dd, $J_{CP} = 2.2$ and 7.6 Hz, CH_3), 30.5 (s, *t*Bu), 47.5 (s, CH), 47.6 (s, CH_2), 47.7 (s, CH), 50.1 (dd, $J_{CP} = 1.5$ and 22.2 Hz, CH), 56.8 (t, $J_{CP} = 1.9$ Hz, CH_3C), 60.4 (dd, $J_{CP} = 42.9$ and 70.1 Hz, PCP), 171.4 ppm (s, *t*BuNC).

Density functional theory (DFT)[22] calculations: All studies were performed at the B3LYP[23] level of theory as implemented in the Gaussian package[24] by using the 6-31 + G(d,f) basis set[25] to describe properly the significant negative charges present along the possible reaction coordinates. All stationary points were subjected to harmonic analysis. Transition structures showed only one imaginary

 © 2006 Wiley-VCH Verlag GmbH & Co. KGaA, Weinheim

frequency associated with nuclear motion along the reaction coordinate under study as verified by intrinsic reaction coordinate (IRC) computations. Total energies were computed, including zero-point vibrational energy (ZPVE) terms.[26] Bond orders and charges were computed by mean of the NBO method.[27]

Received: August 3, 2006
Published online: October 13, 2006

Keywords: carbenes · cycloaddition · density functional calculations · phosphorus · ring contraction

[1] P. J. Richard, *Chem. Rev.* **1989**, *89*, 1111 – 1124.
[2] a) H. Hopf, H. Berger, G. Zimmermmann, U. Nüchter, P. G. Jones, I. Dix, *Angew. Chem.* **1997**, *109*, 1236 – 1238; *Angew. Chem. Int. Ed. Engl.* **1997**, *36*, 1187 – 1190; b) M. Christl, M. Braun, G. Müller, *Angew. Chem.* **1992**, *104*, 471 – 474; *Angew. Chem. Int. Ed. Engl.* **1992**, *31*, 473 – 476.
[3] a) B. Engels, J. C. Schöneboom, A. F. Münster, S. Groetsch, M. Christl, *J. Am. Chem. Soc.* **2002**, *124*, 287 – 297; b) S. Martín-Santamaría, B. lavan, H. S. Rzepa, *Chem. Commun.* **2000**, 1089 – 1090; c) W. Pan, P. B. Shevlin, *J. Am. Chem. Soc.* **1997**, *119*, 5091 – 5094.
[4] a) M. L. McKee, P. B. Shevlin, M. Zottola, *J. Am. Chem. Soc.* **2001**, *123*, 9418 – 9425; b) B. Engels, J. Schöneboom, A. F. Münster, S. Groetsch, M. Christl, *J. Am. Chem. Soc.* **2002**, *124*, 287 – 297; c) C. M. Geise, C. M. Hadad, F. Zheng, P. B. Shevlin, *J. Am. Chem. Soc.* **2002**, *124*, 355 – 364; d) A. F. Nikitina, R. S. Sheridan, *Org. Lett.* **2005**, *7*, 4467 – 4470.
[5] a) M. L. McKee, P. B. Shevlin, M. Zottola, *J. Am. Chem. Soc.* **2004**, *126*, 237 – 249; b) P. Bednarek, C. Wentrup, *J. Am. Chem. Soc.* **2003**, *125*, 9083 – 9089; c) D. Kvaskoff, P. Bednarek, L. George, S. Pankajakshan, C. Wentrup, *J. Org. Chem.* **2005**, *70*, 7947 – 7955.
[6] a) T. Khasanova, R. S. Sheridan, *J. Am. Chem. Soc.* **2000**, *122*, 8585 – 8586; b) R. Warmulth, M. A. Marvel, *Angew. Chem.* **2000**, *112*, 1168 – 1171; *Angew. Chem. Int. Ed.* **2000**, *39*, 1117 – 1119.
[7] a) W. T. Borden, N. P. Gritsan, C. M. Hadad, W. L. Karney, C. R. Kemnitz, M. S. Platz, *Acc. Chem. Res.* **2000**, *33*, 765 – 771; b) A. Maltsev, T. Bally, M.-L. Tsao, M. S. Platz, A. Kuhn, M. Vosswinkel, C. Wentrup, *J. Am. Chem. Soc.* **2004**, *126*, 237 – 249.
[8] Recent review on ylides and carbodiphosphorane chemistry: a) O. I. Kolodiazhnyi, *Tetrahedron* **1996**, *52*, 1855 – 1929; b) O. I. Kolodiazhnyi, *Phosphorus Ylides: Chemistry and Application in Organic Synthesis*, Wiley-VCH, Weinheim, **1999**.
[9] The degradation temperature of cyclic carbodiphosphoranes (R = Ph): 35 °C (X = $(CH_2)_3$), 25 °C (X = $(CH_2)_2$), −30 °C (X = C_6H_4); a) H. Schmidbaur, T. Costa, B. Milewski-Mahrla, U. Schubert, *Angew. Chem.* **1980**, *92*, 557 – 558; *Angew. Chem. Int. Ed. Engl.* **1980**, *19*, 555 – 556; b) G. A. Bowmaker, R. Herr, H. Schmidbaur, *Chem. Ber.* **1983**, *116*, 3567 – 3579.
[10] S. Marrot, T. Kato, H. Gornitzka, A. Baceiredo, *Angew. Chem.* **2006**, *118*, 2660 – 2663; *Angew. Chem. Int. Ed.* **2006**, *45*, 2598 – 2601.
[11] a) G. Alcaraz, U. Wecker, A. Baceiredo, F. Dahan, G. Bertrand, *Angew. Chem.* **1995**, *107*, 1358 – 1359; *Angew. Chem. Int. Ed. Engl.* **1995** *34*, 1246 – 1248; b) V. Piquet, A. Baceiredo, H. Gornitzka, F. Dahan, G. Bertrand, *Chem. Eur. J.* **1997**, *3*, 1757 – 1764.
[12] Ring contraction of small rings (ring size smaller than five) in carbocation or carbene chemistry is well-known: a) G. A. Olah, V. P. Reddy, G. K. S. Prakash, *Chem. Rev.* **1992**, *92*, 69 – 95; synthesis of β-lactams by ring contraction: b) P. S. Baran, R. A. Shenvi, C. A. Mitsos, *Angew. Chem.* **2005**, *117*, 3780 – 3783; *Angew. Chem. Int. Ed.* **2005**, *44*, 3714 – 3717; c) F. M. Cordero, F. Pisaneschi, A. Goti, J. Ollivier, J. Salaün, A. Brandi, *J. Am. Chem. Soc.* **2000**, *122*, 8075 – 8076.
[13] D. B. Puranik, M. J. Fink, *J. Am. Chem. Soc.* **1989**, *111*, 5951 – 5952.
[14] R. Reed, G. Bertrand, *Phosphorus-31 NMR Spectral Properties in Compound Characterization and Structural Analysis* (Eds: L. D. Quin, J. G. Verkade), VCH, New York, **1994**, pp. 189 – 200.
[15] Crystal data for **2a:** $C_{28}H_{51}N_5P_2$, $M_r = 519.68$, monoclinic, space group $P2_1/n$, $a = 9.842(1)$, $b = 29.268(2)$, $c = 10.541(1)$ Å, $\beta = 95.653(2)°$, $V = 3021.8(4)$ Å^3, $Z = 4$, $T = 173(2)$ K. 14789 reflections (4925 independent, $R_{int} = 0.0558$) were collected; largest electron-density residue: 0.242 e Å^{-3}, $R_1 = 0.0510$ (for $I > 2\sigma(I)$) and $wR_2 = 0.1192$ (all data). The structure was solved by direct methods[28] and all nonhydrogen atoms were refined anisotropically using the least-squares method on F^2.[29] CCDC-616067 (**2a**) contains the supplementary crystallographic data for this paper. These data can be obtained free of charge from The Cambridge Crystallographic Data Centre via www.ccdc.cam.ac.uk/data_request/cif.
[16] The rearrangement of transient diphosphinocarbenes to phosphaalkenes has already been reported: A. Baceiredo, A. Igau, G. Bertrand, M. J. Menu, Y. Dartiguenave, J. J. Bonnet, *J. Am. Chem. Soc.* **1986**, *108*, 7868 – 7869.
[17] Even when **2** was exclusively obtained from **1** in the presence of excess benzonitrile (15 equivalents), no trace of the other regioisomers was detected.
[18] For reviews on phosphinocarbenes: a) W. Kirmse, *Angew. Chem.* **2004**, *116*, 1799 – 1801; *Angew. Chem. Int. Ed.* **2004**, *43*, 1767 – 1769; b) D. Bourissou, O. Guerret, F. P. Gabbaï, *Chem. Rev.* **2000**, *100*, 39 – 92.
[19] See the Supporting Information for additional details.
[20] We have found a regioisomeric saddle point **TS2′** that lies 0.6 kcal mol^{-1} above **TS2** in the gas phase and in benzene solution (see the Supporting Information). This difference in energy corresponds to a kinetic formation of 71 % of **2b** with respect to its regioisomeric four-membered cycloadduct, which in turn lies 3.9 kcal mol^{-1} above **2b** in the gas phase. It is expected that when R = *i*Pr the regioselectivity will be higher.
[21] a) J. A. Ross, R. P. Seiders, D. M. Lemal, *J. Am. Chem. Soc.* **1976**, *98*, 4325 – 4327; b) C. Zhou, D. M. Birney, *J. Am. Chem. Soc.* **2002**, *124*, 5231 – 5241.
[22] R. G. Parr, W. Yang, *Density-Functional Theory of Atoms and Molecules*, Oxford, New York, **1989**.
[23] a) W. Kohn, A. D. Becke, R. G. Parr, *J. Phys. Chem.* **1996**, *100*, 12974 – 12980; b) A. D. Becke, *J. Chem. Phys.* **1993**, *98*, 5648 – 5652; c) A. D. Becke, *Phys. Rev. A* **1988**, *38*, 3098 – 3100.
[24] Gaussian 03, Revision C.02, M. J. Frisch et al. Gaussian, Inc., Wallingford, CT, **2004**.
[25] a) W. J. Hehre, L. Radom, P. von R. Schleyer, A. J. Pople, *Ab Initio Molecular Orbital Theory*, Wiley, New York, **1986**, pp. 76 – 87; b) R. Ditchfield, W. J. Hehre, J. A. Pople, *J. Chem. Phys.* **1971**, *54*, 724; c) W. J. Hehre, R. Ditchfield, J. A. Pople, *J. Chem. Phys.* **1972**, *56*, 2257.
[26] a) K. Fukui, *Acc. Chem. Res.* **1981**, *14*, 363 – 368; b) C. Gonzalez, H. B. Schlegel, *J. Chem. Phys.* **1989**, *90*, 2154 – 2161; c) C. Gonzalez, H. B. Schlegel, *J. Phys. Chem.* **1990**, *94*, 5523 – 5527.
[27] a) A. E. Reed, L. A. Curtiss, F. Weinhold, *Chem. Rev.* **1988**, *88*, 899 – 926; b) A. E. Reed, F. Weinhold, *J. Chem. Phys.* **1983**, *78*, 4066 – 4073; c) A. E. Reed, R. B. Weinstock, F. Weinhold, *J. Chem. Phys.* **1985**, *83*, 735 – 740.
[28] SHELXS-97, G. M. Sheldrick, *Acta Crystallogr. Sect. A* **1990**, *46*, 467.
[29] SHELXL-97, Program for Crystal Structure Refinement, G. M. Sheldrick, University of Göttingen, **1997**.

 © 2006 Wiley-VCH Verlag GmbH & Co. KGaA, Weinheim

NO Microsensors

DOI: 10.1002/anie.200601708

Detection of Nitric Oxide Release from Single Cells by Using Constant-Distance-Mode Scanning Electrochemical Microscopy**

*Sonnur Isik and Wolfgang Schuhmann**

Nitric oxide (NO) is involved in many important physiological processes and has been identified to be the endothelium-derived relaxing factor (EDRF).[1] A deficiency in NO plays a role in hypertension, hyperglycaemia, arteriosclerosis, Parkinson's disease, and Alzheimer's disease.[2] Conversely, increased NO levels contribute to arthritis, reperfusion injury, and cancer.[3] Thus, it is important to quantify the details of NO production in biological matrices to elucidate the physiological and pathological processes related to NO production and release.

Electrochemical NO sensors based on platinum-coated or electrocatalyst-modified electrodes often in combination with a permselective and charged membrane for interference elimination have been proposed.[4] Moreover, the determination of NO released upon stimulation from adherently growing cell populations or individual cells has been reported by using electrochemical NO sensors.[5] Recently, release of NO together with oxygen radicals was carefully evaluated by using positioned microelectrodes.[6]

Although NO reacts only very slowly with molecular oxygen at low concentrations, a nonstationary NO concentration zone will be formed above the cell. Assuming the releasing cell to be a point source of NO, any released NO will diffuse rapidly into the bulk of the solution, making it impossible to evaluate the exact concentration values for NO. Thus, it is obvious that the NO signal is extremely distance dependant,[5,6] making accurate positioning of the NO sensor indispensable for reliable experimentation (Figure 1). NO microsensors are positioned at cells by using micromanipulators under visual control by means of an optical microscope. Usually, the sensor is brought in contact with the cell membrane and then retracted to a predefined distance, therefore implying an error of typically at least 1–2 μm. This potentially leads to a contamination of the sensor surface or to unwanted shear-force stimulation of NO release. Conically shaped sensors (Figure 1b) determine values that are only an average of the NO concentration in the diffusion zone above the cells. In contrast, disk-shaped NO sensors (Figure 1a) will act as a sink for the released NO and will rapidly consume all NO within the gap between cell and electrode surface with a high collection efficiency. If the size of active electrode and cell are similar, a collection efficiency of close to 100% can be assumed.

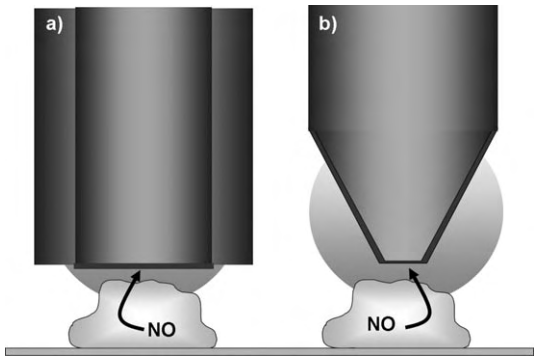

Figure 1. Schematic representation of the diffusion profile of NO upon stimulated release from a single cell. Detection by using a closely positioned a) disk electrode and b) a conically shaped microelectrode.

Recently, we have shown that scanning electrochemical microscopy (SECM) can be successfully used for accurate positioning of disk-shaped NO microsensors at known distances from NO-releasing cells by means of negative-feedback-mode *z*-approach curves based on diffusion-limited reduction of molecular oxygen.[7] Moreover, we have reported on the application of shear-force-dependent constant-distance positioning in SECM,[8] its application to the visualization of the topography of individual adherently growing cells, and the detection of neurotransmitter release upon depolarization of the cell membrane.[9] The shear-force-dependent positioning allows us to maintain a constant damping of the vibration of the SECM tip by means of a feedback loop at a distance of less than 300 nm between the tip and the cell membrane. The interactions between the SECM tip and the sample are sufficiently small to avoid cell damage. In particular, carbon-fiber microelectrodes, insulated with an electrodeposition paint,[10] have been advantageously used in cell measurements.[9]

Herein, highly sensitive disk-shaped NO microsensors are positioned at individual cells by using shear-force positioning in SECM. Upon stimulation, the release of NO from single cells could be detected. Disk-shaped vibrational needle-type carbon-fiber (CF) microelectrodes with a diameter of ≈7–9 μm were produced by following previously reported protocols.[9b,10] For the development of a highly sensitive and highly selective NO-sensor, a CF microelectrode was first coated with platinum by reductive multisweep deposition of Pt clusters from an aqueous solution of $H_2[PtCl_6]$. Coating with platinum significantly increases the surface area of the disk-shaped microelectrode, which is a prerequisite for enhanced sensitivity. Following this, a layer of Ni tetrasulfonate phthalocyanine tetrasodium salt (Ni-TSPc) prepared in a NaOH solution (1M) was polymerized on the microelectrode surface by using cyclic voltammetry in a potential range of 0

[*] Dr. S. Isik, Prof. Dr. W. Schuhmann
Analytische Chemie–Elektroanalytik & Sensorik
Ruhr-Universität Bochum
Universitätsstrasse 150, NC 04/788
44780 Bochum (Germany)
Fax: (+49) 234-321-4683
E-mail: wolfgang.schuhmann@rub.de

[**] The work was supported by the BMBF in the framework of the research area "Nanobiotechnologie" (NBT066). The authors are grateful to Priv.-Doz. Dr. A. Blöchl, Lehrstuhl für Molekulare Neurobiochemie, Ruhr-Universität Bochum, for the supply of the cells and valuable discussions.

© 2006 Wiley-VCH Verlag GmbH & Co. KGaA, Weinheim

to 1.2 V.[11] Finally, a permselective nafion membrane was dip-coated on top of the Ni-TSPc layer to improving the selectivity of the NO sensor against negatively charged interfering compounds. Nafion repels negatively charged interferences like NO_2^-, while simultaneously stabilizing positively charged compounds such as NO^+ (the primary oxidation product of NO). Figure 2 displays the differential pulse voltammograms (DPV) of a bare CF disk electrode, a platinum-coated CF electrode, as well as a platinum-coated CF disk after modification with a Ni-TSPc layer in presence of NO (9.9 μM). All electrodes had been covered with a nafion membrane.

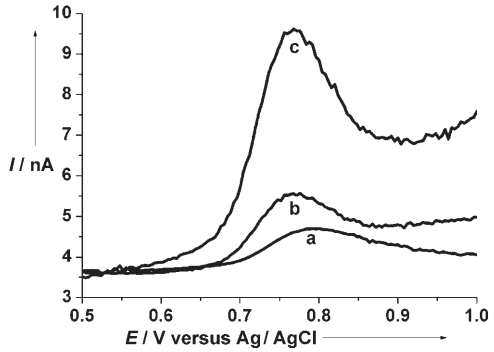

Figure 2. DPV of a) bare CF b) a platinum-coated CF, and c) a platinum-coated CF covered with a layer of polymerized Ni-TSPc in the presence of NO (9.9 μM).

The significant increase in the peak current observed in the DPV obtained with the platinum-coated and Ni-TSPc modified CF disk electrode clearly demonstrates the improved sensitivity of the modified electrode. The detection limit of the developed NO microsensor was determined to be 143 nM for DPV and 25 nM constant-potential amperometry. The selectivity was evaluated with respect to the detection of NO_2^-, which is the most important interference in NO detection owing to its similar oxidation potential. In this way, the reaction of NO_2^- was investigated, through the use of NO microsensors, with and without negatively charged nafion membranes.

Figure 3 demonstrates the improved selectivity of the nafion-coated sensors. The presence of the permselective nafion membrane decreases the peak current in the DPV in the presence of NO_2^- (333 μM) by a factor of two, whereas an approximately 70-times lower concentration of NO is detected with a significantly higher current. Owing to the fact that interferences from compounds such as dopamine or ascorbic acid were not expected in the system in vitro, the selectivity with respect to these compounds was not evaluated.

The properties of the NO microsensors as vibratory SECM tips were evaluated in combination with shear-force-dependent constant-distance positioning. An example of a topographic scan over a single transformed human umbilical vein endothelial cell (T-HUVEC) by using a NO microsensor is shown in Figure 4. The microelectrode was placed left of an individual cell with the aid of an inverted optical microscope.

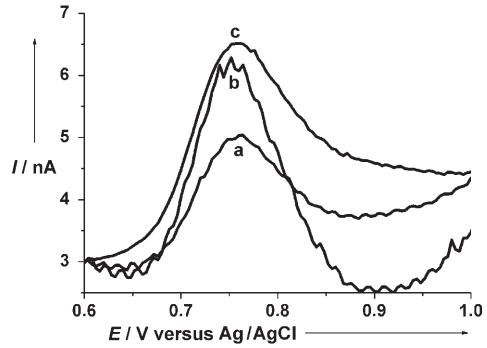

Figure 3. DPV obtained by using a platinum-coated and Ni-TSPc modified CF disk electrode a) covered with nafion in the presence of NO_2^- (333 μM), b) without nafion in the presence of NO_2^- (333 μM), and c) covered with nafion in the presence of NO (4.9 μM).

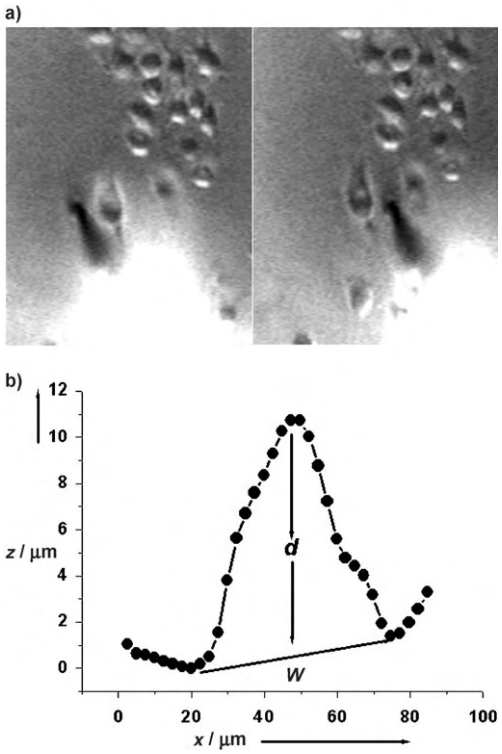

Figure 4. a) Optical images showing the position of the SECM tip before and after scanning of the cell topography. b) Topography line scan over an individual cell by using the shear-force-based constant-distance positioning. d = cell height, W = cell width.

Detection of the damping of the microelectrode vibration caused by shear-force interactions could be detected in close proximity to the glass surface by a z-approach curve. A line scan to the right of the cell follows the topography of the cell and determines the position of the sensor located right of the cell. Figure 4a shows optical microscopy images of the position of the NO sensor before and after scanning of the cell topography, and Figure 4b shows the detected cell topography through shear-force-dependent height control.

In the next step, an individual T-HUVEC was selected and the NO sensor tip was positioned next to the cell by using z-approach curves with shear-force-dependent damping of the

 © 2006 Wiley-VCH Verlag GmbH & Co. KGaA, Weinheim

vibrating SECM tip. As before, a line scan following the cell topography was initiated; however, the scan was stopped once the NO sensor was located exactly on top of the cell at a distance of 100 to 300 nm (Figure 5).

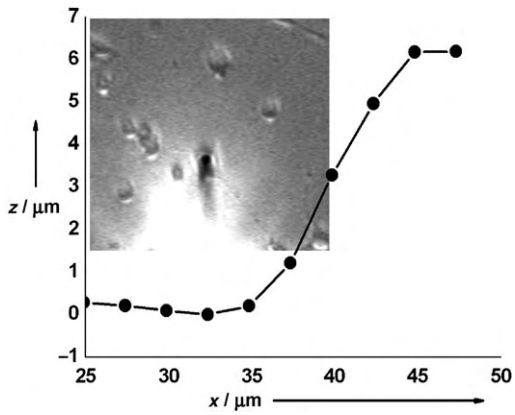

Figure 5. Positioning of the NO sensor over a single T-HUVEC in a line scan under additional visual control. The distance between the sensor surface and the cell membrane (below 300 nm) is defined by the shear-force-based constant-distance mode of SECM.

After exact positioning of the sensor tip over the cell, NO release is stimulated upon addition of 1 μM bradykinin. Prior to this, the NO sensor was poised to its working potential of +750 mV (vs. Ag/AgCl), and the current was detected over time with the help of a highly sensitive potentiostat. An example of an amperometric current trace is displayed in Figure 6. Immediately after stimulation, the release of NO leads to an increase in the oxidation current with a maximum of about 13.9 pA obtained after 5–8 s. Assuming a 100% collection efficiency, the current trace can be regarded as a representation of the total amount of NO produced by the cell upon stimulation. Thus, the total charge can be converted into an amount of NO released by the cell assuming a one-electron oxidation of NO to NO^+ at the sensor surface. For the example shown in Figure 6, a charge of 655 pC and an amount of 6.8 fmol NO was derived.

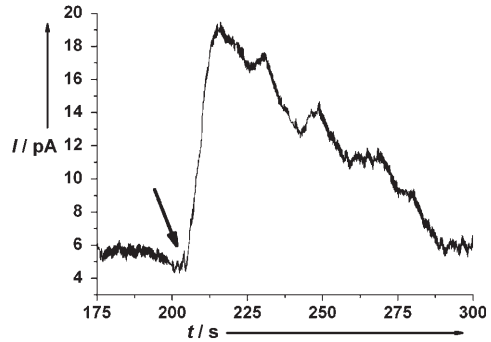

Figure 6. Amperometric current response from a disk-shaped NO sensor accurately positioned over an individual T-HUVEC by using the constant-distance-mode positioning of SECM. The arrow indicates the time of stimulation of the cell by means of addition of bradykinin (1 μM).

Control experiments with buffer solution instead of bradykinin and in the absence of cells unequivocally proved that the observed current is due to a compound released by the cell. Moreover, previous studies[7] that used the same cells in the presence of a NO synthase inhibitor proved that bradykinin stimulation leads to release of NO from the cells. The current fluctuations, which superimpose the current trace, may be due to the release of NO through vacuole openings instead of by diffusion through the cell membrane. However, more work has to be done to prove this assumption.

A sequence of independent measurements at different individual T-HUVECs was performed by positioning the NO sensor tip with shear-force-dependent constant-distance SECM, and the NO oxidation current was amperometrically recorded after stimulation with bradykinin. The maximum current of six different single-cell measurements varied between 5.7 and 13.9 pA, whereas the amount of NO calculated from the charge varied between 1.4 fmol and 10 fmol.

To summarize, single-cell NO detection was achieved with a highly sensitive and selective disk-shaped NO sensor prepared from platinum-coated and Ni-pthalocyanine modified carbon fiber microelectrodes. Accurate positioning of these NO microsensors by using the shear-force-dependent constant-distance mode of SECM is indispensable for reproducibly attaining an extremely small distance of below 300 nm between the NO sensor and the cell membrane without touching the cell.

Experimental Section

Cyclic voltammetry, coating with platinum, and deposition of the NO -selective layer on CF microelectrodes were performed by using a CHI1030 potentiostat (CH Instruments, Austin, TX). Amperometric measurements for detection of NO were carried out in a previously described Bio-SECM[8b] by using a low-noise VA10 potentiostat (npi electronics, Tamm, Germany). Active vibration dampening (TS-140, HWL, Germany) was used to allow for the positioning of the SECM tip at a distance of less than 300 nm.

Ringer buffer solution required for the stability and survival of the living cells was prepared from NaOH, KOH, NaCl, KCl, $MgCl_2$, $CaCl_2$, $NaHCO_3$, glucose, and 2-(4-(2-hydroxyethyl)-1-piperazinyl)-ethanesulfonic acid (HEPES; Riedel-de-Haen, Seelze, Germany) and its pH value was adjusted to 7.4. Bradykinin and Ni tetrasulfonate phthalocyanine tetrasodium salt were purchased from Aldrich (Steinheim, Germany).

Spontaneously transformed human umbilical vein endothelial cells (T-HUVECs, a kind gift from G. Neufeld/Haifa, Israel) were cultured following standard cell-culture protocols. T-HUVECs were seeded on glass cover slips in low density and cultured in RPM-1641 supplemented with fetal calf serum (10%) at 37°C in 10% CO_2 atmosphere. Before the electrochemical experiment, the growth medium was replaced with buffer solution, pH 7.4.

Received: April 30, 2006
Revised: August 9, 2006
Published online: October 13, 2006

Keywords: electrochemistry · nitric oxide · scanning probe microscopy · sensors · single cells

 © 2006 Wiley-VCH Verlag GmbH & Co. KGaA, Weinheim

[1] R. M. J. Palmer, A. G. Ferrige, S. Moncada, *Nature* **1987**, *327*, 524 – 526.

[2] a) L. J. Ignarro in *Nitric Oxide Biology and Pathology* (Ed.: L. J. Ignarro), Academic Press, San Diego, **2000**; b) L. Linder, W. Kiowski, F. R. Buhler, T. F. Luscher, *Circulation* **1990**, *81*, 1762 – 1767; c) H. H. Schmidt, T. D. Warner, K. Ishii, H. Sheng, F. Murad, *Science* **1992**, *255*, 721 – 723; d) P. M. Vanhoute, *J. Cardiovasc. Pharmacol.* **1990**, *16*, 15 – 19; e) S. Moncada, R. M. Palmer, E. A. Higgs, *Biochem. Pharmacol.* **1989**, *38*, 1709 – 1715.

[3] a) D. D. Rees, S. Cellek, R. M. Palmer, S. Moncada, *Biochem. Biophys. Res. Commun.* **1990**, *173*, 541 – 547; b) T. M. Dawson, V. L. Dawson, *Annu. Rev. Med.* **1996**, *47*, 219 – 227; c) S. Moncada, E. A. Higgs, *FASEB J.* **1995**, *9*, 1319 – 1330.

[4] a) F. Bailey, T. Malinski, F. Kiechle, *Anal. Chem.* **1991**, *63*, 395 – 398; b) M. N. Friedemann, S. W. Robinson, G. A. Gerhardt, *Anal. Chem.* **1996**, *68*, 2621 – 2628; c) S. Trevin, F. Bedioui, J. Devynck, *J. Electroanal. Chem.* **1996**, *408*, 261 – 265; d) F. Bedioui, S. Trevin, J. Devynck, *Electroanalysis* **1996**, *8*, 1085 – 1091; e) M. Pontie, F. Bedioui, *Analusis* **2000**, *28*, 465 – 469; f) N. Diab, W. Schuhmann, *Electrochim. Acta* **2001**, *47*, 265 – 273; g) F. Bedioui, N. Villeneuve, *Electroanalysis* **2003**, *15*, 5 – 18; h) V. Ryabova, A. Schulte, T. Erichsen, W. Schuhmann, *The Analyst* **2005**, *130*, 1245 – 1252.

[5] a) K. Shibuki, *Neurosci. Res.* **1990**, *9*, 69 – 76; b) K. Shibuki, D. Okada, *Nature* **1991**, *349*, 326 – 328; c) T. Malinski, Z. Taha, *Nature* **1992**, *358*, 676 – 678; d) T. Malinski, M. W. Radomski, Z. Taha, S. Moncada, *Biochem. Biophys. Res. Commun.* **1993**, *194*, 960 – 965; e) T. Malinski, Z. Taha, S. Grunfeld, A. Burewicz, P. Tomboulian, F. Kiechle, *Anal. Chim. Acta* **1993**, *279*, 135 – 140; f) A. J. Kanai, H. C. Strauss, G. A. Truskey, A. L. Crews, S. Grunfeld, T. Malinski, *Circ. Res.* **1995**, *77*, 284 – 293; g) P. Vallance, S. Patton, K. Bhagat, R. MacAllister, M. Radomski, S. Moncada, T. Malinski, *Lancet* **1995**, *346*, 153 – 154; h) C. Amatore, *C. R. Acad. Sci. Ser. IIb* **1996**, *323*, 757 – 771; i) F. Bedioui, S. Trevin, *Biosens. Bioelectron.* **1998**, *13*, 227 – 230.

[6] a) S. Arbault, P. Pantano, J. A. Jankowski, M. Vuillaume, C. Amatore, *Anal. Chem.* **1995**, *67*, 3382 – 3390; b) C. Amatore, S. Arbault, C. Bouton, K. Coffi, J. C. Drapier, H. Ghandour, Y. Tong, *ChemBioChem* **2006**, *7*, 653 – 661; c) C. Amatore, S. Arbault, Y. Bouret, B. Cauli, M. Guille, A. Rancillac, J. Rossier, *ChemPhysChem* **2006**, *7*, 181 – 187.

[7] a) A. Pailleret, J. Oni, S. Reiter, S. Isik, M. Etienne, F. Bedioui, W. Schuhmann, *Electrochem. Commun.* **2003**, *5*, 847 – 852; b) S. Isik, M. Etienne, J. Oni, A. Blöchl, S. Reiter, W. Schuhmann, *Anal. Chem.* **2004**, *76*, 6389 – 6394; c) S. Isik, M. Etienne, J. Oni, A. Blöchl, S. Reiter, W. Schuhmann, *Anal. Chem.* **2004**, *76*, 6389 – 6394; d) S. Borgmann, I. Radtke, T. Erichsen, A. Blöchl, R. Heumann, W. Schuhmann, *ChemBioChem* **2006**, *7*, 669 – 672.

[8] a) A. Hengstenberg, A. Blöchl, I. D. Dietzel, W. Schuhmann, *Angew. Chem.* **2001**, *113*, 942 – 946; b) L. Pitta Bauermann, W. Schuhmann, A. Schulte, *Phys. Chem. Chem. Phys.* **2004**, *6*, 4003 – 4008.

[9] a) M. Ludwig, C. Kranz, W. Schuhmann, H. E. Gaub, *Rev. Sci. Instrum.* **1995**, *66*, 2857 – 2860; b) A. Hengstenberg, C. Kranz, W. Schuhmann, *Chem. Eur. J.* **2000**, *6*, 1547 – 1554; c) B.Ballesteros Katemann, A. Schulte, W. Schuhmann, *Electroanalysis* **2004**, *16*, 60 – 65.

[10] a) A. Schulte, R. H. Chow, *Anal. Chem.* **1996**, *68*, 3054 – 3058; b) A. Schulte, R. H. Chow, *Anal. Chem.* **1998**, *70*, 985 – 990.

[11] a) F. Bedioui, S. Trevin, J. Devynck, F. Lantoine, A. Brunet, M. A. Devynck, *Biosens. Bioelectron.* **1997**, *12*, 205 – 212; b) S. Isik, L. Berdondini, J. Oni, A. Blöchl, M. Koudelka-Hep, W. Schuhmann, *Biosens. Bioelectron.* **2005**, *20*, 1566 – 1572.

 © 2006 Wiley-VCH Verlag GmbH & Co. KGaA, Weinheim

Enzyme Inhibitors

DOI: 10.1002/anie.200601569

Aryl Indanyl Ketones: Efficient Inhibitors of the Human Peptidyl Prolyl *cis*/*trans* Isomerase Pin1**

*Sebastian Daum, Frank Erdmann, Gunter Fischer, Boris Féaux de Lacroix, Anahita Hessamian-Alinejad, Sabine Houben, Walter Frank, and Manfred Braun**

The rigidity of the amide bond is a feature that distinctly influences the structure of proteins. The rotation about the imidic peptide bond preceding proline has to surmount an activation barrier of 75 to 100 kJ mol^{-1} for the conversion of the *cis*-conformer **1** into *trans*-**3** (Scheme 1). Thereby, the torsion angle ω changes from 0 to 180°. In unfolded proteins, the *trans*-isomer **3** predominates; however, native proteins frequently contain a specific prolyl bond in the *cis* conformation **1**.[1]

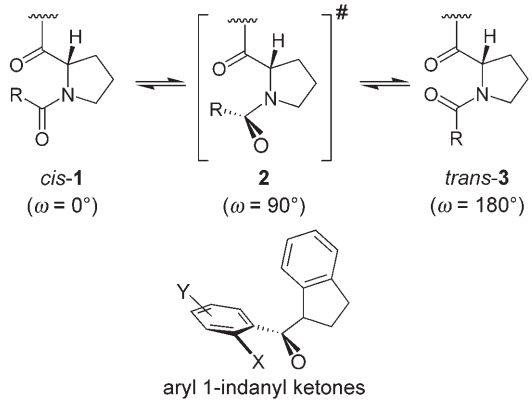

Scheme 1. *Cis–trans* isomerization of peptidyl–prolyl bonds. Aryl 1-indanyl ketones as mimics of the twisted-amide transition state **2**.

Peptidyl prolyl *cis*/*trans* isomerases (PPIases) are enzymes that catalyze the *cis–trans* interconversion of prolyl bonds (**1**⇌**3**).[2] Discovered in 1984, they have been found to be an important group of enzymes with a strong impact on the slow processes involved in protein folding.[3] Concerning the mechanism of the enzymatic catalysis exhibited by PPIases, various hypotheses have been developed to rationalize how

[*] Dipl.-Chem. B. Féaux de Lacroix, Dr. A. Hessamian-Alinejad, S. Houben, Prof. Dr. W. Frank, Prof. Dr. M. Braun
Wissenschaftliche Einrichtung Chemie
Universität Düsseldorf
Universitätsstrasse 1, 40225 Düsseldorf (Germany)
Fax: (+49) 211-811-5079
E-mail: braunm@uni-duesseldorf.de
S. Daum, Dr. F. Erdmann, Prof. Dr. G. Fischer
Max-Planck-Forschungsstelle für Enzymologie der Proteinfaltung
Weinbergweg 22, 06120 Halle (Germany)

[**] This work was supported by the Deutsche Forschungsgemeinschaft (Br 604/14-1,2).

InterScience
© 2006 Wiley-VCH Verlag GmbH & Co. KGaA, Weinheim

the energy of the transition state **2** in the uncatalyzed isomerization of *cis*-**1** and *trans*-**3** is lowered to the experimentally measured values of the enzyme catalyzed reaction.[1,2b]

Among the three families of human PPIases, the parvulin-like Pin1 is unique in its substrate specificity which has made it possible to specifically accelerate the *cis–trans* isomerization of $PO_3H_2Ser(PO_3H_2Thr)$–Pro bonds in short peptides and proteins.[4] Therefore, Pin1 interacts with and regulates many key phosphoproteins of the eukaryotic cell cycle, such as cyclin D1, p53, or β-catenin.[5] In several human cancer cell lines, the depletion of Pin1 causes cell cycle arrest. Moreover, the enzyme has been found to be overexpressed in many tumor cell lines.[6] Pin1 has also been found to be involved in Alzheimer's disease.[7] To date, however, few compounds have been reported to act as inhibitors of Pin1. Among them, the natural naphthoquinone juglone inactivated Pin1 in an irreversible manner by minor structural alterations at the active site after the Michael addition of a thiol group.[8] Several polycyclic aromatic compounds[9] and natural peptide mimetics[10] have also been reported to inhibit Pin1.

In our search for efficient reversible inhibitors of human Pin1 (hPin1), we were guided by the idea that the "twisted-amide" transition-state model **2** along with the concomitant change of hybridization about the ring nitrogen atom might be readily mimicked by aryl 1-indanyl ketones, because we anticipated them to have a twisted conformation in front of the five-membered ring. Its similarity to the "twisted amide" **2** is indicated in Scheme 1.

Despite their relatively simple structure, only a few compounds containing the aryl 1-indanyl-ketone moiety have been synthesized.[11] Most of them served as intermediates for fredericamycin A[11c–g] and, in only a few cases, were nonracemic products synthesized.[11d,i] Thus, general routes to aryl indanyl ketones had to be developed to make the preparation of specifically substituted products possible. As shown in Scheme 2, monoaryl indanyl ketones **7a**,**b** were easily available by coupling lithiated arenes **5a**,**b**, generated by a bromine–lithium exchange from bromoarenes **4a**,**b**, with monodeprotonated indanecarboxylic acid **6a**.[12] As an alternative to the lithium salt **6b**, the Weinreb-type[13] amide **6c** was also found to react readily with aryllithium **5** to deliver the ketones **7**. Generally, this variant provided higher yields. The cleavage of the methyl ether group in compounds **7a**,**b** occurred upon treatment with aluminum chloride[14] to give the phenols **8a**,**b**. For the introduction of a methyl substituent in the α-carbonyl position, the enolate generated from ketone **7b** was treated with methyl iodide to give racemic product **9**.

A novel domino reaction led to the biaryl indanyl ketone **10**, as shown in Scheme 3. When two equivalents of aryllithium **5b**, generated by bromine–lithium exchange from **4b**, were allowed to react with the lithium salt **6b** of indane carboxylic acid, the biaryl indanyl ketone **10** resulted as the only product apart from protonated starting material **5b** (H instead of Li) and carboxylic acid **6a**. Clearly, not only the addition to the carboxylate **6b** had occurred, but also a substitution of the fluorine atom by the second equivalent of the aryllithium **5b** serving as a nucleophile. Although the

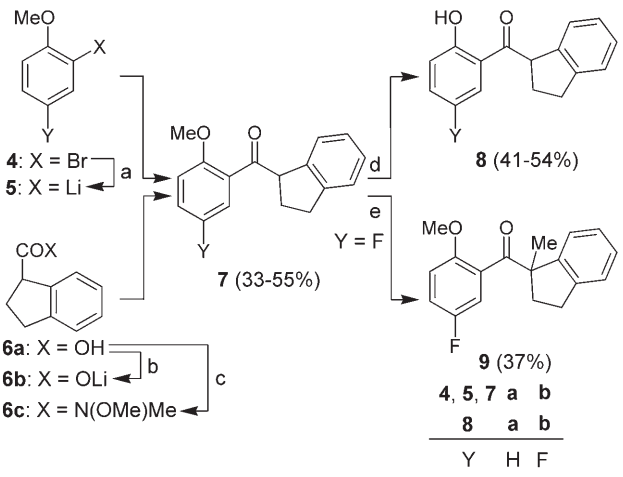

Scheme 2. Synthesis of monoaryl indanyl ketones **7**–**9**. Reagents and conditions: a) *n*BuLi, Et_2O, −78 °C; b) *n*BuLi, Et_2O, −78 to −10 °C; c) 1. $SOCl_2$, reflux; 2. HN(OMe)Me·HCl, pyridine, 0 °C to room temperature; d) $AlCl_3$, CH_2Cl_2, 0 °C; e) 1. LiN*i*Pr$_2$, THF, −78 to 0 °C, 2. MeI, −20 °C to room temperature.

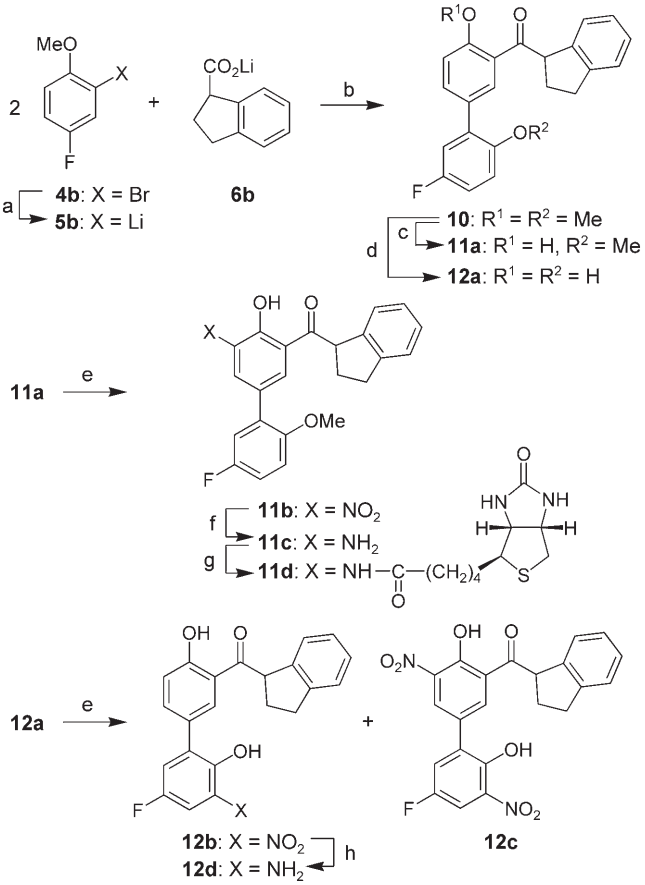

Scheme 3. Domino reaction between aryllithium **5b** and carboxylate **6b**. Synthesis of ketones **11** and **12** derived from **10**. Reagents and conditions: a) *n*BuLi, Et_2O, −78 °C; b) −78 °C to reflux, 27%; c) $AlCl_3$, CH_2Cl_2, 0 °C to room temperature, 59%; d) BBr_3, CH_2Cl_2, 71%; e) HNO_3, HOAc, 10 °C, 79%; f) H_2/Pd/C, THF, 73%; g) biotinyl chloride, pyridine, 8%; h) H_2/Pd/C, EtOH, 95%.

 © 2006 Wiley-VCH Verlag GmbH & Co. KGaA, Weinheim

question remains open whether this step follows an addition–elimination or an aryne pathway, the complete regiocontrol is remarkable. The domino reaction does not occur when, instead of the carboxylate **6b**, the amide **6c** is treated with two equivalents of **5b**.

An unambiguous confirmation of the structure of ketone **10**, which forms as a single isomer, comes from a crystal-structure analysis of phenolic ketone **11a** (Figure 1),[15] the

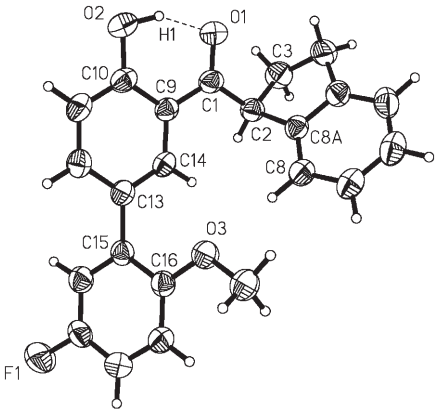

Figure 1. Molecular structure of ketone **11a**. Thermal ellipsoids are set at 30% probability; radii of hydrogen atoms are chosen arbitrarily. Selected interatomic distances [Å] and angles [°]: C1–O1 1.2443(15), C10–O2 1.3570(15), O2–H1 0.996(18), H1···O1 1.639(18), O1···O2 2.5570(15); O2-H1···O1 151.2(15), C3-C2-C8A 101.55(12); O1-C1-C9-C10 5.01(18), O1-C1-C2-C8A 92.15(15), O1-C1-C2-C3 −20.98(19), C2-C1-C9-C10 −174.96(12), C14-C13-C15-C16 57.77(17).

product of a selective demethylation of the methoxy substituent in the position *ortho* to the carbonyl group. Although the yield of the domino reaction is moderate (25–30%), it opens an easy way to the ketone **10** that in turn serves as a starting material for further derivatives. Thus, a regioselective *ortho*-nitration of the phenol **11a** was possible and gave the product **11b** as a single isomer. Catalytic hydrogenation afforded the aromatic amine **11c** that was coupled with biotin-derived acid chloride to give the amide **11d**. A complete demethylation of biaryl indanyl ketone **10** by means of boron tribromide[14] led to the formation of bisphenolic ketone **12a**. Upon treatment with nitric acid in acetic acid, a mixture of nitro compounds **12b** and **12c** was obtained. After separation, the former was reduced to the aromatic amine **12d**.

Whereas all the aryl indanyl ketones described herein were obtained as racemic mixtures, the α-methyl-substituted ketone **9** was chosen to be prepared in an enantiomerically pure form. For this purpose, enantiomeric (*R*)- and (*S*)-1-methyl-1-indanecarboxylic acids[16,17] served as starting materials. Thus, reaction of the corresponding Weinreb-type amides with **5b** delivered (*R*)- and (*S*)-**9**, respectively, in 45 to 48% overall yield.

The inhibition of hPin1 by the aryl indanyl ketones prepared as described above was determined in a protease-free PPIase assay with Suc-Ala-Glu-Pro-Phe-pNA as the substrate.[18] The compounds exhibit substantial inhibition of hPin1. As shown in Table 1, most of the aryl indanyl ketones

Table 1: Inhibition constants of aryl indanyl ketones **7**–**9**, **11**, and **12**.

Entry	Ketone	K_i [μM]	Entry	Ketone	K_i [μM]
1	**7a**	6.2±0.4	9	**11d**	1.4±0.9
2	**7b**	8.7±0.2	10	**12a**	3.1±0.6
3	**8a**	5.1±0.8	11	**12b**	0.5±0.1
4	**8b**	15.0±3.0	12	**12c**	0.2±0.1
5	**9**	19.0±4.9	13	**12d**	0.4±0.1
6	**11a**	1.7±0.2	14	(*R*)-**9**	5.6±0.9
7	**11b**	1.1±0.2	15	(*S*)-**9**	51.0±9.0
8	**11c**	4.9±0.7			

(entries 1–10) have K_i values in the micromolar range. The hydrogen-bonded hydroxy group adjacent to the carbonyl group is not crucial to Pin1 inhibition, although the phenolic derivatives are superior to the phenol ethers. A significant improvement in Pin1 inhibition originates from the introduction of nitro groups. Thus, mono- and dinitro-substituted ketones **12b** and **12c** (Table 1; entries 11 and 12) led to a strong inhibition with K_i values in the sub-micromolar range. Remarkably, the replacement of a nitro group in **12b** by an amino substituent in **12d** did not influence Pin1 inhibition to a major extent (Table 1; entry 13).

Ketone **11d** with a biotin side chain allowed the reversibility of Pin1 inhibition to be demonstrated. For this experiment the activity assay was performed at a fixed concentration of **11d**, leading to 80% inhibition of the Pin1 PPIase activity. The addition of increasing concentrations of streptavidin (a stronger competitive binder for **11d**) resulted in the full return of Pin1 activity whereas the addition of streptavidin presaturated with biotin had no effect (Figure 2). This

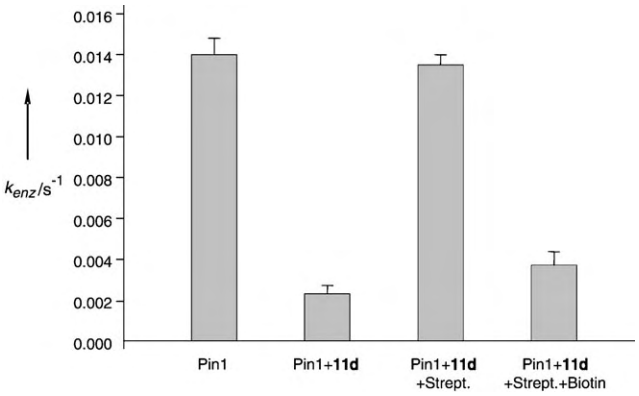

Figure 2. Reversibility of Pin1/**11d** complex formation; PPIase activity of 5 nM Pin1 in the absence and presence of 5 μM **11d**, 10 μM Streptavidin, 30 μM Biotin.

behavior indicates that the inhibitor is noncovalently attached to Pin1 and the concentration-dependent formation of inactive enzyme is not due to irreversible Pin1 denaturation and aggregation.[10c]

As expected, a substantial difference in the inhibition of the enzyme occurred when the two enantiomers of ketone **9** were tested, and the corresponding K_i values differed by an order of magnitude from each other (Table 1; entries 14 and 15). The different behavior of the enantiomers underlines the

 © 2006 Wiley-VCH Verlag GmbH & Co. KGaA, Weinheim

idea of the similarity between the structure of aryl indanyl ketones and the "twisted-amide" transition state, because the binding sites in the transition state of the active center must have a stereochemical component. More support for the hypothesis comes from the crystal structure of ketone **11a** (Figure 1). The torsion angle between the aromatic-carbonyl and the indanyl moiety (O1-C1-C2-C8A) of 92° is in accord with the features of the twisted amide **2**. In addition, homologues of aryl indanyl ketones with four- or six-membered rings instead of a five-membered one do not display substantial Pin1 inhibition, a fact that supports the "twisted-amide" hypothesis (data not shown).

Next we asked whether application of selected compounds of Table 1 would give rise to the same effects in cells as those obtained after the depletion of Pin1 in cells by genetic means. A luciferase reporter gene assay with a p53 response element in MCF-7 cells (breast cancer cell line) was performed. In cells, the phosphorylated form of tumor-suppressor protein p53 interacts with endogenous Pin1 after DNA damage by chemotherapeutic drugs or irradiation. In this pathway, Pin1 induces conformational changes which lead to increased transactivation activity and higher proteolytic stability of p53.[19]

As shown in Figure 3, the compounds (*S*)-**9**, (*R*)-**9**, and *rac*-**9** are able to reduce the stimulated activity of the p53 reporter gene in etoposid treated MCF-7 cells in a concentration-dependent manner and according to their inhibitory potencies. Similarly, cotransfection of Pin1-negative mouse-embryo fibroblasts with the expression construct for an inactive Pin1 variant failed to increase the stability and transactivation activity of p53.[19c]

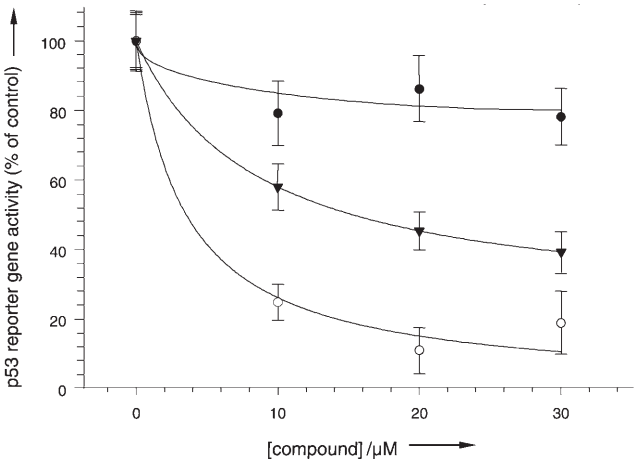

Figure 3. Influence of (*R*)-**9** (○), (*S*)-**9** (●), and *rac*-**9** (▼) on p53 reporter gene activity in etoposid-treated MCF-7 cells. Data are mean values of three independent measurements (± standard deviation).

In a second experiment, we investigated the effect of (*S*)-**9**, (*R*)-**9** and *rac*-**9** on the oncogenic transcriptional activator β-catenin. Several studies could demonstrate that Pin1 regulates the β-catenin turnover in tumor cells. Moreover, the β-catenin level directly correlates with the PPIase activity of Pin1, as shown by using a set of point-mutated Pin1 variants.[20] Cells of the tumor cell line SH-SY5Y were incubated with the compounds and the intracellular β-catenin level was determined by Western blotting with a specific anti-β-catenin antibody and subsequent densitometric analysis (Figure 4). The application of (*R*)-**9** and *rac*-**9** leads to a decreased β-catenin content in the cells, whereas (*S*)-**9** has only a minor effect.

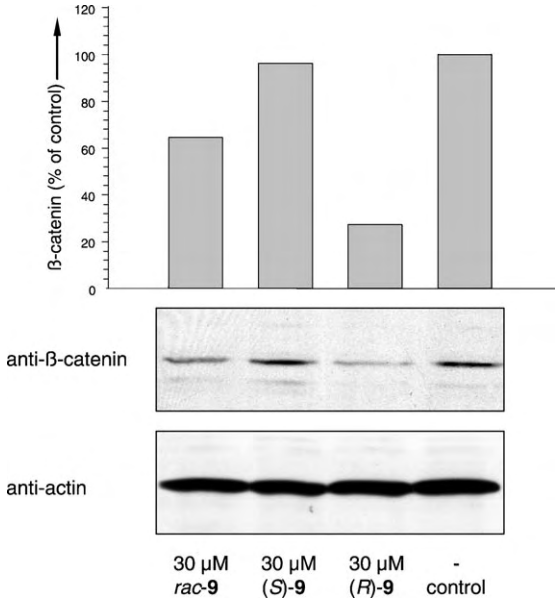

Figure 4. (*S*)-**9**, (*R*)-**9**, and *rac*-**9** decrease the intracellular β-catenin level in SH-SY5Y cells by Pin1 inhibition.

In summary, a new class of efficient, cell-penetrating, reversible inhibitors of human Pin1 has been developed that are based on the structural motif of aryl 1-indanyl ketones. They not only display inhibition constants in sub-micromolar range, but have shown biological activities and seem to be promising candidates for the development of anticancer drugs.

Received: April 20, 2006
Revised: June 22, 2006
Published online: October 18, 2006

Keywords: antitumor agents · biological activity · chirality · enzymes · ketones

[1] Review: J. Fanghänel, *Angew. Chem.* **2003**, *115*, 506; *Angew. Chem. Int. Ed.* **2003**, *42*, 490.
[2] Review: a) G. Fischer, *Angew. Chem.* **1994**, *106*, 1479; *Angew. Chem. Int. Ed. Engl.* **1994**, *33*, 1415; b) G. Fischer, *Chem. Soc. Rev.* **2000**, *29*, 119.
[3] G. Fischer, H. Bang, C. Mech, *Biomed. Biochim. Acta* **1984**, *43*, 1101.
[4] a) M. B. Yaffe, M. Schutkowski, M. Shen, X. Z. Zhou, P. T. Stukenberg, J.-U. Rahfeld, J. Xu, J. Kuang, M. W. Kirschner, G. Fischer, L. C. Cantley, K. P. Lu, *Science* **1997**, *278*, 1957; b) R. Ranganathan, K. P. Lu, T. Hunter, J. P. Noel, *Cell* **1997**, *89*, 875; c) J. D. Joseph, E. S. Yeh, K. I. Swenson, A. R. Means, E. Winkler, *Prog. Cell Cycle Res.* **2003**, *5*, 477.

 © 2006 Wiley-VCH Verlag GmbH & Co. KGaA, Weinheim

[5] A. Ryo, Y.-C. Liou, K. P. Lu, G. Wulf, *J. Cell Sci.* **2003**, *116*, 773.

[6] G. M. Wulf, A. Ryo, G. G. Wulf, S. W. Lee, T. Niu, V. Petkova, K. P. Lu, *Embo J.* **2001**, *20*, 3459.

[7] a) Y.-C. Liou, A. Sun, A. Ryo, X. Z. Zhou, Z.-X. Yu, H.-K. Huang, T. Uchida, R. Bronson, G. Bing, X. Li, T. Hunter, K. P. Lu, *Nature* **2003**, *424*, 556; b) P. J. Lu, G. Wulf, X. Z. Zhou, P. Davies, K. P. Lu, *Nature* **1999**, *399*, 784.

[8] L. Henning, C. Christner, M. Kipping, B. Schelbert, K. P. Rücknagel, S. Grabley, G. Küllertz, G. Fischer, *Biochemistry* **1998**, *37*, 5953.

[9] T. Uchida, M. Takamiya, M. Takahashi, H. Miyashita, H. Ikeda, T. Terada, Y. Matsuo, M. Shirouzu, S. Yokoyama, F. Fujimori, T. Hunter, *Chem. Biol.* **2003**, *10*, 15.

[10] a) H. C. Wang, K. Kim, R. Bakhtiar, J. P. Germanas, *J. Med. Chem.* **2001**, *44*, 2593; b) Y. Zhang, *Mini-Rev. Org. Chem.* **2004**, *1*, 359; c) E. Bayer, M. Thutewohl, C. Christner, T. Tradler, F. Osterkamp, H. Waldmann, P. Bayer, *Chem. Commun.* **2005**, 516; d) D. Wildemann, F. Erdmann, B. Hernandez Alvarez, G. Stoller, X. Z. Zhou, J. Fanghänel, M. Schutkowski, K. P. Lu, G. Fischer, *J. Med. Chem.* **2006**, *49*, 2147.

[11] a) J. K. Stille, R. A. Newsom, *J. Org. Chem.* **1961**, *26*, 1375; b) J. F. Bunnett, J. A. Skorcz, *J. Org. Chem.* **1962**, *27*, 3836; c) D. L. J. Clive, A. G. Angoh, S. M. Bennett, *J. Org. Chem.* **1987**, *52*, 1339; d) W. Trypke, A. Steigel, M. Braun, *Synlett* **1992**, 827; e) D. L. J. Clive, Y. Tao, A. Khodabocus, Y.-J. Wu, A. G. Angoh, S. M. Bennett, C. N. Boddy, L. Bordeleau, D. Kellner, G. Kleiner, D. S. Middleton, C. J. Nichols, S. R. Richardson, P. G. Vernon, *J. Am. Chem. Soc.* **1994**, *116*, 11275; f) D. L. Boger, I. C. Jacobson, *J. Org. Chem.* **1990**, *55*, 1919; D. L. Boger, I. C. Jacobson, *J. Org. Chem.* **1991**, *56*, 2115; g) P. A. Evans, T. A. Brandt, *Tetrahedron Lett.* **1996**, *37*, 1367; h) H. Sakurai, Y. Imamoto, T. Hirao, *Chem. Lett.* **2002**, 44; i) B. Hauer, J. F. Bickley, J. Massue, P. C. A. Pena, S. M. Roberts, J. Skidmore, *Can. J. Chem.* **2002**, *80*, 546.

[12] M. Tiffeneau, A. Orékhoff, *Bull. Soc. Chim. Fr.* **1920**, *27*, 789; L. Fišnerová, B. Kakáč, O. Němeček, A. Šimek, Z. J. Vejdělek, *Collect. Czech. Chem. Commun.* **1967**, *32*, 4082.

[13] For reviews on the use of Weinreb amides in synthesis, see: M. Mentzel, H. M. R. Hoffmann, *J. Prakt. Chem.* **1997**, *339*, 517; J. Singh, N. Satyamurthi, I. S. Aidhen, *J. Prakt. Chem.* **2000**, *342*, 340.

[14] T. W. Greene, P. G. M. Wuts, *Protective Groups in Organic Synthesis*, 2nd ed., Wiley, New York, **1991**, and references therein.

[15] $C_{23}H_{19}FO_3$, $M_r = 362.38$, monoclinic, space group $P2_1/n$, $a = 13.3598(10)$, $b = 7.1470(4)$, $c = 18.9363(17)$ Å, $\beta = 97.202(10)°$, $V = 1793.8(2)$ Å^3, $Z = 4$, $\rho = 1.342$ g cm^{-3}, $\mu = 0.095$ mm^{-1}, $T = 291$ K, crystal dimensions: 0.25 mm × 0.3 mm × 0.3 mm, STOE-IPDS, $Mo_{K\alpha}$ radiation ($\lambda = 0.71073$ Å), $\theta_{max} = 25.65°$, 13715 measured, 3372 unique, and 1924 observed reflections with $I > 2\sigma(I)$, Lorentz polarization correction, direct methods and ΔF synthesis, minimization of $\Sigma w(F_o^2 - F_c^2)^2$, 320 refined parameters, $(\Delta/\sigma)_{max} = 0.000$, $R_1[F_o^2 > 2\sigma(F_o^2)] = 0.029$, $wR_2 = 0.059$ (all data), $w = 1/[\sigma^2(F_o^2) + (0.0215P)^2]$ where $P = (F_o^2 + 2F_c^2)/3$, $S = 1.028$, $\Delta\rho_{max}/\Delta\rho_{min} = 0.122/-0.106$ e Å^{-3}. CCDC-604159 contains the supplementary crystallographic data for this paper. These data can be obtained free of charge from The Cambridge Crystallographic Data Centre via www.ccdc.cam.ac.uk/data_request/cif.

[16] M. Braun, W. Kotter, *Angew. Chem.* **2004**, *116*, 520; *Angew. Chem. Int. Ed.* **2004**, *43*, 514.

[17] Although an enantioselectively catalyzed route to 1-methyl-1-arylindane carboxylic acid has been opened (ref. [16]), it is more readily prepared from the corresponding esters of (*R*)- and (*S*)-1,1,2-triphenyl-1,2-ethanediol; see: H. Sacha, D. Waldmüller, M. Braun, *Chem. Ber.* **1994**, *127*, 1959.

[18] B. Janowski, S. Wöllner, M. Schutkowski, G. Fischer, *Anal. Biochem.* **1997**, *252*, 299.

[19] a) P. Zacchi, M. Gostissa, T. Uchida, C. Salvagno, F. Avolio, S. Volinia, Z. Ronai, G. Blandino, C. Schneider, G. Del Sal, *Nature* **2002**, *419*, 853; b) H. Zheng, H. You, X. Z. Zhou, S. A. Murray, T. Uchida, G. Wulf, L. Gu, X. Tang, K. P. Lu, Z.-X. J. Xiao, *Nature* **2002**, *419*, 849; c) G. M. Wulf, Y.-C. Liou, A. Ryo, S. W. Lee, K. P. Lu, *J. Biol. Chem.* **2002**, *277*, 47976.

[20] A. Ryo, M. Nakamura, G. Wulf, Y.-C. Liou, K. P. Lu, *Nat. Cell Biol.* **2001**, *3*, 793.

 © 2006 Wiley-VCH Verlag GmbH & Co. KGaA, Weinheim

Biomimetic Thin Films

DOI: 10.1002/anie.200602382

Polymer Brushes as Ionotropic Matrices for the Directed Fabrication of Microstructured Calcite Thin Films**

Stefano Tugulu, Marc Harms, Marc Fricke, Dirk Volkmer, and Harm-Anton Klok**

Many biominerals are characterized by complex, hierarchically ordered structures.[1] In nature, the formation of biominerals is guided by matrix macromolecules. For example, acidic biomacromolecules play an important role in directing the mineralization of $CaCO_3$, one of the most abundant biominerals.[2] In addition to the three crystalline polymorphs, biogenic $CaCO_3$ also occurs in two amorphous modifications: a stable hydrated form and a less stable, essentially anhydrous form, which can act as a transient precursor of the thermodynamically stable crystalline modifications.[3,4] The formation of various complex biogenic $CaCO_3$ structures, such as sea urchin spines, has been proposed to proceed via the second, metastable amorphous-$CaCO_3$ (ACC) phase.[5,6] ACC has also been exploited as a

[*] S. Tugulu, Prof. H.-A. Klok
École Polytechnique Fédérale de Lausanne (EPFL)
Institut des Matériaux, Laboratoire des Polymères
Bâtiment MXD, Station 12, 1015 Lausanne (Switzerland)
Fax: (+41) 21-693-5650
E-mail: harm-anton.klok@epfl.ch
Homepage: http://lp.epfl.ch
M. Harms, Dr. M. Fricke, Prof. D. Volkmer
Anorganische Chemie II
University of Ulm
Albert-Einstein-Allee 11, 89081 Ulm (Germany)
Fax: (+49) 731-502-3039
E-mail: dirk.volkmer@uni-ulm.de
Homepage: http://www.uni-ulm.de/ac2/Volkmer_Group/

[**] This work was supported by the VolkswagenStiftung (H.-A.K.) and the Deutsche Forschungsgemeinschaft (DFG priority program 1117 "Principles of biomineralization", Vo 829/2-3, D.V.). The authors thank Priv.-Doz. Dr. A. Ziegler (Central Facility of Electron Microscopy, University of Ulm) for his help with the electron microscopy and to Dr. S. Hild (University of Ulm), Dr. G. Lamarque (Laboratoire des Polymères, EPFL) and WITec GmbH (Ulm) for the AFM studies.

Supporting information for this article is available on the WWW under http://www.angewandte.org or from the author.

WILEY InterScience DISCOVER SOMETHING GREAT
© 2006 Wiley-VCH Verlag GmbH & Co. KGaA, Weinheim

transient precursor in vitro to produce $CaCO_3$ crystals in constrained geometries, to fabricate microstructured calcite single crystals, and to synthesize nacre-type laminated $CaCO_3$ coatings.[7–9] The advantage of the transient ACC phase is that it can be more easily molded into complex structures than the crystalline $CaCO_3$ polymorphs. The amorphous precursor route has also been used to prepare crystalline carbonate apatite films.[10] The application of such concepts to direct the size, shape, and microstructure of synthetic inorganic materials is of great technological importance and could lead to new materials with potential applications in, for example, optical information processing, catalysis, and regenerative medicine.[11–14] A convenient route for the fabrication of microstructured inorganic materials is the use of self-assembled monolayers (SAMs) to create 2D spatially constrained microenvironments for crystallization.[12,14] In this case, crystallization is limited to those regions of the substrate that present the appropriate surface chemistry. Instead of relying on specific chemical surface modification, micrometer scale patterned ceramic thin films can also be prepared by imposing physical boundaries on the crystallization.[13] These boundaries can be achieved using a variety of soft lithography techniques, including, microtransfer molding, micromolding in capillaries, and embossing.

Figure 1. Fabrication of microstructured calcite films. A) Synthesis of PMAA brushes by SI-ATRP of sodium methacrylate from photolithographically patterned ATRP initiator functionalized substrates (bipy = 2,2′-bipyridine). B) Directed deposition of a thin, metastable layer of amorphous calcium carbonate (ACC) and subsequent temperature-induced transformation of the metastable ACC layer into a microstructured, polycrystalline calcite film.

Herein, we present a novel approach for the fabrication of microstructured, crystalline calcite thin films. Our strategy involves the use of photolithographically patterned poly(methacrylic acid) (PMAA) brushes grown by surface-initiated atom-transfer radical polymerization (SI-ATRP). These brushes function as ionotropic[15] matrices to produce crystalline calcite films that are an exact 3D replica of the PMAA brush. One of the attractive features of polymer brushes compared to SAMs is that film thickness and chemical composition can be precisely controlled using a variety of surface-initiated, controlled radical polymerization techniques, including ATRP.[16–18] Herein, we demonstrate for the first time the use of such brushes to act as ionotropic matrices for the directed synthesis of microstructured calcite thin films. The proposed strategy combines three key elements (Figure 1): 1) the use of photolithographic techniques to prepare microstructured PMAA brushes; 2) the ability of the PMAA brushes to stabilize the ACC; and 3) the possibility to convert the metastable ACC phase into a polycrystalline calcite film by thermal treatment.

A first series of mineralization experiments was carried out with 100-nm-thick, unstructured PMAA brushes grafted on glass substrates. The brushes were exposed to a continuous flow of a supersaturated calcium carbonate solution in a perfusion cell. After 30 min, the substrates were taken from the perfusion cell, washed, dried, and subsequently analyzed with various microscopic techniques. The differential interference contrast (DIC) micrograph in Figure 2A shows the formation of a homogeneously flat and unstructured $CaCO_3$ film. The insert in Figure 2A shows an optical micrograph that was taken between crossed polarizers. The absence of birefringence in most of the micrograph indicates that the $CaCO_3$ film is predominantly amorphous. Figure 2A, however, also shows some isolated calcite crystals surrounded by circular features. These circular features can be attributed to the depletion of calcium carbonate around the forming crystal. Further confirmation of the amorphous nature of the $CaCO_3$ film was obtained by determining the optical retardance of the film with a birefringence imaging system (LC-PolScope).[19,20] The optical retardance is a function of the orientation of the crystallographic *c* axis and the thickness of the crystalline film. As shown by the false color image in Figure 2B, the optical retardance of the ACC film varied by less than 1 nm throughout the whole micrograph, which can be attributed to the lack of crystallinity in the film. The small variations that can be observed are due to the residual stress in the film. The amorphous nature of the $CaCO_3$ layer was also confirmed by attenuated total reflection (ATR)-FTIR experiments, which did not reveal the characteristic ν_4 absorption band of calcite at 714 cm^{-1} (Supporting Information).[21] These experiments clearly indicate that the PMAA

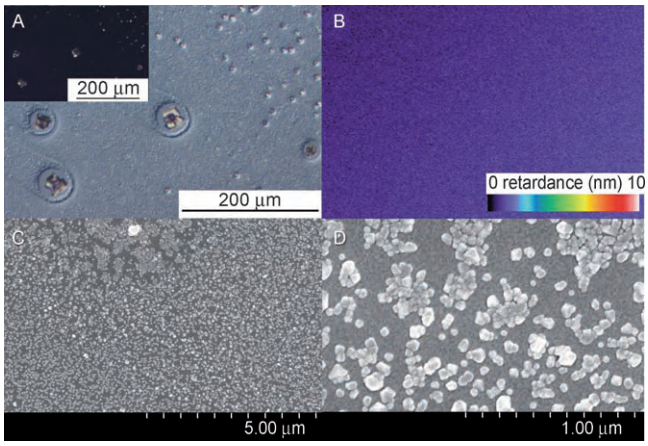

Figure 2. ACC film stabilized by a 100-nm-thick, unstructured PMAA brush. A) Differential interference contrast micrograph (inset: polarized optical micrograph); B) false-color LC-PolScope image; C) low- and D) high-magnification SEM images.

© 2006 Wiley-VCH Verlag GmbH & Co. KGaA, Weinheim

brushes allow the deposition and stabilization of a thin, metastable ACC film. The scanning electron micrographs in Figure 2C and Figure 2D show that the ACC film is composed of spherical particles with diameters ranging from 20 to 100 nm.

The ACC layer was subsequently crystallized by heating the sample to 250 °C for 2 h. The polarized optical micrograph of the resulting film in Figure 3 shows a mosaic structure of discrete domains, each consisting of a flat calcite single crystal. ATR-FTIR spectra revealed a characteristic ν_4 absorption band at 714 cm^{-1}, which supports the identification of the crystalline $CaCO_3$ modification as calcite (Supporting Information).[21] To obtain insight into the crystallographic orientation of the crystalline domains in the calcite film, LC-PolScope experiments were performed. Figure 3B shows an LC-PolScope image, which illustrates that each domain in the polycrystalline film is characterized by a narrow range of optical retardance values. The small variations that can be observed within the individual domains can be ascribed to stress-induced birefringence, which might result from the drying and shrinking of the film during the heating process. Figure 3C is an image of the same area as shown in Figure 3B, however, with the direction of the slow axis of birefringence indicated at several points as small vectors. Within each domain in Figure 3C, the birefringence vectors point in the same direction, which suggests that the polycrystalline film is composed of flat single calcite crystals. Figure 3D shows a scanning electron micrograph, which illustrates that the calcite film consists of coalesced $CaCO_3$ particles.

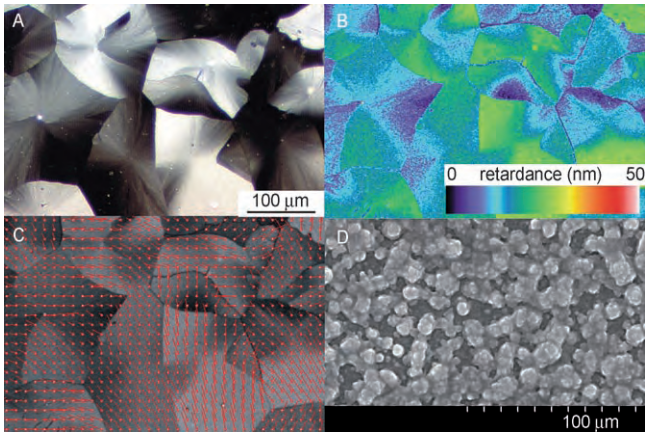

Figure 3. Thin calcite films obtained by heating a PMAA-brush-stabilized ACC film for 2 h at 250 °C. A) Polarized optical micrograph; B) LC-PolScope image (retardance values are indicated as false color); C) retardance gray-scale image (red vector overlay indicates the orientation of the slow birefringence axis); D) high-magnification SEM image.

The experiments discussed so far indicate that PMAA brushes can act as ionotropic matrices for the stabilization of a metastable ACC phase and for the subsequent formation of thin, polycrystalline calcite films by a simple thermal treatment. A subsequent series of experiments addressed whether glass substrates covered with patterned PMAA brushes can be used to fabricate microstructured calcite thin films. Patterned PMAA brushes were prepared by exposing substrates, which were functionalized with the ATRP initiator, to UV irradiation using a TEM grid as a photomask. Photoirradiation leads to decomposition of the ATRP initiator in the exposed regions, and subsequent SI-ATRP of sodium methacrylate only takes place on regions on the substrates that are not irradiated.[22] This effect is illustrated in Figure 4, which shows optical and atomic force microscopy (AFM) images of 90-nm-thick PMAA brushes, which were prepared using photomasks of different mesh sizes.

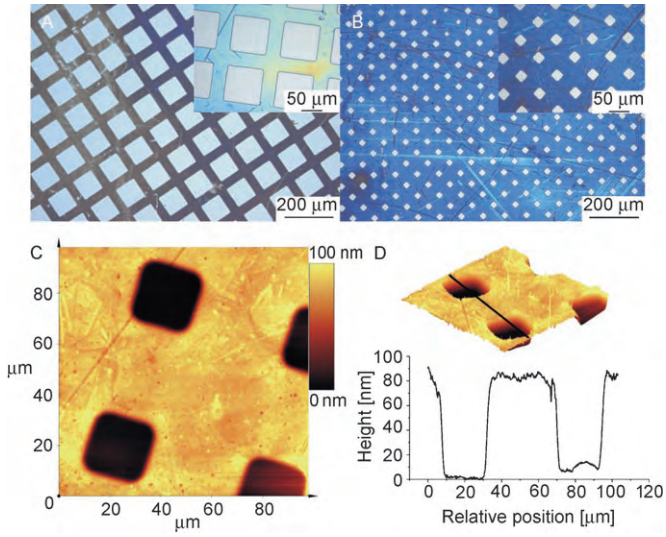

Figure 4. A),B) Reflected light microscopy images of photolithographically patterned PMAA brushes supported on silicon substrates prepared using different photomasks (insets: enlargements); C) topographical AFM image; D) 3D projection of the AFM image and height profile of a photolithographically patterned PMAA brush.

Mineralization experiments with the micropatterned PMAA brushes were carried out as described above with subsequent thermal treatment (2 h, 250 °C) to induce the formation of a thin, polycrystalline calcite film. Figure 5 shows for comparison a DIC micrograph of a layer of ACC that has been formed using a 90-nm-thick, micropatterned PMAA brush with DIC, polarized optical, and LC-PolScope images of the same sample after heating to 250 °C for 2 h. Comparison of Figure 5A and C clearly indicates that deposition of ACC only occurs on regions of the substrate defined by the PMAA brush pattern. This feature is particularly evident from the absence of birefringence in Figure 5C in areas that are not covered with PMAA. Figure 5C also shows that after thermal treatment areas of the substrate that had been covered with PMAA reveal a mosaic-like texture, similar to that shown in Figure 3A, which indicates the formation of a crystalline calcite film. Using AFM, the thickness of the microstructured calcite film could be estimated at approximately 80–90 nm (Supporting Information). This result suggests that mineralization of $CaCO_3$ occurs within the PMAA brush and indicates that the polycrystalline calcite thin film is an exact 3D replica of the

 © 2006 Wiley-VCH Verlag GmbH & Co. KGaA, Weinheim

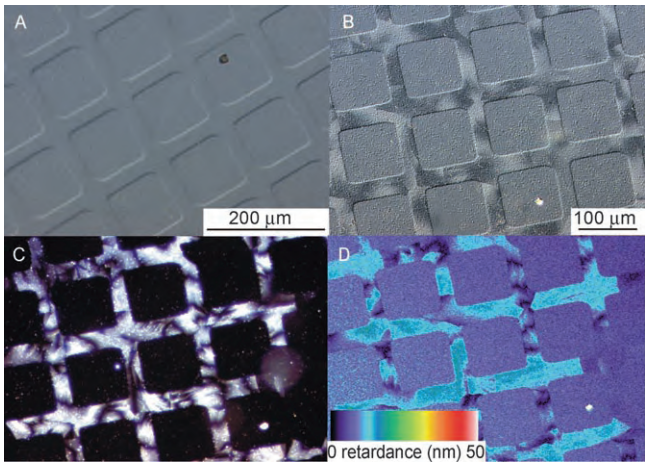

Figure 5. A) DIC micrograph of an ACC film deposited using a patterned 90-nm-thick PMAA brush on a glass substrate; B) DIC, C) polarized optical, and D) false-color LC-PolScope images of the same $CaCO_3$ film after heating for 2 h at 250 °C.

ionotropic PMAA matrix. Information about the crystallographic orientations of the calcite crystals in the microstructured film was obtained from LC-PolScope measurements. Comparison of Figure 3B and Figure 5D indicates a much narrower range of optical retardance values for the microstructured calcite film than for the unstructured sample. This result may be due to stress relaxation during crystallization which is facilitated in the microstructured sample.[8]

In conclusion, we have presented a novel strategy for the fabrication of microstructured calcite thin films. The process bears some resemblance to biological mineralization processes in that acidic macromolecules are used to form an ionotropic gel, which can host and stabilize a transient ACC phase and serve to direct crystal growth into geometries defined by the macromolecular matrix. We have used photolithographically patterned PMAA brushes a as biomimetic, acidic macromolecular matrix to fabricate microstructured calcite films that are an exact 3D replica of the PMAA brush. The success of the strategy relies on three key elements: 1) the use of photolithographic techniques to prepare microstructured PMAA brushes; 2) the ability of PMAA brushes to stabilize ACC and 3) the conversion of the metastable ACC phase into a polycrystalline calcite film by thermal treatment. In contrast to SAMs, $CaCO_3$ mineralization does not occur on a 2D template, but within the ionotropic PMAA brush matrix. Consequently, the PMAA brushes act as a 3D matrix that is copied with high fidelity into the final calcite replica. While the lateral dimensions of the microstructures are defined by the lithographic techniques that are used to prepare the micropatterned PMAA brush, the thickness of the calcite film can be adjusted through the thickness of the PMAA brush, which can be easily controlled owing to the "living" nature of the SI-ATRP procedure. The feasibility of this strategy was demonstrated with the fabrication of relatively simple, microstructured calcite films. It is anticipated, however, that this technique may be readily extended to other inorganic materials and more complex structures by combining the flexibility of SI-ATRP with regards to the chemical composition and architecture of the polymer brush with the numerous lithographic and nonlithographic methods that are available to generate micropatterned surfaces. This approach could lead to the fabrication of a variety of novel microstructured inorganic materials with interesting optical, catalytic, or biological properties.

Experimental Section

Details of the synthesis of the PMAA brushes and the mineralization experiments are given in the Supporting Information. Optical micrographs employing DIC and polarization contrast were recorded with a Hitachi HV-C20 A 3-CCD RGB camera at a resolution of $3 \times 768 \times 576$ pixels mounted on an inverted stage microscope (Olympus IX70). Birefringence measurements were performed with a commercial LC-PolScope imaging system (CRI). Atomic force microscopy was carried out using a Nanoscope II microscope. Electron micrographs were taken from samples that were rotary shadowed with platinum (3 nm) in a Balzers BAF 300 freeze-fracturing device and examined in a Hitachi S-5200 field emission scanning electron microscope. ATR-FTIR spectroscopy was performed on a Nicolet Magna-IR 560 spectrometer equipped with a single-reflection diamond ATR system (Specac Golden Gate).

Received: June 13, 2006
Published online: October 13, 2006

Keywords: biomimetic synthesis · biomineralization · calcium carbonate · polymer brushes · thin films

[1] S. I. Stupp, P. V. Braun, *Science* **1997**, *277*, 1242.
[2] B.-A. Gotliv, L. Addadi, S. Weiner, *ChemBioChem* **2003**, *4*, 522.
[3] L. Addadi, S. Raz, S. Weiner, *Adv. Mater.* **2003**, *15*, 959.
[4] T. Kato, A. Sugawara, N. Hosoda, *Adv. Mater.* **2002**, *14*, 869.
[5] Y. Politi, T. Arad, E. Klein, S. Weiner, L. Addadi, *Science* **2004**, *306*, 1161.
[6] N. Nassif, N. Pinna, N. Gehrke, M. Antonietti, C. Jäger, H. Cölfen, *Proc. Natl. Acad. Sci. USA* **2005**, *102*, 12653.
[7] E. Loste, F. C. Meldrum, *Chem. Commun.* **2001**, 901.
[8] J. Aizenberg, D. A. Muller, J. L. Grazul, D. R. Hamann, *Science* **2003**, *299*, 1205.
[9] D. Volkmer, M. Harms, L. Gower, A. Ziegler, *Angew. Chem.* **2005**, *117*, 645; *Angew. Chem. Int. Ed.* **2005**, *44*, 639.
[10] G. Xu, I. A. Aksay, J. T. Groves, *J. Am. Chem. Soc.* **2001**, *123*, 2196.
[11] D. Braga, *Angew. Chem.* **2003**, *115*, 5702; *Angew. Chem. Int. Ed.* **2003**, *42*, 5544.
[12] J. Aizenberg, *Adv. Mater.* **2004**, *16*, 1295.
[13] C. R. Martin, I. A. Aksay, *J. Electroceram.* **2004**, *12*, 53.
[14] Y. Gao, K. Koumoto, *Cryst. Growth Des.* **2005**, *5*, 1983.
[15] H. Thiele, *Histolyse und Histogenese: Gewebe und ionotrope Gele—Prinzip einer Strukturbildung*, Akademische Verlagsgesellschaft, Frankfurt am Main, **1967**.
[16] S. Edmondson, V. L. Osborne, W. T. S. Huck, *Chem. Soc. Rev.* **2004**, *33*, 14.
[17] B. Zhao, W. J. Brittain, *Prog. Polym. Sci.* **2000**, *25*, 677.
[18] J. Pyun, T. Kowalewski, K. Matyjaszewski, *Macromol. Rapid Commun.* **2003**, *24*, 1043.
[19] R. Oldenbourg, G. Mei, *J. Microsc.* **1995**, *180*, 140.
[20] R. Oldenbourg, *Nature* **1996**, *381*, 811.
[21] E. Beniash, J. Aizenberg, L. Addadi, S. Weiner, *Proc. R. Soc. London Ser. B* **1997**, *264*, 461.
[22] R. Iwata, P. Suk-In, V. P. Hoven, A. Takahara, K. Akiyoshi, Y. Iwasaki, *Biomacromolecules* **2004**, *5*, 2308.

 © 2006 Wiley-VCH Verlag GmbH & Co. KGaA, Weinheim

Molecular Switches

DOI: 10.1002/anie.200602591

Reversible Red Fluorescent Molecular Switches**

*Mariano Bossi, Vladimir Belov, Svetlana Polyakova, and Stefan W. Hell**

Materials with chemical and physical properties that can be optically modulated are of high interest for new optical recording systems, holographic rewriteable media, drug-delivery applications, biosensors, and advanced microscopic techniques.[1] Photochromic compounds readily lend themselves to this purpose, as they can be reversibly converted by light between two states with different spectroscopic properties.[2] This attribute can then be used to modulate or even switch secondary functions at the molecular or supramolecular level by using light as a trigger.

The reversible optical switching of fluorescence forms the foundation of a new physical concept in lens-based optical imaging to break through the resolution limit caused by diffraction (half the light wavelength).[3] In fact, a resolution at 1/46 of the light wavelength, corresponding to 16 nm, has been achieved with stimulated-emission depletion microscopy, a technique in which the fluorescence of molecular labels is reversibly switched off by ultrafast laser pulses, which induce stimulated emission.[3a] The generalization of this concept, termed RESOLFT (reversible saturable optical fluorescent transitions),[3b,c] showed that the use of ultrafast laser pulses can be avoided if photochromic fluorescent labels are used for the fluorescence switching.[3d] This promising method enables imaging and writing on the nanoscale with ultralow intensities of light. Unfortunately, none of the photochromic compounds synthesized so far possess the required optical properties: pronounced fluorescence modulation, high photostability, and fast switching times. Large fluorescence quantum yields (Φ_{fl}) are also highly desirable, as these allow short imaging times and sensitivity down to a single molecule.

A convenient way to modulate the fluorescence signal of a dye[4] is to attach it to a photochromic compound,[5] either directly[6] or through a linker.[7] The fluorescence modulation is effected through resonant energy transfer (RET)[8] from the fluorescent dye (RET donor) to one of the isomers of the photochromic switch (RET acceptor). For high RET efficiency, the absorption band of the RET acceptor must overlap with the emission band of the donor.

Diheteroaryl ethenes display excellent photochromic properties, can be switched many times, and are chemically and thermally stable. They can be reversibly photoswitched between a colorless open form (OF) and a colored closed form (CF).[5a] The forward reaction is driven by UV light and the reverse reaction by visible light (Scheme 1). Hence, the fluorescence of a fluorophore can be "switched off" when its emission band overlaps the absorption band of the CF of a diheteroaryl ethene, which functions as an RET acceptor.

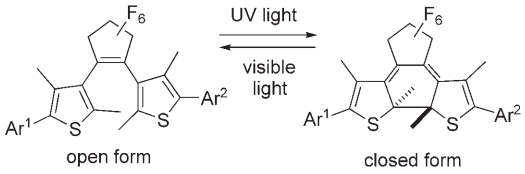

Scheme 1. Photochromism of 1,2-bis(thiophen-3-yl)cyclopentenes.

To control the photochromic reactions and the excitation of the fluorophore specifically, a large separation between the absorption bands of the OF, the CF, and the fluorophore is preferred. However, most of the fluorescent switches reported so far[9] do not fulfill this condition. Most compounds with a high degree of fluorescence modulation have only moderate or low Φ_{fl} values;[6d–f,h,j,n] in some cases, these values have not been reported.[6a–c,i,k,l,7a,b,d] Others possess a relatively low fluorescence modulation, especially when the ring-closing reaction is not activated at short wavelengths (254 or 313 nm).[6c,d,7b] Hence, their use in biological microscopy is precluded by the high autofluorescence background and expected photodamage. Moreover, aberration-corrected lenses with high numerical apertures (1.35–1.45) are only available for wavelengths greater than 360 nm. The goal of the present study was to synthesize photoswitchable fluorescent compounds with substantially improved performance in the visible or near-UV wavelength range. Particular importance was placed on increasing the fluorescence modulation at longer switching wavelengths and at the same time obtaining high Φ_{fl} values. For this purpose, we had to find a robust photochromic compound and a photo- and chemically stable fluorescent dye, and connect the two with a linker that enables effective RET between the donor and acceptor.

Rhodamine dyes are known to be good fluorescent labels that have large absorption coefficients and fluorescent quantum yields and show high photostability and a low rate of triplet formation. Moreover, they are preferred in biological applications because their excitation band between 550 and 600 nm results in lower autofluorescence compared with excitation in the UV or blue region. Owing to its high degree of substitution, the planar molecule rhodamine 101 (Rh 101) is one of the most stable fluorophores with Φ_{fl} close to unity.[10a] Its carboxy group is sterically hindered, and thus coupling

[*] Dr. M. Bossi, Dr. V. Belov, S. Polyakova, Prof. Dr. S. W. Hell
Department of Nanobiophotonics
Max Planck Institute for Biophysical Chemistry
Am Fassberg 11, 37077 Göttingen (Germany)
Fax: (+49) 551-201-2505
E-mail: shell@gwdg.de

[**] The authors are grateful to R. Machinek and co-workers, Dr. H. Frauendorf, G. Udvarnoki, G. Krökel, and F. Hambloch, for analyses performed at the Institut für Organische und Biomolekulare Chemie (Georg-August-Universität Göttingen), and to L. Kastrup, C. Eggeling, and J. Jethwa for critical reading of the manuscript. M.B. and S.W.H. acknowledge the European Commission for a Marie Curie Fellowship and support through the SPOTLITE project (NEST-Adventure).

Supporting information for this article is available on the WWW under http://www.angewandte.org or from the author.

InterScience
© 2006 Wiley-VCH Verlag GmbH & Co. KGaA, Weinheim

reactions with amines require special activation (the amino group is a convenient functional group for attachment to the fluorophore).[10b] The acylation of piperidine (chosen as a prototype for the linker) with Rh 101 to give compound Rh-NC_5H_{10} results in a red shift of the absorption band from 560 to 583 nm and the emission band from 589 to 604 nm without significant change in Φ_{fl} (Tables 1 and 2). This compound was prepared to study the effect on the fluorophore of substitution, and to evaluate the fluorescence of Rh-NC_5H_{10} in the absence of RET. The emission band of Rh-NC_5H_{10} required a photochromic system with an absorption maximum at about 620–640 nm for the CF.

Table 1: Photochemical and photophysical properties of the building blocks **1**–**3** and Rh-NC_5H_{10}.[a]

Compd	λ_{max} [nm] ($\varepsilon\times10^{-4}$ [$M^{-1}cm^{-1}$])		α_{PS}[b]	Φ		R_0 [Å]
	OF	CF		OF→CF[b]	CF→OF	
1	277 (3.0)	578 (1.4)	0.88	0.28	8.2×10^{-3}[c]	44
2	342 (2.4) 308 (2.3)	605 (1.5)	0.95	0.065	7.3×10^{-4}[c]	49
3	345 (4.1)	640 (1.9)	0.96	0.10	2.5×10^{-4}[d]	51
Rh-NC_5H_{10}	583 (10)[e]	–	–	–	–	

[a] Absorption coefficients (ε) were taken from Figure 1, the degree of conversion in the photostationary state (α_{PS}) was measured by HPLC, and quantum yields for the photochromic reactions ($\Phi_{OF\rightarrow CF}$ and $\Phi_{CF\rightarrow OF}$) were calculated from irradiation experiments.[14] Förster radii (R_0) for RET between the corresponding CF and the fluorophore (Rh-NC_5H_{10}) were calculated from the spectral properties of the components (see Figure 1).[16] Errors are approximately 10% for the quantum yields and absorption coefficients, and 2% for the conversion in the photostationary state. [b] Irradiation: 313 nm. [c] Irradiation: 577 nm. [d] Irradiation: 610 nm. [e] Emission maximum: 604 nm.

As a starting point, we chose a system described by the group of Lehn.[11] It consists of a 1,2-bis(2-methyl-3-thienyl)perfluorocyclopentene core with 4-hydroxyphenyl group at the 5-position of one thiophene ring and 4-pyridyl substituent at the 5′-position of the other thiophene ring. Its OF and CF in benzene absorb at 296 and 602 nm, respectively. The degree of conversion into the CF in the photostationary state (α_{PS}) was reported to be greater than 98% (in benzene). To increase the photochemical stability of this system, we blocked each of the unsubstituted thiophene positions with a methyl group[12] to prepare the photochromic compound **1** (Scheme 2). The major absorption maxima of the OF and the CF are at 277 and 578 nm, respectively (in EtOH). To shift the absorption of the CF to longer wavelengths, we inserted a thiophene ring between the pyridyl residue or the phenoxy group and the central core, and thus synthesized compounds **2** and **3** with an extended π system. Extended π conjugation is known to increase the ε value of the closed isomer and improve the conversion into the closed form, owing to a decrease in the quantum yield of the ring-opening reaction.[13] The linker units were synthesized through a Mitsunobu reaction of available *N*-Boc-4-hydroxy(methyl)piperidines with 4-iodophenol.[14] The precursor with a shorter linker (**4**) was obtained from 2-phenoxyethyl amine.[14] The carboxy group of Rh 101 was activated with the peptide coupling

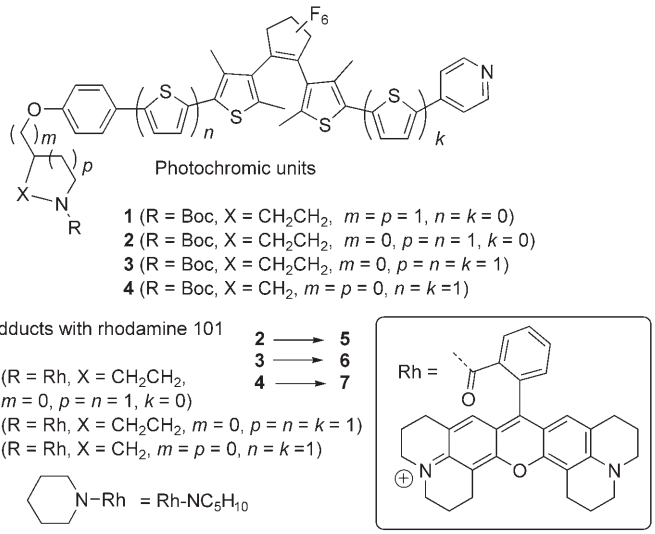

Scheme 2. Photochromic units **1**–**4** and their adducts with rhodamine 101 (**5**–**7**). Boc = *tert*-butyloxycarbonyl.

reagent HATU, and the adducts **5**–**7** were isolated in good yields. The final compounds were purified by HPLC where necessary.

The spectroscopic and photochromic properties of the novel molecular switches **5**–**7** and the building blocks **1**–**4** and Rh-NC_5H_{10} were studied in ethanol by irradiating diluted solutions (ca. 10^{-5} M) with light of different wavelengths.[14] The properties of the building blocks are summarized in Figure 1 and Table 1. The conversion of the parent photochromic compound **1** was incomplete ($\alpha_{PS} = 88\%$ at 313 nm), which is disadvantageous as the highest fluorescence modulation achievable is limited by the conversion of the photochromic unit. We define the fluorescence modulation (FM) as $1-F_{PS}/F_0$, in which F_0 and F_{PS} are the fluorescence signals of the initial and the photostationary (PS) states, respectively. The addition of one or more thiophene rings increases the

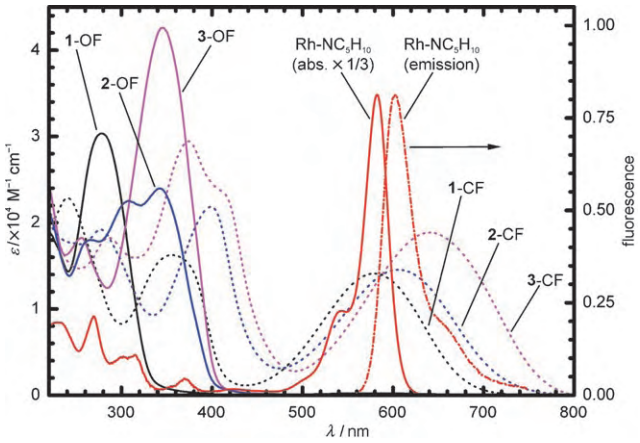

Figure 1. Absorption spectra (left axis) of the photochromic compounds **1**–**3**; open forms (OF) are plotted with full lines and closed forms (CF) with dotted lines (**1**: black, **2**: blue, **3**: purple). Absorption spectrum (solid red line) and fluorescence emission (dotted red line, right axis) for the fluorescent building block Rh-NC_5H_{10} are also shown.

 © 2006 Wiley-VCH Verlag GmbH & Co. KGaA, Weinheim

value of α_{PS} up to nearly 100%. The photocyclization reaction (OF→CF) was performed at 313, 366, and 375 nm, and the values of α_{PS} were found to be independent of the irradiation wavelength. A red shift and a slight increase in the absorption coefficient is observed in the absorption spectra of the CF with increasing number of thiophene rings. The addition of one thiophene ring in the OF (**2**) leads to splitting into two absorption bands, both of which are red-shifted relative to the spectrum of **1**. Compound **3** has only one major band at approximately the same wavelength as the second band of **2** (345 nm). The addition of thiophene units decreased the quantum efficiency of the ring-opening reaction ($\Phi_{CF\rightarrow OF}$), but no clear pattern was observed for the photocyclization reaction ($\Phi_{OF\rightarrow CF}$). The spectroscopic and photochromic properties of compounds **3** and **4** were identical, despite the different linkers involved; therefore, compound **4** is not included in Table 1 and Figure 1.

The photochromic building blocks **2**–**4** were attached to Rh101, whereas compound **1** was disregarded because of its lower α_{PS} value (<0.9). A shorter linker was also used (**4**) to study the effect of a decrease in the distance between the donor and the acceptor. The properties of the final adducts (**5**–**7**) are summarized in Table 2. All the absorption spectra

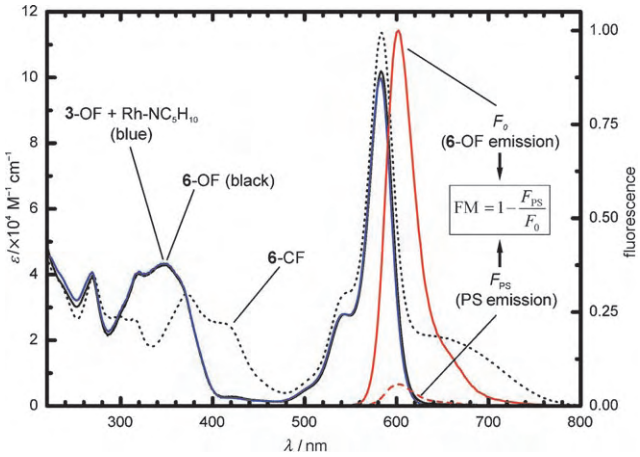

Figure 2. Absorption spectra (left axis) of **6** (solid black line: OF, dotted black line: CF) and the sum of the absorption spectra of compounds **3** and Rh-NC_5H_{10} (blue line). Fluorescence emission (right axis) of **6** in the OF (solid red line) and in the PS state under irradiation at 375 nm (dashed red line, 98% CF); the different intensities demonstrate the fluorescence modulation.

Table 2: Photochemical and photophysical properties of the fluorescent switches **5**–**7**.[a]

Compd	Φ		Φ_{fl}	α_{PS}[b]	FM	τ_{fl} [ns]	E_{RET}[12]	
	OF→CF[b]	CF→OF[c]					E_{OF}	E_{CF}
Rh-NC_5H_{10}	–	–	0.97	–	–	4.5	–	–
5	0.032	5.5×10^{-4}	0.72	0.98	0.86	3.3	0.26	0.91
6	0.063	2.2×10^{-4}	0.72	0.98	0.94	3.3	0.26	0.97
7	0.061	2.2×10^{-4}	0.29	0.98	0.92	1.3	0.72	0.98

[a] The fluorescence modulation (FM), as well as $\Phi_{OF\rightarrow CF}$ and $\Phi_{CF\rightarrow OF}$ values were calculated from irradiation experiments. α_{PS} was measured by HPLC,[14] and Φ_{fl} was measured by stationary methods.[15] Fluorescence lifetimes (τ_{fl}) are given for the OF.[14] See the Supporting Information for details of the calculation of E_{OF} and E_{CF}.[14] Errors are approximately 10% for quantum yields and absorption coefficients, 5% for fluorescence lifetimes, and 2% for the conversion in the photostationary state and fluorescence modulation. [b] Irradiation: 313 nm. [c] Irradiation: 660 nm.

indicate the absence of perturbations due to the binding of donor and acceptor units. The spectra of **6** are given in Figure 2 as an example. The blue line is the sum of the spectra of the components **3**-OF and Rh-NC_5H_{10}. It is identical within experimental errors to the spectrum of **6**-OF (Figure 2, black line). Moreover, the emission spectra of all compounds (**5**–**7** and Rh-NC_5H_{10}) are identical, and a decrease in $\Phi_{OF\rightarrow CF}$ values was observed for each of the final adducts relative to the corresponding photochromic building blocks **2**–**4**. This tendency can be attributed to the fact[7c] that some of the irradiation light is absorbed by the fluorophore and hence cannot contribute to photocyclization. The efficiencies of the reverse reaction ($\Phi_{CF\rightarrow OF}$) are nearly unaffected by coupling to Rh101. The values obtained for α_{PS} were slightly enhanced and are close to 100% for all adducts (**5**–**7**).

FM, Φ_{fl}, fluorescence lifetimes (τ_{fl}), and RET efficiencies of both isomers (E_{OF} and E_{CF}) were measured in dilute solutions (optical density <0.05) to avoid any self-absorption effects.[15] Two important conclusions follow from the results (Table 2): First, comparison of **5** and **6** reveals an increase in FM and E_{CF}. This result correlates with the calculated R_0 value (Table 1), which is slightly larger for **3**, the building block of **6**. Second, a shorter linker results in only a slightly larger E_{CF} value for compound **7** relative to **6**, but a significantly larger E_{OF} value. This increase is responsible for the poorer FM value of **7**. Consequently, a longer linker may be introduced to reduce E_{OF} while leaving E_{CF} unchanged. In other words, the linker may be lengthened without problem to insert a binding unit for attaching the whole fluorescent structure as a label to a substrate.

In summary, we have prepared switchable fluorescent compounds with improved properties in the visible wavelength region which make them suitable for application in information storage and fluorescence microscopy. The photocyclization reaction responsible for quenching the fluorescent signal can be activated by focusable light. The synthesized compounds **5**–**7** possess large fluorescence modulation (>85%) even with irradiation at 375 nm, where many photostable diaryl perfluorocyclopentenes do not absorb.[5a] The photocyclization reaction of these switches can be carried out with laser diodes. Large RET efficiencies for the energy transfer between the fluorophore and the CF of the photochromic moieties account for the strong fluorescence modulations observed. All compounds have good fluorescence quantum yields (≥30%), in particular **5** and **6** (70%). The fluorescence signal can be probed at 550–600 nm and detected between 600 and 700 nm, thereby minimizing the generation of background signal. Further work involves attaching reactive groups to **6** in order to bind it to polymer precursors, nanoparticles, and biomolecules. As a label in a RESOLFT method, this or similar compounds could boost

 © 2006 Wiley-VCH Verlag GmbH & Co. KGaA, Weinheim

the spatial resolution of far-field fluorescence microscopy by at least an order of magnitude.

Received: June 29, 2006
Published online: October 16, 2006

Keywords: fluorescence modulation · heterocycles · molecular switches · photochromism · rhodamines

[1] *Organic Photochromic and Thermochromic Compounds*, *Vol. 1* (Eds.: J. C. Crano, R. J. Guglielmetti), Kluwer/Plenum, New York, **1999**.
[2] *Molecular Switches* (Ed.: B. L. Feringa), Wiley-VCH, Weinheim, **2001**.
[3] a) V. Westphal, S. W. Hell, *Phys. Rev. Lett.* **2005**, *94*, 143903; b) S. W. Hell, *Nat. Biotechnol.* **2003**, *21*, 1347–1355; c) S. W. Hell, M. Dyba, S. Jakobs, *Curr. Opin. Neurobiol.* **2004**, *14*, 599–609; d) S. W. Hell, S. Jakobs, L. Kastrup, *Appl. Phys. A* **2003**, *77*, 859–860.
[4] For a review, see: F. M. Raymo, M. Tomasulo, *J. Phys. Chem. A* **2005**, *109*, 7343–7352.
[5] Photochromic properties of diaryl ethylenes and fulgides have been reviewed: a) M. Irie, *Chem. Rev.* **2000**, *100*, 1685–1716; b) Y. Yokoyama, *Chem. Rev.* **2000**, *100*, 1717–1739; c) a recent report on diaryl ethylenes: Y.-C. Jeong, S. I. Yang, E. Kim, K.-H. Ahn, *Tetrahedron* **2006**, 5855–5861.
[6] a) G. M. Tsivgoulis, J.-M. Lehn, *Angew. Chem.* **1995**, *107*, 1188–1191; *Angew. Chem. Int. Ed. Engl.* **1995**, *34*, 1119–1122; b) G. M. Tsivgoulis, J.-M. Lehn, *Chem. Eur. J.* **1996**, *2*, 1399–1406; c) M. Takeshita, M. Irie, *Chem. Lett.* **1998**, 1123–1124; d) A. Osuka, D. Fujikane, H. Shinmori, S. Kobatake, M. Irie, *J. Org. Chem.* **2001**, *66*, 3913–3923; e) J. Ern, A. T. Bens, H.-D. Martin, S. Mukamel, S. Tretiak, K. Tsyganenko, K. Kuldova, H. P. Trommsdorf, C. Kryshi, *J. Phys. Chem. A* **2001**, *105*, 1741–1749; f) K. Yagi, C. F. Song, M. Irie, *J. Org. Chem.* **2001**, *66*, 5419–5423; g) T. Kawai, T. Sasaki, M. Irie, *Chem. Commun.* **2001**, 711–712; h) H. Cho, E. Kim, *Macromolecules* **2002**, *35*, 8684–8687; i) T. A. Golovkova, D. V. Kozlov, D. C. Neckers, *J. Org. Chem.* **2005**, *70*, 5545–5549; j) A. Fernández-Acebes, J.-M. Lehn, *Chem. Eur. J.* **1999**, *5*, 3285–3292; k) T. B. Norsten, N. R. Branda, *Adv. Mater.* **2001**, *13*, 347–349; l) A. L. Myles, N. R. Branda, *Adv. Funct. Mater.* **2002**, *12*, 167–173; m) M.-S. Kim, T. Kawai, M. Irie, *Chem. Lett.* **2001**, 702–703; n) R. T. F. Jukes, V. Adamo, F. Hartl, P. Besler, L. De Cola, *Inorg. Chem.* **2004**, *43*, 2779–2792.
[7] a) J. M. Endtner, F. Effenberger, A. Hartschuh, H. Port, *J. Am. Chem. Soc.* **2000**, *122*, 3037–3046; b) L. Giordano, T. M. Jovin, M. Irie, E. A. Jares-Erijman, *J. Am. Chem. Soc.* **2002**, *124*, 7481–7489; c) T. Fukaminato, T. Sasaki, T. Kawai, N. Tamai, M. Irie, *J. Am. Chem. Soc.* **2004**, *126*, 14843–14849; d) M. Frigoli, G. H. Mehl, *Chem. Eur. J.* **2004**, *10*, 5243–5250.
[8] B. W. van der Meer, G. Coker III, S.-Y. S. Chen, *Resonance Energy Transfer: Theory and Data*, Wiley-VCH, Weinheim, **1991**.
[9] Outstanding fluorescence modulation was reported for condensed dithieno(thiophenes)[6a,b] or ethinyl-Bodipy[6i] residues as fluorophores directly attached to 1,2-bis(2-alkyl-3-thienyl)perfluorocyclopentenes. The highest conversion to the closed form was 92%[6a,b] and 96%[6i] and was achieved at 365 and 254 nm, respectively. In both cases, the remaining fluorescence was 10–11%. When anthracene was connected through a CH_2 group to an acceptor, 87% conversion to the nonfluorescent CF was observed at the PS state at 355 nm.[7a] Irie and co-workers[7c] used the 1,3-adamantane linker and studied in detail the single molecule properties of the highly fluorescent 2,5-dimethoxy-bis(9,10-phenylethinyl)anthracene. Similar fluorophores connected to two acceptor units displayed around 80% fluorescence modulation and 83% Φ_{fl}.[6g] In another study,[7b] in which Lucifer yellow was connected to different acceptors through relatively long and flexible cadaverine linkers acylated with succinic or butanoic acid residues, the fluorescence decreased by 65 or 84% in the PS state (at 313 and 320 nm, respectively).
[10] a) T. Karstens, K. Kobs, *J. Phys. Chem.* **1980**, *84*, 871–872; b) T. Nguyen, M. B. Francis, *Org. Lett.* **2003**, *5*, 3245–3248.
[11] a) S. H. Kawai, S. L. Gilat, R. Ponsinet, J.-M. Lehn, *Chem. Eur. J.* **1995**, *1*, 285–293; b) S. H. Kawai, S. L. Gilat, J.-M. Lehn, *Eur. J. Org. Chem.* **1999**, 2359–2366.
[12] This substitution pattern is known to increase the photochemical stability against irreversible isomerization: M. Irie, T. Lifka, K. Uchida, S. Kobatake, Y. Shindo, *Chem. Commun.* **1999**, 747–750.
[13] G. M. Tsivgoulis, J.-M. Lehn, *Adv. Mater.* **1997**, *9*, 39–41.
[14] See the Supporting Information for details.
[15] J. R. Lackowicz, *Principles of Fluorescence Spectroscopy*, 2nd ed., Kluwer/Plenum, New York, **1999**.
[16] B. Valeur, *Molecular Fluorescence: Principles and Applications*, Wiley-VCH, Weinheim, **2002**.

 © 2006 Wiley-VCH Verlag GmbH & Co. KGaA, Weinheim

Intermetallic Compounds

DOI: 10.1002/anie.200602712

Transition-Metal Anions in Solids and Their Implications on Bonding**

Myung-Hwan Whangbo, Changhoon Lee, and Jürgen Köhler**

Despite its highly qualitative nature, the concept of oxidation state developed nearly two centuries ago has remained useful, largely because it enables one to predict the major orbital characters of the frontier energy levels for a given compound. The oxidation state of an atom in a compound is determined by counting the valence electrons of the constituent atoms by using a set of commonly accepted rules. This electron counting is most straightforward for two limiting cases of binary compounds: ionic and covalent compounds. When a compound contains several elements with a range of similar

[*] Prof. Dr. M.-H. Whangbo, C. Lee
Department of Chemistry
North Carolina State University
Raleigh, NC 27695-8204 (USA)
Fax: (+1) 919-515-7832
E-mail: mike_whangbo@ncsu.edu
Priv.-Doz. Dr. J. Köhler
Max-Planck-Institut für Festkörperforschung
Heisenbergstrasse 1, 70569 Stuttgart (Germany)
Fax: (+49) 711-689-1091
E-mail: j.koehler@fkf.mpg.de

[**] The work at NCSU was supported by the Office of Basic Energy Sciences, Division of Materials Sciences, US Department of Energy, under grant DE-FG02-86ER45259.

© 2006 Wiley-VCH Verlag GmbH & Co. KGaA, Weinheim

electronegativities, the assignment of oxidation states can be somewhat arbitrary. To correctly predict the nature of the frontier energy levels in such a case, it is necessary to employ a modified electron counting scheme that takes orbital energy differences into consideration.[1]

Intermetallic compounds containing electropositive atoms (for example, alkali, alkaline-earth, or rare-earth metals) exhibit both covalent and ionic components. For example, in NaTl, each sodium atom donates its valence electron to a thallium atom, and the resulting Tl^- ions form a lattice with a diamond structure and covalent bonding.[2,3] In contrast to the case of main-group-element atoms, transition-metal atoms have rarely been considered to form anions. However, the electronegativities of late transition metals, such as gold and platinum, are only slightly lower than that of iodine.[4] It took some years to accept CsAu[5] as an ionic species with Cs^+ and Au^- ions,[6] but now there are several such aurides.[7]

The extension of this finding to other transition metals was first realized in the red, transparent compound Cs_2Pt, which contains Cs^+ and Pt^{2-} ions.[8] The recently discovered compounds $PtIn_7F_{13}$,[9] $PtIn_6Ga_2O_8$,[10] $Pt_2In_{14}Ga_3O_8F_{15}$,[11] and $PtIn_6Ge_2O_9$[12] contain the octahedral cation $[PtIn_6]^{10+}$, in which the Pt–In bonds are strongly covalent, but the oxidation state of platinum is most likely −2.[9,11] There are other known octahedral cluster cations of main-group elements in which the encapsulated late transition metals exist most likely as anions, for example, $[MSn_6]^{14+}$ (M = Fe, Ru)[13] and $[IrBi_6]^{n+}$ ($n = 3, 4$).[11,14] In such cluster cations, the *n*d orbitals of the transition metal act as a reservoir for 10 electrons. The bonding of the transition-metal atom with the surrounding main-group-element ligands, which leads to the frontier energy levels, primarily involves the $(n+1)$s and $(n+1)$p orbitals of the transition metal. Thus, the transition metal behaves like a main-group element.[11] This picture of bonding was also observed in the electronic structures of the highly negative $[MIn_{10}]^{10-}$ ions found in $K_{10}In_{10}M$ (M = Ni, Pd, Pt).[15] Our search for further examples of transition-metal anions has led us to intermetallic compounds containing both electropositive elements (for example, alkaline-earth and rare-earth metals) and late transition metals.

Herein, we discuss the results of our electronic-band-structure calculations for three isostructural intermetallic compounds, La_2Ge_2In,[16] La_2Pt_2In,[17,18] and La_2Cu_2In.[19] In the crystal structures of La_2M_2In (M = Pt, Cu, Ge), layers of composition M_2In alternate with layers of lanthanum atoms along the *c* direction. In each M_2In layer, the indium atoms form a nearly ideal square lattice in which every In_4 "square" contains one M–M dimer (Figure 1a). Every lanthanum atom is located at a 10-coordinate site surrounded by four indium atoms and six M atoms from four M–M dimers (Figure 1b). The M–M distances of La_2M_2In (Pt–Pt = 2.85 Å, Cu–Cu = 2.59 Å, Ge–Ge = 2.54 Å) are slightly longer than those of elemental M (Pt–Pt = 2.775 Å, Cu–Cu = 2.556 Å, Ge–Ge = 2.450 Å).[4] In the following, we show that the transition-metal atoms of La_2M_2In (M = Pt, Cu) exist as anions and discuss their bonding characteristics.

Electronic-band-structure calculations have been reported for the isostructural compounds Ce_2M_2In (M = Ge, Pt)[20] and Gd_2Ge_2Mg.[21] Both studies carried out crystal-orbital Hamiltonian population (COHP) analyses[22] to find that, below the Fermi level, substantial bonding occurs in the RE–M, M–In, and M–M interactions (RE = Ce, Gd; M = Ge, Pt). In the study of Gd_2Ge_2Mg,[21] Choe et al. suggested that the Ge–Ge dimer exists as the Zintl ion $[Ge–Ge]^{6-}$. The main objective of our study is to show that, in intermetallic compounds containing 3d–5d transition metals and electropositive elements, the transition-metal atoms can be regarded as anions with full *n*d orbitals, and their bonding characters can be regarded as similar to those of the late main-group elements of Periods 4–6.

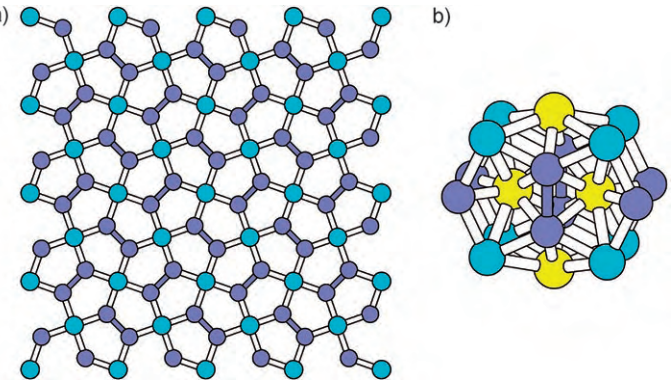

Figure 1. Crystal structure of La_2M_2In (M = Ge, Pt, Cu). a) An M_2In layer (viewed along [001]). b) Coordination environment of the lanthanum atoms. La yellow, M blue, In cyan.

The electronic band structures of La_2M_2In (M = Ge, Pt, Cu) are summarized in Figures 2 and 3; the band dispersion relations are plotted in Figure 2, and the density of states (DOS) in Figure 3. In all three compounds, the lanthanum 5d-, 6s-, and 6p-orbital contributions below the Fermi level are substantial. However, their major contributions lie above the Fermi level, and lanthanum is the least electronegative element in the compound. These factors give rise to an oxidation state of +3 and, hence, to the electron counting $[M_2In]^{6-}$. The indium 5s-orbital contributions occur largely around −5.0 eV for La_2Ge_2In, −6.0 eV for La_2Pt_2In, and −6.5 eV for La_2Cu_2In. The indium 5p-orbital contributions appear mainly above −3.0 eV for La_2Ge_2In, −4.0 eV for La_2Pt_2In, and −5.0 eV for La_2Cu_2In. Namely, the energy regions of the valence 5s- and 5p-orbital contributions of indium are well-separated; thus, there is no 5s/5p orbital hybridization of indium.

The germanium 4s-orbital contributions occur primarily around −7.0 eV, the platinum 6s-orbital contributions between −4.5 and −5.0 eV, and the copper 4s-orbital contributions between −5.5 and −5.0 eV. The germanium 4p-orbital contributions appear largely between −3.5 and −0.5 eV, the platinum 6p-orbital contributions between −4.0 and −1.5 eV, and the copper 4p-orbital contributions between −5.2 and −3.5 eV. Thus, the energy regions of the valence *n*s- and *n*p-orbital contributions of M are well separated, and there is no *n*s/*n*p orbital hybridization of M in La_2M_2In.

The platinum 5d-orbital contributions occur largely between −4.0 and −1.5 eV, and the copper 3d-orbital contributions between −5.2 and −3.5 eV. The *n*d-block

 © 2006 Wiley-VCH Verlag GmbH & Co. KGaA, Weinheim

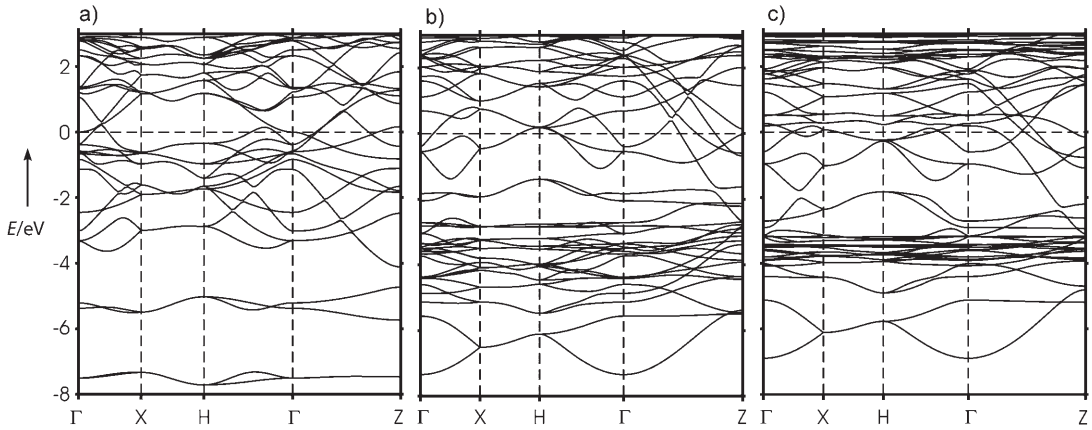

Figure 2. Dispersion relations of the bands near the Fermi level for a) La_2Ge_2In, b) La_2Pt_2In, and c) La_2Cu_2In.

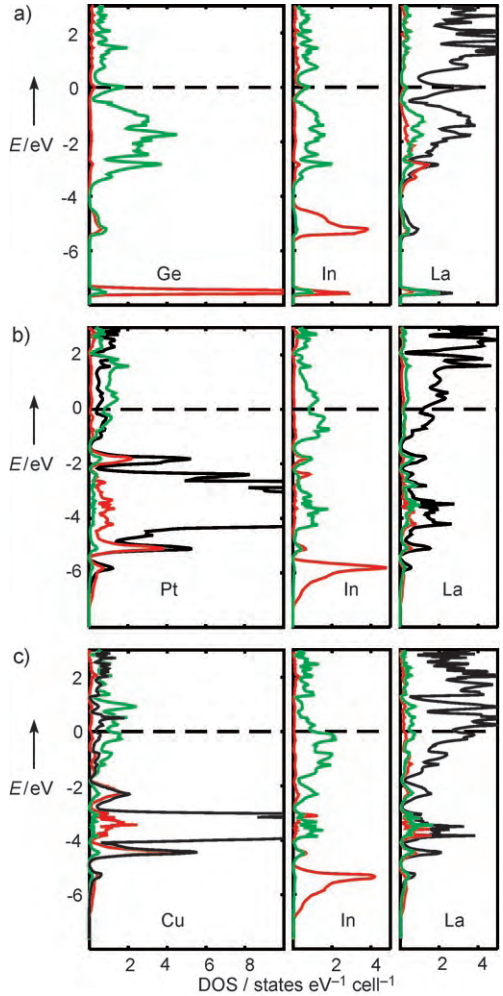

Figure 3. Partial DOS plots for a) La_2Ge_2In, b) La_2Pt_2In, and c) La_2Cu_2In. The red, green, and black curves represent the contributions of the s, p, and d orbitals, respectively.

bands of La_2M_2In (M = Pt, $n = 5$; M = Cu, $n = 3$) are completely filled and occur between the $(n+1)$s- and $(n+1)$p-block bands. The highest occupied bands of La_2M_2In (M = Pt, Cu) are the $(n+1)$p-block bands of M and the 4p-block bands of indium, both of which are partially filled. Since the $(n+1)$s- and nd-block bands of M are completely filled, while the $(n+1)$p-block bands of M are partially filled, the oxidation states of the transition metals are negative (see below). In essence, the energies of the valence atomic orbitals of the transition metals M in La_2M_2In (M = Pt, Cu) increase in the order $(n+1)\text{s} < n\text{d} < (n+1)\text{p}$. This is the sequence found for an isolated transition-metal atom of oxidation state 0. In describing the electronic structures of transition-metal compounds with main-group elements, however, the commonly found orbital sequence is $n\text{d} < (n+1)\text{s} < (n+1)\text{p}$.

It is important to understand why this switching of the orbital sequence takes place. In general, increasing (decreasing) the number of electrons around a system increases (decreases) the extent of electron–electron repulsion and, hence, raises (lowers) the energies of all the orbitals of the system.[23] However, this effect does not affect all the orbitals uniformly; a more contracted orbital is more strongly affected. For a transition metal, the nd orbitals are more contracted than the $(n+1)$s orbital. Thus, unless the atoms surrounding a transition-metal atom lead to strongly preferential orbital interactions with the nd, $(n+1)$s, or $(n+1)$p orbitals, the energy of the nd orbitals is lowered below that of the $(n+1)$s orbital when the oxidation state of the transition metal is positive, and is raised above that of the $(n+1)$s orbital when the oxidation state is zero or negative (Figure 4). In cases where the oxidation state of the transition metal is positive, this effect also explains why the energy difference between the nd and the $(n+1)$s levels of a transition-metal atom decreases on going from the left to the right of the Periodic Table. Owing to the relativistic effect, this trend is more pronounced for the 5d transition metals than for the 3d and 4d transition metals.[24]

It is important to have simple pictures of bonding that capture the essence of the electronic structures of La_2M_2In (M = Ge, Pt, Cu). The M–M bond of La_2M_2In can be regarded as a single bond. Since there is no s/p orbital hybridization of M, the M–M single bond is a σ bond formed between the valence p orbitals of two M atoms that point toward each other. To form such a σ bond, each germanium atom should have the electron configuration $(4s)^2(4p)^5$, which corresponds to a Ge^{3-} ion. Namely, each Ge–Ge dimer of La_2Ge_2In exists as the Zintl ion $[Ge{-}Ge]^{6-}$, as in the isostructural compound

 © 2006 Wiley-VCH Verlag GmbH & Co. KGaA, Weinheim

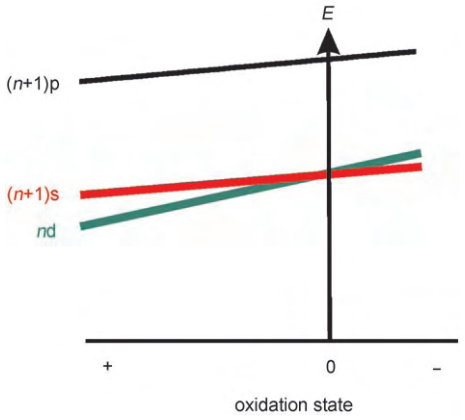

Figure 4. Variation in the sequence of the *n*d, (*n*+1)s, and (*n*+1)p orbitals of a transition metal as a function of oxidation state.

Gd_2Ge_2Mg.[21] Thus, each indium atom of La_2Ge_2In has an oxidation state of 0 and, hence, the electron configuration $(5s)^2(5p)^1$.

As already pointed out, the (*n*+1)s- and *n*d-block bands of La_2M_2In (M = Pt, *n* = 5; Cu, *n* = 3) are completely filled. To form a Pt–Pt σ bond using 6p orbitals, each platinum atom should have the electron configuration $(6s)^2(5d)^{10}(6p)^1$, which corresponds to a Pt^{3-} ion. To a first approximation, therefore, each Pt–Pt dimer of La_2Pt_2In exists as the Zintl ion $[Pt–Pt]^{6-}$, and each indium atom of La_2Pt_2In has an oxidation state of 0. To form a Cu–Cu σ bond using 4p orbitals, each copper atom should have the electron configuration $(4s)^2(3d)^{10}(4p)^1$, which corresponds to a Cu^{2-} ion. Therefore, each Cu–Cu dimer of La_2Cu_2In exists as the Zintl ion $[Cu–Cu]^{4-}$. Each indium atom of La_2Cu_2In has an oxidation state of −2 and, hence, the electron configuration $(5s)^2(5p)^3$.

These simple pictures of bonding are supported by the DOS plots in Figure 3. In the energy region below the Fermi level, where there are strong contributions from M orbitals, the contributions from the lanthanum 5d, 6s, and 6p orbitals, and the indium 5p orbitals are substantial. This observation suggests a stabilization of the Zintl anions by M–La and M–In bonding, as observed in studies of Ce_2M_2In (M = Ge, Pt)[20] and Gd_2Ge_2Mg.[21] Choe et al. considered the electron-counting scheme $(Gd^{3+})_2(Ge_2^{6-})(Mg^{2+})(e^-)_2$ for Gd_2Ge_2Mg. To indicate that the magnesium 3s-block bands are completely filled in Gd_2Ge_2Mg,[21] the alternative description $(Gd^{3+})_2(Ge_2^{6-})(Mg^0)$ might be preferred. An important consequence for a transition-metal anion is that it cannot carry a magnetic moment, because its d-block levels, which are contracted and, hence, can accommodate unpaired electrons, are completely filled.

In summary, our work has shown that the transition-metal atoms in La_2Pt_2In and La_2Cu_2In exist as the Zintl ions $[Pt–Pt]^{6-}$ and $[Cu–Cu]^{4-}$, respectively, and has clarified why the orbital sequence of a transition metal switches from *n*d < (*n*+1)s < (*n*+1)p to (*n*+1)s < *n*d < (*n*+1)p depending on its oxidation state. For a large number of intermetallic compounds containing late 3d–5d transition-metal atoms, the nature of their frontier orbitals and, hence, their electronic properties can be easily understood, once it is recognized that the transition-metal atoms in such compounds can be regarded as anions with bonding characteristics similar to those of the late main-group elements of Periods 4–6.

Experimental Section

First-principles density functional theory (DFT) electronic-band-structure calculations were performed for La_2M_2In (M = Ge, Pt, Cu), using the tight-binding linear muffin-tin orbital (TB-LMTO) method[25] in the atomic-sphere approximation (ASA) and in its scalar relativistic version.[26] The exchange-correlation potential was calculated according to von Barth and Hedin,[27] with 96 k points sampling the irreducible Brillouin zone. The basis sets consisted of s, p, d, and f functions for lanthanum, and of s, p, and d functions for indium, germanium, and platinum. No empty spheres were needed to achieve convergence for La_2Cu_2In and La_2Ge_2In, and the overlap criterion between Wigner–Seitz spheres was set to a maximum of 16%. Only for La_2Pt_2In was the atomic sphere overlap too large; in this case, the insertion of two empty spheres into the interstitial regions was necessary. The k space was integrated using the tetrahedron method, with 1602 k points within the first Brillouin zone, to calculate the DOS plots.

Received: July 7, 2006
Revised: August 29, 2006
Published online: October 6, 2006

Keywords: electronic structure · germanium · intermetallic phases · transition metals · Zintl anions

[1] a) J. A. Paradis, M.-H. Whangbo, R. V. Kasowski, *New J. Chem.* **1993**, *17*, 525; b) K.-S. Lee, H.-J. Koo, D. Dai, J. Ren, M.-H. Whangbo, *Inorg. Chem.* **1999**, *38*, 340; c) K.-S. Lee, H.-J. Koo, D. Dai, J. Ren, M.-H. Whangbo, *J. Solid State Chem.* **1999**, *147*, 11.
[2] a) E. Zintl, W. Dullenkopf, *Z. Phys. Chem. Abt. B* **1932**, *16*, 183; b) E. Zintl, G. Brauer, *Z. Phys. Chem. Abt. A* **1933**, *20*, 241; c) E. Zintl, G. Woltersdorf, *Z. Elektrochem.* **1935**, *41*, 876.
[3] I. Hewaidy, E. Busmann, W. Klemm, *Z. Anorg. Allg. Chem.* **1964**, *326*, 283.
[4] http://www.webelements.com/. The Pauling electronegativities of gold, platinum, and iodine are 2.54, 2.28, and 2.66, respectively.
[5] A. H. Sommer, *Nature* **1943**, *152*, 215.
[6] a) V. E. Wood, J. R. Reitz, *J. Phys. Chem. Solids* **1962**, *23*, 229; b) T. L. Liu, *Phys. Rev.* **1975**, *12*, 3008; c) A. Hasegawa, M. Watabe, *J. Phys. F* **1977**, *7*, 75; d) J. Knecht, R. Fischer, H. Overhof, F. Hensel, *J. Chem. Soc. Chem. Commun.* **1978**, 905; e) G. K. Wertheim, R. L. Cohen, G. Crecelius, K. W. West, J. H. Wemick, *Phys. Rev. B* **1979**, *20*, 860.
[7] a) A. Pantelouris, G. Küper, J. Hormes, C. Feldmann, M. Jansen, *J. Am. Chem. Soc.* **1995**, *117*, 11749; b) A. V. Mudring, M. Jansen, *Z. Naturforsch. B* **2001**, *56*, 433; c) J. Nuss, M. Jansen, *Z. Kristallogr. New Cryst. Struct.* **2002**, *217*, 313.
[8] A. S. Karpov, J. Nuss, U. Wedig, M. Jansen, *Angew. Chem.* **2003**, *115*, 4966; *Angew. Chem. Int. Ed.* **2003**, *42*, 4818.
[9] J. Köhler, J.-H. Chang, *Angew. Chem.* **2000**, *112*, 2077; *Angew. Chem. Int. Ed.* **2000**, *39*, 1998.
[10] H. A. Friedrich, J. Köhler, *Z. Anorg. Allg. Chem.* **2001**, *627*, 144.
[11] J. Köhler, J.-H. Chang, M.-H. Whangbo, *J. Am. Chem. Soc.* **2005**, *127*, 2277.
[12] J. Köhler, H. A. Friedrich, M.-H. Whangbo, A. Villesuzanne, *J. Am. Chem. Soc.* **2005**, *127*, 12990.
[13] a) T. Söhnel, P. Böttcher, W. Reichelt, F. E. Wagner, *Z. Anorg. Allg. Chem.* **1998**, *624*, 708; b) T. Söhnel, W. Reichelt, F. E. Wagner, *Z. Anorg. Allg. Chem.* **2000**, *626*, 223.

 © 2006 Wiley-VCH Verlag GmbH & Co. KGaA, Weinheim

[14] M. Ruck, *Z. Anorg. Allg. Chem.* **1998**, *624*, 521.
[15] S. C. Sevov, J. D. Corbett, *J. Am. Chem. Soc.* **1993**, *115*, 9089.
[16] V. I. Zaremba, A. Stepien-Damm, G. P. Nichiporuk, Yu. B. Tyvanchuk, Ya. M. Kalychak, *Kristallografiya* **1998**, *43*, 13.
[17] D. Kaczorowski, P. Rogl, K. Hiebl, *Phys. Rev. B* **1996**, *54*, 9891.
[18] Ya. V. Galadzhun, R. Pöttgen, *Z. Anorg. Allg. Chem.* **1999**, *625*, 481.
[19] R. Mishra, R.-D. Hoffmann, R. Pöttgen, *Z. Naturforsch. B* **2001**, *56*, 239.
[20] V. I. Zaremba, D. Johrendt, U. Ch. Rodewald, G. P. Nychyporuk, R. Pöttgen, *Solid State Sci.* **2005**, *7*, 998.
[21] W. Choe, G. J. Miller, E. M. Levin, *J. Alloys Compd.* **2001**, *329*, 121.
[22] R. Dronskowski, P. Blöchl, *J. Phys. Chem.* **1993**, *97*, 8617.
[23] T. A. Albright, J. K. Burdett, M.-H. Whangbo, *Orbital Interactions in Chemistry*, Wiley, New York, **1985**.
[24] P. Pyykkö, J. P. Desclaux, *Acc. Chem. Res.* **1979**, *12*, 276.
[25] R. Tank, O. Jepsen, A. Burkhardt, O. K. Andersen, TB-LMTO-ASA, Version 4.7, MPI für Festkörperforschung, Stuttgart, **1998**.
[26] a) O. K. Andersen, *Phys. Rev. B* **1975**, *12*, 3060; b) O. K. Andersen, O. Jepsen, *Phys. Rev. Lett.* **1984**, *53*, 2571; c) O. Jepsen, O. K. Andersen, *Z. Phys. B* **1995**, *97*, 35.
[27] U. von Barth, L. Hedin, *J. Phys. C* **1971**, *4*, 2064.

 © 2006 Wiley-VCH Verlag GmbH & Co. KGaA, Weinheim

Cover Picture

Yoichi Nakao, Satoru Yoshida, Shigeki Matsunaga, Nobuaki Shindoh, Yoh Terada, Koji Nagai, Jun K. Yamashita, A. Ganesan, Rob W. M. van Soest, Nobuhiro Fusetani,*

Irene Izzo,* Nakia Maulucci, Giuseppe Bifulco, and Francesco De Riccardis*

Inhibitory activity against histone deacetylase is displayed by the newly discovered natural products azumamides A–E, isolated from the marine sponge *Mycale izuensis*, shown in the background of the cover picture. The total synthesis of azumamides A and E is reported and has allowed the stereochemical structure of the azumamides to be established. For more information on these natural products, see the Communications by N. Fusetani and co-workers and by I. Izzo, F. De Riccardis et al. on pages 7553 ff. and 7557 ff., respectively.

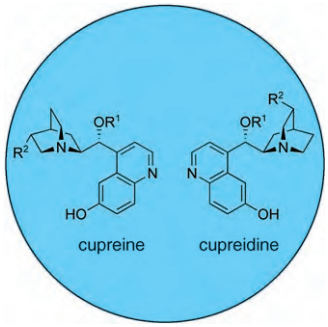

Cinchona Organocatalysts
In their Minireview on page 7496 ff., H. Hiemstra and co-workers describe the scope and mode of action of cupreines and cupreidines, a new class of bifunctional organocatalysts, which are accessible from natural cinchona alkaloids through cleavage of the C6′ methoxy group.

Aldol Reactions
Modern variations of the aldol reaction for natural products synthesis are summarized in the Review by R. Mahrwald and B. Schetter on page 7506 ff. Reactions with metal enolates as well as metal-catalyzed, organocatalytic, and biocatalytic methods are highlighted.

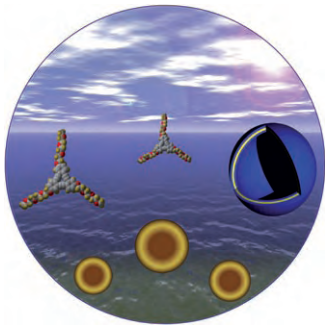

Self-Assembly
In their Communication on page 7526 ff., G. N. Tew and co-workers report the self-assembly of a triangular macrocycle based on *ortho*-phenylene ethynylene into vesicles—the first such example from a discotic liquid-crystalline molecule.

Contents

VIP ***The following Communications have been judged by at least two referees to be "very important papers" and will be published online at www.angewandte.org soon:***

A. Corma, M. Renz**
A General Method for the Preparation of Ethers Using Water-Resistant Solid Lewis Acids

K. Banert, Y.-H. Joo, T. Rüffer, B. Walfort, H. Lang*
The Exciting Chemistry of Tetraazidomethane

B. V. Popp, J. E. Wendlandt, C. R. Landis, S. S. Stahl**
Reaction of Molecular Oxygen with an NHC-Coordinated Pd^0 Complex: Computational Insights and Experimental Implications

R. Martinez, R. Chevalier, S. Darses, J.-P. Genet**
A Versatile Ruthenium Catalyst for C–C Bond Formation through C–H Bond Activation

*H. Nuss, M. Jansen**
$Cs_5([12]crown\text{-}4)_2(O_3)_5$: The First Supramolecular Ozonide Compound Containing $^1{}_\infty\{Cs_8(O_3)_{10}\}^2$ Rods

F. Camerel, R. Ziessel, B. Donnio, C. Bourgogne, D. Guillon, M. Schmutz, C. Iacovita, J.-P. Bucher*
Formation of Gels and Liquid Crystals Induced by Pt···Pt Interactions in Luminescent σ-Alkynyl Platinum(II) Terpyridine Complexes

News

M. Baldus Receives Founders Medal ——— **7490**

Paracelsus Prize for J. E. Baldwin ——— **7490**

P. Gregory Returns to Wiley-VCH ——— **7490**

Books

Determination of Complex Reaction Mechanisms — John Ross, Igor Schreiber, Marcel O. Vlad — *reviewed by O. Steinbock* ——— **7491**

Highlights

Tetrapyrrole Macrocycles

M. O. Senge,*
N. N. Sergeeva ——— **7492 – 7495**

Metamorphosis of Tetrapyrrole Macrocycles

I don't like what I am: An example of ring-size change in tetrapyrroles is found in the ring expansion of corroles to porphyrins (see scheme). These and other recently discovered relationships between tetrapyrrole structures offer the possibility of rapid autoconversion of such macrocycles.

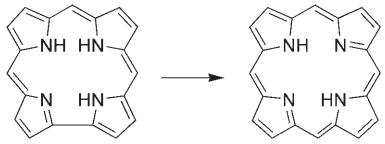

Minireviews

Asymmetric Organocatalysis

T. Marcelli, J. H. van Maarseveen,
H. Hiemstra* ——— **7496 – 7504**

Cupreines and Cupreidines: An Emerging Class of Bifunctional Cinchona Organocatalysts

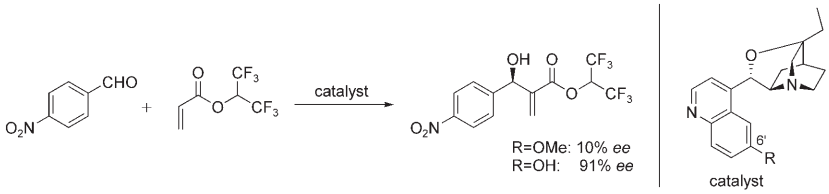

Hidden functionality: Cleavage of the C6′ methoxy group in cinchona alkaloids affords organocatalysts with a phenolic OH group. Despite its position far away from the stereocenters, this hydroxy group proves crucial to obtain high enantioselectivity in many synthetically relevant reactions.

InterScience

© 2006 Wiley-VCH Verlag GmbH & Co. KGaA, Weinheim

Reviews

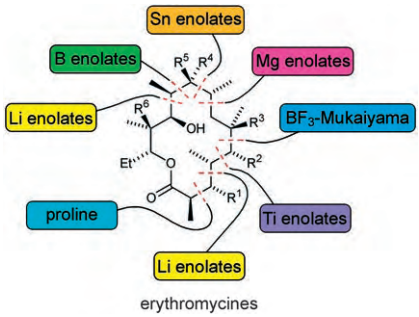

A couple of variations: The aldol reaction is one of the most important methods in organic synthesis for the stereoselective formation of polyketide natural products such as erythromycin (see scheme). This Review presents modern variants of this reaction, including the application of metal enolates as well as metal-catalyzed, organocatalytic, and biocatalytic methods.

Natural Product Synthesis

B. Schetter, R. Mahrwald* ___ **7506 – 7525**

Modern Aldol Methods for the Total Synthesis of Polyketides

Communications

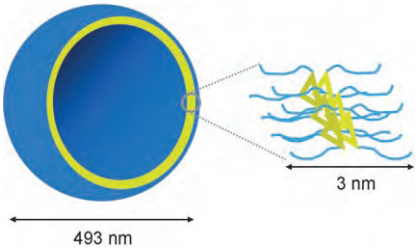

A triangular macrocycle based on *ortho*-phenylene ethynylene with polar ethylene oxide side chains spontaneously self-assembles into vesicles upon exposure of solutions in chloroform to water. These self-assembled structures were characterized by transmission electron microscopy and atomic force microscopy. The self-assembly of disklike macrocycles into spherical vesicles represents a new molecular architecture for vesicle formation.

Vesicles

S. H. Seo, J. Y. Chang, G. N. Tew* ___ **7526 – 7530**

Self-Assembled Vesicles from an Amphiphilic *ortho*-Phenylene Ethynylene Macrocycle

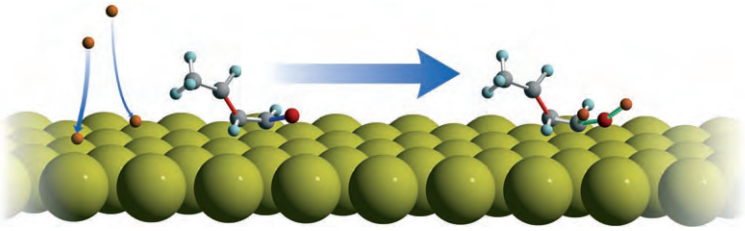

Tilt it a little: X-ray absorption spectroscopy and photoemission were used to elucidate the mechanism of promoter action in the Cu-catalyzed chemoselective hydrogenation of crotonaldehyde. Sulfur adatoms electronically perturb the C=O bond and tilt the C=C bond away from the surface, thus activating the former and rendering the latter inert to hydrogenation. Quantitative conversion of the reactant with 100% selectivity may be achieved.

Chemoselective Hydrogenation

M. E. Chiu, D. J. Watson, G. Kyriakou, M. S. Tikhov, R. M. Lambert* ___ **7530 – 7534**

Tilt the Molecule and Change the Chemistry: Mechanism of S-Promoted Chemoselective Catalytic Hydrogenation of Crotonaldehyde on Cu(111)

For the USA and Canada:
ANGEWANDTE CHEMIE International Edition (ISSN 1433-7851) is published weekly by Wiley-VCH PO Box 191161, D 69451 Weinheim, Germany. Air freight and mailing in the USA by Publications Expediting Inc. 200 Meacham Ave., Elmont, NY 11003. Periodicals postage paid at Jamaica NY 11431. US POSTMASTER: send address changes to *Angewandte Chemie*, Wiley-VCH, 111 River Street, Hoboken, NJ 07030. Annual subscription price for institutions: US$ 5685/5168 (valid for print and electronic / print or electronic delivery); for individuals who are personal members of a national chemical society prices are available on request. Postage and handling charges included. All prices are subject to local VAT/sales tax.

© 2006 Wiley-VCH Verlag GmbH & Co. KGaA, Weinheim

The best in chemistry –

for more than a hundred years

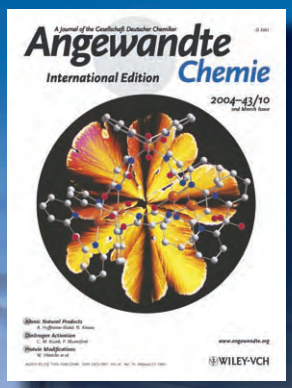

A Journal of the Gesellschaft Deutscher Chemiker

Angewandte
International Edition Chemie

www.angewandte.org

1888: ***The beginning of a success story***

Constant Innovations

1962: *First issue of the International Edition*
1976: *Graphical abstracts*
1979: *Cover pictures*
1988: *Centenary of Angewandte*
1989: *Routine use of color*
1991: *New section: Highlights*
1992: *Computerized editorial tracking system*
1995: *Internet service for readers*
1998: *Regular press service; full-text online*
2000: *New section: Essays; EarlyView: Communications available online ahead of the printed version*
2001: *New section: Minireviews*
2002: *Online submission of manuscripts*
2003: *Weekly publication; new section: News; new layout*
2004: *Backfiles (1962-1997); ManuscriptXpress: Online system for authors and referees*

Angewandte's advisors...

Manfred Reetz
Max-Planck-Institut für Kohlenforschung, Mülheim

*»**Angewandte Chemie** is extremely well-balanced in providing various types of information to the academic and industrial chemical community. If you inadvertently miss an issue, the mishap will catch up with you sooner or later.«*

***Angewandte Chemie International Edition** is a journal of the German Chemical Society (GDCh)*

GDCh

WILEY InterScience® DISCOVER SOMETHING GREAT

WILEY-VCH

1881404_gu

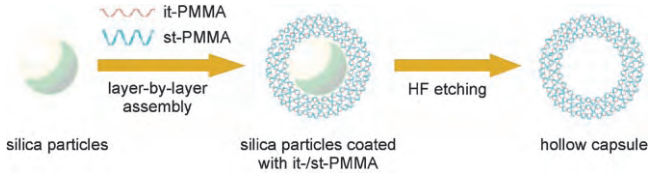

A hollow victory: Hollow capsules of poly(methyl methacrylate) (PMMA) stereocomplex can be fabricated by a combination of the layer-by-layer assembly technique and the silica template method (see scheme; it = isotactic, st = syndiotactic). A hollow nanostructure composed of nonionic multilayers is constructed through van der Waals interactions.

Polymer Nanostructures

T. Kida, M. Mouri, M. Akashi* ——— 7534 – 7536

Fabrication of Hollow Capsules Composed of Poly(methyl methacrylate) Stereocomplex Films

Armed forces: The rolling-circle amplification method has been used to replicate a four-arm DNA nanojunction. Under appropriate conditions, the DNA nanoobjects can be replicated efficiently and correctly, therefore opening a new avenue for large-scale enzymatic synthesis of DNA nanostructures.

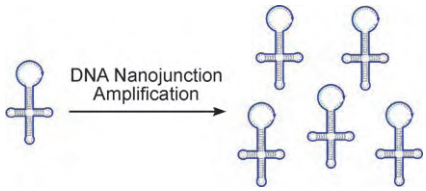

DNA Replication

C. Lin, M. Xie, J. J. L. Chen, Y. Liu, H. Yan* ——— 7537 – 7539

Rolling-Circle Amplification of a DNA Nanojunction

Mix it up a little bit: A diffusive nanomixer for single-molecule studies has been developed that allows single-molecule fluorescence studies to be performed under nonequilibrium conditions in free solution without compromising the signal-to-noise ratio. This method has been used for direct monitoring by single-molecule fluorescence resonance energy transfer of the conformations of a quadruplex during unfolding.

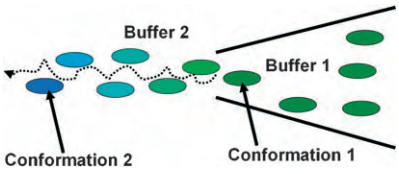

Single-Molecule Studies

S. S. White, S. Balasubramanian, D. Klenerman,* L. Ying* ——— 7540 – 7543

A Simple Nanomixer for Single-Molecule Kinetics Measurements

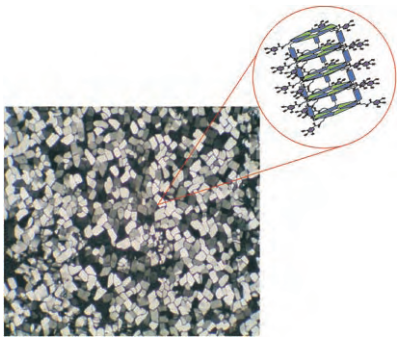

Jewel-box: In a hierarchical process, three molecules of a calix[4]arene (blue) and six of barbituric or cyanuric acid (green) assemble into double-rosette boxes, which assemble into columns, which in turn assemble into columnar liquid-crystalline phases (see picture). The resulting mesophases have a remarkable thermal stability and a high degree of order.

Supramolecular Chemistry

A. Piermattei, M. Giesbers, A. T. M. Marcelis, E. Mendes, S. J. Picken, M. Crego-Calama,* D. N. Reinhoudt* ——— 7543 – 7546

Induction of Liquid Crystallinity by Self-Assembled Molecular Boxes

© 2006 Wiley-VCH Verlag GmbH & Co. KGaA, Weinheim

Contents

Crystal Engineering

T. Friščić, A. V. Trask, W. Jones,*
W. D. S. Motherwell ——— **7546 – 7550**

Screening for Inclusion Compounds and Systematic Construction of Three-Component Solids by Liquid-Assisted Grinding

Back to the grind: Three-component solids are prepared by neat and liquid-assisted grinding. Various solid or liquid guests are incorporated into a caffeine/succinic acid host framework. These grinding methods are superior to solution crystallization for the screening of ternary inclusion compounds.

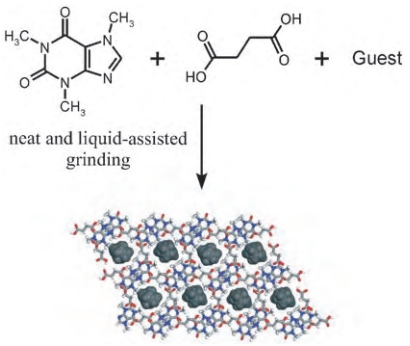

Cluster Compounds

J. R. Butchard, O. J. Curnow,* D. J. Garrett, R. G. A. R. Maclagan ——— **7550 – 7553**

Structure of a Discrete Dichloride Hexahydrate Cube as a Tris(diisopropylamino)cyclopropenium Salt

Overcoming repulsion: Two chloride anions are glued together by six Cl···H–O hydrogen bonds in the stable dichloride hydrate cube $[Cl_2(H_2O)_6]^{2-}$. The solid-state structure of the cluster determined by X-ray diffraction of its salt (see picture; Cl green, O red, H white) is consistent with the gas-phase structures calculated at two levels of theory.

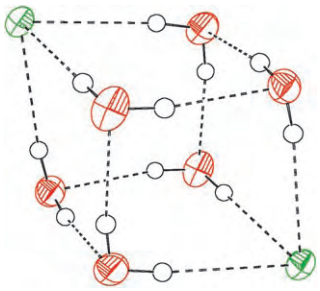

Marine Natural Products

Y. Nakao, S. Yoshida, S. Matsunaga, N. Shindoh, Y. Terada, K. Nagai, J. K. Yamashita, A. Ganesan, R. W. M. van Soest, N. Fusetani* ——— **7553 – 7557**

Azumamides A–E: Histone Deacetylase Inhibitory Cyclic Tetrapeptides from the Marine Sponge *Mycale izuensis*

A zoom in on azumamides (1): Azumamides A–E are five new cyclic tetrapeptides isolated from the marine sponge *Mycale izuensis*. The azumamides display inhibitory activity toward histone deacetylase with IC_{50} values of 0.045–1.3 μg mL^{-1}. Their structures were determined on the basis of spectroscopic analysis and chemical degradation.

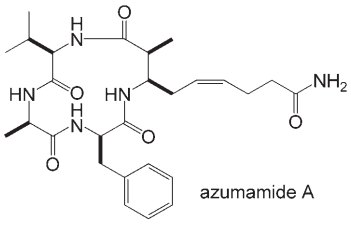

Natural Product Synthesis

I. Izzo,* N. Maulucci, G. Bifulco, F. De Riccardis* ——— **7557 – 7560**

Total Synthesis of Azumamides A and E

A zoom in on azumamides (2): An efficient synthetic route for two of the newly discovered marine natural products, namely azumamides A and E, has been developed (see picture). The present synthesis was followed by determination of the stereochemical structure of the azumamides.

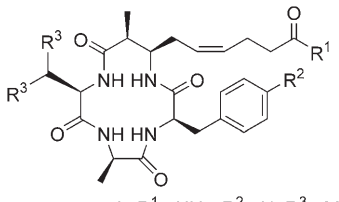

© 2006 Wiley-VCH Verlag GmbH & Co. KGaA, Weinheim

Magnetic ends: By measuring the distribution of distances between two spin labels it is possible to quantify the flexibility of shape-persistent molecules (see picture). It is found that even the flexibility of short oligomers is described well by the wormlike-chain model.

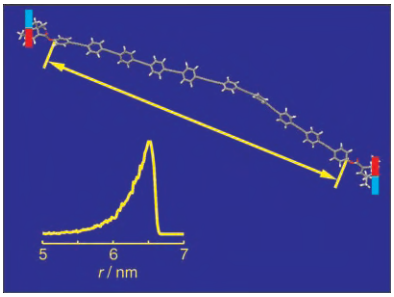

Molecular Dynamics

A. Godt, M. Schulte, H. Zimmermann, G. Jeschke* ——— **7560 – 7564**

How Flexible Are Poly(*para*-phenyleneethynylene)s?

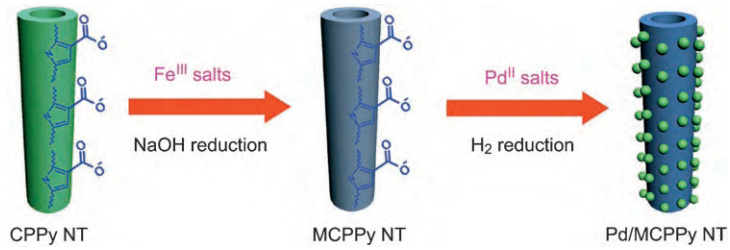

Magnetic and catalytic: Both of these properties are shown by the title system, which can be readily prepared by vapor-deposition polymerization and subsequent chemical reduction of Fe^{III} and Pd^{II} salts on carboxylated polypyrrole nanotubes (CPPy NT; see picture). These supported Pd nanocatalysts exhibit excellent catalytic activity and reusability in the Heck coupling reaction. MCPPy NT: magnetic carboxylated polypyrrole nanotube.

Supported Nanocatalysts

S. Ko, J. Jang* ——— **7564 – 7567**

A Highly Efficient Palladium Nanocatalyst Anchored on a Magnetically Functionalized Polymer-Nanotube Support

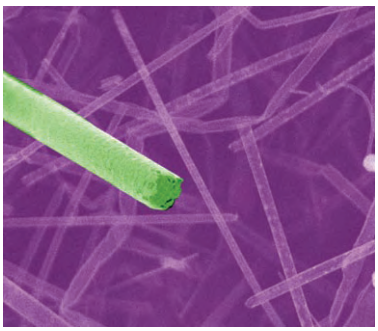

Upon thermal evaporation of a mixture of ZnS or CdS with P and Mn_3P_2 powders, nanotubes of II_3–V_2 semiconductors (Zn_3P_2 or Cd_3P_2) morph around metal nanorods that are formed in situ. These thin-walled nanotubes are single crystals with open ends, circular cross sections, and uniform diameters (see picture).

Nanotubes

G. Shen,* Y. Bando, C. Ye, X. Yuan, T. Sekiguchi, D. Golberg ——— **7568 – 7572**

Single-Crystal Nanotubes of II_3–V_2 Semiconductors

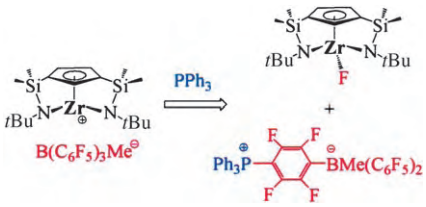

C–F bond activation: In the presence of a phosphane, deactivation of cationic zirconium complexes can occur by direct fluoride migration to the zirconium center, that is, the breaking of a C–F bond—the strongest bond of organic molecules—without previous C_6F_5 transfer to the metal atom (see picture).

Ion Pairs

J. Cano, M. Sudupe, P. Royo,* M. E. G. Mosquera ——— **7572 – 7574**

Evidence of Fluoride Transfer from the Anion of $[Zr\{C_5H_3[SiMe_2(\eta^1\text{-}NtBu)]_2\}]^+$ $[RB(C_6F_5)_3]^-$ Complexes to the Zirconocenium Cation

© 2006 Wiley-VCH Verlag GmbH & Co. KGaA, Weinheim

Contents

Glycosylation

T. Yamada, K. Takemura, J.-i. Yoshida, S. Yamago* ——— 7575 – 7578

Dialkylphosphates as Stereodirecting Protecting Groups in Oligosaccharide Synthesis

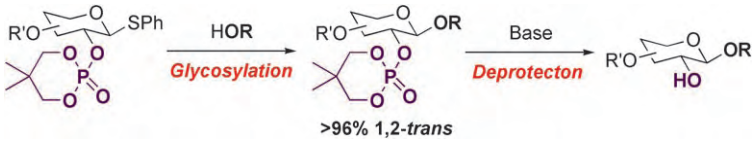

Double duty: A phosphoric ester at the C2 position in glycosyl donors directs the glycosylation to occur selectively at the anomeric carbon atom with complete 1,2-*trans* selectivity. Since the phosphoric ester can be removed to give the hydroxy function, this group serves as a stereodirecting protecting group in oligosaccharide synthesis.

Amphiphiles

Y. Geng,* D. E. Discher, J. Justynska, H. Schlaad* ——— 7578 – 7581

Grafting Short Peptides onto Polybutadiene-*block*-poly(ethylene oxide): A Platform for Self-Assembling Hybrid Amphiphiles

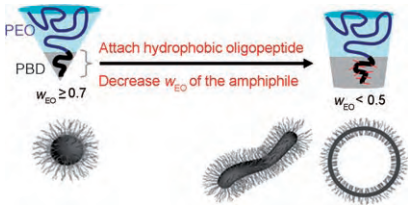

The attachment of a hydrophobic peptide onto polybutadiene-*block*-poly(ethylene oxide) shifts the assembly morphologies in water towards those with lower curvatures, namely, from spherical micelles to wormlike micelles and vesicles (see picture; w_{EO}: weight fraction of the hydrophilic PEO block; PEO = poly(ethylene oxide); PBD = polybutadiene). Helical superstructures also arise from peptide interactions inside the hydrophobic core.

Oxime Ligation

A. Dirksen, T. M. Hackeng, P. E. Dawson* ——— 7581 – 7584

Nucleophilic Catalysis of Oxime Ligation

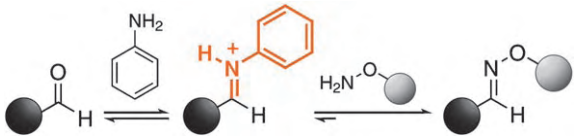

Aniline acts as a nucleophilic catalyst of oxime ligation in aqueous solution through formation of the orange-colored intermediate. The method is demonstrated by acceleration of the oxime ligation of peptides at pH 4.5 and pH 7, which extends the scope of this reaction to conditions relevant for the bioconjugation of macromolecules (see scheme).

Chromium Colloids

E. Breynaert, I. Hermans,* B. Lambie, G. Maes, J. Peeters, A. Maes, P. Jacobs ——— 7584 – 7588

Silica-Immobilized Chromium Colloids for Cyclohexane Autoxidation

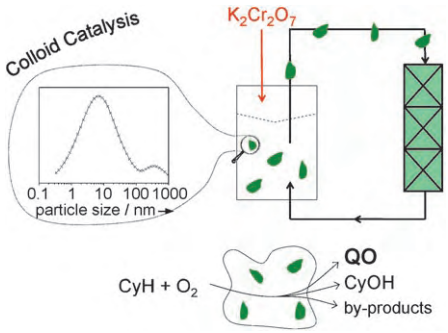

In a stable condition: Oxyhydroxide colloids of chromium deposited on silica gel are selective, stable catalysts for the autoxidation of cyclohexane (CyH). The Cr^{III} colloids, generated in situ, are immobilized by a column precipitation chromatographic technique (see picture). An increased yield of cyclohexanone (QO) is obtained.

© 2006 Wiley-VCH Verlag GmbH & Co. KGaA, Weinheim

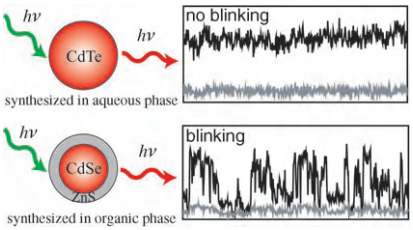

Blinking marvelous! In contrast to quantum dots (QDs) synthesized in organic solutions, CdTe QDs synthesized in aqueous solutions containing thiopropionic acid do not blink. The fluorescence of these QDs is steady under continuous laser excitation (see picture, the gray line is the background intensity). The presence of thio groups on the surface of the QDs is key to their antiblinking behavior.

Fluorescence

H. He, H. Qian, C. Dong, K. Wang, J. Ren* ——— **7588 – 7591**

Single Nonblinking CdTe Quantum Dots Synthesized in Aqueous Thiopropionic Acid

Metathesis takes sides: The scope of asymmetric metathesis has been expanded with the use of chiral ruthenium catalysts for asymmetric ring-opening cross-metathesis and for the first example of an asymmetric cross-metathesis (see scheme, TIPS = triisopropylsilyl). Information about the mechanism of asymmetric ring-opening cross-metathesis should allow the development of more selective catalysts.

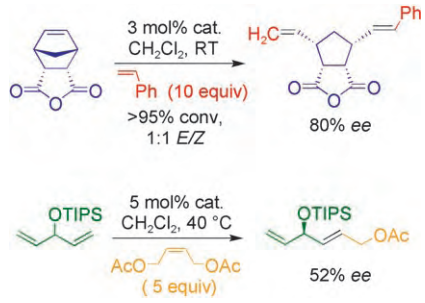

Asymmetric Catalysis

J. M. Berlin, S. D. Goldberg, R. H. Grubbs* ——— **7591 – 7595**

Highly Active Chiral Ruthenium Catalysts for Asymmetric Cross- and Ring-Opening Cross-Metathesis

Chloride ligands are crucial in the gold-catalyzed cycloisomerization of allenynes to give hydrindienes such as **1**, which are formally products of C–H activation and formed completely selectively over the usual Alder-ene products (**2**; see scheme). This effect could be rationalized by a DFT study that sheds new light on the electrophilic metal-catalyzed cycloisomerization of polyunsaturated systems.

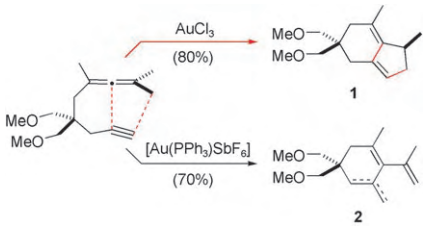

Mechanistic Studies

G. Lemière, V. Gandon, N. Agenet, J.-P. Goddard, A. de Kozak, C. Aubert,* L. Fensterbank,* M. Malacria* ——— **7596 – 7599**

Gold(I)- and Gold(III)-Catalyzed Cycloisomerization of Allenynes: A Remarkable Halide Effect

A simple trick could prove generally valuable for asymmetric copper-catalyzed conjugate addition reactions. It was found that the enantioselectivities of such reactions of dialkyl zinc reagents with α-halo enones in the presence of chiral phosphorimidite ligands were dramatically improved upon the addition of styrene, which acts as a radical scavenger to suppress the competitive non-asymmetric radical pathway (see example).

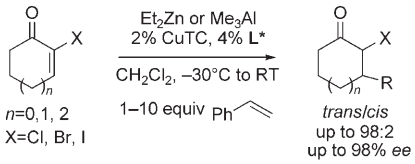

Asymmetric Catalysis

K. Li, A. Alexakis* ——— **7600 – 7603**

Asymmetric Conjugate Addition to α-Halo Enones: Dramatic Effect of Styrene on the Enantioselectivity

© 2006 Wiley-VCH Verlag GmbH & Co. KGaA, Weinheim

Contents

Zeolites

H. Wang, T. J. Pinnavaia* — **7603 – 7606**

MFI Zeolite with Small and Uniform Intracrystal Mesopores

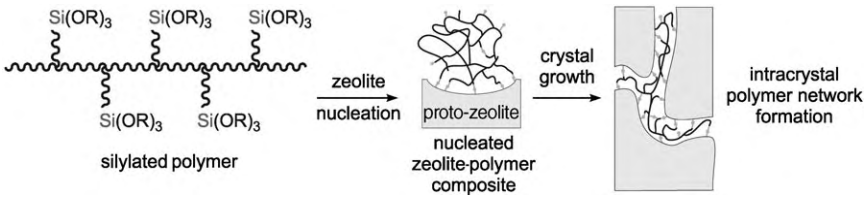

The nucleation of a ZSM-5 zeolite in the presence of silylated polyethylenimine polymers affords composite crystals that contain phase-segregated polymer. Calcination of the crystals results in zeolites with uniform intracrystal mesopores smaller than 10 nm, which are ideally suited for size-selective catalytic conversions of large molecules.

Asymmetric Catalysis

T. Ooi, S. Takada, K. Doda, K. Maruoka* — **7606 – 7608**

Highly Diastereo- and Enantioselective Formal Conjugate Addition of Nitroalkanes to Nitroalkenes by Chiral Ammonium Bifluoride Catalysis

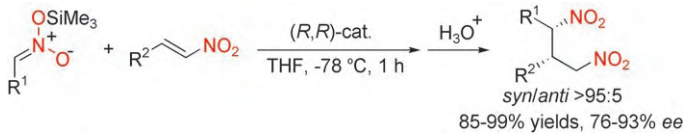

A matter of control: A chiral quaternary ammonium bifluoride catalyst in combination with silyl nitronates results in the highly diastereo- and enantioselective formal conjugate addition of nitroalkanes to nitroalkenes (see scheme). The resulting 1,3-dinitro compounds bear two defined stereocenters, which can serve as versatile chiral building blocks in organic synthesis.

Natural Products Synthesis

W. Li, H. Li, Y. Li, Z. Hou* — **7609 – 7611**

Total Synthesis of (±)-Quadrangularin A

The key to successful coupling in the synthesis of (±)-quadrangularin A (**1**) was the introduction of *tert*-butyl groups in the precursor to block two reactive positions. Thus, the oxidative coupling of 3,5-di-(*tert*-butyl)resveratrol was carried out regioselectively in an efficient total synthesis of the natural product.

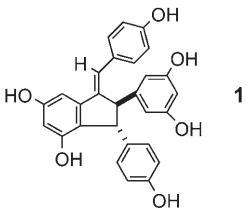

1

Copper-Centered Oxidation

R. Santo, R. Miyamoto, R. Tanaka, T. Nishioka, K. Sato, K. Toyota, M. Obata, S. Yano, I. Kinoshita,* A. Ichimura,* T. Takui* — **7611 – 7614**

Diamagnetic–Paramagnetic Conversion of Tris(2-pyridylthio)methylcopper(III) through a Structural Change from Trigonal Bipyramidal to Octahedral

All change: The stable, diamagnetic, trigonal-bipyramidal Cu^{III} complex (see picture) arising from one-electron oxidation of a Cu^{II} complex undergoes conversion into a paramagnetic octahedral Cu^{III} complex upon addition of Cl^- ions. Characterization of the complexes and density functional calculations indicate that the initial one-electron oxidation is metal- rather than ligand-centered.

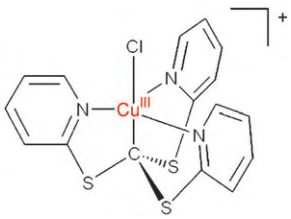

© 2006 Wiley-VCH Verlag GmbH & Co. KGaA, Weinheim

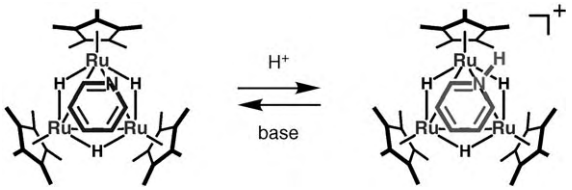

Localized protonation: The title complex was prepared by the reaction of a triruthenium pentahydrido complex with pyridine. This compound is the heterocyclic analogue of the face-capping benzene complex, but its reactivity with a protic acid (see scheme) was considerably different from that of the benzene complex owing to the lone pair of electrons at the nitrogen atom.

Surface Adsorption Models

T. Kawashima, T. Takao, H. Suzuki* ——— 7615 – 7618

Synthesis and Structure of a Triruthenium Complex Containing a Face-Capping Pyridine Ligand

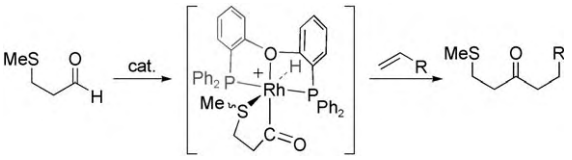

Top of the P-O-Ps: Stabilization of a cationic rhodium catalyst with the hemilabile P-O-P ligand dpephos allows efficient intermolecular hydroacylation of challenging substrates (see scheme). Structural studies have established the role of the coordination of the oxygen atom, and a catalytically competent acyl–hydridorhodium intermediate was fully characterized.

C–H Activation

G. L. Moxham, H. E. Randell-Sly, S. K. Brayshaw, R. L. Woodward, A. S. Weller,* M. C. Willis* — 7618 – 7622

A Second-Generation Catalyst for Intermolecular Hydroacylation of Alkenes and Alkynes Using β-S-Substituted Aldehydes: The Role of a Hemilabile P-O-P Ligand

Heading south: An efficient approach to the FGHI southern ring system of azaspiracid-1 is disclosed. Each of the eight stereogenic centers is generated with excellent diastereoselectivity. In addition, the stereochemical outcome of the ketalization steps could be controlled by careful selection of the conditions. Teoc = 2-(trimethylsilyl)ethoxycarbonyl; TMS = trimethylsilyl; TIPS = triisopropylsilyl; Bn = benzyl.

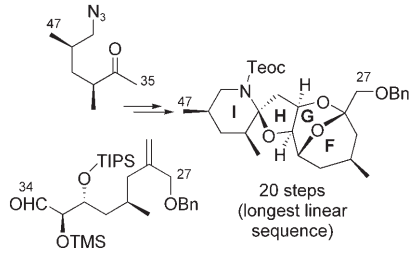

Natural Product Synthesis

X.-T. Zhou, L. Lu, D. P. Furkert, C. E. Wells, R. G. Carter* ——— 7622 – 7626

Synthesis of the Southern FGHI Ring System of Azaspiracid-1 and Investigation into the Controlling Elements of C28- and C36-Ketalization

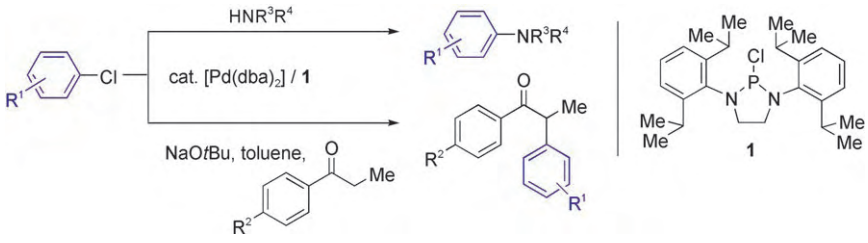

Sterically hindered substituents on a secondary chlorophosphine **1** prevent formation of a diaminooxophosphine, and thereby allow for highly efficient arylation reactions of amines and α-C-H acidic ketones with (hetero)aryl chlorides.

C–N Coupling

L. Ackermann,* J. H. Spatz, C. J. Gschrei, R. Born, A. Althammer ——— 7627 – 7630

A Diaminochlorophosphine for Palladium-Catalyzed Arylations of Amines and Ketones

© 2006 Wiley-VCH Verlag GmbH & Co. KGaA, Weinheim

Contents

[2+2] Cycloadditions

J. Paradies, I. Greger, G. Kehr, G. Erker,* K. Bergander, R. Fröhlich — **7630 – 7633**

Formation of an Organometallic Ladderane Derivative by Dynamic Topochemical Reaction Control

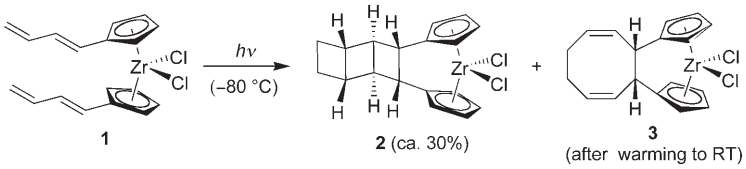

Coming together at the ends: Bis(butadienylcyclopentadienyl) dichlorozirconium (**1**) undergoes dynamic topochemical reactions upon photolysis that eventually lead to the formation of ladderane derivative **2** and the organometallic cyclooctadiene derivative **3**.

Directed Evolution

K. B. M. Sauter, A. Marx* — **7633 – 7635**

Evolving Thermostable Reverse Transcriptase Activity in a DNA Polymerase Scaffold

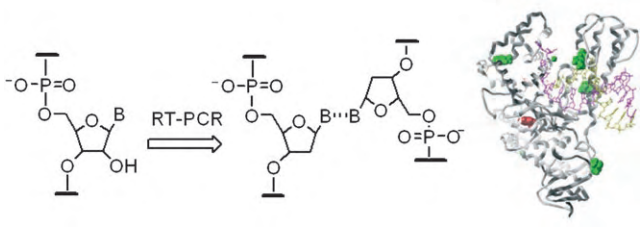

Active mutants: Thermostable DNA polymerases normally exhibit no significant intrinsic activities to reverse transcribe RNA into DNA. We show that enzymes with significantly increased reverse transcription ability can be generated by directed evolution (see picture).

Thin Films

D. Stacchiola, S. Kaya, J. Weissenrieder, H. Kuhlenbeck, S. Shaikhutdinov,* H.-J. Freund, M. Sierka, T. K. Todorova, J. Sauer — **7636 – 7639**

Synthesis and Structure of Ultrathin Aluminosilicate Films

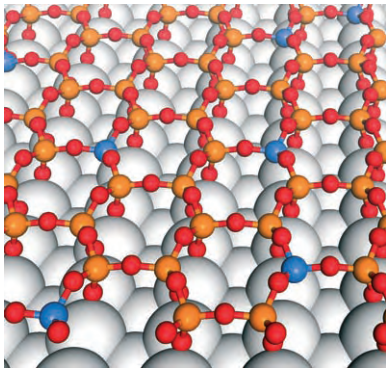

Making films: Ordered aluminosilicate films are grown on a Mo(112) substrate, and their structures are determined through high-resolution experiments and density functional theory calculations. At low Al/Si ratios, aluminum atoms partially replace the silicon atoms of the silica structure. The resulting aluminosilicate film consists of a layer of corner-sharing $\{SiO_4\}$ and $\{AlO_3\}$ units (see picture; Mo gray, Al blue, Si orange, O red).

Supporting information is available on the WWW (see article for access details).

A video clip is available as Supporting Information on the WWW (see article for access details).

The issues for November 2006 appeared online on the following dates
Issue 41: October 17. · Issue 42: October 23. · Issue 43: October 30. · Issue 44: November 6

Sources

Product and Company Directory

You can start the entry for your company in "Sources" in any issue of *Angewandte Chemie*.

If you would like more information, please do not hesitate to contact us.

Wiley-VCH Verlag – Advertising Department
Tel.: 0 62 01 - 60 65 65
Fax: 0 62 01 - 60 65 50
E-Mail: MSchulz@wiley-vch.de

Service

Keywords — *7640*

Authors — *7641*

Preview — *7643*

© 2006 Wiley-VCH Verlag GmbH & Co. KGaA, Weinheim

Retraction

Since publication of this Communication, it has come to the authors' attention that the crystallographically determined structure of $[NEt_4][HgCl_2][HgCl_3]$ has been described previously (*Acta Cryst. E* **2002**, *58*, m534). The cell parameters and structural data are consistent with those of the compound that the authors reported as being $[NEt_4][AuCl_2][AuCl_3]$. Clearly the structure of the mercury compound as an impurity in the reaction product has been determined. Thus, all the conclusions drawn from this data are invalid, although several gold-containing products were derived from the reaction in high overall yields. Accordingly, the authors withdraw this Communication, apologize for these mistakes and that the readership of *Angewandte Chemie* has been misled by the publication of this Communication. They would like to thank Prof. H. Schmidbaur for initially drawing their attention to this matter.

$[NEt_4][AuCl_2][AuCl_3]$: Solid-State Evidence of Essentially Y-Shaped Jahn–Teller-Distorted $AuCl_3$

K. R. Flower,* R. G. Pritchard, A. T. McGown ——— **6535–6537**

Angew. Chem. Int. Ed. **2006**, *45*

DOI 10.1002/anie.200602092

Looking for outstanding employees?

Do you need another expert for your excellent team? ...Chemists, PhD Students, Managers, Professors, Sales Representatives...

Take advantage of our classified sections in ***Angewandte Chemie*** and ***Angewandte Chemie International Edition***.

Place an advert in the printed version and have it made available online for 1 month, free of charge!

Angewandte Chemie International Edition

Advertising Sales Department: Marion Schulz
Phone: 0 62 01 - 60 65 65
Fax: 0 62 01 - 60 65 50
E-Mail: MSchulz@wiley-vch.de

For all customers in Europe !

We, TCI Europe, deliver all our products directly from BELGIUM.

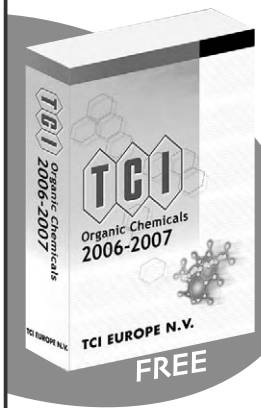

EURO CATALOGUE 2006 - 2007

- 18 000 organic chemicals
- 1000 new products
- more physical properties
- more chemical structures

... and, **LOWER PRICES** for many items!

Ask your free copy today!

TCI EUROPE N.V.
+800 46 73 86 67 • +32 (0)3 735 07 00
Fax +32 (0)3 735 07 01
sales@tcieurope.be • www.tcieurope.be
<Head Office>
TOKYO CHEMICAL INDUSTRY CO., LTD.
www.tokyokasei.co.jp

 © 2006 Wiley-VCH Verlag GmbH & Co. KGaA, Weinheim

M. Baldus Receives Founders Medal

Marc Baldus (Max Planck Institute for Biophysical Chemistry, Göttingen, Germany) has received the Founders Medal at the International Conference on Magnetic Resonance in Biological Systems (ICMRBS) in Göttingen. The US$3000 prize is awarded to a young researcher who has made exceptional contributions to the development of magnetic resonance in biological systems. Baldus was one of the first to solve the three-dimensional structure of a globular protein using solid-state NMR spectroscopy. He has also investigated protein fibrils which appear in neurodegenerative disorders, and the binding behaviors of neuropeptides and membrane proteins. He recently contributed a Highlight in *Angewandte Chemie* discussing current developments in solid-state NMR spectroscopy.[1a] His next Communication concerning the secondary structure, dynamics, and topology of a seven-helix receptor in native membranes, as studied by solid-state NMR spectroscopy,[1b] will be featured on the cover of Issue 3, 2007, of *Angewandte Chemie*.

M. Baldus

Baldus completed his degree in Physics at the Technical University Darmstadt with a research project at the University of Florida in Gainesville (USA). Following studies in Zurich (Switzerland) and in Nijmegen (The Netherlands), Baldus received his PhD from the ETH Zurich under the supervision of R. Ernst (Nobel Prize in Chemistry 1991) and B. Meier. During 1997–99, he worked as a postdoctoral researcher with R. G. Griffin at the Massachusetts Institute of Technology (MIT), Cambridge (USA), before accepting a lectureship at the University of Leiden (The Netherlands). In 2000, he joined the Max Planck Institute for Biophysical Chemistry, where he is currently head of the solid-state NMR spectroscopy group.

Paracelsus Prize for J. E. Baldwin

Jack E. Baldwin (University of Oxford) has been awarded the Paracelsus Prize, worth 20000 Swiss Francs, from the Swiss Chemical Society. The prize was presented at the Society's fall meeting. Baldwin has been chosen for this prize, the highest honor of the Swiss Chemical Society, for his work on the biosynthesis and biomimetic synthesis of natural products. Baldwin completed his undergraduate studies at Imperial College London in 1960 and undertook his postgraduate studies under the supervision of D. Barton (Nobel Prize for Chemistry 1969) and completed his PhD in 1964. He remained with this group until 1967, when he moved to Pennsylvania State University. In 1970, he joined MIT. He returned to England in March 1972 (King's College) only to return to MIT as Assistant Professor a few months later (November 1972). In 1978, he was elected a Fellow of the Royal Society and appointed to the University of Oxford, where he remained until his retirement in 2005. He was awarded a knighthood in 1997.

J. Baldwin

Despite his retirement, Baldwin continues to supervise an active research group, which is interested in the biomimetic synthesis of natural products and also develops new synthetic methods. Baldwin's rules for ring closure, which he first proposed in 1976,[2a] are regularly discussed in textbooks. He recently reported an enhancement of the Stille reaction with a new combination of reagents in *Chemistry—A European Journal*.[2b] Baldwin was a member of the editorial advisory board of *ChemBioChem* during 2000–2004.

P. Gregory Returns to Wiley-VCH

After four years as Director of Publishing for the Royal Society of Chemistry, Peter Gregory returns to his former workplace, Wiley-VCH in Weinheim (Germany). He will take over as Editor-in-Chief of the journals *Advanced Materials* and *Advanced Functional Materials* and will also take responsibility for all the materials science journals at Wiley-VCH, including the polymer journals, such as *Macromolecular Chemistry and Physics*. In addition, he will join the Global STM (Science, Technology, and Medicine) Board of John Wiley & Sons.

Gregory completed his PhD on the electron spin resonance of hydrocarbon radical cations at University College London under the supervision of A. G. Davies and worked from 1986 to 1989 in the group of P. v. R. Schleyer at the University of Erlangen-Nürnberg. He started as an editor at *Advanced Materials* in 1989, a year after the journal was launched, and was promoted to Editor-in-Chief in 1992.

P. Gregory

[1] a) M. Baldus, *Angew. Chem.* **2006**, *118*, 1204; *Angew. Chem. Int. Ed.* **2006**, *45*, 1186; b) M. Etzkorn, S. Martell, O. C. Andronesi, K. Seidel, M. Engelhard, M. Baldus, *Angew. Chem.* **2007**, *119*, DOI: 10.1002/ange.200602139; *Angew. Chem. Int. Ed.* **2007**, *46*, DOI: 10.1002/anie.200602139.

[2] a) J. E. Baldwin, *J. Chem. Soc. Chem. Commun.* **1976**, 734; b) S. P. H. Mee, V. Lee, J. E. Baldwin, *Chem. Eur. J.* **2005**, *11*, 3294.

DOI: 10.1002/anie.200604345

InterScience
© 2006 Wiley-VCH Verlag GmbH & Co. KGaA, Weinheim

Tetrapyrrole Macrocycles

DOI: 10.1002/anie.200603249

Metamorphosis of Tetrapyrrole Macrocycles**

Mathias O. Senge and Natalia N. Sergeeva*

Keywords:
corroles · nitrogen heterocycles · oxidation · photochemistry · porphyrinoids

Tetrapyrroles are some of the most ubiquitous pigments and cofactors in nature with an ever-expanding array of industrial applications.[1] In chemical terms all naturally occurring tetrapyrroles are derived from either the porphyrin skeleton porphyrin(1.1.1.1)[2] with 24 macrocycle atoms (**1**; four pyrrole rings and four methine bridges; for example, hemes and chlorophylls) or the corrin skeleton with 23 macrocycle atoms (four pyrrole rings and three bridging meso carbon atoms; for example, vitamin B_{12}).

There has been an immense surge in the preparation of structural homologues and isomers with different arrangements of the macrocycle atoms of these systems, and significant advances have been made to construct so-called isomeric (for example, N-confused porphyrins or porphycenes),[3] expanded (texaphyrins or octaphyrin **3**),[4] or contracted porphyrins (corrole **2**).[5] This surge was accompanied by significant progress in the synthetic methodology for their preparation as well as for the development of novel hydroporphyrins, nonaromatic tetrapyrroles, and conformationally designed systems.[1,6]

Typically all these different classes of cyclic polypyrrole compounds are accessible through specific and dedicated synthetic routes, and one cannot easily be transformed into another (Scheme 1). A notable exception was the finding that metal complexes of some octaphyrins[4] can undergo a thermal transformation into spirodicorroles **4**.[7] Some of these compounds can be split into two porphyrins in which the expanded porphyrins are linked with "regular" tetrapyrroles.[8,9]

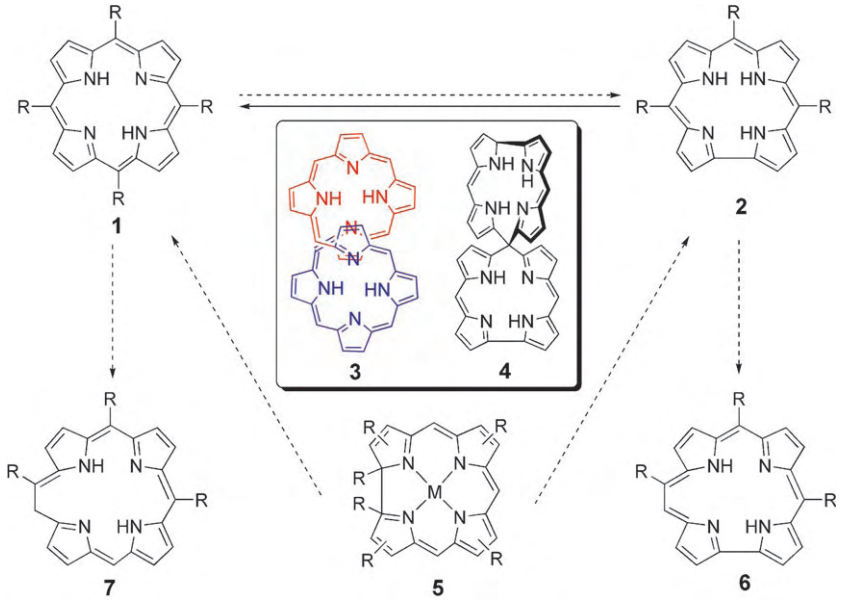

Scheme 1. Selected classes of tetrapyrroles and their possible interconversion routes.

In a recent paper by Gros et al., an intriguing observation was made that further links the different classes of polypyrrolic classes.[10] Upon standing under air at room temperature, a solution of the corrole **8** in $MeOH/C_6D_6$ was slowly converted into the porphyrin **9** (Scheme 2). The reaction was accelerated upon direct illumination and produced **9** in 19% yield within 48 hours.[11] Indeed, corroles are photosensitive and less stable in solution compared to their porphyrin analogues. It was shown earlier that they can easily be transformed into the corresponding biliverdin species in the presence of oxygen.[12] Intriguingly, porphyrin **9** was not the only product of this autoconversion, but was accompanied by the formation of the biliverdin derivative **10**, clearly the product of a similar ring-opening reaction.

Based on these observations and mechanistic studies, a possible mechanism involves a [2+2] cycloaddition to form a spiro intermediate, which is easily oxidized and split into **9** and **10**. Support for this mechanism comes from the behavior of bimetallic [36]octaphyrin(1.1.1.1.1.1.1.1), which splits into the two porphyrin macrocycles via the covalently linked spiro intermediates **13** (Scheme 3).[7,8] Insertion of Pd^{II} into the [34]octaphyrin(1.1.1.0.1.1.1.0) resulted in the formation of the binuclear complex **11** and its isomer, the bisspirodiporphyrin **12**. These two species exist in reversible thermal equilibrium, with **12**

[*] Prof. Dr. M. O. Senge, Dr. N. N. Sergeeva
School of Chemistry
SFI Tetrapyrrole Laboratory
Trinity College Dublin
Dublin 2 (Ireland)
Fax: (+353) 1-896-8536
E-mail: sengem@tcd.ie

[**] Writing of this article was made possible by a Science Foundation Ireland Research Professorship (SFI 04/RP1/B482).

InterScience
© 2006 Wiley-VCH Verlag GmbH & Co. KGaA, Weinheim

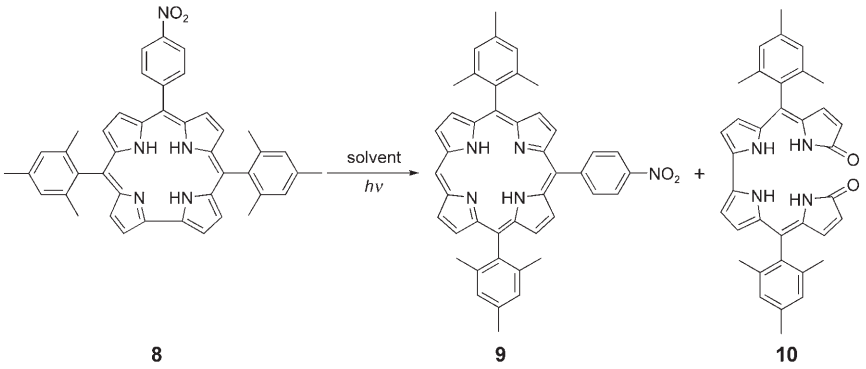

Scheme 2. Room-temperature autoconversion of a free-base corrole into a free-base porphyrin.

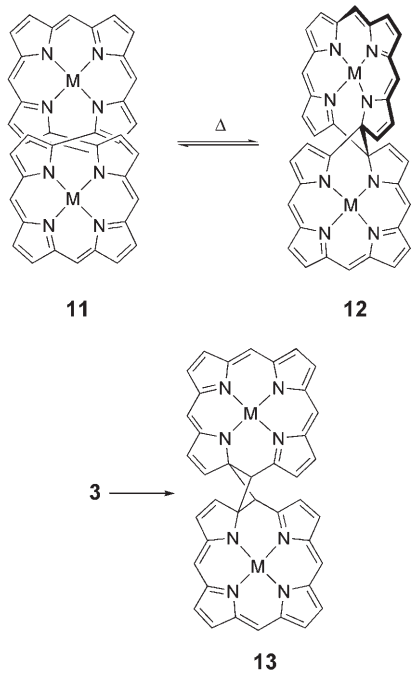

Scheme 3. Putative intermediates of the octaphyrin conversion.

predominating at room temperature, and the equilibrium can be shifted photochemically to **11**.[7]

Osuka and co-workers discovered the ultimate transformation of the copper(II) complex of an octaphyrin into the corresponding spirocyclobutane intermediate **14**, which was split into two porphyrin molecules **15** through a cycloreversion reaction (Scheme 4).[8,9] Although the formation of spiro compounds has so far only been experimentally observed for metal complexes, the close analogy between these reactions indicates the likelihood of their involvement in the reaction **8**→**9** as well.

While nature and synthetic chemists typically use linear synthetic strategies for the construction of individual molecular frameworks, the striking reaction discovered by Gros et al. indicates the conceptional possibility for switching back and forth between different porphyrin macrocycle systems. This becomes even clearer when other macrocycle transformations are taken into account (Scheme 5). In fact, another well-known reaction links the corrole and porphyrin macrocycles. In 1967, Johnson and co-workers described that neutral 1-substituted (tetradehydrocorrinato)nickel(II) complexes can undergo a thermal sigmatropic rearrangement to the respective Ni^{II} corroles.[13] Likewise, thermolysis of 1-methyl-19-alkyl-substituted Ni^{II} tetradehydrocorrin salts **16** yields the respective porphyrins **17**, in which the "new" meso carbon atom is derived from the 1-methyl group.[14] Thus, this reaction is mechanistically quite different from the ones involving spirobistetrapyrroles and involves ring expansion and alkyl migration of the 1-substituent. Related examples are the known porphyrin-to-homoporphyrin ring expansions that are observed upon oxidative cyclizations of *a*,*c*-biladiene salts, where the crucial mechanistic step is the conversion of a 1,20-disubstituted 20-hydroporphyrin through intermediary ring-opening and ring-closure sequences.[15]

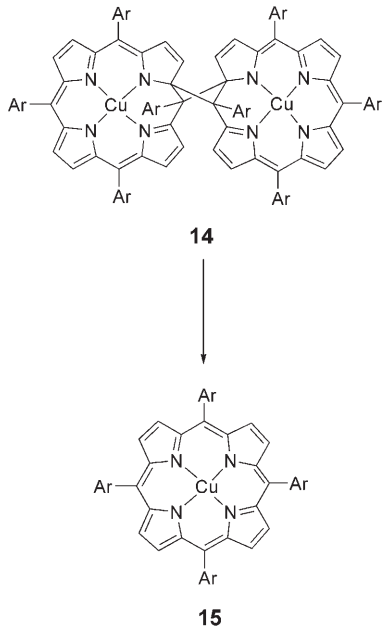

Scheme 4. Cycloreversion of spirocyclobutane intermediate **14** into porphyrin **15**.

Homoporphyrins, that is, porphyrins with a two-carbon-atom meso bridge, are also accessible by stepwise conversion of N-substituted porphyrins. A classic example is the Ni^{II}-catalyzed rearrangement of **18** (Scheme 5) involving first the formation of a Ni^{II} cationic complex, then cyclization to an aziridine, C–C bond migration to a meso position, and subsequent electrocyclic ring opening of the cyclopropanoic intermediate.[16]

Conceptionally, a similar case is the transformation of corroles into hemiporphycenes (formally homocorroles), which was reported here last year by Paolesse et al.[17] Reaction of 5,10,15-triphenylcorrole **20** with diiodocarbene gave the corresponding 5-iodo-10,15,20-triphenylporphyrin in traces and larger amounts of the hemiporphycene **21** (Scheme 5) through a ring-expansion reaction. Such a one-step procedure is more facile than the original total syntheses of hemiporphycenes.[18] Hemiporphycenes are also accessible by ring contraction of homoporphyrins.[19] Likewise, a brominated porphycene has been shown to undergo a thermal ring contraction to isocorrole [porphyrin-(2.0.1.0)] in basic medium.[20]

As corroles can undergo ring expansion to porphyrins, porphyrins can undergo ring contraction to corroles. A few months ago, Callot et al. showed that the Friedel–Crafts acylation of the 5,10,15,20-tetraarylporphyrinnickel(II) compound **22** with aryl anhydrides gives the corrole **23** upon air oxidation in the presence of pyridine (Scheme 5). Mechanistically this reaction most likely involves a pinacol-type rearrangement

© 2006 Wiley-VCH Verlag GmbH & Co. KGaA, Weinheim

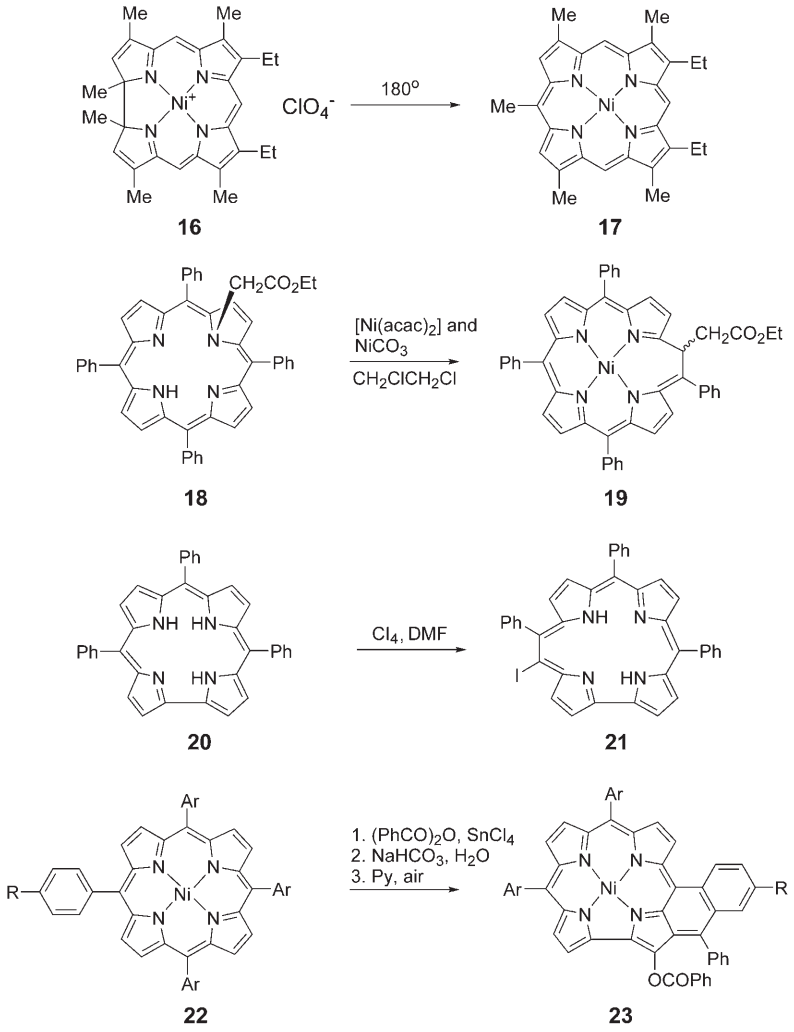

Scheme 5. Selected interconversions of different tetrapyrroles; acac = acetylacetonate.

similar to the one involving the natural formation of corrinoids,[21] and the reaction is a typical example for the synthetic possibilities that result from interactions at the porphyrin periphery.[22]

Thus, porphyrins and related tetrapyrroles not only exist in a wide variety of different structural isomers and homologues, but there is also an increasing body of evidence that members of the individual classes can also be interconverted. Many of these reactions at present will not find large-scale synthetic applications; often they are restricted to specific derivatives, substituents, metal complexes, and reaction conditions. Yet, the observation that some of these reactions, such as the corrole→porphyrin conversion **8**→**9**, can occur at room temperature indicates the synthetic potential of these tetrapyrrole macrocycle interconversion reactions.

The last 25 years have seen an explosion in the number of new, altered, and specifically designed tetrapyrroles, and it might be believed that only structural, mechanistic, and physical details remain to be studied to optimize their technical application potential. Now, links between the different classes of tetrapyrroles are emerging, and it appears possible to develop routes for rapid interconversion.

[1] *The Porphyrin Handbook*, *Vol. 1–10* (Eds.: K. M. Kadish, K. M. Smith, R. Guilard), Academic Press, San Diego, **2000**.

[2] The standard nomenclature for the various cyclic tetrapyrrole systems uses (*a.b.c.d*) to denote the number of bridging meso carbon atoms. The "regular" porphyrin is porphyrin(1.1.1.1), corrole is porphyrin(1.1.1.0), porphycene is porphyrin(2.0.2.0), hemiporphycene is porphyrin(2.1.1.0), etc.

[3] a) E. Vogel, *Pure Appl. Chem.* **1990**, *62*, 557; b) E. Vogel, *Pure Appl. Chem.* **1993**, *65*, 143.

[4] a) E. Vogel, M. Bröring, J. Fink, D. Rosen, H. Schmickler, J. Lex, K. W. K. Chan, D. A. Plattner, M. Nendel, K. N. Houk, *Angew. Chem.* **1995**, *107*, 2705; *Angew. Chem. Int. Ed. Engl.* **1995**, *34*, 2511; b) M. Bröring, J. Jendrny, L. Zander, H. Schmickler, J. Lex, Y.-D. Wu, M. Nendel, J. Chen, D. A. Plattner, K. N. Houk, E. Vogel, *Angew. Chem.* **1995**, *107*, 2709; *Angew. Chem. Int. Ed. Engl.* **1995**, *34*, 2515; c) J.-Y. Shin, H. Furuta, K. Yoza, S. Igarashi, A. Osuka, *J. Am. Chem. Soc.* **2001**, *123*, 7190.

[5] a) J. L. Sessler, S. Weghorn, *Expanded, Contracted and Isomeric Porphyrins*, Elsevier, Oxford, **1997**; b) T. K. Chandrashekar, S. Venkatraman, *Acc. Chem. Res.* **2003**, *36*, 676.

[6] a) K. M. Smith, M. G. H. Vicente in *Science of Synthesis* (Ed.: S. E. Weinreb), Thieme, Stuttgart, **2003**, p. 1081; b) J. L. Sessler, R. S. Zimmerman, C. Bucher, V. Král, B. Andrioletti, *Pure Appl. Chem.* **2001**, *73*, 1041; c) M. O. Senge, *Chem. Commun.* **2006**, 243; d) Y. Inokuma, J. Ho Kwon, T. Kyu Ahn, M. Yoo, D. Kim, A. Osuka, *Angew. Chem.* **2006**, *118*, 975; *Angew. Chem. Int. Ed.* **2006**, *45*, 961.

[7] E. Vogel, M. Michels, L. Zander, J. Lex, N. S. Tuzun, K. N. Houk, *Angew. Chem.* **2003**, *115*, 2964; *Angew. Chem. Int. Ed.* **2003**, *42*, 2857.

[8] Y. Tanaka, W. Hoshino, S. Shimizu, K. Youfu, N. Aratani, N. Maruyama, S. Fujita, A. Osuka, *J. Am. Chem. Soc.* **2004**, *126*, 3046.

[9] Highlight: L. Latos-Grażyński, *Angew. Chem.* **2004**, *116*, 5234; *Angew. Chem. Int. Ed.* **2004**, *43*, 5124.

[10] C. P. Gros, J.-M. Barbe, E. Espinosa, R. Guilard, *Angew. Chem.* **2006**, *118*, 5770; *Angew. Chem. Int. Ed.* **2006**, *45*, 5642.

[11] One of the pieces of experimental proof for the formation of **9** was a single-crystal X-ray analysis of a product fraction that was shown to be a cocrystal of **8** and **9** (1:1 ratio). See Figure 1 in reference [10].

[12] C. Tardieux, C. P. Gros, R. Guilard, *J. Heterocycl. Chem.* **1998**, *35*, 965.

[13] a) R. Grigg, A. W. Johnson, K. Richardson, K. W. Sheldon, *J. Chem. Soc. D* **1967**, 1192; b) R. Grigg, A. W. Johnson, K. Richardson, K. W. Sheldon, *J. Chem. Soc. C* **1970**, 1289.

[14] a) R. Grigg, A. W. Johnson, K. Richardson, K. W. Sheldon, *J. Chem. Soc. D* **1968**, 897; b) R. Grigg, A. W. Johnson,

 © 2006 Wiley-VCH Verlag GmbH & Co. KGaA, Weinheim

K. Richardson, K. W. Sheldon, *J. Chem. Soc. C* **1969**, 655.
[15] a) P. A. Liddell, M. M. Olmstead, K. M. Smith, *Tetrahedron Lett.* **1990**, *31*, 2685; b) P. A. Lidell, K. R. Gerzevske, J. J. Lin, M. M. Olmstead, K. M. Smith, *J. Org. Chem.* **1993**, *58*, 6681; c) J. J. Lin, K. R. Gerzevske, P. A. Liddell, M. O. Senge, M. M. Olmstead, R. G. Khoury, B. E. Weeth, S. A. Tsao, K. M. Smith, *J. Org. Chem.* **1997**, *62*, 4266.
[16] H. J. Callot, T. Tschamber, *J. Am. Chem. Soc.* **1975**, *97*, 6175.
[17] R. Paolesse, S. Nardis, M. Stefanelli, F. R. Fronczek, M. G. H. Vicente, *Angew. Chem.* **2005**, *117*, 3107; *Angew. Chem. Int. Ed.* **2005**, *44*, 3047.
[18] E. Vogel, M. Bröring, S. J. Weghorn, P. Scholz, R. Deponte, J. Lex, H. Schmickler, K. Schaffner, S. E. Braslavsky, M. Müller, S. Pörting, C. J. Fowler, J. L. Sessler, *Angew. Chem.* **1997**, *109*, 1725; *Angew. Chem. Int. Ed. Engl.* **1997**, *36*, 1651.
[19] H. J. Callot, A. Rohrer, T. Tschamber, *New J. Chem.* **1995**, *19*, 155.
[20] S. Will, A. Rahbar, H. Schmickler, J. Lex, E. Vogel, *Angew. Chem.* **1990**, *102*, 1434; *Angew. Chem. Int. Ed. Engl.* **1990**, *29*, 1390.
[21] C. Jeandon, R. Ruppert, H. J. Callot, *J. Org. Chem.* **2006**, *71*, 3111.
[22] Recent reviews on reactions at the porphyrin periphery: a) H. J. Callot, R. Ruppert, C. Jeandon, S. Richeter, *J. Porphyrins Phthalocyanines* **2004**, *8*, 111; b) M. O. Senge, J. Richter, *J. Porphyrins Phthalocyanines* **2004**, *8*, 934; c) M. O. Senge, *Acc. Chem. Res.* **2005**, *38*, 733; d) K. M. Smith, S. H. Lee, M. G. H. Vicente, *J. Porphyrins Phthalocyanines* **2005**, *9*, 769.

 © 2006 Wiley-VCH Verlag GmbH & Co. KGaA, Weinheim

Asymmetric Organocatalysis

DOI: 10.1002/anie.200602318

Cupreines and Cupreidines: An Emerging Class of Bifunctional Cinchona Organocatalysts

*Tommaso Marcelli, Jan H. van Maarseveen, and Henk Hiemstra**

Keywords:
asymmetric catalysis · cinchona alkaloids · enantioselectivity · natural products · organocatalysis

Dedicated to Professor Hans Wynberg

In the steadily expanding field of organocatalysis, cinchona alkaloids play a prominent role. Until the late 1990s, bifunctional catalysts based on this scaffold relied exclusively on the C9-hydroxy group as the hydrogen-bond donor. Recently, new cinchona catalysts have been developed that feature a phenolic OH group in the C6′ position—a structural feature that allows a diverse set of reactions to be catalyzed in a highly stereoselective fashion. This Minireview describes the scope and modes of action of this new class of asymmetric bifunctional organocatalysts.

1. Introduction

Cinchona alkaloids are recognized as a privileged class of compounds in asymmetric catalysis (Figure 1).[1] One of the most interesting features of this well-known family of alkaloids is their availability in two pseudo-enantiomeric forms; cinchona catalysts can therefore provide access to both enantiomers of a product with mostly identical selectivities. Long before the explosion of asymmetric organocatalysis,[2] cinchona alkaloids were already shown to be outstanding catalysts for enantioselective reactions. Although the first report on asymmetric organocatalysis involving the hydrocyanation of aldehydes catalyzed by cinchonidine dates back to 1912,[3] it is only after 1960 that cinchona alkaloids were recognized as useful tools for the highly enantioselective synthesis of chiral molecules. A seminal study by Pracejus on the applications of cinchona alkaloids in ketene chemistry[4] was followed, in the next two decades, by several reports from Wynberg et al.,[5] with the most impressive example being the enantioselective Staudinger-like synthesis of β-lactones.[6] In the 1980s, the popularity of cinchona derivatives in asymmetric catalysis increased considerably, in particular as a result of developments in phase-transfer catalysis[7] and asymmetric dihydroxylation.[8]

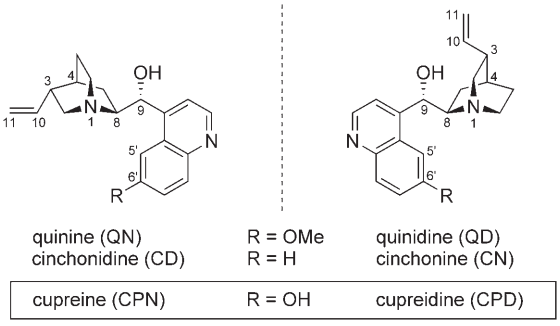

Figure 1. The four main cinchona alkaloids and their C6′–OH derivatives. With regard to the pseudo-enantiomers, the key stereogenic centers (N1, C8, C9) have the opposite absolute configuration while the quinuclidine fragment (C3, C4) is identical in both.

To gain insight into their mode of action, the conformational behavior of the alkaloids was investigated by means of NMR spectroscopic and computational techniques and resulted in the identification of four low-energy cinchona conformers (Figure 2).[9] Molecular mechanics (MM) calculations suggested that quinine and quinidine preferentially adopt a *syn*-closed conformation in the gas phase; however, *anti*-open conformations were observed in nonpolar solvents (by means of ^{1}H NMR spectroscopy) for both alkaloids.[9b] Substituents at C9 play a key role in determining the conformation of cinchona alkaloids; in solution, esters are present in the *anti*-closed form, while C9 methyl ethers prefer an *anti*-open arrangement. More sophisticated ab initio studies revealed that polar solvents stabilize the two closed conformers.[9c] However, many other factors (such as intermolecular interactions) are responsible for the complex conformational behavior of cinchona alkaloids in solution. Furthermore, upon protonation, a C9 *p*-chlorobenzoyl ester was shown to switch from the *anti*-closed to the *anti*-open conformation.

[*] T. Marcelli, Dr. J. H. van Maarseveen, Prof. Dr. H. Hiemstra
Van't Hoff Institute for Molecular Sciences (HIMS)
Universiteit van Amsterdam
Nieuwe Achtergracht 129, 1018WS Amsterdam (The Netherlands)
Fax: (+31) 20-525-5670
E-mail: hiemstra@science.uva.nl

InterScience
© 2006 Wiley-VCH Verlag GmbH & Co. KGaA, Weinheim

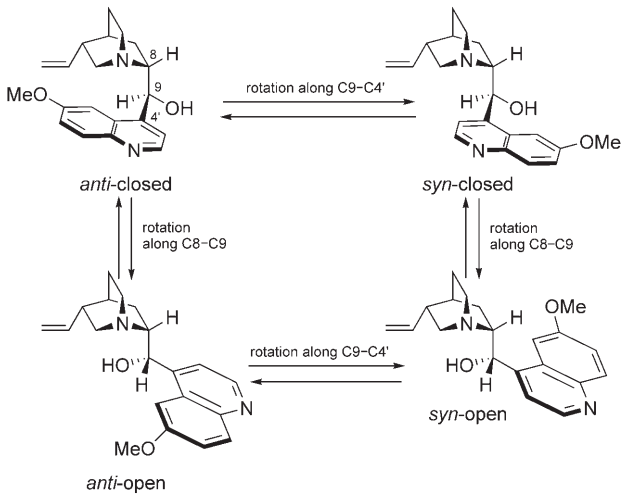

Figure 2. The four low-energy conformers of quinidine.

In recent years, many new applications of cinchona organocatalysts have been reported. In most examples, the alkaloids (or their derivatives) were used as chiral bases.[10] In some cases, however, the bifunctional character of the naturally occurring alkaloids was successfully exploited. The presence of both the quinuclidine basic nitrogen center and a free hydroxy group on C9 was shown to be crucial for some applications; for instance, detailed mechanistic studies on the addition of aromatic thiols to cyclic enones revealed that the β-hydroxyamine motif behaves as a Lewis base/Brønsted acid bifunctional catalyst and is responsible for the good enantioselectivities observed in the reaction (up to 74% *ee*).[11]

Conversion of the methoxy group at the C6′ position of both quinine and quinidine into a reactive functionality did not receive special attention in the early studies on cinchona organocatalysis. Selective cleavage of the carbon–oxygen bond to yield a phenol was first reported in 1979.[12] More recently, Hoffmann and co-workers explored the reactivity of cinchona alkaloids and their conversion into different derivatives, with a special focus on the synthesis of different strained tricyclic structures.[13] To achieve that, several quinidine derivatives were subjected to cyclization under strongly acidic conditions. Of particular interest is the synthesis of the oxazatwistane[14] β-isoquinidine (β-IQD), a compound with limited conformational flexibility and increased basicity and nucleophilicity, mainly due to the reduced steric hindrance of the quinuclidine nitrogen center and the increased ring strain of its tricyclic framework (Figure 3).[13c]

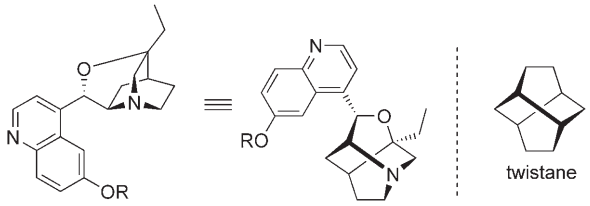

Figure 3. Cinchona oxazatwistanes: β-isoquinidine (β-IQD) and β-isocupreidine (β-ICPD).

The demethylated form of this cinchona derivative, β-isocupreidine (β-ICPD),[15] and other simpler congeners that comprise a C6′-hydroxy group were recently shown to be powerful enantioselective catalysts for a wide array of reactions. These catalysts feature two separated sites for simultaneous activation of both nucleophile and electrophile.[16] The advantage of cupreines and cupreidines over previously reported cinchona bifunctional catalysts (mainly the parent alkaloids or their 10,11-dihydro derivatives) is that they have a free site for further functionalization (C9–OH) which can be exploited to fine tune properties such as basicity and conformation and therefore affect the catalytic performances. This Minireview summarizes the achievements made possible by this new class of bifunctional cinchona organocatalysts, which are referred to as cupreines in the following pages (Table 1).

2. Baylis–Hillman Reactions

The first application of a cinchona organocatalyst that bears a hydroxy moiety at the C6′ position was reported by

Henk Hiemstra was born in Dronrijp, Friesland, The Netherlands, in 1952. He studied chemistry at the University of Groningen and completed his PhD there with Hans Wynberg in 1980. After a postdoctoral stay with Barry M. Trost at the University of Wisconsin, Madison, USA, he was appointed at the University of Amsterdam in 1982. He was promoted to full professor of organic synthesis in 1997. His research areas are new synthetic methodology and the total synthesis of natural products.

Jan van Maarseveen was born in Enschede, The Netherlands, in 1963. He studied chemistry at the University of Nijmegen and completed his PhD there with Binne Zwanenburg and Hans W. Scheeren in 1994. He then joined Solvay Pharmaceuticals (Weesp, The Netherlands) as a group leader in the Medicinal Chemistry Department. He was appointed associate professor at the University of Amsterdam in 1999. His current research interests include the development of novel synthetic methodology to enable difficult peptide cyclizations.

Tommaso Marcelli was born in Milan, Italy, in 1978. He studied industrial chemistry at the University of Bologna and received his MSc in 2002 under the supervision of Goffredo Rosini. He then moved to the Netherlands to join the group of Prof. Hiemstra, where he is currently working on his PhD thesis. His research deals with the design of new cinchona organocatalysts for asymmetric C–C bond-forming reactions.

© 2006 Wiley-VCH Verlag GmbH & Co. KGaA, Weinheim

Table 1: Structures and abbreviations of some cinchona catalysts.

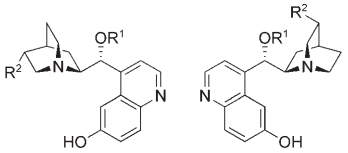

cupreine cupreidine

R^1	R^2	Cupreine	Cupreidine
H	vinyl	CPN	CPD
H	ethyl	DHCPN	DHCPD
benzyl	vinyl	BnCPN	BnCPD
9-phenanthryl	vinyl	PHNCPN	PHNCPD
acetyl	vinyl	AcCPN	AcCPD
benzoyl	vinyl	BzCPN	BzCPD

Hatakeyama and co-workers in 1999.[17a] They showed that β-ICPD is a highly enantioselective catalyst for the Baylis–Hillman reaction[18] of hexafluoroisopropyl acrylate (HFIPA) with various aldehydes. The desired adducts were obtained with excellent enantiomeric excess although in moderate yields only, mainly owing to the formation of a dioxanone by-product (Scheme 1).

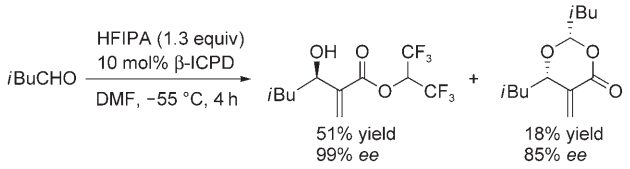

Scheme 1. β-Isocupreidine-catalyzed Baylis–Hillman reaction. DMF = *N*,*N*-dimethylformamide.

Besides its importance from a synthetic point of view (this was the first example of a highly enantioselective catalytic Baylis–Hillman reaction), this study clearly showed that the presence of the phenol was essential for the enantioselectivity. Straightforward yet elegant mechanistic studies provided sufficient information to propose a convincing rational for the observed asymmetric induction. In their model (Figure 4), Hatakeyama and co-workers suggested that after conjugate addition of the catalyst to the Michael acceptor and subsequent reversible attack of the resulting enolate on the aldehyde, several diastereomeric structures are present. Two of these structures benefit from increased stabilization as a result of an intramolecular hydrogen bond between the alcoholate and the phenolic OH group. One of them can easily adopt the antiperiplanar arrangement of the quaternary nitrogen center and the α-hydrogen atom required for the elimination to take place, leading to the preferential formation of one enantiomer. The other structure experiences severe steric repulsions in doing so and therefore reacts with another molecule of aldehyde to yield the dioxanone by-product with occasionally high enantiomeric excess.

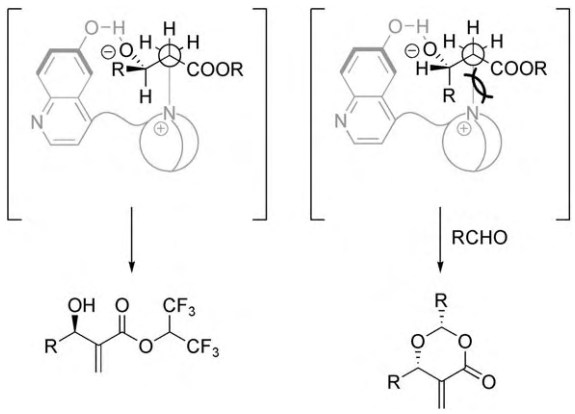

Figure 4. Explanation for the enantioselectivity in the β-isocupreidine-catalyzed Baylis–Hillman reaction.

The use of Michael acceptors other than HFIPA met with limited success. Simple α,β-unsaturated systems such as methyl vinyl ketone gave poor results (< 50 % *ee*), while α-naphthyl acrylate could be converted into the corresponding Baylis–Hillman adducts with variable enantiomeric excesses (33–92 % *ee*) although in low yields (17–68 %).[19] Details on the optimization of catalyst structure, reaction partners, and conditions, as well as an improved experimental protocol for the reaction of HFIPA with aldehydes were reported recently by Hatakeyama and co-workers.[17b]

This methodology was applied to the total synthesis of (−)-mycestericin E[20] and a formal synthesis of epopromycin B[21] (Scheme 2). In this case, β-ICPD was employed to obtain high levels of diastereoselectivity in the reaction of HFIPA with (*S*)-*N*-Fmoc-leucinal. Interestingly, the *R* enantiomer reacted sluggishly under the same conditions and furnished a diastereomeric mixture of dioxanones in low yield.

Shi et al. employed β-ICPD in the aza-Morita–Baylis–Hillman reaction of imines with simple Michael acceptors such as methyl vinyl ketone, methyl acrylate, and acrylonitrile

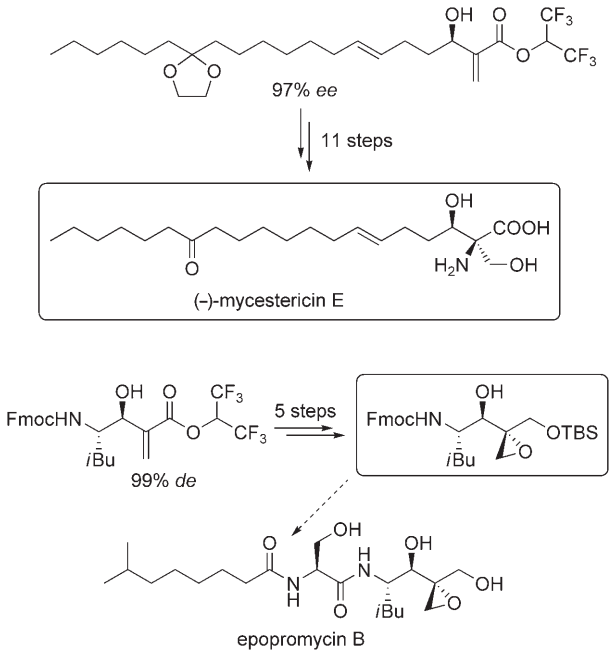

Scheme 2. Applications of Baylis–Hillman adducts. Fmoc = 9-fluorenylmethoxycarbonyl; TBS = *tert*-butyldimethylsilyl.

© 2006 Wiley-VCH Verlag GmbH & Co. KGaA, Weinheim

(Scheme 3).[22,23] The enantioselectivity turned out to be strongly dependent on the reaction conditions and the nature of the reactants; the best combination was when aromatic *N*-sulfonyl imines were used with methyl vinyl ketone. In this case, the aza-Morita–Baylis–Hillman adducts could be obtained in fair to high yields (58–80%) and with synthetically useful enantiomeric excesses (73–99% *ee*).[22]

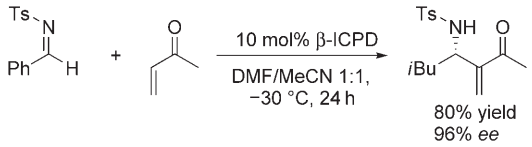

Scheme 3. Enantioselective aza-Baylis–Hillman reaction. Ts = *p*-toluenesulfonyl.

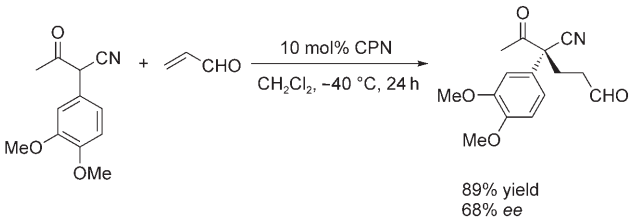

Scheme 4. Cupreine-catalyzed conjugate addition to acrolein.

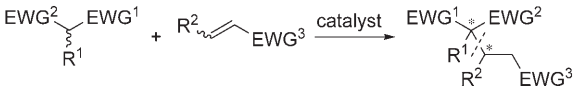

Scheme 5. Asymmetric C–C bond formation through conjugate addition. EWG = electron-withdrawing group.

Hatakeyama and co-workers reported an enantioselective aza-Morita–Baylis–Hillman reaction of HFIPA with *N*-phosphinoyl imines.[24] In this case, enantioselectivities were less impressive (54–72% *ee*); nevertheless, nearly enantiopure products were obtained in satisfactory yields after one recrystallization.

Having successfully developed a one-pot, three-component aza-Baylis–Hillman reaction,[25] Balan and Adolfsson implemented enantioselectivity in their protocol by replacing 1,4-diazabicyclo[2.2.2]octane (DABCO) with cinchona derivatives.[26] *N*-Sulfonyl imines, formed in situ from tosylamide and an aldehyde (in the presence of a small amount of titanium 2-propoxide and molecular sieves), reacted with methyl acrylate in the presence of β-ICPD (15 mol%) to yield the aza-Baylis–Hillman adducts in variable yields (12–95%) and with moderate enantiomeric excesses (49–74% *ee*).

Remarkably, the aza-Baylis–Hillman adducts in all cases have the opposite absolute configuration to the adducts derived from aldehydes.[27] Hatakeyama and co-workers explained this reversal by assuming that the steric hindrance around the imine nitrogen center governs the rate of elimination that leads to the preferential formation of one enantiomer.

3. Conjugate Additions

The ability of phenolic (C6′–OH) cinchona alkaloids to activate Michael acceptors in enantioselective transformations was first demonstrated in 2002,[28] with the asymmetric addition of α-cyanoketones to acrolein catalyzed by cupreine (Scheme 4). Despite the moderate enantiomeric excesses obtained, the reported results are particularly noteworthy considering the ease of polymerization of acrolein in the presence of a nucleophilic catalyst.

Two years later, Deng and co-workers published the first of a series of papers that deal with the use of simple cupreines as catalysts for conjugate additions (Scheme 5).[29–32] They showed that a small set of readily available catalysts can provide excellent enantio- and diastereoselectivity with several combinations of reaction partners, giving access to a notable array of small chiral building blocks. Malonates, β-ketoesters, β-diketones, α-nitroesters, α-cyanoesters, and α-cyanoketones were successfully employed as nucleophiles in the addition to nitroalkenes, vinyl sulfones, and vinyl ketones. In all cases, employment of cinchona alkaloids with a C6′–OMe substituent resulted in considerably lower asymmetric induction. Wang et al. recently extended this concept to the aza-Michael addition of benzotriazole, triazole, and tetrazole to nitroalkenes (Table 2).[33]

In their attempt to rationalize the results obtained for the addition of cyclic ketoesters to nitroalkenes leading to the

Table 2: Scope of cupreine-catalyzed enantioselective conjugate additions.

Nucleophiles (Nu)

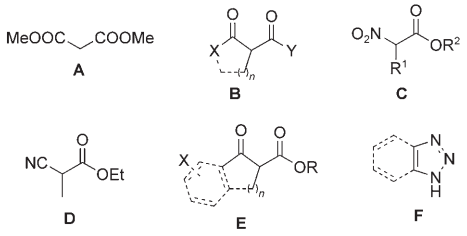

Electrophiles (E)

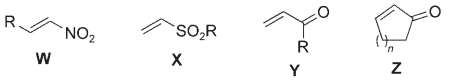

Nu	E	Catalyst (mol%)[a]	Yield [%]	*ee* [%][b]	*de* [%]	Ref.
A	**W**	CPN (10)	71–99	80–99	–	[29]
B	**W**	BzCPN (10)	73–95	99	72–98	[30]
C	**W**	BzCPN (10)	77–78	92–96	84–90	[30]
D	**W**	BzCPN (10)	75–77	98–99	86–98	[30]
D	**X**	PHNCPN (20)	76–96	86–97	–	[31]
E	**Y**	PHNCPN (1–10)	82–100	90–98	–	[32]
E	**Z**	PHNCPN (20)	87–99	85–98	72–92	[32]
F	**W**	CPN (10)	65–90	57–94	–	[33]

[a] The corresponding pseudo-enantiomers afforded the opposite enantiomers with nearly identical selectivities. [b] Enantiomeric excess of the major diastereomer.

 © 2006 Wiley-VCH Verlag GmbH & Co. KGaA, Weinheim

simultaneous generation of two contiguous tertiary and quaternary stereocenters, Deng and co-workers proposed that the phenolic OH group could control the stereochemistry of the resulting product through hydrogen bonding of both nucleophile and electrophile. As similar results were obtained with the conformationally more rigid β-ICPD, they suggested that in this reaction the cinchona catalyst adopts an *anti*-open conformation.[30]

Such mechanistic considerations led the researchers to also investigate the addition of carbon nucleophiles to α-chloroacrylonitrile. In this case, a tandem Michael addition/asymmetric protonation led to the simultaneous generation of two noncontiguous stereocenters (Scheme 6).[34] Excellent

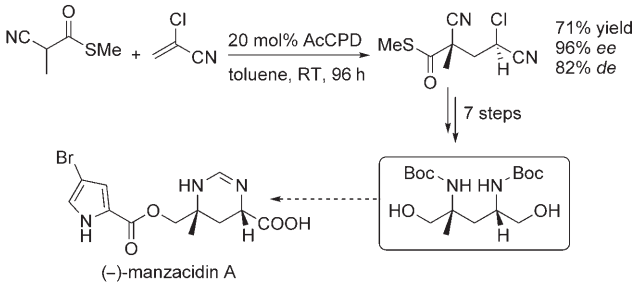

Scheme 6. Tandem Michael addition/asymmetric protonation.

yields (71–96%) and stereoselectivities (78–96% *ee*, 2:1–25:1 d.r.) could be achieved with both cyclic and acyclic donors. Furthermore, the synthetic usefulness of the resulting compounds was highlighted by a formal synthesis of (−)-manzacidin A.

More recently, Deng and co-workers also reinvestigated Michael additions to α,β-unsaturated aldehydes (including acrolein). Careful optimization of the reaction conditions and screening of different substituents at C9 resulted in excellent yields and enantioselectivities with different nucleophiles (β-ketoesters, β-diketones, and α-cyanoacetates).[35] Interestingly, when highly nucleophilic β-ICPD, quinuclidine, or DABCO were employed as catalysts for the same transformation, extensive polymerization of the aldehyde was observed. A concise synthesis of (+)-tanikolide, involving a chiral aldehyde with a quaternary stereocenter as the key intermediate, was also described (Scheme 7).

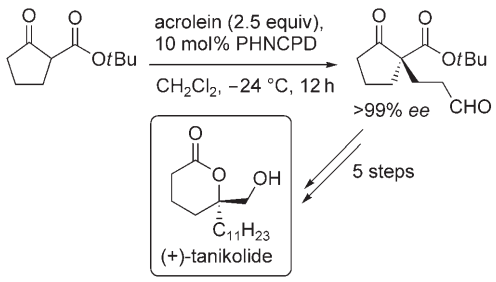

Scheme 7. Cupreidine-catalyzed conjugate addition to acrolein.

4. Electrophilic Aminations

The reaction of a carbon nucleophile with an azodicarboxylate followed by reductive cleavage of the nitrogen–nitrogen bond in the resulting hydrazine represents an elegant approach to the creation of a nitrogen-containing quaternary stereocenter (Scheme 8).[36] Jørgensen and co-workers

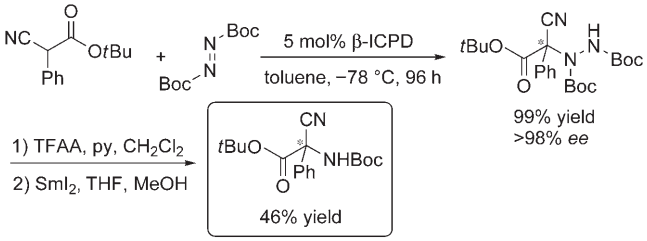

Scheme 8. Asymmetric electrophilic amination of cyanoacetates. Boc = *tert*-butyloxycarbonyl; TFAA = trifluoraacetic anhydride; py = pyridine.

showed that racemic β-ketoesters and α-aryl-α-cyanoacetates can be aminated in excellent yields (84–99%) and with high enantioselectivity (83–99% *ee*) in the presence of a remarkably low amount of β-ICPD (as little as 0.5 mol%).[37] Deng and co-workers expanded the scope of this transformation by replacing β-ICPD with BnCPN and BnCPD.[38] The catalyst loading occasionally had to be increased to obtain acceptable reaction rates. Nevertheless, both product enantiomers could thus be obtained in virtually identical yield (71–99%) and enantiomeric excesses (82–99% *ee*). Unfortunately, the two-step reductive cleavage of the nitrogen–nitrogen bond to yield a carbamate-protected amine (without loss of optical purity) proceeded in somewhat disappointing yield.[36]

Jørgensen et al. also reported the first atroposelective organocatalytic Friedel–Crafts amination of 2-naphthols[39] (Scheme 9). Careful selection of the substituents on the

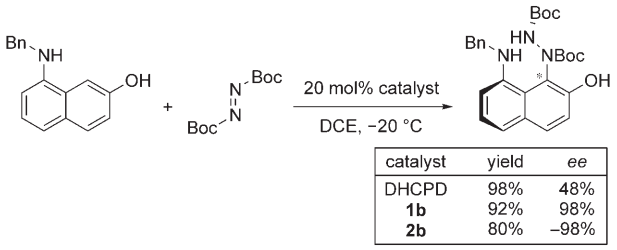

catalyst	yield	*ee*
DHCPD	98%	48%
1b	92%	98%
2b	80%	−98%

Scheme 9. Atroposelective Friedel–Crafts amination. Bn = benzyl; DCE = dichloroethane.

aromatic ring permitted the identification of 8-amino-2-naphthols as precursors for configurationally stable aryl hydrazines. While quinine afforded nearly racemic products, dihydrocupreidine (DHCPD) promoted this reaction with enantiomeric excesses of up to 88%. On the other hand, results obtained with dihydrocupreine (DHCPN) were less satisfactory (≤61% *ee*), thus constituting a rare example of poor pseudo-enantiomeric behavior in cinchona organocatalysis.

© 2006 Wiley-VCH Verlag GmbH & Co. KGaA, Weinheim

Although they are unreactive under the optimized reaction conditions, DHCPN and DHCPD were recognized as potential substrates for this transformation. By changing the solvent and temperature, the autocatalytic amination of these catalysts could be carried out in good yields (80–95%). The C5′-aminated cinchona alkaloids **1b** and **2b** (Figure 5) were found to be excellent pseudo-enantiomeric catalysts for the amination of naphthols, providing access to both atropisomers of the chiral hydrazines with even higher enantiomeric excesses (87–98% *ee*).

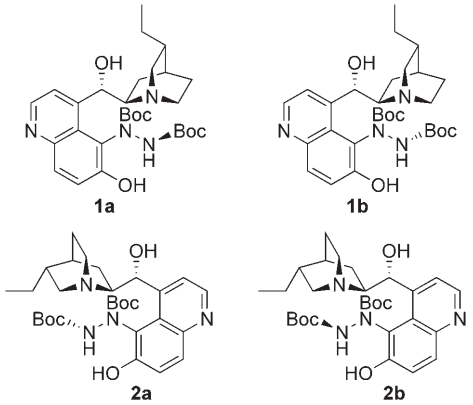

Figure 5. C5′-aminated cinchona alkaloids.

5. Nitroaldol Reactions

The enantioselective addition of a nitroalkane to an aldehyde, known as the nitroaldol (or Henry) reaction,[40] has remained an elusive goal in organocatalysis for many years.[41] Following pioneering studies by Matsumoto and co-workers on the use of cinchona alkaloids in this reaction,[41b] we investigated the use of cupreidines in the reaction of nitromethane with electron-poor aldehydes (Scheme 10). Although only moderate enantioselectivities (up to 45% *ee*) could be obtained, the results showed a clear beneficial effect of the phenol moiety on the asymmetric induction.[42] Replacement of the phenol with an activated thiourea[43,44] provided us with a catalyst that could promote the nitroaldol reaction of various aromatic and heteroaromatic aldehydes in high yields (87–99%) and with high enantiomeric excesses (85–93% *ee*).[45]

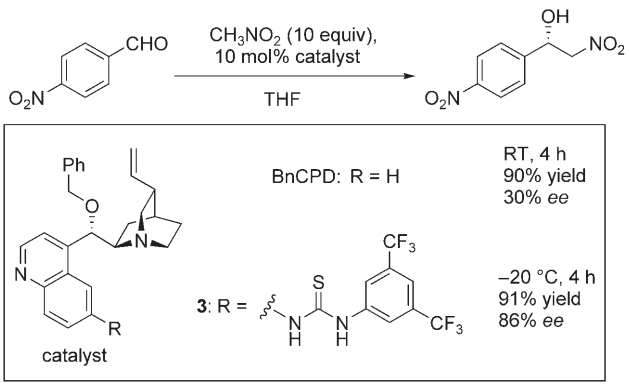

Scheme 10. Enantioselective nitroaldol reaction of aromatic aldehydes.

Deng and co-workers showed that, although not suitable for aldehydes, benzoylcupreine (BzCPN) amd benzoylcupreidine (BzCPD) are excellent enantioselective organocatalysts for the reaction of α-ketoesters with nitromethane.[46] This methodology provides an easy access to small yet densely functionalized molecules that feature a quaternary stereocenter. The usefulness of these building blocks was demonstrated by their straightforward conversion into highly enantioenriched aziridines, β-lactams, and α-alkylcysteines (Scheme 11).

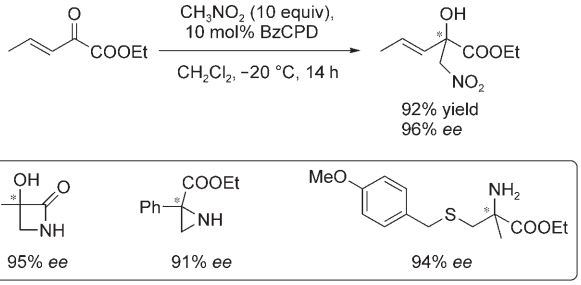

Scheme 11. Asymmetric Henry reaction of α-ketoesters, and further manipulation of the products.

Unlike in the case of conjugate addition, in the nitroaldol reaction β-ICPD afforded products with considerably lower optical purity than those obtained with simpler cupreidines (both with aldehydes and α-ketoesters). Although not supported by direct experimental evidence, this suggests that a "closed" conformation of the catalyst may be required for an efficient asymmetric induction (this conformation is impossible to adopt for β-ICPD owing to its tricyclic structure).

6. Miscellaneous

Romo and co-workers developed an elegant asymmetric organocatalytic protocol for the nucleophile-catalyzed aldol lactonization.[47] Good to excellent enantiomeric excesses were obtained with different quinidine derivatives substituted with a methoxy group at the C6′ position. Interestingly, when β-ICPD was used as the catalyst, a complete reversal in the sense of asymmetric induction was observed (Scheme 12).[47b] Analysis of ^{1}H NMR coupling constants and NOE spectra did not provide the authors with a satisfying explanation for the observed enantioselectivities, but suggested that *O*-acetylquinidine and β-ICPD discriminate between the two prochiral faces according to completely different mechanisms, as previously observed for other reactions, such as the Michael addition of thiols to enones.[10a]

Enantiomerically enriched hydroxylated β-dicarbonyl compounds were obtained by Taylor by reacting a cyclic β-ketoester with *tert*-butyl hydroperoxide in the presence of catalytic amounts of a quinidine derivative (Scheme 13).[48] Although the importance of the phenolic OH in the catalyst

 © 2006 Wiley-VCH Verlag GmbH & Co. KGaA, Weinheim

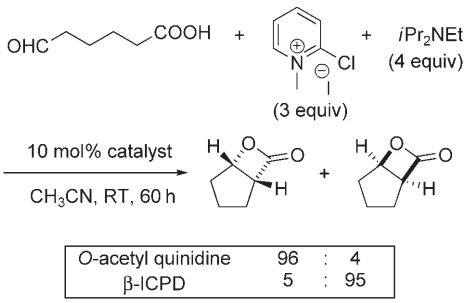

Scheme 12. Asymmetric nucleophile-catalyzed aldol lactonization.

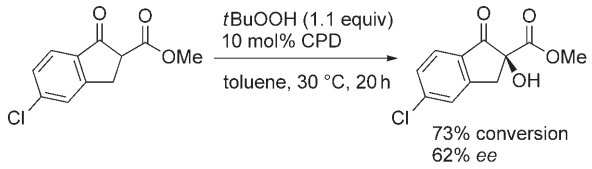

Scheme 13. Enantioselective α-hydroxylation of β-ketoesters.

was not mentioned, cupreidines consistently outperformed their C6′−OMe counterparts in the examples described therein.

Baylis–Hillman adducts, upon conversion of the alcohol into a leaving group, can be substrates for asymmetric allylic substitutions.[49] Trost et al. employed palladium complexes to convert these compounds into highly enantiomerically enriched intermediates for the total synthesis of biologically relevant targets.[50] More recently, Lu and co-workers described the first enantioselective allylic substitution catalyzed by a cinchona alkaloid, namely β-ICPD. *O*-Boc-protected Baylis–Hillman adducts were treated with a variety of nucleophiles to afford chiral α-methylene esters in good yields (84–96%) although with only moderate enantiomeric excesses (51–72% *ee*).[51] According to the proposed mechanism, the presence of an electron-withdrawing ester on the olefin allows β-ICPD to attack the activated double bond (first S_N2' step) and displace the leaving group. The consequent loss of carbon dioxide generates a basic *tert*-butoxide anion, which is able to deprotonate the pro-nucleophile; the second S_N2' step leads to formation of the product and regeneration of the catalyst (Scheme 14).

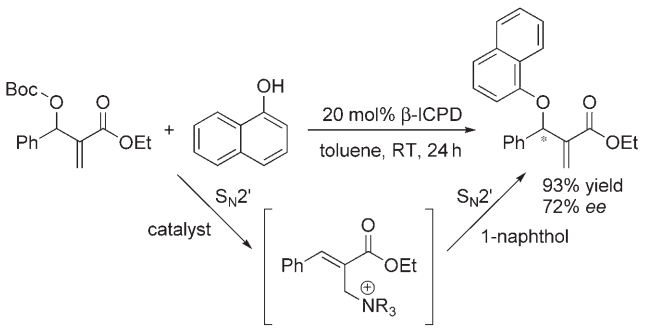

Scheme 14. Organocatalytic asymmetric allylic substitution.

7. Conclusions and Outlook

In only a short time since their first application, cupreines and cupreidines have been shown to be powerful catalysts for a plethora of asymmetric transformations. Note that almost all of the catalysts described in this Minireview can be accessed in one or two easy steps from commercially available alkaloids. In particular, β-ICPD offers an attractive combination of high reactivity and selectivity, therefore allowing reactions to be carried out with minimal catalyst loading and thus overcoming one of the major limitations of most organocatalysts. Also, for many transformations, cupreines display a level of chemo-, regio-, and enantioselective control that is unmatched by metal complexes or other organocatalysts.

To further exploit the potential of these catalysts (and to design new ones), detailed mechanistic investigations would be desirable. While many DFT and NMR studies have been reported for enamine catalysis,[52] the understanding of the processes governing enantioselectivity in cinchona bifunctional organocatalysis is often not satisfactory. We believe that the examples here described represent only a minor portion of the asymmetric catalytic transformations made possible by these alkaloids; it is likely that new cupreine derivatives and combinations of reaction partners have to be expected in the near future.[53]

The National Research School Combination Catalysis (NRSC-C) is gratefully acknowledged for financial support.

Received: June 9, 2006
Published online: October 19, 2006

[1] T. P. Yoon, E. N. Jacobsen, *Science* **2003**, *299*, 1691–1693.
[2] Comprehensive reviews about asymmetric organocatalysis: a) A. Berkessel, H. Gröger, *Asymmetric Organocatalysis*, Wiley-VCH, New York, **2005**; b) P. I. Dalko, L. Moisan, *Angew. Chem.* **2004**, *116*, 5248–5286; *Angew. Chem. Int. Ed.* **2004**, *43*, 5138–5175; c) P. I. Dalko, L. Moisan, *Angew. Chem.* **2001**, *113*, 3840–3864; *Angew. Chem. Int. Ed.* **2001**, *40*, 3726–3748; for a review about cinchona organocatalysts with a special focus on enantioselective phase-transfer catalysis, see: d) S. Kacprzak, J. Gawronski, *Synthesis* **2001**, 961–998.
[3] G. Bredig, P. S. Fiske, *Biochem. Z.* **1912**, *46*, 7.
[4] H. Pracejus, *Justus Liebigs Ann. Chem.* **1960**, *634*, 9–22.
[5] For a review, see: H. Wynberg, *Top. Stereochem.* **1986**, *16*, 87–129.
[6] H. Wynberg, E. G. J. Staring, *J. Am. Chem. Soc.* **1982**, *104*, 166–168.
[7] For reviews, see: a) M. J. O'Donnell, *Acc. Chem. Res.* **2004**, *37*, 506–517; b) C. Najera, *Synlett* **2002**, 1388–1403.
[8] For a review, see: H. C. Kolb, M. S. VanNieuwenhze, K. B. Sharpless, *Chem. Rev.* **1994**, *94*, 2483–2547.
[9] a) G. D. H. Dijkstra, R. M. Kellogg, H. Wynberg, *Recl. Trav. Chim. Pays-Bas* **1989**, *108*, 95; b) G. D. H. Dijkstra, R. M. Kellogg, H. Wynberg, J. S. Svendsen, I. Marko, K. B. Sharpless, *J. Am. Chem. Soc.* **1989**, *111*, 8069–8076; c) T. Bürgi, A. Baiker, *J. Am. Chem. Soc.* **1998**, *120*, 12920–12926.
[10] For reviews, see: a) S.-K. Tian, Y. Chen, J. Hang, L. Tang, P. McDaid, L. Deng, *Acc. Chem. Res.* **2004**, *37*, 621–631; b) S. France, D. J. Guerin, S. J. Miller, T. Letcka, *Chem. Rev.* **2003**, *103*, 2985–3012.

 © 2006 Wiley-VCH Verlag GmbH & Co. KGaA, Weinheim

[11] H. Hiemstra, H. Wynberg, *J. Am. Chem. Soc.* **1981**, *103*, 417 – 430.

[12] L. D. Small, H. Rosenberg, P. U. Nwangwu, T. L. Holcslaw, S. J. Sohs, *J. Med. Chem.* **1979**, *22*, 1014 – 1016. Deng and co-workers recently described a procedure that is compatible with the presence of benzyl and aryl ethers at the C9 position; see Ref. [29].

[13] a) C. Von Riesen, H. M. R. Hoffmann, *Chem. Eur. J.* **1996**, *2*, 680 – 684; b) W. Braje, J. Frackenpohl, P. Langer, H. M. R. Hoffmann, *Tetrahedron* **1998**, *54*, 3495 – 3512; for a review, see: c) H. M. R. Hoffmann, J. Frackenpohl, *Eur. J. Org. Chem.* **2004**, 4293 – 4312.

[14] The synthesis of twistane (tricyclo[4.4.0.$0^{3,8}$]decane) was first reported in 1962: H. W. Whitlow Jr., *J. Am. Chem. Soc.* **1962**, *84*, 3412 – 3413. Unlike its highly symmetrical isomer adamantane (T_d symmetry), twistane (which is composed of four fused twist-boat cyclohexane rings) has D_2 symmetry and is therefore chiral.

[15] Most authors use the abbreviation β-ICD; note, however, that this may lead to ambiguity as CD is the commonly accepted abbreviation for cinchonidine. The main drawback of β-ICPD is the lack of an easily available pseudo-enantiomer. Hatakeyama and co-workers addressed this problem by devising two elegant yet somewhat lengthy synthetic routes: a) A. Nakano, K. Takahashi, J. Ishihara, S. Hatakeyama, *Heterocycles* **2005**, *66*, 371 – 383; b) A. Nakano, M. Ushiyama, Y. Iwabuchi, S. Hatakeyama, *Adv. Synth. Catal.* **2005**, *347*, 1790 – 1796.

[16] For a review on hydrogen-bond donors in asymmetric organocatalysis with a section on bifunctional catalysts (section 3.3), see: a) M. S. Taylor, E. N. Jacobsen, *Angew. Chem.* **2006**, *118*, 1550 – 1573; *Angew. Chem. Int. Ed.* **2006**, *45*, 1520 – 1543; for a review on (metal-based) bifunctional asymmetric catalysis, see: b) J.-A. Ma, D. Cahard, *Angew. Chem.* **2004**, *116*, 4666 – 4683; *Angew. Chem. Int. Ed.* **2004**, *43*, 4566 – 4583.

[17] a) This paper also describes a reliable one-step multigram synthesis of β-ICPD from quinidine: Y. Iwabuchi, M. Nakatani, N. Yokoyama, S. Hatakeyama, *J. Am. Chem. Soc.* **1999**, *121*, 10219 – 10220; b) A. Nakano, S. Kawahara, S. Akamatsu, K. Morokuma, M. Nakatani, Y. Iwabuchi, K. Takahashi, J. Ishihara, S. Hatakeyama, *Tetrahedron* **2005**, *61*, 381 – 389.

[18] For a review, see: D. Basavaiah, A. J. Rao, T. Satyanarayana, *Chem. Rev.* **2003**, *103*, 811 – 892.

[19] M. Shi, J.-K. Jiang, *Tetrahedron: Asymmetry* **2002**, *13*, 1941 – 1947.

[20] Y. Iwabuchi, M. Furukawa, T. Esumi, S. Hatakeyama, *Chem. Commun.* **2001**, 2030 – 2031.

[21] Y. Iwabuchi, T. Sugihara, T. Esumi, S. Hatakeyama, *Tetrahedron Lett.* **2001**, *42*, 7867 – 7871.

[22] a) M. Shi, Y.-M. Xu, *Angew. Chem.* **2002**, *114*, 4689 – 4692; *Angew. Chem. Int. Ed.* **2002**, *41*, 4507 – 4510; b) M. Shi, Y.-M. Xu, Y.-L. Shi, *Chem. Eur. J.* **2005**, *11*, 1794 – 1802.

[23] M. Shi, G.-L. Zhao, *Adv. Synth. Catal.* **2004**, *346*, 1205 – 1219.

[24] S. Kawahara, A. Nakano, T. Esumi, Y. Iwabuchi, S. Hatakeyama, *Org. Lett.* **2003**, *5*, 3103 – 3105.

[25] a) D. Balan, H. Adolfsson, *J. Org. Chem.* **2001**, *66*, 6498 – 6501; b) D. Balan, H. Adolfsson, *J. Org. Chem.* **2002**, *67*, 2329 – 2334.

[26] D. Balan, H. Adolfsson, *Tetrahedron Lett.* **2003**, *44*, 2521 – 2524.

[27] In Ref. [24], Hatakeyama and co-workers unambiguously determined the absolute configuration of the aza-Baylis–Hillman adducts. Therefore, the assigned absolute sterochemistry of the products in Refs. [22], [23], and [26] should be considered erroneous.

[28] T. Morita, H. Yamada, A. Takahashi (Toa Eiyo), JP2002080444, **2002**.

[29] H. Li, Y. Wang, L. Tang, L. Deng, *J. Am. Chem. Soc.* **2004**, *126*, 9906 – 9907.

[30] H. Li, Y. Wang, L. Tang, F. Wu, X. Liu, C. Guo, B. M. Foxman, L. Deng, *Angew. Chem.* **2005**, *117*, 107 – 110; *Angew. Chem. Int. Ed.* **2005**, *44*, 105 – 108.

[31] H. Li, J. Song, X. Liu, L. Deng, *J. Am. Chem. Soc.* **2005**, *127*, 8948 – 8949.

[32] F. Wu, H. Li, R. Hong, L. Deng, *Angew. Chem.* **2006**, *118*, 961 – 964; *Angew. Chem. Int. Ed.* **2006**, *45*, 947 – 950.

[33] J. Wang. H. Li, L. Zu, W. Wang, *Org. Lett.* **2006**, *8*, 1391 – 1394.

[34] Y. Wang, X. Liu, L. Deng, *J. Am. Chem. Soc.* **2006**, *128*, 3928 – 3930.

[35] F. Wu, R. Hong, J. Khan, X. Liu, L. Deng, *Angew. Chem.* **2006**, *118*, 4407 – 4411; *Angew. Chem. Int. Ed.* **2006**, *45*, 4301 – 4305.

[36] Some recent examples: a) N. S. Chowdari, C. F. Barbas III, *Org. Lett.* **2005**, *7*, 867 – 870; b) E. Castellanos, G. Reyes-Rangel, E. Juaristi, *Helv. Chim. Acta* **2004**, *87*, 1016 – 1024; c) M. Marigo, J. Jarsten, K. A. Jørgensen, *Angew. Chem.* **2003**, *115*, 1405 – 1407; *Angew. Chem. Int. Ed.* **2003**, *42*, 1367 – 1369.

[37] S. Saaby, M. Bella, K. A. Jørgensen, *J. Am. Chem. Soc.* **2004**, *126*, 8120 – 8121.

[38] X. Liu, H. Li, L. Deng, *Org. Lett.* **2005**, *7*, 167 – 169.

[39] S. Brandes, M. Bella, A. Kjœrsgaard, K. A. Jørgensen, *Angew. Chem.* **2006**, *118*, 1165 – 1169; *Angew. Chem. Int. Ed.* **2006**, *45*, 1147 – 1151.

[40] For an excellent short feature article, see: C. Palomo, M. Oiarbide, A. Mielgo, *Angew. Chem.* **2004**, *116*, 5558 – 5560; *Angew. Chem. Int. Ed.* **2004**, *43*, 5442 – 5444.

[41] a) R. Chinchilla, C. Najera, P. Sanchez-Agullo, *Tetrahedron: Asymmetry* **1994**, *5*, 1393 – 1402; b) Y. Misuri, R. A. Bulman, K. Matsumoto, *Heterocycles* **2002**, *56*, 599 – 605; c) M. T. Allingham, A. Howard-Jones, P. J. Murphy, D. A. Thomas, P. W. R. Caulkett, *Tetrahedron Lett.* **2003**, *44*, 8677 – 8680.

[42] T. Marcelli, R. N. S. van der Haas, J. H. van Maarseveen, H. Hiemstra, *Synlett* **2005**, 2817 – 2819.

[43] For a review, see: S. J. Connon, *Chem. Eur. J.* **2006**, *12*, 5418 – 5427.

[44] Cinchona catalysts featuring the same thiourea group at the C9 position (with inverted absolute configuration) gave excellent results in different reactions; see: a) B. Vakulya, S. Varga, A. Csámpai, T. Soos, *Org. Lett.* **2005**, *7*, 1967; b) S. H. McCooey, S. J. Connon, *Angew. Chem.* **2005**, *117*, 6525 – 6528; *Angew. Chem. Int. Ed.* **2005**, *44*, 6367 – 6370; c) J. Ye, D. J. Dixon, P. S. Hines, *Chem. Commun.* **2005**, 4481 – 4483; d) J. Song, Y. Wang, L. Deng, *J. Am. Chem. Soc.* **2006**, *128*, 6048 – 6049 (this paper also describes the synthesis of a C6′-thiourea catalyst derived from β-ICPD).

[45] T. Marcelli, R. N. S. van der Haas, J. H. van Maarseveen, H. Hiemstra, *Angew. Chem.* **2006**, *118*, 943 – 945; *Angew. Chem. Int. Ed.* **2006**, *45*, 929 – 931.

[46] H. Li, B. Wang, L. Deng, *J. Am. Chem. Soc.* **2006**, *128*, 732 – 733.

[47] a) G. S. Cortez, R. L. Tennyson, D. Romo, *J. Am. Chem. Soc.* **2001**, *123*, 7945 – 7946; b) G. S. Cortez, S. H. Oh, D. Romo, *Synthesis* **2001**, 1731 – 1736.

[48] E. G. Taylor (DuPont), WO2003040083, **2003**.

[49] a) B. M. Trost, *J. Org. Chem.* **2004**, *69*, 5813 – 5837; b) B. M. Trost, *Chem. Pharm. Bull.* **2002**, *50*, 1 – 14.

[50] a) B. M. Trost, O. R. Thiel, H. C. Tsui, *J. Am. Chem. Soc.* **2002**, *124*, 11616 – 11617; b) B. M. Trost, O. R. Thiel, H. C. Tsui, *J. Am. Chem. Soc.* **2003**, *125*, 13155 – 13164; c) B. M. Trost, M. R. Machacek, H. C. Tsui, *J. Am. Chem. Soc.* **2005**, *127*, 7014 – 7024.

[51] Y. Du, X. Han, X. Lu, *Tetrahedron Lett.* **2004**, *45*, 4967 – 4971.

[52] Some recent examples: a) A. Fu, B. List, W. Thiel, *J. Org. Chem.* **2006**, *71*, 320 – 326; b) A. Bassan, W. Zou, E. Reyes, F. Himo, A. Córdova, *Angew. Chem.* **2005**, *117*, 7190 – 7194; *Angew. Chem. Int. Ed.* **2005**, *44*, 7028 – 7032; c) F. R. Clemente, K. N. Houk, *Angew. Chem.* **2004**, *116*, 5890 – 5892; *Angew. Chem. Int. Ed.* **2004**, *43*, 5766 – 5768.

 © 2006 Wiley-VCH Verlag GmbH & Co. KGaA, Weinheim

[53] Note added in proof: After this manuscript was accepted, three examples of cupreine-catalyzed asymmetric transformations were reported: a) Kornblum–Delamare rearrangement: S. T. Staben, X. Linghu, F. D. Toste, *J. Am. Chem. Soc.* **2006**, *128*, 12658 – 12659; b) Friedel–Crafts reaction of indoles with aldehydes and ketoesters: H. Li, Y.-Q. Wang, L. Deng, *Org. Lett.* **2006**, *8*, 4063 – 4065; c) different applications of C5′-aminated cupreines: S. Brandes, B. Niess, M. Bello, A. Prieto, J. Overgaard, K. A. Jørgensen, *Chem. Eur. J.* **2006**, *12*, 6039 – 6052

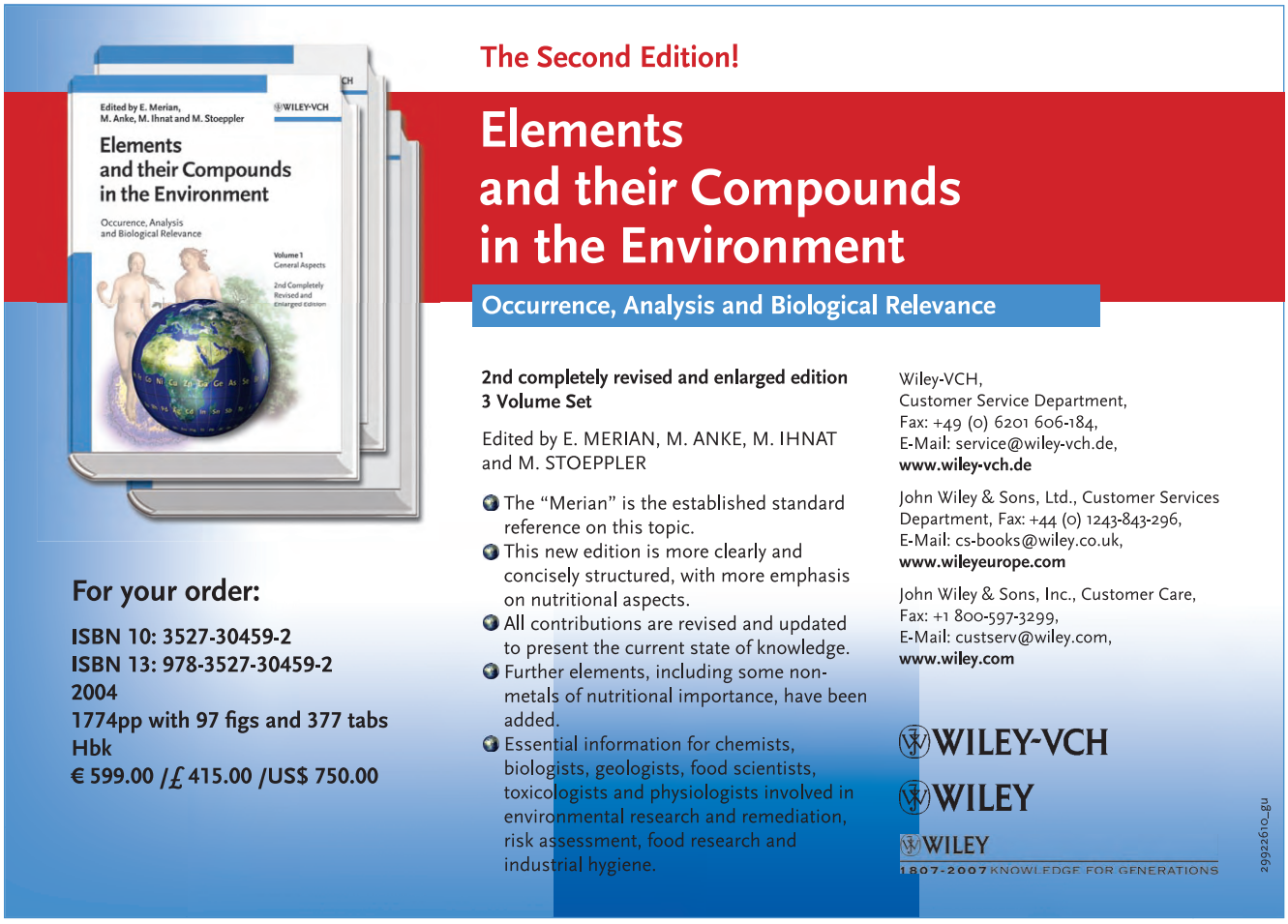

© 2006 Wiley-VCH Verlag GmbH & Co. KGaA, Weinheim

R. Mahrwald and B. Schetter

DOI: 10.1002/anie.200602780

Natural Product Synthesis

Modern Aldol Methods for the Total Synthesis of Polyketides

*Bernd Schetter and Rainer Mahrwald**

Keywords:
aldol reaction · asymmetric synthesis · enantioselectivity · natural products · polyketides

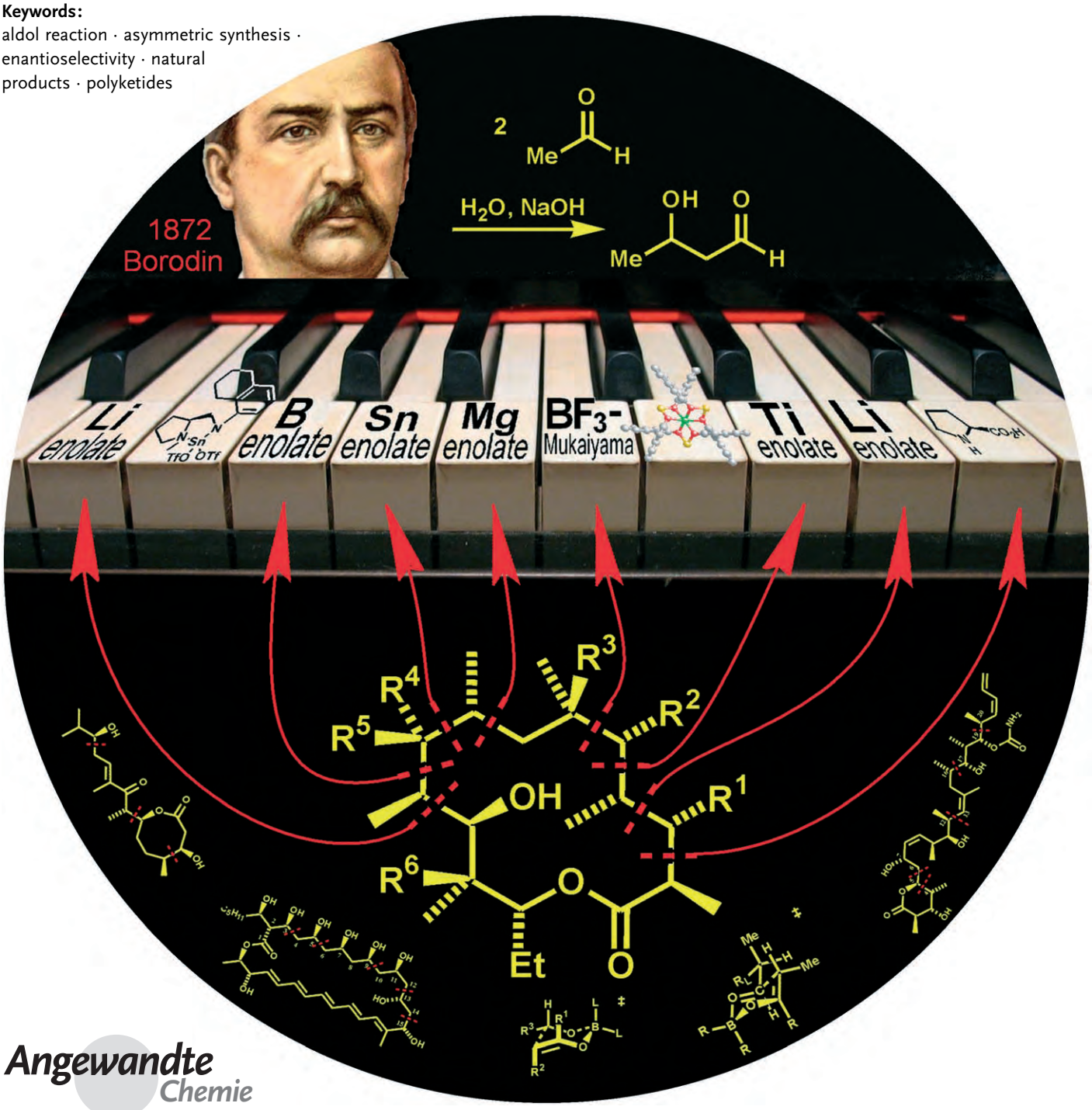

© 2006 Wiley-VCH Verlag GmbH & Co. KGaA, Weinheim

The aldol reaction is one of the most important methods for the stereoselective construction of polyketide natural products, not only for nature but also for synthetic chemistry. The tremendous development in the field of aldol additions during the last 30 years has led to more and more total syntheses of complicated natural products. This Review illustrates by means of selected syntheses of natural products the new variants of the aldol addition. This includes aldol additions with various metal enolates, as well as metal-complex-catalyzed, organocatalytic, and biocatalytic methods.

From the Contents

1. Introduction	7507
2. Aldol Additions of Lithium Enolates	7508
3. Aldol Additions of Titanium Enolates	7510
4. Aldol Additions of Boron Enolates	7513
5. Aldol Additions of Tin Enolates	7514
6. Catalytic Aldol Reactions with Lewis Acids	7516
7. Direct Aldol Additions	7519
8. Catalytic Aldol Reactions with Lewis Bases	7520
9. Organocatalysis	7521
10. Enzyme-Catalyzed Aldol Additions	7522
11. Summary and Outlook	7522

1. Introduction

Erythromycin A, one of the most representative structures of the polyketide family, "*looks at present time quite hopelessly complex, particularly in view of its plethora of asymmetric centers*". This quote by Woodward in 1956[1] illustrates the undeveloped and unsatisfactory state of stereoselective versions C–C bond-formation processes at that time. This situation also applied to the aldol addition, one of the fundamental reactions in the total synthesis of polyketides. The subsequent development of new versions of the aldol reaction over the following decades has kept on increasing the possibilities for the construction of defined, stereogenic centers. As a consequence, more and more total syntheses and approaches to polyketides have been published.[2,3] The Woodward research group itself was the first to succeed in a complete total synthesis of erythromycin A in 1981.[4] They used a stereoselective aldol reaction with lithium enolates for the construction of the C2–C3 bond. Almost at the same time, Masamune et al. described a total synthesis of 6-deoxyerythronolide B by using aldol reactions in the presence of chiral boron enolates.[5]

More and more different enolates have since been tried in aldol reactions for the total syntheses of polyketides. Figure 1 shows an overview of aldol reactions that have been used in total syntheses or in approaches to aglycones of the erythromycin family. Nearly every possible C–C bond has been constructed with the help of aldol additions. The efforts made in this field of aldol additions are briefly summarized in Table 1.

The impressive developments in the field of stereoselective aldol reactions over the last 25 years have come about as a succession of important discoveries that have even advanced the whole field of polyketide total synthesis. This Review presents an overview of modern versions of the aldol reaction and considers the latest developments. It describes the role of the metal enolate structure (lithium, boron, titanium, and tin(II)) in the diastereoselectivity, Lewis acid catalyzed additions of enol silyl ethers to aldehydes (Mukaiyama reaction), and the development of chiral catalysts for direct aldol additions. Moreover, modern methods of proline-catalyzed and even enzyme-catalyzed aldol reactions in the total synthesis of polyketides are also discussed.

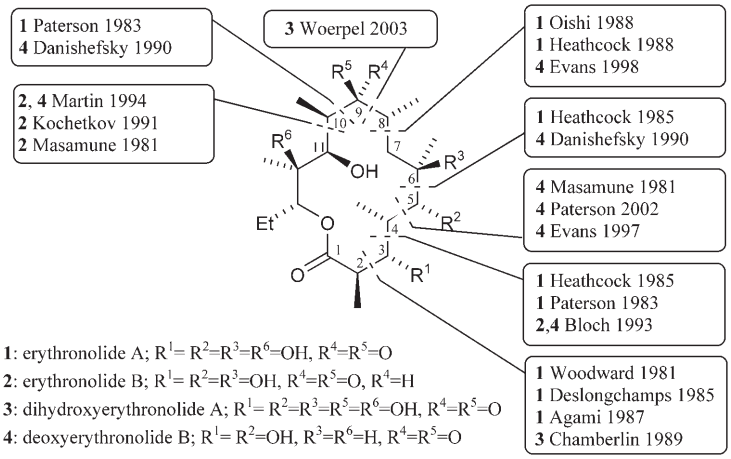

Figure 1. Aldol additions in the total syntheses or partial syntheses of erythromycins.

The tremendous progress in the area of aldol reactions, which has supplied a vast amount of information, means that it is not possible to provide a comprehensive collection of all the total syntheses. For that reason, methods will be demonstrated and discussed using selected, instructive exam-

[*] B. Schetter, Dr. habil. R. Mahrwald
Chemisches Institut
Humboldt-Universität zu Berlin
Brook-Taylor-Strasse 2, 12489 Berlin (Germany)
Fax: (+49) 30-2093-6940
E-mail: rainer.mahrwald@hz.hu-berlin.de

© 2006 Wiley-VCH Verlag GmbH & Co. KGaA, Weinheim

Table 1: Developments in methods for aldol reactions.

Approach	Reagent/method
C2–C3 bond formation	lithium enolates,[4,6] zirconium enolates,[7] proline catalysis[8]
C3–C4 bond formation	lithium enolates,[9,10] boron enolates[11,12]
C4–C5 bond formation	boron enolates,[5,13] titanium enolates[14]
C5–C6 bond formation	lithium enolates,[9] BF_3-catalyzed Mukaiyama reaction[15]
C7–C8 bond formation	lithium enolates,[16] magnesium enolates,[17] BF_3-catalyzed Mukaiyama reactions[18]
C8–C9 bond formation	tin enolates[19]
C9–C10 bond formation	boron enolates,[11] BF_3-catalyzed Mukaiyama reaction[15]
C10–C11 bond formation	lithium and titanium enolates,[20–22] lithium enolates,[23–25] boron enolates[5]

ples of total syntheses and approaches to polyketides or polyketide substructures.

2. Aldol Additions of Lithium Enolates

Very instructive examples of the use of lithium enolates in polyketide syntheses can be found in the total syntheses of erythronolide A and epothilones. Woodward et al. used lithium enolates of *tert*-butyl thiopropionate for the introduction of the C1–C2 unit of the erythronolide A seco acid **7** (Scheme 1). In this way, they exclusively obtained product **6**, which still contains the undesired configuration at C2. The target molecule **7** with the "natural" configuration at C2 was obtained by kinetic protonation of **6**.[4]

The efforts made in the total syntheses of epothilones represent a further instructive example of the use of lithium enolates for stereoselective aldol additions. Epothilones contain a typical polyketide substructure (in the east region; Figure 2) and in the first total synthesis by Nicolaou et al., the construction of this area was achieved by a stereoselective aldol addition. They treated the chiral aldehyde (*S*)-**11** with the ketoacid **10** in the presence of lithium diisopropylamide (LDA; Scheme 2). However, the aldol products were obtained with no stereoselectivity (**12**/**13** = 2:3).[26] Thus, in a

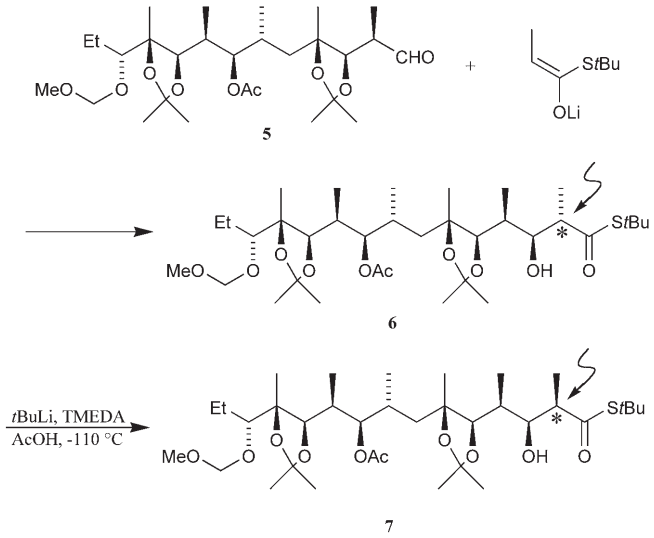

Scheme 1. Synthesis of erythronolide A by Woodward et al.[4] TMEDA = *N*,*N*,*N*′*N*′-tetramethylethylenediamine.

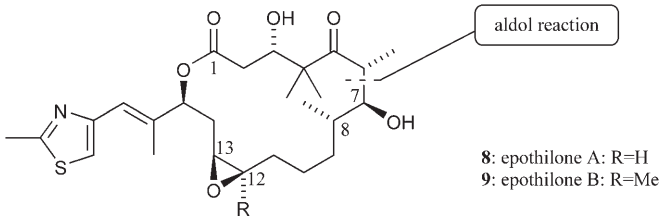

Figure 2. Epothilone A and B.

second attempt, they treated the modified, chiral ketoacid **14** with the same chiral aldehyde (*S*)-**11**, but again almost no selectivity was observed in the aldol addition.[27]

A different approach was taken by the Schinzer research group. They used the corresponding chiral acetonide **17** as the lithium enolate source. Its aldol addition with the chiral aldehyde (*S*)-**11** resulted in the formation of **18** as the major isomer (25:1) (Scheme 3).[28–30] Further attempts with the chiral aldehyde **19** and the lithium enolate of acetonide **17** resulted in a single isomer **20** with the "natural" epothilone configuration. A 10:1 mixture of diastereoisomers favoring triade **22** with the "correct" configuration was isolated

Bernd Schetter studied chemistry at the Eberhardt-Karls University Tübingen, where he obtained his MSc in 2003 under the supervision of Prof. B. Speiser for the development of redox-active modified nanoparticles in the framework of the graduate course "Interphases" (DFG). He subsequently joined the Mahrwald research group at the Humboldt University in Berlin, where he is now involved in the development of new direct aldol methods. He is supported by a PhD scholarship from the the Konrad-Adenauer-Stiftung.

Rainer Mahrwald studied chemistry at the Martin-Luther Universität Halle and subsequently led the synthetic group at the "Manfred von Ardenne" research institute in Dresden. He gained his PhD with Prof. G. Wagner in Leipzig in 1979, and then went to the Institute of Organic Chemistry at the Academy of Sciences in Berlin, where he remained until 1990. Following research at the Philipps-University in Marburg with Prof. M. T. Reetz, he habilitated at the Humboldt University in Berlin, where he is now a private lecturer. His main area of research is the development of stereoselective C–C coupling.

© 2006 Wiley-VCH Verlag GmbH & Co. KGaA, Weinheim

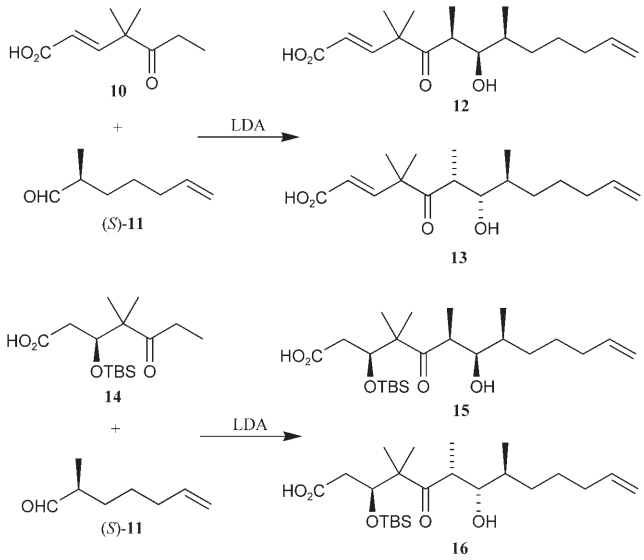

Scheme 2. Synthesis of a substructure of epothilone by Nicolaou et al.[26] TBS = *tert*-butyldimethylsilyl.

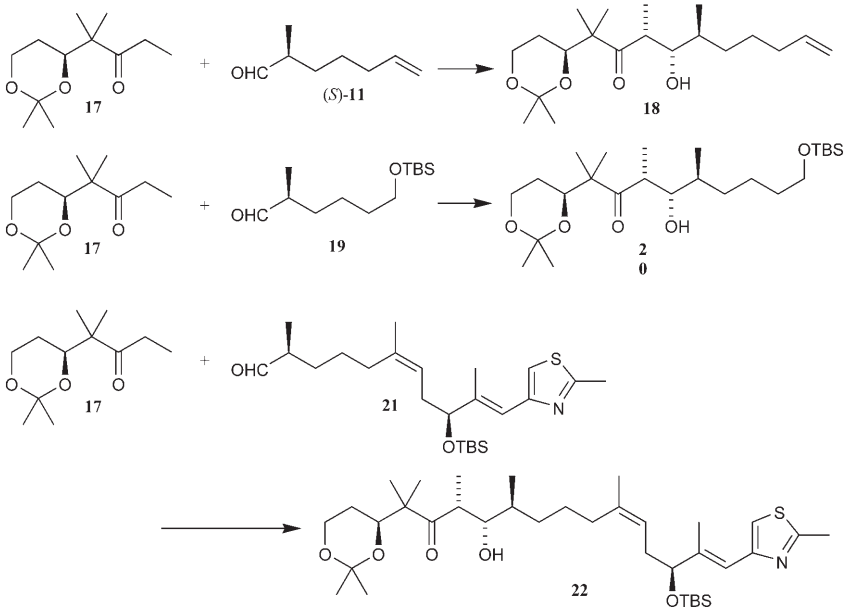

Scheme 3. Double stereodifferentiating aldol additions by Schinzer et al.[28–30]

starting from the highly functionalized aldehyde **21**. An explanation of this remarkable stereochemical result is given by the transition state shown in Figure 3, where two functional peculiarities of the acetonide **17** lead to this chelation-controlled model. First, the influence of the methyl groups on C4 generate a (*Z*)-enolate. Secondly, the oxygen atom at C3 leads to the formation of a rigid bicyclic structure. For related studies see also Refs. [31–34].

The above synthesis of the starting *S*-configured acetonide **17** provides an illustrative example of lithium enolates in stereoselective aldol reactions. In this case, the well-established HYTRA-aldol addition was used, which means aldehyde **24** was treated with the lithium dianion of (*S*)-HYTRA (HYTRA = 1,1,2-triphenyl-1,2-ethanediol acetate) (*S*)-**23** to

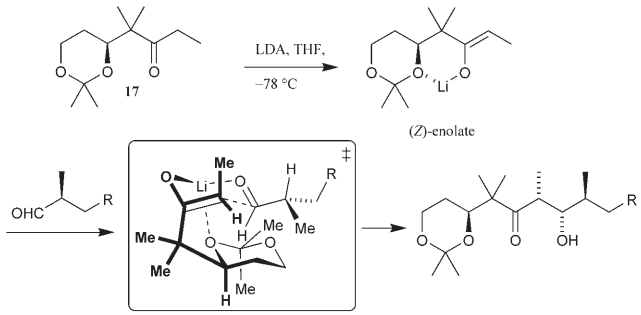

Figure 3. Bicyclic transition state.

give the expected ester **25** with excellent diastereoselectivity (50:1, 75 % yield). Further transformations finally yielded the starting chiral acetonide (*S*)-**17** (Scheme 4).[35] For a comprehensive review of HYTRA-adol additions see Ref. [36].

Kalesse and co-workers used another approach for the aldol addition of the silyl-protected ketone **28** with the chiral aldehyde **29** to yield stereotriade **30** exclusively (Scheme 5).[37,38] Nicolaou et al. treated the same enolate component **28** with the fully functionalized aldehyde **21** in aldol additions. However, only a moderate stereoselectivity of 3:1 in favor of the "natural" configured triade **31** was observed.[39]

Mulzer et al. later published a study of aldol reactions of the same enolate component **28** with the fully functionalized aldehyde **32**. A mixture of stereoisomers was isolated in a ratio of 6:1, with the stereoisomer **33** having the "natural" epothilone configuration favored (Scheme 6).[40,41] The aldol reaction with aldehyde **35**, which contains the natural epoxide functionality, exclusively yielded the desired diastereoisomer **36** in a ratio of 19:1.[42]

Danishefsky and co-workers described double stereodifferentiating aldol additions of both enantiomers of the functionalized ketones (*S*)- and (*R*)-**37** with the unsaturated, chiral aldehyde **38** (Scheme 7). Application of the lithium dianion of (*S*)-**37** in these reactions resulted in the diastereoisomers **39** and **40** being isolated in a ratio of 2:3 (mismatched case), while reactions of (*R*)-**37** gave only one single isomer **41**

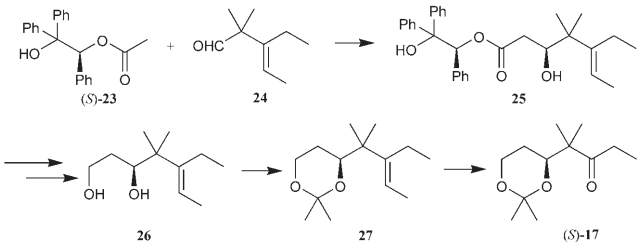

Scheme 4. HYTRA-approach to acetonide (*S*)-**17**.

 © 2006 Wiley-VCH Verlag GmbH & Co. KGaA, Weinheim

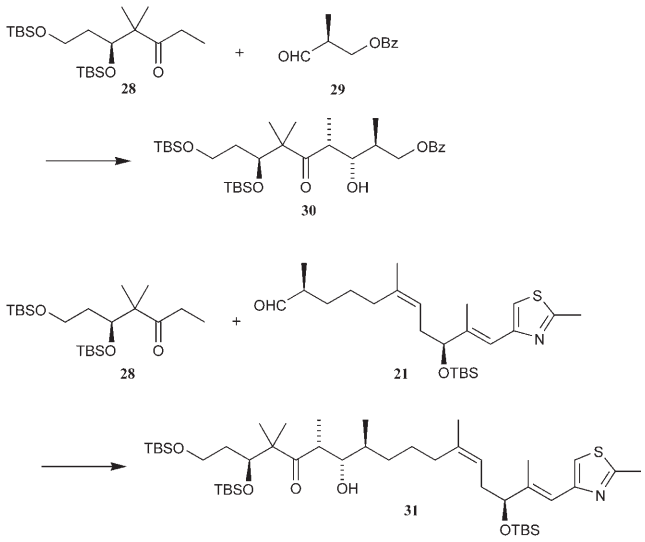

Scheme 5. Syntheses by Kalesse and co-workers[37–38] and Nicolaou et al.[39] Bz = benzoyl.

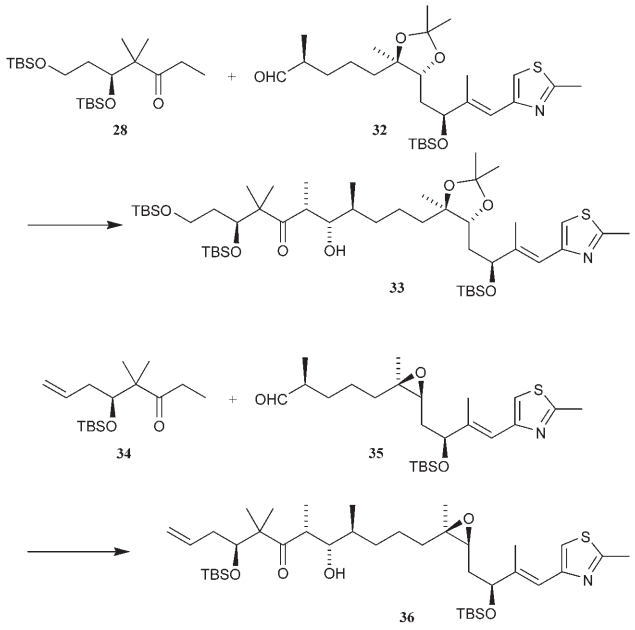

Scheme 6. Double stereodiffenrentiating approach by Mulzer et al.[40,41]

with the "natural" configuration (matched case) of the epothilones.[43,44]

3. Aldol Additions of Titanium Enolates

Nearly 20 years ago stereoselective aldol additions with titanium enolates were reported for the first time (for the use of amino acid derived chiral oxazolinone see Refs. [45–47]; of glucofuranose-derived chiral ligands see Refs. [48–50]; of camphor-derived imidazolidinone see Ref. [51]). The use of chiral titanium enolates in stereoselective adol additions have lasted until today. A comprehensive overview of this topic has

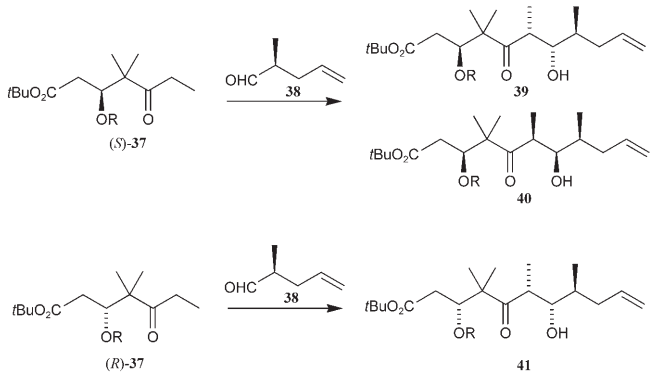

Scheme 7. Double stereodifferentiating synthesis by Danishefsky and co-workers.[43,44]

been reported by Gosh and Shevli.[52] $TiCl_4$ or related titanium(IV) halogen alkoxides and amines were initially used in diastereoselective aldol additions. This method was first described and elaborated by Evans et al. for the polypropionate series. Under the conditions they employed, *syn*-configured aldols were obtained exclusively.[53] An example illustrating this method is the total synthesis of denticulatin B (**45**, Scheme 8).[54] The total synthesis of denticulatin with boron enolates or allylboranes can be found in Refs. [55,56].

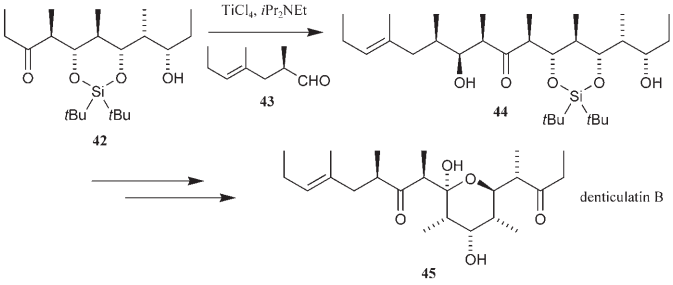

Scheme 8. Total synthesis of denticulatin B.

Another example stems from the total synthesis of stigmatellin A (**49**). In the course of this synthesis, Enders et al. accomplished the aldol addition of benzyloxyacetaldehyde (**47**) with ketone **46** in the presence of $TiCl_4$ and diisopropylethylamine. The aldol adduct **48** was isolated with a high degree of *syn* selectivity (83:17, Scheme 9).[57] Perkins and Sampson published a total synthesis of membrenone C (**55**). Two aldol additions were performed in the presence of $TiCl_4$ and diisopropylethylamine during this synthesis. The products were obtained with a high degree of *syn* selectivity (aldol adduct **52** with 39:1 and diketone **54** with 19:1, Scheme 10).[58]

As a further example, the total synthesis of rapamycin (**57**) by Danishefsky and co-workers demonstrates the successful application of titanium(IV) halogen alkoxides in aldol additions. At a very late stage in this synthesis, the cyclization of acyclic ketoaldehyde **56** was achieved by an aldol addition in the presence of $Ti(OiPr)Cl_3$ and triethylamine. The cyclized product **57** was isolated in 11% yield,

 © 2006 Wiley-VCH Verlag GmbH & Co. KGaA, Weinheim

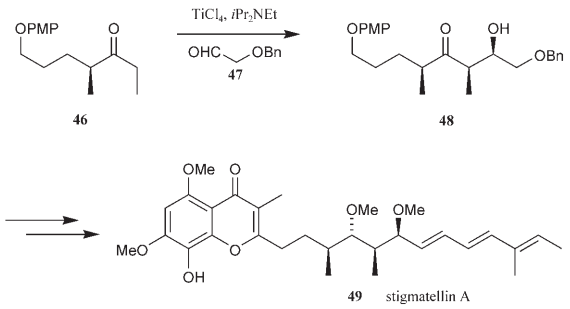

Scheme 9. Total synthesis of stigmatellin A. PMP = p-methoxyphenyl, Bn = benzyl.

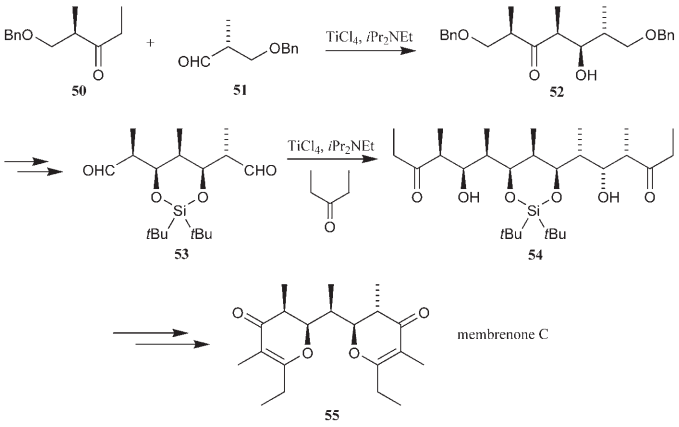

Scheme 10. Total synthesis of membrenone C.

together with 22% of the undesired *syn*-configured aldol product. This result once again underlines the above described *syn* selectivity generally observed in $TiCl_4$/amine-mediated aldol additions (Scheme 11).[59]

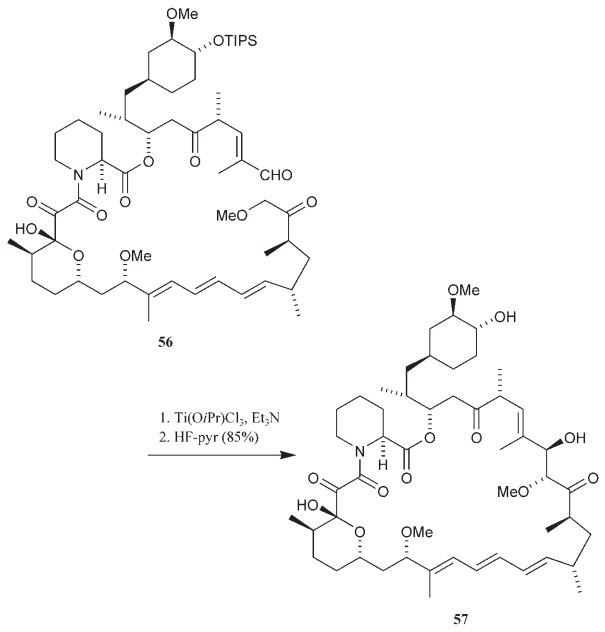

Scheme 11. Total synthesis of rapamycin. TIPS = triisopropylsilyl, pyr = pyridine.

Aldol additions were also carried out with chiral titanium enolates. A first example of this method stems from the total synthesis of epothilone 490 by Danishefsky and co-workers (Scheme 12).[60–63] In their approach, the authors used the

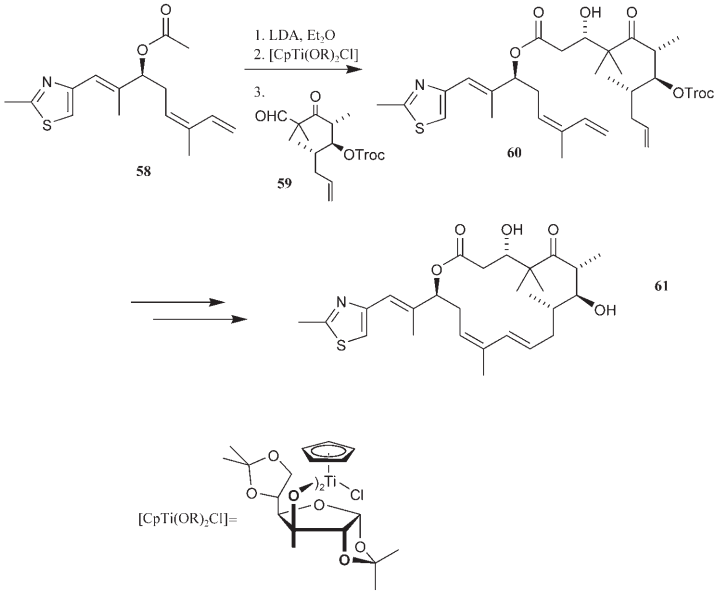

Scheme 12. Total synthesis of epothilone 490 by Danishefsky and co-workers.[60–63] Troc = 2,2,2-trichloroethoxycarbonyl, Cp = cyclopentadienyl.

well-established aldol method with titanium enolate developed by Duthaler. For a comprehensive overview of this method see Ref. [49]. The generation of the chiral titanium enolate was achieved by transmetalation of the lithium enolate of acetate **58** with $[CpTi(OR)_2]Cl$ (R = (*R*)-1,2:5,6-di-*O*-isopropylidene-α-D-glucofuranose). The subsequent aldol addition using aldehyde **59** resulted in aldol adduct **60** as a single isomer in 85% yield. The subsequent ring-closing metathesis finally yielded epothilone 490 (**61**) with 64% yield.

The aldol method developed by Duthaler was in fact used twice in the total synthesis of tautomycin (**67**) by Chamberlin and co-workers.[64] Again, the chiral enolates were generated by transmetalation of the lithium enolates of propionate **62** with Duthaler's reagent $[CpTi(OR)_2]Cl$ (Scheme 13). A $TiCl_4$-catalyzed Mukaiyama approach to tautomycin can be found in Ref. [65].

One of the most frequently employed and most reliable aldol additions in natural product synthesis is the reaction of chiral titanium enolates which are generated from oxazolinone chiral auxiliaries that are derived from amino acids. This method is based on the initial findings of Thornton and co-workers described above.[45–47] Crimmins used this method twice in the total synthesis of callystatin A (**73**, Scheme 14).[66]. The chiral titanium enolates were generated by the use of $TiCl_4$ and (−)-sparteine (Crimmins' procedure). The reaction of the titanium enolate of **68** with (*S*)-2-methylbutanal (**69**) yielded the *syn*-aldol adduct **70** with a selectivity of 98%. Chain elongation was then performed by the same method by using a second aldol addition of the chiral aldehyde **71**. The stereopentade **72** was isolated with a

 © 2006 Wiley-VCH Verlag GmbH & Co. KGaA, Weinheim

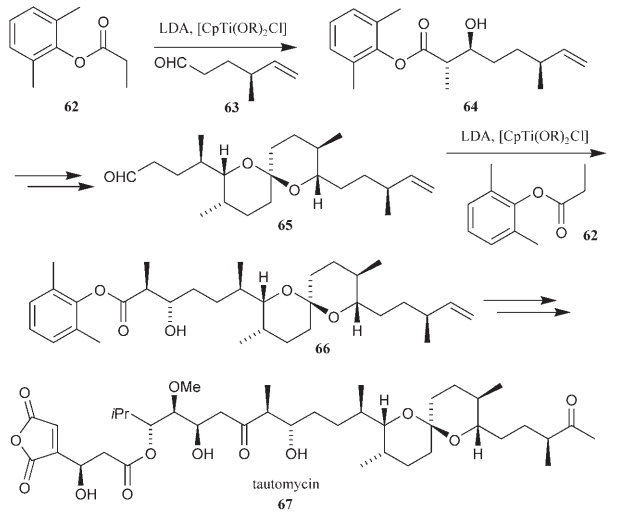

Scheme 13. Synthesis of tautomycin by Chamberlin and co-workers.[64]

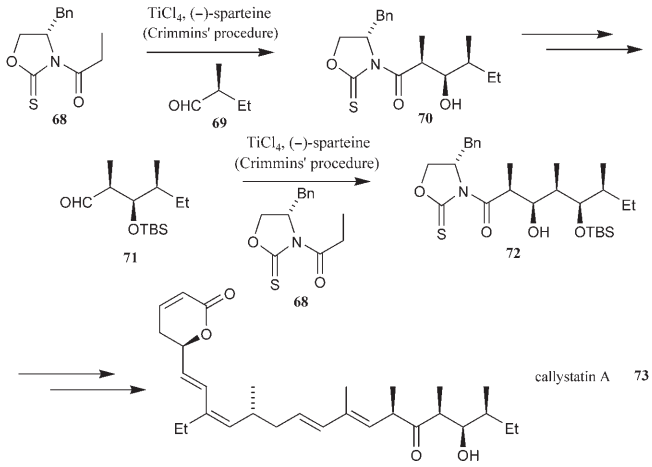

Scheme 14. Total synthesis of callystatin A.

selectivity of 98%. Synthetic routes to callystatin A and 20-*epi*-callystatin A can be found in Ref. [67]. The total synthesis of callystatin using boron enolates and lithium enolates are described in Refs. [68,69]. For an overview of the total syntheses of callystatin A see Ref. [70]. In a later study Crimmins et al. achieved the total synthesis of spongistatin (**76**), by employing the same conditions as above for the aldol reactions. By treating aldehyde **74** with the titanium enolate of **68**, they obtained diol **75** with a high degree of *syn* selectivitiy (96:4, Scheme 15).[71–73]

Chakraborty et al. used the Crimmins' procedure in the total synthesis of crocacin C (**78**). Treatment of cinnamaldehyde with the titanium enolate of **68** led to the isolation of allyl alcohol **77** as a single *syn*-configured isomer (Scheme 16).[74] The total synthesis of crocacin using boron enolate can be found in Ref. [75]. For the first total synthesis of crocacin involving tin enolates see Ref. [76].

The Gosh research group developed several highly selective aldol methods based on aminoindanol chiral auxiliaries.[77,78] In the first total synthesis of amphidinolide T1 (**79**), they demonstrated the usefulness of their methods

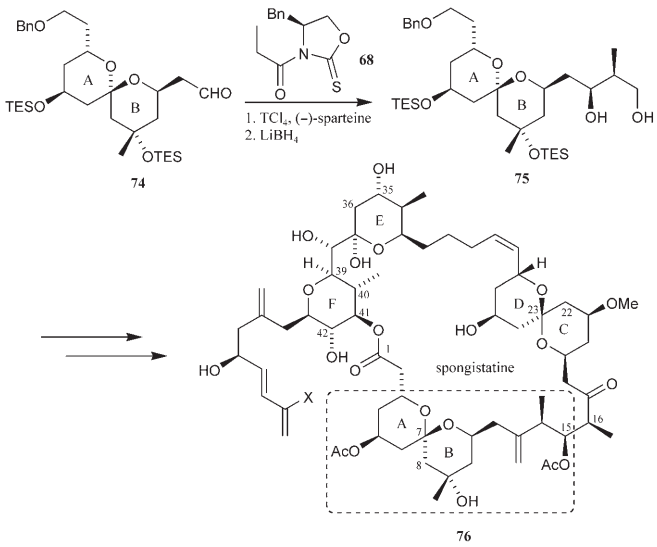

Scheme 15. Total synthesis of spongistatin 1 (X = Cl) and 2 (X = H) by Crimmins et al.[71–73] TES = triethylsilyl.

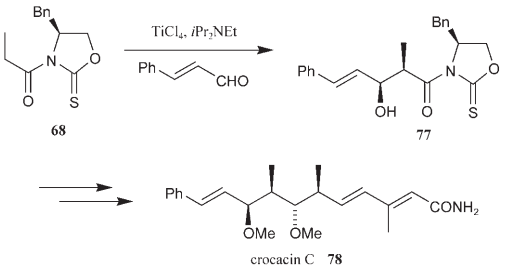

Scheme 16. Total synthesis of crocacin.

(Scheme 17).[79] The construction of the two key intermediates **83** and **84** was performed according to the Gosh method. The aldol reaction of the titanium enolate of chiral ester **80** with 3-benzyloxypropionaldehyde yielded the *syn*-configured

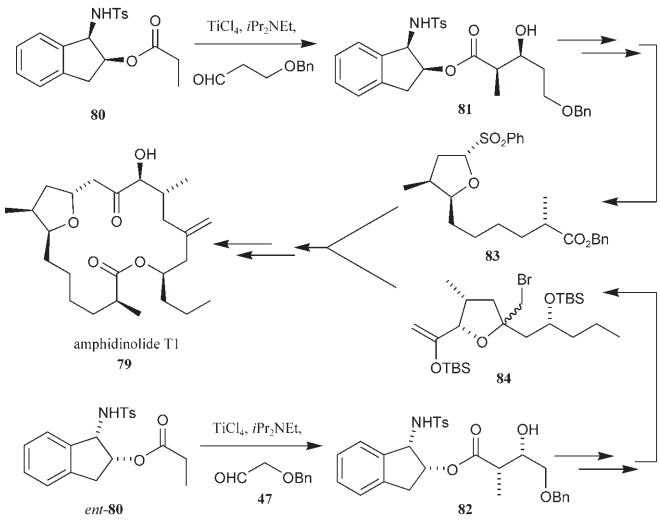

Scheme 17. Synthesis of amphidinolide T1 by Gosh and Liu.[79] Ts = tosylate.

 © 2006 Wiley-VCH Verlag GmbH & Co. KGaA, Weinheim

ester **81**. Alternatively, a single isomer of the *syn*-configured isomer **82** was isolated after treating the titanium enolate of the ester *ent*-**80** with benzyloxyacetaldehyde (**47**). Further transformations of the fragments **83** and **84** finally gave amphidinolide T1 (**79**). These stereochemical outcome of the reactions are explained by the transition states illustrated in Scheme 18. Chelation of the titanium atom leads to *anti*

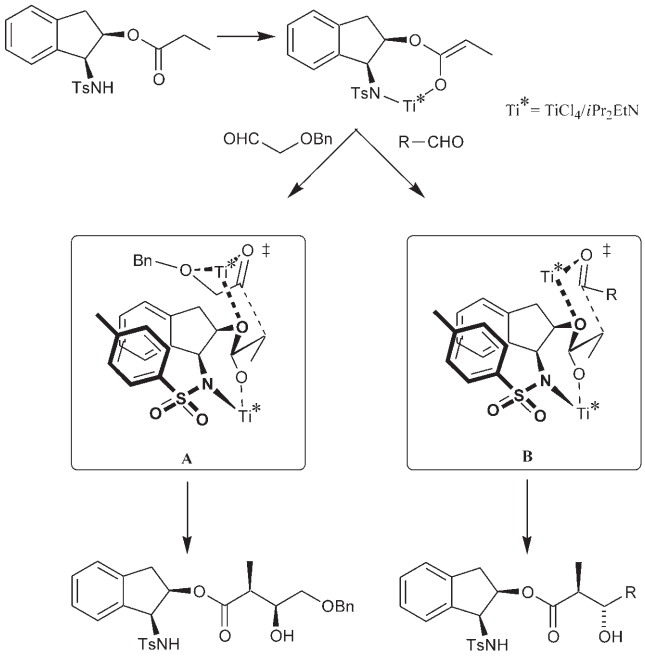

Scheme 18. Asymmetric aldol additions with aminoindanol auxiliaries.

diastereoselectivity via a seven membered Zimmerman–Traxler-like transition state (**B**). In contrast, the excellent *syn* diastereoselectivity that is observed in reactions of aldehydes with an oxygen atom at the α position can be explained by the transition state **A**.

4. Aldol Additions of Boron Enolates

Mukaiyama et al. published several results 30 years ago indicating the possibility of synthesizing boron enolates of carbonyl compounds.[80,81] These studies led to the development of the widely utilized stereoselective aldol reaction with boron enolates. As mentioned in the introduction, Masamune et al. used chiral boron enolates twice in one of the first total synthesis of deoxyerythronolide B (Figure 1). This result demonstrates the usefulness and importance of this aldol method.[6]

The configuration of the aldol product strongly depends on the geometry of the boron enolates used in these reactions: (*E*)-enolates give *anti* aldols whereas (*Z*)-enolates give *syn* aldols. These results can be explained by the transitions states shown in Scheme 19. The aldol addition proceeds via a chairlike, six-membered transition state, which is more rigid than those of alkali metal enolates. This transition state arises from the shorter boron–oxygen bond, which maximizes the

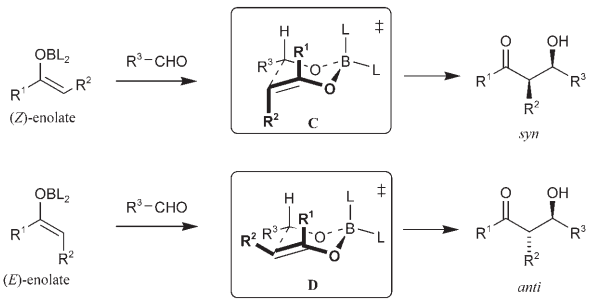

Scheme 19. Aldol reactions of (*Z*)- or (*E*)-boron enolates with aldehydes.

1,3-diaxial interactions ($R^3 \leftrightarrow L$) in the transition state. This strong dependence of the configuration of the aldol adducts on the geometry of the enolates enables *syn*- as well as *anti*-configured aldols to be made as desired. Hence, the method is widely used in the synthesis of polyketides. For several comprehensive reviews in this field see Refs. [82–85].

The convergent synthesis of rutamycin A (**91**) serves as a starting example. Evans and Howard alternately used titanium and boron enolates for the construction of the polyketide fragment **90** (Scheme 20). *Anti*-configured aldol **87** was obtained with a high degree of stereoselectivity (97:3) by treating the (*E*)-boron enolate of **85** with aldehyde **86**. The stereoselectivity observed is a consequence of the matched double stereodifferentiating nature of this bond construction and is controlled by the configuration at C10. The fragment coupling of aldehyde **88** with the titanium enolate of ketone **89** yielded the *syn*-configured aldol **90** in high stereoselectivity (97:3).[86] For an aldol approach to rutamycin B using titanium enolates see Ref. [87].

Another instructive example of the boron enolate method can be found in the total synthesis of discodermolide (**92**, Scheme 21). In the construction of the elaborate stereochemical polyketide structure of that natural product, Paterson and co-workers used their own method based on boron enolates several times.[88–90] The configuration of the products obtained by coupling aldehyde **98** with the boron enolate of ketone **99** can be explained best by transition state **E**. A comprehensive overview of the different strategies used in the total synthesis of discodermolide can be found in Ref. [91]. In a further study, Paterson et al. investigated the total synthesis of spongistatin (**100**). Here, they made extensive use of the boron enolate method for the synthesis of the starting chiral compounds for the total synthesis (Scheme 22).[92,93]

Evans et al. sucessfully used various aldol methods for the total synthesis of spongistatin 2 (**117**). This synthesis represents an impressive example of the usage of various aldol methods (BF_3-catalyzed Mukaiyama reaction of **118** with **119** and of **122** with **123**, tin Lewis acid catalyzed Mukaiyama reaction of **120** with aldehyde **121**, aldol reaction of the boron enolate of **127** with aldehyde **126**, aldol reaction of the lithium enolate of **125** with aldehyde **124**; Scheme 23). They combined the AB and CD fragments by an aldol addition of the (*E*)-boron enolate of ketone **129** with aldehyde **128** (Scheme 23). The desired *anti*-configured aldol adduct was

 © 2006 Wiley-VCH Verlag GmbH & Co. KGaA, Weinheim

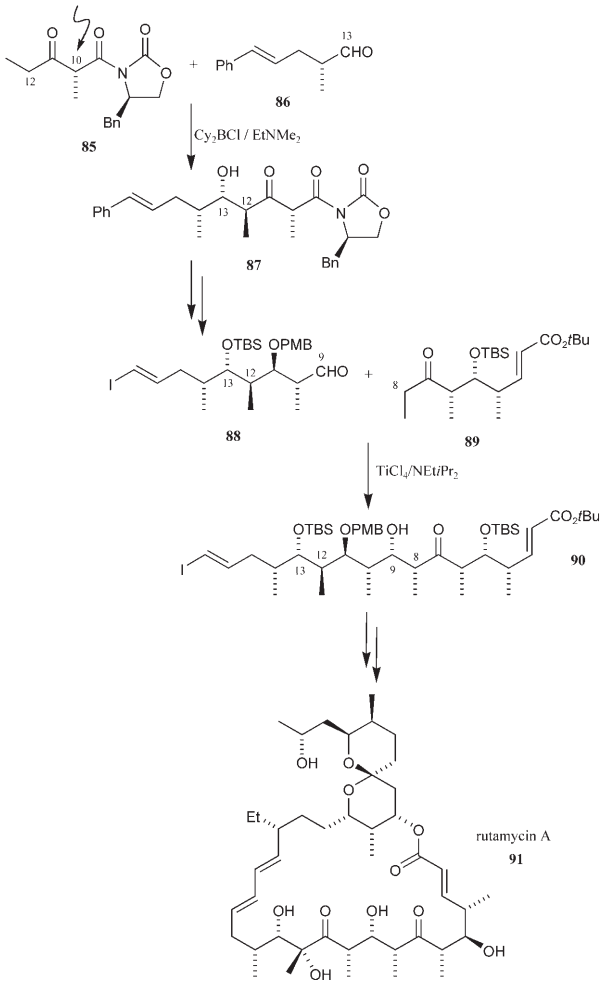

Scheme 20. Total synthesis of rutamycin A by Evans and Howard.[86] Cy = cyclohexyl.

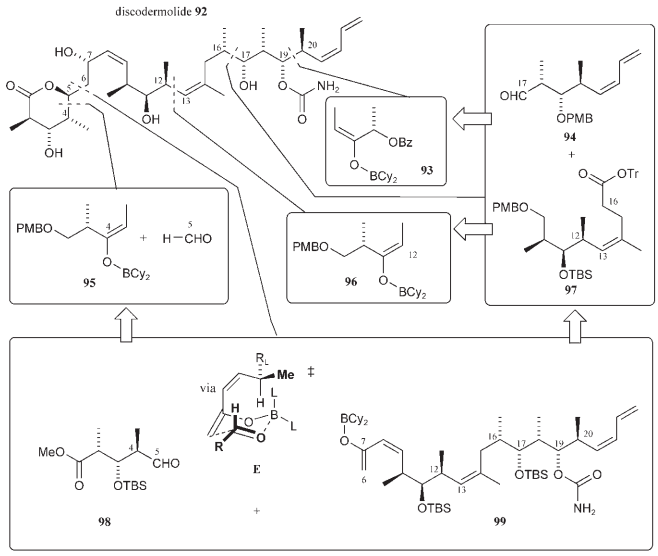

Scheme 21. Total synthesis of discodermolide by Paterson et al.[88–90] Tr = triphenylphenyl.

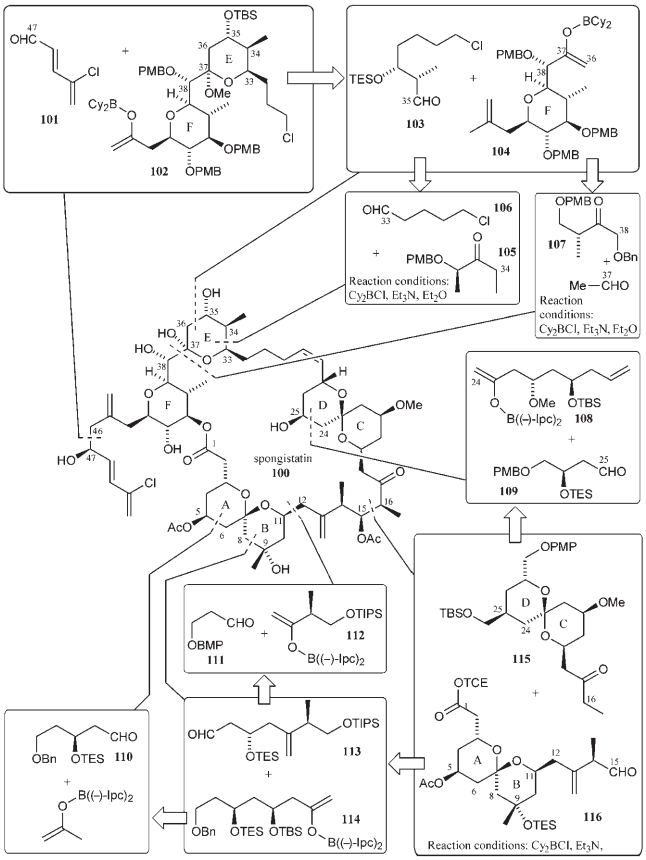

Scheme 22. Total synthesis of spongistatin 1 by Paterson et al.[92, 93] Ipc = isopinocampheyl, TCE = 2,2,2-trichloroethyl.

then isolated with high stereoselectivity.[94–96] This remarkable stereochemical outcome was confirmed by model reactions.

Reactions of (*E*)-boron enolates of isopropyl ethyl ketone **130** with isopropyl methyl ketone **132** with chiral α-substituted aldehyde **134** yielded the desired *anti*-configured aldol product with high stereoselectivity (Scheme 24). The product configuration can be explained best by a destabilization of the *anti*-Felkin transition state **G** through sterically unfavored *syn*-pentane interactions (Scheme 24). Several other research groups also reported successful couplings of the AB and CD fragments under the same conditions.[97–99] Different approaches to spongistatin 1 are described in Refs. [100, 101].

A recent example in which Paterson's boron enolate method was employed extensively described the total synthesis of maurenone (**144**, Scheme 25). By using a cascade of boron enolate aldol additions, differently configured starting chiral aldehydes **138**, *ent*-**138**, **147**, and *ent*-**147** (Scheme 26) as well as chiral ketones **150** and **151** (Scheme 27) were synthesized in high stereoselectivity.[102] In this way, all the possible isomers of maurenone could be obtained.

5. Aldol Additions of Tin Enolates

Mukaiyama, Iwasawa, et al. were the first to develop an aldol addition based on tin(II) enolates. They used $Sn(OTf)_2$ and tertiary amines in their experiments which gave aldol

 © 2006 Wiley-VCH Verlag GmbH & Co. KGaA, Weinheim

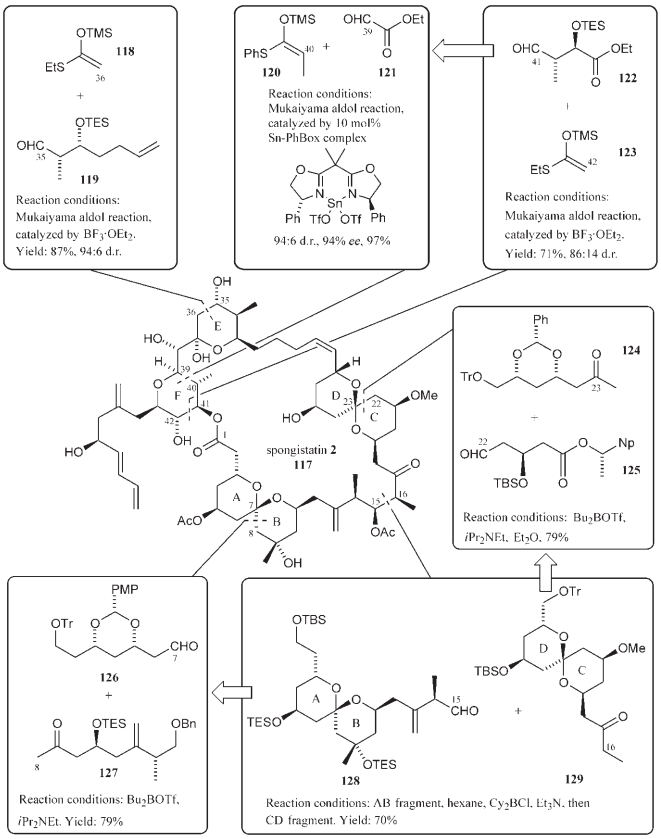

Scheme 23. Total synthesis of spongistatin 2 by Evans et al. [92–94]

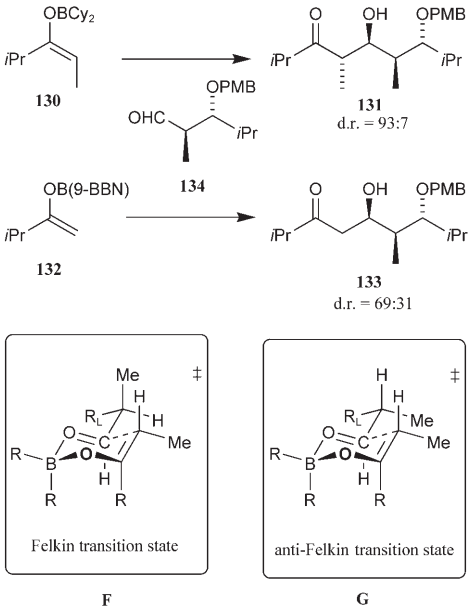

Scheme 24. Transition states of aldol additions of boron enolates of ketones with chiral α-substituted aldehydes. BBN = borabicyclo-[3.3.1]nonane.

adducts with excellent *syn* selectivities.[103–105] This method was used by several other researchers for the total synthesis of natural products.

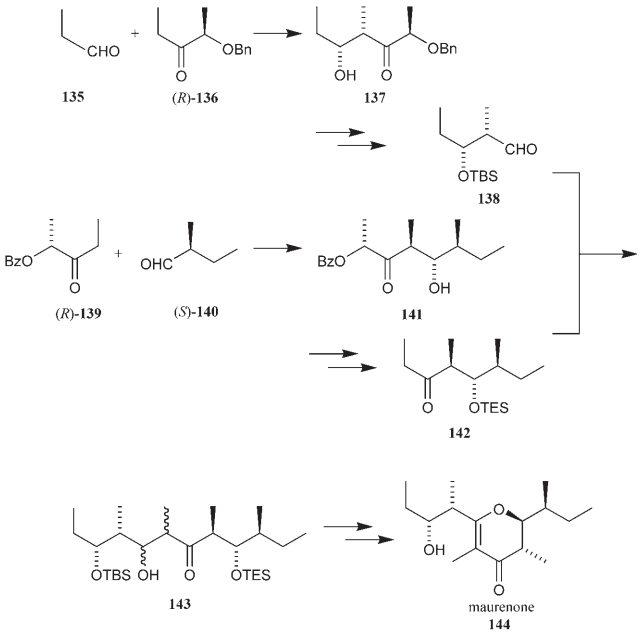

Scheme 25. Synthesis strategy for the total synthesis of maurenone.

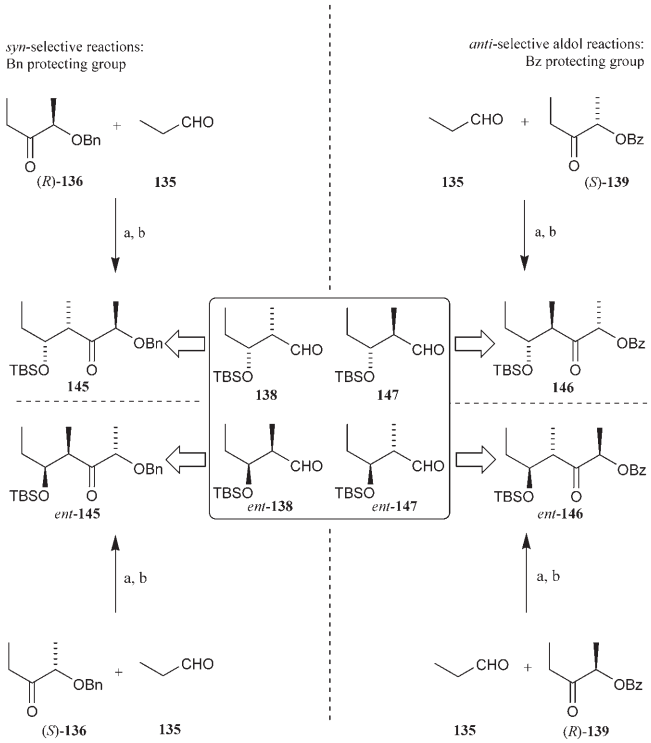

Scheme 26. Total synthesis of maurenone: Preparation of the chiral aldehydes. Reaction conditions: a) Cy_2BCl, Me_2NEt, −80 °C; b) TBSOTf, 2,6-lutidine, −78 °C. Tf = triflate.

As mentioned in the introduction, Peng and Woerpel used a tin enolate aldol addition as the key step to connect the two parts of dihydroerythronolide A (see also Figure 1).[19] Evans et al. used an aldol addition of tin enolates in their total synthesis of calyculin A (**155**). The tin(II) enolate of glycolate imide (**152**) was generated with the help of tin(II) triflate in

 © 2006 Wiley-VCH Verlag GmbH & Co. KGaA, Weinheim

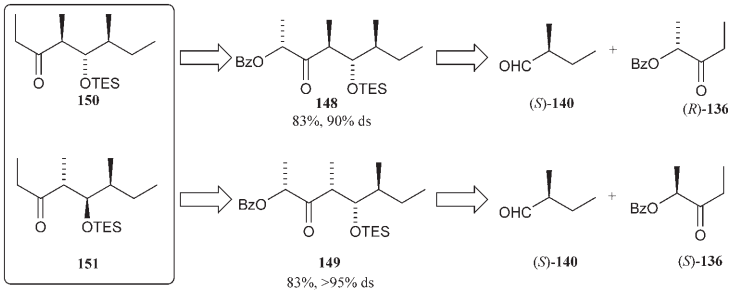

Scheme 27. Total synthesis of maurenone: Preparation of the chiral ketones. Reaction conditions: a) Cy_2BCl, Me_2NEt, −80 °C; b) TESOTf, 2,6-lutidine, −78 °C.

the presence of triethylamine to construct the ketide structure (in the marked region of Scheme 28) of calyculin A (**155**). The

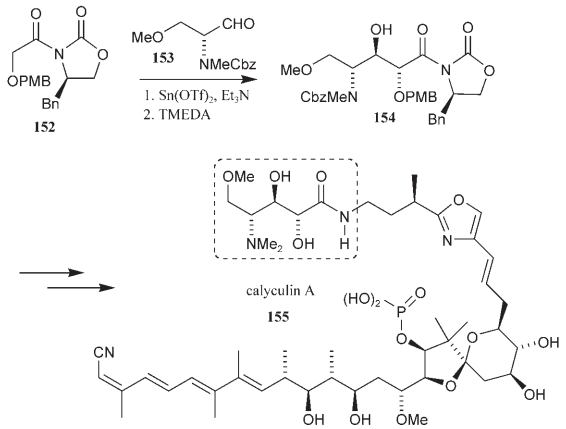

Scheme 28. Total synthesis of calyculin A by Evans et al.[106] Cbz = benzyloxycarbonyl.

observed *anti* selectivity was achieved by an additional treatment of the tin(II) enolate of imide **152** with TMEDA.[106] For an aldol approach to calyculin A using lithium enolates see Ref. [107].

Very recently, the same procedure was again used by Evans et al. for the total synthesis of aflastatin A (**160**). Tin(II) triflate and triethylamine served to establish the desired *anti* configuration in the starting chiral compound **158**. The subsequent aldol addition with boron enolate resulted in the exclusive formation of the *anti-syn-anti* configuration found in the C33–C36 region (Scheme 29).[108,109] The determination of the absolute configuration of aflastatin A is described in Ref. [110].

6. Catalytic Aldol Reactions with Lewis Acids

The syntheses dicussed so far have covered the utilization of different metal enolates and necessitate the use of equimolar amounts of a chiral auxiliary. A catalytic and simultaneously enantioselective performance is never possible under these conditions. Catalytic aldol reactions, on the other hand, do not suffer from these drawbacks. One of the most promising developments in catalytic aldol reactions

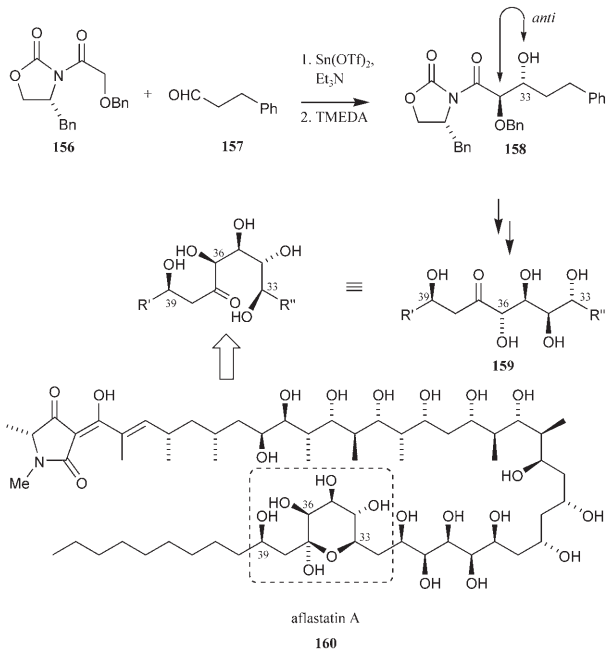

Scheme 29. Total synthesis of aflastatin A by Evans et al.[108,109]

started over 30 years ago when Mukaiyama et al. discovered aldol additions of silyl enol ethers with carbonyl compounds in the presence of Lewis acids.[111,112] For the first time, this method offered the possibility of an enantioselective and at the same time catalytic reaction. In the mid-1980s its full potential was realized by the discoveries of several other research groups, and since then numerous results and publications have accumulated in this field. Many total syntheses are unimaginable without the existence of the so-called Mukaiyama reaction. For several comprehensive overviews see Refs. [113,114]. Examples involving the use of several different Lewis acids will illustrate this development. However, the large number of publications in this field has necessitated that this chapter be especially selective.

6.1. Mukaiyama Reactions with Boron Lewis Acids

In contrast to the thouroughly documented aldol reactions with boron enolates, little has been published on the catalytic use of chiral boron Lewis acids in the Mukaiyama reaction. A very short asymmetric synthesis of a fragment of bryostatin 7 (**169**), which was accomplished by the use of substoichiometric amounts of chiral boron Lewis acid, was described by Kiyooka and Maeda (Scheme 30). This example may serve as a bridge between the boron enolate chemistry (as discussed above) and the catalytic use of boron Lewis acids in Mukaiyama reactions. The authors constructed the triol ester **166** by using three sequential Mukaiyama aldol additions in the presence of chiral oxazaborolidinones (*S*)- and (*R*)-**163** derived from sulfonamides of α-amino acids.[115] Another total synthesis of bryostatin using boron enolates can be found in Ref. [116].

A second example published by Kiyooka et al. demonstrates the power of this aldol method. Filipin III (**180**), a

 © 2006 Wiley-VCH Verlag GmbH & Co. KGaA, Weinheim

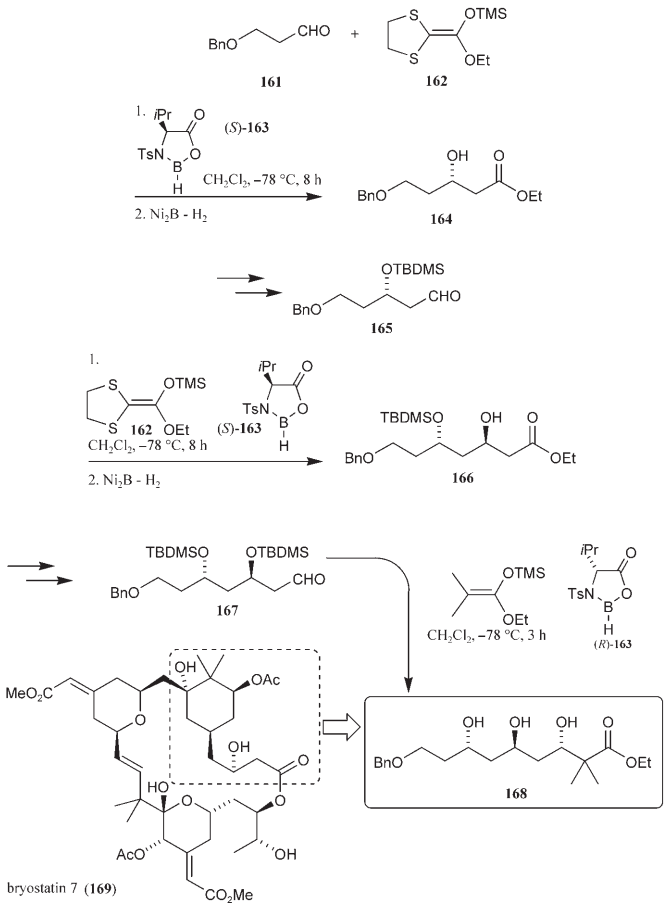

Scheme 30. Total synthesis of bryostatin 7. TMS = trimethylsilyl, TBDMS = *tert*-butyldimethylsilyl.

polyacetate macrolide, was synthesized by using chiral oxazaborolidinones (*S*)-**163** and (*R*)-**163** (Scheme 31).[117]

6.2. Mukaiyama Reactions with Tin Lewis Acids

In their initial studies, Mukaiyama et al. also tested tin(IV) chloride as a Lewis acid.[111,112] Tin(IV) chloride was found to be a useful, mildly active chelating catalyst for the Mukaiyama reaction. These catalytic properties of tin Lewis acids were exploited in a variety of total syntheses.

In 1997 White and Deerberg published a total synthesis of rapamycin (**181**). The polyketide substructure **182** in the eastern part of the molecule was constructed using a chiral tin catalyst. High diastereo- as well as enantioselectivities were observed in the reaction of chiral aldehyde **183** with the enolate component **184** (*syn*/*anti* = 5/95; 92% *ee anti*, Scheme 32).[118] The total synthesis of rapamycin by using conventional boron enolate aldol chemistry can be found in Ref. [119].

Shiina et al. also used chiral tin catalysts to accomplish the total syntheses of octalactin A and B (**186**). The three chiral precursors **187**, **188**, and **189** were synthesized in the presence of chiral tin(II) Lewis acids (*S*)-**190**, (*R*)-**191**, and (*S*)-**191**, respectively, with high enantioselectivities (Scheme 33).[120,121] This work has been summarized in a review.[122]

As a final example, Evans et al. described an approach to spongistatin 2 (**117**). The starting chiral compound **193** was synthesized in a Mukaiyama reaction (Scheme 34) in the presence of the (box)-Sn(OTf)$_2$ complex **192**. The *anti*-configured aldol adduct **193** was obtained in an enantiomeric excess of over 94% (see also Scheme 23).[123]

6.3. Mukaiyama Reactions with Titanium Lewis Acids

In 1994 Carreira et al. described the application of chiral tridentate titanium Lewis acid **194** in enantioselective Mukaiyama reactions.[124] Rychnovsky et al. used these salen–titanium complexes in a total synthesis of the polyunsaturated macrolide roflamycoin (**195**, Scheme 35). The absolute configuration at C29 in the C35–C27 segment **197** of the roflamycoin was established by the use of a chiral titanium(IV) complex **194** in a Mukaiyama reaction.[125]

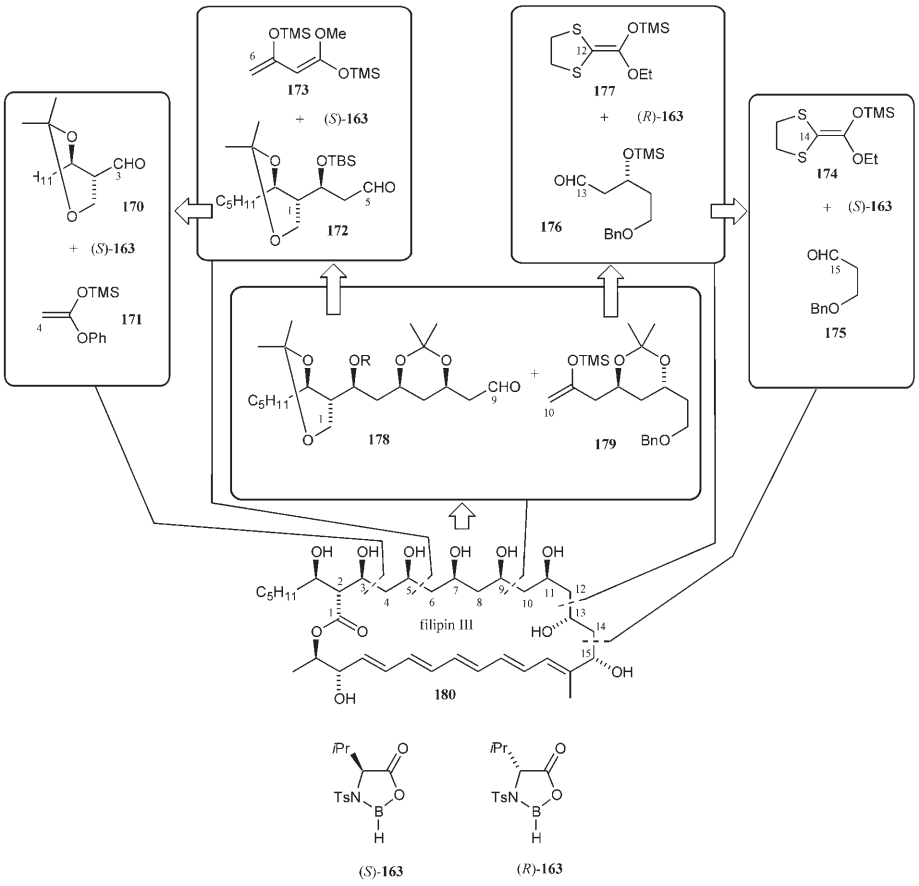

Scheme 31. Total synthesis of filipin III.

© 2006 Wiley-VCH Verlag GmbH & Co. KGaA, Weinheim

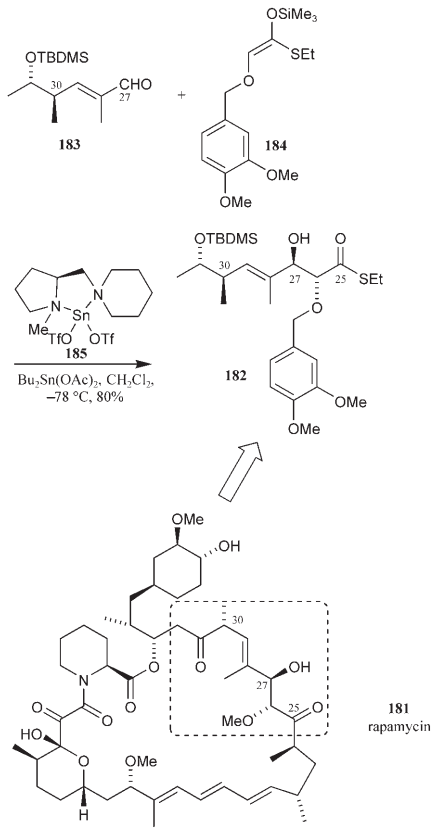

Scheme 32. Tin(II)-catalyzed approach to rapamycin.

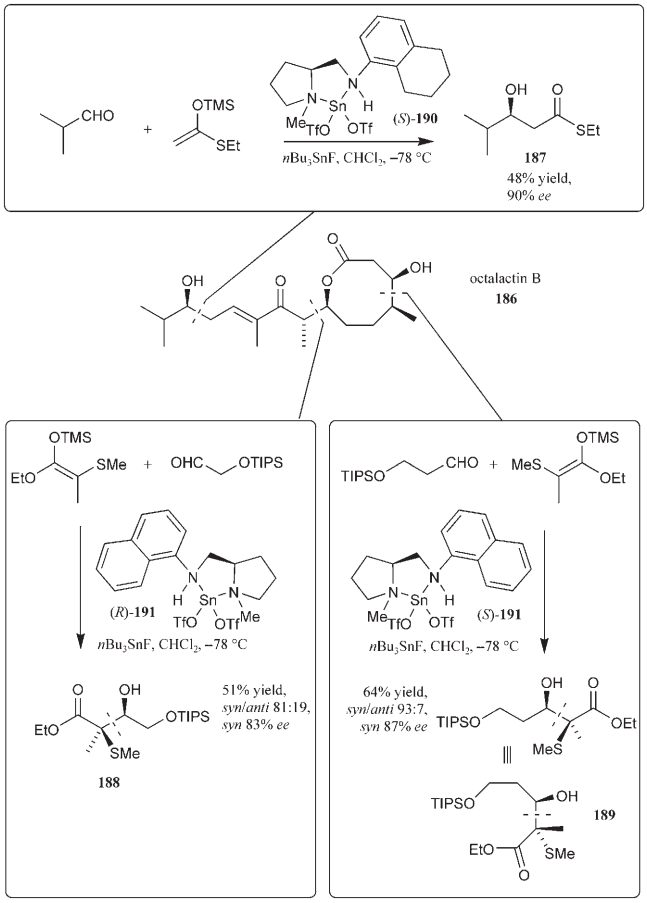

Scheme 33. Total synthesis of octalactin by Shiina et al.[120,121]

A further application of the Carreira catalyst **194** can be found in the total synthesis of macrolactin A (**198**, Scheme 36). The C3–C7 unit (*S*)-**201** was obtained by using the (*S*)-configured titanium catalyst (*S*)-**194**, and the C11–C15 segment (*R*)-**201** was constructed by the use of the (*R*)-configured titanium catalyst (*R*)-**194**. Both segments (*S*)-**201** and (*R*)-**201** were obtained in the same yield and the same enantioselectivity of 92% *ee*.[126]

6.4. Mukaiyama Reactions with Copper Lewis Acids

Ten years ago, Evans et al. reported the first Mukaiyama reaction catalyzed by a chiral copper complex. The aldol adducts were obtained with high enantioselectivities.[127] In general, two different types of copper catalysts are known: chiral pyridylbis(oxazoline)–copper(II) complexes (hereafter pyboxCu) and chiral binap–copper(II) fluorides. The use of [(pybox)Cu(SbF_6)$_2$] (**202**) in the total synthesis of bryostatin 2 (**205**) illustrates the first class. The starting chiral aldol adduct **204** needed was obtained with a high degree of enantioselectivity (> 99% *ee*, Scheme 37).[128]

Another example of the application of chiral copper catalysts is the total synthesis of callipeltoside A (**211**) by Evans et al. The starting chiral δ-hydroxy-α,β-unsaturated ester **210** was isolated with excellent enantioselectivity in a stereoselective, vinyloguos aldol addition catalyzed by the air-stable, chiral [(Ph-pybox)Cu(H_2O)$_2$](SbF_6) complex (**209**,

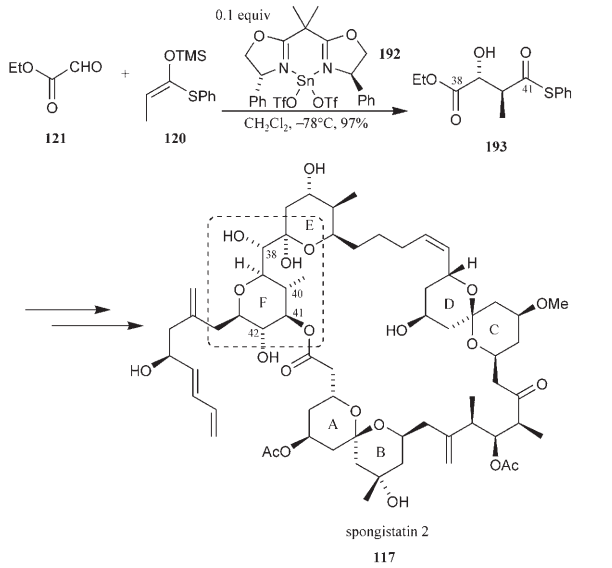

Scheme 34. Total synthesis of spongistatin 2 by Evans et al.[123]

Scheme 38).[129] For further approaches to callipeltoside A (**211**) see Refs. [130–135].

At the same time, Krüger and Carreira developed a copper-catalyzed Mukaiyama reaction based on the use of copper(II) flouride. A representative application can be

 © 2006 Wiley-VCH Verlag GmbH & Co. KGaA, Weinheim

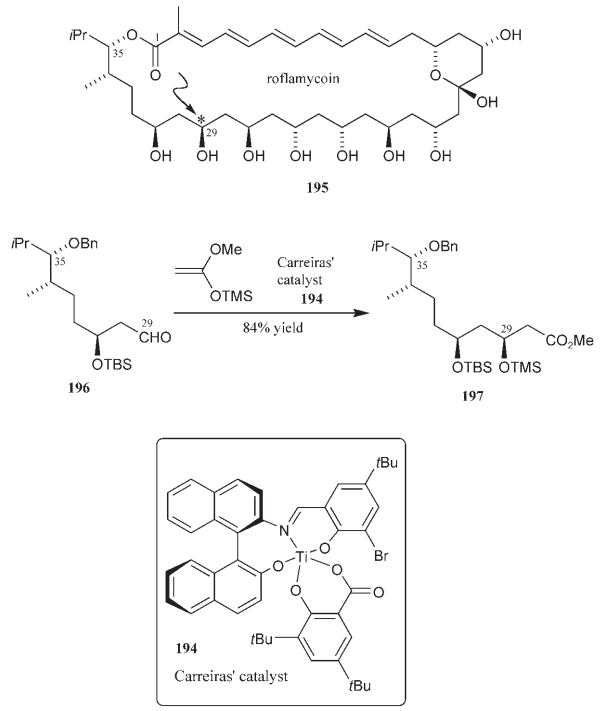

Scheme 35. Total synthesis of roflamycoin by Rychnovsky et al.[125]

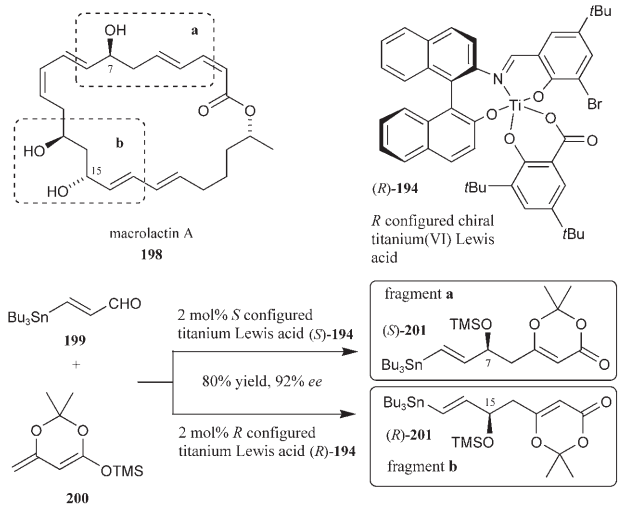

Scheme 36. Total synthesis of macrolactin A by Carreira and co-workers.[126]

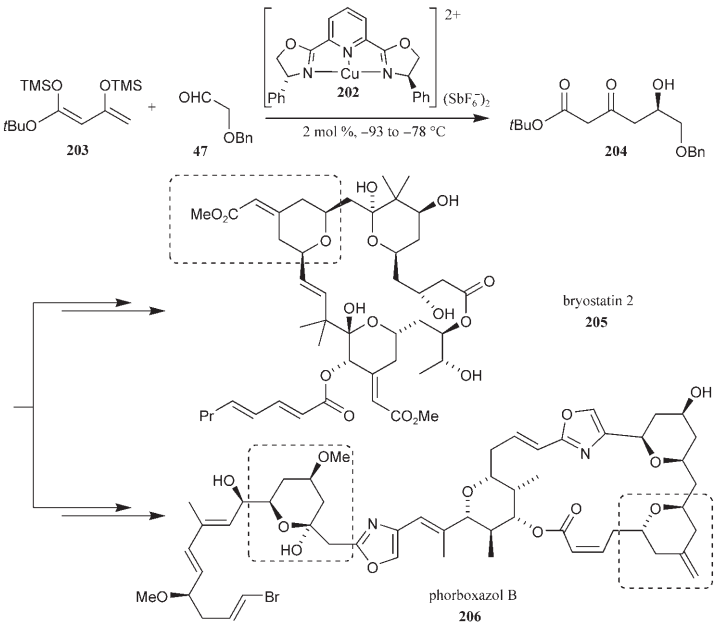

Scheme 37. Total synthesis of bryostatin 2 in the presence of a chiral copper catalyst.

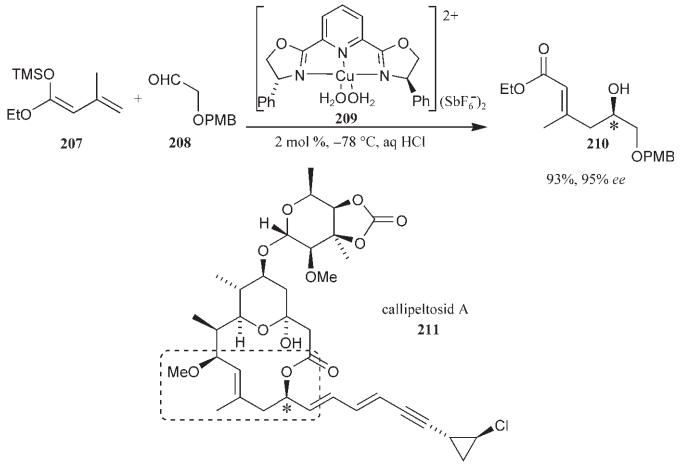

Scheme 38. Total synthesis of callipeltoside A by Evans et al.[129]

found in the total synthesis of amphotericin B (**212**, Scheme 39).[136] Both key fragments (*S*)-**216** and (*R*)-**216** of its polyketide subunit C1–C13 were derived from the same aldol reaction, which differed only in that in one case (*R*)- and in the other (*S*)-configured (Tol-binap)-CuF_2 complex **213** was used.[137]

7. Direct Aldol Additions

A development that was modeled on aldolases in nature, started nearly 10 years ago. In nature, the class II aldolases work by using zinc ions to activate the enolate component, while a tyrosine residue from the adjoining subunit simultaneously assists in the activation of the incoming aldehyde. Thus, a highly catalytic as well as enantioselective aldol reaction is achieved in nature without the need for separate reaction steps to form the enolate or the enol ether.[138]

In 1997 Shibasaki and co-workers described the first catalytic and enantioselective direct aldol addition based on this model. By using substoichiometric amounts of a bimetallic catalyst (*S*)-**217** (lanthanum and lithium), they had no need to prepare preformed enolates.[139] The same authors also found an application of this promising method in the total synthesis of fostriecin (**221**). By using 10 mol% of the bimetallic complex (*S*)-**217**, they were able to isolate the acetylenic ketone **220**, an important intermediate, in 70% yield (Scheme 40).[140] The synthesis of 8-*epi*-fostriecin by the

 © 2006 Wiley-VCH Verlag GmbH & Co. KGaA, Weinheim

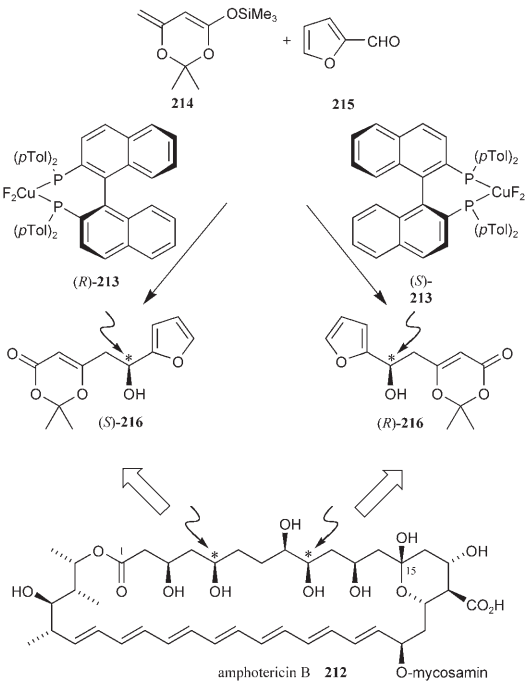

Scheme 39. Total synthesis of amphotericin B.

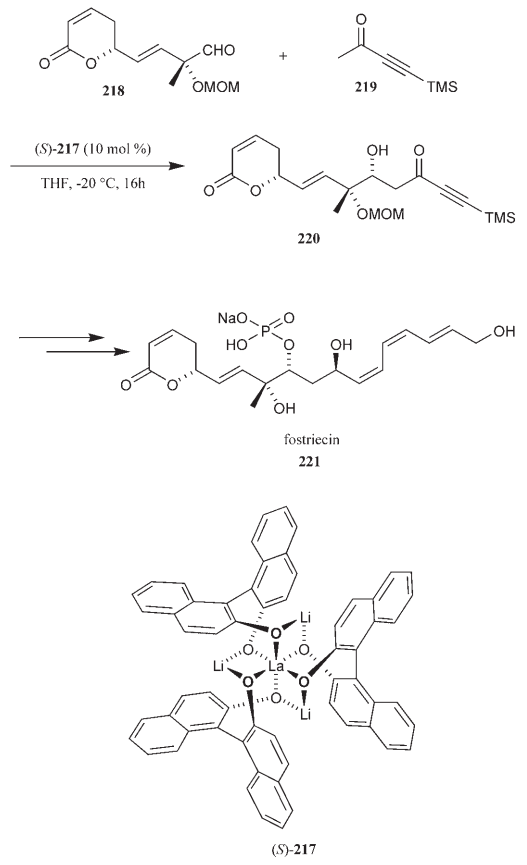

Scheme 40. Total synthesis of fostriecin by Shibasaki and co-workers.[140] MOM = methoxymethyl.

same method is reported in Ref. [141]. For the determination of the absolute configuration of fostriecin see Ref. [142].

In 2001 Trost et al. were able to realize a direct enantioselective aldol addition of enolizable aldehydes with α-hydroxyketones. To achieve this, they used a dinuclear chiral Zn catalyst **224**, which yielded the aldol adducts with a high degree of enantioselectivity.[143] The same authors reported an application of this reaction in the total synthesis of boronolide (**222**), in which the polyketide substructure was achieved by an aldol addition of *n*-pentanal with the α-hydroxyketone **223**. The *syn*-aldol adduct **225** was observed in 96% *ee* (Scheme 41).[144] Very recently Trost et al. also published an asymmetric synthesis of fostriecin (**221**) using the same dinuclear zinc catalyst **224**. The necessary aldol intermediate **228** was obtained with 99% *ee* (Scheme 42).[145]

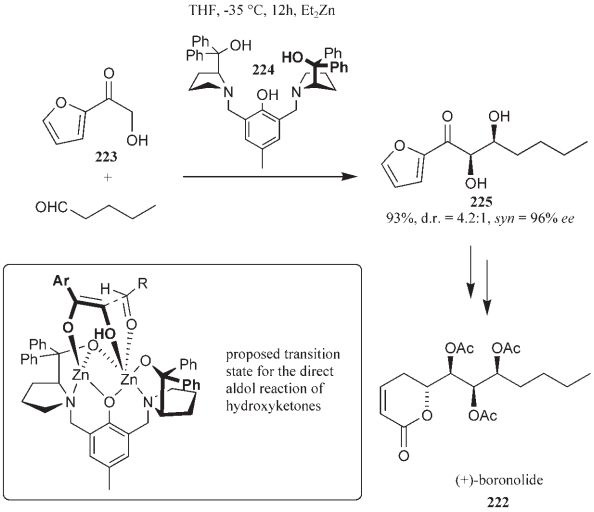

Scheme 41. Total synthesis of boronolide by Trost and Yeh.[144]

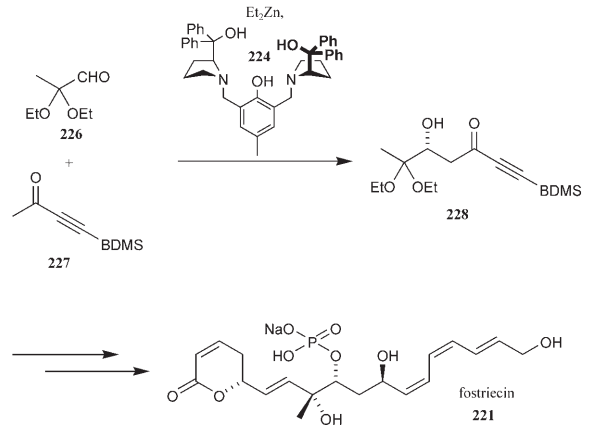

Scheme 42. Total synthesis of fostriecin by Trost et al.[145] BDMS = benzyldimethylsilyl.

8. Catalytic Aldol Reactions with Lewis Bases

In 1996, Denmark et al. described the first aldol reaction of trichlorosilyl enolates with aldehydes.[146] In contrast to the well-established Mukaiyama reaction, in which Lewis acids are deployed, this transformation was catalyzed by Lewis

 © 2006 Wiley-VCH Verlag GmbH & Co. KGaA, Weinheim

bases. By using chiral Lewis bases, aldol adducts could be obtained with a high degree of enantioselectivity. Several comprehensive overviews have been written on this method.[147–149] As an example, Denmark et al. used their own method to synthesize RK-397 (**229**). The starting chiral aldol adduct **230** was obtained by a vinylogous aldol reaction of ketene acetal **231** and α,β-unsaturated aldehyde **232** using chiral phosphoramide **235** in the presence of $SiCl_4$ (96% *ee*, Scheme 43). The second aldol step during this total synthesis was achieved by chiral phosphoramide **236** and $SiCl_4$. Unfortunately, the diastereoselectivity was only 2:1 in favoring of the desired product **237**. Better diastereoselectivities were obtained by using the established boron enolate reactions (19:1).[150] For comprehensive reviews of vinylogous aldol additions see Ref. [151].

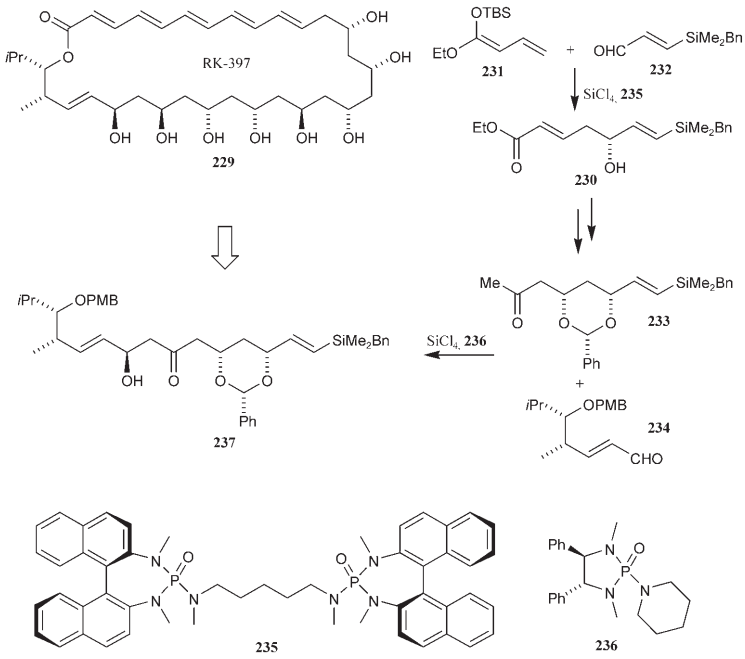

Scheme 43. Total synthesis of RK-397 by Denmark et al.

hydroxydiketone **239** (99% *ee*) by a proline-catalyzed aldol addition of acetone and aldehyde **238** (Scheme 44).[157]

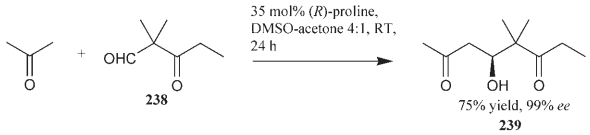

Scheme 44. Proline-catalyzed synthesis of important intermediates of epothilone. DMSO = dimethylsulfoxide.

The simplest polyketides—the triketides—have also been synthesized by proline-catalyzed enantioselective aldol additions. Córdova and co-workers obtained polyketide carbohydrate **241** in high enantioselectivity by treating racemic *anti*-configured β-hydroxyaldehyde **240** with enolizable aldehyde **47** in the presence of catalytic amounts of proline. Even when the benzyloxyacetaldehyde was used only, identically configured polyketide sugars **241** were obtained in a one-pot procedure. Thus, this method gives a way to synthesize carbohydrates (Scheme 45).[158–161] Another proline-catalyzed reaction that leads to the formation of carbohydrates has been reported.[162,163].

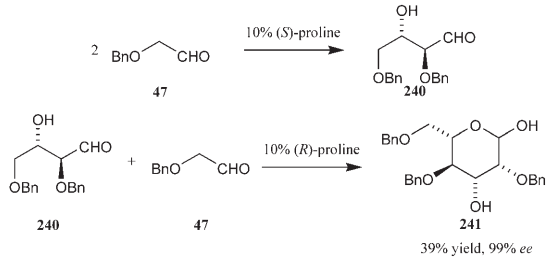

Scheme 45. Proline-catalyzed de novo synthesis of carbohydrates.

9. Organocatalysis

Organocatalysis is a very widely applicable and promising field in asymmetric synthesis.[152,153] For comprehensive overviews of amine catalysis see Refs. [154,155]. A subsection of amine catalysis is the proline-catalyzed aldol reaction, which was used in several total syntheses of natural products. The next examples demonstrate the power of this method and at the same time provides a good connection with the total syntheses of epothilone, discussed in Section 2 on lithium enolates.

Nicolaou et al. used the chiral ketoacid **14** or, later on, the chiral ketone **28** in their total syntheses of epothilone (see Schemes 2 and 5). These compounds were synthesized by using the allyl borane method developed by Brown.[156] A more straighforward approach involving proline catalysis was described by Avery and Zheng. They isolated the chiral

Enders and Grondal developed an elegant approach to carbohydrates in which they used dihydroxyacetone equivalent **242** in a proline-catalyzed aldol addition. In reactions with various aldehydes, selectively protected aldol adducts **243** were isolated with a high degree of enantioselectivities (Scheme 46). These products are valuable intermediates in the total synthesis of various carbohydrates, for example, ribose, lyxose, psicose, and even aminopsicose and aminotagatose.[164,165]

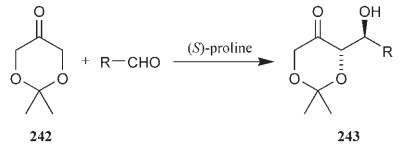

Scheme 46. $C_3 + C_n$ strategy to the synthesis of protected carbohydrates by Enders and Grondal.[164,165]

 © 2006 Wiley-VCH Verlag GmbH & Co. KGaA, Weinheim

10. Enzyme-Catalyzed Aldol Additions

In addition to the chemical methods described above, enzymatic methods have been used more and more as chiral catalysts in asymmetric aldol additions. Several comprehensive overviews have been written on this topic.[138,166–169].

The most important application of enzyme-catalyzed aldol additions is in the de novo synthesis of carbohydrates. Nevertheless, there are some examples of the stereoselective total syntheses of polyketides by enzyme-catalyzed aldol additions. In particular, the high stereoselectivity of aldolases renders them very valuable in catalytic C–C bond-formation processes, as shown in the following two examples.

Chain elongation of the *manno*-configured substrate **244** with pyruvate in the presence of NeuA (NeuA = *N*-acetylneuraminic acid aldolase) yielded the cyclic ketal **245** in good yields and selectivity for the synthesis of amphotericin B (**246** Scheme 47).[170,171] The C9–C16 chain fragment **247** of the

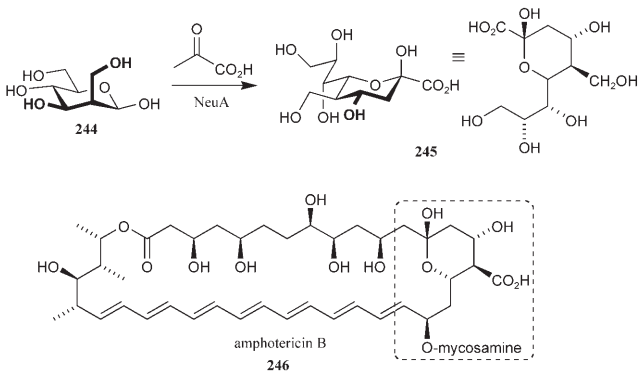

Scheme 47. NeuA catalysis in the total synthesis of amphotericin.

antibiotic pentamycin (**248**) was obtained by a FruA-catalyzed aldol addition of DHAP with the chiral aldehyde **249** (FruA = D-fructose-1,6-bisphosphate aldolase, DHAP = dihydroxyacetone phosphate; Scheme 48).[172,173]

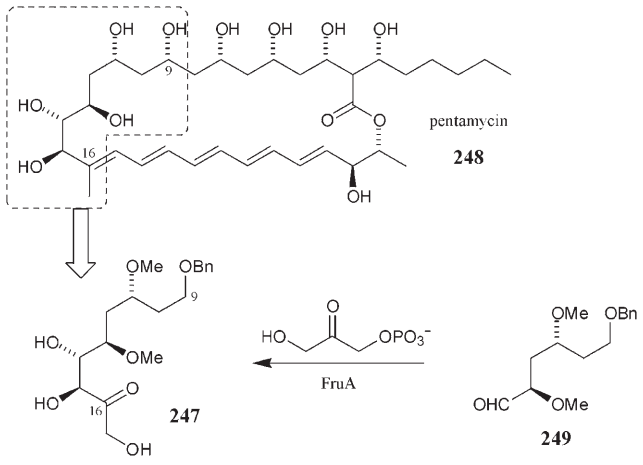

Scheme 48. FruA-catalyzed synthesis of pentamycin.

11. Summary and Outlook

This overview provides an up-to-date discussion of all aspects of modern aldol additions in the total synthesis of polyketides, a highly important class of biological compounds. Different strategies and methods have been applied, including the development of various metal enolate architectures, the use of catalytic aldol additions, and the development of organo- as well as biocatalytical versions. The total syntheses discussed, highlight the contemporary state of the art in controlling the regio-, chemo-, and stereoselectivity in such complex acyclic systems.

The various successful synthetic approaches developed up to now demonstrate the possibility of synthesizing polyketides. This feature has further inspired the development and application of new methods of acyclic stereocontrol: the correct installation of a configuration by exploiting substrate as well as reagent control.

However, these complex natural products continue to act as a challenge for innovative synthetic strategies and methods. Future goals involve the minimization or reduction in the use of protective groups, the effective coupling of highly functionalized intermediates, and the development of new direct syntheses.

The authors grateful acknowledge the financial grants of the Konrad-Adenauer-Stiftung, DFG, and Schering AG.

Received: July 13, 2006

[1] R. B. Woodward in *Perspectives in Organic Chemistry* (Ed.: A. Todd), Wiley-Interscience, New York, **1956**, p. 160.
[2] a) I. Paterson, M. M. Mansuri, *Tetrahedron* **1985**, *41*, 3569–3624; b) S. Masamune, G. S. Bates, J. W. Corcoran, *Angew. Chem.* **1977**, *89*, 602–624; *Angew. Chem. Int. Ed. Engl.* **1977**, *16*, 585–607.
[3] J. Mulzer, *Angew. Chem.* **1991**, *103*, 1484–1486; *Angew. Chem. Int. Ed. Engl.* **1991**, *30*, 1452–1484.
[4] R. B. Woodward, E. Logush, K. P. Nambiar, K. Sakan, D. E. Ward, B. W. Au-Yeung, P. Balaram, L. J. Browne, P. J. Card, C. H. Chen, R. B. Chênevert, A. Fliri, K. Frobel, H.-J. Gais, D. G. Garratt, K. Hayakawa, K. W. Heggie, D. P. Hesson, D. Hoppe, I. Hoppe, J. A. Hyatt, D. Ikeda, P. A. Jacobi, K. S. Kim, Y. Kobuke, K. Kojima, K. Krowicki, V. J. Lee, T. Leutert, S. Malchenko, J. Martens, R. S. Matthews, B. S. Ong, J. B. Press, T. V. Rajan Babu, G. Rousseau, H. M. Sauter, M. Suzuki, K. Tatsuta, L. M. Tolbert, E. A. Truesdale, I. Uchida, Y. Ueda, T. Uyehara, A. T. Vasella, W. C. Vladuchick, P. A. Wade, R. M. Williams, H. N.-C. Wong, *J. Am. Chem. Soc.* **1981**, *103*, 3210–3213.
[5] S. Masamune, M. Hirama, S. Mori, S. A. Ali, D. S. Garvey, *J. Am. Chem. Soc.* **1981**, *103*, 1568–1571.
[6] A. R. Chamberlin, M. Dezube, S. H. Reich, D. Sall, *J. Am. Chem. Soc.* **1989**, *111*, 6247–6256.
[7] B. Bernet, P. M. Bishop, M. Caron, T. Kawamata, B. L. Roy, L. Ruest, G. Sauvé, P. Soucy, P. Deslongchamps, *Can. J. Chem.* **1985**, *63*, 2810–2813.
[8] C. Agami, N. Platzer, C. Puchot, H. Sevestre, *Tetrahedron* **1987**, *43*, 1091–1098.
[9] C. H. Heathcock, S. D. Young, J. P. Hagen, R. Pilli, U. Badertscher, *J. Org. Chem.* **1985**, *50*, 2095–2105.

 © 2006 Wiley-VCH Verlag GmbH & Co. KGaA, Weinheim

[10] M. Ahmar, I. Romain, R. Bloch, *J. Org. Chem.* **1993**, *58*, 2953 – 2957.
[11] I. Paterson, S. K. Patel, J. R. Porter, *Tetrahedron Lett.* **1983**, *24*, 3395 – 3396.
[12] I. Paterson, D. D. P. Laffan, D. J. Rawson, *Tetrahedron Lett.* **1988**, *29*, 1461 – 1464.
[13] I. Paterson, T. Temal-Laib, *Org. Lett.* **2002**, *4*, 2473 – 2476.
[14] D. A. Evans, A. S. Kim, *Tetrahedron Lett.* **1997**, *38*, 53 – 56.
[15] D. C. Myles, S. J. Danishefsky, G. Schulte, *J. Org. Chem.* **1990**, *55*, 1636 – 1648.
[16] T. Nakata, M. Fukui, T. Oishi, *Tetrahedron Lett.* **1988**, *29*, 2223 – 2226.
[17] C. H. Heathcock, see citation in Ref. [2].
[18] D. A. Evans, A. S. Kim, R. Metternich, V. Novack, *J. Am. Chem. Soc.* **1998**, *120*, 5921 – 5942.
[19] Z. H. Peng, K. A. Woerpel, *J. Am. Chem. Soc.* **2003**, *125*, 6018 – 6019.
[20] S. F. Martin, G. J. Pacofsky, R. P. Gist, W. C. Lee, *J. Am. Chem. Soc.* **1989**, *111*, 7634 – 7636.
[21] S. F. Martin, W.-C. Lee, *Tetrahedron Lett.* **1993**, *34*, 2711 – 2714.
[22] S. F. Martin, W.-C. Lee, G. J. Pacofsky, R. P. Gist, T. A. Mulhern, *J. Am. Chem. Soc.* **1994**, *116*, 4674 – 4688.
[23] N. K. Kochetkov, A. F. Sviridov, M. S. Ermolenko, D. V. Yashunsky, V. S. Borodkin, *Tetrahedron* **1989**, *45*, 5109 – 5136.
[24] A. F. Sviridov, M. S. Ermolenko, D. V. Yashunsky, V. S. Borodkin, N. K. Kochetkov, *Tetrahedron Lett.* **1987**, *28*, 3839 – 3842.
[25] A. F. Sviridov, V. S. Borodkin, M. S. Ermolenko, D. V. Yashunsky, N. K. Kochetkov, *Tetrahedron* **1991**, *47*, 2317 – 2336.
[26] K. C. Nicolaou, Y. He, D. Vourloumis, H. Vallberg, Z. Yang, *Angew. Chem.* **1996**, *108*, 2554 – 2556; *Angew. Chem. Int. Ed. Engl.* **1996**, *35*, 2399 – 2401.
[27] K. C. Nicolaou, Y. He, D. Vourloumis, H. Vallberg, F. Roschangar, F. Sarabia, S. Ninkovic, Z. Yang, J. I. Trujillo, *J. Am. Chem. Soc.* **1997**, *119*, 7960 – 7973.
[28] D. Schinzer, A. Limberg, O. M. Böhm, *Chem. Eur. J.* **1996**, *2*, 1477 – 1482.
[29] D. Schinzer, A. Bauer, J. Schieber, *Chem. Eur. J.* **1999**, *5*, 2492 – 2500.
[30] D. Schinzer, A. Bauer, J. Schieber, *Synlett* **1998**, 861 – 864.
[31] C. H. Heathcock, C. T. Buse, W. A. Kleschick, M. C. Pirrung, J. E. Sohn, J. Lampe, *J. Org. Chem.* **1980**, *45*, 1066 – 1081.
[32] C. H. Heathcock, M. C. Pirrung, C. T. Buse, J. P. Hagen, D. S. Young, J. E. Sohn, *J. Am. Chem. Soc.* **1979**, *101*, 7077 – 7079.
[33] C. H. Heathcock, C. T. White, *J. Am. Chem. Soc.* **1979**, *101*, 7076 – 7077.
[34] C. H. Heathcock, *Science* **1981**, *214*, 395 – 400.
[35] D. Schinzer, A. Bauer, O. M. Böhm, A. Limberg, M. Cordes, *Chem. Eur. J.* **1999**, *5*, 2483 – 2491.
[36] M. Braun in *Modern Aldol Reactions*, *Vol. 1* (Ed.: R. Mahrwald), Wiley-VCH, Weinheim, **2004**, pp. 1 – 62.
[37] K. Gerlach, M. Quitschalle, M. Kalesse, *Tetrahedron Lett.* **1999**, *40*, 3553 – 3556.
[38] E. Claus, A. Pahl, P. G. Jones, H. M. Meyer, M. Kalesse, *Tetrahedron Lett.* **1997**, *38*, 1359 – 1362.
[39] K. C. Nicolaou, S. Ninkovic, F. Sarabia, D. Vourloumis, Y. He, H. Vallberg, M. R. V. Finlay, Z. Yang, *J. Am. Chem. Soc.* **1997**, *119*, 7974 – 7991.
[40] J. Mulzer, G. Karig, P. Pojarliev, *Tetrahedron Lett.* **2000**, *41*, 7635 – 7638.
[41] J. Mulzer, A. Mantoulidis, E. Öhler, *Tetrahedron Lett.* **1998**, *39*, 8633 – 8636.
[42] H. J. Martin, M. Drescher, J. Mulzer, *Angew. Chem.* **2000**, *112*, 591 – 593; *Angew. Chem. Int. Ed.* **2000**, *39*, 581 – 583.
[43] A. Balog, C. Harris, K. Savin, X.-G. Zhang, T.-C. Chou, S. J. Danishefsky, *Angew. Chem.* **1998**, *110*, 2821 – 2824; *Angew. Chem. Int. Ed.* **1998**, *37*, 2675 – 2678.
[44] C. B. Lee, Z. Wu, F. Zhang, M. D. Chappel, S. J. Stachel, T.-C. Chou, Y. Guan, S. J. Danishefsky, *J. Am. Chem. Soc.* **2001**, *123*, 5249 – 5259.
[45] M. Nerz-Stormes, E. R. Thornton, *Tetrahedron Lett.* **1986**, *27*, 897 – 900.
[46] S. Shirodkar, M. Nerz-Stormes, E. R. Thornton, *Tetrahedron Lett.* **1990**, *31*, 4699 – 4702.
[47] M. Nerz-Stormes, E. R. Thornton, *J. Org. Chem.* **1991**, *56*, 2489 – 2498.
[48] R. O. Duthaler, P. Herold, W. Lottenbach, K. Oertle, M. Riediker, *Angew. Chem.* **1989**, *101*, 490 – 491; *Angew. Chem. Int. Ed. Engl.* **1989**, *28*, 495 – 497.
[49] R. O. Duthaler, A. Hafner, *Chem. Rev.* **1992**, *92*, 807 – 832.
[50] R. O. Duthaler, F. Bienewald, A. Hafner in *Transition Metals for Organic Synthesis*, *2nd ed.*, *Vol. 1* (Eds.: M. Beller, C. Bolm), Wiley-VCH, Weinheim, **2004**, pp. 491 – 517.
[51] C. Palomo, M. Oiarbide, A. Gonzáles, J. M. García, F. Berrée, A. Linden, *Tetrahedron Lett.* **1996**, *37*, 6931 – 6934.
[52] A. K. Gosh, M. Shevli in *Modern Aldol Reactions*, *Vol. 1* (Ed.: R. Mahrwald), Wiley-VCH, Weinheim, **2004**, pp. 63 – 125.
[53] D. A. Evans, D. L. Rieger, M. T. Bilodeau, F. Urpi, *J. Am. Chem. Soc.* **1991**, *113*, 1047 – 1049.
[54] I. Paterson, M. V. Perkins, *Tetrahedron* **1996**, *52*, 1811 – 1834.
[55] J. De Brabander, W. Oppolzer, *Tetrahedron* **1997**, *53*, 9169 – 9202.
[56] M. W. Andersen, B. Hildebrandt, R. W. Hoffmann, *Angew. Chem.* **1991**, *103*, 90 – 92; *Angew. Chem. Int. Ed. Engl.* **1991**, *30*, 97 – 99.
[57] D. Enders, G. Geibel, S. Osborne, *Chem. Eur. J.* **2000**, *6*, 1302 – 1309.
[58] M. V. Perkins, R. A. Sampson, *Org. Lett.* **2001**, *3*, 123 – 126.
[59] C. M. Hayward, D. Yohannes, S. J. Danishefsky, *J. Am. Chem. Soc.* **1993**, *115*, 9345 – 9346.
[60] K. Biswas, H. Lin, J. T. Njardarson, M. D. Chappell, T.-C. Chou, Y. Guan, W. P. Tong, L. He, S. B. Horwitz, S. J. Danishefsky, *J. Am. Chem. Soc.* **2002**, *124*, 9825 – 9832.
[61] M. D. Chappell, S. J. Stachel, C. B. Lee, S. J. Danishefsky, *Org. Lett.* **2000**, *2*, 1633 – 1636.
[62] C. B. Lee, Z. Wu, F. Zhang, M. D. Chappell, S. J. Stachel, T. C. Chou, Y. Guan, S. J. Danishefsky, *J. Am. Chem. Soc.* **2001**, *123*, 5249 – 5259.
[63] Z. Wu, F. Zhang, S. J. Danishefsky, *Angew. Chem.* **2000**, *112*, 4679 – 4682; *Angew. Chem. Int. Ed.* **2000**, *39*, 4505 – 4508.
[64] J. E. Sheppeck II, W. Liu, A. R. Chamberlin, *J. Org. Chem.* **1997**, *62*, 387 – 398.
[65] M. Oikawa, T. Ueno, H. Oikawa, A. Ichihara, *J. Org. Chem.* **1995**, *60*, 5048 – 5068.
[66] M. T. Crimmins, B. W. King, *J. Am. Chem. Soc.* **1998**, *120*, 9084 – 9085.
[67] D. Enders, J. L. Vicario, A. Job, M. Wolberg, M. Müller, *Chem. Eur. J.* **2002**, *8*, 4272 – 4284.
[68] L. C. Dias, P. R. R. Meira, *J. Org. Chem.* **2005**, *70*, 4762 – 4773.
[69] M. Kalesse, K. P. Chary, M. Quitschalle, A. Burzlaff, C. Kasper, T. Scheper, *Chem. Eur. J.* **2003**, *9*, 1129 – 1136.
[70] M. Kalesse, M. Christmann, *Synthesis* **2002**, 981 – 1003.
[71] M. T. Crimmins, J. D. Katz, D. G. Washburn, S. P. Allwein, L. F. McAtee, *J. Am. Chem. Soc.* **2002**, *124*, 5661 – 5663.
[72] M. T. Crimmins, J. D. Katz, L. C. McAtee, E. A. Tabet, S. J. Kirincich, *Org. Lett.* **2001**, *3*, 949 – 952.
[73] M. T. Crimmins, J. D. Katz, *Org. Lett.* **2000**, *2*, 957 – 960.
[74] T. K. Chakraborty, S. Jayaprakash, P. Laxman, *Tetrahedron* **2001**, *57*, 9461 – 9467.
[75] L. C. Dias, L. G. de Oliveira, *Org. Lett.* **2001**, *3*, 3951 – 3954.
[76] J. T. Feutrill, M. J. Lilly, M. A. Rizzacasa, *Org. Lett.* **2000**, *2*, 3365 – 3367.
[77] A. K. Gosh, M. Onishi, *J. Am. Chem. Soc.* **1996**, *118*, 2527 – 2528.

 © 2006 Wiley-VCH Verlag GmbH & Co. KGaA, Weinheim

[78] A. K. Gosh, S. Fidanze, M. Onishi, K. A. Hussain, *Tetrahedron Lett.* **1997**, *38*, 7171 – 7174.
[79] A. K. Gosh, C. J. Liu, *J. Am. Chem. Soc.* **2003**, *125*, 2374 – 2375.
[80] T. Mukaiyama, T. Inoue, *Chem. Lett.* **1976**, 559 – 562.
[81] T. Inoue, Z. Uchimaru, T. Mukaiyama, *Chem. Lett.* **1977**, 153 – 154.
[82] T. Mukaiyama, *Org. React.* **1982**, *28*, 203 – 331.
[83] B. M. Kim, S. F. Williams, S. Masamune in *Comprehensive Organic Synthesis* (Ed.: B. M. Trost), Pergamon, London, **1993**, pp. 239 – 275.
[84] D. A. Evans, J. V. Nelson, T. R. Taber, *Top. Stereochem.* **1982**, *13*, 1 – 115.
[85] T. Mukaiyama, J.-I. Matsuo in *Modern Aldol Reactions*, *Vol. 1* (Ed.: R. Mahrwald), Wiley-VCH, Weinheim, **2004**, pp. 127 – 160.
[86] D. A. Evans, P. N. Howard, *Tetrahedron Lett.* **1993**, *34*, 2229 – 2232.
[87] J. D. White, R. Hanselmann, R. W. Jackson, W. J. Porter, Y. Ohba, T. Tiller, S. Wang, *J. Org. Chem.* **2001**, *66*, 5217 – 5231.
[88] C. D. Cowden, I. Paterson, *Org. React.* **1997**, *51*, 1 – 200.
[89] I. Paterson, D. C. Wallace, C. D. Cowden, *Synthesis* **1998**, 639 – 652.
[90] I. Paterson, R. D. Norcross, R. A. Ward, P. Romea, M. A. Lister, *J. Am. Chem. Soc.* **1994**, *116*, 11287 – 11314.
[91] I. Paterson, G. J. Florence, *Eur. J. Org. Chem.* **2003**, 2193 – 2208.
[92] I. Paterson, D. Y. K. Chen, M. J. Coster, J. L. Acena, J. Bach, K. R. Gibson, L. E. Keown, R. M. Oballa, A. Trieselmann, D. J. Wallace, A. P. Hodgson, R. D. Norcross, *Angew. Chem.* **2001**, *113*, 4179 – 4184; *Angew. Chem. Int. Ed.* **2001**, *40*, 4055 – 4060.
[93] I. Paterson, M. J. Coster, D. Y. K. Chen, K. R. Gibson, D. J. Wallace, *Org. Biomol. Chem.* **2005**, *3*, 2410 – 2419, and references cited therein.
[94] D. A. Evans, P. J. Coleman, L. C. Dias, *Angew. Chem.* **1997**, *109*, 2951 – 2954; *Angew. Chem. Int. Ed. Engl.* **1997**, *36*, 2738 – 2741.
[95] D. A. Evans, B. W. Trotter, B. Cote, P. J. Coleman, *Angew. Chem.* **1997**, *109*, 2954 – 2957; *Angew. Chem. Int. Ed. Engl.* **1997**, *36*, 2741 – 2744.
[96] D. A. Evans, B. W. Trotter, B. Cote, P. J. Coleman, L. C. Dias, A. N. Tyler, *Angew. Chem.* **1997**, *109*, 2957 – 2961; *Angew. Chem. Int. Ed. Engl.* **1997**, *36*, 2744 – 2747.
[97] C. H. Heathcock, M. McLaughlin, J. Medina, J. L. Hubbs, G. A. Wallace, R. Scott, M. M. Claffey, C. J. Hayes, G. R. Ott, *J. Am. Chem. Soc.* **2003**, *125*, 12844 – 12849.
[98] J. L. Hubbs, C. H. Heathcock, *J. Am. Chem. Soc.* **2003**, *125*, 12836 – 12843.
[99] A. B. Smith III, V. A. Doughty, C. Sfouggattakis, C. S. Bennett, J. Koyanagi, M. Takeuchi, *Org. Lett.* **2002**, *4*, 783 – 786.
[100] J. Guo, K. J. Duffy, K. L. Stevens, P. I. Dalko, R. M. Roth, M. M. Hayward, Y. Kishi, *Angew. Chem.* **1998**, *110*, 198 – 202; *Angew. Chem. Int. Ed.* **1998**, *37*, 187 – 190.
[101] M. M. Hayward, R. M. Roth, K. J. Duffy, P. I. Dalko, K. L. Stevens, J. Guo, Y. Kishi, *Angew. Chem.* **1998**, *110*, 202 – 206; *Angew. Chem. Int. Ed.* **1998**, *37*, 190 – 196.
[102] J. S. Crossman, M. V. Perkins, *J. Org. Chem.* **2006**, *71*, 117 – 124.
[103] T. Mukaiyama, R. W. Stevens, N. Iwasawa, *Chem. Lett.* **1982**, 353 – 356.
[104] T. Mukaiyama, N. Iwasawa, R. W. Stevens, T. Gaga, *Tetrahedron* **1984**, *40*, 1381 – 1390.
[105] T. Mukaiyama, N. Iwasawa, *Chem. Lett.* **1984**, 753 – 756.
[106] D. A. Evans, J. R. Gage, J. L. Leighton, *J. Am. Chem. Soc.* **1992**, *114*, 9434 – 9453.
[107] G. R. Scarlato, J. A. DeMattei, L. S. Chong, A. K. Ogawa, M. R. Lin, R. W. Armstrong, *J. Org. Chem.* **1996**, *61*, 6139 – 6152.
[108] D. A. Evans, F. Glorius, J. D. Burch, *Org. Lett.* **2005**, *7*, 3331 – 3333.
[109] D. A. Evans, W. C. Trenkle, J. Zhang, J. D. Burch, *Org. Lett.* **2005**, *7*, 3335 – 3338.
[110] H. Ikeda, N. Matsumori, M. Ono, A. Suzuki, A. Isogai, H. Nagasawa, S. Sakuda, *J. Org. Chem.* **2000**, *65*, 438 – 444.
[111] T. Mukaiyama, K. Narasaka, K. Banno, *Chem. Lett.* **1973**, 1011 – 1014.
[112] T. Mukaiyama, K. Banno, K. Narasaka, *J. Am. Chem. Soc.* **1974**, *96*, 7503 – 7509.
[113] C. H. Heathcock in *Comprehensive Organic Synthesis*, *Vol. 2* (Eds.: B. M. Trost, I. Fleming, C. H. Heathcock), Pergamon, Oxford, **1993**, chap. 1.6, pp. 181 – 238; B. M. Kim, S. F. Williams, S. Masamune in *Comprehensive Organic Synthesis*, *Vol. 2* (Eds.: B. M. Trost, I. Fleming, C. H. Heathcock), Pergamon, Oxford, **1993**, chap. 1.7, pp. 239 – 275; M. W. Rathke, P. Weipert in *Comprehensive Organic Synthesis*, *Vol. 2* (Eds.: B. M. Trost, I. Fleming, C. H. Heathcock), Pergamon, Oxford, **1993**, chap. 1.8, pp. 277 – 299; I. Paterson in *Comprehensive Organic Synthesis*, *Vol. 2* (Eds.: B. M. Trost, I. Fleming, C. H. Heathcock), Pergamon, Oxford, **1993**, chap. 1.9, pp. 301 – 319; C. Gennari in *Comprehensive Organic Synthesis*, *Vol. 2* (Eds.: B. M. Trost, I. Fleming, C. H. Heathcock), Pergamon, Oxford, **1993**, chap. 2.4, pp. 629 – 660.
[114] M. Braun in *Methoden der Organischen Chemie (Houben-Weyl) 4th ed.* 1952–, Vol. E21b, **1996**, pp. 1603 – 1666.
[115] S. Kiyooka, H. Maeda, *Tetrahedron: Asymmetry* **1997**, *8*, 3371 – 3374.
[116] M. A. Blanchette, M. S. Malamas, M. H. Nantz, J. C. Roberts, R. Somfai, D. C. Whritenour, S. Masamune, *J. Org. Chem.* **1989**, *54*, 2817 – 2825.
[117] S. Kiyooka, M. A. Hena, T. Yabukami, K. Murai, F. Goto, *Tetrahedron Lett.* **2000**, *41*, 7511 – 7516.
[118] D. J. White, J. Deerberg, *Chem. Commun.* **1997**, 1919 – 1920.
[119] K. C. Nicolaou, E. J. Sorensen, *Classics in Total Synthesis*, Wiley-VCH, Weinheim, **1996**, pp. 565 – 631.
[120] I. Shiina, H. Oshiumi, M. Hashizume, Y. Yamai, R. Ibuka, *Tetrahedron Lett.* **2004**, *45*, 543 – 547.
[121] I. Shiina, M. Kubota, H. Oshiumi, M. Hashizume, *J. Org. Chem.* **2004**, *69*, 1822 – 1830.
[122] I. Shiina, M. Hashizume, Y.-S. Yamai, H. Oshiumi, T. Shimazaki, Y.-J. Takasuna, R. Ibuka, *Chem. Eur. J.* **2005**, *11*, 6601 – 6608.
[123] D. A. Evans, B. W. Trotter, P. J. Coleman, B. Cote, L. C. Dias, H. A. Rajapakse, A. N. Tyler, *Tetrahedron* **1999**, *55*, 8671 – 8726.
[124] E. M. Carreira, R. A. Singer, W. Lee, *J. Am. Chem. Soc.* **1994**, *116*, 8837 – 8838.
[125] S. D. Rychnovsky, U. R. Khire, G. Yang, *J. Am. Chem. Soc.* **1997**, *119*, 2058 – 2059.
[126] Y. Kim, R. A. Singer, E. M. Carreira, *Angew. Chem.* **1998**, *110*, 1321 – 1323; *Angew. Chem. Int. Ed.* **1998**, *37*, 1261 – 1263.
[127] D. A. Evans, J. A. Murry, M. J. Kozlowski, *J. Am. Chem. Soc.* **1996**, *118*, 5814 – 5815.
[128] D. A. Evans, P. H. Carter, E. M. Carreira, A. B. Charette, J. A. Prunet, M. Lautens, *J. Am. Chem. Soc.* **1999**, *121*, 7540 – 7552.
[129] D. A. Evans, D. Hu, J. D. Burch, G. Jaeschke, *J. Am. Chem. Soc.* **2002**, *124*, 5654 – 5655.
[130] I. Paterson, R. D. M. Davies, R. Marquez, *Angew. Chem.* **2001**, *113*, 623 – 627; *Angew. Chem. Int. Ed.* **2001**, *40*, 603 – 607.
[131] I. Paterson, R. D. M. Davies, A. C. Heimann, R. Marquez, A. Meyer, *Org. Lett.* **2003**, *5*, 4477 – 4480.
[132] B. M. Trost, O. Dirat, J. L. Gunzner, *Angew. Chem.* **2002**, *114*, 869 – 871; *Angew. Chem. Int. Ed.* **2002**, *41*, 841 – 843.
[133] B. M. Trost, J. L. Gunzner, O. Dirat, Y. H. Rhee, *J. Am. Chem. Soc.* **2002**, *124*, 10396 – 10415.
[134] H. Huang, J. S. Panek, *Org. Lett.* **2004**, *6*, 4383 – 4385.
[135] H. Huang, J. S. Panek, *Org. Lett.* **2003**, *5*, 1991 – 1993.
[136] J. Krüger, E. M. Carreira, *J. Am. Chem. Soc.* **1998**, *120*, 837 – 838.

 © 2006 Wiley-VCH Verlag GmbH & Co. KGaA, Weinheim

[137] J. Krüger, E. M. Carreira, *Tetrahedron Lett.* **1998**, *39*, 7013 – 7016.
[138] T. D. Machajewski, C.-H. Wong, *Angew. Chem.* **2000**, *112*, 1406 – 1430; *Angew. Chem. Int. Ed.* **2000**, *39*, 1352 – 1375.
[139] Y. M. A. Yamada, N. Yoshikawa, H. Sasai, M. Shibasaki, *Angew. Chem.* **1997**, *109*, 1942 – 1944; *Angew. Chem. Int. Ed. Engl.* **1997**, *36*, 1871 – 1873.
[140] K. Fujii, K. Maki, M. Kanai, M. Shibasaki, *Org. Lett.* **2003**, *5*, 733 – 736.
[141] K. Maki, R. Motoki, K. Fujii, M. Kanai, T. Kobayashi, S. Tamura, M. Shibasaki, *J. Am. Chem. Soc.* **2005**, *127*, 17111 – 17117.
[142] D. L. Boger, M. Hikota, B. M. Lewis, *J. Org. Chem.* **1997**, *62*, 1748 – 1753.
[143] B. M. Trost, H. Ito, E. R. Silcoff, *J. Am. Chem. Soc.* **2001**, *123*, 3367 – 3368.
[144] B. M. Trost, Y. S. C. Yeh, *Org. Lett.* **2002**, *4*, 3513 – 3516.
[145] B. M. Trost, M. U. Frederiksen, J. P. N. Papillon, P. E. Harrington, S. Shin, B. T. Shireman, *J. Am. Chem. Soc.* **2005**, *127*, 3666 – 3667.
[146] S. E. Denmark, S. B. D. Winter, X. Su, K.-T. Wong, *J. Am. Chem. Soc.* **1996**, *118*, 7404 – 7405.
[147] S. E. Denmark, R. A. Stavenger, *Acc. Chem. Res.* **2000**, *33*, 432 – 440.
[148] S. E. Denmark, T. Bui, *Proc. Natl. Acad. Sci. USA* **2004**, *101*, 5439 – 5444.
[149] S. E. Denmark, S. Fujimori in *Modern Aldol Reactions*, *Vol. 2* (Ed.: R. Mahrwald), Wiley-VCH, Weinheim, **2004**, pp. 229 – 326.
[150] S. E. Denmark, S. Fujimori, *J. Am. Chem. Soc.* **2005**, *127*, 8971 – 8973.
[151] a) S. E. Denmark, J. R. Heemstra, Jr., G. L. Beutner, *Angew. Chem.* **2005**, *117*, 4760 – 4777; *Angew. Chem. Int. Ed.* **2005**, *44*, 4682 – 4698; b) M. Kalesse, *Top. Curr. Chem.* **2005**, *244*, 43 – 76.
[152] P. I. Dalko, L. Moisan, *Angew. Chem.* **2004**, *116*, 5248 – 5286; *Angew. Chem. Int. Ed.* **2004**, *43*, 5138 – 5175.
[153] A. Berkessel, H. Gröger, *Asymmetric Organocatalysis*, Wiley-VCH, Weinheim, **2005**.
[154] a) B. List, *Tetrahedron* **2002**, *58*, 5573 – 5590; b) B. List, *Acc. Chem. Res.* **2004**, *37*, 548 – 557; c) B. List, *Chem. Commun.* **2006**, 819 – 824.
[155] R. O. Duthaler, *Angew. Chem.* **2003**, *115*, 1005 – 1008; *Angew. Chem. Int. Ed.* **2003**, *42*, 975 – 978.
[156] K. C. Nicolaou, S. Ninkovic, F. Sarabia, D. Vourloumis, D. He, H. Vallberg, M. R. V. Finlay, Z. Zang, *J. Am. Chem. Soc.* **1997**, *119*, 7960 – 7973.
[157] Y. Zheng, M. A. Avery, *Tetrahedron* **2004**, *60*, 2091 – 2095.
[158] E. Reyes, A. Córdova, *Tetrahedron Lett.* **2005**, *46*, 6605 – 6609.
[159] N. S. Chowdari, D. B. Ramachary, A. Córdova, C. F. Barbas III, *Tetrahedron Lett.* **2002**, *43*, 9591 – 9595.
[160] J. Casas, M. Engqvist, I. Ibrahem, B. Kaynak, A. Córdova, *Angew. Chem.* **2005**, *117*, 1367 – 1369; *Angew. Chem. Int. Ed.* **2005**, *44*, 1343 – 1345.
[161] A. Córdova, I. Ibrahem, J. Casas, H. Sundén, M. Engqvist, E. Reyes, *Chem. Eur. J.* **2005**, *11*, 4772 – 4784.
[162] A. B. Northrup, I. K. Mangion, F. Hettche, D. W. C. MacMillan, *Angew. Chem.* **2004**, *116*, 2204 – 2206; *Angew. Chem. Int. Ed.* **2004**, *43*, 2152 – 2154.
[163] A. B. Northrup, D. W. C. MacMillan, *Science* **2004**, *305*, 1725 – 1726.
[164] C. Grondal, D. Enders, *Tetrahedron* **2006**, *62*, 329 – 337.
[165] D. Enders, C. Grondal, *Angew. Chem.* **2005**, *117*, 1235 – 1238; *Angew. Chem. Int. Ed.* **2005**, *44*, 1210 – 1212.
[166] C. H. Wong, G. M. Whitesides, *Enzymes in Synthetic Organic Chemistry*, Pergamon, Oxford, **1994**.
[167] U. Bornscheuer, R. Kazlauskas, *Hydrolases in Organic Synthesis—Regio- and Stereoselective Biotransformations*, Wiley-VCH, Weinheim, **1999**.
[168] *Enzyme Catalysis in Organic Synthesis*, *2nd ed.* (Eds.: K. Drauz, H. Waldmann), Wiley-VCH, Weinheim, **2002**.
[169] W.-D. Fessner in *Modern Aldol Reactions*, *Vol. 1* (Ed.: R. Mahrwald), Wiley-VCH, Weinheim, **2004**, pp. 201 – 272.
[170] K. Koppert, R. Brossmer, *Tetrahedron Lett.* **1992**, *33*, 8031 – 8034.
[171] A. Malleron, S. David, *New J. Chem.* **1996**, *20*, 153 – 159.
[172] K. Matsumoto, M. Shimagaki, T. Nakata, T. Oishi, *Tetrahedron Lett.* **1993**, *34*, 4935 – 4938.
[173] M. Shimagaki, H. Muineshima, M. Kubota, *Chem. Pharm. Bull.* **1993**, *41*, 282 – 286.

© 2006 Wiley-VCH Verlag GmbH & Co. KGaA, Weinheim

Vesicles

DOI: 10.1002/anie.200600688

Self-Assembled Vesicles from an Amphiphilic *ortho*-Phenylene Ethynylene Macrocycle**

*Sang Hyuk Seo, Ji Young Chang, and Gregory N. Tew**

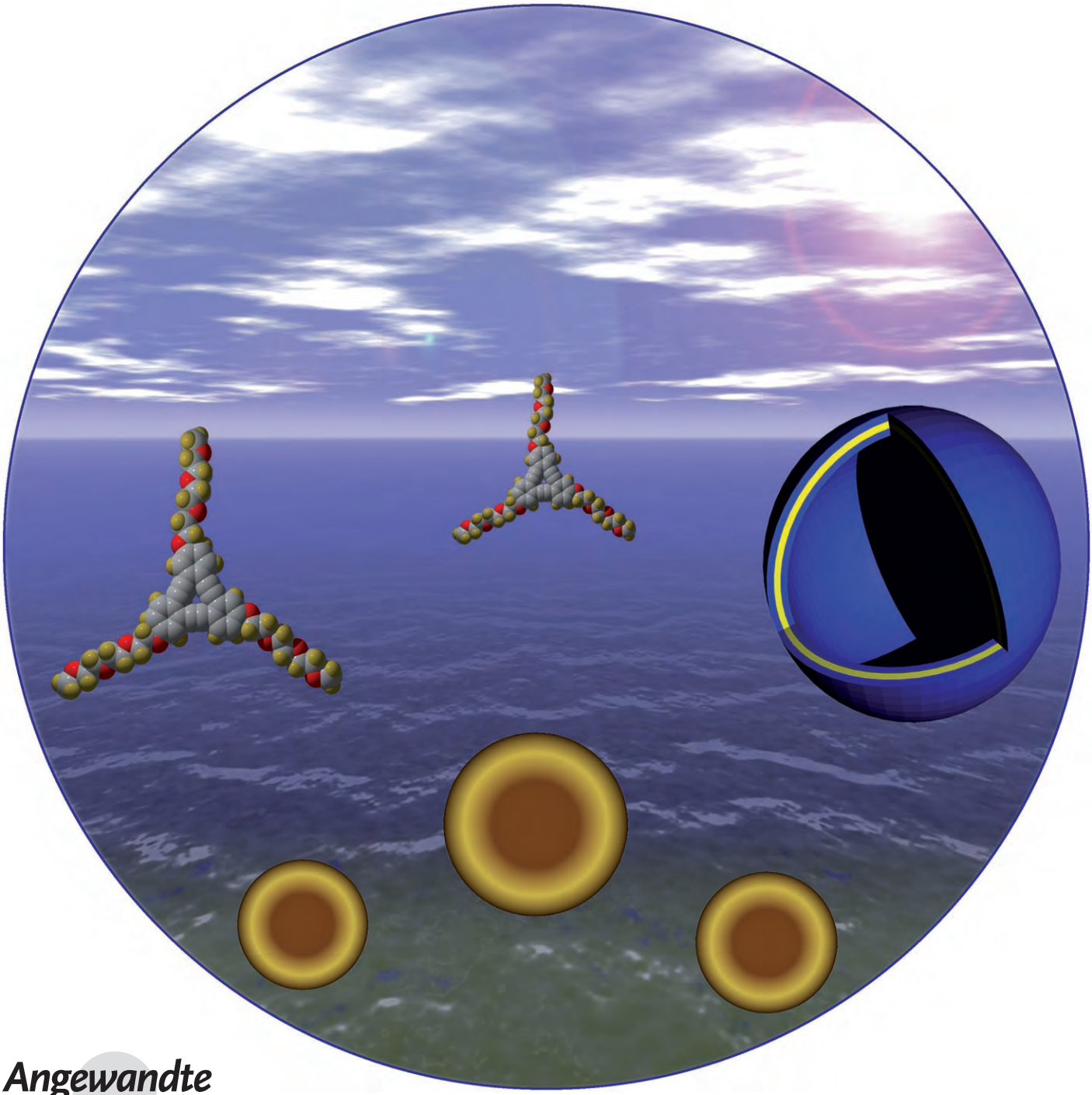

WILEY InterScience DISCOVER SOMETHING GREAT

© 2006 Wiley-VCH Verlag GmbH & Co. KGaA, Weinheim

Amphiphilic molecules, namely those that carry both hydrophilic and hydrophobic parts within one structure, self-assemble into an amazing variety of structures:[1] for example, micellar structures (usually globular), ellipsoids, disks, cylinders, vesicles, and lamellae.[2] This assembly usually depends strongly on the molecular architecture, concentration, and solvent environment. Of these geometric forms, vesicles (enclosed spherical bilayer assemblies) have attracted much attention from a fundamental perspective as well as for their potential applications in drug or gene delivery, nanotechnology, and as model systems of biomembranes.[3,4a] Block copolymers that assemble into vesicles have attracted considerable attention.[4] In contrast, other than classical head-group surfactants and phospholipids, relatively few small synthetic molecules are known that spontaneously self-assemble into vesicles. Recent exceptions include facially amphiphilic segmented dendrimers as well as functionalized calixarenes, cyclodexdrins, and cucurbit[6]urils.[5] The calixarenes, cyclodexdrins, and cucurbit[6]urils all have built-in curvature that promotes vesicle formation. Growing the number of molecular architectures that spontaneously form vesicular structures remains an important goal that will increase understanding and widen applications. Herein we report vesicle formation from a new molecular architecture, an amphiphilic, discotic *ortho*-phenylene ethynylene (*o*-PE) macrocycle.

Phenylene ethynylene and other shape-persistent cyclic structures remain of great interest in the fields of supramolecular chemistry and materials science because of their unique properties.[6] Recently, we reported the synthesis and columnar hexagonal liquid-crystalline properties of this novel triethylene glycol (TEG) substituted triangular-shaped macrocycle.[7] As well as these bulk properties, the rigid, hydrophobic core and polar, flexible side chains suggested that this molecule might display interesting self-assembly behavior in aqueous solutions. This amphiphilic macrocycle self-assembles into vesicles with average diameter of approximately 500 nm from solutions in chloroform/H_2O (1:1).[8] The vesicular morphologies of this amphiphilic macrocycle were studied by atomic force microscopy (AFM) and transmission electron microscopy (TEM). The assembled vesicles are robust enough to be dried onto a carbon surface and examined by AFM without collapse. The vesicles collapsed following exposure to the high vacuum of TEM, as confirmed by AFM, but otherwise the morphology remains unchanged. To our knowledge, this is the first example of a vesicle formed from an amphiphilic discotic macrocycle.

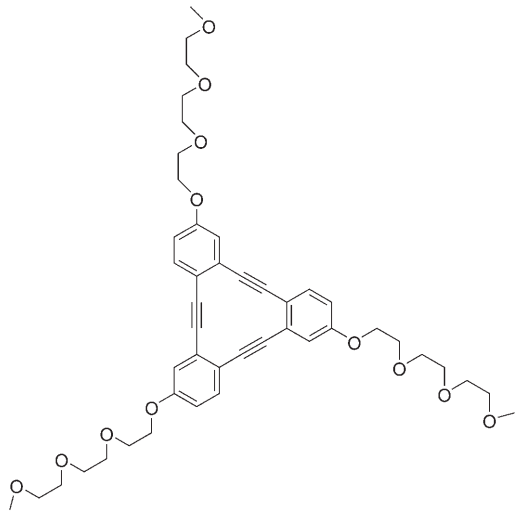

1

The morphological properties of these self-assembled vesicles were initially examined by AFM. Height and phase AFM images of the structures obtained from aqueous solutions of macrocycle **1** at two different magnifications and from two different samples are shown in Figure 1 a–d. These AFM images show spherical aggregates with diameters in the range of 200 nm to 1 μm. AFM cross-sectional analysis (Figure 1 f) of a typical structure shows that the diameters of the vesicles (650 nm) are generally seven- or eight-times larger than the heights of the vesicles (83 nm). This observation is consistent with deformation of a spherical vesicle following adsorption onto the carbon surface of the copper grid and indicates that these structures are robust yet soft enough to deform upon drying.

A histogram of 270 structures collected from several samples gives an average diameter for the vesicles of 493 nm (Figure 2). Light scattering measurements confirm the presence of vesicles in solution and provide an average diameter of 516 nm, which is in excellent agreement with the AFM results. TEM images (Figure 3) reveal structures with diameters of around 500 nm as well as a few larger structures (for example, only 2 of 57 structures in Figure 3 e, or 3.5%, are larger than 1 μm).

Figure 3 shows a series of six TEM images (some stained with RuO_4 for different time periods) and confirms that the structures previously observed by AFM are vesicles. The sizes and diameters of these spherical vesicles observed by TEM are similar to those visualized by AFM. Samples observed without staining (Figure 3 a,b) revealed circular forms with dark outlines, which is consistent with vesicle formation. Images of stained samples (Figure 3 c–f) confirm the presence

[*] Prof. G. N. Tew
Polymer Science and Engineering Department
University of Massachusetts
Amherst, MA 01003 (USA)
Fax: (+1) 413-545-0082
E-mail: tew@mail.pse.umass.edu
Homepage: http://www.pse.umass.edu/tew/
S. H. Seo, Prof. J. Y. Chang
School of Materials Science and Engineering, and
Hyperstructured Organic Materials Research Center
Seoul National University
Seoul 151-742 (Korea)

[**] We thank the NSF for financial support (NSF CAREER CHE-0449663). This work used MRSEC facilities supported by the NSF (DMR 9400488). G.N.T thanks the ARO and ONR Young Investigator programs in addition to the PECASE program, 3M Nontenured faculty grant, and Dupont Young Faculty Award for generous support. The BK 21 Project and HOMRC (S.H.S and J.Y.C) are gratefully acknowledged. The frontispiece was created by Jacob Gagnon.

 © 2006 Wiley-VCH Verlag GmbH & Co. KGaA, Weinheim

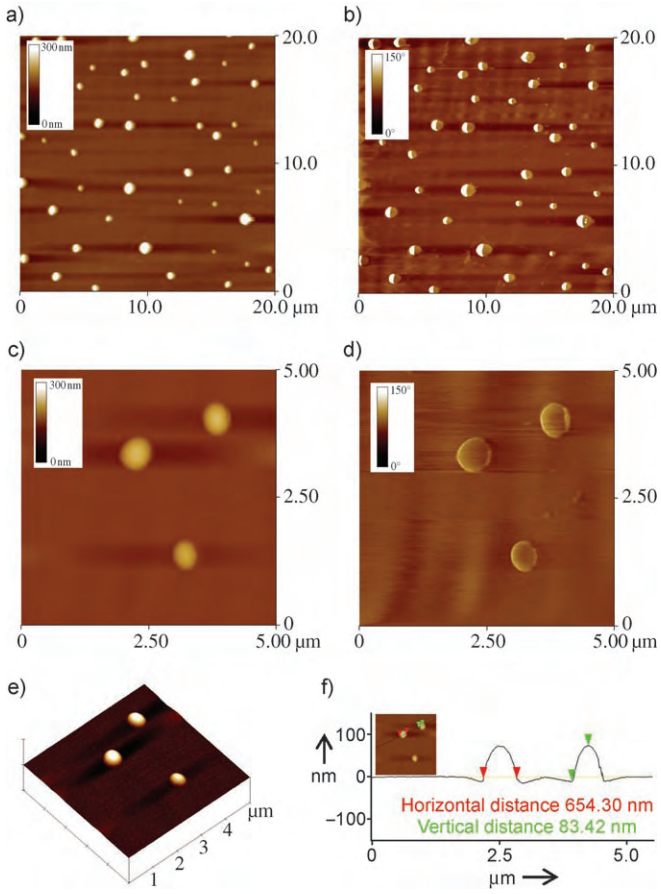

Figure 1. Tapping-mode AFM images of vesicles formed by **1** on a carbon-coated copper grid: a,c) height images; b,d) phase images; e) 3D image; and f) cross-sectional analysis.

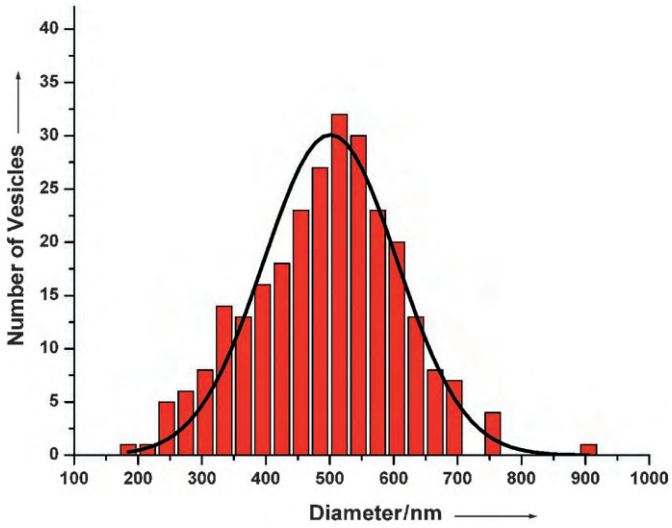

Figure 2. Diameter histogram obtained from 270 vesicles observed by AFM (the maximum of the fitted distribution is at 493 nm).

of spherical assemblies with a dark outer ring expected from the 2D projection of vesicular structures typically observed by TEM.[9] Figure 3d contains one large (ca. 1 µm) vesicle; the image was enlarged approximately 100 times (not shown) so

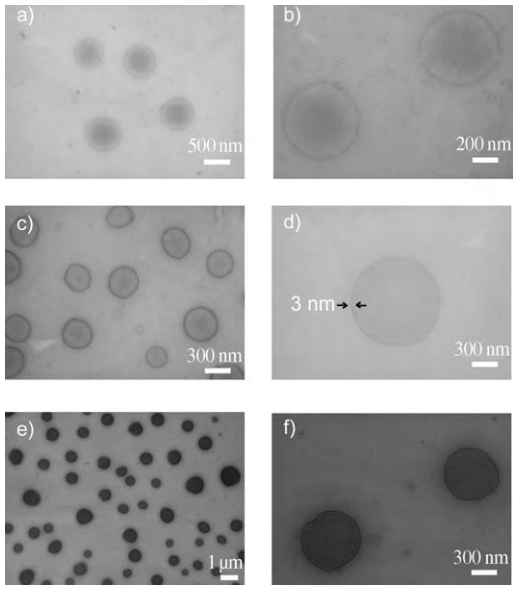

Figure 3. TEM images of vesicles of **1**: a,b) without staining; c,d) stained for 15 minutes; and e,f) stained for 45 minutes [with RuO_4 (0.05 wt% solution)]. d) The bilayer thickness is 3 nm.

that the shell thickness could be measured. The width of the dark line around the exterior is approximately 3 nm. This image provides the clearest measurement of shell thickness of all TEM images collected. Similar shell thicknesses are observed in Figure 3a,b but the shells are lighter because of the lack of staining whereas heavier staining (Figure 3e,f) increases the thickness of the dark line as staining penetrates the collapsed structure. Therefore, this measurement of approximately 3 nm collected from Figure 3d is the most accurate and represents an upper limit of shell dimensions. It is an upper limit because the TEM is a 2D projection of a 3D object in which the maximum contrast corresponds to the thickest part of the structure. As the sample is stained for longer, the contrast is lost as the entire object becomes darker. In view of the wall thickness of approximately 3 nm and the molecular dimensions of macrocycle **1**, we postulate that the macrocycle packs into a bilayer structure with the phenylene ethynylene core toward the interior of the bilayer and the more polar TEG side chains exposed to solvent. This is illustrated schematically in Figure 4 and supported by the TEM, AFM, and light-scattering data.

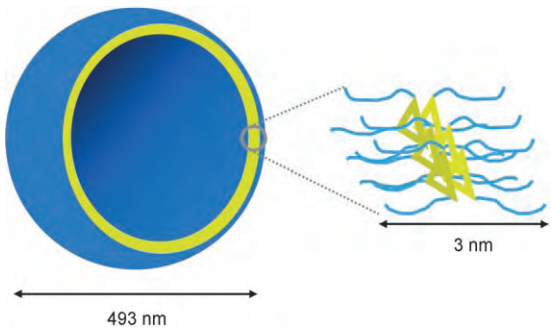

Figure 4. A schematic illustration of the bilayered unilamellar vesicle characterized by AFM and TEM images.

 © 2006 Wiley-VCH Verlag GmbH & Co. KGaA, Weinheim

To collect further evidence for the hollow spherical vesicle, the same samples used previously for AFM and TEM were reinvestigated by AFM. Unlike AFM images obtained before TEM, the 2D and 3D AFM images in Figure 5 show spherical aggregates with collapsed centers.

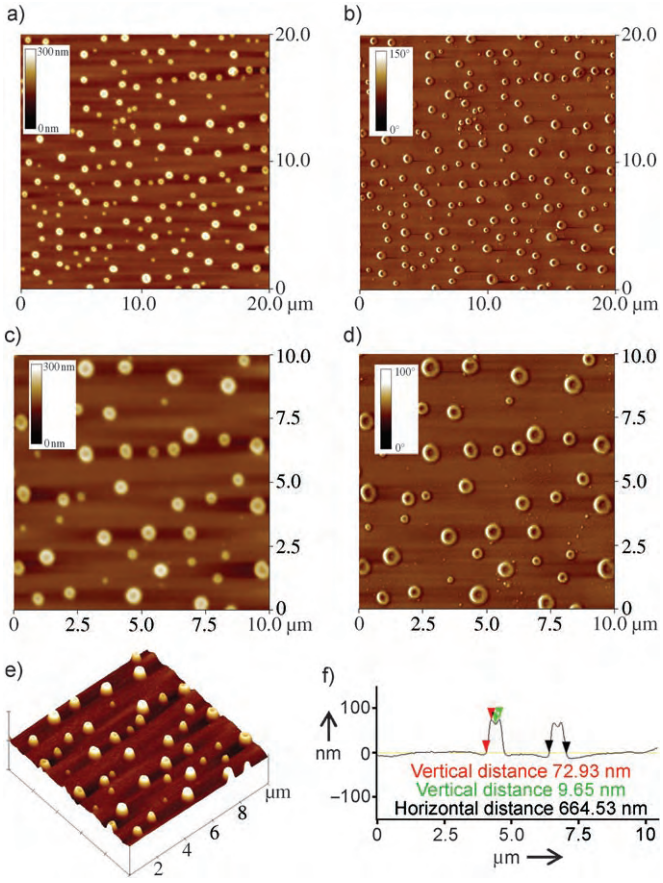

Figure 5. Tapping-mode AFM images of vesicles after TEM measurement: a,c) height images; b,d) phase images; e) 3D image; and f) cross-sectional analysis. These images show that the vesicles have collapsed after exposure to high vacuum.

The diameters of the vesicles are the same before and after exposure to the high vacuum of TEM, which indicates that no significant morphological changes occurred other than the collapse. Figures 1 f and 5 f show the cross-sectional analyses of vesicles with similar sizes (about 650 nm) obtained before and after TEM analysis, respectively. The vertical distance, or height, of the vesicle in Figure 1 f is about 83 nm compared with 73 nm in Figure 5 f, whereas Figure 5 f shows a depressed center consistent with a collapsed vesicle following exposure to high vacuum.[9] AFM was able to capture fractured vesicles before exposure to high vacuum, thus providing additional evidence that the initial structures observed by AFM are vesicles.[9]

In summary, the novel ethylene oxide substituted triangular macrocycle based on *ortho*-phenylene ethynylene was shown to self-assemble from aqueous chloroform into vesicles. AFM and TEM were used to characterize these assemblies with a bilayer wall thickness of about 3 nm and average diameter of around 500 nm. This is the first demonstration of vesicle self-assembly from discotic liquid-crystalline molecules and suggests the design parameters for vesicle formation may be broader than expected.

Received: February 21, 2006
Revised: July 25, 2006
Published online: September 26, 2006

Keywords: amphiphiles · macrocycles · self-assembly · vesicles

[1] a) J. P. Hill, W. Jin, A. Kosaka, T. Fukushima, H. Ichihara, T. Shimomura, K. Ito, T. Hashizume, N. Ishii, T. Aida, *Science* **2004**, *304*, 1481 – 1483; b) V. Percec, A. E. Dulcey, V. S. K. Balagurusamy, Y. Miura, J. Smidrkal, M. Peterca, S. Nummelin, U. Edlund, S. D. Hudson, P. A. Heiney, H. Duan, S. N. Magonov, S. A. Vinogradov, *Nature* **2004**, *430*, 764 – 768; c) L. Chen, Y. Yuan, J. S. Helm, Y. Hu, Y. Rew, D. Shin, D. L. Boger, S. Walker, *J. Am. Chem. Soc.* **2004**, *126*, 7462 – 7463; d) K. Brandenburg, L. Hawkins, P. Garidel, J. Andrä, M. Müller, H. Heine, M. H. J. Koch, U. Seydel, *Biochemistry* **2004**, *43*, 4039 – 4046; e) N. Nuraje, I. A. Banerjee, R. I. MacCuspie, L. Yu, H. Matsui, *J. Am. Chem. Soc.* **2004**, *126*, 8088 – 8089; f) G. Li, W. Fudickar, M. Skupin, A. Klyszcz, C. Draeger, M. Lauer, J.-H. Fuhrhop, *Angew. Chem.* **2002**, *114*, 1906 – 1931; *Angew. Chem. Int. Ed. Angew. Chem. Int. Ed. Engl.* **2002**, *41*, 1828 – 1852; g) M. Lee, J.-W. Kim, S. Peleshanko, K. Larson, Y.-S. Yoo, D. Vaknin, S. Markutsya, V. V. Tsukruk, *J. Am. Chem. Soc.* **2002**, *124*, 9121 – 9128.

[2] a) W. Zhou, W. Gu, Y. Xu, C. S. Pecinovsky, D. L. Gin, *Langmuir* **2003**, *19*, 6346 – 6348; b) M. Kölbel, T. Beyersdorff, C. Tschierske, S. Diele, J. Kain, *Chem. Eur. J.* **2000**, *6*, 3821 – 3837; c) M. Yoshio, T. Mukai, H. Ohno, T. Kato, *J. Am. Chem. Soc.* **2004**, *126*, 994 – 995; d) J. H. Jung, S. Shinkai, T. Shimizu, *Chem. Eur. J.* **2002**, *8*, 2684 – 2690; e) J.-M. Lehn, *Angew. Chem.* **1990**, *102*, 1347 – 1362; *Angew. Chem. Int. Ed. Engl.* **1990**, *29*, 1304 – 1319; f) B. Angelov, A. Angelova, M. Ollivon, C. Bourgaux, A. Campitelli, *J. Am. Chem. Soc.* **2003**, *125*, 7188 – 7189; g) R. Auzély-Velty, T. Benvegnu, D. Plusquellec, G. Mackenzie, J. A. Haley, J. W. Goodby, *Angew. Chem.* **1998**, *110*, 2665 – 2668; *Angew. Chem. Int. Ed.* **1998**, *37*, 2511 – 2515; h) K. Borisch, S. Diele, P. Göring, H. Kresse, C. Tschierske, *Angew. Chem.* **1997**, *109*, 2188 – 2190; *Angew. Chem. Int. Ed. Engl.* **1997**, *36*, 2087 – 2089; i) B. Chen, U. Baumeister, S. Diele, M. K. Das, X. Zeng, G. Ungar, C. Tschierske, *J. Am. Chem. Soc.* **2004**, *126*, 8608 – 8609.

[3] a) T. M. Allen, P. R. Cullis, *Science* **2004**, *303*, 1818 – 1822; b) A. Mueller, D. F. O'Brien, *Chem. Rev.* **2002**, *102*, 727 – 758; c) R. Blumenthal, M. J. Clague, S. R. Durell, R. M. Epand, *Chem. Rev.* **2003**, *103*, 53 – 70.

[4] a) D. E. Discher, A. Eisenberg, *Science* **2002**, *297*, 967 – 973; b) B. M. Discher, Y. Y. Won, D. S. Ege, J. C. M. Lee, F. S. Bates, D. E. Discher, D. A. Hammer, *Science* **1999**, *284*, 1143 – 1146; c) L. Zhang, K. Yu, A. Eisenberg, *Science* **1996**, *272*, 1777 – 1779; d) H. Shen, A. Eisenberg, *Angew. Chem.* **2000**, *112*, 3448 – 3450; *Angew. Chem. Int. Ed.* **2000**, *39*, 3310 – 3312; e) I. Gitsov, K. L. Wooley, J. M. J. Fréchet, *Angew. Chem.* **104**, 1282 – 1285; *Angew. Chem. Int. Ed. Engl.* **1992**, *31*, 1200 – 1202; f) J. P. Spatz, S. Möβmer, M. Möller, *Angew. Chem.* **1996**, *108*, 1673 – 1676; *Angew. Chem. Int. Ed. Engl.* **1996**, *35*, 1510 – 1512; g) A. Harada, K. Kataoka, *Science* **1999**, *283*, 65 – 67; h) F. Chécot, S. Lecommandoux, Y. Gnanou, H.-A. Klok, *Angew. Chem.* **2002**, *114*, 1395 – 1399; *Angew. Chem. Int. Ed.* **2002**, *41*, 1339 – 1343; i) A. Kros, W. Jesse, G. N. Metselaar, J. J. L. M. Cornelissen, *Angew. Chem.* **2005**, *117*, 4423 – 4426; *Angew. Chem. Int. Ed.* **2005**, *44*, 4349 – 4352; j) E. P. Holowka, D. J. Pochan, T. J. Deming, *J. Am. Chem. Soc.* **2005**, *127*, 12423 – 12428; k) J. Du, Y. Chen, Y.

 © 2006 Wiley-VCH Verlag GmbH & Co. KGaA, Weinheim

Zhang, C. C. Han, K. Fischer, M. Schmidt, *J. Am. Chem. Soc.* **2003**, *125*, 14710 – 14711; l) D. M. Vriezema, J. Hoogboom, K. Velonia, K. Takazawa, P. C. M. Christianen, J. C. Maan, A. E. Rowan, R. J. M. Nolte. *Angew. Chem.* **2003**, *115*, 796 – 800; *Angew. Chem. Int. Ed.* **2003**, *42*, 772 – 776; m) A. P. H. J. Schenning, B. de Bruin, M. C. Feiters, R. J. M. Nolte, *Angew. Chem.* **1994**, *106*, 1741 – 1742; *Angew. Chem. Int. Ed. Engl.* **1994**, *33*, 1662 – 1663.

[5] a) M. Yang, W. Wang, F. Yuan, Z. Zhang, J. Li, F. Liang, B. He, B. Minch, G. Wegner, *J. Am. Chem. Soc.* **2005**, *127*, 15107 – 15111; b) Y. Tanaka, M. Miyachi, Y. Kobuke, *Angew. Chem.* **1999**, *111*, 565 – 567; *Angew. Chem. Int. Ed.* **1999**, *38*, 504 – 506; c) M. Lee, S.-J. Lee, L.-H. Jiang, *J. Am. Chem. Soc.* **2004**, *126*, 12724 – 12725; d) H.-K. Lee, K. M. Park, Y. J. Jeon, D. Kom, D. Y. Oh, H. S. Kim, C. K. Park, K. Kim, *J. Am. Chem. Soc.* **2005**, *127*, 5006 – 5007; e) B. J. Ravoo, R. Darcy, *Angew. Chem.* **2000**, *112*, 4494 – 4496; *Angew. Chem. Int. Ed.* **2000**, *39*, 4324 – 4326; f) T. Imura, H. Yanagishita, D. Kitamoto, *J. Am. Chem. Soc.* **2004**, *126*, 10804 – 10805.

[6] a) J. S. Moore, *Acc. Chem. Res.* **1997**, *30*, 402; b) R. Faust, *Angew. Chem.* **1998**, *110*, 2985 – 2988; *Angew. Chem. Int. Ed.* **1998**, *37*, 2825 – 2828; c) U. H. F. Bunz, Y. Rubin, *Chem. Soc. Rev.* **1999**, *28*, 107 – 119; d) S. Höger, *J. Polym. Sci. Part A* **1999**, *37*, 2685 – 2698; e) M. M. Haley, J. J. Pak, S. C. Brand, *Top. Curr. Chem.* **1999**, *201*, 81 – 130; f) S. Shotwell, P. M. Windscheif, M. D. Smith, U. H. F. Bunz, *Org. Lett.* **2004**, *6*, 4151 – 4154; g) S. Höger, D. L. Morrison, V. Enkelmann, *J. Am. Chem. Soc.* **2002**, *124*, 6734 – 6736; h) S. Höger, S. Rosselli, A.-D. Ramminger, V. Enkelmann, *Org. Lett.* **2002**, *4*, 4269 – 4272; i) T. V. Jones, R. A. Blatchly, G. N. Tew, *Org. Lett.* **2003**, *5*, 3297 – 3299; j) R. A. Blatchly, G. N. Tew, *J. Org. Chem.* **2003**, *68*, 8780 – 8785; k) T. V. Jones, M. M. Slutsky, R. Laos, T. F. A. de Greef, G. N. Tew, *J. Am. Chem. Soc.* **2005**, *127*, 17235 – 17240.

[7] S. H. Seo, H. Seyler, J. O. Peters, T. V. Jones, T. H. Kim, J. Y. Chang, G. N. Tew, *J. Am. Chem. Soc.*, **2006**, *128*, 9264 – 9265.

[8] Vesicles were prepared by two separate methods that yield identical structures: 1) A solution of **1** in chloroform (1×10^{-3} M) was dropped on a carbon-coated copper grid and an equal volume of deionized water was subsequently placed on top of the solution. The copper grid was removed and dried under a nitrogen stream at room temperature. 2) A solution of **1** in chloroform (1×10^{-3} M) was mixed with water to yield a 1:1 mixture in a small vial. After manual shaking, the organic solution was taken from the vial and cast onto a carbon-coated copper grid placed on filter paper and dried under a nitrogen stream.

[9] See the Supporting Information for more details.

 © 2006 Wiley-VCH Verlag GmbH & Co. KGaA, Weinheim

Chemoselective Hydrogenation

DOI: 10.1002/anie.200603408

Tilt the Molecule and Change the Chemistry: Mechanism of S-Promoted Chemoselective Catalytic Hydrogenation of Crotonaldehyde on Cu(111)**

*May E. Chiu, David J. Watson, Georgios Kyriakou, Mintcho S. Tikhov, and Richard M. Lambert**

The chemoselective hydrogenation of α,β-unsaturated carbonyl compounds to form unsaturated alcohols is challenging, fundamentally interesting, and important both in the research laboratory and on a technical scale, as these materials are valuable and versatile intermediates in the production of fine chemicals and pharmaceuticals. Thermodynamics favors hydrogenation of the C=C bond to form the (unwanted) saturated aldehyde or ketone as shown in Scheme 1, which refers to the particular case of crotonaldehyde. Thus chemoselective C=O hydrogenation is a demanding process that requires the manipulation of kinetic effects by means of a suitable catalyst.

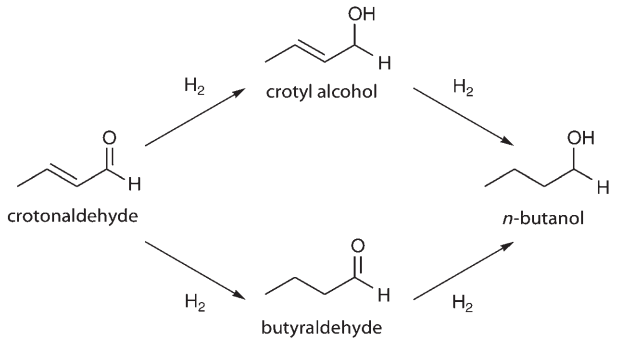

Scheme 1. Possible hydrogenation products of crotonaldehyde.

A variety of supported metal-particle catalysts (including Pt, Pd, Cu, Ag, Au, Ir, and Os) that exhibit a wide range of chemoselectivity have been investigated for this purpose,[1] though very little has emerged in terms of fundamental understanding. Theoretical studies[2] suggest that the adsorption geometry of the reactant molecule may be a key

[*] M. E. Chiu, Dr. D. J. Watson, Dr. G. Kyriakou, Dr. M. S. Tikhov, Prof. R. M. Lambert
Department of Chemistry
University of Cambridge
Lensfield Road
Cambridge CB21EW (UK)
Fax: (+44) 1223-336-362
E-mail: rml1@cam.ac.uk

[**] The authors thank Dr. M. Barnaba, Dr. L. Petaccia, and Dr. S. Lizzit for their support during synchrotron experiments. M.E.C. acknowledges the financial support of the Cambridge University Oppenheimer Trust.

InterScience
© 2006 Wiley-VCH Verlag GmbH & Co. KGaA, Weinheim

parameter in these systems, although direct experimental evidence for such effects is almost wholly lacking. Prompted by the striking findings of Hutchings and co-workers,[3] who reported that adsorbed sulfur strongly promoted the selectivity of practical dispersed Cu catalysts for production of crotyl alcohol from crotonaldehyde, we recently carried out a limited preliminary investigation[4] into the effects of a high coverage of sulfur (κ_S) on the adsorption and reactivity of crotonaldehyde on Cu(111). It was found that at a fractional surface coverage of $\kappa_S = 0.43$, sulfur activated the otherwise inert copper surface towards the formation of crotyl alcohol, albeit with very low efficiency, and an approximate evaluation of its effects on reactant adsorption geometry was performed, however, interpretation was restricted by the presence of a mixture of chemisorbed states.

Here, we present the results of a comprehensive investigation of crotonaldehyde hydrogenation on Cu(111) under very well defined conditions that enable determination of the reaction mechanism and elucidation of the mode of promoter action. By means of high-resolution X-ray photoelectron spectroscopy (XPS) and near-edge X-ray absorption on fine structure (NEXAFS) studies, it is found that a very low sulfur coverage can induce 100% conversion of adsorbed crotonaldehyde into crotyl alcohol, with essentially 100% selectivity. By isolating the S-modified state and by taking advantage of the specificity of NEXAFS for the detection of double bonds and the ability of synchrotron photoemission to resolve chemically distinct species, we were able to follow the conversion of reactant into product and determine the orientation of both species with respect to the surface. This is an unprecedented observation of the evolution of a relatively complex surface-catalyzed reaction by these techniques, or indeed by any other technique.

Synchrotron radiation experiments were performed at the ELETTRA synchrotron radiation facility in Trieste (Italy). Deposition of sulfur and crotonaldehyde was monitored directly by using fast-XPS. Crotonaldehyde was dosed by backfilling the vacuum chamber with an accurately measured pressure of the vapor, and sulfur was produced as a beam of S_2 molecules generated by a solid-state electrochemical source.[5] Because dissociative chemisorption of dihydrogen on Cu(111) is significantly activated, hydrogen was supplied by means of a collimated hot filament atomizer.[6] This delivered a flux of hydrogen atoms directly to the sample surface, thus enabling the deposition of hydrogen with high coverages on a convenient timescale. NEXAFS intensity data were analyzed by following established standard methodology.[7]

Previous work established that the hydrogen-covered Cu(111) surface was completely inert towards crotonaldehyde hydrogenation,[4] and control experiments showed that maximum chemical activity occurred at a sulfur coverage of $\kappa_S = 0.16$ ($\kappa = 1$ corresponds to the atom density of Cu(111), 1.77×10^{15} atoms cm^{-2}). Accordingly, all the data were acquired with $\kappa_S = 0.16$. Figure 1A shows C 1s fast-XPS data acquired during exposure of the sulfur-predosed Cu(111) surface to crotonaldehyde at 153 K. The spectra consist of two peaks in 3:1 intensity ratio, consistent with the presence of intact crotonaldehyde.[4,8] The peak with higher intensity that appears at lower binding energy is assigned to the three

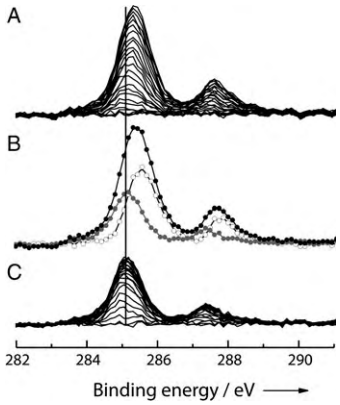

Figure 1. C 1s fast-XPS uptake of crotonaldehyde on the S-promoted Cu(111) surface ($\kappa_S = 0.16$) at 153 K (A) and 173 K (C). The S-bound state is isolated at 173 K. The decomposition of A into two components is shown in B: gray filled circles denote the S-bound state, and unfilled circles denote the unperturbed state.

carbon atoms of the CH_3CHCH moiety: the lower intensity, higher binding energy peak is attributed to the carbonyl carbon atom, in agreement with expectation. It is clear that the molecule binds in two chemically distinct states, one associated with S-modified sites (285.10 eV) and the other being characteristic of adsorption at unperturbed sites (285.55 eV). Figure 1B shows a decomposition of the C 1s spectrum into its two components. The S-modified state, which is populated first, is the more strongly adsorbed state of the two and could therefore be isolated by carrying out the adsorption at 173 K (Figure 1C). Both states exhibit a 3:1 peak intensity ratio, indicating the presence of two distinct kinds of intact crotonaldehyde molecules.

C K-edge NEXAFS spectra for the isolated S-modified state were recorded at five photon-incidence angles (θ, defined relative to the surface plane) to determine the orientation of the C=C and C=O bonds with respect to the surface. (It is known that in the absence of S, the molecule lies essentially flat on Cu(111).[4]) Figure 2A shows the raw data, which exhibit two π^* resonances centered at 282.30 and 284.45 eV: these may be assigned with confidence to the C=C and C=O bonds, respectively.[4,8–9] Simple inspection shows

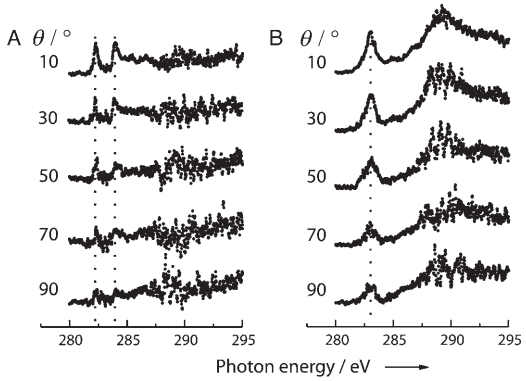

Figure 2. A) C K-edge NEXAFS of crotonaldehyde on Cu(111) predosed with S atoms ($\kappa_S = 0.16$). B) NEXAFS of the same surface taken immediately after dosing H atoms.

 © 2006 Wiley-VCH Verlag GmbH & Co. KGaA, Weinheim

that both resonances are most intense at near-grazing photon incidence; moreover, on going towards normal incidence the relative intensity (I_θ) of the 284.45 eV resonance decreases fastest. We may immediately infer that both double bonds are tilted with respect to the surface, with the C=C bond significantly more tilted more than the C=O bond.

The S-promoted hydrogenation reaction was studied by preadsorbing crotonaldehyde at 173 K followed by dosing with atomic hydrogen ($\kappa_H \approx 0.7$), immediately after which the XPS and NEXAFS data were recorded. Hydrogen treatment caused a remarkable change in the NEXAFS spectra (Figure 2B). The resonances at 282.30 and 284.45 eV corresponding to C=C and C=O bonds, respectively, were replaced by a single resonance at 282.92 eV. Clearly, a reaction had occurred leading to the hydrogenation of one of the double bonds: the question is, which one? XPS provided an unambiguous answer as illustrated in Figure 3, which shows

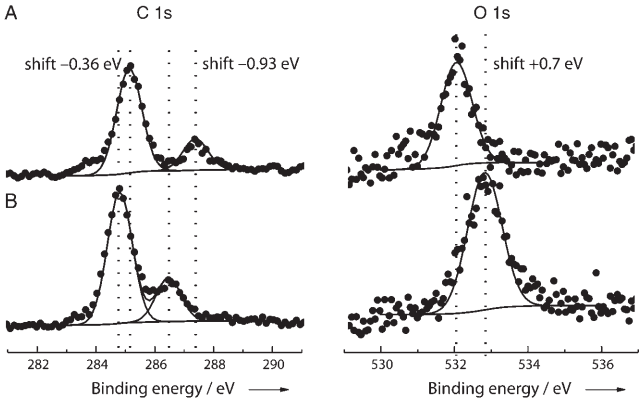

Figure 3. C 1s and O 1s XPS recorded before (A) and after (B) the hydrogen dose. Clear shifts in the spectra indicate that the formation of crotyl alcohol is achieved with 100% conversion and selectivity.

C 1s and O 1s XPS before (top) and after (bottom) addition of hydrogen. The spectra obtained before addition of hydrogen are exactly as expected for crotonaldehyde; the positions of the carbonyl C 1s emission peak and the O 1s emission are characteristic of the C=O double bond.[10] After dosing with hydrogen, the C 1s and O 1s spectra were both markedly different: the entire C 1s spectrum shifts to lower binding energy, and crucially, the carbonyl peak shifts by a substantially greater amount. Conversely, the O 1s emission shifted to higher binding energy, consistent with S-induced valence charge transfer away from the oxygen atom thus activating the C=O bond towards hydrogenation. Both observations are diagnostic of the formation of a C–O single bond,[10] demonstrating unequivocally that chemoselective hydrogenation to form crotyl alcohol had occurred. We may therefore assign the single NEXAFS resonance in Figure 2B to the C=C bond of the unsaturated alcohol. Note that the chemoselective reaction occurred on a timescale that was short compared with the observation time ($\approx$10 min) with 100% conversion of the reactant at 100% selectivity.

The tilt angles of all three double bonds were evaluated by standard procedures,[9] which involved fitting the observed photon-incidence-angle dependence (normalized to $I_{10°}$) to the theoretically calculated dependence for a series of trial bond orientations. The optimum fits are shown in Figure 4, from which it is apparent that the C=C bond in crotonaldehyde is tilted with respect to the surface by approximately 36°

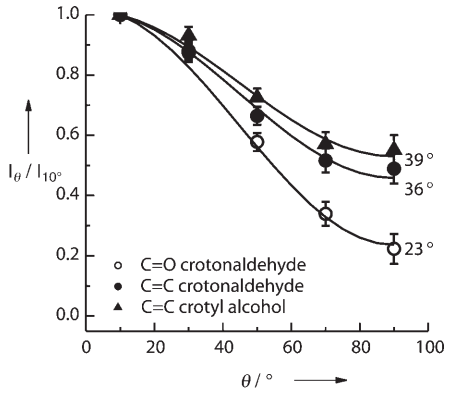

Figure 4. Full analysis of normalized π* intensities plotted against the photon-incidence angle (θ), showing the tilt angles of each double bond with respect to the surface.

whereas the C=O bond is tilted by about 23°. These results, taken with the XPS data, provide a plausible explanation for the activation of Cu by S and the observed 100% selectivity towards crotyl alcohol formation (see below). Sulfur strongly perturbs the carbonyl function of crotonaldehyde (XPS), activating it towards hydrogenation whilst also inducing a pronounced tilt of the C=C function away from the surface (NEXAFS), rendering it immune from attack by hydrogen atoms, thus favoring formation of the unsaturated alcohol. Interestingly, a similar pronounced C=C tilt angle is also present in the crotyl alcohol product ($\approx$39°) suggesting that this bond in the unsaturated alcohol should also be protected against hydrogenation, inhibiting its further hydrogenation to yield *n*-butanol, which would be the thermodynamically favored product. As we shall see, this ultraselective behavior was observed over the entire range of reactant conversion. (Note that Wahlström et al.[11] reported an ordered $(\sqrt{43} \times \sqrt{43})R7.5°$ S overlayer structure in the sulfur coverage regime relevant to the present work. Whether S-crotonaldehyde steric repulsion or some other type of interaction is responsible for C=C tilting can only be determined by theory, and such calculations are planned.[12])

The S-promoted surface reaction was studied in more detail by stepwise incremental addition of hydrogen atoms to preadsorbed crotonaldehyde at 173 K, with XPS and grazing-incidence NEXAFS data recorded after each dose of hydrogen (Figure 5). It is apparent that successive doses of hydrogen resulted in progressive changes in shapes and positions of the π* resonances. At 4 minutes hydrogen exposure, the intensity of the C=O peak diminished whilst the C=C resonance broadened. Eventually, with increasing amounts of added hydrogen, the carbonyl resonance disappeared altogether and the C=C resonance shifted to 282.92 eV, characteristic of crotyl alcohol.

The corresponding C 1s and O 1s XPS data shown in Figure 6A and C are in excellent accord with the NEXAFS

 © 2006 Wiley-VCH Verlag GmbH & Co. KGaA, Weinheim

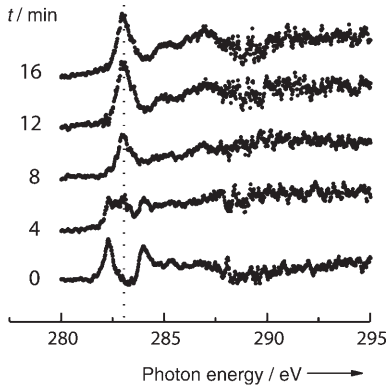

Figure 5. C K-edge NEXAFS acquired at $\theta = 10°$ after each hydrogen atom dose.

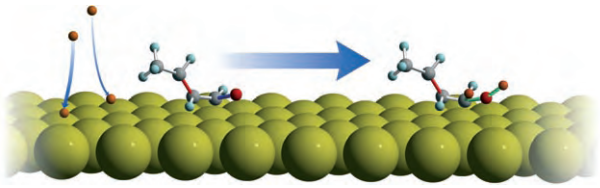

Figure 7. Schematic representation of the surface-mediated hydrogenation of crotonaldehyde to crotyl alcohol. The C=C and C=O bonds of crotonaldehyde are colored red and blue, respectively. When hydrogen atoms (orange) impinge upon the surface, the C=O bond is hydrogenated while the C=C bond is left intact; the newly formed single bonds are shown in green. Note that in this mechanism the geometry of the reactively formed crotyl alcohol is essentially the same as that of its parent crotonaldehyde.

results and serve to illustrate the changes in electronic structure of the surface species during progressive conversion of reactant into product. As the conversion proceeds, both the C 1s and the O 1s emission initially broaden and then converge on the characteristic spectra of crotyl alcohol. These results permit estimation of the reaction selectivity. By fitting the spectra with two Gaussian components, the separate contributions from crotonaldehyde and crotyl alcohol may be quantified. The corresponding integrated intensities are plotted in Figure 6B, from which it is clear that at every stage of reaction, conversion of crotonaldehyde into crotyl alcohol proceeds with 100% chemoselectivity, leading ultimately to 100% conversion of the reactant. Note that C 1s and O 1s data mirror each other extremely closely, providing strong confirmation of these conclusions. Finally, Figure 7 shows a plausible structural model that is consistent with our findings.

In summary, we have shown that X-ray absorption spectroscopy and photoemission may be used to elucidate the mechanism of a demanding, interesting, and relatively complex catalytic reaction in considerable detail. The chemoselective process in question is prototypical of an important class of heterogeneous reactions that are of potential technical importance. Sulfur strongly promotes catalytic activity by electronically perturbing the target C=O bond and at the same time strongly tilting the C=C bond away from the surface, rendering it immune to attack by hydrogen adatoms, thus favoring chemoselective hydrogenation. The strongly tilted C=C configuration is retained in the product molecule, similarly inhibiting its further hydrogenation to the thermodynamically favored saturated alcohol. The success of the strategy used here suggests that many other catalytic systems of fundamental interest and practical importance could be similarly investigated.

Experimental Section

High-resolution XPS and NEXAFS were used to examine surface composition, adsorbate electronic structure, and orientation of the C=C and C=O bonds in crotonaldehyde in the presence of hydrogen atoms. These measurements were carried out on the SuperESCA beamline at the ELETTRA synchrotron radiation facility in Trieste (Italy). XPS and NEXAFS spectra were collected using a double-pass 32-channel hemispherical electron analyzer. The degree of linear polarization of the photons was 0.99. The angle between the entrance lens of the analyzer and the incoming photon beam was 70° in the horizontal plane. Photon-incidence and photon-detection angles during XPS experiments were fixed at 8° and 78°, respectively. The data were processed in accordance with standard methodology.[7] Note that the XPS binding-energy scale is referenced to the Cu $3p_{3/2}$ line at 75.0 eV (the NEXAFS photon-energy scale is uncor-

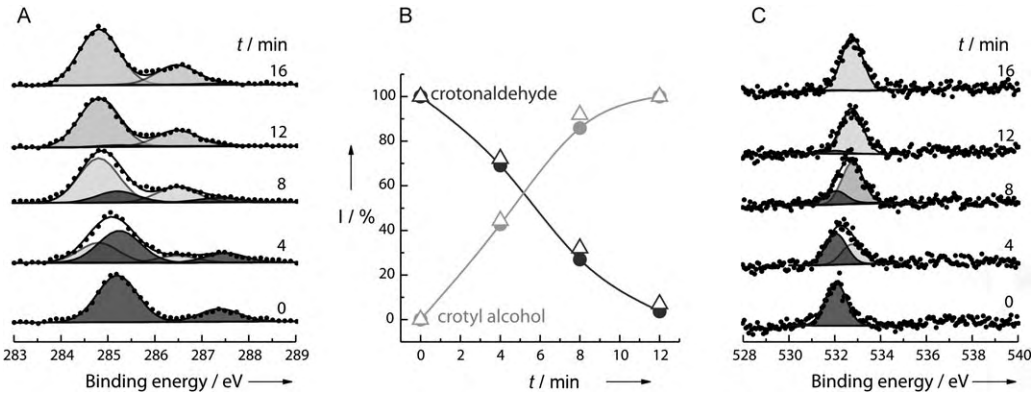

Figure 6. C 1s (A) and O 1s (C) XPS spectra acquired after each hydrogen dose; crotonaldehyde peaks are shaded dark gray, and crotyl alcohol peaks are shaded light gray. B) Normalized integrated XPS peak intensities (I) showing the evolution of crotyl alcohol with the consumption of crotonaldehyde (time of hydrogen dose plotted). Circles denote C 1s data, and triangles correspond to O 1s data.

© 2006 Wiley-VCH Verlag GmbH & Co. KGaA, Weinheim

rected). The Cu(111) surface was cleaned by Ar^+ bombardment at 800 K, followed by annealing in vacuum at 800 K. Reagent-grade crotonaldehyde (> 99.9 %, Sigma Aldrich) was purified before use by means of freeze–pump–thaw cycles and dosed by backfilling the vacuum chamber with an accurately measured vapor pressure; surface coverages were calibrated by fast XPS. Crotonaldehyde was dosed at 173 K to ensure the isolation of the desired surface state; subsequent XPS and NEXAFS spectra were recorded at 168 K to limit desorption from the surface. Dissociative chemisorption of dihydrogen on Cu(111) is activated and therefore extremely slow under ultrahigh-vacuum conditions; accordingly a hot filament source[6] was used to generate a flux of hydrogen atoms, thus enabling the required hydrogen coverages to be achieved on a convenient timescale (173 K). Sulfur was deposited (298 K) using a solid-state electrochemical source[5] that produced a beam of S_2 molecules, enabling precise control of S coverage.

Received: August 20, 2006
Published online: October 24, 2006

Keywords: heterogeneous catalysis · hydrogenation · reaction mechanisms · sulfur · X-ray absorption spectroscopy

[1] P. Gallezot, D. Richard, *Catal. Rev. Sci. Eng.* **1998**, *40*, 81.
[2] F. Delbecq, P. Sautet, *J. Catal.* **2002**, *211*, 398.
[3] G. J. Hutchings, F. King, I. P. Okoye, M. B. Padley, C. H. Rochester, *J. Catal.* **1994**, *148*, 453.
[4] M. E. Chiu, G. Kyriakou, F. J. Williams, D. J. Watson, M. S. Tikhov, R. M. Lambert, *Chem. Commun.* **2006**, 1283.
[5] a) C. Wagner, *J. Chem. Phys.* **1953**, *21*, 1819; b) W. Heegemann, K. H. Meister, E. Bechtold, K. Hayek, *Surf. Sci.* **1975**, *49*, 161.
[6] a) M. F. Luo, D. A. MacLaren, I. G. Shuttleworth, W. Allison, *Chem. Phys. Lett.* **2003**, *381*, 654; b) T. Kammler, J. Kuppers, *J. Chem. Phys.* **1999**, *111*, 8115.
[7] a) D. A. Outka, J. Stohr, *J. Chem. Phys.* **1988**, *88*, 3539; b) J. Stohr, D. A. Outka, *Phys. Rev. B* **1987**, *36*, 7891.
[8] A. J. Urquhart, F. J. Williams, O. P. H. Vaughan, R. L. Cropley, R. M. Lambert, *Chem. Commun.* **2005**, 1977.
[9] F. Bournel, C. Laffon, Ph. Parent, G. Tourillon, *Surf. Sci.* **1996**, *350*, 60.
[10] J. F. Moulder, W. F. Stickle, P. E. Sobol, K. D. Bomben, *Handbook of X-ray Photoelectron Spectroscopy* (Eds.: J. C. Chastain, R. C. King), Perkin Elmer Corporation, Physical Electronics, **1992**.
[11] E. Wahlström, I. Ekvall, H. Olin, S.-A. Lindgren, L. Walldén, *Phys. Rev. B* **1999**, *60*, 10699.
[12] C. Kolczewski, K. Hermann, unpublished results.

 © 2006 Wiley-VCH Verlag GmbH & Co. KGaA, Weinheim

Polymer Nanostructures

DOI: 10.1002/anie.200602116

Fabrication of Hollow Capsules Composed of Poly(methyl methacrylate) Stereocomplex Films**

*Toshiyuki Kida, Masataka Mouri, and Mitsuru Akashi**

Considerable effort has been devoted to the development of nanostructured particles constructed by the self-assembly of polymeric systems.[1] In particular, polymeric hollow capsules have attracted much attention in the biomedical and pharmaceutical fields,[2] since they can be utilized as drug carriers and containers in which sensitive biomolecules can be preserved. The construction of hollow capsules of uniform size and controlled film thickness has been efficiently carried out by the deposition of polymer films onto the surface of colloidal core templates through the layer-by-layer (LbL) technique and the subsequent removal of the template cores.[3] However, this method has been limited to the preparation of hollow capsules composed of polyelectrolyte multilayers based on electrostatic interactions,[4] except for a few cases reported by Zhang et al.[5] and Sukhishvili et al.[6] where hollow capsules were prepared using the hydrogen-bonding interactions between the uncharged polymers.[7] Much less attention has been paid to hollow capsules composed of nonionic multilayers constructed through their van der Waals interactions, possibly because these hollow capsules were believed to be easily ruptured after the removal of the template core on account of the much weaker van der Waals interactions. Hollow capsules composed of nonionic multilayers can be expected to possess a shell permeability and morphology unlike those of conventional hollow capsules composed of polyelectrolyte multilayers.

Poly(methyl methacrylate) (PMMA) has found many applications in the biomedical field as a result of its excellent biocompatibility. The stereoregular PMMA stereocomplex, which is a double-stranded helical assembly formed with van der Waals interactions between isotactic (it) and syndiotactic

[*] Dr. T. Kida, M. Mouri, Prof. M. Akashi
Department of Applied Chemistry
Graduate School of Engineering
Osaka University
2-1 Yamadaoka, Suita, Osaka 565-0871 (Japan)
Fax: (+81) 6-6879-7359
E-mail: akashi@chem.eng.osaka-u.ac.jp
Homepage: http://www.chem.eng.osaka-u.ac.jp/~akashi-lab/

[**] The authors appreciate the technical support for the living anionic polymerization by Prof. Tatsuki Kitayama (Osaka University) and the TEM observations by Prof. Akio Takaoka and Toshiaki Hasegawa (Research Center for Ultrahigh-Voltage Electron Microscopy, Osaka University). This work was financially supported by a Grant-in-Aid for Scientific Research (No. 15655041) from the Ministry of Education, Culture, Sports, Science, and Technology of Japan.

Supporting information for this article is available on the WWW under http://www.angewandte.org or from the author.

WILEY InterScience DISCOVER SOMETHING GREAT
© 2006 Wiley-VCH Verlag GmbH & Co. KGaA, Weinheim

(st) PMMA units,[8] has been used as a component of hollow-fiber membranes for artificial dialysis.[9] Recently, our research group prepared stable, ultrathin films of double-stranded PMMA stereocomplex by the alternate LbL assembly of it- and st-PMMA on a solid substrate.[10] The application of these it-/st-PMMA stereocomplex films to the hollow capsule shell allows the construction of novel hollow capsules of nonionic multilayers based on their van der Waals interactions. Herein, we report the preparation of hollow capsules composed of PMMA stereocomplex multilayer shells by a combination of the alternate LbL assembly of it- and st-PMMA and the silica template method.

The fabrication of hollow capsules of it-/st-PMMA stereocomplex was carried out according to the process shown in Figure 1. We chose silica particles as the template core, as

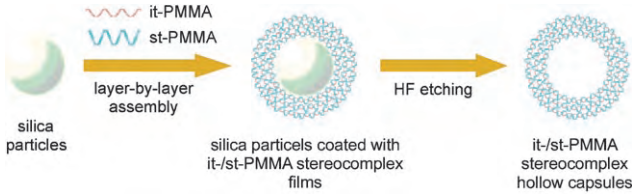

Figure 1. Fabrication process of it-/st-PMMA stereocomplex hollow capsules.

silica can be readily removed from the particles coated with polymer films by treatment with aqueous HF.[5,11] Acetonitrile/water (9:1) was chosen as the immersion solvent, since this solvent should make it possible to deposit a relatively large amount of the LbL assembly composed of PMMA stereocomplex onto the silica particles, in accordance with previous results on the alternate LbL assembly of it- and st-PMMA onto a Au plate.[10] Silica nanoparticles with a diameter of 330 nm were alternately immersed in acetonitrile/water (9:1) solutions (25 mL) of it-PMMA ($M_n = 20400$, $M_w/M_n = 1.21$; isotactic (mm)/heterotactic (mr)/syndiotactic (rr) triads = 99:1:0) and st-PMMA ($M_n = 73200$, $M_w/M_n = 1.20$; mm/mr/rr = 1:9:90). The immersion process was continued for ten cycles to afford ten double layers of it- and st-PMMA. The resulting particles were then treated with 2.3% aqueous HF to remove the silica cores. Inductively coupled plasma (ICP) emission analysis of the obtained particles indicated that more than 99.8% of the Si atoms were removed from the film-coated silica particles by HF etching.

Figure 2b and c shows the transmission electron microscopic (TEM) images of silica particles coated with PMMA film and PMMA hollow capsules, respectively. These images clearly indicate that the PMMA films were constructed on the surface of the silica particles, and PMMA hollow capsules were successfully fabricated by the removal of the silica core from the core–shell particles without any damage to the shell. The PMMA hollow capsules have a spherical shape with an average diameter of 510 nm, and their shell thickness is approximately 90 nm. The scanning electron microscope (SEM) images of silica particles coated with PMMA film and PMMA hollow capsules are shown in the Supporting Information. Self-assembled multilayer films of it- or st-

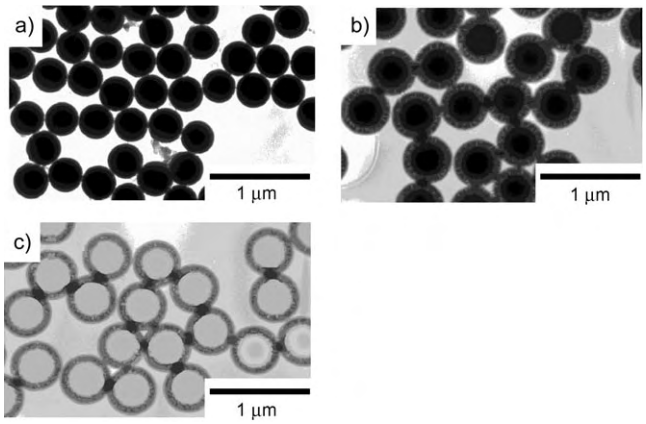

Figure 2. TEM images of a) bare silica particles, b) PMMA film-coated silica particles, and c) PMMA hollow capsules obtained after HF etching.

PMMA alone were not formed on the silica particles, in accordance with the previous result on the LbL assembly of it- or st-PMMA onto a Au plate.[10] This finding shows that the formation of a stereocomplex between it- and st-PMMA is a crucial driving force for the construction of the PMMA multilayered film on a silica particle.

X-ray diffraction (XRD) analysis and infrared (IR) spectroscopy are effective methods for evaluating the formation of a stereocomplex between stereoregular PMMAs. The XRD patterns of the particles before (Figure 3b) and after the HF etching of PMMA film-coated silica particles (Figure 3a) showed two peaks characteristic of the PMMA stereocomplex ($2\theta = 11$ and 15°),[12] whose peaks were significantly different from those of it- and st-PMMA. This result clearly indicates that films of PMMA stereocomplex were formed on the silica surface by the LbL assembly of it- and st-PMMA. This stereocomplex structure was maintained even after the removal of the silica template. In the FTIR/

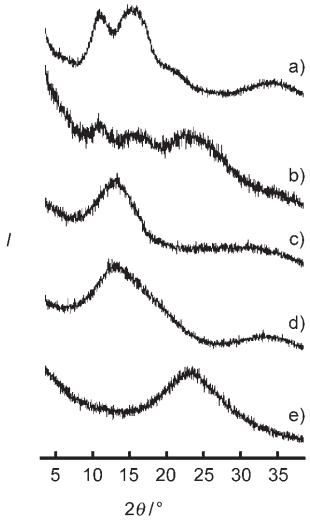

Figure 3. XRD patterns of a) PMMA hollow capsules obtained after HF etching, b) PMMA film-coated silica particles, c) it-PMMA, d) st-PMMA, and e) bare silica particles.

© 2006 Wiley-VCH Verlag GmbH & Co. KGaA, Weinheim

attenuated total reflection (ATR) spectra of the PMMA hollow capsules obtained after removal of the silica core (Figure 4a), absorption peaks corresponding to the C=O stretching vibrations and the main-chain CH_2 rocking vibrations of the PMMA stereocomplex were observed at around 1750 and 860 cm^{-1}, respectively,[8,10,13] thus strongly supporting the formation of hollow capsules of the PMMA stereocomplex.

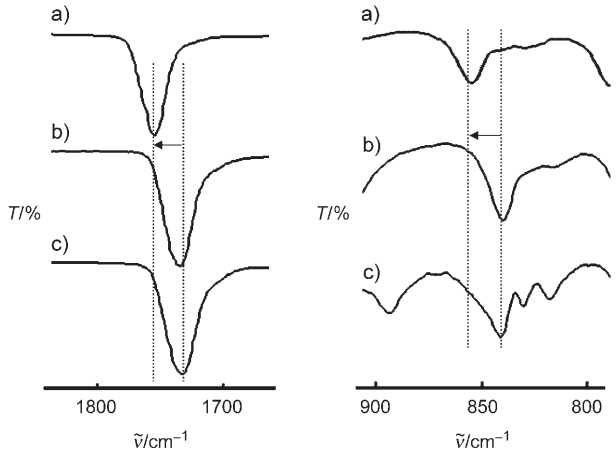

Figure 4. FTIR/ATR spectra of a) PMMA hollow capsules, b) it-PMMA, and c) st-PMMA.

In conclusion, we have demonstrated that hollow capsules of PMMA stereocomplex were successfully fabricated by a combination of LbL assembly of the stereocomplex and the silica template method. To the best of our knowledge, this is the first example of hollow capsules composed of nonionic multilayers constructed through van der Waals interactions. We believe that these PMMA stereocomplex hollow capsules are potentially applicable as drug carriers and containers. Replacement of the st-PMMA with st-poly(methacrylic acid) (st-PMAA) in the stereocomplex shell will allow construction of pH-responsive hollow capsules, as the st-PMAA is readily and selectively extracted from the it-PMMA/st-PMAA stereocomplex shell by an alkaline aqueous solution.[14]

Experimental Section

it-PMMA ($M_n = 20400$, $M_w/M_n = 1.21$; mm/mr/rr = 99:1:0) and st-PMMA ($M_n = 73200$, $M_w/M_n = 1.20$; mm/mr/rr = 1:9:90) were synthesized by conventional anionic polymerization using MMA monomers and the appropriate initiators (t-C_4H_9MgBr and t-$C_4H_9Li/(C_2H_5)_3Al$ for it- and st-PMMA, respectively).[15] Silica nanoparticles with a diameter of 330 nm (180 mg) were alternately immersed in acetonitrile/water (9:1) solutions (25 mL) of it- and st-PMMA (both concentrations were 1.7 mg mL^{-1}) for 15 min at 25 °C under gentle shaking. After each immersion, the silica nanoparticles were rinsed with acetonitrile/water (9:1). The immersion process was continued for ten cycles to afford ten double layers of it- and st-PMMA. The resulting particles were then treated with 2.3 % aqueous HF for 12 h at 25 °C to remove the silica cores.

Received: May 27, 2006
Revised: July 29, 2006
Published online: October 20, 2006

Keywords: multilayers · nanostructures · polymers · template synthesis · thin films

[1] a) D. E. Discher, A. Eisenberg, *Science* **2002**, *297*, 967–973; b) L. M. Bronstein in *Encyclopedia of Nanoscience and Nanotechnology*, *Vol. 7* (Eds.: H. S. Nalwa), American Scientific Publishers, Los Angeles, **2004**, 193–206.
[2] W. Meier, *Chem. Soc. Rev.* **2000**, *29*, 295–303, and references therein.
[3] a) F. Caruso, *Chem. Eur. J.* **2000**, *6*, 413–419; b) P. T. Hammond, *Adv. Mater.* **2004**, *16*, 1271–1293.
[4] a) A. A. Antipov, G. B. Sukhorukov, *Adv. Colloid Interface Sci.* **2004**, *111*, 49–61; b) L. Dähne, C. S. Peyratout, *Angew. Chem.* **2004**, *116*, 3850–3872; *Angew. Chem. Int. Ed.* **2004**, *43*, 3762–3783.
[5] Y. Zhang, Y. Guan, S. Yang, J. Xu, C. C. Han, *Adv. Mater.* **2003**, *15*, 832–835.
[6] a) V. Kozlovskaya, S. Ok, A. Sousa, M. Libera, S. A. Sukhishvili, *Macromolecules* **2003**, *36*, 8590–8592; b) E. Kharlampieva, V. Kozlovskaya, J. Tyutina, S. A. Sukhishvili, *Macromolecules* **2005**, *38*, 10523–10531.
[7] W. B. Stockton, M. F. Rubner, *Macromolecules* **1997**, *30*, 2717–2725.
[8] a) J. Spěváček, B. Schneider, *Adv. Colloid Interface Sci.* **1987**, *27*, 81–149; b) E. Schomaker, G. Challa, *Macromolecules* **1989**, *22*, 3337–3341.
[9] B. Bikson, J. K. Nelson, N. Muruganandam, *J. Membr. Sci.* **1994**, *94*, 313–328.
[10] T. Serizawa, K. Hamada, T. Kitayama, N. Fujimoto, K. Hatada, M. Akashi, *J. Am. Chem. Soc.* **2000**, *122*, 1891–1899.
[11] a) P. Schuetz, F. Caruso, *Adv. Funct. Mater.* **2003**, *13*, 929–937; b) Y. Itoh, M. Matsusaki, T. Kida, M. Akashi, *Chem. Lett.* **2004**, *33*, 1552–1553.
[12] E. J. Vorenkamp, F. Bosscher, G. Challa, *Polymer* **1979**, *20*, 59–64.
[13] a) J. Spěváček, B. Schneider, *J. Polym. Sci. Part C* **1974**, *12*, 349–353; b) J. Dybal, J. Stokr, B. Schneider, *Polymer* **1983**, *24*, 971–980; c) J. Spěváček, B. Schneider, *J. Polym. Phys. Ed.* **1984**, *22*, 617–635; d) J. Dybal, J. Spěváček, B. Schneider, *J. Polym. Sci. Part B* **1986**, *24*, 657–674; e) O. N. Tretinnikov, K. Nakano, K. Ohta, R. Iwamoto, *Macromol. Chem. Phys.* **1996**, *197*, 753–765.
[14] T. Serizawa, K. Hamada, T. Kitayama, M. Akashi, *Angew. Chem.* **2003**, *115*, 1150–1153; *Angew. Chem. Int. Ed.* **2003**, *42*, 1118–1121.
[15] a) K. Hatada, K. Ute, K. Tanaka, Y. Okamoto, T. Kitayama, *Polym. J.* **1986**, *18*, 1037–1047; b) T. Kitayama, T. Shinozaki, T. Sakamoto, M. Yamamoto, K. Hatada, *Makromol. Chem.* **1989**, *15*, 167–185; c) K. Hatada, T. Kitayama, *Polym. Int.* **2000**, *49*, 11–47.

 © 2006 Wiley-VCH Verlag GmbH & Co. KGaA, Weinheim

DNA Replication

DOI: 10.1002/anie.200602113

Rolling-Circle Amplification of a DNA Nanojunction**

*Chenxiang Lin, Mingyi Xie, Julian J. L. Chen, Yan Liu, and Hao Yan**

The field of structural DNA nanotechnology has seen exciting progress in recent years in using branched DNA junctions as building blocks for nanoconstruction.[1,2] One limiting factor in scaling up this technology is the cost of synthesizing DNA oligonucleotides. Thus, an immediate challenge is to develop efficient strategies to replicate branched DNA nanojunctions. However, the presence of a junction structure and the topology of the branched DNA nanostructure make it difficult for polymerase enzymes to pass through, preventing PCR from being a viable approach for this purpose. Prior outstanding efforts toward replicating DNA nanostructures involved either applying chemical copying mechanisms[3] or generating a long scaffolding DNA strand (through a plasmid DNA cloning method) that can fold into a unique nanostructure[4] through the assistance of added smaller synthetic DNA oligonucleotides. To date, the whole structure of branched DNA has not been replicated by using only enzymatic reactions.

Rolling-circle amplification (RCA) is an isothermal enzymatic DNA replication process that uses certain DNA polymerases to generate long single-stranded DNA (ssDNA) with tandem repeats of the complementary sequence of a single-stranded circular DNA template.[5] Such a process is initiated by the hybridization of a linear DNA primer to the circular DNA template. In the presence of dNTP, ϕ29 DNA polymerase adds nucleotides to the 3′ end of the primer strand and replicates the DNA around the template circle continuously with the preceding strand displaced from the template. The linear ssDNA product synthesized by RCA consists of several hundred tandem repeats of the template sequence. Recently, Mao and co-workers[6] and Simmel and co-workers[7] have used RCA to obtain long linear DNA strands to organize metallic nanoparticles into one-dimensional arrays with well-defined interparticle distances.

Previous studies demonstrated that the ϕ29 DNA polymerase can unwind DNA duplexes efficiently and is capable of strand displacement for processive DNA synthesis on a circular DNA template.[8–11] It has been shown that the ϕ29 DNA polymerase can overcome certain local topological constraints, such as circular padlock DNA probes hybridized with a linear DNA target or catenated to a circular DNA strand. The DNA strands causing the topological constraints can be displaced when ϕ29 DNA polymerase processes along the circle template. As the circle DNA templates themselves do not contain stable secondary structures or topological constraints, it is still not clear if RCA can work effectively on a circular template that has a stable secondary structures.

In this study, we chose a four-arm DNA junction as a target to replicate by using RCA. We aim to address the following two critical questions: 1) can RCA replicate a DNA junction that contains a specific secondary structure and topology, and 2) how efficient would the replication be? Our data suggest that this DNA polymerase can readily overcome the stable Holliday junction structure in the single-stranded circular template and replicate the DNA nanostructure efficiently.

Scheme 1 illustrates the amplification cycle of the four-arm DNA strand by using the RCA strategy. This 93-nucleotide ssDNA, termed as the sense (+) strand, folds into a Holliday four-way junction.[12] This cloverleaf-shaped structure contains two 5-base-pair (bp) arms, a 9-bp arm, and

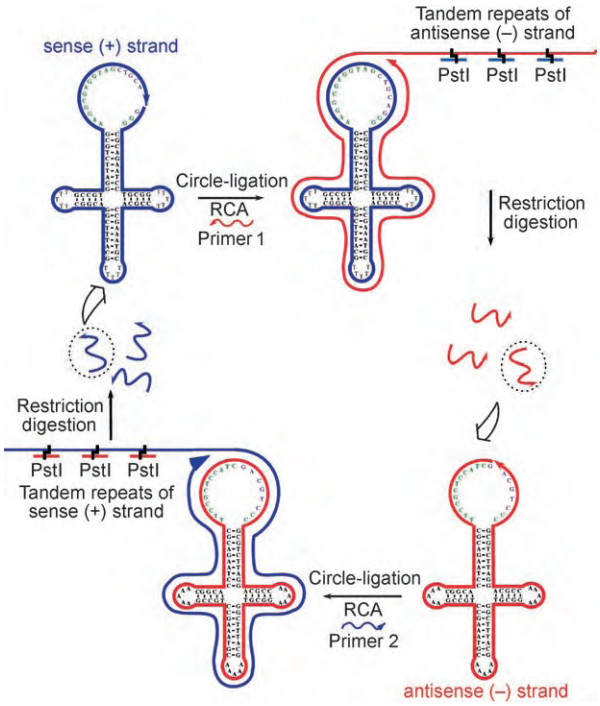

Scheme 1. Schematic diagram of the DNA nanojunction amplification cycle.

[*] C. Lin, M. Xie, Prof. Dr. J. J. L. Chen, Dr. Y. Liu, Prof. Dr. H. Yan
Department of Chemistry and Biochemistry
Arizona State University
Tempe, AZ 85287 (USA)
Fax: (+1) 480-727-2378
E-mail: hao.yan@asu.edu
C. Lin, Dr. Y. Liu, Prof. Dr. H. Yan
The Biodesign Institute
Arizona State University
Tempe, AZ 85287 (USA)
Prof. Dr. J. J. L. Chen
School of Life Sciences
Arizona State University
Tempe, AZ 85287 (USA)

[**] This work has been supported by grants from the NSF (CCF-0453685, CCF-0453686, and CTS-0545652) and research grants from the Biodesign Institute at ASU to H.Y.

Supporting information for this article is available on the WWW under http://www.angewandte.org or from the author.

© 2006 Wiley-VCH Verlag GmbH & Co. KGaA, Weinheim

a 10-bp arm. The three shorter arms are each enclosed with a TTTTT pentaloop. The 10-bp arm has a 5′ overhang of three nucleotides (nt) and a 3′ overhang of 17 nt. The 5′ and 3′ ends of the DNA can be covalently ligated by a ssDNA ligase, CircLigase (Epicentre Biotech). Once closed, this 20-nt single-stranded loop serves as a primer-binding site for the RCA reaction. This loop also contains a restriction site (purple-colored bases) for the restriction enzyme PstI. To replicate the sense (+) DNA strand, two sequential RCA reactions need to be carried out. In the first phase of the cycle, ϕ29 DNA polymerase synthesizes a linear strand of DNA from the circularized sense (+) strand template following the hybridization of the primer 1 (red). This long ssDNA product consists of tandem repeats of a DNA sequence that is complementary to the template. To convert these tandem repeats to its monomeric units, the restriction helper strand 1 (a 15-base oligonucleotide) was annealed to the DNA product to form cleavable restriction sites for the PstI enzyme along the repeating sequences. After the restriction digestion by the PstI enzyme, individual copies of the antisense (−) DNA strands were released and purified by denaturing PAGE. In the second phase of the cycle, the antisense (−) strands were circularized and used as a template in the next RCA reaction to generate sense (+) DNA strands. The antisense:sense amplification uses primer 2 and restriction helper strand 2 and follows the same procedures described above.

To determine the efficiency of the RCA replication, DNA samples from each step of the amplification cycles were analyzed by denaturing PAGE (Figure 1). The yield of the circularization reaction by CircLigase is near 100% for both the sense (+) and antisense (−) DNA strands (see Figure 1a and 2b, compare lanes 1 and 2). The long DNA products amplified by RCA reactions (Figure 1a and b, lane 3) were digested by PstI enzyme to give rise to monomers of the linear DNA nanojunction with an expected size (lane 4). The amplification yield of RCA is about 12-fold for the sense:antisense reaction, and about 200-fold for the antisense:sense reaction. The difference in amplification efficiency is speculated to result from the difference in the sequence between the sense (+) and antisense (−) strands. The overall yield could be further improved by optimizing the digestion conditions as a fraction of DNA products were not fully digested (Figure 1b, lane 4). Different restriction enzymes could also be chosen to achieve higher digestion efficiency. Under optimal condition, one full cycle of two sequential RCA reactions is expected to amplify the DNA sense strands at least 2400-fold.

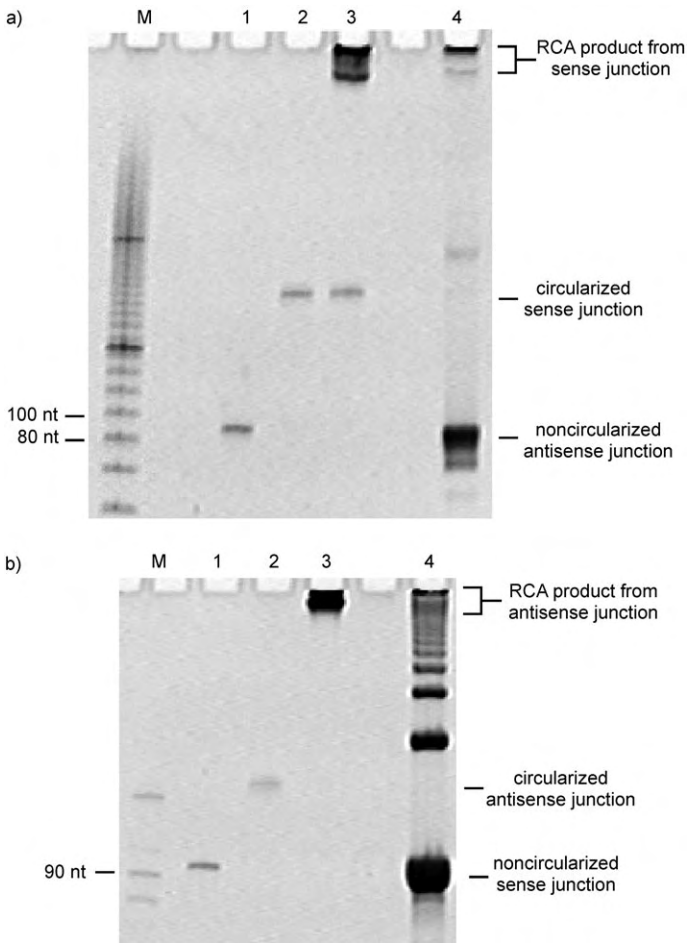

Figure 1. Amplification efficiency of DNA nanojunction through RCA. a) The first phase of the RCA cycle. Lane M: 20-bp ladder; lane 1: linear sense strand (LSS; 1 pmol); lane 2: after circle ligation; lane 3: after RCA; lane 4: after PstI digestion. Lanes 2–4 each contain products started from LSS (1 pmol). The major band in lane 4 was cut and eluted, yielding linear antisense strand (LAS, 12.3 pmol). b) The second phase of the RCA cycle. Lane M: 10-nt ssDNA ladder; lane 1: LAS (2 pmol); lane 2: after circle ligation; lane 3: after RCA products; lane 4; after PstI digestion. Lanes 2 and 4 each contain products that started from LAS (2 pmol), and lane 3 contains products from LAS (0.5 pmol). The major band in lane 4 was cut and eluted, yielding LSS (420 pmol).

Three control experiments were performed to confirm the expected formation of the four-way junction in the amplified DNA nanostructure. First, proper folding of the DNA strand was tested by a gel-mobility shift assay (Figure 2a). The DNA with a nanojunction showed a slower gel mobility compared with linear DNA with the same length but a random sequence, suggesting that the strand folds into a stable secondary structure. Next, we performed an Endo VII enzyme digestion experiment to detect the Holliday-junction structure in the DNA products. Endo VII is an endonuclease that specifically cleaves DNA with a Holliday-junction structure at well-defined positions.[12] The ^{32}P-labeled 5′-end DNA strand was cleaved by Endo VII at the Holliday-junction structure and gave rise to the correct bands corresponding to the expected 29/30-nt ^{32}P-labeled products for the sense strand and 39/40-nt products for the antisense strand (see Figure 2b and the Supporting Information for the cleavage sites). This result supports the theory that RCA-replicated DNA nanojunctions can fold into Holliday-junction structures as expected. The melting curve of the DNA products provides another line of evidence for a stable secondary structure in the DNA nanojunction. The sense junction exhibits a melting temperature at 77 °C (Figure 2c), which is consistent with the melting temperature that was predicted by using Mfold[14] based on this particular sequence.

 © 2006 Wiley-VCH Verlag GmbH & Co. KGaA, Weinheim

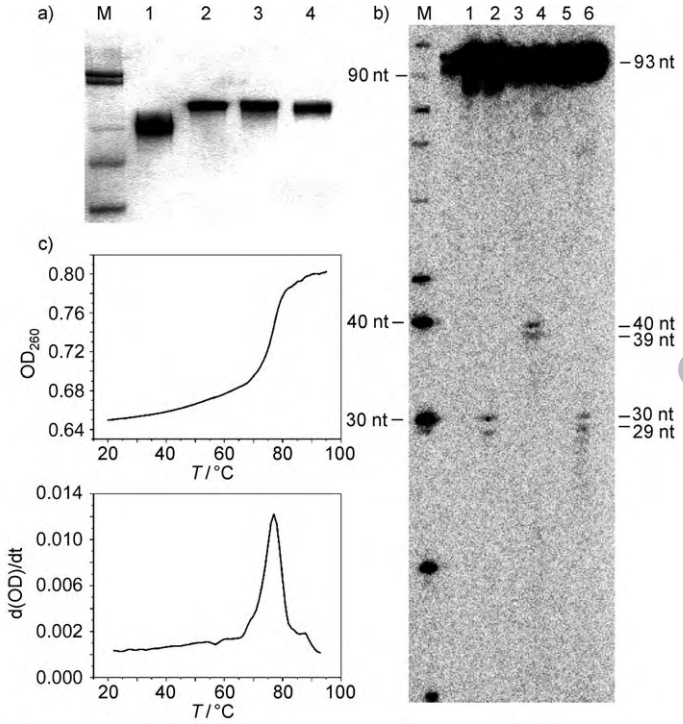

Figure 2. Analysis of the Holliday-junction structure of the DNA nanojunction. a) Native PAGE analysis of the DNA nanojunction. Lane M: 10-nt ssDNA ladder; lane 1: annealed random sequenced 93 mer ssDNA; lane 2: annealed LSS; lane 3: annealed LAS; lane 4: annealed LSS (final product after the complete replication cycle). b) Endonuclease cleavage of DNA with a Holliday junction. DNA samples treated with T4 Endonuclease VII (lane 2: LSS; lane 4: LAS; lane 6: LSS (final product)) or without T4 Endonuclease VII (lane 1, LSS; lane 3: LAS; lane 5: LSS (final product)). Lane M: 10-nt ssDNA ladder. c) Melting-curve profile of the sense junction (top) and the differential melting curve (bottom). OD = optical density.

We expect that the RCA reaction strategy could be employed to replicate and amplify other DNA nanostructures with different structures and more complicated topology (see the examples in the Supporting Information). The replication concept utilized herein is straightforward for single-stranded templates that can be easily circularized. A variety of ssDNA nanostructures can be designed by utilizing paranemic-crossover (PX) DNA structures.[15] Even periodic 2D structures could possibly be achieved by PX cohesion[16] after replicating DNA nanostructures. Multistranded structures can also be replicated separately for each strand and then combined together.

To compare the replication efficiency of the RCA reaction with that of PCR, we have tested asymmetric PCR on the sense strand (see the Supporting Information). Owing to the secondary structure, significant amounts of truncated products can also be seen, thus the amplification efficiency (approximately five times more of the correct-length product) is lower. Most DNA nanostructures constructed so far contain strands both with secondary structures and strands without secondary structures. It is possible to combine RCA with PCR for multistranded DNA nanoarchitectures.[17]

In summary, we have successfully demonstrated the use of RCA as a strategy to amplify a four-arm branched nanojunction. This is the first time that a four-arm junction has been replicated by using an enzymatic reaction. The fact that a nanojunction can be replicated by the RCA opens a new avenue for large-scale enzymatic synthesis of DNA nanoconstruction.

Received: May 26, 2006
Revised: July 20, 2006
Published online: October 18, 2006

Keywords: DNA junctions · DNA replication · nanotechnology · rolling-circle amplification

[1] N. C. Seeman, *Nature* **2003**, *421*, 427–431.
[2] U. Feldkamp, C. M. Niemeyer, *Angew. Chem.* **2006**, *118*, 1888–1910; *Angew. Chem. Int. Ed.* **2006**, *45*, 1856–1976.
[3] L. H. Eckardt, K. Naumann, W. M. Pankau, M. Rein, M. Schweitzer, N. Windhab, G. Kiedrowski, *Nature* **2002**, *420*, 286.
[4] W. M. Shih, J. D. Quispe, G. F. Joyce, *Nature* **2004**, *427*, 618–621.
[5] D. Liu, S. L. Daubendiek, M. A. Zillman, K. Ryan, E. T. Kool, *J. Am. Chem. Soc.* **1996**, *118*, 1587–1594.
[6] Z. X. Deng, Y. Tian, S. H. Lee, A. E. Ribbe, C. D. Mao, *Angew. Chem.* **2005**, *117*, 3648–3651; *Angew. Chem. Int. Ed.* **2005**, *44*, 3582–3585.
[7] S. Beyer, P. Nickels, F. C. Simmel, *Nano Lett.* **2005**, *5*, 719–722.
[8] L. Blanco, A. Bernad, J. M. Lazaro, G. Martin, C. Garmendia, M. Salas, *J. Biol. Chem.* **1989**, *264*, 8935–8940.
[9] J. Baner, M. Nilson, M. Mendal-Hartvig, U. Landegren, *Nucleic Acids Res.* **1998**, *26*, 5073–5078.
[10] C. Larsson, J. Koch, A. Nygren, G. Janssen, A. K. Raap, U. Landegren, M. Nilson, *Nat. Methods* **2004**, 1, 227–232.
[11] H. Kuhn, V. V. Demidov, M. D. Frank-Kamenetskii, *Nucleic Acids Res.* **2002**, *30*, 574–580.
[12] N. R. Kallenbach, R. I. Ma, N. C. Seeman, *Nature* **1983**, *305*, 829–831.
[13] J. E. Mueller, C. J. Newton, F. Jensch, B. Kemper, R. P. Cunningham, N. R. Kallenbach, N. C. Seeman, *J. Biol. Chem.* **1990**, *265*, 13918–13924.
[14] M. Zuker, *Nucleic Acids Res.* **2003**, *31*, 1–10.
[15] Z. Shen, H. Yan, T. Wang, N. C. Seeman, *J. Am. Chem. Soc.* **2004**, *126*, 1666–1674.
[16] X. Zhang, H. Yan, Z. Shen, N. C. Seeman, *J. Am. Chem. Soc.* **2002**, *124*, 12940–12941.
[17] H. Yan, S. H. Park, G. Ginkelstein, J. H. Reif, T. H. LaBean, *Science* **2003**, *301*, 1882–1884.

 © 2006 Wiley-VCH Verlag GmbH & Co. KGaA, Weinheim

Single-Molecule Studies

DOI: 10.1002/anie.200602289

A Simple Nanomixer for Single-Molecule Kinetics Measurements**

Samuel S. White, Shankar Balasubramanian, David Klenerman, and Liming Ying**

Single-molecule experiments have enabled the study of subpopulations and multiple reaction pathways by removing the ensemble averaging in bulk experiments.[1] However, to date most single-molecule fluorescence experiments have been performed under equilibrium conditions, which limits the range of measurements for protein and nucleic acid folding or unfolding and precluded the study of weakly bound complexes that would dissociate under equilibrium conditions. One methodology to perform single-molecule studies far from equilibrium is by using a micro- or nanofluidic mixing device.[2,3] Eaton and co-workers coupled a microfabricated laminar-flow mixer to a confocal microscope to examine the folding kinetics of an individual cold shock protein (Csp).[2] Their device offers a time resolution of around 100 ms and can study reactions as long as 10 s. Herein we present a new methodology for studying reaction kinetics at the single-molecule level by incorporating a 100-nm-diameter glass pipette into a confocal optical system to form a quasi-continuous-flow nanomixer, as shown in Figure 1. Our nanomixer offers a slightly better time resolution and approximately the same time-scale as Eaton's system.[2] This new methodology has the added advantages of a reduced background, as measurements are made in free solution, and more importantly simple device fabrication, which should make the method widely applicable.

The nanomixer is based around a nanopipette that we previously developed for the controlled delivery and nanowriting of biomolecules.[4] As almost the entire electric field drop occurs at the tip, when a moderate potential difference is applied across the pipette, biomolecules (in buffer 1) are driven from the tip by a combination of electrophoretic, dielectrophoretic, and electroosmotic forces (see the Supporting Information for a schematic of the basic principle of the device).[4c] Measurements of the diffusion constant by fluorescence correlation spectroscopy near the opening of the pipette tip showed that there was no detectable net flow at a distance 2 μm away from the pipette tip.

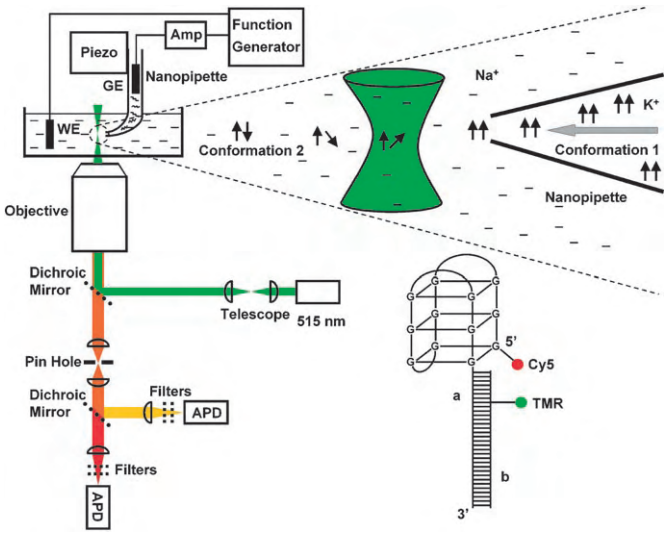

Figure 1. Experimental setup and quadruplex used. Amp = current and voltage amplifier ($\times 10^8$), WE = working electrode, GE = ground electrode.

We approximated the motion of the biomolecules outside the pipette as radial diffusion by using a simple "single-pore" model.[5] The concentration profile $C(r)$ at a radius r away from the pipette opening can be described by Equation (1), in which C_S represents the concentration of the molecule at the pipette tip.[5,6]

$$C(r) = \left(\frac{r_0}{r}\right) C_S \qquad (1)$$

For a disk-shaped pore, such as for the pipettes used in this study, with radius a, the radius of the corresponding hemispherical pore r_0 can be described by Equation (2).[5]

$$r_0 = \frac{2a}{\pi} \qquad (2)$$

To verify this model the fluorescence of Alexa-647 in Alexa-647-labeled yellow-fluorescent protein (YFP), which is proportional to the YFP concentration, was measured as a function of distance from the pipette tip. The data were fitted to Equation 1 by using the radius of the nanopipette for a (50 nm); the fitted data are shown as the gray line in Figure 2. The "single-pore" model fits the data well, which further supports the assumption that the mixing of biomolecules with the bulk solution (buffer 2) is predominately by diffusion.

As biomolecules diffuse through buffer 2, their conformation changes as a result of the difference in buffer

[*] Dr. S. S. White, Dr. S. Balasubramanian, Dr. D. Klenerman, Dr. L. Ying[+]
Department of Chemistry
University of Cambridge
Lensfield Road, Cambridge CB21EW (UK)
Fax: (+44) 1223-336-362
E-mail: dk10012@cam.ac.uk
ly206@cam.ac.uk

[+] Current Address:
Biological Nanoscience Section
National Heart and Lung Institute
Imperial College London
London SW72AZ (UK)

[**] We thank Joe Piper for the help in diffusion-constant measurements, and Andreas Bruckbauer and Victor Ostanin for constructive discussions about diffusion from the pipette. This work was funded by the Biotechnology and Biological Sciences Research Council, UK.

Supporting information (experimental details, device schematic, derivation of Equation (3), and population assignment) for this article is available on the WWW under http://www.angewandte.org or from the author.

WILEY InterScience DISCOVER SOMETHING GREAT
© 2006 Wiley-VCH Verlag GmbH & Co. KGaA, Weinheim

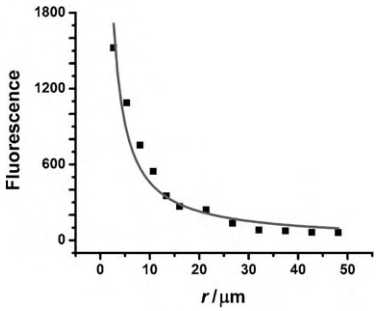

Figure 2. Fluorescence/concentration variation of YFP with distance from the pipette tip. The gray line is a fit of Equation (1) with $r_0 = 0.032$ μm ($a = 50$ nm).

conditions, and this change can be probed by fluorescence spectroscopy. Molecules are probed at different distances x from the pipette tip, and the time t_{max} at which there is maximal probability to observe the molecules is related to x by Equation (3).

$$x^2 = 6\,D\,t_{max} \tag{3}$$

D is the one-dimensional diffusion constant (see the Supporting Information for the derivation, which is based on Einstein's relation for 3D diffusion). This relationship allows kinetic measurements to be made. The dead time of the nanomixer, which limits the time resolution possible, is about 10 ms and depends on how close to the pipette tip it is possible to make measurements without directional flow and the diffusion coefficient of the biomolecule of interest.

We first tested the nanomixer by measuring the dissociation rate constant of an eight-base-pair duplex DNA molecule labeled with a donor and acceptor dye pair. The two complementary strands stay associated inside the pipette, where the sample concentration is well above K_d in 100 mM NaCl. When the duplex DNA is driven out of the pipette, its concentration quickly decreases to well below K_d, which results in dissociation of the two strands. A typical fluorescence resonance energy transfer (FRET) decay curve as a function of reaction time is shown in Figure 3. The dissociation rate constant measured by the nanomixer is $2.6 \pm 0.4\ s^{-1}$ in comparison to the value of $1.2 \pm 0.2\ s^{-1}$ observed from

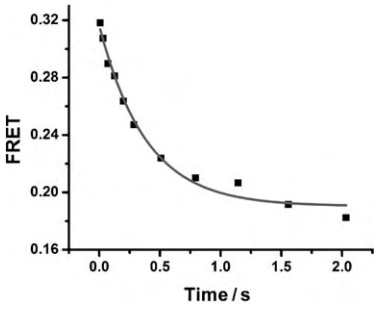

Figure 3. FRET decay as a function of reaction time after a model duplex DNA labeled with Rhodamine green and Alexa-647 at a concentration of 100 nM was quickly diluted by the nanomixer into a buffer (100 mM Na^+).

kinetics measurement of the same sequence of duplex DNA by Bayley and co-workers using a protein nanopore.[7] This slightly faster dissociation time is expected, as the DNA we used was labeled with fluorophore at both ends of the duplex, which marginally destabilizes the duplex.

We then applied the nanomixer to study the unfolding kinetics of the human telomeric DNA quadruplex at the single-molecule level. We studied a quadruplex system (Figure 1) that has been previously investigated in detail under equilibrium conditions by single-molecule FRET between a TMR donor and a Cy5 acceptor.[8] In these experiments, the quadruplex was attached to a 35-bp duplex DNA molecule so that there is no change in diffusion coefficient in its different conformations. This situation was confirmed by experiment by using fluorescence correlation spectroscopy (see the Supporting Information). The human intramolecular telomeric G-quadruplex (HITQ) comprises the repeat sequence d(TTAGGG) and has been the subject of considerable study during the past decade because of its links with telomere regulation and cancer.[9] The HITQ can adopt two principal conformations, parallel and antiparallel, which are to a degree dependent on the monovalent cation present and its concentration.[10,11] It is now recognized that in both sodium and potassium buffers, HITQ forms a mixture of parallel and antiparallel quadruplexes but with different ratios,[8,12] although a very recent paper has reported that in potassium solution, HITQ may adopt a hybrid structure with parallel and antiparallel strands.[13]

An equilibrium single-molecule FRET histogram of the HITQ in 1 mM Na^+ buffer is shown in the lower panel of Figure 4 (magenta histogram). Two peaks can be clearly seen, one with a center at a transfer efficiency of 0.32 and another near zero. The FRET peak centered near zero is a combination of the unfolded quadruplex (see the Supporting Information) and inactive Cy5.[8] The HITQ in 100 mM K^+ buffer is shown in the upper panel of Figure 4 (cyan histogram). This histogram again shows two peaks, but the low FRET peak (**II**) at 0.32 has now shifted to a high FRET peak (**I**) centered at 0.78. Although we cannot unequivocally assign the high and low FRET HITQ structures, one possible scenario is that the structure of the low FRET form (**II**) is a type of antiparallel quadruplex and the high FRET form (**I**) is a mixture of a different type of antiparallel and a parallel quadruplex (see the Supporting Information).[8,12,14] This conclusion is supported by the size of the FRET efficiency for these different structures (see the Supporting Information). Representative FRET histograms measured at different distances/times after diffusion out of the pipette are shown in Figure 4. The kinetics experiments were performed with 100 mM K^+ buffer in the nanopipette and 1 mM Na^+ buffer in the bath.[15] The high FRET peak rapidly decreases with time and the low FRET form correspondingly increases in magnitude. The kinetics for the conformational change can be obtained by assuming a minimal two-state model [Equation (4)].

$$\text{structure } \mathbf{I} \xrightarrow{k_1} \text{structure } \mathbf{II} \tag{4}$$

The decrease in structure **I** was fitted to a first-order rate equation, and the increase in structure **II** of the HITQ was

 © 2006 Wiley-VCH Verlag GmbH & Co. KGaA, Weinheim

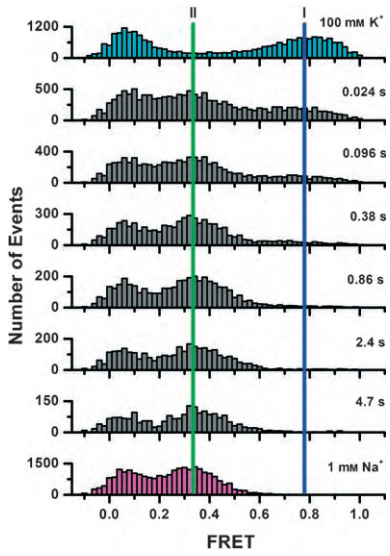

Figure 4. Single-molecule FRET histograms of HITQ during conversion from the high FRET structure to the low FRET structure with 100 mM K^+ buffer and 200 nM HITQ in the pipette and 1 mM Na^+ buffer in the bath. The cyan FRET histogram is the distribution in 100 mM K^+ at equilibrium (top). The magenta FRET histogram is the distribution in 1 mM Na^+ at equilibrium (bottom). The green (structure **II**) and blue (structure **I**) solid lines are the centers of the Gaussian function fitted to each population. Data for the FRET histograms were collected for 15 min at different distances from the pipette tip, converted to time by using Equation (3), and represent time after mixing. All experiments were performed at 37 °C.

also fitted to a first-order rate equation (Figure 5). Identical rates were obtained for the decrease in structure **I** and the increase in structure **II** ($k_1 = 5.8 \pm 1.8\ s^{-1}$). The only data available for the unfolding kinetics of the HITQ were obtained at high salt concentration by us[8,16] and Zhao et al.[17] by using the indirect hybridization method. These measurements gave slower unfolding, probably owing to the higher salt concentration used, and the later work was also carried out on a surface-immobilized quadruplex, the kinetics of which may be hindered by the surface. Ha and co-workers also studied surface-immobilized HITQ folding and unfolding; these experiments were carried out under equilibrium conditions in 2 mM K^+ solution and gave a unfolding rate of approximately $0.35\ s^{-1}$ at 37 °C.[18] Thus, in view of these differences, our results are consistent with the limited data available for comparison, and importantly our single-molecule measurements allow us to identify any potential intermediate species involved.

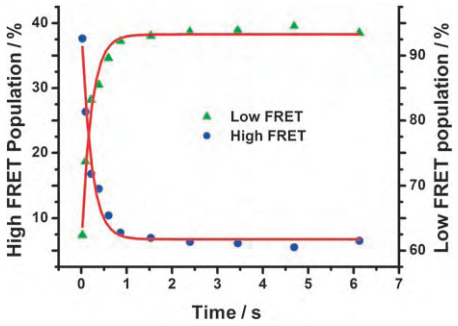

Figure 5. Population variation of the high and low FRET structures with time after mixing. The population of each species was calculated from the area of the Gaussian fits to the FRET histograms in Figure 4. Green triangles represent the low FRET population and blue circles represent the high FRET population. The solid red lines are fits of the data to a first-order rate equation.

In conclusion, a fully functional diffusive nanomixer for single-molecule studies has been developed that allows single-molecule fluorescence studies to be performed under non-equilibrium conditions in free solution without compromising the signal-to-noise ratio. The use of this method has been demonstrated by directly monitoring the subpopulations of the different conformations of a quadruplex during unfolding by using single-molecule FRET to provide complementary kinetic information to previous work.[16–18] Our nanomixer should allow studies of important biological process, such as protein folding, under nonequilibrium conditions in an experimentally simple way.

Received: June 7, 2006
Revised: September 9, 2006
Published online: October 19, 2006

Keywords: DNA · FRET (fluorescence resonant energy transfer) · kinetics · single-molecule studies

[1] a) S. Weiss, *Science* **1999**, *283*, 1676–1683; b) X. S. Xie, J. Trautman, *Annu. Rev. Phys. Chem.* **1998**, *49*, 441–480.
[2] E. A. Lipman, B. Schuler, O. Bakajin, W. A. Eaton, *Science* **2003**, *301*, 1233–1235.
[3] a) D. E. Hertzog, X. Michalet, M. Jäger, X. X. Kong, J. G. Santiago, S. Weiss, O. Bakajin, *Anal. Chem.* **2004**, *76*, 7169–7178; b) J. B. Knight, A. Vishwanath, J. P. Brody, R. H. Austin, *Phys. Rev. Lett.* **1998**, *80*, 3863–3866; c) E. Kauffmann, N. C. Darnton, R. H. Austin, C. Batt, K. Gerwert, *Proc. Natl. Acad. Sci. USA* **2001**, *98*, 6646–6649.
[4] a) L. M. Ying, A. Bruckbauer, A. M. Rothery, Y. E. Korchev, D. Klenerman, *Anal. Chem.* **2002**, *74*, 1380–1385; b) A. Bruckbauer, L. M. Ying, A. M. Rothery, D. J. Zhou, A. I. Shevchuk, C. Abell, Y. E. Korchev, D. Klenerman, *J. Am. Chem. Soc.* **2002**, *124*, 8810–8811; c) L. M. Ying, S. S. White, A. Bruckbauer, L. Meadows, Y. E. Korchev, D. Klenerman, *Biophys. J.* **2004**, *86*, 1018–1027; d) K. T. Rodolfa, A. Bruckbauer, D. J. Zhou, Y. E. Korchev, D. Klenerman, *Angew. Chem.* **2005**, *117*, 7014–7019; *Angew. Chem. Int. Ed.* **2005**, *44*, 6854–6859.
[5] A. Kueng, C. Kranz, A. Lugstein, E. Bertagnolli, B. Mizaikoff, *Angew. Chem.* **2005**, *117*, 3485–3488; *Angew. Chem. Int. Ed.* **2005**, *44*, 3419–3422.
[6] E. R. Scott, H. S. White, J. B. Phipps, *Anal. Chem.* **1993**, *65*, 1537–1545.
[7] S. Howorka, L. Movileanu, O. Braha, H. Bayley, *Proc. Natl. Acad. Sci. USA* **2001**, *98*, 12996–13001.
[8] L. M. Ying, J. J. Green, H. T. Li, D. Klenerman, S. Balasubramanian, *Proc. Natl. Acad. Sci. USA* **2003**, *100*, 14629–14634.
[9] S. Neidle, G. Parkinson, *Nat. Rev. Drug Discovery* **2002**, *1*, 383–393.
[10] Y. Wang, D. J. Patel, *Structure* **1993**, *1*, 263–282.
[11] G. N. Parkinson, M. P. H. Lee, S. Neidle, *Nature* **2002**, *417*, 876–880.
[12] a) Y. J. He, R. D. Neumann, I. G. Panyutin, *Nucleic Acids Res.* **2004**, *32*, 18, 5359–5367; b) I. Ourliac-Garnier, M. A. Elizondo-Riojas, S. Redon, N. P. Farrell, S. Bombard, *Biochemistry* **2005**,

 © 2006 Wiley-VCH Verlag GmbH & Co. KGaA, Weinheim

44, 10620 – 10634; c) J. Li, J. J. Correia, L. Wang, J. O. Trent, J. B. Chaires, *Nucleic Acids Res.* **2005**, *33*, 4649 – 4659.
[13] A. Ambrus, D. Chen, J. Dai, T. Bialis, R. A. Jones, D. Yang, *Nucleic Acids Res.* **2006**, *34*, 9, 2723 – 2735.
[14] A. Siddiqui-Jain, C. L. Grand, D. J. Bearss, L. H. Hurley, *Proc. Natl. Acad. Sci. USA* **2002**, *99*, 11593 – 11598.
[15] Under these conditions, the kinetics was sufficiently fast for our instrument. It was too slow at higher sodium concentrations.
[16] J. J. Green, L. M. Ying, D. Klenerman, S. Balasubramanian, *J. Am. Chem. Soc.* **2003**, *125*, 3763 – 3767.
[17] Y. Zhao, Z. Y. Kan, Z. X. Zeng, Y. H. Hao, H. Chen, Z. Tan, *J. Am. Chem. Soc.* **2004**, *126*, 13255 – 13264.
[18] J. Y. Lee, B. Okumus, D. S. Kim, T. Ha, *Proc. Natl. Acad. Sci. USA* **2005**, *102*, 18938 – 18943.

 © 2006 Wiley-VCH Verlag GmbH & Co. KGaA, Weinheim

Supramolecular Chemistry

DOI: 10.1002/anie.200602870

Induction of Liquid Crystallinity by Self-Assembled Molecular Boxes

Alessio Piermattei, Marcel Giesbers, Antonius T. M. Marcelis, Eduardo Mendes, Stephen J. Picken, Mercedes Crego-Calama, and David N. Reinhoudt**

The self-assembly of small molecular building blocks into supramolecular aggregates through noncovalent interactions has been used extensively for the formation of nanoscale structures.[1] For self-organization into highly ordered nanoarchitectures, the building blocks require well-defined structures with high thermodynamic stabilities.[2] Hydrogen bonding is a powerful tool for the construction of such structures, owing to its directional and dynamic nature,[3] and its capability for error correction.[4] A variety of liquid-crystalline materials[5] have been prepared by self-assembly through hydrogen-bond formation.[6] Rodlike[7] and disklike[8,9] low-molecular-weight complexes, and polymers[10] with side-chain,[11] main-chain,[12] network, host–guest[9,13] arrangements, and single building blocks[14] have been reported.

The shape of the mesogenic molecule is one of the factors that determine the packing and order in the liquid-crystalline phase. Recently, unconventional shapes, such as bananas,[15] dendrons,[16] cones,[5] shuttlecocks,[5] rod-dendrons,[5] and rings[5] have been reported. The self-assembly of these unconventional mesogenic supramolecules has produced new phases of supramolecular liquid crystals.[17] To our knowledge, there have been no reports of hydrogen-bonded 3D nano-objects composed of different building blocks with the capability to form liquid crystals.

Herein, we report the first example of a liquid-crystalline material based on the self-organization of self-assembled molecular boxes. Each box consists of two rosette motifs connected through three calix[4]arene dimelamine molecules (**1**). The circular motifs (rosettes)[18] are formed by hydrogen bonding between the melamine moieties of **1** and a barbituric or cyanuric acid (Figure 1). The mesogenic double-rosette assemblies $\mathbf{1}_3\cdot(\mathrm{DEB})_6$ (DEB = 5,5-diethylbarbituric acid) and $\mathbf{1}_3\cdot(\mathrm{BuCYA})_6$ (BuCYA = *N*-butylcyanuric acid) form spontaneously upon mixing **1** with 2 equiv of either DEB or BuCYA in an apolar solvent (Figure 1).[19] The assemblies, which are held together by 36 hydrogen bonds, are thermodynamically stable, even at a concentration of 5 μM.[20] The calix[4]arene dimelamine **1** was functionalized with octadecyl chains to promote the self-organization of the double-rosette assemblies into a liquid-crystalline phase. The long alkyl chains are connected to the terminal benzamide moieties of **1** to prevent their interference with the network of hydrogen bonds that holds the double rosette together.[21]

The formation of the self-assembled mesogens was confirmed by ^{1}H NMR spectroscopy in solution (Figure 2). The signals assigned to the imide protons (a, b) of DEB and BuCYA at $\delta_{NH} = 15$–14 ppm are diagnostic of the formation of the assemblies; upon hydrogen-bond formation, the signals of these protons undergo a strong downfield shift (in free DEB, $\delta_{NH} = 8.40$ ppm; in free BuCYA, $\delta_{NH} = 11.2$ ppm).[19]

The thermal behavior of the assembly and of the isolated component **1** was determined by polarized optical microscopy (POM) and differential scanning calorimetry (DSC; Table 1). The DSC thermograms of the assemblies each exhibit two peaks associated with phase transitions. In the case of $\mathbf{1}_3\cdot(\mathrm{DEB})_6$, the first (low-temperature) peak is attributed to a reversible transition between an unidentified columnar ($\mathrm{Col_x}$) phase and a hexagonal columnar ($\mathrm{Col_h}$) phase. However, no differences were observed between the optical textures and the X-ray diffraction (XRD) patterns of the two phases. In the case of $\mathbf{1}_3\cdot(\mathrm{BuCYA})_6$, the first peak is attributed to a crystal–liquid crystal ($\mathrm{Col_h}$ phase) transition. For both double-rosette assemblies, the second peak is attributed to a transition between a liquid-crystalline ($\mathrm{Col_h}$) and an isotropic phase. The thermotropic $\mathrm{Col_h}$ phase exists over a wide temperature range for both assemblies (16–173 °C for $\mathbf{1}_3\cdot(\mathrm{DEB})_6$; 31–233 °C for $\mathbf{1}_3\cdot(\mathrm{BuCYA})_6$; Table 1). The thermal stability of the liquid-crystalline phase is remarkable, considering the dimensions (1.2 nm in height; 3.3 nm in

[*] A. Piermattei, Dr. M. Crego-Calama, Prof. D. N. Reinhoudt
Laboratory of Supramolecular Chemistry & Technology
MESA$^+$ Institute for Nanotechnology
University of Twente
P.O. Box 217, 7500 AE Enschede (The Netherlands)
Fax: (+31) 534-894-645
E-mail: m.cregocalama@utwente.nl
d.n.reinhoudt@utwente.nl
Dr. M. Giesbers, Dr. A. T. M. Marcelis
Laboratory of Organic Chemistry
Wageningen University
P.O. Box 8026, 6700 EG Wageningen (The Netherlands)
Dr. E. Mendes, Prof. S. J. Picken
Nanostructured Materials (NSM-DCT)
Faculty of Applied Sciences
Julianalaan 136, 2628 BL Delft (The Netherlands)

Supporting information for this article (Experimental Section) is available on the WWW under http://www.angewandte.org or from the author.

 © 2006 Wiley-VCH Verlag GmbH & Co. KGaA, Weinheim

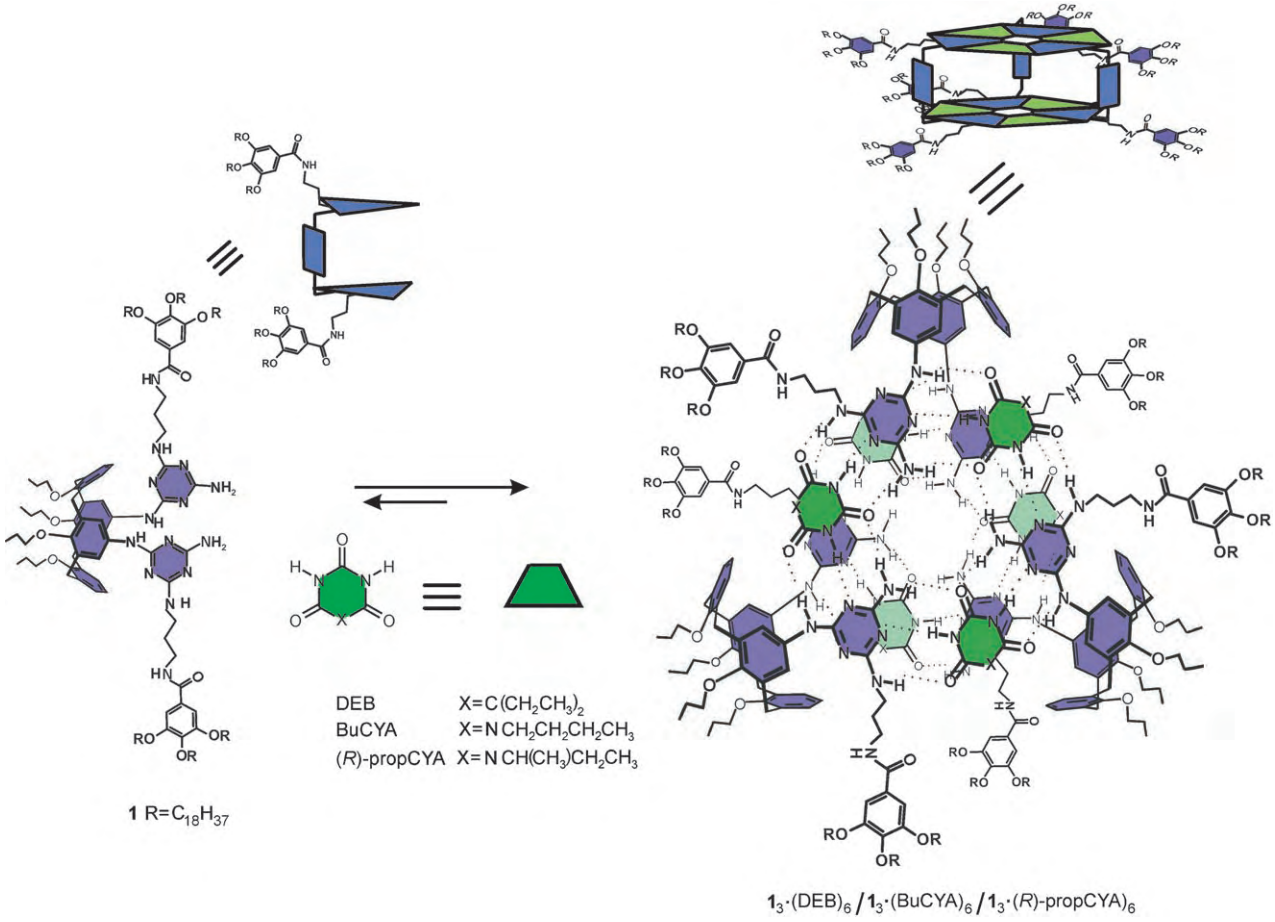

Figure 1. Self-assembly of $\mathbf{1}_3\cdot(DEB)_6$, $\mathbf{1}_3\cdot(BuCYA)_6$, and $\mathbf{1}_3\cdot((R)\text{-propCYA})_6$.

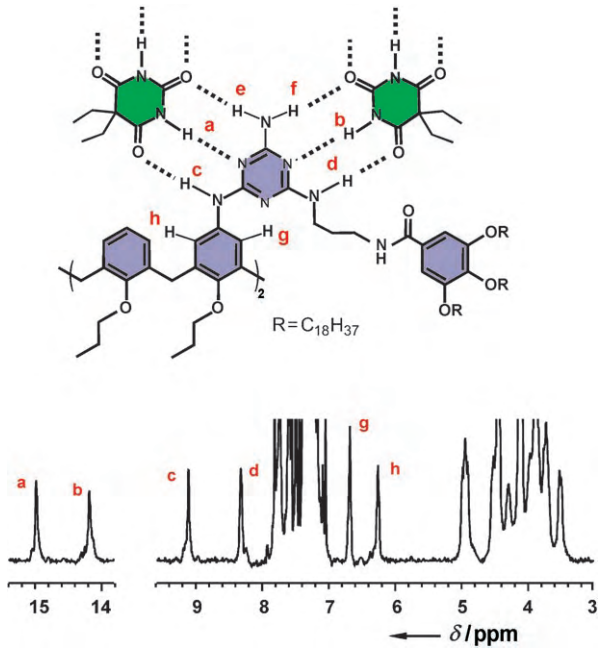

Figure 2. Sections of the ^{1}H NMR spectrum (400 MHz) of $\mathbf{1}_3\cdot(DEB)_6$ (1 mM in [D_8]toluene) at 298 K.

Table 1: Thermal properties of **1**, $\mathbf{1}_3\cdot(DEB)_6$, and $\mathbf{1}_3\cdot(BuCYA)_6$.

Compound	Phase transition[a]						
1	Cr	17	(59.8)	Iso			
$\mathbf{1}_3\cdot(DEB)_6$	Col_x	16	(18.7)	Col_h	173	(35.0)	Iso
$\mathbf{1}_3\cdot(BuCYA)_6$	Cr	31	(167.5)	Col_h	233	(70.1)	Iso

[a] Phase-transition temperatures [°C] and enthalpy changes [kJ mol^{-1}] (in parentheses); Cr = crystalline phase, Col_x = unidentified columnar phase, Col_h = hexagonal columnar phase, Iso = isotropic phase.

width) and the noncovalent nature (12 DAD·ADA hydrogen bonds; D = donor, A = acceptor) of the double-rosette assembly.[19] In contrast, the DSC thermogram of **1** exhibits only one peak. This peak is attributed to a transition between a crystalline phase and an isotropic phase on the basis of POM, which reveals the spherulite texture of the crystalline phase. It is remarkable that the liquid-crystalline phase is observed for the double-rosette assemblies, even though none of the isolated building blocks are mesogenic.

To exclude the possibility of thermal degradation of the double-rosette assemblies during the heating process, circular dichroism (CD) studies on thin layers of the optically active assembly $\mathbf{1}_3\cdot((R)\text{-propCYA})_6$ ((*R*)-propCYA = *N*-[(*R*)-1-methylpropyl]cyanuric acid) were performed (not

 © 2006 Wiley-VCH Verlag GmbH & Co. KGaA, Weinheim

shown).[20,22,23] The optically active double-rosette assemblies (with *P* or *M* helicity) exhibit a very strong induced CD signal at a wavelength of 350–250 nm,[20] owing to the dissymmetric arrangement of the many chromophoric units, whereas the building block **1** is nearly CD inactive. The intensity of the CD signal of $\mathbf{1}_3$·((*R*)-propCYA)$_6$ does not decrease after several thermal cycles, evidencing the high thermal stability of the assembly.

POM suggests that the liquid-crystalline phase of the assemblies is a columnar mesophase: a mosaic texture showing birefringent areas is observed for $\mathbf{1}_3$·(DEB)$_6$ and $\mathbf{1}_3$·(BuCYA)$_6$ after cooling from the isotropic melt (Figure 3).

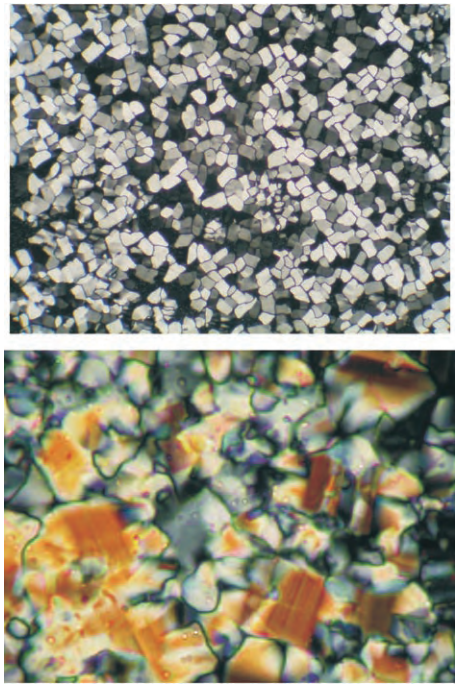

Figure 3. POM images of $\mathbf{1}_3$·(DEB)$_6$ at 120 °C (top) and of $\mathbf{1}_3$·(BuCYA)$_6$ at 180 °C (bottom).

Note that the assemblies $\mathbf{1}_3$·(DEB)$_6$ and $\mathbf{1}_3$·(BuCYA)$_6$ have very different isotropization temperatures (ΔT_{iso} = 60 °C; Table 1). Melamines form stronger hydrogen bonds with cyanurates than with barbiturates,[24] resulting in the higher thermal stability of $\mathbf{1}_3$·(BuCYA)$_6$. Furthermore, cyanuric acids have a nitrogen atom with trigonal coordination geometry at position 5 of the heterocycle. As a result, in $\mathbf{1}_3$·(BuCYA)$_6$, the butyl substituent and the heterocycle are in the same plane. Consequently, the rosette faces of the assembly can be considered as flat surfaces, which allow efficient stacking in the columnar phase. In contrast, barbituric acids have a carbon atom with tetrahedral coordination geometry at the 5 position. As suggested by molecular simulation studies,[25] the ethyl substituents at this carbon atom point to the top and bottom faces of the double-rosette assembly, which may weaken the interaction between neighboring assemblies within the columns and contribute to a lower thermal stability.

The powder XRD pattern for the Col$_h$ phase of $\mathbf{1}_3$·(DEB)$_6$ is shown in Figure 4. In the small-angle region, the relatively sharp reflections at 37.3 (100), 21.9 (110), 19.1 (200), and 14.0 Å (210) are characteristic of the hexagonal arrangement.

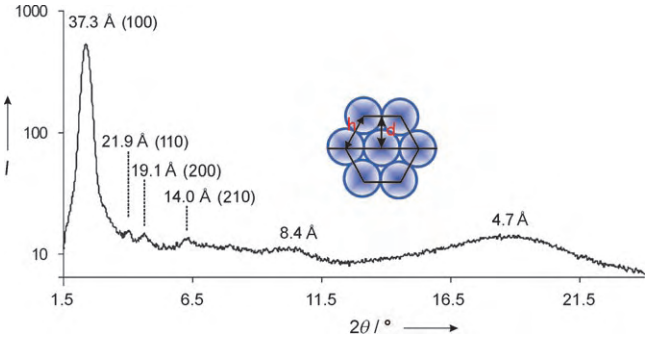

Figure 4. Powder XRD pattern of $\mathbf{1}_3$·DEB$_6$ at 120 °C, and schematic of the columnar organization in the Col$_h$ phase (see text for details).

A broad reflection at 8.4 Å corresponds to the distance between the bottom rosette faces of neighboring assemblies. In the wide-angle region, the diffuse halo near 4.7 Å arises from the disordered terminal alkyl chains and is characteristic of their liquid-like arrangement.

The double rosettes stack in an ordered columnar fashion. The driving force for the self-assembly of the columns is the nanoscale segregation of the double rosette cores and the lipophilic alkyl chains.[26] The intercolumn distance is h = 43.0 Å (Figure 4).[27] A comparable distance was found by atomic force microscopy (AFM) for similar assemblies.[28] Their deposition onto highly ordered pyrolytic graphite (HOPG) showed that the double-rosette assemblies self-organize by face-to-face arrangement into rodlike structures. A hierarchical process leads from the self-assembly of double rosettes, to the assembly of the double rosettes into columns, and to the self-organization of the columns into a Col$_h$ liquid-crystalline phase, as demonstrated by XRD.

The powder XRD pattern of the Col$_h$ phase of $\mathbf{1}_3$·(BuCYA)$_6$ is very similar to that observed for $\mathbf{1}_3$·(DEB)$_6$. This observation indicates that the side-chains of the cyanuric acid components do not interfere with the self-organization and packing, probably because the dimensions of the double-rosette scaffold are much larger than those of the side chains.[19]

Herein, we have demonstrated that the self-assembled double rosettes $\mathbf{1}_3$·(DEB)$_6$ and $\mathbf{1}_3$·(BuCYA) are able to form liquid crystals. The strength of the hydrogen bonds within the double-rosette assemblies and the spatial disposition of the side chains of the barbituric and cyanuric acid derivatives are crucial factors for the stability of the mesophase. The lateral substituents on the double-rosette building blocks do not seem to affect the hierarchical organization of the mesophase. The remarkable thermal stability and the high degree of order of these mesophases, as well as the easy introduction of chemical diversity, make them a potentially good platform for the self-assembly of new nanomaterials.

Received: July 18, 2006
Published online: October 17, 2006

 © 2006 Wiley-VCH Verlag GmbH & Co. KGaA, Weinheim

Keywords: hydrogen bonds · liquid crystals · nanotechnology · self-assembly · supramolecular chemistry

[1] J.-M. Lehn, *Supramolecular Chemistry: Concepts and Perspectives*, VCH, Weinheim, **1995**.

[2] D. N. Reinhoudt, *Supramolecular Materials and Technologies*, Wiley, Chichester, **1999**.

[3] L. J. Prins, D. N. Reinhoudt, P. Timmerman, *Angew. Chem.* **2001**, *113*, 2446 – 2492; *Angew. Chem. Int. Ed.* **2001**, *40*, 2383 – 2426.

[4] D. N. Reinhoudt, M. Crego-Calama, *Science* **2002**, *295*, 2403 – 2407.

[5] T. Kato, N. Mizoshita, K. Kishimoto, *Angew. Chem.* **2006**, *118*, 44 – 74; *Angew. Chem. Int. Ed.* **2006**, *45*, 38 – 68.

[6] C. M. Paleos, D. Tsiourvas, *Liq. Cryst.* **2001**, *28*, 1127 – 1161.

[7] C. A. Schalley, *Adv. Mater.* **1999**, *11*, 1535 – 1537.

[8] a) T. Kato, T. Matsuoka, M. Nishii, Y. Kamikawa, K. Kanie, T. Nishimura, E. Yashima, S. Ujiie, *Angew. Chem.* **2004**, *116*, 2003 – 2006; *Angew. Chem. Int. Ed.* **2004**, *43*, 1969 – 1972; b) J. van Gestel, A. R. A. Palmans, B. Titulaer, J. Vekemans, E. W. Meijer, *J. Am. Chem. Soc.* **2005**, *127*, 5490 – 5494; c) M. Suarez, J.-M. Lehn, S. C. Zimmerman, A. Skoulios, B. Heinrich, *J. Am. Chem. Soc.* **1998**, *120*, 9526 – 9532; d) G. Proni, G. P. Spada, G. Gottarelli, F. Ciuchi, P. Mariani, *Chirality* **1998**, *10*, 734 – 741.

[9] J. Barberá, M. Bardají, J. Jiménez, A. Laguna, M. P. Martínez, L. Oriol, J. L. Serrano, I. Zaragozano, *J. Am. Chem. Soc.* **2005**, *127*, 8994 – 9002.

[10] T. Kato, N. Mizoshita, K. Kanie, *Macromol. Rapid Commun.* **2001**, *22*, 797 – 814.

[11] M. Ikeda, T. Nobori, M. Schmutz, J.-M. Lehn, *Chem. Eur. J.* **2005**, *11*, 662 – 668.

[12] a) L. Brunsveld, E. W. Meijer, R. B. Prince, J. S. Moore, *J. Am. Chem. Soc.* **2001**, *123*, 7978 – 7984; b) J. Hirschberg, R. A. Koevoets, R. P. Sijbesma, E. W. Meijer, *Chem. Eur. J.* **2003**, *9*, 4222 – 4231.

[13] a) S. Yagai, T. Nakajima, K. Kishikawa, S. Kohmoto, T. Karatsu, A. Kitamura, *J. Am. Chem. Soc.* **2005**, *127*, 11134 – 11139; b) F. Wurthner, S. Yao, B. Heise, C. Tschierske, *Chem. Commun.* **2001**, 2260 – 2261.

[14] a) S. Bonazzi, M. M. Demorais, G. Gottarelli, P. Mariani, G. P. Spada, *Angew. Chem.* **1993**, *105*, 251 – 254; *Angew. Chem. Int. Ed. Engl.* **1993**, *32*, 248 – 250; b) M. Nishii, T. Matsuoka, Y. Kamikawa, T. Kato, *Org. Biomol. Chem.* **2005**, *3*, 875 – 880.

[15] D. M. Walba, E. Korblova, R. Shao, J. E. Maclennan, D. R. Link, M. A. Glaser, N. A. Clark, *Science* **2000**, *288*, 2181 – 2184.

[16] G. Ungar, Y. Liu, X. Zeng, V. Percec, W.-D. Cho, *Science* **2003**, *299*, 1208 – 1211.

[17] V. Percec, M. Peterca, M. J. Sienkowska, M. A. Ilies, E. Aqad, J. Smidrkal, P. A. Heiney, *J. Am. Chem. Soc.* **2006**, *128*, 3324 – 3334.

[18] C. T. Seto, G. M. Whitesides, *J. Am. Chem. Soc.* **1993**, *115*, 905 – 916.

[19] P. Timmerman, R. H. Vreekamp, R. Hulst, W. Verboom, D. N. Reinhoudt, K. Rissanen, K. A. Udachin, J. Ripmeester, *Chem. Eur. J.* **1997**, *3*, 1823 – 1832.

[20] L. J. Prins, C. Thalacker, F. Wurthner, P. Timmerman, D. N. Reinhoudt, *Proc. Natl. Acad. Sci. USA* **2001**, *98*, 10042 – 10045.

[21] H. J. van Manen, V. Paraschiv, J. J. García-López, H. Schönherr, S. Zapotoczny, G. J. Vancso, M. Crego-Calama, D. N. Reinhoudt, *Nano Lett.* **2004**, *4*, 441 – 446.

[22] L. J. Prins, J. Huskens, F. de Jong, P. Timmerman, D. N. Reinhoudt, *Nature* **1999**, *398*, 498 – 502.

[23] The double-rosette assembly, in which the two melamine rings of each calix[4]arene molecule are antiparallel to one another, has D_3 symmetry. In the absence of chiral centers, the assemblies are present as a racemic mixture of *P* and *M* helices. If one enantiomer of a barbituric or cyanuric acid with a chiral center is used in the self-assembly, only one diastereoisomer of the double rosette (of *P* or *M* helicity) is formed, which represents an induction of supramolecular chirality. The diastereoisomerism of the double-rosette assemblies allows them to be studied by CD.

[24] A. G. Bielejewska, C. E. Marjo, L. J. Prins, P. Timmerman, F. de Jong, D. N. Reinhoudt, *J. Am. Chem. Soc.* **2001**, *123*, 7518 – 7533.

[25] M. G. J. ten Cate, J. Huskens, M. Crego-Calama, D. N. Reinhoudt, *Chem. Eur. J.* **2004**, *10*, 3632 – 3639.

[26] T. Kato, *Science* **2002**, *295*, 2414 – 2418.

[27] The intercolumn distance h is calculated with the formula $h = d/\cos(\pi/6)$, where d is the distance between the (100) planes, which corresponds to the distance between adjacent layers of double-rosette columns.

[28] H. A. Klok, K. A. Jolliffe, C. L. Schauer, L. J. Prins, J. P. Spatz, M. Möller, P. Timmerman, D. N. Reinhoudt, *J. Am. Chem. Soc.* **1999**, *121*, 7154 – 7155.

 © 2006 Wiley-VCH Verlag GmbH & Co. KGaA, Weinheim

Crystal Engineering

DOI: 10.1002/anie.200603235

Screening for Inclusion Compounds and Systematic Construction of Three-Component Solids by Liquid-Assisted Grinding**

Tomislav Friščić, Andrew V. Trask, William Jones, and W. D. Samuel Motherwell*

The rational construction of cocrystals (crystalline solids made up of more than one molecular component) has recently attracted the attention of solid-state scientists and materials chemists.[1] The interest, founded on the growing number of applications of multicomponent solids, includes the discovery of new cocrystals, as well as the development of efficient methods for cocrystal synthesis and screening.[2,3] Whereas reliable strategies have been developed to design and construct two-component (binary) cocrystals by using hydrogen bonds,[4] halogen bonds,[5] $\pi\cdots\pi$[6] or van der Waals forces,[7] the construction of ternary and higher-order cocrystals still presents a challenge.[8,9]

[*] Dr. T. Friščić, Dr. A. V. Trask, Dr. W. Jones
Pfizer Institute for Pharmaceutical Materials Science
Department of Chemistry, University of Cambridge
Lensfield Road, Cambridge CB21EW (UK)
Fax: (+44) 01223-762-829
E-mail: wj10@cam.ac.uk
Dr. W. D. S. Motherwell
Cambridge Crystallographic Data Centre
12 Union Road, Cambridge CB21EZ (UK)

[**] John E. Davies is gratefully acknowledged for collecting the single-crystal X-ray diffraction data. The authors thank Neil Feeder and Pete Marshall for fruitful discussions. The Pfizer Institute for Pharmaceutical Materials Science is acknowledged for funding.

Supporting information for this article is available on the WWW under http://www.angewandte.org or from the author.

WILEY InterScience DISCOVER SOMETHING GREAT
© 2006 Wiley-VCH Verlag GmbH & Co. KGaA, Weinheim

One possible strategy towards three-component solids is a host–guest design, wherein the host is a crystalline lattice assembled using two molecular species.[10] Traditionally, inclusion compounds have been synthesized by crystallizing the host and guest compounds from a solution.[11] Whereas the choice of components available for the construction of such systems is limited by the solubilities of the host and the guest, the limitations become more severe in multicomponent systems that require balancing the solubilities of several molecular species.

A possible way to circumvent such solubility issues is through the use of mechanochemical methods.[12] Notably, our group, and others, have reported that binary cocrystals can readily be constructed by grinding together individual components, either neat or in the presence of a small amount of a liquid phase (liquid-assisted grinding).[13,14] That the amounts of liquid involved in liquid-assisted grinding experiments are typically very small suggests that the solubilities of individual components are not decisive for cocrystal formation by grinding. Consequently, neat and liquid-assisted grinding methods are expected to be more efficient than solution crystallization in recognizing guests available to a particular host. Indeed, such a possibility has already been hinted at by Toda and co-workers in the case of the inclusion compound of 1,1-di(*o*-hydroxyphenyl)cyclohexane and naphthoquinone.[15]

With our interest in three-component systems, we have decided to explore neat and liquid-assisted grinding as screening and synthetic methods that would identify guest molecules compatible with a particular two-component host and, correspondingly, facilitate the systematic construction of three-component solids.[9] We were encouraged in our efforts by the recent report of Braga and co-workers on the mechanochemical synthesis of metal–organic intercalation compounds.[16] We now communicate the use of grinding methods for the efficient screening of guests in inclusion compounds, as well as for the deliberate construction of ternary solids independent of the state of aggregation of the guest (that is, liquid or solid).

We have focused our attention on the novel two-component host **1**, which is assembled from caffeine (caf) and succinic acid (sa) in a 1:1 stoichiometric ratio (Scheme 1). Host **1** can be obtained as an inclusion compound with 1,4-dioxane by cocrystallizing caf and sa from the solvent. Whereas the attempted cocrystallization of caf and sa from common organic solvents results in the precipitation of the individual components, mechanical agitation in 1,4-dioxane affords the recrystallization of the initially precipitated caf into cocrystals composed of caf, sa, and 1,4-dioxane. The stoichiometric ratio of the components in the cocrystal is 1:1:0.66 caf/sa/1,4-dioxane, as established by ^{1}H NMR spectroscopy and thermal analysis.

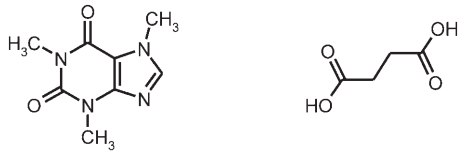

Scheme 1.

As determined by single-crystal X-ray diffraction, caf and sa molecules form layers held together by O–H···O, O–H···N, and pairs of C–H···O hydrogen bonds. Stacking of the layers produces the framework **1**. The framework contains channels, which are occupied by columns of disordered 1,4-dioxane molecules so as to give a solid of composition **1**·0.66 $C_4H_8O_2$ (Figure 1). The synthesis of **1**·0.66 $C_4H_8O_2$ was also achieved

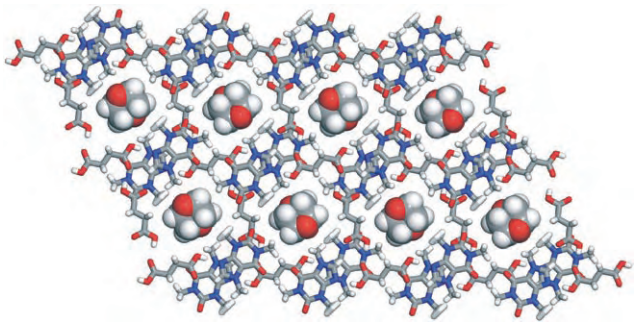

Figure 1. Fragment of the **1**·0.66 $C_4H_8O_2$ structure. The host framework is shown in a wire-frame representation, and the guest molecules in a space-filling representation. C gray, H white, N blue, O red.

by the neat grinding of caf and sa with 1,4-dioxane. That the products obtained by the two methods both correspond to **1**·0.66 $C_4H_8O_2$ was established by comparing the measured powder X-ray diffraction (PXRD) patterns to that calculated on the basis of the crystal structure (Figure 2), as well as by solid-state cross-polarization (CP) magic-angle-spinning (MAS) ^{13}C NMR spectroscopy.

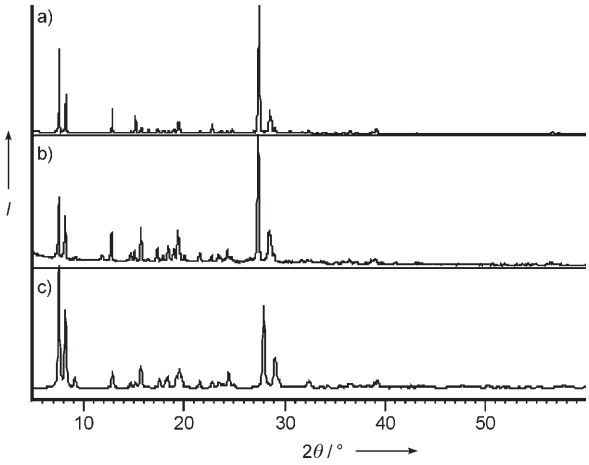

Figure 2. PXRD patterns of a) solution-grown **1**·0.66 $C_4H_8O_2$ and b) the product of the neat grinding of caf, sa, and 1,4-dioxane. c) Simulated PXRD pattern of **1**·0.66 $C_4H_8O_2$.

To compare the efficiencies of neat grinding, liquid-assisted grinding, and crystallization from solution in identifying guests for **1**, 20 liquid compounds were selected as potential guests (Table 1, entries 1–20).[17] The ability of a molecule to act as a guest was recognized by the formation of a solid isomorphous to **1**·0.66 $C_4H_8O_2$, as determined by PXRD.[18] The observation that inclusion compounds were

 © 2006 Wiley-VCH Verlag GmbH & Co. KGaA, Weinheim

Table 1: Formation of **1**·guest by different synthetic methods

Entry	Guest	State of aggregation[a,b]	From solution	Neat grinding[d]	Liquid-assisted grinding[e]
1		L	Yes	Yes	Yes
2		L	Yes	Yes	Yes
3		L	Yes[c]	Yes	Yes
4		L	No	Yes	Yes
5		L	Yes[c]	Yes	Yes
6		L	No	No	Yes
7		L	No	Yes	Yes
8		L	No	Yes	Yes
9	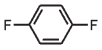	L	No	Yes	Yes
10		L	No	Yes	Yes
11		L	No	Yes	Yes
12		L	No	Yes	Yes
13		L	No	Yes	Yes
14	CCl_4	L	No	Yes	Yes
15	CH_3NO_2	L	No	Yes	Yes
16	Hexane	L	No	No	No
17	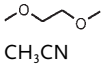	L	No	No	No
18	CH_3CN	L	No	No	No
19	CH_3OH	L	No	No	No
20	Acetone	L	No	No	No
21		S	No	No	Yes
22		S	No	No	Yes
23		S	No	Yes	Yes
24	Ferrocene	S	No	No	No
25	CHI_3	S	No	No	No

[a] At ambient conditions. [b] L = liquid, S = solid. [c] Very low yields.[18] [d] Approximately 2 equiv guest were used. [e] Acetonitrile was used as the liquid phase.

not formed in any experiments involving only caf, sa, and acetonitrile led to the selection of acetonitrile as the liquid phase for liquid-assisted grinding.

Screening by solution crystallization provided **1**·guest in only four cases: 1,4-dioxane, 1,4-thioxane, tetrahydropyran, and 3,4-dihydropyran (Table 1, entries 1–3 and 5).[18] Thermal analysis and ^{1}H NMR spectroscopy revealed the composition of the 1,4-thioxane cocrystals to be **1**·0.54 C_4H_8OS, while a crystal-structure analysis revealed that the framework **1** remained largely unchanged with respect to **1**·0.66 $C_4H_8O_2$ (see Supporting Information). However, the 1,4-thioxane guest molecules are much more disordered within the channels.

In contrast to crystallization from solution, neat and liquid-assisted grinding identified 11 additional molecules that form complexes with **1** (Table 1, entries 4, 6–15). As evidenced from the relative intensities of signals in the PXRD patterns, a small amount of liquid can improve the yield of the ternary solid up to the quantitative level and, in some cases, enable the formation of cocrystals not obtained by neat grinding. In particular, the addition of acetonitrile enabled the formation of **1**·C_6H_{12} (Table 1, entry 6). This observation demonstrates that liquid-assisted grinding can be more efficient than neat grinding in identifying potential guests, and indicates that the role of the liquid is more than simply providing a lubricant for the reaction. The success of grinding as a screening method encouraged us to explore compounds that are solids at ambient conditions as guests. Liquid-assisted grinding readily provided three such cocrystals, involving 1,4-dithiane, norbornane, and norbornylene (Table 1, entries 21–23).[19]

The inability to form an inclusion compound of **1** by crystallization from a liquid guest does not imply that the inclusion compound of the guest cannot be obtained from solution. For example, the complex of **1** and nitromethane forms readily by grinding, but not by crystallization from liquid nitromethane (Table 1, entry 15). However, subsequent exploration of different solvent systems provided crystals of **1**·CH_3NO_2 by the slow evaporation of a solution of caf and sa in a 1:1 CH_3NO_2/CH_3OH mixture (which allowed the structure of **1**·CH_3NO_2 to be determined; see Supporting Information).

Exploring the diversity of guests by neat and liquid-assisted grinding provides an opportunity to understand better the inclusion properties of **1**. Assuming that the formation of cocrystals is governed largely by the host–guest compatibility, rather than solubility, guest inclusion appears to be independent of the flexibility or electronic structure of the guest. Aromatic and fluorinated aromatic molecules, as well as saturated and unsaturated aliphatic molecules perform equally well as guests (Table 1, entries 6–10). The presence of heteroatoms does not seem to inhibit cocrystal formation (Table 1, entries 1–5, 11–13). The host also accommodates molecules that do not contain a six-membered ring (Table 1, entries 11–15). Consequently, the likelihood of a molecule to be incorporated in **1** seems to be determined largely by size. The inability to use hexane or 1,2-dimethoxyethane as guests, as opposed to cyclohexane and 1,4-dioxane, suggests that shape is also relevant for the formation of **1**·guest.

The inclusion versatility of **1** contrasts with our inability to obtain a binary cocrystal of caf and sa.[20] Removal of the guest from **1**·0.66 $C_4H_8O_2$, **1**·0.54 C_4H_8OS, or **1**·CH_3NO_2 by heating results in the separation of caf and sa. In contrast, homologues of sa readily form binary cocrystals with caf.[21] In an attempt to rationalize such behavior, we have structurally characterized the 1:1 caf/adipic acid cocrystal (**2**; see Supporting Information).

Structural comparison of **2** and **1**·guest suggests a reason for the instability of a binary solid involving caf and sa (Figure 3). Namely, **2** consists of hydrogen-bonded chains of adipic acid, which are laterally decorated with caf groups and are analogous to the sa chains observed in the complexes of **1**. In **2**, the caf molecules of neighboring chains interdigitate to

 © 2006 Wiley-VCH Verlag GmbH & Co. KGaA, Weinheim

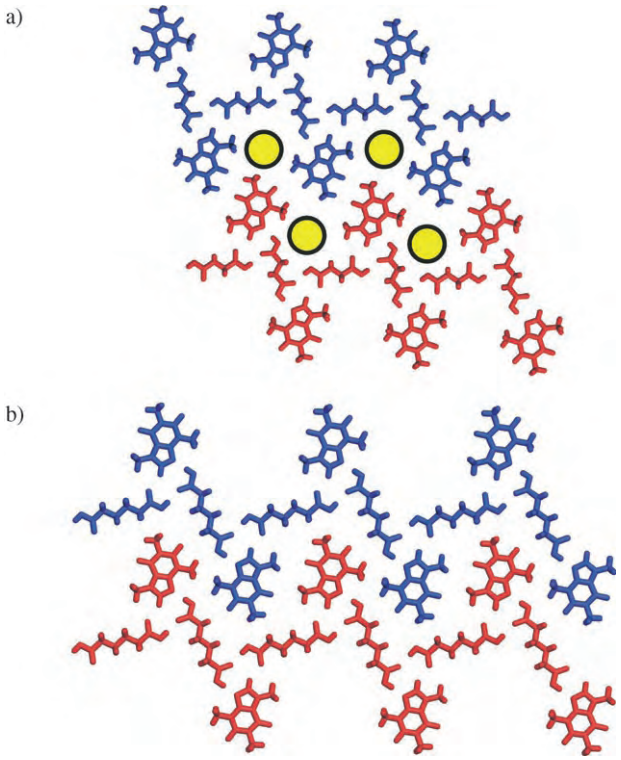

Figure 3. Comparison of the structures of a) **1**·guest and b) **2**. Two interdigitated hydrogen-bonded chains are shown in red and blue; the guests in **1**·guest are indicated by yellow circles.

form sheets with short (3.3 Å) contacts between methyl groups in adjacent chains. Presumably, an analogous structure with sa would lead to shorter, repulsive contacts. As a result, the caf molecules in the host **1** connect by pairs of C–H···O hydrogen bonds and interdigitate only partially, providing room for guest inclusion.

In summary, neat and liquid-assisted grinding have proven advantageous over solution crystallization as methods of screening for three-component inclusion compounds. Crystallization from solution identified 4 (22%) of the 18 inclusion guests recognized by grinding. In addition, the small amounts of liquid involved render grinding methods environmentally more acceptable.[22] From the synthetic aspect, liquid-assisted grinding circumvents the limitations imposed by the solubilities of the cocrystal components, providing a simple and efficient way to systematically construct ternary solids. In particular, liquid-assisted grinding enabled the construction of three ternary cocrystals by introducing solids as guests in a host–guest design. With the guidelines for the construction of inclusion compounds already established, grinding becomes particularly appealing as a tool to construct multicomponent solids.[23] We anticipate that grinding will open new avenues in the construction of cocrystals, in spite of the inability to characterize the products by single-crystal X-ray diffraction. With this limitation in mind, we are currently exploring the characterization of complexes of **1** by spectroscopic and computational methods,[24] as well as the determination of their structures from PXRD data.[25]

Experimental Section

Details of the experimental procedures are given in the Supporting Information, along with PXRD patterns of the products, thermal decomposition curves and solution ^{1}H NMR spectra of **1**·0.66 $C_4H_8O_2$, **1**·0.54 C_4H_8OS, and **1**·CH_3NO_2, as well as solid-state CP-MAS ^{13}C NMR spectra of **1**·0.66 $C_4H_8O_2$ obtained by crystallization from solution, or by neat or liquid-assisted grinding

CCDC-616667 (**1**·0.66 $C_4H_8O_2$), CCDC-616668 (**1**·0.54 C_4H_8OS), CCDC-616669 (**1**·CH_3NO_2), and CCDC-616670 (**2**) contain the supplementary crystallographic data for this paper. These data can be obtained free of charge from The Cambridge Crystallographic Data Centre via www.ccdc.cam.ac.uk/data_request/cif.

Received: August 9, 2006
Published online: October 19, 2006

Keywords: crystal engineering · grinding · host–guest systems · inclusion compounds · screening

[1] a) G. M. J. Schmidt, *Pure Appl. Chem.* **1971**, *27*, 647–678; b) M. C. Etter, S. M. Reutzel, *J. Am. Chem. Soc.* **1991**, *113*, 2586–2598; c) M. D. Hollingsworth, *Science* **2002**, *295*, 2410–2413; d) C. B. Aakeröy, D. J. Salmon, *CrystEngComm* **2005**, *7*, 439–448.
[2] a) P. Vishweshwar, J. A. McMahon, J. A. Bis, M. J. Zaworotko, *J. Pharm. Sci.* **2006**, *95*, 499–516; b) L. S. Reddy, N. J. Babu, A. Nangia, *Chem. Commun.* **2006**, 1369–1371.
[3] a) C. B. Aakeröy, A. M. Beatty, B. A. Helfrich, *J. Am. Chem. Soc.* **2002**, *124*, 14425–14432.
[4] T. L. Nguyen, F. W. Fowler, J. W. Lauher, *J. Am. Chem. Soc.* **2001**, *123*, 11057–11064.
[5] a) A. Sun, J. W. Lauher, N. S. Goroff, *Science* **2006**, *312*, 1030–1034; b) T. Caronna, R. Liantonio, T. A. Logothetis, P. Metrangolo, T. Pilati, G. Resnati, *J. Am. Chem. Soc.* **2004**, *126*, 4500–4501.
[6] J. H. Kim, S. V. Lindemann, J. K. Kochi, *J. Am. Chem. Soc.* **2001**, *123*, 4951–4959.
[7] M. W. Hosseini, A. De Cian, *Chem. Commun.* **1998**, 727–733.
[8] a) C. B. Aakeröy, A. M. Beatty, B. A. Helfrich, *Angew. Chem.* **2001**, *113*, 3340–3342; *Angew. Chem. Int. Ed.* **2001**, *40*, 3240–3242; b) B. R. Bhogala, S. Basavoju, A. Nangia, *CrystEngComm* **2005**, *7*, 551–562.
[9] a) E. J. Cheung, S. J. Kitchin, K. D. M. Harris, Y. Imai, N. Tajima, R. Kuroda, *J. Am. Chem. Soc.* **2003**, *125*, 14658–14659.
[10] a) K. T. Holman, A. M. Pivovar, M. D. Ward, *Science* **2001**, *294*, 1907–1911; b) L. R. MacGillivray, J. L. Atwood, *J. Am. Chem. Soc.* **1997**, *119*, 6931–6932; c) K. Ochiai, Y. Mazaki, K. Kobayashi, *Tetrahedron Lett.* **1995**, *36*, 5947–5950; d) N. Shan, W. Jones, *Tetrahedron Lett.* **2003**, *44*, 3687–3689.
[11] a) V. S. S. Kumar, F. C. Pigge, N. P. Rath, *Cryst. Growth Des.* **2004**, *4*, 1217–1222; b) L. R. Nassimbeni, *Acc. Chem. Res.* **2003**, *36*, 631–637; c) S. Hirano, S. Toyota, M. Kato, F. Toda, *Chem. Commun.* **2005**, 3646–3648.
[12] D. Braga, F. Grepioni, *Angew. Chem.* **2004**, *116*, 4092–4102; *Angew. Chem. Int. Ed.* **2004**, *43*, 4002–4011.
[13] a) N. Shan, F. Toda, W. Jones, *Chem. Commun.* **2002**, 2372–2373; b) A. V. Trask, N. Shan, W. D. S. Motherwell, W. Jones, S. Feng, R. B. H. Tan, K. J. Carpenter, *Chem. Commun.* **2005**, 880–882.
[14] a) A. V. Trask, W. Jones, *Top. Curr. Chem.* **2005**, *254*, 41–70; b) A. O. Patel, D. Y. Curtin, I. C. Paul, *J. Am. Chem. Soc.* **1984**, *106*, 348–353.
[15] F. Toda, K. Tanaka, A. Sekikawa, *J. Chem. Soc. Chem. Commun.* **1987**, 279–280.

 © 2006 Wiley-VCH Verlag GmbH & Co. KGaA, Weinheim

[16] D. Braga, M. Curzi, A. Johansson, M. Polito, K. Rubini, F. Grepioni, *Angew. Chem.* **2006**, *118*, 148 – 152; *Angew. Chem. Int. Ed.* **2006**, *45*, 142 – 146.
[17] A. Nangia, G. Desiraju, *Chem. Commun.* **1999**, 605 – 606.
[18] The use of PXRD to detect the formation of **1** in the product is supported by the appearance of reflections corresponding to either 1) α- or β-caf, caf hydrate, sa and solid guest or 2) a solid isomorphous with **1**·0.66 $C_4H_8O_2$ or 3) a mixture of both.
[19] A similar strategy has been applied to provide a quaternary cocrystal from solution: B. R. Bhogala, S. Basavoju, A. Nangia, *Cryst. Growth Des.* **2005**, *5*, 1683 – 1686.
[20] V. R. Pedireddi, W. Jones, A. P. Chorlton, R. Docherty, *Chem. Commun.* **1996**, 987 – 988.
[21] A. V. Trask, W. D. S. Motherwell, W. Jones, *Cryst. Growth Des.* **2005**, *5*, 1013 – 1021.
[22] N. Shan, W. Jones, *Green Chem.* **2003**, *5*, 728 – 730,.
[23] a) D. V. Soldatov, *J. Inclusion Phenom.* **2004**, *48*, 3 – 9; b) R. Bishop, *Chem. Soc. Rev.* **1996**, *25*, 311 – 319; c) K. T. Holman, A. M. Pivovar, J. A. Swift, M. D. Ward, *Acc. Chem. Res.* **2001**, *34*, 107 – 118; d) V. S. S. Kumar, F. C. Pigge, N. P. Rath, *Cryst. Growth Des.* **2006**, *6*, 193 – 196.
[24] G. M. Day, J. Chisholm, N. Shan, W. D. S. Motherwell, W. Jones, *Cryst. Growth Des.* **2004**, *4*, 1327 – 1340.
[25] A. V. Trask, J. van de Streek, W. D. S. Motherwell, W. Jones, *Cryst. Growth Des.* **2005**, *5*, 2233 – 2241.

 © 2006 Wiley-VCH Verlag GmbH & Co. KGaA, Weinheim

Cluster Compounds

DOI: 10.1002/anie.200603547

Structure of a Discrete Dichloride Hexahydrate Cube as a Tris(diisopropylamino)cyclopropenium Salt**

James R. Butchard, Owen J. Curnow, David J. Garrett, and Robert G. A. R. Maclagan*

The aqueous solvation of halide anions, and the chloride anion in particular, is a highly active area of research, since these are among the most common anions in nature. The energetics and structures of chloride–water clusters are important to our understanding of solvation phenomena.[1] For example, solvated anions are relevant to the study of the interfaces of aqueous salt solutions with air, biologically important water–membrane interfaces, electrical phenomena in the troposphere and ionosphere, and the mobility of ions. Consequently, chloride hydrates have been investigated by a large number of experimental and theoretical techniques.[2] Almost all of these studies have focused on monochloride hydrates $[Cl(H_2O)_n]^-$, and they have addressed issues such as the stabilities and structures (including the coordination number and location of the chloride anion) of the complexes, as well as their infrared spectra. Owing to the tendency of chloride anions to be located on the cluster surfaces, these monochloride hydrate clusters invariably have low-energy polar structures.[2]

In contrast, the study of dichloride hydrates is almost unknown. To our knowledge, no theoretical studies and only one brief structural report of a discrete dichloride hydrate cluster have been published.[3] Dichloride clusters have a greater potential to form nonpolar clusters. They are relevant in concentrated solutions and may be even more relevant in hydrophobic and low-polarity environments. We now report on structural and theoretical studies of the nonpolar cluster $[Cl_2(H_2O)_6]^{2-}$ ($\mathbf{1}^{2-}$).

The solid-state structure of $[C_3(NiPr_2)_3]Cl{\cdot}3H_2O$ was initially determined to investigate the effect of anticipated steric interactions between the isopropyl groups in the previously unknown tris(diisopropylamino)cyclopropenium cation (Figure 1). Other aminocyclopropenium cations contain nitrogen atoms in planar coordination environments; however, steric interactions in $[C_3(NiPr_2)_3]^+$ force two of the isopropyl groups out of the C_3N_3 plane, and one of the nitrogen atoms (N2) assumes a distorted tetrahedral coordination geometry. The structure of this and related cations will be discussed elsewhere.[4]

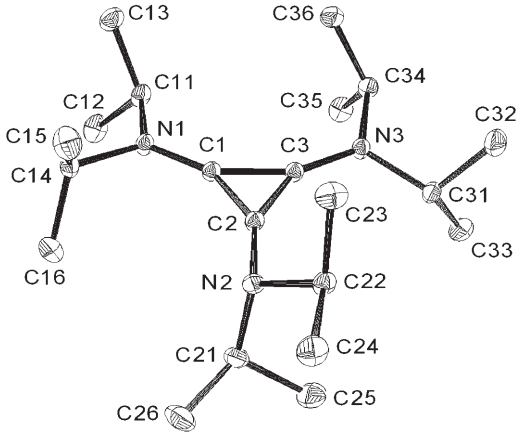

Figure 1. The cation in $[C_3(NiPr_2)_3]Cl{\cdot}3H_2O$. Hydrogen atoms are omitted for clarity. Thermal ellipsoids are set at 50% probability. Selected interatomic distances [Å] and angles [°]: C1–C2 1.3861(8), C1–C3 1.4316(9), C2–C3 1.3881(8), N1–C1 1.3219(7), N2–C2 1.3928(8), N3–C3 1.3260(8); C2-N2-C21 109.57(5), C2-N2-C22 113.83(5), C21-N2-C22 118.99(5).

To our surprise, the chloride anion in $[C_3(NiPr_2)_3]Cl{\cdot}3H_2O$ was found as the discrete dichloride hexahydrate cluster $\mathbf{1}^{2-}$ (Figure 2), in which the chloride anions occupy opposite corners of the Cl_2O_6 cube. Effectively, each chloride anion has

[*] J. R. Butchard, Dr. O. J. Curnow, D. J. Garrett, Prof. R. G. A. R. Maclagan
Department of Chemistry
University of Canterbury
Private Bag 4800, Christchurch (New Zealand)
Fax: (+64) 3-364-2110
E-mail: owen.curnow@canterbury.ac.nz
Homepage:
http://www.chem.canterbury.ac.nz/people/curnow.shtml

[**] Dr. Lourdes Infantes (Instituto de Química-Física Rocasolano, Spain) is thanked for her assistance in identifying other ion hydrate cubes. Prof. Ward Robinson is thanked for his crystallographic assitance.

InterScience
© 2006 Wiley-VCH Verlag GmbH & Co. KGaA, Weinheim

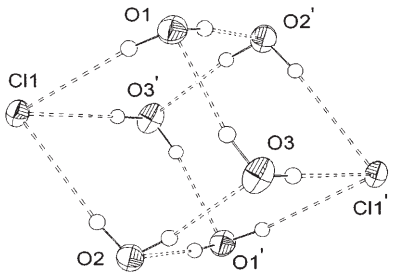

Figure 2. The cluster $\mathbf{1}^{2-}$ in $[C_3(NiPr_2)_3]Cl{\cdot}3\,H_2O$. One of the two possible hydrogen-bonding arrangements is shown; dashed lines indicate hydrogen bonds. Thermal ellipsoids are set at 50% probability. Selected interatomic distances [Å] and angles [°]: Cl1—O1 3.2529(8), Cl1—O2 3.2413(8), Cl1—O3′ 3.1860(8), O1—O3 2.8345(11), O2—O3 2.8245(11), O1—O2′ 2.8379(11), Cl1—Cl1′ 6.3212(5); O1-Cl1-O2 77.02(2), O1-Cl1-O3′ 74.07(2), O2-Cl1-O3′ 72.56(2), O1-O3-O2 91.21(3), O3-O1-O2′ 84.22(3), O3-O2-O1′ 86.46(3).

another chloride anion in its third solvation sphere. Every edge of the cube contains one hydrogen atom, and there are no hydrogen atoms exterior to the cluster. Thus, each chloride anion is involved in three hydrogen bonds. Each oxygen atom has one hydrogen bond to a chloride anion, one hydrogen bond to an oxygen atom, and one hydrogen bond from another oxygen atom. There are two possible hydrogen-bonding arrangements around the O_6 ring (one is shown in Figure 2), each with (noncrystallographic) S_6 symmetry. If the hydrogen-atom positions are averaged, the symmetry of the ring is D_{3d}. The O_6 cluster has a distorted chair conformation, with the axial hydrogen atoms hydrogen bound to the chloride anions. Note that the chloride anions are not encapsulated by water molecules, but can be considered as surface anions.

There has been one report of such a discrete cube:[3] Dalley and co-workers reported $\mathbf{1}^{2-}$ as a salt of sodium [2.2.2]cryptand (Crypt-222; Cambridge Structural Database (CSD) reference code ZOMBAE).[5] A dichloride hexahydrate cube with hydrogen bonding to a cationic complex has been characterized (CHYDNI),[6] and a dibromide hexahydrate cube has also been reported as part of a hydrogen-bonding network (KIQVAH).[7] The salt $[K(Crypt\text{-}222)]Br{\cdot}3.5\,H_2O$ has disordered cubes of water molecules and bromide anions as part of a hydrogen-bonding network.[8] An interesting "inverted" $[Na_2(H_2O)_6]^{2+}$ cube within a network of hydrogen bonds has also been reported.[9]

Table 1 gives selected distances and angles for our $\mathbf{1}^{2-}$ anion and for other $[X_2(H_2O)_6]^{2-}$ (X = Cl, Br) cubes. The Cl—O distances for the three chloride cubes are similar, with the distances in CHYDNI being approximately 0.1 Å shorter than those in the other two. The O—O distances in three of the cubes are very similar (2.790–2.888 Å), but those in ZOMBAE (3.063 Å) are noticeably longer. The $[Na_2(H_2O)_6]^{2+}$ cube has an average O—O distance of 2.787 Å.[9] A crystallographically characterized $(H_2O)_8$ water cube also has a similar average O—O distance (2.85 Å), although considerable variation in the distances (2.750–2.929 Å) results from the interaction of the exterior hydrogen atoms with the cocrystallized cobalt complexes.[10] The most remarkable difference between the chloride cubes lies with the Cl—Cl distance, for which ours is the longest at 6.3212(5) Å, compared to 5.953 Å in ZOMBAE and 5.204 Å in CHYDNI. These differences largely result from the differing angles in the cubes: the O-Cl-O angles in our structure are approximately 10° smaller than those in the two other chloride cubes; the O-O-O angles in our structure are approximately 10° smaller than those in CHYDNI, but are more similar to those in ZOMBAE. The origin of the structural differences between the three $\mathbf{1}^{2-}$ clusters must be a combination of crystal-packing forces (differing electrostatic arrangements) and steric interactions, as well as the external hydrogen-bonding interactions in CHYDNI.

As can be seen in Figure 3, $\mathbf{1}^{2-}$ is well-isolated from the cationic centers in $[C_3(NiPr_2)_3]Cl{\cdot}3\,H_2O$: the chloride anions are surrounded by isopropyl groups, and the closest interactions between the cluster and the C_3^+ ring involve O1 and

Table 1: Selected average structural parameters for $[X_2(H_2O)_6]^{2-}$ clusters.

	This work	ZOMBAE[5]	CHYDNI[6]	KIQVAH[7]
X	Cl^-	Cl^-	Cl^-	Br^-
X—X [Å]	6.321	5.953	5.204	7.057
X—O [Å]	3.227	3.206	3.120	3.428
O—O [Å]	2.832	3.063	2.790	2.888
O-X-O [°]	74.55	83.11	85.63	68.41
O-O-O [°]	87.30	87.96	98.96	83.57

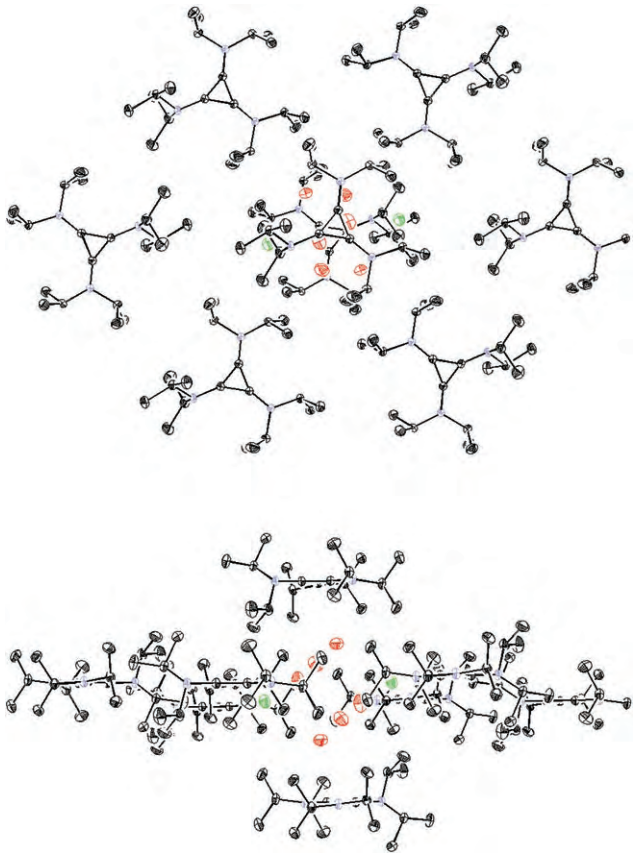

Figure 3. Two orthogonal views of $[C_3(NiPr_2)_3]Cl{\cdot}3\,H_2O$ illustrating the environment of $\mathbf{1}^{2-}$ (Cl green, O red, N blue, C black). Hydrogen atoms are omitted for clarity. Thermal ellipsoids are set at 50% probability.

© 2006 Wiley-VCH Verlag GmbH & Co. KGaA, Weinheim

O1′ (above and below the ring; O1–C1 = 3.1488(9) Å, O1–C2 = 3.5190(9) Å, and O1–C3 = 3.2460(9) Å). Most of the contacts between the chloride anion and the cyclopropenium cation involve the methyl groups (C12, C24, C25, and C33 at C–Cl distances of 3.85–4.0 Å), with the exception of a contact to the hydrogen atom on C34, which is in the α position with respect to a nitrogen atom. For this contact, the Cl–H distance is 2.94 Å, and the C-H-Cl angle is 146.6°. Weiss and coworkers have commented on the electron-rich nature of tris(dialkylamino)cyclopropenium cations and the resultant ion-pair strain between the cations and halide anions, which leads to isolated anions.[11] We might, therefore, expect our cluster to be less distorted from the ideal gas-phase structure than the other known clusters, especially that in CHYDNI, which is involved in external hydrogen bonding.

To investigate the low-energy gas-phase structure of $\mathbf{1}^{2-}$ and its stability, calculations were performed at both the MP2/aug-cc-pVDZ and the B3LYP/aug-cc-pVDZ levels of theory (Table 2). The structures were shown to be true minima by calculation of the harmonic vibrational frequencies. The calculations assumed S_6 symmetry for the structure of $\mathbf{1}^{2-}$. When the calculations were repeated starting with C_1 symmetry, they converged to the S_6 structure. Both calculations give structural parameters that are significantly closer to those found in our X-ray study than to those found in ZOMBAE and CHYDNI. The structural parameters obtained from the MP2 calculation match the experimental values reported herein most closely: the Cl–Cl distance differs by only 0.12 Å, the O–O distances by only 0.004 Å, and the Cl–O distances by only 0.058 Å. Similarly, the angles are in excellent agreement, with less than 1° difference. Apparently, ion-pair strain has resulted in a relatively isolated and undistorted $\mathbf{1}^{2-}$ cluster.

Table 2: Structural parameters and standard enthalpies of formation calculated for $[Cl_2(H_2O)_6]^{2-}$ ($\mathbf{1}^{2-}$) and $[Cl(H_2O)_3]^-$ ($\mathbf{2}^-$).

	$[Cl_2(H_2O)_6]^{2-}$ ($\mathbf{1}^{2-}$)			$[Cl(H_2O)_3]^-$ ($\mathbf{2}^-$)	
	X-ray	B3LYP[a]	MP2[b]	B3LYP[a]	MP2[b,c]
Cl–Cl [Å]	6.321	6.554	6.441	–	–
Cl–O [Å]	3.227	3.312	3.285	3.231	3.222
O–O [Å]	2.832	2.869	2.836	3.025	3.009
O-Cl-O [°]	74.55	73.10	73.61	55.82	55.68
O-O-O [°]	87.30	86.85	87.91	60.00	60.00
ΔH^0 [kJ mol^{-1}]	–	−173.3	−222.0	−159.3	−176.7

[a] B3LYP/aug-cc-pVDZ. [b] MP2/aug-cc-pVDZ. [c] Also see reference [12].

Since the corresponding monomer of $\mathbf{1}^{2-}$, $[Cl(H_2O)_3]^-$ ($\mathbf{2}^-$), has been extensively investigated,[2,12] similar calculations were also performed on this cluster for comparison. The Cl–O distances calculated for $\mathbf{1}^{2-}$, which has no net dipole moment, and the polar pyramidal monomer differ by less than 0.07 Å; however, the O–O distances calculated for $\mathbf{1}^{2-}$ are significantly shorter (by 0.18 Å) than those calculated for $\mathbf{2}^-$. This shortening can be attributed to the more favorable O-H-O hydrogen-bonding angle in the O_6H_6 ring of $\mathbf{1}^{2-}$ (171.7°) than in the O_3H_3 ring of $\mathbf{2}^-$ (144.0°). The calculated O-H-Cl angle for $\mathbf{1}^{2-}$ (173.5°) compares more favorably than that for $\mathbf{2}^-$ (179.5°) to the O-H-Cl angle calculated by Xantheas for $[Cl(H_2O)]^-$ (168.0°).[12]

The strongly negative standard enthalpy of formation (ΔH^0) calculated for $\mathbf{1}^{2-}$ attests to its gas-phase stability. Clearly, the six Cl···H–O hydrogen bonds are sufficient to overcome the electrostatic repulsion between the chloride anions. Note that $\mathbf{1}^{2-}$ is not as stable as its monomer $\mathbf{2}^-$ (for comparison, the ΔH^0 for $\mathbf{2}^-$ should be multiplied by 2).[12] This result is not surprising, given the electrostatic repulsion in $\mathbf{1}^{2-}$, even though the hydrogen-bonding interactions may be stronger in the dianion.

In summary, we have described a well-isolated dichloride hydrate cluster in the solid state and have presented the first calculations for such a species, which indicate that it should also be stable in the gas phase. The presence of such dianionic species in hydrated halide phases should, therefore, be considered, particularly in studies involving concentrated solutions and low-polarity environments, even though local polarizations are likely to be important. Spectroscopic studies of $\mathbf{1}^{2-}$ and investigations of other dichloride hydrates remain to be carried out.

Experimental Section

$[C_3(NiPr_2)_3]Cl{\cdot}3H_2O$ was prepared by addition of $NHiPr_2$ (20.2 g, 0.200 mol) to C_3Cl_5H (3.28 g, 0.0153 mol) at 0 °C in 1,2-$C_2Cl_2H_4$ (100 mL). The solution was stirred overnight and allowed to warm to ambient temperature. It was then heated under reflux for 2 days. A precipitate of $[NH_2iPr_2]Cl$ was separated by filtration. The solvent was then removed to give a brown oil, which was washed with aqueous HCl (100 mL) and then water (200 mL). The organic component was extracted with $CHCl_3$, and after solvent removal, a brown crystalline mass entrained in oil remained. Addition of diethyl ether caused the mass to become an oil, from which crystals were obtained upon cooling (0.52 g, 8% yield). ^{1}H NMR (300 MHz, $CDCl_3$, 23 °C, TMS): $\delta = 3.59$ (septet, ^3J(H,H) = 6.8 Hz, 1H; C*H*-$(CH_3)_2$), 1.27 ppm (d, ^3J(H,H) = 6.8 Hz, 6H; CH(CH_3)$_2$). The chemical shift for the water molecules is highly concentration-dependent, but indicative of free water. ^{13}C{^{1}H} NMR (75 MHz, $CDCl_3$, 23 °C, TMS): $\delta = 117.6$ (s; C_3), 49.5 (s; *C*H(CH$_3$)$_2$), 22.5 ppm (s; CH(*C*H$_3$)$_2$). ES-MS (CH_3CN/H_2O, 20 V): *m/z* (%): 336 (100) $[C_3(NPr_2)_3]^+$, 253 (25) $[C_3(NPr_2)_2OH]^+$. Elemental analysis (%) calcd for $C_{21}H_{48}ClN_3O_3$: C 59.20, H 11.35, N 9.86; found: C 59.53, H 11.25, N 9.71.

X-ray diffraction data for a single crystal of $[C_3(NiPr_2)_3]Cl{\cdot}3H_2O$ was collected using an APEX II diffractometer equipped with a Bruker SMART CCD area detector. The structure was solved by direct methods and refined by least-squares methods on F^2, with anisotropic thermal parameters for all non-hydrogen atoms. The water hydrogen atoms were refined isotropically with O–H distances of 0.84 Å, and the hydrogen atoms in the O_6H_6 ring were refined with equal distributions over the two possible hydrogen-bonding networks. Crystallographic data and refinement parameters: $C_{21}H_{48}ClN_3O_3$, crystal size $0.85 \times 0.26 \times 0.18$ mm^3, $M_r = 426.07$ g mol^{-1}, triclinic, space group $P\bar{1}$, $a = 9.9248(6)$, $b = 10.1879(6)$, $c = 13.1210(7)$ Å, $\alpha = 82.683(3)$, $\beta = 81.063(3)$, $\gamma = 88.233(3)$°, $V = 1299.84(13)$ Å^3, $Z = 2$, $\rho_{calcd} = 1.089$ g cm^{-3}, $\mu = 0.170$ mm^{-1}, $Mo_{K\alpha}$ radiation ($\lambda = 0.71073$ Å), $T = 93(2)$ K, $2\theta_{max} = 69.92$°, 34404 reflections collected, 10109 independent reflections ($R_{int} = 0.0310$), $R_1(I \geq 2\sigma(I)) = 0.0342$, $wR_2(I \geq 2\sigma(I)) = 0.0946$, R_1(all) = 0.0427, wR_2(all) = 0.1029, residual electron density = 0.451/−0.209 e Å^{-3}. CCDC-615639 contains the supplementary crystallographic data for this paper. These data can be

 © 2006 Wiley-VCH Verlag GmbH & Co. KGaA, Weinheim

obtained free of charge from The Cambridge Crystallographic Data Centre via www.ccdc.cam.ac.uk/data_request/cif.

Received: August 31, 2006
Revised: September 11, 2006
Published online: October 16, 2006

Keywords: chlorine · cluster compounds · hydrates · hydrogen bonds · water

[1] a) H. Ohtaki, T. Radnai, *Chem. Rev.* **1993**, *93*, 1157; b) Y. Marcus, *Ion Solvation*, Wiley, Chichester, **1986**; c) D. T. Richens, *The Chemistry of Aqua Ions*, Wiley, Chichester, **1997**.
[2] See, for example: a) D. D. Kemp, M. S. Gordon, *J. Phys. Chem. A* **2005**, *109*, 7688; b) W. H. Robertson, M. A. Johnson, *Annu. Rev. Phys. Chem.* **2003**, *54*, 173; c) R. Ayala, J. M. Martínez, R. R. Pappalardo, E. S. Marcos, *J. Chem. Phys.* **2003**, *119*, 9538; d) R. Custelcean, M. G. Gorbunova, *J. Am. Chem. Soc.* **2005**, *127*, 16362; e) P. S. Lakshminarayanan, E. Suresh, P. Ghosh, *Angew. Chem.* **2006**, *118*, 3891; *Angew. Chem. Int. Ed.* **2006**, *45*, 3807.
[3] Note that searching for hydrogen-bonding motifs can be fraught with difficulties: M. Mascal, L. Infantes, J. Chisholm, *Angew. Chem.* **2006**, *118*, 36; *Angew. Chem. Int. Ed.* **2006**, *45*, 32.
[4] J. R. Butchard, O. J. Curnow, D. J. Garrett, unpublished results.
[5] N. K. Dalley, K. E. Krakowiak, J. S. Bradshaw, X. Kou, R. M. Izatt, *J. Heterocycl. Chem.* **1995**, *32*, 1201.
[6] K. F. Belyaeva, V. N. Biyushkin, V. A. Neverov, L. A. Nezhel'-skaya, N. I. Belichuk, T. I. Rozhdestvenskaya, *Koord. Khim.* **1981**, *7*, 433.
[7] J. Springbord, B. Nielsen, C. E. Olsen, I. Søtofte, *J. Chem. Soc. Perkin Trans. 2* **1999**, 2701.
[8] A. N. Chekhlov, *Russ. J. Coord. Chem.* **2005**, *31*, 230.
[9] C. Chulvi, M. C. Muñoz, L. Perelló, R. Ortiz, M. I. Arriortua, J. Via, K. Urtiaga, J. M. Amigó, L. E. Ochando, *J. Inorg. Biochem.* **1991**, *42*, 133.
[10] W. B. Blanton, S. W. Gordon-Wylie, G. R. Clark, K. D. Jordan, J. T. Wood, U. Geiser, T. J. Collins, *J. Am. Chem. Soc.* **1999**, *121*, 3551.
[11] R. Weiss, T. Brenner, F. Hampel, A. Wolski, *Angew. Chem.* **1995**, *107*, 481; *Angew. Chem. Int. Ed. Engl.* **1995**, *34*, 439.
[12] S. S. Xantheas, *J. Phys. Chem.* **1996**, *100*, 9703.

 © 2006 Wiley-VCH Verlag GmbH & Co. KGaA, Weinheim

Marine Natural Products

DOI: 10.1002/anie.200602047

Azumamides A–E: Histone Deacetylase Inhibitory Cyclic Tetrapeptides from the Marine Sponge *Mycale izuensis***

*Yoichi Nakao, Satoru Yoshida, Shigeki Matsunaga, Nobuaki Shindoh, Yoh Terada, Koji Nagai, Jun K. Yamashita, A. Ganesan, Rob W. M. van Soest, and Nobuhiro Fusetani**

In memory of Takahiro Yamashita

Histone acetylation and deacetylation, which are catalyzed by histone acetyltransferases (HATs) and histone deacetylases (HDACs), respectively, play important roles in transcriptional regulation.[1] Inhibitors of these enzymes induce cell-cycle arrest,[2] p53-independent induction of the cyclin-dependent kinase inhibitor p21,[3] tumor-selective apoptosis,[4] and differentiation of normal and malignant cells.[5] Recently, HDAC inhibitors such as trichostatin A (TSA) and suberoylanilide hydroxamic acid (SAHA) were demonstrated to exert potent anti-angiogenic effects through the alteration of vascular endothelial growth factor signaling.[6] These direct and

[*] Prof. Y. Nakao, S. Yoshida, Prof. S. Matsunaga, Prof. N. Fusetani
Graduate School of Agricultural and Life Sciences
The University of Tokyo
Bunkyo-ku, Tokyo 113–8657 (Japan)
Fax: (+81) 3-5841-8166
E-mail: anobu@mail.ecc.u-tokyo.ac.jp

N. Shindoh, Y. Terada
Molecular Medicine Research Labs
Drug Discovery Research, Astellas Pharma Inc.
21 Miyukigaoka, Tsukuba, Ibaraki 305-8585 (Japan)

Dr. K. Nagai
Fermentation Research Labs
Drug Discovery Research, Astellas Pharma Inc.
5-2-3 Toukoudai, Tsukuba, Ibaraki 305-2698 (Japan)

Prof. J. K. Yamashita
Institute for Frontier Medical Sciences, Kyoto University
53 Kawahara-cho, Shogoin, Sakyo-ku, Kyoto 606-8507 (Japan)

Dr. A. Ganesan
School of Chemistry, University of Southampton
Southampton SO17 1BJ (UK)

Prof. R. W. M. van Soest
Institute for Systematics and Ecology, University of Amsterdam
1090 GT Amsterdam (The Netherlands)

[**] We thank Dr. Kazuo Furihata (University of Tokyo), Prof. Norikazu Nishino (Kyushu Institute of Technology), Dr. Minoru Yoshida (RIKEN), and Prof. Francesco De Riccardis (University of Salerno) for valuable discussions. Samples of authentic (2*S*,3*S*)-, (2*S*,3*R*)-, (2*R*,3*R*)-, and (2*R*,3*S*)-3-amino-2-methyl hexanoic acids were kindly provided by Prof. Junji Kimura (Aoyama Gakuin University). Financial support through a Grant-in-Aid for Scientific Research from the Ministry of Education, Culture, Sports, Science, and Technology of Japan is gratefully acknowledged.

Supporting information for this article is available on the WWW under http://www.angewandte.org or from the author.

© 2006 Wiley-VCH Verlag GmbH & Co. KGaA, Weinheim

indirect effects on tumor growth and metastasis indicate that HDAC inhibitors are potential anticancer agents. In fact, HDAC inhibitors such as valproic acid, SAHA, and FR901228 (FK228) have entered clinical trials as anticancer drugs.[3]

In the course of our search for antitumor leads from Japanese marine invertebrates, we found two HDAC inhibitory sponges among 167 species of marine invertebrates tested. We reported the isolation of cyclostellettamines as active substances from *Xestospongia* sp.[7] Subsequently, we isolated five new cyclic tetrapeptides named azumamides A–E (**1**–**5**) from *Mycale izuensis* (Table 1). Herein, we report the isolation, structure elucidation, and biological activities of these compounds.

Table 1: Azumamides A–E (**1**–**5**).

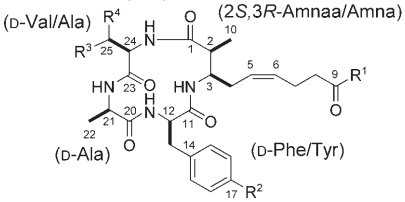

Azumamide	R^1	R^2	$R^3 = R^4$	Yield[a] [mg]	Yield[a] [%]	IC_{50} (HDAC) [μM][b]
A (**1**)	NH_2	H	Me	2.7	1.2×10^{-4}[c]	0.045
B (**2**)	NH_2	OH	Me	1.6	7.3×10^{-5}	0.11
C (**3**)	OH	OH	Me	1.4	6.4×10^{-5}	0.11
D (**4**)	NH_2	H	H	0.6	2.7×10^{-5}	1.3
E (**5**)	OH	H	Me	0.9	4.1×10^{-5}	0.064

[a] Yield of azumamide isolated by extraction from marine sponge (see text for details). [b] Against the crude enzymes extracted from K562 cells. [c] Yield based on wet weight.

Frozen samples (2.2 kg) were exhaustively extracted with EtOH and MeOH. The combined extracts were partitioned between H_2O and Et_2O, and the aqueous layer was further extracted with *n*BuOH. The active *n*BuOH layer was successively subjected to ODS (octadecylsilane) flash chromatography, gel filtration, and ODS HPLC to afford azumamides A–E (Table 1).

Azumamide A (**1**) was obtained as an optically active colorless solid ($[\alpha]_D^{23} = +33°$) with a molecular formula of $C_{27}H_{39}N_5O_5$ as established by high-resolution fast atom bombardment mass spectrometry (HR-FABMS). The peptidic nature of **1** was readily inferred from exchangeable proton signals at $\delta = 7.63$, 7.85, 8.00, and 8.15 ppm, and methine proton signals at $\delta = 3.60$, 4.13, 4.17, and 4.29 ppm in the ^{1}H NMR spectrum. Two-dimensional NMR analysis including COSY, HOHAHA,[8] HMQC,[9] and HMBC[10] led to identification of three usual amino acids, namely alanine (Ala), valine (Val), and phenylalanine (Phe), as well as an unusual β-amino acid residue (see the Supporting Information).

The β-amino acid was assigned as 3-amino-2-methyl-5-nonenedioic acid, 9-amide (Amnaa) on the basis of the following observations: The spin system from H-2 to H_2-8 through two olefinic protons at $\delta = 5.38$ (H-5) and 5.50 ppm (H-6) was readily obtained by COSY analysis; the *Z* geometry of the double bond was deduced from the coupling constant of 11 Hz. COSY cross-peaks CH_3-10/H-2 and NH-3/H-3 placed a CH_3 group and an NH group on C-2 and C-3, respectively. HMBC cross-peaks from the α- and β-methine (H-2 and H-3) and CH_3-10 protons to the carbonyl carbon atom at $\delta = 176.9$ ppm placed this carbonyl group at C-1. On the other hand, HMBC correlations from H_2-8 to the carbonyl carbon atom at $\delta = 178.4$ ppm could place an amide or a carboxylate group at the terminus of the side chain. The molecular formula and two broad proton signals at $\delta = 7.58$ and 6.76 ppm, which were correlated with each other in the HOHAHA spectrum, indicated the amidated terminus of the side chain (Figure 1).

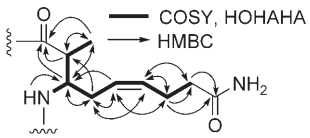

Figure 1. 3-Amino-2-methyl-5-nonenedioic acid, 9-amide (Amnaa). HOHAHA = Homonuclear Hartman–Hahn; HMBC = heteronuclear multiple bond coherence.

The connectivities of these four amino acids were established by analysis of the HMBC spectrum (Figure 2).

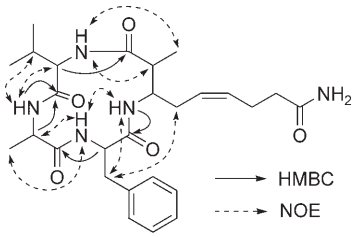

Figure 2. Interresidual HMBC and ROESY correlations for **1**.

An HMBC correlation between NH-3 ($\delta = 7.63$ ppm) and C-11 ($\delta = 174.0$ ppm) connected Amnaa to Phe, while that between H-24 ($\delta = 3.60$ ppm) and C-1 ($\delta = 176.9$ ppm) established the linkage between Amnaa and Val. HMBC cross-peaks H-12/C-20, H-21/C-23, and NH-21/C-23 placed the Ala residue between Val and Phe, thus completing the overall structure, which was also confirmed by ROESY correlations NH-3/H-13a and NH-12, NH-12/H-21 and H-22, NH-21/H-24 and H-25, and NH-24/H-2 and H-10 (Figure 2).

Azumamide B (**2**) has a molecular formula of $C_{27}H_{39}N_5O_6$ as established by HR-FABMS. The ^{1}H NMR spectrum of **2** was almost superimposable on that of **1**, except for signals in the aromatic region. Two doublet signals ($\delta = 7.02$ and 6.66 ppm), each of which was integrated as two protons, implied that the Phe residue in **1** was replaced by tyrosine (Tyr) in **2**.

In the ^{1}H NMR spectrum of azumamide C (**3**), the mutually coupled amide protons of Amnaa in **2** were not observed, suggesting that the terminal amide group of Amnaa in **2** was the free carboxylic acid, hence the relevant amino acid being 3-amino-2-methyl-5-nonenoic-1,9-diacid (Amnda)

 © 2006 Wiley-VCH Verlag GmbH & Co. KGaA, Weinheim

in **3**. The molecular formula of **3** was established as $C_{27}H_{38}N_4O_7$ on the basis of HR-FABMS ($[M+H]^+$ m/z 531.2811; $\Delta = -0.7$ mmu) in accordance with the proposed structure.

Azumamide D (**4**; $C_{25}H_{35}N_5O_5$) was smaller than **1** by a C_2H_4 unit. The presence of Ala in **4** was established in straightforward manner by the presence of a doublet methyl group at $\delta = 1.49$ ppm (H-25) in the ^{1}H NMR spectrum instead of the two doublet methyl signals around $\delta = 0.95$ ppm in **1**, thus suggesting that Val residue in **1** was replaced by Ala in **4**. As in the case of **2** and **3**, azumamide E (**5**; $C_{27}H_{38}N_4O_6$) was related to **1** as its free acid form.

The absolute configuration of the α-amino acids in **1**–**5** was determined by Marfey analysis[11] to be the all-D form, while the stereochemistry of the β-amino acid (Amnaa) in **1** was determined as follows (Scheme 1): To prevent side

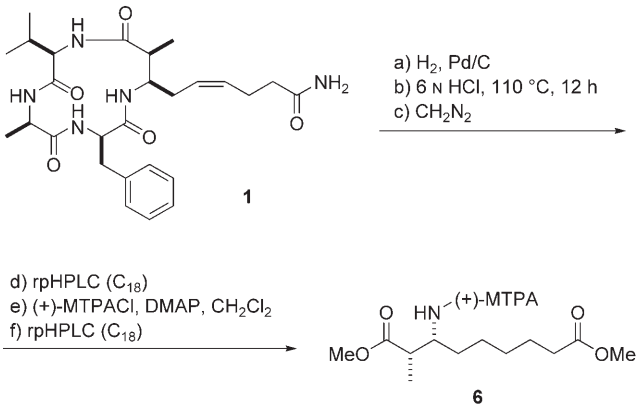

Scheme 1. Degradation and derivatization of **1**. rp = reversed phase; MTPA = α-methoxy-α-(trifluoromethyl)phenylacetic acid; DMAP = 4-(dimethylamino)pyridine.

reactions during acid hydrolysis, **1** was hydrogenated over Pd/C, followed by acid hydrolysis. The hydrolyzed residues were esterified with CH_2N_2 and separated by reversed-phase HPLC. Then, the fraction containing the desired methyl ester was derivatized with (+)-MTPACl in the presence of DMAP in CH_2Cl_2, followed by reversed-phase HPLC to obtain the desired MTPA ester **6** (m/z 484 $[M+Na]^+$). Comparison of the spectrum of this MTPA ester **6** with those of the model compounds derived from four stereoisomers of 3-amino-2-methylhexanoic acids suggested its 2*S*,3*R* configuration (see the Supporting Information). Although the limited amounts of samples prevented us from applying the same strategy for **2**–**5**, the similar chemical shifts and coupling constant values for these units allowed us to infer the same 2*S*,3*R* configuration for **1**–**5**.

Azumamides A–E (**1**–**5**) showed potent HDAC inhibitory activity with IC_{50} values of 0.045 to 1.3 μM in an assay using enzymes prepared from K562 human leukemia cells (Table 1). The effect of azumamide A (**1**) on histone deacetylation at the cell level was also evaluated. After incubation during 6 h of K562 cells with **1**, acetylation of histones H3 and H4 was detected by western blot analysis, which clearly showed a dose-dependent inhibition of the deacetylation of Ac-H3 (Lys9 and Lys14) and Ac-H4 (Lys8) by **1** in the concentration range 0.19–19 μM (Figure 3). In accordance with the cell-based assay, azumamide A showed moderate cytostatic effects on WiDr (human colon cancer) cells and K562 (human leukemia) cells with IC_{50} values of 5.8 and 4.5 μM, respectively.

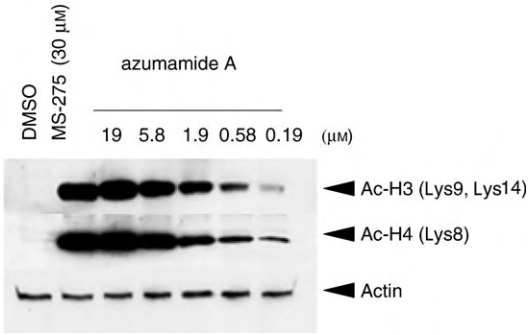

Figure 3. Western blot analysis following the treatment of azumamide A on K562 cells (MS-275: positive control; DMSO = dimethyl sulfoxide).

Furthermore, the anti-angiogenic effect of azumamide A was tested by the in vitro vascular organization model using mouse ES cells.[12] Azumamide A (**1**) at 19 μM significantly inhibited the vascular formation from aggregates of vascular progenitor cells in three-dimensional culture using type-I collagen gel (Figure 4).

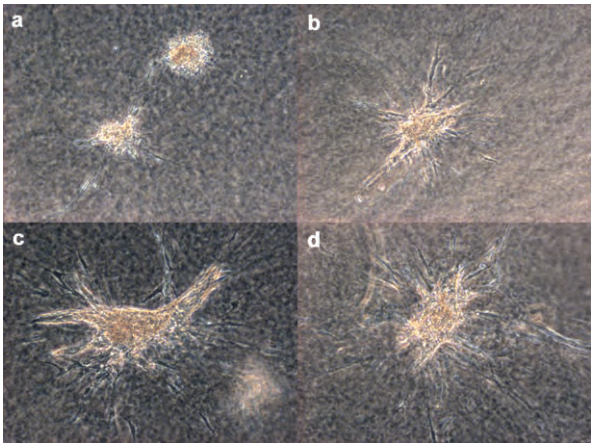

Figure 4. Anti-angiogenic effects of azumamide A (**1**) at a) 19 μM, b) 1.9 μM, and c) 0.19 μM. d) Control (MeOH only).

Only a few examples of marine HDAC inhibitors are known to date; psammaplin obtained from marine sponge *Pseudoceratina purpurea* inhibited HDAC with IC_{50} values of 2.1–327 nM,[13] while azumamides A–E (**1**–**5**) are the first examples of cyclic peptides with HDAC inhibitory activity isolated from marine organisms. Recently, the crystal structure of the complex between a histone deacetylase like protein (HDLP) and trichostatin A (TSA)[14] was solved.[15] The crystal structure provides interesting insights into the binding modes of HDAC inhibitors. According to this

 © 2006 Wiley-VCH Verlag GmbH & Co. KGaA, Weinheim

structure, TSA binds to the enzyme by inserting its long aliphatic chain into the hydrophobic pocket. The hydroxamic acid group at one end of the aliphatic chain reaches the polar bottom of the pocket, where it coordinates with a zinc ion in a bidentate fashion. The aromatic dimethylaminophenyl portion at the other end of the TSA chain makes contacts with the pocket entrance and in an adjacent surface groove, thereby capping the pocket (Figure 5).

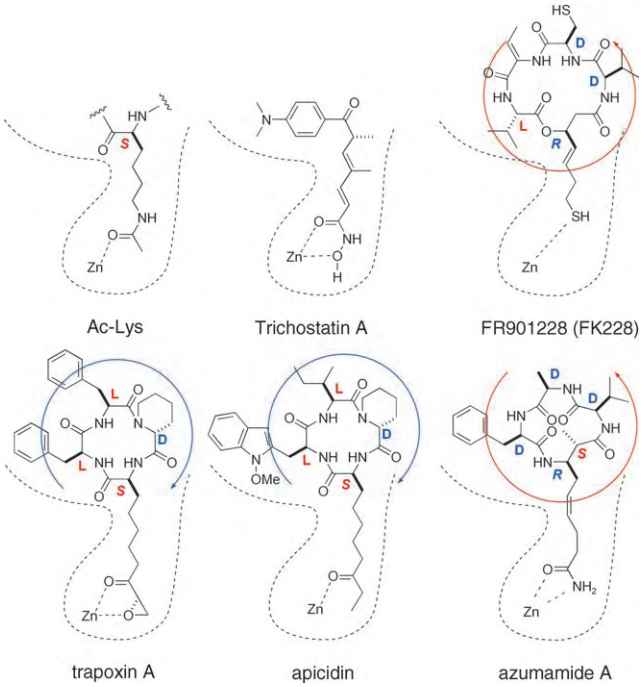

Figure 5. Comparison of plausible binding modes.

Trapoxins (Tpx)[16] and apicidins,[17] two classes of HDAC inhibitory cyclic tetrapeptides, contain groups that may be analogous to the aliphatic chain, the active-site/zinc-binding group, and the cap of TSA. Trapoxins contain a 2-amino-8-oxo-9,10-epoxy-decanoic acid (Aoeda), in which the epoxide group is thought to irreversibly bind to the enzyme,[14b] while the apicidins comprise a 2-amino-8-oxo-decanoic acid (Aoda), with the ketone group being responsible for zinc chelation.[18] The corresponding terminal functions for azumamides are the amide or carboxylate group. Generally, the affinity of an amide group to zinc is much weaker than that of a carboxylic acid. Therefore, it is quite interesting that azumamides A (**1**) and C (**3**) with an amide end showed the equivalent level of HDAC inhibitory activity as azumamides B (**2**) and E (**5**), which have a carboxylate moiety.

Hydrophobic amino acids in Tpx and apicidins may play a role of the dimethylaminophenyl group in trichostatin A. The reversed absolute stereochemistry of Phe/Tyr, Ala, and β-carbon atoms of Amnaa/Amnda in azumamides to that of the corresponding residues of Phe, Phe/Ile, Aoeda/Aoda in trapoxin A/apicidin suggest the possibility that azumamides are retro-enantio types of HDAC inhibitors of trapoxins or apicidins (Figure 5).

Azumamides are the first cyclic peptides from marine invertebrates that exhibit anti-HDAC inhibitory activity. Potent inhibitory activity against HDACs prepared from K562 cells was observed for azumamide A (**1**), while the activity for induction of histone acetylation in K562 cells of **1** remained moderate. The reason for the difference between these results is not yet clear.[19]

Received: May 23, 2006
Published online: September 18, 2006

Keywords: angiogenesis · enzymes · inhibitors · natural products · peptides

[1] J. H. Bayle, G. R. Crabtree, *Chem. Biol.* **1997**, *4*, 885 – 888.
[2] a) L. Sambucetti, D. D. Fischer, S. Zabludoff, P. O. Kwon, H. Chamberlin, N. Trogani, H. Xu, D. Cohen, *J. Biol. Chem.* **1999**, *274*, 34940 – 34947; b) N. Sato, T. Ohta, H. Kitagawa, M. Kayahara, I. Ninomiya, S. Fushida, T. Fujimura, G. Nishimura, K. Shimizu, K. Miwa, *Int. J. Oncol.* **2004**, *24*, 679 – 685.
[3] a) S. Minucci, P. G. Pelicci, *Nat. Rev. Cancer* **2006**, *6*, 38 – 51; b) J.-W. Han, S. H. Ahn, S. H. Park, S. Y. Wang, G.-U. Bae, D.-W. Seo, H.-K. Kwon, S. Hong, H. Y. Lee, Y.-W. Lee, H.-W. Lee, *Cancer Res.* **2000**, *60*, 6068 – 6074; c) R. Ju, M. T. Muller, *Cancer Res.* **2003**, *63*, 2891 – 2897.
[4] a) A. Insinga, S. Monestiroli, S. Ronzoni, V. Gelmetti, F. Marchesi, A. Viale, L. Altucci, C. Nervi, S. Minucci, P. G. Pelicci, *Nat. Med.* **2005**, *11*, 71 – 76; b) A. Nebbioso, N. Clarke, E. Voltz, E. Germain, C. Ambrosino, P. Bontempo, R. Alvarez, E. M. Schavone, F. Ferrara, F. Bresciani, A. Weisz, A. R. de Lera, H. Gronemeyer, L. Altucci, *Nat. Med.* **2005**, *11*, 77 – 84.
[5] a) P. N. Munster, T. Troso-Sandoval, N. Rosen, R. Rifkind, P. A. Marks, V. M. Richon, *Cancer Res.* **2001**, *61*, 8492 – 8497; b) M. Jung, G. Brosch, D. Kölle, H. Scherf, C. Gerhäuser, P. Loidl, *J. Med. Chem.* **1999**, *42*, 4669 – 4679.
[6] C. F. Deroanne, K. Bonjean, S. Servotte, L. Devy, A. Colige, N. Clausse, S. Blacher, E. Verdin, J.-M. Foidart, B. V. Nusgens, V. Castronovo, *Oncogene* **2002**, *21*, 427 – 436.
[7] N. Oku, K. Nagai, N. Shindoh, Y. Terada, R. W. M. van Soest, S. Matsunaga, N. Fusetani, *Bioorg. Med. Chem. Lett.* **2004**, *14*, 2617 – 2620.
[8] A. Bax, M. F. Summers, *J. Am. Chem. Soc.* **1986**, *108*, 2093 – 2094.
[9] M. F. Summers, L. G. Marzilli, A. Bax, *J. Am. Chem. Soc.* **1986**, *108*, 4285 – 4294.
[10] A. Bax, A. Azolos, Z. Dinya, K. Sudo, *J. Am. Chem. Soc.* **1986**, *108*, 8056 – 8063.
[11] P. Marfey, *Carlsberg Res. Commun.* **1984**, *49*, 591 – 596.
[12] J. Yamashita, H. Itoh, M. Hirashima, M. Ogawa, S. Nishikawa, T. Yurugi, M. Naito, K. Nakao, S.-I. Nishikawa, *Nature* **2000**, *408*, 92 – 96.
[13] I. C. Piña, J. T. Gautschi, G. Y. S. Wang, M. L. Sanders, F. J. Schmitz, D. France, S. Cornell-Kennon, L. C. Sambucetti, S. W. Remiszewski, L. B. Perez, K. W. Bair, P. Crews, *J. Org. Chem.* **2003**, *68*, 3866 – 3873.
[14] a) V. G. Allfrey, R. Faulkner, A. E. Mirsky, *Proc. Natl. Acad. Sci. USA* **1964**, *51*, 786 – 794; b) M. Yoshida, M. Kijima, M. Akita, T. Beppu, *J. Biol. Chem.* **1990**, *265*, 17174 – 17179.
[15] M. S. Finnin, J. R. Donigian, A. Cohen, V. M. Richon, R. A. Rifkind, P. A. Marks, R. Breslow, N. P. Pavletich, *Nature* **1999**, *401*, 188 – 1193.
[16] a) H. Itazaki, K. Nagashima, K. Sugita, H. Yoshida, Y. Kawamura, Y. Yasuda, K. Matsumoto, K. Ishii, N. Uotani, H. Nakai, A. Terui, S. Yoshimatsu, Y. Ikenishi, Y. Nakagawa, *J. Antibiot.* **1990**, *43*, 1524 – 1532; b) M. Kijima, M. Yoshida, K. Sugita, S.

 © 2006 Wiley-VCH Verlag GmbH & Co. KGaA, Weinheim

Horinouchi, T. Beppu, *J. Biol. Chem.* **1993**, *268*, 22429 – 22435; c) J. Taunton, C. A. Hassig, S. L. Schreiber, *Science* **1996**, *272*, 408 – 411; d) J. Taunton, J. L. Collins, S. L. Schreiber, *J. Am. Chem. Soc.* **1996**, *118*, 10412 – 10422.

[17] S. B. Singh, D. L. Zink, J. D. Polishook, A. W. Dombrowski, S. J. Darkin-Rattray, D. M. Schmatz, M. A. Goetz, *Tetrahedron Lett.* **1996**, *37*, 8077.

[18] a) S. L. Colletti, R. W. Myers, S. J. Darkin-Rattray, A. M. Gurnett, P. M. Dulski, S. Galuska, J. J. Allocco, M. B. Ayer, C. Li, J. Lim, T. M. Crumley, C. Cannova, D. M. Schmatz, M. J. Wyvratt, M. H. Fisher, P. T. Meinke, *Bioorg. Med. Chem. Lett.* **2001**, *11*, 107 – 111; b) S. L. Colletti, R. W. Myers, S. J. Darkin-Rattray, A. M. Gurnett, P. M. Dulski, S. Galuska, J. J. Allocco, M. B. Ayer, C. Li, J. Lim, T. M. Crumley, C. Cannova, D. M. Schmatz, M. J. Wyvratt, M. H. Fisher, P. T. Meinke, *Bioorg. Med. Chem. Lett.* **2001**, *11*, 113 – 117.

[19] The potency of azumamides varied with HDACs of different origins. These results will be published elsewhere.

 © 2006 Wiley-VCH Verlag GmbH & Co. KGaA, Weinheim

ment of new anticancer agents.[2] Recently, Fusetani and coworkers isolated azumamides A–E (**1**–**5**; Table 1) from the marine sponge *Mycale izuensis*;[3] they represent five unusual cyclic peptides that show potent inhibitory activity on histone deacetylase (HDAC) enzymes (IC_{50}: 0.045–1.3 μM).

Table 1: The azumamides A–E (**1**–**5**).

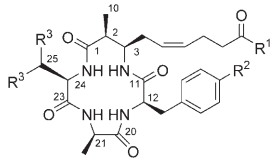

azumamides A–E

Azumamide	R^1	R^2	R^3
A (**1**)	NH_2	H	Me
B (**2**)	NH_2	OH	Me
C (**3**)	OH	OH	Me
D (**4**)	NH_2	H	H
E (**5**)	OH	H	Me

Natural Product Synthesis

DOI: 10.1002/anie.200602033

Total Synthesis of Azumamides A and E**

Irene Izzo, Nakia Maulucci, Giuseppe Bifulco, and Francesco De Riccardis**

In memory of Luigi Gomez-Paloma and Guido Sodano

In the last years, marine invertebrates have yielded some of the most interesting and biologically important secondary metabolites.[1] Among these fascinating structures, cyclic peptides demonstrate impressive antiproliferative properties and considerable promise as lead structures for the development of new anticancer agents.[2] Recently, Fusetani and coworkers isolated azumamides A–E (**1**–**5**; Table 1) from the marine sponge *Mycale izuensis*;[3] they represent five unusual cyclic peptides that show potent inhibitory activity on histone deacetylase (HDAC) enzymes (IC_{50}: 0.045–1.3 μM).

Histone acetylation plays a fundamental role in gene expression, interfering with transcription-based processes and the regulation of the cell cycle.[4] The modulation of histone-modifying enzymes is recognized as a critical factor for the epigenetic control of oncogene transcription and the activation of tumor repressors.[4b] These combined effects can force cancer cells toward differentiation and growth arrest, rendering HDAC inhibitors as unique leads for the development of specific, noncytotoxic antitumor antibiotics.

Azumamides belong to the rare class of HDAC inhibitors typified by a cyclic tetrapeptide core.[4b] Structurally, they include four nonribosomal amino acid residues, three of which are α-amino acids belonging to the D series (D-Phe, D-Tyr, D-Ala, D-Val), while the fourth one is a unique β-amino acid assigned as (*Z*)-(2*S*,3*R*)-3-amino-2-methyl-5-nonenedioic acid, 9-amide (Amnaa) in azumamides A (**1**), B (**2**), and D (**4**), and as (*Z*)-(2*S*,3*R*)-3-amino-2-methyl-5-nonendioic acid (Amnda) in azumamides C (**3**) and E (**5**).[3]

The configurations at C2 and C3 of the Amnaa residue in azumamide A (**1**) were determined through derivatization with (+)-MTPA-Cl of the free α-methyl-β-amino acid, once isolated and after minor modifications.[3] Comparison of the ^{1}H NMR spectrum of the MTPA amide with those recorded for the stereochemically defined 3-amino-2-methylhexanoic acid models indicated a 2*S*,3*R* pattern. The same configurations were proposed for the remaining azumamides (**2**–**5**) on the basis of their similar chemical shifts and coupling constant values observed in their NMR spectra.[3]

The novel molecular features and the interesting bioactivity of azumamides prompted us to embark on an integrated project consisting of 1) the elaboration of a potentially stereodivergent route for the synthesis of the cyclopeptide architecture of the azumamides and 2) the search of the solution structure for azumamide E (**5**). The first objective served to unequivocally establish the stereochemistry of the Amnaa and Amnda residues, while the second goal was a prerequisite for the inhibitor–enzyme docking studies.

[*] Dr. I. Izzo, Dr. N. Maulucci, Prof. F. De Riccardis
Department of Chemistry
University of Salerno
Via Ponte Don Melillo, 84084 Fisciano/Salerno (Italy)
Fax: (+39) 89-969-603
E-mail: iizzo@unisa.it
dericca@unisa.it
Prof. G. Bifulco
Department of Pharmaceutical Sciences
University of Salerno
Via Ponte Don Melillo, 84084 Fisciano/Salerno (Italy)

[**] Financial support from the MIUR ("Sintesi di Sostanze Naturali e di loro analoghi sintetici con attività antitumorale") and the Università degli Studi di Salerno is acknowledged. Both the institutions are also gratefully acknowledged. We thank Prof. Nobuhiro Fusetani and Dr. Yoichi Nakao (University of Tokyo) and A. Ganesan (University of Southampton) for valuable discussions, and Prof. Agostino Casapullo and Dr. Patrizia Iannece for the mass spectra.

Supporting information for this article is available on the WWW under http://www.angewandte.org or from the author.

 © 2006 Wiley-VCH Verlag GmbH & Co. KGaA, Weinheim

Initially, we investigated the possible synthesis of azumamide A (**1**). Our convergent approach is shown in Scheme 1 and featured the β-amino acid **7** and the *all*-D tripeptide **8** as key synthons. The synthesis of the α-methyl-β-amino-ω-

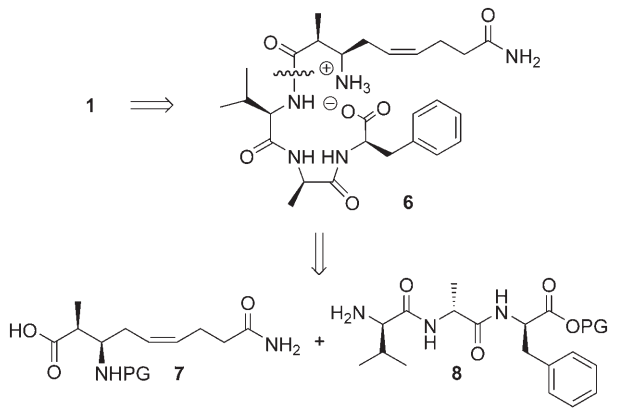

Scheme 1. Retrosynthetic plan for azumamide A. PG = protecting group.

carbamoyl acid **7** relied on the stereochemically flexible Brown's crotylboration reaction[5] and started from the commercially available 3-benzyloxypropanol (**9**, Scheme 2).[6] The homoallylic acetate[7] **11** was obtained through a highly diastereo- and enantioselective (d.r. > 99%; 98% *ee*[8]) crotylation performed with the chiral reagent (+)-(*E*)-crotyl-Ipc_2-borane on the readily available 3-benzyloxypropanal (**10**). The subsequent reductive ozonolysis[9] furnished variable ratios of the regioisomeric acetates **12** and **13**. K_2CO_3-mediated hydrolysis of the mixture of acetates

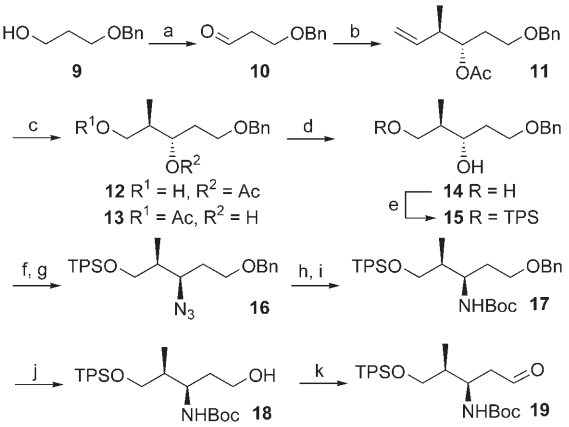

Scheme 2. Reagents and conditions: a) oxalyl chloride, DMSO, Et_3N, CH_2Cl_2, 98%; b) i) (+)-Ipc_2BOMe, (*E*)-2-butene, *t*BuOK, *n*BuLi, $BF_3{\cdot}Et_2O$, THF, −78°C; ii) Ac_2O, py, CH_2Cl_2, 80%; c) O_3, CH_2Cl_2, then PPh_3; $NaBH_4$, EtOH; d) K_2CO_3, MeOH, 61% over three steps; e) TPSCl, DMAP, py, CH_2Cl_2, 90%; f) MsCl, Et_3N, THF; g) NaN_3, DMF, 60°C, 89% over two steps; h) H_2, Pt_2O, EtOAc; i) Boc_2O, Et_3N, CH_2Cl_2, 92% over two steps; j) H_2, Pd/C, EtOH; k) oxalyl chloride, DMSO, Et_3N, CH_2Cl_2, 93% over two steps. Bn = benzyl; DMSO = dimethyl sulfoxide; Ipc = isopinocampheyl; py = pyridine; TPS = *tert*-butyldiphenylsilyl; DMAP = 4-dimethylaminopyridine; Ms = mesyl; DMF = *N*,*N*-dimethylformamide; Boc = *tert*-butyloxycarbonyl.

and regioselective silylation of the diol **14** produced the requested (2*R*,3*S*)-1-[(*tert*-butyldiphenylsilyl)oxy]-5-benzyloxy-2-methyl-3-pentanol (**15**).

Three-step stereospecific amination at C3 and Boc-protection furnished the orthogonally triprotected aminodiol **17** in good overall yield. Pd-mediated hydrogenation and sequential Swern oxidation afforded the (3*R*,4*S*)-3-[(*tert*-butyloxycarbonyl)amino]-5-[(*tert*-butyldiphenylsilyl)oxy]-4-methylpentanal (**19**) in 93% yield over two steps. With the aldehyde in hand, we were ready to complete the synthesis of the key intermediate (*Z*)-(2*S*,3*R*)-3-[(*tert*-butyloxycarbonyl)amino]-2-methyl-5-nonenedioic acid, 9-amide (**25**, Scheme 3).

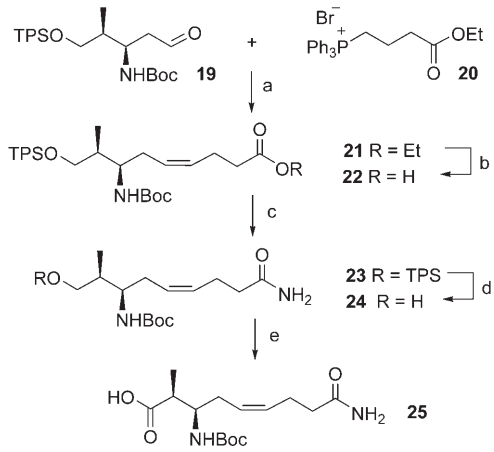

Scheme 3. Reagents and conditions: a) KHMDS, THF, −78°C→RT, 76%; b) LiOH, H_2O/THF, 70°C, 91%; c) DPPA, NH_4Cl, Et_3N, DMF, 79%; d) HF/py, py, 60%; e) TEMPO, phospate buffer, $NaClO_2$, NaClO, CH_3CN, 37%. KHMDS = potassium 1,1,1,3,3,3-hexamethyldisilazane; DPPA = diphenylphosphorylazide; TEMPO = 2,2,6,6-tetramethyl-1-piperidinyloxy, free radical.

We thus performed a highly stereoselective Wittig olefination[10] by reacting the diprotected aldehyde **19** with the ylide formed from the phosphonium salt **20**.[11] The *Z*-alkene **21** was obtained in good yield and with no detectable accompanying *E* isomer (^{1}H NMR spectroscopy). Lithium hydroxide mediated ester hydrolysis and concurrent DPPA[12] carboxyl group activation gave, in the presence of ammonium chloride, the amide **23** in 72% yield over two steps. Finally, HF-induced desilylation and a disappointingly low-yielding oxidation of the primary alcohol to the carboxylic acid[13] afforded the desired N-protected acid **25** in a modest yield of 22% for two steps.

With fragment **25** in hand, we were ready for the synthesis of the linear tetrapeptide **6**. Its preparation relied on solution-phase peptide synthesis (Scheme 4) and gave key zwitterion **6**, which was ready for the macrolactamization reaction required to produce azumamide A (**1**). Although the linear zwitterion **6** contained the Amnaa residue, which was expected to facilitate the ring closure,[14,15] the macrolactamization reaction performed with the most commonly used reagents for the cyclization of homodetic peptides (DPPA,[12] FDPP,[16] and EDC/HOBt;[15] see Supporting Information)[17] did not give

 © 2006 Wiley-VCH Verlag GmbH & Co. KGaA, Weinheim

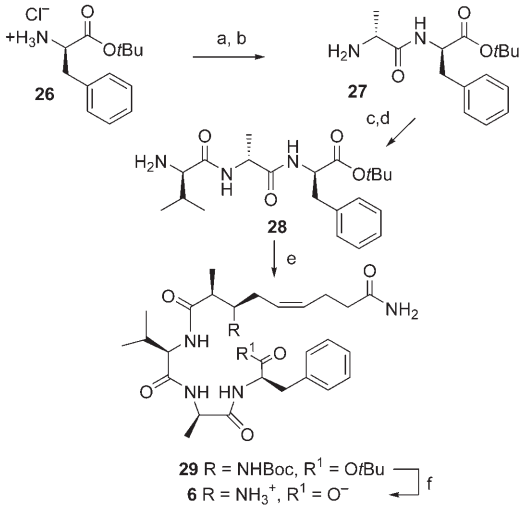

Scheme 4. Reagents and conditions: a) *N*-Fmoc-D-Ala, EDC, HOBt, DIPEA, CH_2Cl_2; b) Et_2NH, CH_3CN, 93% over two steps; c) *N*-Fmoc-D-Val, EDC, HOBt, DIPEA, CH_2Cl_2; d) Et_2NH, CH_3CN, 89% over two steps; e) **25**, EDC, HOBt, DIPEA, CH_2Cl_2, 61%; f) TFA/CH_2Cl_2 (1:1), quant. Fmoc = 9-fluorenylmethoxycarbonyl; EDC = *N*-(3-dimethylaminopropyl)-*N'*-ethylcarbodiimide; HOBt = 1-hydroxybenzotriazole; DIPEA = diisopropylethylamine; TFA = trifluoroacetic acid.

the expected azumamide A (**1**). Considering that the number of variables associated with the cyclization step implies a "test it and see" approach, we decided to steer away from the synthetically bothersome carbamoyl function present in the β-amino acid residue, postponing its introduction to a later stage of the synthesis. Thus, we chose to transform the ethyl ester **21**, an intermediate in the synthesis of **25**, into the corresponding (*Z*)-(2*S*,3*R*)-3-[(*tert*-butyloxycarbonyl)amino]-2-methyl-5-nonenedioic acid, 9-ethyl ester (**31**, Scheme 5), a

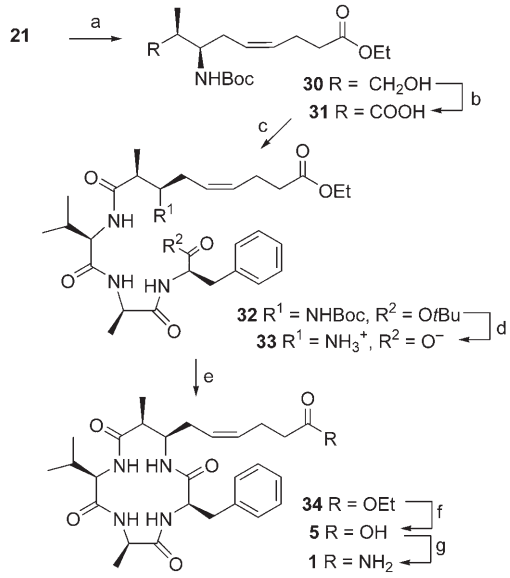

Scheme 5. Reagents and conditions: a) HF/py, py, quant.; b) TEMPO, phospate buffer, $NaClO_2$, NaClO, CH_3CN, 75%; c) **28**, EDC, HOBt, DIPEA, CH_2Cl_2, 86%; d) TFA/CH_2Cl_2 (1:1), quant.; e) FDPP, DIPEA, DMF, 3 days, 37%; f) LiOH, H_2O/THF, 0°C, 75%; g) DPPA, NH_4Cl, Et_3N, DMF, 54%; FDPP = pentafluorophenyl diphenylphosphinate.

protected form of the Amnda residue, and proceed toward the elaboration of azumamide E (**5**).

As expected, better results were obtained both in the desilylation and in the oxidation[13] steps in the absence of carboxamide. We isolated the protected β-amino acid **31** in a satisfying overall yield of 75%. The C9,N-diprotected Amnda (**31**) was then coupled with the *all*-D tripeptide **28** to give the linear tetrapeptide **32**. Treatment of **32** with a mixture of trifluoroacetic acid/dichloromethane (1:1) led to quantitative deprotection of its carboxylate and amino groups to give **33**. This time, we were delighted to find that the FDPP-mediated macroclactamization reaction performed on **33** produced the C9-protected cyclotetrapeptide **34** in 37% yield.[18] The ethyl ester present in **34** was easily hydrolyzed in the presence of LiOH, and the target azumamide E (**5**) was thus isolated in 75% yield.

Azumamide A (**1**) was subsequently obtained in 54% yield through DPPA-induced amidation of azumamide E (**5**) in the presence of ammonium chloride and a non-nucleophilic base. The analytical data for **1** and **5** ($[\alpha]_D$ values, electrospray mass spectrometry and ^1H and ^{13}C NMR spectroscopy data) measured on the synthetic samples were almost identical to those reported by Fusetani and co-workers[3] for the natural products.[19] A conformational analysis aimed to obtain the experimental structure for azumamide E (**5**) was carried out by means of restrained molecular mechanics (MM) and molecular dynamics (MD) calculations (10 ns, see Supporting Information). The solution-state structure determined from NMR spectroscopy (Figure 1) was obtained by using 17

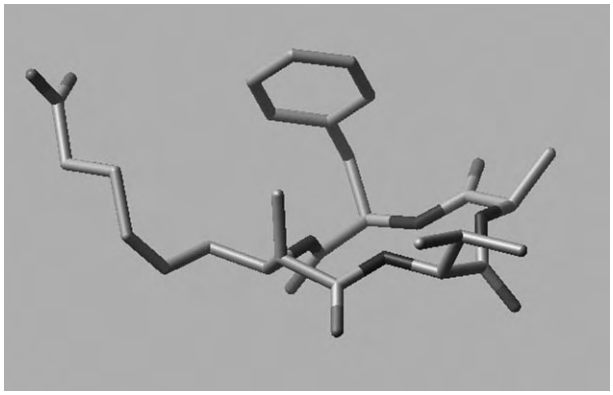

Figure 1. NMR solution-state conformation of azumamide E (**5**) obtained by restrained MD calculations using ROESY data (t_{mix} = 100 ms, 600 MHz, [D_6]DMSO, 300 K). O mid-gray, N dark gray, C pale gray; H atoms omitted.

spatial restraints previously collected in the ROESY spectra ([D_6]DMSO, 600 MHz, t_{mix}: 50, 100, and 150 ms); a careful analysis of its backbone did not reveal the presence of any identifiable turns or defined secondary structure. The presentation of this structure may be considered as an introduction to structural studies of drug–receptor interactions that will follow in due course.

In summary we have developed a successful protocol for the solution-phase synthesis of azumamides A (**1**) and E (**5**),

 © 2006 Wiley-VCH Verlag GmbH & Co. KGaA, Weinheim

establishing unequivocally the configurations of the azumamides, and presented a three-dimensional NMR solution-state structure of azumamide E (**5**). Modification of the core structure of the azumamides and evaluation of their effects on the three HDAC enzymes is currently underway.

Received: May 22, 2006
Published online: September 8, 2006

Keywords: inhibitors · macrolactamization · natural products · peptides · total synthesis

[1] For recent reviews, see: J. W. Blunt, B. R. Copp, M. H. G. Munro, P. T. Northcote, M. R. Prinsep, *Nat. Prod. Rep.* **2006**, *23*, 26–78, and references therein.
[2] For recent reviews, see: Y. Hamada, T. Shiori, *Chem. Rev.* **2005**, *105*, 4441–4482, and references therein.
[3] Y. Nakao, S. Yoshida, S. Matsunaga, N. Shindoh, Y. Terada, K. Nagai, J. K. Yamashita, A. Ganesan, R. W. M. van Soest, N. Fusetani, *Angew. Chem.*, DOI: 10.1002/ange.200602047; *Angew. Chem. Int. Ed.*, DOI: 10.1002/anie.200602047.
[4] a) S. Minucci, P. G. Pelicci, *Nat. Rev. Cancer* **2006**, *6*, 38–51; b) M. Biel, V. Washolowski, A. Giannis, *Angew. Chem.* **2005**, *117*, 3248–3280; *Angew. Chem. Int. Ed.* **2005**, *44*, 3186–3216; c) T. A. Miller, D. J. Witter, S. Belvedere, *J. Med. Chem.* **2003**, *46*, 5097–5116; note that the HDAC inhibition profiles observed for azumamides E and C contradict the assumption that carboxylic acids at the "zinc binding" domain give poor enzymatic activity. See Ref. [4b].
[5] H. C. Brown, K. S. Bhat, *J. Am. Chem. Soc.* **1986**, *108*, 5919–5923; for recent reviews, see: M. Lei, M. P. Sibi, *Tetrahedron* **2002**, *58*, 7991–8035, and references therein.
[6] Experimental procedures and spectroscopic data can be found in the Supporting Information.
[7] The acetylation was necessary for purification purposes.
[8] The enantiomeric excess of compound **11** was evaluated by Mosher ester analysis of the alcohol resulting from acetate hydrolysis (see Supporting Information).
[9] A. B. Benowitz, S. Fidanze, P. L. C. Small, Y. Kishi, *J. Am. Chem. Soc.* **2001**, *123*, 5128–5129.
[10] D. R. Williams, K. Shamim, J. P. Reddy, G. S. Amato, S. M. Shaw, *Org. Lett.* **2003**, *5*, 3361–3364.
[11] Compound **20** was easily prepared from commercially available ethyl 4-bromobutyrate.
[12] K. Uwai, K. Ohashi, Y. Takaya, T. Ohta, T. Tadano, K. Kisara, K. Shibusawa, R. Sakakibara, Y. Oshima, *J. Med. Chem.* **2000**, *43*, 4508–4515.
[13] M. Zhao, J. Li, E. Mano, Z. Song, D. M. Tschaen, E. J. J. Grabowski, P. J. Reider, *J. Org. Chem.* **1999**, *64*, 2564–2566; the oxidation reaction on **24** proved to be capriciously batch-dependant. It is reported therein that the presence of carbon–carbon double bonds can be troublesome. Two-step procedures (from the alcohol to the aldehyde and from the aldehyde to the carboxylic acid) gave yields of less than 30%. Fewer problems were observed for the oxidation of **30** (Scheme 5).
[14] M. P. Glenn, M. J. Kelso, J. T. A. Tyndall, D. P. Fairlie, *J. Am. Chem. Soc.* **2003**, *125*, 640–641.
[15] For recent reviews on peptide cyclizations, see: a) J. W. Davies, *J. Pept. Sci.* **2003**, *9*, 471–501; b) P. Li, P. P. Roller, J. Xu, *Curr. Org. Chem.* **2002**, *6*, 411–440, and references therein.
[16] a) S. Chen, J. Xu, *Tetrahedron Lett.* **1991**, *32*, 6711–6714; b) J. Dudash, Jr., J. Jiang, S. C. Mayer, M. M. Joullie, *Synth. Commun.* **1993**, *23*, 349–356.
[17] In the macrolactamization reaction, the reagents DPPA (the successor of the conventional "azide" coupling methods) and FDPP (inducing the formation of an activated pentafluorophenyl ester) are preferred to carbodiimide-based coupling reagents, whose urea group is difficult to remove (the only exception is the water soluble carbodiimide, EDC), and to "uronium" activators (for the concurrent end-capping through tetramethylguanidylation of the amino group).
[18] Using DPPA and BOP-Cl [bis(2-oxo-3-oxazolidinyl)phosphinic chloride (see: C. van der Auwera, M. J. O. Anteunis, *Int. J. Pept. Protein Res.* **1987**, *29*, 574–588), we observed the formation of trace amounts (ESI-MS analysis) of the cyclotetrapeptide **34** (see Supporting Information).
[19] The small variations in the values in the NMR spectra observed for synthetic azumamide E (**5**) were attributed to its the sensitivity to the apparent pH value of the CD_3OD solutions (see Supporting Information).

 © 2006 Wiley-VCH Verlag GmbH & Co. KGaA, Weinheim

Molecular Dynamics

DOI: 10.1002/anie.200602807

How Flexible Are Poly(*para*-phenyleneethynylene)s?**

*Adelheid Godt, Miriam Schulte, Herbert Zimmermann, and Gunnar Jeschke**

Molecules are often seen as geometrically well-defined building blocks for nanosized objects. Prominent examples are oligo(*para*-phenyleneethynylene)s (oligoPPEs), which are viewed as molecular rods despite their distinct flexibility.[1] Quantitative knowledge about intrinsic flexibility is required for designing functional nanostructures as well as for understanding the mechanical and dynamic properties of molecules. This knowledge can, in principle, be gained from the end-to-end-distance distribution.[2] Information about distance dis-

[*] Prof. Dr. G. Jeschke[+]
Max-Planck-Institut für Polymerforschung
Postfach 3148, 55131 Mainz (Germany)
Fax: (+49) 6131-379-100
E-mail: gunnar.jeschke@uni-konstanz.de
Prof. Dr. A. Godt, M. Schulte
Universität Bielefeld, Fakultät für Chemie
Universitätsstrasse 25, 33615 Bielefeld (Germany)
Dr. H. Zimmermann
Max-Planck-Institut für medizinische Forschung
Jahnstrasse 29, 69120 Heidelberg (Germany)
[+] Current address:
Universität Konstanz, Fachbereich Chemie
Universitätsstrasse 10, 78457 Konstanz (Germany)

[**] This work was supported by the Deutsche Forschungsgemeinschaft. The authors thank M. K. Bowman for an insightful discussion on orientation selection and C. Bauer for technical assistance.

Supporting information for this article is available on the WWW under http://www.angewandte.org or from the author.

WILEY InterScience DISCOVER SOMETHING GREAT
© 2006 Wiley-VCH Verlag GmbH & Co. KGaA, Weinheim

tributions in the nanometer range has recently become accessible by techniques that measure the dipole–dipole interaction between two spin labels.[3] Such measurements can be performed with high precision by pulsed electron–electron double resonance (ELDOR) methods.[4] Recently, this technique was used to characterize the flexibility of bispeptide nanostructures on the basis of the standard deviation of the label-to-label distance distribution.[5] Quantification in terms of a reliable persistence length does, however, require elimination of the contribution of the labels to the distance distribution. Herein we show that such an elimination is possible and that the end-to-end distance distribution $P(r_{EE})$ of oligoPPE backbones can be obtained from pulsed ELDOR data to provide an estimate of the persistence length of polyPPEs.

We concentrate on oligomers because their comparatively small size allows their step-by-step synthesis and therefore a better control of the molecular structure than is possible for polymers. Side products that result from oxidative alkyne dimerization and carbometalation during the Sonogashira–Hagihara coupling, the key reaction for the synthesis of these oligomers and polymers, can be separated from the product.[6] Additionally, the limited purity of the monomers speaks in favor of oligomers: If one assumes that the monomers 1,4-diiodobenzene and 1,4-diethynylbenzene are contaminated with only 0.1% of the constitutional 1,3-isomers, nearly all chains of a polymer batch with a polymerization degree of 1000 contain one *meta* linkage. This polymerization degree is typical for samples used in light-scattering experiments,[7] which is the standard technique for determining the persistence length. *Meta* linkages will reduce the radius of gyration and hence the apparent persistence length.[8] In contrast, only one out of 100 molecules has this defect in the case of a decamer.

Pulsed electron paramagnetic resonance (EPR) techniques[9] are well suited for characterizing structures of 2–8 nm in length.[4,10] At these distances backbone flexibility strongly influences the shape of $P(r_{EE})$ for persistence lengths of the order of 15 nm. Such a persistence length is expected for polyPPEs on the basis of an earlier extensive light-scattering study.[7] The principal limitation of EPR techniques is their requirement for spin labeling, so that the label-to-label-distance distribution $P(r_{LL})$ rather than $P(r_{EE})$ is measured (Scheme 1). The contribution of the labels to $P(r_{LL})$ can be eliminated and thus $P(r_{EE})$ obtained by synthesizing[11] and measuring a series of compounds with the same labeling pattern and backbone structure but different backbone length.

Elimination of the label contribution requires a model for the distribution of conformations of both the label and the backbone. It is necessary to model the backbone, as $P(r_{EE})$ can only be obtained from $P(r_{LL})$ when the distribution of the relative orientations of the backbone ends is also known. We model the backbone as a sequence of jointed stiff segments. As segments we define the phenylene ring, the bond between a phenylene and an ethynylene unit, the triple bond, and the bond between two ethynylene units. The relative segment lengths r_j are taken from the MMFF force field.[12] The angle θ_j at the joint between two segments (Figure 1) is determined by a harmonic bending potential. The bending potential for joints at a phenylene segment is half as large as that for all other joints within the backbone. All torsion angles φ_j are equally likely; that is, the chain rotates freely at its joints, which agrees well with our molecular dynamics (MD) simulations of oligoPPEs. A general stretch factor s for the segment length and the bending potential F_B for the non-phenylene joints are the two fit parameters of the backbone model. The labels are modeled as additional stiff segments of

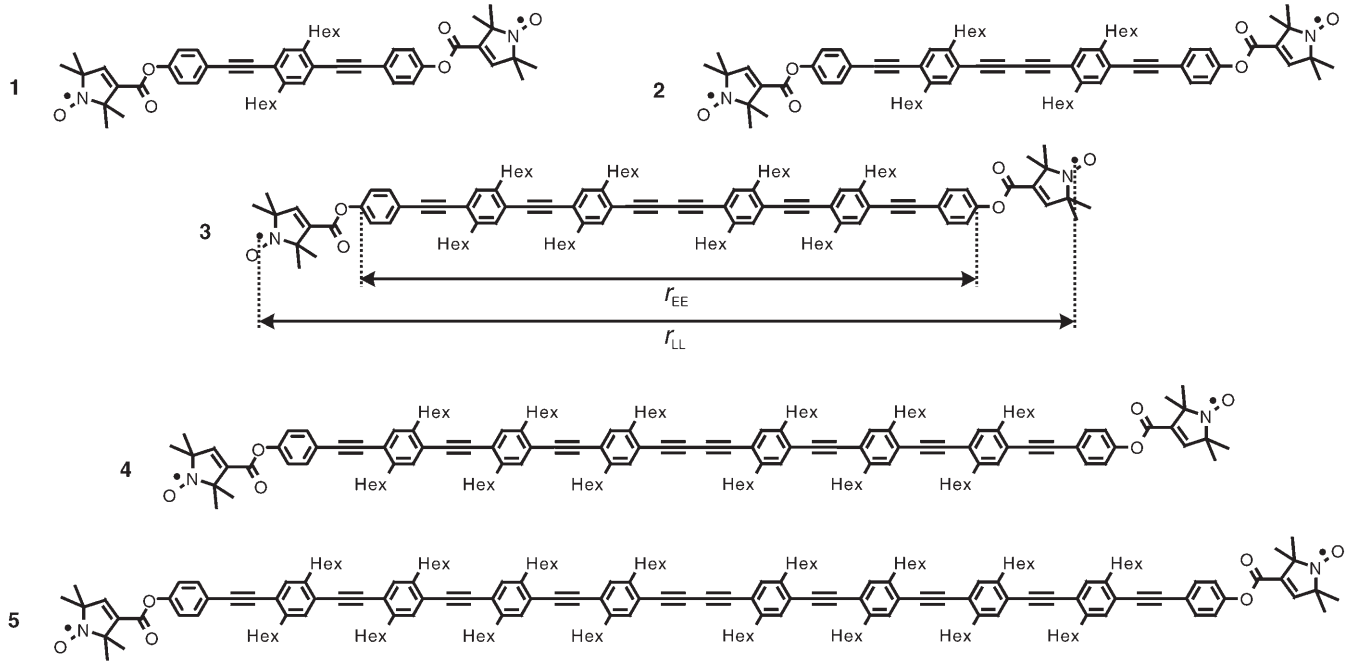

Scheme 1. Structures of the biradicals used and definition of the label-to-label distance r_{LL} and backbone end-to-end distance r_{EE}.

 © 2006 Wiley-VCH Verlag GmbH & Co. KGaA, Weinheim

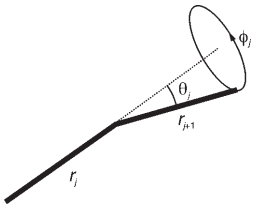

Figure 1. Coarse-grained model for the conformation of the PPE backbone consisting of consecutive segments j and $j+1$ with lengths r_j and r_{j+1}. The segment $j+1$ rotates freely about the dotted axis. For angle θ_j, a normal distribution with a mean value of zero is assumed. The same model is used for the end labels.

length l jointed to the first and last phenylene unit of the backbone with an effective bending potential B. The distribution of label conformations is thus accounted for by two additional fit parameters l and B.

To test whether this model properly separates the label and backbone contribution to $P(r_{LL})$, we applied it to results of MD simulations for **2**–**4** that were obtained with the PCFF force field. The $P(r_{LL})$ and the true $P(r_{EE})$ were extracted from the MD trajectories. The model was fitted to the $P(r_{LL})$ of the three compounds simultaneously. Fit parameters are given in Table 1, and the apparent $P(r_{EE})$ for the ensemble of

Table 1: Best-fit values of the stretch factor s, backbone bending potential F_B, label length l, and effective label bending potential B in the conformational model for oligoPPEs.

Fitted data	s	F_B [k_BT]	l [nm]	B [k_BT]
MD	0.993	38.4	0.650	2.023
DEER	0.991	20.0	0.646	2.019

modeled conformations is compared to the true $P(r_{EE})$ in Figure 2 for each compound. The good agreement justifies the use of the same model for extracting $P(r_{EE})$ from pulsed ELDOR data.

In earlier four-pulse double electron–electron resonance (DEER) measurements on compounds **1** and **3**[3a,4d] we noticed that effects of orientation selection[13] were apparent

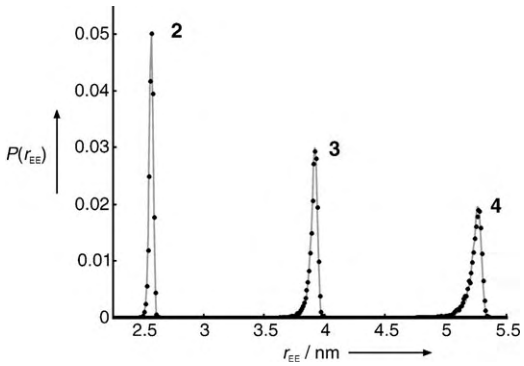

Figure 2. End-to-end distance distributions $P(r_{EE})$ from MD simulations of compounds **2**–**4**. Black dots correspond to the true $P(r_{EE})$ extracted directly from the MD trajectories and gray solid lines to the apparent $P(r_{EE})$ obtained by model-based elimination of the label contribution from the label-to-label distance distribution $P(r_{LL})$.

in dipolar spectra and caused a systematic deviation of the experimental time-domain data from fits during the first dipolar oscillation. Such a systematic deviation might compromise the fitting of the conformational model, in particular for the longer oligomers **4** and **5**, for which only few oscillations can be observed. We therefore introduce orientation averaging by varying the magnetic field so that the observer position is swept between the low-field maximum of the nitroxide spectrum and the global maximum in 23 steps of 0.1 mT. The difference between pump and observer frequency is kept constant at 65 MHz. This procedure virtually eliminates orientation selection and systematic deviations of the fit (Figure 3).

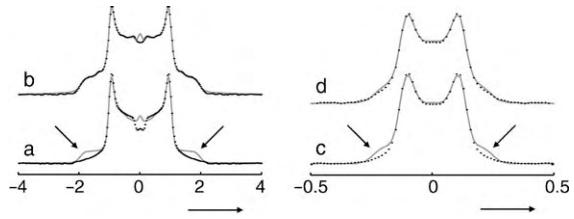

Figure 3. Improved orientation averaging in dipolar spectra obtained by the four-pulse DEER experiment on **2** (a,b) and **5** (c,d). Black dots correspond to experimental data and gray solid lines to simulations for which an ideal powder average is assumed. a,c) Fixed observer and pump positions. Arrows mark deviations due to the suppression of orientations along the spin–spin vector. b,d) Orientation averaging.

To obtain the end-to-end distance distributions $P(r_{EE})$ from the orientation-averaged DEER data, we simultaneously fitted the conformational model to the experimental form factors $F(t)$ of all five compounds. The $F(t)$ values were obtained from the primary experimental data by correcting for the intermolecular background. In our approach the label-to-label distance distributions $P(r_{LL})$ computed with the conformational model are converted into simulated form factors by straightforward matrix multiplication. The other possible approach of converting the experimental $F(t)$ values into distance distributions $P(r_{LL})$ would require the solution of an ill-posed inverse problem and thus compromise the reliability of the fit.[3]

Our conformational model with four variable parameters fits the experimental form factors of all five compounds quite closely (Figure 4). Furthermore, the label length l and

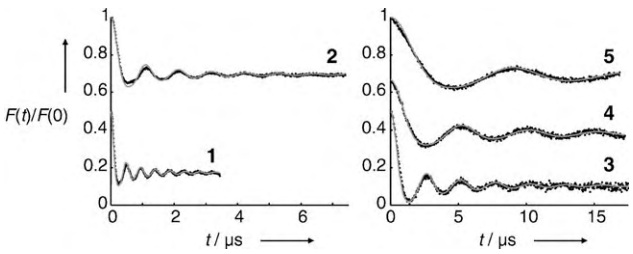

Figure 4. Global fit of the conformational model for oligoPPEs to experimental form factors $F(t)$. Black dots represent experimental data, gray solid lines simulations corresponding to the parameters in Table 1.

 © 2006 Wiley-VCH Verlag GmbH & Co. KGaA, Weinheim

effective label bending potential B agree nicely with the results for the MD data (Table 1), which suggests that an MD simulation in vacuo describes the conformational distribution of the nitroxide end labels quite well. Likewise, good agreement between the MD and DEER data was found for the stretch factor s for the contour length of the backbone. The stretch factor s is close to the ideal value of unity.

In contrast, the bending potential F_B of the backbone joints is smaller for the DEER than for the MD data by almost a factor of two (Table 1). This deviation by far exceeds experimental error. We therefore conclude that the backbone of oligoPPEs is significantly more flexible than suggested by our MD simulations (Figure 2). This greater flexibility is in line with calculation-based predictions for related semiflexible polymers.[14]

The experimental $P(r_{EE})$ results for all compounds are shown in Figure 5 together with a global fit by the Kratky–Porod wormlike-chain (WLC) model; an analytical expression[2] for $P(r_{EE})$ has been used. Within the limits of experimental precision our data agree with this model. The best-fit persistence length is 17.5 nm.

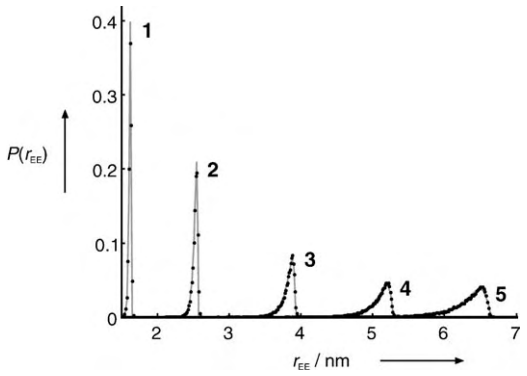

Figure 5. End-to-end distance distributions $P(r_{EE})$ for oligoPPE backbones. Black dots correspond to $P(r_{EE})$ extracted from DEER data, and gray solid lines show a global fit by the WLC model.

If we fit the WLC model to the individual $P(r_{EE})$ of the five compounds, we find persistence lengths of 14.3, 16.9, 18.2, 19.2, and 19.1 nm for **1**, **2**, **3**, **4**, and **5**, respectively. This trend is probably due to the fact that our conformational model, unlike the WLC model, allows for some variation in the contour length by bond-stretching vibrations. The longer the oligomer, the more backbone flexibility dominates the broadening of the distance distribution, so that the data for **4** and **5** are more reliable. Apparently, the persistence length approaches an asymptotic limit of about 19 nm for theses two oligomers. From the contour lengths obtained by the WLC fits we find that one *para*-phenyleneethynylene repeat unit increases the contour length by 0.688 nm.

Although the investigation is restricted to oligomers with a length of up to 8 nm, it provides the persistence length of polyPPE, because the persistence length is a property that depends only on the structure of the repeating units and not on the length of the molecule. Light-scattering experiments on polydisperse polyPPEs gave distinctly shorter persistence lengths of between 13.5 and 16 nm.[7] The difference between the two sets of results may be partially due to the different side groups.[15] It may also hint at the presence of constitutional defects, such as *meta* linkages. For validation, samples of polyPPEs of different origin formed by different synthetic routes[16] need to be investigated.

In summary, we have introduced a new approach for the experimental characterization of the flexibility of shape-persistent molecules. This approach is based on the synthesis of a series of oligomers, spin labeling, the measurement of spin-to-spin distance distributions, and the extraction of the end-to-end distance distribution of the backbone by modeling the conformational ensemble. As information on the residual flexibility of shape-persistent molecules is a key requirement for the rational design of well-defined nanostructures, this approach should find applications well beyond the determination of the persistence length of semiflexible polymers.

Experimental Section

Synthesis: Compounds **1**–**3** were synthesized as described previously.[11] Compounds **4** and **5** were synthesized analogously. Synthetic procedures and analytical data are given in the Supporting Information.

DEER measurements: Glassy frozen solutions of biradical (**1**, **2**: 1.5 mmol L^{-1}; **3**, **4**, **5**: 0.4 mmol L^{-1}) in perdeuterated *o*-terphenyl were analyzed by a variable-time four-pulse DEER experiment on a Bruker E580 spectrometer at a temperature of 50 K.[4b,c,d] Details are given in the Supporting Information.

Modeling: Molecular-dynamics simulations were run for a total time of 2 ns with the program package Cerius2 (v.3.8, Molecular Simulations, Inc.) by using the PCFF force field and a Nosé–Hoover thermostat to generate a canonical ensemble. Distance distributions $P(r_{LL})$ and $P(r_{EE})$ within our conformational model were computed by Monte Carlo simulations by using a home-written Matlab (The MathWorks, Inc., Natick, MA, USA) program. Details are given in the Supporting Information.

Received: July 14, 2006
Published online: October 18, 2006

Keywords: chain model · EPR spectroscopy · polymers · shape persistence · spin labeling

[1] See, for example: a) S. Rucareanu, O. Mongin, A. Schuwey, N. Hoyler, A. Gossauer, *J. Org. Chem.* **2001**, *66*, 4973–4988; b) A. Khatyr, R. Ziessel, *J. Org. Chem.* **2000**, *65*, 3126–3134; c) J. S. Moore, *Acc. Chem. Res.* **1997**, *30*, 402–413; d) V. Hensel, A. Godt, R. Popovitz-Biro, H. Cohen, T. R. Jensen, K. Kjaer, I. Weissbuch, E. Lifshitz, M. Lahav, *Chem. Eur. J.* **2002**, *8*, 1413–1423; e) U. H. F. Bunz, *Adv. Polym. Sci.* **2005**, *177*, 1–52; f) P. F. H. Schwab, M. D. Levin, J. Michl, *Chem. Rev.* **1999**, *99*, 1863–1933; g) C. Grave, A. D. Schlüter, *Eur. J. Org. Chem.* **2002**, 3075–3098.

[2] J. Wilhelm, E. Frey, *Phys. Rev. Lett.* **1996**, *77*, 2581–2584.

[3] a) G. Jeschke, A. Koch, U. Jonas, A. Godt, *J. Magn. Reson.* **2002**, *155*, 72–82; b) M. K. Bowman, A. G. Maryasov, N. Kim, V. J. DeRose, *Appl. Magn. Reson.* **2004**, *26*, 23–29; c) G. Jeschke, G. Panek, A. Godt, A. Bender, H. Paulsen, *Appl. Magn. Reson.* **2004**, *26*, 223–244; d) A. D. Milov, Y. D. Tsvetkov, F. Formaggio, S. Oancea, C. Toniolo, J. Raap, *Phys. Chem. Chem. Phys.* **2004**, *6*, 3596–3603; e) W.-Y. Chiang, P. P. Borbat, J. H. Freed, *J. Magn. Reson.* **2005**, *172*, 279–295; f) G. Jeschke, V. Chechik, P. Ionita,

 © 2006 Wiley-VCH Verlag GmbH & Co. KGaA, Weinheim

A. Godt, H. Zimmermann, J. Banham, C. R. Timmel, D. Hilger, H. Jung, *Appl. Magn. Reson.* in press.
[4] a) A. D. Milov, K. M. Salikhov, M. D. Shirov, *Fiz. Tverd. Tela* **1981**, *23*, 975 – 982; b) R. E. Martin, M. Pannier, F. Diederich, V. Gramlich, M. Hubrich, H. W. Spiess, *Angew. Chem.* **1998**, *110*, 2994 – 2998; *Angew. Chem. Int. Ed.* **1998**, *37*, 2834 – 2837; c) M. Pannier, S. Veit, A. Godt, G. Jeschke, H. W. Spiess, *J. Magn. Reson.* **2000**, *142*, 331 – 340; d) G. Jeschke, A. Bender, H. Paulsen, H. Zimmermann, A. Godt, *J. Magn. Reson.* **2004**, *169*, 1 – 12.
[5] S. Pornsuwan, G. Bird, C. E. Schafmeister, S. Saxena, *J. Am. Chem. Soc.* **2006**, *128*, 3876 – 3877.
[6] H. Kukula, S. Veit, A. Godt, *Eur. J. Org. Chem.* **1999**, 277 – 286.
[7] a) P. M. Cotts, T. M. Swager, Q. Zhou, *Macromolecules* **1996**, *29*, 7323 – 7328; b) compounds **2**–**5** differ, for synthetic reasons, from polyPPEs by one ethynylene unit. Nevertheless, a comparison of the data seems admissible.
[8] a) Y. Zhou, G. S. Chirikjian, *Macromolecules* **2006**, *39*, 1950 – 1960; b) D. Hu, J. Yu, K. Wong, B. Bagchi, P. J. Rossky, P. F. Barbara, *Nature* **2000**, *405*, 1030 – 1033.
[9] A. Schweiger, G. Jeschke, *Principles of Pulse Electron Paramagnetic Resonance*, Oxford University Press, Oxford, **2001**.
[10] a) D. Hinderberger, O. Schmelz, M. Rehahn, G. Jeschke, *Angew. Chem.* **2004**, *116*, 4716 – 4721; *Angew. Chem. Int. Ed.* **2004**, *43*, 4616 – 4621; b) O. Schiemann, N. Piton, Y. G. Mu, G. Stock, J. W. Engels, T. F. Prisner, *J. Am. Chem. Soc.* **2004**, *126*, 5722 – 5729; c) P. P. Borbat, J. H. Davis, S. E. Butcher, J. H. Freed, *J. Am. Chem. Soc.* **2004**, *126*, 7746 – 7747; d) J. E. Banham, C. R. Timmel, R. J. M. Abbott, S. M. Lea, G. Jeschke, *Angew. Chem.* **2006**, *118*, 1074 – 1077; *Angew. Chem. Int. Ed.* **2006**, *45*, 1058 – 1061.
[11] A. Godt, C. Franzen, S. Veit, V. Enkelmann, M. Pannier, G. Jeschke, *J. Org. Chem.* **2000**, *65*, 7575 – 7582.
[12] a) T. A. Halgren, *J. Comput. Chem.* **1996**, *17*, 490 – 519; b) T. A. Halgren, *J. Comput. Chem.* **1996**, *17*, 520 – 552; c) T. A. Halgren, *J. Comput. Chem.* **1996**, *17*, 553 – 586; d) T. A. Halgren, R. B. Nachbar, *J. Comput. Chem.* **1996**, *17*, 587 – 615; e) T. A. Halgren, *J. Comput. Chem.* **1996**, *17*, 616 – 641.
[13] a) R. G. Larsen, D. J. Singel, *J. Chem. Phys.* **1993**, *98*, 5134 – 5146; b) A. Maryasov, Y. Tsvetkov, J. Raap, *Appl. Magn. Reson.* **1998**, *14*, 101 – 113; c) E. Narr, A. Godt, G. Jeschke, *Angew. Chem.* **2002**, *114*, 4063 – 4066; *Angew. Chem. Int. Ed.* **2002**, *41*, 3907 – 3910.
[14] B. L. Farmer, B. R. Chapman, D. S. Dudis, W. W. Adams, *Polymer* **1993**, *34*, 1588 – 1601.
[15] R. A. Vaia, D. Dudis, J. Henes, *Polymer* **1998**, *39*, 6021 – 6036.
[16] a) U. H. F. Bunz, *Acc. Chem. Res.* **2001**, *34*, 998 – 1010; b) R. Pizzoferrato, M. Berliocchi, A. Carlo, P. Lugli, M. Venanzi, A. Micozzi, A. Ricci, C. Lo Sterzo, *Macromolecules* **2003**, *36*, 2215 – 2223.

 © 2006 Wiley-VCH Verlag GmbH & Co. KGaA, Weinheim

Supported Nanocatalysts

DOI: 10.1002/anie.200602456

A Highly Efficient Palladium Nanocatalyst Anchored on a Magnetically Functionalized Polymer-Nanotube Support**

*Sungrok Ko and Jyongsik Jang**

Heterogeneous catalysts have been extensively employed in various fields because they have fewer of the drawbacks of homogeneous catalysts, such as the difficulties in recovery and regeneration.[1] Nanometer-sized catalyst supports have recently attracted a great deal of interest because of their high surface area and outstanding stability and activity in the liquid phase.[2,3] In particular, nanotube-supported catalysts have been selected for highly efficient catalysis because they provide different contact areas that can be functionalized in various ways.[3a] Even though several significant studies regarding nanotube supports have been reported, their complicated functionalization and a lack of surface-functionality control remain major obstacles to practical applications. Magnetic supports have been used as an effective tool for convenient catalyst recycling by applying an external magnetic field.[2a,b] However, most of these examples suffer from the need for a sophisticated synthetic procedure for surface deposition and the aggregation of magnetic particles in the infiltration approach.[3b] Therefore, it is still important to develop a reliable synthetic route to highly efficient reusable catalysts.

Herein, we report a novel approach for the facile fabrication of magnetic polypyrrole nanotubes and subsequent controlled deposition of Pd nanocatalysts on the nanotube surface. Carboxylated pyrrole monomers are chemically polymerized in the presence of iron(III) chloride as an oxidizing agent, and magnetic phases are readily introduced into the nanotubes by precipitation of residual iron salt complexes during the template removal process. These magnetic carboxylated polypyrrole nanotubes (MCPPy NTs) provide the anchoring sites for metal salts, thus making it possible to generate Pd nanocatalyts quantitatively at room temperature without tedious surface functionalization. This is the first demonstration of the fabrication of a magnetically separable polymer nanotube support containing intrinsically functionalized repeating units.

[*] S. Ko, Prof. Dr. J. Jang
Hyperstructured Organic Materials Research Center and
School of Chemical and Biological Engineering
Seoul National University
San 56-1 Shinlim Kwanak, Seoul 151-742 (Korea)
Fax: (+82) 2-888-1604
E-mail: jsjang@plaza.snu.ac.kr

[**] This work was supported in part by the Brain-Korea 21 Program of the Korea Ministry of Education and by the Hyperstructured Organic Materials Research Center of Seoul National University.

Supporting information for this article is available on the WWW under http://www.angewandte.org or from the author.

WILEY InterScience DISCOVER SOMETHING GREAT
© 2006 Wiley-VCH Verlag GmbH & Co. KGaA, Weinheim

Scheme 1 describes the synthetic route to Pd nanocatalysts supported on magnetically functionalized nanotubes (Pd/MCPPy NTs). MCPPy NTs were first prepared by vapor-deposition polymerization (VDP).[4] Vaporized pyrrole-3-carboxylic acid monomers were chemically polymerized by

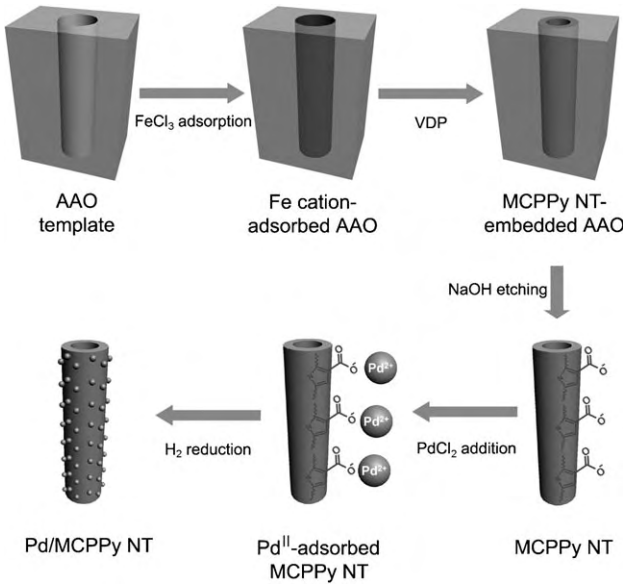

Scheme 1. Synthetic route to Pd/MCPPy NTs.

Fe cations adsorbed on an anodic aluminum oxide (AAO) membrane at 150 °C and 10^{-2} Torr. The magnetic phases were introduced into the polymer during template removal by treatment with a base.[5] Typically, the conducting polymers exist in their oxidized forms owing to electron localization by the dopants (Fe salts).[6] These Fe salt complexes in the polymer backbone were reduced to magnetites by treatment with sodium hydroxide (0.1 M).

The MCPPy NTs provide a defined number of homogeneous surface carboxylate groups since the polymer nanotubes consist of pyrrole monomers with a carboxylic acid moiety. These surface functional groups were subsequently used as the nucleation sites for metal ions.[7] Thus, Pd cations were electrostatically bound to the carboxylate groups of the MCPPy NTs. The carboxylate groups induce electron transfer to Pd^{II} to form Pd^0 in the presence of H_2 as the reducing species.[8] The Pd nanoparticles were retained on the nanotubes because the carbonyl groups of MCPPy NTs coordinate strongly to the surface atoms of the nanoparticles.[9] Surface carboxylate groups therefore enhance the stability of Pd nanoparticles anchored by this salt reduction method.

The successful polymerization to form MCPPy NTs was confirmed by Raman spectroscopy (Supporting Information). The characteristic bands of polypyrrole at 930, 1332, and 1580 cm^{-1} were attributed to the C–H, C–N, and C=C stretching modes, respectively. The peaks of the symmetrical C–H in-plane bending between 930 and 981 cm^{-1} were assigned to the dications (bipolaron) and radical cations (polaron). The relatively high intensity of the bipolaron peak at 930 cm^{-1} indicates a high charge-carrier density, as corroborated by the high electrical conductivity of 3×10^{-2} S cm^{-1}.

Figure 1 shows TEM images of MCPPy NTs and Pd/MCPPy NTs. The MCPPy NTs (Figure 1 A) have a tailored

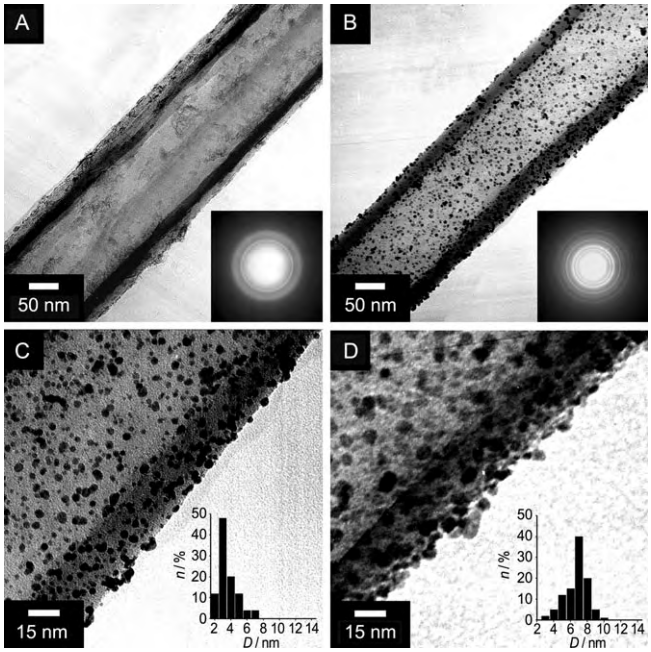

Figure 1. TEM images of A) a MCPPy NT and B) a Pd/MCPPy NT prepared with a dilute $PdCl_2$ solution (1×10^{-4} M). The inset images are the SAED patterns; C) and D) magnified TEM images of Pd/MCPPy NTs obtained using different $PdCl_2$ concentrations (1×10^{-4} and 1×10^{-3} M, respectively). The Pd nanoparticle size was determined by counting 100 Pd nanoparticles by TEM and is illustrated in the inset histogram (C: (3.6 ± 1.3) nm; D: (6.7 ± 3.1) nm).

nanotube morphology, with a diameter of around 100 nm, a uniform wall thickness of 10–20 nm, and an inner vacant volume. The selected area electron diffraction (SAED) pattern confirmed the presence of magnetites. Figures 1 B–D show TEM images of Pd/MCPPy NTs prepared using different $PdCl_2$ solutions. As the $PdCl_2$ concentration increases from 1×10^{-4} to 5×10^{-3} M (not shown), the size of the deposited Pd nanoparticles increases from a lower limit of 3.6 to an upper limit of 9.8 nm. Fast nucleation relative to growth produces a small particle size at low concentrations of Pd salt.[10] Figures 1 B and 1 C show that relatively uniform Pd nanoparticles are formed on the surface of the MCPPy NTs. The SAED pattern (inset in Figure 1 B) of the Pd/MCPPy NTs also shows the presence of Pd on the nanotube. These Pd nanoparticles have a narrow size distribution (the inset histogram of Figure 1 C). However, the nanoparticle size distribution becomes large as the concentration of Pd precursor increases (Figure 1 D).

The fraction of Pd deposited from solution onto the nanotubes was calculated by thermogravimetric analysis. Almost 99 % of the Pd ions in solution were deposited from a 10^{-4} M $PdCl_2$ solution, whereas only 69 % of the Pd in

 © 2006 Wiley-VCH Verlag GmbH & Co. KGaA, Weinheim

solution were deposited with a 5×10^{-3} M $PdCl_2$ solution, a consequence of the excess of Pd ions. This novel synthetic route to Pd/MCPPy NTs may provide a facile means of synthesizing other metal nanoparticles on MCPPy NTs.

The Pd/MCPPy NTs were also characterized by powder X-ray diffraction (XRD) analysis (Supporting Information) and X-ray photoelectron spectroscopy (XPS). The sharp O peak in Figure 2 demonstrates the presence of carbonyl groups in the Pd/MCPPy NTs and the two peaks at 335 and 341 eV for Pd 3d show that Pd is present as Pd^0. The XPS

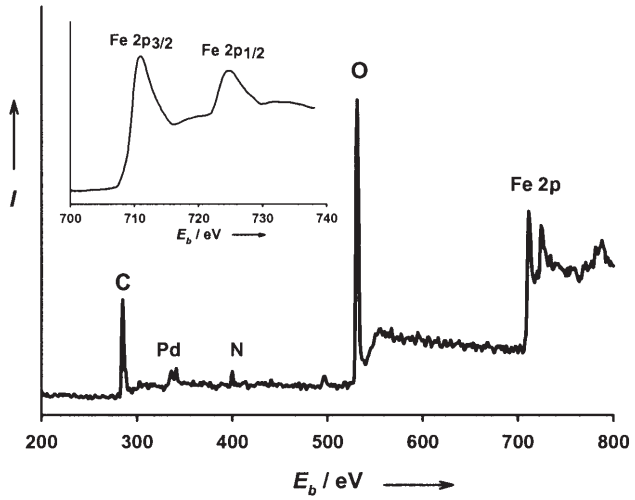

Figure 2. XP spectra of Pd/MCPPy NTs. The inset shows the spectrum in the Fe 2p region.

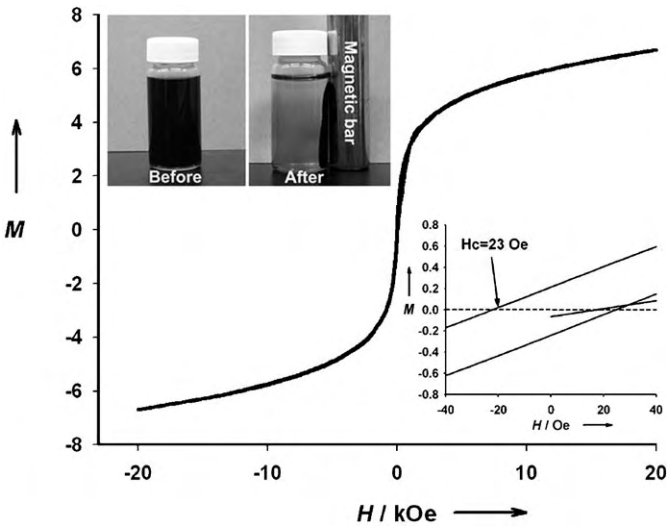

Figure 3. Magnetic behavior of Pd/MCPPy NTs at 300 K between −20 and +20 kOe (M in emu g^{-1}). The inset shows the magnified area between −40 and +40 Oe. The photographs demonstrate that MCPPy NTs in aqueous solution can be attracted and arranged vertically by a magnetic bar (0.3 T). MCPPy NTs completely suspended in aqueous solution can be harvested within 10 s.

spectrum of the Fe 2p region (Figure 2, inset) clearly indicates that the magnetic phases are magnetites.

The magnetic properties of the MCPPy NTs were investigated with a SQUID magnetometer. The magnetization curve exhibits typical ferromagnetic behavior (Figure 3), and saturation of the magnetization (6.7 emu g^{-1}) was found above 1.5 kOe. The coercivity (Hc) of the MCPPy NTs was observed at a field of 23 Oe. A significant enhancement of coercivity was observed relative to the value for bulk iron (Hc = 1 Oe) owing to the anisotropy of the magnetite embedded in the MCPPy NTs.[11] The photographs in Figure 3 demonstrate that the Pd/MCPPy NTs in aqueous solution can be harvested and separated by a magnetic field; this process takes about ten seconds.

To investigate the catalytic activity of Pd/MCPPy NTs three types of olefination of aryl iodides were investigated (Table 1). 4-Iodoanisole and 2-iodotoluene (entries 1 and 2) were chosen as activated aryl halides with an electron-withdrawing group and a methyl group, respectively, and butyl acrylate was used as a model aliphatic olefin as it a precursor of cinnamic ester derivatives. Cinnamic esters are used as UV absorbers in industry.[12] Iodobenzene and styrene were selected (Table 1; entry 3) as a non-activated aryl iodide and aromatic olefin, respectively. It has been reported that non-activated aryl halides are converted with only a low conversion yield.[13] The reaction was carried out in *N*,*N*-dimethylacetamide (DMA) in the presence of tributylamine and 3.6-nm Pd/MCPPy NTs.

Table 1: Olefination of aryl iodides.[a]

Entry	Aryl iodide	Olefin	t [h]	Product	Yield[b] [%]
1		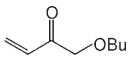	3	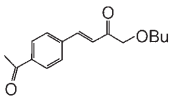	99
2		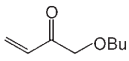	3	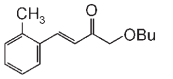	98
3			3	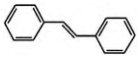	97

[a] The reaction was carried out in DMA (20 mL) at 120 °C with tributylamine (3.0 mmol), aryl iodide (2.0 mmol), and olefin (2.6 mmol) in the presence of 3.6-nm Pd/MCPPy NTs (0.01 g, 21 wt% Pd). [b] The yield was calculated by GC analysis, as described elsewhere.[1f,3a]

When the activated aryl iodides and butyl acrylate were coupled, the yields were approximately 99 and 98%, respectively. More importantly, the non-activated aryl iodide was also converted with a high yield of 97% under the same experimental conditions. The reaction yield with a conventional carbon-supported Pd catalyst is approximately 53%.[3a] This remarkable increase in yield is due to the higher

 © 2006 Wiley-VCH Verlag GmbH & Co. KGaA, Weinheim

available surface area of the Pd nanoparticles, where edge and vertex sites are abundant.[14] Importantly, there was no loss of catalytic activity for conversion of the non-activated aryl iodide and no morphological change of the Pd/MCPPy NTs after recycling and repeating the reaction five times. On the basis of these data, the Pd/MCPPy NTs are excellent potential candidates for reusable and recoverable catalysts.

In conclusion, Pd/MCPPy NTs have been successfully fabricated by the chemical reaction of iron and palladium salts immobilized on a polymer-nanotube support prepared by vapor-deposition polymerization. In particular, the template removal process endows the Pd/MCPPy NTs with enhanced magnetic performance without the need for a complicated attachment of magnetic particles. The Pd/MCPPy NTs show excellent catalytic activity (above 97%) for the Heck coupling of aryl iodides resulting from the narrow size distribution and high surface area of the Pd nanocatalyst. In addition, these Pd/MCPPy NTs show excellent behavior as reusable catalysts of the Heck coupling. This facile methodology could be expanded to allow the fabrication of organic and inorganic nanocarriers in fields such as chemical and biosensors, data storage, separation, and drug-delivery systems.

Experimental Section

MCPPy NTs: Fe cations were adsorbed onto an AAO membrane by immersing the membrane in an $FeCl_3$ solution (0.1M) for 5 min and then drying it in a vacuum oven for 5 h. Residual Fe cations were removed by absorbing three times with disposable sorbents to reduce the possible closing and interconnecting of the nanotubular edges. The Fe-cation-adsorbed AAO membrane and pyrrole-3-carboxylic acid (0.14 mmol) were placed into a reactor which was evacuated at 10^{-2} Torr for 15 min. The monomer (Acros Organics) was purified by distillation. Vapor-deposition polymerization was performed at 150°C for 5 h. The AAO template was removed by treatment with NaOH solution (0.1M) at room temperature for 3 h and the MCPPy NTs were collected by applying an external magnetic field. The detailed procedure is given in the Supporting Information.

Pd/MCPPy NTs: An MCPPy NTs solution (5 mL, 0.5 mg mL^{-1}) was added to a solution $PdCl_2$ (30 mL; 1×10^{-4} to 5×10^{-3} M). Pd salts conjugated to the carboxylate moieties on the nanotube surface were reduced in the presence of an excess of H_2 gas at room temperature. The H_2 gas was bubbled through the mixture for 2 min at a rate of 0.5 L min^{-1}. Residual $PdCl_2$ was removed by washing with distilled water. The detailed procedure is described in the Supporting Information.

Received: June 19, 2006
Published online: October 16, 2006

Keywords: heterogeneous catalysis · magnetic properties · nanotubes · palladium · supported catalysts

[1] a) M. Zhao, R. M. Crooks, *Angew. Chem.* **1999**, *111*, 375–377; *Angew. Chem. Int. Ed.* **1999**, *38*, 364–366; b) J. Grunes, J. Zhu, G. A. Somorjai, *Chem. Commun.* **2003**, 2257–2259; c) R. Narayanan, M. A. El-Sayed, *J. Am. Chem. Soc.* **2003**, *125*, 8340–8347; d) D. Astruc, F. Lu, J. R. Aranzaes, *Angew. Chem.* **2005**, *117*, 8062–8083; *Angew. Chem. Int. Ed.* **2005**, *44*, 7852–7872; e) J. M. Thomas, R. Raja, D. W. Lewis, *Angew. Chem.* **2005**, *117*, 6614–6641; *Angew. Chem. Int. Ed.* **2005**, *44*, 6456–6482; f) R. G. Heidenreich, J. G. E. Krauter, J. Pietsch, K. Köhler, *J. Mol. Catal. A* **2002**, *182–183*, 499–509.

[2] a) A.-H. Lu, W. Schmidt, N. Matoussevitch, H. Bönnemann, B. Spliethoff, B. Tesche, E. Bill, W. Kiefer, F. Schüth, *Angew. Chem.* **2004**, *116*, 4403–4406; *Angew. Chem. Int. Ed.* **2004**, *43*, 4303–4306; b) S. C. Tsang, V. Caps, I. Paraskevas, D. Chadwick, D. Thompsett, *Angew. Chem.* **2004**, *116*, 5763–5767; *Angew. Chem. Int. Ed.* **2004**, *43*, 5645–5649; c) Y. Jiang, Q. Gao, *J. Am. Chem. Soc.* **2006**, *128*, 716–717.

[3] a) B. Yoon, C. M. Wai, *J. Am. Chem. Soc.* **2005**, *127*, 17174–17175; b) G. Korneva, H. Ye, Y. Gogotsi, D. Halverson, G. Friedman, J.-C. Bradley, K. G. Kornev, *Nano Lett.* **2005**, *5*, 879–884.

[4] a) J. Jang, B. Lim, *Angew. Chem.* **2003**, *115*, 5758–5761; *Angew. Chem. Int. Ed.* **2003**, *42*, 5600–5603; b) J. Jang, S. Ko, Y. Kim, *Adv. Funct. Mater.* **2006**, *16*, 754–759; c) S. Yu, N. Li, J. Wharton, C. R. Martin, *Nano Lett.* **2003**, *3*, 815–818; d) M. Steinhart, R. B. Wehrspohn, U. Gösele, J. H. Wendorff, *Angew. Chem.* **2004**, *116*, 1356–1367; *Angew. Chem. Int. Ed.* **2004**, *43*, 1334–1344.

[5] a) D. L. Leslie-Pelecky, *Chem. Mater.* **1996**, *8*, 1770–1783; b) D. K. Kim, M. Kikhaylova, Y. Zhang, M. Muhammed, *Chem. Mater.* **2003**, *15*, 1617–1627.

[6] a) J. Jang, *Adv. Polym. Sci.* **2006**, *199*, 189–259; b) J. Jang, J. H. Oh, G. D. Stucky, *Angew. Chem.* **2002**, *114*, 4188–4191; *Angew. Chem. Int. Ed.* **2002**, *41*, 4016–4019.

[7] D. L. Huber, *Small* **2005**, *1*, 482–501.

[8] M. T. Reetz, E. Westermann, *Angew. Chem.* **2000**, *112*, 170–173; *Angew. Chem. Int. Ed.* **2000**, *39*, 165–168.

[9] E. Bekyarova, A. Hashimoto, M. Yudasaka, Y. Hattori, K. Murata, H. Kanoh, D. Kasuya, S. Iijima, K. Kaneko, *J. Phys. Chem. B* **2005**, *109*, 3711–3714.

[10] C. B. Murray, D. J. Norris, M. G. Bawendi, *J. Am. Chem. Soc.* **1993**, *115*, 8706–8715.

[11] a) J. Jang, H. Yoon, *Small* **2005**, *1*, 1195–1199; b) J. Jang, H. Yoon, *Adv. Mater.* **2003**, *15*, 2088–2091.

[12] W. A. Herrmann, V. P. W. Böhm, C.-P. Reisinger, *J. Organomet. Chem.* **1999**, *576*, 23–41.

[13] A. Perosa, P. Tundo, M. Selva, S. Zinovyev, A. Testa, *Org. Biomol. Chem.* **2004**, *2*, 2249–2252.

[14] a) O. M. Wilson, M. R. Knecht, J. C. Garcia-Martinez, R. M. Crooks, *J. Am. Chem. Soc.* **2006**, *128*, 4510–4511; b) T. Teranishi, M. Miyake, *Chem. Mater.* **1998**, *10*, 594–600.

 © 2006 Wiley-VCH Verlag GmbH & Co. KGaA, Weinheim

Nanotubes

DOI: 10.1002/anie.200602636

Single-Crystal Nanotubes of II_3–V_2 Semiconductors**

Guozhen Shen, Yoshio Bando, Changhui Ye, Xiaoli Yuan, Takashi Sekiguchi, and Dmitri Golberg*

In recent years, considerable attention has been paid to 1D nanostructures, such as wires, rods, belts, ribbons, and tubes owing to their unique physical and chemical properties and potential applications in nanoscale devices with diverse functions.[1] In particular, since the first identification of carbon nanotubes in 1991,[2] much effort has been made to synthesize inorganic nanotubes controllably. A variety of nanotubes based on layered, or pseudolayered materials have been prepared, which include transition-metal chalcogenides (for example, MX_2,[3,4] where M is Mo or W, X is S or Se; and others[5,6]), $NiCl_2$,[7] BN,[8] vanadium oxide,[9] and Bi.[10] Synthesis of single-crystal nanotubes with nonlayered crystal structures was pioneered by Yang and co-workers, who prepared single-crystal GaN nanotubes by an "epitaxial casting" template process;[11] other nanotubes, such as Si and ZnS,[12] have since been obtained by using the same concept.

Semiconducting II_3–V_2 compounds are of scientific and technological importance because they have narrow band gaps. For example, the band gap of Cd_3P_2 is 0.55 eV and Zn_3P_2 has a band gap of 1.55 eV.[13] Owing to the large excitonic radii of these materials, they are expected to exhibit pronounced size quantization effects. The electrons in such a semiconductor will be confined in crystals that are much larger than if they were in analogous II–VI or III–V semiconductors. Bulk II_3–V_2 semiconductors have many potential applications in infrared detectors, lasers, solar-cell technology, ultrasonic multipliers, and Hall generators.[14] However, compared with the significant progress in 1D nanoscale II–VI and III–V semiconductors, research on nanoscale II_3–V_2 semiconductors has been lagging far behind because of the lack of general synthetic methods. To date, there are only a few reports on the synthesis of 0D II_3–V_2 nanoparticles by using metal–organic processes,[15] and no reports on 1D II_3–V_2 nanostructures. Very recently, we synthesized 1D trumpetlike Zn_3P_2 nanostructures by using a thermochemical process.[16] This success inspired us to attempt further efforts in synthesizing hollow nanotubes of II_3–V_2 semiconductors because nanotubes have certain properties that are superior to their nanowire counterparts. For example, hollow nanotubes can serve as nanoscale containers or pipes to deliver fluids and molecular species. They are excellent building blocks for the construction of large-scale nanofluidic systems.[17]

Herein, we report the first synthesis of single-crystal II_3–V_2 nanotubes. Nanotubes of Cd_3P_2 and Zn_3P_2 semiconductors are synthesized by a template process, in which the in situ formed Cd or Zn nanorods act as the self-sacrificing templates for the growing nanotubes. By carefully controlling the experimental parameters, II_3–V_2 nanotube-based 1D heterostructures are also fabricated by using this simple method.

Single-crystal Cd_3P_2 and Zn_3P_2 nanotubes were synthesized at 1350 °C under ambient pressure in a vertical induction furnace from a mixture of CdS (or ZnS), P, and Mn_3P_2 powders. After the reaction had finished, woollike material was collected from the inner wall of the graphite cylinder of the apparatus. The phase composition and structure of the product were examined by powder X-ray diffraction (XRD; Figure 1). As shown in Figure 1a, all the reflection peaks in

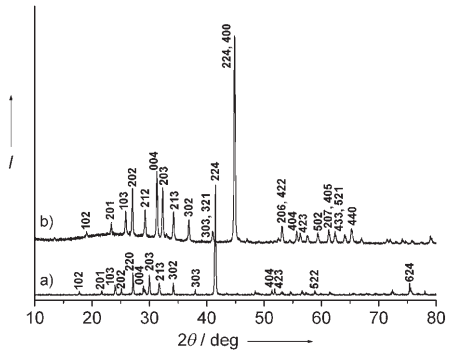

Figure 1. XRD patterns of a) Cd_3P_2 nanotubes and b) Zn_3P_2 nanotubes.

this pattern can be readily indexed to tetragonal phase (space group $P4_2/nmc$) of Cd_3P_2 phase (JCPDS Card No. 65-2856). The pattern in Figure 1b can be indexed to tetragonal (space group $P4_2/nmc$) Zn_3P_2 (JCPDS Card no. 65-2854). During XRD, no characteristic peaks from other crystalline impurities, such as Mn_3P_2, MnP, Zn, ZnS, (or Cd, CdS), were detected, thus indicating the formation of pure products.

Field-emission scanning electron microscopy (FESEM) was used to examine the morphology of the products. Figure 2a shows a low-magnification SEM image of as-synthesized Cd_3P_2 product. The product consists exclusively of 1D wirelike nanostructures with lengths ranging from several tens to hundreds of micrometers. A high-magnification SEM image (Figure 2b) reveals hollow 1D nanostructures. Typically, these Cd_3P_2 nanotubes have outer diameters of 80–250 nm and very thin walls. All the obtained nanotubes had open ends without any attached particles (inset of

[*] Dr. G. Shen, Prof. Y. Bando, Dr. C. Ye, Prof. D. Golberg
Nanoscale Materials Center
National Institute for Materials Science (NIMS)
Namiki 1-1, Tsukuba, Ibaraki 305-0044 (Japan)
Fax: (+81) 298-513-354
E-mail: shen.guozhen@nims.go.jp
Dr. X. Yuan, Prof. T. Sekiguchi
Advanced Electronic Materials Center
National Institute for Materials Science (NIMS)
Namiki 1-1, Tsukuba, Ibaraki 305-0044 (Japan)

[**] We thank Y. Uemura and K. Kurashima for their help in the setup of experiments and TEM work, and Dr. C. Y. Zhi for helpful discussions. II and V indicate elements of Group II and Group V, respectively, of the periodic table.

Supporting information for this article is available on the WWW under http://www.angewandte.org or from the author.

© 2006 Wiley-VCH Verlag GmbH & Co. KGaA, Weinheim

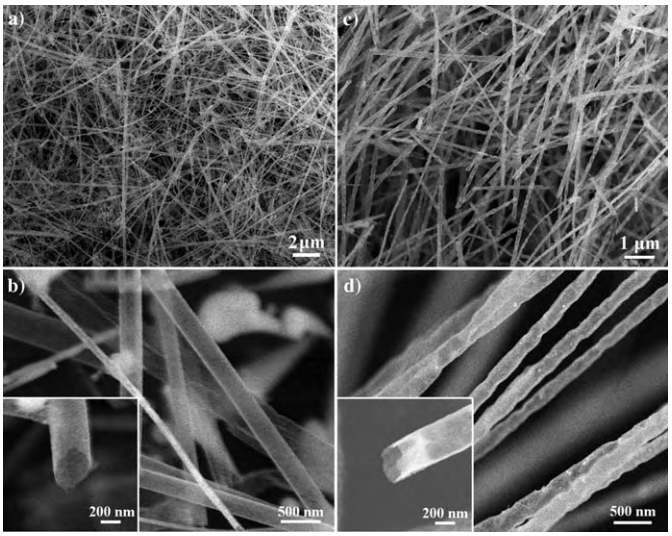

Figure 2. SEM images of a,b) Cd_3P_2 nanotubes and c,d) Zn_3P_2 nanotubes at different magnifications, see text for details.

Figure 2b). An SEM image of the Zn_3P_2 product is shown in Figure 2c, which also documents the formation of 1D wirelike nanostructures with lengths of tens of micrometers. High-magnification SEM images give clear evidence of Zn_3P_2 nanotube formation (Figure 2d and inset). The nanotube outer diameters are in the range of 100–200 nm. As with the Cd_3P_2 nanotubes, all the Zn_3P_2 nanotubes had open tips without any attached particles.

The morphology and composition of the products were further investigated by using transmission electron microscopy (TEM) and energy-dispersive X-ray spectrometry (EDS). Figure 3a shows the low-magnification TEM image of the Cd_3P_2 product and the formation of smooth nanotubes with outer diameters of 80–250 nm, which is in accordance with the SEM results. Figures 3b and c depict the tip ends of the Cd_3P_2 nanotubes: the nanotubes have circular cross sections, open ends without any attached particles, uniform diameters along their entire lengths, and very thin walls. Some partially filled nanotubes were also found (TEM images in Figures 3d and e). EDS spectra of the nanotube walls and the inner filler material were analyzed to check their compositions. The EDS spectrum of a nanotube in Figure 3f shows that the nanotube is composed of Cd and P atoms with an approximate atomic ratio of 1.62:1, which is close to the stoichiometry of Cd_3P_2. In this spectrum, the signals corresponding to Cu arise from the TEM grid. No other impurity was detected. Figure 3g shows the main signal of elemental Cd as well as a weak signal of P, which indicates that the filler material is Cd. Thus, the partially filled structures are Cd-filled Cd_3P_2 nanotubes.

Further detailed structural analysis of the products was carried out by using high-resolution TEM (HRTEM) and selected-area electron diffraction (SAED). Figures 4a and b are the low-magnification TEM images of two typical Cd_3P_2 nanotubes without any filling material. The corresponding SAED pattern in the inset of Figure 4b indicates their single-crystal nature. TEM confirmed that all the Cd_3P_2 nanotubes have very thin walls with respect to their diameters. Figure 4c

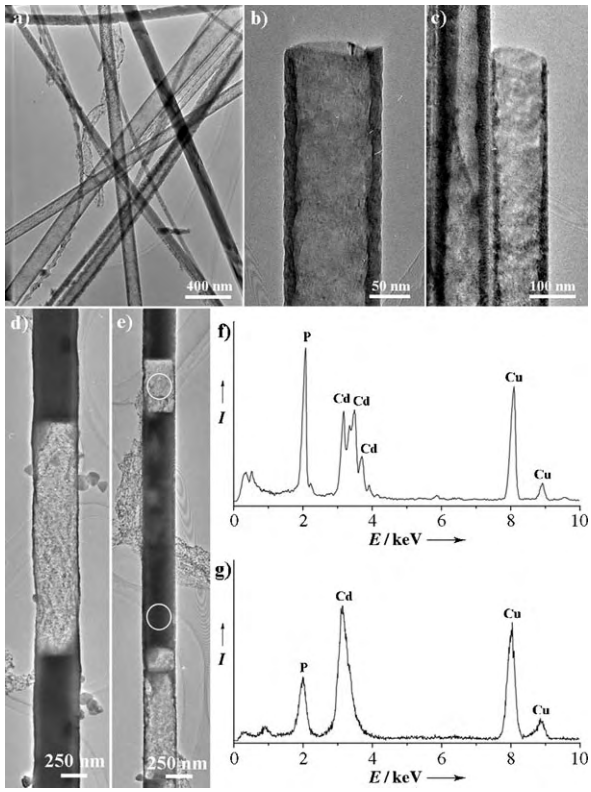

Figure 3. a) TEM image of Cd_3P_2 nanotubes. b,c) TEM images showing the tips of the Cd_3P_2 nanotubes. d,e) TEM images of Cd-filled Cd_3P_2 nanotubes. f,g) EDS spectra of the parts circled in (e), see text for details.

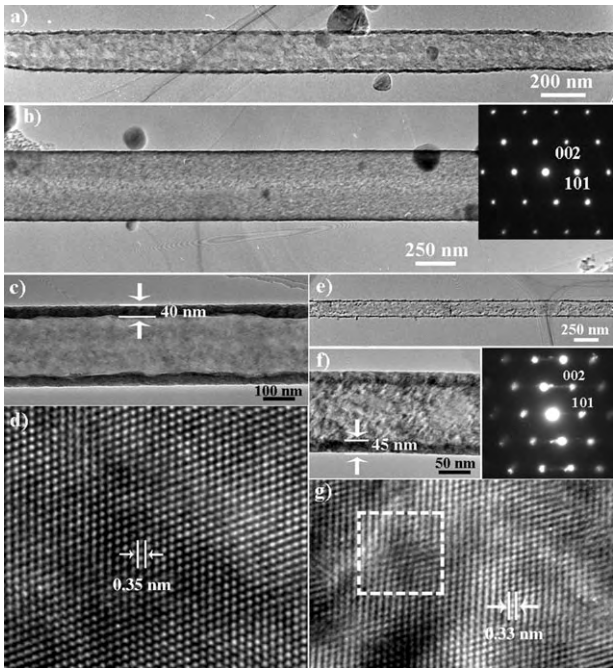

Figure 4. a,b) TEM image of Cd_3P_2 nanotubes and corresponding SAED pattern (inset). c) HRTEM image showing the wall thickness of a Cd_3P_2 nanotube. d) Lattice-resolved HRTEM image of a Cd_3P_2 nanotube. e) Low-magnification TEM image of a Zn_3P_2 nanotube. f) HRTEM image showing the wall thickness of a Zn_3P_2 nanotube and its SAED pattern. g) Lattice-resolved HRTEM image of a Zn_3P_2 nanotube, marked area shows evidence of defects.

 © 2006 Wiley-VCH Verlag GmbH & Co. KGaA, Weinheim

shows a high-magnification (HR) TEM image of a single Cd_3P_2 nanotube with a diameter around 250 nm and wall thickness around 40 nm. A lattice-resolved HRTEM image of the Cd_3P_2 nanotube is given in Figure 4d; the clearly marked interplanar *d* spacing is 0.35 nm, which corresponds to that of the {202} lattice planes of tetragonal Cd_3P_2. In light of the SAED pattern in Figure 4b, the HRTEM result indicates that each Cd_3P_2 nanotube is a single crystal with the preferred growth direction perpendicular to the (101) planes.

Structural information on the Zn_3P_2 nanotubes was obtained by HRTEM analysis. Figure 4e is the TEM image of a single Zn_3P_2 nanotube with an outer diameter of approximately 150 nm; the hollow cavity can be clearly seen. All of the nanotubes are thin, with wall thickness of 5–50 nm. An HRTEM image (Figure 4f) shows a nanotube with a wall thickness of approximately 45 nm. An SAED pattern of the Zn_3P_2 (inset of Figure 4f) confirms that the nanotubes are single-crystalline. Streaks parallel to the growth direction of the Zn_3P_2 nanotube are visible, which indicates the presence of defects within the nanotube. Figure 4g is a lattice-resolved HRTEM image taken of the Zn_3P_2 nanotubes. The lattice spacing of 0.33 nm perfectly matches the {202} lattice planes of tetragonal Zn_3P_2. These fringes are perpendicular to the nanotube axis. The results indicate that the Zn_3P_2 nanotube also has a preferred growth direction perpendicular to the (101) planes, which is similar to that of the Cd_3P_2 nanotubes. Defects, such as dislocations were observed in the nanotube as see in the marked area of the image.

To gain insight into the growth process of II_3–V_2 nanotubes, we performed a series of experiments in which the quantity of reagents, reaction temperature, and time were varied. Figure 5a shows an SEM image of a product when a mixture of ZnS, P, and Mn_3P_2 with a molar ratio of 5:1:1 was used. 1D nanostructures were still formed under these conditions. However, a high-magnification SEM image (Figure 5b) shows that they are of hierarchical branch–stem morphology. TEM and EDS analyses demonstrate interesting hierarchical ZnS nanowire (branches) and Zn_3P_2 nanotube (stems) heterostructures (see Supporting Information). When the amount of ZnS in the mixture was further increased, Zn_3P_2 nanotubes coated with ZnS nanoparticles were obtained instead of pure Zn_3P_2 nanotubes (Figures 5c and d). The reaction temperature is another key factor that influences product morphology. Figures 5e and 5f depict the SEM images of a product synthesized at about 1500 °C. Clearly, the products comprise Zn_3P_2 microtubes with open tips and diameters around 1 μm.

During the formation of Zn_3P_2 nanotubes, most of the nanotubes obtained 20 min after the start of the reaction were filled with Zn metal (Figures 5g and h). With a prolongation of the reaction time, the Zn inside the nanotubes was consumed through evaporation to leave hollow nanotubes. Similar processes were also observed for the formation of Cd_3P_2 nanotubes. Based on these findings, we propose a self-sacrificing template mechanism to explain the formation of the nanotubes. At a high temperature, M′S (M′ = Zn, Cd) reacts with C (from the graphite crucible) by the reaction $2M'S + C \rightarrow 2M' + CS_2$ to produce gaseous M′. Gaseous M′ is transferred by the carrier gas (N_2) to the low-temperature region, where it is deposited on the graphite crucible (Figure 6a). Owing to the anisotropic nature of wurtzite M′ phases, 1D M′ nanorods are rapidly formed (Figure 6b). At the same time, Mn_3P_2 also decomposes to generate gaseous P, which is also transferred to the low-temperature region, where it reacts with the M′ nanorods by $3M' + 2P \rightarrow M'_3P_2$, and thus coaxial M'/M'_3P_2 nanocables are produced (Figure 6c). During this process, the dislocations formed in the M'_3P_2 relax the built-in strain, which is confirmed by the presence of dislocations in the synthesized

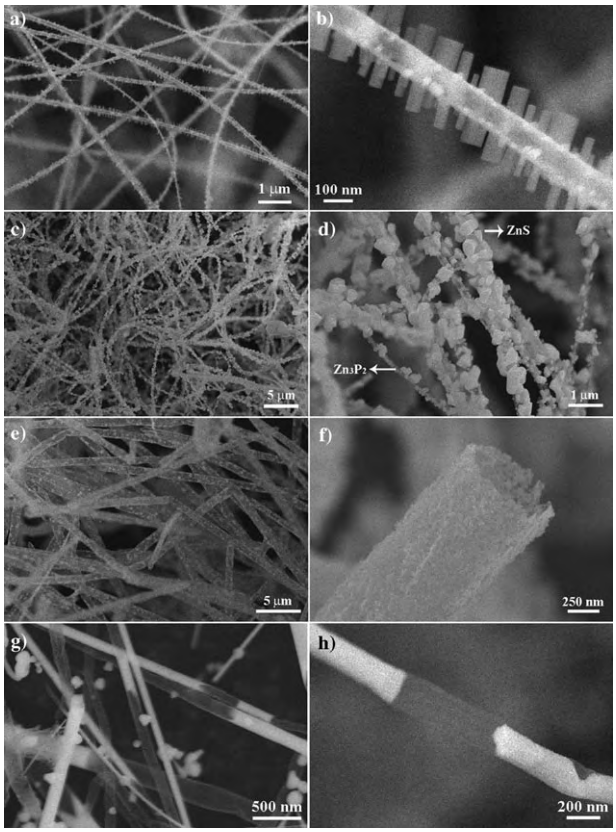

Figure 5. FESEM images of Zn_3P_2 products prepared under different conditions (see text for details): a,b) hierarchical structures of Zn_3P_2 nanotubes with ZnS nanowire branches; c,d) Zn_3P_2 nanotubes coated with ZnS nanoparticles; e,f) Zn_3P_2 microtubes. g,h) SEM images of the partially filled Zn_3P_2 nanotubes.

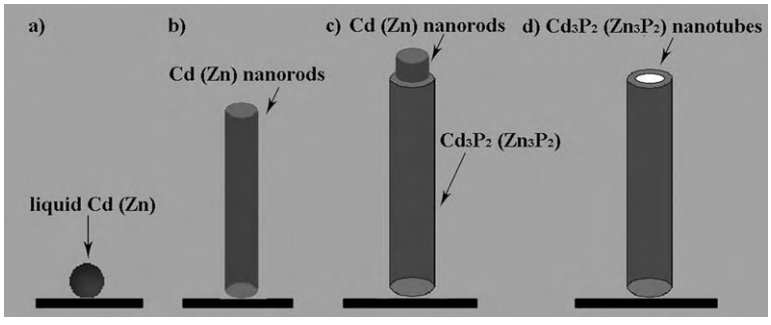

Figure 6. Proposed growth mechanism of the II_3–V_2 nanotubes, see text for details.

 © 2006 Wiley-VCH Verlag GmbH & Co. KGaA, Weinheim

products (Figure 4g). After a reaction time, the M′ species is partially consumed through evaporation out of the coaxial nanocables, whereas the M'_3P_2 shell remains intact, and single-crystalline M'_3P_2 nanotubes with circular cross sections are formed (Figure 6d).

The cathodoluminescence (CL) properties of II_3–V_2 nanotubes have been studied at 16 K. The samples were first deposited on a standard copper TEM grid and thoroughly characterized by TEM before they were set into the CL system. CL spectra from individual nanotubes were obtained with a high-resolution CL system that operates at an accelerating voltage of 5 kV and a current of 1.2 nA in a low-energy CL system inside a thermal field-emission scanning electron microscope (TFESEM, Hitachi S4200). Figure 7

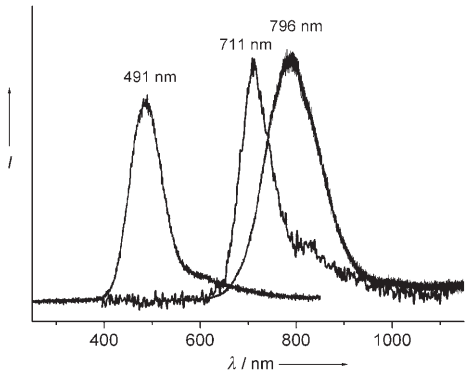

Figure 7. CL spectra of II_3–V_2 nanotubes with wall thicknesses of about 10, 20, and 45 nm, with emissions at 491, 711, and 796 nm, respectively.

shows the CL spectra taken from Zn_3P_2 nanotubes with different wall thickness of about 10, 20, and 45 nm; emissions centered at about 491, 711, and 796 nm were observed, respectively. Emissions from nanotubes with wall thickness of 10 and 20 nm were blue-shifted with respect to the emission of bulk Zn_3P_2 (1.55 eV, 802 nm). It has been reported that the emission values increase from nanoparticles with respect to those from the bulk crystal because of quantum confinement in the nanoparticles.[15c] For example, photoluminescence (PL) studies indicate that Zn_3P_2 quantum dots with different diameters show emissions ranging from 2.74 eV (450 nm) to 3.55 eV (349 nm), which are greatly blue-shifted compared to the standard emission values from bulk crystals.[15c] For synthesized Zn_3P_2 nanotubes, we think that the blue-shift of emissions observed for nanotubes with thin walls is caused by quantum confinement.[15] For the nanotubes with thicker walls (45 nm), no appreciable shift is observed as the walls are larger than the excitonic radii. CL properties of the Cd_3P_2 nanotubes were also checked, but no obvious CL emission was observed.

In conclusion, we have synthesized single-crystal II_3–V_2 nanotubes (Cd_3P_2 and Zn_3P_2) through a thermochemical process and characterized them by XRD, SEM, TEM, and EDS studies. A self-sacrificing template mechanism is proposed to explain nanotube formation, which involves the in situ step-by-step formation of Group IIB metal nanorods, Group IIB metal cores, II_3–V_2 semiconductor shells, and finally II_3–V_2 nanotubes. By carefully controlling the experimental parameters, this simple method can be used to prepare diverse II_3–V_2 nanotube-based 1D heterostructures. Furthermore, with judicious choice of source materials, II_3–V_2 nanotubes with compositions other than Cd_3P_2 and Zn_3P_2, such as Cd_3As_2 and Zn_3As_2, may be fabricated.

Experimental Section

Single-crystal nanotubes of Zn_3P_2 and Cd_3P_2 semiconductors were synthesized in a vertical induction furnace, which consists of a fused-quartz tube and an induction-heated cylinder made of high-purity graphite coated with a carbon-fiber thermo-insulating layer. The furnace has one inlet C pipe and one outlet C pipe on its base. In a typical process, a graphite crucible that contains a mixture of ZnS (or CdS), P, and Mn_3P_2 powders with a molar ratio of 3:1:1 was placed in the center cylinder. After evacuation of the quartz tube to approximately 20 Pa, a flow of pure N_2 was introduced and maintained through the inlet at a flow rate of 50 standard cubic centimeters per minute (sccm) at ambient pressure in the furnace, and the crucible was rapidly heated and kept around 1350 °C for 1 h. After the reaction was terminated and the furnace cooled to room temperature, woollike products had deposited on the inner wall of the graphite cylinder. The collected products were characterized by X-ray diffraction (XRD, RINT 2200HF), SEM (JSM-6700F), and HRTEM (JEM-3000F) equipped with an energy-dispersive X-ray spectrometer (EDS).

Received: July 3, 2006
Revised: August 23, 2006
Published online: October 18, 2006

Keywords: chemical vapor deposition · nanotechnology · nanotubes · scanning probe microscopy · template synthesis

[1] a) J. T. Hu, T. W. Odom, C. M. Lieber, *Acc. Chem. Res.* **1999**, *32*, 435–445; b) Y. N. Xia, P. D. Yang, Y. Sun, Y. Wu, B. Mayers, B. Gates, Y. Yin, F. Kim, H. Yan, *Adv. Mater.* **2003**, *15*, 353–389.
[2] S. Iijima, *Nature* **1991**, *354*, 56–58.
[3] a) R. Tenne, L. Margulis, M. Genut, G. Hodes, *Nature* **1992**, *360*, 444–446; b) Y. Feldman, E. Wasserman, D. J. Srolovitz, R. Tenne, *Science* **1995**, *267*, 222–225.
[4] a) R. Tenne, *Prog. Inorg. Chem.* **2001**, *50*, 269–315; b) R. Tenne, A. Zettl, *Top. Appl. Phys.* **2001**, *80*, 81–112; c) R. Tenne, *Chem. Eur. J.* **2002**, *8*, 5297–5304.
[5] a) M. Nath, C. N. R. Rao, *J. Am. Chem. Soc.* **2001**, *123*, 4841–4842; b) M. Nath, C. N. R. Rao, Angew. Chem. **2002**, *114*, 3601–3604; *Angew. Chem. Int. Ed.* **2002**, *41*, 3451–3454; c) U. K. Gautam, S. R. C. Vivekchand, A. Govindaraj, G. U. Kulkarni, N. R. Selvi, C. N. R. Rao, *J. Am. Chem. Soc.* **2005**, *127*, 3658–3659.
[6] a) C. H. Ye, G. W. Meng, Z. Jiang, Y. H. Wang, G. Wang, L. D. Zhang, *J. Am. Chem. Soc.* **2002**, *124*, 15180–15181; b) J. Yang, Y. C. Liu, H. M. Lin, C. C. Chen, *Adv. Mater.* **2004**, *16*, 713–716.
[7] Y. R. Hacohen, E. Grunbaum, R. Tenne, J. Sloan, J. L. Hutchison, *Nature* **1998**, *395*, 336–337.
[8] N. G. Chopra, R. J. Luyken, K. Cherrey, V. H. Crespi, M. L. Cohen, S. G. Louie, A. Zettl, *Science* **1995**, *269*, 966–967.
[9] a) M. E. Spahr, P. Bitterli, R. Nesper, M. Müller, F. Krumeich, H.-U. Nissen, *Angew. Chem.* **1998**, *110*, 1339–1342; *Angew. Chem. Int. Ed.* **1998**, *37*, 1263–1266; b) G. R. Patzke, F. Krumeich, R. Nesper, *Angew. Chem.* **2002**, *114*, 2554–2571; *Angew. Chem. Int. Ed.* **2002**, *41*, 2446–2453.
[10] Y. D. Li, J. W. Wang, Z. X. Deng, Y. Y. Wu, X. M. Sun, D. P. Yu, P. D. Yang, *J. Am. Chem. Soc.* **2001**, *123*, 9904–9905.

 © 2006 Wiley-VCH Verlag GmbH & Co. KGaA, Weinheim

[11] J. Goldberger, R. He, Y. Zhang, S. Lee, H. Q. Yan, H. J. Choi, P. D. Yang, *Nature* **2003**, *422*, 599 – 602.
[12] a) Z. Q. Liu, D. H. Zhang, S. Han, C. Li, B. Lei, W. G. Lu, J. Y. Fang, C. W. Zhou, *J. Am. Chem. Soc.* **2005**, *127*, 6 – 7; b) J. Q. Hu, Y. Bando, Z. W. Liu, J. H. Zhan, D. Golberg, T. Sekiguchi, *Angew. Chem.* **2004**, *116*, 65 – 68; *Angew. Chem. Int. Ed.* **2004**, *43*, 63 – 66; c) J. Q. Hu, Y. Bando, J. H. Zhan, D. Golberg, *Angew. Chem.* **2004**, *116*, 4706 – 4709; *Angew. Chem. Int. Ed.* **2004**, *43*, 4606 – 4609.
[13] O. Madelung, *Data in Science and Technology: Semiconductors other Than Group IV Elements and III–V Compounds*, Springer, Berlin.
[14] a) W. Zdanowicz, L. Zdanowicz, *Annu. Rev. Mater. Sci.* **1975**, *5*, 301 – 328; b) E. K. Arushanov, *Prog. Cryst. Growth Charact.* **1980**, *3*, 211 – 255; c) V. B. Larzarev, V. Y. Schevchenka, Y. H. Greenberg, V. V. Sobolein, *II–V Semiconducting Compounds*, Nauska, Moscow, **1978**; d) M. Bushan, A. Catalano, *Appl. Phys. Lett.* **1981**, *38*, 39 – 41.
[15] a) M. Green, P. O'Brien, *Adv. Mater.* **1998**, *10*, 527 – 528; b) M. Green, P. O'Brien, *J. Mater. Chem.* **1999**, *9*, 243 – 247; c) M. Green, P. O'Brien, *Chem. Mater.* **2001**, *13*, 4500 – 4505; d) H. Weller, A. Fojtik, A. Henglein, *Chem. Phys. Lett.* **1985**, *117*, 485 – 487; e) S. C. Goel, M. Y. Chang, W. E. Buhro, *J. Am. Chem. Soc.* **1990**, *112*, 5636 – 5637.
[16] G. Z. Shen, Y. Bando, J. Q. Hu, D. Golberg, *Appl. Phys. Lett.* **2006**, *88*, 143105.
[17] a) R. Fan, R. Karnik, M. Yue, D. Y. Li, A. Majumdar, P. D. Yang, *Nano Lett.* **2005**, *5*, 1633 – 1637; b) J. Goldberger, R. Fan, P. D. Yang, *Acc. Chem. Res.* **2006**, *39*, 239 – 248; c) R. Fan, M. Yue, R. Karnik, A. Majumdar, P. D. Yang, *Phys. Rev. Lett.* **2005**, *95*, 086607.

 © 2006 Wiley-VCH Verlag GmbH & Co. KGaA, Weinheim

Ion Pairs

DOI: 10.1002/anie.200602694

Evidence of Fluoride Transfer from the Anion of $[Zr\{C_5H_3[SiMe_2(\eta^1\text{-}NtBu)]_2\}]^+[RB(C_6F_5)_3]^-$ Complexes to the Zirconocenium Cation**

Jesús Cano, María Sudupe, Pascual Royo, and Marta E. G. Mosquera*

Cationic Group 4 metal complexes of the type $[L_2MR']^+$ generated by activation of the corresponding dialkyl compounds with $B(C_6F_5)_3$ are active homogeneous catalysts for olefin polymerization.[1] Weakly coordinating anions are required to minimize the ion-pairing interactions, which are crucial in determining the properties of the resulting polymeric materials and the characteristics of the polymerization processes. These counteranions frequently contain fluoroorganic moieties to reduce interactions by dissipating the negative charge and decreasing the nucleophilicity. However, $[RB(C_6F_5)_3]^-$ groups can still be responsible for deactivation processes.

The carbon–fluorine bond is the strongest and least reactive bond found in organic molecules and its activation is a chemical challenge,[2] whereas the boron–carbon bond is more reactive and C_6F_5 transfer to the cationic metal center is the most commonly observed deactivation pathway for $[L_2MR'][RB(C_6F_5)_3]$ catalysts.[3] Ziegler and co-workers recently reported calculations on different competing thermal deactivation pathways for the $[L_2MR'][RB(C_6F_5)_3]$ ion pair.[4]

We previously reported[5] Group 4 metal complexes with doubly silyl-amido-bridged chelating tridentate ligands. Complexes of this type, when activated with methylaluminoxane (MAO), are efficient catalysts for ethene polymerization despite generating cationic species free of the alkyl group required for the insertion reaction. Similar observations were made for a related singly silyl-η-amido bridged zirconium dicyclopentadienyl compound[6] and for cationic Co^I species,[7] which also show activity towards ethene polymerization.

We report herein the reaction pathways that are followed when the cationic complexes $[Zr\{C_5H_3[SiMe_2(\eta^1\text{-}NtBu)]_2\}][RB(C_6F_5)_3]$ (["Zr"][$RB(C_6F_5)_3$], R = CH_2Ph (**1**), Me (**2**)) are heated in the presence of triphenylphosphane. Using reported synthetic methods,[5a] we synthesized the cationic zirconium compounds **1** and **2**[8] as barely soluble oils or oily solids by adding one equivalent of $B(C_6F_5)_3$ to C_6D_6 solutions of the corresponding alkyl complexes ["Zr"R] in sealed NMR tubes. The same products were observed when similar reactions were carried out on a preparative scale. Complexes **1** and **2** were thermally stable upon heating them in solution up to 80 °C for several hours. However, the addition of one equivalent of PPh_3 to C_6D_6 solutions of **1** and **2** at room temperature gave a suspension of an insoluble solid, which upon heating at 80 °C for several days afforded a mixture that contained compounds ["Zr"F] (**3**) and ["Zr"(C_6F_5)] (**4**). The insoluble solid was separated by filtration, suspended in fresh C_6D_6, and heated at 80 °C for 7 days to give compound **3**.

Compounds **3** and **4** were generated by the transfer of F and C_6F_5 groups, respectively, to the Zr atoms of the starting complexes although their formation and structure were only confirmed when they were obtained by alternative synthetic methods. So compound **3** was prepared by treating ["Zr"-(CH_2Ph)] with $FSnPh_3$[9] in toluene at 80 °C for 5 h; the product was characterized by elemental analysis and NMR spectroscopy.[10] The resultant ($PhCH_2$)$SnPh_3$ was also identified by ^1H NMR spectroscopy [δ_{CH_2} = 2.81 ppm (1 s + 2 d, 2 H, $J_{H,Sn^{119}}$ = 68, $J_{H,Sn^{117}}$ = 65 Hz].

The reaction of the same benzyl complex with the Lewis acid $Al(C_6F_5)_3$ proceeded at 25 °C with abstraction of the benzyl ligand to give the cationic zirconium complex, ["Zr"]-[($PhCH_2$)$Al(C_6F_5)_3$], with simultaneous formation of a small amount of **4**. Quantitative C_6F_5 transfer was completed after

[*] Dr. J. Cano, M. Sudupe, Prof. P. Royo, Dr. M. E. G. Mosquera
Departamento de Química Inorgánica
Universidad de Alcalá
Campus Universitario, 28871 Alcalá de Henares (Spain)
Fax: (+34) 918-854-683
E-mail: pascual.royo@uah.es

[**] Financial support by the Spanish MEC (project MAT2004-02614) and DGUI/CM (program S/0505/PPQ-0328) is acknowleged. R = Me, CH_2Ph.

Supporting information for this article is available on the WWW under http://www.angewandte.org or from the author.

InterScience DISCOVER SOMETHING GREAT
© 2006 Wiley-VCH Verlag GmbH & Co. KGaA, Weinheim

12 h to give **4** as the unique reaction product,[11] which was isolated as a crystalline solid.

The chemical shifts in the ^{1}H NMR spectra for complexes **3** and **4** were identical to those observed for the same products isolated by thermal transformation of **1** and **2** in the presence of PPh_3, which demonstrates that they were formed by F and C_6F_5 transfer to the metal center, respectively (Scheme 1). A

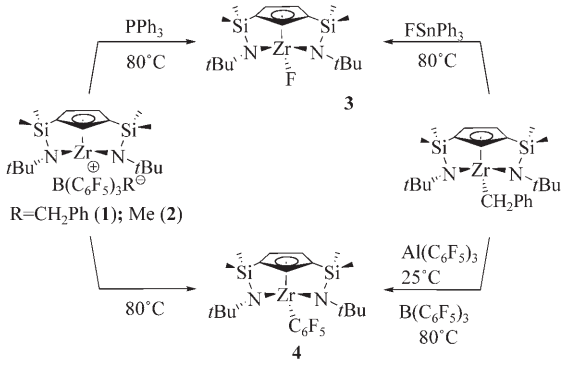

Scheme 1. Thermal transformations observed for complexes **1** and **2**.

significant upfield shift of the signals arising from the *o*-fluorine atoms was observed in the ^{19}F NMR spectrum of **4** ($\delta = 109.1$ ppm) with respect to the corresponding signals observed for $B(C_6F_5)_3$ ($\delta = 132.1$ ppm). The molecular structure of **4** was determined by X-ray diffraction.[3d,12] The structure agrees with the spectroscopic data and shows clearly the C_6F_5 moiety coordinated to the metal center (see Supporting Information). The Zr coordination sphere is completed by the $\{C_5H_3[SiMe_2(\eta^1\text{-}NtBu)]_2\}$ ligand with no other groups bonded to the Zr center. The precision of this study was limited by the poor quality of the crystal set.

Formation of an alkyl-bridged ion-pair system,[3b] ["Zr"{μ-$RB(C_6F_5)_3$}], could be responsible for the intramolecular B–C_6F_5 bond activation and the C_6F_5 transfer to the Zr center with elimination of the neutral borane, $RB(C_6F_5)_2$.[13] This reaction is slow when the cationic complexes **1** and **2** are heated at 80 °C for 7 days to give complex **4** (Scheme 1).

In the presence of a phosphane, a different deactivation process occurs by transfer of a *p*-fluoro substituent of one of the pentafluorophenyl borate rings to the Zr center. The decomposition of the zirconocenium cation [(1,2-$Me_2C_5H_3)_2$ZrMe][$RB(C_6F_5)_3$] has been reported[3a,14] and two possible pathways for fluoride transfer,[3a] both based on the same migration of C_6F_5 to the metal center with subsequent activation of the *o*-fluorine atom or direct fluoride migration to the zirconium cation, were proposed although no experimental evidence of the reaction mechanism was given. A similar fluoride transfer was reported very recently for the reaction of the dinuclear hydride complex [{*rac*-(ebthi)ZrH-(μ-H)}$_2$] with $B(C_6F_5)_3$.[15]

The thermal fluoride transfer observed for complexes **1** and **2** may occur by nucleophilic addition of PPh_3 to the *p*-C–F bond of one of the electron-deficient C_6F_5 rings of the metal-coordinated alkylborate counteranion $[RB(C_6F_5)_3]^-$ with immediate transfer of the generated fluoride to the zirconocenium cation to give **3**.[16] Supporting this proposal, we note that **4** is not converted into **3**. In addition, we were able to isolate a colorless single crystal of the μ-F complex [("Zr")$_2$(μ-F)][$(PhCH_2)B(C_6F_5)_3$] (**5**) from the mixture of compounds obtained when an equimolar mixture of **1** and PPh_3 was warmed at 50 °C for 7 days.[17] An X-ray diffraction study (Figure 1) revealed that **5** consists of a separate dinuclear cation, $[("Zr")_2F]^+$, and the free $[(PhCH_2)B(C_6F_5)_3]^-$ anion.

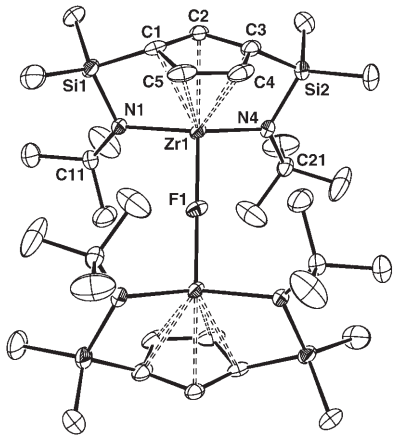

Figure 1. ORTEP view of **5** with thermal ellipsoids set at 30% probability. The complex crystallizes with two independent cations in the unit cell {Zr1-F1-Zr1#} and {Zr2-F2-Zr2#} (not shown). Only half of each cation is present in the asymmetric unit, the other half (Zr#) is generated in each case by crystallographic inversion. The separations Zr1-F1 and Zr2-F2 (2.1393(4), 2.1416(5) Å) are within the range for a Zr–F bond (2.02–2.29 Å). The Zr-F-Zr moiety is linear (180.000(8)° Zr1-F1-Zr1# and 180.000(1)° Zr2-F2-Zr2#), which agrees with results from other complexes with bridging fluorine atoms. The Cp rings are mutually *trans*. The anion is omitted for clarity.

Further confirmation of this reaction pathway was obtained by the isolation of the zwitterionic compound [4-Ph_3P]$^+$[C_6F_4{$BMe(C_6F_5)_2$}]$^-$ (**6**).[18] Crystals of **6** suitable for X-ray diffraction studies were obtained when equimolar amounts of **2** and PPh_3 were heated at 80 °C for 7 days. The molecular structure of compound **6** (Figure 2) demonstrates

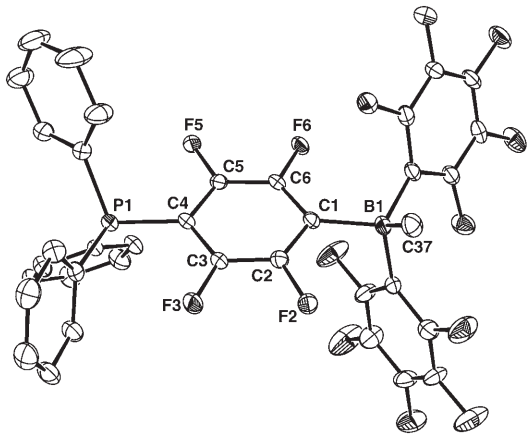

Figure 2. ORTEP view of **6** with thermal ellipsoids set at 30% probability. Both P–C (1.811(3) Å) and B–C (1.680(4) Å) interatomic distances are within the range for single bonds.

 © 2006 Wiley-VCH Verlag GmbH & Co. KGaA, Weinheim

that the triphenylphosphonium and the methylbis(pentafluorophenyl)borate fragments are the *para*-substituents of the resulting tetrafluorophenyl activated ring.[17]

In summary, we have found experimental evidence to support a reaction pathway involving direct fluoride migration to the zirconium cation without previous transfer of C_6F_5. It is noteworthy that the opening of the silyl–amido bridge was not observed in the course of these activations. Experiments with other donor ligands are in progress to investigate the conditions under which the ion pairs **1** and **2** may follow different decomposition routes and the possible mechanisms of these reactions.

Received: July 6, 2006
Published online: October 20, 2006

Keywords: homogeneous catalysis · ion pairs · polymerization · reaction mechanisms · zirconium

[1] a) M. Bochmann, *J. Chem. Soc. Dalton Trans.* **1996**, 255; b) E. Y. X. Chen, T. J. Marks, *Chem. Rev.* **2000**, *100*, 139; c) G. Erker, *Dalton Trans.* **2005**, 1883.

[2] a) J. L. Kiplinger, T. G. Richmond, C. E. Osterberg, *Chem. Rev.* **1994**, *94*, 373; b) J. Burdeniuc, B. Jedlicka, R. H. Crabtree, *Chem. Ber.* **1997**, *130*, 145; c) T. G. Richmond, *Topics in Organometallic Chemistry*, *Vol. 3*, Springer, New York, **1999**, p. 243.

[3] a) X. M. Yang, C. L. Stern, T. J. Marks, *J. Am. Chem. Soc.* **1994**, *116*, 10015; b) T. Wondimagegn, Z. T. Xu, K. Vanka, T. Ziegler, *Organometallics* **2004**, *23*, 3847; c) T. J. Woodman, M. Thornton-Pett, M. Bochmann, *Chem. Commun.* **2001**, 329; d) V. Amo, R. Andres, E. de Jesús, F. J. de la Mata, J. C. Flores, R. Gómez, M. P. Gómez-Sal, J. F. C. Turner, *Organometallics* **2005**, *24*, 2331; e) R. Gómez, P. Gómez-Sal, P. A. del Real, P. Royo, *J. Organomet. Chem.* **1999**, *588*, 22.

[4] a) T. Wondimagegn, K. Vanka, Z. T. Xu, T. Ziegler, *Organometallics* **2004**, *23*, 2651; b) T. Wondimagegn, Z. T. Xu, K. Vanka, T. Ziegler, *Organometallics* **2005**, *24*, 2076.

[5] a) J. Cano, P. Royo, M. Lanfranchi, M. A. Pellinghelli, A. Tiripicchio, *Angew. Chem.* **2001**, *113*, 2563; *Angew. Chem. Int. Ed.* **2001**, *40*, 2495; b) J. Cano, P. Royo, H. Jacobsen, O. Blacque, H. Berke, E. Herdtweck, *Eur. J. Inorg. Chem.* **2003**, 2463; c) M. Sudupe, J. Cano, P. Royo, E. Herdtweck, *Eur. J. Inorg. Chem.* **2004**, 3074; d) J. Cano, M. Sudupe, P. Royo, M. E. G. Mosquera, *Organometallics* **2005**, *24*, 2424.

[6] J. Z. Jin, D. R. Wilson, E. Y. X. Chen, *Chem. Commun.* **2002**, 708.

[7] a) V. C. Gibson, M. J. Humphries, K. P. Tellmann, D. F. Wass, A. J. P. White, D. J. Williams, *Chem. Commun.* **2001**, 2252; b) T. M. Kooistra, Q. Knijnenburg, J. M. M. Smits, A. D. Horton, P. H. M. Budzelaar, A. W. Gal, *Angew. Chem.* **2001**, *113*, 4855; *Angew. Chem. Int. Ed.* **2001**, *40*, 4719; c) W. Steffen, T. Blömker, N. Kleigrewe, G. Kehr, R. Fröhlich, G. Erker, *Chem. Commun.* **2004**, 1188; d) N. Kleigrewe, W. Steffen, T. Blömker, G. Kehr, R. Fröhlich, B. Wibbeling, G. Erker, J. C. Wasilke, G. Wu, G. C. Bazan, *J. Am. Chem. Soc.* **2005**, *127*, 13955.

[8] **2:** ^{1}H NMR (300 MHz, C_6D_6): $\delta = 0.21$, 0.33 (2 s, 2×6 H, $SiMe_2$), 0.94 (s, 18 H, N*t*Bu), not observed (BCH_3), 6.31 (m, 1 H, C_5H_3), 6.48 ppm (m, 2 H, C_5H_3). ^{13}C NMR (75 MHz, C_6D_6): $\delta = 1.5$ ($2 \times SiMe_2$), 34.8 ($NCMe_3$), 58.6 ($NCMe_3$), 127.5 ($3 \times C_5H_3$), 136.5 ppm ($4 \times C_6F_5$). ^{19}F NMR (280 MHz, C_6D_6): $\delta = 132.1$ (m, 2 F, *o*-C_6F_5), 163.6 (m, 1 F, *p*-C_6F_5), 167.2 ppm (m, 2 F, *m*-C_6F_5). Elemental analysis (%) calcd: C 49.65, H 3.97, N 2.76; found: C 50.51, H 3.71, N 3.35.

[9] H. Hatop, H. W. Roesky, T. Labahn, A. Fischer, H. G. Schmidt, M. Noltemeyer, *Organometallics* **2000**, *19*, 937.

[10] **3:** ^{1}H NMR (300 MHz, C_6D_6): $\delta = 0.53$, 0.61 (2 s, 2×6 H, $SiMe_2$), 1.31 (s, 18 H, N*t*Bu), 6.69 (m, 1 H, C_5H_3), 6.88 ppm (m, 2 H, C_5H_3). ^{13}C NMR (75 MHz, C_6D_6): $\delta = 2.4$, 5.1 ($2 \times SiMe_2$), 36.4 ($NCMe_3$), 56.7 ($NCMe_3$), 120.7, 124.1, 127.7 ppm ($3 \times C_5H_3$). ^{19}F NMR (280 MHz, C_6D_6): $\delta = -24.9$ ppm. Elemental analysis (%) calcd: C 47.28, H 7.70, N 6.49; found: C 47.90, H 7.11, N 6.36.

[11] **4:** ^{1}H NMR (300 MHz, C_6D_6): $\delta = 0.45$, 0.53 (2 s, 2×6 H, $SiMe_2$), 1.25 (s, 18 H, N*t*Bu), 6.37 (m, 1 H, C_5H_3), 6.69 ppm (m, 2 H, C_5H_3). ^{13}C NMR (75 MHz, C_6D_6): $\delta = 1.9$, 2.5 ($2 \times SiMe_2$), 35.5 ($NCMe_3$), 57.2 ($NCMe_3$), 116.9, 124.4, 125.0 ($3 \times C_5H_3$), 135.8, 139.1, 147.9, 150.1 ppm ($4 \times C_6F_5$). ^{19}F NMR (280 MHz, C_6D_6): $\delta = 109.1$ (m, 2 F, *o*-C_6F_5), 155.9 (m, 1 F, *p*-C_6F_5), 162.4 ppm (m, 2 F, *m*-C_6F_5). Elemental analysis (%) calcd: C 47.64, H 5.74, N 4.83; found: C 47.92, H 5.27, N 4.63.

[12] a) V. Tabernero, C. Maestre, G. Jiménez, T. Cuenca, C. R. de Arellano, *Organometallics* **2006**, *25*, 1723; b) K. Phomphrai, A. E. Fenwick, S. Sharma, P. E. Fanwick, J. M. Caruthers, W. N. Delgass, M. M. Abu-Omar, I. P. Rothwell, *Organometallics* **2006**, *25*, 214.

[13] S. Dagorne, I. A. Guzei, M. P. Coles, R. F. Jordan, *J. Am. Chem. Soc.* **2000**, *122*, 274.

[14] L. Jia, X. M. Yang, C. L. Stern, T. J. Marks, *Organometallics* **1997**, *16*, 842.

[15] P. Arndt, U. Jäger-Fiedler, M. Klahn, W. Baumann, A. Spannenberg, V. V. Burlakov, U. Rosenthal, *Angew. Chem.* **2006**, *118*, 4301; *Angew. Chem. Int. Ed.* **2006**, *45*, 4195; ebthi = 1,2-ethylene-1,1′-bis(η^5-tetrahydroindenyl).

[16] S. Döring, G. Erker, R. Fröhlich, O. Meyer, K. Bergander, *Organometallics* **1998**, *17*, 2183.

[17] CCDC-613558 (**4**), CCDC-613223 (**5**), and CCDC-613224 (**6**) contain the supplementary crystallographic data for this paper. These data can be obtained free of charge from The Cambridge Crystallographic Data Centre via www.ccdc.cam.ac.uk/data_request/cif.

[18] **6:** ^{1}H NMR (300 MHz, C_6D_6): $\delta = 1.47$ ppm (s, BMe); ^{13}C NMR (75 MHz, C_6D_6): $\delta = 29.2$ ppm (BMe); ^{19}F NMR (280 MHz, C_6D_6): $\delta = 124.5$, 128.4, 131.8, 162.5, 165.8 ppm ($3 \times C_6F_5$, $2 \times C_6F_4$).

 © 2006 Wiley-VCH Verlag GmbH & Co. KGaA, Weinheim

Glycosylation

DOI: 10.1002/anie.200602699

Dialkylphosphates as Stereodirecting Protecting Groups in Oligosaccharide Synthesis**

*Takeshi Yamada, Kazunobu Takemura, Jun-ichi Yoshida, and Shigeru Yamago**

The stereoselective formation of the glycosidic linkage is one of the most important tasks in synthetic carbohydrate chemistry, because the glycoside structure plays a crucial role in many important biological processes involving oligosaccharides.[1] To date, 1,2-*trans*-glycosides have been prepared through the intramolecular participation of the acyl protecting groups at the neighboring C2 position.[2] However, this method has serious drawbacks owing to the formation of orthoester side products.[3] The formation cannot be completely surpressed even when sterically and electronically protected pivalates are used.[4] While the orthoester can be isomerized to give the 1,2-*trans*-glycoside, the isomerization frequently results in low efficiency[3f,j,k,5] or formation of the undesired stereoisomer.[3i,6] During our studies to develop an iterative glycosylation,[7,8] we faced the same problem, which limited the generality of the method. Therefore, the development of a general and high-yielding method for the synthesis of 1,2-*trans*-glycosides would considerably increase the generality of both the iterative as well as conventional glycosylations to access to certain complex oligosaccharides.

Here we report the first use of dialkylphosphates as stereodirecting groups for the synthesis of 1,2-*trans*-glycosides. As the phosphates can be removed after glycosylation, they can be used as stereodirecting protecting groups (Scheme 1). In addition, we found that these protecting groups can be used in iterative glycosylation reactions. Therefore, a variety of oligosaccharides that possess the 1,2-*trans*-glycosidic linkage can be synthesized under a set of glycosylation conditions. Although dialkylphosphinamides have been used for the protection of amines,[9] there is no report on the use of dialkylphosphates for the protection of alcohols. Furthermore, while there are a few examples of the use of diphenylphosphinamides as stereodirecting protecting groups in glucosamine synthesis,[10] their synthetic potential has not been well recognized.

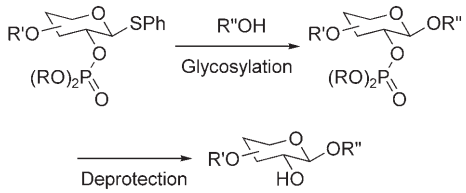

Scheme 1. Dialkylphosphates as stereodirecting protecting groups.

Thioglycoside **1a**, which has a 2,2-dimethyltrimethylene (DMTM) phosphate group at the C2 position, was activated by treatment with benzenesulfenylpiperidine (BSP) and triflic anhydride (Tf_2O) in the presence of 2,6-di-*tert*-butyl-4-methylpyridine (DTBMP) at −60 °C,[11] and cyclohexanol was added to this reaction mixture. The desired 1,2-*trans*-glycoside β-**2a** formed as the sole product in 76% yield (Scheme 2). The formation of α-**2a** and the corresponding orthophosphorate product was not detected. The same glycosylation of **1a** by reaction with *N*-iodosuccinimide and triflic acid activators in the presence of cyclohexanol also afforded β-**2a** exclusively in 79% yield.[12] The DMTM phosphate group in **2a** was removed by treatment with sodium hydroxide (10 equiv) in an ethanol/water mixture at 60 °C for 1.0 h to give the free alcohol **3** in 95% yield.

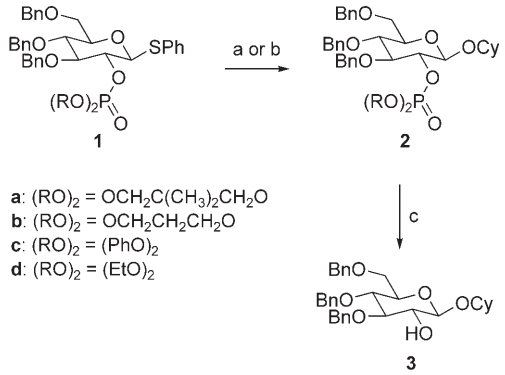

Scheme 2. Effects of dialkylphosphates. Reagents and conditions: a) **1** (1.0 equiv), BSP (1.1 equiv), Tf_2O (1.4 equiv), DTBMP (2.0 equiv), CH_2Cl_2, MS (4 Å), −60 °C for 30 min, then cyclohexanol (1.5 equiv), −60 °C for 30 min, **2a**; 76% (>99% β), **2b**; 84% (>99% β), **2c**; 77% (>99% β), **2d**; 84% (89% β). b) **1a** (1.0 equiv), NIS (1.1 equiv), TfOH (0.1 equiv), cyclohexanol (1.5 equiv), CH_2Cl_2, MS (4 Å), −45 °C, 60 min, 79% (99% β). c) **2** (1.0 equiv), NaOH (10 equiv), EtOH/H_2O, 60 °C, 1 h. Bn = benzyl, Cy = cyclohexyl, NIS = *N*-iodosuccinimide, Tf = trifluoromethylsulfonyl.

With dialkylphosphates in hand, we next examined the structural effects of the phosphates on the selectivity and deprotection efficiency. Trimethylene phosphate **1b** reacted with similar efficiencies to **1a** in both the glycosylation (84%, >99% β) and the deprotection (84%). Diphenyl phosphate **1c** also showed high glycosylation efficiencies (77%, >99% β), but the deprotection was

[*] K. Takemura, Prof. S. Yamago[+]
Division of Molecular Materials Science
Graduate School of Science, Osaka City University
Osaka 558-8585 (Japan)
Dr. T. Yamada,[+] Prof. J.-i. Yoshida
Department of Synthetic Chemistry and Biological Chemistry
Graduate School of Engineering, Kyoto University
Kyoto 615-8510 (Japan)
[+] Current address:
Institute for Chemical Research, Kyoto University
Kyoto 611-0011 (Japan)
Fax: (+81) 774-38-3067
E-mail: yamago@scl.kyoto-u.ac.jp

[**] This work was supported in part by a Shiseido Grant for Science Research. The authors thank Prof. Kawabata of Kyoto University for the measurement of optical rotation.

Supporting information for this article is available on the WWW under http://www.angewandte.org or from the author.

© 2006 Wiley-VCH Verlag GmbH & Co. KGaA, Weinheim

sluggish (< 30 % yield). The selectivity eroded in the glycosylation of diethyl phosphate **1d** (89 % β). We selected DMTM phosphate for the following studies since in the protection of the C2 hydroxy group it was more efficient than the corresponding trimethylene analogue (see the Supporting Information).

The synthetic scope of the current phosphate protecting group has been examined by changing the structure of donors as well as acceptors (Table 1, Scheme 3). We employed a binary activation system using BSP and Tf_2O[11] because these conditions could be applied for the iterative glycosylation of thioglycosides derived from 2-deoxy-2-aminoglycosides.[7a,b] The glycosylation of **1a** with **4e**, which has a hydroxy group at C6, proceeded smoothly and afforded the desired *O*-glycoside with complete β selectivity in quantitative yield (entry 1, Table 1). The glycosylation of **1a** with **4f** and **4g**, which have the sterically hindered hydroxyl groups at C3 and C4, respectively, also afforded **6** and **7** in good yields (entries 2 and 3, Table 1). While small quantities of the 1,2-*cis* isomers were formed in both cases, sufficiently high levels of selectivity were observed (> 96 %). Thioglycosides with a DMTM protecting group at C2 could also be used as glycosyl acceptors. Thus, the coupling of **1a** with **8** afforded β-**9h** in quantitative yield (entry 4, Table 1). Iterative glycosylation using **9h** as a donor and **8** as an acceptor afforded trisaccharide **9i** (entry 5, Table 1), which was further glycosylated with **8** to give tetrasaccharide **9j** (entry 6, Table 1). The desired 1,2-*trans*-glycosides formed in good yields with excellent selectivities in all cases. As the glycosyl donor was activated prior to the coupling reaction, the armed glycoside **10** could be used as a glycosyl acceptor (entry 7, Table 1).[13,14] As all the products are thioglycosides, they could be directly used for the next iterative or armed–disarmed glycosylation reaction as glycosyl donors.

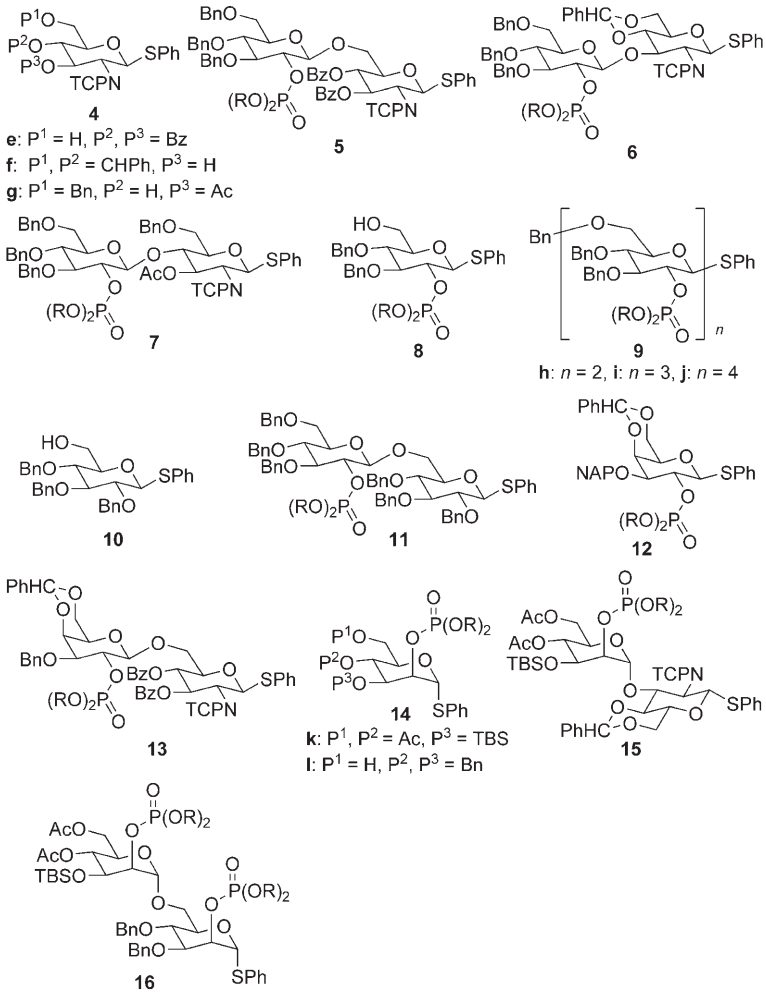

Scheme 3. Examples of donors and acceptors used in the glycosylation and the resulting products; see Table 1. Bz = benzoyl, NAP = 2-naphthylmethyl, $(RO)_2 = OCH_2C(CH_3)_2CH_2O$, TCPN = *N*-tetrachlorophthalimide, TBS = *tert*-butyldimethylsilyl.

Table 1: Stereoselective glycosylation of thioglycosides.[a] For structures see Scheme 3.

Entry	Donor	Acc.	Prod.	Yield [%]	Sel. (α:β)
1	**1a**	**4e**	**5**	98	1:>99
2	**1a**	**4f**	**6**	75	2:98
3	**1a**	**4g**	**7**	71	4:96
4	**1a**	**8**	**9h**	100	1:>99
5	**9h**	**8**	**9i**	80	1:99
6	**9i**	**8**	**9j**	80	1:>99
7	**1a**	**10**	**11**	85	2:98
8	**12**	**4e**	**13**	100	2:98
9	**14k**	**4f**	**15**	81	99:1
10	**14k**	**14l**	**16**	76	96:4

[a] Donor (1.0 equiv), BSP (1.1 equiv), Tf_2O (1.4 equiv), DTBMP (2.0 equiv), CH_2Cl_2, MS (4 Å), −60 °C, 10–30 min, then acceptor (1.5 equiv) at −60 °C, 15–60 min.

This method could be extended to the use of glycosides other than glucose derivatives. Galactose derivative **12** afforded exclusively β isomer **13** (entry 8, Table 1). Mannose donor **14k** gave exclusively α isomers **15** and **16** upon coupling with acceptors **4f** and **14l**, respectively, as a result of the 1,2-*trans*-directing effect of the axial DMTM group at C2 (entries 9 and 10, Table 1).

Potential intermediates in the current glycosylation reaction were analyzed to understand the remarkable 1,2-*trans* selectivity. Thus, **1a** was activated by BSP and Tf_2O in CD_2Cl_2 at −80 °C, and the resulting reaction mixture was analyzed by ^1H, ^{13}C, and ^{31}P NMR spectroscopy at the same temperature. We were surprised to find that the α-glycosyl triflate **17** formed as the sole product.[15] The anomeric carbon in **17** resonates at $\delta =$ 105 ppm in the ^{13}C NMR spectra, which strongly indicates the formation of a neutral species rather than a cationic species.[15,7a] The α stereochemistry was suggested by the ^1H NMR spectra, in which the

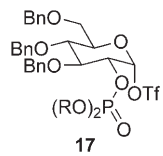

 © 2006 Wiley-VCH Verlag GmbH & Co. KGaA, Weinheim

C1 proton gives rise to a doublet at $\delta = 6.40$ ppm with a coupling constant of 2.4 Hz. The phosphorus signal in **17** occurs at $\delta = -8.9$ ppm, a chemical shift virtually identical to that of **1a** ($\delta = -8.8$ ppm). The results clearly indicate that the phosphorus atom in **17** does not bear a positive charge.[16] These results are in sharp contrast to the formation of the orthoester cation intermediate in C2 acyl-protected glycosyl donors.[17] Therefore, the lack of the formation of orthophosphate product must be attributed to the lack of positive charge on the phosphorus atom in **17**.

A possible explanation for the observed 1,2-*trans* selectivity is the "S_N2-like" attack of the acceptor alcohol on the α-triflate intermediate (Scheme 4, path A) in analogy to the β-mannoside synthesis developed by Crich.[15] However, Crich

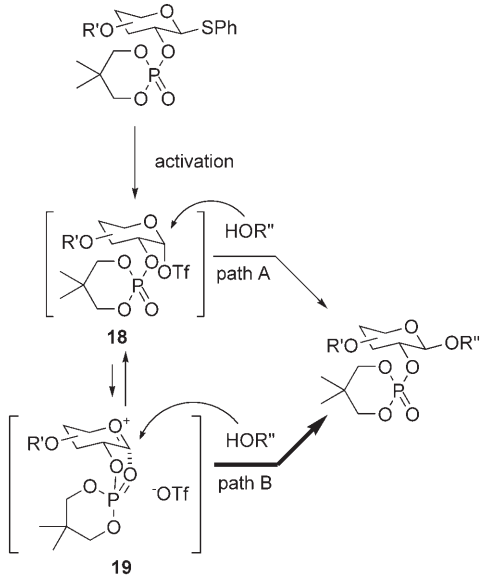

Scheme 4. Plausible mechanism.

also reported that α-triflate intermediates, which possess a nonparticipative protecting group at C2, show low or moderate 1,2-*trans* selectivity.[18] We also reported that a β-triflimide intermediate of *N*-phthaloyl-protected glucosamine exclusively afforded the β-glycosides,[7a] suggesting that the α-triflates do not always react in an "S_N2-like" manner. An alternative and more plausible mechanism involves intermediate **19**, which would arise through neighboring group participation of the phosphorus ester. This intermediate would be short-lived and exist in equilibrium with **18**. The alcohol reacts at less hindered side in **19** to give 1,2-*trans*-glycoside (path B). While there is no direct evidence for the involvement of **19**, we believe that the latter is more plausible for the formation of 1,2-*trans*-glycosides.[19,20] Further synthetic and mechanistic elaborations of this new stereodirecting protecting group are currently underway.

Experimental Section

Typical glycosylation procedure (synthesis of **5**): A solution of a glycosyl donor **1a** (69.1 mg, 0.10 mmol), BSP (23.0 mg, 0.11 mmol), DTBMP (41.1 mg, 0.20 mmol), and molecular sieves 4 Å (ca. 100 mg) in CH_2Cl_2 (1.0 mL) was treated with Tf_2O (38.4 mg, 0.14 mmol) at −60 °C. After 10 min, glycosyl acceptor **4e** (112 mg, 0.15 mmol) was added at this temperature. The reaction mixture was at this temperature for 15 min, then quenched by addition of Et_3N (0.1 mL), and warmed to room temperature. To this solution was added saturated aqueous $NaHCO_3$ solution, and organic phase was separated. The aqueous phase was extracted three times with ethyl acetate, and the combined organic extracts were washed with saturated aqueous NaCl solution, dried with $MgSO_4$, filtered, and concentrated under reduced pressure by rotary evaporator to give the crude product. Purification by flash column chromatography (silica gel 10 g; elution with 30% ethyl acetate in hexane) afforded **5** in 98% (92.1 mg, α:β = < 1:99) as a white amorphous substance. $[\alpha]_D^{20} = +59.8$ (*c* 0.4, $CHCl_3$); IR (KBr): $\tilde{\nu} = 1732$(s), 1389, 1354, 1301, 1271, 1068, 1010, 740, 711; ^{1}H NMR (400 MHz, $CDCl_3$): $\delta = 0.81$ (s, 3H, CH_3), 1.17 (s, 3H, CH_3), 3.44 (dt, $J = 9.7$, 3.1 Hz, 1H, H-5′), 3.58–3.68 (m, 3H, H-4′, H-6′) 3.83 (t, $J = 9.0$ Hz, 1H, H-3′), 3.89–4.18 (m, 6H, H-6, P(O){OCH_2C-(CH_3)$_2$CH_2O}), 4.24–4.36 (m, 2H, H-2′, H-5), 4.41 (d, $J = 12.4$ Hz, 1H, CH_2Ph), 4.50 (d, $J = 12.4$ Hz, 1H, CH_2Ph), 4.81 (d, $J = 10.8$ Hz, 1H, CH_2Ph), 4.56 (t, $J = 10.4$ Hz, 1H, H-2), 4.71 (d, $J = 8.0$ Hz, 1H, H-1′), 4.77 (d, $J = 10.8$ Hz, 1H, CH_2Ph), 4.78 (d, $J = 10.4$ Hz, 1H, CH_2Ph), 4.96 (d, $J = 10.4$ Hz, 1H, CH_2Ph), 5.46 (t, $J = 9.8$ Hz, 1H, H-4), 5.88 (d, $J = 10.4$ Hz, 1H, H-1), 6.17 (dd, $J = 9.8$, 9.4 Hz, 1H, H-3), 7.09–7.53 (m, 26H, Ar), 7.69–7.74 (m, 2H, Ar), 7.85–7.91 ppm (m, 2H, Ar); ^{13}C NMR (100 MHz, $CDCl_3$): $\delta = 20.41$ (CH_3), 21.49 (CH_3), 32.05 (C, $J_{CP} = 5.3$ Hz), 54.49 (CH, C2), 67.53 (CH_2, C-6), 68.37 (CH_2, C6′), 69.54 (CH, C4), 72.11 (CH, C3), 73.42 (CH_2, *C*H_2Ph), 74.85 (CH_2, *C*H_2Ph), 75.02 (CH, C5′), 75.28 (CH_2, *C*H_2Ph), 77.60 (CH, C4), 77.59–77.70 (CH_2, 2C, P(O){O*C*H_2C(CH_3)$_2$*C*H_2O}), 78.60 (CH, C5), 79.27 (CH, $J_{CP} = 6.9$ Hz, C2′), 82.04 (CH, C1), 83.04 (CH, $J_{CP} = 3.0$ Hz, C3′), 100.71 (CH, $J_{CP} = 3.1$ Hz, C1′), 126.75 (C), 127.05 (C), 127.54 (CH), 127.61 (CH), 127.72 (CH, 2C), 127.81 (CH, 2C), 128.16 (CH, 2C), 128.16 (C), 128.27 (CH, 2C), 128.30 (CH, 4C), 128.32 (CH, 4C), 128.38 (CH, 2C), 128.59 (C), 129.25 (CH, 2C), 129.72 (CH, 2C), 129.80 (CH, 2C), 129.91 (C), 130.02 (C), 130.90 (C), 132.30 (CH, 2C), 133.46 (CH), 133.49 (CH), 137.90 (C), 137.98 (C), 138.11 (C), 140.37 (C), 140.61 (C), 162.05 (C=O), 163.20 (C=O), 165.31 (C=O), 165.90 (C=O); HRMS (FAB) *m*/*z*: calcd for $C_{66}H_{61}Cl_4NO_{16}PS$: 1326.2203 $[M+H]^+$; found: 1326.2195.

Received: July 7, 2006
Revised: August 15, 2006
Published online: October 20, 2006

Keywords: carbohydrates · glycosylation · oligosaccharides · protecting groups · stereoselective synthesis

[1] a) *Carbohydrates in Chemistry and Biology* (Eds.: B. Ernst, G. W. Hart, P. Sinaÿ), Wiley-VCH, Weinheim, **2000**; b) A. Varki, *Glycobiology* **1993**, *3*, 97.

[2] Other stereodirecting groups except acyl group have been recently reported. a) J.-H. Kim, H. Yang, J. Park, G.-J. Boons, *J. Am. Chem. Soc.* **2005**, *127*, 12090; b) J. T. Smoot, P. Pornsuriyasak, A. V. Demchenko, *Angew. Chem.* **2005**, *117*, 7285; *Angew. Chem. Int. Ed.* **2005**, *44*, 7123.

[3] Selected recent examples: a) P. H. Seeberger, M. Eckhardt, C. E. Gutteridge, S. J. Danishefsky, *J. Am. Chem. Soc.* **1997**, *119*, 10064; b) Y. Konda, T. Toida, E. Kaji, K. Takeda, Y. Harigaya, *Carbohydr. Res.* **1997**, *301*, 123; c) X.-S. Ye, C.-H. Wong, *J. Org. Chem.* **2000**, *65*, 2410; d) F. W. Lichtenthaler, M. Oberthür, S. Peters, *Eur. J. Org. Chem.* **2001**, 3849; e) Y. Du, M. Zhang, F. Kong, *J. Chem. Soc. Perkin Trans. 1* **2001**, 2289; f) M. Mach, U. Schluester, F. Mathew, B. Fraser-Raid, K. C. Hazen, *Tetrahedron* **2002**, *58*, 7345; g) H. Amer, A. Hofinger, P. Kosma, *Carbohydr. Res.* **2003**, *338*, 35; h) A. Fürstner, F. Jeanjean, P. Razon, C.

 © 2006 Wiley-VCH Verlag GmbH & Co. KGaA, Weinheim

Wirtz, R. Mynott, *Chem. Eur. J.* **2003**, *9*, 320; i) J. Ning, W. Zhang, Y. Yi, G. Yang, Z. Wu, J. Yi, F. Kong, *Bioorg. Med. Chem.* **2003**, *11*, 2193; j) N. Pleuss, H. Kunz, *Angew. Chem.* **2003**, *115*, 3282; *Angew. Chem. Int. Ed.* **2003**, *42*, 3174; k) H. A. Orgueira, A. Bartolozzi, P. Schell, R. E. J. N. Litjens, E. R. Palmacci, P. H. Seeberger, *Chem. Eur. J.* **2003**, *9*, 140; l) S. Dziadek, C. Brocke, H. Kunz, *Chem. Eur. J.* **2004**, *10*, 4150; m) S. M. Rele, S. S. Iyer, S. Baskaran, E. L. Chaikof, *J. Org. Chem.* **2004**, *69*, 9159; n) X. Zhu, B. Yu, Y. Hui, R. R. Schmidt, *Eur. J. Org. Chem.* **2004**, 965.

[4] a) A. Harreus, H. Kunz, *Liebigs Ann. Chem.* **1986**, 717; b) K. W. Neumann, J. Tamura, T. Ogawa, *Bioorg. Med. Chem.* **1995**, *3*, 1637; c) O. J. Plante, E. R. Palmacci, R. B. Andrade, P. H. Seeberger, *J. Am. Chem. Soc.* **2001**, *123*, 9545; d) J. D. C. Codée, J. van den Bos, R. E. J. N. Litjens, H. S. Overkleeft, J. H. van Boom, G. A. van der Marel, *Org. Lett.* **2003**, *5*, 1947.

[5] a) T. Ogawa, K. Katano, M. Matsui, *Carbohydr. Res.* **1978**, *64*, C3; b) K. Zegelaar-Jaarsveld, H. I. Duynstee, G. A. van der Marel, J. H. van Boom, *Tetrahedron* **1996**, *52*, 3575.

[6] Y. Zeng, J. Ning, F. Kong, *Tetrahedron Lett.* **2002**, *43*, 3729.

[7] a) S. Yamago, T. Yamada, T. Maruyama, J. Yoshida, *Angew. Chem.* **2004**, *116*, 2197; *Angew. Chem. Int. Ed.* **2004**, *43*, 2145; b) T. Yamada, S. Kinjo, J. Yoshida, S. Yamago, *Chem. Lett.* **2005**, *34*, 1556; c) S. Yamago, T. Yamada, O. Hara, H. Ito, Y. Mino, J. Yoshida, *Org. Lett.* **2001**, *3*, 3867; d) S. Yamago, T. Yamada, H. Ito, O. Hara, Y. Mino, J. Yoshida, *Chem. Eur. J.* **2005**, *11*, 6159.

[8] a) J. D. C. Codée, R. E. J. N. Litjens, L. J. van der Bos, H. S. Overkleeft, G. A. van der Marel, *Chem. Soc. Rev.* **2005**, *34*, 769; b) See also, X. Huang, L. Huang, H. Wang, X.-S. Ye, *Angew. Chem.* **2004**, *116*, 5333; *Angew. Chem. Int. Ed.* **2004**, *43*, 5221.

[9] *Protective Groups in Organic Synthesis*, 3rd ed. (Eds.: T. W. Greene, P. G. M. Wuts), Wiley, New York, **1999**, pp. 598–600.

[10] a) L. Zervas, S. Konstas, *Chem. Ber.* **1960**, *93*, 435; b) J. Banoub, P. Boullanger, D. Lafont, *Chem. Rev.* **1992**, *92*, 1167.

[11] D. Crich, M. Smith, *J. Am. Chem. Soc.* **2001**, *123*, 9015. Several attempts to utilize 2-acyl protected thioglycoside donors for the iterative glycosylation under Crich's conditions failed.

[12] a) P. Konradsson, U. E. Udodong, B. Fraser-Reid, *Tetrahedron Lett.* **1990**, *31*, 4313; b) G. H. Veeneman, S. H. van Leeuwen, J. H. van Boom, *Tetrahedron Lett.* **1990**, *31*, 1331.

[13] Competition experiments indicated that **1a** could be classified into disarmed glycoside (See Supporting Information).

[14] D. R. Mootoo, P. Koradsson, U. Udodong, B. Fraser-Reid, *J. Am. Chem. Soc.* **1988**, *110*, 5583.

[15] D. Crich, S. Sun, *J. Am. Chem. Soc.* **1997**, *119*, 11217.

[16] The ^{31}P NMR resonances shift downfield when trialkylphosphates are converted to tetraalkyl phosphonium ions. J. H. Finley, D. Z. Denney, D. B. Denney, *J. Am. Chem. Soc.* **1969**, *91*, 5826.

[17] D. Crich, Z. M. Dai, S. Gastaldi, *J. Org. Chem.* **1999**, *64*, 5224.

[18] a) D. Crich, W. Cai, *J. Org. Chem.* **1999**, *64*, 4926; b) D. Crich, T. K. Hutton, A. Banerjee, P. Jayalath, J. Picione, *Tetrahedron: Asymmetry* **2005**, *16*, 105.

[19] It is unlikely that the excellent selectivity is attributed to the steric effect because the use of steric hindered alcohols showed lower selectivity than one of less hinder alcohols (Table 1, entries 1–3).

[20] Thiomannoside **14k** gave the corresponding α-triflate intermediate upon activation by BSP and Tf_2O as judged by the low temperature ^{1}H NMR study, and the intermediate selectively afforded α-glycoside upon treatment of alcohol. The result absolutely denies the path A and is consistent with the path B.

 © 2006 Wiley-VCH Verlag GmbH & Co. KGaA, Weinheim

Amphiphiles

DOI: 10.1002/anie.200602739

Grafting Short Peptides onto Polybutadiene-*block*-poly(ethylene oxide): A Platform for Self-Assembling Hybrid Amphiphiles**

Yan Geng, Dennis E. Discher, Justyna Justynska, and Helmut Schlaad**

The peptide in peptide-containing hybrid amphiphiles usually plays the role of a hydrated hydrophilic headgroup rather than that of a hydrophobic tail.[1–3] However, chiral peptide interactions within a dense hydrophobic core of an amphiphile assembly might better mimic the hydrophobic interactions that drive the collapse and ordering in protein folding and highly specific protein–protein associations.[4] The goal of this study was therefore to make self-assembling hybrid amphiphiles that integrate peptides within the hydrophobic core. More-practical reasons for attaching short peptides onto synthetic polymers involve biomedical applications: 1) amino acids chosen from those often found in protein cores (cysteine, phenylalanine, tryptophane, etc.) can help to tune the solubility of hydrophobic drugs, and 2) short peptides with less than six repeat units are less antigenic[5,6] than long polypeptides[7] or proteins.[8]

Purely synthetic block copolymer amphiphiles can self-assemble into various mesostructures (e.g. spherical micelles, wormlike micelles, and vesicles) in aqueous solutions[9–11] by similar principles to the hydrophobic effect operative for surfactants (i.e. minimization of the contact of the hydrophobic blocks with water).[12,13] Morphological phase diagrams mapped out for nonionic block copolymers of polybutadiene-*block*-poly(ethylene oxide) (PBD-*b*-PEO) show that their self-assembly structures in water are largely determined by the weight fraction of the hydrophilic PEO

[*] Prof. Y. Geng
Department of Chemistry
University of Georgia
Athens, GA 30602 (USA)
Fax: (+1) 706-542-9454
E-mail: ygeng@chem.uga.edu
Homepage: http://www.chem.uga.edu/ygeng
J. Justynska, Dr. H. Schlaad
Max-Planck-Institut für Kolloid- und Grenzflächenforschung
Wissenschaftspark Golm, 14424 Potsdam (Germany)
Fax: (+49) 331-567-9502
E-mail: schlaad@mpikg-golm.mpg.de
Prof. D. E. Discher
University of Pennsylvania
Philadelphia, PA 19104-6315 (USA)

[**] We thank Reinhard Sigel, Hans Börner, and Markus Antonietti (MPI-KG) for their help and useful discussions. We also thank the Bates group at the University of Minnesota for cryo-TEM measurements. Grants were provided by the NSF, the Deutsche Forschungsgemeinschaft, and the Max-Planck-Gesellschaft.

Supporting information for this article is available on the WWW under http://www.angewandte.org or from the author.

WILEY InterScience DISCOVER SOMETHING GREAT
© 2006 Wiley-VCH Verlag GmbH & Co. KGaA, Weinheim

block (w_{EO}) and that decreasing w_{EO} disfavors spherical micelles and favors structures with lower mean curvature such as wormlike micelles and vesicles.[9] Although the structures of synthetic block copolymers can be tuned, the hybridization of synthetic copolymers with peptides leads to a further level of sophistication and functionality of the self-assembled structures.[1,2] Helical superstructures have recently been prepared from peptide hybrid amphiphiles, typically using long polypeptides as the hydrophilic block, such as polystyrene-*block*-poly(isocyanodipeptide)[14] and polybutadiene-*block*-poly(L-glutamate).[15,16] These peptide hybrids were generally synthesized by advanced techniques such as metal-catalyzed polymerization of isocyanopeptides or ring-opening polymerization of the α-amino acid *N*-carboxyanhydride.

Herein, we introduce a new type of self-assembling peptide hybrid amphiphiles by using synthetic PBD-*b*-PEO as the backbone and grafting cysteine-containing oligopeptides onto the hydrophobic PBD segment through a free-radical addition reaction. Modification with difluorocarbene was used in the solid-state to tune the self-assembly behavior of block copolymers;[17] in aqueous solutions, attaching short hydrophobic peptides decreases the w_{EO} value of the amphiphile and thus shifts the preferred self-assembly morphology towards those with lower curvatures, namely, from spherical micelles to wormlike micelles and vesicles (Scheme 1). Initial studies also suggest that chiral peptide interactions within the hydrophobic core foster the formation of helical superstructures.

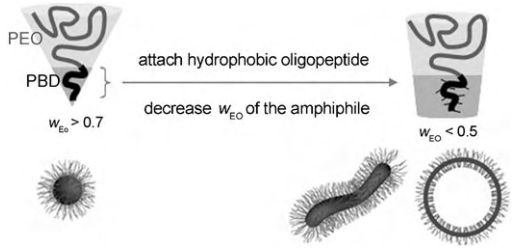

Scheme 1. Change of the morphology towards lower curvature structures through the attachment of a hydrophobic peptide onto PBD-*b*-PEO.

Two PBD-*b*-PEO copolymer samples with similar number-average molecular weight (M_n) but different weight fractions of PEO were used: PBD_{14}-*b*-PEO_{93} (**1**, M_n = 4900 g mol^{-1}, w_{EO} = 0.83) and PBD_{25}-*b*-PEO_{75} (**2**, M_n = 4700, w_{EO} = 0.70). As reported earlier, PBD-*b*-PEO can be functionalized through free-radical addition of ω-functional mercaptans (RSH) without altering the molecular-weight distribution (MWD).[18,19] The number of functional groups attached to the PBD chain is usually lower than the number of converted double bonds owing to a side reaction of the radical species, namely, the formation of six-membered cyclic units (Scheme 2a). We have extended the radical addition route from mercaptans to chiral cysteine-containing oligopeptides. The route was first tested on an L-cysteine derivative (**C**) and then on the dipeptide (L,L)-cysteine-phenylalanine (**CF**) as a model oligopeptide to prove the applicability of this route (Scheme 2b).

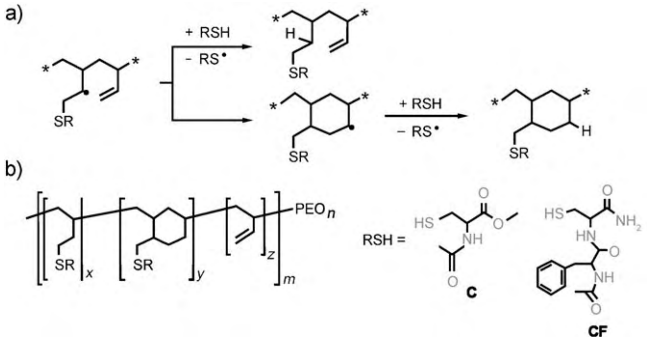

Scheme 2. a) Possible reaction pathway of the intermediate radicals formed by the addition of RS· onto PBD. b) Chemical structure of **C**- and **CF**-grafted PBD-*b*-PEO.

Addition reactions of **C** onto **1** and **2** were performed in refluxing tetrahydrofuran (THF) using azoisobutyronitrile (AIBN) as the radical source ($[C{=}C]_0/[\mathbf{C}]_0/[AIBN]_0$ = 1:10:0.33). Conversion of PBD double bonds came to completion within 24 h and products **1**-**C** and **2**-**C** exhibited the same narrow MWDs as the precursors (PDI ≤ 1.05; see NMR spectroscopy and size-exclusion chromatography (SEC) in the Supporting Information).[18] In the case of **CF**, the molar ratio was chosen to be $[C{=}C]_0/[\mathbf{CF}]_0/[AIBN]$ = 1:2.5:0.33 for economic reasons. Further decreasing the amount of **CF** bears the risk that the PBD chains will undergo intermolecular cross-linking. Because of the poor solubility of **CF** in THF, the radical addition reaction was carried out in *N*-methylpyrrolidone (NMP) as the solvent. The ^{1}H NMR spectra (**1**-**CF** shown in Figure 1a, **2**-**CF** given in the Supporting Information) shows signals of the dipeptide at δ = 4.3, 4.5 (α-CH), 7.1–7.3 (phenyl), and 8.1 ppm (NH); the signals of the thioether linkage -CH_2SCH_2- arise at $\delta \approx 2.7$ and 2.9 ppm. Resonances at δ = 4.8–5.6 ppm indicate the presence of residual double bonds. Quantitative analysis of signal intensities relative to that of PEO ($\delta \approx 3.6$ ppm) suggested that both samples contain about 10 **CF** units and 2–3 unreacted butadiene units. SEC (with differential refractive

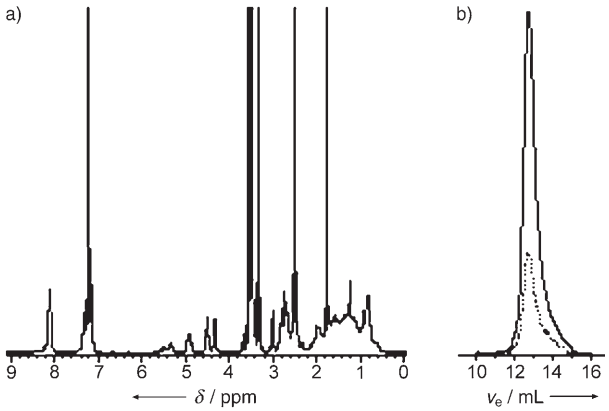

Figure 1. a) ^{1}H NMR spectrum (solvent: $[D_6]$DMSO) and b) SEC (eluent: NMP; solid line: RI; dashed line: UV, λ = 270 nm) of **1**-**CF**.

 © 2006 Wiley-VCH Verlag GmbH & Co. KGaA, Weinheim

index (RI) and UV detectors) of **1-CF** (Figure 1b) confirmed the attachment of **CF** units onto the polymer (UV absorption at 270 nm) and the preservation of the narrow MWD (polydispersity index < 1.2).

As mentioned above, the morphology of the PBD-*b*-PEO self-assembled structures in water is dictated by the w_{EO} value. Spherical micelles predominate when $w_{EO} > 0.55$, whereas wormlike micelles form when $w_{EO} \approx 0.50$–0.55 and vesicles form when w_{EO} is well below 0.5.[9] The precursor PBD-*b*-PEO samples **1** ($w_{EO} = 0.83$) and **2** ($w_{EO} = 0.70$) form spherical micelles at 0.1% w/w in water, as visualized by cryogenic transmission electron microscopy (cryo-TEM; Figure 2). The dark spots observed in the micrographs correspond to the hydrophobic cores of the micelles, which are about 12 and 20 nm in diameter for **1** and **2**, respectively. The hydrodynamic diameters of the micelles determined by dynamic light scattering (DLS) are 27 and 45 nm, respectively.

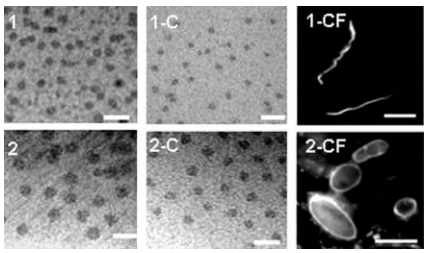

Figure 2. Visualization of self-assembled structures of PBD-*b*-PEO (**1**, **2**) and **C**-grafted hybrids (**1-C**, **2-C**) by cryo-TEM (scale bars = 50 nm) and **CF**-grafted hybrids (**1-CF**, **2-CF**) by FM (scale bars = 5 μm) in water.

Grafting **C** onto **1** and **2** had no effect on the shape of micelle cores, yet decreased their size by 10–30% (Figure 2). The hydrodynamic diameters of the micelles also decreased to about one third that of the precursor micelles. The formation of smaller-sized micelles can be attributed to the slight hydrophilic nature of cysteine, which increases the overall hydrophilic fraction of the hybrids and the corresponding interfacial curvature.

In contrast, dipeptide **CF** is hydrophobic, and grafting **CF** onto **1** and **2** leads to a decrease of w_{EO} and shifts the morphology towards those with smaller curvatures, that is, wormlike micelles and vesicles. Fluorescence microscopy (FM) revealed giant wormlike micelles with contour lengths of 10–15 μm for **1-CF** ($w_{EO} = 0.54$) and vesicles with diameters of 2–5 μm for **2-CF** ($w_{EO} = 0.43$) (Figure 2). FM is widely used to study cellular structures and dynamics, but has recently been established also as a reliable and convenient technique for visualizing micrometer-sized wormlike micelles and vesicles.[20–22] Unlike cryo-TEM, FM allows direct observation of samples in aqueous solutions without requiring fixation and constraint in thin films, and thus provides more equilibrated and convenient access to length and dynamic measurements of soft objects. The w_{EO} values of the **CF**-grafted PBD-*b*-PEO that correspond to wormlike micelles and vesicles are quantitatively comparable to the PBD-*b*-PEO morphological phase diagram,[9] thus suggesting that the self-assembly of such hybrids in water is likewise dictated by the hydrophobic–hydrophilic balances.

Integrating the dipeptide **CF** into PBD-*b*-PEO not only changed the hydrophobic–hydrophilic ratio of the amphiphile, but also introduced hydrogen-bonding, π–π, and chiral interactions into the hydrophobic core of the assembly, which might induce the formation of helices. Helices often emerge in nature from such interactions, for example, in proteins and DNA. As helices are generally more observable in fibrous structures, we then examined the giant **1-CF** wormlike micelles in more detail. FM revealed the existence of both right- and left-handed defected helical structures with supermolecular pitches of a few micrometers (Figure 3a). Sequen-

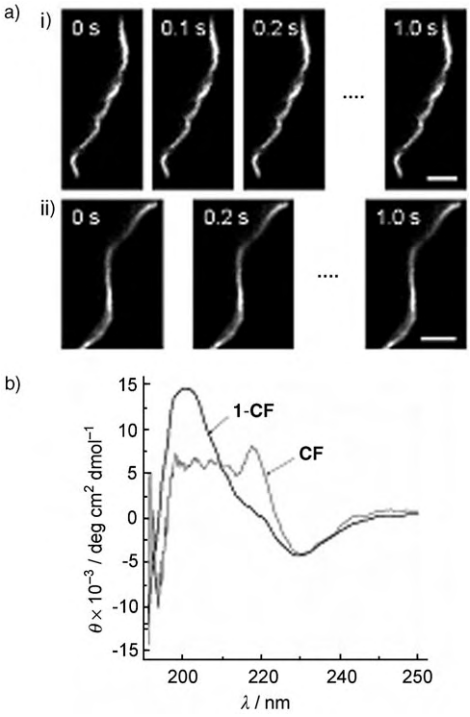

Figure 3. a) FM snapshots of i) right-handed and ii) left-handed distorted helical structures (scale bars = 2 μm); and b) CD spectrum of **1-CF** wormlike micelles in water.

tial snapshots of individual **1-CF** wormlike micelles confirm that their helical curvature is rigid, whereas pristine PBD-*b*-PEO wormlike micelles are extremely soft and flexible and exhibit large thermal fluctuations.[23] Analysis of the circular dichroism (CD) spectrum of an aqueous solution of **1-CF** wormlike micelles (Figure 3b) indicates a near racemic mixture of helices with right-handed and left-handed screw senses (see the Supporting Information). Although investigations continue, the capability of such amphiphilic hybrids that contain hydrophobic peptides to self-assemble into helical superstructures is evident.

In conclusion, we report a new type of peptide hybrid amphiphiles by directly grafting cysteine-containing oligopeptides onto synthetic PBD-*b*-PEO copolymers. The morphologies (spherical micelles, wormlike micelles, and vesicles) of such self-assembled hybrid amphiphiles may be tuned by

 © 2006 Wiley-VCH Verlag GmbH & Co. KGaA, Weinheim

controlling the hydrophobic–hydrophilic ratios. Helical superstructures also arise from the chiral peptide interactions inside the assembly core. This new class of hybrids allows the integration of functionalities into the assembly core for various applications. Future investigations will likely include exploring the attachment of different functional oligopeptides, studying their self-assembly and superstructures, and pursuing their biomedical applications.

Received: July 10, 2006
Published online: October 20, 2006

Keywords: amphiphiles · helical structures · micelles · self-assembly · vesicles

[1] J. D. Hartgerink, E. Beniash, S. I. Stupp, *Science* **2001**, *294*, 1684 – 1688.
[2] H. Schlaad, M. Antonietti, *Eur. Phys. J. E* **2003**, *10*, 17 – 23.
[3] H. Schlaad, *Adv. Polym. Sci.* **2006**, *202*, 53 – 74.
[4] J. Miao, J. Klein-Seetharaman, H. Meirovitch, *J. Mol. Biol.* **2004**, *344*, 797 – 811.
[5] A. Y. Rudensky, P. Preston-Hurlburt, S.-C. Hong, A. Barlow, C. A. Janeway, *Nature* **1991**, *353*, 622 – 627.
[6] J. W. Yewdell, J. R. Bennink, *Curr. Opin. Immunol.* **2001**, *13*, 13.
[7] T. J. Deming, *Adv. Drug Delivery Rev.* **2002**, *54*, 1145 – 1155.
[8] K. Velonia, A. E. Rowan, R. J. M. Nolte, *J. Am. Chem. Soc.* **2002**, *124*, 4224 – 4225.
[9] S. Jain, F. S. Bates, *Science* **2003**, *300*, 460 – 464.
[10] S. Förster, M. Zisenis, E. Wenz, M. Antonietti, *J. Chem. Phys.* **1996**, *104*, 9956 – 9970.
[11] D. E. Discher, A. Eisenberg, *Science* **2002**, *297*, 967 – 973.
[12] J. N. Israelachvili, *Intermolecular and Surface Forces*, Academic Press, London, **1985**.
[13] P. Alexandridis, B. Lindman, *Amphiphilic Block Copolymers: Self-assembly and Applications*, Elsevier, New York, **2000**.
[14] J. J. L. M. Cornelissen, M. Fischer, N. A. J. M. Sommerdijk, R. J. M. Nolte, *Science* **1998**, *280*, 1427 – 1430.
[15] H. Kukula, H. Schlaad, M. Antonietti, S. Förster, *J. Am. Chem. Soc.* **2002**, *124*, 1658 – 1663.
[16] F. Chécot, S. Lecommandoux, Y. Gnanou, H.-A. Klok, *Angew. Chem.* **2002**, *114*, 1395 – 1399; *Angew. Chem. Int. Ed.* **2002**, *41*, 1339 – 1343.
[17] Y. Ren, T. P. Lodge, M. A. Hillmyer, *Macromolecules* **2000**, *33*, 866 – 876.
[18] J. Justynska, Z. Hordyjewicz, H. Schlaad, *Polymer* **2005**, *46*, 12057 – 12064.
[19] J. Justynska, H. Schlaad, *Macromol. Rapid Commun.* **2004**, *25*, 1478 – 1481.
[20] B. M. Discher, Y.-Y. Won, D. S. Ege, J. C.-M. Lee, F. S. Bates, D. E. Discher, D. A. Hammer, *Science* **1999**, *284*, 1143 – 1146.
[21] P. Dalhaimer, H. Bermudez, D. E. Discher, *J. Polym. Sci. Part B* **2004**, *42*, 168 – 176.
[22] Y. Geng, D. E. Discher, *J. Am. Chem. Soc.* **2005**, *127*, 12780 – 12781.
[23] P. Dalhaimer, F. S. Bates, D. E. Discher, *Macromolecules* **2003**, *36*, 6873 – 6877.

 © 2006 Wiley-VCH Verlag GmbH & Co. KGaA, Weinheim

Oxime Ligation

DOI: 10.1002/anie.200602877

Nucleophilic Catalysis of Oxime Ligation**

*Anouk Dirksen, Tilman M. Hackeng, and Philip E. Dawson**

Imine-based reactions have found wide application in the conjugation of biomolecules as a result of their high chemoselectivity.[1–8] Aldehydes and ketones can be readily introduced into biomolecules and are virtually inert towards reaction with other functional groups in these molecules. Under acidic conditions the carbonyl group reacts with primary amines to form a reversible imine (Scheme 1a), and the equilibrium favors the free carbonyl. However, when α-effect nitrogens[9] such as aminooxy groups and hydrazides are used, the equilibrium favors the imine.[1–8]

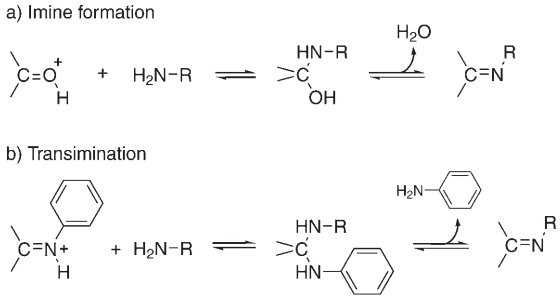

Scheme 1. a) Imine formation and b) transimination under acidic conditions.

Oxime ligations are often called upon to link complex and precious macromolecules.[7,8] The oxime bond is stable under physiological conditions, whereas more dynamic imines, such as hydrazones, are often reduced to obtain a stable linkage. Oxime ligations proceed with modest reaction rates in acidic solution but are poorly reactive at pH 7. which limits their use in many biological applications. To improve the reaction rate, oxime ligations typically require millimolar concentrations of

[*] Dr. A. Dirksen, Dr. P. E. Dawson
Departments of Cell Biology and Chemistry
Skaggs Institute for Chemical Biology
The Scripps Research Institute
10550 North Torrey Pines Road, La Jolla, CA 92037 (USA)
Fax: (+1) 858-784-7319
E-mail: dawson@scripps.edu
Dr. A. Dirksen, Dr. T. M. Hackeng
Cardiovascular Research Institute Maastricht
University Maastricht
P.O. Box 616, 6200 MD Maastricht (The Netherlands)

[**] This work was supported by the Netherlands Organization for Scientific Research (NWO; to A.D.) and by the National Institutes of Health (GM059380 to P.E.D.).

Supporting information for this article is available on the WWW under http://www.angewandte.org or from the author.

 © 2006 Wiley-VCH Verlag GmbH & Co. KGaA, Weinheim

each reactant or a large excess of one component to establish pseudo-first-order kinetics.

Here we show that oxime ligations can be significantly accelerated by using aniline as a nucleophilic catalyst. Rate enhancements are achieved by changing the electrophile from a weakly populated protonated carbonyl (Scheme 1a) to a more highly populated protonated aniline Schiff base[10] (Scheme 1b).[11] The transimination ("trans-Schiffization")[11] of the protonated aniline Schiff base to the oxime proceeds rapidly under acidic aqueous conditions. The resulting ligation rates (k_{obs}) are increased up to 400-fold in aqueous solution at pH 4.5 and up to 40-fold at pH 7. Such rate enhancements enable the use of equimolar reactants at submillimolar concentrations, meeting the stringent requirements of challenging macromolecular ligation.

To illustrate the method, two unprotected peptides, glyoxylyl-LYRAG **1** and aminooxyacetyl-GRGDSGG **2** (Scheme 2) were ligated in the presence and absence of aniline at pH 4.5. The ligation reactions were performed at ambient temperature with each peptide at a concentration of 1 mM. The reactions were followed by HPLC, the ligation product **3** was quantitated by integration (214 nm), and the resulting data were fit to the second-order rate equation. In the absence of a catalyst, the half-time ($t_{1/2}$) of the reaction, that is, the time required to reach 50% conversion, is 310 min ($k_{obs} = 0.057 \pm 0.010\,M^{-1}s^{-1}$; Figure 1). However, in the presence of 10 mM aniline $t_{1/2}$ is reduced to 25 min ($k_{obs} = 0.68 \pm 0.05\,M^{-1}s^{-1}$). A further increase in the reaction rate is established by using a 100 mM anilinium acetate buffer (pH 4.6; Figure 1). Consistent with the proposed mechanism of nucleophilic catalysis, aniline does not change the equilibrium for the oxime ligation, and all reactions eventually reach over 99% conversion to **3**.

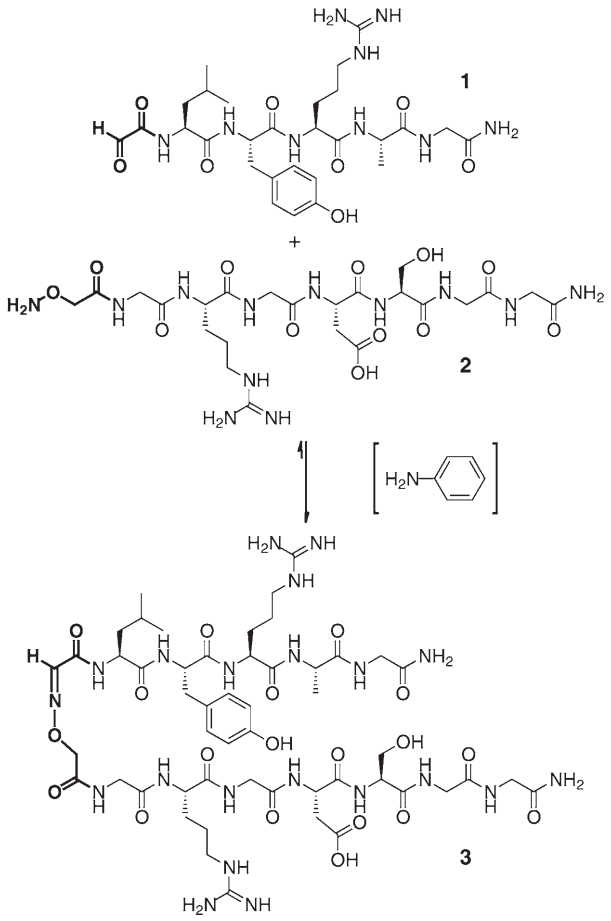

Scheme 2. Oxime ligation between glyoxylyl-LYRAG **1** and aminooxyacetyl-GRGDSGG **2** performed in either the absence or the presence of aniline.

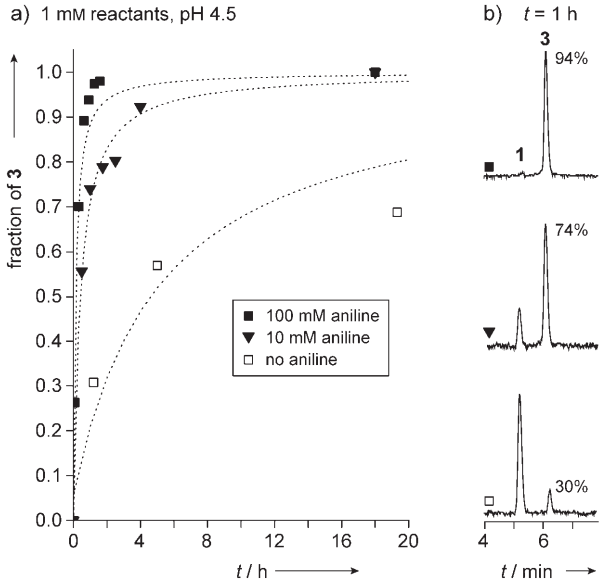

Figure 1. a) Formation of ligation product **3** over time at a reactant concentration of 1 mM in 0.1 M ammonium acetate buffer (pH 4.5) in the absence (□) and in the presence of 10 mM aniline (▼), and in 100 mM anilinium acetate buffer (pH 4.6; ■) ([**1**] = [**2**] = 1 mM; RT). b) RP HPLC traces recorded after 1 h for the three ligation reactions (gradient: 5–15% 9:1 v/v MeCN/H_2O in H_2O, 0.1% TFA in 10 min).

The solubility of large macromolecules is frequently limited to 0.1 mM concentrations owing to their high molecular weight, low availability, and tendency to aggregate. The enhanced ligation rates achieved through catalytic transimination suggested that oxime bonds could be formed efficiently at these low concentrations. Indeed, when the ligation is performed at pH 4.5 and at 0.1 mM of each peptide, the $t_{1/2}$ for oxime formation is reduced 30-fold from 8200 minutes (5.7 d; $k_{obs} = 0.020 \pm 0.001\,M^{-1}s^{-1}$) in the absence of aniline to 270 min ($k_{obs} = 0.62 \pm 0.03\,M^{-1}s^{-1}$) in the presence of 10 mM aniline (Figure 2). The ligation rate was further increased to a total of more than 400-fold using a 100 mM anilinium acetate buffer (pH 4.6); thus the peptides could be ligated with a $t_{1/2}$ of just 19 min ($k_{obs} = 8.6 \pm 2.0\,M^{-1}s^{-1}$) (Figure 2).

Since many biological macromolecules are conformationally unstable at low pH, it is often desirable to perform ligation reactions at pH 7. As shown in Figure 3, the uncatalyzed ligation is very slow under these conditions; $t_{1/2}$ is 11000 min (7.6 days; $k_{obs} = 0.0015 \pm 0.0001\,M^{-1}s^{-1}$), and competition is observed with the slow intramolecular ring closure of the glyoxylyl-functionalized peptide **1** to its corresponding cyclic isomers.[12] In contrast, oxime ligation

 © 2006 Wiley-VCH Verlag GmbH & Co. KGaA, Weinheim

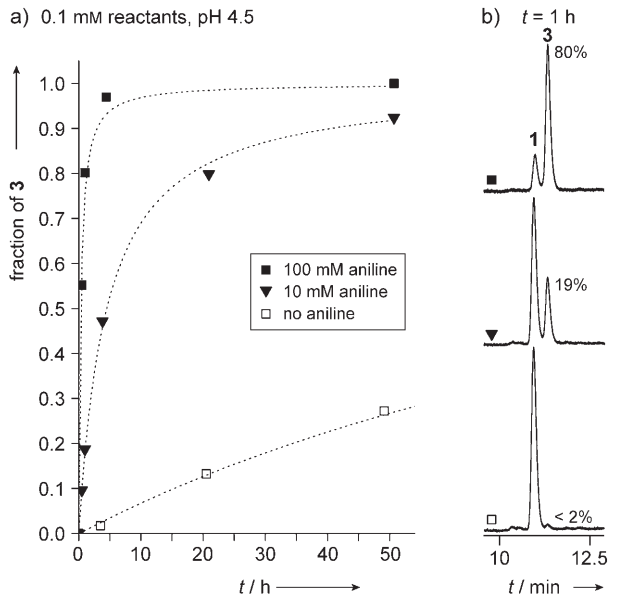

Figure 2. a) Formation of ligation product **3** over time at a reactant concentration of 0.1 mM in a 0.1 M ammonium acetate buffer (pH 4.5) in the absence (□) and in the presence of 10 mM aniline (▼), and in a 100 mM anilinium acetate buffer (pH 4.6; ■) ([**1**] = [**2**] = 0.1 mM; RT). b) RP HPLC traces recorded after 1 h for the three ligation reactions (gradient: 0–33.5 % 9:1 v/v MeCN/H_2O in H_2O, 0.1 % TFA in 15 min).

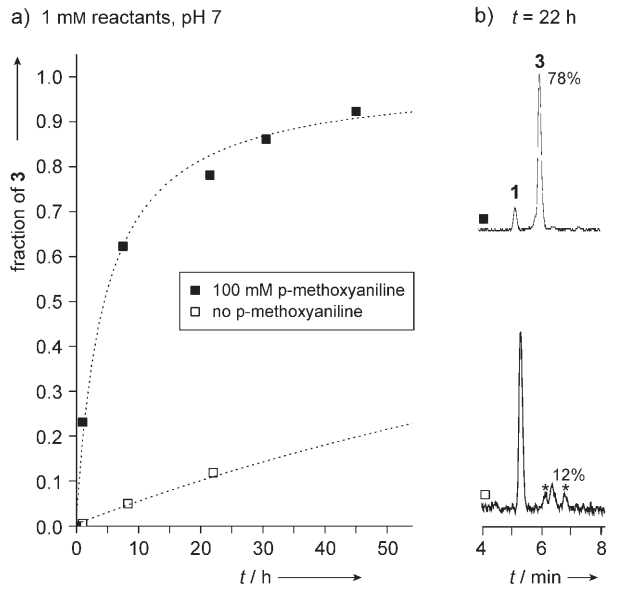

Figure 3. a) Formation of ligation product **3** over time at a reactant concentration of 1 mM in a 0.1 M sodium phosphate buffer (pH 7) in the absence (□) and in the presence of 100 mM *p*-methoxyaniline (▼) ([**1**] = [**2**] = 1 mM; RT). b) RP HPLC traces recorded after 22 h for the two ligation reactions (gradient: 5–15 % 9:1 v/v MeCN/H_2O in H_2O, 0.1 % TFA in 10 min); the peaks marked with an asterisk correspond to two isomers of the cyclization product of **1** (confirmed by ESI-MS).

at neutral pH can be achieved by using 100 mM *p*-methoxyaniline as a catalyst (selected because of its elevated pK_a of 5.3). In the presence of the *p*-methoxyaniline catalyst, the $t_{1/2}$ is 280 min ($k_{obs} = 0.061 \pm 0.006\ M^{-1}s^{-1}$; Figure 3), similar to the rate observed for the uncatalyzed oxime ligation at pH 4.5. These reaction conditions could find utility in the ligation or labeling of folded protein domains.

The application of aniline as a nucleophilic catalyst extends the scope of oxime ligations to new conditions highly relevant for bioconjugation. The rate enhancement can be attributed to the in situ generation of a comparatively high concentration of a reactive electrophile, the protonated aniline Schiff base, without affecting the equilibrium for oxime formation. It has been established that imine formation involves the nucleophilic attack of a free amine on the protonated carbonyl followed by dehydration (Scheme 1 a).[13,14] Since the pK_a of a protonated carbonyl is in the range of −4 to −10,[15] the concentration of this highly reactive electrophile is extremely low at pH 4.5. Although lowering the pH would lead to an increase in protonated carbonyl, the concomitant protonation of the reacting amine counteracts this effect.

Aniline and its derivatives meet the unique requirements for nucleophilic catalysis of oxime ligations.[11] Aniline (pK_a = 4.6; *p*-methoxyaniline: pK_a = 5.3)[11a] has a pK_a similar to that of α-effect nitrogens, such as the amine of the aminooxy group (p$K_a \approx 4.6$).[16] However, the pK_a of an imine formed with an α-effect nitrogen is typically 5–6 units below the pK_a of the parent amine, whereas the pK_a of the aniline Schiff base is only 2 units below that of aniline.[17] Consequently, the aniline Schiff base is significantly protonated under ligation conditions, whereas the imine formed with the α-effect nitrogen is almost completely deprotonated. In addition, the small equilibrium constant (K_{eq}) for the formation of the aniline Schiff base[11] allows the use of an excess of aniline without having it compete with the formation of the oxime. At neutral pH, aniline derivatives with a high pK_a should be more effective catalysts, establishing higher concentrations of the protonated aniline Schiff base. The ability to generate a reactive species without competing with the desired product is a key property of any nucleophilic catalyst.

Nucleophilic catalysis using aniline or other appropriate amine derivatives should be applicable to any reaction for which imine formation or transimination is the rate-determining step. Aniline is a mild, fairly unreactive nucleophile and is therefore compatible with many functional groups as demonstrated here by the use of unprotected peptides. Furthermore, aniline is soluble in a range of solvents and can be used as a convenient aqueous buffer with acetic acid, and both its solubility and nucleophilicity can be tuned through the introduction of substituents on the aromatic ring. Aniline catalysis will have a major impact on the numerous applications of imine chemistry including bioconjugation,[1–8] cellular labeling,[18,19] surface immobilization,[20] and dynamic combinatorial libraries.[21,22]

Received: July 19, 2006
Published online: October 19, 2006

Keywords: bioconjugation · nucleophilic catalysis · peptides · Schiff bases · transimination

 © 2006 Wiley-VCH Verlag GmbH & Co. KGaA, Weinheim

[1] H. F. Gaertner, K. Rose, R. Cotton, D. Timms, R. Camble, R. E. Offord, *Bioconjugate Chem.* **1992**, *3*, 262 – 268.
[2] K. Rose, *J. Am. Chem. Soc.* **1994**, *116*, 30 – 33.
[3] L. E. Canne, A. R. Ferré-D'Amaré, S. K. Burley, S. B. H. Kent, *J. Am. Chem. Soc.* **1995**, *117*, 2998 – 3007.
[4] J. Shao, J. P. Tam, *J. Am. Chem. Soc.* **1995**, *117*, 3893 – 3899.
[5] L. K. Mahal, K. J. Yarema, C. R. Bertozzi, *Science* **1997**, *276*, 1125 – 1128.
[6] Y. Singh, O. Renaudet, E. Defrancq, P. Dumy, *Org. Lett.* **2005**, *7*, 1359 – 1362.
[7] P. E. Dawson, S. B. H. Kent, *Annu. Rev. Biochem.* **2000**, *69*, 923 – 960.
[8] J. A. Borgia, G. B. Fields, *Trends Biotechnol.* **2002**, *18*, 243 – 251.
[9] E. G. Sander, W. P. Jencks, *J. Am. Chem. Soc.* **1968**, *90*, 6154 – 6162.
[10] H. Schiff, *Ann. Chem. Pharm.* **1864**, *131*, 118 – 119.
[11] a) E. H. Cordes, W. P. Jencks, *J. Am. Chem. Soc.* **1962**, *84*, 826 – 831; b) W. P. Jencks, *Catalysis in Chemistry and Enzymology*, Dover Publications, New York, **1986**, pp. 72 – 73.
[12] K. Rose, J. Chen, M. Dragovic, W. Zeng, D. Jeannerat, P. Kamalaprija, U. Burger, *Bioconjugate Chem.* **1999**, *10*, 1038 – 1043.
[13] F. A. Carey, R. J. Sundberg, *Advanced Organic Chemistry Part A: Structure and Mechanisms*, 3rd ed., Plenum, New York, **1990**, pp. 447 – 453.
[14] a) S. Rosenberg, S. M. Silver, J. M. Sayer, W. P. Jencks, *J. Am. Chem. Soc.* **1974**, *96*, 7986 – 7998; b) J. M. Sayer, B. Pinsky, A. Schonbrunn, W. Washtien, *J. Am. Chem. Soc.* **1974**, *96*, 7998 – 8009.
[15] E. M. Arnett, R. P. Quirk, J. W. Larsen, *J. Am. Chem. Soc.* **1970**, *92*, 3977 – 3984.
[16] T. C. Bissot, R. W. Parry, D. H. Campbell, *J. Am. Chem. Soc.* **1957**, *79*, 796 – 800.
[17] E. H. Cordes, W. P. Jencks, *J. Am. Chem. Soc.* **1962**, *84*, 832 – 837.
[18] J. A. Prescher, C. R. Bertozzi, *Nat. Chem. Biol.* **2005**, *1*, 13 – 21.
[19] I. Chen, M. Howarth, W. Lin, A. Y. Ting, *Nat. Methods* **2005**, *2*, 99 – 104.
[20] K. Larsen, M. B. Thygesen, F. Guillaumie, W. G. T. Willats, K. J. Jensen, *Carbohydr. Res.* **2006**, *341*, 1209 – 1234.
[21] S. J. Rowan, S. J. Cantrill, G. R. L. Cousins, J. K. M. Sanders, J. F. Stoddart, *Angew. Chem.* **2002**, *114*, 938 – 993; *Angew. Chem. Int. Ed.* **2002**, *41*, 898 – 952.
[22] O. Ramström, J.-M. Lehn, *Nat. Rev. Drug. Discovery* **2002**, *1*, 26 – 36.

 © 2006 Wiley-VCH Verlag GmbH & Co. KGaA, Weinheim

Chromium Colloids

DOI: 10.1002/anie.200602736

Silica-Immobilized Chromium Colloids for Cyclohexane Autoxidation**

Eric Breynaert, Ive Hermans, Bert Lambie, Guido Maes, Jozef Peeters, André Maes, and Pierre Jacobs*

The selective oxidation of cyclohexane (CyH) with molecular oxygen still constitutes a major challenge for chemists.[1] The synthesis of cyclohexanone (QO) is of special interest,[2] as it is a key chemical for the production of polyamides such as nylon 6 and nylon 6,6. It is generally recognized that the thermal reaction of CyH with O_2 proceeds via a complex radical chain mechanism, with a limit of 5% on the conversion to prevent overoxidation of the desired products.[3–5] Currently, the industrial autoxidation of CyH is often carried out in the presence of small amounts of dissolved cobalt salts.[3,4] Cobalt ions are able to assist in the generation of new radicals from the primary chain-propagation product, cyclohexyl hydroperoxide (CyOOH), via a Haber–Weiss catalytic cycle [reactions (1) and (2)].[1,3–8] This catalytic decomposition is indeed much faster than thermal initiation through a bimolecular reaction of CyOOH with CyH or QO.[9]

$$CyOOH + Co^{2+} \rightarrow CyO^{\cdot} + Co^{3+}OH^{-} \quad (1)$$

$$CyOOH + Co^{3+}OH^{-} \rightarrow CyOO^{\cdot} + H_2O + Co^{2+} \quad (2)$$

Chromium, however, is known to catalyze additionally the dehydration of CyOOH to QO, which results in a much more favorable product distribution.[3,4] Our recently developed insights into the mechanism of CyH autoxidation[10–12] prompted us to look at the opportunities for using Cr as a catalyst. The earlier mechanistic view,[3–5] which assumes that QO is responsible for the majority of by-products, is at odds with our results that stem from a combined experimental and theoretical approach to the subject.[10,11]

[*] E. Breynaert, Dr. I. Hermans, Prof. Dr. A. Maes, Prof. Dr. P. Jacobs
Centrum voor Oppervlaktechemie en Katalyse
K. U. Leuven
Kasteelpark Arenberg 23, 3001 Heverlee (Belgium)
Fax: (+32) 16-321-998
E-mail: ive.hermans@biw.kuleuven.be
B. Lambie, Prof. Dr. G. Maes, Prof. Dr. J. Peeters
Departement Chemie
K. U. Leuven
Celestijnenlaan 200F, 3001 Heverlee (Belgium)

[**] This work was performed in the frame of IAP, GOA, IDECAT, and CECAT projects. E.B., I.H., and B.L. acknowledge fellowships from K. U. Leuven, FWO-Vlaanderen, and IWT, respectively.

Supporting information for this article is available on the WWW under http://www.angewandte.org or from the author.

WILEY InterScience DISCOVER SOMETHING GREAT
© 2006 Wiley-VCH Verlag GmbH & Co. KGaA, Weinheim

On the one hand, QO was found to be barely more reactive than CyH, which indicates that its overoxidation can only account for a small fraction of the by-products. On the other hand, CyOOH was identified as being very reactive towards the chain-carrying peroxyl radicals, on account of its weakly bonded α-H atom.[13] This hitherto overlooked, though very fast, α-H abstraction results in the formation of QO, cyclohexanol (CyOH), and the majority of the by-products (Scheme 1).[10,11] It can therefore be rationalized that

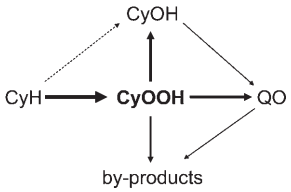

Scheme 1. Formation of QO, CyOH, and by-products via fast propagation reactions in the CyH autoxidation.[10,11]

the catalytic dehydration of CyOOH to QO can boost the selectivity of the reaction. Equally important is that the use of Cr could eliminate the need for a separate decomposition step of CyOOH. However, given its noxious nature, immobilization of Cr is an important prerequisite to its industrial breakthrough.

Retention of (isomorphically) substituted Cr in Cr/$AlPO_4$-*n* under autoxidation conditions was difficult.[1,14] Despite several attempts, the heterogeneous nature of the active site in Cr/$AlPO_4$-*n* or Cr/silicalite-like materials could not always be established unambiguously. Indeed, rigorous testing for the heterogeneity of so-called heterogeneous Cr catalysts is crucial, as many of these materials slowly release Cr under oxidizing conditions.[14] For the conventional Cr/$AlPO_4$-5, experimental evidence was found that the Cr is not incorporated in the framework, but rather is present as octahedral Cr^{III} ions at the surface of the zeolite crystal.[15] However, it cannot be excluded that changing the synthesis conditions[16,17] might result in stable, supported, Cr-based autoxidation catalysts. The performance of recently discovered three-dimensional mesoporous chromium oxide in autoxidation reactions remains to be examined.[18] Alternatively, Cr immobilization is possible by covalent anchoring of its complexes to a solid support.[19] Although these materials are more resistant to leaching, labile C–H bonds in the organic spacer can be slowly oxidized under the severe autoxidation conditions.

Herein, a new approach to the immobilization of Cr is presented, aimed at the design of stable autoxidation catalysts. Use is made of a novel column precipitation chromatographic (CPC) technique, which was recently developed to quantify oxidic eigencolloids of Tc^{IV}.[20] Cr^{III} eigencolloids, generated in situ by reduction of dosed $K_2Cr_2O_7$ with hydrazine, were precipitated onto a silica support in a chromatography column. The deposition of colloids flowing over a support column is interpreted mechanistically as a combination of coagulation of the colloids and heterocoagulation and heteroadagulation onto the packed bed.[20] As it is known that polyvalent ions can induce flocculation and facilitated deposition in a colloidal system,[20] and that sulfate ions can influence the Cr^{III} hydrolysis,[21] $CaSO_4$ was premixed with the dry silica support. The synthesis was carried out in a CPC system characterized by a high collector-particle radius and superficial velocity, in combination with a column flow reversal cycle, to achieve a homogeneous distribution of chromium. After chromium deposition, the column packing was vacuum-dried to remove water and residual hydrazine.

Dynamic light scattering (DLS) analysis of a liquid sample from the recirculation reactor reveals the presence of 6-nm particles that are reasonably stable in time (Figure 1). These nanosized Cr colloids are fixed on the silica gel by the CPC technique, and they remain invisible by SEM. It should be emphasized that our synthesis procedure yields nanoparticles that are much smaller than those commonly reported.[21,22]

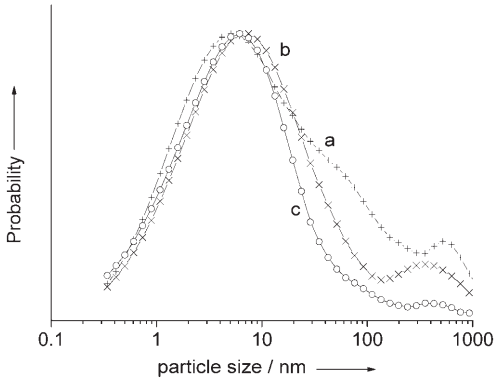

Figure 1. Particle size distribution as determined by DLS. Liquid sample withdrawn from the recirculation reactor without passing over the CPC column, measured after a) 4, b) 8, and c) 12 days (initially filtered over a 0.22-μm filter to remove dust particles).

The UV/Vis spectra of the green aqueous phase (Figure 2) are characteristic of octahedral Cr^{3+} ions.[23] The Cr speciation in solution does not change significantly over the range of free chromium concentrations used (10–40 mM).[24] The average extinction coefficients of (23 ± 5) and $(17 \pm 5)\,M^{-1}\,cm^{-1}$ at 422

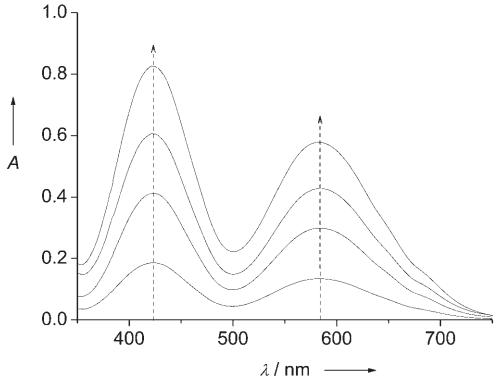

Figure 2. UV/Vis spectra of the solution phase depending on the amount of $K_2Cr_2O_7$ added to the CPC system (0.25, 0.50, 0.75, 1.5 mmol).

 © 2006 Wiley-VCH Verlag GmbH & Co. KGaA, Weinheim

and 582 nm, respectively,[24] are in good agreement with reported values for (oligomeric) chromium species.[25]

Column precipitation[20] is the dominant immobilization mechanism, as the achieved loadings of up to 13 mg g^{-1} are higher than the maximal loading one could possibly obtain with ion exchange.[24,26] The diffuse reflectance spectra (DRS) of the dry chromium-loaded solids[24] are very similar to the liquid-phase UV/Vis spectra and also reveal the presence of octahedral Cr^{3+} species.[23]

The X-band EPR spectra of Cr-loaded silica gel and a liquid aliquot from the recirculation reactor are analogous (Figure 3 a and b). The intense and broad β signal around $g = 2$ is characteristic for Cr^{3+} ions surrounded by six oxygen

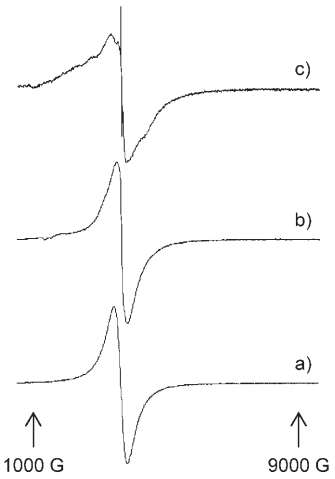

Figure 3. EPR spectra of a) a liquid sample withdrawn from the CPC reactor, b) Cr-loaded silica gel (1.60 mg Cr per g gel), and c) sample (b) after an autoxidation reaction at 403 K. All spectra were recorded at 110 K (9.588 GHz).

ligands in an octahedral coordination.[23,28] This finding, in combination with the UV/Vis and DRS information, indicates that the chromium nanoparticles identified in solution are immobilized on the silica support. No change in the surface area upon Cr loading was observed with N_2 adsorption.[29] X-ray diffraction showed no sign of a crystalline chromium oxide phase, and small-angle X-ray scattering (SAXS) was unable to characterize nanoparticles because of the structure of the silica support (broad peak below $2\theta = 8°$).[24]

The catalytic performance of the new Cr-on-silica catalyst was evaluated in the autoxidation of CyH with 30 ppm of Cr, at a temperature of 403 K where thermal autoxidation is very slow. It was found that the new material (13.0 mg Cr g^{-1}) is slightly more active than homogeneous [Cr(acac)$_3$] (acac = acetylacetonate; $\Delta p(O_2)$ after 300 min equals 1.6 and 1.4 MPa, respectively), which should be ascribed to an ideal dispersion of Cr colloids with a high surface area. The turnover frequency (TOF) of the immobilized Cr species was fairly independent of their loading. The CyOOH concentration remained very low throughout the reaction,[24] compared to that in the pure autoxidation reaction at the same temperature (Table 1).[11,24] This low concentration is the result of the catalytic dissociation and catalytic dehydration of

Table 1: Product yield at 3% conversion during the autoxidation of CyH at 403 K.

Experiment	QO	CyOH	CyOOH	By-products
pure[a]	23.5	31.0	40.0	5.5
new Cr catalyst[b]	60.0	24.3	1.2	14.5
Co catalyst[c]	37.5	50.5	1.5	10.5

[a] Pure CyH autoxidation, reaction time = 1150 min. [b] Cr-catalyzed autoxidation (30 ppm Cr as 13.0 mg Cr per g silica gel), reaction time = 150 min. [c] Co-catalyzed autoxidation (homogeneous reaction with 5 ppm Co^{II} octoate (2-ethylhexanoate), ICN Pharmaceuticals), reaction time = 150 min.

CyOOH,[30] also explaining the rather remarkable linear O_2 consumption (Figure 5 a). Normally the CyOOH concentration initially increases almost exponentially,[9,10] thus causing a large increase in the rate of initiation, which results in an exponential increase in the O_2 consumption. The high QO yield relative to that of by-products compensates the slightly higher by-product yield that results from overoxidation of QO.

Immediately after a catalytic run, an EPR analysis of the catalyst with 1.60 mg Cr g^{-1} reveals the presence of an additional sharp γ signal (Figure 3 c), often assigned to a single Cr^{V} species.[23,28] However, other studies attribute this signal to a mixed-valence trinuclear cluster of the type $Cr^{VI}OCr^{III}OCr^{VI}$ (pseudo Cr^{5+}).[31] Such in situ generated Cr^{VI} species could be the actual active sites of the catalyst. Indeed, a study of the CyOOH dehydration activity of chromium demonstrated the formation of an intermediate cyclohexyl peroxychromate ester between CyOOH and Cr^{VI}, which is able to decompose to QO.[30] When the used catalyst is stored for a few days in a desiccator, the sharp γ signal disappears, which suggests that it corresponds to a very reactive Cr species.

To evaluate the stability of the catalyst, the solid was separated at 353 K from the liquid phase after approximately 5% conversion (reaction at 403 K), to avoid re-adsorption of potentially leached Cr species. The liquid phase was checked for Cr by electrothermal vaporization (ETV) atomic absorption spectroscopy (AAS) and the concentration was below 5 ppb for all tested samples. Important is the fact that the same amount of Cr was measured when the catalysts were stirred for the same time at the same temperature in CyH, without O_2. Meanwhile, DLS analysis of this CyH liquid revealed particles of several hundred nanometers, probably caused by abrasion and attrition of the silica powder in the batch reactor.

This finding presents strong evidence that the new Cr catalyst is chemically stable under the current process conditions, and that the very small amount of Cr detected in the liquid phase is a result of physical impact of the stirrer on the material. It is expected that these effects will be absent if the reaction is carried out in a tubular reactor. Anyway, the (remaining) activity of the supernatant at 403 K can be safely attributed to the oxidation-enhancing nature of the products. Indeed, Figure 4 illustrates that an artificial autoxidation mixture, devoid of any chromium and mimicking the supernatant composition, exhibits the same activity, thus pointing to the heterogeneous nature of the new colloid-based system.

 © 2006 Wiley-VCH Verlag GmbH & Co. KGaA, Weinheim

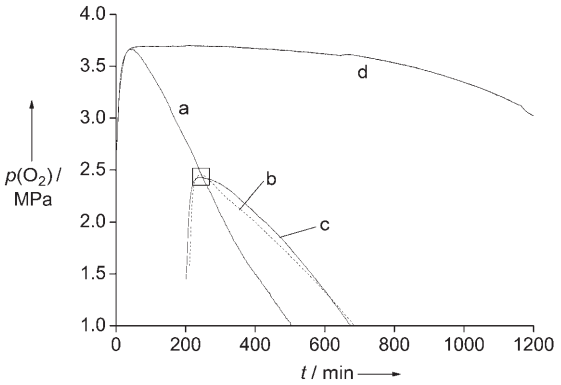

Figure 4. The activity at 403 K of a) fresh Cr catalyst (5.5 mg Cr g^{-1}), b) the hot-filtered supernatants (separated after 210 min), c) an artificial mixture containing the same amount of CyOOH (ca. 1 mM), CyOH (34 mM), QO (99 mM), and adipic acid (ca. 1 mM), and d) pure CyH autoxidation.

Probably, the stability can be attributed to the amorphous nature of the oxyhydroxide Cr colloids, which allows the accommodation of different coordination modes of Cr during a redox cycle.

As can be seen in Figure 5, the activity of the recycled catalyst is slightly lower than that of the fresh catalyst, although the oxidation remains much faster than a pure CyH autoxidation. After this initial decrease in performance, the activity is maintained during several recycles. The initial loss in activity before reaching a steady conversion points to the existence of a short transient period, the details of which are not well understood at this moment.

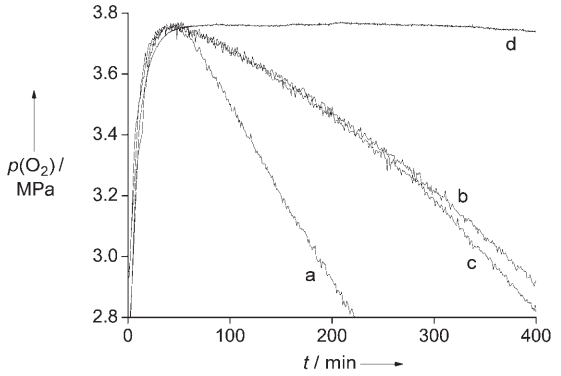

Figure 5. Comparison of the activity at 403 K of a) fresh CPC-synthesized catalyst (2.5 mg Cr g^{-1}), b) after one catalytic run, c) after four recycles, and d) the pure CyH autoxidation.

In conclusion, we have presented a new approach to the synthesis of heterogeneous chromium catalysts, based on the immobilization of Cr colloids generated in situ. The active materials are demonstrated to increase the yield of cyclohexanone in the autoxidation of cyclohexane. Strong evidence for the heterogeneous nature of the catalysis is supplied. More work is in progress to assess the nature of the support for heterogeneous chromium colloids in autoxidation catalysis, as well as that of colloids in other (liquid phase) reactions.

Experimental Section

In the CPC system, the content of a 100-mL stirred reactor was recirculated over a 25-mm-diameter column packed with silica powder (20 g) containing $CaSO_4 \cdot 2H_2O$ (10 wt%, dry premixed), at a flow rate of 20 mL min^{-1}. Silica 60 from Fluka with a particle size of 40–63 μm and a BET specific surface of 440 $m^2 g^{-1}$ was used as inert support material. A flow reversal was automatically initiated every 10 min to target a homogeneous Cr distribution over the column. After an initial equilibration of the column with the reactor volume (pH set at 4.0 ± 0.1 with HCl), the formation of chromium(III) colloid was achieved in situ by dosing the desired amount of $K_2Cr_2O_7$ at a rate of 3 μmol min^{-1} to the reducing stirred tank, which contained excess hydrazine (ratio $N_2H_2/Cr^{VI} \geq 1.3{:}1$). A synthesis pH of 4 was chosen, as PHREEQC modeling of the solution speciation indicates a mainly oligomeric nature of oversaturated Cr^{III} solutions, which favors the formation of Cr colloids.[32] The Cr content was measured by flame AAS after microwave digestion of the solid material.[33]

The autoxidation of CyH (50 mL, HPLC grade) was studied in a 100-mL stainless-steel Parr reactor, stirred at 500 rpm. The headspace was filled with O_2 at an initial room-temperature pressure of 2.75 MPa. The pressure was monitored continuously during the experiment. Products and by-products were collected in excess acetone and analyzed by GC (CP-Sil5 column, Chrompack), after silylation with *N*-methyl-*N*-(trimethylsilyl)trifluoroacetamide (MSTFA).[24] 1-Heptanol was used as external standard to correct for sensitivity differences in the flame ionization detector.

UV/Vis, diffuse reflectance, and X-band EPR spectra were recorded on a Perkin–Elmer Lambda 12 spectrometer, a Cary 5 UV/Vis/NIR spectrophotometer, and a Bruker ESP 300E instrument with a rectangular TE104 cavity, respectively.

Received: July 10, 2006
Published online: October 16, 2006

Keywords: autoxidation · chromium · colloids · radicals · supported catalysts

[1] U. Schuchardt, D. Cardoso, R. Sercheli, R. Pereira, R. S. da Cruz, M. C. Guerreiro, D. Mandelli, E. V. Spinacé, E. L. Pires, *Appl. Catal. A* **2001**, *211*, 1.
[2] a) T. Maschmeyer, R. D. Oldroyd, G. Sankar, J. M. Thomas, I. J. Shannon, J. A. Klepetko, A. F. Masters, J. K. Beattie, C. R. Catlow, *Angew. Chem.* **1997**, *109*, 1713; *Angew. Chem. Int. Ed. Engl.* **1997**, *36*, 1639; b) V. Kesavan, P. S. Sivanand, S. Chandrasekaran, Y. Koltypin, A. Gedanken, *Angew. Chem.* **1999**, *111*, 3729; *Angew. Chem. Int. Ed.* **1999**, *38*, 3521.
[3] R. A. Sheldon, J. K. Kochi, *Metal-Catalyzed Oxidations of Organic Compounds*, Academic Press, New York, **1981**.
[4] G. Franz, R. A. Sheldon in *Ullmann's Encyclopedia of Industrial Chemistry*, Wiley-VCH, Weinheim, **2000**.
[5] S. Bhaduri, D. Mukesh, *Homogeneous Catalysis: Mechanisms and Industrial Applications*, Wiley, New York, **2000**.
[6] N. M. Emanuel, Z. K. Maizus, I. P. Skibida, *Angew. Chem.* **1969**, *81*, 91; *Angew. Chem. Int. Ed. Engl.* **1969**, *8*, 97.
[7] D. L. Vanoppen, D. E. De Vos, M. J. Genet, P. G. Rouxhet, P. A. Jacobs, *Angew. Chem.* **1995**, *107*, 637; *Angew. Chem. Int. Ed. Engl.* **1995**, *34*, 560.
[8] M. Nowotny, L. N. Pedersen, U. Hanefeld, T. Maschmeyer, *Chem. Eur. J.* **2002**, *8*, 3724.
[9] I. Hermans, P. A. Jacobs, J. Peeters, *Chem. Eur. J.* **2006**, *12*, 4229.
[10] I. Hermans, T. L. Nguyen, P. A. Jacobs, J. Peeters, *ChemPhysChem* **2005**, *6*, 637.
[11] I. Hermans, P. A. Jacobs, J. Peeters, *J. Mol. Catal. A* **2005**, *251*, 221.

 © 2006 Wiley-VCH Verlag GmbH & Co. KGaA, Weinheim

[12] I. Hermans, P. A. Jacobs, J. Peeters, *ChemPhysChem* **2006**, *7*, 1142.
[13] L. Vereecken, T. L. Nguyen, I. Hermans, J. Peeters, *Chem. Phys. Lett.* **2004**, *393*, 432.
[14] R. A. Sheldon, M. Wallau, I. W. C. E. Arends, U. Schuchardt, *Acc. Chem. Res.* **1998**, *31*, 485.
[15] B. M. Weckhuysen, R. A. Schoonheydt, *Zeolites* **1994**, *14*, 360.
[16] J. Kornatowski, G. Zadrozna, M. Rozwadowski, B. Zibrowius, F. Marlow, J. A. Lercher, *Chem. Mater.* **2001**, *13*, 4447.
[17] A. M. Baele, D. Grandjean, J. Kornatowski, P. Glatzel, F. M. F. de Groot, B. M. Weckhuysen, *J. Phys. Chem. B* **2006**, *110*, 716.
[18] A. K. Sinha, K. Suzuki, *Angew. Chem.* **2005**, *117*, 275; *Angew. Chem. Int. Ed.* **2005**, *44*, 271.
[19] See, for example: I. C. Chisem, J. Rafelt, M. T. Shieh, J. Chisem, J. H. Clark, R. Jachuck, D. Macquarrie, C. Ramshaw, K. Scott, *Chem. Commun.* **1998**, 1949.
[20] E. Breynaert, A. Maes, *Anal. Chem.* **2005**, *77*, 5048.
[21] S. Music, M. Maljkovic, S. Popovic, R. Trojko, *Croat. Chem. Acta* **1999**, *72*, 789, and references therein.
[22] See, for example: a) T. Tsuzuki, P. G. McCormick, *Acta Mater.* **2000**, *48*, 2795; b) M. Ocaña, *J. Eur. Ceram. Soc.* **2001**, *21*, 931; c) M. Bañobre-López, C. Vázquez, J. Rivas, M. A. López-Quintela, *Nanotechnology* **2003**, *14*, 318; d) M. V. Borysenko, V. M. Bogatyrov, E. N. Poddenezhny, A. A. Boiko, A. A. Chuiko, *J. Sol–Gel Sci. Technol.* **2004**, *32*, 327; e) D.-W. Kim, S.-I. Shin, J.-D. Lee, S.-G. Oh, *Mater. Lett.* **2004**, *58*, 1894; f) W. S. Zhang, E. Brück, Z. D. Zhang, O. Tegus, W. F. Li, P. Z. Si, D. Y. Geng, K. H. J. Buschow, *Phys. B* **2005**, *358*, 332.
[23] B. M. Weckhuysen, I. E. Wachs, R. A. Schoonheydt, *Chem. Rev.* **1996**, *96*, 3327.
[24] See Supporting Information.
[25] H. Stünzi, W. Marty, *Inorg. Chem.* **1983**, *22*, 2145.
[26] For example, at pH 4.68 the ion-exchange capacity (determined with $CrCl_3$) was found to be 0.024 meq g^{-1}, in good agreement with those determined for Pb^{II}, Cu^{II}, and Ni^{II} at the same pH value.[27] The pH value of 4.68 is above that of our synthesis (4.0), and more than twice that of the point of zero charge (PZC), determined to be 2.12 by potentiometric titration.
[27] H. H. Tran, F. A. Roddick, J. A. O'Donnell, *Water Res.* **1999**, *33*, 2992.
[28] B. M. Weckhuysen, R. A. Schoonheydt, F. E. Mabbs, D. Collison, *J. Chem. Soc. Faraday Trans.* **1996**, *92*, 2431.
[29] Even if the Cr colloids have a specific surface area as high as 1000 $m^2 g^{-1}$, a loading of 5 mg Cr per g support would induce only a negligible increase in surface area.
[30] W. Buijs, R. Raja, J. M. Thomas, H. Wolters, *Catal. Lett.* **2003**, *91*, 253.
[31] P. G. Harrison, N. C. Lloyd, W. Daniell, *J. Phys. Chem. B* **1998**, *102*, 10672, and references therein.
[32] The Cr speciation in solution was modeled using PHREEQC, in combination with the Lawrence Livermore National Library (LLNL 85 2005-02-02) database; precipitation was disabled during the modeling because of the slow kinetics. http://www.geo.vu.nl/users/posv/phreeqc/index.html (PHREEQC for Windows, version 2.12.04 built using PREEQC 2.12.1-669).
[33] Powder (ca. 200 mg) was dissolved in concentrated perchloric acid (1 mL), HNO_3 (2 mL), and HCl (1 mL).

 © 2006 Wiley-VCH Verlag GmbH & Co. KGaA, Weinheim

Fluorescence

DOI: 10.1002/anie.200602758

Single Nonblinking CdTe Quantum Dots Synthesized in Aqueous Thiopropionic Acid**

*Hua He, Huifeng Qian, Chaoqing Dong, Kanglin Wang, and Jicun Ren**

Colloidal semiconductor nanocrystals, also known as quantum dots (QDs), have received considerable attention in recent years because of their unique optical properties including photostability, brightness, narrow but tunable emission spectra, and a broad spectral excitation cross section. These properties make them promising candidates for optoelectronic and biological applications.[1,2] At the single-particle level, however, QDs exhibit severe fluorescence intermittence or blinking (i.e., bright "on" intervals with fluorescence alternate with almost dark "off" intervals without fluorescence or with fluorescence of reduced intensity under continuous laser excitation) on a wide time scale from milliseconds to minutes, and in most cases, on/off events follow an inverse power-law probability distribution.[3] This phenomenon has been ubiquitously observed for luminescent nanocrystal samples of different compositions and structures[4] and represents an intrinsic limitation for certain practical uses, especially as a single-photon light source for quantum information processing and continuous monitoring of single labeled biomolecules. It is very important to develop new approaches for the synthesis of nonblinking QDs or to suppress blinking.

The optical properties of luminescent QDs, such as quantum yield, photostability, and blinking statistics, are highly dependent on their surface chemistry and synthesis conditions.[5,6] At present, most semiconductor QDs are prepared almost to completion in an organic phase by using solvents with high boiling points, such as trioctylphosphane (TOP) or trioctylphosphane oxide (TOPO) or a mixture of TOP and TOPO, and the QDs have to be modified by using surface-chemistry methods to make the surfaces hydrophilic before they are coupled to biomolecules. To date, it is accepted wisdom that all QDs synthesized in organic phases exhibit blinking that is difficult to overcome. In recent years, methods of preparing fluorescent QDs in aqueous phases

[*] H. He, H. Qian, C. Dong, K. Wang, Prof. Dr. J. Ren
College of Chemistry & Chemical Engineering
Shanghai Jiaotong University
800 Dongchuan Road, Shanghai 200240 (China)
Fax: (+86) 21-54741297
E-mail: jicunren@sjtu.edu.cn

[**] The authors thank Prof. Andong Xia for helpful discussions and for measuring fluorescence spectra of single CdTe quantum dots. This work was financially supported by NSFC (No. 90408014, 20335020), and the Nano-Science Foundation of Shanghai (0452M052, 05M05002).

Supporting information for this article is available on the WWW under http://www.angewandte.org or from the author.

WILEY InterScience DISCOVER SOMETHING GREAT
© 2006 Wiley-VCH Verlag GmbH & Co. KGaA, Weinheim

have been significantly improved.[7] Aqueous syntheses provide certain advantages, compared with those of organic phases, such as low toxicity, inexpensiveness, and especially that the products have high quantum yields (40–67%), excellent water-solubility, and biological compatibility such that some have been used in fixed- and live-cell imaging.[8] Aqueous syntheses of luminescent QDs are receiving more and more attention.[9] However, the optical properties of single QDs synthesized in the aqueous phase remain unclear. It is a question of nature as to whether single QDs synthesized in the aqueous phase blink, as do those prepared in the organic phase. Herein, we study the luminescent properties of individual CdTe QDs, synthesized in aqueous solutions, by using total internal reflection fluorescence microscopy (TIRFM). Surprisingly, we found that individual CdTe QDs synthesized in thiopropionic acid (TPA) aqueous solutions did not blink, which is in contrast to those synthesized in organic phases.

CdTe QDs in this study were synthesized in aqueous phases by using the reaction between Cd^{2+} ions and NaHTe in solution in the presence of TPA as a stabilizer; quantum yields of the products were 40–50%. Figure 1 shows a 500 ms exposure–time fluorescence image of single CdTe QDs, embedded in a poly(ethylene oxide) (PEO) matrix, at room temperature. In the fluorescence images, individual QDs are shown to be distributed homogeneously in the PEO matrix and no aggregation is observed. The non-uniform spatial distribution of spot intensities is a consequence of the exponential decay of the evanescent field generated upon total internal reflection at the coverslip–PEO interface and brightness variations of different QDs, and these do not influence the time dependence of the fluorescent behavior of each spot, which was also observed and discussed previously.[10] Water-soluble PEO was used to disperse QDs onto coverslips to avoid aggregation of CdTe QDs during sample preparation. We found that PEO is a good matrix to disperse water-soluble CdTe QDs on coverslips for obtaining high-quality fluorescence images of individual QDs (Figure 1). Furthermore, fluorescence spectroscopy also confirms that PEO, unlike polyvinylpyrrolidone (PVP), does not quench the fluorescence of CdTe QDs (data not shown). A typical fluorescence spectrum of single CdTe QDs is given in the Supporting Information). Figure 2 shows the fluorescence intensity trajectories, together with background intensity, of five random individual CdTe QDs with a time resolution of 200 ms for durations of 500 s under continuous wave excitation. Continuous fluorescence emission of individual CdTe QDs is clearly visible. Indeed, all individual CdTe QDs in the field of view, which could be traced simultaneously by TIRFM, did not blink (see Supporting Information for the corresponding video). To rule out possible influence from the integration time scale, the fluorescence intensity trajectory with a time resolution of 50 ms was also recorded, which showed a similar continuous fluorescence emission (see Supporting Information). For comparison, we also imaged individual CdSe/ZnS QDs prepared in an organic phase (Jiayuan Quantun Dots Co.). Fluorescence blinking for these CdSe/ZnS QDs was observed, which is consistent with previous reports.[3] The intensity trajectories and the corresponding videos are available in the Supporting Information. These data demonstrate that our TIRFM system is a very powerful tool for the characterization of blinking of QDs. Why do CdTe QDs synthesized in the aqueous phase not blink? To date, the blinking mechanism of QDs is not clear but thought to arise from electron (or hole) ejection from an Auger process, pure electron tunneling into the surrounding matrix, or electron capture in trap states of the surface of the particle.[3a,c,11] It was shown that blinking may exhibit unique kinetics by different degrees of surface passivation or by altering synthesis conditions and that the associated mechanism is related to defect sites or unsaturated dangling bonds located at the surface of the QDs.[6a,b] CdTe QDs used in our study were synthesized in aqueous phases in the presence of TPA as a stabilizer and their surfaces were well coated with TPA. We speculate that TPA has a critical effect on the optical properties of CdTe QDs synthesized in aqueous solution. The thio moiety in TPA is an excellent electron donor and donates electrons to the surface traps, thus rendering them incapable of accepting electrons from the carrier or serving as channels

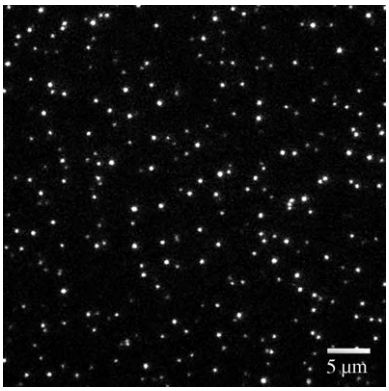

Figure 1. TIRFM image ($45 \times 45\ \mu m^2$) of single CdTe QDs embedded in a PEO matrix at room temperature. Emission peak at 689 nm; exposure time: 500 ms.

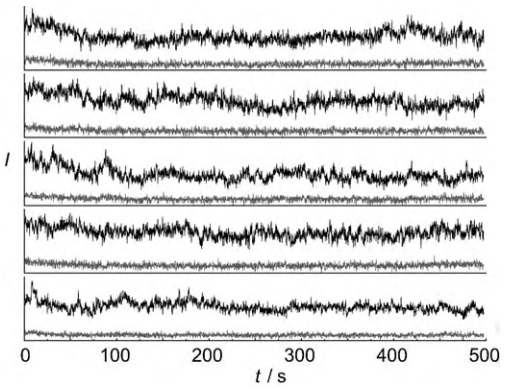

Figure 2. Fluorescence-intensity trajectories of five random individual CdTe QDs (emission peak at 689 nm) with a temporal resolution of 200 ms for durations of 500 s. The local background (gray) was extracted from the average intensity around each spot.

 © 2006 Wiley-VCH Verlag GmbH & Co. KGaA, Weinheim

for efficient charge tunneling from the interior of the QDs to the surrounding matrix. Recently, it was reported that the blinking of QDs can be suppressed by antiblinking agents, such as β-thioethanol (BTE) and thioethylamine (TEA), or when the surfaces of QDs were coordinated with organic ligands, such as oligo(phenylene vinylene) (OPV).[6c–e] To confirm the role of TPA on the surface of the QDs used in our study, TPA on the surfaces of CdTe QDs was exchanged with citrate, and the fluorescence-intensity trajectories of citrate-coated QDs were recorded (Figure 3); surprisingly, blinking

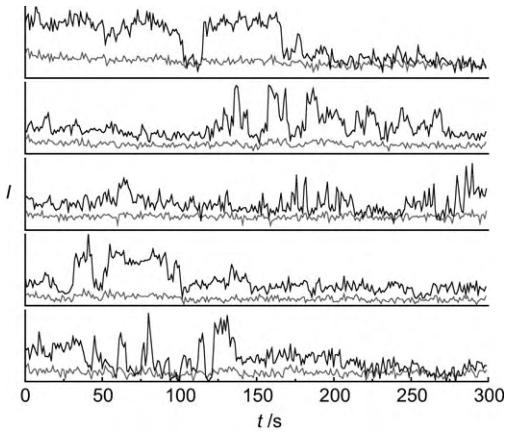

Figure 3. Fluorescence-intensity trajectories of five random individual citrate-coated CdTe QDs with a temporal resolution of 1000 ms for durations of 500 s. The local background (gray) was extracted from the average intensity around each spot.

was observed. In addition, the fluorescence of citrate-coated QDs decreases significantly and photobleaches rapidly under continuous laser excitation. This result is attributed to ligand exchange or surface damage of the CdTe QDs. Furthermore, we investigated the fluorescent emission of individual CdTe QDs synthesized in an aqueous phase in the presence of glutathione, another stabilizer that contains a thio group.[12] The results show that glutathione-coated CdTe QDs also do not blink (data not shown). Our data illustrate that thio-based compounds, such as TPA and glutathione, play a key role in suppressing the blinking of CdTe QDs and improving their photostability. So far, the synthesis of QDs such as CdTe, CdSe, ZnSe, and HgTe in aqueous solutions has involved the use of thio-containing compounds as stabilizers, which coat the surface of these QDs.

In conclusion, we have used TIRFM to observe individual CdTe QDs synthesized in aqueous solution and have investigated their fluorescence-emission behavior. We have found that individual CdTe QDs synthesized in TPA solution do not blink. Our experiments have confirmed that the TPA coating on the CdTe QDs plays a key role in suppressing blinking. We believe that these CdTe QDs are suitable for use in single-molecule imaging and single-molecule detection as fluorescent probes as they are water-soluble, biocompatible, bright, and do not blink. However, CdTe QDs, especially after purification, photobleach more rapidly than CdSe/ZnS QDs prepared in an organic phase (see Supporting Information). For individual purified CdTe QDs, fluorescence emission was beyond detection after about 15 min under continuous wave excitation. We speculate that this deterioration is due to the damage of TPA or photooxidation of CdTe. We are working to improve the photostability of the CdTe QDs synthesized in an aqueous phase.

Experimental Section

CdTe QDs were prepared in the presence of TPA (Fluka) as described previously.[7d,e] Briefly, Cd precursor solutions were prepared by mixing a solution of $CdCl_2$ (1.25×10^{-3} M) with a solution of TPA and this mixture was adjusted to a pH of 8–9 with NaOH (1M). The solution was purged with N_2 then vigorously stirred while oxygen-free NaHTe (or NaHSe) solution was injected; the molar ratio of Cd/Te/TPA was 2.5:1:6. The resulting mixture was heated to reflux for different periods of time to control the size of QDs. UV/Vis absorption spectra of TPA-stabilized QDs were obtained by using a Lambda 20 UV/Vis spectrophotometer (Perkin-Elmer). Photoluminescence spectra were recorded on a Varian Cary Fluorescence Spectrophotometer. CdTe QDs with emission peaks at 689 nm or 625 nm were used. Citrate-coated CdTe QDs were prepared by adding purified QDs to a citrate solution (10 mM; pH 8.3) to induce ligand exchange. Glutathione-coated CdTe QDs were synthesized in glutathione solution as described previously.[12]

Coverslips ($24 \times 32 \times 0.17$ mm^3) were thoroughly cleaned prior to sample preparation by sonication in chromic acid mixture, NaOH solution (0.1M), ethanol, and ultrapure water (Millipore), each for 15 min, then dried in a jet of N_2. An aqueous solution of CdTe QDs (about 1.0×10^{-8} mol L^{-1}, estimated by the fluorescence correlation spectroscopy) and an aqueous solution of PEO (1%; MW 100000, Sigma) were mixed in a 1:1 ratio. CdSe/ZnS QDs (emission peak at 625 nm, Wuhan Jiayuan Quantum dots Co. Ltd., China) were dispersed in a chloroform solution of PMMA (poly(methyl methacrylate); 2%, Sigma). A small drop of this mixture was carefully coated onto the coverslips by rolling with a clean cylindrical glass rod.

CdTe QDs were imaged by a total internal reflection fluorescence microscope based on an Olympus IX 71 inverted fluorescence microscope (Olympus Optical Co.). A schematic diagram of the TIRFM setup is given in the Supporting Information. Samples were excited with a He–Ne laser operating at 543.5 nm (5 mW, Coherent) and the laser power monitored in front of the microscopy objective (numerical aperture (NA) = 1.45, 60×, Olympus) was measured to be 0.65 mW. Fluorescence from the sample was collected by the same objective, separated from the excitation light by a suitable dichroic mirror (570 nm) and emission filters (long-pass filter, 590 nm), and then focused into a cooled-CCD (charged coupled device) camera with a frame-transfer device (Cascade 650, Photometrics). The frame-transfer device has an imaging array of 653×492 with 7.4×7.4 μm^2/pixel. As the image can be quickly transferred from the sensor area to the frame transfer area, there is no need for a mechanical shutter. When operated in overlap mode, the camera is extremely useful in applications requiring continuous imaging (100% duty cycle) and can capture all the light emitted from the specimen. Image acquisition and processing were performed using the MetaMorph program (Universal Imaging). The local background was extracted from the average intensity around each spot. All measurements were performed at room temperature.

Received: July 11, 2006
Revised: September 3, 2006
Published online: October 20, 2006

Keywords: colloids · fluorescence · nanostructures · quantum chemistry · semiconductors

 © 2006 Wiley-VCH Verlag GmbH & Co. KGaA, Weinheim

[1] a) W. C. W. Chan, S. M. Nie, *Science* **1998**, *281*, 2016 – 2018; b) M. Bruchez, M. Moronne, P. Gin, S. Weiss, A. P. Alivisatos, *Science* **1998**, *281*, 2013 – 2016; c) B. Dubertret, P. Skourides, D. J. Norris, V. Noireaux, A. H. Brivanlou, A. Libchaber, *Science* **2002**, *298*, 1759 – 1762; d) P. Alivisatos, *Nat. Biotechnol.* **2004**, *22*, 47 – 52; e) X. Michalet, F. F. Pinaud, L. A. Bentolila, J. M. Tsay, S. Doose, J. J. Li, G. Sundaresan, A. M. Wu, S. S. Gambhir, S. Weiss, *Science* **2005**, *307*, 538 – 544.

[2] a) M. C. Schlamp, X. G. Peng, A. P. Alivisatos, *J. Appl. Phys.* **1997**, *82*, 5837 – 5842; b) A. Kiraz, M. Atature, A. Imamoglu, *Phys. Rev. A* **2004**, *69*, 032305.

[3] a) M. Nirmal, B. O. Dabbousi, M. G. Bawendi, J. J. Macklin, J. K. Trautman, T. D. Harris, L. E. Brus, *Nature* **1996**, *383*, 802 – 804; b) M. Kuno, D. P. Fromm, H. F. Hamann, A. Gallagher, D. J. Nesbitt, *J. Chem. Phys.* **2000**, *112*, 3117 – 3120; c) M. Kuno, D. P. Fromm, H. F. Hamann, A. Gallagher, D. J. Nesbitt, *J. Chem. Phys.* **2001**, *115*, 1028 – 1040; d) K. T. Shimizu, R. G. Neuhauser, C. A. Leatherdale, S. A. Empedocles, W. K. Woo, M. G. Bawendi, *Phys. Rev. B* **2001**, *63*, 205316; e) M. Kuno, D. P. Fromm, S. T. Johnson, A. Gallagher, D. J. Nesbitt, *Phys. Rev. B* **2003**, *67*, 125304.

[4] a) M. Kuno, D. P. Fromm, A. Gallagher, D. J. Nesbitt, O. I. Micic, A. J. Nozik, *Nano Lett.* **2001**, *1*, 557 – 564; b) I. Sychugov, R. Juhasz, J. Linnros, J. Valenta, *Phys. Rev. B* **2005**, *71*, 115331; c) F. Cichos, J. Martin, C. von Borczyskowski, *Phys. Rev. B* **2004**, *70*, 115314; d) J. J. Peterson, T. D. Krauss, *Nano Lett.* **2006**, *6*, 510 – 514.

[5] a) B. O. Dabbousi, J. Rodriguez Viejo, F. V. Mikulec, J. R. Heine, H. Mattoussi, R. Ober, K. F. Jensen, M. G. Bawendi, *J. Phys. Chem. B* **1997**, *101*, 9463 – 9475; b) L. H. Qu, X. G. Peng, *J. Am. Chem. Soc.* **2002**, *124*, 2049 – 2055.

[6] a) V. Biju, Y. Makita, T. Nagase, Y. Yamaoka, H. Yokoyama, Y. Baba, M. Ishikawa, *J. Phys. Chem. B* **2005**, *109*, 14350 – 14355; b) D. E. Gomez, J. van Embden, J. Jasieniak, T. A. Smith, P. Mulvaney, *Small* **2006**, *2*, 204 – 208; c) S. Hohng, T. Ha, *J. Am. Chem. Soc.* **2004**, *126*, 1324 – 1325; d) A. Biebricher, M. Sauer, P. Tinnefeld, *J. Phys. Chem. B* **2006**, *110*, 5174 – 5178; e) N. I. Hammer, K. T. Early, K. Sill, M. Y. Odoi, T. Emrick, M. D. Barnes, *J. Phys. Chem. B* **2006**, *110*, 14167 – 14171.

[7] a) M. Y. Gao, S. Kirstein, H. Möhwald, A. L. Rogach, A. Kornowski, A. Eychmüller, H. Weller, *J. Phys. Chem. B* **1998**, *102*, 8360 – 8363; b) N. Gaponik, D. V. Talapin, A. L. Rogach, K. Hoppe, E. V. Shevchenko, A. Kornowski, A. Eychmüller, H. Weller, *J. Phys. Chem. B* **2002**, *106*, 7177 – 7185; c) H. Zhang, Z. Zhou, B. Yang, M. Y. Gao, *J. Phys. Chem. B* **2003**, *107*, 8 – 13; d) L. Li, H. F. Qian, J. C. Ren, *Chem. Commun.* **2005**, 528 – 530; e) L. Li, H. F. Qian, N. H. Fang, H. C. Ren, *J. Lumin.* **2006**, *116*, 59 – 66.

[8] a) J. F. Weng, X. T. Song, L. Li, H. F. Qian, K. Y. Chen, X. M. Xu, C. X. Cao, J. C. Ren, *Talanta* **2006**, *70*, 397 – 402; b) Z. H. Li, K. M. Wang, W. H. Tan, J. Li, Z. Y. Fu, C. B. Ma, H. M. Li, X. X. He, J. B. Liu, *Anal. Biochem.* **2006**, *354*, 169 – 174.

[9] a) J. Lee, A. O. Govorov, N. A. Kotov, *Nano Lett.* **2005**, *5*, 2063 – 2069; b) D. M. Guldi, G. M. A. Rahman, V. Sgobba, N. A. Kotov, D. Bonifazi, M. Prato, *J. Am. Chem. Soc.* **2006**, *128*, 2315 – 2323; c) A. Wolcott, D. Gerion, M. Visconte, J. Sun, A. Schwartzberg, S. W. Chen, J. Z. Zhang, *J. Phys. Chem. B* **2006**, *110*, 5779 – 5789.

[10] A. Y. Kobitski, C. D. Heyes, G. U. Nienhaus, *Appl. Surf. Sci.* **2004**, *234*, 86 – 92.

[11] U. Banin, M. Bruchez, A. P. Alivisatos, T. Ha, S. Weiss, D. S. Chemla, *J. Chem. Phys.* **1999**, *110*, 1195 – 1201.

[12] H. F. Qian, C. Q. Dong, J. F. Weng, J. C. Ren, *Small* **2006**, *2*, 747 – 751.

 © 2006 Wiley-VCH Verlag GmbH & Co. KGaA, Weinheim

Asymmetric Catalysis

DOI: 10.1002/anie.200602469

Highly Active Chiral Ruthenium Catalysts for Asymmetric Cross- and Ring-Opening Cross-Metathesis**

*Jacob M. Berlin, Steven D. Goldberg, and Robert H. Grubbs**

Olefin metathesis has found widespread application in small-molecule synthesis.[1] Its use can be subclassified into three transformations[1a]—ring-opening metathesis, ring-closing metathesis, and cross-metathesis—and one can readily envision an asymmetric variant of each of these reactions (Scheme 1). We report herein the use of highly active chiral ruthenium catalysts for asymmetric ring-opening cross-metathesis (AROCM) and the first example of an asymmetric cross-metathesis (ACM) reaction.

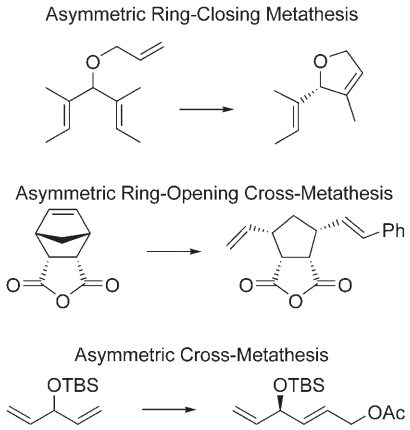

Scheme 1. Three classes of asymmetric metathesis. TBS = *tert*-butyldimethylsilyl.

Chiral molybdenum catalysts have been developed for asymmetric ring-closing metathesis (ARCM) and AROCM.[2–4] These catalysts lack extensive tolerance of functional groups and require rigorous exclusion of air and moisture. The use of more stable enantioselective ruthenium metathesis catalysts, which have a greater tolerance of

[*] J. M. Berlin, Dr. S. D. Goldberg, Prof. R. H. Grubbs
Arnold and Mabel Beckman Laboratories of Chemical Synthesis
California Institute of Technology
Division of Chemistry and Chemical Engineering
Mail Code 164-30, Pasadena, CA 91125 (USA)
Fax: (+1) 626-564-9297
E-mail: rhg@its.caltech.edu

[**] We gratefully acknowledge Prof. F. D. Toste for early experimental work.

Supporting information for this article is available on the WWW under http://www.angewandte.org or from the author.

© 2006 Wiley-VCH Verlag GmbH & Co. KGaA, Weinheim

functional groups, would dramatically expand the scope and utility of these transformations, as has been the case in other areas of olefin metathesis. We have recently prepared a series of highly active chiral ruthenium catalysts (Scheme 2, **2a**,**b**–**6a**,**b**).[5] The chirality in these catalysts is transferred from the backbone of the N-heterocyclic carbene (NHC) to the metal center through differentially substituted aryl rings on the NHC. The *ortho*-isopropyl groups lie on the opposite sides of the catalyst to the phenyl rings in the backbone of the NHC, thus creating a chiral C_2-symmetric environment around the metal center. Catalysts **2a**,**b**, **3a**,**b**, **5a**,**b**, and **6a**,**b** have been used in ARCM to form oxygen-containing heterocycles in good yields (64–98%) and with high *ee* values (76–92%).[6] These catalysts bearing monodentate chiral NHCs proved to be much more active and selective for ARCM than catalyst **7**, which possesses a bidentate chiral NHC and is stereogenic directly at the metal center.[7] We now report the application of our highly active catalysts to asymmetric ring-opening cross-metathesis and asymmetric cross-metathesis.

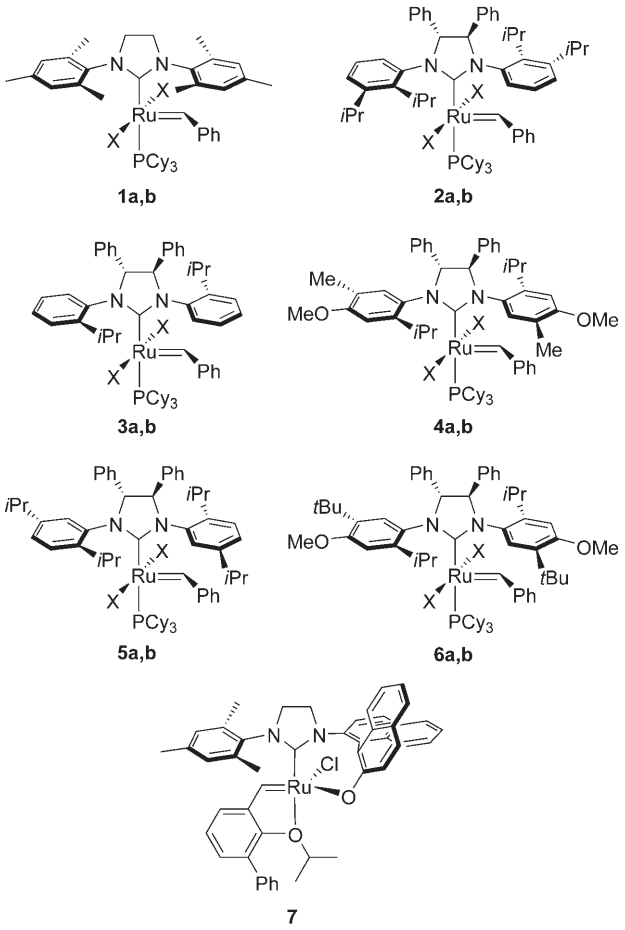

Scheme 2. Ruthenium–olefin metathesis catalysts (**a**: X = Cl, **b**: X = I). Cy = cyclohexyl.

Encouraged by our results for ARCM, we turned our attention to AROCM. Catalyst **7** and related complexes have been successfully employed in AROCM for a number of norbornenes and related strained bicycles.[8] In our initial studies, anhydride **8** was treated with one mole percent of the catalysts **2a**, **3a**, **5a**, and **6a** in CH_2Cl_2 in the presence of ten equivalents of styrene (Table 1). Catalyst **6a** was the most selective of the dichloride catalysts, and no change in enantioselectivity was observed upon variation of the solvent

Table 1: AROCM with chiral ruthenium catalysts.

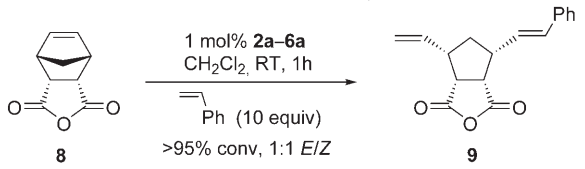

Catalyst	Product	*ee* [%]
2a	*ent*-**9**	47
3a	*ent*-**9**	29
5a	**9**	62
6a	**9**	76

(CH_2Cl_2, $CHCl_3$, THF, Et_2O, benzene, toluene, and with no solvent) or of the equivalents (1, 3, 5, and 10) of cross-partner. In our studies on ARCM, the diiodide catalysts **2b**–**6b** were found to be dramatically more enantioselective than the dichloride catalysts **2a**–**6a**.[6b] For AROCM, the use of diiodide catalyst **6b** in place of dichloride catalyst **6a** slightly improved the *ee* value to 80% and cooling the reaction to 0°C gave **9** in 82% *ee*. The diiodide catalysts are generally less reactive than the dichloride catalysts; therefore, the loading of **6b** was increased to 3 mol% to achieve activity similar to that observed with **6a**. Since catalysts **6a** and **6b** gave the highest *ee* value for substrate **8**, they were employed in studies to explore the substrate scope (Table 2). The *E*/*Z* ratio was close to 1:1 for all of the substrates examined, but we initially focused our attention on discovering trends within the *trans* series of products because in all cases the *ee* values of the *cis* products were lower than those of the *trans* products. Replacement of the anhydride oxygen atom with a *tert*-butylamine group to give **10** reduced the enantioselectivity to 57% for **6a** and 75% for **6b**, but both catalysts gave quantitative yields. Introducing heteroatoms into the norbornene skeleton **11** slightly reduced the *ee* value to 68%, and surprisingly catalysts **6a** and **6b** afforded products with the same *ee* value. When diols **12** and **13** were used, the yields were dramatically reduced to 30% and 10%, respectively. In these cases, substrate coordination to the catalyst may inhibit the reaction. In addition, the stereochemistry of the norbornene diols affected the *ee* values: the *endo* diol **13** gave 81% *ee* while the *exo* diol **12** gave only 33% *ee*. To prevent coordination to the catalyst, diol **13** was protected as a bisacetate **14**, which resulted in a decrease in the *ee* value to 60% accompanied by a large increase in the yield to 99%; the use of catalyst **6b** improved the *ee* value to 72%, but slightly reduced the yield to 78%. The *cis* series of products exhibited different trends in selectivity than the *trans* series (Table 2). The *ee* values for the *cis* products increased when those for the *trans* products decreased (**8** versus **10** with **6a**) and decreased when the *ee* values for *trans* products increased (**10**

 © 2006 Wiley-VCH Verlag GmbH & Co. KGaA, Weinheim

Table 2: AROCM with catalysts **6a** and **6b**.

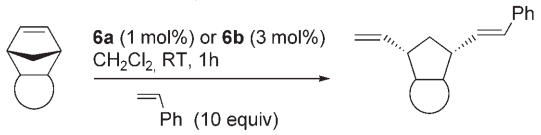

Substrate		Cat.[a,b]	*ee* [%] *E* (*Z*)	Yield [%] (*E*/*Z*)
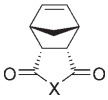	**8** X = O	**6a**	76 (4)	95 (1:1)
		6b	80 (n.d.)	96 (1:1)
	10 X = N-*t*Bu	**6a**	57 (33)	99 (1.4:1)
		6b	75 (50)	99 (1.2:1)
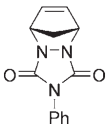	**11**	**6a**	68 (15)	99 (1.2:1)
		6b	68 (10)	99 (1.2:1)
	12	**6a**	33 (29)	30 (1.1:1)
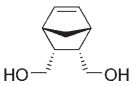	**13**	**6a**	81 (20)	10 (n.d.)
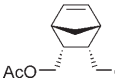	**14**	**6a**	60 (10)	99 (1.4:1)
		6b	72 (40)	78 (1.4:1)

[a] Conditions for **6a**: 1 mol% catalyst, CH_2Cl_2, RT, 10 equiv styrene, 1 h. [b] Conditions for **6b**: 3 mol% **6a**, 1 equiv NaI, CH_2Cl_2, RT, 10 equiv styrene, 1 h. n.d. = not determined.

compared to **11** with **6a**). In addition, when catalysts **2a**,**b**–**5a**,**b** were examined with these substrates, catalysts **6a** and **6b** always gave the *trans* product with the highest *ee* value. However, catalysts **5a** and **5b** often gave the *cis* product with the highest *ee* value.

Careful evaluation of the data obtained thus far elucidates some aspects of the mechanism for AROCM and allows for a proposal as to the origin of enantioselectivity. No change in the *E*/*Z* ratio or *ee* value was observed on monitoring the reactions of **8** and **10** over 3 h. Moreover, the reactive terminal olefin in the products is never observed to undergo further cross-metathesis reactions at room temperature. These findings indicate that the products are not reactive towards secondary metathesis and therefore that the *ee* values and *E*/*Z* ratios observed are the direct result of a singular interaction with the catalysts. Of primary importance to the development of a mechanism for AROCM is to distinguish between the two possible ruthenium–alkylidene propagating species (Scheme 3). In pathway 1, the norbornene reacts with a ruthenium–methylidene intermediate and this ring-opening step determines the *ee* value of the products. Then in the cross-metathesis step the products are released, thereby determining the olefin geometry of the products and regenerating the ruthenium–methylidene species. This pathway requires that the *ee* value of both the *E* and *Z* products be identical. In pathway 2, the norbornene reacts with a ruthenium–benzylidene intermediate and both the *ee* value and olefin geometry of the products are determined concurrently in this ring-opening step. The products are then released in the cross-metathesis step that regenerates the ruthenium–benzylidene species. The *ee* values of the *E* and *Z* products are independent in this reaction pathway. Since the observed *ee* values of the *E* and *Z* products are significantly different, we propose that it is likely that the ruthenium–benzylidene is the propagating species in this system.

There has been a long-standing debate regarding the site of olefin coordination to the ruthenium catalyst that leads to metallocyclobutane formation. There is experimental evidence that supports olefin binding either *cis* or *trans* to the NHC.[9] In the most recent report on this issue,[9c] Romero and Piers provide compelling evidence for the observation of a 14-electron ruthenium species in which the metallocycle lies *trans* to the NHC. Computational studies also support olefin binding *trans* to the NHC;[10] in fact, calculations from a recent computational study of the use of catalyst **3b** in ARCM, showed olefin coordination *trans* to the NHC to be the lower energy pathway.[10a]

In our system, catalyst **2a** yields *ent*-**9**, and catalyst **6a** yields **9** as the major *trans* product.[11] Moreover, the propagating species is believed to be a benzylidene species, and norbornenes are well known to react preferentially on the *exo* face of the olefin.[12] With these caveats in mind, a *cis*-coordination pathway would require that the norbornene would approach catalyst **2a** from the face that is shielded by the *ortho*-isopropyl group, and catalyst **6a** from the face that

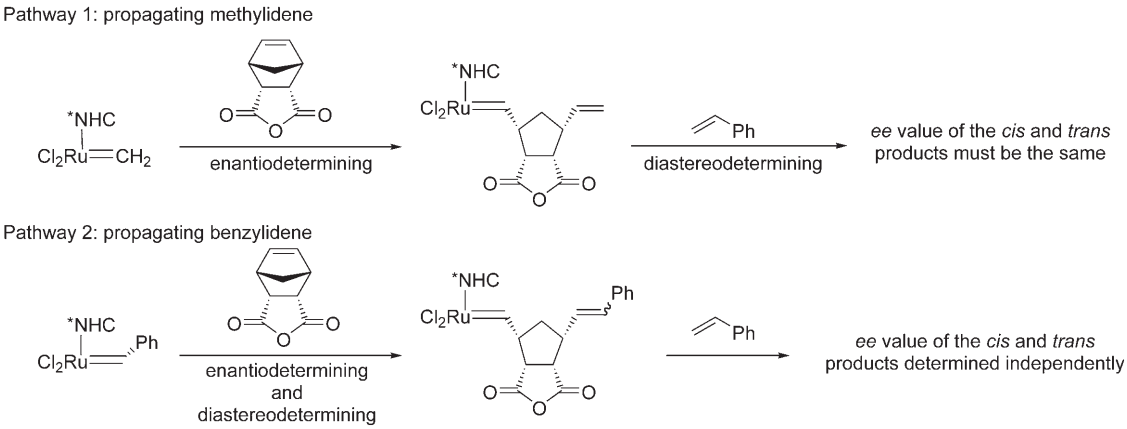

Scheme 3. Comparison of propagating species. *NHC = chiral N-heterocyclic carbene.

 © 2006 Wiley-VCH Verlag GmbH & Co. KGaA, Weinheim

possesses the *meta-tert*-butyl group (Scheme 4). It is most likely that introducing a *tert*-butyl group in the *meta* position increases the steric bulk of that side of the ring. Therefore, the *cis*-coordination pathway seems unlikely as it requires the norbornene to approach both catalyst **2a** and **6a** from the more hindered side.

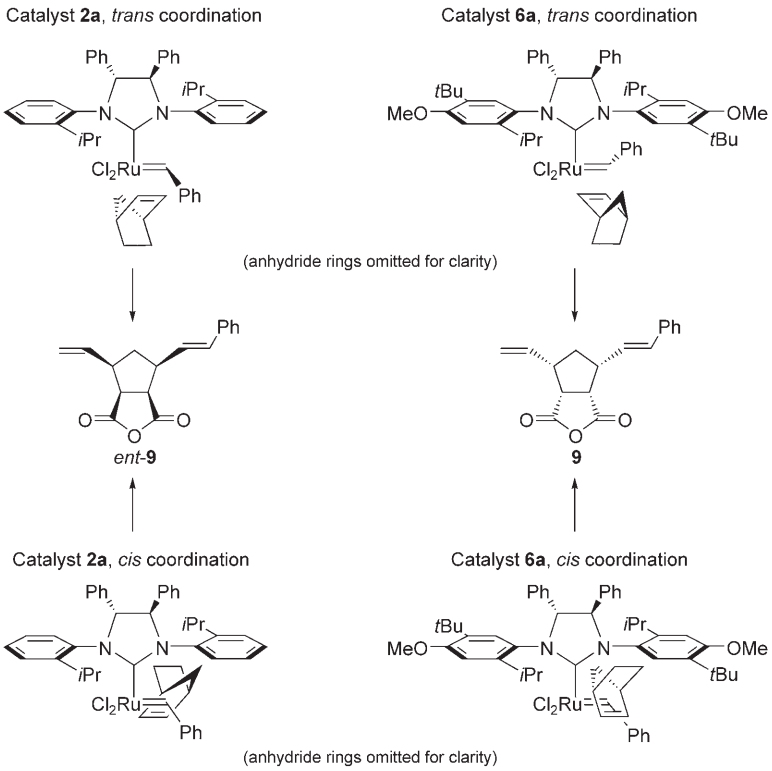

Scheme 4. Olefin approaches for **2a** and **6a** which afford the major *trans* enantiomer.

We propose that a *trans*-coordination pathway is more consistent with the observed data. This pathway would require that the benzylidene unit of catalyst **2a** sit under the unsubstituted side of the aryl ring and the benzylidene unit of catalyst **6a** sit under the side bearing an *ortho*-isopropyl group (Scheme 4). Thus, increasing the steric bulk of the *tert*-butyl side of the ring causes the benzylidene unit to move to the opposite side of the ring, thereby explaining the observed reversal of enantioselectivity between these two catalysts. We expect that our continued work on asymmetric metathesis will allow us to further develop this mechanistic insight.

Catalyst **1a** has been used extensively in cross-metathesis,[13] and a chiral variant of this transformation would provide a powerful new synthetic tool for the construction of stereochemically complex targets. However, ACM is also the most challenging of the asymmetric metathesis transformations, as all three factors—the propagating species, its orientation, and enantiotopic olefin selection—must be controlled. In ARCM, there is only one possible propagating species which leads to productive metathesis, so only the orientation of that species and the selection of an enantiotopic olefin must be controlled. AROCM requires both control of the propagating species and its orientation, but facial selectivity of the enantiotopic olefin is easily controlled in the norbornene substrate. To address the enantiotopic olefin selection in ACM, we focused on *meso*-diene substrates which contained distinct small (H), medium (vinyl), and large (OR; for example, R = TBS) substituents at the allylic carbon atom. To address the nature of the propagating species, we employed the TBS-protected 1,4-pentadien-3-ol **15a** and *cis*-1,4-diacetoxy-2-butene (**16**) as substrates (Table 3). It was expected that the use of an excess of **16**, which is more active in metathesis than **15a**, would predominantly afford a ruthenium–acetoxyethylidene complex as the propagating species. This supposition was supported by the fact that the initial benzylidene unit of **2a** was observed to react exclusively with **16** to give cinnamyl acetate. Thus, we controlled the propagating species and achieved the first asymmetric olefin cross-metathesis reaction, although the results are certainly not optimized, with yields and *ee* values lower than expected. One systemic problem causing the low yield is that the terminal olefin present in the product is similar in reactivity to the starting material, thus resulting in consumption of the desired product and formation of a significant amount of symmetrical bis-cross-product (15%). Complexes **2a** and **5a** emerged as the most enantioselective catalysts for this reaction. For catalysts **3a**–**6a**, the enantioselectivity increased as the *meta* substitution increased in size from a proton through a methyl group to an isopropyl group, but a *tert*-butyl group proved to be too large and eroded the enantioselectivity. However, moving the isopropyl group to the opposite *meta* position to give **2a** proved to be equally as effective as **5a**. Since the use of catalyst **5a** gave slightly better yield than **2a**, we explored the use of **5a** with a number of other prochiral diene substrates (Table 4). Increasing the size of the protecting group by using the TIPS-protected 1,4-pentadien-3-ol **15b** (Table 4) resulted in a modest increase in the *ee* value from 44% to 52%. We also examined the use of the protected 1,2-diol **18** and the protected 1,3-diol **20**, which afforded *ee* values similar to those obtained with **15a**. In an attempt to improve the enantioselectivity of ACM we further reduced the reactivity of the diene substrate by preparing both 1,1- and 1,2-disubstituted olefins. Unfortunately, diene **22** proved to be unreactive under these conditions and diene **23** gave only 4% *ee*. The poor result for **23** could result from

Table 3: ACM with catalysts **2a**–**6a**.

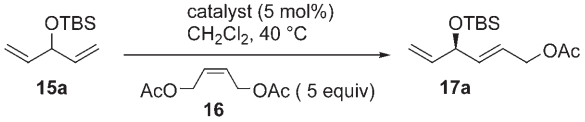

Catalyst	*ee* [%]	Yield [%]
2a	44	20
3a	22	15
4a	34	20
5a	44	28
6a	37	12

 © 2006 Wiley-VCH Verlag GmbH & Co. KGaA, Weinheim

Table 4: ACM with *cis*-1,4-diacetoxy-2-butene using catalyst **5a**.

Substrate	Product	*ee* [%]	Yield [%]
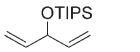	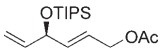	52	54[a]
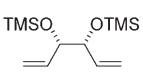	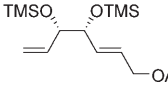	40	17[b]
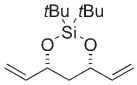	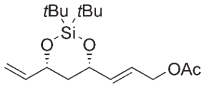	37	48[c]
	–	n.r.	n.r.
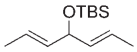	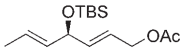	4	23[c]

[a] 5 mol% **5a**, 5 equiv of **15b** relative to **16**, no solvent, 40°C, 6 h. [b] 5 mol% **5a**, 5 equiv of **16**, no solvent, 40°C, 6 h. [c] 5 mol% **5a**, 5 equiv of **16**, 0.25 M in CH_2Cl_2, 40°C, 6 h. TIPS = triisopropylsilyl, TMS = trimethylsilyl, n.r. = no reaction.

the medium and large groups ($CHCHCH_3$ and OTBS, respectively) being too similar in size. This initial report into ACM sets the stage for future catalyst and substrate design to make this transformation synthetically useful.

In conclusion, we have reported an expansion in scope for asymmetric metathesis using highly active ruthenium catalysts with chiral monodentate NHCs. These catalysts showed excellent activity in ring-opening cross-metathesis reactions, and enantioselectivities ranged from 68% to 82%. These investigations allowed us to develop a working model for the mechanism of AROCM, from which we are working to design more-selective metathesis catalysts. We have achieved the first asymmetric cross-metathesis reactions, in which we obtained *ee* values ranging from 37% to 52%. These reactions represent an important proof of principle, and we are working to improve the yields and enantioselectivities for ACM.

Received: June 19, 2006
Published online: October 20, 2006

Keywords: asymmetric catalysis · carbenes · metathesis · reaction mechanisms · ruthenium

[1] For recent reviews on olefin metathesis, see: a) R. H. Grubbs, *Handbook of Metathesis*, Wiley-VCH, Weinheim, **2003**; b) A. Fürstner, *Angew. Chem.* **2000**, *112*, 3140–3172; *Angew. Chem. Int. Ed.* **2000**, *39*, 3012–3043; c) R. H. Grubbs, S. Chang, *Tetrahedron* **1998**, *54*, 4413–4450; d) K. J. Ivin, *J. Mol. Catal. A* **1998**, *133*, 1–16.

[2] For reviews of molybdenum-catalyzed enantioselective metathesis, see: a) R. R. Schrock, A. H. Hoveyda, *Angew. Chem.* **2003**, *115*, 4740–4782; *Angew. Chem. Int. Ed.* **2003**, *42*, 4592–4633; ; b) A. H. Hoveyda, R. R. Schrock, *Chem. Eur. J.* **2001**, *7*, 945–950.

[3] a) S. J. Dolman, K. C. Hultzsch, F. Pezet, X. Teng, A. H. Hoveyda, R. R. Schrock, *J. Am. Chem. Soc.* **2004**, *126*, 10945–10953; b) J. A. Jernelius, R. R. Schrock, A. H. Hoveyda, *Tetrahedron* **2004**, *60*, 7345–7351; c) S. J. Dolman, R. R. Schrock, A. H. Hoveyda, *Org. Lett.* **2003**, *5*, 4899–4902; d) W. C. P. Tsang, J. A. Jernelius, G. A. Cortez, G. S. Weatherhead, R. R. Schrock, A. H. Hoveyda, *J. Am. Chem. Soc.* **2003**, *125*, 2591–2596.

[4] For a preparation of chiral molybdenum catalysts in situ, see: S. L. Aeilts, D. R. Cefalo, P. J. Bonitatebus, J. H. Houser, A. H. Hoveyda, R. R. Schrock, *Angew. Chem.* **2001**, *113*, 1500–1504; *Angew. Chem. Int. Ed.* **2001**, *40*, 1452–1456.

[5] Catalysts **4a**,**b** have not been previously reported, but were prepared analogously to **2a**,**b**, **3a**,**b**, **5a**,**b**, and **6a**,**b**. For full experimental details, see the Supporting Information.

[6] a) T. W. Funk, J. M. Berlin, R. H. Grubbs, *J. Am. Chem. Soc.* **2006**, *128*, 1840–1846; b) T. J. Seiders, D. W. Ward, R. H. Grubbs, *Org. Lett.* **2001**, *3*, 3225–3228.

[7] On comparison with the results from references [6a] and [8c].

[8] a) J. J. Van Veldhuizen, J. E. Campbell, R. E. Giudici, A. H. Hoveyda, *J. Am. Chem. Soc.* **2005**, *127*, 6877–6882; b) D. G. Gillingham, O. Kataoka, S. B. Garber, A. H. Hoveyda, *J. Am. Chem. Soc.* **2004**, *126*, 12288–12290; c) J. J. Van Veldhuizen, D. G. Gillingham, S. B. Garber, O. Kataoka, A. H. Hoveyda, *J. Am. Chem. Soc.* **2003**, *125*, 12502–12508; d) J. J. Van Veldhuizen, S. B. Garber, J. S. Kingsbury, A. H. Hoveyda, *J. Am. Chem. Soc.* **2002**, *124*, 4954–4955.

[9] For evidence for *cis* coordination, see: a) T. M. Trnka, M. W. Day, R. H. Grubbs, *Organometallics* **2001**, *20*, 3845–3847; for evidence for *trans* coordination, see: b) J. A. Tallarico, P. J. Bonitatebus, Jr., M. L. Snapper, *J. Am. Chem. Soc.* **1997**, *119*, 7157–7158; c) P. E. Romero, W. E. Piers, *J. Am. Chem. Soc.* **2005**, *127*, 5032–5033.

[10] a) C. Costabile, L. Cavallo, *J. Am. Chem. Soc.* **2004**, *126*, 9592–9600; b) C. Adlhart, P. Chen, *J. Am. Chem. Soc.* **2004**, *126*, 3496–3510; c) S. Fomine, S. M. Vargas, M. Tlenkopatchev, *Organometallics* **2003**, *22*, 93–99; d) L. Cavallo, *J. Am. Chem. Soc.* **2002**, *124*, 8965–8973; e) S. F. Vyboishchikov, M. Bühl, W. Thiel, *Chem. Eur. J.* **2002**, *8*, 3962–3975.

[11] The absolute stereochemistry of **9** has been determined by analysis of the X-ray crystal structure of an imide derivative (see the Supporting Information). From the comparison of HPLC traces run under identical conditions,our studies indicate that the incorrect absolute stereoisomer was reported in reference [8d].

[12] For example, see: H. C. Brown, N. R. Ayyangar, G. Zweifel, *J. Am. Chem. Soc.* **1964**, *86*, 397–403.

[13] A. K. Chatterjee, T.-L. Choi, D. P. Sanders, R. H. Grubbs, *J. Am. Chem. Soc.* **2003**, *125*, 11360–11370, and references therein.

 © 2006 Wiley-VCH Verlag GmbH & Co. KGaA, Weinheim

Mechanistic Studies

DOI: 10.1002/anie.200602189

Gold(I)- and Gold(III)-Catalyzed Cycloisomerization of Allenynes: A Remarkable Halide Effect**

Gilles Lemière, Vincent Gandon, Nicolas Agenet, Jean-Philippe Goddard, Ariel de Kozak, Corinne Aubert, Louis Fensterbank,* and Max Malacria**

Dedicated to Professor K. Peter C. Vollhardt on the occasion of his 60th birthday

Electrophilic metal halides, also referred to as π Lewis acids, are exquisite catalysts for the selective and efficient cycloisomerization of polyunsaturated precursors into highly valuable carbo- or heterocyclic derivatives.[1] The diversity of the substrates that have been examined, mainly under platinum(II) and (IV) catalysis,[2] as well as gold(I) and (III) catalysis,[3] not only illustrates the versatility of these processes, but also renders the proposed mechanistic scenarios more plausible. In the case of enynes,[4] electrophilic activation of the alkyne triggers a nucleophilic attack by the alkene to give a metallacyclopropyl carbene intermediate that can evolve along different pathways.[5] Alternatively, metallacyclopentene intermediates have been invoked to give Alder-ene types of products.[6] In this context, because of their high degree of unsaturation, allenynes are very interesting substrates.[7]

Our initial experiments with $PtCl_2$ and precursors **1** (Tables 1 and 2) gave three types of reaction evolution depending upon the substitution pattern of the starting material.[8] To rationalize the formation of products **2**–**4**, we proposed the intervention of a common platinacyclopentene intermediate. This suggestion was later supported by the DFT calculations of Soriano and Marco-Contelles.[9] Nevertheless, some new data did not completely fit with this mechanistic rationale. For example, we noticed that the formation of hydrindiene **2a** from **1a** could also be promoted by $PtCl_4$ (Table 1, entry 2) in a more rapid reaction than that with

Table 1: Reactivity of **1** in the presence of platinum and gold catalysts.[a]

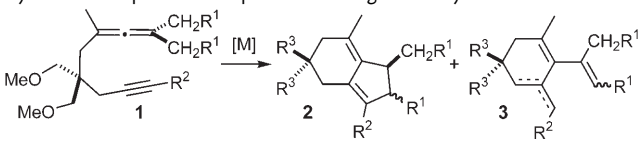

Entry	Catalyst	Conditions	**2** [%]	**3** [%]	*exo*/*endo*
1a: $R^1 = R^2 = H$					
1	$PtCl_2$, 5 mol%	toluene, RT, 24 h	80	–[b]	–
2	$PtCl_4$, 5 mol%	toluene, RT, 1 h	80	–[b]	–
3	$AuCl_3$, 1 mol%	CH_2Cl_2, 0°C, 0.5 h	80	–[b]	–
4	$NaAuCl_4$, 1 mol%	CH_2Cl_2, 0°C, 1 h	75	–[b]	–
5	AuCl, 1 mol%	CH_2Cl_2, 0°C, 0.5 h	79	–[b]	–
6	$[Au(PPh_3)SbF_6]$, 1 mol%	CH_2Cl_2, 0°C, 0.25 h	0	70	1:1
7	$[Au(PPh_3)NTf_2]$, 1 mol%	CH_2Cl_2, 0°C, 6 h	5	68	2:1
8	$[Pt(PhCN)_2dppp](BF_4)_2$, 5 mol%	CH_2Cl_2, 35°C, 0.3 h	–[b]	57	3:1
1b: $R^1 = Me$, $R^2 = H$					
9	$AuCl_3$, 1 mol%	CH_2Cl_2, 0°C, 0.5 h	64[c]	–[b]	–
1c: $R^1 = H$, $R^2 = SiMe_3$					
10	$AuCl_3$, 1 mol%	CH_2Cl_2, 0°C to RT	no reaction		
11	AuCl, 1 mol%	CH_2Cl_2, 0°C to RT	no reaction		
12	$[Au(PPh_3)SbF_6]$, 1 mol%	CH_2Cl_2, 0°C, 0.25 h	complex mixture of isomers		

[a] $R^3 = CH_2OMe$. [b] Traces were observed. [c] Two diastereomers (55:45).

$PtCl_2$; this result would imply an unlikely Pt^{IV}–Pt^{VI} catalytic couple if a platinacyclopentene pathway were involved (Table 1, entry 2).[10] Furthermore, although, to the best of our knowledge, auracyclopentenes are unknown species, gold(III) and gold(I) chloride catalysts also afforded hydrindienes **2a** and **2b** in high yield and after short reaction times at 0°C (Table 1, entries 3–5 and 9). Two other observations shed additional light on this transformation. In the presence of a cationic gold(I) complex generated in situ from the reaction of $[AuCl(PPh_3)]$ with $AgSbF_6$, a dramatic change in reactivity occurred, and only the regioisomers **3** were isolated (Table 1, entry 6). This reactivity was further confirmed when we used $[Au(PPh_3)NTf_2]$[11] and $[Pt(PhCN)_2dppp](BF_4)_2$[12] (dppp = 1,3-bis(diphenylphosphanyl)propane, two other cationic halide-free metal catalysts (Table 1, entries 7–8). In general, alkynes with a trimethylsilyl (TMS) substituent react sluggishly in $PtCl_2$-catalyzed processes.[13] Accordingly, allenyne **1c** did not react under $AuCl_3$ or AuCl catalysis (Table 1,

[*] G. Lemière, Dr. V. Gandon, N. Agenet, Dr. J.-P. Goddard, Dr. C. Aubert, Prof. Dr. L. Fensterbank, Prof. Dr. M. Malacria
Laboratoire de Chimie Organique, UMR CNRS 7611
Institut de Chimie Moléculaire, FR 2769
Université Pierre et Marie Curie, Paris 6, case 229
4, place Jussieu, 75005 Paris (France)
Fax: (+33) 1-4427-7360
E-mail: aubert@ccr.jussieu.fr
fensterb@ccr.jussieu.fr
malacria@ccr.jussieu.fr
Prof. Dr. A. de Kozak
Laboratoire de Chimie de la Matière Condensée
UMR CNRS 7574
Université Pierre et Marie Curie, Paris 6, case 176
4, place Jussieu, 75005 Paris (France)

[**] M.M. is a member of the Institut Universitaire de France (IUF). The authors thank the IUF, the Ministère de la Recherche, and the CNRS for financial support.

Supporting information for this article is available on the WWW under http://www.angewandte.org or from the author.

InterScience © 2006 Wiley-VCH Verlag GmbH & Co. KGaA, Weinheim

entries 10–11). When a gold(I) source was used instead, a complex mixture of unidentified products resulted (Table 1, entry 12).[14] In contrast, unambiguous reactivity was observed for precursor **1d** in the presence of the previously used catalysts (Table 2). In all cases, vinyl allene **4** was formed in high yield.

Table 2: Formation of vinyl allene **4**.

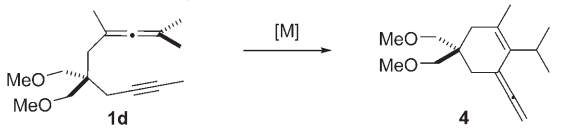

Entry	Catalyst	Conditions	**4** [%]
1	$PtCl_2$, 5 mol%	toluene, RT, 24–48 h	84
2	$AuCl_3$, 1 mol%	CH_2Cl_2, RT, <5 min	92
3	AuCl, 1 mol%	CH_2Cl_2, RT, <5 min	89
4	$[Au(PPh_3)SbF_6]$, 1 mol%	CH_2Cl_2, RT, <5 min	79

As no metallacyclic pathway could explain these new findings with gold, we suspected the occurrence of a cationic event.[15] To probe this hypothesis, we monitored the reaction of **1a** in CD_3OD in the presence of $AuCl_3$ (1 mol%) by ^1H and ^{13}C NMR spectroscopy. The conversion of **1a** was complete within 10 minutes, and compound **5** was formed as a single diastereomer (Scheme 1). The stereochemical assignment of the exocyclic double bond was based on an NOE experiment. The structure of compound **5** supports the existence of a carbocationic intermediate in which the carbon–gold bond is *anti* to the cationic center.

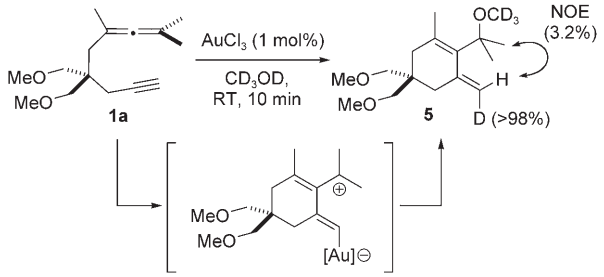

Scheme 1. Trapping of a key intermediate with deuterated methanol.

We also wanted to probe the occurrence of a cationic route in non-oxygenated solvents. Echavarren and co-workers showed that a metallacyclic pathway can be disfavored artificially in the presence of oxygen-containing nucleophilic solvents.[6] Therefore, we introduced a phenyl group at the internal allene position to give **1e** (Table 3). This substrate proved to be highly reactive and provided in good yield the expected Friedel–Crafts product **6** with an exocyclic methylene group, accompanied by the endocyclic isomers **7** and **8**.[16] In the presence of platinum(II) the reaction was much slower, and a large amount of hydrindiene **2e** was formed.

We next performed an isotope-labeling experiment with compound $[D_5]$-**1e** (Scheme 2). As a result of the facile isomerization of the exocyclic double bond, it was not possible to assign the configuration of compound $[D_5]$-**6**. However, it was evident from ^1H NMR spectroscopy that a deuterium atom had been transferred from the phenyl ring to the exocyclic double bond.

Table 3: Intervention of an aromatic ring.

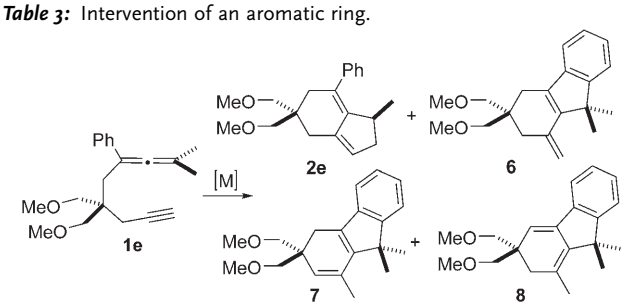

Entry	Catalyst	Cond.	Yield [%]	Products	Ratio
1	$AuCl_3$, 1 mol%	CH_2Cl_2, 0°C, 15 min	98	**6/7/8**	67:27:6
2	$[Au(PPh_3)SbF_6]$, 1 mol%	CH_2Cl_2, 0°C, 15 min	87	**6/7/8**	65:30:5
3	$PtCl_2$, 5 mol%	toluene, RT, 30 h	84	**2e/6/7/8**	38:44:11:7

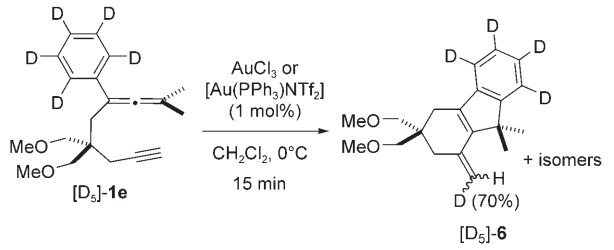

Scheme 2. Deuterium-transfer experiment.

This valuable set of information drove us to analyze the mechanism in more detail. The reactivity of allenynes toward $AuPH_3^+$ and $AuCl_3$ was studied by means of DFT computations. $AuCl_3$ was chosen as a unique model for gold halide species since it is assumed to be the dominant catalyst after chloride substitution in $AuCl_4^-$ or after the dismutation of AuCl into $AuCl_3$ and Au^0 in CH_2Cl_2.[17] The latter assertion derives from our observation of a brown powder that forms instantaneously when AuCl is added to a solution of any allenyne. An X-ray powder diffraction study confirmed the presence of pure gold(0) unambiguously (see Supporting Information for details). Along with the results of computational studies dealing with the gold-catalyzed cyclization of enynes,[18] we could locate neither auracyclopentenes nor their hypothetical η^4-complexed precursors. Instead, cationic species of type **B** or **D** (Scheme 3) were found and linked to alkyne–gold complexes **A** via reasonably low lying transition states ($\Delta G^{\ddagger}_{298} \approx 5$–$15$ kcal mol^{-1}; see Supporting Information).[19] In all cases, *exo* cyclizations, which lead to a *trans* arrangement of the C2–C7 and C1–M bonds, were found to be favored kinetically over *endo* cyclizations by nearly a factor of two.

 © 2006 Wiley-VCH Verlag GmbH & Co. KGaA, Weinheim

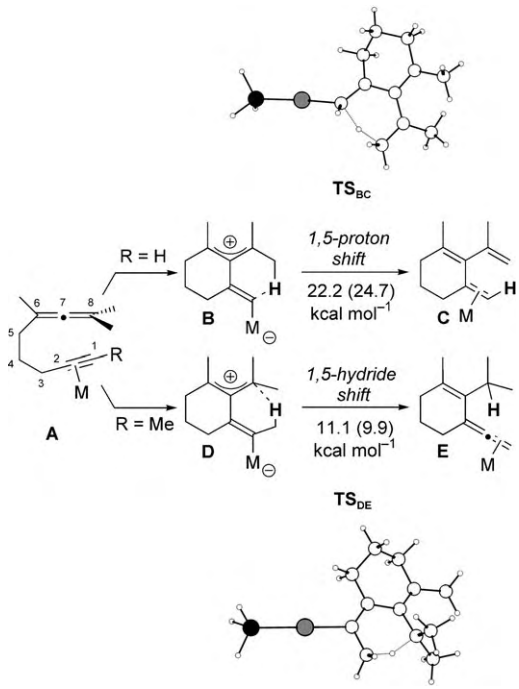

Scheme 3. Mechanistic proposal for the formation of Alder-ene and vinyl allene products: $\Delta G^{\ddagger}_{298}$ values were calculated at the DFT/B3LYP/LACVP(d,p) level for M = $AuCl_3$ (and $AuPH_3^+$). Representative geometries of transition states are given for M = $AuPH_3^+$. P (black), Au (dark gray), Cl (light gray).

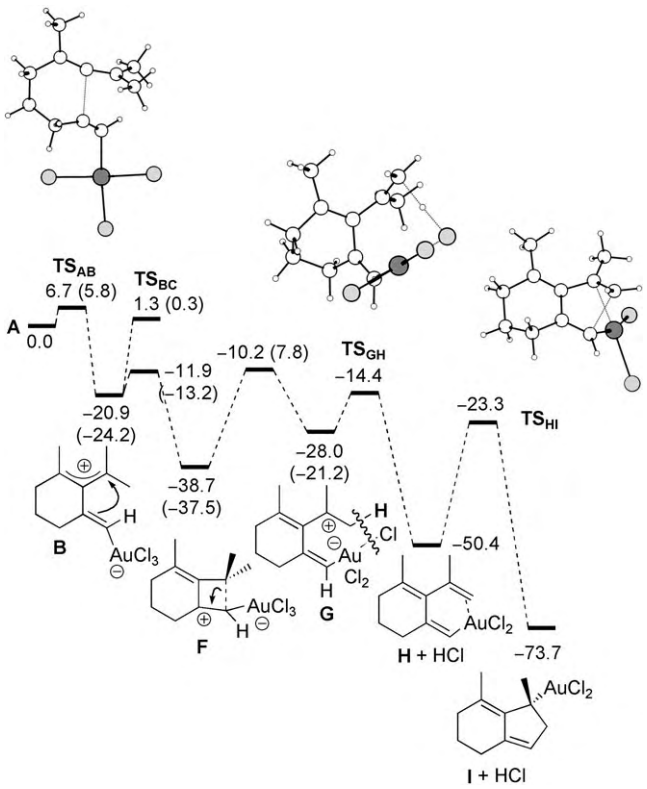

Scheme 4. Energy profile [kcal mol^{-1}] for the transformation of **A** (R = H, M = $AuCl_3$) into the hydrindiene precursor **I**: Geometries of key transition states are depicted. Energy values for the transformation of **A** into **G** with M = $AuPH_3^+$ are also indicated in parentheses.

The formation of Alder-ene products **C** was only computationally possible when R = H, by a direct 1,5-proton shift. These transformations require a free energy of activation of 22.2 kcal mol^{-1} ($AuCl_3$) or 24.7 kcal mol^{-1} ($AuPH_3^+$) and are exothermic by 27.7 kcal mol^{-1} ($AuCl_3$) or 25.1 kcal mol^{-1} ($AuPH_3^+$). The formation of vinyl allene **E** from **D** (R = Me) is also possible in a single step by a 1,5-hydride shift.[20] Free energies of activation of 11.1 kcal mol^{-1} ($AuCl_3$) and 9.9 kcal mol^{-1} ($AuPH_3^+$) were calculated for these exothermic processes ($\Delta G_{298} = -5.0$ kcal mol^{-1} ($AuCl_3$) and −6.0 kcal mol^{-1} ($AuPH_3^+$)).

To account for the formation of hydrindienes,[21] we noticed that only chloride-containing catalysts could promote this specific cycloisomerization (see Table 1).Therefore, we envisaged a mechanism for the transformation of **B** into **I** that involves isomerization of the vinyl metal moiety followed by the elimination of HCl. From a thermodynamic point of view, the isomerization of **B** into **G** is favorable with $AuCl_3$ ($\Delta G_{298} = -7.1$ kcal mol^{-1} (R = H) and −7.2 kcal mol^{-1} (R = Me)), but not with $AuPH_3^+$ ($\Delta G_{298} = 3.0$ kcal mol^{-1} (R = H) and 1.5 kcal mol^{-1} (R = Me)). Manifold efforts failed to locate a transition state corresponding to the direct transformation of **B** into **G**. However, we were able to find a two-step mechanism for this isomerization (Scheme 4). When R = H and M = $AuCl_3$ (or $AuPH_3^+$), a free energy of activation of 9.0 (11.0) kcal mol^{-1} is sufficient to convert **B** into intermediate **F**, which is more stable than **B** by 17.8 (13.3) kcal mol^{-1}. In this case, the quite low free energies of activation make this step faster than the 1,5-proton shifts described above. On the other hand, when R = Me ($\Delta G^{\ddagger}_{298} = 17.1$ kcal mol^{-1} ($AuCl_3$) and 38.1 kcal mol^{-1} ($AuPH_3^+$)) the 1,5-hydride shift is still the fastest process. Therefore, the rest of the discussion will be restricted to the case R = H. Complexes of type **F** would result from a formal [2+2] cycloaddition of the starting compounds **A**.[22] Although the C1–C8 bond is especially long (≈1.59 Å), ring opening at C1–C8 is kinetically difficult. With $AuCl_3$, a free energy of activation of 28.5 kcal mol^{-1} was found for the endothermic transformation of **F** into **G** ($\Delta G_{298} = 10.7$ kcal mol^{-1}). However, **G** would readily undergo elimination of HCl with concomitant formation of an Au–C bond to give **H** ($\Delta G^{\ddagger}_{298} = 13.6$ kcal mol^{-1}). This step is appreciably exothermic by 22.4 kcal mol^{-1}.

The resulting alkene–gold complex **H** could then undergo a 5-*endo*-trig carboauration to give complex **I**. This transformation requires quite a high free energy of activation of 27.1 kcal mol^{-1} but is also characterized by a large exothermicity of 23.3 kcal mol^{-1}. The last step could then be the cleavage of the Au–C bond by HCl, to liberate the final product and regenerate the catalyst. Overall, the formation of **I** from **A** has a thermodynamic driving force greater than that corresponding to the transformation of **A** into **C** (ΔG_{298}(**AI**) = −73.7 kcal mol^{-1}; ΔG_{298}(**AC**) = −48.6 kcal mol^{-1}). Thus, with $AuCl_3$, the two-step isomerization of the vinyl metal moiety positions the metal suitably for the elimination of HCl. On the other hand, the isomerization of **B** into **G** is much more difficult with $AuPH_3^+$. Although the first step to give **F** can be quite fast ($\Delta G^{\ddagger}_{298} = 11.0$ kcal mol^{-1}) and thermodynamically favorable ($\Delta G_{298} = -13.3$ kcal mol^{-1}),

 © 2006 Wiley-VCH Verlag GmbH & Co. KGaA, Weinheim

the energy requirement for the transformation of **F** into **G** seems to be prohibitively high ($\Delta G^{\ddagger}_{298} = 45.3$ kcal mol^{-1}, $\Delta G_{298} = 16.3$ kcal mol^{-1}).[23] As **F** was not found to evolve in any other way, we believe that the formation of the Alder-ene product **C** arises from the 1,5-proton shift described above, despite a higher activation energy (24.7 kcal mol^{-1} for **B**→**C** versus 11.0 kcal mol^{-1} for **B**→**F**). The greater stability of **C** relative to that of **F** (ΔG_{298}(**AF**) = −37.5 kcal mol^{-1}; ΔG_{298}(**AC**) = −49.3 kcal mol^{-1}) should funnel the reaction toward the Alder-ene product.

Thus, gold catalysis has provided deeper insight into the mechanism of the cycloisomerization of allenynes. Because no standard metallacyclic route could be envisaged, two unusual mechanistic pathways which take into account the presence of cationic intermediates have been proposed: a 1,5-proton shift for the Alder-ene products and a 1,5-hydride shift for the vinyl allenes. We also found evidence for an intriguing halide effect that completely alters the cycloisomerization process (Alder-ene versus hydrindiene products), presumably through the elimination of HCl as a key step for the formation of hydrindienes. Finally, physical evidence has been found for the dismutation of AuCl into Au and $AuCl_3$. A comprehensive experimental and computational study will be reported in due course.

Received: June 1, 2006
Revised: August 4, 2006
Published online: October 18, 2006

Keywords: allenynes · cycloisomerization · gold · halides · homogeneous catalysis

[1] For reviews, see: a) S. T. Diver, A. J. Giessert, *Chem. Rev.* **2004**, *104*, 1317 – 1382; b) G. C. Lloyd-Jones, *Org. Biomol. Chem.* **2003**, *1*, 215 – 236.
[2] a) M. Méndez, V. Mamane, A. Fürstner, *Chemtracts: Org. Chem.* **2003**, *16*, 397 – 425; b) L. Anorbe, G. Dominguez, J. Pérez-Castells, *Chem. Eur. J.* **2004**, *10*, 4938 – 4943.
[3] a) G. Dyker, *Angew. Chem.* **2000**, *112*, 4407 – 4409; *Angew. Chem. Int. Ed.* **2000**, *39*, 4237 – 4239; b) A. M. Echavarren, C. Nevado, *Chem. Soc. Rev.* **2004**, *33*, 431 – 436; c) C. Bruneau, *Angew. Chem.* **2005**, *117*, 2380 – 2386; *Angew. Chem. Int. Ed.* **2005**, *44*, 2328 – 2334; d) S. Ma, S. Yu, Z. Gu, *Angew. Chem.* **2006**, *118*, 206 – 209; *Angew. Chem. Int. Ed.* **2006**, *45*, 200 – 203.
[4] C. Aubert, O. Buisine, M. Malacria, *Chem. Rev.* **2002**, *102*, 813 – 834.
[5] a) A. Fürstner, P. W. Davies, T. Gress, *J. Am. Chem. Soc.* **2005**, *127*, 8244 – 8245; b) C. Nieto-Oberhuber, S. Lopez, M. P. Muñoz, D. J. Cárdenas, E. Buñuel, C. Nevado, A. M. Echavarren, *Angew. Chem.* **2005**, *117*, 6302 – 6304; *Angew. Chem. Int. Ed.* **2005**, *44*, 6146 – 6148.
[6] M. Méndez, M. P. Muñoz, C. Nevado, D. J. Cárdenas, A. M. Echavarren, *J. Am. Chem. Soc.* **2001**, *123*, 10511 – 10520.
[7] a) A. S. K. Hashmi in *Modern Allene Chemistry* (Eds.: N. Krause, A. S. K. Hashmi), Wiley-VCH, Weinheim, **2004**, pp. 877 – 923; b) K. M. Brummond, H. Chen in *Modern Allene Chemistry* (Eds.: N. Krause, A. S. K. Hashmi), Wiley-VCH, Weinheim, **2004**, pp. 1041 – 1089; c) S. Ma, *Chem. Rev.* **2005**, *105*, 2829 – 2871.
[8] N. Cadran, K. Cariou, G. Hervé, C. Aubert, L. Fensterbank, M. Malacria, J. Marco-Contelles, *J. Am. Chem. Soc.* **2004**, *126*, 3408 – 3409.
[9] E. Soriano, J. Marco-Contelles, *Chem. Eur. J.* **2005**, *11*, 521 – 533.
[10] The observed reaction times presumably exclude a similar catalytic system derived from the reduction of $PtCl_4$ to $PtCl_2$.
[11] N. Mézailles, L. Ricard, F. Gagosz, *Org. Lett.* **2005**, *7*, 4133 – 4136.
[12] S. Oi, I. Tsukamoto, S. Miyano, Y. Inoue, *Organometallics* **2001**, *20*, 3704 – 3709.
[13] See, for example: a) T. J. Harrison, G. R. Dake, *Org. Lett.* **2004**, *6*, 5023 – 5026; b) K. Cariou, E. Mainetti, L. Fensterbank, M. Malacria, *Tetrahedron* **2004**, *60*, 9745 – 9755.
[14] To avoid the use of a fluoride source along with the TMS-substituted allenyne **1c**, we also tried the [AuCl(PPh_3)]/AgOTf catalytic system; however, a complex mixture was still formed. Compound **1c** proved unreactive toward $AgSbF_6$ and AgOTf.
[15] To the best of our knowledge, the notion that noble-metal-catalyzed cycloisomerizations proceed via intermediates that behave like cations was first proposed in: A. Fürstner, H. Szillat, B. Gabor, R. Mynott, *J. Am. Chem. Soc.* **1998**, *120*, 8305 – 8314.
[16] For the intramolecular trapping by Friedel–Crafts reactions of putative cations formed in transition-metal-catalyzed cycloisomerizations, see: A. Fürstner, C. Aïssa, *J. Am. Chem. Soc.* **2006**, *128*, 6306 – 6307.
[17] The disproportionation of AuCl into $AuCl_3$ and Au in CH_2Cl_2 or CH_3CN has been described; see: a) A. Vogler, H. Kundely, *Coord. Chem. Rev.* **2001**, *219–221*, 489 – 507; b) T. C. Wabnitz, J.-Q. Yu, J. B. Spencer, *Chem. Eur. J.* **2004**, *10*, 484 – 493.
[18] C. Nieto-Oberhuber, M. P. Muñoz, E. Buñuel, C. Nevado, D. J. Cárdenas, A. M. Echavarren, *Angew. Chem.* **2004**, *116*, 2456 – 2460; *Angew. Chem. Int. Ed.* **2004**, *43*, 2402 – 2406.
[19] The cyclizations are exothermic by 15–25 kcal mol^{-1}.
[20] a) For a related cationic extension of a suprafacial sigmatropic shift, see: R. Hoffmann, D. J. Tantillo, *Angew. Chem.* **2003**, *115*, 6057 – 6062; *Angew. Chem. Int. Ed.* **2003**, *42*, 5877 – 5882; b) for a related quantum-chemical study of 1,5-hydride shifts in 2,6-dimethyl-2-heptyl cations, see: V. Vrček, I. Vinkovič Vrček, H.-U. Siehl, *J. Phys. Chem. A* **2006**, *110*, 1868 – 1874.
[21] We have confirmed that Alder-ene products are not precursors to hydrindienes. For example, under gold(III) catalysis, compound **3a** was not converted into **2a**.
[22] For examples of the transition-metal-catalyzed [2+2] cycloaddition of allenynes, see: C. H. Oh, A. K. Guptar, D. I. Park, N. Kim, *Chem. Commun.* **2005**, 5670 – 5672, and references therein.
[23] It is not clear why the transformation of **F** into **G** is kinetically much more difficult with $AuPH_3^+$ than with $AuCl_3$.

 © 2006 Wiley-VCH Verlag GmbH & Co. KGaA, Weinheim

Asymmetric Catalysis

DOI: 10.1002/anie.200602417

Asymmetric Conjugate Addition to α-Halo Enones: Dramatic Effect of Styrene on the Enantioselectivity**

*Kangying Li and Alexandre Alexakis**

Aiming to enlarging the scope of potential Michael acceptors in the copper-catalyzed asymmetric conjugate addition,[1,2] we regarded the class of α-halo enones as being attractive, because the resulting α-halo ketones are versatile intermediates that are widely used in organic synthesis, for example, in the synthesis of a variety of heterocycles,[3] in cross aldol condensations,[4] in the synthesis of enaminoketones,[5] and in Favorskii rearrangements.[6] Of particular interest was the reactivity of the resulting α-halogenated enolate, which could be seen as a carbenoid that might undergo inter- or intramolecular cyclopropanation reactions in the presence of a copper catalyst (Scheme 1).[7]

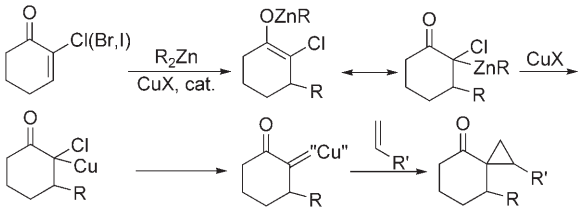

Scheme 1. Potential pathway for cyclopropanation.

There are scarce examples of the conjugate addition of allyllithium,[8] cuprates,[9] or organometallic reagents that react under copper catalysis, such as Grignard[10e] and organozinc reagents,[11] to α-halogenated Michael acceptors. However, no results have been reported so far for the asymmetric conjugate addition of dialkyl zinc or trialkyl aluminum reagents to α-halo enones, despite all the recent progress in this research area.[1b] We describe herein the results of our research on this topic, including an interesting observation of an improvement in enantioselectivity when styrene is employed as a radical scavenger.

With respect to the proposed reaction in Scheme 1, there were three main points to address: 1) the reactivity of α-halo enones, 2) the level of enantioselectivity that could be attained in an enantioselective process, and 3) the feasibility of the cyclopropanation. First, we compared the reactivity of the α-halo cyclohexenones **1**–**3** (Scheme 2) with that of

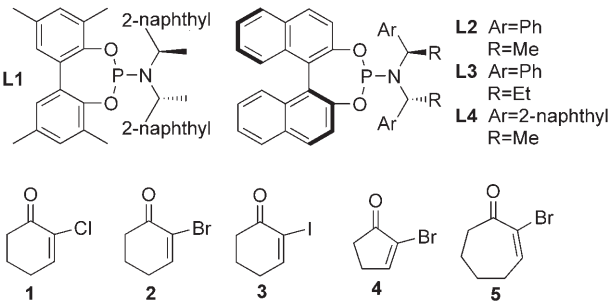

Scheme 2. Chiral ligands and substrates used in this study.

cyclohexenone. The conjugate addition reactions carried out in parallel in the presence of Et_2Zn and ligand **L4** (see details in the Supporting Information) showed that α-halogenated enones were less reactive than cyclohexenone and that the reactivity of the three substrates **1**, **2**, and **3** decreased mildly with increasing electronegativity of the halogen (Scheme 3).

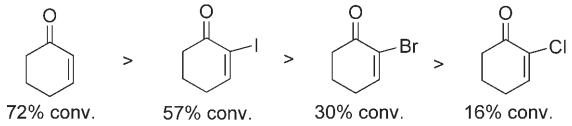

Scheme 3. Relative reactivity of **1**–**3**: % conversion after a reaction time of 10 min at −30 °C in diethyl ether.

A variety of reaction conditions was tested for their effect on the enantioselectivity of the reaction (Table 1). The ligand

Table 1: Asymmetric conjugate addition of diethylzinc to compounds **1**–**3** in diethyl ether.

Entry	Substrate	CuX[d]	Ligand	*trans*/*cis*[a]	*ee* [%][b]	Config.[c]
1	**1**	CuTC	**L1**	71:29	77 (77)	(2*R*,3*S*)
2	**1**	CuTC	*ent*-**L2**	70:30	80 (84)	(2*S*,3*R*)
3	**1**	CuTC	**L4**	70:30	83 (83)	(2*R*,3*S*)
4[e]	**1**	CuTC	**L4**	69:31	87 (80)	(2*R*,3*S*)
5[f]	**1**	CuTC	**L4**	71:29	78 (69)	(2*R*,3*S*)
6	**1**	$Cu(OTf)_2$	**L4**	70:30	90 (92)	(2*R*,3*S*)
7	**2**	CuTC	**L1**	68:32	77 (76)	(2*R*,3*S*)
8	**2**	CuTC	*ent*-**L2**	69:31	63 (64)	(2*S*,3*R*)
9	**2**	CuTC	**L4**	70:30	88 (88)	(2*R*,3*S*)
10	**2**	$Cu(OTf)_2$	**L4**	71:29	86 (86)	(2*R*,3*S*)
11	**3**	CuTC	**L1**	18:82	73 (65)	(2*S*,3*S*)
12	**3**	CuTC	*ent*-**L2**	18:82	79 (74)	(2*R*,3*R*)
13	**3**	CuTC	**L4**	18:82	84 (83)	(2*S*,3*S*)
14	**3**	$Cu(OTf)_2$	**L4**	18:82	84 (83)	(2*S*,3*S*)

[a] Determined by GC-MS and/or NMR spectroscopy. [b] Determined by GC on a chiral phase; the *ee* value of the minor diastereomer is given in parentheses. [c] Configuration of the major product. [d] CuTC stands for copper thiophene carboxylate, Tf for trifluoromethanesulfonyl. [e] Toluene was used as the solvent. [f] CH_2Cl_2 was used as the solvent.

[*] Dr. K. Li, Prof. Dr. A. Alexakis
Département de chimie organique
Université de Genève
30 quai E. Ansermet, 1211 Genève 4 (Switzerland)
Fax: (+41) 223-793-215
E-mail: alexandre.alexakis@chiorg.unige.ch

[**] The authors thank the Swiss National Research Foundation (no. 200020-105368) and COST Action D24/003/01 (OFES contract no. C02.0027) for financial support, and BASF for their generous gift of chiral amines.

Supporting information for this article is available on the WWW under http://www.angewandte.org or from the author.

InterScience
© 2006 Wiley-VCH Verlag GmbH & Co. KGaA, Weinheim

L4 was slightly better than **L1** and **L2**. All reactions were carried out to full conversion. (The mixture was maintained at −30 °C for 2 h, then warmed to room temperature.) The reactions were very clean, and all products were isolated in greater than 85 % yield. The only by-product detected (5–10 %) was 3-ethylcyclohexanone, which results from an iodine–zinc exchange with 2-iodocyclohexenone (**3**).[12] After quenching the reaction with an acid, two diastereomers were obtained. The major diastereomer was the *trans* diastereomer in the case of the α-chloro and α-bromo products **6** and **7**.[10a] Isomerization with DBU (1,8-diazabicyclo[5.4.0]undec-7-ene) gave the *cis* isomer as the thermodynamically more stable (*cis*/*trans* 63:37 for **6** and 79:21 for **7**). This isomerization is not unexpected in view of the favored axial orientation of the halo substituent of α-halo cyclohexanones.[10b–d] In the case of the α-iodo product **8**, the more stable *cis* isomer was obtained directly.[10e]

As seen in Table 1, the enantioselectivity is good in most cases. In CH_2Cl_2, however, a clear drop in enantioselectivity was observed (78 % *ee*; Table 1, entry 5). This was an unfortunate result because CH_2Cl_2 is the best solvent for copper-catalyzed cyclopropanations, which we intended to investigate next. Nevertheless, we proceeded to examine the behavior of the resulting enolate. When the copper-catalyzed conjugate addition was carried out with 10 equivalents of styrene, cyclopropanation was observed neither at room temperature, nor after prolonged heating at reflux (Scheme 4). Only the hydrolyzed conjugate adduct **6** was

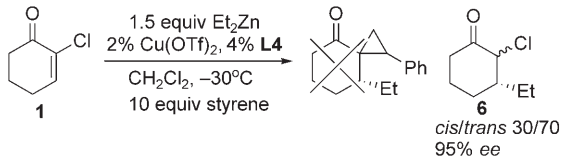

Scheme 4. Attempted cyclopropanation.

obtained, but its *ee* value had jumped from 78 % to 95 %! This remarkable effect of the addition of styrene may have two causes. First, π coordination of Cu to the double bond of styrene results in a favorable modification of the environment of the organometallic species. Such an effect has been observed by Knochel and co-workers,[13] who reported that *para*-trifluorostyrene is helpful in a Ni-catalyzed cross-coupling reaction. The second possibility is that styrene may prevent an alternative non-asymmetric conjugate-addition pathway.

Indeed, it was demonstrated by Bertrand et al. that ethyl radicals could be generated from diethylzinc in the presence of oxygen and added to cyclohexenone.[14a] They also showed that when *i*PrI or *t*BuI were added, the ethyl radical reacted to generate the more stable isopropyl or *tert*-butyl radical, which underwent the conjugate addition instead. Therefore, a simple way to detect a possible radical pathway was to run the copper-catalyzed reaction in the presence of *i*PrI (6 equiv). The presence of the isopropyl conjugate adduct would provide evidence that such a radical pathway exists (Scheme 5). In our case, the radical process could be initiated

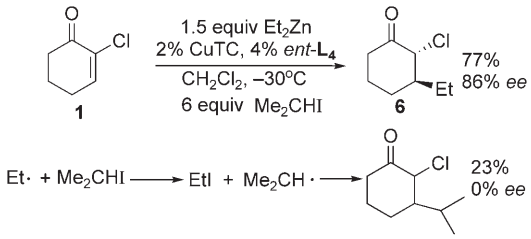

Scheme 5. Reaction sequence in the presence of *i*PrI that is indicative of a radical pathway with **1**.

by traces of oxygen, but also by the reduction of a Cu^{II} salt to Cu^{I} by diethylzinc. We also could not exclude an SET mechanism in the reaction of α-halo enones.[14b,c]

As suspected, the experiment in dichloromethane afforded the *i*Pr adduct and the desired ethylated product in the ratio 23:77, respectively. However, most striking was the observation that the desired product **6** was formed with 86 % *ee*, as opposed to 78 % *ee* in the absence of *i*PrI (Table 1, entry 5), whereas the *i*Pr adduct was racemic. Thus, the copper-catalyzed conjugate addition might actually proceed with higher enantioselectivity than that usually observed.

It seems clear that the role of styrene is to inhibit a non-asymmetric conjugate addition by trapping the initial Et radical. The radical polymerization of styrene is a well-known process.[15] The high enantioselectivity of the reaction shown in Scheme 4 implies that the addition of an ethyl radical to styrene is faster than its addition to 2-chlorocyclohexenone (**1**). Furthermore, the resulting phenylbutyl radical appears to be sufficiently inert not to add to **1**. To check this point, we repeated the experiment of Bertrand et al. (Et_2Zn, air, no copper, substrate **1**) in the presence of styrene. Only traces of adduct **6** were found, along with a visible cloud of polymerized styrene.

This "styrene effect" was investigated more thoroughly with 2-bromocyclohexenone (**2**; Table 2). In CH_2Cl_2, in the absence of styrene, the *ee* value of the product was 85 %. In the presence of styrene (10 equiv), the *ee* value increased to 95 %; complete conversion was observed, and the reaction was not slower. The high enantioselectivity was maintained even with just 0.1 equivalents of styrene. This is a remarkable effect, which shows the true enantioselectivity of the copper-catalyzed pathway. It may be assumed that many results in the literature on this topic could be improved just by adding styrene! Indeed, several reports point to "slightly improved"

Table 2: Effect of styrene on the enantioselectivity in the reaction of **2**.[a]

Entry	Styrene [equiv]	*trans*/*cis*[b]	*ee* %[c]
1	–	70:30	85 (87)
2	10	70:30	95 (95)
3	5	71:29	96 (95)
4	1	76:24	97 (94)
5	0.5	75:25	98 (96)
6	0.1	74:26	96 (94)

[a] The reaction conditions were the same as those given in Scheme 5. [b] Determined by GC-MS. [c] Determined by GC on a chiral phase; *ee* value of the minor diastereomer is given in parentheses.

 © 2006 Wiley-VCH Verlag GmbH & Co. KGaA, Weinheim

enantioselectivity when a Cu^{I} salt, such as $[CuOTf]_2$·benzene, is employed instead of a Cu^{II} salt, such as $Cu(OTf)_2$.[16] The reduction of the Cu^{II} catalyst, present in 2 mol%, with diethylzinc generates 2 mol% of ethyl radical and corresponds to at least a 2% loss in enantioselectivity. If the radical propagation is not stopped, the loss in enantioselectivity may be much higher. Thus, it is only the initial radical-formation step that has to be prevented. Nevertheless, most other experiments were run with 1–10 equivalents of styrene.

We repeated our experiments with all enones **1**–**5** under these new conditions (Table 3). The results clearly show the beneficial effect of added styrene on the reactions of the three α-halo cyclohexenones **1**–**3**, whatever the solvent (see Table 3, entry 2, footnote [c]). With 2-bromocyclopentenone (**4**), this

Table 3: Asymmetric conjugate addition of diethylzinc to compounds **1**–**5**.

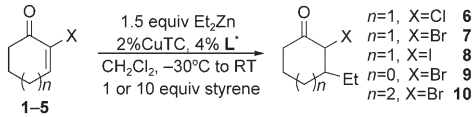

1–5

Entry	Substrate	L*	Styrene [equiv]	Product	*trans*/*cis*[a]	*ee* [%][b]
1	**1**	**L4**	–	**6**	71:29	78 (69)
2[c]	**1**	**L4**	10	**6**	70:30	98 (97)
3	**2**	**L4**	–	**7**	70:30	85 (87)
4	**2**	**L4**	1	**7**	76:24	97 (94)
5	**3**	**L4**	–	**8**	18:82	88 (87)
6	**3**	**L4**	1	**8**	19:81	95 (92)
7	**4**	**L4**	–	**9**	71:29	05 (05)
8	**4**	**L4**	10	**9**	70:30	79 (78)
9	**5**	**L4**	–	**10**	2:98	21
10[d]	**5**	*ent*-**L2**	–	**10**	5:95	75 (74)
11[d]	**5**	*ent*-**L2**	10	**10**	5:95	78 (78)

[a] Determined by GC-MS and/or NMR spectroscopy. [b] Determined by GC on a chiral phase; the *ee* value of the minor diastereomer is given in parentheses. [c] The same results were obtained in toluene and in Et_2O. [d] Et_2O was used as the solvent.

"styrene effect" is even more spectacular: In the absence of styrene, the adduct **9** was formed in almost racemic form, whereas it was formed with 79% *ee* in the presence of styrene![17] In the reaction of 2-bromocycloheptenone (**5**), the ligand **L4** was not as good as **L2**, and the "styrene effect" was not so pronounced when the reaction was performed in Et_2O in the presence of **L2**.

The successful application of diethylzinc in this reaction prompted us to try another dialkyl zinc reagent. Unfortunately, no reaction took place between **2** and dimethylzinc under the same conditions, probably as a result of the low reactivity of the latter. Recently, triorganoaluminum reagents have been shown to be good replacements for dialkyl zinc reagents in asymmetric copper-catalyzed conjugate additions.[2a,b,18] To our pleasure, the addition of Me_3Al to **2** proceeded very well (Scheme 6). The desired 1,4-adduct **11** was formed with moderate diastereoselectivity and excellent enantioselectivity. In this case, the best ligand appeared to be **L3**. The addition of styrene did not improve this result.

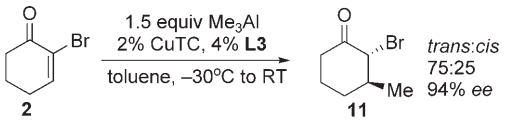

2 11

Scheme 6. Addition of Me_3Al to **2**.

In summary, we have shown that high enantioselectivities can be attained in the copper-catalyzed conjugate addition of Et_2Zn and Me_3Al to α-halogenated enones. We also found evidence of an achiral radical pathway by carrying out the reaction with isopropyl iodide, and demonstrated that it is possible to stop this radical process by adding styrene, which acts as a radical scavenger. It may be assumed that many conjugate addition reactions described previously could be improved if they were carried out in the presence of styrene.

Experimental Section

Typical procedure: Dry diethyl ether (2 mL) was added to a mixture of copper thiophene carboxylate (CuTC; 1.9 mg, 0.01 mmol) and ligand **L4** (12.8 mg, 0.02 mmol) under nitrogen. The solution was stirred at room temperature for 30 min and was then cooled to −30 °C. Diethylzinc (1 M in hexane, 0.75 mL) was added dropwise, with the temperature maintained below −30 °C. The resulting solution was stirred for 5 min, and a solution of 2-bromocyclohexenone (**2**; 0.5 mmol) in diethyl ether (0.5 mL) was then added dropwise. The reaction mixture was stirred at −30 °C for 2 h and then allowed to warm up to room temperature. The reaction mixture was stirred at room temperature until all the starting material had been consumed. The solution was then diluted with diethyl ether (20 mL) and washed successively with 2 N HCl and brine. The organic layer was dried over anhydrous sodium sulfate. Removal of the solvent gave the crude product, which was subjected to flash chromatography. The product was then analyzed by GC on a chiral stationary phase (or supercritical fluid chromatography) and NMR spectroscopy to determine the ratio of diastereomers and the *ee* values.

7: *trans*/*cis* 76:24 (crude), 72:28 (after chromatography), light-yellow oil; Mixture of isomers: ^{1}H NMR (400 MHz, $CDCl_3$): $\delta = 0.88$–0.95 (dt, 3H, CH_3), 1.36–1.80 (m, 5H, $2CH_2$, CH), 1.99–2.07 (m, 2H, CH_2), 2.27–2.34 (m, 1H, CH), 2.84–3,15 (m, 1H, CH), 4.25 (d, $^3J_{H,H} = 7.6$ Hz, 0.73H, CH), 4.28–4.29 ppm (d, $^3J_{H,H} = 1.28$ Hz, 0.27H, CH); ^{13}C NMR (100 MHz, $CDCl_3$): $\delta = 10.82$, 23.55, 25.18, 25.92, 26.46, 26.99, 35.58, 38.69, 44.66, 47.64, 58.89, 59.61, 203.29, 204.87 ppm; IR (neat): $\tilde{\nu} = 2962$, 2936, 2874, 1715, 1458, 1424, 1313, 1221, 1174, 1093, 962, 927, 757, 668 cm^{-1}; MS (ESI): *m*/*z* (%): 206 (8), 204 (8), 125 (34), 107 (13), 81 (19), 69 (16), 55 (100); HRMS (EI): $[M+Na]^+$ calcd for $C_8H_{13}BrO$: 227.0047; found: 227.0049.

Received: June 15, 2006
Revised: September 7, 2006
Published online: October 19, 2006

Keywords: asymmetric synthesis · conjugate addition · copper · homogeneous catalysis · radicals

[1] a) N. Krause in *Modern Organocopper Chemistry*, Wiley-VCH, Weinheim, **2001**; b) A. Alexakis, C. Benhaim, *Eur. J. Org. Chem.* **2002**, 3221–3236; c) T. Hayashi, *Acc. Chem. Res.* **2000**, *33*, 354–362.

[2] a) M. D'Augustin, L. Palais, A. Alexakis, *Angew. Chem.* **2005**, *117*, 1400–1402; *Angew. Chem. Int. Ed.* **2005**, *44*, 1376–1378; b) D. Polet, A. Alexakis, *Tetrahedron: Asymmetry* **2005**, *16*,

 © 2006 Wiley-VCH Verlag GmbH & Co. KGaA, Weinheim

1529 – 1532; c) A. Alexakis, D. Polet, S. Rosset, S. March, *J. Org. Chem.* **2004**, *69*, 5660 – 5667, and references therein.
[3] a) M. Kodomari, T. Aoyama, Y. Suzuki, *Tetrahedron Lett.* **2002**, *43*, 1717 – 1720; b) F. Kunckell, *Ber. Dtsch. Chem. Ges.* **1901**, *34*, 637; c) H.-J. Lohrisch, L. Kopanski, R. Herrmann, H. Schmidt, W. Steglich, *Liebigs Ann. Chem.* **1986**, 177 – 194.
[4] J.-E. Dubois, G. Axiotis, E. Bertounesque, *Tetrahedron Lett.* **1985**, *26*, 4371 – 4372.
[5] K. Van Sant, S. M. South, *Tetrahedron Lett.* **1987**, *28*, 6019 – 6020.
[6] A. E. Favorskii, *J. Prakt. Chem.* **1913**, *88*, 658.
[7] a) A. Pfaltz in *Comprehensive Asymmetric Catalysis*, *Vol. 2* (Ed.: E. N. Jacobsen, A. Pfaltz, H. Yamamoto), Springer, Berlin, **1999**, pp. 513 – 538; b) W. Kirmse, *Angew. Chem.* **2003**, *115*, 1120 – 1125; *Angew. Chem. Int. Ed.* **2003**, *42*, 1088 – 1093.
[8] H. J. Klemeyer, L. A. Paquette, *J. Org. Chem.* **1994**, *59*, 7924 – 7927.
[9] a) C. Chuit, R. Sauvetre, D. Masure, J. F. Normant, *Tetrahedron* **1979**, *35*, 2645 – 2653; b) C. J. Kowalski, A. E. Weber, K. W. Fields, *J. Org. Chem.* **1982**, *47*, 5088 – 5093.
[10] a) The *cis* and *trans* isomers of **6** could be separated and their configuration assigned unambiguously by the comparison of their NMR spectra with that reported by: S. E. Denmark, M. S. Dappen, N. S. Sear, R. T. Jacobs, *J. Am. Chem. Soc.* **1990**, *112*, 3466 – 3474; b) E. J. Corey, *J. Am. Chem. Soc.* **1953**, *75*, 2301 – 2304; c) C. A. Horiuchi, S. Kiji, *Chem. Lett.* **1988**, 31 – 34; d) E. L. Eliel, S. H. Wilen, *Stereochemistry of Organic Compounds*, Wiley, New York, **1994**. e) When the reaction was quenched under neutral conditions (aqueous NH_4Cl), *trans*-**8** was formed as the major isomer; see: C. K. Sha, C. T. Tseng, W. S. Chang, *Tetrahedron Lett.* **2001**, *42*, 683 – 685.
[11] S. Carret, A. Blanc, Y. Coquerel, M. Berthod, A. E. Greene, J.-P. Deprés, *Angew. Chem.* **2005**, *117*, 5260 – 5263; *Angew. Chem. Int. Ed.* **2005**, *44*, 5130 – 5133.
[12] P. Knochel, N. Millot, A. L. Rodrigues, *Org. React.* **2001**, *58*, 417 – 731.
[13] a) R. Giovannini, T. Stüdemann, G. Dussin, P. Knochel, *Angew. Chem.* **1998**, *110*, 2512 – 2515; *Angew. Chem. Int. Ed.* **1998**, *37*, 2387 – 2390; b) R. Giovannini, T. Stüdemann, A. Devasagayaraj, G. Dussin, P. Knochel, *J. Org. Chem.* **1999**, *64*, 3544 – 3553.
[14] a) M. P. Bertrand, L. Feray, R. Nouguier, P. Perfetti, *J. Org. Chem.* **1999**, *64*, 9189 – 9189; b) H. O. House, *Acc. Chem. Res.* **1976**, *9*, 59 – 67; c) M. D. Murphy, C. A. Ogle, S. H. Bertz, *Chem. Commun.* **2005**, 854 – 856.
[15] a) G. Moad, E. Rizzardo, D. H. Solomon, *Macromolecules* **1982**, *15*, 909 – 914; b) A. Studer, *Chem. Eur. J.* **2001**, *7*, 1159 – 1164, and references therein.
[16] a) K. S. Lee, M. K. Brown, A. W. Hird, A. H. Hoveyda, *J. Am. Chem. Soc.* **2006**, *128*, 7182 – 7184; b) Y. H. Choi, J. Y. Choi, H. Y. Yang, Y. H. Kim, *Tetrahedron: Asymmetry* **2002**, *13*, 801 – 804; c) M. Shi, W. Zhang, *Adv. Synth. Catal.* **2005**, *347*, 535 – 540; d) M. Shi, C. J. Wang, W. Zhang, *Chem. Eur. J.* **2004**, *10*, 5507 – 5516; e) T. Morimoto, N. Mochizuki, M. Suzuki, *Tetrahedron Lett.* **2004**, *45*, 5717 – 5722; f) Y. Takahashi, Y. Yamamoto, K. Katagiri, H. Danjo, K. Yamaguchi, T. Imamoto, *J. Org. Chem.* **2005**, *70*, 9009 – 9012; g) R. R. Cesati III, J. de Armas, A. H. Hoveyda, *J. Am. Chem. Soc.* **2004**, *126*, 96 – 101; h) S. Ongeri, U. Piarulli, R. F. W. Jackson, C. Gennari, *Eur. J. Org. Chem.* **2001**, 803 – 807; i) L. Wang, Y. M. Li, C. W. Yip, L. Qiu, Z. Zhou, A. S. C. Chan, *Adv. Synth. Catal.* **2004**, *346*, 947 – 953; j) L. Liang, T. T.-L. Au-Yeung, A. S. C. Chan, *Org. Lett.* **2002**, *4*, 3799 – 3801.
[17] A similar experiment to that in Scheme 5 with 2-bromocyclopentenone (**4**) afforded the ethylated product along with the racemic isopropylated product in a 16:84 ratio.
[18] a) P. K. Fraser, S. Woodward, *Chem. Eur. J.* **2003**, *9*, 776 – 783; b) L. Su, X. Li, W. L. Chan, X. Jia, A. S. C. Chan, *Tetrahedron: Asymmetry* **2003**, *14*, 1865 – 1869; c) Y. Takemoto, S. Kuraoka, N. Hamaue, C. Iwata, *Tetrahedron: Asymmetry* **1996**, *7*, 993 – 996.

 © 2006 Wiley-VCH Verlag GmbH & Co. KGaA, Weinheim

Zeolites

DOI: 10.1002/anie.200602595

MFI Zeolite with Small and Uniform Intracrystal Mesopores**

*Hui Wang and Thomas J. Pinnavaia**

The catalytic activity of zeolites[1] often is limited by the diffusion of reagents and reaction products through the framework pore network. Recently, several efforts have been made to reduce the diffusion path length in zeolites by confining crystal growth to a nanometer length scale[2–8] or by providing intracrystal mesopores during synthesis.[9–13] The latter strategy is intrinsically appealing, in part, because it precludes the need for colloidal crystal formation and avoids the drawbacks associated with nanoparticle processing. Moreover, the presence of mesopores in zeolite crystals offers the possibility of improving product selectivity in the catalytic cracking of polymeric molecules.[14]

The embedding of carbon nanoparticles and certain polymers into zeolites crystals during synthesis has been shown to be an effective means of generating intracrystal mesopores.[9–13] These templating methods provide much better control of pore size than conventional steaming and chemical leaching approaches to mesopore formation in zeolites.[15] However, particle templates typically afford average pore sizes that are too large (≥ 10 nm) and pore size distributions that are too broad (> 10 nm widths at half maximum) for catalytic cracking reactions with high product selectivity.

Herein we report a method to prepare templated zeolites with small intracrystal mesopores (average pore size 2.0–3.0 nm) and narrow pore size distributions (ca. 1.0–1.5 nm width at half maximum). We selected the MFI zeolite ZSM-5 to illustrate our approach, in part, because it is widely recognized for its unique properties as a catalyst for NO_x reduction, Fisher–Tropsch chemistry, and toluene disproportionation, and as an additive for petroleum cracking. Scheme 1 illustrates our synthetic strategy for templating uniform mesopores within a zeolite matrix. In this scheme, a silane-functionalized polymer is used as a porogen for the formation of intracrystal mesopores. The presence of -SiO_3 units on the polymer allows it to be integrated into a silica–alumina sol–gel reaction mixture. Nucleation of the zeolite phase in the presence of the silylated polymer is accompanied by the grafting of the polymer to the zeolites surface through covalent Si-O-Si linkages. As the zeolite crystal grows, the

[*] H. Wang, Professor T. J. Pinnavaia
Department of Chemistry
Michigan State University
East Lansing, MI 48824 (USA)
Fax: (+1) 517-432-1225
E-mail: pinnavaia@chemistry.msu.edu

[**] The support of this research through NSF grant CHE-0211029 is gratefully acknowledged.

© 2006 Wiley-VCH Verlag GmbH & Co. KGaA, Weinheim

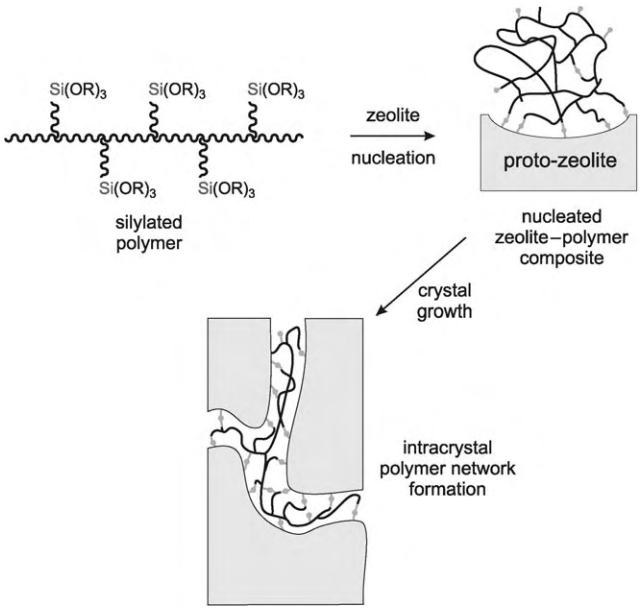

Scheme 1. Conceptional approach to the synthesis of a zeolite with intracrystal mesopores using a silylated polymer as the mesoporogen.

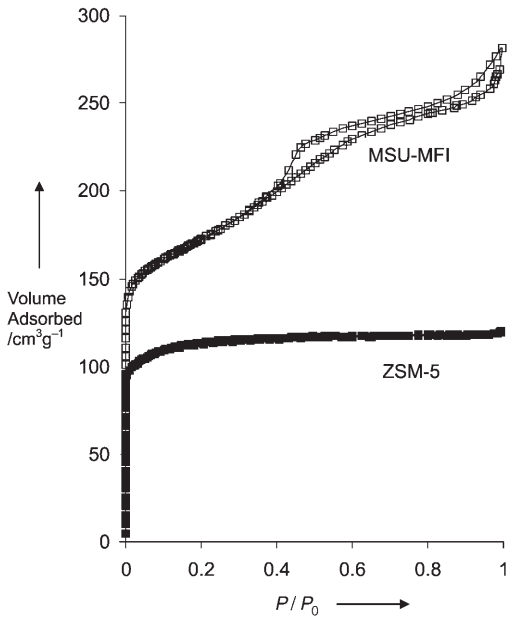

Figure 1. Nitrogen adsorption/desorption isotherms for MSU-MFI zeolites prepared in the presence of a silylated polyethylenimine oxide as an intracrystal porogen. The initial molecular weight of the polymer was 25 000, and silylation was carried out by reaction with (3-glycidoxypropyl)trimethoxysilane at a Si/NH molar ratio of 1.0:5.0. Included for comparison are the isotherms for ZSM-5 zeolite prepared under equivalent conditions in absence of the silylated porogen.

incorporated polymer becomes phase-segregated from the zeolite matrix, forming an intracrystal polymer network that is covalently linked to the zeolite framework. Calcination of the composite crystals removes the polymer porogen and forms a zeolite with uniform intracrystal mesopores.

Verification of the above synthetic scheme was obtained using a silane-fuctionalized polyethylenimine as the mesoporogen for the preparation of mesoporous forms of zeolite ZSM-5. The silylated polymer, formed from the reaction of (3-glycidoxypropyl)trimethoxysilane and polyethylenimine PEI at a Si/NH ratio of 0.20, was combined with tetraethylorthosilicate and aluminum tri-*sec*-butoxide to form a reaction mixture with the molar oxide composition $1.00\,Al_2O_3{:}100\,SiO_2{:}18.5\,[TPA]_2O{:}2000\,H_2O{:}10\,SiO_2$ as silylated PEI. Digestion of the mixture at 150 °C, followed by calcination at 600 °C to remove both the framework template and the mesoporogen yielded the final mesoporous zeolite, denoted MSU-MFI.

Figure 1 provides the nitrogen adsorption/desorption isotherms for a representative mesoporous ZSM-5 made from a silylated form of PEI with an initial molecular weight of 25 000. Included for comparison are the isotherms for conventional ZSM-5 prepared under equivalent conditions in the absence of silylated polymer. The near-linear uptake of nitrogen by MSU-MFI over the range $P/P_0 = 0.10$ to 0.60 is indicative of the presence of small mesopores. The conventional form of MFI lacks this adsorption feature. Direct evidence for the presence of intracrystal mesopores is provided by the TEM images shown in Figure 2 for whole-particle and thin-sectioned specimens. Each particle is permeated by randomly oriented small mesopores of nearly the same size. Higher resolution images reveal lattice fringes that extend over the entire particle, thus indicating that each particle is a single crystal and not an aggregate of nanocrystals.

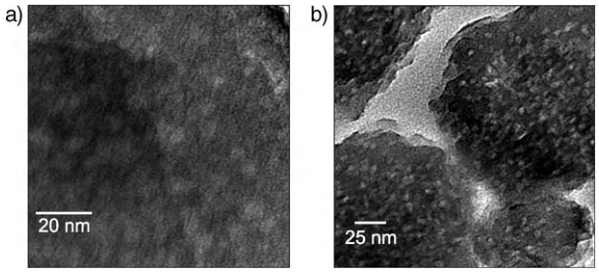

Figure 2. TEM images of the MSU-MFI zeolite prepared in the presence of silylated polyethylenimine with an initial molecular weight of 25 000: a) whole-particle specimen; b) thin-sectioned sample. The light contrast areas are intracrystal mesopores.

Figure 3 provides the mesopore size distributions and corresponding mesopore volumes for MSU-MFI zeolites prepared in the presence of PEI polymers with initial molecular weights of 600, 1800, and 25 000. For each derivative, the pore size distribution is confined to values below 8 nm, and the distribution of pores is centered between 2.0 and 3.0 nm with a width at half maximum less than 1.5 nm. These mesopore size distributions, which are in the range anticipated for selective polymer cracking, are unprecedented among all previously reported mesoporous forms of ZSM-5 or any other zeolite structure type. Also, the corresponding mesopore volumes for these new ZSM-5 derivatives (0.07–0.11 cm^3g^{-1}) compare favorably with the micropore volume of the zeolite framework (0.12 cm^3g^{-1}).

 © 2006 Wiley-VCH Verlag GmbH & Co. KGaA, Weinheim

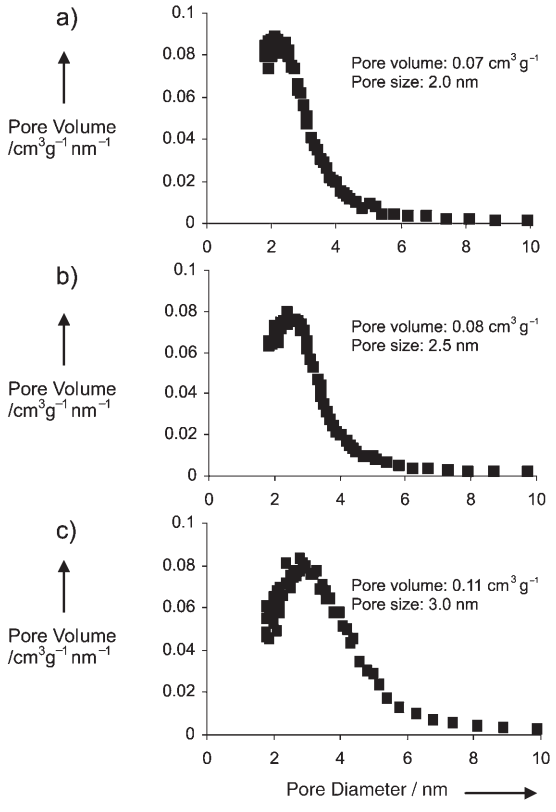

Figure 3. BJH mesopore size distributions, obtained from nitrogen adsorption isotherms, for MSU-MFI zeolites prepared from polyethylenimine polymers with initial molecular weights of a) 600, b) 1800, and c) 25 000. For each silylated porogen the Si/N ratio was 1.0:5.0. The mesopore volumes are reported for the corresponding mesopore size distributions.

The 50% increase in average mesopore size observed upon increasing the polyethylenimine molecular weight from 600 to 25 000 is substantially lower than the approximately 3.4-fold increase expected for a 40-fold increase in polymer molecular weight. This latter observation indicates the zeolite matrix greatly alters the solvation and conformation of the phase-segregated polymer embedded in the crystal. Further evidence for confinement effects on the polymer is provided by a comparison of the hydrodynamic radius of the free polymer with the pore sizes of the templated material. For example, the hydrodynamic radius of polyethylenimine with molecular weight of 25 000 is around 6.6 nm,[16] whereas the average radius of the mesopores templated by the silylated form of this polymer is about 1.5 nm.

Non-silylated forms of polyethylenimine do not inhibit zeolite nucleation nor do they act as intracrystal mesoporogens. Thus, silylation is essential for effective incorporation of the polymer into a growing zeolite matrix. However, also the degree of polymer silylation is important in forming intracrystal mesopores. For example, silylated polyethylenimines formed from a Si/NH ratio of 1:1 in the reaction mixture are ineffective in templating intracrystal mesopores. Instead, fully silylated PEI derivatives limit crystal growth to the sub-micrometer size domain, thus giving rise to zeolites with interparticle mesopores far larger than the intracrystal mesopores formed at a Si/NH ratio of 1.0:5.0 in the reaction mixture. Even simple organosilanes of the type $RSi(OR)_3$ are known to limit the growth of zeolites crystals,[17] but none have resulted in zeolites with intracrystal mesopores.

Finally, our molecular approach to the formation of zeolites with small and uniform mesopores is not limited to MFI framework structures. We have been successful in forming intracrystal mesopores also in FAU frameworks, particularly zeolite Y, which also is an important zeolite for the catalytic cracking of large polymers. Further, other forms of silylated polymers are showing promise as intracrystal mesoporogens in zeolite synthesis, thus indicating that our approach is quite general and not limited to one zeolite structure type nor to one type of silylated polymer.

Experimental Section

The silylated polymer was formed by reaction of (3-glycidoxypropyl)trimethoxysilane with polyethylenimine PEI at a Si/NH ratio of 0.20. The epoxide ring opening and the formation of hydrolytically stable C–N bonds was completed within 24 h at 80 °C. The transparent polymer gel was evacuated under vacuum to remove ethanol and then stored in a sealed vial to prevent hydrolysis of the Si-OCH_3 groups in the polymer. The silylated polymer in tetrapropylammonium hydroxide solution was combined with tetraethylorthosilicate and aluminum tri-*sec*-butoxide to form a reaction mixture with the molar oxide composition $1.00\,Al_2O_3$:100 SiO_2:18.5 $[TPA]_2O$:2000 H_2O:10 SiO_2 as silylated PEI. The mixture was heated at 150 °C for 48 h to form the zeolite–silylated PEI composite. ^{29}Si MAS NMR spectroscopy verified the presence of Q^4 SiO_4 groups characteristic of the zeolite lattice (100–120 ppm) and of T^3 and T^2 SiO_3 moieties indicative of silylated PEI (65–75 ppm). Essentially all the silylated polymer was incorporated into the zeolites matrix, as judged from the relative intensities of the Q and T resonances.

Received: June 29, 2006
Published online: October 17, 2006

Keywords: mesoporous materials · templating methods · zeolites

[1] A. Corma, *Chem. Rev.* **1997**, *97*, 2373–2420.
[2] G. Reding, T. Maurer, B. Kraushaar-Czarnetzki, *Microporous Mesoporous Mater.* **2003**, *57*, 83–92.
[3] S. Mintova, N. H. Olson, J. Senker, T. Bein, *Angew. Chem.* **2002**, *114*, 2670–2673; *Angew. Chem. Int. Ed.* **2002**, *41*, 2558–2561.
[4] C. E. A. Kirschhock, V. Buschmann, S. Kremer, R. Ravishankar, C. J. Y. Houssin, B. L. Mojet, R. A. van Santen, P. J. Grobet, P. A. Jacobs, J. A. Martens, *Angew. Chem.* **2001**, *113*, 2707–2710; *Angew. Chem. Int. Ed.* **2001**, *40*, 2637–2640.
[5] I. Schmidt, C. Madsen, C. J. H. Jacobsen, *Inorg. Chem.* **2000**, *39*, 2279–2283.
[6] D. On, S. Kaliaguine, *Angew. Chem.* **2001**, *113*, 3348–3351; *Angew. Chem. Int. Ed.* **2001**, *40*, 3248–3251.
[7] S. S. Kim, J. Shah, T. J. Pinnavaia, *Chem. Mater.* **2003**, *15*, 1664–1668.
[8] M. J. Verhoef, P. J. Kooyman, J. C. van der Waal, M. S. Rigutto, J. A. Peters, H. van Bekkuum, *Chem. Mater.* **2001**, *13*, 683–687.
[9] C. J. H. Jacobsen, C. Madsen, J. Houzvicka, I. Schmidt, A. Carlsson, *J. Am. Chem. Soc.* **2000**, *122*, 7116–7117.
[10] A. H. Janssen, I. Schmidt, C. J. H. Jacobsen, A. J. Koster, K. P. de Jong, *Microporous Mesoporous Mater.* **2003**, *65*, 59–75.

 © 2006 Wiley-VCH Verlag GmbH & Co. KGaA, Weinheim

[11] I. Schmidt, A. Boisen, E. Gustavsson, K. Stahl, S. Pehrson, S. Dahl, A. Carlsson, C. J. H. Jacobsen, *Chem. Mater.* **2001**, *13*, 4416 – 4418.
[12] Y. Tao, H. Kanoh, K. Kaneko, *J. Am. Chem. Soc.* **2003**, *125*, 6044 – 6045.
[13] F. Xiao, L. Wang, C. Yin, K. Lin, Y. Di, J. Li, R. Xu, D. S. Su, R. Schlogl, T. Yokoi, T. Tatsumi, *Angew. Chem.* **2006**, *118*, 3162 – 3165; *Angew. Chem. Int. Ed.* **2006**, *45*, 3090 – 3093.
[14] J. Aguao, J. L. Sotelo, D. P. Serrano, J. A. Calles, J. M. Escola, *Energy Fuels* **1997**, *11*, 1225 – 1231.
[15] S. van Donk, A. H. Janssen, J. H. Bitter, K. P. de Jong, *Catal. Rev.* **2003**, *45*, 297 – 319.
[16] M. M. Andersson, R. Hatti-Kaul, W. Brown, *J. Phys. Chem. B* **2000**, *104*, 3660 – 3667.
[17] D. P. Serrano, J. Aguado, J. M. Escola, J. M. Rodriguez, A. Peral, *Chem. Mater.* **2006**, *18*, 2462 – 2464.

 © 2006 Wiley-VCH Verlag GmbH & Co. KGaA, Weinheim

Asymmetric Catalysis

DOI: 10.1002/anie.200602787

Highly Diastereo- and Enantioselective Formal Conjugate Addition of Nitroalkanes to Nitroalkenes by Chiral Ammonium Bifluoride Catalysis**

*Takashi Ooi, Saki Takada, Kanae Doda, and Keiji Maruoka**

The conjugate addition of reactive nucleophiles to electron-deficient alkenes (the Michael addition reaction) is an important and reliable tool for the construction of highly functionalized carbon skeletons. Among the various candidates for this bond-forming process, nitro compounds are particularly attractive because of the strong electron-withdrawing property of the nitro group and their versatility as a masked functionality.[1] Indeed, it is well documented that nitroalkenes serve as excellent Michael acceptors[2] and the anions of nitroalkanes (nitronates) as prominent Michael donors.[3] Surprisingly, however, despite its potential use for the synthesis of optically active 1,3-diamines, carbon–carbon coupling between nitroalkanes and nitroalkenes is extremely rare,[4] and catalytic enantioselective systems have so far been limited to the recent contribution reported by Du and co-workers[5]. This is partly because of the inherent difficulty of controlling the addition of nitronate **3** to nitroalkene **4**. The initial product formed is the nitronate **5**, which is sufficiently reactive to also undergo conjugate addition to **4**, thus resulting in a mixture of oligomerization products [Eq. 1].

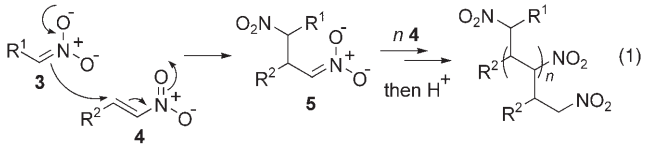

Our strategy toward overcoming this methodological deficiency involves the use of chiral ammonium bifluoride catalysis in combination with silyl nitronates (**6**, Scheme 1).[6] The chiral ammonium nitronate **8**, generated in situ from **6**, and chiral ammonium bifluoride of type **1**[7] or **2** would be responsible for controlling the relative and absolute stereochemistry in the addition to the nitroalkene **4**, to afford the corresponding chiral nitronate **9** of the stereochemically defined conjugate adduct. If the reaction of **9** with residual **6** is

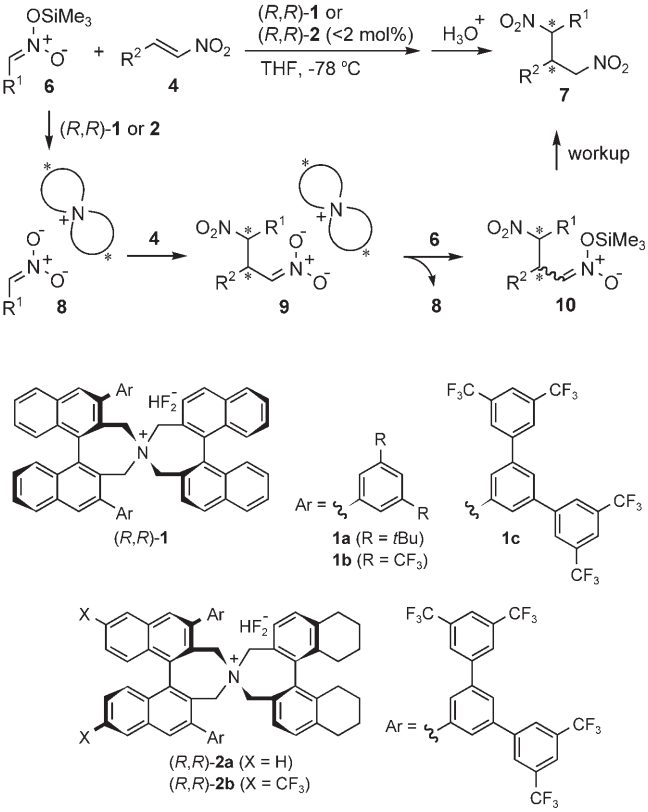

Scheme 1. Selective conjugate addition of silyl nitronates to nitroalkenes under chiral ammonium bifluoride catalysis.

[*] Dr. T. Ooi,[+] S. Takada, K. Doda, Prof. K. Maruoka
Department of Chemistry
Graduate School of Science
Kyoto University
Sakyo, Kyoto, 606-8502 (Japan)
Fax: (+81) 75-753-4041
E-mail: maruoka@kuchem.kyoto-u.ac.jp

[+] Current address:
Department of Applied Chemistry
Graduate School of Engineering
Nagoya University
Chikusa, Nagoya, 464-8603 (Japan)

[**] This work was partially supported by a Grant-in-Aid for Scientific Research on Priority Areas "Advanced Molecular Transformation of Carbon Resources" from the Ministry of Education, Culture, Sports, Science, and Technology, Japan.

Supporting information for this article is available on the WWW under http://www.angewandte.org or from the author.

InterScience
© 2006 Wiley-VCH Verlag GmbH & Co. KGaA, Weinheim

faster than its further addition to **4**, the requisite chiral nucleophile **8** would be regenerated along with derivatization of the desired product **7** as the silyl nitronate **10**. This process would thereby allow the asymmetric formal conjugate addition of nitroalkanes to nitroalkenes with ideal stoichiometry. Herein, we describe the realization of this hypothesis by using the N-spiro C_2-symmetric chiral quaternary ammonium bifluoride **2b**.

We began our studies by examining the reaction of nitropropane-derived silyl nitronate **6a** with β-nitrostyrene (**4a**) using the chiral quaternary ammonium bifluoride **1a**.[7b,c] When **4a** was treated with **6a** (1.2 equiv) in the presence of **1a** (2 mol%) in toluene (0.1M substrate concentration) at −78°C, an almost instantaneous consumption of **4a** was observed along with the formation of totally insoluble white precipitate, and the one-to-one adduct **7a** was isolated in only 7% yield. This finding implied the predominant intervention of the rapid oligomerization process under the reaction conditions. However, we were encouraged by the fact that **7a** thus obtained was diastereomerically homogeneous and it was determined to have 58% *ee* (entry 1, Table 1). We next screened reaction variables and found initially that switching the solvent to THF under otherwise similar conditions significantly augmented the desired pathway to furnish **7a** in 73% yield, although the enantioselectivity decreased to 29% *ee* (entry 2, Table 1). On the basis of this result, we evaluated the effect of the catalyst structure mainly on the enantioselectivity. Although the electron-withdrawing 3,5-bis(trifluoromethyl)phenyl-substituted **1b**[7a,b] exhibited comparable chiral efficiency to that of **1a**, modification of the 3,3′-aromatic substituent to the *meta*-terphenyl-type structure **1c**[7] led to a dramatic improvement in selectivity (entries 3 and 4, Table 1). Furthermore, we assembled the chiral ammonium bifluoride **2a**, which consisted of a chiral octahydrobinaphthyl subunit, with the expectation that its steric and electronic effects would help control stereoselectivity. Fortunately, the conjugate addition of **6a** to **4a** proceeded smoothly under the influence of **2a** in a highly diastereoselective manner, affording *syn*-**7a** in 78% yield with 89% *ee* (entry 5, Table 1). Moreover, introduction of a trifluoromethyl group in the 6,6′ position of the binaphthyl core of **2b** delivered even higher enantioselectivity (91% *ee*, entry 6, Table 1).[8] Here, the use of two equivalents of silyl nitronate **6a** allowed near quantitative production of **7a**, and the slight erosion in enantiomeric excess was recovered by performing the reaction at a lower substrate concentration (entries 7 and 8, Table 1). It should be noted that the catalyst loading can be reduced to 0.5 mol% without substantial loss of reactivity and stereoselectivity (entries 9 and 10, Table 1).

Having established the optimized conditions,[9] the scope of the reaction was investigated using silyl nitronate **6a** and a variety of nitroalkenes (Table 2). With aromatic nitroalkenes, the reaction efficiency and diastereoselectivity were relatively insensitive to the electronic properties of the aromatic ring, although the presence of electron-withdrawing substituents seemed to be associated with slightly lower enantioselectivity (entries 1–4, Table 2). This protocol proved to be compatible with heteroaromatic nitro-

Table 1: Screening of the reaction variables in the conjugate addition reaction of silyl nitronate **6a** to β-nitrostyrene (**4a**), catalyzed by chiral quaternary ammonium bifluoride.[a]

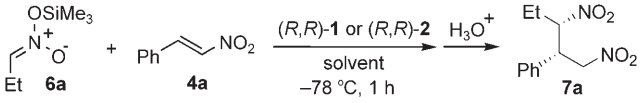

Entry	**6a** (equiv)	Catalyst	mol%	Solvent	Conc. [M]	Yield [%][b]	[%] *ee*[c]
1	1.2	(*R*,*R*)-**1a**	2	toluene	0.1	7	58
2		(*R*,*R*)-**1a**		THF		73	29
3		(*R*,*R*)-**1b**				67	32
4		(*R*,*R*)-**1c**				80	80
5		(*R*,*R*)-**2a**				78	89
6		(*R*,*R*)-**2b**				85	91
7	2.0	(*R*,*R*)-**2b**				97	85
8		(*R*,*R*)-**2b**			0.04	97	91
9		(*R*,*R*)-**2b**	1			99	90
10		(*R*,*R*)-**2b**	0.5			86	90

[a] The reaction was carried out at −78°C for 1 h using (*R*,*R*)-**1** or (*R*,*R*)-**2** as catalyst. [b] Yield of isolated product. The ratio *syn*/*anti* was determined by ^{1}H NMR analysis to be >95:5, which means that the minor isomer could not be detected by NMR analysis (the authentic sample of *anti* isomer was prepared by a literature procedure[4a]). [c] The enantiopurity of **7a** was determined by HPLC analysis on a chiral stationary phase using hexane-2-propanol as the solvent. The relative and absolute configurations were assigned by ^{1}H NMR analysis after derivatization to the corresponding cyclic thiourea and diamide compounds. For further details, see the Supporting Information.

Table 2: Stereoselective conjugate addition of silyl nitronates **6** to nitroalkenes **4** catalyzed by chiral quaternary ammonium bifluoride (*R*,*R*)-**2b**.[a]

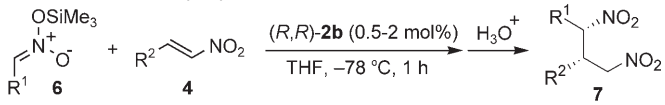

Entry	R^1 (**6**)	R^2 (**4**)	(*R*,*R*)-**2b** [mol%]	Yield [%][b]	*syn*/*anti*[c]	*ee* [%] [d]	Prod.
1	Et (**6a**)	*p*-MeO-C_6H_4	1	99	>95:5	91	**7b**
2		*o*-MeO-C_6H_4	0.5	99	>95:5	87	**7c**
3		*o*-Cl-C_6H_4	0.5	98	>95:5	80	**7d**
4		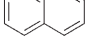	0.5	95	>95:5	89	**7e**
5			2	92	>95:5	93	**7f**
6			2	85	>95:5	91	**7g**
7		*c*-Hex	1	99	>95:5	92	**7h**
8		$CH_3(CH_2)_5$	1	93	>95:5	76	**7i**
9	Pr (**6b**)	Ph	1	99	>95:5	91	**7j**
10	$MeOCH_2$ (**6c**)	Ph	1	99	82:18	83	**7k**

[a] The reaction was carried out using 2 equiv of silyl nitronate **6** in the presence of (*R*,*R*)-**2b** in THF (0.04M substrate concentration) at −78°C for 1 h. [b] Yield of isolated product. [c] Determined by ^{1}H NMR analysis. [d] The enantiopurity of major product *syn*-**7** was determined by HPLC analysis on a chiral stationary phase using hexane-2-propanol or ethanol as the solvent. *c*-Hex = cyclohexyl.

© 2006 Wiley-VCH Verlag GmbH & Co. KGaA, Weinheim

alkenes and the corresponding 1,3-dinitro compounds were obtained in high yield with excellent diastereo- and enantioselectivities by employing 2 mol% of **2b** (entries 5 and 6, Table 2). Aliphatic nitroalkenes also appeared to be good acceptors, further expanding the generality of the substrates (entries 7 and 8, Table 2). The present method was applicable to other silyl nitronates derived from simple nitroalkanes, where eminent catalytic activity and a high level of stereoselectivity were attained (entries 9 and 10, Table 2).

The resulting 1,3-dinitro compounds with two consecutive stereochemically defined stereocenters can be readily converted into the corresponding 1,3-diamines, which are versatile chiral building blocks from synthetic as well as pharmaceutical viewpoints.[10] For example, exposure of a mixture of **7a** in THF to a hydrogen atmosphere in the presence of a catalytic amount of Raney Nickel at 45 °C for 36 h resulted in the formation of **11** in 75% yield with complete preservation of the stereochemical integrity (Scheme 2).[11]

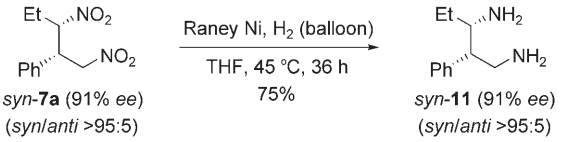

syn-**7a** (91% *ee*) (*syn*/*anti* >95:5)

syn-**11** (91% *ee*) (*syn*/*anti* >95:5)

Scheme 2. Derivatization of 1,3-dinitroalkane *syn*-**7a** into the corresponding 1,3-diamine *syn*-**11**.

In conclusion, we have achieved an efficient, highly diastereo- and enantioselective formal conjugate addition of nitroalkanes to nitroalkenes by the catalysis with the novel chiral quaternary ammonium bifluoride **2b** in combination with silyl nitronates. This strategy greatly expands the use of conjugate addition chemistry involving organonitro compounds and provides a reliable route to optically active 1,3-dinitro compounds, which are synthetically useful intermediates for a wide range of valuable 1,3-difunctionalized organic molecules.

Received: July 13, 2006
Published online: October 18, 2006

Keywords: 1,3-dinitro compounds · asymmetric catalysis · C—C coupling · conjugate addition · homogeneous catalysis

[1] a) N. Ono, *The Nitro Group in Organic Synthesis*, Wiley-VCH, New York, **2001**, chaps. 4 and 6; for a recent example of facile transformations of optically active organonitro compounds, see: b) C. Czekelius, E. M. Carreira, *Angew. Chem.* **2005**, *117*, 618; *Angew. Chem. Int. Ed.* **2005**, *44*, 612.

[2] a) O. M. Berner, L. Tedeschi, D. Enders, *Eur. J. Org. Chem.* **2002**, 1877; for recent examples, see: b) D. J. Dixon, R. D. Richardson, *Synlett* **2006**, 81; c) S. B. Tsogoeva, S. Wei, *Chem. Commun.* **2006**, 1451; d) M. Terada, H. Ube, Y. Yaguchi, *J. Am. Chem. Soc.* **2006**, *128*, 1454; e) P. J. Nichols, J. A. DeMattei, B. R. Barnett, N. A. LeFur, T.-H. Chuang, A. D. Piscopio, K. Koch, *Org. Lett.* **2006**, *8*, 1495; f) H. Huang, E. N. Jacobsen, *J. Am. Chem. Soc.* **2006**, *128*, 7170, and references therein.

[3] a) M. Yamaguchi in *Comprehensive Asymmetric Catalysis*, *Vol. 3* (Eds.: E. N. Jacobsen, A. Pfaltz, H. Yamamoto), Springer, Berlin, **1999**, chap. 31.2; b) M. Yamaguchi in *Comprehensive Asymmetric Catalysis Supplement 1* (Eds.: E. N. Jacobsen, A. Pfaltz, H. Yamamoto), Springer, Berlin, **2004**, p. 151; c) R. Ballini, G. Bosica, D. Fiorini, A. Palmieri, M. Petrini, *Chem. Rev.* **2005**, *105*, 933.

[4] For a few examples of non-stereoselective reactions, see: a) M. D. Alcántara, F. C. Escribano, A. Gómez-Sánchez, M. J. Diánez, M. D. Estrada, A. López-Castro, S. Pérez-Garrido, *Synthesis* **1996**, 64; b) R. Ballini, G. Bosica, D. Fiorini, A. Palmieri, *Synthesis* **2004**, 1938.

[5] S.-F. Lu, D.-M. Du, J. Xu, S.-W. Zhang, *J. Am. Chem. Soc.* **2006**, *128*, 7418.

[6] For an account of chiral ammonium fluoride catalysis, see: T. Ooi, K. Maruoka, *Acc. Chem. Res.* **2004**, *37*, 526.

[7] a) T. Ooi, K. Doda, K. Maruoka, *J. Am. Chem. Soc.* **2003**, *125*, 2054; b) T. Ooi, K. Doda, K. Maruoka, *J. Am. Chem. Soc.* **2003**, *125*, 9022; c) T. Ooi, K. Doda, S. Takada, K. Maruoka, *Tetrahedron Lett.* **2006**, *47*, 145.

[8] When the reaction was quenched with an excess amount of D_2O, approximately 60% of deuterium incorporation was observed at the C1 methylene center of *syn*-**7a**, thereby suggesting the intervention of a silyl nitronate intermediate of type **10**. We assume that the low deuterium incorporation could be ascribed to the high susceptibility of the silyl nitronate, generated in situ, to protonation from a small amount of water or methanol.

[9] Although 1.2 equiv of silyl nitronate **6** seemed to be sufficient, we decided to use 2 equiv of **6** at 0.04 M substrate concentration for further investigations to constantly attain excellent yields.

[10] For selected examples, see: a) C. F. Bigge, J.-P. Wu, J. T. Drummond, *Bioorg. Med. Chem. Lett.* **1992**, *2*, 207; b) G. H. P. Roos, A. R. Donovan, *Tetrahedron: Asymmetry* **1999**, *10*, 991; c) S. E. Denmark, J.-H. Kim, *Can. J. Chem.* **2000**, *78*, 673; d) M. M. Kabat, *Tetrahedron Lett.* **2001**, *42*, 7521; e) F. Cohen, L. E. Overman, *J. Am. Chem. Soc.* **2001**, *123*, 10782.

[11] The *ee* value of *syn*-**11** was confirmed by HPLC analysis after derivatization to the corresponding cyclic thiourea. See the Supporting Information.

 © 2006 Wiley-VCH Verlag GmbH & Co. KGaA, Weinheim

Natural Products Synthesis

DOI: 10.1002/anie.200603097

Total Synthesis of (±)-Quadrangularin A**

*Wenling Li, Hao Li, Ying Li, and Zijie Hou**

Pais and co-workers isolated (−)-quadrangularin A (**1**) from the stem of *Cissus quadrangularis* in 1999.[1] Several analogues of **1**, compounds **2**–**6**, have been obtained from other plants (Scheme 1).[1,2] These molecules are all dimers or substituted dimers of resveratrol (**7**) with an indane skeleton. To date, no synthetic effort towards this family of compounds has been reported. Although cyclodimerizations of stilbene under acidic conditions to form indanes and/or tetralins have been studied extensively,[3] this strategy is not generally applicable to the synthesis of natural oligostilbenes owning to poor stereoselectivity and the limitation to stilbene substrates. Therefore, it remained a significant challenge for chemists to develop new strategies for the synthesis of these compounds. As part of a program to study the biomimetic synthesis of stilbene oligomers,[4] we report herein an approach to the synthesis of compound **1** based on regioselective oxidative coupling.

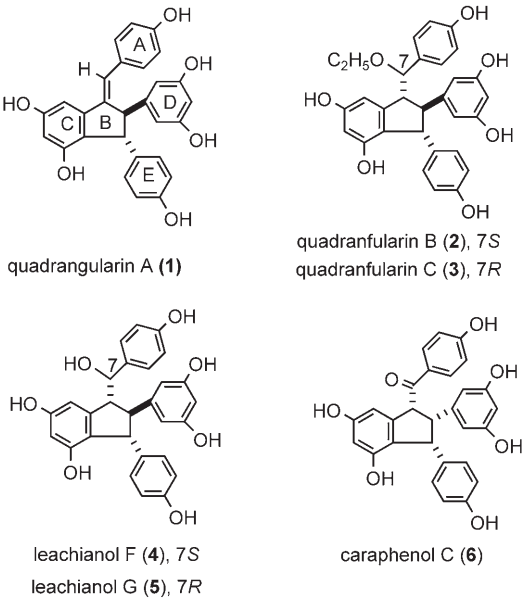

Scheme 1. Quadrangularin A (**1**) and analogues **2**–**6**.

To design a synthetic route to **1**, it is essential to understand the possible biosynthetic mechanism for the dimerization of **7** in vivo. At least three important mesomers, M_5, M_8, and M_{10}, have been identified as being derived from **7** under enzymatic catalysis in the organism.[5] Coupling reactions between these radical mesomers could produce various resveratrol dimers, such as the natural products **1**, **8**, and **9** (Scheme 2). The structural complexity of the oligomers results from the diversity of the coupling modes, which also increases the difficulty of their regiocontrolled biomimetic synthesis in vitro.

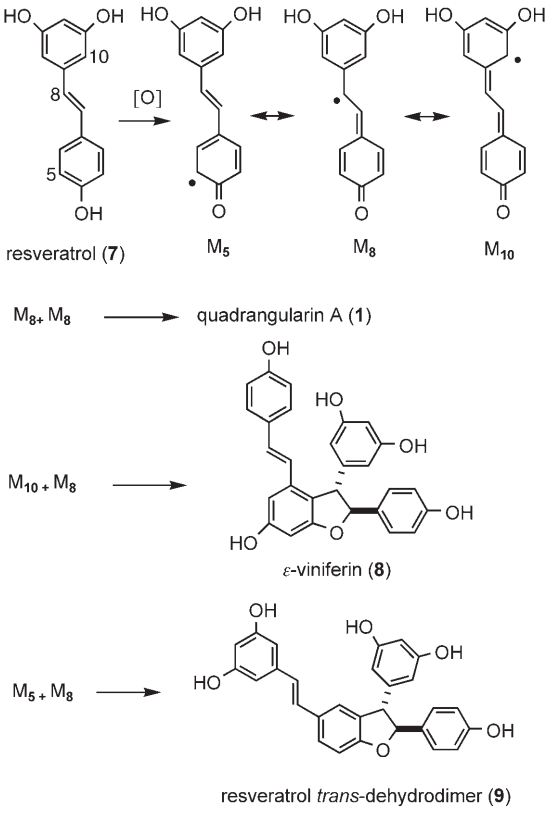

Scheme 2. Possible biosynthetic pathways of resveratrol dimers.

Resveratrol oligomers have novel structures and a wide range of biological activity but low natural abundance; therefore, many chemists have studied the oxidative coupling of resveratrol under a variety of conditions since ε-viniferin (**8**) was first isolated in 1977 by Langcake and Pryce.[6] However, the major product obtained was mostly the 5–8-coupling product, that is, resveratrol *trans*-dehydrodimer (**9**), regardless of whether enzymes (peroxidase[7] or laccase[8]) or inorganic oxidants ($FeCl_3$, $K_3(FeCN)_6$, or Ag_2O) were used.[9] Thus, we deduced that the 5–8-coupling mode occurs predominantly and that its product **9** is stable under the oxidative conditions employed. We believed that the critical step for the synthesis of the 8–8-coupling product **1** could be

[*] W. Li, H. Li, Prof. Y. Li, Prof. Z. Hou
State Key Laboratory of Applied Organic Chemistry and
Department of Chemistry
Lanzhou University
222 Tianshui Street S., Lanzhou 730000 (P.R. China)
Fax: (+86) 931-891-2582
E-mail: houzj@lzu.edu.cn
W. Li
Department of Chemical and Biological Engineering
Lanzhou Railway University
Lanzhou 730000 (P.R. China)

[**] We are grateful to Prof. H.-L. Zhang and Dr. J.-C. Liao for helpful discussions.

Supporting information for this article is available on the WWW under http://www.angewandte.org or from the author.

 © 2006 Wiley-VCH Verlag GmbH & Co. KGaA, Weinheim

made possible by impeding the formation of the 5–8-coupling product **9**.

Enlightened by the work of Sarkanen and Wallis, who found that the presence of non-hydrogen substituents (OMe or *tert*-butyl) adjacent to the phenolic hydroxy group of some phenylpropanoids hindered the undesired 5–8 and 8–O coupling and greatly enhanced the chance of the 8–8 coupling (Scheme 3),[10] we decided to introduce *tert*-butyl protecting groups at C3 and C5 of resveratrol to favor a regioselective coupling reaction. The advantage of this method is that *tert*-butyl substituents can be conveniently incorporated into and efficiently removed from aromatic substrates.[11] Thus, the synthetic route to **1** was designed and carried as shown in Scheme 4.

The coupling precursor 3,5-di-(*tert*-butyl)resveratrol (**17**) was prepared in seven steps from 3,5-dihydroxybenzoic acid (**10**). First, the dibenzyl alcohol **11** was made from **10** through a straightforward three-step sequence of esterification, benzyl protection, and reduction.[12] Compound **11** was then converted into the dibenzyl chloride **12**,[13] and **12** was transformed into the phosphonium salt **13**. To form the second substrate for the planned olefination, **14** was oxidized with Br_2 in *tert*-butanol to produce the aldehyde **15**.[14] A Wittig reaction between **13** and **15** in toluene at reflux afforded the *E* stilbene **16** in good yield; it was not necessary to protect the phenolic hydroxy group of **15**. Finally, the benzyl protecting groups were removed[4] from **16** to give the coupling precursor **17** in 53% overall yield.

Next, the treatment of **17** with horseradish peroxidase (HRP) and H_2O_2[15] in aqueous acetone at room temperature under an argon atmosphere for 48 h gave the 8–8-coupling product **18** in 35% yield. This result validated our original hypothesis. It was noted that the prolonged reaction time or the large amount of H_2O_2 used resulted in the formation of minor trimeric products.[16] The structure of **18** was established on the basis of HRMS, ^{1}H NMR, ^{13}C NMR, and 2D correlation NMR spectral data. The presence of a quinone methide moiety in **18** was supported by the existence of three mutually coupled signals corresponding to methine hydrogen atoms (8-H, 8′-H, 7′-H) and a signal corresponding to an olefinic hydrogen atom (7-H) in the ^{1}H NMR spectrum, as well as a signal corresponding to a carbonyl carbon atom (C4) in the ^{13}C NMR spectrum. The HMBC cross peaks of 7-H/C2, 8′-H/C10′,C1′,C7, and 7′-H/C9,C9′,C2′ further confirmed the positions of the aromatic rings on the indane moiety. Furthermore, the relative *trans* configuration of the three methine hydrogen atoms 8-H, 8′-H, and 7′-H was established by an NOE difference experiment, which showed NOE correlations at 8-H/10′-H and 7′-H/10′-H.

Finally, **18** underwent a prototropic rearrangement in the presence of Al_2O_3,[10] and the *tert*-butyl protecting groups were removed from the resulting compound **19**[11] to provide the target racemic product **1**. All spectral data of **1** were in good agreement with the data reported in the literature for the natural product.[1] The relative stereochemistry of **19** was also assigned by an NOE difference experiment. The key NOE correlation between 7-H and 14-H indicated an *E* configuration of the double bond, and NOE interactions

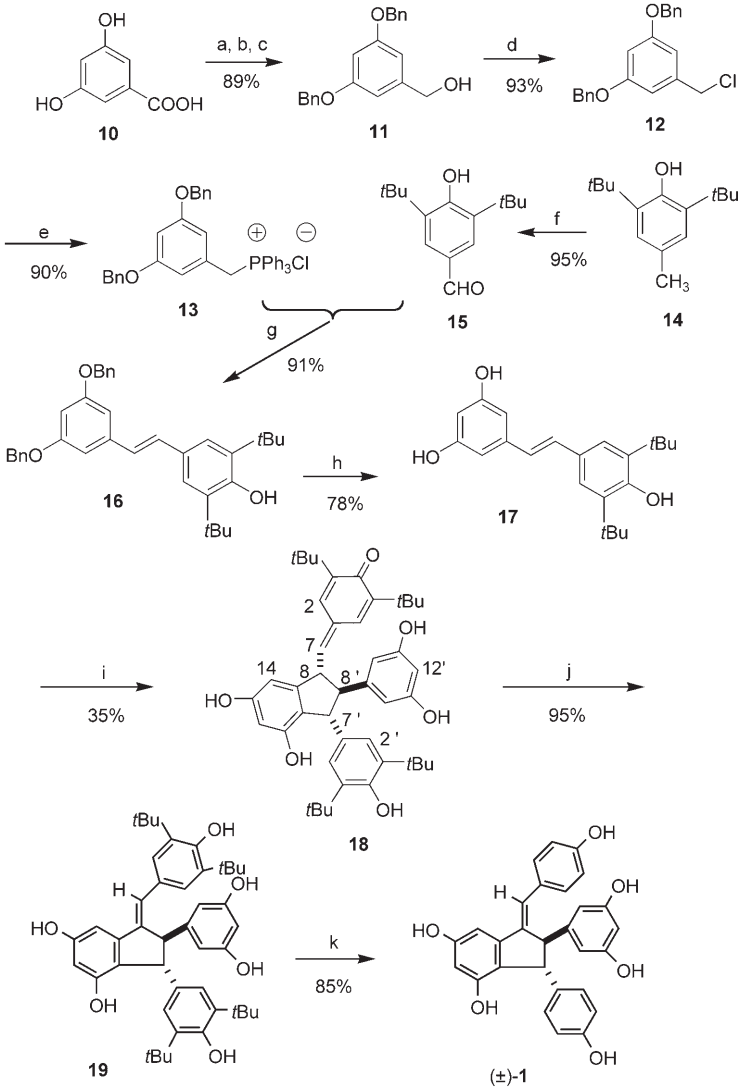

Scheme 4. Total synthesis of (±)-**1**. Reagents and conditions: a) CH_3OH, H_2SO_4, reflux; b) $PhCH_2Br$, K_2CO_3, DMF, RT; c) $LiAlH_4$, Et_2O, RT; d) $SOCl_2$, Et_3N, benzene, 0°C→RT; e) PPh_3, xylene, reflux; f) Br_2, *tert*-butanol, RT; g) *n*BuLi, toluene, RT→reflux; h) $AlCl_3$, $PhNMe_2$, CH_2Cl_2, 0°C; i) HRP/H_2O_2, acetone/water (3:1), RT; j) Al_2O_3, benzene, RT; k) $AlCl_3$, CH_3NO_2, toluene, 60°C. Bn = benzyl, DMF = *N*,*N*-dimethylformamide.

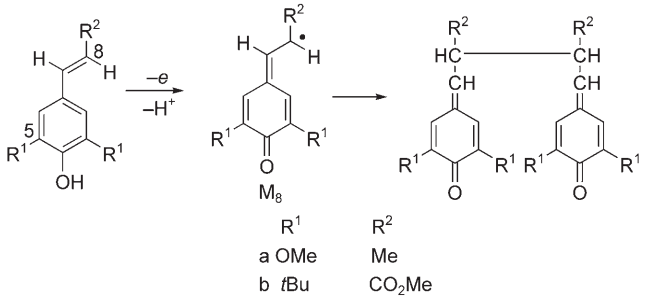

Scheme 3. Proposed coupling mechanism of some phenylpropanoids.

 © 2006 Wiley-VCH Verlag GmbH & Co. KGaA, Weinheim

at 8′-H/2′-H and 7′-H/10′-H suggested that rings D and E have a *trans* relationship.

In summary, we have completed the first total synthesis of (±)-quadrangularin A (**1**) in 11 steps and 15% overall yield from 3,5-dihydroxybenzoic acid (**10**). The key coupling reaction could be carried out regioselectively by introducing *tert*-butyl groups to protect alternative reactive positions in the coupling precursor. Most importantly, this strategy may be used as an efficient general method for the synthesis of other naturally occurring oligostilbenes. The application of this synthetic route to analogues of **1** is currently in progress in our laboratory.

Received: July 31, 2006
Published online: October 19, 2006

Keywords: biomimetic synthesis · natural products · oligostilbenes · oxidative coupling · total synthesis

[1] S. A. Adesanya, R. Nia, T. M. Martin, N. Boukamcha, A. Montagnac, M. Pais, *J. Nat. Prod.* **1999**, *62*, 1694.
[2] a) M. Ohyama, T. Tanaka, M. Iiuma, *Phytochemistry* **1995**, *38*, 73; b) H.-F. Luo, L.-P. Zhang, C.-Q. Hu, *Tetrahedron* **2001**, *57*, 4849.
[3] a) M. Hiscock, G. B. Porter, *J. Chem. Soc. Perkin Trans. 2* **1972**, 79; b) J. M. Aguirre, E. N. Alesso, *J. Chem. Soc. Perkin Trans. 1* **1999**, 1353.
[4] W.-L. Li, K.-K. He, Y. Li, Z.-J. Hou, *Acta Chim. Sin.* **2005**, *63*, 1607.
[5] X.-C. Li, D. Ferreira, *Tetrahedron* **2003**, *59*, 1501.
[6] P. Langcake, R. J. Pryce, *Experientia* **1977**, *33*, 151.
[7] a) P. Langcake, R. J. Pryce, *J. Chem. Soc. Chem. Commun.* **1977**, 208; b) Y. Hirano, R. Kondo, K. Sakai, *J. Wood Sci.* **2002**, *48*, 64; c) Y. Takaya, K. Terashima, J. Ito, Y.-H. He, M. Tateoka, N. Yamaguchi, M. Niwa, *Tetrahedron* **2005**, *61*, 10285.
[8] a) A. C. Breuil, M. Adrian, N. Pirio, P. Meunier, R. Bessis, P. Jeandet, *Tetrahedron Lett.* **1998**, *39*, 537; b) R. H. Cichewicz, S. A. Kouzi, M. T. Hamann, *J. Nat. Prod.* **2000**, *63*, 29; c) S. Nicotra, M. R. Cramarossa, A. Mucci, U. M. Pagnoni, S. Riva, L. Forti, *Tetrahedron* **2004**, *60*, 595.
[9] a) K.-S. Huang, M. Lin, Y.-H. Wang, *Chin. Chem. Lett.* **1999**, *10*, 817; b) M. Sako, H. Hosokawa, T. Ito, M. Iinuma, *J. Org. Chem.* **2004**, *69*, 2598; c) Y. Takaya, K. Terashima, J. Ito, Y.-H. He, M. Tateoka, N. Yamaguchi, M. Niwa, *Tetrahedron* **2005**, *61*, 10285.
[10] a) K. V. Sarkanen, A. F. A. Wallis, *J. Chem. Soc. Perkin Trans. 1* **1973**, 1869; b) K. V. Sarkanen, A. F. A. Wallis, *J. Chem. Soc. Perkin Trans. 1* **1973**, 1878.
[11] a) M. Tashiro, T. Itoh, H. Yoshiya, G. Fukata, *Org. Prep. Proced. Int.* **1984**, *16*, 155; b) G. Sartori, F. Bigi, R. Maggi, C. Porta, *Tetrahedron Lett.* **1994**, *35*, 7073; c) S. A. Saleh, H. L. Tashtoush, *Tetrahedron* **1998**, *54*, 14157.
[12] K. Thakkar, R. L. Geahlen, M. Cushman, *J. Med. Chem.* **1993**, *36*, 2950.
[13] M. M. Abelman, L. E. Overman, V. D. Tran, *J. Am. Chem. Soc.* **1990**, *112*, 6959.
[14] T. H. Coffield, A. H. Filbey, G. G. Ecke, A. J. Kolka, *J. Am. Chem. Soc.* **1957**, *79*, 5019.
[15] HRP is a heme-containing enzyme that catalyzes the oxidation of phenolic substrates; H_2O_2 serves as the ultimate electron acceptor; see: a) S. Kobayashi, H. Higashimura, *Prog. Polym. Sci.* **2003**, *28*, 1015, and references therein; b) D. M. X. Donelly, F. G. Murphy, *J. Chem. Soc. Perkin Trans. 1* **1987**, 2719; c) J. C. Pew, W. J. Connors, *J. Org. Chem.* **1969**, *34*, 580.
[16] In the enzyme-catalyzed coupling reaction of **17**, the 8–8-coupling product **18** reacted further with **17** to form two minor trimers **20** and **21** because of the prolonged reaction time or the large amount of H_2O_2 used. The structures of **20** and **21** were determined by 1D and 2D NMR spectroscopy.

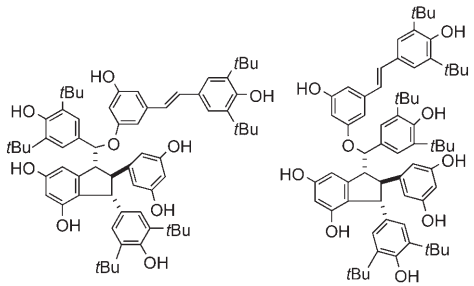

 © 2006 Wiley-VCH Verlag GmbH & Co. KGaA, Weinheim

Copper-Centered Oxidation

DOI: 10.1002/anie.200603127

Diamagnetic–Paramagnetic Conversion of Tris(2-pyridylthio)methylcopper(III) through a Structural Change from Trigonal Bipyramidal to Octahedral**

Ryoko Santo, Riichi Miyamoto, Rika Tanaka, Takanori Nishioka, Kazunobu Sato, Kazuo Toyota, Makoto Obata, Shigenobu Yano, Isamu Kinoshita, Akio Ichimura,* and Takeji Takui**

The coordination chemistry of copper(III) is of great importance for the understanding of dioxygen cleavage in enzymatic systems[1] and allyl cross-coupling reactions.[2] However,

[*] R. Santo, R. Miyamoto, Dr. R. Tanaka, Dr. T. Nishioka, Prof. Dr. K. Sato, Dr. K. Toyota, Prof. Dr. I. Kinoshita, Prof. Dr. A. Ichimura, Prof. Dr. T. Takui
Departments of Chemistry and Material Science
Graduate School of Science
Osaka City University
3-3-138 Sugimoto, Sumiyoshi-ku, Osaka, 558-8585 (Japan)
Fax: (+81) 6-6605-2553
E-mail: isamu@sci.osaka-cu.ac.jp
ichimura@sci.osaka-cu.ac.jp
takui@sci.osaka-cu.ac.jp
Dr. M. Obata, Prof. Dr. S. Yano
Division of Material Science
Graduate School of Human Culture
Nara Women's University
Kitauoyanishimachi, Nara, 630-8506 (Japan)

[**] This work was supported financially by a Sasagawa Scientific Research Grant from the Japan Science Society and Grants-in-Aid for Scientific Research from the Ministry of Education, Culture, Sports, Science and Technology (no. 18350033 and area no. 769, no. 15087209). The X-ray absorption spectral study was performed with the approval of the Photon Factory Program Advisory Committee (proposal no. 2004G290).

Supporting Information for this article is available on the WWW under http://www.angewandte.org or from the author.

 © 2006 Wiley-VCH Verlag GmbH & Co. KGaA, Weinheim

there are still only a few examples of structurally characterized Cu^{III} complexes,[3] most of which have a square-planar structure. The Cu^{III} state is stabilized by strong coordinating ligands, and its complexes have been isolated as carboxylates,[4] thiolates,[5] deprotonated amides,[6] carbamates,[7] and N-confused porphyrins.[8] The Cu–C(sp^2) bonds in the N-confused porphyrins are stabilized by the π-delocalization effect in the porphyrin ring aided by protonation–deprotonation of the peripheral nitrogen atoms.[8] Nonplanar Cu^{III} complexes are rare, and only a few structures have been reported,[3] namely square-pyramidal $[Cu(PhCO_2)_2(pyridine)_2Cl]$[9] and an octahedral moiety in a $Co^{III}Cu^{III}Co^{III}$ heterometallic cluster bridged by 1,4,7-tris(4-*tert*-butyl-2-sulfidobenzyl)-1,4,7-triazacyclononane.[10]

Herein, we report the synthesis and electronic properties of a Cu^{III} complex with a trigonal-bipyramidal (tbp) structure. This is the first report of a tbp Cu^{III} complex that has been structurally and spectroscopically well defined. We also report the diamagnetic–paramagnetic conversion of the Cu^{III} complex which accompanies a change from a trigonal-bipyramidal to an octahedral structure.

We have reported the complexes $[Cu^{II}(tptm)X]$ (tptm = tris(2-pyridylthio)methanide; X = F, Cl, Br, I), which have a novel Cu^{II}–C(sp^3) bond and a tbp structure.[11] These complexes show a highly reversible one-electron oxidation process at around +0.1 V versus the redox potential of ferrocenium/ferrocene, $E^{o\prime}(Fc^+/Fc)$, in CH_2Cl_2.[11a] These electrochemical results suggested that the one-electron-oxidized complexes retain their tbp structures in the Cu^{III} state, as predicted by density functional theory (DFT) calculations.[11a] The oxidation of $[Cu^{II}(tptm)Cl]$ (**1**) with one equivalent of $[Ce^{IV}(NH_4)_2(NO_3)_6]$ in the presence of KPF_6 produces the stable complex $[Cu^{III}(tptm)Cl]PF_6$ (**2**-PF_6), which was crystallized from CH_2Cl_2/cyclohexane. The crystal structure of this complex is shown in Figure 1. The asymmetric unit of **2**-PF_6 contains an independent complex cation. There are four independent complex molecules in the asymmetric unit of the crystal of **1**. These have a similar structure, with only small deviations of the bond parameters due to the crystal packing (See Supporting Information for selected bond lengths and angles).[12] Both complexes **1** and **2** have a tbp geometry with relatively little distortion. The Cu–Cl bond lengths in **2** are 0.05–0.06 Å shorter than those in **1**. The Cu–N bond lengths also shrink, from 2.074(7)–2.142(7) Å in **1** to 2.028(3)–2.074(3) Å in **2**, upon oxidation. Although the Cu–C bond lengths in **1** and **2** are identical within the experimental error (2.005(9)–2.020(7) Å and 2.038(4) Å respectively), complex **2** has shorter Cu–Cl and Cu–N bonds than those in **1** owing to the smaller ionic radius of the copper ion in **2**. These results suggest that complex **2** contains a copper(III) ion rather than an oxidized ligand moiety. The experimental bond lengths around the Cu atom could be reproduced by DFT calculations.[13]

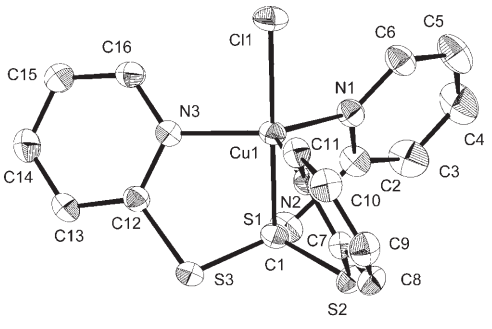

Figure 1. ORTEP drawing of **2** (thermal ellipsoids set at 50% probability). Selected bond lengths and angles are given in the Supporting Information.

The electronic spectrum of **1** in CH_2Cl_2 has two absorption maxima at 385 and 529 nm ($\varepsilon = 1.98 \times 10^3$ and $1.46 \times 10^3\ M^{-1}cm^{-1}$), while the spectrum of **2** has three maxima at 351, 463, and 550 nm ($\varepsilon = 2.52 \times 10^3$, 4.37×10^3, and $5.24 \times 10^3\ M^{-1}cm^{-1}$; Figure 2). The molar absorption coefficients of **2** are larger than those of **1** in this region because of the presence of the vacant d_{z^2} orbital of the Cu^{III} atom, which accepts charge from the ligands. This result also suggests that complex **2** contains Cu^{III} (see Supporting Information).[14]

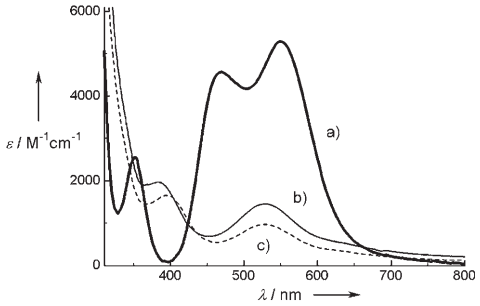

Figure 2. UV/Vis spectra of **2**-PF_6 (a), **1** (b), and **3** (c) recorded at room temperature in CH_2Cl_2. Spectrum (c) is obtained from a solution of **2** treated with an excess of chloride ions.

Metal K-edge X-ray absorption near-edge spectra were measured for the copper in **1** and **2**-PF_6. As shown in Figure 3, the energy in **2** is 8994.6 eV, which is 1.3 eV higher than that in

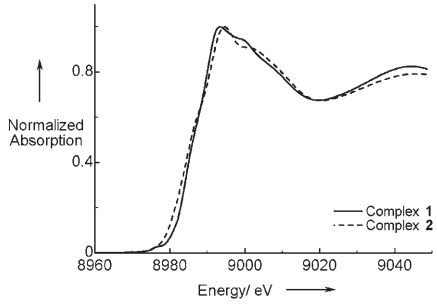

Figure 3. Metal K-edge X-ray absorption spectra of **1** and **2**-PF_6.

1. This result supports the proposed metal-centered one-electron oxidation of **1** to **2**. Such an energy difference between the Cu^{II} and Cu^{III} states and the spectral shape resemble those of the octahedral Cu^{II} and Cu^{III} complexes reported by Krebs et al.[15]

The ^1H NMR spectrum of **2** (Figure 4) shows well-resolved signals for the protons of the pyridine rings and

 © 2006 Wiley-VCH Verlag GmbH & Co. KGaA, Weinheim

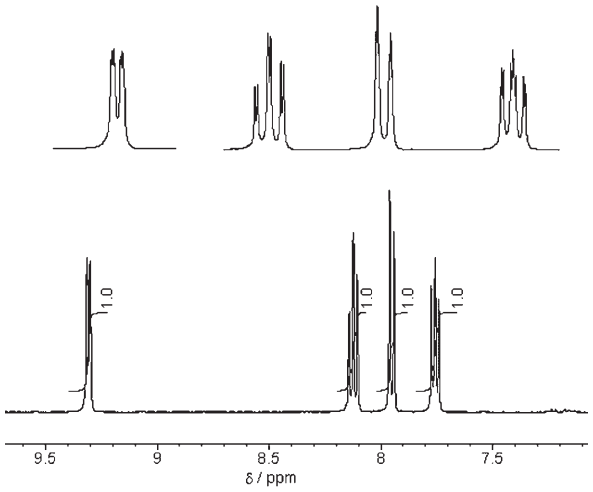

Figure 4. ^{1}H NMR spectra of **2** in CD_2Cl_2 and expansions of the signals. ^{1}H NMR (400 MHz, CD_2Cl_2): $\delta = 7.76$ (3H, $^3J = 7.6$, 5.6, $^4J \approx 0.9$ Hz; H5), 7.95 (3H, $^3J = 8.1$, $^4J = 0.9$ Hz; H3), 8.12 (3H, $^3J = 7.6$, 8.1, $^4J \approx 1.0$ Hz; H4), 9.31 ppm (3H, $^3J = 5.6$, $^4J \approx 0.9$ Hz; H6) H3–H6 are on C3–C6 (Figure 1), respectively.

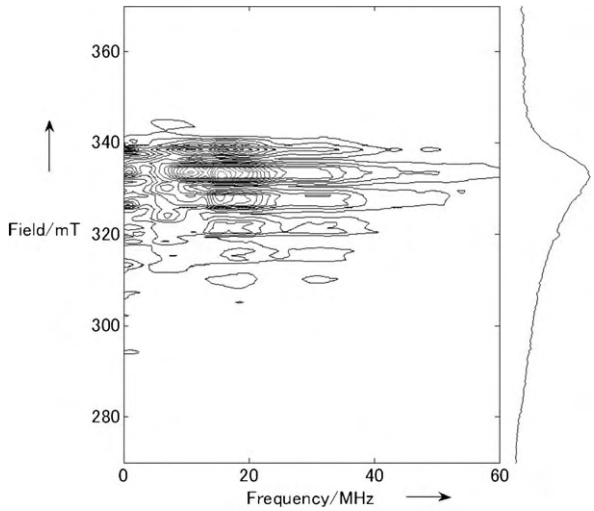

Figure 5. 2D-ESTN contour plot of **3** (that is, of a solution of **2** in CH_2Cl_2 containing one equivalent of chloride ions) recorded at 4 K. On the right is an electron-spin-echo-detected ESR spectrum.

signals for the pyridine carbon atoms are seen in the ^{13}C NMR spectra. The ^{1}H NMR spectrum, which shows an almost complete set of $^3J_{H,H}$ to $^4J_{H,H}$ couplings, demonstrates the diamagnetism of complex **2**. In the ^{13}C NMR spectrum, the signal of the carbon atom connected to copper is missing owing to the large quadrupole moment of the copper ion. The addition of chloride ions to the probe causes a significant broadening of the signals and a change in the chemical shifts. Thus, in the presence of one equivalent of chloride ions all the signals of the protons of the pyridine rings disappear. Such a remarkable change indicates that the addition of a chloride ion to complex **2** produces the paramagnetic Cu^{III} complex $[Cu(tptm)Cl_2]$ (**3**) with an octahedral geometry.[16] The absorption spectrum of **2** also changes upon addition of chloride ions: with increasing concentration of chloride ion the absorbance between 450 and 800 nm decreases in intensity. Figure 2c shows the spectrum of **3** which is obtained from a solution of **2** treated with an excess of chloride ions.[17]

To identify the paramagnetic Cu^{III} species we measured the pulse-ESR-based two-dimensional electron spin transient nutation (2D-ESTN) spectrum[18] of a rigid-glass sample containing both **2** and one equivalent of chloride ions at 4 K.[18c–e] 2D-ESTN spectroscopy gives unequivocal information on the electron-spin multiplicity of paramagnetic entities, even in non-oriented media.[18] The contour plot (Figure 5) shows two nutation peaks (10.8 and 15.5 MHz) corresponding, respectively, to spin-doublet ($S = 1/2$) and spin-triplet ($S = 1$) entities in the ground state with the spin-triplet dominating in the glass sample. The ratio of the two peak-frequencies ($15.5/10.8 = 1.45$) agrees with the theoretical one ($2^{1/2}$ to the first order of the perturbation theory for the ESR-allowed transition $Ms = 0$ to $Ms = \pm 1$). Thus, we can unequivocally conclude that **2** reacts with a chloride ion to produce a ground-state triplet complex with a small *g*-anisotropy, which suggests a highly symmetric molecular structure, such as a pseudo-octahedron. The DFT calculations predict the possible occurrence of an octahedral Cu^{III} complex in the triplet ground-state with a tptm ligand,[19] as described below. The 2D-ESTN spectrum also shows that the fine-structure parameters of the triplet-state complex **3** are small, thus indicating a minimal departure from complete octahedral symmetry at the copper site of **3**.

The ^{1}H ENDOR spectrum of the ESR sample of **2** with one equivalent of chloride ions showed signals arising from the protons of the ligands, that is, the three pyridine rings (See Figure S1 and Tables S3 and S4 in the Supporting Information). The spin-density distribution estimated from the ENDOR measurements is consistent with that predicted by the DFT calculations with the assumed octahedral structure for **3** in the triplet ground-state ($S = 1$; Supporting Information Tables S3 and S4).[16,20] The *g*-values calculated for the triplet-state octahedral structure are 2.0413, 2.0513, and 2.0598, which are close to that observed (2.0899) for to the strong central peak (see the electron-spin-echo detected ESR spectrum in Figure 5).[21] All the ESR/ENDOR-based data and the DFT calculations safely exclude the possible occurrence of a square-pyramidal structure for **3** in the triplet ground-state. The minority spin-doublet species corresponding to the nutation peak at 10.8 MHz is due to the products of the disproportionation reaction, namely complex **1** and the further oxidized product.

In conclusion, the unique coordination between Cu and C produces a stable copper complex in the +3 oxidation state with a tbp structure. The structural and spectroscopic data for **2** unambiguously indicate that complex **2** is a diamagnetic copper(III) complex with a tbp structure. Complex **2** reacts with an additional chloride ion to produce a paramagnetic octahedral complex **3** with a triplet ground-state. Complete analysis of the products of further electrode oxidation of the Cu^{III} complex in the presence of chloride ions and investigation of the properties of the paramagnetic Cu^{III} species by cw-ENDOR spectroscopy are underway.

 © 2006 Wiley-VCH Verlag GmbH & Co. KGaA, Weinheim

Experimental Section

Complex **1** was synthesized as reported previously.[11b] Green-black crystals of **1** were grown from a CH_2Cl_2 solution layered with hexane. It crystallizes in the monoclinic system, space group $P2_1/n$, with $a = 15.2610(4)$, $b = 8.7545(2)$, $c = 54.6327(12)$ Å, $\beta = 91.7111(9)°$, and $Z = 16$ ($R_1 = 0.0774$, $wR_2 = 0.1556$).

2-PF_6·CH_2Cl_2: Complex **1** (20.1 mg) and cerium(IV) ammonium nitrate (29.5 mg) were mixed in the presence of KPF_6 (9.9 mg) in acetonitrile. The solvent was evaporated, the crystals obtained were redissolved in CH_2Cl_2, and the solution purified by filtration. Reddish-black crystals of **2**-PF_6 were obtained from a CH_2Cl_2 solution layered with cyclohexane. The absorption spectrum of **2**-PF_6 agrees with that of the product obtained from electrochemical oxidation of **1**. Elemental analysis (%) calcd for $C_{17}H_{14}Cl_3CuF_6N_3PS_3$: C 30.41, H 2.10, N 6.26; found: C 30.65, H 2.04, N 6.35. ^{13}C NMR (100 MHz, CD_2Cl_2): $\delta = 124, 126, 142, 154, 162$ ppm. **2**-PF_6·CH_2Cl_2 crystallized in the monoclinic system, space group $P2_1/c$, with $a = 10.910(2)$, $b = 19.638(4)$, $c = 11.910(2)$ Å, $\beta = 94.677(5)°$, and $Z = 4$ ($R_1 = 0.0624$, $wR_2 = 0.1040$).

Received: August 2, 2006
Published online: October 20, 2006

Keywords: copper · density functional calculations · electrochemistry · N ligands · oxidation

[1] a) J. A. Halfen, S. Mahapatra, E. C. Wilkinson, S. Kaderli, V. G. Young, Jr., L. Que, Jr., A. D. Zuberbühler, W. B. Tolman, *Science* **1996**, *271*, 1397 – 1400; b) H. Hayashi, S. Fujinami, S. Nagatomo, S. Ogo, *J. Am. Chem. Soc.* **2000**, *122*, 2124 – 2125; c) K. Yoshizawa, N. Kihara, T. Kamachi, Y. Shiota, *Inorg. Chem.* **2006**, *45*, 3034 – 3041.

[2] A. S. E. Karlström, J. Bäckvall, *Chem. Eur. J.* **2001**, *7*, 1981 – 1989.

[3] a) M. Melnik, M. Kabesova, *J. Coord. Chem.* **2000**, *50*, 323 – 338; b) T. V. Popova, N. V. Aksenova, *Russ. J. Coord. Chem.* **2003**, *29*, 743 – 765.

[4] L. L. Diaddario, W. R. Robinson, D. W. Margerum, *Inorg. Chem.* **1983**, *22*, 1021 – 1025.

[5] J. Hanss, H.-J. Krüger, *Angew. Chem.* **1996**, *108*, 2989 – 2991; *Angew. Chem. Int. Ed. Engl.* **1996**, *35*, 2827 – 2830.

[6] a) J. S. Rybka, J. L. Kurtz, T. A. Neubecker, D. W. Margerum, *Inorg. Chem.* **1980**, *19*, 2791 – 2796; b) F. C. Anson, T. J. Collins, T. G. Richmond, B. D. Santarsiero, J. E. Toth, B. G. R. T. Treco, *J. Am. Chem. Soc.* **1987**, *109*, 2974 – 2979; c) R. Ruiz, C. Surville-Barland, A. Aukauloo, E. Anzolabehere-Mallart, Y. Journaux, J. Cano, M. C. Muñoz, *J. Chem. Soc. Dalton Trans.* **1997**, 745 – 751; d) J. Hanss, A. Beckmann, H. J. Krüger, *Eur. J. Inorg. Chem.* **1999**, 163 – 172.

[7] M. A. Willert-Porada, D. J. Burton, N. C. Baenziger, *J. Chem. Soc. Chem. Commun.* **1989**, 1633 – 1634.

[8] a) H. Maeda, Y. Ishikawa, T. Matsuda, A. Osuka, H. Furuta, *J. Am. Chem. Soc.* **2003**, *125*, 11822 – 11823; b) H. Maeda, A. Osuka, H. Furuta, *J. Am. Chem. Soc.* **2003**, *125*, 15690 – 15691.

[9] G. Speier, V. Fülöp, *J. Chem. Soc. Chem. Commun.* **1990**, 905 – 906.

[10] C. Krebs, T. Glaser, E. Bill, T. Weyhermüller, W. Meyer-Klaucke, K. Wieghardt, *Angew. Chem.* **1999**, *111*, 370 – 372; *Angew. Chem. Int. Ed.* **1999**, *38*, 359 – 361.

[11] a) I. Kinoshita, L. J. Wright, S. Kubo, K. Kimura, A. Sakata, T. Yano, R. Miyamoto, T. Nishioka, K. Isobe, *Dalton Trans.* **2003**, 1993 – 2003; b) R. Miyamoto, R. Santo, T. Matsushita, T. Nishioka, A. Ichimura, Y. Teki, I. Kinoshita, *Dalton Trans.* **2005**, 3179 – 3186; c) R. Miyamoto, R. T. Hamazawa, M. Hirotsu, T. Nishioka, I. Kinoshita, L. J. Wright, *Chem. Commun.* **2005**, 4047 – 4049.

[12] The axial bond angles Cl–Cu–C_{ax} are close to 180° for both oxidation states (i.e. in **1** and **2**). The N–Cu–N angles for **1** are in the range 106.2(2)–131.5(2)° and these values vary more widely than those found in **2**, which are in the range 114.88(13)–124.32(13)°. The copper atom in **2** is located 0.2187(17) Å out of the trigonal plane formed by the three nitrogen atoms of pyridine units in the direction of the chloride ligand.

[13] The electronic configurations for complexes **1** and **2** were calculated by DFT methods (B3LYP) with the 6-31g(d) basis set using the Gaussian 03 program package. Gaussian 03 (Revision B.05): M. J. Frisch et al., see Supporting Information. See also reference [11b].

[14] The calculation reproduces the tbp structure and the electronic transition of **2** (TD method).

[15] Krebs et al. have also reported the Cu K-edge spectrum of a paramagnetic octahedral Cu^{III} complex. The energy of the Cu^{III} complex is higher than that of the Cu^{II} complex by 0.7 eV. See reference [10].

[16] The calculation of the expected octahedral structure for **3** was optimized and the paramagnetic data was also obtained. The DFT calculation of the octahedral Cu^{III} complex was performed at the B3LYP level of theory using the Gaussian 03 program package.[13] Selected calculated bond lengths and angles for **3** are also listed in the Supporting Information, Table S3. An unrestricted DFT calculation of **3** ($S = 1$) with the TZ2P basis set was carried out to estimate magnetic parameters, such as the hyperfine interaction terms. A VWN density functional was used as the local density approximation with Becke and Perdew functionals as generalized gradient approximations. See Table S4 in the Supporting Information for the hyperfine terms.

[17] Spectral data of **3** were obtained in CH_2Cl_2 solutions of **2** containing an excess of chloride ions (29 mM tetrabutylammonium chloride). The electronic spectrum of **3** has two absorption maxima at 396 and 527 nm ($\varepsilon_{max} = 1.6 \times 10^3$ and 9.7×10^2 $M^{-1}cm^{-1}$, respectively).

[18] a) J. Isoya, H. Kanda, J. R. Norris, J. Tang, M. K. Bowman, *Phys. Rev. B* **1990**, *41*, 3905 – 3913; b) A. V. Astashkin, A. Schweiger, *Chem. Phys. Lett.* **1990**, *174*, 595 – 602; c) K. Sato, D. Shiomi, T. Takui, K. Itoh, T. Kaneko, E. Tsuchida, H. Nishide, *J. Spectrosc. Soc. Jpn.* **1994**, *43*, 280 – 291; d) K. Sato, M. Yano, M. Furuichi, D. Shiomi, T. Takui, K. Abe, K. Itoh, A. Higuchi, K. Katsuma, Y. Shirota, *J. Am. Chem. Soc.* **1997**, *119*, 6607 – 6613; e) H. Tomioka, M. Hattori, K. Hirai, K. Sato, D. Shiomi, T. Takui, K. Itoh, *J. Am. Chem. Soc.* **1998**, *120*, 1106 – 1107.

[19] A bromide-bridged dinuclear Ni^{II} dimer complex with a tptm ligand has an octahedral geometry, as determined crystallographically (K. Kitano, R. Tanaka, N. Kuwamura, R. Santo, R. Miyamoto, T. Nishioka, A. Ichimura, I. Kinoshita, unpublished data).

[20] a) G. te Velde, F. M. Bickelhaupt, S. J. A. van Gisbergen, C. F. Guerra, E. J. Baerends, J. G. Snijders, T. Ziegler, *J. Comput. Chem.* **2001**, *22*, 931 – 967; b) C. F. Guerra, J. G. Snijders, G. te Velde, E. J. Baerends, *Theor. Chem. Acc.* **1998**, *99*, 391 – 403; c) ADF2006.01, SCM, Theoretical Chemistry, Vrije Universiteit, Amsterdam, The Netherlands.

[21] S. Patchkovskii, T. Ziegler, *J. Phys. Chem. A* **2001**, *105*, 5490 – 5497.

 © 2006 Wiley-VCH Verlag GmbH & Co. KGaA, Weinheim

Surface Adsorption Models

DOI: 10.1002/anie.200603447

Synthesis and Structure of a Triruthenium Complex Containing a Face-Capping Pyridine Ligand**

*Takashi Kawashima, Toshiro Takao, and Hiroharu Suzuki**

The chemistry of organic molecules on a metal surface has been attracting considerable attention with regard to the mechanistic study of heterogeneous catalysis.[1] Polynuclear organometallic molecules have often served as an appropriate model for the adsorbed organic molecules on a metal surface and have made important contributions to surface science. Coordination of an arene on a polynuclear organometallic compound is one of the most intensively studied subjects.[2] Various coordination modes of arenes, such as μ_3-,[3] μ_4-,[4] and μ_5-benzyne complexes[4a,b], as well as trimetallic face-capping arene complexes,[5] have been elucidated by means of diffraction studies, and transformation of a face-capping μ_3-benzene ligand to a μ_3-benzyne ligand as a consequence of double C–H bond activation has also been demonstrated.[5b] These results afford not only information on the structure of the arene species on the metal surface, but also provide information about the reactivity of the absorbed arene.

In contrast to arenes, pyridine has been shown to coordinate to a multimetallic core in quite limited modes. In relation to the hydrodenitrogenation process and poisoning of catalysis, it is important to understand the interaction of pyridine with a polynuclear compound. Since Yin and Deeming synthesized a trimetallic μ-pyridyl complex, $[Os_3(CO)_{10}(\mu\text{-}H)(\mu\text{-}C_5H_4N)]$, by the reaction of $[Os_3(CO)_{12}]$ with pyridine,[6a] several trimetallic complexes containing a μ-pyridyl ligand have been prepared.[6] However, a polynuclear complex containing a face-capping μ_3-pyridine ligand has so far never been prepared, although the face-capping mode has been proposed in surface science on the basis of spectroscopic studies.[7] We report herein the first synthesis of a μ_3-η^2:η^2:η^2-pyridine complex and its protonation to yield a μ_3-pyridinium complex.

[*] T. Kawashima, T. Takao, Prof. H. Suzuki
Department of Applied Chemistry
Graduate School of Science and Engineering
Tokyo Institute of Technology
O-okayama, Meguro-ku, Tokyo 152-8552 (Japan)
Fax: (+81) 3-5734-3913
E-mail: hiroharu@n.cc.titech.ac.jp

[**] This work was partially supported by Grants-in-Aid for Scientific Research on Priority Areas (Grant Nos. 15205009 and 14078101, "Reaction Control of Dynamic Complexes") and the 21st Century COE program from the Ministry of Education, Culture, Sports, Science and Technology, Japan. We acknowledge Kanto Chemical Co., Inc., for generous gifts of pentamethylcyclopentadiene.

Supporting information for this article is available on the WWW under http://www.angewandte.org or from the author.

The reaction of the triruthenium pentahydrido complex $[\{Cp^*Ru(\mu\text{-}H)\}_3(\mu_3\text{-}H)_2]$ (**1**; $Cp^* = \eta^5\text{-}C_5Me_5$) with pyridine in toluene at 100 °C afforded the face-capping pyridine complex $[(Cp^*Ru)_3(\mu_3\text{-}\eta^2\text{:}\eta^2\text{:}\eta^2\text{-}C_5H_5N)(\mu\text{-}H)_3]$ (**2**) with liberation of H_2 [Eq. (1)].[8] Complex **2** was characterized by ^1H and ^{13}C NMR spectra and elemental analysis, and the structure was determined by means of an X-ray diffraction study.

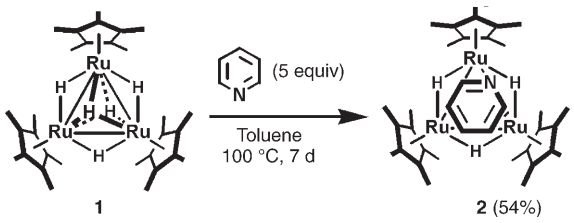

1 **2** (54%) (1)

The X-ray diffraction study of **2** was performed by using a red single crystal that was obtained from a toluene solution at −30 °C (Figure 1).[9] The structure clearly demonstrates that the pyridine ligand is coordinated to the $\{Ru_3\}$ core in a μ_3-η^2:η^2:η^2 fashion. To the best of our knowledge, complex **2** is the first example of a polynuclear complex with a face-capping pyridine ligand.

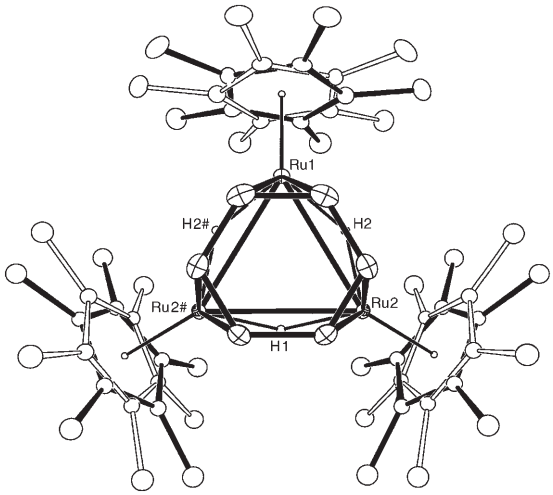

Figure 1. Molecular structure of **2** with thermal ellipsoids at the 30% level of probability. Selected bond lengths [Å] and angles [°]: Ru1-Ru2 3.0346(3), Ru2-Ru2# 3.0298(3); Ru2-Ru1-Ru2# 59.895(6), Ru1-Ru2-Ru2# 60.053(6).

The pyridine ligand in **2** is located parallel to the $\{Ru_3\}$ plane. Although the position of the nitrogen atom was not determined as a result of disorder over the six-membered ring, the average value of the "coordinated" C=C and C=N bond lengths (1.395(6) Å) is shorter than the average of the "uncoordinated" C–C and C–N bond lengths (1.446(5) Å). This difference shows that the pyridine ligand has Kekulé distortion as an azacyclohexatriene-type ring. The Ru–Ru bond lengths (av. 3.0315 Å) correspond to an Ru–Ru single bond.

 © 2006 Wiley-VCH Verlag GmbH & Co. KGaA, Weinheim

In the ^{1}H NMR spectrum, measured at room temperature, the five signals stemming from the pyridine ligand appear at $\delta = 2.36$, 2.42, 2.52, 3.47, and 3.60 ppm. These signals resonate in a significantly higher magnetic field in comparison with the free pyridine molecule ($\delta = 7.28$–8.61 ppm). This upfield shift is likely a result of the strong back-donation from the ruthenium centers and the ring-current shielding effect that is caused by the three surrounding Cp* ligands. Signals for the μ_3-benzene ligand of the face-capping benzene complex $[(Cp^*Ru)_3(\mu_3\text{-}\eta^2\text{:}\eta^2\text{:}\eta^2\text{-}C_6H_6)(\mu\text{-}H)_3]$ (**4**) were also observed at higher field ($\delta = 2.43$ ppm).[10] The ^{13}C NMR signals of the pyridine ligand similarly appeared at significantly higher field ($\delta = 34.5$, 35.2, 35.7, 58.5, and 60.3 ppm).

The three sharp signals for the Cp* groups were observed at $\delta = 1.66$, 1.67, and 1.78 ppm. These shifts clearly demonstrate that the μ_3-pyridine ligand of **2** does not rotate on the NMR timescale. This finding is in contrast with the corresponding trimetallic μ_3-η^2:η^2:η^2-arene complex, which is fluxional through the motion of the μ_3-arene ligand.[11]

Heating of **1** in pyridine at 120 °C resulted in quantitative formation of **2** in 48 hours, whereas a face-capping benzene complex **4** was obtained in relatively low yield (32 %) under similar conditions in the analogous reaction of **1** with benzene.[10b] This difference implies that the initial coordination through the lone pair of electrons at the nitrogen atom is a crucial step for the formation of the μ_3-pyridine complex. However, the lone pair of electrons does not participate in the face-capping coordination, as confirmed by the formation of a μ_3-pyridinium complex **3** upon protonation.

Addition of an equimolar amount of $HBF_4{\cdot}OMe_2$ to **2** in diethyl ether immediately afforded a precipitate of the monocationic face-capping pyridinium complex $[(Cp^*Ru)_3(\mu_3\text{-}\eta^2\text{:}\eta^2\text{:}\eta^2\text{-}(C_5H_5NH)(\mu\text{-}H)_3]BF_4$ (**3**) in 62 % yield [Eq. (2)].[12] In the ^{1}H NMR spectrum of **3** in

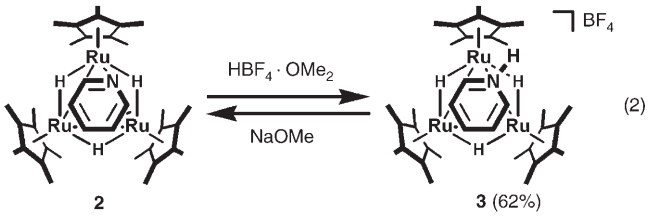

(2)

$[D_2]$dichloromethane, a broad signal from the NH group was observed at $\delta = 5.33$ ppm, which was diminished upon addition of D_2O. A stretching vibration assignable to the N–H bond appeared at 3256 cm^{-1} in the IR spectrum.

Treatment of **3** with a base, such as NaOMe, resulted in complete regeneration of **2**. When the protonation was performed by the use of deuterated tetrafluoroboric acid, a deuterium atom was incorporated only at the NH site. This observation shows that protonation of **2** did not proceed by way of an initial attack at the metal center, but by a direct attack at the nitrogen atom. This fact strongly supports the assertion that the lone pair of electrons was not involved in the bonding with the metal centers. Similar behavior has been observed in the protonation of a perpendicularly coordinated nitrile complex, $[(Cp^*Ru)_3(\mu_3\text{-}\eta^2\text{:}\eta^2(\perp)\text{-}PhCN)(\mu\text{-}H)_2(\mu_3\text{-}H)]$, which resulted in formation of the cationic μ_3-iminoacyl complex $[(Cp^*Ru)_3(\mu_3\text{-}\eta^2\text{:}\eta^2(\perp)\text{-}PhCNH)(\mu\text{-}H)_2(\mu_3\text{-}H)]^+$.[13]

In contrast, protonation of the corresponding μ_3-benzene complex **4** exclusively proceeded at the ruthenium center. A dicationic complex, $[(Cp^*Ru)_3(\mu_3\text{-}\eta^3\text{:}\eta^3\text{-}C_6H_6)(\mu\text{-}H)_3]^{2+}$ (**5**), was formed as a result of liberation of dihydrogen subsequent to protonation [Eq. (3)]. Thus, exclusive formation of the μ_3-

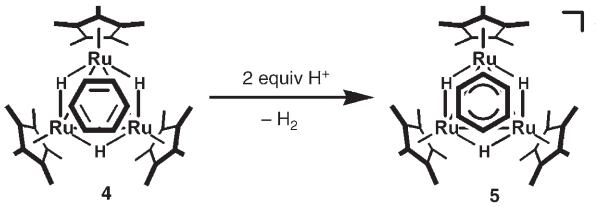

(3)

pyridinium complex is attributed to the presence of the lone pair of electrons at the nitrogen atom, and the cationic μ_3-pyridinium complex does not undergo further protonation at the ruthenium center.

The molecular structure of **3** was determined by an X-ray diffraction study (Figure 2).[9] The position of the nitrogen

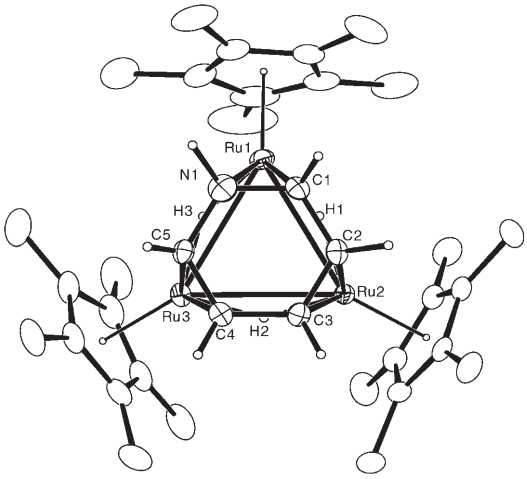

Figure 2. Molecular structure of $3{\cdot}C_3H_8O$ with thermal ellipsoids at the 30 % level of probability. The BF_4^- ion and 2-propanol are omitted for clarity. Selected bond lengths [Å] and angles [°]: Ru1-Ru2 3.0321(6), Ru2-Ru3 3.0273(8), Ru1-Ru3 3.0331(6), Ru1-N1 2.131(4), Ru1-C1 2.148(5), Ru2-C2 2.157(4), Ru2-C3 2.165(4), Ru3-C4 2.157(4), Ru3-C5 2.139(4), N1-C1 1.385(6), N1-C5 1.433(6), C1-C2 1.440(7), C2-C3 1.405(6), C3-C4 1.447(6), C4-C5 1.393(6); Ru2-Ru1-Ru3 59.884(17), Ru1-Ru2-Ru3 60.075(13), Ru1-Ru3-Ru2 60.041(14), C1-N1-C5 120.3(4), N1-C1-C2 120.5(4), C1-C2-C3 119.4(4), C2-C3-C4 119.8(4), C3-C4-C5 119.9(4), N1-C5-C4 120.1(4).

atom was determined on the basis of the hydrogen bond between the NH group and one of the fluorine atoms of the BF_4^- ion. The short H···F separation (1.99(5) Å) strongly suggests a hydrogen–fluorine bonding interaction (see the Supporting Information). This hydrogen atom was also observed by NMR spectroscopy. In the ^{19}F{^{1}H} NMR spectrum in $[D_2]$dichloromethane, two signals from the BF_4^- ion appeared at $\delta = -154.02$ and -153.96 ppm with an intensity

 © 2006 Wiley-VCH Verlag GmbH & Co. KGaA, Weinheim

ratio of 1:3. All of the ^{1}H NMR signals of **3** become broader in a more polar solvent, such as acetone or methanol. This broadening is probably a result of an equilibrium between the hydrogen-bonded species and the solvent-separated ion pair.

Addition of a proton to the face-capping pyridine ligand did not cause considerable changes in the structure. The average of the "coordinated" C=C and C=N bond lengths (1.394(6) Å) and the average of the "uncoordinated" C–C and C–N bond lengths (1.440(7) Å) are comparable to those of **2**. Although the bond lengths between the ruthenium atoms and the coordinated carbon and nitrogen atoms differ only slightly (shortened by ca. 0.02 Å), a significant upfield shift of the signals of the pyridine ring was observed in the ^{13}C NMR spectrum. The pyridinium carbon atoms were observed at $\delta =$ 24.8, 25.6, 31.7, 39.4, and 44.3 ppm. These values are shifted upfield by about 10–20 ppm in comparison with those of **2**. The ^{1}H NMR signals of the μ_3-pyridinium ligand also exhibited a slight upfield shift ($\delta = 1.78$, 2.47, 2.59, 3.30, and 3.50 ppm) relative to those of **2**.

It is interesting that the ^{13}C NMR signals of the μ_3-pyridinium ligand underwent an upfield shift in spite of the reduction of the electron density. This shift implies that the cationic charge is localized mainly at the nitrogen atom, and the bonding interaction between the triruthenium core and the pyridinium ring would be considerably different from that of the neutral complex.

Density functional theory (DFT) calculations for the adsorbed pyridine ring on an MoS_2 catalyst with 25% hydrogen coverage demonstrated that the pyridinium ion was readily formed by the migration of hydrogen from the neighboring SH group, which interacts with an Mo edge more tightly than pyridine itself.[14] Strong poisoning of the hydrodesulfurization process by pyridine has been ascribed to the formation of a pyridinium ion. Thus, formation of **3** by protonation of **2** must be an appropriate model of an adsorbed pyridine molecule.

In summary, face-capping pyridine complex **2** was formed by the reaction of triruthenium complex **1** with pyridine. Compound **2** is the first example of a pyridine ligand that exhibits μ_3-η^2:η^2:η^2 coordination to a trinuclear complex. The face-capping pyridinium complex **3** was obtained upon protonation of **2**. These results reproduce the behavior of an adsorbed pyridine molecule on a metal surface.

Received: August 23, 2006
Published online: October 6, 2006

Keywords: cluster compounds · protonation · pyridine · ruthenium · structure elucidation

[1] a) E. L. Muetterties, T. N. Rhodin, E. Band, C. F. Brucjer, W. R. Pretzer, *Chem. Rev.* **1979**, *79*, 91; b) E. L. Muetterties, *Pure Appl. Chem.* **1982**, *54*, 83; c) J. U. Mach, E. Bertel, F. P. Netzer, *Surf. Sci.* **1985**, *159*, 265; d) F. Zaera, *Chem. Rev.* **1995**, *95*, 2651.

[2] a) D. Braga, P. J. Dyson, F. Grepioni, B. F. G. Johnson, *Chem. Rev.* **1994**, *94*, 1585; b) M. A. Bennett, H. P. Schwemlein, *Angew. Chem.* **1989**, *101*, 1349; *Angew. Chem. Int. Ed. Engl.* **1989**, *28*, 1296.

[3] a) M. I. Bruce, G. Shaw, F. G. A. Stone, *J. Chem. Soc. Dalton Trans.* **1972**, 2094; b) C. W. Bradford, R. S. Nyholm, *J. Chem. Soc. Dalton Trans.* **1973**, 529; c) A. J. Deeming, R. E. Kimber, M. Underhill, *J. Chem. Soc. Dalton Trans.* **1973**, 2589; d) K. A. Azam, C. C. Yin, A. J. Deeming, *J. Chem. Soc. Dalton Trans.* **1978**, 1201; e) J. Evans, S. C. Brown, *J. Chem. Soc. Chem. Commun.* **1980**, 1021; f) P. A. Jackson, B. F. G. Johnson, J. Lewis, A. D. Massey, D. Braga, C. Gradella, F. Grepioni, *J. Organomet. Chem.* **1990**, *391*, 225; g) K. H. Chan, W. K. Leong, K. H. G. Mak, *Organometallics* **2006**, *25*, 250.

[4] a) S. A. R. Knox, B. R. Lloyd, A. G. Orpen, J. M. Viñas, M. Weber, *J. Chem. Soc. Chem. Commun.* **1987**, 1498; b) S. A. R. Knox, B. R. Lloyd, D. A. V. Morton, S. M. Nicholls, A. G. Orpen, J. M. Viñas, M. Weber, G. K. Williams, *J. Organomet. Chem.* **1990**, *394*, 385; c) M. I. Bruce, P. A. Humphrey, O. bin Shawkataly, M. R. Snow, E. R. T. Tiekink, W. R. Cullen, *Organometallics* **1990**, *9*, 2910; d) W. R. Cullen, S. J. Rettig, T. C. Zheng, *Organometallics* **1995**, *14*, 1466; e) M. I. Bruce, P. A. Humphrey, S. Okucu, R. Schmutzler, B. W. Skelton, A. H. White, *Inorg. Chim. Acta* **2004**, *357*, 1805.

[5] a) B. F. G. Johnson, J. Lewis, C. Housecroft, M. Gallup, M. Mrtinelli, D. Braga, F. Grepioni, *J. Mol. Catal.* **1992**, *74*, 61; b) M. A. Gallop, B. F. G. Johnson, J. Lewis, A. McCamley, R. N. Perutz, *J. Chem. Soc. Chem. Commun.* **1988**, 1071; c) H. Wadepohl, K. Büchner, H. Pritzkow, *Angew. Chem.* **1987**, *99*, 1294; *Angew. Chem. Int. Ed. Engl.* **1987**, *26*, 1259.

[6] a) C. C. Yin, A. J. Deeming, *J. Chem. Soc. Dalton Trans.* **1975**, 2091; b) A. J. Deeming, R. Peters, M. B. Hursthouse, J. D. J. Backer-Dirks, *J. Chem. Soc. Dalton Trans.* **1982**, 787; c) G. A. Foulds, B. F. G. Johnson, J. Lewis, *J. Organomet. Chem.* **1985**, *294*, 123; d) A. Eisenstadt, C. M. Giandomenico, M. F. Fredrick, R. M. Laine, *Organometallics* **1985**, *4*, 2033; e) M. I. Bruce, M. G. Humphrey, M. R. Snow, E. R. T. Tiekink, R. C. Wallis, *J. Organomet. Chem.* **1986**, *314*, 311; f) R. H. Fish, T.-J. Kim, J. L. Stewart, J. H. Bushweller, R. K. Rosen, J. W. Dupon, *Organometallics* **1986**, *5*, 2193.

[7] a) N. J. DiNardo, Ph. Avouris, J. E. Demuth, *J. Chem. Phys.* **1982**, *81*, 2189; b) G. D. Waddill, L. L. Kesmodel, *Chem. Phys. Lett.* **1986**, *128*, 208; c) R. M. Wexler, M.-C. Tsai, C. M. Friend, E. L. Muetterties, *J. Am. Chem. Soc.* **1982**, *104*, 2034; d) M. Surman, S. R. Bare, P. Hofmann, D. A. King, *Surf. Sci.* **1987**, *179*, 243.

[8] A 20-mL glass tube equipped with a greaseless valve was charged with **1** (206.1 mg, 0.289 mmol) and toluene (10 mL). Pyridine (0.12 mL, 1.44 mol) was added, and the reaction mixture was heated at 100 °C for seven days. Toluene and the remaining pyridine were removed under reduced pressure. The residual solid was purified by the use of column chromatography on alumina with tetrahydrofuran. The second purple band containing **2** was collected, and the solvent was removed under reduced pressure. Complex **2** was obtained as a purple solid (123.0 mg, 0.155 mmol, 54% yield). ^{1}H NMR (400 MHz, [D$_6$]benzene, 23 °C, TMS): $\delta = -21.50$ (dd, ^2J(H,H) = 3.8, 3.4 Hz, 1H, RuH), −19.68 (dd, ^2J(H,H) = 4.6, 3.8 Hz, 1H, RuH), −19.65 (dd, ^2J(H,H) = 4.6, 3.4 Hz, 1H, RuH), 1.66 (s, 15H, Cp*), 1.67 (s, 15H, Cp*), 1.78 (s, 15H, Cp*), 2.36 (dd, ^3J(H,H) = 6.0, 4.4 Hz, 1H, C$^\beta$H), 2.42 (dd, ^3J(H,H) = 6.0, 4.4 Hz, 1H, C$^\beta$H), 2.52 (dd, ^3J(H,H) = 6.0, 6.0 Hz, 1H, C$^\gamma$H), 3.47 (d, ^3J(H,H) = 4.4 Hz, 1H, C$^\alpha$H), 3.60 ppm (d, ^3J(H,H) = 4.4 Hz, 1H, C$^\alpha$H); ^{13}C{^{1}H} NMR (100 MHz, [D$_6$]benzene, 23 °C, TMS): $\delta =$ 10.89 (C$_5$*Me*$_5$), 10.93 (C$_5$*Me*$_5$), 11.2 (C$_5$*Me*$_5$), 34.5 (C$^\beta$ or C$^\gamma$), 35.2 (C$^\beta$ or C$^\gamma$), 35.7 (C$^\beta$ or C$^\gamma$), 58.5 (C$^\alpha$), 60.3 (C$^\alpha$), 89.5 (*C*$_5$Me$_5$), 89.6 (*C*$_5$Me$_5$), 90.5 ppm (*C*$_5$Me$_5$).

[9] X-ray crystallography: All data were collected on a Rigaku R-Axis RAPID imaging plate diffractometer with graphite-monochromated Mo$_{K\alpha}$ radiation ($\lambda = 0.71069$ Å) at 153 K. Crystal data for **2**: orthorhombic, space group *Pbcn* (No. 57), $a = 10.8241(16)$, $b = 16.270(3)$, $c = 17.841(3)$ Å, $V = 3141.9(8)$ Å^3, $Z = 4$, $\rho_{calcd} =$

 © 2006 Wiley-VCH Verlag GmbH & Co. KGaA, Weinheim

1.672 $Mg\,m^{-3}$, $\mu(Mo_{K\alpha}) = 1.448\ mm^{-1}$; of the 36407 reflections that were collected, 5092 were unique ($R_{int} = 0.0221$), $R_1 = 0.0357$ [$I > 2\sigma(I)$], $wR_2 = 0.0952$ [$I > 2\sigma(I)$]. Crystal data for **3**·C_3H_8O: monoclinic, space group $P2_1/n$ (No. 14), $a = 16.880(3)$, $b = 14.785(2)$, $c = 17.401(4)$ Å, $\beta = 117.060(8)°$, $V = 3867.5(13)$ $Å^3$, $Z = 4$, $\rho_{calcd} = 1.613\ Mg\,m^{-3}$, $\mu(Mo_{K\alpha}) = 1.206\ mm^{-1}$; of the 44592 reflections that were collected, 11697 were unique ($R_{int} = 0.0740$), $R_1 = 0.0517$ [$I > 2\sigma(I)$], $wR_2 = 0.0998$ [$I > 2\sigma(I)$]. CCDC-617366 (**2**) and CCDC-617367 (**3**) contain the supplementary crystallographic data for this paper. These data can be obtained free of charge from The Cambridge Crystallographic Data Centre via www.ccdc.cam.ac.uk/data_request/cif.

[10] a) A. Inagaki, Y. Takaya, T. Takemori, H. Suzuki, *J. Am. Chem. Soc.* **1997**, *119*, 625; b) H. Suzuki, T. Kakigano, K. Tada, M. Igarashi, K. Matsubara, A. Inagaki, M. Oshima, T. Takao, *Bull. Chem. Soc. Jpn.* **2005**, *78*, 67.

[11] a) M. A. Gallop, B. F. G. Johnson, J. Lewis, P. R. Raithby, *J. Chem. Soc. Chem. Commun.* **1987**, 1809; b) M. A. Gallop, B. F. G. Johnson, J. Keeler, J. Lewis, S. J. Heyes, C. M. Dobson, *J. Am. Chem. Soc.* **1992**, *114*, 2510; c) H. Wadepohl, K. Bühner, M. Herrmann, H. Pritzkow, *Organometallics* **1991**, *10*, 861.

[12] A 50-mL Schlenk tube was charged with **2** (20.5 mg, 0.026 mmol) and diethyl ether (20 mL). HBF_4·OMe_2 (3.2 μL, 0.026 mmol) was added with vigorous stirring at room temperature. A purple precipitate was immediately formed. After 30 min of stirring, the purple precipitate was separated by removing the supernatant and was washed four times with diethyl ether (5 mL). The residual solid was then dried under reduced pressure, and complex **3** was obtained as a purple solid (14.1 mg, 0.016 mmol, 62% yield). ^{1}H NMR (400 MHz, [D_2]dichloromethane, 23 °C, TMS): $\delta = -20.69$ (dd, ^2J(H,H) = 4.8, 3.0 Hz, 1H, RuH), −20.15 (dd, ^2J(H,H) = 4.8, 3.4 Hz, 1H, RuH), −19.67 (dd, ^2J(H,H) = 3.4, 3.0 Hz, 1H, RuH), 1.70 (s, 15H, Cp*), 1.71 (s, 15H, Cp*), 1.75 (s, 15H, Cp*), 1.78 (dd, ^3J(H,H) = 6.0, 4.4 Hz, 1H, $C^{\beta}H$), 2.47 (dd, ^3J(H,H) = 6.4, 4.4 Hz, 1H, $C^{\beta}H$), 2.59 (dd, ^3J(H,H) = 6.4, 6.0 Hz, 1H, $C^{\gamma}H$), 3.30 (d, ^3J(H,H) = 4.4 Hz, 1H, $C^{\alpha}H$), 3.50 (d, ^3J(H,H) = 4.4 Hz, 1H, $C^{\alpha}H$), 5.33 ppm (br s, $\Delta\nu_{1/2} = 16.4$ Hz, 1H, NH); $^{13}C\{^1H\}$ NMR (100 MHz, [D_2]dichloromethane, 23 °C, TMS): $\delta = 9.8$ (C_5Me_5), 9.9 (C_5Me_5), 10.1(C_5Me_5), 24.8 (C^{β} or C^{γ}), 25.6 (C^{β} or C^{γ}), 31.7 (C^{β} or C^{γ}), 39.4 (C^{α}), 44.3 (C^{α}), 91.3 (C_5Me_5), 92.2 (C_5Me_5), 95.6 ppm (C_5Me_5); $^{19}F\{^1H\}$ NMR (376 MHz, [D_2]dichloromethane, 23 °C, $CFCl_3$): $\delta = -154.02$ (BF_4), −153.96 ppm (BF_4).

[13] T. Takao, T, Kawashima, H. Suzuki, *Organometallics* **2005**, *24*, 3371.

[14] Á. Logadóttir, P. G. Moses, B. Hinnemann, N.-Y. Topsøe, K. G. Knudsen, H. Topsøe, J. K. Nørskov, *Catal. Today* **2006**, *111*, 44.

 © 2006 Wiley-VCH Verlag GmbH & Co. KGaA, Weinheim

C–H Activation

DOI: 10.1002/anie.200603133

A Second-Generation Catalyst for Intermolecular Hydroacylation of Alkenes and Alkynes Using β-S-Substituted Aldehydes: The Role of a Hemilabile P-O-P Ligand**

Gemma L. Moxham, Helen E. Randell-Sly, Simon K. Brayshaw, Robert L. Woodward, Andrew S. Weller, and Michael C. Willis**

Hydroacylation reactions of alkenes and alkynes catalyzed by transition metals are examples of the growing number of transformations which form carbon–carbon bonds based on C–H-bond activation.[1] In particular, hydroacylation reactions offer an atom-economic entry to a variety of ketone-containing products.[2,3] Although intramolecular reactions that afford cyclopentanones are well established,[4] access to larger ring systems[5] and intermolecular reactions remain a considerable challenge.[6] We recently described a intermolecular rhodium-catalyzed reaction based on the use of β-S-substituted aldehydes.[7] Although this method had advantages over previous protocols, in that the use of alkyl aldehydes under mild reaction conditions (55–65 °C) is permitted, several limitations remained. Paramount among these were the need to use electron-poor alkenes to achieve good reactivity (Scheme 1) and the use of [Rh(dppe)-(acetone)$_2$]ClO$_4$[4a] as the catalyst. Although this catalyst performs relatively well in intermolecular reactions, the need to generate it immediately before use from the hydrogenation of [Rh(dppe)(nbd)]ClO$_4$ (nbd = norbornadiene) considerably detracts from its utility.[8] We document herein the development of a highly active hydroacylation catalyst that can be

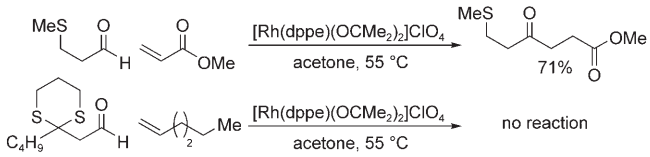

Scheme 1. Intermolecular hydroacylation. dppe = 1,2-bis(diphenylphosphanyl)ethane.

[*] G. L. Moxham, H. E. Randell-Sly, Dr. S. K. Brayshaw, Dr. R. L. Woodward, Dr. A. S. Weller, Dr. M. C. Willis
Department of Chemistry
University of Bath
Bath, BA2 7AY (UK)
Fax: (+44) 1225-386-568
E-mail: a.s.weller@bath.ac.uk
m.c.willis@bath.ac.uk

[**] This work was supported by the EPSRC and AstraZeneca. The EPSRC Mass Spectrometry Service at the University of Wales, Swansea, is also thanked for their assistance.

Supporting information for this article is available on the WWW under http://www.angewandte.org or from the author.

© 2006 Wiley-VCH Verlag GmbH & Co. KGaA, Weinheim

generated using commercial components without recourse to hydrogenation. In addition, we provide a structural study accounting for the enhanced reactivity of our new system, including the characterization of a rare acyl–rhodium hydride intermediate.

To achieve successful metal-catalyzed hydroacylation reactions, the intermediate acyl–metal species must be stabilized. Although the β-S-substituents on S-substituted aldehydes perform this function well with activated compounds,[9] the system fails with less reactive substrates such as unfunctionalized alkenes; in these cases decarbonylation of the putative five-coordinate acyl hydride intermediate and catalyst decomposition results (**I**→**II**, Scheme 2). We reasoned that use of a ligand capable of providing additional

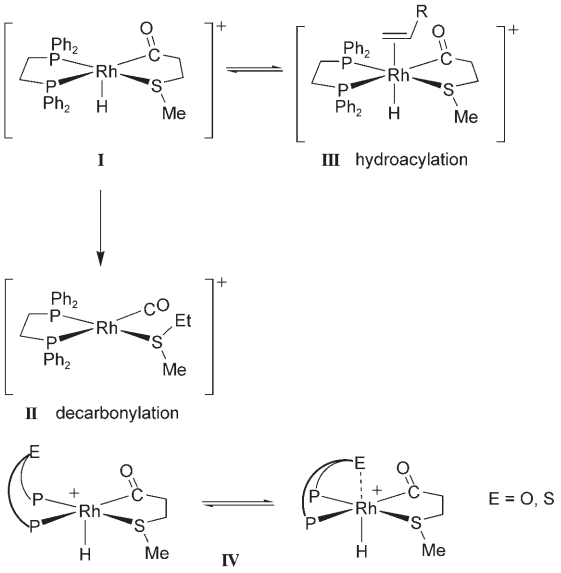

Scheme 2. Intermediate cationic rhodium species.

coordinative stabilization to the acyl–metal intermediate should deliver a more robust system, and speculated that incorporation of a hemilabile[10] substitutent on the ligand would provide extra stabilization to the cationic rhodium center while still allowing the necessary latent-vacant coordination site for the reaction to proceed (**IV**, Scheme 2). Related arguments have been used to account for the higher turnover numbers that have been observed when excess alkene was employed.[11] In our system, the use of additional alkene provided no benefit.

To explore this idea, we studied the union of the thioether-substituted aldehyde **1** and methyl acrylate, and employed a variety of catalysts (Table 1). The reaction using the standard catalyst $[Rh(dppe)(acetone)_2]ClO_4$ takes 90 minutes (entry 1, Table 1). Replacing dppe with the rigid P-O-P ligand xantphos (Figure 1) resulted in complete loss of reactivity. However, by using the more flexible variant, dpephos, complete conversion was achieved in only 60 minutes (entries 2 and 3, Table 1). The analogous thio- and methylene-bridged versions of dpephos (ligands **3** and **4**) failed to generate active catalysts (entries 4 and 5, Table 1).

Table 1: Catalyst investigation.[a]

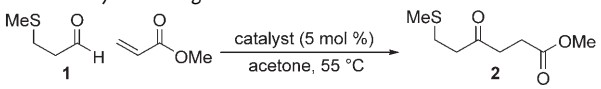

Entry	Catalyst	Conv. [%][c]	*t*
1	$[Rh(dppe)(nbd)]ClO_4$	100[b]	90 min
2	$[Rh(xantphos)(nbd)]ClO_4$	0	48 h
3	$[Rh(dpephos)(nbd)]ClO_4$	100	60 min
4	[Rh(**3**)(nbd)]ClO_4	0	48 h
5	[Rh(**4**)(nbd)]ClO_4	0	48 h
6	$[Rh(dpephos)(nbd)]PF_6$	100	4 h
7	$[Rh(dpephos)[nbd)]BAr^F{}_4$	100	75 min
8	$[Rh(dpephos)(nbd)]CB_{11}H_6Cl_6$	100	30 min
9	$[Rh(dpephos)(nbd)]CB_{11}H_6Br_6$	100	45 min
10[d]	$[\{Rh(cod)Cl\}_2]$/dpephos/$Ag(CB_{11}H_6Cl_6)$	100	45 min
11[d]	$[\{Rh(cod)Cl\}_2]$/dpephos/$Ag(ClO_4)$	100	90 min

[a] Conditions: aldehyde (1.0 equiv), methyl acrylate (2.0 equiv), catalyst (5 mol%), acetone, 55 °C. The catalyst was generated by addition of H_2 (1 atm, 5 min, acetone), except for entries 10 and 11, for structures of the ligands tested, see Figure 1. [b] Product obtained as a 4:1 mixture of linear and branched regioisomers. Exclusive formation of the linear isomer was observed for all other entries. [c] Determined by ^1H NMR spectroscopy. [d] Catalyst generated from the simple combination of the three components.

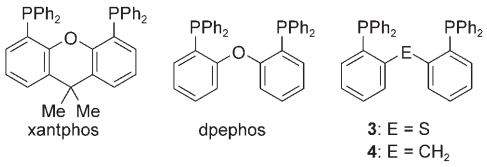

Figure 1. Ligands tested in Table 1

In an attempt to further increase the catalyst activity, we explored the use of alternative counterions. A screening of possible anion combinations showed that the weakly coordinating carborane anions $(CB_{11}H_6X_6)^-$ (X = Cl, Br)[12] gave the best turnovers, with reaction completion in only 30 and 45 minutes respectively, while use of $(BAr^F{}_4)^-$, $(ClO_4)^-$ and $(PF_6)^-$ gave no advantage (entries 6–9, Table 1). Monitoring the reactions by GC demonstrated that the relative rates showed the same variation on changing the anion. The rate enhancement for reactions catalyzed by cationic transition-metal centers partnered with weakly coordinating anions such as monoanionic carboranes is now well established,[13] and arises from a combination of the availability of reactive vacant sites and the stabilization of the active catalyst by the anion. At this stage, the active catalysts were being generated by hydrogenation of the [Rh(nbd)(phosphine)](anion) precursors, and, although we had identified several highly reactive systems, we still considered the need to activate with hydrogen gas a practical limitation. The use of the chelating aldehyde **1** now proved to be a real advantage, as simply combining $[\{Rh(cod)Cl\}_2]$ (cod = cycloocta-1,5-diene), dpephos, and $Ag(CB_{11}H_6Cl_6)$ generated an active catalyst that achieved complete conversion in only 45 minutes (entry 10, Table 1). A catalyst incorporating the $(ClO_4)^-$ counterion could be generated in a similar way, and 100% conversion was reached in 90 minutes (entry 11, Table 1).[14] Using the ligand

 © 2006 Wiley-VCH Verlag GmbH & Co. KGaA, Weinheim

dpephos provides an additional advantage, in that the reactions with methyl acrylate were now completely selective for the linear regioisomer; use of the original dppe-derived catalyst resulted in a 4:1 mixture of linear and branched isomers.[7a]

As we could generate a highly active catalyst without the need for hydrogen activation, we briefly evaluated the scope of the reactions promoted by these systems. From a practical standpoint, we elected to use the catalyst featuring the perchlorate anion as opposed to the more expensive carborane systems, even though use of the latter gave the best rates. Table 2 demonstrates that a catalyst generated from $[\{Rh(cod)Cl\}_2]$, dpephos, and $Ag(ClO_4)$ is effective at promoting the union of a variety of aldehyde, alkene, and alkyne components. In all cases, the efficiency of the reactions matches or surpasses that achieved previously. Of particular note are the reactions employing octene (entries 4, 8 and 12, Table 1); the products from these reactions were either inaccessible or only available in low yield[15] using the original catalyst system.

Encouraged by the fact that use of dpephos resulted in the best catalytic performance, we looked in more detail at the catalytic cycle. The active catalyst species $[Rh(dpephos)(OCMe_2)_2]CB_{11}H_6Cl_6$ (**A**, Scheme 3) was generated by hydrogenation of $[Rh(dpephos)(nbd)]CB_{11}H_6Cl_6$ in acetone. The solid-state structure of **A** (Figure 2) shows a square-planar Rh^I motif, with no close Rh···O interactions from the P-O-P ligand (O(3)–Rh 3.562(2) Å). The NMR spectroscopic data of a solution of the complex are in full accord with this structure. Addition of one equivalent of aldehyde **1** to catalyst **A** immediately generates a complex which was identified by spectroscopic methods as the acyl hydride $[Rh(dpephos)(H)(MeSCH_2CH_2CO)]CB_{11}H_6Cl_6$ (**B**). The room-temperature ^1H NMR spectrum shows a broadened hydride signal at $\delta = -8.75$ ppm as a doublet of triplets ($J(RhH) = 23$ Hz, $J(PH) \approx 1$ Hz) and a doublet in the $^{31}P\{^1H\}$ NMR spectrum, suggesting a fluxional process that renders the phosphine atoms equivalent. On cooling (−93 °C), the $^{31}P\{^1H\}$ NMR spectrum displays tightly coupled AB systems that show *trans* PP coupling, at $\delta = 26.8$, 25.9 ppm ($J(RhP) = 125$ Hz, $J(PP) = 303$ Hz), while the ^1H NMR spectrum reveals a single hydride resonance at $\delta = -8.62$ ppm that shows *cis* coupling to phosphorus. On the basis of this data, we assign the structure at low-temperature to be **B**, in which the dpephos coordinates *mer* with the metal, possibly with a coordinated oxygen atom. Complexes containing *trans*-spanning dpephos with a coordinated oxygen are known.[16] We assign the hydride as being opposite to the sulfur, as it is unlikely to reside opposite to the highly *trans*-influencing acyl ligand. The relatively large $J(RhH)$ coupling constant (23 Hz) is consistent with this. The fluxional processes at room temperature could possibly proceed via a five-coordinate intermediate with either the oxygen or sulfur atoms not

Table 2: Intermolecular hydroacylation using the new catalyst system.[a]

Entry	Aldehyde	Alkene/ alkyne	Product	*t* [h]	Yield [%][b]
1	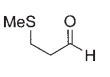		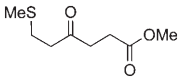	1	74
2			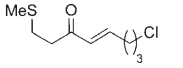	1	82
3			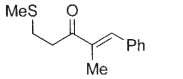	16	80
4		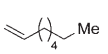	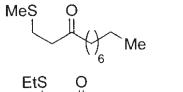	24	70
5	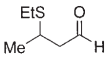		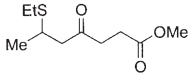	16	81
6			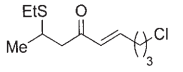	16	97
7			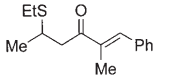	24	73
8		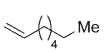	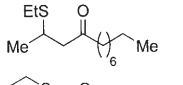	48	61
9	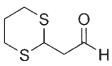		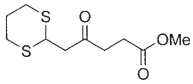	4	75
10			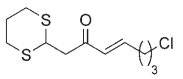	4	87
11			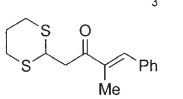	24	82
12			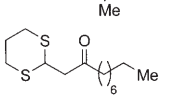	48	89

[a] Conditions: aldehyde (1.0 equiv), alkene, or alkyne (2.0 equiv), $[\{Rh(cod)Cl\}_2]$ (2.5 mol%), dpephos (5 mol%), $Ag(ClO_4)$ (5 mol%), acetone, 55 °C. [b] Yields of isolated single isomers.

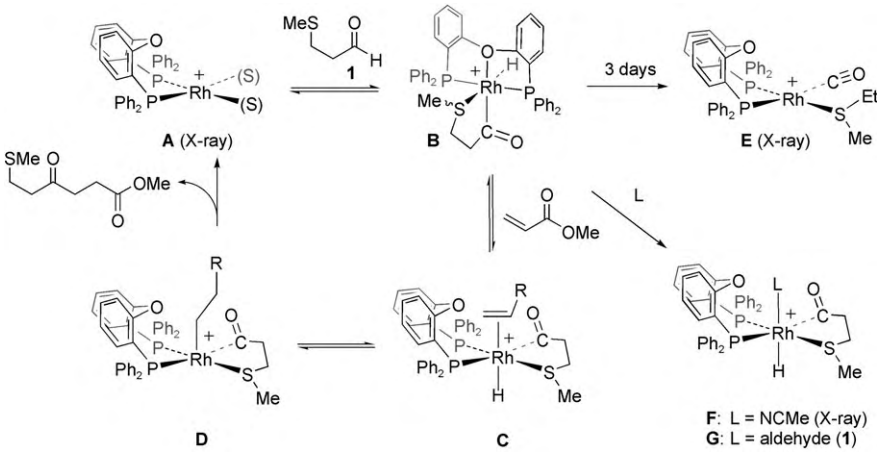

Scheme 3. Proposed mechanism for the hydroacylation reaction. Compound structures confirmed by X-ray analysis are indicated.

 © 2006 Wiley-VCH Verlag GmbH & Co. KGaA, Weinheim

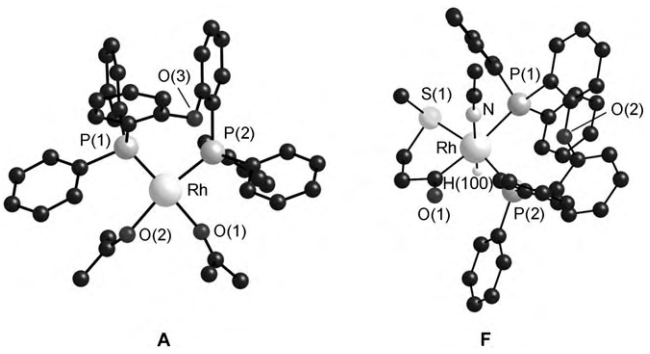

Figure 2. Solid-state structures of **A** and **F**. Selected bond distances [Å] and angles [°]: **A** Rh–O(1) 2.154(2), Rh–O(2) 2.126(4), Rh–O(3) 3.562(1), Rh–P(1) 2.202(5), Rh–P(2) 2.198(1), P(1)-Rh-P(2) 96.23(2); **F** Rh–C(41) 2.039(4) Rh–P(1) 2.508(1), Rh–P(2) 2.305(1), Rh–S(1) 2.372(1), Rh–O(2) 4.271(1), P(1)-Rh-P(2) 100.37(3).

bound, although we favor the former because of the isolation of complex **F** (described below). Complex **B** is stable to decarbonylation in solution at room temperature for an appreciable time ($t_{1/2} = 24$ h), although after three days smooth conversion of **B** into the decarbonylated product **E** is observed, and attempts to recrystallize **B** also led to the decarbonylated product **E** (see the Supporting Information for the solid-state structure).

Support for the facile decoordination of the oxygen atom in the dpephos ligand comes from addition of a slight excess of aldehyde **1** or acetonitrile to **B** which results in the instant formation of [Rh(dpephos)(L)(H)($MeSCH_2CH_2CO$)]-$CB_{11}H_6Cl_6$ **F** (L = MeCN) or **G** (L = **1**), in which the oxygen atom is no longer bound. The solid-state structure of **F** (Figure 2) confirms the acyl–hydride motif, with the acetonitrile ligand *trans* to the (located) hydride ligand. The strong *trans* influence of the acyl ligand is clearly demonstrated in the two Rh−P bond lengths that differ by 0.2 Å. NMR data suggest two isomers in solution. Given that in the $^{31}P\{^1H\}$ NMR spectrum there is a large difference in the J(RhP) coupling constants for the two inequivalent phosphines (that is: 150 and 65 Hz), this suggests that the acyl ligand lies *trans* to a phosphine, and therefore we assign structures to these isomers in which either the hydride and ligand (L), or the sulfur and L have swapped places.

Compound **F** is a model for the putative alkene adduct **C** in the hydroacylation cycle (Scheme 3). Moreover, **B** and **F** can enter directly into the catalytic cycle, as addition of alkene immediately results in catalytic turnover. Acyl–hydridorhodium complexes resulting from the addition of simple aldehydes are rare[17] as they generally suffer from decarbonylation,[18] and as far as we are aware **B** and **F** represent true examples (rather than model systems) of such species, which are also competent in the catalytic hydroacylation of useful substrates.[19] Such complexes have often been suggested but not experimentally observed. Presumably the dpephos ligand temporarily blocks a vacant site on **B** necessary for decarbonylation[17d,18] but it is able to move aside to allow the coordination of substrate, whereas in **F** the acetonitrile fulfils this role.

Support for this hypothesis comes from varying the ligand set to change the coordinating properties of the ligand. Use of ligand **3**, in which the thioether would be expected to bind strongly, results in the complex, [Rh(**3**)(nbd)]$CB_{11}H_6Cl_6$ (**H**, Scheme 4), in which the sulfur binds so effectively that the

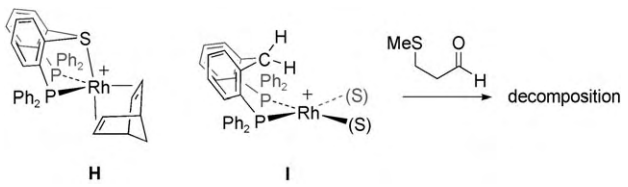

Scheme 4. Additional complexes evaluated as hydroacylation catalysts. (S) = acetone solvent.

resulting 18-electron complex does not react with H_2 (see the Supporting Information for the X-ray structure). Conversely, the methylene-bridged ligand **4**, which can provide no additional stabilization, can be used to form [Rh(**4**)-$(acetone)_2$]$CB_{11}H_6Cl_6$ (**I**, Scheme 4), but on addition of aldehyde **1**, very rapid (5 min) decomposition results and we observe no acyl hydride intermediate. Finally, [Rh(dppe)-$(acetone)_2$]$CB_{11}H_6Cl_6$ reacts with **1** to form an acyl hydride intermediate that decomposes within one hour to afford a mixture of products—one of which we have identified as the product of decarbonylation, [Rh(dppe)(CO)(SMeEt)]-$CB_{11}H_6Cl_6$.

In conclusion, we have reported a new, more efficient catalyst for intermolecular hydroacylation reactions of alkenes and alkynes employing β-S-substituted aldehydes. The catalyst can be generated from the simple combination of Rh^I salt, counterion, and ligand, and hydrogenation is unnecessary. The catalyst so formed allows previously unreactive substrates to participate in efficient coupling processes. Mechanistic studies have established the intermediacy of a key acyl–hydridorhodium species, and have also demonstrated that a hemilabile[10] oxygen atom of the P-O-P ligand is responsible for the increased stability of the active catalyst. Application of this catalyst-stabilization/activation concept to alternative processes is underway and will be reported in due course.

Experimental Section

Representative procedure using the catalyst generated from [{Rh(cod)Cl}$_2$], dpephos, and Ag(ClO_4) to prepare ketone **2** (Table 2, entry 1): Acetone (1.5 mL) was added under argon to [{Rh(cod)Cl}$_2$] (3.7 mg, 0.0075 mmol) followed by silver perchlorate (3.1 mg, 0.015 mmol). The resulting mixture was stirred at room temperature for 10 min. After this time dpephos (8 mg, 0.015 mmol) was added and the mixture was stirred for a further 15 min. Subsequently 3-(methylthio)propionaldehyde (**1**, 30 μL, 0.3 mmol) was added, immediately followed by methyl acrylate (54 μL, 0.6 mmol). The resulting solution was heated and stirred at 55 °C for 90 min. The solution was then cooled to room temperature, concentrated in vacuo, and purified by flash chromatography (4:1 Hexane/EtOAc) giving **2** as a colorless oil (42 mg, 74 % yield); ^1H NMR (300 MHz, $CDCl_3$): $\delta = 3.68$ (3H, s), 2.71–2.81 (6H, m), 2.61 (2H t, $J = 6.3$ Hz), 2.11 ppm (3H, s); ^{13}C NMR (101 MHz, $CDCl_3$):

 © 2006 Wiley-VCH Verlag GmbH & Co. KGaA, Weinheim

δ = 207.1, 173.2, 51.9, 42.5, 37.3, 27.9, 27.7, 15.79 ppm. The data was consistent to those reported in the literature.[7a]

Received: August 2, 2006
Published online: October 17, 2006

Keywords: C–H activation · hemilabile ligands · homogeneous catalysis · intermolecular hydroacylation · rhodium

[1] For recent reviews on C–H activation, see: a) V. Ritleng, C. Sirlin, M. Pfeffer, *Chem. Rev.* **2002**, *102*, 1731; b) J. A. Labinger, J. E. Bercaw, *Nature* **2002**, *417*, 507; c) G. Dyker, *Angew. Chem.* **1999**, *111*, 1808; *Angew. Chem. Int. Ed.* **1999**, *38*, 1698; d) *Handbook of C–H Transformations: Applications in Organic Synthesis* (Ed.: G. Dyker), Wiley-VCH, Weinheim, **2005**.
[2] K. Sakai, J. Ide, O. Oda, N. Nakamura, *Tetrahedron Lett.* **1972**, 1287.
[3] B. M. Trost, *Acc. Chem. Res.* **2002**, *35*, 695.
[4] For selected examples, see: a) D. P. Fairlie, B. Bosnich, *Organometallics* **1988**, *7*, 936; b) K. P. Gable, G. A. Benz, *Tetrahedron Lett.* **1991**, *32*, 3473; c) T. Sattelkau, P. Eilbracht, *Tetrahedron Lett.* **1998**, *39*, 9647; d) J. P. Morgan, K. Kundu, M. P. Doyle, *Chem. Commun.* **2005**, 3307.
[5] For selected examples, see: a) Y. Sato, Y. Oonishi, M. Mori, *Angew. Chem. Int. Ed.* **2002**, *41*, 1218; b) A. D. Aloise, M. E. Layton, M. D. Shair, *J. Am. Chem. Soc.* **2000**, *122*, 12610; c) H. D. Bendorf, C. M. Colella, E. C. Dixon, M. Marchetti, A. N. Matukonis, J. D. Musselman, T. A. Tiley, *Tetrahedron Lett.* **2002**, *43*, 7031.
[6] For selected examples, see: a) T. B. Marder, D. C. Roe, D. Milstein, *Organometallics* **1988**, *7*, 1451; b) T. Kondo, N. Hiraishi, Y. Morisaki, K. Wada, Y. Watanabe, T.-a. Mitsudo, *Organometallics* **1998**, *17*, 2131; c) C. P. Lenges, P. S. White, M. J. Brookhart, *J. Am. Chem. Soc.* **1998**, *120*, 6965; d) C.-H. Jun, D.-Y. Lee, H. Lee, J.-B. Hong, *Angew. Chem. Int. Ed.* **2000**, *39*, 3070; e) M. Tanaka, M. Imai, Y. Yamamoto, K. Tanaka, M. Shimowatari, S. Nagumo, N. Kawahara, H. Suemune, *Org. Lett.* **2003**, *5*, 1365.
[7] a) M. C. Willis, S. J. McNally, P. J. Beswick, *Angew. Chem. Int. Ed.* **2004**, *43*, 340; b) M. C. Willis, H. E. Randell-Sly, R. L. Woodward, G. S. Currie, *Org. Lett.* **2005**, *7*, 2249; c) M. C. Willis, H. E. Randell-Sly, R. L. Woodward, S. J. McNally, G. S. Currie, *J. Org. Chem.* **2006**, *71*, 5291.
[8] Although the dimer $[\{Rh(dppe)\}_2](ClO_4)_2$ (Ref. [4a]) can be isolated, it is relatively air sensitive, and in our hands its use led to variable results.
[9] M. C. Willis, S. Sapmaz, *Chem. Commun.* **2001**, 2558.
[10] P. Braunstein, F. Naud, *Angew. Chem.* **2001**, *113*, 702; *Angew. Chem. Int. Ed.* **2001**, *40*, 680.
[11] a) C. F. Lochow, R. G. Miller, *J. Am. Chem. Soc.* **1976**, *98*, 1281; b) D. P. Fairlie, B. Bosnich, *Organometallics* **1988**, *7*, 946.
[12] a) C. A. Reed, *Acc. Chem. Res.* **1998**, *31*, 133; b) C. A. Reed, *Chem. Commun.* **2005**, 1669.
[13] a) A. Macchioni, *Chem. Rev.* **2005**, *105*, 2039; b) E. Y. X. Chen, T. J. Marks, *Chem. Rev.* **2000**, *100*, 1167.
[14] A catalyst generated from the direct combination of $[\{Rh(cod)Cl\}_2]$, dppe, and $Ag(ClO_4)$ was also active, although the reaction required 4 h to reach completion.
[15] The product from entry 4 (Table 2) was obtained in 33% yield with the original catalyst. See Ref. [7a].
[16] S.-M. Kuang, P. E. Fanwick, R. A. Walton, *Inorg. Chem.* **2002**, *41*, 405.
[17] a) J. W. Suggs, *J. Am. Chem. Soc.* **1978**, *100*, 640; b) C. Bianchini, A. Meili, M. Peruzzini, F. Vizza, F. Bachechi, *Organometallics* **1991**, *10*, 820; c) K. Wang, T. J. Emge, A. S. Goldman, C. Li, S. P. Nolan, *Organometallics* **1995**, *14*, 4929; d) R. Goikhman, D. Milstein, *Angew. Chem.* **2001**, *113*, 1153; *Angew. Chem. Int. Ed.* **2001**, *40*, 1119.
[18] D. Milstein, *Acc. Chem. Res.* **1984**, *17*, 221.
[19] For an example of a spectroscopically characterized acyl–hydrido species that undergoes intramolecular hydroacylation, see: D. Milstein, *J. Chem. Soc. Chem. Commun.* **1982**, 1357.

 © 2006 Wiley-VCH Verlag GmbH & Co. KGaA, Weinheim

Natural Product Synthesis

DOI: 10.1002/anie.200603353

Synthesis of the Southern FGHI Ring System of Azaspiracid-1 and Investigation into the Controlling Elements of C28- and C36-Ketalization**

*Xiao-Ti Zhou, Liang Lu, Daniel P. Furkert, Charles E. Wells, and Rich G. Carter**

The azaspiracid family of natural products has stimulated significant interest in both the synthetic[1–3] and biological communities[4] due to their complex structural architecture and toxicity (Figure 1). We were initially drawn toward

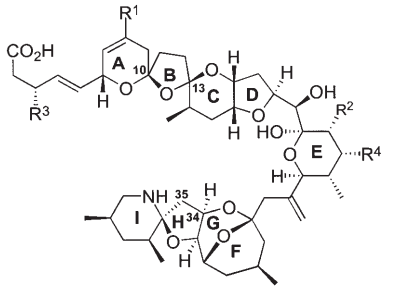

azaspiracid-1 (**1**): R^1 = H, R^2 = Me, R^3 = R^4 = H
azaspiracid-2 (**2**): R^1 = R^2 = Me, R^3 = R^4 = H
azaspiracid-3 (**3**): R^1 = R^2 = R^3 = R^4 = H
azaspiracid-4 (**4**): R^1 = R^2 = H, R^3 = OH, R^4 = H
azaspiracid-5 (**5**): R^1 = R^2 = R^3 = H, R^4 = OH

Figure 1. The azaspiracids.

[*] Dr. X.-T. Zhou, L. Lu, Dr. D. P. Furkert, Dr. C. E. Wells, Prof. R. G. Carter
Department of Chemistry
Oregon State University
Corvallis, OR 97331 USA
Fax: (+1) 541-737-9496
E-mail: rich.carter@oregonstate.edu

[**] Financial support was provided by the National Institutes of Health (GM63723). The authors would also like to thank Prof. Max Deinzer (OSU) and Dr. Jeff Morré (OSU) for mass spectral data, Rodger Kohnert (OSU) and Dr. Clemens Anklin (Bruker Biospin) for NMR assistance, Damien L. Kupier (OSU) for his synthetic assistance toward aldehyde **18**, David J. Weldon (University of Mississippi) for his early work on the synthesis of **32**, and Dr. Roger Hanselmann (Rib-X Pharmaceuticals) for helpful discussions.

Supporting information for this article is available on the WWW under http://www.angewandte.org or from the author.

© 2006 Wiley-VCH Verlag GmbH & Co. KGaA, Weinheim

azaspiracid-1 (**1**) by the C10,C13-bis-spiroketal portion of the molecule. Our endeavors have led to a better understanding of the controlling elements behind this structural motif.[1] Herein, we detail our successful construction of the FGHI ring system present in the southern portion of azaspiracid.

Our retrosynthetic strategy for the southern portion of azaspiracid disconnected FGHI ring system **6** at the C34–35 linkage to yield aldehyde **7** and allyl silane **8** (Scheme 1). To establish the correct stereochemistry at C34, this key coupling would need to proceed via a Cram-chelated intermediate with aldehyde **7**. The allyl silane portion would be available from the known Myers alkylation product **9**.[5] The aldehyde **7** should be accessible from the Andrus aldol adduct **10**, which in turn could be constructed from the sultam **11** and the chloride **12**.

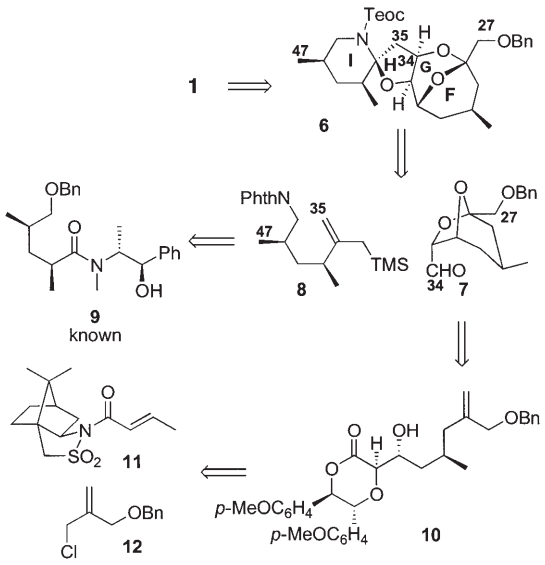

Scheme 1. Retrosynthetic analysis of azaspiracid-1 (**1**). Teoc = 2-(trimethylsilyl)ethoxycarbonyl, Bn = benzyl, TMS = trimethylsilyl, PhthN = phthalimido.

The synthesis of the allyl silane **8** is shown in Scheme 2. The Myers alkylation adduct **9** was prepared in four steps from the commercially available oxazolidinone **13**.[5] Treatment of **9** with methyllithium yielded the methyl ketone **14**. Next, conversion of **14** into the enol triflate followed by palladium-catalyzed coupling gave the allyl silane **15**. Removal of the benzyl ether was accomplished by using sodium naphthalenide. Finally, Mitsunobu reaction gave the phthalimide **8**.

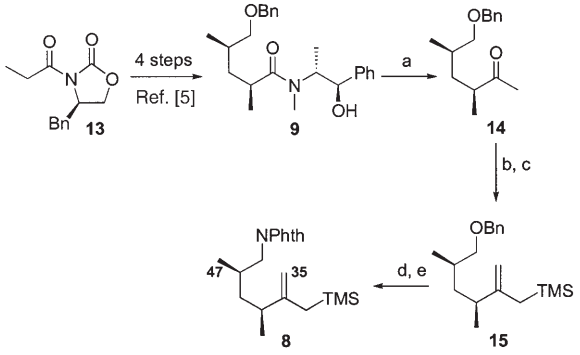

Scheme 2. Synthesis of allyl silane **8**. Reagents and conditions: a) MeLi, Et_2O, 82%; b) KHMDS, Comins' reagent, THF, 91%; c) $[Pd(PPh_3)]_4$, LiCl, $TMSCH_2MgBr$, Et_2O, 77%; d) Na, naphthalene, THF, −78→−40°C, 72%; e) phthalimide, DEAD, PPh_3, THF, 96%. HMDS = hexamethyldisilazide, DEAD = diethyl azodicarboxylate.

Synthesis of the aldehyde fragment **7**[6] was accomplished in eight steps (Scheme 3). After monobenzylation of the commercially available dichloride **16**, cuprate addition to the known sultam **11**, under similar conditions described by Paquette and Boulet,[7] led to generation of the stereocenter at C30 with excellent diastereoselectivity (d.r. > 20:1). Direct reduction of the product to the aldehyde **18** followed by boron-mediated aldol reaction with the Andrus dioxanone (**19**)[8] resulted in the adduct **10** again with excellent selectivity (d.r. > 10:1). Ring opening of the lactone **10** to its methyl ester **20** followed by CAN oxidative cleavage provided the diol **21**. The key [3.2.1] bicyclic ketal moiety could be constructed through ozonolysis of **21** with DMS workup, which induced spontaneous C28-ketal formation. This ketalization process could be driven to completion by the addition of Amberlyst-15. Finally, reduction with DIBAL-H proceeded cleanly to give the aldehyde **7**. The stereochemistry of aldehyde **7** was conclusively established through X-ray crystal structure assignment of the 2,4-dinitrohydrazone derivative **22**.[9]

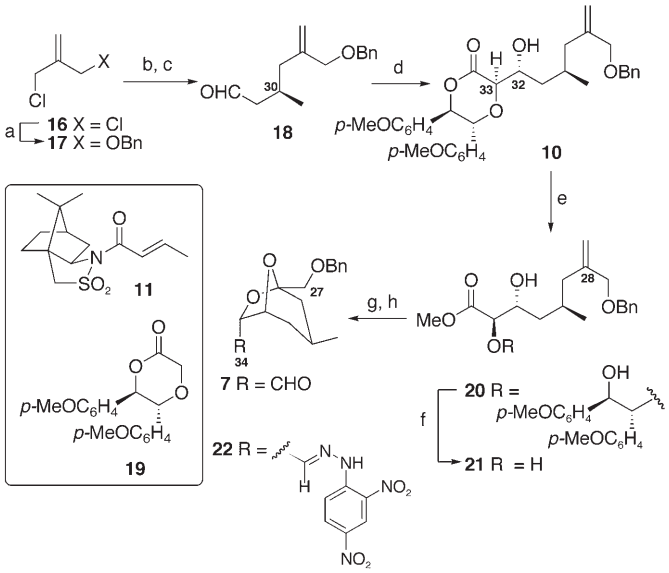

Scheme 3. Synthesis of bicyclic aldehyde **7**. Reagents and conditions: a) NaH, BnOH, THF, DMF, 77%; b) Mg, $BrCH_2CH_2Br$, CuBr·DMS, **11**, LiCl, TMSCl, THF, 90%; c) DIBAL-H, CH_2Cl_2, −78°C, 84%; d) **19**, $(c\text{-}C_6H_{11})_2BOTf$, Et_3N, CH_2Cl_2; −78→−20°C, 86%; e) NaOMe, MeOH, 0°C, 90%; f) CAN, MeCN/H_2O (9:1), 72%; g) O_3, CH_2Cl_2, DMS then Amberlyst-15, 80%; h) DIBAL-H, CH_2Cl_2, −78°C, 87%. DMF = *N*,*N*-dimethylformamide, DMS = dimethyl sulfide, DIBAL-H = diisobutylaluminum hydride, OTf = trifluoromethanesulfonate, CAN = ceric ammonium nitrate.

With the two major subunits in hand, we shifted our focus to their combination (Scheme 4). Treatment of a precooled solution of aldehyde **7** with Lewis acids ($TiCl_4$ or $SnCl_4$)

 © 2006 Wiley-VCH Verlag GmbH & Co. KGaA, Weinheim

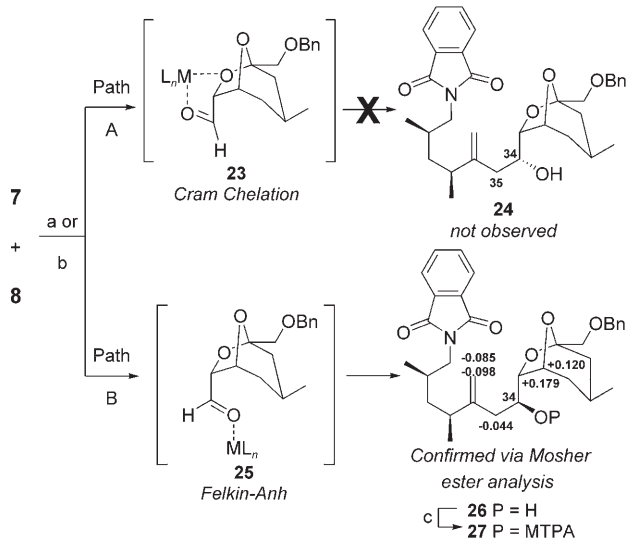

Scheme 4. First-generation coupling. Reagents and conditions: a) $SnCl_4$, CH_2Cl_2, 54% (**26**); b) $BF_3{\cdot}Et_2O$, CH_2Cl_2, 52% (**26**); c) (*R*)/(*S*)-Mosher acid chloride, DMAP, CH_2Cl_2, 45–51%. Representative data points for the difference in NMR chemical shift values [ppm], that is, δ(*S*)-Mosher ester−δ(*R*)-Mosher ester, are shown for ester **27** (400 MHz, $CDCl_3$). MTPA = α-methoxy-α-trifluoromethylphenylacetic acid (Mosher), DMAP = 4-(dimethylamino)pyridine.

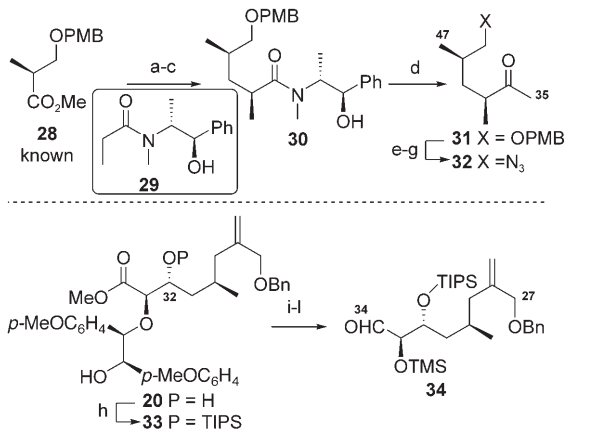

Scheme 5. Synthesis of revised coupling partners **32** and **34**. Reagents and conditions: a) $LiAlH_4$, Et_2O, 0°C, 99%; b) Ph_3P, I_2, imid., CH_2Cl_2, 86%; c) **29**, LDA, LiCl, THF, 90%; d) MeLi, Et_2O, 92%; e) DDQ, CH_2Cl_2, H_2O; f) TsCl, Et_3N, CH_2Cl_2, 64% (over 2 steps); g) NaN_3, DMF, 92%; h) TIPSOTf, 2,6-lut., CH_2Cl_2, −78°C, 83%; i) CAN, MeCN/H_2O (9:1), 98%; j) TMSOTf, 2,6-lut., CH_2Cl_2, −78°C, 86%; k) DIBAL-H, CH_2Cl_2, −78°C; l) DMP, CH_2Cl_2, 76% (over 2 steps). imid. = imidazole, LDA = lithium diisopropylamide, DDQ = 2,3-dichloro-5,6-dicyano-1,4-benzoquinone, Ts = *para*-toluenesulfonyl, TIPS = triisopropylsilyl, lut. = lutidine, DMP = Dess–Martin periodinane, PMB = *para*-methoxybenzyl.

followed by the addition of allyl silane **8** provided the coupled material as a single diastereomer at C34. We had hypothesized that chelating Lewis acids such as titanium or tin would proceed via the intermediate **23** to give the desired stereochemical outcome (**24**). We were surprised to find, upon conversion of the intermediate into its Mosher ester **27**,[10] that the C34 stereochemistry was in fact that of the undesired isomer. Further support for this assignment can be found in the fact that treatment of **7** with $BF_3{\cdot}Et_2O$ (a Lewis acid incapable of proceeding via intermediate **23**) also gave alcohol **26**, again as a single diastereomer. Despite our considerable efforts, we were unable to devise a viable route to invert the stereochemistry at C34.

It would appear from our efforts that the encumbered nature of alcohol **26** made it impossible to properly install the C34 stereogenic center. On the basis of this setback, we chose to revise our approach (Scheme 5). Starting from the known PMB-protected ester **28**,[11] DIBAL-H reduction, iodination, and Myers alkylation gave **30**. Conversion of **30** into the methyl ketone followed by DDQ deprotection and two-step azide incorporation gave **32**.

For the aldehyde component **34**, selective protection at C32 was required. Triisopropylsilylation of aldol adduct **10** did yield the corresponding silyl ether; however, methanolysis of the lactone proved unsuccessful. Fortunately, treatment of **20** with TIPSOTf and 2,6-lutidine at low temperature gave selectively the C32-OTIPS product **33**. None of the corresponding benzyl OTIPS ether was observed. Finally, deprotection with CAN, protection with TMS, and reduction produced the aldehyde **34**.

Next, our efforts returned to the combination of the subunits **32** and **34** (Scheme 6). Aldol reaction of ketone **32** and aldehyde **34** gave the coupled adduct **35** in excellent yield

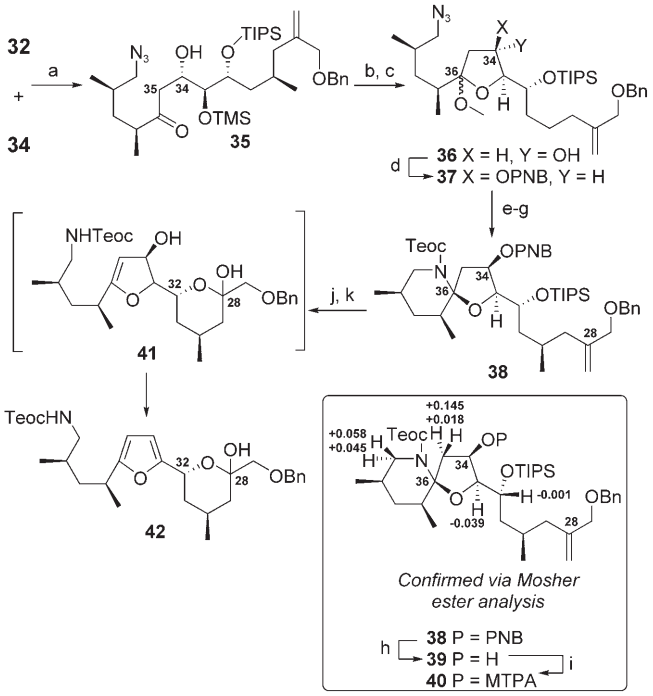

Scheme 6. Formation of unwanted furan **42**. Reagents and conditions: a) LDA, THF, −78°C, 94%; b) TBAF, HOAc, THF, 99%; c) PPTS, MeOH, 94%; d) *p*-NO_2-$C_6H_4CO_2H$, DEAD, PPh_3, THF, 53%; e) PPh_3, THF, H_2O; f) Teoc-O-(C_6H_4-*p*-NO_2), Et_3N, EtOAc, 71% (over two steps); g) Yb(OTf)$_3$, MeCN, 78%; h) K_2CO_3, MeOH, 75%; i) (*R*)/(*S*)-Mosher acid chloride, DMAP, CH_2Cl_2, 68–72%; j) TBAF, THF, 81%; k) O_3, CH_2Cl_2, −78°C; DMS then Amberlyst-15, CH_2Cl_2. Representative data points for the difference in chemical shift values [ppm], that is, δ(*S*)-Mosher ester−δ(*R*)-Mosher ester, are shown for ester **40** (400 MHz, $CDCl_3$). TBAF = tetra-*n*-butylammonium fluoride, PPTS = pyridinium *para*-toluenesulfonate, PNB = *para*-nitrobenzoate.

 © 2006 Wiley-VCH Verlag GmbH & Co. KGaA, Weinheim

as a single diastereomer. On the basis of precedent from us and others,[2e,3e,g] we suspected that the C34 stereochemistry was once again incorrect. Fortunately, after removal of the TMS group at C33 and mixed ketal formation at C36, we were able to cleanly invert the C34 stereochemistry using Martin's modified Mitsunobu conditions.[12] Staudinger reduction of the azide followed by Teoc protection and cyclization[2e] using $Yb(OTf)_3$ gave the HI ring system in **38**. The desired stereochemistry at C34 was confirmed through modified Mosher ester analysis.[10] Treatment of **38** with TBAF in THF induced selective removal of the TIPS (C32) and PNB (C34) protecting groups in the presence of the Teoc moiety. With only alkene cleavage at C28 and [3.3.1] bicyclic ketal formation remaining, we believed that the completion of the FGHI ring system was within reach. We were surprised to find that despite considerable experimentation, we consistently observed degradation of the material during ozonolysis. Small amounts of a minor product could be isolated for which the spectral data was supportive of furan structure **42**, which presumably formed via the enol ether intermediate **41**.

Thwarted by the unexpected furan formation, we reexamined the ordering of cyclization events (Scheme 7). Starting from the C34 inversion product **37**, C28 alkene dihydroxylation and cleavage yielded the ketone **43**. Removal of the TIPS ether at C32 as well as the *p*-nitrobenzoate group at C34 with TBAF yielded the diol **44**. While non-alcoholic solvents proved problematic in the formation of the [3.3.1] bicyclic structure, use of methanol as a solvent cleanly led to formation of the desired FGH ring system of **45**. The use of a hydrogen-bonding solvent moderates the acidity of the system, thereby preventing formation of the destructive C35–36 enol ether. Finally, azide reduction and Teoc protection provided compound **46**.

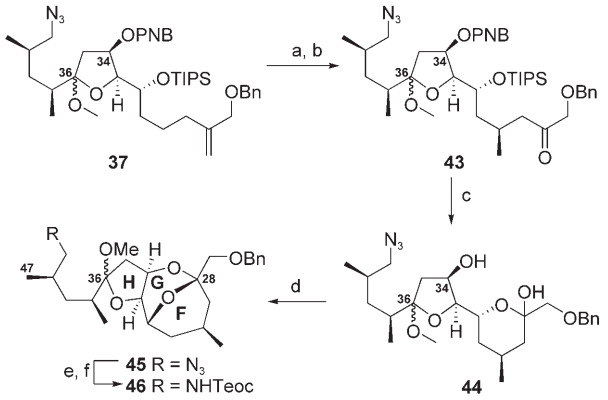

Scheme 7. Incorporation of FGH ring system. Reagents and conditions: a) $K_2OsO_4 \cdot 2H_2O$, NMO, acetone, H_2O; b) $NaIO_4$, THF, H_2O, 87% (over two steps); c) TBAF, THF, 85%; d) CSA, MeOH, 79%; e) PPh_3, THF, H_2O; f) Teoc-O-(C_6H_4-*p*-NO_2), Et_3N, EtOAc, 86% (over two steps). NMO = *N*-methylmorpholine-*N*-oxide, CSA = camphorsulfonic acid.

With the FGH rings now in place, the final challenge remaining was the formation of the azaspiro HI ring system (Scheme 8). Initial attempts to form C36 azaspiroketal using acidic media (e.g. CSA, MeOH) led to extensive decomposition. Interestingly, treatment of **46** with $Yb(OTf)_3$[2e,3e,g,p] in PhMe led to rapid formation (30 min, room temperature) of a single new product **47**. Careful analysis by 2D NMR spectroscopy revealed that **47** possessed the undesired stereochemistry at C36. Use of extended reaction times led to formation of a second compound, compound **6**; however, decomposition was a competitive pathway under these conditions. Fortunately, use of an alternate solvent (THF) at room temperature led to the desired C36 spiroaminal **6** as the major product (74% yield, **6**/**47** 4:3 ratio). The minor product **47** could be recycled by resubmission to identical reaction conditions to generate the same thermodynamic 4:3 ratio. As we have previously demonstrated in our synthesis of the C1–C26 northern portion of azaspiracid-1 (**1**),[1h] we are able to control the stereochemical outcome during ketalization through the proper choice of conditions. We did find the formation of the unwanted spiroaminal **47** as the kinetic product to be surprising, as the anomerically stabilized axial orientation is typically kinetically favored as a result of a presumed lower transition-state energy. We attribute this unusual behavior to a severe steric interaction between the NTeoc group and the fused GH ring system.

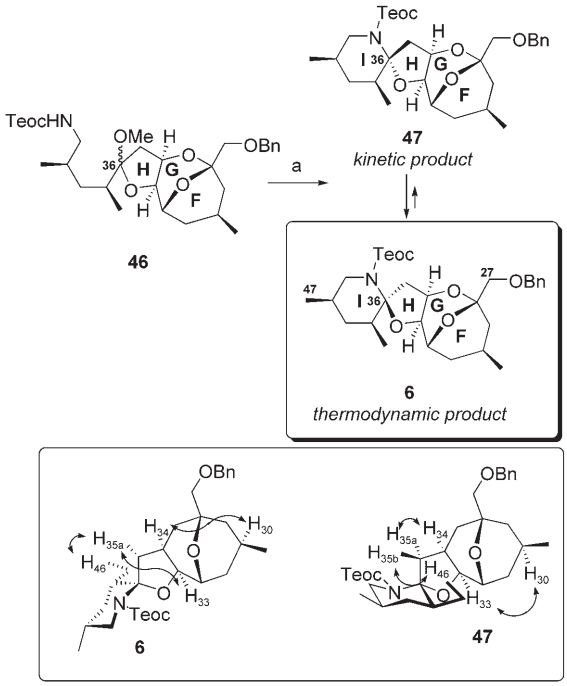

Scheme 8. Completion of the southern fragment. Reagents and conditions: a) $Yb(OTf)_3$, THF, 30 min, 74% (4:3 **6**/**47**). Key NOE interactions in **6** and **47** are indicated by double-ended arrows in the lower part of the scheme.

In summary, an efficient synthesis of the C27–C47 southern portion (**6**) has been achieved in 20 steps from commercially available dichloride **16**. The outlined approach represents the shortest route to the FGHI ring system reported to date.[2e,3e,g,p] In addition, we have demonstrated that careful selection of conditions for the ketalization steps allows control over the stereochemical outcome of the reaction.

 © 2006 Wiley-VCH Verlag GmbH & Co. KGaA, Weinheim

Completion of the total synthesis of azaspiracid-1 (**1**) will be reported in due course.

Received: August 17, 2006
Published online: October 17, 2006

Keywords: aldol reaction · azaspiracids · fused-ring systems · ketalization · natural products

[1] a) R. G. Carter, D. J. Weldon, *Org. Lett.* **2000**, *2*, 3913 – 3916; b) R. G. Carter, D. J. Weldon, T. C. Bourland, 221st National ACS Meeting, **2001**, San Diego, ORG-479; c) R. G. Carter, D. E. Graves, *Tetrahedron Lett.* **2001**, *42*, 6035 – 6039; d) R. G. Carter, T. C. Bourland, D. E. Graves, *Org. Lett.* **2002**, *4*, 2177 – 2179; e) R. G. Carter, D. E. Graves, M. A. Gronemeyer, G. S. Tschumper, *Org. Lett.* **2002**, *4*, 2181 – 2184; f) R. G. Carter, T. C. Bourland, X.-T. Zhou, M. A. Gronemeyer, *Tetrahedron* **2003**, *59*, 8963 – 8974; g) X.-T. Zhou, R. G. Carter, *Chem. Commun.* **2004**, 2138 – 2140; h) X.-T. Zhou, R. G. Carter, *Angew. Chem.* **2006**, *118*, 1819 – 1822; *Angew. Chem. Int. Ed.* **2006**, *45*, 1787 – 1790.

[2] a) K. C. Nicolaou, Y. Li, N. Uesaka, T. V. Koftis, S. Vyskocil, T. Ling, M. Govindasamy, W. Qian, F. Bernal, D. Y.-K. Chen, *Angew. Chem.* **2003**, *115*, 3771 – 3776; *Angew. Chem. Int. Ed.* **2003**, *42*, 3643 – 3648; b) K. C. Nicolaou, D. Y.-K. Chen, Y. Li, W. Qian, T. Ling, S. Vyskocil, T. V. Koftis, M. Govindasamy, N. Uesaka, *Angew. Chem.* **2003**, *115*, 3777 – 3781; *Angew. Chem. Int. Ed.* **2003**, *42*, 3649 – 3653; c) K. C. Nicolaou, S. Vyskocil, T. V. Koftis, Y. M. A. Yamada, T. Ling, D. Y.-K. Chen, W. Tang, G. Petrovic, M. O. Frederick, Y. M. Satake, *Angew. Chem.* **2004**, *116*, 4412 – 4418; *Angew. Chem. Int. Ed.* **2004**, *43*, 4312 – 4318; d) K. C. Nicolaou, T. V. Koftis, S. Vyskocil, G. Petrovic, T. Ling, Y. M. A. Yamada, W. Tang, M. O. Frederick, *Angew. Chem.* **2004**, *116*, 4418 – 4424; *Angew. Chem. Int. Ed.* **2004**, *43*, 4318 – 4324; e) K. C. Nicolaou, P. M. Pihko, F. Bernal, M. O. Frederick, W. Qian, N. Uesaka, N. Diedrichs, J. Hinrichs, T. V. Koftis, E. Loizidou, G. Petrovic, M. Rodriquez, D. Sarlah, N. Zou, *J. Am. Chem. Soc.* **2006**, *128*, 2244 – 2257; f) K. C. Nicolaou, D. Y.-K. Chen, Y. Li, N. Uesaka, G. Petrovic, T. V. Koftis, F. Bernal, M. O. Frederick, M. Govindasamy, T. Ling, P. M. Pihko, W. Tang, S. Vyskocil, *J. Am. Chem. Soc.* **2006**, *128*, 2258 – 2267; g) K. C. Nicolaou, T. V. Koftis, S. Vyskocil, G. Petrovic, W. Tang, M. O. Frederick, D. Y.-K. Chen, Y. Li, T. Ling, Y. M. A. Yamada, *J. Am. Chem. Soc.* **2006**, *128*, 2859 – 2872; h) K. C. Nicolaou, M. O. Frederick, G. Petrovic, K. P. Cole, E. Z. Loizidou, *Angew. Chem.* **2006**, *118*, 2671 – 2677; *Angew. Chem. Int. Ed.* **2006**, *45*, 2609 – 2615.

[3] a) A. B. Dounay, C. J. Forsyth, *Org. Lett.* **2001**, *3*, 975 – 978; b) J. Aiguade, J. Hao, C. J. Forsyth, *Org. Lett.* **2001**, *3*, 979 – 982; c) J. Aiguade, J. Hao, C. J. Forsyth, *Tetrahedron Lett.* **2001**, *42*, 817 – 820; d) J. Hao, J. Aiguade, C. J. Forsyth, *Tetrahedron Lett.* **2001**, *42*, 821 – 824; e) K. C. Nicolaou, P. M. Pihko, N. Diedrichs, N. Zou, F. Bernal, *Angew. Chem.* **2001**, *113*, 1302 – 1305; *Angew. Chem. Int. Ed.* **2001**, *40*, 1262 – 1265; Erratum: K. C. Nicolaou, P. M. Pihko, N. Diedrichs, N. Zou, F. Bernal, *Angew. Chem.* **2001**, *113*, 1621; *Angew. Chem. Int. Ed.* **2001**, *40*, 1573; f) K. R. Buszek, 221st National ACS Meeting, **2001**, San Diego, ORGN-570; g) C. J. Forsyth, J. Hao, J. Aiguade, *Angew. Chem.* **2001**, *113*, 3775 – 3779; *Angew. Chem. Int. Ed.* **2001**, *40*, 3663 – 3667; h) K. C. Nicolaou, W. Qian, F. Bernal, N. Uesaka, P. M. Pihko, J. Hinrichs, *Angew. Chem.* **2001**, *113*, 4192 – 4195; *Angew. Chem. Int. Ed.* **2001**, *40*, 4068 – 4071; i) M. Sasaki, Y. Iwamuro, J. Nemoto, M. Oikawa, *Tetrahedron Lett.* **2003**, *44*, 6199 – 6201; j) K. R. Buszek, T. S. Gibson, B. C. Reinhardt, J. R. Sunde, 226th ACS National Meeting, **2003**, New York, ORGN-179; k) Y. Ishikawa, S. Nishiyama, *Tetrahedron Lett.* **2004**, *45*, 351 – 354; l) Y. Ishikawa, S. Nishiyama, *Heterocycles* **2004**, *63*, 539 – 565; m) Y. Ishikawa, S. Nishiyama, *Heterocycles* **2004**, *63*, 885 – 893; n) L. K. Geisler, S. Nguyen, C. J. Forsyth, *Org. Lett.* **2004**, *6*, 4159 – 4162; o) S. Nguyen, J. Xu, C. J. Forsyth, *Tetrahedron* **2006**, *62*, 5338 – 5346; p) M. Oikawa, T. Uehara, T. Iwayama, M. Sasaki, *Org. Lett.* **2006**, *8*, 3943 – 3946.

[4] a) T. MacMahon, J. Silke, *Harmful Algae News* **1996**, *14*, 2; b) M. Satake, K. Ofuji, H. Naoki, K. J. James, A. Furey, T. McMahon, J. Silke, T. Yasumoto, *J. Am. Chem. Soc.* **1998**, *120*, 9967 – 9968.

[5] a) G. Mas, L. Gonzalez, J. Vilarrasa, *Tetrahedron Lett.* **2003**, *44*, 8805 – 8809; b) B. G. Vong, S. Abraham, E. A. Theodorkis, *Org. Lett.* **2003**, *5*, 1617 – 1620.

[6] Independently and concurrently to our effort, Nicolaou and coworkers reported the synthesis of this aldehyde. See Reference [2f].

[7] a) S. L. Boulet, L. A. Paquette, *Synthesis* **2002**, 895 – 900; b) B. H. Lipshutz, C. Hackmann, *J. Org. Chem.* **1994**, *59*, 7437 – 7444.

[8] M. B. Andrus, E. L. Meredith, E. J. Hicken, B. L. Simmons, R. R. Glancey, W. Ma, *J. Org. Chem.* **2003**, *68*, 8162 – 869, and references therein.

[9] See Supporting Information for the ORTEP representation of **22**. CCDC-605862 (**22**) contains the supplementary crystallographic data for this paper. These data can be obtained free of charge from The Cambridge Crystallographic Data Centre via www.ccdc.cam.ac.uk/data_request/cif.

[10] a) I. Ohtani, T. Kusumi, Y. Kashman, H. Kakisawa, *J. Am. Chem. Soc.* **1991**, *113*, 4092 – 4096; b) J. A. Dale, H. S. Mosher, *J. Am. Chem. Soc.* **1973**, *95*, 512 – 519; c) G. R. Sullivan, J. A. Dale, H. S. Mosher, *J. Org. Chem.* **1973**, *38*, 2143 – 2147.

[11] N. Nakajima, K. Horita, R. Abe, O. Yonemitsu, *Tetrahedron Lett.* **1988**, *29*, 4139 – 4142.

[12] S. F. Martin, J. A. Dodge, *Tetrahedron Lett.* **1991**, *32*, 3017 – 3020.

 © 2006 Wiley-VCH Verlag GmbH & Co. KGaA, Weinheim

C–N Coupling

DOI: 10.1002/anie.200602222

A Diaminochlorophosphine for Palladium-Catalyzed Arylations of Amines and Ketones**

Lutz Ackermann, Julia H. Spatz, Christian J. Gschrei, Robert Born, and Andreas Althammer*

Palladium-catalyzed amination reactions of aryl halides are indispensable tools for the synthesis of compounds with N–C(sp^2) linkages.[1–4] Iodides and electronically activated bromides can be successfully transformed by employing simple palladium salts. Aryl chlorides, however, are arguably the most useful single class of substrates because of their lower cost and the wider diversity of available compounds. The conversion of aryl chlorides usually requires recently developed stabilizing ligands.[5] The ligand design has been focused predominantly on electron-rich tertiary phosphines.[6,7] Owing to their electron-rich nature tertiary phosphines and their transition-metal complexes are often prone to oxidation. An alternative approach makes use of complexes derived from air-stable secondary phosphine oxides.[8] However, applications of these catalysts to more challenging substrates, such as *ortho*-substituted aryl chlorides or acyclic alkyl amines,[9,10] have so far not been reported.[11]

Recently, we described the diaminooxophosphine (daop) ligand **2**, which allowed for palladium-catalyzed amination reactions of electronically deactivated aryl chlorides.[12,13] During studies on the in situ generation of daop ligand **2** through salt elimination from the corresponding chlorophosphine **1**,[14] we observed an initial oxidative addition of chloride **1** to a low-valent palladium species, thereby giving rise to a phosphenium cation.[12] Phosphenium cations are isolobal to N-heterocyclic singlet carbenes,[15,16] which are frequently employed in transition-metal catalysis.[7] Therefore, we wondered if a catalyst with a superior reactivity profile could be developed by preventing salt elimination and daop formation. Herein, we present a sterically hindered diaminochlorophosphine as ligand for efficient arylation reactions of amines and α-C–H acidic ketones with ample scope.

[*] Dr. L. Ackermann, Dipl.-Chem. J. H. Spatz, Dipl.-Chem. C. J. Gschrei, Dipl.-Chem. R. Born, Dipl.-Chem. A. Althammer
Department Chemie und Biochemie
Ludwig-Maximilians-Universität München
Butenandtstrasse 5–13, Haus F, 81377 München (Germany)
Fax: (+49) 89-2180-77425
E-mail: lutz.ackermann@cup.uni-muenchen.de
Homepage: http://www.cup.uni-muenchen.de/oc/ackermann/

[**] Support by the DFG (Emmy Noether-Programm), the Fonds der Chemischen Industrie, Professor Paul Knochel, and the Ludwig-Maximilians-Universität is gratefully acknowledged. We thank Saltigo GmbH (Leverkusen) for the generous gift of chemicals.

Supporting information for this article is available on the WWW under http://www.angewandte.org or from the author.

Initial experiments were directed at probing the reactivity of various diaminochlorophosphines with respect to salt elimination with NaO*t*Bu (Scheme 1). While diaminochlorophosphine **1** was quantitatively converted to daop **2** within two hours, no reaction occurred when using bulky chloride **3**[17] under otherwise identical reaction conditions.

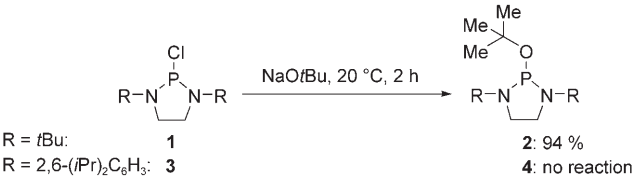

Scheme 1. Salt elimination from diaminochlorophosphines with NaO*t*Bu.

The catalytic activity of sterically congested **3** was tested in the amination of electronically deactivated aryl chloride **5a** (Table 1). A palladium complex of **3** (Table 1, entry 3) proved more active than the ones generated from either chlorophosphine **1** or daop **2**[12] (Table 1, entries 1 and 2). The superior catalytic performance allowed for a significant reduction of catalyst loading (Table 1, entries 5 and 6), with an optimal palladium/ligand ratio of 1:2 (Table 1, entries 4 and 5). Importantly, a complex derived from the corresponding daop **4** displayed a considerably reduced efficacy (Table 1, entry 7). These experiments highlight a different working mode for sterically hindered ligand **3**, when compared with the one observed for preligand **1**.[18]

Table 1: Ligand studies for the amination of aryl chloride **5a**.[a]

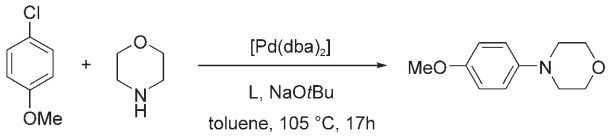

5a **6a** **7a**

Entry	[Pd(dba)$_2$][b] (mol%)	L (mol%)	Yield [%][c]
1	5.0	**1** (10.0)	63
2	5.0	**2** (10.0)	62
3	5.0	**3** (10.0)	98
4	1.0	**3** (1.0)	32
5	1.0	**3** (2.0)	93
6	0.5	**3** (1.0)	86
7	5.0	**4** (10.0)	31

[a] Reaction conditions: **5a** (1.0 mmol), **6a** (1.2 mmol), NaO*t*Bu (1.3 mmol), toluene (3.0 mL), 105 °C, 17 h. [b] dba = dibenzylideneacetone. [c] Yield of isolated product.

Subsequently, the scope of the amination reaction with aryl chlorides was studied, with particular emphasis on more demanding substrate combinations (Table 2). Sterically hindered aniline derivatives were efficiently converted (Table 2, entries 1, 2, 5, 8, 9, and 13). Furthermore, high yields of isolated product were obtained using electron-rich, thereby electronically deactivated, aryl chlorides and bromides, even

 © 2006 Wiley-VCH Verlag GmbH & Co. KGaA, Weinheim

Table 2: Amination reactions with challenging substrates.[a]

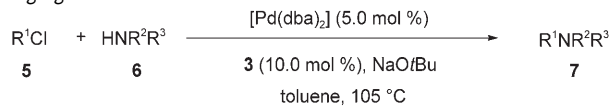

Entry	Chloride	Amine	Product	Yield [%][b]	Entry	Chloride	Amine	Product	Yield [%][b]
1	**5b**	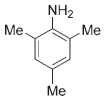 **6b**	**7b**[c]	97	8	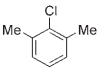 **5e**	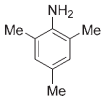 **6b**	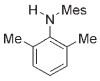 **7i**[c]	98
2	**5c**	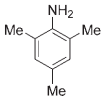 **6b**	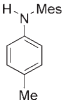 **7c**[c]	97	9	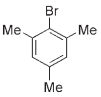 **10a**	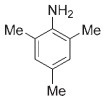 **6b**	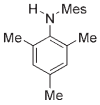 **7j**[c]	87
3	**5d**	**6c**	**7d**	93	10	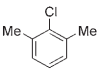 **5e**	**6f**	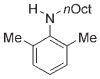 **7k**	94
4	**5d**	**6d**	**7e**	96	11	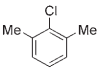 **5e**	**6g**	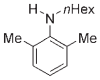 **7l**	85
5	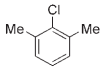 **5e**	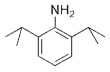 **6e**	**7f**[d]	91	12	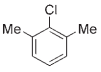 **5e**	**6h**	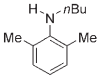 **7m**	80
6	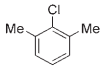 **5e**	**6c**	**7g**	93	13	**5f**	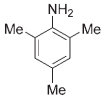 **6b**	**7n**[c]	85
7	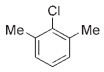 **5e**	**6d**	**7h**	88	14	**5b**	**6i**	**7o**	91

[a] Reaction conditions: **5** (1.0 mmol), **6** (1.2 mmol), NaO*t*Bu (1.3 mmol), [Pd(dba)$_2$] (5.0 mol %), **3** (10.0 mol %), toluene (3.0 mL), 105 °C, 2–21 h. [b] Yield of isolated product. [c] Mes = 2,4,6-$Me_3C_6H_2$. [d] Ar = 2,6-($iPr)_2C_6H_3$.

when bearing *ortho* substituents (Table 2, entries 3–12). Thus, tetra-*ortho*-substituted diaryl amines were prepared in high yields (Table 2, entries 5, 8, and 9). Acyclic alkyl amines are difficult substrates, as the palladium amide complexes derived thereof easily undergo β-hydride elimination.[3] Nonetheless, the catalyst formed from bulky **3** performed well in arylation reactions of alkyl amines (Table 2, entries 10–12). Also the synthesis of a heteroaromatic species or of a tertiary amine proceeded well (Table 2, entries 13, and 14, respectively).

Among representative secondary chlorophosphines, sterically hindered diaminochlorophosphine **3** exhibited superior catalytic performance in the α-arylation[19] of ketone **8a** with aryl chloride **5a** (Table 3, entry 1, and the Supporting Information).

A palladium complex that was generated from ligand **3** proved applicable to the α-arylation employing iodides, bromides, and chlorides (Table 3, entries 1–3). With respect to aryl chlorides, electronically deactivated electrophiles were efficiently converted, thus giving rise to the corresponding ketones with high yields of isolated product (Table 3, entries 4–11).

 © 2006 Wiley-VCH Verlag GmbH & Co. KGaA, Weinheim

Table 3: Scope of the α-arylation using electron-rich chlorides.[a]

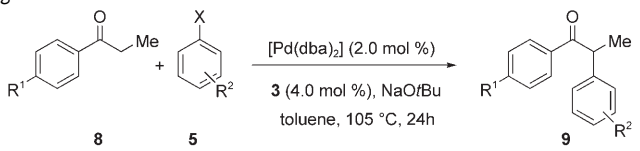

8 5 9

Entry	R^1	Halide	Product	Yield [%][b]	Entry	R^1	Halide	Product	Yield [%][b]
1	H			90	7	OMe		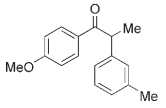	89
	8a	**5a**				**8c**	**5g**	**9e**	
2	H	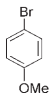	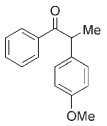	98	8	F		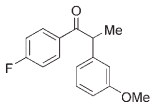	80
	8a	**10b**	**9a**			**8b**	**5h**	**9f**	
3	H			96	9	OMe		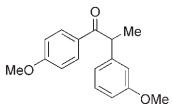	78
	8a	**11a**				**8c**	**5h**	**9g**	
4	F		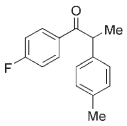	92	10	H	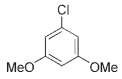	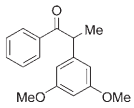	75
	8b	**5c**	**9b**			**8a**	**5i**	**9h**	
5	OMe		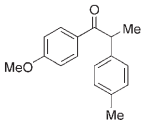	90	11	OMe	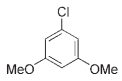	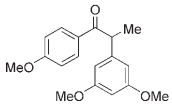	87
	8c	**5c**	**9c**			**8c**	**5i**	**9i**	
6	F		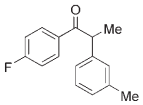	90					
	8b	**5g**	**9d**						

[a] Reaction conditions: **8** (1.2 mmol), **5** (1.0 mmol), NaO*t*Bu (1.3 mmol), [Pd(dba)$_2$] (2.0 mol%), **3** (4.0 mol%), toluene (2.5 mL), 105°C, 24 h. [b] Yield of isolated product.

In summary, we have demonstrated that sterically hindered substituents on the nitrogen atoms of secondary chlorophosphines prevent formation of diaminooxophosphines and thereby facilitate efficient palladium-catalyzed arylation reactions of amines and α-C–H acidic ketones with ample scope.

Experimental Section

Representative procedure for the palladium-catalyzed amination of aryl chlorides (Table 1, entry 3): A solution of [Pd(dba)$_2$] (29 mg, 0.05 mmol, 5.0 mol%) and **3** (44 mg, 0.10 mmol, 10.0 mol%) in toluene (3.0 mL) was stirred for 10 min at room temperature under N_2. NaO*t*Bu (125 mg, 1.30 mmol), **6a** (103 mg, 1.18 mmol), and **5a** (147 mg, 1.03 mmol) were added, and the resulting mixture was stirred at 105°C for 17 h. Et_2O (50 mL) and brine (50 mL) were added to the cooled reaction mixture. The separated aqueous phase was extracted with Et_2O (3×50 mL). The combined organic layers were dried over $MgSO_4$ and concentrated in vacuo. The remaining residue was purified by column chromatography on silica gel (*n*-pentane/Et_2O, 5:1→4:1) to yield **7a** as an orange solid (199 mg, 98%).

Received: June 2, 2006
Revised: July 25, 2006
Published online: October 17, 2006

 © 2006 Wiley-VCH Verlag GmbH & Co. KGaA, Weinheim

Keywords: arylation · C—N coupling · cross-coupling · palladium · phosphane ligands

[1] B. Schlummer, U. Scholz, *Adv. Synth. Catal.* **2004**, *346*, 1599 – 1626.
[2] J. F. Hartwig in *Modern Arene Chemistry* (Ed.: D. Astruc), Wiley-VCH, Weinheim, **2002**, pp. 107 – 168.
[3] L. Jiang, S. L. Buchwald in *Metal-Catalyzed Cross-Coupling Reactions*, 2nd ed. (Eds.: A. de Meijere, F. Diederich), Wiley-VCH, Weinheim, **2004**, pp. 699 – 760.
[4] A. Zapf, M. Beller, T. Riermeier in *Transition Metals for Organic Synthesis*, 2nd ed. (Eds.: M. Beller, C. Bolm), Wiley-VCH, Weinheim, **2004**, pp. 231 – 256.
[5] A. F. Littke, G. C. Fu, *Angew. Chem.* **2002**, *114*, 4350 – 4386; *Angew. Chem. Int. Ed.* **2002**, *41*, 4176 – 4211.
[6] Selected recent examples: a) E. R. Strieter, S. L. Buchwald, *Angew. Chem.* **2006**, *118*, 939 – 942; *Angew. Chem. Int. Ed.* **2006**, *45*, 925 – 928; b) Q. Shen, S. Shekhar, J. P. Stambuli, J. F. Hartwig, *Angew. Chem.* **2005**, *117*, 1395 – 1399; *Angew. Chem. Int. Ed.* **2005**, *44*, 1371 – 1375; c) F. Rataboul, A. Zapf, R. Jackstell, S. Harkal, T. Riermeier, A. Monsees, U. Dingerdissen, M. Beller, *Chem. Eur. J.* **2004**, *10*, 2983 – 2990; d) M. Nishiyama, T. Yamamoto, Y. Koie, *Tetrahedron Lett.* **1998**, *39*, 617 – 620.
[7] For the use of N-heterocyclic carbenes in catalysis, see: W. A. Herrmann, *Angew. Chem.* **2002**, *114*, 1342 – 1363; *Angew. Chem. Int. Ed.* **2002**, *41*, 1290 – 1309.
[8] G. Y. Li, *Angew. Chem.* **2001**, *113*, 1561 – 1564; *Angew. Chem. Int. Ed.* **2001**, *40*, 1513 – 1516.
[9] G. Y. Li, G. Zheng, A. F. Noonan, *J. Org. Chem.* **2001**, *66*, 8677 – 8681.
[10] G. Burton, P. Cao, G. Li, R. Rivero, *Org. Lett.* **2003**, *5*, 4373 – 4376.
[11] L. Ackermann, *Synthesis* **2006**, 1557 – 1571.
[12] L. Ackermann, R. Born, *Angew. Chem.* **2005**, *117*, 2497 – 2500; *Angew. Chem. Int. Ed.* **2005**, *44*, 2444 – 2447.
[13] For the use of a triaminophosphine ligand, see: S. Urgaonkar, J.-H. Xu, J. G. Verkade, *J. Org. Chem.* **2003**, *68*, 8416 – 8423.
[14] Examples for transition-metal-catalyzed coupling reactions employing air-stable heteroatom-substituted secondary phosphine oxides: a) L. Ackermann, R. Born, J. H. Spatz, D. Meyer, *Angew. Chem.* **2005**, *117*, 7382 – 7386; *Angew. Chem. Int. Ed.* **2005**, *44*, 7216 – 7219; b) L. Ackermann, *Org. Lett.* **2005**, *7*, 3123 – 3125; c) L. Ackermann, C. J. Gschrei, A. Althammer, M. Riederer, *Chem. Commun.* **2006**, 1419 – 1421; d) L. Ackermann, A. Althammer, R. Born, *Angew. Chem.* **2006**, *118*, 2681 – 2685; *Angew. Chem. Int. Ed.* **2006**, *45*, 2619 – 2622; e) L. Ackermann, A. Althammer, *Org. Lett.* **2006**, *8*, 3457 – 3460.
[15] D. Gudat, *Coord. Chem. Rev.* **1997**, *163*, 71 – 106.
[16] H. Nakazawa, *Adv. Organomet. Chem.* **2004**, *50*, 107 – 143.
[17] M. B. Abrams, B. L. Scott, R. T. Baker, *Organometallics* **2000**, *19*, 4944 – 4956.
[18] Studies directed towards elucidating the catalyst's working mode were performed by employing either $[Pd(dba)_2]$ or $[PdCl_2(PhCN)_2]$. Accordingly, addition of chlorophosphine **3** to a solution of $[PdCl_2(PhCN)_2]$ in toluene yielded the catalytically active homobimetallic chlorophosphine complex $[\{LPdCl_2\}_2]$ (L = **3**). For relevant coordination chemistry, see, for example: a) D. E. Berry, K. A. Beveridge, G. W. Bushnell, K. R. Dixon, *Can. J. Chem.* **1985**, *63*, 2949 – 2957; b) reference [11].
[19] D. C. Culkin, J. F. Hartwig, *Acc. Chem. Res.* **2003**, *36*, 234 – 245.

 © 2006 Wiley-VCH Verlag GmbH & Co. KGaA, Weinheim

[2+2] Cycloadditions

DOI: 10.1002/anie.200601592

Formation of an Organometallic Ladderane Derivative by Dynamic Topochemical Reaction Control**

Jan Paradies, Ingo Greger, Gerald Kehr, Gerhard Erker, Klaus Bergander, and Roland Fröhlich*

Dedicated to Professor Manfred Christl on the occasion of his 65th birthday

Topochemical reaction control offers unique possibilities for carbon–carbon coupling reactions.[1] Typical examples include the formation of cyclobutane or even ladderane[2,3] (annelated oligocyclobutane) derivatives by photochemical [2+2] cycloaddition reactions of substituted alkenes in suitably orientated spatial arrangements in a crystal lattice,[4] on rigid organic frameworks,[5] or through hydrogen-bridged scaffolds.[6] Essentially, cyclobutane ring formation by photolytic [2+2] cycloaddition often readily takes place in such a situation when the distance between the neighboring π systems involved is close enough (≤ 3.6 Å separation), but may not occur at larger distances between the individual conjugated oligo-ene chains in the crystal or in solution.[5] An alternative approach might be to attach, for example, butadienyl chains at the Cp rings of a bent metallocene ($\Theta < 180°$; see Scheme 1). In these conformationally flexible systems[7] the pairs of dienyl substituents may come into close enough proximity (< 3.6 Å) to potentially allow for cyclobutane or even ladderane formation by photochemical [2+2] cycloaddition.

On the basis of related *ansa*-metallocene work[8] we have now found and studied an example of the formation of an

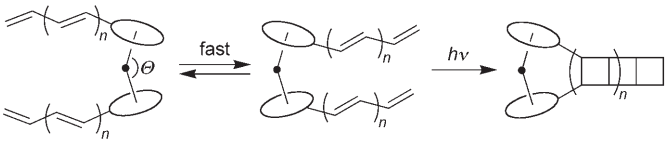

Scheme 1.

[*] Dr. J. Paradies, Dipl.-Chem. I. Greger, Dr. G. Kehr, Prof. Dr. G. Erker, Dr. K. Bergander, Dr. R. Fröhlich[+]
Organisch-Chemisches Institut
Universität Münster
48149 Münster (Germany)
Fax: (+49) 251-83-36503
E-mail: erker@uni-muenster.de

[+] X-Ray crystal structure analyses

[**] Financial support from the Fonds der Chemischen Industrie and the Deutsche Forschungsgemeinschaft is gratefully acknowledged.

Supporting information for this article is available on the WWW under http://www.angewandte.org or from the author.

WILEY InterScience DISCOVER SOMETHING GREAT
© 2006 Wiley-VCH Verlag GmbH & Co. KGaA, Weinheim

organometallic cyclooctadiene derivative and an isomeric small ladderane system by means of such a dynamic topochemical reaction at a substituted Group 4 bent-metallocene system. The synthesis of the bis(butadienylcyclopentadienyl) dichlorozirconium complex (**5**) was carried out by the fulvene route.[9] Fulvene **2** was prepared by condensation of crotonic aldehyde with sodium cyclopentadienide and hydrolytic work up.[10] Subsequent deprotonation was cleanly effected by treatment with potassium hexamethyldisilazide (**3**) in diethyl ether at 0 °C. The resulting potassium butadienylcyclopentadienide (**4**) was then transmetalated to the zirconium center by treatment with zirconium tetrachloride in THF at −78 °C to yield **5** as a yellow solid (78 % isolated; Scheme 2).

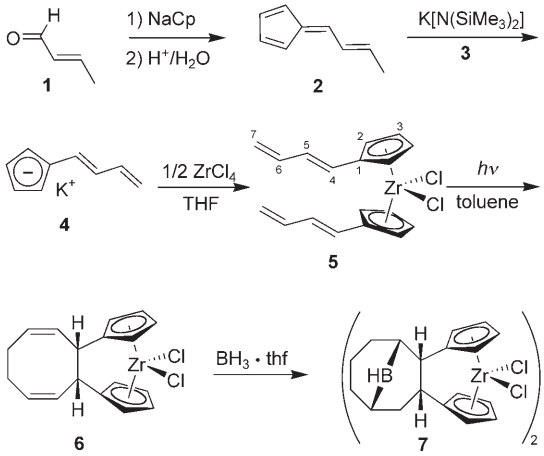

Scheme 2.

Photolysis of complex **5** at ambient temperature (Philips HPK 125, pyrex filter, toluene) resulted in consumption of the starting material within about one hour. From the resulting reaction mixture complex **6** was isolated as the product of a formal intramolecular [4+4] cycloaddition. Complex **6** was characterized by X-ray diffraction (Figure 1; single crystals from toluene). The system features a C_1-symmetric, cyclooctadienylene-bridged *ansa*-metallocene framework. The C_2 bridge (C6–C13 1.556(4) Å) is located at the narrow side of the bent-metallocene wedge ($Cp_{centroid}$-Zr-$Cp_{centroid}$ 125.0°). The doubly unsaturated C_8 ring is found in a distorted tub-shaped cisoid conformation with both the internal double bonds (C7–C8 1.328(4) Å, C11–C12 1.319(4) Å) orientated toward the same lateral metallocene sector.

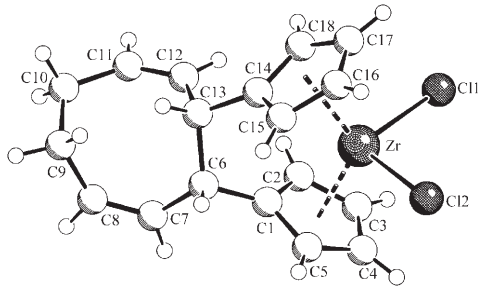

Figure 1. Molecular structure of the cyclooctadienylene-bridged *ansa*-metallocene **6** in the solid state.

Complex **6** behaves like a typical cyclooctadiene derivative. Upon treatment with the borane·thf complex it adds BH_3. From the reaction mixture the respective organometallic 9-BBN derivative **7** was isolated as a [B]-(μ-H)$_2$-[B] dimer as shown by an X-ray crystal structure analysis (Figure 2).

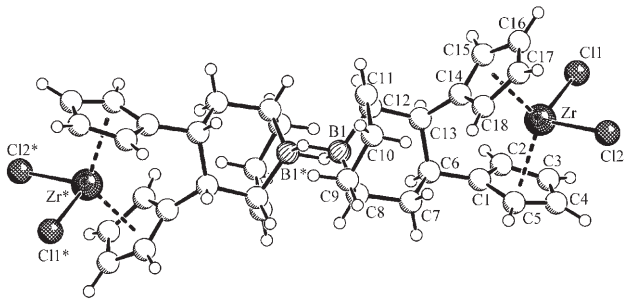

Figure 2. Molecular structure of the organometallic 9-BBN derivative **7** in the solid state.

Photolysis of **5** in dichloromethane at low temperature revealed a rather complex system of product-forming reactions. The ratio of the obtained products depended critically on the actual reaction conditions. In a typical experiment, irradiation of **5** at −80 °C (quartz filter, CD_2Cl_2, four hours) and subsequent NMR analysis at room temperature showed the formation of a mixture of four products. A major product (ca. 35 %) was assigned the structure of the C_s-symmetric ladderane derivative **8** according to its characteristic NMR spectra. The ^{1}H NMR spectrum features an ABCD pattern of a pair of symmetry-equivalent Cp ligands. The bridging C_8H_{10} ladderane moiety gives rise to a set of five groups of ^{1}H NMR signals in equal intensity: three of the cyclobutane tertiary CH resonances and two of the *exo*/*endo* protons of the CH_2CH_2 unit of the terminal ladderane four-membered ring. A detailed NMR analysis (including NOE experiments) indicated an all-*exo* stereochemical connectivity of **8** (for details, see the Experimental Section and the Supporting Information).

A second product (yield ca. 20 %) was assigned the structure of the isomer **9**, as it exhibits a pair of non-symmetry-related Cp ligands, each featuring an AA′BB′ ^{1}H NMR pattern. The bridging tricyclo[4.1.1.0^{2,5}]octandiyl moiety features a set of six ^{1}H NMR resonances in a 2:2:2:2:1:1 intensity ratio and five corresponding ^{13}C NMR signals (2:2:2:1:1; for details, see the Experimental Section and the Supporting Information). Moreover, the cyclooctadiene (cod) product **6** was formed (ca. 25 %), and there is a fourth minor isomer that is yet to be identified.

Photolysis of **5** at −80 °C (quartz filter, CD_2Cl_2, one hour) with subsequent NMR monitoring at low temperature helped to reveal which primary products were formed in this reaction (Scheme 3). Again, formation of the ladderane derivative **8** is observed (ca. 30 %) and is accompanied by a new major product (**10**, ca. 60 %), which is also C_s-symmetric. This compound features the typical NMR resonances of a cyclobutane ring (^{13}C NMR: $\delta = 44.1$ (C8), 23.7 ppm (C9); ^{1}H NMR: $\delta = 2.35$, 2.08 (H9^a/H9^b), 3.41 ppm (H8)) that was formed by photochemical [2+2] cycloaddition between the

 © 2006 Wiley-VCH Verlag GmbH & Co. KGaA, Weinheim

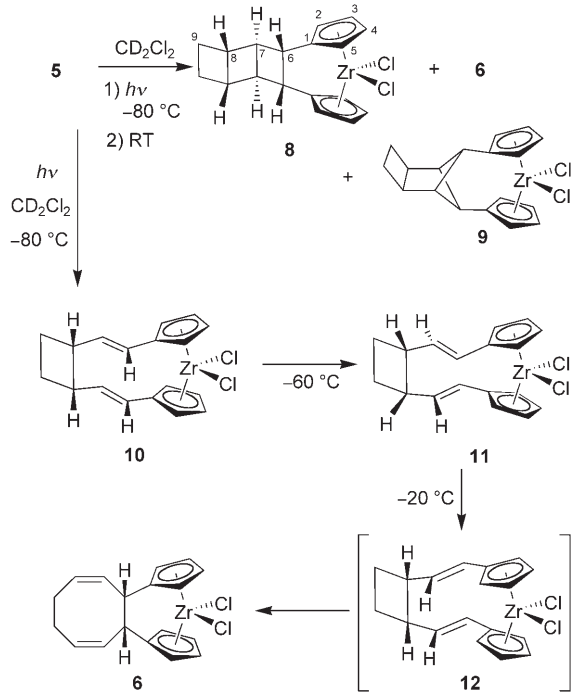

Scheme 3.

pair of H_2C=CH end groups of the butadienyl moieties of **5**, while the pair of internal *trans*-CH=CH groups remained unreacted (^{1}H NMR: $\delta = 5.68/6.07$ ppm (*trans*-$^3J_{HH} = 16.3$ Hz, H6/H7); ^{13}C NMR: $\delta = 122.5$, 137.5 ppm). As expected, compound **10** features a set of four methine signals for the pair of symmetry-equivalent Cp ligands (^{1}H NMR: $\delta = 6.81$, 6.72, 6.59, 6.01 ppm (H2–H5); for further details, see the Supporting Information). At higher monitoring temperatures up to room temperature the ladderane derivative **8** remained unchanged, but a stepwise conversion of **10** resulted. At about −60 °C complex **10** rearranged to an isomer for which we have assigned the structure of the C_1-symmetric conformer **11**. The isomer features two different internal *trans*-C=C bonds (^{1}H NMR: $\delta = 5.90/6.29$ ($^3J = 16.5$ Hz, H6/H7), $\delta = 6.16/5.86$ ppm ($^3J = 16.6$ Hz, H6′/H7′); ^{13}C NMR: $\delta = 124.1/139.8$ (C6/C7), $\delta = 123.2/135.7$ ppm (C6′/C7′)) in addition to the corresponding pairs of distal cyclobutane ring signals (^{13}C NMR: $\delta = 42.8/42.3$ ppm (C8/C8′), $\delta = 23.3/21.0$ ppm (C9/C9′)). Raising the temperature further to −20 °C led to subsequent formation of the cod derivative **6**. Presumably this reaction takes place through a further conformational rearrangement to the organometallic "(s-*cis*)-*cis*-divinylcyclobutane" derivative **12**, which is unstable under the applied reaction conditions and rapidly undergoes a thermally induced Cope rearrangement to form **6**. Possibly, the product **9** is formed from a subsequent photoreaction of the intermediate **11**, but this needs to be confirmed by further detailed mechanistic investigations.

The photolysis of **5** was carried out on a preparative scale (18 hours, −80 °C, CH_2Cl_2, pyrex filter). From the resulting mixture the cod derivative **6** was removed by the hydroboration reaction (see Scheme 2). Subsequent crystallization from *n*-heptane gave a mixture of the ladderane derivative **8** and its isomer **9** (ca. 1:1 ratio, ca. 40 % yield).

We have favorably used the special features of the conformationally rapidly equilibrating bent-metallocene framework to bring conjugated diene chains into sufficiently close proximity to allow C–C coupling reactions to take place that are otherwise typically observed under the conditions of topochemical reaction control. In our case the photochemical [2+2] cycloaddition reaction between the distal butadiene CH=CH_2 units takes place readily to form the cyclobutane derivative **10** and represents a *dynamic topochemical reaction* (to eventually yield the novel organometallic cod derivative **6** in a series of subsequent thermally induced reaction steps). A probable competing reaction even leads to the formation of the unique organometallic ladderane derivative **8**. The observed reaction pathways at the Group 4 bent-metallocene framework may indicate that carrying out intramolecular C–C coupling reactions at suitable dynamic frameworks may be an interesting methodological extension of the topochemical reaction principle.

Experimental Section

5: ^{1}H NMR (599.8 MHz, C_7D_8, 25 °C): $\delta = 6.32$ (m, 2H, H5), 6.21 (m, 2H, H6), 6.07 (d, $J = 15.6$ Hz, 2H, H4), 5.97 (m, 4H, H2), 5.78 (m, 4H, H3), 5.12 (dd, 2H, $H7_{cis}$), 4.97 ppm (dd, 2H, $H7_{trans}$); ^{13}C NMR (150.8 MHz, C_7D_8, 25 °C): $\delta = 126.8$ (C1), 115.2/114.9 (C2/C3 of Cp), 125.8, 132.1, 137.1, 118.3 ppm (C4–C7, butadienyl); decomp: 126 °C. Elemental analysis (%) calcd for $C_{18}H_{18}ZrCl_2$: C 54.53, H 4.58; found: C 54.74, H 4.65.

6: ^{1}H NMR (599.8 MHz, C_7D_8, 25 °C): $\delta = 6.46$ (m, 2H, H4), 6.31 (m, 2H, H3), 5.70 (m, 2H, H2), 5.40 (m, 2H, H5), 5.32 (m, 2H, H8), 5.28 (m, 2H, H7), 4.01 (m, 2H, H6), 2.13 (m, 2H, H9^a), 1.70 ppm (m, 2H, H9^b); ^{13}C{^{1}H} NMR (150.8 MHz, C_7D_8, 25 °C): $\delta = 136.9$ (C1), 130.4 (C7), 129.3 (C8), 124.8 (C4), 121.6 (C3), 110.5 (C2), 109.3 (C5), 46.2 (C6), 27.9 ppm (C9); m.p.: 128 °C. Elemental analysis (%) calcd for $C_{18}H_{18}ZrCl_2$: C 54.53, H 4.58; found: C 54.58, H 4.92.

8: ^{1}H NMR (599.8 MHz, CD_2Cl_2, −60 °C): $\delta = 6.68$, 6.61, 6.37, 6.24 (each m, each 2H, Cp), 4.01 (m, 2H, H6), 3.13 (m, 2H, H7), 2.78 (m, 2H, H8), 2.52, 2.02 ppm (each m, each 2H, H9^a, H9^b); ^{13}C NMR (150.8 MHz, CD_2Cl_2, −60 °C): $\delta = 140.1$ (C1), 124.1, 121.7, 110.1, 109.2 (C2–C5 of Cp), 48.3 (C6), 44.7 (C7), 41.5 (C8), 25.3 ppm (C9).

9: ^{1}H NMR (599.8 MHz, CD_2Cl_2, 25 °C): $\delta = 6.72$, 6.02 (each m, each 2H, Cp), 6.66, 5.90 (each m, each 2H, Cp′), 3.65 (d, $J = 4.9$ Hz, 1H, CH), 3.02 (m, 2H, CH), 2.77 (m, 2H, CH), 2.63 (d, $J = 4.9$ Hz, 1H, CH), 2.35, 1.70 ppm (each m, each 2H, CH_2); ^{13}C{^{1}H} NMR (150.8 MHz, CD_2Cl_2, 25 °C): $\delta = 124.0$, 111.6 (Cp′), 124.0, 111.3 (Cp), 50.7 (CH), 49.6 (CH), 39.1 (CH), 38.7 (CH), 22.8 ppm (CH_2).

X-ray crystal structure analysis of **6**: $C_{18}H_{18}Cl_2Zr$, $M_r = 396.44$, $a = 7.981(1)$, $b = 8.030(1)$, $c = 13.336(1)$ Å, $\alpha = 102.14(1)$, $\beta = 106.37(1)$, $\gamma = 94.89(1)$°, $V = 792.1(2)$ Å^3, $\rho_{calcd} = 1.662$ g cm^{-3}, $\mu = 1.021$ mm^{-1}, empirical absorption correction ($0.629 \le T \le 0.749$), $Z = 2$, triclinic, space group $P\bar{1}$ (No. 2), $\lambda = 0.71073$ Å, $T = 198$ K, ω and ϕ scans, 9869 reflections collected ($\pm h$, $\pm k$, $\pm l$), $[(\sin\theta)/\lambda] = 0.67$ Å^{-1}, 3848 independent ($R_{int} = 0.34$) and 3531 observed reflections ($I \ge 2\sigma(I)$), 190 refined parameters, $R = 0.034$, $wR^2 = 0.084$.

X-ray crystal structure analysis of **7**: $C_{36}H_{40}B_2Cl_4Zr_2{\cdot}2CHCl_3$, $M_r = 1057.28$, $a = 7.332(1)$, $b = 14.562(1)$, $c = 18.614(1)$ Å, $\beta = 90.82(1)$°, $V = 1987.2(3)$ Å^3, $\rho_{calcd} = 1.767$ g cm^{-3}, $\mu = 1.228$ mm^{-1}, empirical absorption correction ($0.640 \le T \ge 0.941$), $Z = 2$, monoclinic, space group $P2_1/n$ (No. 14), $\lambda = 0.71073$ Å, $T = 198$ K, ω and ϕ scans, 12978 reflections collected ($\pm h$, $\pm k$, $\pm l$), $[(\sin\theta)/\lambda] = 0.65$ Å^{-1}, 4541 independent ($R_{int} = 0.043$) and 3681 observed reflections ($I \ge 2\sigma(I)$), 255 refined parameters, $R = 0.064$, $wR^2 = 0.204$.

 © 2006 Wiley-VCH Verlag GmbH & Co. KGaA, Weinheim

For additional information, including the programs used, see the Supporting Information.

Received: April 23, 2006
Revised: July 31, 2006
Published online: October 20, 2006

Keywords: cycloadditions · ladderanes · photochemistry · topochemical reactions · zirconocenes

[1] a) M. D. Cohen, G. M. J. Schmidt, *J. Chem. Soc.* **1964**, 1996–2000; b) G. M. J. Schmidt, *J. Chem. Soc.* **1964**, 2014–2021; c) J. Bregman, K. Osaki, G. M. J. Schmidt, F. I. Sonntag, *J. Chem. Soc.* **1964**, 2021–2030; see also: D. J. Tantillo, R. Hoffmann, *Angew. Chem.* **2002**, *114*, 1075–1078; *Angew. Chem. Int. Ed.* **2002**, *41*, 1033–1036.

[2] H. Hopf, *Angew. Chem.* **2003**, *115*, 2928–2931; *Angew. Chem. Int. Ed.* **2003**, *42*, 2822–2825.

[3] a) J. S. S. Damsté, M. Strous, W. I. C. Rijpstra, E. C. Hopmans, J. A. J. Geenevasen, A. C. T. Duin, L. A. van Niftrik, M. S. M. Jetten, *Nature* **2002**, *419*, 708–712; b) M. M. M. Kuypers, A. O. Sliekers, G. Lavik, M. Schmidt, B. B. Jorgensen, J. G. Kuenen, J. S. S. Damsté, M. Strous, M. S. M. Jetten, *Nature* **2003**, *422*, 608–611; c) V. Mascitti, E. J. Corey, *J. Am. Chem. Soc.* **2004**, *126*, 15664–15665.

[4] X. Gao, T. Friščić, L. R. MacGillivray, *Angew. Chem.* **2004**, *116*, 234–238; *Angew. Chem. Int. Ed.* **2004**, *43*, 232–236.

[5] a) H. Hopf, H. Greiving, P. G. Jones, P. Bubenitschek, *Angew. Chem.* **1995**, *107*, 742–744; *Angew. Chem. Int. Ed. Engl.* **1995**, *34*, 685–687; b) H. Zitt, I. Dix, H. Hopf, P. G. Jones, *Eur. J. Org. Chem.* **2002**, 2298–2307; c) H. Greiving, H. Hopf, P. G. Jones, P. Bubenitschek, J.-P. Desvergne, H. Bouas-Laurent, *Eur. J. Org. Chem.* **2005**, 558–566; d) H. Hopf, H. Greiving, C. Beck, I. Dix, P. G. Jones, J.-P. Desvergne, H. Bouas-Laurent, *Eur. J. Org. Chem.* **2005**, 567–581.

[6] D. B. Varshney, X. Gao, T. Friščić, L. R. MacGillivray, *Angew. Chem.* **2006**, *118*, 662–666; *Angew. Chem. Int. Ed.* **2006**, *45*, 646–650.

[7] a) C. Krüger, M. Nolte, G. Erker, S. Thiele, *Z. Naturforsch. B* **1992**, *47*, 995–999; b) M. Knickmeyer, G. Erker, T. Fox, *J. Am. Chem. Soc.* **1996**, *118*, 9623–9630; c) T. Jödicke, F. Menges, G. Kehr, U. Höweler, R. Fröhlich, *Eur. J. Inorg. Chem.* **2001**, 2097–2106.

[8] a) G. Erker, S. Wilker, C. Krüger, R. Goddard, *J. Am. Chem. Soc.* **1992**, *114*, 10983–10984; b) G. Erker, S. Wilker, C. Krüger, M. Nolte, *Organometallics* **1993**, *12*, 2140–2151; c) W.-L. Nie, G. Erker, G. Kehr, R. Fröhlich, *Angew. Chem.* **2004**, *116*, 313–317; *Angew. Chem. Int. Ed.* **2004**, *43*, 310–313.

[9] a) K. Ziegler, W. Schäfer, *Justus Liebigs Ann. Chem.* **1934**, *511*, 101–109; b) K. Ziegler, H.-G. Gellert, H. Martin, K. Nagel, J. Schneider, *Justus Liebigs Ann. Chem.* **1954**, *589*, 91–121; c) M. F. Sullivan, W. F. Little, *J. Organomet. Chem.* **1967**, *8*, 277–285; d) P. Renaut, G. Tainturier, B. Gautheron, *J. Organomet. Chem.* **1978**, *148*, 43–51; e) J. Okuda, *Chem. Ber.* **1989**, *122*, 1075–1077; f) G. Erker, R. Nolte, Y.-H. Tsay, C. Krüger, *Angew. Chem.* **1989**, *101*, 642–644; *Angew. Chem. Int. Ed. Engl.* **1989**, *28*, 628–629; g) G. Erker, R. Nolte, R. Aul, S. Wilker, C. Krüger, R. Noe, *J. Am. Chem. Soc.* **1991**, *113*, 7594–7602; h) R. R. Squires, *Acc. Chem. Res.* **1992**, *25*, 461–467.

[10] M. Neuenschwander, D. Meuche, H. Schaltegger, *Helv. Chim. Acta* **1964**, *47*, 1022–1032.

 © 2006 Wiley-VCH Verlag GmbH & Co. KGaA, Weinheim

Directed Evolution

DOI: 10.1002/anie.200602772

Evolving Thermostable Reverse Transcriptase Activity in a DNA Polymerase Scaffold**

*Katharina B. M. Sauter and Andreas Marx**

DNA polymerases are involved in all DNA synthesis that occurs in nature.[1] Furthermore, DNA polymerases are the workhorses in numerous important molecular biological core technologies like the widely applied polymerase chain reaction (PCR), cDNA cloning, genome sequencing, and diagnostics based on nucleic acids.[2] In each of these processes the DNA polymerase requires a DNA strand as a template for directing DNA synthesis. In contrast, RNA templates are processed with marginal activity.[1] Nevertheless, it has been reported that some DNA polymerases like *Thermus thermophilus* (*Tth*) exhibit increased reverse transcriptase (RT) activity exclusively in the presence of Mn^{2+} ions.[3] However, for many applications in mRNA diagnosis, for example, in pathogen detection or gene expression analysis, employment of Mn^{2+} is not suited.[4] Thus, we asked whether one is able to generate a DNA polymerase that is proficient to first reverse transcribe RNA into DNA and subsequently amplify the DNA by PCR without the requirement of Mn^{2+} ions. Through this approach, new insights into DNA polymerase substrate recognition and valuable tools for applications should be gained.

Methods of directed evolution have been shown to be promising to engineer nucleic acid polymerases with altered properties.[5] Alterations have mainly been achieved by directed molecular evolution by using genetic complementation and/or screening,[6] phage display,[7] or in vitro compartmentalization.[8] Herein, we show that the generation of a new DNA polymerase function, that is, RT-PCR activity, is achievable through iterative screening of small libraries of DNA polymerases. Our example is one of the rare examples where using an arbitrary randomized (nonfocused) library was sufficient to identify a new DNA polymerase activity.

To evolve reverse transcriptase activity in an N-terminal, shortened form of DNA polymerase from *Thermus aquaticus* (*Klentaq*)[9] we randomized the open reading frame by error-prone PCR (epPCR).[10] Protein expression was conducted in 96-well plates, and enzymes were screened for PCR activity

[*] Dipl.-Chem. K. B. M. Sauter, Prof. Dr. A. Marx
Fachbereich Chemie
Universität Konstanz
Universitätsstrasse 10, M 726, 78457 Konstanz (Germany)
Fax: (+49) 7531-88-5140
E-mail: andreas.marx@uni-konstanz.de

[**] We gratefully acknowledge financial support by the DFG and Volkswagen Foundation. Samuel Weisbrod is gratefully acknowledged for his assistance in the preparation of the manuscript.

Supporting information for this article is available on the WWW under http://www.angewandte.org or from the author.

© 2006 Wiley-VCH Verlag GmbH & Co. KGaA, Weinheim

on DNA templates directly after heat denaturation of host proteins and lysis without the requirement of further purification steps. All procedures were performed by automated liquid handling, thus enabling high throughput if required. DNA polymerase activities were monitored using SYBR-green I for parallel quantification of PCR product formation and fluorescent readout in 384-well plates. Subsequently, the active variants were tested for their RT-PCR activity by employing a natural RNA target from bacteriophage MS2. RT-PCR activities were quantified with SYBRgreen I by melting-curve analysis of PCR product using a conventional real-time PCR-cycler in 96-well plates.

Already after screening 768 PCR-active variants derived from about 2000 initially collected clones, we identified a mutant (termed M1) that shows promising features in RT-PCR and was therefore further studied. M1 was subsequently purified to homogeneity (see the Supporting Information) for functional characterization, and we found that this mutant exhibits strikingly increased RT-PCR activity in comparison to the wild-type enzyme (Figure 1 a). While the parental

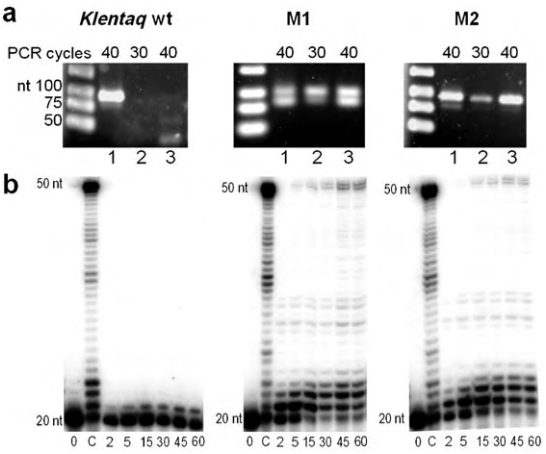

Figure 1. Analysis of the selected variants in comparison to the wild type. a) PCR activity of the respective enzyme using either a DNA target (lanes 1) or RNA target (lanes 2, 3). All reactions were conducted under identical reaction conditions (nt = nucleotides). b) Reverse transcriptase activity conducted with the indicated enzyme for the indicated reaction times [min] under identical reaction conditions. C = control reaction conducted with the corresponding DNA template.

enzyme was unable to form any significant PCR product from RNA after 40 cycles, under identical conditions M1 is clearly competent. All reactions were conducted by employing originally described PCR buffer and reaction conditions that were used for *Klentaq* and enable PCR product formation when DNA amplification is performed using a DNA target.[6c,9] Primer strands were designed to anneal at the 3′-terminus of the RNA target, and their design was not further optimized. However, the enzyme yields two products that are distinguishable through analysis by gel electrophoresis. The major product has the desired length and the expected sequence. However, this feature seems to be sequence-dependent, since when using RNA templates from different origin, for example, *E. coli* S16 mRNA, M1 yields the desired product exclusively (see the Supporting Information).

Next, we conducted a second round of randomization by employing epPCR, parallel expression, and screening as described above. After screening of approximately 2000 PCR-active mutants we identified one variant (termed M2) that was purified and further analyzed. M2 has RT-PCR activity and yields the desired PCR product (Figure 1 a).

Sequencing of the variant M1 revealed that six mutations have occurred that are distributed throughout the enzyme: L322M, L459M, S515R, I638F, S739G, and E773G (Figure 2 a). M2 bears only one additional mutation compared to the mutations already present in M1 (L789F).

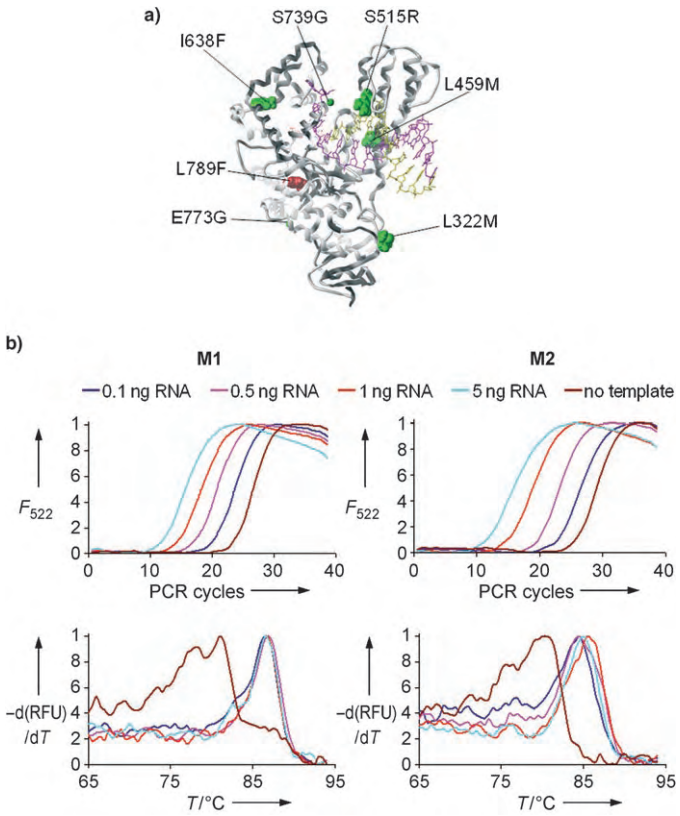

Figure 2. a) Mutations in the evolved RT-PCR-active DNA polymerases M1 (green) and M2 (green and red) are mapped on a ribbon representation of *Klentaq* (PDB code 1QSS).[11] The DNA template strand is shown in magenta, the primer strand in yellow. b) Upper: Results of real-time RT-PCR experiments using M1 and M2 with various amounts of RNA employing conventional real-time PCR equipment. Lower: Melting-curve analysis of the reaction products employing conventional real-time PCR equipment.

To further investigate the properties of M1 and M2 in comparison to the wild-type enzyme, we conducted primer-extension experiments (Figure 1 b). A DNA primer strand was annealed to its complementary site on a 50-nucleotide RNA template strand. When the primer/template complex was incubated with the wild-type *Klentaq*, the extension of the DNA primer by only one nucleotide was detected after gel analysis. Interestingly, similar low activity of *Tth* DNA polymerase in the absence of Mn^{2+} is observed when copying

 © 2006 Wiley-VCH Verlag GmbH & Co. KGaA, Weinheim

the RNA template (Supporting Information). However, both mutants M1 and M2 reverse transcribe RNA significantly more efficiently. Quantification of the respective activities under steady-state conditions indicates that the M1 and M2 mutants are about 40- and 22-fold, respectively, more active on the RNA template than the wild-type enzyme (Supporting Information). In marked contrast, the variants M1 and M2 are able to yield significantly longer reaction products that are sufficient for RT-PCR under identical conditions. However, quantification of the activity on DNA-directed primer extension indicates that both mutants have about twice the activity of the wild-type enzyme (Supporting Information). Thus, a clear activity gain for RNA-directed DNA synthesis was achieved by two rounds of iterative randomization and screening. Further assessment of the mutants in comparison to the wild-type enzyme indicates that this gain was not accompanied by a loss in thermostability, but by a loss of some selectivity (Supporting Information).

The specific detection of RNA through reverse transcription and subsequent cDNA amplification is fundamental for many applications in diagnosis, for example, pathogen detection or gene expression analysis.[4] To amplify RNA by RT-PCR, usually two enzymes have to be employed: a reverse transcriptase that synthesizes the complementary DNA strand and a thermostable DNA polymerase for PCR amplification. However, the first step is prone to failure owing to formation of stable RNA secondary structures and the diminished thermostability of the employed reverse transcriptases.[3] Thermostable M1 and M2 might be particularly interesting for a one-step RT-PCR approach. Thus, we investigated whether the mutants are applicable in quantitative detection of RNA by real-time one-step RT-PCR.[12] This method is extensively used for pathogen and gene expression diagnosis.[4] We followed the reactions by employing varied RNA concentrations in a conventional real-time PCR cycler with SYBRgreenI for detection of double-stranded DNA. Indeed, M1 and M2 are able to amplify DNA starting from RNA targets at various concentrations under standard conditions (Figure 2b). The observed RNA detection limit using the evolved enzyme is comparable to the performance of commercially available kits. When the wild-type enzyme was used, no such amplification curves were detected.

In summary, through screening of DNA polymerase libraries that contain arbitrary randomized mutants generated by epPCR, we were able to identify enzymes that exhibit RT-PCR function, a function that is imperceptible in the wild-type enzyme. As demonstrated, the identified mutants might find immediate applications and provide the basis for the development of new means for single-step RT-PCR technologies like pathogen RNA detection or gene expression analysis in real time. Functional and structural studies to elucidate the origin of the new function are underway.

Received: July 12, 2006
Published online: October 20, 2006

Keywords: directed evolution · DNA polymerase · DNA recognition · polymerase chain reaction · reverse transcriptase

[1] A. Kornberg, T. A. Baker, *DNA Replication*, 2nd ed., Freeman, New York, **1991**.
[2] J. Sambrook, D. W. Russell, *Molecular Cloning: A Laboratory Manual*, Cold Spring Harbor Laboratory Press, Cold Spring Harbor, **2001**.
[3] a) T. W. Myers, D. H. Gelfand, *Biochemistry* **1991**, *30*, 182–192; b) M. D. Jones, *Methods Enzymol.* **1993**, *218*, 413–419; c) V. I. Grabko, L. G. Chistyakova, V. N. Lyapustin, V. G. Korobko, A. I. Miroshnikov, *FEBS Lett.* **1996**, *387*, 189–192.
[4] a) S. A. Bustin, R. Mueller, *Clin. Sci.* **2005**, *109*, 365–379; b) A. K. Sandvik, B. K. Alsberg, K. G. Nørsett, F. Yadetie, H. L. Waldum, A. Lægreid, *Clin. Chim. Acta* **2006**, *363*, 157–164; c) S. Mocellin, C. R. Rossi, P. Pilati, D. Nitti, F. M. Marincola, *Trends Mol. Med.* **2003**, *9*, 189–195.
[5] a) A. A. Henry, F. E. Romesberg, *Curr. Opin. Biotechnol.* **2005**, *16*, 370–377; b) S. Brakmann, *Cell. Mol. Life Sci.* **2005**, *62*, 2634–2646; c) E. Loh, L. A. Loeb, *DNA Repair* **2005**, *4*, 1390–1398.
[6] a) P. H. Patel, L. A. Loeb, *J. Biol. Chem.* **2000**, *275*, 40266–40272; b) P. H. Patel, H. Kawate, E. Adman, M. Ashbach, L. A. Loeb, *J. Biol. Chem.* **2001**, *276*, 5044–5051; c) S. Brakmann, S. Grzeszik, *ChemBioChem* **2001**, *2*, 212–219; d) M. B. Kermekchiev, A. Tzekov, W. M. Barnes, *Nucleic Acids Res.* **2003**, *31*, 6139–6147; e) D. Summerer, N. Z. Rudinger, I. Detmer, A. Marx, *Angew. Chem.* **2005**, *117*, 4791–4794; *Angew. Chem. Int. Ed.* **2005**, *44*, 4712–4715.
[7] a) M. Fa, A. Radeghieri, A. A. Henry, F. E. Romesberg, *J. Am. Chem. Soc.* **2004**, *126*, 1748–1754; b) A. M. Leconte, L. Chen, F. E. Romesberg, *J. Am. Chem. Soc.* **2005**, *127*, 12470–12471; c) G. Xia, L. Chen, T. Sera, M. Fa, P. G. Schultz, F. E. Romesberg, *Proc. Natl. Acad. Sci. USA* **2002**, *99*, 6597–6602.
[8] a) F. J. Ghadessy, J. L. Ong, P. Holliger, *Proc. Natl. Acad. Sci. USA* **2001**, *98*, 4552–4557; b) F. J. Ghadessy, N. Ramsay, F. Boudsocq, D. Loakes, A. Brown, S. Iwai, A. Vaisman, R. Woodgate, P. Holliger, *Nat. Biotechnol.* **2004**, *22*, 755–759.
[9] W. M. Barnes, *Gene* **1992**, *112*, 29–35.
[10] R. C. Cadwell, G. F. Joyce, *PCR Methods Appl.* **1992**, *2*, 28–33.
[11] Y. Li, V. Mitaxov, G. Waksman, *Proc. Natl. Acad. Sci. USA* **1999**, *96*, 9491–9496.
[12] J. Wilhelm, A. Pingoud, *ChemBioChem* **2003**, *4*, 1120–1128.

 © 2006 Wiley-VCH Verlag GmbH & Co. KGaA, Weinheim

Thin Films

DOI: 10.1002/anie.200602670

Synthesis and Structure of Ultrathin Aluminosilicate Films**

Dario Stacchiola, Sarp Kaya, Jonas Weissenrieder, Helmut Kuhlenbeck, Shamil Shaikhutdinov, Hans-Joachim Freund, Marek Sierka, Tanya Kumanova Todorova, and Joachim Sauer*

Inorganic-chemistry textbooks define aluminosilicates as silicates in which some of the Si^{4+} ions are replaced by Al^{3+} ions. The excess negative charge arising from the replacement is balanced by positive ions, such as H^+ or alkali-metal cations. Zeolites are important microporous members of the aluminosilicate family, which have a large variety of applications ranging from catalysis and adsorption to agriculture and construction.[1] Both experimental and theoretical studies of zeolites, in particular, the precise determination of the catalytically active sites, are often hampered by the structural and chemical complexity of these compounds.[2] The employment of surface-sensitive techniques to elucidate the mechanism of catalytic reactions on zeolites at a fundamental level is challenging. Owing to the insulating properties of aluminum–silicon oxides, this approach can only be successful when applied to thin films grown on conducting metal substrates, as demonstrated for many binary oxides (for example, alumina, silica, magnesia, or iron oxides).[3–6] Thin zeolite films are also currently used in membrane technology,[7] chemical sensors,[8] and optoelectronic devices.[9]

Herein, we report the preparation of ordered ultrathin aluminosilicate films on a metal substrate. The atomic structure of the films was determined using scanning tunneling microscopy (STM), infrared reflection absorption spectroscopy (IRAS), photoelectron spectroscopy (PES) with synchrotron radiation, and density functional theory (DFT) calculations. This approach can be further developed for the preparation of thin zeolite films as model systems for atomistic studies of zeolite surfaces.

We have recently shown that an ordered thin silica film consisting of a two-dimensional (2D) network of corner-sharing $\{SiO_4\}$ tetrahedra can be grown on a Mo(112) substrate.[10–13] One oxygen atom of each $\{SiO_4\}$ tetrahedron in the film points towards molybdenum atoms in the substrate. Deposition of aluminum onto the film and subsequent annealing in vacuum leads to a partial reduction of the silica, as evidenced by X-ray photoelectron spectroscopy (XPS). This sequential preparation destroys the long-range order in the original silica film, as shown by low-energy electron diffraction (LEED). STM inspection of the product revealed a rough surface with particle-like features, which were interpreted as alumina nanoparticles embedded in the silica film. This observation is consistent with the results of Gründling et al., who obtained disordered Al_2O_3–SiO_2 films by vacuum annealing samples consisting of aluminum deposited onto approximately 3-nm-thick silica films on Mo(100) substrates.[14]

To facilitate the intermixing of aluminum and silicon in the film, we codeposited aluminum and silicon onto an O/Mo(112) surface in an oxygen environment (see Experimental Section). In the subsequent annealing in vacuum, the temperature was increased in steps, until LEED analysis of the film indicated an ordered structure.

After annealing films with low Al/Si ratios (less than 0.2) at 1100 K, a sharp LEED pattern corresponding to a c(2×2) structure on the Mo(112) surface, similar to that of the pure silica film, was observed. XPS investigation of these films indicated that the silicon and aluminum atoms are in fully oxidized states.

STM images of the mixed-oxide films reveal atomically flat terraces with only a few nanoparticles at their edges (Figure 1a). High-resolution images show the same honeycomb structure and antiphase domain boundaries reported

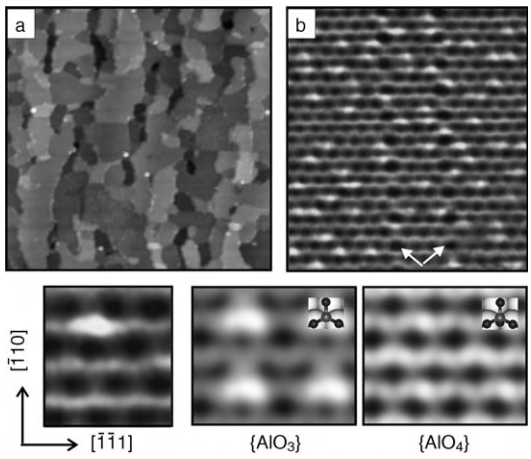

Figure 1. Top: STM images of an aluminosilicate film (Al/Si ≈ 1:5) on a Mo(112) substrate. Sizes and tunneling parameters: a) 100×100 nm^2, $V_s = 1.6$ V, $I = 0.2$ nA; b) 8×6 nm^2, $V_s = 1.2$ V, $I = 0.3$ nA. The arrows in (b) indicate antiphase domain boundaries along the molybdenum [$\bar{1}$10] direction. Bottom: simulated STM images for the $\{AlO_3\}$ and $\{AlO_4\}$ models are compared with an enlarged section of image (b). The $\{AlO_3\}$ and $\{AlO_4\}$ units are superimposed on the simulated images.

[*] Dr. D. Stacchiola, S. Kaya, Dr. J. Weissenrieder, Dr. H. Kuhlenbeck, Dr. S. Shaikhutdinov, Prof. H.-J. Freund
Department of Chemical Physics
Fritz-Haber-Institut der Max-Planck-Gesellschaft
Faradayweg 4–6, Berlin 14195 (Germany)
Fax: (+49) 30-84134105
E-mail: shaikhutdinov@fhi-berlin.mpg.de
Homepage: http://www.fhi-berlin.mpg.de/cp
Dr. M. Sierka, T. K. Todorova, Prof. J. Sauer
Humboldt-Universität zu Berlin
Institut für Chemie
Unter den Linden 6, Berlin 10099 (Germany)

[**] We acknowledge financial support from the Fonds der Chemischen Industrie and the EU Project GSOMEN. D.S. and J.W. thank the Alexander von Humboldt Foundation for fellowships. T.K.T. and S.K. acknowledge the International Max Planck Research School "Complex Surfaces in Materials Science". We also thank the Norddeutscher Verbund für Hoch- und Höchstleistungsrechnen (HLRN) for computing time.

WILEY InterScience DISCOVER SOMETHING GREAT
© 2006 Wiley-VCH Verlag GmbH & Co. KGaA, Weinheim

for the silica films (Figure 1b).[11,12] However, in contrast to the pure silica films, numerous bright spots were detected on the surface of the aluminosilcate films. These spots are approximately 0.2 Å higher than the neighboring protrusions. The density of the spots correlates well with the aluminum coverage determined by XPS, and their random distribution indicates a random distribution of the aluminum atoms in the film. The protrusions are slightly elongated along one of the principal directions of the silica lattice, which coincides with the $[\bar{1}\bar{1}1]$ direction of the Mo(112) surface (additional experiments demonstrated that this is not a tip artifact).

On the basis of these LEED and STM results, we propose that the structure of the aluminosilicate film consists of a 2D network of corner-sharing $\{SiO_4\}$ tetrahedra, in which some Si^{4+} ions are replaced by Al^{3+} ions. The charge defects introduced by the Al^{3+} ions must be compensated. In bulk aluminosilicates, this compensation is achieved by the intercalation of H^+ or alkali-metal cations. Alkali metals were not present during the film preparation, and H^+ ions were not detected by vibrational or electron spectroscopy. However, the extra charge in thin films can be easily accommodated by the electron reservoir of the metal substrate. In this $\{AlO_4\}$ model, the Al^{3+} ions are each coordinated to four O^{2-} ions in the same geometry as the Si^{4+} ions in the pure silica film (Figure 2). Another possibility is that the Al^{3+} ions are coordinated by three O^{2-} ions from the top layer of the film, but are not bonded to an O^{2-} ion at the substrate interface ($\{AlO_3\}$ model; Figure 2).

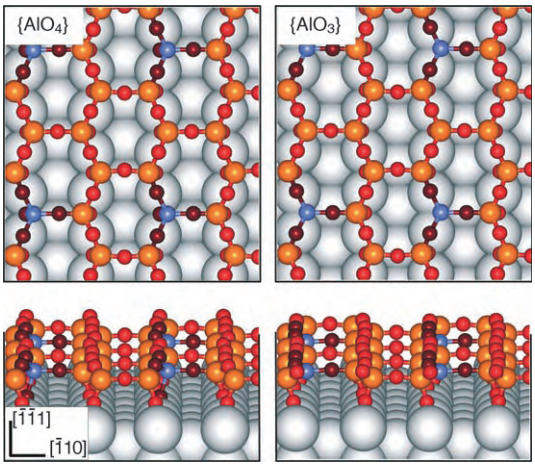

Figure 2. Top and side views of the $\{AlO_4\}$ and $\{AlO_3\}$ models of aluminosilicate films on a Mo(112) substrate. Mo gray, Al blue, Si orange, O red.

These two models were examined with DFT calculations by considering a (4×2) surface cell, in which one of the eight silicon atoms was replaced by an aluminum atom, resulting in compositions of $AlSi_7O_{20}$ for the $\{AlO_4\}$ model and $AlSi_7O_{19}$ for the $\{AlO_3\}$ model. Both models are minima on the potential energy surface.[15]

For the STM image shown in Figure 1b, the tunneling parameters were chosen such that the oxygen atoms in the topmost layer of the film are detected as protrusions.[11,12] In the images simulated from the DFT-optimized structures of the $\{AlO_4\}$ and $\{AlO_3\}$ models, the aluminum-bonded surface oxygen atoms, which have a higher corrugation amplitude, are brighter than the silicon-bonded oxygen atoms (Figure 1). This effect is more pronounced for the $\{AlO_3\}$ model, because of the enhanced relaxation associated with the absence of aluminum-bonded interface oxygen atoms. Comparison of the experimental and simulated STM images, therefore, favors the $\{AlO_3\}$ model.

Further support for the $\{AlO_3\}$ model comes from high-resolution PES. In PE spectra of the silica films (Figure 3, top spectra), the O 1s region, which is much better resolved than

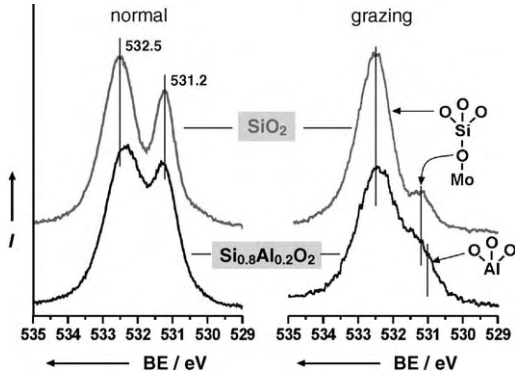

Figure 3. O 1s region of the PE spectra of silica (top) and aluminosilicate (bottom: Al/Si ≈ 1:5) films recorded at normal and grazing emission angles.

by conventional XPS,[11–13] comprises two distinct peaks, which are assigned to oxygen species in the top layer (at 532.5 eV) and in the molybdenum-bonded interface layer (at 531.2 eV).[11] The signal at lower binding energy (BE) is strongly attenuated when the spectrum is measured at a grazing emission angle, confirming that the associated oxygen species are located in the subsurface region. The presence of interface oxygen atoms is also manifested by a well-resolved signal at 228.2 eV in the Mo 3d region (not shown), which is attributed to partially oxidized molybdenum atoms at the substrate surface (a signal at 228.0 eV is also observed, which is assigned to metallic molybdenum).

As a result of the presence of approximately 20 mol% aluminum in the aluminosilicate film, the O 1s signals in the PE spectra broaden (see Figure 3, bottom spectra), because the oxygen atoms (which are bonded to silicon and/or aluminum atoms) occupy a variety of environments. Our DFT calculations revealed that the oxygen atoms in Si-O-Al units have a BE of 531 eV, which overlaps with that of the interface oxygen atoms in Si-O-Mo units. As a result, the intensity of the lower-BE O 1s signal is notably higher in the PE spectrum of the aluminosilicate film than in that of the pure silica film. Because the aluminum-bonded oxygen atoms are in the top layer of the film, this signal is less attenuated in the aluminosilicate spectrum recorded at a grazing emission angle. According to our calculations, the oxygen atoms in the

 © 2006 Wiley-VCH Verlag GmbH & Co. KGaA, Weinheim

Al-O-Mo units of the $\{AlO_4\}$ model should be manifested by a signal at 530 eV, which is not observed experimentally. Therefore, our PES results also favor the $\{AlO_3\}$ model.

The IR spectra of the silica and aluminosilicate films, as well as the calculated frequencies for the $\{AlO_3\}$ model are presented in Figure 4. Note that only vibrations resulting in

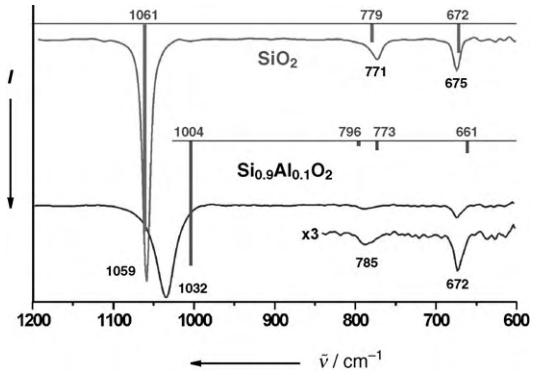

Figure 4. IR spectra of silica and aluminosilicate (Al/Si ≈ 1:9) films. An enlargement of the low-frequency region of the aluminosilicate spectrum is also shown. Bars indicate the frequencies calculated for the $\{AlO_3\}$ model; the height of the bars is proportional to the signal intensity.

changes in the dipole moment that are perpendicular to the surface can be detected, owing to the presence of the metal substrate. The main peak at 1059 cm^{-1} in the spectrum of the silica film appears as a significantly broadened peak at 1032 cm^{-1} in the spectrum of the aluminosilicate film. This signal originates from asymmetric Si-O-Mo stretching vibrations[11,12] and is, therefore, strongly influenced by the partial replacement of silicon by aluminum. The line broadening in the aluminosilicate spectrum is consistent with the less-ordered structure of the film relative to that of the pure silica film. The weak IR features at 771 and 675 cm^{-1} in the silica spectrum, which are assigned to symmetric stretching and bending modes, are also altered in the aluminosilicate spectrum.

The agreement between the calculated and experimental frequencies is not as good as for the silica films. This discrepancy can be partially explained by the relatively small (4×2) unit cell used in the calculations, which results in an ordered superstructure, whereas in the real film the aluminum atoms are randomly dispersed. Nonetheless, the calculations correctly predict the direction of the energy shift of the main signal, as well as the splitting of the signal near 770 cm^{-1}.

In summary, the preparation of an ordered aluminosilicate film on a metal substrate has been achieved through the codeposition of aluminum and silicon onto a Mo(112) surface in an O_2 atmosphere and subsequent vacuum annealing. Experimental and theoretical results show that, in aluminosilicate films with low Al/Si ratios, aluminum atoms partially replace the silicon atoms of the silica structure to form a 2D network of corner-sharing $\{AlO_3\}$ and $\{SiO_4\}$ units.

Experimental Section

The experiments were carried out in an ultra-high vacuum (UHV) chamber (base pressure 2×10^{-10} mbar) equiped with LEED, XPS, IRAS, and STM. The aluminosilicate films were prepared by a method similar to that described for the preparation of silica films.[11,12] Aluminum and silicon were codeposited onto a p(2×3)-O-Mo(112) surface at 900 K in an O_2 atmosphere (5×10^{-8} mbar). The total amounts of aluminum and silicon at different Al/Si ratios corresponded to slightly more than one monolayer (relative to the Mo(112) substrate). The mixed-oxide overlayer was then annealed at 1100 K in vacuum for 5 min. The PES experiments using synchrotron radiation were performed in a UHV chamber at BESSY II (beamline UE52-PGM1) with a Scienta R4000 analyzer (energy resolution below 200 meV).

The methodology applied in the DFT calculations was described previously.[11–13] The Vienna ab initio simulation package (VASP)[16,17] was used with the Perdew–Wang (PW91) exchange-correlation functional[18] and the projector augmented wave (PAW) method.[19,20] The basis set consisted of plane waves with energies up to 400 eV, and a $4\times4\times1$ Monkhorst–Pack grid was used for the generation of k points.[21] The vibrational spectra were calculated using the central finite-difference method; intensities were determined from the derivative of the dipole-moment component perpendicular to the surface. To compensate for systematic errors of DFT, we applied an empirical scaling factor of 1.0312 to the calculated frequencies.[11,22] Core-level binding energies including final state effects were calculated using a modified PAW method. STM images were simulated from the self-consistent charge density by employing the Tersoff–Hamann approach.[23]

Received: July 5, 2006
Revised: August 17, 2006
Published online: October 19, 2006

Keywords: aluminosilicates · mixed oxides · thin films · zeolites

[1] *Introduction to Zeolite Science and Practice* (*Studies in Surface Science and Catalysis*, *Vol. 137*), (Eds.: H. van Bekkum, P. A. Jacobs, E. M. Flanigen, J. C. Jansen), Elsevier, Amsterdam, **2001**.
[2] M. Sierka, J. Sauer, *J. Phys. Chem. B* **2001**, *105*, 1603.
[3] M. Bäumer, H.-J. Freund, *Prog. Surf. Sci.* **1999**, *61*, 127.
[4] S. Chambers, *Surf. Sci. Rep.* **2000**, *39*, 105.
[5] S. Wendt, Y. D. Kim, D. W. Goodman, *Progr. Surf. Sci.* **2003**, *74*, 141.
[6] W. Weiss, W. Ranke, *Progr. Surf. Sci.* **2002**, *70*, 1.
[7] J. Choi, S. Ghosh, Z. Lai, M. Tsapatsis, *Angew. Chem.* **2006**, *118*, 1172; *Angew. Chem. Int. Ed.* **2006**, *45*, 1154.
[8] J. Coronas, J. Santamaria, *Top. Catal.* **2004**, *29*, 29.
[9] G. Shu, J. Liu, A. S. T. Chiang, R. W. Thompson, *Adv. Mater.* **2006**, *18*, 185.
[10] T. Schroeder, M. Adelt, B. Richter, M. Naschitzki, J. B. Giorgi, M. Bäumer, H.-J. Freund, *Surf. Rev. Lett.* **2000**, *7*, 7.
[11] J. Weissenrieder, S. Kaya, J. L. Lu, H. J. Gao, S. Shaikhutdinov, H. J. Freund, M. Sierka, T. K. Todorova, J. Sauer, *Phys. Rev. Lett.* **2005**, *95*, 076103.
[12] T. K. Todorova, M. Sierka, J. Sauer, S. Kaya, J. Weissenrieder, J.-L. Lu, H.-J. Gao, S. Shaikhutdinov, H.-J. Freund, *Phys. Rev. B* **2006**, *73*, 165414.
[13] M. Sierka, T. K. Todorova, S. Kaya, D. Stacchiola, J. Weissenrieder, J.-L. Lu, H.-J. Gao, S. Shaikhutdinov, H.-J. Freund, J. Sauer, *Chem. Phys. Lett.* **2006**, *424*, 115.
[14] Ch. Gründling, J. A. Lercher, D. W. Goodman, *Surf. Sci.* **1994**, *318*, 97.
[15] Because of the different chemical compositions of the models, their relative stabilities may depend on the oxygen partial

 © 2006 Wiley-VCH Verlag GmbH & Co. KGaA, Weinheim

pressure. A full DFT analysis will be presented in future publications.
[16] G. Kresse, J. Furthmüller, *Comput. Mater. Sci.* **1996**, *6*, 15.
[17] G. Kresse, J. Furthmüller, *Phys. Rev.* B **1996**, *54*, 11169.
[18] J. P. Perdew, J. A. Chevary, S. H. Vosko, K. A. Jackson, M. R. Pederson, D. J. Singh, C. Fiolhais, *Phys. Rev. B* **1992**, *46*, 6671.
[19] P. E. Blöchl, *Phys. Rev. B* **1994**, *50*, 17953.
[20] G. Kresse, D. Joubert, *Phys. Rev. B* **1999**, *59*, 1758.
[21] H. J. Monkhorst, J. D. Pack, *Phys. Rev. B* **1976**, *13*, 5188.
[22] A. P. Scott, L. Radom, *J. Phys. Chem.* **1996**, *100*, 16502.
[23] J. Tersoff, D. R. Hamann, *Phys. Rev. B* **1985**, *31*, 805.

 © 2006 Wiley-VCH Verlag GmbH & Co. KGaA, Weinheim